

NASA Conference Publication 2220

Proceedings of the Thirteenth Annual  
Precise Time and Time Interval (PTTI)  
Applications and Planning Meeting

A meeting held at the  
Naval Research Laboratory  
Washington, D.C.  
December 1—3, 1981



**NASA Conference Publication 2220**

**Proceedings of the Thirteenth Annual  
Precise Time and Time Interval (PTTI)  
Applications and Planning Meeting**

**A meeting held at the  
Naval Research Laboratory  
Washington, D.C.  
December 1—3, 1981**

Sponsored by

Naval Observatory  
NASA Goddard Space Flight Center  
Naval Electronic Systems Command  
Naval Research Laboratory  
Defense Communications Agency  
Chief of Naval Operations  
National Bureau of Standards  
Army Electronics Technology  
and Devices Laboratory  
Rome Air Development  
Center



National Aeronautics and  
Space Administration

**Scientific and Technical  
Information Branch  
1982**





## EXECUTIVE COMMITTEE

Schuyler C. Wardrip, Chairman  
NASA Goddard Space Flight Center

Ralph T. Allen  
Naval Electronic Systems Command

Charles A. Bartholomew  
Naval Research Laboratory

Andrew R. Chi  
NASA Goddard Space Flight Center

LCDR Glen E. Eubanks  
Chief of Naval Operations

Dr. Arthur O. McCoubrey  
National Bureau of Standards

James A. Murray, Jr.  
Naval Research Laboratory

Kenneth Putkovich  
Naval Observatory

Dr. Samuel R. Stein  
National Bureau of Standards

Dr. Harris A. Stover  
Defense Communications Agency

Straton M. Spyropoulos  
Naval Observatory

Dr. John R. Vig  
Army Electronics Technology  
and Devices Laboratory

Dr. Nicholas F. Yannoni  
Rome Air Development  
Center

GENERAL CHAIRMAN

ANDREW R. CHI  
NASA Goddard Space Flight Center

PTTI 1981

TECHNICAL PROGRAM COMMITTEE

DR. RICHARD L. SYDNOR, CHAIRMAN  
Jet Propulsion Laboratory

DAVID W. ALLAN  
National Bureau of Standards

PAUL F. KUHNLE  
Jet Propulsion Laboratory

DR. CARROLL O. ALLEY  
University of Maryland

DR. HARRIS A. STOVER  
Defense Communications Agency

DR. ROGER BEEHLER  
National Bureau of Standards

DR. ROBERT F. C. VESSOT  
Smithsonian Astrophysical Observatory

EDITORIAL COMMITTEE

L. J. RUEGER, CHAIRMAN  
Johns Hopkins University  
Applied Physics Laboratory

DR. JAMES BARNES  
National Bureau of Standards

DR. JOHN R. VIG  
Army Electronics Technology  
and Devices Laboratory

ERIC BLOMBERG  
Kernco, Inc.

SCHUYLER C. WARDRIP  
NASA Goddard Space Flight Center

PAUL F. KUHNLE  
Jet Propulsion Laboratory

DR. NICHOLAS F. YANNONI  
Rome Air Development Center

O. JAY OAKS  
Naval Research Laboratory

CHARLOTTE M. HARRIGAN — SECRETARY  
Applied Physics Laboratory

SESSION CHAIRMEN

SESSION I

DR. HARRIS A. STOVER  
Defense Communications Agency

SESSION II

PAUL F. KUHNLE  
Jet Propulsion Laboratory

SESSION III

DR. ROGER BEEHLER  
National Bureau of Standards

SESSION IV

DAVID W. ALLAN  
National Bureau of Standards

SESSION V

DR. ROBERT F. C. VESSOT  
Smithsonian Astrophysical Observatory

SESSION VI

DR. CARROLL O. ALLEY  
University of Maryland

#### ARRANGEMENTS

Charles A. Bartholomew, NRL  
James A. Murray, Jr., NRL  
Joseph White, NRL

#### FINANCE COMMITTEE

Straton M. Spyropoulos, USNO  
Schuyler C. Wardrip, GSFC

#### PUBLICATIONS

Charlotte M. Harrigan, APL  
L. J. Rueger, APL  
Schuyler C. Wardrip, GSFC

#### TECHNICAL ASSISTANCE

Fredrick Danzy, NRL  
Stan Falvey, NRL  
Robert Hersh, NRL  
Chester Kleczek, NRL  
Wayne Lloyd, NRL

#### PRINTING

Charles V. Hardesty, GSFC  
Donald E. Ellis, GSFC

#### RECEPTIONISTS

Sheila Faulkner, USNO  
Kathy Gifford, NRL  
Donna Kline, NBS  
Kathy McDonald, NRL  
Marie Nader, GSFC  
Dorothy Outlaw, USNO  
Stella Scates, NRL  
Emma Thomas, GSFC

#### BANQUET SPEAKER

Astronaut Guy S. Gardner, Major USAF  
Subject: Overview of Space Shuttle and  
Future Pay Loads



## FOREWORD

These proceedings contain the papers accepted by the Technical Program Committee for the 13th Annual Precise Time and Time Interval Applications and Planning Meeting. In addition, these proceedings include the discussions following the presentations. There were 200 registered attendees; of this number 17 were from 9 foreign countries.

The objective of the meeting was to provide an opportunity for the program planners to meet those who are engaged in research and development and to keep abreast of the state-of-the-art of the technological development. At the same time, it provided an opportunity for the engineers and scientists to meet the program planners and to learn what technology can be applied. This objective is clearly reflected by the title of the meeting. While the intent of the meeting was designed for logical evolution of technology and program development, it has not been easy, indeed, to reduce it into practice.

Since the first meeting, held informally at the U.S. Naval Observatory in 1969, we have had 12 years of experience and growth. As we reach the tender age of the teens, we begin to find support from the sponsors as well as from the participants. It will always remain a challenge to us all and, in particular, to those who have the responsibility of managing and steering the meetings to achieve our stated goals.

The Executive Committee has been fortunate in attracting new and able leaders to organize and plan the meetings. Their rewards are reflected by the increasing number, and the continuing support of the sponsors. On behalf of the Executive Committee, I want to recognize the excellent effort of the Technical Program Committee and the Session Chairmen for their leadership and contributions to make this meeting a success. Finally, I want to express our appreciation to the host for 1981, the Naval Research Laboratory, the many people behind the scene, and the secretaries, whose support was vital to conduct the meeting smoothly.



Andrew R. Chi  
General Chairman





## CONTENTS

	<u>Page</u>
CALL TO SESSION. . . . . <i>Andrew R. Chi</i>	1
WELCOME ADDRESS. . . . . <i>Dr. Bruce Wald</i>	3
OPENING COMMENTS . . . . . <i>Dr. John McElroy</i>	5
OPENING COMMENTS . . . . . <i>Dr. Gernot Winkler</i>	7
OPENING COMMENTS . . . . . <i>Rear Admiral J. B. Mooney, Jr.</i>	9
OPENING COMMENTS . . . . . <i>Rear Admiral C. J. Moore</i>	11
OPENING COMMENTS . . . . . <i>Captain Raymond A. Vohden</i>	13
OPENING COMMENTS . . . . . <i>Dr. Richard L. Sydnor</i>	15

## SESSION I PTTI REQUIREMENTS AND SPECIFICATIONS

Precise Time and Time Interval Users, Requirements and Specifications . . . . . <i>James R. Bowser</i>	27
Requirements and Specifications. Forum with Audience Participation . . . . .	45

## CONTENTS (continued)

Page

### SESSION II NETWORK CLOCK OPERATIONS

Precise Time Dissemination via Portable Atomic Clocks . . . . .	87
<i>Kenneth Putkovich</i>	
Loran-C, An Overview . . . . .	121
<i>Lt. William J. Thrall</i>	
Using the NAVSTAR Global Positioning System as a Global Timing System . . . . .	133
<i>Karl L. Kovach</i>	
A History and Analysis of Hydrogen Maser Reliability . . . . .	167
<i>J. B. Curtright</i>	
Field Operations with Cesium Clocks in HF Navigation Systems . . . . .	175
<i>E. H. Christy and D. A. Clayton</i>	
High Accuracy Omega Timekeeping . . . . .	187
<i>Edward A. Imbier</i>	
Time Information Distribution at White Sands Missile Range . . . . .	199
<i>R. A. Stimets, Jr.</i>	
Relationships Between US Naval Observatory, LORAN-C and Defense Satellite Communication System . . . . .	201
<i>Laura G. Charron</i>	
LORAN-C Prediction Problems. . . . .	217
<i>Carl F. Lukac</i>	

### SESSION III LOCAL TIME AND FREQUENCY TRANSFER

Comparison of VLBI, TV and Traveling Clock Techniques for Time Transfer . . . . .	231
<i>J. H. Spencer, E. B. Waltman, K. J. Johnston N. J. Santini, W. J. Klepczynski, D. Matsakis P. Angerhofer, and G. Kaplan</i>	
Development of Optical Fiber Frequency and Time Distribution Systems . . . . .	243
<i>George Lutes</i>	

## CONTENTS (continued)

	<u>Page</u>
Low Noise Buffer Amplifiers and Buffered Phase Comparators for Precise Time and Frequency Measurement and Distribution . . . . .	263
<i>R. A. Eichinger, P. Dachel, W. H. Miller, and J. S. Ingold</i>	
Time Transfer of IRIG-B Time Code Via Dedicated Telephone Link. . . . .	281
<i>G. Missout, J. Beland, D. Lebel, G. Bedard and P. Bussiere</i>	
Variations in Propagation Delay Time for Line Ten (TV) Based Time Transfers . . . . .	299
<i>M. C. Chiu and B. W. Shaw</i>	
The Role of Precise Time in IFF . . . . .	309
<i>William Bridge</i>	
Digital Processing Clock. . . . .	325
<i>David H. Phillips</i>	
Time Comparison via OTS-2 . . . . .	347
<i>G. de Jong and R. Kaarls</i>	

## SESSION IV GLOBAL TIME AND FREQUENCY TRANSFER

Design Approach for a Microprocessor Based GPS Time Transfer Receiver . . . . .	373
<i>P. C. Ould and R. J. Van Wechel</i>	
Time Transfer Using NAVSTAR GPS . . . . .	389
<i>A. J. Van Dierendonck, Q. D. Hua, J. R. McLean and A. R. Denz</i>	
Global Positioning System Time Transfer Receiver (GPS/TTR) Prototype Design and Initial Test Evaluation . . . . .	419
<i>J. Oaks, A. Frank, S. Falvey, M. Lister J. Buisson, C. Wardrip, and H. Warren</i>	
Long Term Frequency Stability Analysis of the GPS NAVSTAR 5 and 6 Cesium and Rubidium Clocks . . . . .	451
<i>Thomas B. McCaskill, Sarah Stebbins, Clarence Carson, and James Buisson</i>	

## CONTENTS (continued)

	<u>Page</u>
Time Code Dissemination Experiment Via The SIRIO-1 VHF Transponder. . . . .	469
<i>E. Detoma, G. Gobbo, S. Leschiutta, and V. Pettiti</i>	
VLBI Clock Synchronization Measurements With the Block I System . . . . .	489
<i>M. G. Roth</i>	
Maintaining Highly Accurate Global Syntonization Using the Hydrogen Line . . . . .	503
<i>Samuel C. Ward</i>	
Clocks for Airborne Systems. . . . .	505
<i>Norman Houlding</i>	
Unprecedented Syntonization and Synchronization Accuracy via Simultaneous Viewing with GPS Receivers and Construction Characteristics of an NBS/GPS Receiver . . . . .	527
<i>Dick D. Davis, Marc Weiss, Alvin Clements and David W. Allan</i>	

## SESSION V INNOVATIVE FREQUENCY STANDARDS

Cryogenic Masers . . . . .	547
<i>A. J. Berlinsky and W. N. Hardy</i>	
A Trapped Mercury 199 Ion Frequency Standards. . . . .	563
<i>Leonard S. Cutler</i>	
Prospects for Stored Ion Frequency Standards . . . . .	579
<i>D. J. Wineland</i>	
Recent Developments and Proposed Schemes for Trapped Ion Frequency Standards . . . . .	593
<i>L. Maleki</i>	
A Rubidium Clock for GPS. . . . .	609
<i>W. J. Riley</i>	

## CONTENTS (continued)

	<u>Page</u>
Investigations of Laser Pumped Gas Cell Atomic Frequency Standard . . . . .	631
<i>C. H. Volk, J. C. Comparo and R. P. Frueholz</i>	
Magnetic State Selection in Atomic Frequency and Time Standards. . . . .	645
<i>H. E. Peters</i>	
Frequency Stability of Maser Oscillators Operated With Enhanced Cavity Q . . . . .	667
<i>Michel Tetu, Pierre Tremblay, Patrick Lesage and Pierre Petit</i>	

## SESSION VI RELATIVITY AND GRAVITY WAVES

Introduction to the Fundamental Concepts of General Relativity and to Their Required Use In Some Modern Timekeeping Systems . . . . .	687
<i>C. O. Alley</i>	
The Role of the Deep Space Network's Frequency and Timing System in the Detection of Gravitational Waves . . . . .	729
<i>John C. Mankins and John LuValle</i>	
The Implication of Precise Timekeeping for Doppler Gravitational Wave Observations. . . . .	757
<i>John R. Anderson, F. B. Estabrook and J. W. Armstrong</i>	
Lamp Reliability Studies for Improved Satellite Rubidium Frequency Standard . . . . .	767
<i>R. P. Frueholz, M. Wun-Fogle, H. U. Eckert, C. H. Volk and P. F. Jones</i>	
Magnetic Shielding and Vacuum Test for Passive Hydrogen Masers . . . . .	791
<i>D. U. Gubser, S. A. Wolf A. B. Jacoby and L. D. Jones</i>	

## CONTENTS (concluded)

	<u>Page</u>
A Phase-Coherent Link Using the ANIK-B Satellite for Geodetic VLBI. . . . .	801
<i>W. B. Waltman, S. H. Knowles, W. H. Cannon, D. A. Davidson, W. T. Petrachenko, J. L. Ven, J. Popelar, D. N. Fort and J. Galt</i>	
Composite-Type <sup>87</sup> Rb Optical-Pumping Light Source for the Rubidium Frequency Standard. . . . .	803
<i>Nobunori Oura, Naimu Kuramochi, Shiegeya Naritsuka and Teruhiko Hayashi</i>	
An NNSS Satellite Timing Receiver. . . . .	817
<i>C. L. Jain, K. Kumar, H. I. Andharia, Mohan Singh, V. D'Souza, V. K. Goel and A. K. Sisodia</i>	
No Warmup Crystal Oscillator . . . . .	831
<i>David H. Phillips</i>	
CONCLUSION . . . . .	851
13th Annual PTTI Registration . . . . .	853

CALL TO SESSION  
Mr. Andrew Chi  
General Chairman  
NASA Goddard Space Flight Center

CHAIRMAN CHI: It is my pleasant duty to officially open this Thirteenth Annual Precise Time and Time Interval Applications and Planning Meeting.

In retrospect, it is indeed a record for us to have had 12 meetings in the past dozen years. As we reach adolescence, we cannot help but look forward to the future, toward maturity, and to look backward with pride and appreciation for our accomplishments and for the generous support of our sponsors. And especially those who contribute so much of their time and resources to foster our growth.

Although the number 13 is ominously associated with omen by some who are superstitious, it is really a number associated with growth. Like the number of the moons around the Jupiter, it was always 13 until 1979, when the Voyagers I and II flew by the planet and discovered that there are now at least 16.

I propose that we continue to grow and to strive toward our objectives. Who knows from this year on, we may, like JPL, someday reach the stars like Canis Major. It is certainly appropriate for us to dream along these lines from this year, the year of the Canine, according to the Chinese calendar.

I would like to use this opportunity to welcome our two new sponsors, the United States Army Electronics Technology and Devices Laboratory of Fort Monmouth, New Jersey; and the United States Air Force Research and Development Command of the Rome Air Development Center, Hanscom Air Force Base, Massachusetts.

It is again my pleasure to introduce to your our host, the Associate Director of Research of the Naval Research Laboratory, Dr. Bruce Wald who will give us the welcome remarks.





## WELCOME ADDRESS

Dr. Bruce Wald  
Associate Director of Research  
Naval Research Laboratory

DR. WALD: For those of you who are paying too much attention to the program, and not enough to the person who spoke, I am not Alan Berman. Alan, unfortunately has a boss and the Chief of Naval Research called him away on very short notice to attend an O & R retreat this morning.

Unfortunately, I have a boss, too, and he asked me to come here and substitute for him. But I am not at all disappointed that he asked me to do it, because it has occurred to me from time to time "isn't it too bad that I am not alive at the time that the fundamental breakthroughs in science are being made", that I could not have been alive at the time of Newton, or Galileo.

But if we take a historical perspective, this is the century of time. In many respects the 18th Century was the century in which precision in the measurement of mass first had its impact. I am thinking of the classical chemists, the name of Lavoisier comes to mind because he was also the executive secretary to the French Commissions on Weights and Measures, and he also improved gun powder so his science would have some military relevance.

But by the use of the chemical balance, he really reversed the concepts of the time on which were elements and which were compounds, which were the ores and which were the names of metals. He did this with precision in mass.

I think the 19th Century was the century of precision in length and in angular measurement. This not only had tremendous economic impact in the industrial revolution, interchangeable machinery, mass production, but it also had great scientific impact in spectroscopy in which precision in measurement in length and small changes and little fine spectra, things that could not be measured before, provided the clues that are helping to unlock some fairly fundamental questions on the nature of matter.

I think the 20th Century has been the century of time. When historians a few hundred years from now look back at the 20th Century they may think that the effect of this revolution about time may be just as profound. But in order to check that thesis, I went last night looking for as current -- well, not as current, but as important a book as I could find on perspective of science around the turn of the century.

What I found is Carl Pearson's Grammar of Science, First Edition, 1892, in which he discusses the problem of time. He spends a chapter, and I think what he is saying is despite all the triumphs of observational astronomy, that time is purely a psychological concept, because after all there is no real standard and there is no way of telling the tidal friction hasn't slowed down the planets. If the number of days in the year are changed we don't know if the days are getting shorter or the year is getting longer. And that time is purely a psychological concept.

I wish I could have Carl Pearson attending this conference and hearing some of the things that have been done by the precise time, not only in the engineering sense, but the things that have been made possible in communications and navigation, and the fundamental physics sense for improving our understanding about the fabric of space.

So, perhaps in the future people will look back on the 20th Century and say that the revolution in time was as important as the one in the 18th Century on mass, and in the 19th Century on length.

But since I can't have Carl Pearson here, I am going to listen with interest, as long as I can this morning, on behalf of the Commanding Officer and the Director of Research, I want to welcome you to NRL. I want to say as an institution, we are proud to have been the sponsor of the early conferences and to have so many distinguished colleagues and sister organizations cosponsor them. And we are looking forward to a very productive meeting.

## OPENING COMMENTS

Dr. John McElroy  
Deputy Director  
NASA Goddard Space Flight Center

DR. McELROY: I am really delighted to have this opportunity to welcome you here to this 13th Conference. I was fortunate enough to attend the one last year, and my own association with the conference goes back from colleagues of mine who have participated in this over many years.

If you look back over the past dozen or so years, at this conference as measured in many respects, we have seen numerous, extremely exciting breakthroughs which have been brought forth here. And I think if you look back over the conference proceedings you can get a tremendous measure of the dynamic nature of this subject and its technology.

In the beginning, when the meeting was originally sponsored by the Naval Observatory and NRL, and the Naval Electronics Systems Command, it was known as the PTTI - Strategic Planning Meeting. Later on that was shortened to simply the Planning Meeting. And in about 1975 it took on this current title, reflecting both the planning nature, as well as the achievement nature of the meeting.

If the number of sponsors is any measure of interest, obviously you have been highly successful. Certainly starting off with just the three, we have gradually expanded the sponsorship up to the present number listed on the brochure, with some nine sponsors being currently listed.

I notice that Fort Monmouth is now here, as one of the sponsors. I will try not to hold any grudges against Fort Monmouth -- some more than 25 years ago, I had the experience of going through the radar school there, and later served under a lieutenant who had learned very well the first rule of leadership, which is namely when faced with a difficult problem, to tell the sergeant to get that radar up on top of that mountain.

I came to appreciate transportable in a way in which I have never since -- I have never quite not been able to react to the word "transportable" since my experience at Monmouth.

But, perhaps, those of you who go back that far will remember that there was a precision time interval measurement system in the old "Topsy Dog" called a mercury delay line, which took a phenomenal amount of period to settle down.

If I look back over the years of achievement of the group here, basically, I see that you have advanced the state-of-the-art a decade-per-decade. We keep increasing, and increasing the frequency stability of our standards and thereby the scientific and technical payoff that we can get from those standards.

And I look forward to hearing the results of the most recent measurements that have been made and the most recent developments. You have paralleled the NASA program, going back to Apollo 11 when we were talking about 10 to the minus 12 and 10 to the minus 13th, and gradually moving up to 10 to the minus 14th, 10 to the minus 15th these days.

So, with a little bit of luck, another decade will see at least another decade of improvement and with a little bit of luck, all of us will still be here to share in some of the excitement.

So, I welcome you to the conference, Goddard intends to keep right on sponsoring it. We think it is a highly productive exercise.

Thank you.

## OPENING COMMENTS

Dr. Gernot Winkler  
Director, Time Service Division  
United States Naval Observatory

Dr. WINKLER: It is not quite correct that I was the founder on the PTTI Strategic Planning Meeting in 1969. Back in that year the Observatory was faced with the responsibility of coordinating the overall DoD PTTI operations, but with practically no way of finding out what is going on and no way of influencing these. And so somebody in my group, I think it was Nick Acrivos, who has since retired, had a terrific idea, why don't we call a conference. And that is how it all started.

At that time, if I may use this opportunity to make a comment about it, we had actually two conferences one for discussion and review of progress to provide an overview of the state-of-the-art for our managers. But we also had a second part where a smaller group met, where plans were discussed.

I think we have lost the second part, but the Executive Committee and the Conference Committee have come up with something which I think should serve the same purpose. I am very curious to see how this will work out.

My main concern, as I look back over these years, is that in order to be successful, we must have audience participation. We must hear from you, who are much closer to the actual needs of the area, we must hear from you what is needed, how could things be improved.

So I am asking you during this conference to do your very best by asking questions and by giving your opinions. This is one of very few conferences which records and prints at least the more important comments. I think they are only slightly edited. And from many users I have been told that this is one of the better features of the proceedings, that we get the comments afterwards, so they are not just made and forgotten, but they are somehow documented.

So, please participate.



## OPENING COMMENTS

Rear Admiral J. B. Mooney, Jr.  
Director of the Naval Oceanographic Division  
Office of the Chief of Naval Operations

REAR ADMIRAL J. B. MOONEY, JR.: Being in a new position of oceanographer of the Navy has some pluses and minuses, and one of the pluses is that I am expected to give short greetings to important assemblies, such as this, without inadvertently shaking the foundations upon which these meetings were founded.

My responsibilities as oceanographer include resource sponsorship for the Naval Observatory and the precise time and time interval coordination.

It is a pleasure for me to work very, very closely with these folks at the Naval Observatory, the timekeepers of the nation, and also folks who have many other illustrious achievements over the more than 150 years.

I think it is appropriate that the various efforts now the responsibility of the oceanographer of the Navy conducted from the shared location of the Observatory. Our predecessor started out together in 1830 and now we are back together, and the old things that were done at the depot with charts and instruments are now coordinated and consolidated at the Observatory where we have meteorology, oceanography, MC&G and time and astronomy, all at the same place.

I am pleased to know that your conference this year is placing emphasis on tasking requirements, and planning and management PTTI activities. Precise time and time interval play an essential role in naval operations. However, the clear articulation of requirements is a problem for us because we need to have them defined so that we can properly document our resource needs.

I hope that you will find Mr. Bowser's paper on DoD PTTI requirements to be a contribution to our planning for our future needs. The study conducted by Automation Industries, also addresses DoD PTTI management problems. It is already being used to generate a revised DoD directive on precise time.

A significant event will take place at the Observatory commencing in 1982, and we will begin procurement of hydrogen masers for upgrading the Naval Observatory master clock system.

All four of the PTTI sponsors in the Navy have been involved in the upgrade of this master clock, NAVELEX, NRL and the Naval Observatory, and my own division, 952.



The purpose of this meeting is to help all of us managers make better use of our time and to manage our PTI activities.

I hope that our objectives for these meetings are realized and our bonds of communication are strengthened by sharing the common challenges and achievements. I will be with you sometime this morning and I hope to join with you at various times throughout the time that you are here.

Thank you for coming.

## OPENING COMMENTS

Rear Admiral C. J. Moore  
Deputy Commander  
Naval Electronic Systems Command

REAR ADMIRAL C. J. MOORE: Good morning, ladies and gentlemen.

It is a great pleasure that I welcome you on behalf of the Naval Electronic Systems Command to the 13th Annual Precise Time and Time Interval Applications and Planning Meeting.

As you have heard, and as many of you already knew, NAVELEX engineers have been associated with this meeting from its inception in the late 1960s. The system we have provided to the fleet, the systems we are providing to the fleet and the systems that we will provide to the fleet tomorrow demand the best time and frequency precision we can achieve, both on a global and on a local level.

Command, control, communications and intelligence systems and the ability of a fleet to wage a successful electronic battle are intimately tied to cesium clocks dispersed throughout the fleet and synchronized to permit a rapid real time interference-free flow of tactical data and command decisions.

Today we have to be satisfied with atomic frequency standards which precisions of a few parts in  $10^{11}$  and time synchronization to 100 nanoseconds, this only on a local level.

Through joint planning meetings, such as this, we hope to develop ideas and techniques that will allow the fleet to have rugged frequency standards with much greater long-term stability and with global time synchronization to 100 nanoseconds.

In line with these future goals, I would like to mention two things that are happening around the Naval Electronic Systems Command in PTTI. First, my director, which is the Command Control Communications and Intelligence Systems and Technology Director, has assumed responsibility for supporting research and exploratory developments at the Naval Observatory starting in FY 82.

Hopefully, we can improve the financial support of the Naval Observatory's PTTI R&D efforts.

Second, our Navy PTTI manager, which is PME-110, has recently established plans of action and milestones leading to the development of the next generation of Navy cesium beam frequency standards and a time distribution amplifier, both of which are slated for production in the FY 86 and 87 timeframe.

This cesium beam standard we intend to militarize, so that it will have long-term stability to satisfy the needs which I mentioned earlier.

Again, let me say that it is a pleasure to be here and for NAVELEX to support this effort.

Thank you.

## OPENING COMMENTS

Captain Raymond A. Vohden  
Superintendent of the Naval Observatory

CAPTAIN VOHDEN: Good morning. As Superintendent of the United States Naval Observatory, it is gratifying to see so many of you here today. The Naval Observatory was the sponsor and originator of the first Annual PTTI Conference 13 years ago. And, as the Superintendent of the Observatory, it is a real pleasure to welcome the Army Electronics Technology and Devices Laboratory and the Air Force Rome Air Development Center, as the eighth and ninth sponsors of this annual meeting.

I consider this a very significant event because it is the first time that all three services have joined in sponsorship of a PTTI meeting. I hope this is the forerunner of greater participation by the Army and Air Force in future PTTI meetings, and that eventually your services will have an even more active role in the sponsorship of these annual conferences.

In February 1965, the Department of Defense delegated responsibility to the Naval Observatory for PTTI. On 28 April 1969, the first PTTI conference was held at the Observatory. The purpose of that conference was to reveal if we were meeting all the requirements and to determine what we could do better than we were doing then.

Four specific goals were set, the first one was to establish a sound working relationship between the Observatory and each DoD component, contractor and other interested agencies. The second was to review existing PTTI requirements and examine possible future requirements. The third was to provide advice and guidance to all PTTI users. The fourth was to promote and establish the means for maintaining operational uniformity of PTTI functions.

In review, it appears that the PTTI conferences have been very successful in accomplishing the original purpose and goals. It must be credited with providing the major means to accomplish technical coordination.

Without the conference we would find the PTTI area in much worse shape than it actually is. If then the conference has been at least reasonably successfully, can anything be done to improve it further?

The answer which I received to this question is that several steps could be taken. One step is that today you will find a major effort to solicit audience participation in what has been called from the beginning a strategic planning meeting.

Secondly, we should increase our efforts to bring higher-level managers from the various agencies to this conference. If they are too busy to attend, at least attempt to better inform them about time.

The importance of PTI, as evidenced by this large gathering of distinguished scientists from government and industry, from the four corners of the world, is probably not well understood by many higher-level management officials.

Consequently, they are not aware of how important our discussions are for their own operations and management decisions. And this unawareness is probably the main reason why the Observatory, as the DoD PTI manager, frequently does not receive pertinent information and requirements on time, and sometimes not at all.

I suggest that you give this matter your thoughts and bring forth any suggestions you may have at a later time.

Fortunately, the Observatory is now in the process of getting the DoD PTI instruction revised, which, if approved, will require PTI coordination within the agencies and services. This new effort can now be justified on the basis of an extensive analysis of the overall PTI requirements, which is near its completion.

I trust that you will be interested in hearing more about this effort, which will be the subject of the first session.

One final note is that the Naval Observatory, located on Massachusetts Avenue, Northwest, Washington is well worth a visit for those of you who may not have been there already. Besides being a place of considerable scientific interest, it is a rather pleasant place to visit.

A tour of the Naval Observatory is scheduled for 8:00 o'clock this evening. I am sure you will find the tour a very interesting and worthwhile experience.

I wish you full success at this important conference.

## OPENING COMMENTS

Dr. Richard L. Sydnor, Chairman  
Technical Program Committee  
Jet Propulsion Laboratory

DR. SYDNOR: As you already heard, we have a slightly different kind of session this first session, we would like to have everybody participate. There are questions raised in the program, you can read them on the program and discuss them during coffeebreak, and we will be back for a discussion later on.

The first chairman is Harris Stover, from Defense Communications Agency, and he will introduce the first session.

Thank you.



SESSION I

PTTI REQUIREMENTS AND SPECIFICATIONS

Dr. Harris A. Stover, Chairman  
Defense Communications Agency





DR. STOVER: Good Morning! Each year when the committee selects a new Program Chairman, they ask him to emphasize requirements and applications. Having been Program Chairman, I know that it can be difficult.

This year, we are trying something different. In this session, we have only one paper -- on users and requirements. After discussing that paper, we will have a break.

After the break, there will be an audience participation discussion related to applications. Some of the questions to be discussed are listed on page XVIII of the program that you received when you registered. You also received a copy of DoD Directive 5160.51. This was because we learned that some of you were not aware of its existence, and it is the subject of one of the questions.

I want to point out that the discussions are being recorded for publication in the proceedings. It is the responsibility of each individual to be sure that classified material is not discussed.

When you participate in the discussions, please use the microphones and identify yourself and your organization.

The paper for this session is titled, "Precise Time and Time Interval -- Users, Requirements, and Specifications". It will be presented by Mr. James R. Bowser of VITRO Laboratories.





August 31, 1971  
NUMBER 5160.51

ATSD(T)

## Department of Defense Directive

**SUBJECT** Precise Time and Time Interval (PTTI) Standards and Calibration Facilities for Use by Department of Defense Components

- Refs.:**
- (a) DoD Directive 5160.51, "Time and Time Interval Standards and Calibration Facilities for Use by Department of Defense Components," February 1, 1965 (hereby cancelled)
  - (b) DoD Instruction 4630.4, "Support and Management Services for Precise Time and Time Interval Standards," June 22, 1966 (hereby cancelled)
  - (c) DoD Directive 4000.19, "Basic Policies and Principles for Interservice and Interdepartmental Logistic Support," August 5, 1967

### I. REISSUANCE

This Directive reissues reference (a) and consolidates references (a) and (b) which are hereby cancelled. Revisions occasioned by organizational and administrative changes are also included. There are no substantive changes.

### II. PURPOSE AND APPLICABILITY

This Directive establishes policy and assigns responsibility to a single Department of Defense Component for establishing, coordinating, and maintaining capabilities for time and time interval (astronomical and atomic) for use by all DoD Components, DoD contractors, and related scientific laboratories.

### III. DEFINITIONS

For purposes of this Directive, the following definitions will apply.

WCS # \_\_\_\_\_  
Action # 0486  
R S # 17507

Department of Defense Directive 5160.51

Continuation of III.

- A. Time signifies epoch, that is, the designation of an instant on a selected time scale, astronomical or atomic. It is used in the sense of time of day.
- B. Time Interval indicates the duration of a segment of time without reference to when the time interval begins and ends. Time interval may be given in seconds of time.
- C. Standards signifies the reference values of time and time interval. These standards are determined by astronomical observation and by the operation of atomic clocks. They are disseminated by transport of clocks, radio transmissions, and by other means.
- D. Precise Frequency signifies a frequency requirement to within one part in  $10^9$  of an established time scale.
- E. Precise Time signifies a time requirement within ten milliseconds.

IV. POLICY

- A. Resources for uniform and standard time and time interval operations and research shall be the responsibility of a single DoD Component.
- B. The maximum practicable interchange of time and time interval information shall be effected throughout the DoD.
- C. Maximum practical utilization of interservice support will be achieved as prescribed in reference (c).

V. RESPONSIBILITIES

- A. The U. S. Naval Observatory (hereafter referred to as the "Observatory") is assigned the responsibility for insuring:
  - 1. Uniformity in precise time and time interval operations including measurements.
  - 2. The establishment of overall DoD requirements for time and time interval.

Department of Defense Directive 5160.51

Aug 31, 71

5160. 51

**Continuation of V.**

3. The accomplishment of objectives requiring precise time and time interval with minimum cost.
- B. In carrying out the above responsibilities, the Observatory shall:**
1. Derive and maintain standards of time and time interval, both astronomical and atomic.
  2. Provide coordination of such standards with recognized national and international standards to insure world-wide continuity of precision.
  3. Monitor conferences concerning time and time interval standards.
  4. Advise and provide guidance to DoD Components, contractors, and scientific laboratories on matters concerning time and time interval, and their measurement.
- C. All DoD Components which require, utilize, or distribute time and time interval information or have a need for a specific time scale shall:**
1. Refer time and time interval to the standards established by the Observatory.
  2. Maintain specific time scales such that relationship to the standard established by the Observatory is known.
  3. Prescribe technical requirements for the coordination of techniques, procedures and periodic calibrations of systems.
  4. Promote economy by prescribing requirements for precise time that are consistent with operational and research needs for accuracy.

Department of Defense Directive 5160.51

## VI. DELINEATION OF FUNCTIONS

- A. The Observatory is the single DoD Component responsible for PTTI management control functions. This responsibility encompasses overall activities requiring time to within ten milliseconds and frequency to within one part in  $10^9$  of an established time scale. In carrying out these PTTI functions on a common-servicing basis, the Observatory will:
1. Issue detailed information concerning reference values for PTTI and distribute them by means of controlled radio transmissions and portable atomic clocks.
  2. Promote (a) operational uniformity of PTTI functions, including measurements; (b) establishment of overall DoD PTTI requirements; and (c) accomplishment of objectives requiring PTTI at minimum cost.
  3. Monitor DoD research programs concerning PTTI (frequency), in coordination with the Office of the Director of Defense Research and Engineering.
  4. Review (a) existing and future PTTI (frequency) requirements of the DoD user components in order to establish overall DoD requirements and to provide adequate supporting services; and (b) existing PTTI operations conducted by DoD user components to provide guidance and recommendations to the Assistant to the Secretary of Defense (Telecommunications).
  5. Establish relationships between the DoD and other Federal Government agencies on PTTI matters.
  6. Provide advice and guidance concerning requests for unilateral PTTI (frequency) programs at the direction of Assistant to the Secretary of Defense (Telecommunications).
  7. Participate in PTTI policy negotiations between the DoD and other Federal Government agencies and international organizations.

Department of Defense Directive 5160.51

Aug 31, 71  
5160. 51

Continuation of VI. A.

8. Maintain records of PTTI (frequency) arrangements between the DoD and its contractors and other Federal Government agencies, with the exception of radio frequency assignments.

B. DoD User Components

1. DoD Components presently conducting Precise Time and Time Interval operations and research may continue these activities unless otherwise instructed by the Assistant to the Secretary of Defense (Telecommunications).
2. The Military Departments will assist the Observatory by (a) providing technical information on current and prospective programs involving PTTI applications; and (b) distributing, monitoring and controlling PTTI services on request, subject to the provisions of this Directive and the availability of funds.

C. DoD User Components and contractors will:

1. Consult the Observatory on any technical and logistic problems arising from obtaining a particular accuracy through radio transmissions and portable atomic clocks.
2. Use DoD-controlled transmissions to the maximum extent practicable. Other transmissions of time and frequency which have been coordinated with the Observatory may be used when DoD transmissions do not provide adequate coverage.
3. Refer measurements and contract specifications to DoD standards determined by the Observatory.
4. Use techniques and procedures described in information documents issued by the Observatory in all cases where such documents satisfy the need.
5. Notify the Observatory of:
  - a. Existing and planned PTTI requirements, including information as to accuracy and stability of needs,

Department of Defense Directive 5160.51



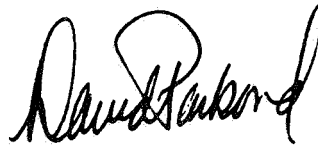
Continuation of VI. C. 5. a.

measurement techniques planned or in operation,  
and continuity of service required of the applicable  
distribution transmission.

- b. PTTI (frequency) arrangements between DoD user  
components and contractors and other Federal  
Government agencies (see paragraph VI. A. 8. above);  
and
  - c. Scheduled scientific and technical meetings on PTTI  
(frequency).
6. Consult the Observatory prior to entering into contracts  
for equipment, research, studies, or services involving  
PTTI (frequency) in order that maximum use of existing  
facilities may be assured.

**VII. EFFECTIVE DATE AND IMPLEMENTATION**

This Directive is effective immediately. It shall be given full  
distribution by all DoD Components. Two copies of each  
implementing document shall be forwarded to the ATSD(T)  
within 90 days.



Deputy Secretary of Defense

Department of Defense Directive 5160.51

## PRECISE TIME AND TIME INTERVAL USERS, REQUIREMENTS AND SPECIFICATIONS

James R. Bowser, Automation Industries, Inc., Vitro Laboratories  
Division, Silver Spring, Maryland

### ABSTRACT

Concurrent with the advanced technology for providing more accurate PTTI through improved devices and a greater variety of dissemination systems, the functional areas of application of Precise Time and Time Interval (PTTI) have also expanded. A comprehensive overview of the PTTI requirements and applications would provide an opportunity for individuals working in a specific functional area to identify mutual problems, requirements, applications or successes shared by those in other functional areas.

Based upon the results of a two year study conducted under the sponsorship of the USNO, this paper presents a compendium of PTTI requirements, applications and the means of meeting the requirements among Department of Defense components, other government agencies and major commercial users. In the course of the investigation it was found that the planning process for PTTI support for new acquisitions or new programs was less than a well defined, coordinated process. This paper describes the processes in general terms and presents a generic model for requirements determination and subsequent coordination which may enhance the planning process and introduce cost benefits to the program.

### INTRODUCTION

In January of 1980, functioning in the role of the Department of Defense PTTI Manager, the U. S. Naval Observatory initiated a study of PTTI requirements. Although the central focus of the study was the DOD requirements, the scope of the effort was expanded to include the requirements of the other government agencies and significant commercial users of PTTI since many of them must maintain reference to the U. S. Naval Observatory master clock time. The purpose of the study was to gain an insight into the magnitude of current uses of PTTI, and

projected requirements, in order to determine the objectives for upgrading the master clock system to provide the most accurate and cost effective service to the users. The identification of the users and their broad requirements were deemed sufficient to meet the objectives. Consequently, the details of specific systems equipments and wiring diagrams were not necessary. Key elements such as accuracy required, the type of standard used, the reference system for maintaining the standard and the functional areas of operation (e.g. communications, navigation etc.) provide sufficient information to establish the USNO objectives for improvements in the master clock.

#### APPROACH

The first step in determining the broad user requirements was to identify the users themselves. This effort had a two-pronged approach best described as a "top-down" and "bottom-up" approach.

The top-down approach began at the top level headquarters of the respective DOD components and other user agencies. In most cases the contact was made by a personal office call. However, some contacts were in group meetings and in a few cases where follow up action was not deemed necessary, contact was made by telephone only. The DOD Directive governing precise time and time interval (DOD DIR 5160.51) required the various components to issue implementing directives and provide copies of these directives to the OSD(C<sup>3</sup>I). By tracing the implementing directive to the responsible staff agencies in each component the personnel most involved in PTTI matters were located. This approach also identified the next lower echelon assigned responsibilities for PTTI matters and lead ultimately down to the field activities maintaining PTTI. At first glance, the top-down technique exhibited all the promise of the most efficient and economical means of gathering the desired information. It was envisioned that within each component the higher level staff would have at hand the aggregate requirements of subordinate commands. These would then be available at a central location and serve to identify the PTTI users at the next lower echelon as well as the quantitative requirements as approved/understood by the higher authority. If the level of detail concerning the requirement was insufficient, it would at least provide the investigator with the identity of the source of further details. By virtue of centralized data sources, the top-down technique would economize on time and travel expenses as well as facilitate the compilation process for displaying the data and the subsequent analysis process. By definition, the top down approach would appear to be the best means to work down to the investigator's perception of "broad" requirements without becoming enmeshed in the diverse details of a multitude of users and their overlapping requirements.

In some instances this technique did not provide a well defined track to the individuals who had a comprehension of PTTI requirements. In many instances, although well aware of an overall program and an appreciation of a need for PTTI, the quantitative aspects of the requirement, and the means whereby it would be satisfied, were not clearly visible at the upper echelon of authority.

In an effort to isolate the elusive requirements information, a questionnaire was designed. Conceptually, the questionnaire would be directed to the PTTI participants identified in the top-down approach with the idea that they in turn would forward it down through the staff or command chain to the various levels where the requirements data were more accessible and better understood. It was a multipurpose questionnaire. A portion of it was designed to gather information on the management structure and organizational relationships and the remainder addressed the requirements.

Although the responses to the questionnaire proved informative in certain areas, they were not 100% effective in filling the gaps.

The combination of the initial staff contacts and a preliminary analysis of the responses to the questionnaire indicated that there existed a level of PTTI requirements that was eluding scrutiny. Those were the requirements associated with systems in the hierarchy of the planning and programming system which were not yet operational. In an effort to ferret out the PTTI requirements in this category, another format was designed with the intent of circulating it to selected program, acquisition, or system managers to provide the specifics on their respective PTTI requirements. Preliminary discussions with selected program sponsors and others in senior staff positions created some reservations about the circulation of the revised format as an augmentation to the questionnaire. In general, it was concluded that it would not be propitious to encumber an already overburdened system with the additional administrative details of responding to yet another inquiry. However, the search for the basic information was not abandoned. The data for selected systems were derived through research of various documents, papers presented at symposia, and through contact with knowledgeable individuals directly associated with these programs.

Concurrent with the "top-down" approach described above, a "bottom-up" approach was implemented. The basic philosophy supporting the bottom-up approach was to identify the myriad of PTTI users, aggregate their requirements and divide them into specific functional categories of use such as navigation, communications, etc. Having developed an aggregate display by category, then seek to identify the operational capabilities which established the PTTI requirements. As a departure point, the computer printout of the distribution list for time service announcements from the USNO was reviewed. Each user, by DOD component,

was listed along with the type of announcements received. The objective here was to try to determine the principal functional category in which that user was operating by the very nature of the time service announcements received. In some instances the title of the using unit provided an insight to their principal functional category.

As an adjunct to the techniques applied in the top-down and bottom-up approaches, every effort was made to investigate all available data sources. Other sources of data included periodicals, individual papers published for symposia, government reports, directives and support agreements, contractors equipment specifications, and vendors editorial observations related to innovative means of dealing with PTTI requirements.

## FINDINGS

Figure 1 presents a summary display of the DOD PTTI requirements compiled from the results of the investigative process described above. Also included in the summary are some other selected major users who are external to the Department of Defense. The first section of the display shows the major dissemination systems. These are referenced throughout the chart as the means whereby the users are calibrating their respective systems. Each component's data is provided under a separate heading.

Although the requirements vary over a wide range, many of the requirements are common to several components. In some instances the means of satisfying the requirement must vary due to the operational environment. Of particular note is the Navy's requirements. The Navy's requirements were compiled in a display which shows the separate requirement by ship class, aircraft class and shore installations. However the data in that form is classified and is available at the Naval Observatory in a separate report. By virtue of long term deployment covering most of the globe and independent operations, the Navy operational requirements are probably the most complex. The National Security Agency's requirements are also classified and are incorporated in the same report at the USNO.

Generally speaking, the most stringent requirements are associated with research and calibration facilities. Fortunately these activities are fixed installations and can provide controlled, stable environments for their standards. Most of the requirements range from 1 part in  $10^{12}$  to 1 part in  $10^{14}$  for frequency stability. The principal means of monitoring these systems is by portable clock, TV-10 and Loran-C. NASA presents the most stringent requirements, both current and projected, for a variety of programs such as space tracking, geodesy, and other investigative projects.

USER	PRECISION REQUIRED	REFERENCED TO	STANDARD	PRINCIPAL USE
DISSEMINATION SYSTEMS				
TIME OF				
	FREQ.	DAY		
Portable Clock	1X10 <sup>-13</sup>	100ns		Calibration/Synchr.
Defense Satellite Comm. System (SATCOM)	1X10 <sup>-11</sup>	100ns	Cs	COMM
Navy Navigation Satellite System (TRANSIT)	1X10 <sup>-11</sup>	100ns	Rb	NAV
Geostationary Operational Environment Satellite (GOES)	3X10 <sup>-11</sup>		Cs	NAV
OMEGA	1X10 <sup>-11</sup>	30µs	Cs	NAV
LORAN-C	1X10 <sup>-11</sup>	1µs Gnd 50µs Sky	Cs	NAV
TV-10	1X10 <sup>-12</sup>	1µs	Cs	Calibration
Global Positioning System (GPS/NAVSTAR)		1µs	Cs	COMM/NAV
HF Radio	1X10 <sup>-7</sup>	1000µs	Hm, Cs	Calibration
VLF	1X10 <sup>-12</sup>	1-10ms		Calibration
NOTSS (Richmond)	1X10 <sup>-12</sup>		Cs	Calibration
U.S. AIR FORCE				
Aerospace Guidance and Metrology Center (AGMC)	1X10 <sup>-12</sup>		Cs	Calibration/Reference
Precise Time Reference Stations (PTRS) (24 in number)		2-40µs	XTAL	Calibration/Reference
Precision Measurement Equipment Laboratories (PMELS) (117 in number)	1X10 <sup>-10</sup> to 5X10 <sup>-11</sup>		VLF Phase Comp. (Cs)	Calibration

REQUIREMENTS SUMMARY  
Figure 1

USER	PRECISION REQUIRED	REFERENCED TO	STANDARD	PRINCIPAL USE
TIME OF DAY				
U.S. AIR FORCE (Cont'd)	FREQ.			
Hanscom AFB	1X10 <sup>-11</sup>	LORAN-C	Cs	Research
AF Communications Facilities	5X10 <sup>-10</sup>	Self-Sync.	XTAL Oscill.	Communications
AF Aeronautical Laboratory	1X10 <sup>-11</sup>	PC	Cs	Calibration/Research
MSL Warning Squadron	1X10 <sup>-11</sup>	PC	Cs	Synchronization/ Time
Eastern Test Range	1X10 <sup>-11</sup>	PC, LORAN-C, VLF	Cs	Range Tracking/Time
Western Test Range	+ 2 $\mu$ s	PC, LORAN-C, VLF TV-10	Cs, Rb	Range Tracking
Air Defense Command	1X10 <sup>-10</sup>	PC	Rb	Communications/Time
FUTURE SYSTEMS				
SEEK TALK I & II	3ms	-	Rb or XTAL	Secure Tactical Comm.
HAVE QUICK	3ms	Transit Satellite	Rb	Tactical Comm.
MEECN			Cs	Emergency Comm.

REQUIREMENTS SUMMARY (Continued)  
Figure 1

USER	PRECISION REQUIRED	REFERENCED TO	STANDARD	PRINCIPAL USE
	FREQ. TIME OF DAY			
U.S. ARMY				
U.S. Army Metrology & Calibration Center (USAMCC)	1X10 <sup>-11</sup>	WWV, VLF	Cs	Frequency Calibration
U.S. Army Electronics Research & Development Cmd (ERADCOM)	1X10 <sup>-11</sup>	LORAN-C	Cs	Frequency Calibration
U.S. Army Communications Cmd Timing Division (Code CCNC-TWS-T) White Sands, NM	+1us(USNO)	LORAN-C	Cs (Four)	Range Timing
U.S. Army White Sands Missile Range (Code QA-CB)	1X10 <sup>-11</sup>	LORAN-C, PC	Cs (Three) Rb (Two)	Range Tracking
U.S. Army Test & Evalua- tion Cmd Yuma Proving Gds, (Code STEYP-MOP-E)	1X10 <sup>-11</sup>	PC (USNO)	Cs (Two)	Range Timing
U.S. Army Area Calibration & Repair Center, Aberdeen Proving Gds, MD	1X10 <sup>-11</sup>	VLF, WWV	Cs (on order ETA 11/81)	Calibration
U.S. Army Area Calibration Laboratory, Lexington Bluegrass Dept., Lexington, KY	1X10 <sup>-12/13</sup>	VLF	Quartz Crystal (Victorian 33)	Calibration

REQUIREMENTS SUMMARY (Continued)  
Figure 1



USER	PRECISION REQUIRED	REFERENCED TO	STANDARD	PRINCIPAL USE
<u>FUTURE SYSTEMS</u>				
Modular Integrated Communications & Navigation System (MICNS)	FREQ. 1X10 <sup>-10</sup>	-	Rb	Navigation & Communications Data Link
Single Channel Objective Tactical Terminal (SCOTT)	+ 20μs/7 days	-		Armored Vehicles Tactical Satellite Link
Single Channel Ground Air Radio System (SINCCARS)		-	Cs	Tactical Communications
Advanced Quick Look	(in Bidders Competition)	-		EW
<u>NATIONAL AERONAUTICS &amp; SPACE ADMINISTRATION</u>				
Space Tracking & Data Network	1X10 <sup>-14</sup> 25μs	PC, LORAN-C, HF	Cs	Space Tracking
Tracking & Data Relay Satellite System (TDRSS)	1X10 <sup>-14</sup> 40ns	PC, LORAN-C	Cs, Hm	Space Tracking
Laser Ranging Network	1X10 <sup>-14</sup> + 1μs	PC, LORAN-C, TV	Cs, Hm, Rb	Laser Range
Space Shuttle	1X10 <sup>-15</sup> < 1μs	PC, LORAN-C, TV	Cs, Hm, Rb	Shuttle, VLBI Lasers
SIRIO/LASSO	1X10 <sup>-15</sup> ns	TDRSS, GPS, Laser, TV, PC	Cs, Hm, Hg	VLBI, Crustal Dynamics Scientific Satellites Deep Space Mission GRAVSAT

REQUIREMENTS SUMMARY (Continued)  
Figure 1

USER	PRECISION REQUIRED	REFERENCED TO	STANDARD	PRINCIPAL USE
U. S. Navy				
Ship Platform	FREQ. -10 1X10-12 to 1X10-12	PC, DSCS	Cs, Crystals	COMM. NAV
Air Platforms	1X10-11	PC, VLF	Rb	
SHORE Installations	1X10-12	PC, LORAN-C TV-10, Hm	Cs, Hm	COMM, Calibration, Research
DEFENSE MAPPING AGENCY				
Elmendorf AFB, AK	1X10-11	PC	Cs	Geodesy
Herndon, VA	1X10-11	PC	Cs	Geodesy
Warren AFB, Geodetic Squadron, WY	1X10-11	PC	Cs	Geodesy
DMAAC/RDGS, St. Louis, MO	1X10-11	WWV	Crystal Oscillator	Geodesy
DMA, New York, NY	1X10-10	VLF	Crystal Oscillator	Geodesy
DMA, Thule, Greenland	1X10-10	VLF	Crystal Oscillator	Geodesy
DMA, Mahe Island, India	1X10-10	VLF	Crystal Oscillator	Geodesy

REQUIREMENTS SUMMARY (Continued)  
Figure 1

USER	PRECISION REQUIRED	TIME OF DAY	REFERENCED TO	STANDARD	PRINCIPAL USE
<u>FEDERAL AVIATION ADMINISTRATION</u>					
FAA Technical Center, Atlantic City, NJ	FREQ $1 \times 10^{-10}$		WWVB (Switching to GOES)	Cs	Navigation Test Range
<u>U. S. COAST GUARD</u>					
LORAN C	$1 \times 10^{-11}$		PC	Cs	
OMEGA	$1 \times 10^{-11}$		PC	Cs	
<u>SMITHSONIAN INSTITUTION</u>					
Astrophysics Lab		+ 2-6 $\mu$ s	PC, OMEGA LORAN-C	Cs/Rb	Satellite Tracking

REQUIREMENTS SUMMARY (Continued)  
Figure 1

USER	PRECISION REQUIRED	REFERENCED TO	STANDARD	PRINCIPAL USE
FUTURE SYSTEMS JOINT				
	FREQ.	TIME OF DAY		
HAVE QUICK		3ms	Transit Satellite	Communications
MEECN (616A)		3ms		Communications
TRI-TAC	(a) $1 \times 10^{-11}$	Autonomous	(a) Cs	Communications
	(b) $1 \times 10^{-10}$		(b) Quartz XTAL Oscillator #1	
	(c) $1 \times 10^{-7}$		(c) Quartz XTAL Oscillator #2	
CIS		10 $\mu$ s	Rb	Identification
DCS TIMING	$1 \times 10^{-11}$	LORAN-C	AN/GSQ 183	Communications

REQUIREMENTS SUMMARY (Continued)  
Figure 1

The next level in the hierarchy of requirements appears to be at the test ranges, Eastern and Western test ranges under the Air Force, and Yuma and White Sands under the Army. The requirement is in the order of 1 part in  $10^{11}$  and time of the day to within  $\pm 2$  microseconds of the USNO master clock. Again portable clocks, Loran-C and TV-10 are the principal sources of reference. Very close to this level of accuracies,  $10^{-11}$  to  $10^{-10}$ , is a wide range of communication systems and data links which relies on timing for security of digital transmission of large volumes of data. Fortunately, all of the components share these requirements. Since the systems are tactical or strategic systems deployed with operational forces, the standards which support the system seldom enjoy the luxury of a controlled environment. Additional performance criteria must be considered such as size, weight, acceleration sensitivity, temperature range, warm up time and power supply. Delicate trade offs are necessary to achieve the operational objective at a reasonable cost. For some of the "future systems" listed in the chart, these tradeoffs are currently in process and the data needed to fill in the chart are not readily available.

The Air Force has widely-dispersed forces. However, their facilities are geographically fixed in nature and independent deployments are of relatively short duration. They have structured their PTTI facilities to cover their needs through the geographical distribution of some 24 Precise Time Reference Stations, each equipped with a standard Time Console unit containing two reference clocks, Loran-C receivers and VLF receivers. In addition there are one hundred and seventeen Precision Measurement Equipment Laboratories worldwide. Their equipments vary in nature from VLF comparators to cesium standards depending upon the nature of the facility being supported.

If one focuses on the future requirements of the Services, it becomes apparent that the operational requirements and the nature of PTTI problems are converging to a common ground. This is driven primarily by sophisticated communication systems and position location equipment which will be widely dispersed in tactical deployments. For example the Army is developing the Single Channel Objective Tactical Terminal (SCOTT) which will require time of day within  $\pm 20$  us and may conceivably require the deployment of several hundred cesium or rubidium clocks. Other future Army systems such as Single Channel Ground Air Radio System (SINCGARS) and Modular Integrated Communication System (MICN) may also add cesium or rubidium clocks to the operational forces. These deployments will clearly change the complexion of the program from that of a laboratory, fixed-installation problem to those problems similar to the Navy's in support of deployed operational forces. There are many joint systems under development which will inexorably spread the problem uniformly among the services as common users.

## PTTI REQUIREMENTS PLANNING

The investigations implemented in researching the requirements, revealed some interesting facts regarding the PTTI requirements planning process. For the purposes of this discussion the PTTI users within the components can be divided into three functional communities; the R&D community, the Logistics community, and the Operational community. PTTI requirements are viewed from a different perspective in each of these communities. One of the first key observations which can be made with few exceptions is that there is no central overseer in the components who transcends the individual boundaries of these communities in order to translate the separate requirements into a common statement of the overall component requirements. Consequently, in researching requirements, each community within the components had to be queried separately. With different perspectives, the statement of requirements takes on a different form. A statement of requirements from the operational community is in operational terms. For example, the requirement may be to achieve secure communications between points A and B, or determine position location, worldwide, to a specified accuracy. The operational representative may or may not be aware of the fact that precise time or time interval is a necessary element of the system to achieve the objective. The investigation then shifts to the logistics community and specifically the acquisition manager; or for systems currently operational, to the metrology and calibration support agencies. The acquisition manager, on the logistics side, is more technically oriented and will generally acknowledge the need for PTTI. However, the manner in which it is to be provided and the specific criteria are not always known. The PTTI portion is viewed as a subsystem to the prepared design which will meet the operational requirement. As we follow the track to the design engineer, to subsystem engineer, etc. the availability of data on PTTI increases considerably. In some instances the final answer rests with the commercial contractor who is assembling the entire system and knows precisely how the timing problem is to be solved. The R&D community has a split view of the issue. On the one hand their attention is directed to their own internal PTTI requirements, on site, for use in research. On the other hand they must be constantly aware of the operational objectives to insure that they keep pace with the requirements. This community shares the frustration of not having a central point of contact which can bring together information regarding PTTI requirements and related activity in the other communities. The net result of the current process is a somewhat fragmented process in PTTI requirements development.

Given the above facts, we might well question how the PTTI program continues to function as well as it does. It does so through the initiative and dedication of the participants who are willing to override the lack of a formalized staffing system and to communicate with one another

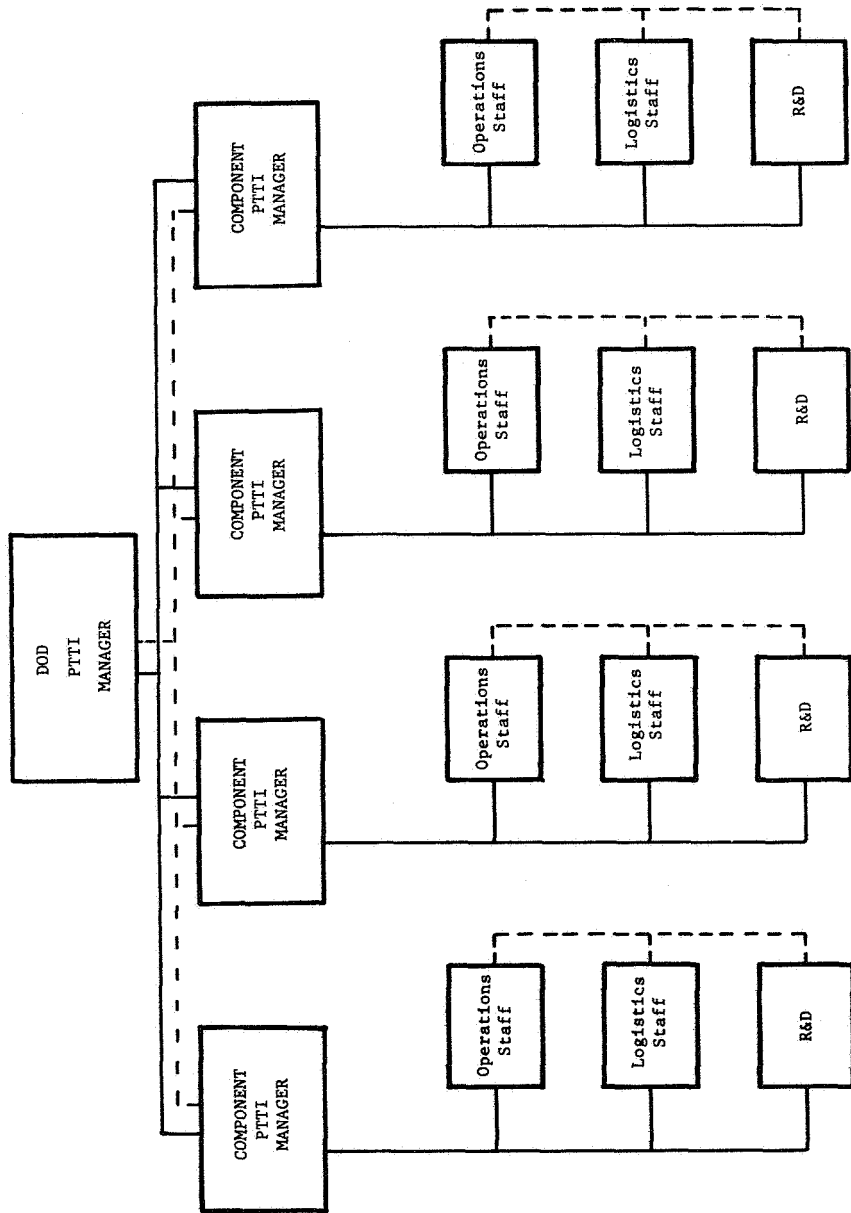
to the degree necessary to accomplish their tasks. There is a complex information exchange network among components, among communities, and even from one component's community to a different community in another component. Although functional, it is time consuming and less than efficient.

A clearly-defined PTTI requirements development process requires a well-delineated organizational structure within which it operates. One such structure is depicted in Figure 2. Each component would have a central PTTI manager assigned, preferably operating on the highest staff level in order to exercise coordination over the separate communities in each component. This is not essential if the necessary coordination authority is unequivocally established in the governing directives and clearly recognized by all participants. A central point of contact is available, and known, to the DOD PTTI manager. Within each component the requirements are brought to a central point where the activities of the other communities are also known. The manager would be able to match current metrology and calibration capabilities with new requirements; provide feedback to the R&D community as to operational requirements and insure that the operational community is afforded the most cost effective and efficient support for his system. By requiring formal coordination with the PTTI manager, early identification of PTTI needs is achieved. All participants become aware of the requirements and a solution is drawn from a full knowledge of the technology available to the entire program. This in turn would tend to converge on standard equipments and common techniques for accessing dissemination systems and maintaining standards. Production line items would begin to replace development models thus providing for economies in acquisition cost, commonality of maintenance and support, uniform training, and a basis for gathering meaningful statistical data on performance parameters which in turn can be used to focus the efforts of the R&D community on the problem areas.

The DOD PTTI Manager would become an active participant in the planning process with well-established lines of communication to centrally-managed programs. With better visibility of the DOD requirements and active participation in the process, the DOD PTTI manager will be better able to meet his responsibilities of providing an efficient and cost-effective DOD program.

#### SUMMARY

Current PTTI requirements cover a wide range of criteria with space systems and basic research heading the list of the most stringent demands for accuracy and stability. Users' requirements are being accommodated through a variety of time dissemination means. The reliance on portable clocks is declining as improved systems and techniques are developed. Almost uniformly throughout the user



— Formal Staffing Lines

- - - Informal Lines of Communication

CONCEPTUAL PROGRAM STRUCTURE

Figure 2



community, GPS/NAVSTAR and the realization of its full potential is viewed as one of the most important factors in future planning. With the advent of the more sophisticated communications systems and data links which are becoming common to all components, the character of the components programs are merging to a single identity. The time is propitious to institute management initiatives which will insure a fully coordinated DOD program. This can be accomplished without any great reorganization or cost and the return on the investment can be realized in all aspects of the program.

## QUESTIONS AND ANSWERS

DR. NICK YANNONI, Rome Air Development Center

What is your time table for completing your current activity? What do you expect to do?

MR. BOWSER:

The time table for me to publish a final report, Dr. Yannoni?

DR. YANNONI:

You said you had been doing something for 18 or 20 months, and I am interested in when you will be completed and what you will achieve?

MR. BOWSER:

The date that we must turn in the final report to Dr. Winkler is the 27th of December. He has seen most of it, except for one chapter of the management report and the final elements of the requirements analysis. I am still out on the search for a number of systems, and trying to establish what those requirements might be. And some of them -- they had promised me the information late in September, but they were still in bidder's competition and that sort of thing, and I would like to fold them in, if I can uncover them.

But the whole report will be finished and turned in to the Observatory prior to the 27th of December, this month.

MR. KELLOGG, Lockheed

On some of these peculiar frequency requirements, is there any effort made to validate, or did you just call somebody and he said 10<sup>11</sup> and you said that is a little less than 14th, or something and stick it in, or is there a common basis on which these can be validated?

MR. BOWSER:

In the cases that I have up here, I was able to validate them, except the one that I showed for the FAA, and that is in the process right now with Mr. Edwards trying to validate that one for me.

And that's a very good point, previous documentation of these requirements did reveal that people would say they had a requirement because that was the most accurate system they had available. So, they would say, "I need one part in  $10^{13}$  that is because I have a cesium beam and that is what I can maintain"; when, in fact, they really didn't need it.

And that is one of the more difficult aspects of trying to track these down.

What I did try to do is say, okay, if that is what you needed, what are you using it for and where does it fit in, and try to find out what it was that drove the requirement.

Now, I was unable to do that in a lot of cases, and this was an endeavor to uncover the broad requirements.

We had conducted a study for the Navy on their specific detailed requirements in which you go down to the level that you are discussing. And that ended up in five volumes that covers a shelf that thick (indicating). And to do that for all of DoD, would take more than a year and a half.

*The following questions were presented to the audience, both orally and through viewgraphs to encourage their participation in the discussion of applications and requirements.*

QUESTION #1: "WHAT ADDITIONAL METHODS CAN BE USED TO DETERMINE PRESENT AND FUTURE PTTI REQUIREMENTS"?

DR. STOVER:

Mr. Bowser has already given us a good start at how this is done, or how he approached it. He has also discussed the difficulties he had in doing it.

Can some of you give us some suggestions as to any other methods that could be used, that might enable us to better determine present and future PTTI requirements?

MR. CLINT FRIEND, Defense Communications Engineering Center

I am in satellite systems engineering requirements. I think that Bob Bowser indicated that there was a lack of organization as far as PTTI and the various components are concerned. If we put out a directive, or perhaps a revision of the present directive, directing everybody to establish a representative at all levels of command, then we would have an organizational path through the chain of command whereby we could collect the requirements which are now known, as he put it, at a technical level -- you know people in other organizations that are doing the same kind of work that you are doing, and they could all be drawn together through a directed organization for PTTI.

QUESTION #2: "ARE THERE OTHER POTENTIAL APPLICATIONS OF PTTI, IN ADDITION TO NAVIGATION, COMMUNICATION OR RESEARCH?"

DR. STOVER:

Most of the people I talked to felt that most of the various applications would fall under one of these three headings, but if we have missed any, we would like to pick them up.

Are there any suggestions as to other potential applications of PTTI -- other than these three, navigation, communication and research?

MR. MACHERSKI, National Research Council

Geo-physics of timing, for example, if you set off an explosion and you tried to get seismic waves propagating in various spaces, you would like to get the timing fairly accurately. That is another very possible application.

MR. Bill BRIDGE, Mitre Corporation

In the tactical situation you certainly could use time differences of arrival systems for locating emitters.

DR. STOVER:

Well, Mr. Bridge, just mentioned position location. I made a note to myself that another possibility might be system monitoring. For various types of systems, knowing precise time might be useful in system monitoring and control.

Actually, in some cases it might be useful for prediction of events that might occur later, if you know the precise time when each of a sequence of similar or related events that occurred previously. Collision avoidance for aircraft is a possibility. In some cases diagnostics of electronic or mechanical failures in large systems could be aided by PTTI.

QUESTION #3: "WHY DO SOME POEPL E WHO SHOULD BE USING PTTI AVOID ITS USE, SOMETIMES GREATLY REDUCING SYSTEM FUNCTIONAL CAPABILITY, SYSTEM FLEXIBILITY, SYSTEM ENDURANCE, RELIABILITY AND SURVIVABILITY?"

QUESTION FROM UNIDENTIFIED PARTICIPANT:

Do they avoid or do they just neglect to?

DR. STOVER:

Would you like to answer your question?

REPLY:

No, you assume that people are actually avoiding.

DR. STOVER:

You are right, I made that assumption when I asked the question. Now, what is your answer?

REPLY:

I suspect it is just lack of knowledge very often, rather than avoiding such use.

DR. STOVER:

I think that that may be true. Some of my own opinion is that in many cases it is due to their being somewhat afraid of the unfamiliar. Again, that is a lack of knowledge, but it is more than just a lack of knowledge. It is a psychological thing. They are afraid of the unfamiliar.

MR. PETE OULD, Interstate Electronics in Anaheim

I am not a user, I am a builder of equipment, but it would strike me that one of the reasons would be the cost of your clocks or your receiving equipment, whether it be LORAN or Transit, or GPS. The basic cost of the thing -- men might sit out there and say, yes, I could use it, but the budget is limited and we can't afford it.

DR. STOVER:

Don't you think there are some possibilities, some situations, where he actually is picking a more expensive alternative because he has not looked at all of the things that the PTTI could do for him?

MR. OULD:

That is possible, but not being a user, I don't know.

DR. VICTOR REINHARDT, NASA/Goddard Space Flight Center

In many cases it is a lack of appreciation or understanding of the time dependent nature of errors. Many people outside the frequencies end of business only understand white noise, stationary noise and drifts, and the middle ground is not appreciated. Therefore, the specifications are not realistic, or they don't understand the problem. They avoid its use, again, out of lack of knowledge, not out of willful acts.

For example, in the tracking business, this is one of the problems, in orbit determination all models are based on stationary statistics and there is lack of understanding of the effect of correlated noise on those models.

DR. STOVER:

So far we have lack of knowledge being very important, either knowledge of what it can do for you, or knowledge of the cost.

LT. ROB CONWAY, Space Division

I think that all of these comments are hitting little specific portions of real general problems, that are becoming increasingly widespread, and that is the fact that all of the people that understand PTTI, or specific examples of the frequency standard applications, are engineers and scientists who have spent many years in development of the fringes of scientific progress. Unfortunately, those people who are spending all these years in development are not the people that are making the decisions on its use and its application in space technology, communications, development, navigation and all this kind of thing.

The people who are making the management decisions are just like you have said before, and several other gentlemen have said before. They are afraid of the use, do not know of the use, are ignorant of the capabilities, are using more expensive methods of solving their problems. -- They are not really educated in the possible ramifications of using PTTI to further their own missions.

I think that you have a problem in management because the managers do not know what the engineers and scientists know. And the engineers and scientists are not in the position to apply their knowledge in a managerial sense.

MR. DAVE PHILLIPS, Naval Research Laboratory

Many people who really know about precision time are afraid to use it in their system, as long as they are not really part of the PTTI community. They feel that their system may be somewhat compromised. They want their system to work alone under all circumstances.

If they can be made to be part of the PTTI community, where their timekeeping capability is actually used in maintaining time, then they will be less likely to not use it.

Many times they want just a stand alone system that works under all conditions, and they are afraid that if they have to use PTTI, this will compromise their system at some point.

DR. STOVER:

Do you also think that in some cases it may just be that they don't want to take the time to put it into their system? They think it will take too long? Or other cases that they may think that their application would be very special, rather than something off the shelf and they may even be mistaken -- are those possibilities, also?

DR. ART MCCOUBREY, National Bureau of Standards

I think Mr. Bowser put his finger on much of the problem in his talk, when he pointed out that there is a lack of really effective advanced planning for the use of PTTI. As a result, I think you find many times that the problems of incorporating PTTI into systems come up late in the development cycle for those systems. Therefore they tend to influence completion dates and things of that sort.

As a consequence, I think people may believe that there are more problems in incorporating PTTI into systems than there actually are, simply because there is not sufficient advanced planning to get the ground established for putting the systems in.



QUESTION #4: "HOW SHOULD PEOPLE WHO SHOULD BE USING PTTI, BUT DON'T KNOW IT, BE PROVIDED WITH INFORMATION NEEDED TO COMPARE ITS ADVANTAGES AND DISADVANTAGES FOR THEIR APPLICATIONS?"

DR. STOVER:

How are these people going to find out that they should be using it? The people who have this ignorance of PTTI capabilities that several of you have mentioned.

Do meetings like this help?

DR. VICTOR REINHARDT, NASA/GSFC

Unfortunately, not that much --

One of the problems is that there is very little communication between the precise time and time interval community and the others -- the users. We should be going out and giving papers at the navigation meetings and the tracking meetings and the other meetings, if we are interested in spreading the use of PTTI, not only in this meeting.

DR. STOVER:

How are we going to promote that?

DR. REINHARDT:

It is up to individuals or groups encouraging that sort of thing, from the individual PTTI laboratories.

MR. DAVID ALLAN, National Bureau of Standards

Periodically, the Bureau of Standards holds seminars, training sessions and so forth which we find are very well attended and very productive in terms of helping people appreciate the advantages, disadvantages of clocks and PTTI matters.

Last year, for example, there was a special session, an evening session at the Frequency Control Symposium, and there will be one again this year. I think the attendance at that and, hopefully, again, this year will help communicate and educate people in this field.

DR. STEVE CRESWELL, FEC, Vandenburg

Twice a year there is a meeting called JRIAIG, which is Joint Range Instrumentation Accuracy Improvement Group, and the inter-range

elements get together and discuss trajectory, reconstruction and timing is a very important part of that. So PTTI just evolves and gets into these types of meetings and it gets discussed rather extensively.

DR. STOVER:

If you will recall from Mr. Bowser's paper, one of the items he mentioned was a lack of PTTI standards. If we had such standards would that help this problem? Help to remove the ignorance?

DR. FRED WALLS, NBS, Boulder

We have a number of reprints describing general characteristics of clocks, their uses, size, weight and volume, projections on these. So, if some of you would like those reprints, maybe we can put up a sign-up list and if you are not on our mailing list, we will send you some of these copies.

We also have some reprints describing the short session that was put on at the last Symposium on Frequency Control (SFC) and that will help, at least for people who are represented here.

DR. STOVER:

Going back, just briefly to Dr. Reinhardt's statements, he mentioned giving papers at other meetings and conferences. How about getting some publications in some of the other journals that aren't specifically related to timing? Is there some way that we can promote that?

MR. ANDY CHI, NASA/GSFC

It sounds to me that we need a clearinghouse, perhaps the U.S. Naval Observatory could act as such a center, through which we could identify not only the reprints of past publications, but also, perhaps, organizing groups of speakers from among this group, so that they can be suggested at different meetings, to present the up-to-date information regarding the PTTI.

MR. BILL BRIDGE, Mitre Corporation

I think there are a great many untapped users of PTTI in the tactical weapons community and I think one of the things that we could do to improve their knowledge of it is to really work on the aspects of tactical environmental problems with PTTI instrumentation.

In other words, show them that they can get the kind of precision time that they need, in a tactical environment, not a laboratory curiosity.

DR. STOVER:

How do we get this information to them?

MR. BRIDGE:

If you just tell them that they have it, in a tactical environment, I think they will come to you.

MR. H. STROCKER, Navy Metrology Engineering Center, Pomona, California

I think the problem of design engineers who are people who conceptualize systems, not using PTTI, is very similar to the same situation that happens in the automated test equipment world, ATE world, as far as the use of built-in test standards, BITE and BIT, built-in test circuits and also built-in test equipment.

One of the things that this community is doing to encourage and promote the use of built-in tests, is to develop testability guides, guides for testability, where a design engineer, or a systems engineer could see what is available in the way of the technology in order to implement this, and what he would have to do to accomplish it.

I think what is needed, in the PTTI area of course, is more dissemination of knowledge, information. But how do you do that? Through meetings and conferences, that is fine.

I think there could also be some DoD documents with NAV Air, Army or Air Force numbers, TO numbers on it, whatever, which could be disseminated to the systems contractors to make them aware of what is available and how you can get traceability for your systems, and what you have to use.

DR. TOM ENGLISH, Efratom

There is an abundance of literature on the subject of time and frequency, but unfortunately it is scattered over a very large area. Anybody going into that field has to put in a great deal of leg work in order to sift through it, even to decide what he needs.

I would like to suggest that if there were a book available giving the fundamentals and still comprehensive and also, bibliography, that that might be a help to potential users.

Let me give an example, in the field of vacuum technique, Dushman's book would probably be one of the first that you would go to a very comprehensive book and very helpful to the user. It is all in one place. Maybe something like that would be helpful for time and frequency. Of course, you need somebody to write it though.

PROFESSOR C. ALLEY, University of Maryland

There is a very nice book by Kartaschoff, published several years ago, a bit outdated, but it has all the fundamentals in it. I don't remember who published it or what the exact title is.

INFORMATION FROM UNIDENTIFIED PARTICIPANT:

Academic Press, Frequency and Time, 1978, New York and San Francisco.

MR. FRANK KOIDE, Rockwell International

I am both a user and a developer of frequency standards. I find that we have many programs within Rockwell -- we have Navy contracts, Air Force contracts and things like that. The requirements are there, but nobody really knows the requirements of the PTTI until they get to the right type of source, and it takes an abundance of effort to get to the right people.

I think some of the literature is available -- there is one that I know of that is very useful, the one that NBS put out, the Monograph 140. And I think that is very helpful in the PTTI world.

DR. FRED WALLS, National Bureau of Standards

It seems to me one of the greatest inhibitors is lead time, by the time the system has decided exactly what their needs are, they are so close to the delivery time, they are unable to backtrack and develop a specific frequency standard or PTTI hardware in order to accomplish what they need.

One of the things we need to do in planning is to develop building blocks, so that they are well characterized. Rather than systems insisting on odd frequency, 4, 3, 9 and 10, 23 and such, you develop very stable frequency sources and then put some effort in low noise synthesis, so that you can go from a standard frequency with known characteristics, that are well characterized and the reliability is well taken care of; then you put in a synthesizer to produce that odd frequency that you need to make your system run.

In that way you can have these building blocks on the shelf and when you finally decide you really need  $10^{-11}$ , you know where to go; if you need  $10^{-13}$ , that is another set of building blocks.

But, basically, most of the effort when using the building block is already done -- you just need that interface to your specific requirement. I think that will greatly speed up the utilization of PTTI in new systems. And that is what we need to concentrate on in the planning.

MR. KELLOG, Lockheed

The Bureau of Standards Monograph 140 was mentioned. I don't know whether it is apparent, or not, to the Bureau of Standards, but the Government Printing Office thinks that that is unavailable under any circumstances and it is regarded more or less as a classic document. Why don't you contact the Bureau of Standards?

If there is a document of use and it is not readily available, this could account for some of the lack of appreciation of what it could do for you.

QUESTION #5: "WHAT ITEMS SHOULD BE ON A CHECKLIST TO HELP A SYSTEM DESIGNER DETERMINE WHETHER HE SHOULD BE USING PTTI?"

MR. AL BARTHOLOMEW, NRL

I shudder to make this observation, but it seems like when you get ready to do some systems, at least in the NAVY and in DoD, you have to file certain documents for frequency usage, whether you buy a receiver, build one or develop it. Maybe that is the kind of thing that has to be introduced to people that start out in a system that requires PTTI.

DR. STOVER:

File a document? Is that what you are saying?

MR. BARTHOLOMEW:

Right.

MR. ANDY CHI, Goddard Space Flight Center

When you specify, I think one should be very careful to distinguish the need, whether it is precise time, or it is time interval. Although they are combined in this meeting, they don't always mean the same thing.

DR. STOVER:

In other words, is it frequency, or is it phase or time?

How about knowing what the stability requirements are for phase or frequency, is that important?

DR. JOHN VIG, Frequency Control Branch at Fort Monmouth, U.S. Army

Yes, I think knowing it is certainly important.

I think it is also important to have a standard way of specifying frequency stability and some of the other parameters of frequency standards.

If you look at manufacturers' literature today, unfortunately, it is very difficult to determine how two frequency standards compare because different manufacturers use different numbers to specify frequency stability. And I think it would be helpful to have a standard way of specifying the performance of a frequency standard.

DR. STOVER:

Are you saying there should be a DoD standard, or an NBS standard?

DR. VIG:

I think that would be very helpful, yes.

DR. FRED WALLS, NBS, Boulder

To build on what John Vig has said, you should also specify the environment in which you are going to use it, because many systems which work by specs on the lab bench don't work in the field because you haven't specified or even thought about the vibration sensitivity, the temperature transients, or that you are in the humidity, and other kinds of things.

Part of the checklist should definitely be the environment in which this system is going to work.

The particular device that you use for PTI depends on the environment. Some systems are much less susceptible to a particular environmental situation than others. And so that is one of the things you must consider.

MR. BOB BOWSER, VITRO Laboratories

When you talk about specifications for a system, I was thinking about that very question before I came down. I was looking through last year's symposium notes and I found one on the systems specifications for a communications system -- it was SEEKTALK, I believe. And there are seven sheets of specifications. So, that when we are talking about specifications, it is not just a frequency stability, or a time plus or minus two microseconds to time of day. But there are seven full sheets of performance characteristics to which this engineer is trying to design a system.

The output, input power, transient protection, warmup characteristics, long-term drift, short-term stability, trim, voltage variation, magnetic field, signal-to-noise, temperature, and you go on and on. And there are seven sheets of those.

So, the design engineer needs a lot of information, as Dr. Vig pointed out, when he is talking about an operational system, where it is going to be subjected to a wide variety of conditions. Specifications in seven sheets for one system, are pretty detailed for some of them. There are Mil standards for a lot of those, temperature characteristics, and operating range, susceptibility to magnetic fields and all of that, but I think that a design engineer

has to have a start point and get the framework within which he has to design his system.

Then he has got to make all the trade-offs, he may not be able to have a system that will give him the duration or the long-term stability for his mission duration and he may even have to shorten the scenario of how the mission is going to be accomplished, or he may have to make a trade-off in power requirements, versus weight. You know, redundancy in the system, whether he is going to have two batteries, or three.

He has got to take into account all of the specifications in an operational environment.

DR. JOHN VIG, U. S. Army

To amplify a little bit on the point Fred Walls made about the environment, I would like to give a couple of examples, horror stories.

For example, one manufacturer specifies the acceleration sensitivity of a standard as parts of  $10^{12}$  per G and you could take that standard and turn it upside down and sure enough, it might change parts in  $10^{12}$  per G, but if you put it in a helicopter, or tank and it is vibrating, you will find that instead of parts in  $10^{12}$  per G, it is more like parts in  $10^9$  per G.

Similarly for phase noise, the specs on phase noise might read 130 dB down at X number of hertz from the carrier. That is nice. If you put it on a vibration-free environment, you probably will see that it meets the specs. If you put that same oscillator into a helicopter, you will find that you have degradations in a phase noise of up to 60 dB or even more sometimes.

So, it is extremely important to specify the environment, and I couldn't agree more with what Fred Walls just stated before.

DR. STOVER:

You know this, but how do you tell that design engineer?

DR. VIG:

That is why I said before that it is very important to specify, because we have had some people for example, who were designing a Doppler radar system that was intended to work in a helicopter.



When they went out initially, they looked at the manufacturers' specs, and they found that they could meet the phase noise requirement with off the shelf oscillators. They bought some oscillators, they mounted them on the bench, and lo and behold, it met the phase noise requirements.

They went ahead with the system and eventually they put it together and put it in the helicopter and the system would not work, because that low-noise oscillator when in a helicopter became an oscillator such that you couldn't see anything on the battlefield, because of the vibration and noise.

Therefore, it is extremely important to have the manufacturers specify the stability in some standard way, both at rest and under various environmental conditions, so that when a system designer is looking for a standard of a certain characteristic, he can look at that spec sheet and tell right away whether or not that device will meet his needs, rather than having to wait until much later and find out the hard way that some of the specs were omitted, unfortunately, from the spec sheet.

MR. BALTER, TRACOR, Incorporated

In addition, to the clock or the oscillator, there is also the problem of how the clock is set, or how the oscillator is synchronized or calibrated. This should also be part of the specifications. It does no good to specify an extremely accurate oscillator, or a clock, unless there is also a means of specifying how it will be periodically calibrated and/or synchronized.

DR. STOVER:

Most of the discussion has been on the basis that the fellow knows that he will have a precise time requirement with a known specification; But what about some of the things he looks at to determine whether he needs that, whether he really should be using precise time, or whether it is important to him, or not?

How does he look at the question of whether or not precise time or frequency will add some potential for future improvements in his system, or how does he look at the advantages versus disadvantages of even getting into a precise time requirement, versus other options that are available to him?

In many cases there are other ways of accomplishing what he wants to do, without getting into a precise time situation.

How does he approach that?

DR. VICTOR REINHARDT, NASA/GSFC

At NASA, what I have found is that the only system that really works is for the users inter-act actively with the builders and the experts of PTTI, because nobody wants to design a system that goes beyond the state-of-the-art in anything. Everbody develops their requirements for practical systems, based on what is available.

Then the people like us go around and try to look for requirements, and we contact them.

Unless there is an informal channel back and forth, you get into all kinds of crazy things because, in fact, what is going on is a loop and we can't say that they are going to give us requirements, because the requirements are going to be based, at anytime, on what they think we can do.

Again, the problem is communication. If they don't know what we can do, they will never give us the proper requirements. I think what should be on a checklist for the designer is to contact the people in the field and find out what is available.

I think that when there are problems, they are contacting the wrong people.

QUESTION FROM AN UNIDENTIFIED PARTICIPANT:

We just wonder in the precise time theory if a lot of the requirements are for long-term stability. We make things that transfer information from WWV and have millisecond accuracy that you can start up cold, such as in an airplane sitting out on a runway, and have it work and you are still within a millisecond or two of the actual time. And these are relatively cheap systems and not, you might say in the so-called precise time community, but we wonder if there are not a lot of requirements in the military of this nature, so that you know that you are actually on time, within a few milliseconds, as opposed to buying very expensive oscillators for long-term stability?

QUESTION #6: "IS THERE A NEED FOR MORE EXTENSIVE COORDINATION OF PTTI APPLICATIONS AND IS THE NAVAL OBSERVATORY THE BEST CHOICE FOR SUCH COORDINATION?"

DR. STOVER:

I think that certainly Mr. Bowser's paper made it clear that there is a need for more coordination. Don't we have some comments on this question?

The previous question we had a great deal of discussion about standards and the need for having some standards and for our specifications.

Should the Observatory be providing guidance on how the specifications should be written for military applications?

No comments?

(No response.)

QUESTION #7: "WHAT CRITERIA SHOULD THE DESIGNER OF A DoD SYSTEM USE TO DETERMINE WHETHER HIS SYSTEM REQUIRES NOTIFICATION AND CONSULTATION WITH THE NAVAL OBSERVATORY RELATIVE TO PTTI REQUIREMENTS, UNDER DoD DIRECTIVE 5160.51?"

DR. STOVER:

Now, this is the question that prompted the committee to have the DoD directive handed to you as you registered. So, all of you should have some idea of what is in the DoD directive. It does say that DoD users should consult with the Naval Observatory relative to PTTI requirements. It also defines what it means by PTTI. Is that adequate criteria, the definition of precise time and the definition of precise frequency?

QUESTION FROM AN UNIDENTIFIED PARTICIPANT:

It is not a very long directive, could you read it, because not all of us got a copy?

DR. STOVER:

I can read a couple of points here, like the definition of precise time and precise frequency. If I can find them.

It defines precise time as a time requirement within 10 milliseconds; it defines precise frequency as a frequency requirement within one part in  $10^9$  of an established time scale. Over under section c, as to what different people do, it says, "All DoD components which require, utilize or distribute time and time interval information -- note those words "utilize" and "distribute" -- "or have a need for a specific time scale, shall: (1) refer time and time interval to the standards established by the Observatory; (2) maintain specific time scales such that the relationship to the standard established by the Observatory is known; (3) prescribe technical requirements for the coordination of techniques, procedures and periodic calibrations of systems, (4) promote economy by prescribing requirements for precise time that are consistent with operational and research needs for accuracy".

Now, that can be interpreted, and I do interpret it to say that anything that falls within a requirement for -- a timing requirement of 10 milliseconds, or a frequency requirement of one part in  $10^9$  should be referred to the Naval Observatory. But if for every  $10^9$  oscillator you put into any radio or piece of equipment

which you build, you go to the Naval Observatory and ask them if it is all right to use it, they are going to be overwhelmed, isn't that right?

Can you handle that, Dr. Winkler?

DR. WINKLER, Naval Observatory

If it goes along like it has for the last 20 years, yes.

I don't think the intent of DoD instruction is to do what you just said. The idea is to bring out, as early as possible, requirements for the provision of standards.

A new system, for instance, which plans to use precise time in a remote corner, which will need the precision of one microsecond, we should know about that, as early as possible. Because it will influence project decisions and it will influence strategic decisions between systems for timing and so on.

It may also, if brought to the attention of similar systems, in other services, establish a cooperation to the extent that they can both supplement each other.

So, the essence of the DoD instruction, in my view, is that timing is a two-way affair, when each user enters that so-called timing community or PTTI community, he can benefit and he can also provide benefits to others from being in a coordinated system.

Now, how does he accomplish that? To what degree should management exercise control? That is what we have, in one way or another, been talking about all morning. To what degree is it necessary to plan such a huge thing as the use of precise time and time intervals for DoD?

That is the big question. You can understand the possible range if you go from one extreme to the other. One extreme is complete chaos, where everybody does what he pleases and we don't have that.

The other extreme would be strict funding authority and line item funding from DoD through the services. It requires a huge management effort. And I think the size of the PTTI effort simply would not support such an approach.

Let's not forget about it, but the use of clocks and frequency standards is a very small item -- it is important, but it is a small item when it comes to the size of modern systems.

Today it is so small that, in fact, its smallness may be the major problem which we have; it is too small to catch the attention of high enough management levels to do something about certain things which have to be done.

As I mentioned before, there is a joke which goes around which says "if you want to have the attention of any real high management official, the cost must be at least \$50 million".

Well, we just don't reach that threshold. And the question is what should we do? To which of these two extremes should an improved management tilt, to a very strict one, or to a complete chaos?

And it appears to me that one has to sort out two things, and keep them as separate as possible in our minds. Number one, the technical details, coordination at the technical level where there is no help unless we have educated engineers and managers. And as we provide better information, we provide handbooks and possibly standards, this will be helpful.

But, make no mistake, the main reason why people do not get information, is not that it is not available, but in fact there is too much paper. In fact, Dr. English, before when he said such a book would be needed, did not know of the existence of quite a number of these books. And I don't blame him, because today every system designer who talks about a system concept has to absorb an absolutely incredible amount of information, of technical details.

And, again, the question of oscillators, timing and so on, is a small item. Unfortunately, however, as small as it is, it requires coordination because otherwise we would have chaos if everybody provides for his own timing, globally with systems of his own making, it would be increasingly expensive.

So, what I think we have to do, and have to accomplish, is to prevent unnecessary duplication. And, again, the best way to do that is to keep our lines of communications free, refrain from unnecessary things which also means unnecessary paperwork. Every sheet of paper today that you cause to be printed is a load, an increasing burden on everybody who is in the system.

I do not think that, therefore, in view of the size of the overall PTTI effort, which is very small and in view of the necessity to provide technical information communication, that we should further load down the system with paper requirements.

But what is necessary, however, and has come out very clearly in Mr. Bowser's talk, and that is that we provide for shorter lines of communication by strong suggestion in the form of regulation, that each service, each agency, which uses precise time and time interval must establish their own internal communication and coordination by appointing clearly visible PTTI manager.

That, in many cases, could be a part-time proposition for somebody. And in agencies, such as DCA, for instance, I think such an appointment is very, very necessary.

The same situation exists for the military services. The only service which today has such a PTTI manager is the Navy, and I think we have benefited very greatly from that. The fact that such an office exists, that things can be referred to that office, that office has the information about similar systems, what they do, that they can plan for certain equipment development which is common to everybody, such as the platform distribution system, for instance, which is an important item -- maybe the most important item in the Navy PTTI.

That is what I think we can and must accomplish in the next phase of management improvements.

Much beyond, that, I don't know. I don't think the Observatory has to know about every crystal -- to come back to your question. That is the function of the service PTTI manager which has to be established.

DR. STOVER:

Let me try a summary on you now. If it is within  $10^9$  in frequency, or 10 milliseconds, and it is also a new type of system or it is a system that interfaces with other systems, or may in the future interface with other systems, then they should come and consult with you, is that your answer?

DR. WINKLER:

Yes.

DR. STOVER:

Thank you.

MR. SAMUEL WARD, Jet Propulsion Laboratory, California

I think that this document could be improved tremendously and serve the purpose of educating the user that doesn't know he needs this by spelling out in terms of location, or velocity acceleration parameters how these translate to those things.

The man who is designing a collision avoidance system may not know that he needs precision time or very accurate frequency in order to do that. And so in navigation we spell it out in terms of how many kilometers at such a distance and translate these frequency and time parameters into others and make them a part of such a document.

If you have a system that must measure location, to whatever level you spell out, then you also have a timing problem, a need for precision time.

DR. STOVER:

Thank you.

Perhaps those people who are working on a revision of this directive will take your remarks into consideration.

DR. VICTOR REINHARDT, NASA/GSFC

I don't think this problem will ever be solved at the management-administrative level. It is a technical problem and unless technical people go out and educate other technical people as to what the problems are, things will not be solved.

You have to get in at the early design phase, at the early idea phase. You have to go out and show people what range rate tracking errors are, as a function of precise time, so that whatever the other people are use to using in terms of requirements are known in terms of precise time, before you get anywhere.

I don't think putting books or directives together will mean anything, unless they are educational on a technical level.

And I just want to reiterate what Sam Ward is saying, that these documents should be highly educational and try to translate as best as possible from the precise time domain into the radar domain, or whatever domain people use in the field.

DR. STOVER:

So, you are saying that standards or any directives should be made educational tools?



DR. REINHARDT:

Yes.

DR. STOVER:

Thank you.

MR. KELLOGG, Lockheed

I don't understand why the burden of the responsibility gets down on the technical people, when one can review in the immediate past a rather large system which at present nobody would argue depends basically on the precise time and time interval accuracy. That is the GPS satellite system.

Before DoD started out to make equipment and test it, it would seem the responsibility should at least be considered as whether or not there should be some kind of conference with the Naval Observatory as to whether, (a) this was a reasonable system to try to inaugurate; (b) whether the equipment could do what it was intended -- that it was suppose to provide; and (c) whether or not it could be tested; and (d) whether the Navy Observatory was in a position to be able to assist in the testing.

At the present moment one could at least entertain the proposition that great effort has been made to exclude the greatest source of help for something which is the greatest advantage to quite a few people who use time and time interval.

DR. STOVER:

Thank you.

QUESTION #8: "WHAT ADVANTAGES OF COORDINATING WITH NATIONAL AND INTERNATIONAL STANDARDS ARE MISSED BY THE SYSTEM DESIGNER THAT SAYS, 'I AM ONLY INTERESTED IN MAINTAINING A CONSISTENT PHASE OR FREQUENCY WITHIN MY SYSTEM; I DON'T CARE ABOUT OTHER SYSTEMS'?"

DR. STOVER:

This was a point that was brought out by Mr. Bowser in his talk. Let me suggest a couple to get thing started since no one offered a response.

It can provide an external reference for monitoring purposes for one thing, so the system can use the timing in a different system for monitoring what is going on in his own system.

It can accommodate future operations requiring the cooperation among different systems.

It can provide an alternate or fallback timing capability.

It also can provide for a possible improvement in performance or reduction in cost by using cooperation among different systems.

These are all points that Dr. Winkler mentioned in his answer to the previous question. Apparently these are points that are frequently overlooked by the person who goes off on his own. Mr. Bowser pointed out in his talk that this is an important thing, but it seems to be the standard procedure for each project, to just go off on its own.

I felt that it was an important question to get in here.

MR. LAUREN RUEGER, JHU/APL

One of the major advantages of tying into the national and international standards is to get rid of some false sense of security. You can run your time instruments, you think everything is working beautifully, you have tested the instrument in your laboratory, side-by-side; and you come to find out that the instrument is pressure sensitive, or sensitive to some kind of environmental factor that you never see because your measurements were not made relative to the more anchored national standards.

DR. STOVER:

Thank you.

DR. SAM STEIN, National Bureau of Standards

I think the principal advantage in coordination between systems comes from an ability to evaluate systems, but we shouldn't overlook the fact that most of the time people who are taking maximum advantage of precise time and time interval technology are doing so in order to guarantee system independence and in order to be able to deny the use of the system to other people.

There is, therefore, a conflicting approach between, say, providing frequency syntonization and timing synchronization between nodes of a system the way the telephone company would do through coordination, and providing the same functions the way the military would do, by having independent high quality standards.

DR. STOVER:

Dr. Stein, don't you believe that he can have that independence and still have it coordinated with the standard? Can't he have both, can't he have the best of both worlds?

DR. STEIN:

The answer is a partial yes, but the two approaches provide totally different aspects and totally different qualities to the system, and they can't be combined to provide a single aspect to the system.

DR. STOVER:

Thank you.

QUESTION #9: "WHEN A SYSTEM DESIGNER RECOGNIZES THAT THERE MIGHT BE ADVANTAGES TO REFERENCING THE PHASE OR FREQUENCY OF HIS SYSTEM TO A NATIONAL AND INTERNATIONAL STANDARD, WHAT METHODS SHOULD HE CONSIDER FOR PROVIDING SUCH A REFERENCE?"

DR. STOVER:

I am going to pass over this question, because I think it will be covered adequately in some of the papers in other sessions.

So, let's go on to the next one.

QUESTION #10: "WITH LIMITED RESOURCES FOR MILITARY TIME REFERENCES, IS IT BEST TO USE THOSE RESOURCES FOR REDUNDANCY IN A SINGLE SYSTEM, OR TO DIVIDE THEM AMONG REDUNDANT SYSTEMS?"

DR. STOVER:

Let me word that question a little bit differently. Is it better to spend all of your money on one very good basket to put your eggs in, or is it better to use that same amount of money on several, perhaps not so good baskets?

DR. WINKLER, Naval Observatory

That is an extremely important basic strategic decision. And in the case of PTTI, fortunately, it is not a very difficult one to make. The reason for that is that with so many time systems in existence today, the additional expense to use one or any one of them to provide time is very, very small. It is merely a management effort. Where costs come in would be the development of the receiving equipment, or of user equipment to interface with these systems.

But, again, most of our users have to do that anyway. Most military users have to interface with some navigation equipment, with some communication equipment and to have several avenues available by which time can be picked up, I think it is an absolutely indispensable principle.

So, again, here I think one can have both advantages without having to pay an inordinate penalty in cost.

DR. STOVER:

Thank you.

QUESTION #11: "WHAT CHARACTERISTICS ARE IMPORTANT FOR A USER TO CONSIDER IN SELECTING A SOURCE OF REFERENCE TO A NATIONAL OR INTERNATIONAL STANDARD, AND WHAT SOURCES BEST PROVIDE THESE CHARACTERISTICS?"

DR. LESCHIUTTA, Istituto Elettrotecnico Nazionale, Torino, Italy

I just remembered that the main basis for international comparisons is relying on the books of the CCIR, the International Committee for Radio Communication, whose group is dealing with frequency and time topics. Thank you.

DR. STOVER:

Thank you.

Since there doesn't seem to be any more comments, I will make a couple of suggestions of things that you might want to consider: Convenience, continuity of service, accuracy or stability, geographical coverage, time when it is available, cost, reliability, survivability, or any unusual requirement.

Let's go on to the next question.

QUESTION #12: "DOES THE EQUIPMENT PROVIDED BY MANUFACTURERS MAKE IT  
CONVENIENT TO APPLY PTTI TO NEW SYSTEMS?"

DR. VICTOR REINHARDT, NASA/Goddard

I think it is very convenient, there are lots of sources, lots of different types, but I just want to address something that happened in connection with this.

I think a lot of users think it is not convenient because of the philosophy of designing many systems, especially military systems in which they say, gee, that box is beautiful, but it is four foot by five foot, or four inches by five inches and we would like it five inches by four inches. They don't realize the implications of redesigning a system, and the impacts on reliability or performance of what seems to them slight changes in size, weight, electrical characteristics.

I think there isn't enough use made of off-the-shelf equipment in many of these fields. This also happens in the satellite field. Risks are taken that don't have to be taken because people insist on making changes which are critical to performance.

DR. STOVER:

Do you think a set of standards for PTTI equipment and PTTI applications would help alleviate this problem?

DR. REINHARDT:

Yes. I think especially a set of standard frequency boxes, clock boxes that meet the kind of requirements people need in critical applications, such as satellite work, military applications.

DR. STOVER:

Can you suggest who might be a desirable choice to produce such standards?

DR. REINHARDT:

I think that it has to come from DoD, if DoD is the user. The way to do that is to get some standards groups, get some Mil standards and to encourage manufacturers, which of course, requires money, to produce some sort of standard box.

But I think it is never going to be successful if the users of these devices don't listen to these standards. I think there is going to be a lot of communication required before this kind of thing happens.

NASA has gone towards these standardizations and standard buses for satellites and whatever, they are only beginning now to address the problems of standardized clocks.

For example, right now every satellite builds its own clock from scratch. And I think because of that, especially in the crystal business, the devices that they use are just behind the state-of-the-art, because they don't take advantage of the commercial standards that I think are better performance than some of their satellite standards that they use now.

DR. STOVER:

Thank you.

DR. SAM STEIN, National Bureau of Standards

I think we should try to learn from past experience in other fields where these same types of problems have been addressed. I think the situation that we are looking at here is one which can be characterized in that the government is at least viewed to be the principal user of a certain type of equipment.

That did happen before in the early 1950s in the computer field, where it was decided that the government would develop the technology in the field.

Now, in that case the preception turned out to be incorrect in the long-term.

In order to provide an orderly marketplace and to prevent the government from overly distorting private competition in the computer field, it was decided to develop both government use standards and government procurement standards for computers.

I can only say that -- this is just a purely personal opinion on my part -- the result of an overly rigid process of government regulations, is that the government has an inventory of computers which is more than one generation out of date, on the average. That is the average government computer is more than seven years old at this time.

I don't think we can afford to produce this kind of result in the precise time field. I think, therefore, we need to tend much more in the direction that you mentioned before, of improved education and improved coordination, and communication of information, and less in the direction of developing standards boxes, or standards for the utilization, standard interfaces, or things which tie down the ability of systems to change and react to changing demands.



DR. WINKLER, Naval Observatory

I concur completely with that comment, in fact, there is a basic directive out in the Department of Defense for quite a few years for system designers to design as much as possible their systems around the available equipment, on the shelf items. And to stay away from custom design models.

And there are several reasons for that, in my mind maybe the most important one is that by using modules which are available, which have been designed and tested in the field, you obtain greater reliability and lower costs. There is no question about that.

That directive stands, in fact, it goes back to David Parker's time as Deputy Secretary of Defense. Those instances which we have in mind when we talk about boxes not being three by four, but four by three, and so on, these are simply cases where this basic directive has been almost deliberately disregarded.

I completely agree with Dr. Stein about his comments that if you overly restrict by regulations the use of frequency standards, you will have the same situation as in other areas, that you are 10 years behind the state-of-the-art.

In addition, you apply a management effort to an area which does not really merit it by its small size.

What we have to attempt, however, is, again, let me repeat that, is to cut out the bad instances to achieve some overall improvement of communication. This can be accomplished. And I think the proposals which the Observatory will make very shortly, will go in that direction and I think they will be successful.

DR. STOVER:

Thank you.

QUESTION #13: "ARE THERE A NUMBER OF OSCILLATORS AVAILABLE AT LOW COST FOR A WIDE SELECTION OF FREQUENCIES WHICH CONVENIENTLY PHASE LOCK TO ONE PULSE PER SECOND SIGNALS?"

DR. STOVER:

Now, let me explain why this question is in this list.

Phase lock oscillators are usually locked to references of their own frequency, and if a 5 megahertz reference were unavailable for an extended period of time, then an oscillator locked to that 5 megahertz reference would drift. If it drifts more than 200 nanoseconds, then when the reference becomes available again, the oscillator will lock to the wrong cycle.

If the reference is one pulse per second, there is very little likelihood that it is going to drift a full second in the period of time that the reference is unavailable. So that when it comes back it will lock onto the correct cycle.

That is the reason for this question. I don't know whether such equipment is conveniently available, or not. But I suggest that there are many applications for which this characteristic is very important. And when we need something of a longer period of time, it seems natural that the definition of time, the second, be the best interval to choose.

Those are my opinions. Now, I would like to hear some of yours.

FROM AN UNIDENTIFIED PARTICIPANT:

There is a technical invitation to this, if you try to use 1 PPS as the standard lock frequency, many crystals would not be capable of keeping this without introducing glitches into the system. That is you have to pick locked time constants on the order of 10 to 100 seconds if you want to avoid the granularity of hitting a crystal with 1 PPS. Many crystals are not capable of doing that, due to vibration and other factors.

You really need an intermediate frequency, 5 megahertz or 1 megahertz, as well as 1 PPS to do the job.

DR. STOVER:

I guess maybe I didn't give my proposition quite correctly. I am assuming that the 1 pulse per second would be used to select the right cycle of some other frequency that might be used. And I think that is what you are saying, is that you need that other frequency.

FROM AN UNIDENTIFIED PARTICIPANT:

You need a reference at 5 megahertz or 1 megahertz, or something, as well as the 1 PPS to do the job, technically, with crystals.

QUESTION #14: "ARE THERE A NUMBER OF EQUIPMENTS AVAILABLE AT LOW COST WHICH PROVIDE PRECISE PHASE ADJUSTMENT OF THEIR OUTPUT, RELATIVE TO THEIR INPUT AND THEREBY PERMIT PHASE LOCKING THE OUTPUT OF AN OSCILLATOR WITHOUT DISTURBING OSCILLATOR PARAMETERS?"

DR. STOVER:

I think the answer to that question is, yes, they are available, so let's move on to the next question.

QUESTION #15: "IS THERE GUIDANCE AVAILABLE TO SHOW POTENTIAL USERS HOW PRECISION CLOCKS, SOURCES OF UTC PHASE REFERENCE, FREQUENCY DIVIDERS, FREQUENCY MULTIPLIERS, MIXERS, PHASE SHIFTERS, ET CETERA, CAN BE CONVENIENTLY CONNECTED INTO SYSTEMS AND THAT THESE DIFFERENT DEVICES HAVE COMPATIBLE INTERFACES FOR BEING CONNECTED INTO THE SYSTEMS?"

DR. STOVER:

Are there any comments on that question?

(No response.)

DR. STOVER:

I can't stimulate a comment, I guess.

Let's go on to the next question.

QUESTION #16: "ARE THERE PTTI DEVICES AVAILABLE WHICH ARE DESIGNED TO PERMIT CONVENIENT INTERFACES WITH MICROPROCESSORS?"

LT. KARL KOVACK, GPS Program Office

The answer is yes, and it is called GPS.

DR. STOVER:

That sounds like a commercial. Maybe somebody would like to comment on what it takes to make a PTTI device convenient to interface with a microprocessor? What characteristics are required in a PTTI device to make it convenient to interface with a microprocessor?

Surely we must visualize that there are going to be some situations in the future where we are going to want to interface PTTI devices with systems that are employing microprocessors for a wide variety of purposes.

DR. EDMUND CHRISTY, Offshore Navigation

Just to name a few devices that are available without being exhaustive about it, there are, in fact, precision phase shifting devices that are available with RS232 and HPIB type interfaces, and there are microprocessors available which also support RS232 and HPIB interfaces.

Likewise, you can now buy direct digital synthesizers which can be phase locked to a cesium standard or some other standard. These are available with microprocessor S100 bus.

So, that is three items right there that I know of, which are easy to connect to microprocessor systems.

I can give someone details on specific part numbers or things like that, if they are interested, later.

DR. STOVER:

I think you answered the question, yes, there are devices available and you also named some of the factors that should be considered, those things that would make them compatible.

With that, let's go on to the last question.

QUESTION #17: "WHAT IS THE MOST PRESSING NEED IN THE FIELD OF PTTI APPLICATIONS?"

DR. WINKLER:

I should say money. Curiously, I think the most pressing need is not the development of small demanding specifications, but greater reliability. Timekeeping stands and falls with reliability and, in fact, when we discussed before what are the difficulties, why don't more people use precise time and time interval, I think many of them are simply afraid that more complexity, more equipment will bring an impairment in the reliability of time systems.

So, clocks and connected equipment, such as distribution amplifiers, what have you, must have extreme reliability in order to be useful as clocks.

And I would suggest that this is the most important answer, and not greater performance. Thank you.

MR. BILL BRIDGE, MITRE Corporation

I would agree with the need for the reliability, but I would like to see that reliability in a tactical environment which includes all the Gs that are involved in aircraft and all the temperature and vibration problems involved with tank-type environment.

DR. SAM WARD, JPL

I think one word says it "education".

DR. STOVER:

I think that has come out throughout the whole session, everybody has discussed the lack of PTTI knowledge that many people have.

DR. FRED WALLS, NBS

The greatest inhibitor to reliability is lack of number and the insistence on specialized packages for new systems and the insistence on odd-ball frequencies. Those things drive a company to put their best engineers, their best people on producing custom changes, rather than working on reliability and improved performance and other things.

If you want reliability, you have got to get the numbers up, there is no way to make two or three, or even 10 of a device and have enough money and time to test it, and to get the data to

prove that it is reliable. If you want reliability, you need to standardize some frequencies, you need to get configuration that you are willing to accept on a number of systems, so you can go to multiple units. I believe that is the only way.

MR. FRANK KOIDE, Rockwell International

I think system reliability comes from system maturity, maturity of the system. If you would look in a spacecraft type world, you take the cesiums or the rubidiums, they have very little system maturity in respect to transmitters, multiplex systems, and things like that, that are on other types of space vehicles.

We have to get maturity into the system, before we get the reliability.

DR. STOVER:

Thank you very much.

I want to thank all of you for your comments and discussion, and I think that this turned out very well. I was very nervous when we started, for fear that we wouldn't get this kind of response. Thank you very much.





SESSION II

NETWORK CLOCK OPERATIONS

Mr. Paul F. Kuhnle  
Jet Propulsion Laboratory



CHAIRMAN KUHNLE: Good afternoon.

This session is on Network Clock Operations and is intended to describe operating clocks and timing systems, and methods currently in use in the field.

Nine papers are scheduled for this session. Unfortunately, paper No. 8 has asked to withdraw. Bob Steimets at White Sands sends his regrets, due to travel funding shortages and reorganization activities.

We have substituted paper No. 39, which is described on page 45 of your program.

The first presentation, paper No. 2, titled Precise Time Dissemination via Portable Atomic Clocks, by Kenneth Putkovich, who is with the United States Naval Observatory. He is Branch Chief of the Precise Time and Time Interval Branch, and he is in charge of the hardware, clocks and portable clocks, portable clock trips, and collection and publication of data relative to LORAN-C and Omega transit and GPS.



## PRECISE TIME DISSEMINATION VIA PORTABLE ATOMIC CLOCKS

Kenneth Putkovich  
U. S. Naval Observatory  
Washington, D. C. 20390

### ABSTRACT

The most precise operational method of time dissemination over long distances presently available to the Precise Time and Time Interval (PTTI) community of users is by means of portable atomic clocks. The many attempts that have been made in the past to devise operational systems for submicrosecond time dissemination to supplant portable clocks largely have been unsuccessful. Many excellent techniques have been developed which are capable of the required precision. In some cases, the cost and burden of utilizing these techniques in a world-wide, operational time dissemination network have proved to be far greater than the portable clock costs. In other cases, the geographical coverage has been limited. In many cases, however, the managers of systems capable of being economically utilized for PTTI dissemination have been reluctant and, in some cases, adamantly opposed to even considering use of their systems for PTTI. In no case have the proposals for a system or a system modification solely for PTTI dissemination been seriously considered. The Global Positioning System (GPS) is the latest system showing promise of replacing portable clocks for global PTTI dissemination. Although GPS has the technical capability of providing superior world-wide dissemination, the question of present cost and future accessibility may require a continued reliance on portable clocks for a number of years. For these reasons it was felt that a discussion of portable clock operations as they are carried out today would be of some value. This paper describes the portable clock system that has been utilized by the U. S. Naval Observatory (NAVOBSY) in the global synchronization of clocks over the past 17 years, explains the concepts on which it is based and examines some of its capabilities and limitations.

### INTRODUCTION

This paper provides a brief background description of the NAVOBSY portable clock service, including some historical information, and a description of the planning that is required, the hardware that is used, the services provided and the areas that are covered by regularly scheduled trips. The body of the paper concerns the acquisition,

reduction, analysis and reporting of portable clock data and the procedures that must be used to insure the veracity of the data. Included are a discussion of the assumptions on which portable clock operations are based, the assignment of uncertainties to reported data and the process used in reducing data from trips. Finally some improvements that have been implemented and others that are under consideration for enhancing the quality of the service provided are presented.

## BACKGROUND

Atomic clocks were first used in a "portable" sense by Reder and Winkler in experiments conducted in 1959 and 1960.<sup>1</sup> The clocks used were the early Atomichrons (Figure 1.), which were seven feet high and weighed several hundred pounds. They were portable only in the sense that they could be transported (with great difficulty) while running and required extensive support in the form of external power when being moved.

A significant reduction in the size of cesium beam frequency standards in the early sixties resulted in the design of a more compact, self contained clock (Figure 2.) that was truly portable in a practical sense in that two men could (with some difficulty) transport the clock to any location using readily available means of transportation. Its use was first demonstrated by Bagley and Cutler in 1964 and again by Baugh and Bodily in 1965.<sup>2,3</sup>

As a result of these demonstrations, a portable clock service was established by the NAVOBSY in 1965 in order to meet world-wide requirements for PTTI. Since that time, several thousand clock synchronizations have been done (Figure 3.). Figure 4 shows an early version of the portable clocks presently used by the portable clock service. This service has proved to be of immense value to U. S. Navy, Department of Defense, NASA and other national and international programs which require PTTI in their operations. It is one of the primary reasons why the many, widespread timekeeping activities that exist today maintain such a relatively high degree of synchronization.

Although a number of techniques have been demonstrated which allow time dissemination over fixed, long baselines to a precision as great or greater than can be achieved with portable clocks, there are no other operational systems which can routinely provide synchronizations to any spot on the globe. The only system with the demonstrated potential for surpassing portable clocks on a global, high availability basis is GPS. Unfortunately, the uncertainty of the future of the system and its accessibility to non-Department of Defense PTTI users has had a significant, negative impact on the development of commercial GPS timing equipment.

## PORTABLE CLOCK OPERATIONS

The effort required to plan and execute a portable clock trip is quite extensive and requires a coordinated effort on the part of a number of people and organizations to insure a reasonable probability of success. Although a tentative schedule is prepared over a year in advance of departure, detailed planning begins about thirty to forty days in advance when an itinerary (including cost estimates, planned activities and personnel assignments) is circulated to cognizant personnel for approval. Once this is completed, detailed planning begins in earnest as outlined in the standard operating procedures in Appendix I. In many cases, the itinerary has to be built around one or two key events which are outside the planner's control - Military Airlift Command (MAC) flights, foreign custom's assistance, local support at remote sites, etc. Throughout the entire planning and execution cycle, an attempt is made to strike a reasonable balance among the often conflicting requirements of the various parties involved - the best possible data from the scientific viewpoint, the most cost effective execution from the management viewpoint, and some reasonable travel conditions from the clock teams viewpoint. The first is the primary responsibility of the clock team leader and personnel in the NAVOBSY Time Service Data Reduction Branch. The second is the joint responsibility of the Precise Time Operations Officer, NAVOBSY management and the clock team. The third evolves from compromises worked out among all those involved in the process.

In addition to clock synchronizations, several other functions may be performed, depending on the requirements of the site visited. If valid requirements exist and are known and trip arrangements properly made to allow sufficient time on site, frequency offsets can be determined, clock adjustments made, maintenance performed, training given and any other PTTI related functions carried out. Unfortunately, in most instances, the pressing business of clock synchronization precludes spending any significant amount of time at sites other than those specifically identified in the itinerary. When requirements develop at sites near to those regularly serviced by NAVOBSY teams, little or no compensation is required from a qualified requestor. In cases where additional, significant cost and time are involved or the requestor is not qualified by virtue of being a U. S. government agency or contractor, the requestor is required to fund any additional expenses.

The NAVOBSY has several "standard" itineraries which are executed on a regular, yearly basis, many in cooperation with and supported by other agencies. A listing of these trips can be found in Table II. The itineraries are designed to cover the largest number of required sites in as short a time as possible without exceeding an approximate 21 day limit or overtaxing the clock team.

In order for the clock team to maximize the possibility of securing valid clock data, they must, as part of their pre-trip procedures, test



the clock and any ancillary equipment required to support their efforts in the field. This involves testing and exercising the standby power system for the clock, testing the time interval counter to be carried on the trip, and assuring that the clock kit contains the connectors, adapters, cables, spare parts and tools that are necessary to assure continued operation of the clock throughout the trip. Thorough preparation, combined with adept, creative personnel, are vital if the team is going to overcome the unexpected events that are certain to occur in an undertaking of this kind.

#### DATA ACQUISITION AND RECORDING

The primary purpose of portable clock operations is to gather data which will allow the determination of a remote clock's time relative to that of an established time scale. In the case of the U.S. Naval Observatory clock operations, the time scale is Coordinated Universal Time (UTC) as generated and maintained by the Master Clock system in Washington, D.C.

The collection of portable clock data actually begins several days in advance of departure. As a matter of policy, atomic clocks designated for use as portable clocks are adjusted and kept as close in frequency to the Master Clock as possible and the time set such that the difference between the portable and Master Clock passes through zero at the midpoint of the trip. All operational NAVOBSY clocks are monitored continuously by an automated data acquisition system (DAS) in order to ~~characterize their performance~~. A special effort is made to assure that clock performance data are taken for a period of five to ten days prior to and after the trip and that the data collection process is undisturbed over this period.

On the day of departure, clock measurements are made against the two reference clock systems in the Master Clock with both the permanent, high resolution (nanosecond or smaller) counter in the measurement console at NAVOBSY and the small, portable, ten nanosecond counter taken on the trip. A 1 PPS time tick to zero crossing of the 1 MHz signal from the portable clock is made on the portable counter to establish a reference value for use during the trip. All these data are recorded on a standard data form shown in Figure 5. Detailed measurement procedures and techniques employed in portable clock operations are not provided in this paper as the subject has been adequately covered previously.<sup>4,5</sup> However, some mention of the rationale behind them is warranted.

NAVOBSY portable clock operations are a significant undertaking. In 1980, for example, 302 clocks were synchronized during 120 site visits. This effort consumed 227 man-days of effort at a cost of over \$95,000. These expenditures were those required to support clock teams while in the field and do not include initial equipment costs, pre and post trip data analysis, reduction and reporting costs, or the cost of supporting

and planning the trips. Thus, the cost per clock synchronized is considerable, over \$320 in 1980. It is imperative under these circumstances that procedures are used that yield consistent, unambiguous, correct data. Although the standard procedures employed by the NAVOBSY in taking clock data appear rather simplistic, they are based on many years of field experience and are designed to minimize loss of data due to poor procedures. In order to be effective, the procedures had to be designed such that they could be carried out under the stressful conditions frequently encountered in portable clock travel. Many are obvious, common sense steps - use of a uniform set of cables, standard measurement parameters, a single set of measurement equipment, etc. Others - tick-to-phase measurements, measurement system reconfiguration to eliminate arithmetic and reduce number size, system designs to reduce measurement ambiguities, etc., are more subtle.

Clock data in the field are recorded on a data form which is prepared for each individual clock measured. Measurement of the primary clock at each site is required immediately on arrival, daily and prior to departure. Additional measurements on other clocks and timekeeping systems and measurements utilizing on-site equipment are made as required. As previously mentioned, depending on site requirements, equipment adjustments, maintenance, training or a variety of other functions may be performed. The primary responsibility of the clock team, however, is the acquisition and recording of valid clock data.

Regardless of the length of the clock trip, it must end with the same steps with which it began, comparison and evaluation against the NAVOBSY Master Clock. Once enough post-trip data are available to characterize the frequency offset of the portable clock, reduction and analysis of the trip data can be completed.

#### DATA REDUCTION AND ANALYSIS

One of the keys to successful portable clock operations is the proper reduction, interpretation and analysis of the data developed over the entire span of the trip, including the pre- and post-trip segments. In the past, when requirements were less stringent and capabilities more limited, a simple interpolation between trip end points was used to determine estimates of portable clock differences. However, increased requirements for higher precision time transfers necessitated improvement in portable clock data, particularly where perturbations in portable clock performance raised questions as to the accuracy of the resultant time transfers.

The pre- and post-trip portions are generally no problem as the data are readily available, stable, well defined and amenable to simple analysis. If the portable clock performs well during the pre-trip and post-trip segments, well defined, straight line fits can be made to the pre-trip and post-trip data. Extrapolation of these straight line fits through

the trip period results in a single line defined by

$$y = mx + b,$$

where  $y$  = Master Clock - Portable Clock time difference (usec),  
 $x$  = Time elapsed (days),  
 $m$  = Offset of Portable Clock from Master Clock (usec/day),  
 $b$  = Constant defined by actual pre- and post-trip data (usec).

Ideally, the portable clock is set so that  $m = 0$ . Failing this, the clock is set so that  $y = 0$  at the midpoint of the trip.

Figure 6 is a simple illustration of the concepts presented above. Figures 7 through 9 are several variations that can occur. In these illustrations the solid lines represent the pre- and post-trip comparisons of the portable clock against the Master Clock. The dashed lines are extrapolations of the pre- and post-trip clock performance data and the associated limits on the estimates of uncertainty which must be assigned to the data, given only the information on clock performance developed during those periods.

Figure 6 illustrates a best case condition where the portable clock performed exceptionally well and experienced no perturbations in operation during the trip. As a consequence, the uncertainty estimates are small and can be predicted with a high degree of confidence.

Figure 7 shows the result of an assumed, single, permanent change in the output frequency of the portable clock. Although a rigorous analysis of the situation might lead to a more refined performance model, this simple technique provides sufficient insight into performance with a minimum amount of effort. Propagating the uncertainties forward and back from the trip end points to a point of apparent discontinuity leads to an acceptable, conservative uncertainty estimate.

Figure 8 illustrates the result of an apparent step in time. In the absence of any additional information, one must assume a worst case condition where the discontinuity occurs at either end of the trip. Under these conditions, the extrapolation results in a large area of uncertainty which is compounded by the need to extend uncertainty estimates over the full length of the trip.

Figure 9 shows a situation where the likelihood of the occurrence of both a step in time and a change in frequency is high. Here again, in the absence of additional information on the performance of the portable clock during the trip, the uncertainty associated with the estimate of the portable clock values could be so high as to render the data worthless.

Under certain conditions the data from the last two cases sometimes can be salvaged. If portable clock measurements were made at a site whose clock had been recently synchronized by another portable clock or by satellite time transfer, or whose time is known to a relatively high precision at all times by virtue of it being a NAVOBSY Precise Time Reference Station (PTRS) or equivalent, then a point or several points can be determined at which the NAVOBSY - Site Clock difference is known to a better precision than that determined from the extrapolation process. The extrapolation and uncertainty determination are then adjusted to reflect this situation.

Thus, for any site clock measurement,  $M_i$ , made with the portable clock at time,  $x_i$ , during the trip, a post trip correction,  $y_i$ , is calculated and applied to the measured value to establish the difference,  $D_i$ , between the Master Clock and the measured clock, so that

$$D_i = M_i + y_i.$$

Associated with each measurement is an empirically determined estimate of uncertainty,  $u_i$ . The uncertainty consists of a fixed component which is associated with the measurement system and technique used, and a time dependent component or prediction uncertainty which increases with time, due to both the random and systematic performance characteristics of the portable clock. The uncertainty is at a minimum at the beginning and end points of the trip as the time dependent component is zero. In most cases, it is at a maximum at the midpoint of the trip, where the time dependent component is largest. In cases where a discontinuity occurs, the uncertainty is propagated over the entire trip. Additional information on these uncertainties can be found in references 5 and 6.

## REPORTS

Dissemination of portable clock data is accomplished by several means and includes current trip schedules, future trip itineraries, and clock data from recent trips. All of this information is available electronically via the NAVOBSY Time Service Automated Data Service (ADS). The ADS consists of an extensive data base and the hardware and software to make it continuously available via telephone to any user with a compatible modem and computer terminal. A full description of the ADS is available from NAVOBSY on request.<sup>7</sup>

Individual clock reports are automatically prepared by a computer from the results of the reduction and analysis of all portable clock measurements made. After a multi-step review, these are mailed to the cognizant agency or personnel. An example of this report is shown in Figure 10. Those clocks that have significance with respect to international timekeeping activities receive additional scrutiny and additional certification is made (Figure 11). These results are published in the current Time Service Announcement, Series 4. In all cases, portable

clock data go through several, distinct, independent levels of analysis and verification to assure the validity of what is published.

#### FUTURE IMPORVEMENTS

Improvements to portable clock operations can be viewed from two inter-related standpoints - cost and quality. As portable clock operations are manpower intensive, the only way to reduce recurring costs is to reduce the number of manhours required to acquire and process data while simultaneously maintaining or improving data quality. Trip lengths and itineraries have been examined and analyzed to the point where little else can be gained in this area without the risk of causing some degradation in overall operations and, specifically, in data quality. Two areas that offer some promise of success are (1) the reduction of the size of portable clock hardware to the point where one person clock trips would be possible and (2) the incorporation of more automation in the acquisition, reduction and analysis of clock data to reduce the time required for processing and to improve the data quality.

Information on a smaller clock and an improved, portable time interval counter for use in NAVOBSY operations was published in 1980.<sup>8</sup> The counter is presently used in all portable clock operations. The small clock has been successfully carried on several one and two person clock trips. It appears, however, that routine, one person clock trips on an operational basis will require further refinements in clock and power supply hardware.

A small, microprocessor-based measurement system for automatic acquisition and storage of portable clock data in the field appears feasible in the near future. Such a system would allow the automation of measurements, entry of clock identification and location information, back-up hard copy output of measurement data, and storage of measured data in a format and form that is suitable for direct, machine processing at the end of the trip. Further enhancements along these lines could include monitoring and determining the reserve capacity of the standby power system, measuring pertinent, ambient, environmental conditions and allowing the input and storage of flight parameters for use in evaluating clock performance over an entire trip. This would allow the implementation of routine correction for relativistic effects and provide the means of pinpointing perturbations in clock operations which currently cause serious problems in data reduction.

#### CONCLUSION

In spite of the fact that the NAVOBSY routinely maintains a widespread network of synchronized clocks utilizing a variety of PTTI dissemination systems other than portable clocks, portable clocks presently provide the only operational means of routinely synchronizing networks of clocks on a totally global basis. It appears that this situation will

continue to exist for several years into the future. Improvements to both portable clock hardware and operation will be necessary in order to meet the current and upcoming requirements for synchronization.<sup>9</sup>

#### REFERENCES

1. F.H. Reder and G.M.R. Winkler "Preliminary Flight Tests of an Atomic Clock in Preparation of Long-Range Clock Synchronization Experiments," Nature, Vol. 186, No. 4725, pp. 592-593, May 21, 1960.
2. A.S. Bagley and L.S. Cutler, "A New Performanc of the Flying Clock Experiment," Hewlett-Packard Journal, Vol. 15, No. 11, July, 1964.
3. L.N. Bodily, "Correlating Time from Europe to Asia with Flying Clocks," Hewlett-Packard Journal, Vol. 16, No. 8 April, 1966.
4. Operating Procedures, Precise Time and Time Interval Equipments, NAVOBSY - TS/PTTI SOP-81, February, 1981.
5. K. Putkovich, "High Precision Time Transfer Methods," Proc. of Seventh Annual PTTI Applications and Planning Meeting, December, 1975.
6. L.G. Charron and R.T. Clarke, III, "Evaluation of Predictability of Quartz-Crystal Oscillators and Other Devices," USNO-TS-01-81, January, 1981.
7. G.M.R. Winkler, "The U.S. Naval Observatory Data Services," 1981. (Available on request from Time Service, U.S. Naval Observatory, Washington, D.C. 20390).
8. K. Putkovich, "Time Dissemination - An Update," Proc. of the Eleventh Annual PTTI Applications and Planning Meeting, November, 1979.
9. Precise Time and Time Interval (PTTI) Program Improvement Plan, U.S. Naval Observatory Report, December, 1981.

<b>Factor System</b>	<b>Capability (μsec)</b>	<b>Cost (\$K)</b>	<b>Coverage</b>	<b>User Skill L-Low, M-Moderate, H-High</b>	<b>Daily Availability</b>
<b>HF Radio</b>	<b>1000</b>	<b>3</b>	<b>Limited Global</b>	<b>M</b>	<b>M</b>
<b>LORAN(sky)</b>	<b>10-30</b>	<b>10</b>	<b>Limited</b>	<b>H</b>	<b>H</b>
<b>GOES</b>	<b>20</b>	<b>7</b>	<b>Limited</b>	<b>L</b>	<b>H</b>
<b>TRANSIT (NOVA)</b>	<b>10 '0.3'</b>	<b>10</b>	<b>Global</b>	<b>L</b>	<b>H</b>
<b>LORAN(Gnd)</b>	<b>1</b>	<b>10</b>	<b>Limited</b>	<b>H</b>	<b>H</b>
<b>LORAN(Auto)</b>	<b>1</b>	<b>10</b>	<b>Limited</b>	<b>H</b>	<b>H</b>
<b>TV Line 10</b>	<b>&lt;0.1</b>	<b>5</b>	<b>Local</b>	<b>H</b>	<b>M</b>
<b>Portable Cs</b>	<b>&lt;0.1</b>	<b>30</b>	<b>Global</b>	<b>M</b>	<b>L</b>
<b>GPS</b>	<b>&lt;0.1</b>	<b>80</b>	<b>Global</b>	<b>L</b>	<b>H</b>

**Table 1. Operational PTTI Dissemination Systems**

**Table 2. Portable Clock Trip Schedule (FY 82)**

OCTOBER	NOVEMBER	DECEMBER
FAR EAST	WEST COAST - 1	SO EUR
TOKYO, JA	SANTA CLARA, CA	NEA MARKI, GR
TAEJUE, KO	SUNNYVALE, CA	NAPLES, IT
TAEJON, KO	CP ROBERTS, CA	SAN VITO, IT
FT BUCKNER, OKI, JA	VANDENBER AFB, CA	TURINO, IT
HANZA, OKI, JA	PT MUGU, CA	MADRID, SP
WAIKAWA, HI	PASADENA, CA	SAN FERNANDO, SP
HAIKU, HI	WHITE SANDS, NM	LANDSTUHL, GE
BELJING, CH	LAS CRUSES, NM	LONDON, UK
SHANGHAI, CH	SORRORO, NM	
XIAN, CH	BOULDER, CO	
JANUARY	FEBRUARY	MARCH
NE - 1		WEST COAST - 2
OTTAWA, CN		FLAGSTAFF, AZ
BOSTON, MA		YUMA, AZ
PROSPECT HARBOR, ME		SAN DIEGO, CA
COREA, ME		PT MUGU, CA
CUTLER, ME		VANDENBERG, CA
NEWARK, OH		SANTA CLARA, CA
IOWA CITY, IO		BOULDER, CO
MINN/ST PAUL, MN		LOS ANGELES, CA
APRIL	MAY	JUNE
CEN EUR		NO EUR
HAMBURG, GE		HOLY LOCH, UK
BRAUNSCHWEIG, GE		THURSO, UK
BERLIN, GE		EDZELL, UK
WETZEL, GE		AMSTERDAM, NE
GRAZ, AU		BRUSSELS, BE
VIENNA, AU		PARIS, FR
NEUCHATEL, SW		LONDON, UK
GENEVA, SW		HERSTMONCEAU, UK
LONDON, UK		NEW DELHI, IN
JULY	AUGUST	SEPT
WEST COAST - 3	NE - 2	SE USA/CUBA
SANTA CLARA, CA	OTTAWA, CN	MIAMI, FL
STOCKTON, CA	BOSTON, MA	KINGS BAY, GA
OSO, WA	PROSPECT HARBOR, ME	CHARLESTON, SC
SPOKANE, WA	COREA, ME	NORFOLK, VA
BOULDER, CO	CUTLER, ME	GUANTANAMO BAY, CUBA
CHEYENNE, WY	NEW PORT, RI	PATRICK AFB, FL
LA MOURE, ND	NEW LONDON, CN	
MINN/ST PAUL MN	FT MONMOUTH, NJ	
PC TRAVEL BY BENDIX		
JAN	MAY	AUG
AUSTRALIA	AUSTRALIA	AUSTRALIA
SYDNEY	SYDNEY	SYDNEY
PERTH	PERTH	PERTH
YARRAGADGEE	YARRAGADGEE	YARRAGADGEE
CANBERRA	PHILLIPINES IS	KAWALEIN IS
MELBOURNE	CLARK AB	HAWAII IS
ADELAIDE	SUBIC BAY	KAUIA
EXMOUTH	DIEGO GARCIA	MAUI
HAWAII	GUM	LUALUALAET
WAIKAWA	HAWAII	HAIKU
	WAIKAWA	WAIKAWA



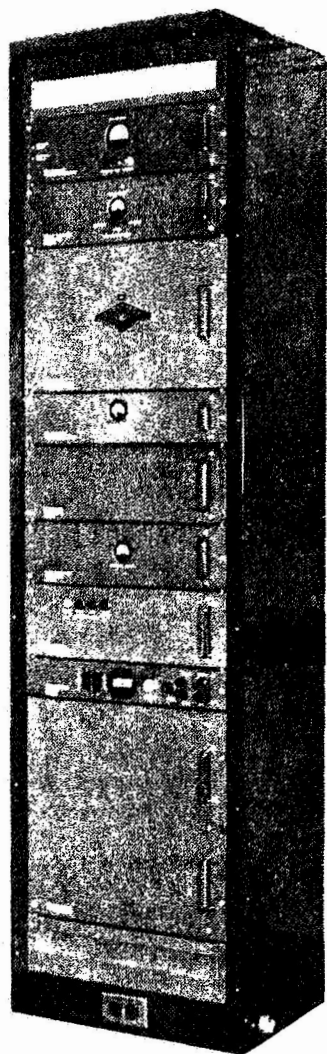


**Figure 1. Atomicchron "Portable" Clock (1959)**

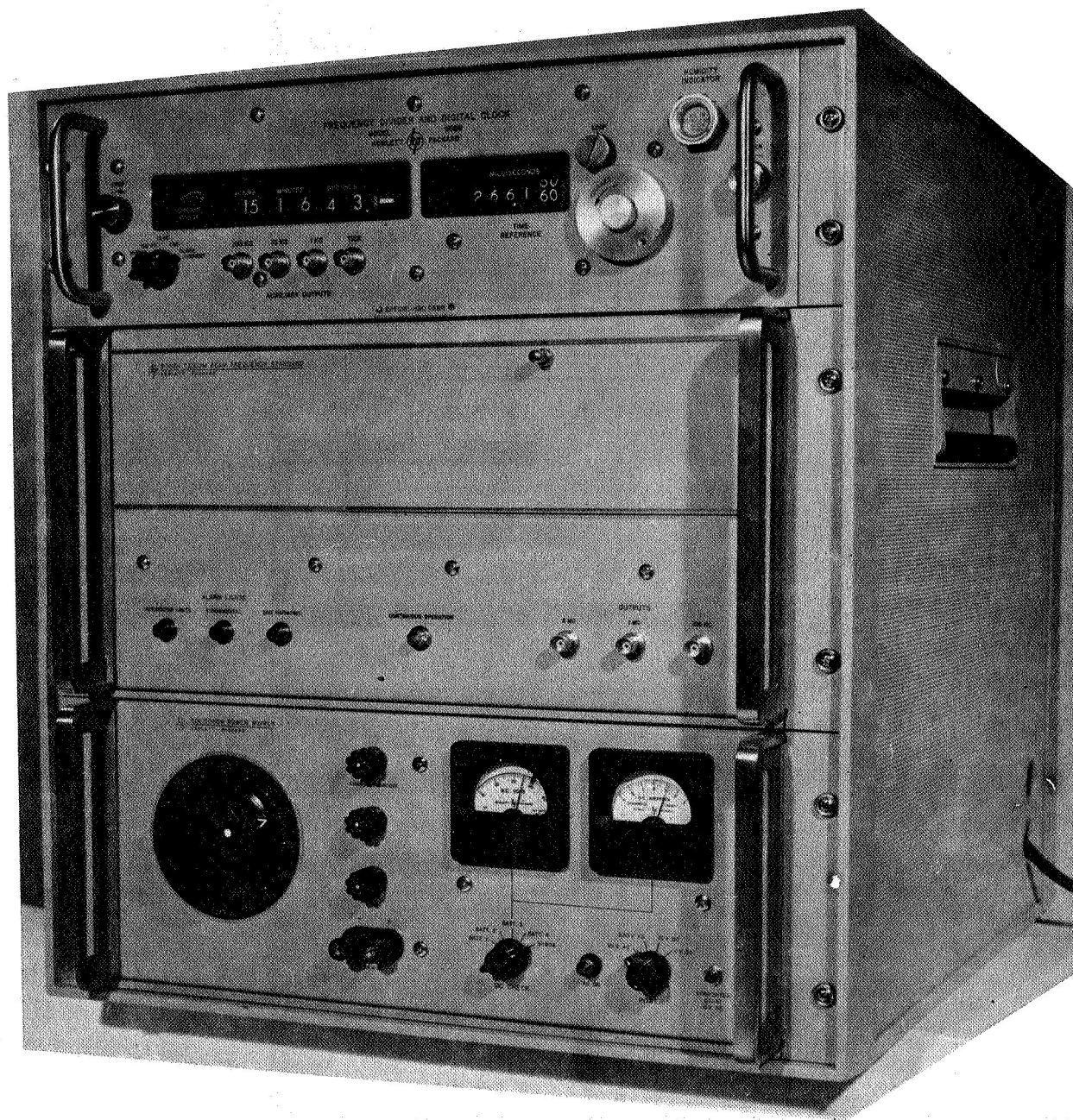


Figure 2. Hewlett-Packard Portable Clock (1964)

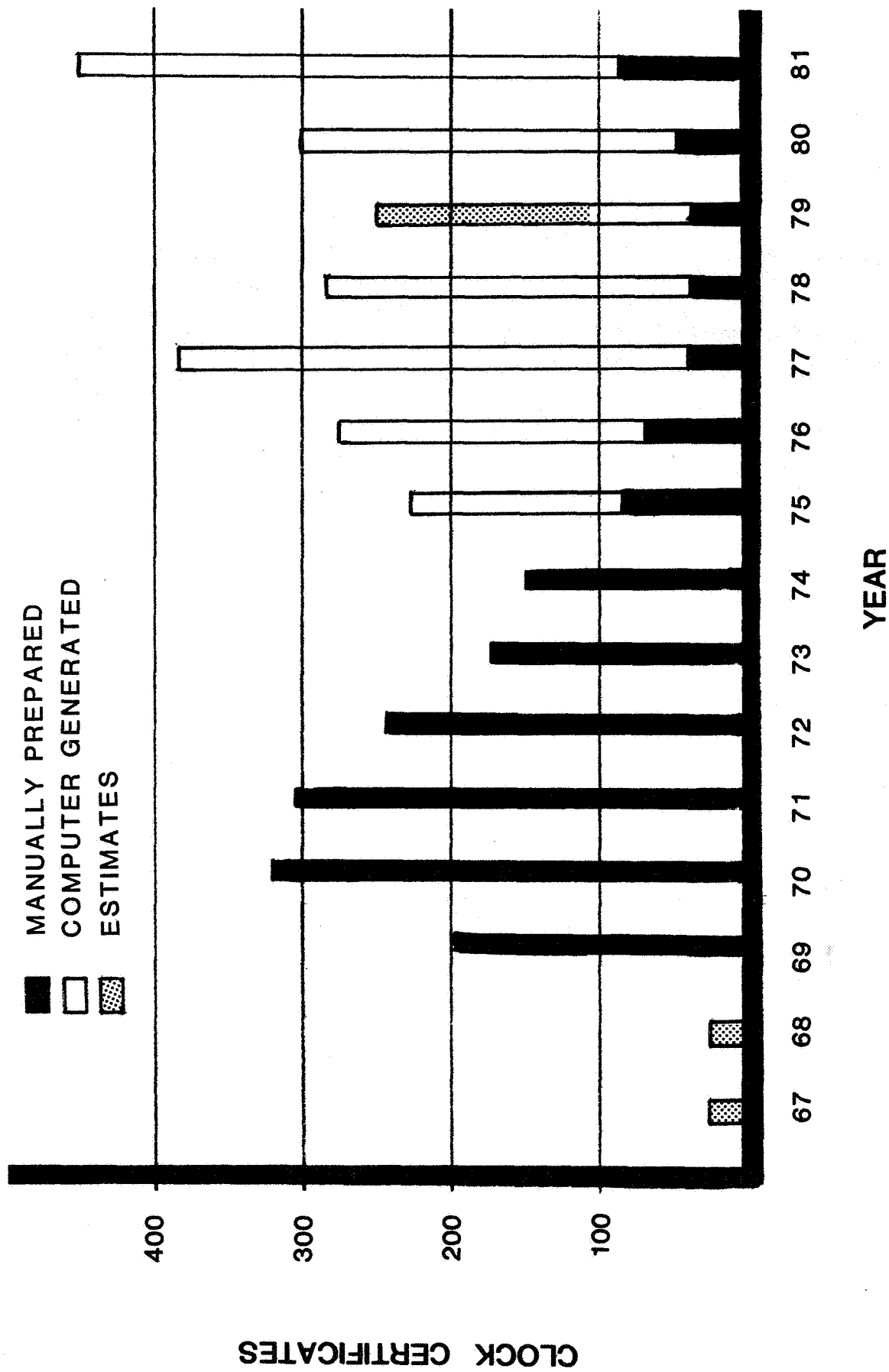


Figure 3. U. S. Naval Observatory Clock Certifications (1967-1981)

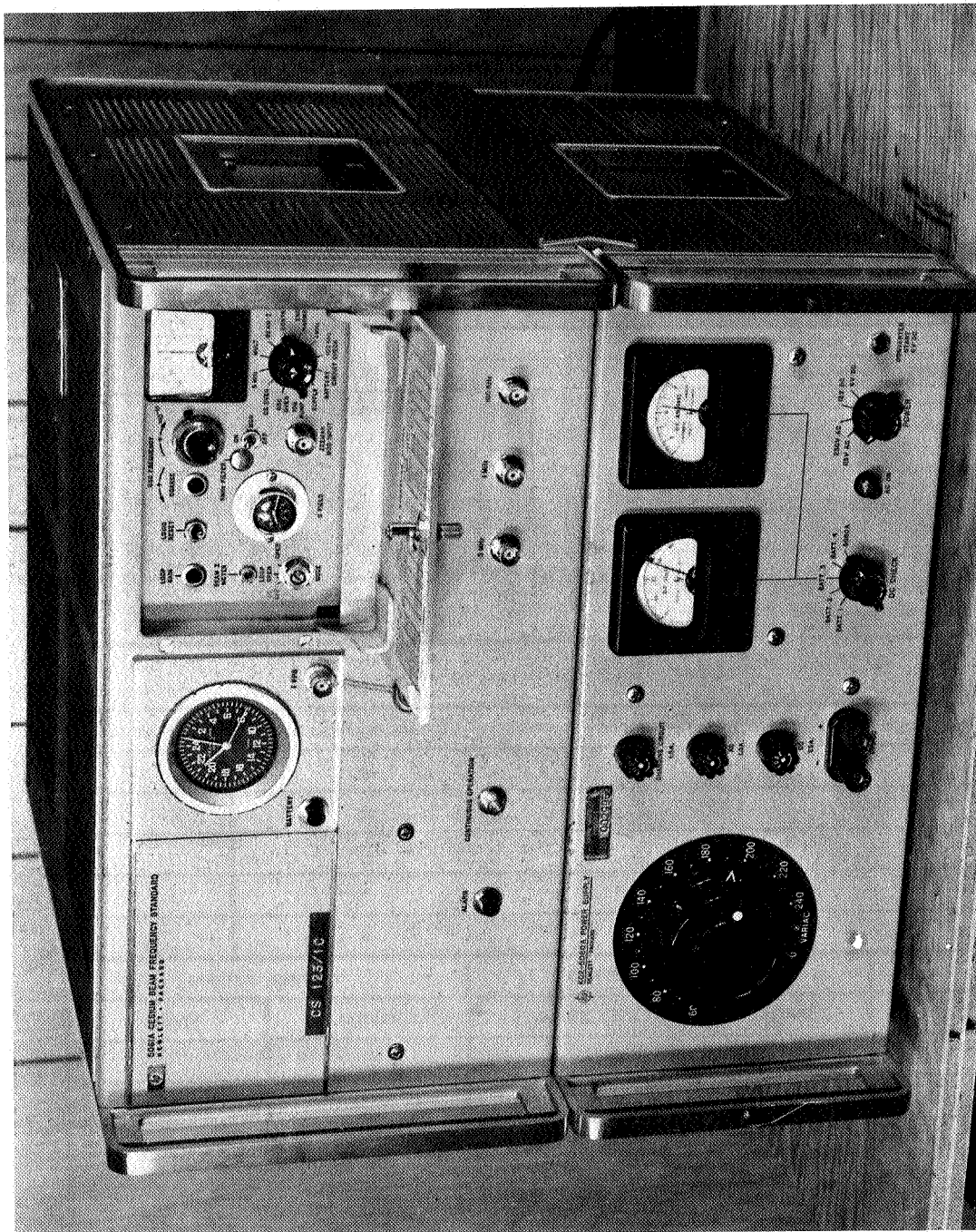


Figure 4. Hewlett-Packard Portable Clock (1968)

<b>Activity &amp; Location:</b>			<b>Personnel Making Measurement:</b>	
<b>Time Standard</b>	<b>Measured Clock</b>	<b>Reference Clock</b>	<b>Time Display Agreement</b>	
<b>Clock Designation</b>			<b>Remarks</b> Hours <input type="checkbox"/> Yes <input type="checkbox"/> No Minutes <input type="checkbox"/> Yes <input type="checkbox"/> No Seconds <input type="checkbox"/> Yes <input type="checkbox"/> No	
<b>Osc.</b>	Manufacturer		<b>PORTABLE CLOCK TICK CHECK</b> (1 pps to 100 kHz crossover) Positive-going 0 volt crossing <input type="checkbox"/> Yes <input type="checkbox"/> No Day/Mon/Yr(ZULU) _____ Hours/Mins(ZULU) _____ PC - CS = _____ $\mu$ sec	
	Model No.			
	Serial No.			
<b>Clock</b>	Manufacturer			
	Model No.			
<b>1PPS</b>	Polarity & Voltage			
	Slope			
	Input Impedance			
<b>Calibration Certificate Mailing Addresses:</b> <b>ORIGINAL TO:</b> _____ _____ _____ <b>COPIES TO:</b> _____ _____			<b>1 PPS Sketch &amp; Characteristics:</b>  Amplitude: _____ volts, into _____ ohms Polarity: _____ rise time _____ $\mu$ sec Pulse Length: _____ $\mu$ sec	
<b>PTTI FIELD MEASUREMENT DATA</b>				
<b>START CLOCK - STOP CLOCK</b>	<b>COUNTER READING + START DELAY - STOP DELAY = RESULTS (USEC)</b>			<b>DATE/TIME (UTC)</b>
-	+      -      =			
-	+      -      =			
-	+      -      =			
-	+      -      =			
-	+      -      =			
	+      -      =			
	<b>THUMBWHEEL SETTING</b>		<b>"C" FIELD SETTING</b>	
<b>CLOCK</b>	<b>INITIAL</b>	<b>FINAL</b>	<b>INITIAL</b>	<b>FINAL</b>
<b>COMMENTS</b>				

Figure 5. Portable Clock Data Sheet

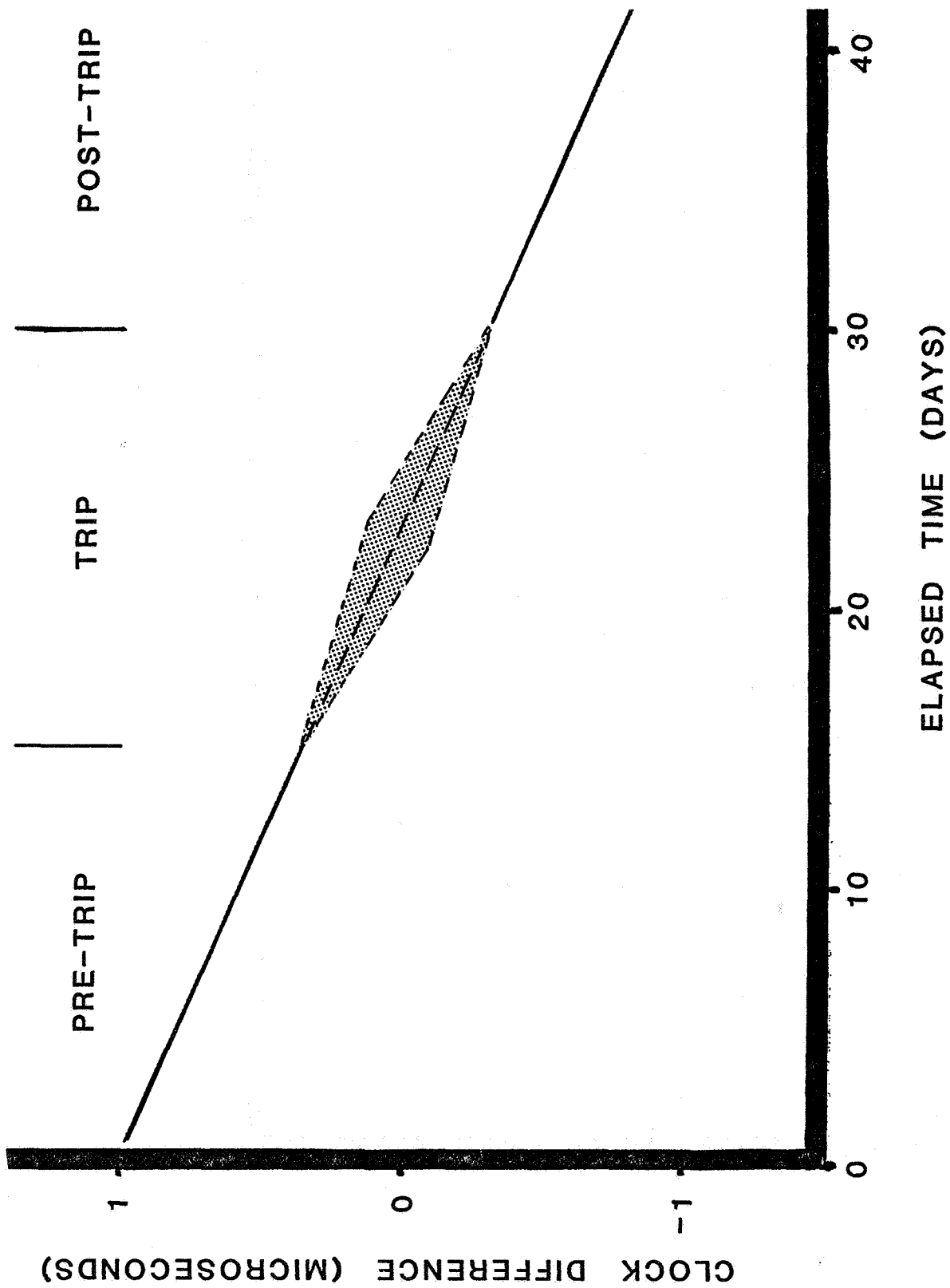


Figure 6. Portable Clock Performance (No Problem)

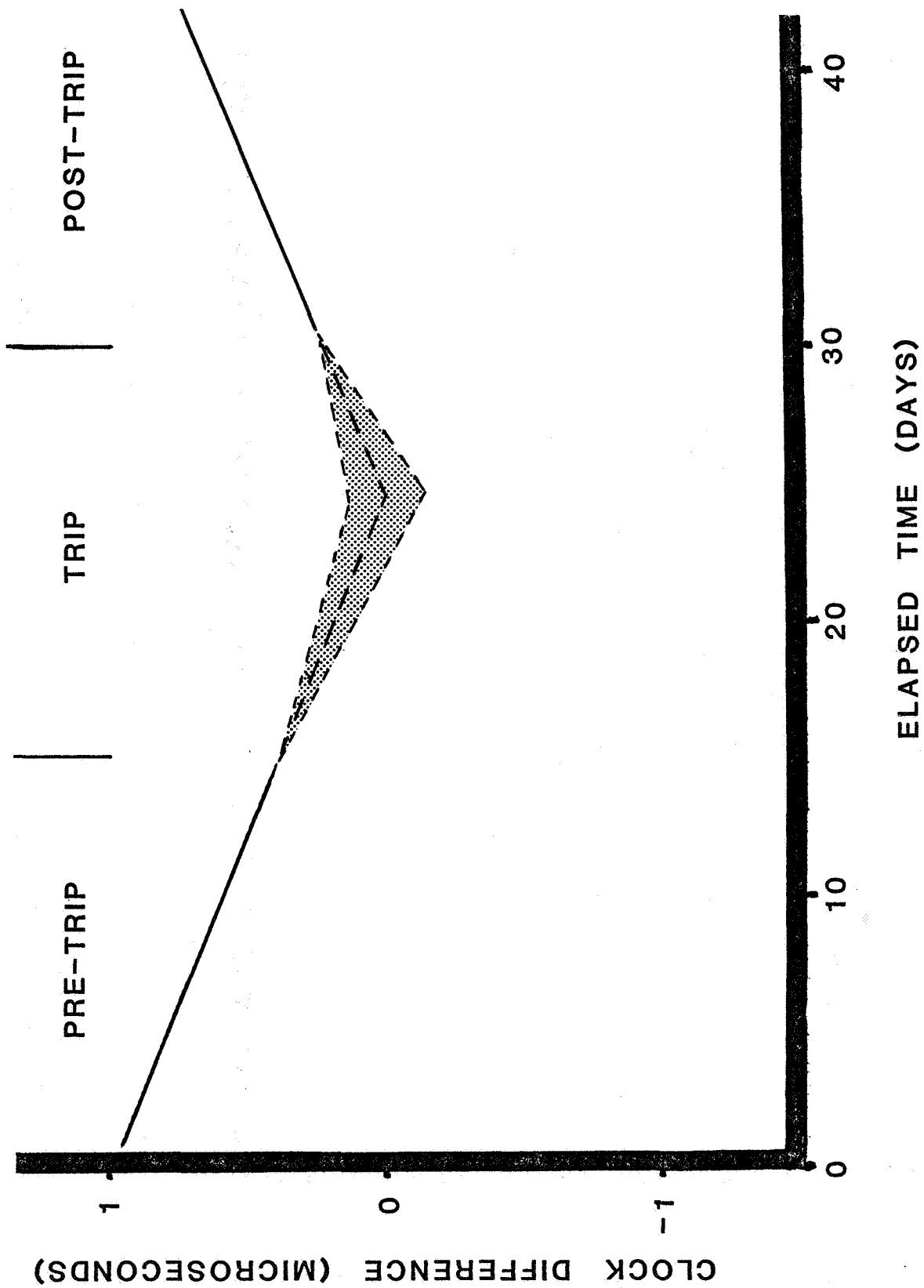


Figure 7. Portable Clock Performance (Frequency Shift)

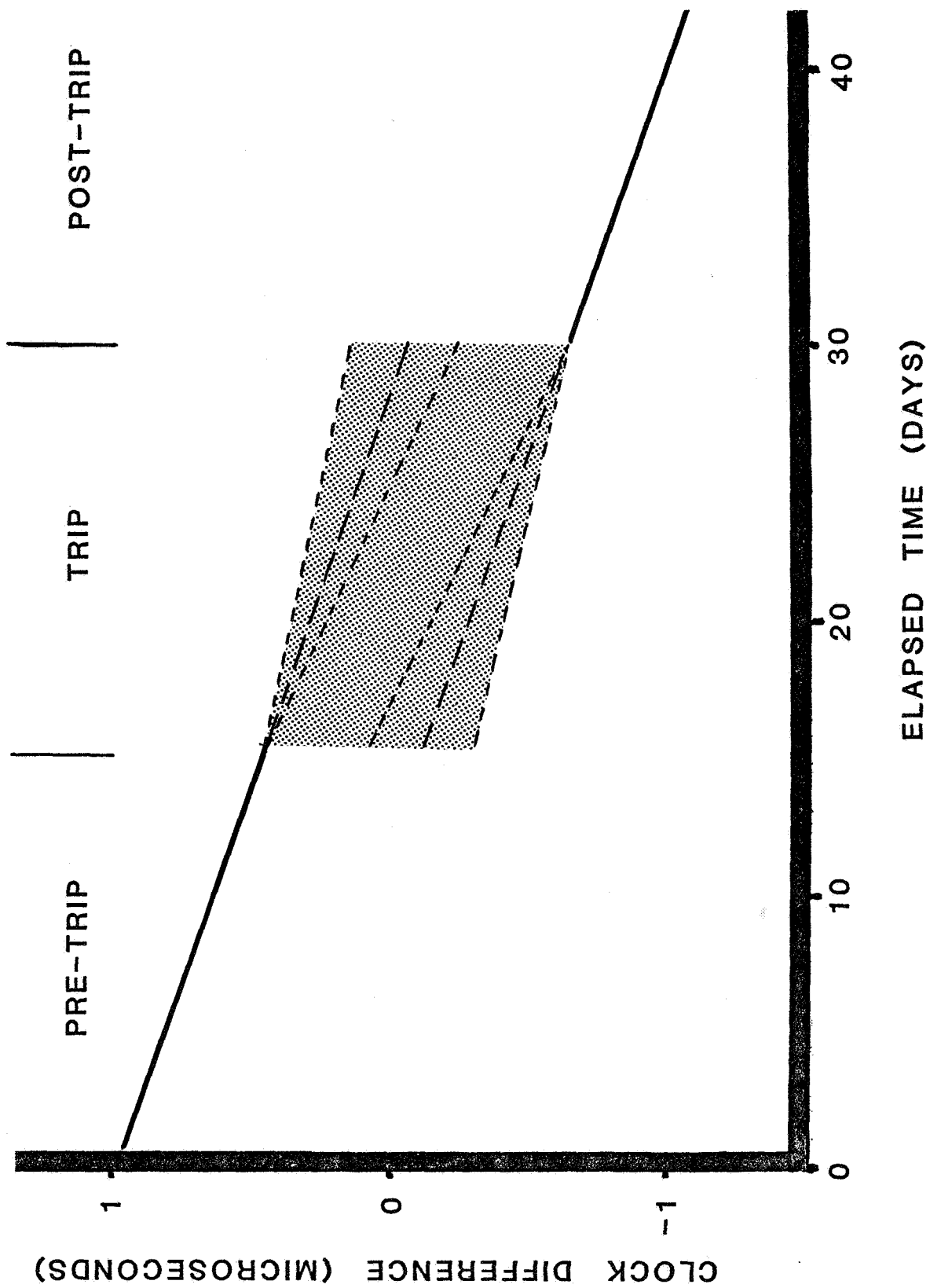


Figure 8. Portable Clock Performance (Time Step)





U. S. NAVAL OBSERVATORY  
WASHINGTON, D.C. 20390

REPORT OF PRECISE TIME MEASUREMENT

1981 FEB. 1981

THE DESIGNATED CLOCK WAS MEASURED BY COMPARING ITS TIME OF DAY  
TO THE U. S. NAVAL OBSERVATORY MASTER CLOCK.

DESIGNATION AND LOCATION OF CLOCK MEASURED

CS651 COMSAT  
GAITHERSBURG, MD

DATE AND TIME OF MEASUREMENT 1981 FEB. 13, 1853 UT, MJD 44648.786806

MEASUREMENT

UTC(USNO MC) - UTC(CS651) =  $0.2 \pm 0.2$  MICROSECONDS

SPECIFICATIONS

TRANSFER TECHNIQUE UTC(PC1452)

ANDREW C. JOHNSON  
PRECISE TIME OPERATIONS OFFICER



U.S. NAVAL OBSERVATORY  
34th and Massachusetts Ave., NW  
Washington, D.C. 20390

IN REPLY REFER TO

REPORT OF PRECISE CLOCK TIME MEASUREMENT

Designation of Clock Measured

UTC (NBS)

Location of Measurement

NBS, Boulder, CO

This clock was measured by comparing its time of day to the U. S. Naval Observatory Master Clock.

Date and Time of Measurement: 24 January 1973, 1818 UT, MJD 41,706.762500

Measurement: UTC(USNO MC) - UTC(NBS) = - 0.2 us  $\pm$  0.2 us

Specifications:

Transfer Technique: UTC(USNO PC 580)

Measured Clock Pulse Characteristics:

Amplitude = 1.3 volts into 50 ohms

Polarity = positive Rise Time:  $\sim$  0.006

Pulse Measured At:

Amplitude: 1.0 volt Polarity: positive Slope: positive

Last Measurement Made Was:

UTC(USNO MC) - UTC(NBS) = 5.8 us  $\pm$  0.3 us

at 1510 UT on 11 May 1972

Date of This Report: 6 February 1973

By: JEAN D. LAVANCEAU  
Section Chief  
Control of Time and Time Interval  
Time Service Division

Control No: A1169

**Figure 11. Manually Prepared Clock Report**

APPENDIX I

STANDARD OPERATING PROCEDURES

FOR

PORTABLE CLOCK OPERATIONS

I. PRECISE TIME OPERATIONS SECTION

RESPONSIBLE FOR THE FOLLOWING:

1. INITIATE TRIP
  - A. ITINERARY
  - B. ESTIMATE COST OF TRIP
2. ASSIGNMENT OF PERSONNEL
3. CLEARANCE MESSAGES AND CORRESPONDENCE
4. PREPARE AND ALSO MONITOR TO ENSURE ALL DOCUMENTS ARE COMPLETED ON TIME.
  - A. TRAVEL ORDERS
  - B. TRAVEL ADVANCES
  - C. TICKETS AND MTAS
  - D. PASSPORT W/VISA UP TO DATE
  - E. IMMUNIZATION RECORD UP TO DATE
  - F. DATA FOLDER W/INFO SHEETS
  - G. FIELD MEASUREMENT SHEETS
  - H. CUSTOMS FORMS
  - I. EQUIPMENT
5. PORTABLE CLOCK
  - A. OFFSET
  - B. ON TIME
  - C. TEST
6. KO-2 POWER SUPPLY
  - A. TEST
7. COUNTER
  - A. TEST
8. TOOL BAG
  - A. MULTIMETER
  - B. CORRECT FUSES
  - C. PROPER AC ADAPTERS FOR TRIP
  - D. TOOL KIT
  - E. AC EXTENSION (50')
  - F. DC CABLE FOR CAR BATTERY
  - G. FLASHLIGHT
  - H. RAINCOAT

### III. PRECISE TIME AND TIME INTERVAL BRANCH

RESPONSIBLE FOR THE FOLLOWING:

1. CHECK AND VERIFY ALL DATA AND REPORTS
2. PREPARE ADDITIONAL CLOCK REPORTS AS NECESSARY
3. PUBLISH PERTINENT RESULTS IN TIME SERVICE SERIES 4
4. SEND CLOCK REPORTS TO COGNIZANT PERSONNEL

### IV. PORTABLE CLOCK TEAM

TEAM LEADER HAS OVERALL RESPONSIBILITY AND THEREFORE SHOULD ENSURE TIMELY COMPLETION OF THE FOLLOWING:

1. DATA REDUCTION BRANCH
  - A. RATE OF CLOCK
    1. ADJUSTMENT IF REQUIRED
  - B. ESTIMATE PC AGAINST LORAN-C AND CESIUM AT SELECTED SITES
  - C. PROBLEMS WITH SITES THAT NEED TO BE INVESTIGATED
2. OPERATIONS GROUP
  - A. PASSPORT W/VISAS
  - B. IMMUNIZATIONS UP TO DATE
  - C. OBTAIN CLEARANCE MESSAGES AND CORRESPONDENCE
  - D. OBTAIN TRAVEL INFORMATION SHEETS AND PTTI FIELD MEASUREMENT DATA SHEETS
  - E. MONITOR PROGRESS OF DOCUMENTS
  - F. REVIEW CORRECT PROCEDURES
    1. MEASUREMENTS
    2. MESSAGES
3. CAR RENTALS
4. LIVING ACCOMMODATIONS

9. REVIEW CORRECT PROCEDURES
  - A. MEASUREMENTS
  - B. MESSAGES
10. ENSURE FOLLOWING IS OBTAINED FROM MS. CHARRON OR MR. CLARK
  - A. PORTABLE CLOCK FREQUENCY OFFSET ESTIMATE
  - B. PERFORMANCE ESTIMATE FOR PERIOD OF TRIP
  - C. ESTIMATE READINGS OF PC AGAINST STATION CLOCKS AND LORAN-C AT SELECTED SITES

## II. ASTRONOMICAL OBSERVATION AND DATA REDUCTION BRANCH

RESPONSIBLE FOR THE FOLLOWING:

1. ESTABLISH OFFSET OF CLOCK
2. ESTIMATE CLOCK PERFORMANCE FOR TRIP PERIOD
3. ESTIMATE PC AGAINST LORAN-C AND CESIUM AT SELECTED SITES
4. PROVIDE ABOVE INFORMATION BOTH TO OPERATIONS SECTION AND TEAM LEADER
5. ADVISE PC TEAM OF ANY PROBLEM AT SITES THAT NEED TO BE INVESTIGATED
6. ENSURE INPUT PORT FOR DATA ACQUISITION SYSTEM IS OPEN AND BEING SCANNED ON RETURN OF PORTABLE CLOCK TO NAVOBSY
7. ANALYZE AND REDUCE DATA AND PREPARE COMPUTER GENERATED CLOCK REPORTS

5. RECHECK
  - A. OFFSET OF CLOCK
  - B. POWER SUPPLY
  - C. COUNTER
6. IF REQUIRED, TRAINING FOR ASSISTANT TO ENSURE HE/SHE IS ABLE TO TAKE READINGS AND HANDLE POWER REQUIREMENTS FOR PORTABLE CLOCK
7. TAG PC FOUR DAYS PRIOR TO DEPARTURE SO FINAL RATE CAN BE TAKEN---SAME HOLDS TRUE ON RETURN

#### V. FIELD OPERATIONS OF PORTABLE CLOCK TEAM

#### OPERATIONS AND RESPONSIBILITIES AS FOLLOWS:

1. DEPARTURE FROM USNO
  - A. ENSURE DATA REDUCTION BRANCH RECEIVES COPY OF READINGS AGAINST SYSTEM 1,2, & 4
  - B. START LOG ON CLOCK PERFORMANCE
    1. DAILY METER READINGS
    2. DAILY TICK TO PHASE
    3. TIME ON BATTERY VERSUS TIME ON CHARGE
    4. TEMPERATURE CHANGES
    5. ANY UNUSUAL PHYSICAL VIBRATIONS/SHOCKS
    6. ALARMS (INDICATE CONDITIONS, DATE AND TIME)
    7. LAST ENTRY SHOULD INCLUDE BOTH DEPARTURE READINGS AND READINGS UPON RETURN TO USNO (AGAINST SYS 1,2,4)
2. ALL MEASUREMENTS TO BE DONE AS FOLLOWS:
  - A. TAKE READINGS AND ENTER ON DATA SHEET. INCLUDE ALL PERTINENT INFORMATION
  - B. HAVE ABOVE RECHECKED BY ASSISTANT
  - C. READ "C-FIELD" AND WHERE POSSIBLE THUMBWHEEL SETTINGS
3. UPON ARRIVAL AT SITES, CARRY OUT THE FOLLOWING:
  - A. OBTAIN INFORMATION ON POWER AVAILABLE
    1. ENSURE POWER/VOLTAGE SETTINGS ON BOTH POWER SUPPLY AND COUNTER ARE CORRECT



2. IF EQUIPMENT MUST REMAIN OVER-NIGHT, EXPLAIN OPERATION OF BOTH POWER SUPPLY AND CESIUM OSCILLATOR, INCLUDING ALARM CONDITIONS. LEAVE WRITTEN INSTRUCTION SHEET WITH PLACE OF LODGING AND PHONE NUMBERS. REVISIT SITE BEFORE TURNING IN IF POSSIBLE
4. TAKE READINGS PER INSTRUCTION FOUND IN NAVOBSY TS/PTTI SOP-81, 6-1 PORTABLE CLOCK OPERATIONS
5. ASSISTANT IS TO VERIFY AND CORRECT, OR FILL OUT NEW TRAVEL INFORMATION SHEET
6. WHERE POSSIBLE, MESSAGES SHOULD BE SENT BACK TO INCLUDE:
  - A. READINGS
  - B. QUESTIONS PC TEAM WERE UNABLE TO ANSWER
  - C. CHANGES IN THUMBWHEEL/C-FIELD SETTINGS
  - D. OVERTIME/COMPTIME
7. AT SELECTED SITES INSURE READINGS ARE WITHIN ACCEPTABLE LIMITS OF ESTIMATED VALUES. IF NOT, TRY TO DETERMINE SOURCE OF ERROR
8. UPON RETURN TO USNO, TRIP REPORT MUST BE FILLED OUT WITHIN FIVE WORKDAYS AND DAILY LOG ON PC SHOULD BE TURNED OVER TO OPERATIONS GROUP AND DATA SHEETS SUBMITTED AS SOON AS POSSIBLE

\*\*\*\* EMERGENCY PROCEDURES FOR PORTABLE ATOMIC CLOCK \*\*\*\*

CLOCK TEAM MEMBERS: \_\_\_\_\_

LODGING: \_\_\_\_\_

PHONE \_\_\_\_\_

IF ANY OF THE FOLLOWING SHOULD OCCUR PLEASE NOTIFY ONE OF THE CLOCK TEAM MEMBERS IMMEDIATELY.

1. KO-2 POWER SUPPLY
  - A. AC POWER LIGHT GOES OUT
  - B. IF POWER SUPPLY DC AMP METER IS READING GREATER THAN 0.6 AMPS.
2. 5061A CESIUM BEAM FREQUENCY STANDARD.
  - A. IF BATTERY LIGHT (YELLOW) COMES ON.
  - B. IF CONTINUOUS OPERATION LIGHT (GREEN) GOES OUT.
  - C. IF ALARM LIGHT (YELLOW) COMES ON.
3. STATION POWER FAILURE.

IF PRIMARY POWER REMAINS OFF FOR A PERIOD OF TWO HOURS AND YOU ARE UNABLE TO REACH ONE OF THE PORTABLE CLOCK TEAM MEMBERS, PLEASE DO THE FOLLOWING. IF ANY DC SOURCES 6V, 12V, 24 TO 30V RATED AT 120 WATTS ARE AVAILABLE AT YOUR LOCATION, CONNECT THE CLOCK TO THE SOURCE USING THE PROCEDURES LISTED BELOW. IF THESE DC SOURCES ARE UNAVAILABLE AT YOUR LOCATION YOU CAN RELOCATE TO ANOTHER BUILDING OR USE AN AUTOMOBILE BATTERY.

- A. LOCATE PORTABLE CLOCK TEAM'S TOOL BAG AND REMOVE THE DC POWER CORD. (IT WILL HAVE TWO BATTERY CLIPS ON ONE END)
- B. ON THE POWER SUPPLY, WHICH IS THE LOWER HALF OF THE PORTABLE CLOCK UNIT, TURN DOWN VARIAC TO ZERO AND REMOVE AC CORD FROM OUTLET.
- C. TURN SWITCH MARKED POWER (LOWER RIGHT FRONT PANEL, LEFT OF CONVERTER START BUTTON) TO EITHER 6V OR 12 V, DEPENDING ON VOLTAGE OF AVAILABLE SOURCE.
- D. FOR EITHER 6V OR 12V CONNECT DC POWER CORD TO POWER SUPPLY CONNECTOR WHICH IS MARKED DC IN. (REAR PANEL OF POWER SUPPLY LEFT HAND SIDE FROM REAR)
- E. CONNECT RED CLIP TO POSITIVE AND BLACK CLIP TO NEGATIVE TERMINALS OF SOURCE.

- F. CHECK FOR AC LIGHT. IF ON, ADJUST VARIAC UNTIL DC AMP METER READS 0.4 AMP.
- G. IF 6 VOLTS DC IS USED, IT MIGHT BE NECESSARY TO PRESS CONVERTER START BUTTON. (LOCATED ON RIGHT HAND SIDE FRON PANEL OF POWER SUPPLY.)
- H. IF 24 TO 30V DC IS TO BE USED, YOU WILL NEED 2 BANANA PLUGS OR OTHER MEANS OF CONNECTING INTO POWER SUPPLY VIA DUAL CONNECTOR ON FRONT PANEL. IF 24 TO 30V DC IS USED, VARIAC IS OUT OF THE CIRCUIT AND AC ON LIGHT WILL NOT LIGHT AS THE VOLTAGE ONLY OPERATES THE CLOCK FROM DC AND DOES NOT CHARGE THE BATTERIES.
- I. KEEP TRYING TO REACH THE PORTABLE CLOCK TEAM.



## QUESTIONS AND ANSWERS

MR. SAM WARD, JPL

Is that form that you used for the clocks which the team carries, is that available for use?

MR. PUTKOVICH:

Sure, everything -- all our data is available, anything we have is available.

MR. WARD:

I didn't mean the data, just the form.

MR. PUTKOVICH:

Sure, no problem.

MR. KLASKE:

It should be pointed out as portable clocks get better and better, actually you expect to see it looking like a time step, if you had a perfect clock, it would appear as a time step, simply because of the relativity.

MR. PUTKOVICH:

Nothing of the magnitude that I showed, it is very much smaller scale.

VOICE: Computer Science

How are clock visits initiated?

MR. PUTKOVICH:

Well, there are several ways, the best way to do it is to write a letter to the Superintendent, Naval Observatory, stating your needs, what your relation to DoD or the Navy is, and where you would like to have portable clock measurements made. And then you will get an answer back.

If you are on our usual route, you will get a portable clock measurement without too much trouble. If you are off our usual route, you are going to have to kick in a few bucks to pay for transportation and per diem and that sort of thing.

But it is available to components of DoD and DoD contractors. And if you are not off the beaten track, you can get a freebie.

MR. AL SWALGE, Frequency and Time Systems

You asked or indicated you were looking for improved clock power supply, could you elaborate a little on that?

MR. PUTKOVICH:

Yes, one of the problems is that the supplier that we are using now has been the workhorse and has been very good, I have not too much of a problem with that, but it requires -- it has idiosyncrasies like when you take it to Northwestern Australia where the power goes up to 270 volts in the evening, you tend to have smoke and bad things happen to your power supply.

QUESTION:

I don't know whose clock that might be.

MR. PUTKOVICH:

Well, that is a K02 power supply, it is a fantastic power supply, but it requires care and attention. It has sealed NiCd batteries in it, they have the memory problem, if you don't keep track of your discharge and charge cycles, you may end up on the short end of a power failure and that is bad for our clocks. Because once they stop, you are sort of out of luck and you might have \$10,000 worth of effort down the tubes.

MR. ANDY CHI:

Do you care to tell us how the long-term, at-rest, data of the portable clock compares with the data when the portable clock is on the trip? Does it look continuous or are there many downs, as it goes through the trips.

Is the data continuous while the clock is in the laboratory and when you take it out to the trips, on a long-term basis, what do the data look like?

MR. PUTKOVICH:

Generally, I think, we could say that you see things as they were in the first two slides, either the frequency stays pretty much same, or you do occasionally get frequency changes. You rarely see the steps in time that occurred on the last two slides, unless something is wrong with the clock; and then you have a problem. You have taken a clock that is not performing well out on a trip and you get degradation of your data accordingly.

The high performance tubes that we are using in the portable clocks that we have now, perform quite well in that regard. The clocks that have the double loop integrators also show some improvement. So, they are performing fairly well.

DR. VICTOR REINHARDT, NASA/Goddard

Do you have a feel for the RMS frequency jumps that you see moving them around?

MR. PUTKOVICH:

No.

## LORAN-C, AN OVERVIEW

LT William J. THRALL  
U.S. Coast Guard  
Washington, D.C. 20593

### Abstract

In 1974 Loran-C was selected to be the government-provided radionavigation system for the U.S. Coastal Confluence Zone and the Great Lakes. Title 14, USC 81 states that the U.S. Coast Guard may establish and maintain electronic aids to operate marine navigation required to serve the needs of the military and commerce of the United States.

Loran-C is a highly accurate positioning system. It operates at an assigned frequency of 100 kHz, and provides phase-coded pulses to develop hyperbolic time-difference lines-of-position (LOP's). In addition to providing for radionavigation, Loran-C also provides precise time and time interval to within  $\pm 5$  microseconds of UTC. The paper discusses the steps taken to plan, install, operate and maintain the Loran-C system up to the year 2000. The following topics are included in the discussion: theory of operation, timing, chain planning, group repetition interval, coding delay versus emission delay, chain calibration, chart verification, system accuracy, signal reliability, and future developments.

The opinions or assertions contained herein are the private ones of the writer and are not to be construed as official or reflecting the views of the Commandant or the Coast Guard at large.

### BACKGROUND

Coast Guard operated since 1958, Loran-C has been providing highly accurate and reliable radionavigation service and Precise Time and Time Interval (PTTI) dissemination through pulsed transmissions in the 90-110 kHz band. A nominal 1200 nautical mile range, coupled with a positioning accuracy of  $1/4$  nautical mile, tested repeatability of up to 15 meters, and a documented availability of greater than 99.7%, has made Loran-C a reliable radionavigation system. Loran-C is



a system that can be used in many land, sea, and air positioning applications.

In 1974 Loran-C was designated as the navigation system for the Great Lakes and Coastal Confluence Zone (CCZ) of the continental United States and Southwest Alaska. This zone extends fifty (50) miles from the harbor entrance or to the 100 fathom curve, whichever is further.

To provide such coverage, it was necessary to construct 12 new Loran-C stations on the East, West, and Gulf coasts and Great Lakes as well as along the Gulf of Alaska and the Bering Sea. This expansion of Loran-C service was called NIP - National Implementation Plan. This together with the Loran Improvement Program (LIP) ensured that not only was the CCZ covered, but that the coverage extended well beyond the CCZ and still maintained the high degree of accuracy and reliability originally advertised. In fact, reliability has continued to improve through equipment advancements to the point where, today, 99.9% availability and greater is enjoyed by the Loran user community.

#### Theory of Operation

Loran-C navigation is made possible by user equipment that measures the difference of time of arrival (TOA) in microseconds between two fixed transmitting locations. This measurement does not, however, define a unique point on the earth. It describes instead, a unique hyperbolic line-of-position or LOP. In theory, each unique time difference (TD) describes one classical hyperbolic LOP that is generated relative to the two fixed transmitting locations.

By introducing another transmitting station a different set of LOP's is created. Where an LOP of one set crosses an LOP of another set, a "fix" can be obtained. This fix is defined by the simultaneous time difference numbers of intersecting LOP's.

Theoretically, there are an infinite number of classical hyperbolic LOP's between transmitting sites and each LOP is defined by its own unique TOA difference. However, real world measurements indicate that

the actual LOP's are far from classical. They're actually warped and bent in some areas, not at all like classical hyperbolic lines.

This warping and bending of the LOP's is caused by the different impedances encountered by the Loran-C transmissions as they propagate across different and varying terrains. For instance, there is virtually no warping or bending of transmissions as they travel over salt water, but across land, which is non-homogeneous, the transmissions are randomly affected, thus causing varying degrees of warpage and coverage loss.

### Chain Planning

The primary purpose of a Loran-C chain is to provide the optimum coverage in a predetermined geographic area. Coverage includes not only signal strength, but also position geometry necessary to obtain the required accuracy. The primary considerations when designing a Loran-C chain are:

- (1) desired signal strength
- (2) background noise level
- (3) system geometric constraints
- (4) Group Repetition Interval (GRI) selection
- (5) specific station positioning

The signal strength at a specific location in the Loran-C service area is dependent upon the transmitted power and the conductivity of the path over which the signal must propagate to reach the observer. Transmitted power is primarily a function of both antenna and antenna current; the greater the power radiated, the further away the signal can be received.

Signal attenuation is a function of the conductivity of the surface over which the signal must propagate. When the path is homogeneous in conductivity as in propagation over sea water, the signal level can be easily computed. However, when the propagation paths are mixed in conductivity as they are in land masses, Millington's Method is used to compute signal strength. The usable coverage area is limited by both the signal strength and the geometric relationship of the LOP's. To be useful to the navigator, intersecting LOP's should cross at 30 degrees or greater. This

is necessary to provide a 2 drms accuracy of 1/4 nautical mile.

The transmitting sites chosen with regard to the previously discussed constraint can vary up to 25-30 miles without an appreciable effect on system coverage. The final site selection becomes one that must consider both electronic and civil constraints.

#### Timing

Group Repetition Interval (GRI) is the interval between successive pulse groups measured at any one station in a chain. In general, the goal of GRI selection is to select a minimum GRI that causes minimum mutual interference between Loran-C GRI's in the coverage area. A consideration in the selection of a GRI is that it be as fast as possible, since increased duty cycle will provide a relative signal to noise improvement. For example, a difference between a GRI of 100,000  $\mu$ sec (GRR=10CPS) and one of 50,000  $\mu$ sec (GRR=20CPS) would show an apparent gain in signal to noise equal to +3db.

$$S/N = 20 \log GRR1/GRR2 + 20 \log 20/10 = +3db$$

This is equivalent to an increase in power by a factor of 2.

Factors governing the determination of minimum GRI are:

- (1) pulse spacing
- (2) receiver recovery time
- (3) coding delays

The current Loran-C format provides for a master pulse group of nine pulses. The first eight of which are spaced 1000  $\mu$ sec apart and a ninth pulse occurring 2000  $\mu$ sec after the start of the eighth pulse. The secondary pulse groups are all identical in format but consist of only eight pulses spaced 1000  $\mu$ sec apart; no ninth pulse. The width of the individual pulses are a nominal 300  $\mu$ sec. Therefore, the elapsed time from the start of the first pulse of a group to the end of the group is 9300  $\mu$ sec for the master and 7300  $\mu$ sec for the secondary groups.

In addition to the time period occupied by either the master or secondary group, an additional time increment must be included to allow the receiving equipment at the Loran station sufficient time to process the group information. This additional time increment is identified as receiver recovery time. Since the absolute minimum of time of occurrence between any two successive pulse groups takes place at a transmitting site, it becomes necessary to consider the minimum receiver recovery time. The recovery time varies between signals received: 4000  $\mu$ sec for M to X and 3000  $\mu$ sec for X to Y, Y to Z, and Z to M.

### Coding Delay

The purpose of the coding delay assigned to each secondary station is to allow the stations of a chain to transmit sequentially in time and to prevent overlap of the different signal groups anywhere in the system. The Coding Delay takes into account baseline lengths in usec, distances between secondaries, and the number of secondaries in the chain.

To meet the foregoing criteria it is necessary to consider the propagation time between stations, the length of the signal group (in time) and coding delay assigned to the preceeding secondary. For example, a pulse repetition period commences with the transmission of the master's group of nine pulses. The master group is then received at each secondary (W, X, Y, & Z), delayed in time by the amount of the individual baseline distances. The first secondary (Xray), upon receipt of the master group's first pulse initiates a countdown, or fixed delay, to when it will commence its transmission of pulses. This fixed delay allows for reception of all nine of the master's pulses plus recovery time needed by the secondary equipment. The signal transmitted by the first secondary must travel to the next secondary (Yankee) in the proper sequence. Yankee must process the master pulse group, the Xray pulse group and its own delay before it initiates its own transmission. This sequence is repeated throughout the chain until, finally, the master must receive the last secondary's pulse group before it can begin a new cycle of operation.

At the first secondary the minimum allowable cod-

ing delay is determined only by the length (time period) of the master pulse group and the secondary equipment recovery time. The master pulse group requires a time period of approximately 7000  $\mu$ sec between the start of the first pulse and the start of the eighth pulse. The recovery time for the receiver of a master pulse group is 4000  $\mu$ sec. Therefore, the minimum allowable coding delay for the first secondary becomes the elapsed time from the beginning of the first pulse to the end of the receiver recovery time or 11000  $\mu$ sec.

At the second secondary, the minimum allowable coding delay is governed by the time required for the propagation, and receipt of the master and the first secondary pulse group plus the equipment recovery time.

In developing Coding Delay assignments, the computed result is rounded off to the next higher 1000  $\mu$ sec increment (unless it computes to an even thousand usec value). In assigning the order of secondary functions it is well to try all possible combinations at each location since significant differences in the calculated minimum GRI may be realized.

#### Calibration

Once a Loran-C chain is established and initial coding delays are assigned to all of the secondaries, it becomes necessary to check or calibrate the entire chain and make minor corrections. The primary purpose of a Loran-C chain calibration is to ensure that the Emission Delay (ED) of each secondary station is set to the value published by the U.S. Coast Guard. Emission Delay is the time interval between the master station's transmission and the secondary station's transmission in the same GRI (both stations using a common time reference). This calibration technique is accomplished using a portable cesium oscillator or "Hot Clock", which is synchronized to Universal Time Coordinated (UTC). The time of each station's respective Time of Transmission (TOT) is measured against the chain's GRI when synchronized to UTC. The Hot Clock is used to provide the extremely accurate frequency for the Repetition Rate Generator and to provide the one pulse per second (1PPS) for Time of

Coincidence (TOC) determination and synchronization. This is basically a hardware implementation of the definition of Emission Delay (ED).

Data is collected first at the master, then at each secondary station and, finally, at the master again. The collection is performed at the base of the transmitting antenna. A clamp-on current transformer is installed and the signal is coupled directly to a common mode rejection filter, then to a coupler unit. The signal is then fed to an oscilloscope and the Computing Counter.

The TOC for the GRI being measured is calculated and the reference GRI is synchronized to it. A pulse, corresponding to the beginning of the reference GRI, is coupled to the Computing Counter.

Time of Transmission (TOT) readings are recorded for each pulse. Each TOT is the mean value of 100 separate samples of the time difference between the beginning of the reference GRI and the standard Zero crossover (SZC) of the pulse being measured. Then the TOT of the next pulse is measured.

The purpose of the two visits to the master station is to set a start time for the calibration and to determine the frequency offset between the master operated oscillator and the Hot Clock. The clock error rate, expressed in nanoseconds per hour (the rate at which the Hot Clock 1PPS output is shifting in time, with respect to that of the master operate oscillator) is calculated by measuring the timing offset between the two visits and dividing by the elapsed time from the first to the second measurement.

Using the Clock Error Rate and the period of the time between the first master data collection and the data collection at the secondaries, a correction to the secondary TOT's is determined and applied. The effect of this correction is to get an actual TOT which has been corrected for Hot Clock drift.

The Controlling Standard Time Difference (CSTD) offset for the baseline, as seen at the monitor site in control of the pair, is algebraically subtracted from the TOT's to correlate the measured TOT with the assigned CSTD. Then the individual pulse TOT's for

each station are adjusted to the first pulse of the respective phase code groups. The mean is taken of the adjusted TOT's, yielding the final TOT for the station.

The Emission Delay of each secondary is calculated as follows:

$$\text{EDs} = \text{TOTs} - \text{TOTm}$$

The CSTD correction is determined as

$$\text{COR} = \text{EDp} - \text{EDs}$$

where EDp is the published ED for the baseline. The correction is added algebraically to the presently assigned CSTD to arrive at the value for the new CSTD.

#### Chart Verification

The Coast Guard is aware that the user may still find incorrect positioning information. This is caused by the varying attenuation of the signal previously mentioned that cannot be accurately predicted. However, the Coast Guard performs surveys to verify the published chart grids against actual received Loran-C signals. The Coast Guard has been verifying, and will continue to verify, the Loran-C navigation charts until satisfied that the information published is valid when compared to the actual signal received. Through the accumulation of Loran-C data, collected simultaneously with information from either Navsat, radio triangulation, or their combination, and the eventual, comparison of this data to published charts, LOP perturbations are identified and charted and a new, more accurate navigational chart is published through DMA.

#### Future Developments

What about Loran-C for the future? Obviously, much, if not all, of the growth of Coast Guard operated Loran-C is over. The CCZ is covered. However, certain international developments have created a need and a desire to install Loran-C chains in various locations: the Suez Canal for one, the Bay of Biscay for another. These chains are paid for and operated by other foreign governments for their own purposes. The GRI selection is normally coordinated through the U.S. Coast Guard. And the Coast Guard does provide,

when asked, any technical or operational information deemed necessary or helpful.

Internally, the Coast Guard is preparing for anticipated hardware improvements, which could allow for almost complete automated Loran-C operations. Through the distribution of Hewlett-Packard 9825's and specially prepared Calculator Assisted Loran Controller (CALOC) software, much of the transmitting station monitoring functions will become automated. Further, the use of Hewlett-Packard 9845 calculators promises to allow many of the monitoring sites to be automated and remoted to the control stations, allowing a substantial decrease in the number of personnel required to monitor the transmitted signals.

The Solid-state Transmitter (AN/FPN-64), along with special Remote Operating System (ROS) hardware, promises further personnel reductions. Crews of 11 or more can be effectively reduced to 4. The Coast Guard is presently planning to replace the old AN/FPN-42 transmitters with the AN/FPN-64.

Yet all of this hardware improvement and subsequent personnel reduction is being planned and coordinated so there will be no degradation in signal or service. The established goals of 1200 nautical mile range, 1/4 mile accuracy, 15 meter repeatability, and 99.7% availability will continue to be met or exceeded well into the next decade.



## QUESTIONS AND ANSWERS

MR. NICK YANNONI, Rome Air Development Center

Just two questions, one was your availability figure. What do you mean by that, 99. something?

LT. THRALL:

Okay, we compute our availability based on what we call a "Loran Month", which is calculated on the number of possible minutes in a month, and then we divide that by the total number of minutes that we are available, and come up with a particular availability figure.

MR. KUHNLE:

So, that is your downtime, sort of?

LT. THRALL:

Right.

MR. YANNONI:

The other question is can you tell me anything about the relationship of LORAN-C to LORAN-A, what has happened to LORAN-A, or is it gone? I understand it is going, or not quite gone, what can you tell me about that?

LT. THRALL:

For a long period of time it was considered to be the longest living corpse in the Coast Guard.

And I don't mean that derogatorily at all, in fact LORAN-A provided very good navigation coverage for a long time. But we turned the last LORAN-A station off December 31st, last year. That is U.S. Coast Guard LORAN-A stations. There are other LORAN-A stations that are apparently still operating in other parts of the world that are not Coast Guard operated or maintained.

MR. NICK YANNONI:

What about the Skywave, do people work with that or not?

LT. THRALL:

Some people do work with Skywaves, we are always trying to fight it in our particular applications. We don't want to see it, it interferes with our purpose. But there are people who are using Skywave. And I am not familiar with their application to be able to discuss it at any length, other than to say, yes, they do use it.

MR. CARL LUCAS, Naval Observatory

From time-to-time you have a reconfiguration in the LORAN chain, could you tell me what goes on during that period? I have a lot of trouble with that.

LT. THRALL:

It is a secret. I don't know of too much in the Coast Guard that would be considered a real secret.

When we do a chain reconfiguration and we are anticipating to be doing one relatively soon, it is done so that one particular station can be turned off completely for a number of days. In the case of our present reconfigurations that are being proposed, we are turning off the station to replace the antennae or to work on the antennae, or to replace transmitting equipment. And it just doesn't happen overnight, we are dealing with very large equipment, and just the effort itself requires that we turn it off.



# USING THE NAVSTAR GLOBAL POSITIONING SYSTEM AS A GLOBAL TIMING SYSTEM

KARL L. KOVACH, ILT, USAF  
SPACE DIVISION/YEE  
P.O. BOX 92960  
WORLDWAY POSTAL CENTER  
LOS ANGELES AFS CA 90009

## ABSTRACT

The Navstar Global Positioning System (GPS), although primarily designed for three dimensional position and velocity determination, is uniquely capable of providing highly accurate and stable timing information to users. This capability is derived from the time delay pseudo ranging concept which forms the basis for GPS navigation. The combination of navigation and timing together in one system will make GPS the Precise Time and Time Interval (PTTI) source of choice for the foreseeable future. Only GPS can supply continuous timing data world wide, in any weather, to a dynamically moving user at a previously unsurveyed site, with submicrosecond accuracy traceable to an established reference.

This paper discusses the application of Navstar GPS to the problems of PTTI dissemination. A short review of the GPS concept leads to a detailed description of the implementation of time transfer through Navstar GPS. Time is followed from the U.S. Naval Observatory (USNO) through the ground control, satellite, and receiving segments of GPS to the user's clock system. The three options by which a user's system can receive from the GPS receivers, currently under development by the DOD, are defined in detail. The electrical/digital/mechanical interface parameters along with suggested methods for their use are outlined for each option.

A detailed error model is also presented for the traceability of UTC (GPS) to UTC (USNO). Although absolute accuracy of UTC (GPS) provided to a user is specified to be slightly over 100 nanoseconds rms, substantially better accuracies can be easily achieved. By understanding and working around some of the GPS error uncertainties, real time synchronization between stationary users on the same continent can be controlled to within a few nanoseconds, and absolute post processed time offset with UTC (USNO) measured within 25 nanoseconds or better. A discussion of some of the potential work around techniques and their applications conclude this paper.

## I. INTRODUCTION

The fundamental concepts of the Navstar Global Positioning System (GPS) have been well described in several excellent papers presented at recent Precise Time and Time Interval (PTTI) meetings, Frequency Control Symposia (FCS), and other conferences. The reader is referred to the bibliography at the end of the article for a short list of those papers available for a detailed definition of GPS navigation principles.

### A. REVIEW

#### 1. Operation in a Nutshell

GPS utilizes a constellation of satellites surrounding the earth in 10,900 nautical mile orbits. Each satellite transmits two "pseudorandom noise" (PRN) timing codes on each of two L-band carrier frequencies towards the earth. Because the frequencies and timing codes used in the transmission are coherently derived from an on-board highly stable atomic frequency standard, by observing the transmitted signals and correcting for path delays (i.e. line-of-sight distance atmospheric and relativistic effects, etc.) the on-board atomic frequency standard's phase and frequency may be accurately determined by a ground based observer. This determination of the satellite frequency standard phase and frequency is the responsibility of the GPS ground control and tracking network, known collectively as the Control Segment. The Control Segment's observation of satellite frequency standard "time" (timing code epoch time or  $T_Z$ ) is compared against the GPS system time ( $T_{GPS}$ ) as kept by the Control Segment. From this comparison, a "satellite clock state" (i.e. time bias, drift and drift rate between  $T_Z$  and  $T_{GPS}$ ) is computed.

The clock state terms which relate the timing code epoch time to  $T_{GPS}$  (See Table 2, equations 1,4) as well as the position of the satellite as a function of  $T_{GPS}$  are uploaded into the satellite as digital data by the Control Segment. The uploaded information is then added onto the PRN codes as a 50 bit per second data stream by the satellite and the resulting satellite data, PRN timing codes, and carrier frequencies are transmitted towards the earth's surface as the satellite's useful navigation signals.

#### 2. Satellite-Control Feedback Loop Operation

When both the satellite's frequency standard time ( $T_Z$ ) and the satellite's position are unknown (as they are for the Control Segment) merely observing the satellite's transmitted frequencies and timing codes provide insufficient information to independently determine either of the two unknown quantities (e.g. is  $T_Z$  three nanoseconds ahead

of the observer or is the satellite one meter further away?). But if a fairly good initial estimate of the unknowns can be determined, detailed state and error models plus Kalman filtering can be used to separate and estimate the two unknown quantities based upon the one observation. This is exactly the method by which the Control Segment does its determination of the satellite's clock and position values. The Control Segment uses extrapolated values of  $T_z$  and satellite position from a previous time as current initial estimates of the unknown quantities and, in essence, the control segment - satellite system operates as a discrete cycle feedback loop (see Figure 1, Loop  $L_1$ ).

During each nominally eight hour period (for example, the period  $P_0$ ), the Control Segment uses its Monitor Stations (MSs) to track the satellite as it moves through its orbit. The tracking data during this period is sent to the Control Segment computation center where it is corrected for propagation delays, and coarsely modeled into satellite position and  $T_z$  states. These states are then compared with the data being transmitted by the satellite during the period (which were based on the previous period,  $P_{-1}$ ) to develop precise current error state estimates and filtered to predict the satellite's future position and clock states. These predicted future states, known as ephemerides and space vehicle time ( $T_{SV}$ ) state terms, are uploaded near the end of the current period for transmission by the satellite during the following period  $P_1$ . Thus, the process will repeat itself cyclicly, feeding forward a previous estimate to be used in determining current values. The satellite begins each period by transmitting the fresh ephemerides and  $T_{SV}$  terms uploaded from the Control Segment. As the period progresses, the satellite continues transmitting the same data with which it started. This data however has "aged" and become less accurate because of the time dependent growth of non-deterministic factors which affect the satellite's ephemeris and  $T_{SV}$  term accuracies. The satellite's data will continue to age throughout the period until it is replaced at the start of the next period with fresh data and the satellite's transmission accuracy is, in effect, reset to its optimal value.

To provide continuous worldwide availability of sufficient satellites for users, there will be at least eighteen satellites in orbit at all times. The GPS Control Segment will continuously repeat the above feedback process with each of the on-orbit satellites to assure that every satellite's ephemeris and  $T_{SV}$  terms are updated on schedule so as to provide the specified accuracy to users. Thus, there will be eighteen simultaneous feedback loops operating, tied together by a common navigation time reference -  $T_{GPS}$ , and position reference - WGS-72.

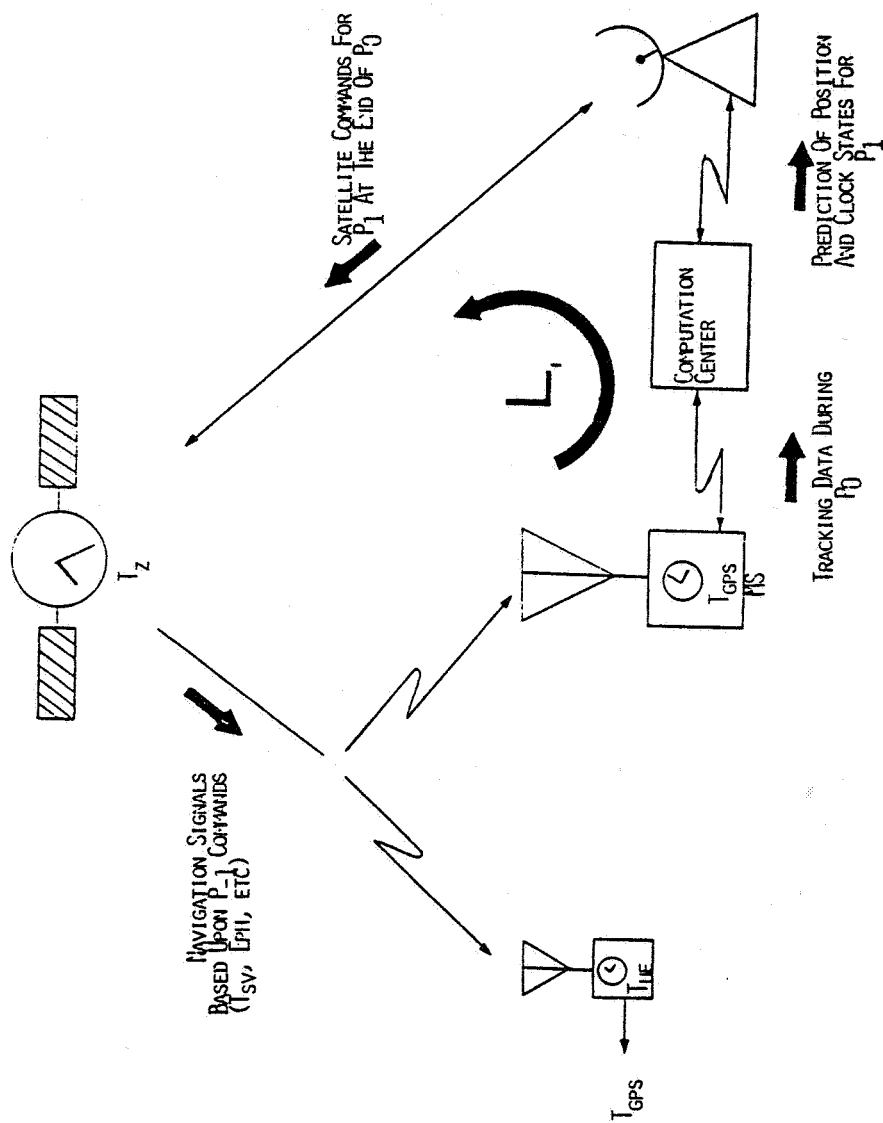


Fig. 1 - Navigation Time Feedback Loop

### 3. User Operation

The beneficiary of the eighteen Control Segment/satellite feedback loops is the GPS navigation user. Unlike the Control Segment tracking stations, the user is not at a known location nor does he have with him an atomic clock to independently keep  $T_{GPS}$ , but he is able to take the satellite's navigation data as truth for  $T_{SV}$  and satellite position. The User Equipment (UE) receiver on the ground has four unknown quantities it must determine to provide a navigation solution; the UE's position vector components (x, y, and z) and its local clock offset from each  $T_{SV}$  (Since each  $T_{SV}$  is approximately equal to  $T_{GPS}$  (modulo one week), the UE need only determine one satellite's  $T_{SV}$  to establish the clock offset). This then is the classical problem; faced with four unknown quantities, the UE must track four satellites (e.g. "eavesdrop" on four of the Control Segment/Satellite feedback loops) simultaneously to obtain the four independent range equations necessary for a position solution.

As widely reported in the literature, the GPS UE receiver does this solution process well. Accuracies of 2 to 3 meters in x, y, and z have been achieved and 16 meters spherical error probable (SEP) worldwide is promised operational users against the reference truth, WGS-72. But these are only three dimensional position accuracies, what about the fourth dimension of the solution - the dimension of time?

#### B. TIMES IN GPS.

##### 1. Navigation Time

The GPS UE, in computing its four dimensional navigation solution, treats its unknown time coordinate just as it treats its position coordinates. The Geometric Dilution of Precision (GDOP), which effects navigation accuracy due to non-orthogonality of the satellite-user ranging vectors, also affects the navigation time accuracy (See Section III.B). If the time and three position errors are normalized for geometric effects, the resulting Control/Satellite -UE ranging errors are found to be approximately equal in magnitude and uncorrelated. The ranging error between each satellite and the UE has been demonstrated to be within 5.3 meters or 17.5 nanoseconds ( $1\sigma$ ), with the units being used interchangeably. These control/satellite -UE ranging errors are known as User Equivalent Ranging Errors (UERE) and more about them will be said later.

The value of the time error as defined above is critical to the understanding of GPS's PTTI applications. The error of 17.5 nanoseconds is (neglecting amplification due to GDOP) the error the UE experiences in determining its local clock's offset from  $T_{GPS}$  averaged over some period of time and averaged over a number of satellites



(i.e., the error the UE has in determining the navigation time). This navigation time,  $T_{GPS}$ , is of little value to most PTTI users however. It is not necessarily stable nor tied to any accepted standard.  $T_{GPS}$  need only be continuous and without major steps in phase or frequency to maintain navigation performance of the system. The way that the GPS Control Segment determines  $T_{GPS}$  (as a paper clock based upon the ensemble of all monitor station frequency standards and driven by one of the MS standard's reference frequency (the GPS Master Clock)) satisfies the requirements for continuity and being without steps, but carries any and all Master Clock frequency instabilities throughout the entire system as instabilities in  $T_{GPS}$ . Thus,  $T_{GPS}$  is quite insufficient for many timing applications but, for the purposes of a navigation time,  $T_{GPS}$  serves it's function well.

## 2. "Time Dissemination" Time.

To solve the problem of supplying a useful time (in the PTTI sense of the word) to using systems when all that is necessarily available from GPS is  $T_{GPS}$ , the designers of GPS have also included terms in the 50 bit per second navigation data message to relate  $T_{GPS}$  to UTC. These terms accompany those for  $T_{SV}$  and the ephemerides as functions of  $T_{GPS}$ . They will be located in page 18 of subframe 4 of each satellite's message and include; time bias and drift rate terms between  $T_{GPS}$  and  $T_{UTC}$ , an accumulative integral second offset term to account for leap seconds, and a future impending leap second change value as well as the UTC time of applicability of the future leap second value change (See Table 2, equations 4,5,6).

The reader should note that this is a major change in GPS approach to the problems of time transfer. The original concept, as widely reported, was to steer  $T_{GPS}$  into direct synchronization with UTC. Repetitive leaps in  $T_{GPS}$  or step changes in the GPS Master Clock's frequency to achieve synchronization with UTC were found to have major, although transient, effects on the quality of GPS user's navigation solutions. Thus the decision was made to allow GPS time to be semi-free running (within an operational bound of 1 microsecond (modulo one second)) relative to UTC and accomplish precise time dissemination with a correction algorithm operating much the same way as the correction from  $T_Z$  to  $T_{SV}$  ( $T_{GPS}$ ).

This time dissemination technique may be similarly viewed as a discreet cycle feedback loop ( $L_2$ ) as shown in Figure 2. A GPS UE set has been selected in lieu of a monitor station for location at USNO because of it's lower cost and ease of maintenance. This loop operates at a nominal one week cycle period. During each period (e.g.  $P_0$ ) the UE set will track a series of single satellites. The UE set's computed UTC (based upon  $T_Z$ ,  $T_{SV}$  terms,  $T_{GPS-UTC}$  terms, etc., being transmitted by each satellite during  $P_0$ ) will be compared to UTC as kept by USNO (UTC(USNO)). The resulting array of measured UTC(GPS)-UTC (USNO)



differences for the tracking period will be transmitted during the period to the Control Segment computation center for modeling the drifts and offsets in UTC(GPS) and  $T_{GPS}$  versus UTC(USNO) as well as computing the new  $T_{GPS}$  to UTC (GPS) correction terms. At the start of the next one week period ( $P_1$ ), these new terms will be uploaded into the satellites for transmission to precise time users during  $P_1$ ; and so, as for  $T_{SV}$ , the closed cycle feedback loop repeats ad infinitum.

### C. Summary.

In summary, the definitions of the types of "time" used in GPS are given in Table 1. The equations used to get from time to time are summarized in Table 2, and applied as follows:

- a.  $T_{Z_i}$  is the PRN code phase time as it leaves the  $i$ th satellite.
- b. Each  $T_{SV}$  is  $T_{Z_i}$  plus correction terms (eqs 1,2) from the navigation data message.  $T_{SV}$  is approximately  $T_{GPS}$  modulo one week.
- c. The UE calculates  $T_{GPS}$  as the average  $T_{SV}$  plus accumulated weeks since midnight 5/6 January 1980 (eq 3).
- d. The UE calculates UTC based on the average satellite's  $T_{GPS}$  (eqs 4,5). Note that this UTC is a 24 hour count only and is corrected for leap second adjustments. (See ICD-GPS-200 for additional details).

## II. TIME FROM GPS USER EQUIPMENT

A user of GPS fits in one of two categories; (a) those who will design and build their own equipment to receive the satellite signals and process navigation/time data to their own specifications, and (b) those who will utilize the DOD procured User Equipment (UE) receivers to obtain navigation and time data in a readily useable format. The first section of this paper addressed how the first category of user can recover UTC from the GPS satellite signals. This section deals with the second category - users who can use UE as a black box source of precise navigation and time for their own system or application and how they can directly receive UTC from the UE.

### A. User Equipment Program

The GPS UE is presently in it's Full Scale Engineering Development (FSED) cycle or Phase II of a three phase program. During Phase I, four U.S. contractors developed and demonstrated UE sets to validate the GPS concept. Most of the UE testing was conducted at Yuma Proving Ground in Arizona utilizing limited satellite coverage from a maximum of four Navigation Development Satellites (Block I type). This

<u>Symbol</u>	<u>Definition</u>	<u>LSB</u>	<u>Modulus</u>	<u>Limit of Resolution</u>	<u>Absolute Reference</u>
$T_{Z_i}$	$i^{th}$ Satellite frequency standard time represented by the PRN code phase or carrier phase.	1 P chip =97.75 nSec	1 week (604,800 sec)	0.05 P chip=5 nSec or 0.1 carrier cycle=0.6 nSec	None
$T_{SV_1}$	$T_{Z_1}$ plus navigation message clock state correction terms ( $\approx T_{GPS}$ Modulo one week)	$2^{-31}$ seconds	1 week	Same as above	GPS time
$T_{GPS}$	Time as kept by GPS Control Segment	$2^{-31}$ seconds	20 years	N/A	UTC (USNO) at midnight 5/6 Jan 80
UTC(GPS)	GPS's estimate of UTC	$2^{-30}$ seconds	24 hours	N/A	UTC(USNO)
$T_{UE}$	UE Clock Time	N/A	N/A	500 pSec	None

TABLE 1 TIMES IN GPS

A. From  $T_{Z_1}$  to  $T_{SV_1}$ :  $T_{SV_1} = T_{Z_1} - \Delta T_{SV_1}$  (1)

$$\Delta T_{SV_1} = a_{f0} + a_{f1} (T_{GPS} - T_{OC_1}) + a_{f2} (T_{GPS} - T_{OC_1})^2 + \Delta t_{r_1} \quad (2)$$

Where: a.  $a_{f0}$ ,  $a_{f1}$ ,  $a_{f2}$ =clock correction coefficients contained in the navigation data message.

b.  $T_{OC_1}$  = clock data reference time for the  $i^{th}$  satellite contained in the navigation data message.

c.  $\Delta t_{r_1} = F e_1 (A_1)^{\frac{1}{2}} \sin E_K$  = relativistic correction ( $e$ ,  $A$ , and  $E_K$  are orbital parameters contained in the navigation data message,  $F$  is a constant equal to  $-4.443 \text{ E-10 sec/(meter)}^{\frac{1}{2}}$ ).

B. From  $T_{SV1}$  to  $T_{GPS}$ :  $T_{GPS} = (1/n_{12-1}^{\frac{1}{2}} T_{SV_1}) + WN + (\text{midnight 5/6 Jan 80})$  (3)

Where: a.  $n$ =number of GPS satellites being averaged by the UE.

b.  $WN$  = week number (contained in the navigation message).

c. (midnight 5/6 Jan 80) = the GPS-UTC zero reference time.

C. From  $T_{GPS}$  to UTC (GPS):  $UTC (GPS) = (T_{GPS} - \Delta t_{UTC}) \left[ \text{MOD } 86400 \right]$  (4)

$$\Delta t_{UTC} = \Delta t_{LS} + A_0 + A_1 (T_{GPS} - t_{ot} + 604800 (WN - WN_t)) \quad (5)$$

Where: a.  $\Delta t_{LS}$  = a value for future for leap second corrections to

be applied at UTC zero hour of the effectivity date indicated by the Week Number ( $WN_{LSF}$ ) and Day Number (DN) ( $\Delta t_{LS}$ ,  $WN_{LSF}$ , DN are contained in the navigation data message).

b.  $A_0$ ,  $A_1$  = UTC correction coefficients contained in the navigation data message.

c.  $t_{ot}$  = reference GPS time for time data,  $WN_t$ =the week number for time data (both in navigation data message).

TABLE 2 TIME EQUATIONS

testing included some limited testing of the time transfer capabilities of GPS. Those test results showed that  $\pm 25$  nanosecond ( $1\sigma$ ) real-time time transfer accuracy was achievable using GPS in a benign field test environment, and that the operational GPS should definitely include time transfer as one of its goals.

The present Phase II began after a favorable Defense Systems Acquisition Council decision on GPS was reached in June 1979. Two UE contractors (Magnavox and Rockwell Collins) were selected out of the original four to develop preproduction prototype UE sets and further demonstrate the military utility and mission enhancing capability of GPS. The competitive environment established between the two contractors during Phase II is expected to produce the most effective UE set designs. But because of the competition between the two designs, this paper is restricted in its discussion of the UE design details to standardized or non competition sensitive characteristics.

Development Test and Evaluation (DT&E) and Initial Operational Test and Evaluation (IOT&E) will be conducted on the two families of equipment from 1982 through 1984. These contractor and government test activities will be conducted at a number of test facilities on land, sea, and airborne test platforms. Five of the Block II type satellites (new navigation message structure) are expected to be available to support this testing. This new type of satellite navigation message will allow testing of the time dissemination procedures discussed in Section 1, including the UTC synchronization parameters which were not present in the Block I navigation message.

Production of GPS UE sets will occur during the Phase III portion of the Navstar program beginning in 1985. Full system capability will be achieved in 1987 when 18 operational satellites will be deployed in orbit. Integration of production UE into military host vehicles and availability of UE for operational time dissemination will begin in 1985 and continue through the 1990's.

#### B. User Equipment Functional Characteristics

The application of GPS UE to various types of military missions under a wide variety of operational conditions has led to the development of three types of UE sets - low dynamic (single satellite channel), medium dynamic (two channel), and high dynamic (five channel) units. The following discussion focuses on the high dynamic (HD) UE set since it is of most interest to a precise time user. Deviations of the low dynamic (LD) and medium dynamic (MD) sets from the HD sets exist primarily in size and in range of host platform dynamic tracking ability and are not further discussed here.

The HD UE set has been designed for operation in the most severe avionic environments and for rigorous shipboard operation. Part of the

IOT&E test program will be to unconditionally qualify the equipment for service use aboard virtually any manned military platform. This is a significant point, in that the performance specifications cited herein apply throughout the entire military environment range. Unlike some of the non DOD utilizer designed equipment whose performance is defined only for laboratory conditions, the GPS UE will perform to specification over any combination of the stated environmental conditions - a significant advantage for the military field user.

Typical functional characteristics of the HD user set are defined in Table 3. The weight and power values include the required antennas, mounts, operator control/display units, interface units, power supplies, etc.

### C. Time Interface Characteristics

If, say, a user has one of these UE sets and it is supposed to provide him with position/navigation and time data - how does he access the data? For position/navigation data, the manner is straight forward: if the user wants the data sent to the operator - the UE's control/display unit displays the requested data "real time" (i.e., real time enough for a man/machine interface) or the UE set will drive the operator's flight instruments directly. For the data to be sent to the host platform's computer - a digital data link (e.g., NTDS or MIL-STD-1553) along with a time tagging scheme (e.g., "real time", 64 mSec counter, "slow strobe") is used. For either of these two approaches, the senescence of data is not particularly critical. A delay of 64 mSec in making the position data available to the using system only induces 7.7 cm worth of transmission uncertainty into the perceived position accuracy (at a host vehicle velocity of 1200 m/Sec). This is a negligible error source when compared with a 15 m SEP.

Senescence of time data is another story however. A time uncertainty of 64 mSec across a digital data bus, will produce a transmission uncertainty of 64 m/Sec at the receiving device -certainly a significant error when compared with 0.1 mSec potential accuracy. Thusly, a separate analog signal is the only way to communicate time to precision levels. The designers of GPS have recognized this and have included three primary analog signal methods to accomplish time dissemination/communication to a using system. These are in order of their accuracy:

- (A) Time Mark Signal
- (B) Reset Pulse (limited implementation)
- (C) Data Capture Pulse

The first two are output analogs from the UE, the last is an input analog to the UE. Digital data is required for all three to resolve modulus and definition uncertainties. These signals are

Size:	7.62 x 7.5 x 19.52 inches (Receiver, etc) 6 x 5.75 x 8 inches (Control display Unit) 14 x 14 x 2 inches (Antenna)
Total Weight;	≤ 66 lbs
Total Power:	< 300 watts, MIL-STD-704A 115 Vac 60/400Hz or 28 Vac
Environmental Characteristics:	MIL-E-5400, MIL-E-16400, MIL-E-4158, etc. (F-16, Surface/subsurface ship typical)
Mean Time Between Maintenance:	1500 hr
Dynamic Range:	Velocity = 1200 m/sec Acceleration = 90 m/sec <sup>2</sup> Jerk = 100 m/sec <sup>3</sup>
Time from Power On Until First Fix:	7 minutes
Rate of Subsequent Fixes:	Once per second
Threat Survivability:	Very High
Accuracies*:	Position (3 dimensional) = 15m (SEP) Velocity (3 dimensional) = 0.1 m/Sec(RMS) Time (to UTC) = 0.1 μSec (1σ)

(\*worst case environment, average satellite visibility)

TABLE 3 - Typical HD UE Set Characteristics



further defined in the following paragraphs.

# 1. Time Mark Signal (TMS)

The Time Mark Signal is a very sharp rise time discreet pulse which coincides with the precise moment in UTC of applicability of each Time Mark Data Block (TMDB). It is the most accurate signal available from the UE to allow the host vehicle's GPS utilizing subsystems to maintain UTC. The TMS occurs at a nominal once per second rate, but does not, itself, represent UTC one-second rollovers!

This analog TMS signal should be construed to be only half of the most precise time interface from the UE. The other half is a simple unidirectional data link which supplies data (the TMDB) to identify the meaning of the analog pulse. This data link is known as the GPS instrumentation port. Each GPS UE has an instrumentation port (IP), and each provides time in this combinational manner. An error of less than 111 nSec (1σ) true accuracy to UTC (USNO) is promised to the user of these signals under any/all combinations of UE design environments (accuracy of the LD UE set's TMS is somewhat less however).

## TMS Operational Use

The operational manner in which this approach works is as shown in Figure 3. A using system will first detect the incoming TMS and will time tag the TMS leading edge against its own internal clock ( $T_{us}$ ). Within 450 mSec, the UE set will transmit the TMDB across the IP. The using system will read this data and parse the CUT Time into two pieces, one for integer number of UTC one second rollovers and one for the fraction of seconds after the last UTC one second rollover that the TMS was issued by the UE set. The using system can now compute its internal clock offset from UTC (USNO) by using the following equations:

$$T_{us} @ \text{TMS issuance} = T_{us}(\text{TMS}) = T_{us}(\text{TMS}) \text{ integer} + T_{us}(\text{TMS})_{\text{fraction}} \quad (7)$$

$$UTC_{\text{TMDB}} = UTC \text{ integer} + UTC \text{ fraction} \quad (8)$$

$$UTC \text{ integer} - T_{us}(\text{TMS}) \text{ integer} = \text{leap second or integral second offset between } UTC \text{ and } T_{us} @ T_{us}(\text{TMS}) \quad (9)$$

$$UTC \text{ fraction} - T_{us}(\text{TMS}) \text{ fraction} = \text{fractional second offset between } UTC \text{ and } T_{us} @ T_{us}(\text{TMS}) \quad (10)$$

Note though, that the offsets computed above are valid only at  $T_{us}(\text{TMS})$ . The reason for this is that although the TMS occurs at a nominal 1 Hz rate, there is substantial noise about that 1 Hz between subsequent TMS's and the UTC fractions reflect the magnitude and sign of that noise.

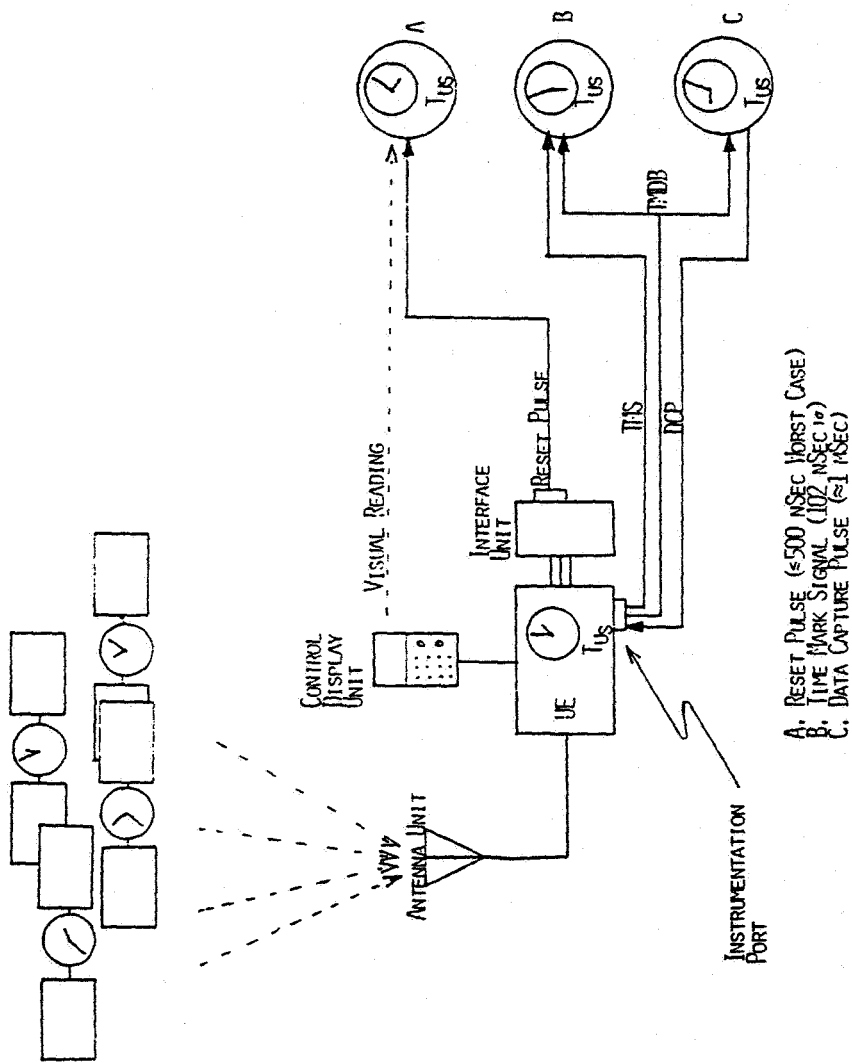


Fig. 3 - Time Interfacing Methods

### Analog Signal Characteristics

Functionally, the TMS is essentially the UE set's own internal time strobe used for keeping  $T_{UE}$  and strobing the internal navigation processing. It is a countdown of the set's Master Reference Oscillator (MRO) frequency and so is coherent with all frequencies (e.g.  $L_1$ ,  $L_2$ , IF  $L_0$ , etc.) used internal to the set. Although the set's MRO is a high precision ( $\sigma(t) = 10^{-12}$ ,  $t = 1$  sec) ovenized quartz oscillator, it is not itself tuned operationally to a precision nominal frequency. For signal tracking-VCO's and DCO's are used, and for processing tasks - the precise frequency is not important since as long as the deviation is known it can be accounted for with software corrections. This and the environmental effects (acceleration sensitivity of  $6 \times 10^{-10}/g$ , temperature sensitivity over  $+71^\circ C$  to  $-54^\circ C$  of  $1 \times 10^{-9}/range$ , etc) on the MRO frequency are the cause of (a) TMS to TMS noise, (b) the non-alignment of the TMS with the UTC one second rollover, (c) non-alignment of TMS's between UE sets, and (d) the reason GPS UE provides only Time-of-Day and not frequency to using systems. See Table 4 for definition of the electrical characteristics of the time mark signal.

### TMDB Digital Characteristics

The instrumentation port is a bidirectional Universal Asynchronous Receiver/Transmitter (UART) device used in a simplex mode for time dissemination purposes. The UE transmits the TMS time data to any listener using this device as an asynchronous serial stream using an RS-422 electrical structure operating at 76.8 Kilobaud (maximum). The UART has been chosen for the data link because of the low cost, high reliability and simplicity of the technique.

The data in the TMDB comes to the using system as a 70 sixteen bit word data block. The 64 words of data are shown in Figure 4 (message headers and checks are omitted). As can be seen, there is quite a bit more in this data block than just time information. All the data is valid exactly at the rise time of the immediately preceeding TMS. For additional details of this data block and how to use the IP, refer to ICD-GPS-204, Navstar GPS Instrumentation and Connector standards available from the GPS Program Office. This document defines the UE design details and also specifies how a MIL-STD-1553 data bus can be alternatively used by a using system to receive the TMDB.

#### 2. Reset Pulse

While the Time Mark Signal is the most accurate method of receiving time out of the UE set, not all using systems are sophisticated enough to utilize that method (e.g. a stand alone atomic clock). As an alternative for those systems, some GPS UE have built-in interface modules to provide a direct reset pulse to be used for clock synchronization (currently only submarine type UE incorporate this

- a. Amplitude: 3 volt minimum into 50 ohm load  
5 volt maximum into an open circuit
- b. Width: 20 microseconds  $\pm$  20%
- c. Rise-time:  $\leq$  20 nanoseconds nominal (ambient temperature), 50 nanoseconds maximum
- d. Fall-time:  $<$  1 microsecond
- e. Connector Type: MIL-C-38994/201B35PN (13 PIN)
- f. Wire Type: COAX
- g. Pin Assignment: See ICD-GPS-204

TABLE 4 - Time Mark Signal Interface Characteristics

- a. Signal Type Positive Going Pulse
- b. Frequency 1 Pulse Per Minute
- c. Amplitude 10 v  $\pm$  10%
- d. Width 20 mSec  $\pm$  10%
- e. Risetime  $\approx$  20 nSec
- f. Falltime  $<$  1 $\mu$ Sec

TABLE 5 - Typical Reset Pulse Interface Characteristics

<u>Data Item</u>	<u>No. of Parameters</u>	<u>Data Type</u>	<u>No. of Words</u>	<u>Units</u>
GPS Time	1	DPFP*	4	seconds
► CUI Time	1	DPFP	4	seconds
Δ T from GPS Time	1	Integer	1	10 milliseconds
Time Mark Counter	1	Integer	1	NA
Position (Lat, Lon)	2	FP	4	radians
Position (x,y,z)	3	FP	6	meters
Altitude (MSL & Absolute)	2	FP	4	meters
Velocity	3	FP	6	meters/seconds
Acceleration (E,N,Up)	3	FP	6	meters/sec/sec
Attitude (Pitch, Roll)	2	FP	4	radians
True Heading	1	FP	2	radians
Magnetic Variation	1	FP	2	radians
Measurement Channel Status	5	Binary	10	NA
Position Error Std. Dev. (N,E,Up)	3	FP	6	meters
RSS (N,E,Up) Pos. Error of Std. Dev.	1	FP	2	meters
Equipment Configuration	1	Binary	2	NA

\*Double Precision Floating point

Fig. 4 - Time Mark Data Block

feature since they are the only types of vehicles which have an on-board installed atomic clock).

This reset pulse is a very fast rise time analog signal which occurs nearly (within approximately 500 nSec worst case) on the UTC (USNO) one minute rollovers. Utilizing this signal and the integer second UTC data displayed on the control/display unit, an operator can utilize the synchronization circuitry in an atomic cesium/rubidium clock to reset the clock to UTC. Details of this signal are shown in Table 5.

### 3. Data Capture Pulse

The Data Capture Pulse (DCP) is the least precise method of receiving time out of the UE set - accurate only to 1 mSec of UTC. It's primary use is in test instrumentation applications of GPS where time and location of "significant events" aboard a platform are to be instrumented. The using system supplies a 28 v positive going pulse to the UE instrumentation port at a maximum rate of 2Hz to mark the significant events (See Figure 3). The UE responds with the time and location of the "significant event" over the IP data link (the UART device). The format and content of the data block thus returned to the using system is identical to that used for the Time Mark Signal (Figure 4) except that it's time of applicability is the "significant event" of interest (the significant event may also be a clock pulse). ICD-GPS-204 contains additional details of this UE function.

## III. Error Model Specification

The error sources which effect a using system's reception of UTC (GPS) from UE are many. They are both deterministic and random, geometrically independent and highly geometric dependent, constant and time varying, independent of environment and environmentally sensitive. This section characterizes some of these factors (UERL, GDOP), shows how they combine, and ultimately how they can be managed for higher accuracy UTC (GPS) reception by the using system.

### A. System Error Budget - UERE

The GPS system error budget has been widely cited in prior analyses of the time accuracy of GPS. It serves as a convenient starting point in this analysis as well. The budget, as shown in Table 6, is divided into system segment allocations and totals up to a 5.3 meter ( $1\sigma$ ) User Equivalent Ranging Error (UERE). This total UERE can be interpreted to be the average error a using system would perceive in the spherical loci of potential location points resulting from a single satellite ranging operation as output by the GPS UE against the absolute reference frame, WGS-72 ("average" as used here means averaged over using systems uniformly distributed in both time and space).

SEGMENT	ERROR SOURCES	SYSTEM BUDGET (METERS $1\sigma$ )
SPACE	Clock & Navigation Subsystem Stability	2.7
	Predictability of SV Perturbations	1.0
	Other	0.5
	Total Segment	2.9
CONTROL	Ephemeris Prediction and Model Implementation	2.5
	Other	0.5
	Total Segment	2.6
USER	Ionospheric Delay Compensation	2.3
	Tropospheric Delay Compensation	2.0
	Receiver Noise and Resolution	1.5
	Multipath	1.2
	Other	0.5
	Total Segment	3.6
SYSTEM	Total $1\sigma$ UERE =	5.3

GPS System Error Budget

TABLE 6

## 1. Satellite Segment

The GPS Space Segment contributions to UERE are primarily due to stability limits in the on board atomic frequency standards. Both rubidium and cesium standards are in use aboard the space vehicles and, despite some early hardware failures, the satellite clocks are performing quite well and have generally exceeded their performance specifications. It is difficult to say however, just how well the onboard clock/navigation subsystems are behaving. It is extraordinarily difficult to separate the effects of the clock/navigation subsystem from the second error source allocated to the satellite - the perturbations about the nominal orbit/ephemeris due to solar pressure variations, satellite outgassing, and attitude control activities on-board the satellite.

Both sources of error have the same net effect as perceived by the ground based observers (the control segment and the users): the apparent line-of-sight difference between the signal tracking derived range and the satellite ephemeris minus user location computed range as was also discussed in the first section of this paper. The definition of exactly which source is the major contributor to the induced UERE has been a hotly debated topic, but the question is moot from the using systems point of view. The user still perceives a total error attributable to the satellite of 2.9 meters (RSS of the three errors including "other"). This total error has some significant characteristics which are worthy of note:

- a. The error value specified is the total induced error bound at the end of an upload applicability period. Immediately after a new upload the error is near zero and grows as a function of time towards the specified limit at the end of the period.
- b. The error of one satellite is uncorrelated with the error of another satellite (except some small coupling due to common solar pressure effects and other environmental factors)
- c. The error is random and is a zero mean process in the long term. All deterministic effects are accounted for in the Control Segment's ephemeris and clock correction models. The remaining errors are random and all biases are accounted for.

## 2. Control Segment

The GPS Control Segment Errors are characteristically much like the Satellite Segment errors although they stem from imprecise modeling as opposed to physical factors in and on the satellite. The Control Segment cannot physically track the satellite across the heavens, but instead must rely on navigation signal tracking of the satellites. This



fact imposes two fundamental characteristics on the quality of the derived ephemerides uploaded to the satellites: a) the Control Segment corrects the navigation signals for net effect -exactly the same net effect the UE will see in the field, thus resulting in the combined satellite derived ranging signals/Control Segment derived ephemerides being optimally corrected for the field user, and b) the Control Segment cannot precisely predict future satellite ephemerides because the input satellite position tracking data has residual SV clock/navigation subsystem, SV perturbation, and signal path delay model noise imposed on it (as was seen in section one of this paper). In summary, the Control Segment errors can be said to have the following characteristics:

a. The 2.6 meter (total) error value specified for the control segment is the total induced error bound at the end of the upload period. The error has the same time dependent characteristics as the space segment errors.

b. The ephemeris errors for one satellite are partially correlated with those for another satellite. Each satellite is modeled independently but residual effects of the tracking and estimation process induce some small correlation.

c. The errors are generally not random due to the imprecise modeling processes. As GPS matures and additional refinements are made to the models, the deterministic effects should decrease in size. Steady state biases are definitely part of the modeling process and affect all satellites uniformly. The biases discovered so far have been minor and have been related to tracking station location errors.

### 3. User Segment

The GPS User Segment error sources are quite unlike the Space and Control segment errors. They do not depend on the upload period nor are they otherwise time dependent. The UE UERE contributions are due to either path delay uncertainties or hardware noise, both of which are environmentally dependent.

Hardware - The hardware noise specification value of 1.6 meters (includes "other") is sized for code tracking in an operational, high threat, jammed environment. It is a random zero mean process noise and, between different tracking channels in the receiver, is uncorrelated.

Path Delays - The path delays that the satellite's navigation signal experiences before reaching the user's antenna are determined by the earth's atmosphere and by reflective surfaces in the vicinity of the user's antenna (multipath). The UE use a dual frequency ( $L_1/L_2$ ) correction algorithm to correct for

ionospheric delays, a geometric correction algorithm for the tropospheric delays, and a combination of search algorithm and judicious antenna placement to minimize multipath errors. The specified values for each of these error sources are the residual errors after making the corrections and reflect on the accuracy of the algorithms used. These errors are generally quite correlated among visible satellites and have both random and bias components.

## B. GDOP

Given that each segment of GPS is performing within its system error budget allocation, the navigation accuracy available to a using system from the GPS UE can be determined by the instantaneous UERE's of the four control/satellite - UE receiver links being used and the Geometric Dilution of Precision (GDOP) between the satellites and the user. This GDOP is a measure of how the satellite geometry affects user accuracy. It's mathematical development and interpretation have been rigorously described several times in recent literature and do not bear repeating here. Suffice it to say that GDOP and its related HDOP (Horizontal Dilution of Precision) act as amplification factors of UERE to give the resulting navigational errors due to the effect of the three dimensional geometry of the satellites and user position as well those due to the four dimensional navigation solution. As a result of this definition and its underlying assumptions the following relationships can be shown to hold:

$$GDOP^2 = HDOP^2 + VDOP^2 + TDOP^2$$

$$\text{Horizontal Position Error} = \text{UERE} \times \text{HDOP}$$

$$\text{Vertical Position Error} = \text{UERE} \times \text{VDOP}$$

$$\text{Navigation Time Error} = \text{UERE} \times \text{TDOP}$$

For specification purposes, for UE solving the four dimensional navigation equations (four equations, four unknowns), the following values of the GDOPs are used (based on the 50th percentile values for a nominal constellation of satellites):

$$GDOP = 3.56$$

$$HDOP = 1.58$$

$$VDOP = 2.71$$

$$TDOP = 1.68$$

And thus, the specified value for average time error for GPS UE is:

$$\text{UERE} \times \text{TDOP} = (5.3\text{m})(3.3\text{nSec/m})(1.68) = 27.9 \text{ nSec}(1\sigma) \quad (11)$$

or the accuracy of navigation time in the GPS UE is  $T_{\text{GPS}} \pm 27.9 \text{ nSec}(1\sigma)$ .

### C. UTC Accuracy

The time error induced in the UE due to UERE and TDOP of  $\pm 29.7$  nSec ( $1\sigma$ ) is only part of the error which a using system will perceive in the time it receives from the UE. Superimposed on the navigation time error are errors due to the  $T_{GPS}$  to UTC (USNO) correction model and errors due to the UE hardware in handling it's analog time signals. Both these errors are independent of geometry and so GDOP or TDOP do not affect them. Each can be characterized as follows:

#### 1. $T_{GPS}$ to UTC (USNO) model

As described in section I.B.2, the Control Segment will be cooperating with USNO in operating a specially calibrated UE set at USNO to receive UTC(GPS) and communicate time differences to the Control Segment on a twenty-four hour cycle. The Control Segment will model these errors and upload the correction terms on a weekly basis into the satellites. The choice of upload periods strongly influences the accuracy provided to users at the end of the weekly upload period. The GPS system specification only calls for this value to be within 100 nSec( $1\sigma$ ). It is this value which has dictated the upload cycle period. Substantially better accuracies could be achieved with more rapid updates -but as yet, no military using command has expressed a requirement which would necessitate a more rapid update cycle. Thus, the current GPS baseline is weekly time uploads.

This time upload procedure error budget at the end of each prediction period has been allocated among the various sources as follows:

(UTC(GPS)-UTC(USNO)) @ USNO (measurement):	31 Nanoseconds ( $1\sigma$ )
( $T_{SVi} - T_{GPS}$ ) at Control Segment (measurement):	14 Nanoseconds( $1\sigma$ )
RSS of Measurement Errors:	34 Nanoseconds ( $1\sigma$ )
Projection/Extrapolation of Previous Measurements 6 days into future:	x 5
UTC (USNO) - $T_{GPS}$ error:	76 Nanoseconds ( $1\sigma$ )
Stability of $T_{GPS}$ versus UTC(USNO):	47 Nanoseconds ( $1\sigma$ )
Total Error of UTC(GPS) versus UTC (USNO):	90 Nanoseconds ( $1\sigma$ )

## 2. UE hardware time handling errors

The GPS UE has been optimized for navigation computation and not specifically for absolute time synchronization. As a result, a rather large error tolerance has been specified for the total UE induced error in time dissemination: 38 nSec ( $1\sigma$ ). This is the additional hardware error the UE can allow to be induced in the final time accuracy output to a using system for its most accurate time interface, the Time Mark Signal. The specified tolerances for the other time interfaces, the Reset Pulse and the Data Capture Pulse, are higher as previously mentioned (primarily due to the additional hardware uncertainties associated with additional analog signal handling).

The major limiting factors which causes such a large error in the UE handling of timing are the acceleration and other environmental sensitivities of the UE Master Reference Oscillator. The value of 38 nSec( $1\sigma$ ) is specified over the environment of the UE and this environment includes up to 9 g's steady state and 15 g transient accelerations,  $+71^{\circ}\text{C}$  to  $-54^{\circ}\text{C}$  temperature range and transient power excursions. Other hardware delays (such as the temperature dependent amplifier and antenna delays, installation peculiar cable delays, and short term electromagnetic interference noise) as well as software (Kalman filter transient response) effects are also included in the factors which limit the UE's ability to provide a well regulated analog signal to a using system.

### D. Combination of errors

Thusly, the final UTC(GPS) provided to a using system using the TMS in the field at an unknown location and operating in a severe military environment is accurate to UTC (USNO) within the following bound:

T <sub>GPS</sub> Errors:	29.7 Nanoseconds ( $1\sigma$ )
T <sub>GPS</sub> to UTC (USNO) Errors:	90.0 Nanoseconds ( $1\sigma$ )
UE Interface/Hardware Time Handling Errors to using system:	<u>37.9 Nanoseconds (<math>1\sigma</math>)</u>
Total UTC (GPS) Error Bound Estimated:	102 Nanoseconds ( $1\sigma$ )
Specified UTC (GPS) Error Bound:	111 Nanosecond ( $1\sigma$ )

## IV. What If 102 nSec Isn't Good Enough?

There are several techniques one may apply to the operation of the GPS UE to achieve much better time dissemination performance. Each technique makes use of particular characteristics of the error inducing sources to either have the errors cancel out with a common mode

technique or make the error source irrelevant to the problem at hand. A few of these techniques are described below along with their effect on the error sources. These techniques are also applied to two specific using system cases as examples of what can be achieved using GPS in a realistic scenario rather than the preceeding worst case specification value discussion.

A. Error Source Reduction Techniques

1. Multipath error reduction:

The Multipath error allocation can be eliminated by judicious placement of the GPS UE antenna to avoid hard surface reflections of satellite signals.

2. Receiver noise reduction:

The receiver noise value of 5 nSec (1.5m) can be reduced to 0.6 nSec by operating in a less jammed environment (i.e. not operating in the middle of a high power jammer field). The lesser levels of jamming will allow precision carrier phase tracking of the signal rather than just P-code tracking and so a corresponding decrease in receiver noise can be achieved.

3. Operate the UE in a stationary mode:

This technique includes both true stationary (velocity of the UE=0) and receiver velocity aiding with minimal acceleration modes. Utilization of either of these modes allows the UE to reduce it's own UERE components (and it's time estimation errors), by approximately  $1/\sqrt{2}$ . These modes also allow reduction of the acceleration induced errors in the master reference oscillator to zero with a corresponding increase in the precision control of the analog time signal output (depending on design peculiarities this can reduce the analog handling error by about  $1/\sqrt{2}$  or more).

4. Operate the User Equipment at a known location:

Utilizing a surveyed location can reduce the UE's perceived TDOP to unity. This results from the fact that only the UE's time is an unknown and only one satellite need be tracked - so geometry has no effect. A previously determined GPS navigation solution is sufficiently precise to enable this technique to work.

5. Average over several satellites in view at known location.

This will reduce the independent and uncorrelated error contributions to UERE and  $T_{GPS-UTC}$  (USNO) by approximately  $1/\sqrt{4} = \frac{1}{2}$ .

6. Calibrate the user hardware errors and operate in a stable environment:

This technique is applicable to all types of using systems. It requires a one time calibration with an independent UTC (USNO) source and can be done prior to fielding of the UE. The improvement is design dependent but can potentially reduce the analog signal handling errors to the order of a few nanoseconds.

7. Post processing:

Post processing of field data for using system applications which do not require real time synchronization with USNO can effectively eliminate the much of the 90 nSec of the UTC(GPS)-UTC(USNO) error source. The necessary data could be had by accessing a planned USNO data bank which will contain the satellite UTC(GPS)-UTC(USNO) data or the using system could use independently measured UTC(GPS) -UTC (using system) data collected at a laboratory site with a second UE and the using system's reference clock (which may or may not be synchronized with UTC (USNO)).

8. Co-regional operation (Common Mode):

With this technique, relative synchronization of two using systems can be improved. Common mode effects (e.g. both UE's tracking the same satellites and both experiencing approximately the same satellite ephemeris, ionospheric, etc. error sources) can be canceled or reduced between the two using systems if relative synchronization between the two is the desired effect.

9. Net Time Synchronization:

If synchronization between two using systems (net time) is all that is desired and absolute UTC traceability is relatively unimportant, then  $T_{GPS}$  can be used in lieu of UTC(GPS) and synchronization between the systems can be within the  $T_{GPS}$  plus UE hardware/analog signal errors.

B. Practical Examples

The foregoing techniques are in general non-exclusive and can be applied independently or in combination (depending on exact circumstance and user application). Two examples of user applications are given below to demonstrate the power of these techniques.

Example 1: Joint Tactical Information Distribution System (JTIDS) type of net synchronization. In this example, two using systems wish to real time control the absolute time bias between their clocks. Assumptions:

- a. An F-16 type aircraft and ground terminal are the two systems.
- b. The F-16 can partially velocity aid his GPS UE, the Ground Terminal is stationary and is at known site.
- c. Moderate jamming environment.
- d. Co-regional operation.

In this case the error reduction techniques that can be applied are: numbers 1,2,3,4,6,8,9. The resulting errors between the two user clocks can be conservatively estimated as 26 nSec ( $1\sigma$ ) as shown by Table 7.

Example 2: A forward observer near a protected target is acquiring data which must be related to UTC (USNO) for subsequent analysis. For this example the following assumptions apply:

- a. The observer is in a highly jammed environment.
- b. He is stationary but at a unknown location.
- c. He has a very precisely calibrated UE.
- d. Post processing reference data is available.
- e. The user utilizes GPS to determine his position.

In this example the following error reduction techniques may be applied: Numbers 1,3,4,5,6,7. Applying these techniques to this example, the UTC (USNO) time accuracy of the collected data would be within approximately 16 nSec ( $1\sigma$ ) as given by Table 8.

## V. Conclusion

The Navstar Global Positioning System has been shown to be a truly integrated timing system. Although some user may choose to build their own satellite timing receivers because of availability constraints or unusual applications, the majority of users can utilize the DOD developed User Equipment and the applicable techniques described in this paper to satisfy their current and future system time-of-day requirements.

In addition, GPS also supplies it's utilizing systems with precise position information. This is a key point in that precise time without precise position information is useless for many military and civilian applications (e.g., time-of-arrival locating, net synchronization, code validity interval communication security, etc.). GPS is unique in supplying both time and position to the same order of accuracy (102 nSec at the speed of light equals 31 meters) real time, anywhere, and in an operational environment.

TABLE 7  
Practical Example 1

Error Source	Nominal Error Value (nSec, 1 $\sigma$ )	Error Value with Applied Techniques (nSec, 1 $\sigma$ )	
		Ground Terminal	Aircraft
Space Segment Errors	9.6	(0) <sup>8</sup>	(0) <sup>8</sup>
Control Segment Errors	8.6	(0) <sup>8</sup>	(0) <sup>8</sup>
User Errors:			
Ionospheric	7.6	$7.6 \times (\frac{1}{2})^3 \times (\frac{1}{2})^8$	$7.6 \times (\frac{1}{2})^8$
Tropospheric	6.6	$6.6 \times (\frac{1}{2})^3 \times (\frac{1}{2})^8$	$6.6 \times (\frac{1}{2})^8$
Receiver Noise	5	(0.6) <sup>2</sup>	(0.6) <sup>2</sup>
Multipath	4	(0) <sup>1</sup>	(0) <sup>1</sup>
Other	1.7	1.7	1.7
URE (RSS of above)	17.7	5.3	7.3
x TDOP	x1.68	x (1.0) <sup>4</sup>	x 1.68
$\sigma_{GPS}$ Error	29.7	5.3	12.3
$\sigma_{GPS}$ to UTC (USNO)	90.0	(0) <sup>9</sup>	(0) <sup>9</sup>
UE Hardware Errors	37.9	(10) <sup>6</sup>	(20) <sup>6</sup>
<hr/>			
Total Time Error (RSS of Above)	102	11.3	23.5

$$\begin{aligned} \text{Synchronization error between Ground Terminal and Aircraft} &= \sqrt{11.3^2 + 13.5^2} \\ &= 26 \text{ nSec (1}\sigma\text{)} \end{aligned}$$

Note: (x)<sup>n</sup> = value of error when technique n is applied



TABLE 8

Practical Example 2

<u>Error Source</u>	<u>Nominal Error Value (nSec, 1<math>\sigma</math>)</u>	<u>Error Value with Applied Technique(nSec, 1<math>\sigma</math>)</u>
Space Segment Errors	9.6	9.6 ( $\frac{1}{2}$ ) <sup>5</sup>
Control Segment Errors	8.6	8.6 ( $\frac{1}{2}$ ) <sup>5</sup>
User Errors:		
Ionospheric	7.6	7.6 x ( $\frac{1}{2}$ ) <sup>3</sup>
Tropospheric	6.6	6.6 x ( $\frac{1}{2}$ ) <sup>3</sup>
Receiver Noise	5	5 x ( $\frac{1}{2}$ ) <sup>3</sup>
Multipath	4	(0) <sup>1</sup> x ( $\frac{1}{2}$ ) <sup>3</sup>
Other	1.7	1.7 x ( $\frac{1}{2}$ ) <sup>3</sup>
URE (RSS of Above)	17.7	10.3
x TDOP	x 1.68	x (1) <sup>4</sup>
T <sub>GPS</sub> Error	29.7	10.3
T <sub>GPS</sub> to UTC (USNO)	90.0	(6) <sup>7</sup>
UE Hardware Errors	37.9	(10) <sup>6</sup>
<hr/>		
Total Time Error (RSS of above)	102	16 (1 $\sigma$ )

Note: (x)<sup>n</sup> = value of error when technique n is applied

#### REFERENCES

1. NAVIGATION, Journal of the Institute of Navigation, Vol 25, No.2 Summer 1973. A special Issue devoted to Navstar GPS
2. Spilker, J.J. , Global Positioning System, "Signal Structure and Performance Characteristics", The Institute of Navigation, 1980.
3. D.J. Henson, et al., "The Navstar Global Positioning System and Time", Proceedings of the National Aerospace Symposium, Springfield, VA 6-8 March 1979, pp 65-73.
4. "System Specification for the Navstar Global Positioning System", SS- GPS-300B, 3 March 1980.
5. "Navstar GPS Instrumentation and Connector Standards", ICD-GPS-204, 5 June 1981
6. M.D. Yakos and E.H. Hirt, "Time Dissemination Using Navstar Global Positioning System (GPS) Phase IIB User Equipment", Proceedings of the 35th Annual Frequency Control Symposium, Philadelphia PA, (as yet unpublished).
7. K. Putkovich, "USNO GPS Program", Proceedings of the Twelfth Annual PTTI Applications and Planning Meeting, Greenbelt, MD, 2-4 December 1980, pp 387-413.
8. "Navstar GPS Space Segment/Navigation User Interfaces", ICD-GPS-200 (DRAFT), 15 December 1981.

## QUESTIONS AND ANSWERS

MR. EDMUND CHRISTY, Offshore Navigation

Lieutenant, you mentioned that something was going to happen next week or so, and it sounded like "launch", could you repeat that?

LT. KOVACH:

December 10th, NAVSTAR 7 is scheduled to be launched, that's next Thursday. And if we are lucky, everything will go all right.

DR. VICTOR REINHARDT, NASA/Goddard

Just a comment, Councilman at M.I.T. has been building VLBI devices using the GPS signal as noise sources and has been able to do multipath experiments on the picosecond level and he is finding out that the multipath problem is much less than people think due to nearby cars or towers, or things like that. I just wanted to mention that.

LT. KOVACH:

Multipath is typical on a very small level, although in a lot of our tests when we set up the inverted range, which real time computes the net satellite accuracy at Yuma, we found that we had a guide wire holding up one of the posts for the tower. And that was producing three to four meters worth of error, just from that one guide wire. It is kind of a black art situation, you really can't analyze it, you just have to try it and see how it works.

MR. KUHNLE:

When he was here last year, Capt. Doug. Tennant, said something about possibly the CA code might not be available to us sometime in the future, is that really true at this time?

LT. KOVACH:

The Federal Navigation Plan which came out early or late last year, calls for that CA code to be always available to all users. It might not be as accurate as some people would like, but they are like 200 meters CEP.

MR. NORM HOULDING, MITRE

What do you mean by jamming environment? Numerically?

LT. KOVACH:

That value is classified, but let me give you a practical example that you might find enlightening in this regard. It turns out that flying against a jamming field, the power necessary to run that jamming field tells how big the plant would necessarily be, either a hydro-electric plant, or a nuclear power plant. It turns out that the power you need to protect the size of the plant that is needed to produce the power that you are protecting it with, it turns out to be pretty linear. I mean, you have got to go to the big plant just to protect itself, so it can output the power to protect itself, you don't have any surplus power you can use anywhere else.

GPS is very jam resistant especially when combined with a controlled reception pattern antenna, one is able to null jammers and interial navigation systems which provide good benefits.



# A HISTORY AND ANALYSIS OF HYDROGEN MASER RELIABILITY

J. B. Curtright  
Jet Propulsion Laboratory\*  
California Institute of Technology, Pasadena, California

## ABSTRACT

Hydrogen masers are an integral part of the Deep Space Network. Their use provides extremely accurate navigation about the outer planets, as well as precise location of tracking stations. To provide accurate measurements over extended periods of time, reliability of equipment plays an important role. The Deep Space Network has a number of hydrogen masers deployed and in the test cycle, which enables an analysis of reliability of several generations and breeds of construction.

A history and analysis of hydrogen maser reliability are given over a three-year period on several types of masers.

## INTRODUCTION

The Deep Space Network (DSN), operated by Jet Propulsion Laboratory, California Institute of Technology for NASA, requires extremely accurate oscillators and timing systems. Navigation of spacecraft to the outer planets and Very Long Baseline Interferometry (VLBI) require long term accuracies and reliability to obtain precise spacecraft location. To that end, the DSN utilizes hydrogen masers as the precision oscillator. This paper reports the results of several years experience with hydrogen maser reliability in a field environment, and suggests modification and changes that could result in even more reliable oscillator operation.

The DSN consists of complexes located around the globe at approximately 120 degree intervals. The complexes are specifically located near Canberra, Australia, Madrid, Spain and Goldstone, California (about 120 miles from Los Angeles in the Mojave Desert). The complexes consist of one 64 meter parabolic antenna and one each 26 meter and 34 meter parabolic antenna.

\*This paper presents results of one phase of research carried out at the Jet Propulsion Laboratory, California Institute of Technology, under Contract No. NAS 7-100, sponsored by the National Aeronautics and Space Administration.

The 64 meter antenna is considered the prime location for each complex, and the location of the hydrogen maser for that complex. There is at least one hydrogen maser at each complex and at times two, depending upon mission criticality and condition of the hydrogen masers.

## Background

This study compiles data taken from several different types of hydrogen masers, that is, manufacturers and models. Specific names of manufacturers are omitted, as they serve no purpose for this study. As the analysis was taking place, it became evident that all hydrogen masers shared similar if not identical characteristics, therefore, categorizing by the manufacturer is not necessary.

The study considered the following, which will be discussed in further detail below: (1) the population of hydrogen masers in the DSN, (2) length of service of instruments, (3) categories of failures, (4) number of failures in each category, (5) MTBF of each category and total MTBF of all instruments in all categories, and (6) conclusion and recommendations.

## Population of Hydrogen Masers

The population of hydrogen masers used in the study was a total of fourteen. The locations of the masers varied from the field environment at the complexes to laboratory environment at JPL in Pasadena, California.

The data taken on each of the masers was from log books, files and requisitions for repair service and parts. Each maser is assigned a log book when it arrives at JPL, and a file is also maintained as a back-up source of data and as a chronological summary of events for a particular instrument.

Data presented in this study is that which was taken while the instruments were under JPL cognizance, and that which caused or resulted in failure of the units.

## Length of Service of Instruments

A total of 533 months of instrument data is utilized in this study. For the 14 units, an average of 38 months, or more than three years per instrument, is the resultant data base. The longest instrument history in this study is 72 months and the shortest is seven months. Two instruments were under study for 54 months.

The 533 months of instrument history represents over 44 years of hydrogen maser data, which is believed to be the largest and longest data base on maser reliability in the industry.

### Categories of Failures

Two major categories of failures became evident as data was gathered and segregated. A major contribution to failure was the VACION pumps that are used to pump the hydrogen gas from the system. All other failures were classified as OTHER, and include Autotuners, Power Supplies, Heaters and external Magnetic Fields.

The VACION pump failures consisted of two modes and totaled 21. The first type, arcing, is caused by "whiskers" growing on the titanium elements, which in turn cause temporary high voltage arcs. This indication is prevalent in older pumps and contaminated elements; that is, elements that may contain impurities in the titanium.

The second type of VACION pump failure is that which is a total short of the elements. This usually happens, again, in the older elements.

In all cases above, the eventual or immediate action was to replace the VACION pump elements. To replace the elements, the maser must be taken off line and major disassembly of the instrument is required to get to the pump elements. The maser must then be turned back on, allowed to stabilize, calibrated and put back on line. The Mean Time To Repair (MTTR) for this type of failure is 1.8 months. It must be noted, however, that the MTTR has lessened in the past two years and is now taking slightly less than 1.5 months. The reason for the MTTR being less is because more is known about the systems and procedure utilization.

The Mean Time Between Failures (MTBF) of the 21 hydrogen masers VACION pumps is slightly more than 25 months. Therefore, one would expect to have a replacement approximately every two years, taking about six weeks to repair and regain on line performance. This result is considered to be less than adequate, in particular the MTBF. A possible solution to the problem is addressed in more detail later in concluding remarks.

In the category of "Other Failures," a total of 12 were accounted for. Those failures are of the electronic type, such as Power Supply failures, Autotuner not reacting, changes in Magnetic Field Compensation and Heater failing. On only two occasions was the hydrogen dissociator found to be low or contaminated.



The reliability factor of the electronics parts of the masers is very satisfactory. With a MTBF of 44.5 months, the apparent useful time of a maser in service for four years is about 3.7 years, including the MTTR of 1.5 months.

The indications are that with an MTBF of 44.5 months and a MTTR of 1.5 months for the electronic components, the physics portion of the Hydrogen Maser is more susceptible to failure, and possibly could prosper from indepth research.

#### Reliability of Total Instrument Population

By combining the MTBF numbers for the VACION pump and all other failures, a total of 33 failures ensues. With the 533 month history of the 14 Hydrogen Masers, a totl MTBF of slightly more than 16 months evolves, with the accompanying MTTR of 1.7 months. It is easily recognized that the 21 failures of the pumps seriously impaired the usefulness of the instruments. Assuming the electronics and pump were equally reliable, one could expect to use a maser for nearly two years without failure, with a repair time of just over 1.5 months. This in itself improves the over all reliability by 6 months.

#### Conclusion

The data base implies that the Hydrogen Maser is vulnerable from a reliability stand point, from VACION pump failure, causing a very low MTBF. When the pumps were first utilized, a 4 year MTBF was advertised by the manufacturer. The first elements were in fact more reliable than the current product, which implies a very fast degradation in the element usefulness in the past 3 to 4 years. We must explore a more reliable pumping process or possibly consider lower source pressure or better quality products from the element manufacturer

It is entirely possible that the titanium plates are manufactured with a contaminant. A close Quality Control by the manufacturer could eliminate early pump failure. Also, the manufacturer could impose very stringent requirements on the supplier of titanium used during element manufacture.

Another possibility would be to refit the instruments with chemical filter pumps, which are passive. A test instrument should be utilized and tested for all known possible failure conditions with chemical pumps. It is proported that if chemical pumps were used, two could be placed in the instrument and switched in and out as required without disrupting maser performance. The advent of this configuration could strongly enhance the current reliability figures presented in this paper.

Maser manufacturers must seriously consider improving the overall performance of Hydrogen Masers. The initial costs as well as maintenance costs and reliability, are not conducive to high performance systems in todays market. A MTBF of 36 months would entice possible users of masers, and reduce maintenance costs as well as time lost due to failures.

The history and analysis of the data presented indicates that a concerted effort be made by manufacturers to improve the reliability of the Hydrogen Maser VACION pump process. All other operations of instruments appear to be adequately reliable to serve its users in a reliable manner.

## QUESTIONS AND ANSWERS

DR. VESSOT:

I think your observations are quite valid insofar as those pump elements are concerned. There is something squirrely going on, either the metallurgy is suffering, or we are doing something we don't know about when we replace pump elements.

It is not likely that we are doing worse than we were before, we are being cleaner and more careful. So, I think it points to the fact that the titanium, as we receive it in the form of pump plates is different now than it was before.

MR. CURTRIGHT:

You mean the titanium as it is placed on the elements or the titanium prior to the placement on the elements?

DR. VESSOT:

Well, generally speaking, the material would be available in sheet form, it is chopped into plates. First, we don't know what alloy is being currently used or what grade of titanium -- there is a great demand for titanium and it seems to be rather difficult material to get.

So, what is happening now, I suspect, is that they are using whatever they can.

Secondly, the chief supplier of the pump elements moved his plant and I suspect his processing may have changed.

MR. CURTRIGHT:

I wonder if it might be advisable to look into some quality control, or quality assurance to the activities they have. I wonder if that would help?

DR. VESSOT:

That might.

Dick Sydnor has initiated an assaying of the material to see what impurities there might be in the metal itself, which I think is a very valid route to take.

As for the hydrogen, I honestly believe that the hydrogen that we have now is as good as it was before. We pass it through palladium diaphragms which are traditionally one of the best means of purifying hydrogen. So that much I think is out.

As far as sorption methods are concerned, I believe that is the way of the future. In the distant past, and we launched a clock that would run for -- Michele Tetu was in on the test, it must have been back in 1976, but clocks had run for a year effectively on a single sorption cartridge made by the SAES company in Italy.

This technology is, I think, becoming better and we will be hearing more of this tomorrow and later in the work that has been done here at the Naval Research Lab.

This technique is that of a sponge-like material that just selectively absorbs hydrogen and you have to cope with the non-hydrogen species with a different pump. And fortunately, for us, we are working on just such a pump to retrofit the clocks that we have now in the field.

MR. CURTRIGHT:

I understand.

One of the problems I see is that when we first went into the vacation world we were led to believe that they were off the shelf items and there was no problem in getting the material, and all sorts of swell things. And I don't want to get into the same situation with the sorption pumps, where we are led to believe that this is an off the shelf item and there is no problem in replacing them, and all of a sudden we see them end up in the canoe that we are in today, with the vacation pumps.

DR. VESSOT:

Well a lot can be avoided if you are willing to inventory a fair amount of spare parts. You can't expect these companies to do so because the volume, as you have shown us, is not a very large volume. Nobody is going to get rich supplying titanium to ion pump makers.

So, I suspect that in this rather competitive economy right now, your best bet is to hedge the market and go into the metals -- this is a strategic metal, I think it is probably not a bad investment -- get it in the form of pure plates an eighth of an inch thick and see what happens. It could be better than some other investments that have been suggested.

MR. CURTRIGHT:

Definitely. Thank you.

MR. PETERS:

I think there is an obvious solution to the finite lifetime of pump elements in hydrogen masers. And this is because of developments in state selection and redesign of the overall system. It is quite clear that we can operate with the factor of at least 10 lower beam flux and therefore -- and also a pump that operates at a lower flux has much longer lifetime, does not have the sputtering problem that a pump that operates at a high flux.

We can and I am giving a paper on it later, so I won't carry on at this time -- state select much more efficiently, use less hydrogen and get more power out of a maser if we modify the beam trajectory and the overall design slightly.

MR. TOM ENGLISH:

I just wondered if you had some, at least rough idea, of what the hydrogen load on your pumps was in moles per year, or some other appropriate units? And, also, specifically, what pumps did you use on your devices?

MR. CURTRIGHT:

The pump elements are Perk and Elmer, eight-element pumps and it is a 200 liter per second pump we are using. How many moles we use per year? I don't have that information with me.

DR. REINHARDT:

Just a comment on the pump problem. We have seen similar results with the varian triode pumps, so I don't think it is manufacture unique. That points to the fact that it is the titanium that everybody is getting.

FIELD OPERATIONS WITH CESIUM CLOCKS  
IN HF NAVIGATION SYSTEMS

E. H. Christy and D. A. Clayton

OFFSHORE NAVIGATION, INC.  
P. O. BOX 23504  
HARAHAN, LOUISIANA 70123

ABSTRACT

For over 10 years, Offshore Navigation, Inc. (ONI) has operated and maintained networks of HF phase comparison marine navigation stations employing cesium clocks. The largest permanent network is in the Gulf of Mexico where some fourteen base stations are continuously active and others are activated as needed. As these HF phase comparison systems, which operate on a single transmission path, require a clock on the mobile unit as well, the ONI inventory consists of upwards of 70 clocks from two different manufacturers.

The maintenance of this network as an operating system requires a coordinated effort involving clock preparation, clock environment control, station performance monitoring and field service.

EQUIPMENT CONFIGURATIONS

The ONI ACS (Atomic Clock Systems) network is comprised of the base stations shown in Figure 1. In addition, other networks may be established temporarily in various coastal areas of the U. S. and elsewhere around the world as required by the on-going search for energy. Each of these base stations is comprised typically of a CW transmitter driven by a synthesized signal generator locked to a cesium standard. As shown in Figure 2 provision is included for automatic transmitter switchover should that unit fail, and battery backup to keep the CS standard alive during power failure. These base stations are situated in locations that have all degrees of access, from easy to difficult, including offshore platforms.

The mobile station configuration, also shown in Figure 2, is comprised of a Cs clock and synthesizer providing local phase reference to a narrow band receiver. The mobile equipment also has battery backup provisions for the clock. The oven is not generally necessary as the equipment is frequently in the conditioned equipment room of the vessel.

The clock environmental chamber (oven) is actually an insulated plywood box fabricated at ONI. Equipped with a thermostatic heater the temperature of the clock inside is maintained at about  $38 \pm 3^{\circ}\text{C}$  ( $100 \pm 5^{\circ}\text{F}$ ), somewhat above ambient. Early base station huts were uninsulated and the higher temperature was what could be maintained easily. Figure 3 shows a picture of the oven and Figure 4 is a typical base station hut.

Sixteen roving technicians, seven on call at all times, are strategically located from Florida to Mexico to perform normal maintenance and emergency repairs. Additionally, a helicopter is continually available for service calls to offshore platforms.

#### CLOCK TYPES AND PREPARATION

ONI employs clocks manufactured by both HP and FTS. The model type and age distribution of these is broken down according to the following table:

<u>TYPE</u>	<u>DATE PURCHASED</u>	<u>QTY</u>	
HP 5061A	1970	1	
	1971	7	
	1972	7	
	1973	3	
	1974	18	
	1975	6	
	1978	3	
	1979	<u>4</u>	49
FTS 4000	1979	<u>2</u>	2
FTS 5000	1980	<u>12</u>	12
FTS 4050	1980	6	
	1981	<u>8</u>	14
			<hr/>
	TOTAL COMPLEMENT		77

Prior to their deployment, clocks are rated in-house for a minimum of 24 hours and, frequently, 48 hours to observe their general stability and suitability for field use. Any clock whose last service record is 3 months or more old is subjected to a routine series of electronic checks at various test points. These readings are written down and kept as part of that unit's record.

At installation time on board ship, the clock is rated by the navigation operator against the navigation net. Final adjustments to the C-field are made at that time and the clock is left undisturbed throughout the voyage, usually 14 days. A typical seismic operation may last from one, to many such voyages.



## BASE STATION PERFORMANCE MONITORING

Base station performance is monitored by two land-based "mobile" stations equipped with strip chart recorders, each station looking at a different section of the net. Note that absolute accuracy is not important; it is only necessary that the net maintain zero relative drift of one station with respect to another. The transmission monitoring here is basically across land at 1700 kHz so one can expect to see substantial short term variations in recording during the course of a day. These may be due to skywaves, weather fronts, etc.

Efforts are made to observe these recordings at regular times every day and thereby ascertain relative drift, if any. It is believed that the 24 hour observations can reliably detect errors of .05 lane (25 nanoseconds) of one station with respect to the "master". At present, when this amount is reached, a technician is dispatched to the station to make a C-field adjustment.

Newly installed clocks require close attention for about two weeks. Thereafter the average clock will remain within plus or minus 2 one hundredths of a lane (10 nanoseconds) without requiring a C-field correction for 6 to 12 months. Adjustments to the beam current, second harmonic content, and control voltage are performed once every 3 to 6 months.

Plans are being made to implement a semi-automatic clock adjustment scheme. This scheme employs "phase microsteppers" such as the Austron 2055A which can be remotely controlled over telephone or radio linkages to implement step/drift corrections as small as  $10^{-5}$  nanoseconds.

## FIELD PERFORMANCE SUMMARY

Of the 49 active standards 12 have thus far undergone tube replacement at ONI. Additionally there have been 5 warranty repairs effected at HP. Figure 5

lists the dates of purchase and replacement together with the approximate months of tube life realized (non-warranty). Over one-half of the clocks dating from 1974 or earlier are still performing with original tubes. Thus our average realized tube life is significantly greater than the 74.6 mos average service life of the failed tubes.

By way of comparison we find the HP standard easier to service and more universally understood by our field operators. The FTS standards are more difficult to repair but they come with a 5 year warranty and appear more temperature-stable. We have no quantitative data to present in that regard, however.

In our experience the parts which fail most often in the HP unit are listed below in order:

1. 5 mHz oscillators
2. operational amplifier      A9
3. synthesizer                      A1
4. multiplier                      A3
5. oven controller

Troubles with the FTS units appear primarily power supply related. Since all FTS units are in warranty, no failure records are on hand.

Several aspects of clock operation and maintenance are perhaps peculiar to our operating environment and will be described here briefly.

Recently HP has recommended higher C-field levels attendant to operating with the higher Zeeman frequency of 53 kHz as opposed to the older 42 kHz. Though there may be some improvement in stability with this modification the C-field adjustment resolution is

decreased to  $8 \cdot 10^{-14}$  from its present  $5 \cdot 10^{-14}$ . ONI thus would run the risk of having field operators make improper C-field adjustments depending upon whether or not their particular clock had been modified. This we have chosen not to do as there were plenty of mistakes made some years ago when the C-field resolution was again changed by HP.

A common occurrence in shipboard operations is the switching of ship's generators on-line. This action frequently results in severe power surges of the AC line. As the 5061A oven control operates from the unregulated supply voltage it is a frequent casualty in the mobile systems.

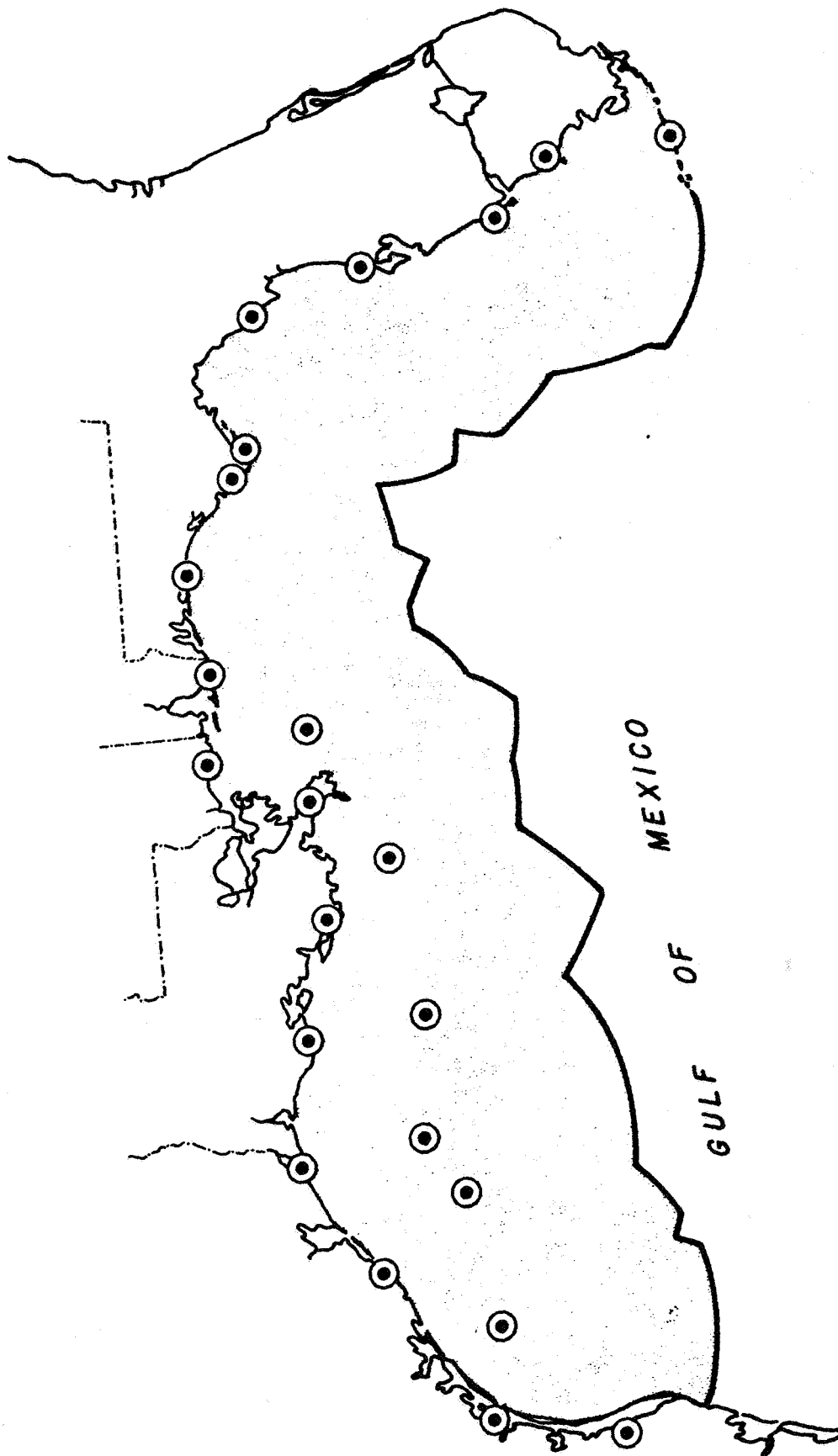
All clocks have been equipped with Sonalert audible alarms indicating power or logic failure. This will alert the mobile operator immediately, even if he is in a noisy environment, as he cannot always observe the clock itself.

We have had several instances wherein the standard was stored without power for extended periods. In these cases, with the ion pump inoperative, tube leakage can become so great that subsequent operation is impossible. In two cases of roughly six-months inadvertent storage, the tubes were unrecoverable.

In a third case the standard was a casualty of a severe fire aboard ship, the insides and outsides of the instrument becoming charred and fire blackened. The unit was subsequently dismantled and left in pieces around the shop for over a year while the technicians worked to refurbish it in spare time. The Cesium tube was reinstalled in the refurbished unit and rejuvenated with a high voltage power supply. That unit is now fully functional and serves as our in-house standard.

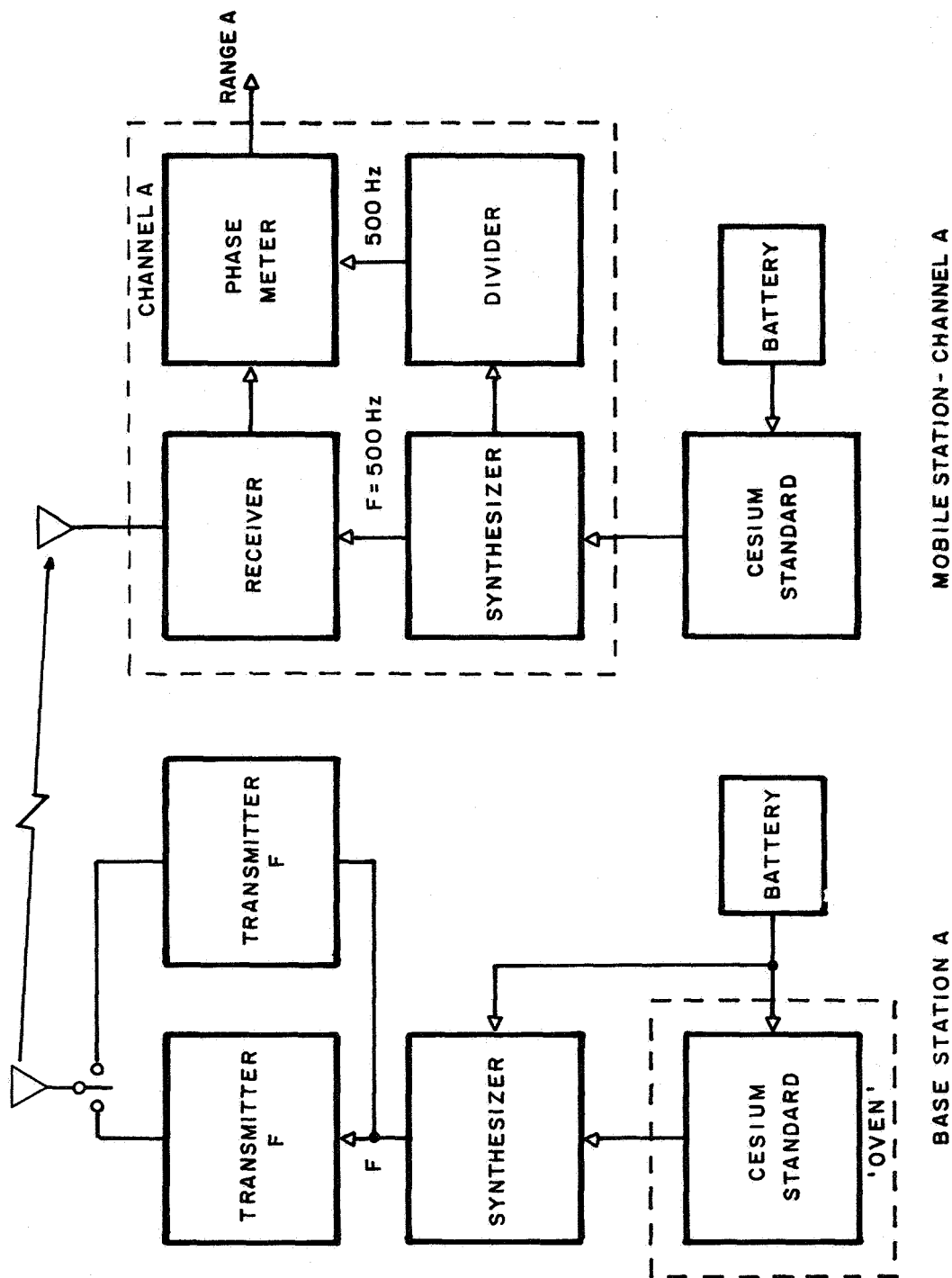
### Summary

The Cesium standard has proven to be a reliable component in providing a system of navigation not achievable by other means to date. Whether or not GPS receivers can perform as reliably and economically remains to be determined. With it's complete in-house service capability, ONI will be maintaining it's clocks for years.



ON I 24 HOUR MICROPHASE COVERAGE  
Figure 1

● BASE STATION



ONI ACS EQUIPMENT CONFIGURATION  
Figure 2

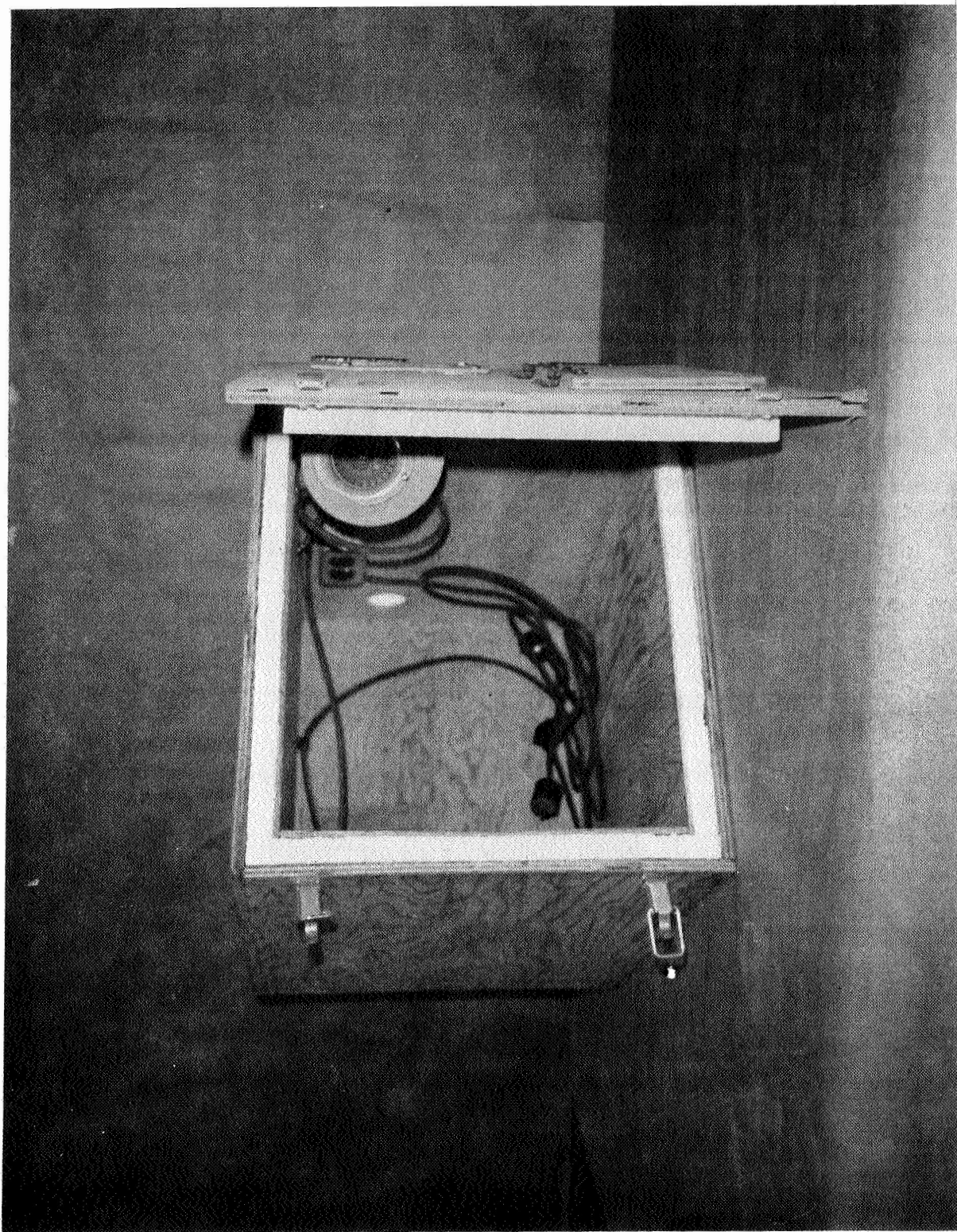


FIGURE 3

THERMOSTATICALLY-CONTROLLED OVEN FOR Cs STD.



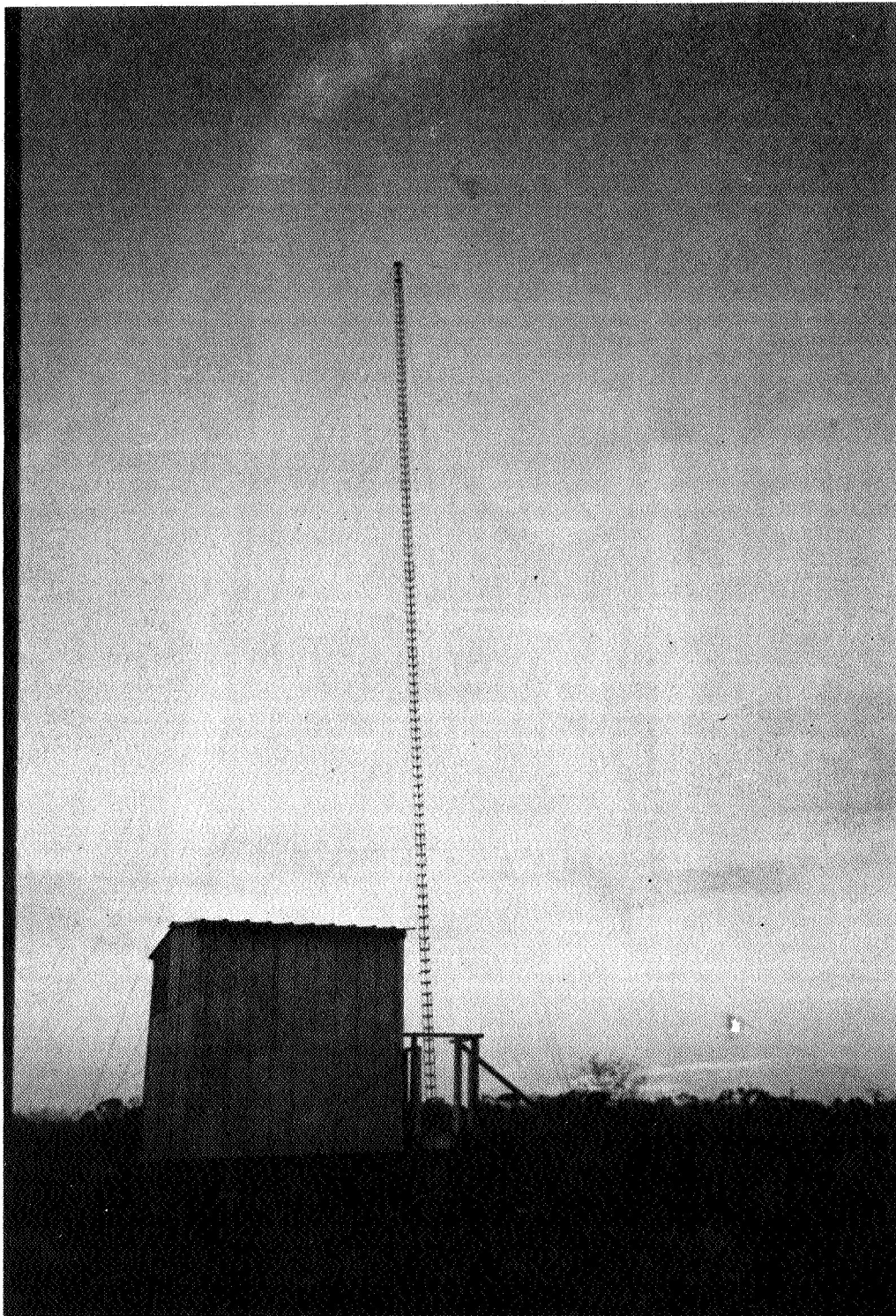


FIGURE 4

TYPICAL REMOTE BASE STATION INSTALLATION

<u>UNIT #</u>	<u>DATE/PURCH</u>	<u>DATE/REPL</u>	<u>No. Mos.</u>	
007	12/13/71	09/24/81	117	
009	10/01/71	07/28/75	46	
011	04/05/72	06/12/81	110	
014	07/06/72	04/08/80	93	
015	08/03/72	08/16/78	72	
016	11/10/73	09/02/81	94	
017	11/10/73	05/20/76	30	H.P. WARRANTY
020	02/01/74	09/27/79	67	
021	02/01/74	06/25/80	76	
022	02/01/74	10/25/76	32	H.P. WARRANTY
023	02/01/74	06/20/80	76	
024	02/01/74	11/08/77	45	H.P. WARRANTY
025	02/01/74	12/09/76	34	H.P. WARRANTY
025		07/17/79	31	
029	04/30/74	02/16/79	58	
031	05/08/74	02/14/77	33	H.P. WARRANTY
031		11/19/81	55	
		AVERAGE	74.6	

# CESIUM BEAM TUBE REPLACEMENT SUMMARY

FIGURE 5



## QUESTIONS AND ANSWERS

DR. LESCHIUTTA, Torina, Italy

Two questions, one your CW positioning system, is it similar to DECCA? Is the CW system hyperbolic?

MR. CHRISTY:

Well, some CW systems are hyperbolic. In fact, DECCA offers one and there was a system hyperbolic rated which was CW. But, no, this is the technique called Rho-Rho or Range-Range. So you carry your reference with you, that is why you take a clock along on the mobile unit.

DR. LESCHIUTTA:

The second one, how do you cope with the skywave signal?

MR. CHRISTY:

The skywave signal in high frequency navigation systems cannot normally be coped with, you cope with it by simply not going out that far, past 130 nautical miles at nighttime.

And that is true of virtually all high frequency base comparison navigation systems by any manufacturer.

## HIGH ACCURACY OMEGA TIMEKEEPING

Edward A. Imbier  
Smithsonian Astrophysical Observatory  
Cambridge, Massachusetts

### ABSTRACT

The Smithsonian Astrophysical Observatory (SAO) operates a worldwide satellite tracking network which uses a combination of OMEGA as a frequency reference, dual timing channels, and portable clock comparisons to maintain accurate epoch time. Propagational charts from the U.S. Coast Guard OMEGA monitor program minimize diurnal and seasonal effects. Daily phase value publications of the U.S. Naval Observatory provide corrections to the field collected timing data to produce an averaged time line comprised of straight line segments called a time history file (station clock minus UTC). Depending upon clock location, reduced time data accuracies of between two and eight microseconds are typical.

### INTRODUCTION

The purpose of this report is to provide a user's report on maintaining high quality time using OMEGA transmissions. This approach has evolved through the years taking accuracy, cost, reliability and quality of reference signals, and ease of time reduction into account. The equipment and timekeeping methods used to keep at least 6 microsecond reduced epoch time at two somewhat remote sites from the standpoint of precise time availability is the subject of this paper. The two sites are both located in South America, one at Natal, Brazil and the other at Arequipa, Peru.

### SAO SATELLITE TRACKING NETWORK

Since 1957, the Smithsonian Astrophysical Observatory has operated a network of astrophysical observing stations

to provide satellite observations in support of evolving scientific programs in geodesy, geophysics, celestial mechanics, the upper atmosphere, and earth and ocean dynamics. These came under NASA sponsorship in 1957. In geodesy and geophysics, the data acquired by the network of satellite tracking stations has been used to develop accurate mathematical models of the earth's size, shape, and gravity field.

#### THE OMEGA NAVIGATIONAL NETWORK

Maintained by the U.S. Coast Guard, a network of eight transmitting stations in the VLF frequency band provides location information to a certainty of 1 to 2 nautical miles with some correctional data. This OMEGA network provides near global coverage. All stations transmit five frequencies which are time sequenced during a ten second interval, each frequency being broadcast in a pattern for about one second each. In this way only one of the eight OMEGA transmitters operates on a particular frequency at a time. Using a time sequenced receiver, individual transmitter locations and frequencies may be selected for navigational or frequency reference use. Each OMEGA transmitter site is referenced to UTC and is maintained to UTC to better than 2 microseconds by portable clock trips and one-way phase measurements between OMEGA transmitter sites. Thus, OMEGA transmissions have proved to be quite valuable in maintaining a continuous frequency reference for a timekeeping system, especially where other time reference signals such as Loran-C and TV time techniques are unavailable.

#### THE TIMING SYSTEM

Fundamental to a satellite tracking operation where range and positional data is taken is time and frequency. All tracking stations have a timekeeping system to provide epoch time data for each satellite observation. Since these sites are usually many hours by car and airplane from a time and frequency laboratory, utmost precautions have been taken to maintain continuous epoch and frequency signals for the tracking site. To insure the site be self-sufficient for as long as possible, a dual timekeeping system was provided to guard against loss of epoch time due to signal interruptions or equipment malfunctions. In addition, a battery backup

system capable of withstanding a power blackout of up to two days is included (in the event that even the electric generator is not operational). For instance, it is not unusual for local power to be interrupted in Peru at least twice per week.

Figures 1 and 2 show the make up the timing system. At the present time a satellite receiver and a Loran receiver are not in either South American sites. In the main timing channel a cesium frequency standard is used. In the other redundant channel a rubidium is sufficient. A high frequency receiver is included to verify epoch to the millisecond level. An OMEGA receiver in each timing channel selects a different OMEGA station, one which is also monitored by the U.S. Naval Observatory. Duplicate time accumulators are used in the main timing channel. Digital phase shifting circuitry permits timing epoch adjustments in 0.1 microsecond steps. Crystal oscillators are running in case of any timing channel oscillator failure. In addition, an OMEGA monitor receiver is used to provide data to the global OMEGA transmission model being generated by the US Coast Guard, as well as provide a backup for the other OMEGA receivers on site. This monitor is capable of receiving transmissions from eight transmitter sites at three different frequencies each.

#### TIMEKEEPING METHODS USING OMEGA

In order for OMEGA to be used for timekeeping, a clock trip to the site is necessary to initialize the timekeeping system and the OMEGA receiver. The OMEGA receiver must have all of its divider chains reset. A reference value of phase shift from the master clock set coincident to UTC must then be determined. A propagation correction chart calculated from a worldwide OMEGA transmission model for the tracking site is used to determine the GMT that has the least variation seasonally. The PPC chart, so called, is available from the U.S. Coast Guard and is shown in Figure 3 for Peru. Also a PPC chart is needed to check the seasonal variation of the OMEGA phase as received by USNO for the frequency and transmitter site used. Strong diurnal phase shifts occur during transition from night to day along the OMEGA transmission path from the transmitter to the receiving site. A GMT time for making OMEGA reading is best during the middle of an all night time or all daylight transmission path. Also a choice of an OMEGA station which is oriented so that the transmission path is in a

North-South orientation provides the longest reliable reading time. That is why the Peru site uses the OMEGA transmission from North Dakota and the Brazil site uses an Argentina transmission. Data from both timing channels is recorded twice per day during the selected best GMT times. Since the OMEGA transmitter site is maintained very closely to UTC(USNO), the propagation phase corrections as recorded by USNO are factored into calculating the final reduced epoch data usually about one month after the fact.

#### WHAT CAN GO WRONG

Timekeeping using OMEGA as a reference has proved to provide rather troublefree service for periods of about two months. Problems can result from the following occurrences:

- Clock jumps or malfunctions at the tracking site
- Cycle jump due to a low signal or storm
- Drift in the main channel oscillator
- Drift or step in the OMEGA transmitter relative to

UTC

- Station off air

Most of these circumstances may be dealt with without any loss in timekeeping uncertainty, especially where the servo controlled OMEGA receiver may be slewed or reset to previous setup reference values.

#### RESULTS OF THE BRAZIL AND PERU TIMEKEEPING SYSTEMS

See figures 4 and 5 for the received phase values for Brazil and Peru.

Data for the past year from May, 1980 to May, 1981 is provided in table 1.

All data is long term averaged and straight line segments are assumed to produce a time line relative to UTC.

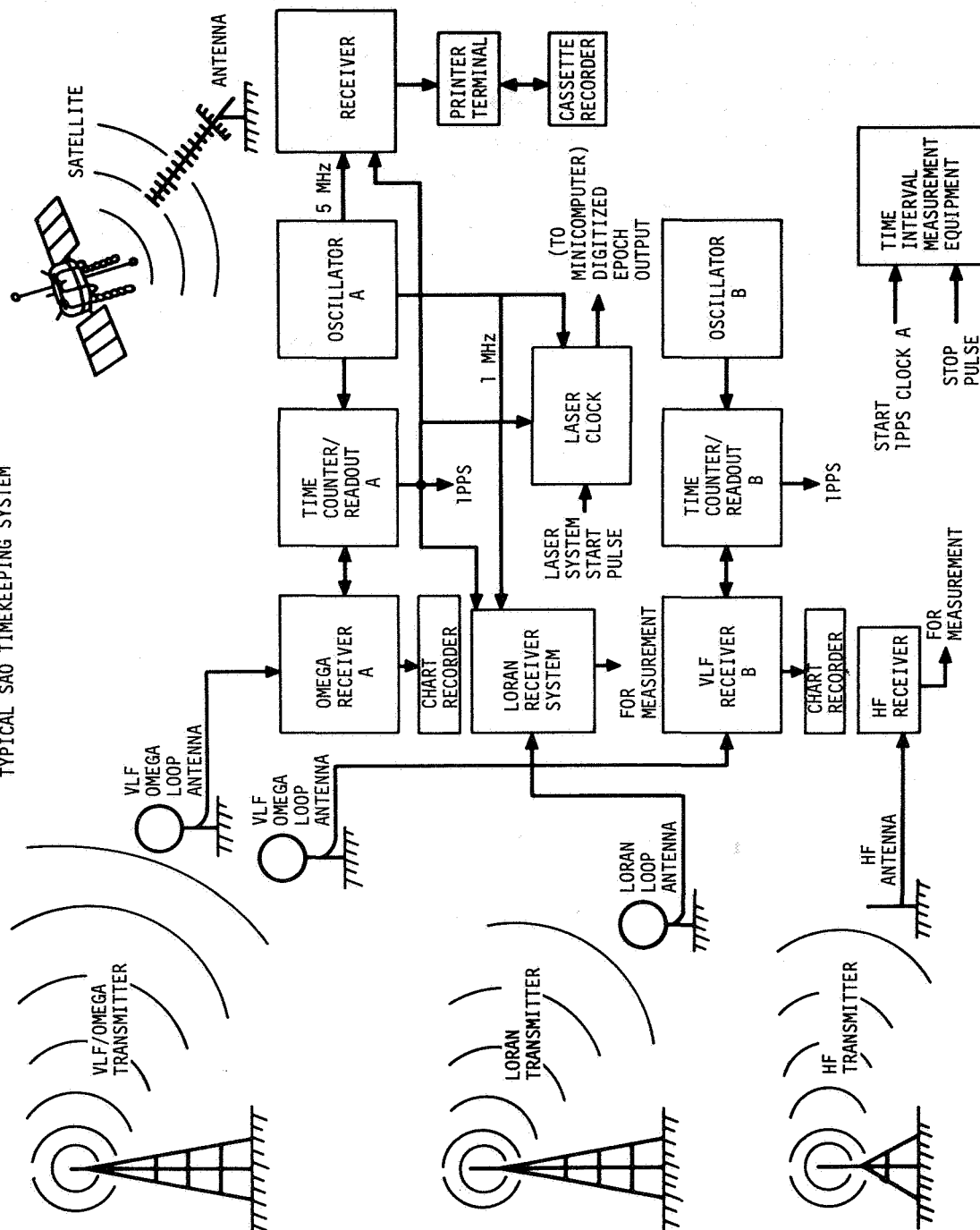
#### CONCLUSIONS

OMEGA as a timekeeping reference has proved to be very reliable and accurate to 2 to 8 microseconds for the SAO sites in South America. When the timing uncertainty becomes greater than 6 microseconds, a clock trip would be planned other than the yearly clock check. However, this

has rarely been necessary for maintaining time to the five microsecond level.

It is anticipated that the range tracking accuracy will improve threefold next year due to improvements in laser pulse width and higher pulse repetition rate. Then a greater timing accuracy will be required, perhaps better than what OMEGA can provide. Then for the short term more clock trips will be necessary and the clock trip fuse perhaps set for an uncertainty of 4 microseconds will have to be adopted until an alternative improved timing reference is adopted. GPS, high accuracy spread spectrum Nova/Transit, or a devoted satellite such as proposed by Dr. Vessot of SAO (orbiting maser) are possibilities to make this improvement. (I would like to thank the US Coast Guard ONSOD branch for their assistance.)

FIGURE 1  
TYPICAL SAO TIMEKEEPING SYSTEM



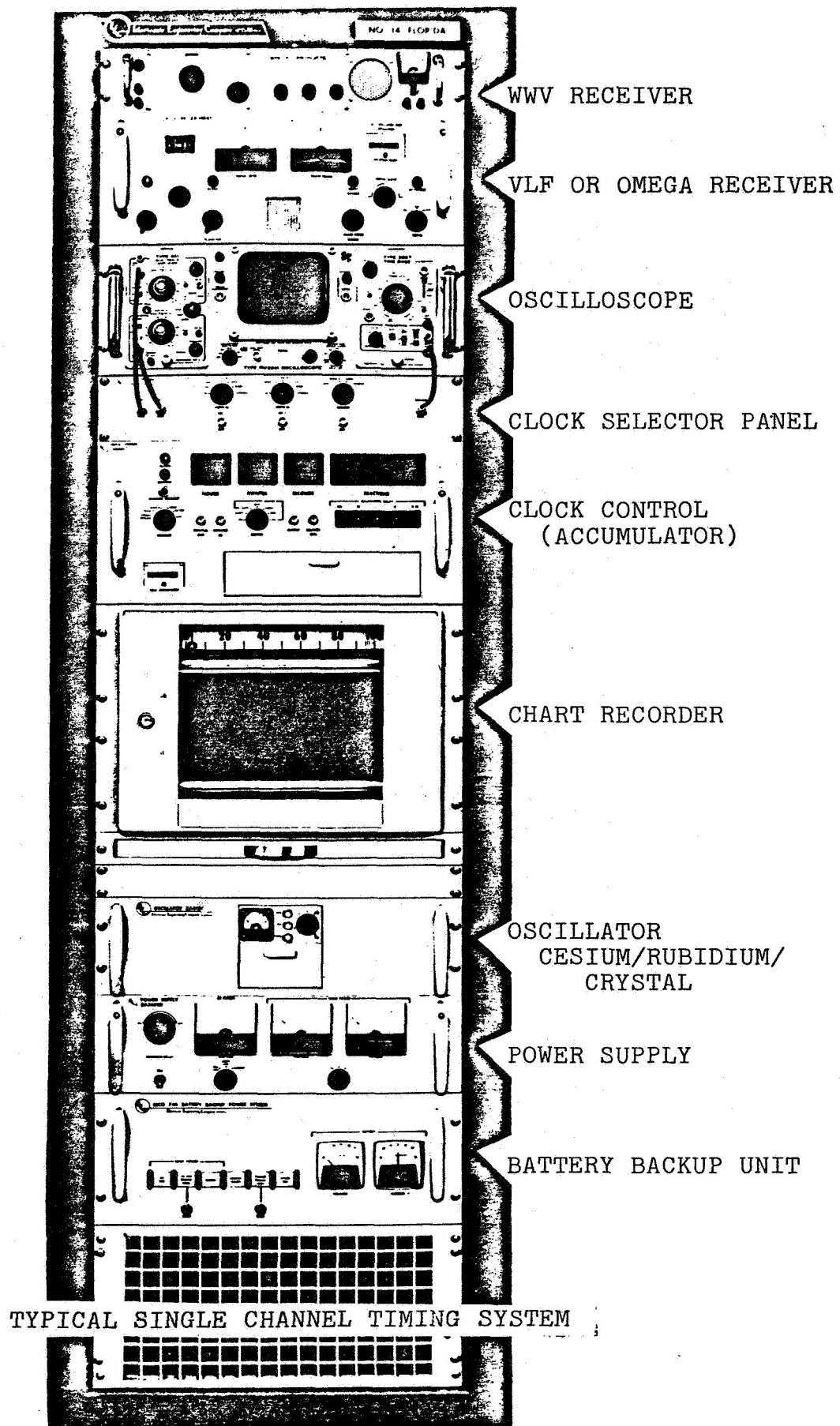


FIGURE 2.



13.6 KHZ OMEGA PROPAGATION CORRECTIONS IN UNITS OF CECS

**ALL DAY**

FIGURE 4. TIME DRIFT REPORT      September, 1981  
                                  Natal, Brazil  
                                  SAO Tracking Site

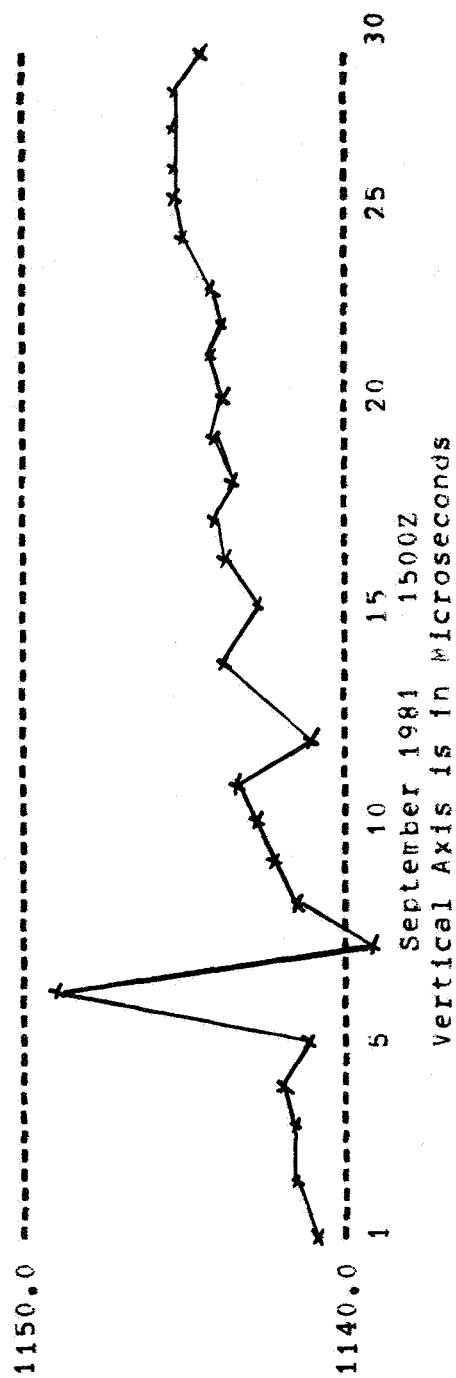


FIGURE 5: TIME DRIFT REPORT September, 1981

Arequipa, Peru  
SAC Tracking Site

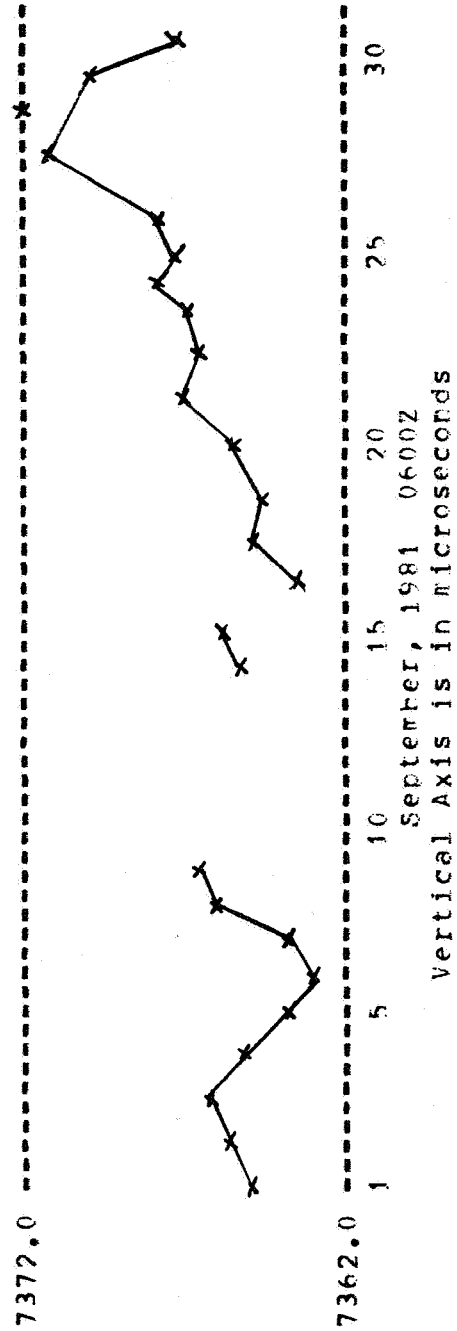


TABLE 1. SAG NETWORK TIMEKEEPING STATUS  
for July 1980 thru May 1981

STATION	REDUCTION PERIOD		STAT - UTC	REDUCTION UNCERTAINTY
BRAZIL	JUL 1	DEC 31, 80	-4 TC 16	3 TC 5
	JAN 1	FEB 9, 81	13 TC 19	3
	FEB 9	MAY 1, 81	-6 TC 0	3
	EXCEPT JULY 15		3 TC 16	22
	JULY 22		-64628	64630
PERU	JUL 1	DEC 31, 80	-9 TC 19	2 TC 3
	JAN 1	JAN 17, 81	19 TC 24	4
	JAN 17	MAY 1, 81	-8 TC -2	4 TC 5



TIME INFORMATION DISTRIBUTION  
AT WHITE SANDS MISSILE RANGE

R. A. Stimets, Jr.  
Timing Division  
U.S. Army Communications Command  
White Sands, White Sands Missile Range, New Mexico

ABSTRACT

At White Sands Missile Range (WSMR), there are several hundreds of instruments and instrumentation sites which require some type of "range time" information to allow correlation of the data they collect.

The instruments and sites are scattered over the 4000 square mile area of the Range. The requirements range from visual indications of range time to the nearest second to time of year to within tens of microseconds. The requirements for an individual user (instrument or site) may vary from mission to mission. Since the Timing System supports an average of seven missions a day and since users may frequently move from site to site over the Range, the goal for Timing at WSMR has been established as having the capability to meet the most stringent requirements at any site on the Range.

This paper presents the methods used by the WSMR Timing System to meet these Requirements. Also included is an analysis of the effectiveness of these methods for some critical instrumentation systems at the Range.

(ABSTRACT ONLY)

PAPER NOT PRESENTED



RELATIONSHIPS BETWEEN U.S. NAVAL OBSERVATORY, LORAN-C  
and  
THE DEFENSE SATELLITE COMMUNICATION SYSTEM

Laura G. Charron  
U.S. Naval Observatory  
Washington, D.C.

ABSTRACT

Department of Defense (DoD) Directive 5160.51 of 31 August 1971 states that "All DoD components ... refer time and time interval to the standards established by the (U.S. Naval) Observatory." To obtain the required traceability, the most widely used system for time dissemination has been the navigational system of the U.S. Coast Guard - Loran-C. When the only chain available for timing was the East Coast chain, monitored by the Observatory, there was no problem in publishing comparisons of that chain to the U.S. Naval Observatory's Master Clock (USNO MC) with a fair degree of reliability. By 1981, however, thirteen chains, covering a substantial portion of the Northern Hemisphere, were in use. The question of how the time comparisons were to be obtained, the chains calibrated, and the results published for chains not directly monitored by USNO then arose.

During this same period, the number of links permitting time transfers point-to-point over the Defense Satellite Communication System (DSCS) were being expanded. In addition, at some selected sites, Loran-C monitoring equipment was installed. It was now possible to have values of USNO MC - DSCS Monitoring Site and thus to be able to determine USNO MC minus Loran-C.

This paper addresses, in general terms, the methods used in forming time scales for distant sites monitoring Loran-C. Particular emphasis will be given to the time transfers obtained via the DSCS and on how the data provided by this system is used to calibrate these remote time scales. The errors involved will be discussed.



INTRODUCTION: Closely related to the U.S. Naval Observatory's (NAVOBSY) basic mission of providing astronomical and time data to all "who avail themselves thereof" are the additional functions imposed by DoD Directive 5160.51 of 31 August 1971. The imposition of these functions required (1) an upgrading of the Master Clock system, (2) improvement in distribution services and (3) an expanded means of maintaining traceability to USNO MC.

The upgrading included such items as purchase of additional cesium clocks, improved Data Acquisition and Control (DAC) systems - an IBM Series 1 and a Hewlett-Packard 1000 - installation of better environmental chambers and improved algorithms for the formation of the USNO MC time scale. To improve the distribution services, an increased number of Time Service Announcements were made available. More than 1000 pieces of mail are now distributed weekly. This mail service is supplemented by telephone voice announcements and more recently (albeit on an experimental basis) by the Digital Data Access System (1,2). Traceability to the USNO MC, for the greatest number of users, is still provided by the Loran-C system maintained by the U.S. Coast Guard. During the period 1967-1981, NAVOBSY expanded the Loran-C timing information it provided to the user community. From providing data only for the East Coast chain, monitored at NAVOBSY, the differences between USNO MC and thirteen Loran-C chains are now routinely published. The body of this paper will deal with how these daily relationships are determined (in particular for the distant chains) and how these relationships are calibrated.

NAVOBSY MONITORING SITE: Presently NAVOBSY monitors four Loran-C chains. These chains are the Northeast USA (9960), the Southeast USA (7980), the Great Lakes (8970) and the East Coast of Canada (5930). The daily times of reception from several receivers for each of the four chains are collected, the delays subtracted, and the values averaged by the HP1000 DAC. This information is then published. By using these data and measurements from monitoring sites (Table 1) which contribute to the NAVOBSY data base, relationships between USNO MC and more distant chains are determined and published. For example, the U.S. Coast Guard station at Cape Race, Newfoundland provides the daily difference between the East Coast of Canada (5930) and the North Atlantic (7930) chains. By a simple calculation, then, of  $USNO\ MC - LC/5930$  plus  $LC/5930 - LC/7930$  one obtains  $USNO\ MC - LC/7930$ . This procedure continues for other eastern chains.

A difficulty arises in this 'linking' - seasonal effects as large as one microsecond have been seen in propagation path delays at NAVOBSY. These effects will be reflected in Loran-C data where 'linking' is used. Some recent analyses by Monger (3) of the U.S. Naval Observatory Time Service Substation (NOTSS) confirmed the earlier propagation studies by Charron (4). In Figure 1 the differences  $USNO\ MC - NOTSS$  via the Southeast USA chain are plotted. It appears that the NOTSS time scale changed in fre-

quency with respect to USNO MC. This change, however, is deceptive - it is not a change in the NOTSS time scale (which was calibrated through portable clock visits during this period) but instead is due to a change in the propagation path delay between NAVOBSY and Carolina Beach, NC, a transmitting station of the 7980 chain.

PRECISE TIME REFERENCE STATION (PTRS), according to Ref. 5, "by agreement, maintains at least one atomic clock coordinated with the NAVOBSY Master Clock; is linked to the NAVOBSY via portable clock and at least one other high precision time transfer technique; can transfer time with a precision of 100 nanoseconds...". These stations, having been established for their own organizational requirements, are all independent of one another and of NAVOBSY. Only by agreement do they transmit data to NAVOBSY. Even though NAVOBSY has no official control of the operation of these stations, the data received from them provides another method of providing comparisons between USNO MC and a Loran-C chain. NAVOBSY adopts the daily values of USNO MC - PTRS (as determined by the PTRS) and its monitored Loran-C data. This is what is done for the West Coast USA (9940) and the West Coast of Canada (5990). Frequent portable clock visits are the means used to calibrate the PTRS, and thus these Loran-C chains. That portable clock visits alone are insufficient for calibration may be seen in the fact that discontinuities as small as 0.3 microsecond and as large as 1.5 microseconds have been reported in the Time Service Announcements Series 4. The discontinuities or jumps seen in Figure 2 are not due to changes or discontinuities at the Loran-C station but are due to undetected frequency changes in the PTRS time scale. Since both chains are dependent upon the same PTRS, any error in the calculation at the PTRS will be seen as discontinuities in both chains. In developing the method of remote time scale determination of Loran-C, a comparison of the values as calculated at the PTRS (and then published by NAVOBSY) and those values obtained using the remote time scale were examined (Figure 3). As can be seen in this plot, each jump that occurred in the Series 4 data brought the values of USNO MC - LC/9940 (as published) into agreement with those obtained using the time scale method.

REMOTE TIME SCALES: Farther west, greater difficulties are encountered in determining daily values of USNO MC - Loran-C chains, namely, the Central Pacific (4990), the Gulf of Alaska (7960), the Northern Pacific (9990) and the Northwest Pacific (9970). Dependence upon a PTRS, calibrated through frequent portable clock visits, is not practical. The distance and resulting costs may allow only yearly trips. The method now used to obtain values for these chains - to a greater or lesser degree - consists of forming a time scale for each Loran-C chain using the average of a number of atomic clocks which will be more uniform and stable than any clock contributing to the time scale.

To implement this approach for a particular chain, a search is made of the pertinent data bases (Table 2) to locate the required data which in-

cludes approximately 18 months of daily Loran-C measurements from as many monitoring sites as possible and several portable clock measurements made at the different sites at different times during that period.

From these data, a delay (sum of delays from propagation path, receiver, antenna, etc) is determined for each site. A series of straight lines then gives values of USNO MC - Site for all sites. The measurement, Site - Loran-C, minus appropriate delay are added to the USNO MC - Site values. This allows one to obtain a comparison of USNO MC - Loran-C via each site. These individual values are then averaged to form a MEAN and the difference between the individual values and the MEAN is calculated. As necessary, new series of straight lines are determined so that the individual values of USNO MC - Loran-C agree with the MEAN to within some specified tolerance. Values of USNO MC minus each Site are calculated using the MEAN value of USNO MC - Loran-C. These values must agree with the values obtained by portable clock measurements. In this reiterative process, it is assumed (a) that the cesiums used for measurements are 'free-running', that is, that none are, for example, steered to follow the published values of Loran-C and (b) that cesiums will not spontaneously change, by the same amount, in time and/or frequency simultaneously.

Once a time scale is formed for an individual chain, a great deal of judgement must be exercised in continuing the process. What has changed with respect to what must be decided (rate correlation)? Did a cesium at a particular monitoring site change frequency? Did one or more fail? Were some adjusted, replaced or removed? These are recurring questions and must be dealt with as each new piece of information is received. Current data from more than one site are always needed but seldom obtained. The continued accuracy of the chain is maintained by reliance upon the occasional clock trip and time transfers from DSCS terminals.

DEFENSE SATELLITE COMMUNICATION SYSTEM (DSCS): Thus far, the only means of calibrating the Loran-C chains mentioned has been portable clock visits to some monitoring sites. However, the trips are infrequent, costly and the measurements made are also subject to error. Examples include incorrect identification of site, of cesium/measured reference, of date/time, and/or start/stop pulse. In addition, during the trip, changes of the portable clock in time and/or frequency with respect to USNO MC are not uncommon. In Figure 4, values of USNO MC minus PC1368 as collected by the DAC before and after a portable clock trip are plotted. If an extrapolation of the frequency offset was used in determining USNO MC minus - Site during the trip, an error as large as 0.300 microsecond could have resulted.

A second means of calibration is possible by use of the DSCS. By the mid-1970's, time transfers between earth terminals were being regularly performed. The differences between the cesiums at each terminal, as deter-

mined from the time transfers, were regularly transmitted via teletype to NAVOBSY and became part of a data base. (Reference 6 details the procedures used in processing these data.) Some terminals were either monitoring Loran-C or had a connection via cable/portable clock to a monitoring site (Figure 5). Such was the case at Elmendorf AFB, AK.

Prior to 1979, the Precise Measurement Electronics Laboratory (PMEL) at Elmendorf AFB acted as a PTRS, described earlier, for the Northern Pacific (9990) chain. (Data for the untimed Gulf of Alaska (7960), although monitored by PMEL, was not used by NAVOBSY.) Transmitted to NAVOBSY were (a) the daily measures of the LC/9990 and the LC/7960 chains, (b) the daily intercomparisons of on-site cesiums and (c) the weekly portable clock measurements between PMEL and the satellite terminal (ELM).

At the same time NAVOBSY also received the time transfer data between the Elmendorf (ELM) satellite terminal and the Ft. Detrick, Md (FDS) terminal. One, therefore, had

	USNO MC	-	FDS	via TV line 10	
+		FDS	-	ELM	via time transfer
-		PMEL	-	ELM	via portable clock visits
	USNO MC	-	PMEL		

By adding the on-site intercomparisons to this value, a relationship between USNO MC and all of the on-site cesiums was obtained.

A time scale, as described earlier, was formed for each PMEL cesium and an averaged value of USNO MC - LC/9990 and USNO MC - LC/7960 was calculated. It was noted that the averaged determination of USNO MC - LC/9990 not only did not agree in time but that the frequency offset differed (Figure 6). It was decided that publication of data for this chain would be suspended temporarily and that a portable clock team knowledgeable in Loran-C operations would visit Elmendorf AFB as soon as possible. The trip was made in December 1978. A thorough examination of sites at PMEL and ELM and also at a NASA site in Fairbanks, AK was made. Delays in the monitoring systems were calibrated. It was found that the Loran-C determinations via the time scale, calibrated by using the weekly DSCS time transfers, were accurate. Since then, the values published in Time Service Announcement Series 4 have been determined in this manner. In addition, the 7960 chain was set on time and publication of USNO MC - LC/7960 began. In Figure 7, the values determined using the time scale are plotted. The DSCS time transfers, used as calibration points, also are seen. The differences between USNO MC and the cesiums at the PMEL, calculated via the remote time scale and a recent portable clock measurement, agreed to within 0.090 microsecond.

The combination of remote time scales and time transfers is a very useful tool. Besides being routinely used in Alaska for the 9990 and 7960 chains, it is also now used for the 9970 chain and to some degree for the 4990 chain.

In determining the feasibility of this method for Loran-C timing and for possible further applications, a time scale also was formed for the 9940 chain. The MEAN, or averaged value, of USNO MC - LC/9940 was used to determine the relationship between NAVOBSY and the National Bureau of Standards (NBS). In Figure 8, values of USNO MC - NBS via (a) 9940 Loran-C time scale, (b) portable clock measurements, (c) DSCS time transfers and (d) Bureau International de l'Heure (BIH) are plotted. It appears that there is some seasonal effect on the order of 0.5 microsecond in the values obtained using the BIH Circular D data.

**CONCLUSIONS:** Each method of determining the relationships between USNO MC and Loran-C and each method of calibrating that relationship is subject to possible error. Dependence upon one data point, whether it be a portable clock measurement, a DSCS time transfer or a Loran-C measurement, can result in erroneous conclusions. In Figure 9, a means of relating Loran-C chains to each other and USNO MC through DSCS terminals and some strategically located monitoring stations (nodal points) can be seen. The expansion and strengthening of the relationships shown can only serve to improve traceability to USNO MC for those users of Loran-C.

More extensive use of remote time scales and greater correlation of the information contained in the data bases make possible:

- 1) Better determinations of USNO MC - Loran-C and thus better world-wide synchronization for those users of Loran-C
- 2) Better determination of time and/or frequency changes in the cesiums at distant sites. It is possible to resolve ambiguities in data. Use of remote time scales provides information necessary to respond quickly to requirements for cesium adjustments at DSCS terminals.
- 3) Improvements in total delay determinations.
- 4) Some monitoring of portable clock behavior in the field.
- 5) Further studies of seasonal and annual terms in propagation path delays.
- 6) Further studies of the relationships between international time scales (USNO, NBS, BIH, etc).

**Acknowledgements:** I wish to thank Dr. R. Glenn Hall, retired Chief of Scientific Operations, for the many discussions and suggestions over the years. I also wish to thank the following members of the Astronomical Programs and Data Analysis Branch for their assistance - R.E. Keating, P.E. Lloyd, E. Bermudez and C.F. Lukac.

#### REFERENCES

1. Time Service Announcement, Series 14, No. 27, 23 June 1980, "Telephone Time Service Announcements".
2. Winkler, Gernot M.R., "The U.S. Naval Observatory Data Services", Proceedings ISOSO 81, November 1981, New York, New York.
3. Monger, Donald, "NOTSS Clock System", Time Service Memorandum, 10 July 1981
4. Charron, Laura G., Internal Memorandum, 10 September 1978.
5. Operating Procedures Precise Time and Time Interval Equipments, NAVOBSY - TS/PTTI SOP 81.
6. Fisher, Laura Charron, "Precise Time and Time Interval Data Handling and Reduction", Proceedings of the Fifth Annual Precise Time and Time Interval (PTTI) Applications and Planning Meeting, December 1973, Washington, D.C.

TABLE 1

## REPRESENTATIVE SAMPLE of MONITORING STATIONS

7970 <u>NORWEGIAN SEA</u>	7980 <u>SOUTHEAST USA</u>	7990 <u>MEDITERRANEAN SEA</u>
OP FRANCE	NAVOBSY	OP FRANCE
HP SWITZERLAND	NOTSS RICHMOND, FL	HP SWITZERLAND
ON SWITZERLAND	AGMC NEWARK AFS, OH	ON SWITZERLAND
NPL ENGLAND	WHITE SANDS MISSILE	IEN ITALY
RGO ENGLAND	RANGE, NM	RGO ENGLAND
NAVSECGRU SCOTLAND		NAVSECGRU ITALY
8970 <u>GREAT LAKES</u>	9960 <u>NORTHEAST USA</u>	9990 <u>NORTH PACIFIC</u>
NAVOBSY	NAVOBSY	PMEL ELMENDORF
	NOTSS RICHMOND, FL	NASA FAIRBANKS
	AGMC NEWARK AFS, OH	SHEMYA AFB, AK
	NBS BOULDER, CO	*DSCS ELMENDORF

\*INDIRECT MEASURE

TABLE 2

## U.S. NAVAL OBSERVATORY DATA BASES

INTERCOMPARISONS OF CESIUM CLOCKS	NAVOBSY TIME SCALES
OMEGA MEASUREMENTS	SATELLITE TIMING INFORMATION (DSCS, TRANSIT)
LORAN-C MEASUREMENTS	UTC(BIH) - UTC(i)
REMOTE TIME SCALES FOR MONITORING SITES	EARTH ORIENTATION PARAMETERS (UT1, POLAR COORDINATES)
PORTABLE CLOCK REDUCTIONS	ASTRONOMICAL OBSERVATIONS

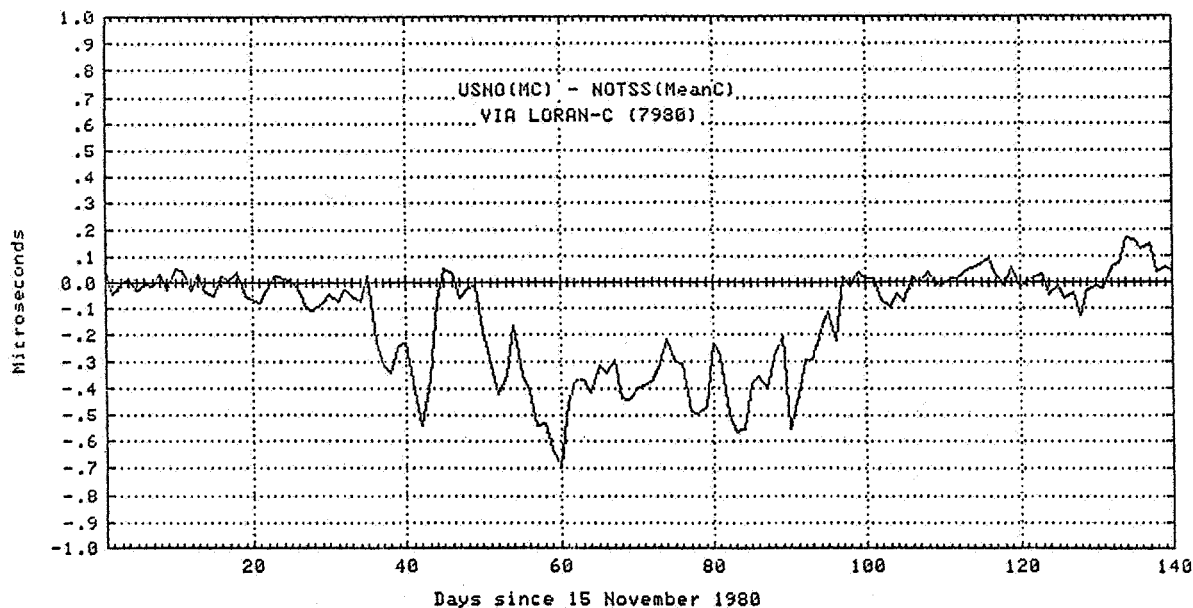


FIGURE 1

COMPARISON OF USNO MC - NOTSS  
via 7980 Loran-C

The change of approximately 0.4 microsecond seen in this figure from Reference 3 is not due to changes in the time scale at NOTSS but, rather, is due to the seasonal effect on the propagation path delay between USNO and the transmitting station of the 7980 chain.



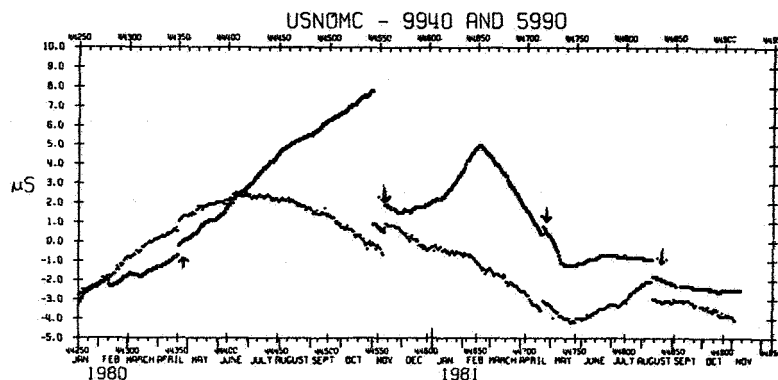


FIGURE 2

These are the published Series 4 values for the 9940 (darker trace) and the 5990 chains. The discontinuities (marked by arrows) seen in both chains occur after portable clock calibrations of the PTRS which determine the values for these chains.

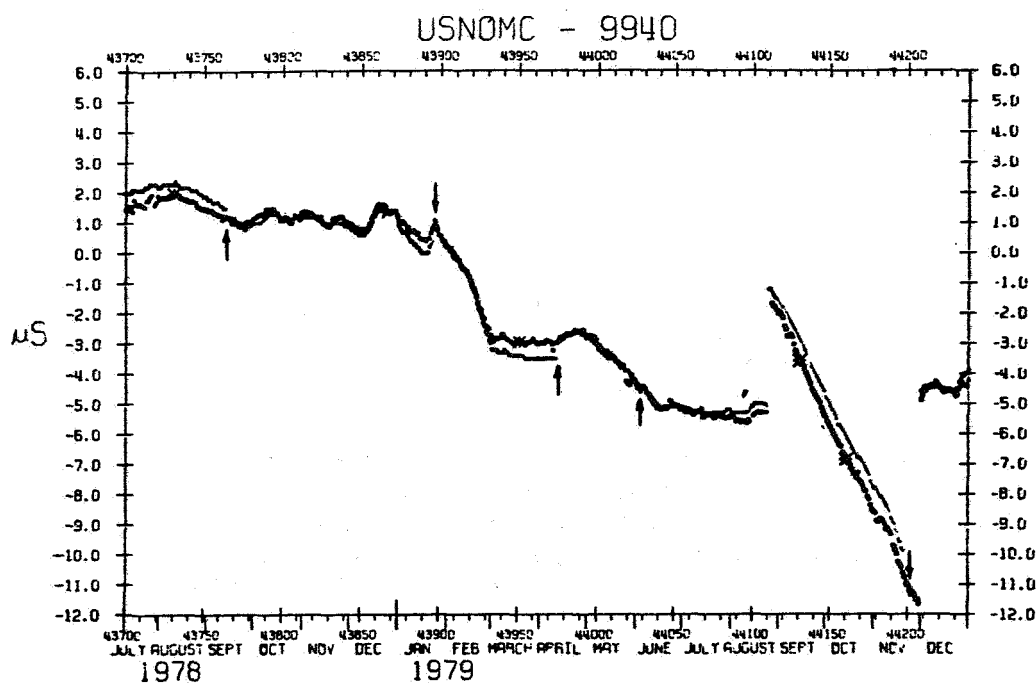


FIGURE 3

The heavy tracing is composed of the averaged values obtained using the time scale reduction method. The second trace consists of the values which were published in Series 4 obtained using the PTRS procedure. The discontinuities, marked with an arrow, are the results of portable clock calibrations at the PTRS. Note that after each discontinuity, the Series 4 values become co-incident with the time scale values.

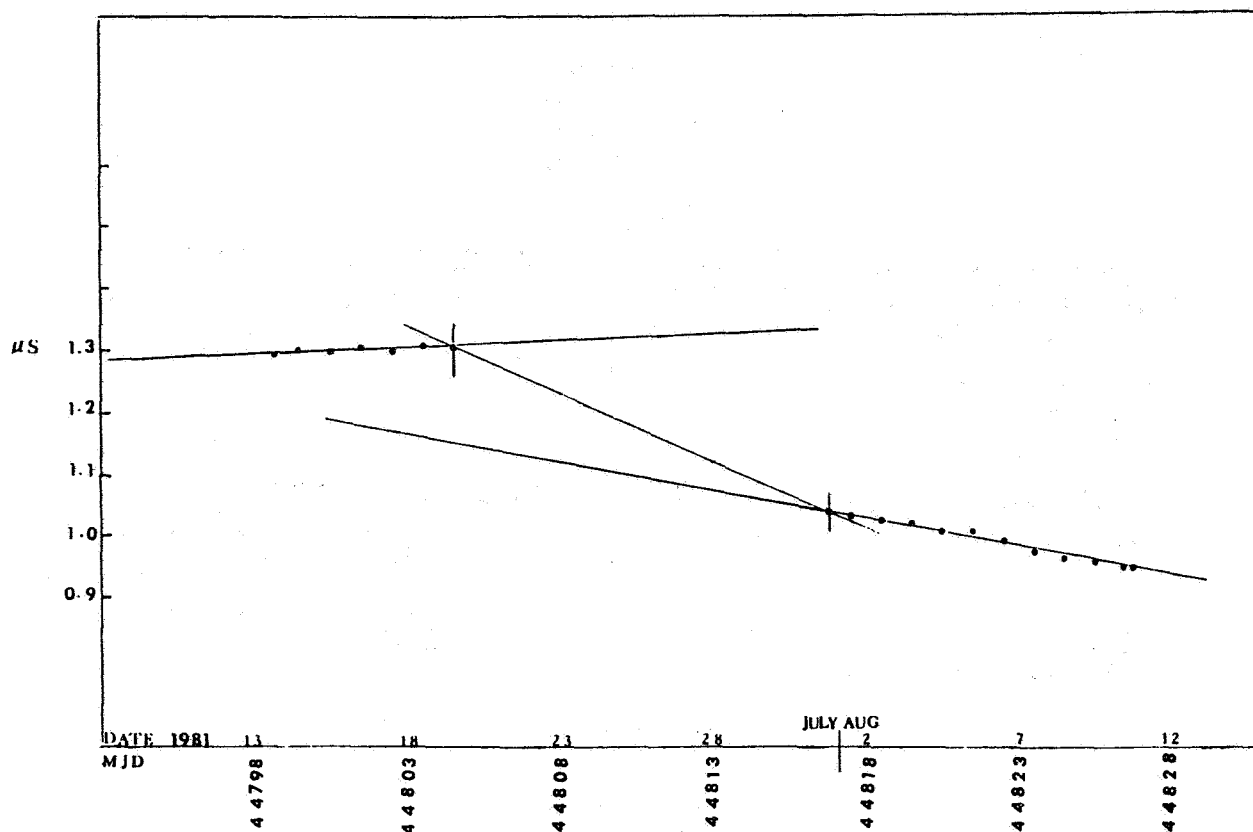
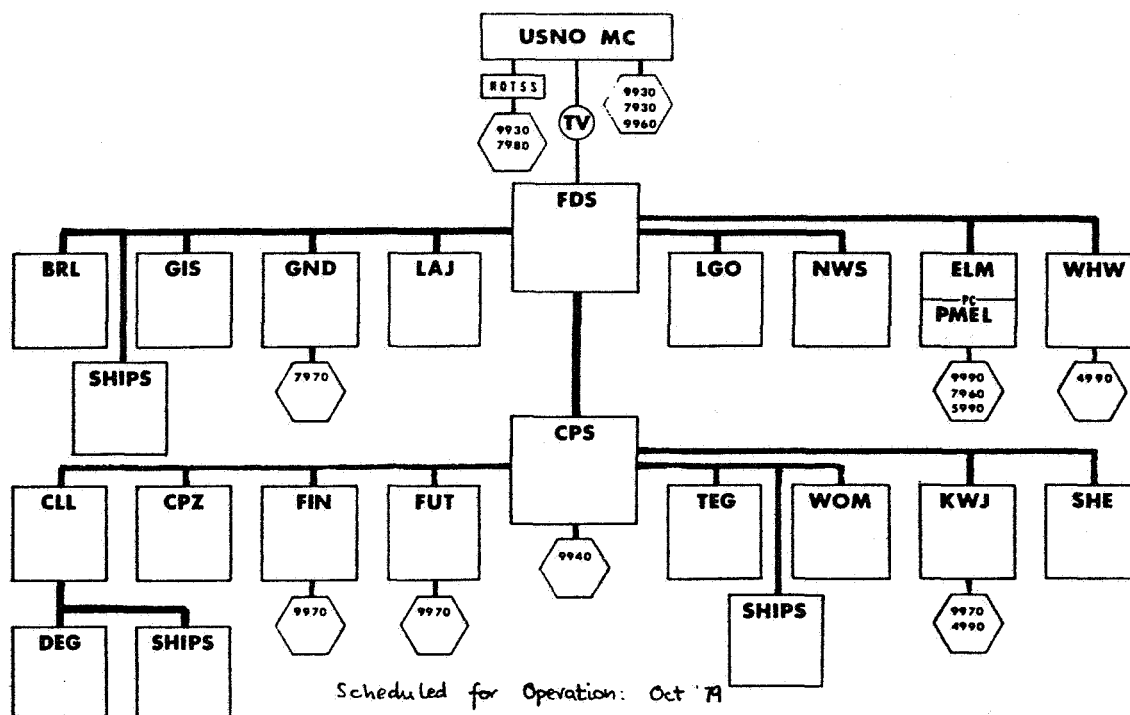


FIGURE 4

COMPARISON: USNO MC - PC1368  
Trip of 13 July - 10 August 1981

The DAC system collected these data before and after a recent portable clock trip. Time and/or frequency change(s) occurred: such changes are not uncommon.



Croughton, UK  
Sunnyvale, CA

FIGURE 5

# HIERARCHY OF TIME TRANSFERS PERFORMED BY THE DSCS TERMINALS

FDS	FT. DETRICK, MD	CLL	CLARK AFB, PHILIPPINES
BRL	BERLIN, GERMANY	CPZ	CP ZAMA, JAPAN
GIS	GUANTANAMO BAY, CUBA	FIN	FINEGAYAN, GUAM
GND	LANDSTUHL, GERMANY	FUT	FUTEMA, OKINAWA
LAJ	LAJES AFB, AZORES	TEG	TAEGU, KOREA
LGO	LAGO DI PATRIA, ITALY	WOM	WOMERA, AUSTRALIA
NWS	NORTHWEST, VA	KWJ	KWAJALEIN, MI
ELM	ELMENDORF AFB, AK	SHE	SHEMYA, AK
WHW	WAHIAWA, HI	DEG	DIEGO GARCIA
CPS	CP ROBERTS, CA		

USNO MC	U.S. NAVAL OBSERVATORY MASTER CLOCK
NOTSS	NAVAL OBSERVATORY TIME SERVICE SUBSTATION, RICHMOND, FL
PMEL	PRECISE MEASUREMENT ELECTRONIC LABORATORY, ELMENDORF AFB, AK
TV	CHANNEL 5 WTTG WASHINGTON, D.C.
◇	LORAN-C CHAINS

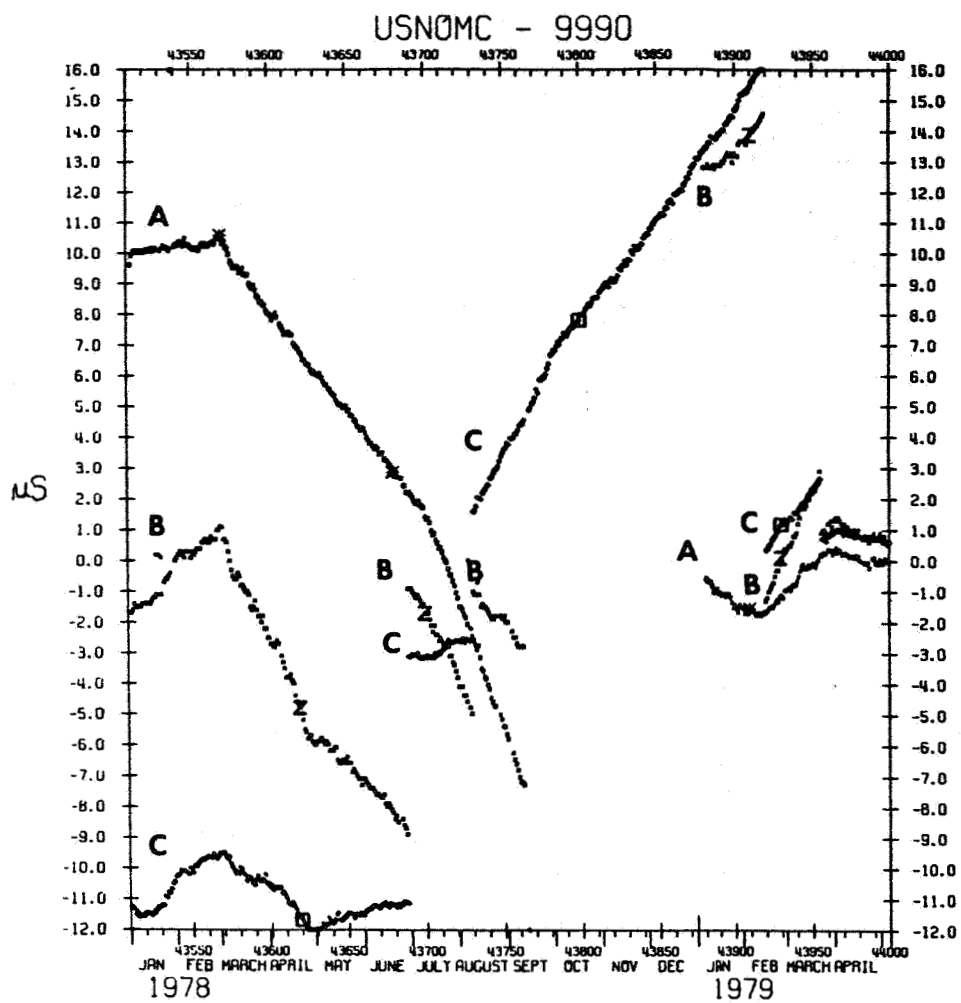


FIGURE 6

The trace labelled, A, is the difference between values determined a PTRS (Trace B) and those obtained from the time scale method (Trace C).

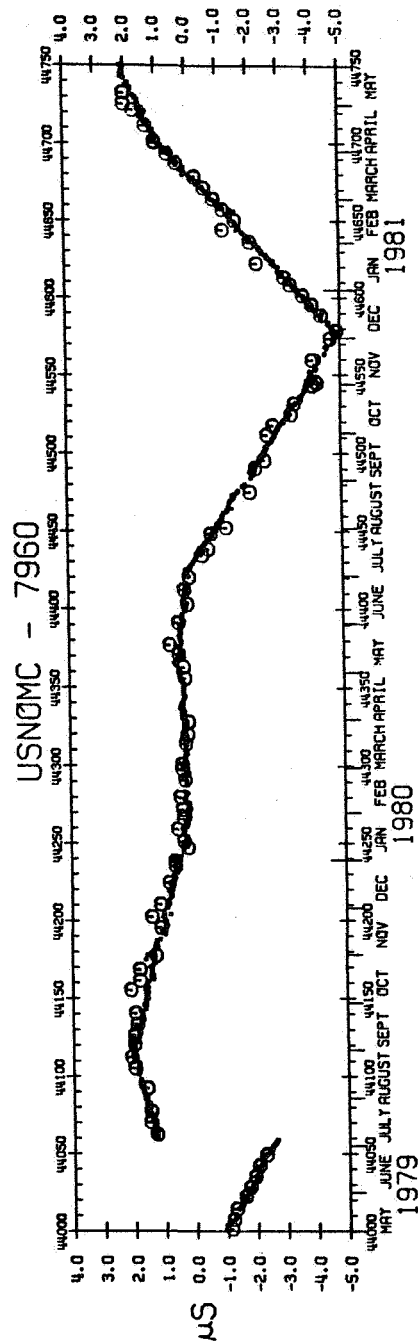


FIGURE 7

After the portable clock calibration discussed in the text, the 7960 chain was set on time and the values published since that time are those determined using the time scale method. The large symbols are calibration points obtained using DSCS time transfers.

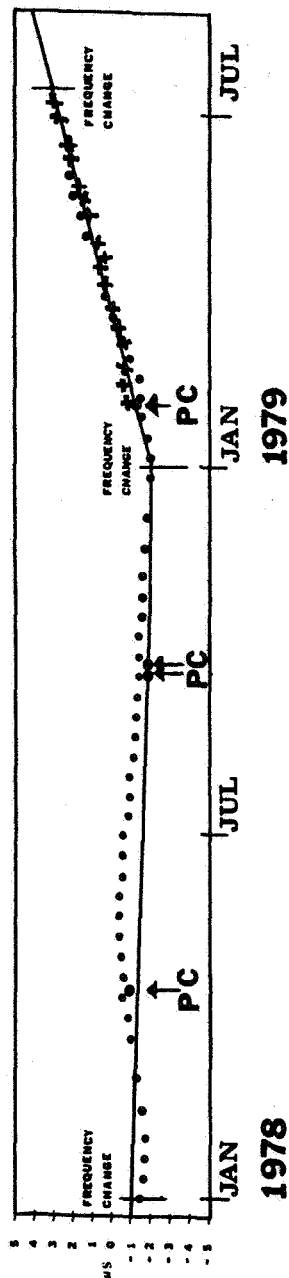


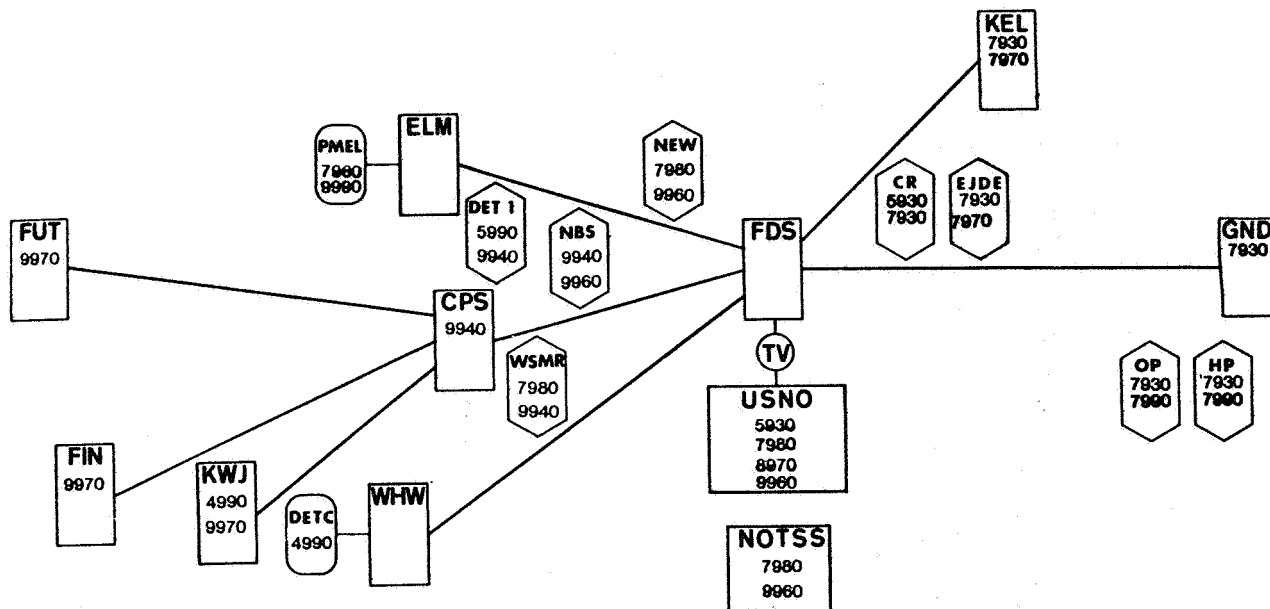
FIGURE 8

USNO MC - NBS

Four methods of determining the relationship USNO MC - NBS have been plotted:

- a) VIA A TIME SCALE - SOLID LINE
- b) VIA PORTABLE CLOCK - INDICATED BY ARROWS
- c) VIA BIH CIRCULAR D - DOTS
- d) VIA DSCS TIME TRANSFER - INDICATED BY + SIGNS

The frequency changes indicated were those made in the NBS time scale.



**RELATIONSHIPS: USNO, LORAN-C, DSCS**

FIGURE 9

#### DSCS TERMINALS

FUT	FUTEMA, OKINAWA
FIN	FINEGAYAN, GUAM
KJW	KWAJALEIN, MI
WHW	WAHIAWA, HI
ELM	ELMENDORF AFB, CA
CPS	CP ROBERTS, CA
FDS	FT. DETRICK, MD
KEL	KEFLAVIK, ICELAND
GND	LANDSTUHL, GERMANY

#### NODAL POINTS

DET1	FAIRCHILD AFB, WA
WSMR	WHITE SANDS MISSILE RANGE, NM
NBS	NATL BUREAU OF STANDARDS BOULDER, CO
NEW	AEROSPACE GUIDANCE METROLOGY CENTER, NEWARK AFS, OH
CP	U.S. COAST GUARD, CAPE RACE, NEWFOUNDLAND
EJDE	U.S. COAST GUARD, EJDE, FAEROE IS.
OP	PARIS OBSERVATORY, PARIS, FRANCE
HP	PTRS - HEWLETT-PACKARD CO. GENEVA, SWITZERLAND

USNO	U.S. NAVAL OBSERVATORY, WASHINGTON, D.C.
NOTSS	NAVAL OBSERVATORY TIME SERVICE SUBSTATION, RICHMOND, FL
TV	Channel 5, WTTG WASHINGTON, D.C.

## LORAN-C PREDICTION PROBLEMS

Carl F. Lukac  
U. S. Naval Observatory  
Washington, D. C.

### ABSTRACT

Control of time and frequency at remote stations and the maintenance of a constant time scale for Loran-C chains are problems of practical importance. The stability of stations monitoring a Loran-C chain is analyzed - in particular, those stations monitoring the Northwest Pacific chain (LC/9970). Part of the analysis consists of comparing individual determinations of the quantity, U. S. Naval Observatory Master Clock (USNO MC) - LC/9970, with an averaged value and in making intercomparisons of monitored data.

The values for the relationship

USNO MC - LC/9970

are published weekly in the Time Service Series 4 announcements to enable users to establish and maintain traceability to the USNO MC. These values also are available on a daily basis by telephonic communication with an HP 1000 computer located in the Time Service building. Details of some of the work done and problems encountered in the determination of USNO MC - LC/9970 are illustrated here.

How does one keep a chain on time? Some chains are monitored at the Naval Observatory and the differences, USNO MC minus the chains, are published in Series 4 as direct measures. However, the Observatory cannot receive the Loran-C signals of most chains, especially the Northwest Pacific chain. Nonetheless, even at a distance of some 8,000 miles from Washington, it is possible to determine and publish the result of emission time of LC/9970 to a high degree of accuracy.

Figure 1 compares the values of USNO MC - LC/9970 for both the published data in Series 4 and the computed average values. The computed values are represented by the curve which has been labelled periodically with large symbols for easier recognition. The difference between the two curves, which has been plotted against an offset zero line, appears near the bottom of the plot. The x axis units are in terms of Modified Julian Day and the y axis units are microseconds. These axis designations are the same for all plots used in this paper. It is obvious that the two curves do not always agree and can be more than  $0.5\mu\text{s}$  apart, but generally the residual is less than  $0.5\mu\text{s}$ .



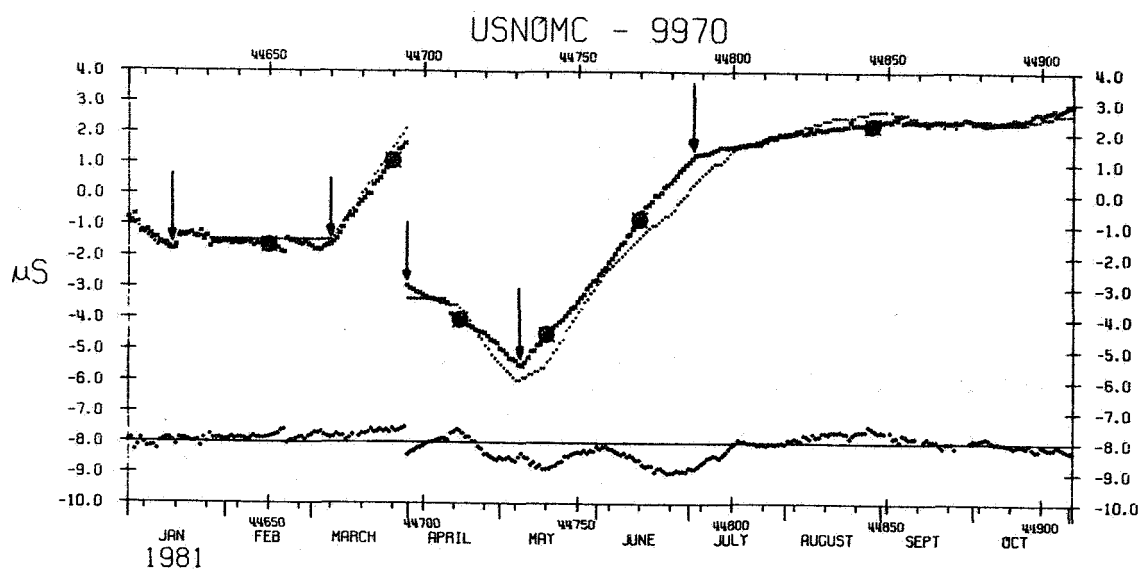


Figure 1.

The upper curves are values as published in Series 4 and as determined from the computed average (traced with large symbols). The lower plot is the difference between the two curves. Announced frequency changes are indicated by arrows.

The published values of USNO MC - LC/9970 are based on extrapolation of the time scales for several monitoring sites. Run-offs occur when additional data is received from other monitoring stations which do not send their Loran readings to the Observatory on a daily basis. If, after new data is received, the computed average curve takes a new direction, then the published values will be steered to the correct value over a period of a week or two rather than have a jump of a fraction of a microsecond.

Figure 1 also shows announced frequency changes (indicated by arrows) in the Loran as well as some discontinuities which will be discussed later. In what follows, attention will be given to the data sources used in generating the computed average and to some of the factors which affect the relative displacement of the two curves.

The Northwest Pacific chain is tied to the Naval Observatory by

1. Portable clocks,
2. Defense Satellite Communication System (DSCS) time transfers, and
3. The rate correlation method.

Each of these methods has advantages and drawbacks, the ideal situation employing all three simultaneously. Using LC/9970 transmissions,

differences of USNO MC - station are seen in Figure 2. In this case, the data is for a cesium at the DSCS terminal in Finegayan, Guam. As with all Loran data, the readings taken by the station are forwarded to the Observatory and calculations made to reduce all the data to USNO MC - station.

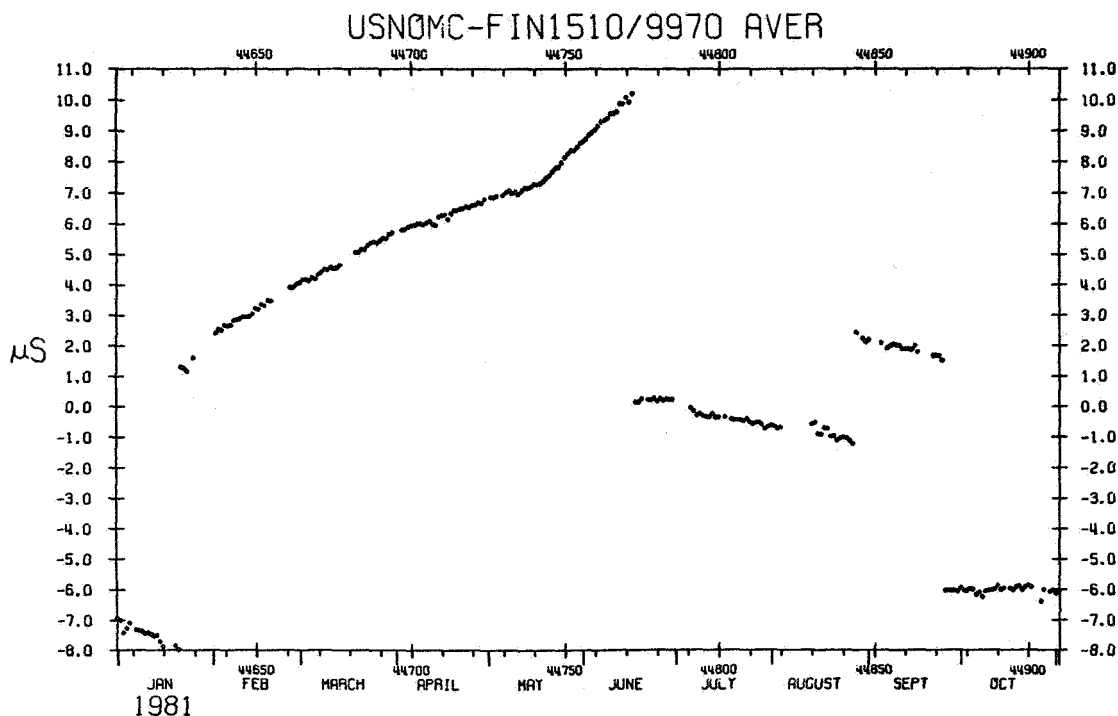


Figure 2.

#### Performance of Cesium 1510

In January, this particular clock was stepped per instruction from the Observatory; later, there were several spontaneous rate changes. Another step was programmed in June as well as a frequency change. In August, the clock jumped and changed rate. In September, it jumped again with another corresponding rate change. There are frequent power outages which contribute to missing data. This plot shows that a clock trip once or twice a year (a typical average for this chain) is far from adequate to tie the LC/9970 chain to the USNO time scale when a clock performs in the manner of cesium 1510.

A better behaved clock in terms of long time spans is cesium 211 at NASA, Guam, whose performance is shown in Figure 3. Here is a clock with reasonably small scatter, no discontinuities and relatively few rate changes. This clock is heavily relied upon for the determination of USNO MC - LC/9970 not only because of performance but also because

its Loran values are reported daily.

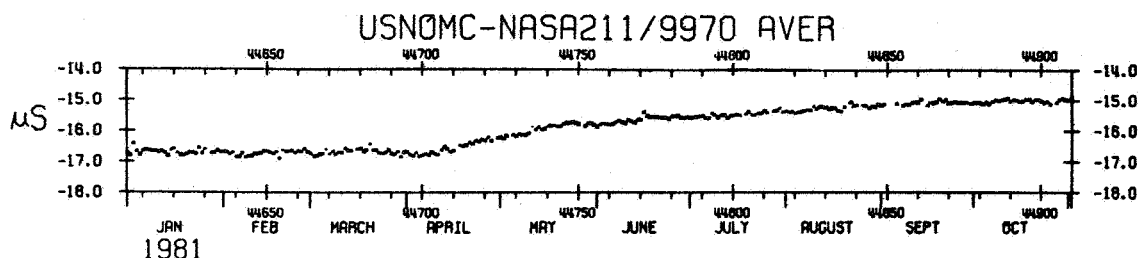


Figure 3.

Performance of Cesium 211. A constant of  $19\mu\text{s}$  has been subtracted from values of USNO MC-Cs 211.

From a practical point of view, satellite time transfers are more useful in establishing the relationship between a Loran chain and the Naval Observatory Master Clock than are portable clock trips, by virtue of the greater frequency of the satellite time transfers. There are three DSCS terminals which can monitor the LC/9970 chain. These terminals are located at:

1. Futema, Okinawa,
2. Finegayan, Guam, and
3. Kwajalein, Marshall Islands.

Time transfers from Futema were resumed in late 1980 after a long absence. The transfers are done on a weekly basis and would normally be quite useful were it not for the fact that no Loran receiver was operating at the site. Recently, Loran-C monitoring has resumed but the data is erratic and equipment problems may still exist. Thus, it is presently impossible to use the Futema time transfers directly.

The DSCS terminal at Finegayan, data from which are presented in Figure 4, is the present 'workhorse' for satellite time transfers in the Pacific. Here, using LC/9970 transmissions, differences of USNO MC - Cs 1061 are plotted along with the intermittent time transfers shown by the large symbols. The satellite points have relatively low scatter and are extremely useful for predicting the direction in which the system should be moving. Cesium 1061 also serves as the primary through which two other clocks at Finegayan are monitored. The drawback is that time transfers are not regular enough due to higher priority requirements at Finegayan. Also, equipment problems tend to produce frequent gaps in the Loran data resulting in cesiums being reset--usually, one to another.

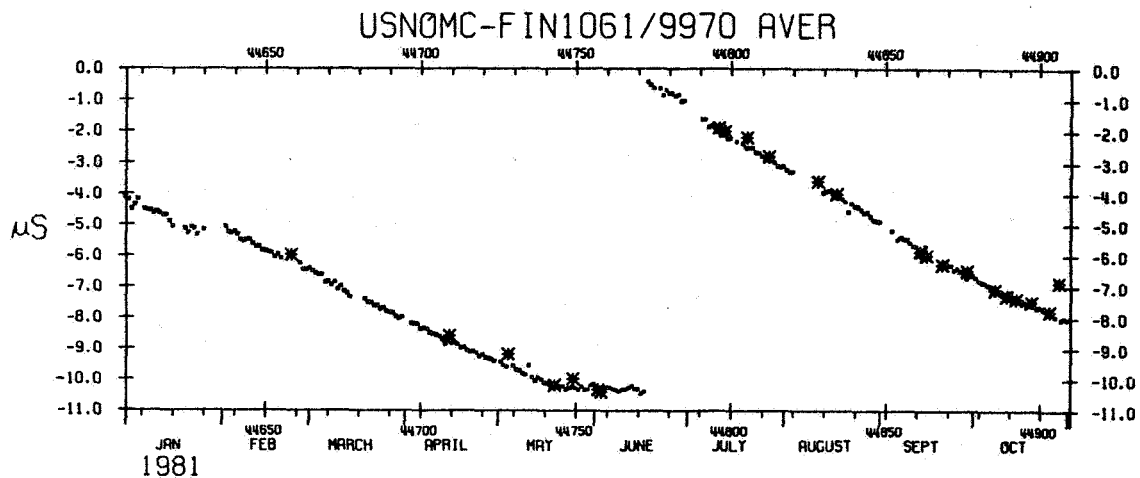


Figure 4.

Performance of Cesium 1061. The large symbols indicate satellite time transfers. A constant of  $1\mu s$  has been subtracted from the values of USNO MC - Cs 1061.

The third DSCS terminal is located at Kwajalein. Even though there is considerable scatter in the Loran data (Figure 5), the large symbolized time transfers were very useful until approximately June 1981. At that

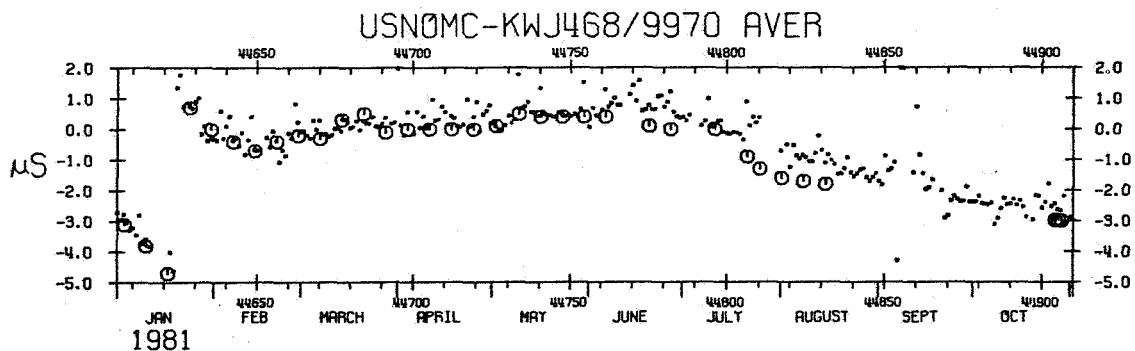


Figure 5.

Performance of Cesium 468 at Kwajalein. Large symbols indicate satellite time transfers.

time the satellite points departed from the Loran system (defined by the many other clocks which make up the MEAN). In fact, there seems to be an offset of about  $1\mu s$ . No transfers were performed after August due to problems with a time transfer modem at the DSCS terminal at Camp Roberts, California. Hence, Kwajalein is temporarily unavailable in helping to determine USNO MC - LC/9970 from a time transfer point of view. This is an example of why one cannot rely exclusively upon any one source of data!

Scatter problems of Loran monitored data in Kwajalein are illustrated in Figure 6 which is obtained by subtracting USNO MC - LC/9970 via each station from USNO MC - LC/9970 as determined by the average of all clocks in the MEAN. Here, NASA (with relatively low scatter) and

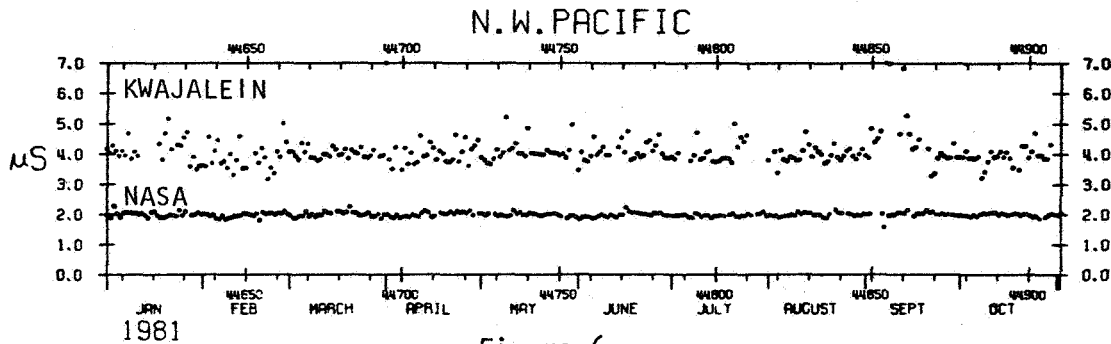


Figure 6.

Relative scatter about an offset zero line of Loran-C signals as observed at two separate monitoring sites in the Pacific.

Kwajalein (with relatively high scatter) are being compared. The scatter in Kwajalein may be a combination of skywave contamination, oscillator or receiver problems, or personnel. Previously, Kwajalein's scatter was much less.

Figure 7 illustrates Loran data for NASA again but this time the x axis has been compressed to go back two years. Also, the time transfers at

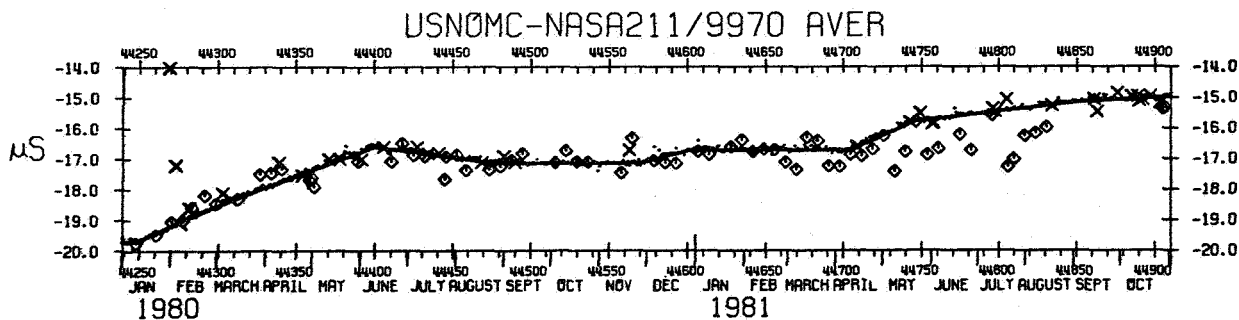


Figure 7.

Values obtained through the computed average of LC/9970, using the satellite time transfers at Finegayan (X) and Kwajalein (◊). A constant of  $19\mu\text{s}$  has been subtracted from these data.

Finegayan and Kwajalein (large symbols) have been reduced to obtain values of USNO MC - NASA through the commonly monitored Loran data. In addition to the usual scatter of Loran-C, a solid line is plotted which

is the adopted frequency offset for USNO MC - station. These are straight lines, changing slope only when indicated by the raw data. It is evident that Kwajalein was definitely better before May of 1981, even though it shows somewhat more scatter than Finegayan. This plot demonstrates that a good clock with several sources of time transfers is a powerful tool for remote time scale determination.

A similar situation (Figure 8) is that in which satellite time transfers from the Finegayan and Kwajalein terminals have been reduced to obtain USNO MC minus Tokyo Astronomical Observatory (TAO) and USNO MC minus Radio Research Laboratory (RRL) via the Loran. These time systems (both located in Tokyo, Japan) are very good members of the clock ensemble which is used in determining the average, but their Loran data are usually two or three weeks behind. Notice the discontinuity in RRL during April. This type of break is easily identified with the actual problem clock if that clock is constantly intercompared with a tightly bound system of clocks, as is maintained for the Northwest Pacific chain.

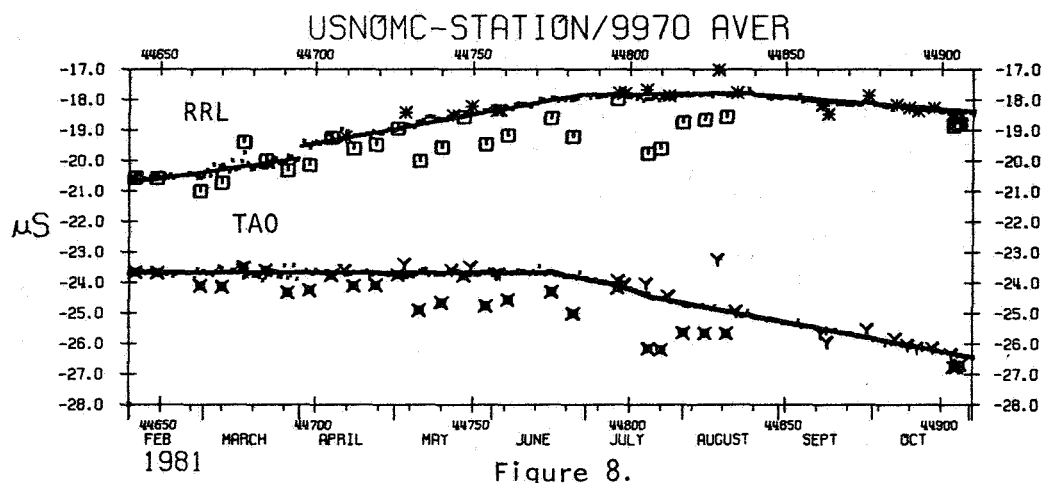


Figure 8.

Values obtained through the computed average of LC/9970 using the satellite time transfers at Finegayan (\*, Y) and Kwajalein (□, X). A constant of  $13\mu\text{s}$  was subtracted from the values of RRL. A constant of  $20\mu\text{s}$  was subtracted from TAO.

When all else fails and there are no portable clock or satellite time transfer values available, the course a system should be taking can be deduced by an intercomparison scheme called rate correlation. This is simply a method which says that if one clock changes in frequency, that change should appear in any differences measured with respect to that clock. For instance, if one has the differences A-B and A-C and A changes by five parts in  $10^{13}$ , both differences should also change by five parts in  $10^{13}$  whereas B-C should not exhibit any changes. This technique requires at least three oscillators but usually is employed

with as many as possible. The method works very well in the Pacific and is easily capable of  $1/2\mu\text{s}$  accuracy.

In Figure 9, Loran data for the National Research Laboratory of Metrology (NRLM) located in Tokyo, Japan, has been subtracted from that obtained at NASA, TAO, and RRL. A change in frequency is clearly evident during July which is attributed to NRLM--the station common to all three differences.

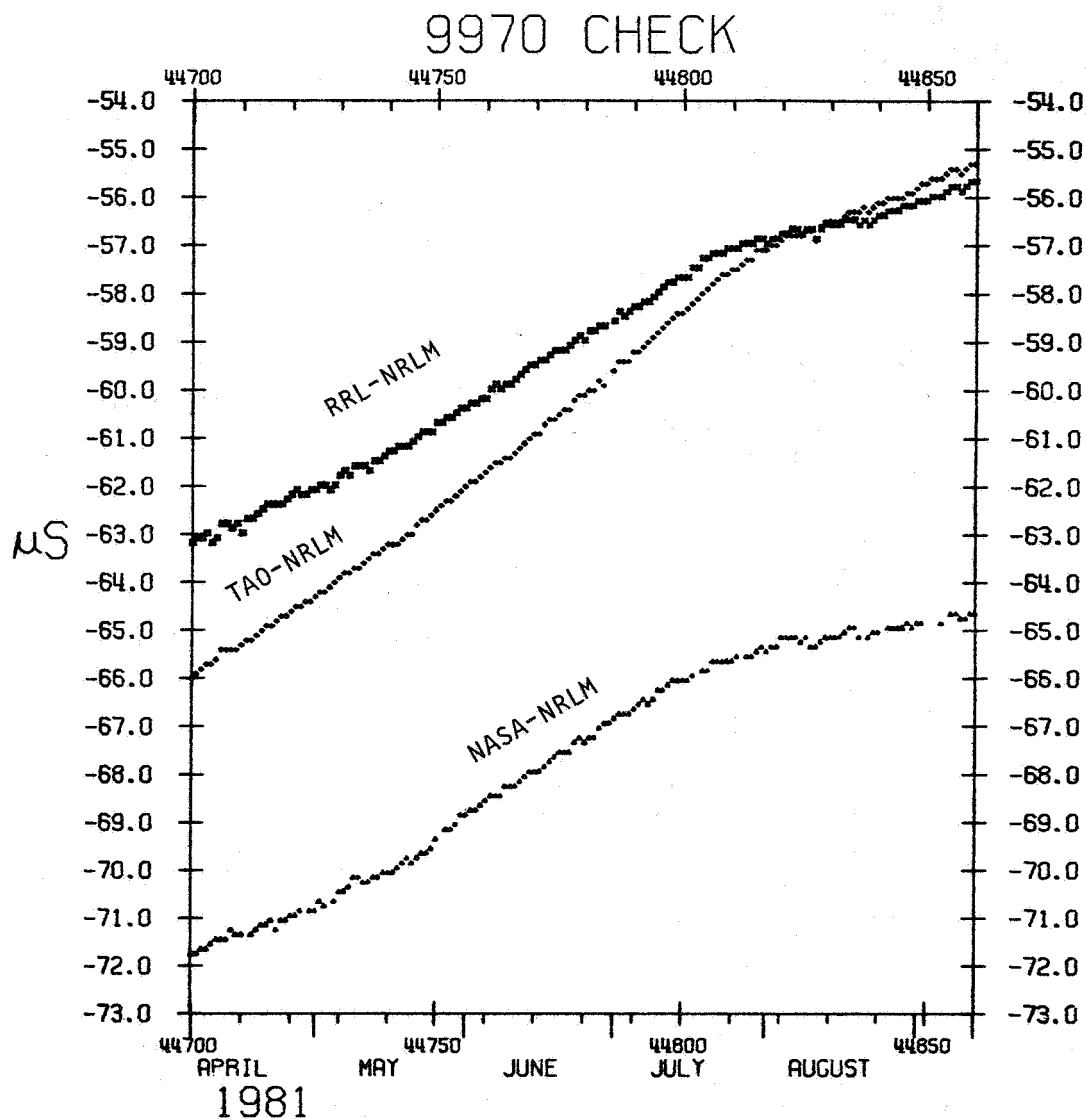


Figure 9.

Differences in rates between pairs of cesiums can detect a rate change in a single clock.

There are approximately 21 cesium clocks monitoring Loran-C in the Northwest Pacific. Eleven of these cesiums are currently in the MEAN. The relationship USNO MC - LC/9970 via each station contributing to the MEAN is plotted in Figure 10. The scatter produced by these different sites is about 0.2 to 0.3  $\mu\text{s}$ .

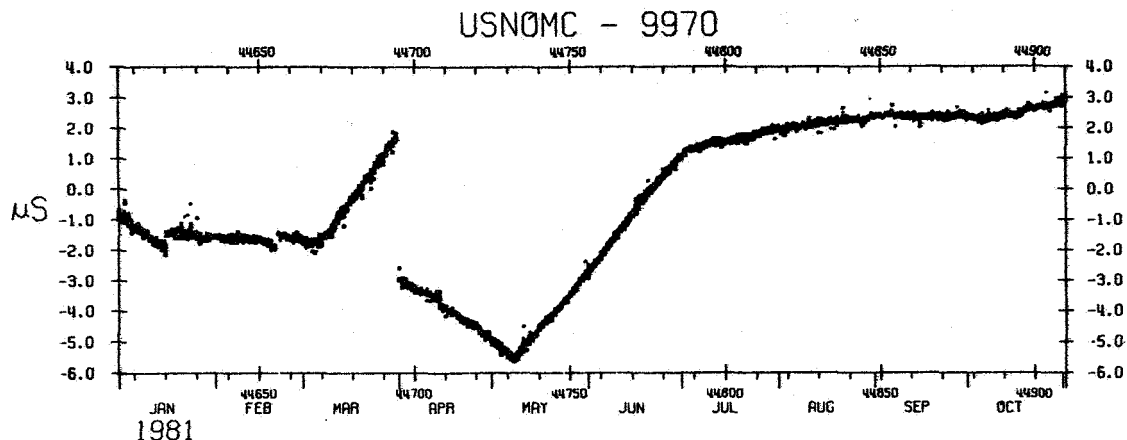


Figure 10.

Scatter of clocks used in the ensemble determining the time scale for LC/9970.

It is the average of the better stations which are used to compute the values published in Series 4. Since not all stations report their data on a daily basis, evaluation of the adopted time scale is continuously being made as additional data are received. Final values may differ from those published. Sometimes revision of Series 4 values becomes necessary and is done automatically if differences between computed and published values approach 0.7  $\mu\text{s}$ . An example of just such a revision is given in Figure 11.

The interval from roughly January through April that appears in Figure 1 is examined more closely in Figure 11. On the left are the original Series 4 values (represented by the curve marked with large symbols) plotted with the final (not original) average. On the right are the revised Series 4 values (again labelled with large symbols) plotted with the same final average. The drastic change in Series 4 values has two primary causes: Chain reconfiguration and insufficient data.



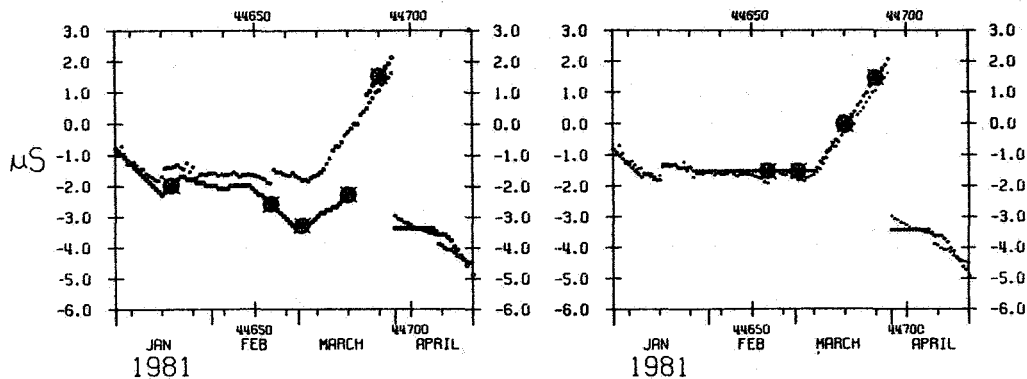


Figure 11.

Original values of USNO MC - LC/9970 published in Series 4 are in the left figure (curve marked with large symbols). The revised values (again marked with large symbols) are in the right figure. The second curve in each figure is the final computed average.

In mid-January an oscillator change occurred. It apparently caused a discontinuity and a frequency change in the Loran data. On 21 February, a chain reconfiguration began--at which something happened, producing a second discontinuity. Another frequency change occurred in early March. Then, a step adjustment and an additional frequency change took place on 1 April. During the reconfiguration, there were no time transfers from Finegayan. Kwajalein was noisy and data was not coming in on a current basis. In addition to the delay change at the beginning of the reconfiguration, Finegayan Loran-C data jumped and changed delay within the reconfiguration. Some monitoring sites stopped sending in data altogether for a while! Hence, Series 4 had to be revised during this period with the final result appearing as in the right-hand figure. It is planned that final revised Series 4 values for the entire year will be available as part of the annual Time Service report (Series 11). Information also will include any revisions for chains other than LC/9970.

It is apparent that a remote Loran-C chain can be kept on time if there is an abundance of data. Control points such as those furnished by satellite time transfers and portable clocks are most useful in helping to remove prediction and system errors. However, care must be exercised in using the control points as they themselves are subject to error. For instance, weekly time transfers can show scattering of  $\pm 0.3\mu\text{s}$ .

Portable clock measurements also are affected by various types of errors--many of which could have gone unnoticed if the data were not

correlated to the Loran-C chain reduction procedures that are described herein. A major problem with reducing portable clock measurements to USNO MC is how to characterize the portable clock's performance during a trip. From the time it leaves the Observatory, or any other controlled environment, little is known about a clock's operation until it returns and monitoring resumes again.

The major difficulty in this work is insufficiently trained personnel. Some specific problems affecting remote time scales are:

1. Insufficient clock trips,
2. Insufficient satellite time transfers,
3. Long-term interruptions of satellite time transfers due to high priority missions,
4. Lack of operational Loran-C receivers at DSCS terminals.
5. Insufficient knowledge of propagation delays,
6. Skywave contamination of signals,
7. Reconfigurations,
8. Constant steering of cesiums, and
9. Delay in receiving monitored data.

Despite these and other problems, the Northwest Pacific chain is kept within  $0.5\mu\text{s}$  of the USNO MC on a routine basis.

#### ACKNOWLEDGEMENT

The author is grateful to Mr. Patrick Lloyd who manages the huge Loran-C database and prepares the data for computation and to Mrs. Edna Bermudez who has produced many of the invaluable charts used constantly in the analysis. Thanks also are expressed to Dr. R. G. Hall and Ms. Laura Charron who have provided considerable assistance through technical discussions concerning data interpretation.



SESSION III

LOCAL TIME AND FREQUENCY TRANSFER

Mr. Roger Beehler, Chairman  
National Bureau of Standards



## COMPARISON OF VLBI, TV, AND TRAVELING CLOCK TECHNIQUES FOR TIME TRANSFER

J. H. Spencer, E. B. Waltman, K. J. Johnston, N. J. Santini (E. O. Hulburt Center for Space Research, Naval Research Laboratory, Washington, D. C. 20375)

W. J. Klepczynski, D. N. Matsakis, P. E. Angerhofer, G. H. Kaplan (U. S. Naval Observatory, Washington, D. C. 20375)

### ABSTRACT

A three part experiment was conducted to develop and compare time transfer techniques. The experiment consisted of: I. a VLBI between Maryland Point Observatory at Riverside, Maryland and NRAO at Green Bank, West Virginia; II. a high precision portable clock time transfer system between the two sites coordinated by the U. S. Naval Observatory in Washington, D. C.; and III. a television time transfer between the U. S. Naval Observatory and the Maryland Point Observatory using a local Washington, D. C. television station, WTTG.

A comparison of the VLBI and traveling clock shows each technique can perform satisfactorily at the five nsec level. There was a systematic offset of 59 nsec between the two methods, which we attributed to a difference in epochs between VLBI formatter and station clock.

The VLBI method had an internal random error of one nsec at the three-sigma level for a two-day period. Thus, the Mark II system performed well, and VLBI shows promise of being an accurate method of time transfer.

The TV system, which had technical problems during the experiment, transferred time with a random error of about 50 nsec.

### INTRODUCTION

An experimental time transfer was conducted between the hydrogen maser clocks at the Maryland Point Observatory of the Naval Research Laboratory (NRL) and the National Radio Astronomy Observatory\* (NRAO), and the U. S.

---

\*The National Radio Astronomy Observatory is operated by Associated Universities, Incorporated, under contract with the National Science Foundation.

---

Naval Observatory's master clock to develop and compare time transfer

techniques. The experiment consisted of three parts: i) a very long baseline interferometer (VLBI) between the Maryland Point Observatory at Riverside, Maryland and NRAO at Green Bank, West Virginia; ii) a high precision portable clock system time transfer between the three sites; and iii) a television time transfer between the U. S. Naval Observatory and the Maryland Point Observatory using television channel 5 in Washington, D. C., WTTG. The purpose of the experiment was to compare each method of time transfer; to evaluate the errors, internal and systematic, of each method; and to isolate problem areas in the VLBI technique, a time transfer technique that is not fully developed, but has the most promise.

It is interesting to note that while one method transports high precision atomic clocks between sites, the other two methods have "no moving parts". Electronic equipment remains stationary in controlled environments. These two methods reference to external radio signals, one local and man made, the other a celestial radio galaxy or quasar. The TV system, while simpler, has a fixed frequency and therefore cannot overcome propagation delay variations. The reference signal of the VLBI system, however, only propagates through one to two atmospheres and can be at frequencies selected for best results. It has the greatest potential.

#### THE VLBI TECHNIQUE

The VLBI experiment was conducted February 19-22, 1980 at 1670 MHz between the 26-meter antenna of the Naval Research Laboratory and the NRAO 43-meter antenna with a bandwidth of 2 MHz. The Mark II data recording system we used has been described by Clark (1973). Bandwidth synthesis, a technique which improves the ability to determine the delay between the two antennas by the ratio of synthesized to actual bandwidth, was not used in these observations, which were designed to be a basic, proto-type experiment. Bandwidth synthesis could improve the internal errors in direct proportion to bandwidth, but was not compatible with the other observations that occurred simultaneously.

The Mark II recording system was used because, while it is not now the most advanced system available, it is the most widely used system for VLBI experiments. Therefore it has the greatest potential for distributing time around the world, if it can transfer time with adequate accuracy.

The observations were correlated on the NRAO processor in Charlottesville, Virginia, and then further reduced with a series of programs developed for the TI-ASC computer at the Naval Research Laboratory. The sources used for this study were 3C273, 3C345, 3C120, 3C84, and 4C39.25. We assumed their positions as given by Wade and Johnston (1977). The initial value of the NRL-NRAO baseline was that given by

a 1976 VLBI (Waltman *et al.* 1982), but it was later updated by less than one meter to remove systematic differences between sources.

Because VLBI transfers time by measuring the time of arrival of wavefronts from a distant celestial radio source such as a radio galaxy or quasar, the reference time of these wavefronts must be tied to the local station clock, a hydrogen maser standard. This is done by measuring the wavefront delay from fiducial marks on the telescope through the receivers, cables, and backends to the local video tape recorder. Unfortunately, for the 2 MHz bandwidth of the Mark II recorder, the fundamental clock of the tape is the 4 MHz formatter clock. We found it to be impossible to precisely measure this clock with respect to the 5 MHz station clock using standard equipment.

The delay between video tapes was found by performing a Fourier transform in lag to get the bandpass at the peak fringe rate frequency. A straight line fit to the phase across the bandpass then yielded the delay. After the data was corrected for atmospheric effects, retarded baseline, antenna geometry, and earth tides, a least-squares solution for the clock rate and offset was found using paired observations of the same source from February 20 and 21. The use of paired scans on consecutive days minimized the error contributed by the atmosphere, source structure, and other repeatable error sources and allowed the baseline to be determined more precisely.

We measured the cable delays through the receivers to the formatters at each telescope and corrected for this effect. The result is that the time difference for NRL-NRAO is shown in Figure 1 after removal of a straight line with a slope of 5.509 psec per second and an offset of  $-14.397 \pm 0.005$   $\mu$ sec at 0<sup>h</sup> UT on 21 February. In this figure the different symbols indicate the source of the data. The sources are coded: 3C273 observations by  $\cdot$ ; 3C84 by X; 3C345 by  $\square$ ; and traveling clock by  $\odot$ . The one sigma errors are shown for each 3 minute scan of the VLBI data except near February 20 where the one error bar at 12:30 is representative.

The sources of error are uncertainty in the formatter clock synchronization, uncertainty in the cable delay measurements, and the internal VLBI random errors. We estimate the error in the cable delay measurements to be 2 nsec (1 sigma). The random error of the VLBI fit was 1 nsec at the three sigma level. Thus, the random internal errors in the VLBI solution made a negligible contribution to the error assigned to the final VLBI result.

While each formatter was "synchronized" to the station clock, this is usually to only a fraction of a microsecond. A correction was made for the offset between the formatter 1 pulse per second and the station clock, but we do not know the timing between that formatter 1 pps and



the internal 4 MHz clock used to record and time the video signals on tape.

#### THE TRAVELING CLOCK TECHNIQUE

A high precision portable clock time transfer system consisting of four cesium clocks (three of which were "super tubes") and a data acquisition system were transported by van between the three observatories almost continuously during the period of the VLBI observations. This resulted in one measurement per day at each radio observatory and three per day at the USNO Master Clock. The four traveling clocks were intercompared continuously using an HP-9815 computer that also traveled in the van in order to form a mean-time scale through which we monitored the performance of the individual cesium clocks. Comparison of the mean time scale, based on the four cesium clocks, with the USNO Master Clock indicated that it remained stable over the period of the experiment. Figure 2 shows the behavior of each of the four clocks compared to the mean after a best fit straight line has been subtracted. Clock 2 is not a super tube. The results of the traveling clock are summarized in Table 1 and the clock difference of NRL-NRAO is plotted in Figure 1 after an offset of  $-14,339 \pm 3.4$  nsec at 0<sup>h</sup> UT on February 21 and a clock rate of 5.509 psec per second have been removed.

#### THE TV TIME TRANSFER TECHNIQUE

It is possible to transfer time by synchronizing to the television signal transmitted by a local commercial station. In the Washington, D. C. area, channel 5, WTTG, broadcasts a signal that is phase locked to a cesium frequency standard and monitored daily by the Naval Observatory. Since this signal can be received at the Maryland Point Observatory, about 70 kilometers from the transmitter, it can be used to transfer time from the USNO to the Maryland Point Observatory.

Unfortunately, as shown in Figure 3, the behavior of the cesium standard at the transmitter was erratic during the period of the experiment. We are therefore limited to simultaneous measurements at both observatories in order to eliminate the large randomness of the transmitter signal. This reduces the data to four measurements where the TV and van can be directly compared. These results are shown in Table 2. The data point for February 19 is almost 900 nsec different from the mean of the other three (approximately 19 standard deviations). We can not explain this except to point out the erratic behavior of the TV cesium standard for this day and that during this period the TV signal was frequently not locked to the standard as a result. Because the clock rate differences at the transmitter and Maryland Point Observatory are not of direct interest, the most interesting method to compare van and TV time transfer methods is to compute the difference

of USNO master clock minus Maryland Point Observatory via TV and via "traveling" clock. The result of 230.119  $\mu$ sec is largely due to the free space propagation delay, but also includes antenna, cable, and receiver delays of the system at the Maryland Point Observatory. The standard deviation of this mean is 50 nsec, much larger than the error of the van alone or when compared to VLBI. We therefore conclude that for a 70 kilometer transmission, 50 nsec represents the short term (1-3 day) standard deviation of a time transfer. Seasonal effects could be expected to degrade this value further for time transfers that last longer.

#### DISCUSSION

For the NRL-NRAO time transfer, the final clock rate determined from the VLBI experiment is in agreement with the traveling clock rate calculated for the same two-day time period. The VLBI data yielded a clock rate of  $5.483 \pm 0.013$  psec per second (2 sigma error); the traveling clock experiment gave  $5.5 \pm 1.0$  psec per second, which is within the quoted error.

Incorporating the residuals of Figure 1 into the offsets removed, we find the clock comparison between NRL and NRAO has an unexpected systematic offset of 59 nsec between the VLBI and traveling clock methods of time transfer. This is probably due to the difference in epochs of the 4 MHz formatter clock used to write the video tape and the 5 MHz station frequency standard as used in the VLBI system. In future experiments, equipment must be developed to measure the 4 MHz formatter clock signal relative to the 5 MHz frequency standard.

The comparison of the TV to traveling clock techniques between the USNO and NRL shows the TV method to be good to  $\sim 50$  nsec over 70 kilometers as given in the last section. The simplicity of this method may make this technique attractive where precise time transfer is not required.

#### CONCLUSIONS

The Mark II VLBI system performed well in the time-transfer experiment, and a comparison of the VLBI results with the traveling clock experiment was useful in identifying possible problem areas in developing the VLBI technique of time transfer.

In the future the use of bandwidth synthesis and better formatter synchronization should greatly improve the VLBI results, making the widely used Mark II system a promising technique for time transfer.

The intercomparison of the VLBI and the four traveling clocks shows each technique can perform satisfactorily at the 5 nsec level. This

supports claims made in the past as to the accuracy of traveling clocks.

The television transfer system was shown to work over 70 kilometers with short term errors of 50 nsec.

The VLBI method of time transfer had an internal random error to the solution for a two-day period of one nsec at the three sigma level. Thus, VLBI shows promise of being an accurate method of time transfer.

#### REFERENCES

- Clark, B.G. 1973, Proceedings of the IEEE, 61, 1242.  
Wade, C. M., and Johnston, K. J. 1977, Astronomical Journal, 82, 791.  
Waltman, E. B., Spencer, J. H., Johnston, K. J. 1982, in preparation.

TABLE 1

NRL -NRAO Via Traveling Clock and VLBI

Date	Time	Traveling Clock ( $\mu$ sec)	VLBI ( $\mu$ sec)	VLBI -Traveling Clock ( $\mu$ sec)
Feb. 18	08 <sup>h</sup> 54 <sup>m</sup> 44 <sup>s</sup>	-15.554		
Feb. 19	09 29 00	-15.088	-15.141	-0.053
Feb. 20	09 45 13	-14.619	-14.680	-0.061
Feb. 21	09 28 28	-14.152	-14.209	-0.057
Feb. 22	06 16 55	-13.742	-13.796	-0.054

TABLE 2

TV Experiment Compared to Traveling Clock Experiment

Date <sup>a</sup>	USNO -TV ( $\mu$ sec)	Via TV ( $\mu$ sec)	USNO -NRL Via Traveling Clock ( $\mu$ sec)	Traveling Clock -TV ( $\mu$ sec)
Feb. 19	2.0003	-218.083	+11.154	229.237
Feb. 20	0.678	-219.519	10.615	230.134
Feb. 21	0.214 <sup>b</sup>	-220.081	10.075	230.156
Feb. 22	-0.251	-220.531 <sup>b</sup>	9.536	230.067

<sup>a</sup>Corrected to 17:00 UT.<sup>b</sup>See text.

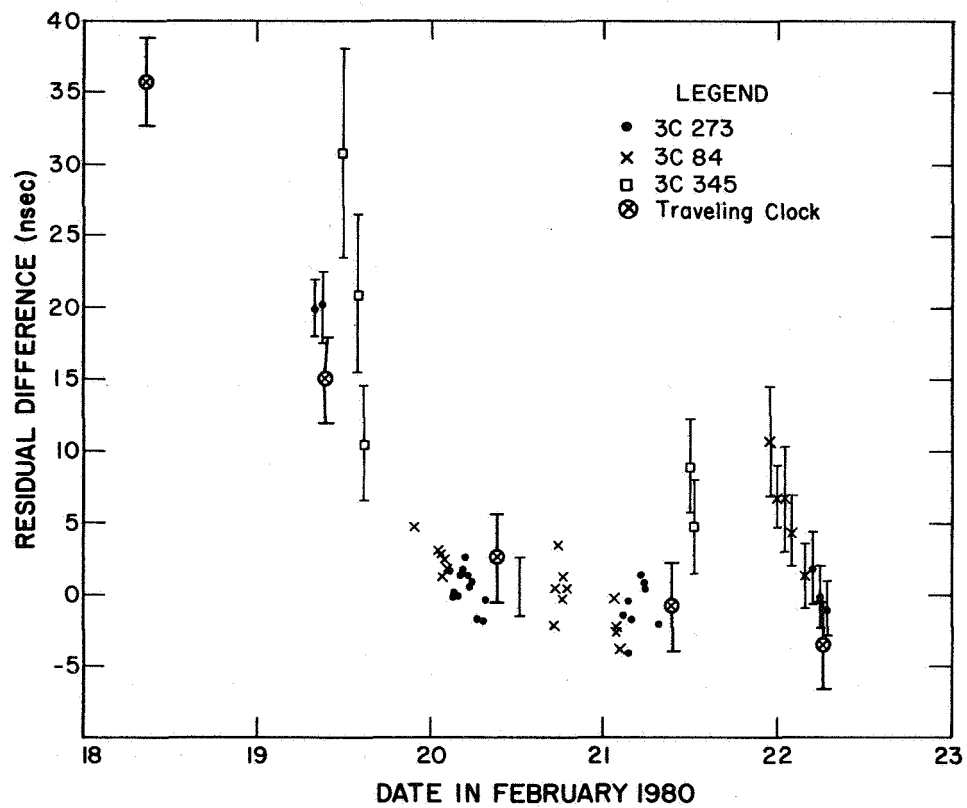


Fig. 1--VLBI and traveling clock results from NRL -NRAO

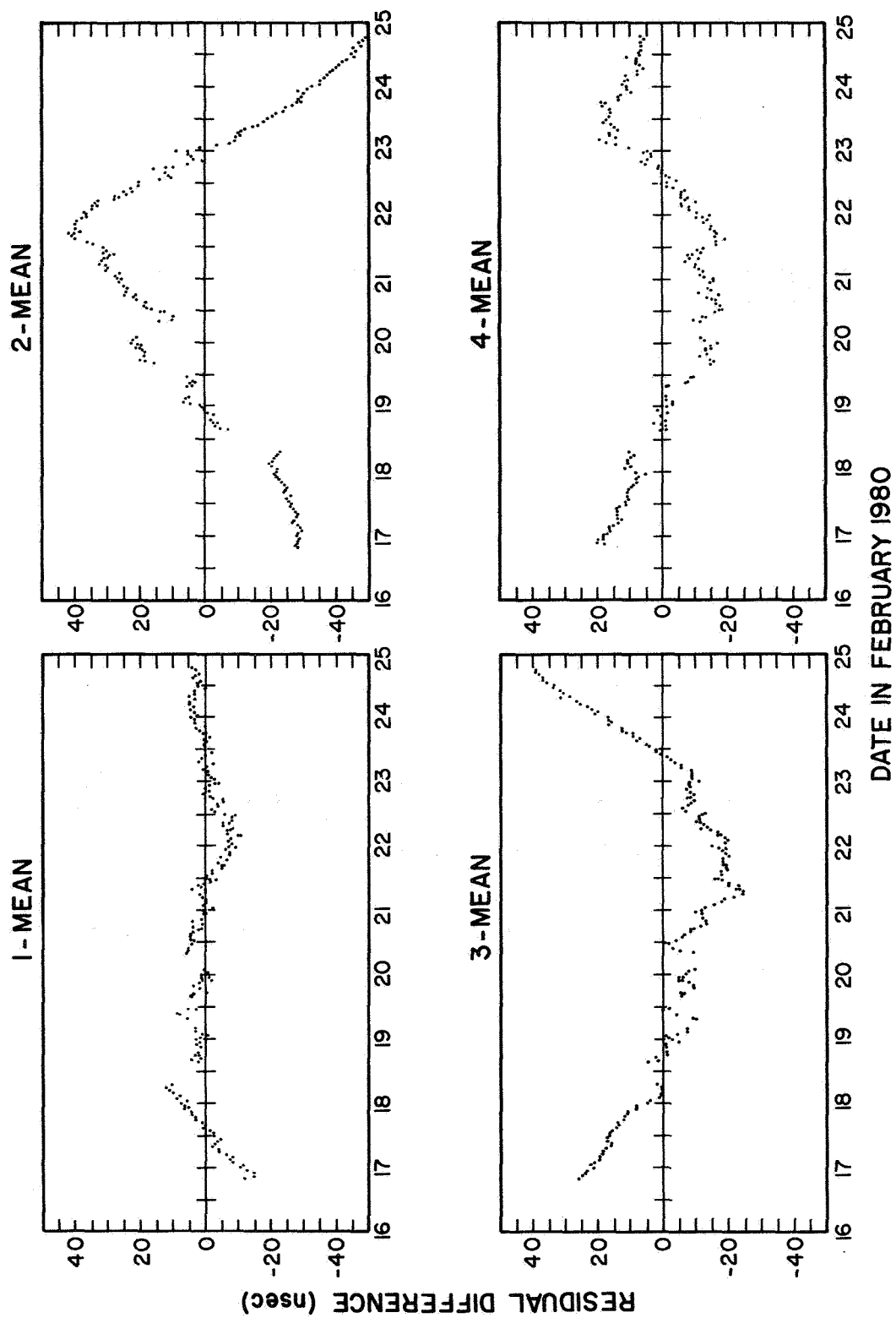


Fig. 2--The traveling clock performance

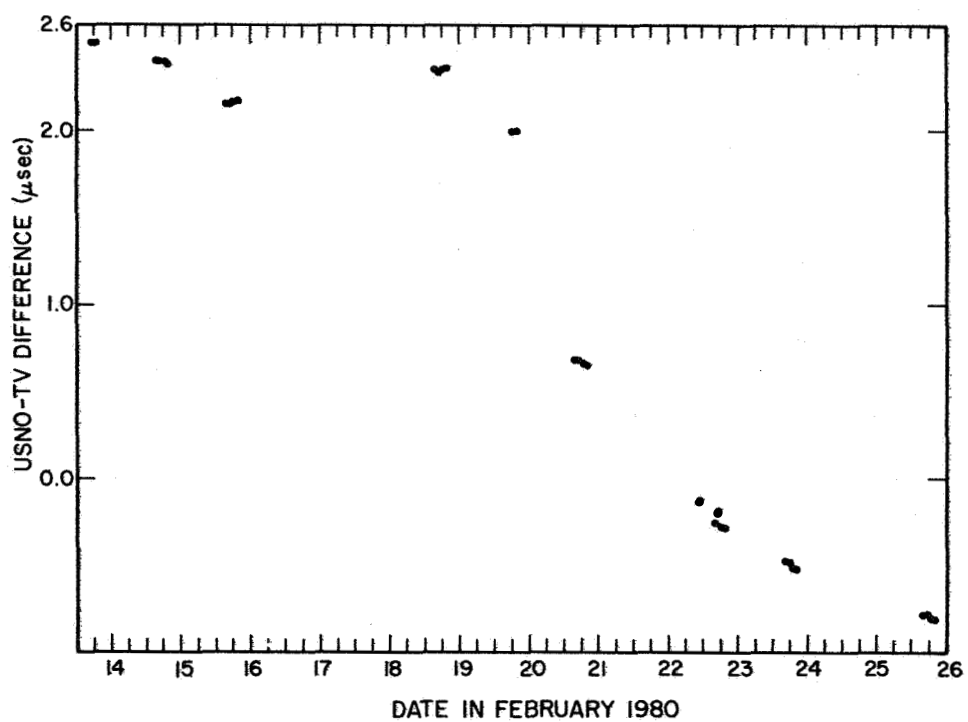


Fig. 3--Behavior of the cesium standard at the TV station

## QUESTIONS AND ANSWERS

MR. CLARK, Naval Observatory

I'm just curious. What do you mean by the temperature stability in the van? Was that just the normal heating system?

MR. SPENCER:

Well, it was February; so, the outside temperature was quite cold, and we tried to keep the environment for the cesium as friendly as possible; so, we had the van in the heated vice president's garage at night, which was about a six-hour interval, and then during the day while it was on the road, the drivers kept the heater in the system at what they considered a comfortable temperature. So, it wasn't really laboratory stabilized, but it was better than sitting on the runway of the airport, or something like that.





## DEVELOPMENT OF OPTICAL FIBER FREQUENCY AND TIME DISTRIBUTION SYSTEMS\*

George Lutes  
Jet Propulsion Laboratory, Pasadena, California

### ABSTRACT

The Jet Propulsion Laboratory is engaged in the development of ultra stable optical fiber distribution systems for the dissemination of frequency and timing references. The ultimate design goals for these systems are a frequency stability of  $10^{-17}$  for  $\tau \geq 100$  sec and time stability of  $\pm 0.1$  ns for 1 year and operation over distances  $\geq 30$  km. This paper will review last years report, describe a prototype system being implemented and discuss progress made in the past year.

### INTRODUCTION

Preliminary work on an optical fiber reference frequency distribution system was reported at last year's PTTI conference. This paper is a progress report on this effort and will begin with a brief review, followed by a description of the prototype system and progress made in the last year.

### REVIEW

It was reported at last year's PTTI conference that a 3-km experimental multimode optical fiber link operating at 850 nm wavelength was installed at JPL. It was to be used in the development of ultra-stable frequency and timing distribution systems.

The link was stabilized using the conjugation method, reference 1, and achieved a stability of  $4 \times 10^{-15}$  for  $\tau = 100$  seconds.

Several problems with this link were reported. The stability was limited by the optical transmitters and receivers. Delay changes as a result of bending multimode fibers are nonreciprocal under some circumstances, and excessively large. This precludes their use for frequency

---

\* This paper presents the results of one phase of research carried out at the Jet Propulsion Laboratory, California Institute of Technology, under Contract No. NAS 7-100, sponsored by the National Aeronautics and Space Administration.

and time reference distribution in non-stationary environments. The minimum loss in optical fibers operating at 850 nm wavelength is about 3 dB/km, which is too large to achieve a 30 km operating distance. The bandwidth of currently available multimode fibers, about 1.5 GHz-km, is not adequate for this use over these distances.

It was concluded in last year's report that, although the results obtained were encouraging, there was still a lot of work to be done.

#### PROTOTYPE SYSTEM

A prototype system, 8 km in length, will be installed between two stations in the Deep Space Communications Complex (DSCC) at Goldstone, California. It will be a single-mode fiber system and will operate at 1300 nm wavelength. The conjugation type of stabilization that will be used in this system will be an improved version of the one used in the experimental system reported last year.

The goal for frequency stability for distances up to 30 km is shown in Figure 1. With this stability the distribution system will not excessively degrade the stability of future frequency references having a stability of up to  $10^{-17}$  for  $\tau = 100$  seconds.

The time distribution stability goal is  $\pm 0.1$  ns for 1 year. This goal has not yet been addressed in detail because it can probably be met with minor additions to the frequency distribution system. In any case, most of the problems will have been resolved in the implementation of the more difficult frequency distribution system.

Another goal, not directly related to frequency and timing distribution, is the capability to distribute 400 MHz bandwidth IF signals over 20 km. This goal will be met as a consequence of the frequency and timing distribution work.

These goals can be approached using single-mode optical fibers operating at 1300 nm wavelength. The delay through such fibers is affected very little by bending and the modulation bandwidth is much wider than that of multimode fibers. Also, 1300 nm is near the wavelength which gives minimum dispersion (equivalent to the widest bandwidth) and lowest loss ( $\leq 1$  dB/km).

A block diagram of the system is shown in Figure 2. In this system, a signal is sent to the far end of the cable where it is turned around and returned to the near end. The transmitted signal,  $\sin(\omega t + \tau)$ , is forced by the control circuit to be the conjugate of the return signal,  $\sin(\omega t - \tau)$ . Since the forward and return paths have equal delays - being the same path - the phase at the far end of the cable is halfway between the transmitted phase and the return phase or  $\omega t$ . The phase of

the input reference is also  $\omega t$ , therefore the phase at the output is the same as the phase at the input.

In Figure 3 the calculated signal-to-noise ratio (S/N) (reference 2) for such a system is shown as a function of the loss in the cable. An operating frequency of 100 MHz and a bandwidth of 10 Hz are assumed. The calculations are supported by measurements made on the 3-km experimental link. The difference between single-mode and multimode fibers is due to greater signal loss in multimode fibers caused by dispersion.

The cable connecting the two stations will contain two single-mode and two multimode optical fibers designed to operate at 1300 nm wavelength. These fibers will be used to develop frequency and timing distribution systems and wideband communications systems. The cable will also contain two multimode optical fibers designed to operate at 850 nm wavelength which will be used for utility communications services between the two stations. The cable will be received in 1- or 2 km lengths and will be plowed into the ground to a depth of 1.5 meters.

The degradation of the stability of a frequency reference signal passing through this cable, without stabilization, has been estimated as follows.

The stability of frequency references is specified at JPL in terms of the square root of the Allan variance (reference 3). The algorithm for computing it is:

$$\sigma = \frac{1}{\sqrt{2} \omega_0 \tau} \sqrt{\frac{1}{N} \sum_{n=1}^N (f_n - f_{n+1})^2}, \quad (1)$$

where:

$f_n$  = average frequency in the interval between  $t_n$  and  $t_{n+1}$

$f_{n+1}$  = average frequency in the interval between  $t_{n+1}$  and  $t_{n+2}$

$t_n$  = the  $n^{\text{th}}$  sampling time

$\tau$  = the interval between samples,

$\omega_0$  = the nominal angular frequency and,

$N$  = the number of samples of  $(f_n - f_{n+1})$ .

Only the degradation caused by ambient temperature variations will be considered since this is the predominate source of instability. We consider first sinusoidal variations in temperature and then a step change in temperature.

Assume that a perfectly stable reference frequency is disseminated over a long single-mode optical fiber cable which is buried in the ground. Also assume that the cable is buried deeply enough that the diurnal change in temperature is essentially sinusoidal.

At time (t) the varying component of temperature (T) of the cable is,

$$T = T_p \sin \omega t \quad (2)$$

where

$T_p$  = the peak temperature variation,

P = the period of one cycle of the temperature variation and

$\omega = \frac{2\pi}{P}$  = the frequency of the temperature variation.

The delay ( $\beta$ ) in radians through the transmission line as a function of temperature is,

$$\beta = \frac{\omega_0 l}{v} + \frac{\omega_0 l \alpha T}{v} \quad (3)$$

where

$\frac{\omega_0 l}{v}$  = the delay at the mean temperature in radians,

$\omega_0$  = the nominal angular frequency of the disseminated signal,

$l$  = the length of the line in meters,

$v$  = the velocity of propagation in the line ( $\approx 2.1 \times 10^8$  m/s for optical fiber) and,

$\alpha$  = the cable's temperature coefficient of delay  
( $\approx 10^{-5}/^{\circ}\text{C}$ ).

The phase ( $\beta$ ) as a function of time ( $t$ ) is from (2) and (3),

$$\beta = \frac{\omega_0^l}{v} + \frac{\omega_0^l \alpha T_P}{v} \sin \omega t. \quad (4)$$

The average frequency ( $f$ ) over a time interval ( $\tau$ ) is the total phase accumulated ( $\beta_A$ ) during the time interval divided by the time interval ( $\tau$ ),

$$f = \frac{\beta_A}{\tau} \quad (5)$$

Therefore from (4) and (5), the average frequency ( $f_n$ ) in the interval ( $t_n, t_n + \tau$ ) is

$$f_n = \left[ \frac{\beta(t)}{\tau} \right]_{t_n}^{t_n + \tau} = \frac{1}{\tau} \left[ \frac{\omega_0^l}{v} + \frac{\omega_0^l \alpha T_P}{v} \sin \omega t \right]_{t_n}^{t_n + \tau} \quad (6)$$

and the average frequency ( $f_{n+1}$ ) in the next interval ( $t_n + \tau, t_n + 2\tau$ ) is,

$$f_{n+1} = \left[ \frac{\beta(t)}{\tau} \right]_{t_n + \tau}^{t_n + 2\tau} = \frac{1}{\tau} \left[ \frac{\omega_0^l}{v} + \frac{\omega_0^l \alpha T_P}{v} \sin \omega t \right]_{t_n + \tau}^{t_n + 2\tau}. \quad (7)$$

The absolute value of the difference between these average frequencies is from (6) and (7),

$$\begin{aligned}
|f_n - f_{n+1}| &= \left| \frac{\omega_0 \ell \alpha T_P}{v\tau} \left[ 2 \sin \omega(t_n + \tau) - \sin \omega t_n - \sin \omega(t_n + 2\tau) \right] \right| \\
&= \left| \frac{4\omega_0 \ell \alpha T_P}{v\tau} \left[ \sin^2 \frac{\omega\tau}{2} \sin \omega(t_n + \tau) \right] \right|.
\end{aligned} \tag{8}$$

Then, from (1) and (8), the square root of the Allan variance of a signal passing through a transmission line having a sinusoidal variation in delay becomes,

$$\sigma = \frac{4\ell\alpha T_P}{\sqrt{2}\tau v} \sqrt{\frac{1}{N} \sum_{n=1}^N \left[ \sin^2 \frac{\omega\tau}{2} \sin \omega(t_n + \tau) \right]^2}. \tag{9}$$

This equation is evaluated in Figure 4, for values of  $\tau$  from 1 second to  $10^6$  seconds and variables  $\ell = 10^4$  meters,  $\alpha = 10^{-5}/^\circ\text{C}$ ,  $T_P = 1^\circ\text{C}$ ,  $v = 2.1 \times 10^8$  meters per second and  $\omega = 2\pi/86400$  radians per second (diurnal variation). These are realistic values based on measurements made at JPL and at the Goldstone Deep Space Complex.

Now consider a cable that is subjected to a step change in ambient temperature. The change is assumed to be much faster than the time constant of the cable. The relative temperature ( $T$ ) of the cable at time ( $t$ ) is,

$$T = T_S \left( 1 - e^{-t/\tau_c} \right) \tag{10}$$

where

$T_S$  = the step change in ambient temperature,

$t$  = the time elapsed since a step change in ambient temperature and,

$\tau_c$  = the time constant of the cable.

The phase ( $\beta$ ) as a function of time ( $t$ ) is from (3) and (10),

$$\beta = \frac{\omega_0^2}{v} + \frac{\omega_0^2 \alpha T_S}{v} \left( 1 - e^{-t/\tau_c} \right). \quad (11)$$

Therefore, from (11) and (5), the average frequency ( $f_n$ ) in the first interval ( $t_n, t_n + \tau$ ) is,

$$f_n = \left[ \frac{\beta(t)}{\tau} \right]_{t_n}^{t_n + \tau} = \frac{1}{\tau} \left[ \frac{\omega_0^2}{v} + \frac{\omega_0^2 \alpha T_S}{v} \left( 1 - e^{-t/\tau_c} \right) \right]_{t_n}^{t_n + \tau}, \quad (12)$$

and the average frequency ( $f_{n+1}$ ) in the second interval ( $t_n + \tau, t_n + 2\tau$ ) is,

$$f_{n+1} = \left[ \frac{\beta(t)}{\tau} \right]_{t_n + \tau}^{t_n + 2\tau} = \frac{1}{\tau} \left[ \frac{\omega_0^2}{v} + \frac{\omega_0^2 \alpha T_S}{v} \left( 1 - e^{-t/\tau_c} \right) \right]_{t_n + \tau}^{t_n + 2\tau}. \quad (13)$$

The absolute value of the difference between the average frequencies ( $f_n$ ) and ( $f_{n+1}$ ) is from (12) and (13),

$$\begin{aligned} |f_n - f_{n+1}| &= \left| \frac{\omega_0^2 \alpha T_S}{\tau v} \left[ 2e^{-\frac{t_n + \tau}{\tau_c}} - e^{-\frac{t_n}{\tau_c}} - e^{-\frac{t_n + 2\tau}{\tau_c}} \right] \right| \\ &= \left| \frac{\omega_0^2 \alpha T_S}{\tau v} e^{-\frac{t_n + \tau}{\tau_c}} \left[ 2 - e^{-\frac{\tau}{\tau_c}} - e^{-\frac{\tau}{\tau_c}} \right] \right| \end{aligned} \quad (14)$$

Thus, the algorithm for the square root of the Allan variance of a signal passing through a transmission line having an exponential change in delay becomes from (1) and (14),



$$\sigma = \frac{\ell \alpha T_S}{\sqrt{2} \tau v} \sqrt{\frac{1}{N} \sum_{n=1}^N \left[ e^{-\frac{t_n + \tau}{\tau_c}} \left\{ 2 - e^{-\frac{\tau}{\tau_c}} - e^{-\frac{\tau}{\tau_c}} \right\} \right]^2} \quad (15)$$

This equation is evaluated in Figure 5 for values of  $\tau$  from 1 second to  $10^6$  seconds and variables  $N=1$  to  $10^7$ ,  $\ell = 10$  meters,  $\alpha = 10^{-5}/^\circ\text{C}$ ,  $T_S = 10^\circ\text{C}$ ,  $v = 2.1 \times 10^8$  meters per second and  $\tau_c = 600$  seconds. These are estimated values for the case where 10 meters of cable are suspended in a rack cooled by plenum air and the door of the rack is opened.

These estimates indicate that the correction factor of the stabilization system will have to be between  $10^3$  and  $10^4$ , for a 10-km optical fiber link, in order to meet the goals.

Since no suitable commercial optical transmitters and receivers operating at 1300 nm wavelength are available, they are being developed at JPL. Circuitry for the cable stabilization system is also being developed. Prototypes of this equipment should be ready by the time the cable is installed in March of 1982.

A block diagram of the laser transmitter being developed is shown in Figure 6. It consists of the laser diode, a temperature stabilizer, an optical carrier level stabilizer and a modulation phase stabilizer.

The temperature of the laser is held near normal room temperature ( $\approx 25^\circ\text{C}$ ). This stabilizes its operating characteristics and extends its life. It is purposely not cooled to below room temperature because water from the surrounding air would condense on the laser eventually causing problems. In the future we plan to seal the laser in an inert gas, in which case we could cool it to a lower temperature and the lifetime would be extended appreciably. Our goal of 50,000 hours mean time to failure appears to be readily achievable once the lasers go into full scale production and the bugs are worked out.

The optical carrier level stabilizer stabilizes the optical carrier power which tends to decrease with age for a given current.

The modulation phase stabilizer locks the phase of the detected output to the phase of the input signal.

There are two areas of concern at this time. Single-mode fiber directional couplers are not available and there is a problem coupling the laser output to a single-mode fiber efficiently.

## PROGRESS

The optical fiber cable has been ordered and will be received in the first quarter of 1982.

Temperature coefficient of delay has been measured at JPL (reference 4) for various optical fibers. One result is shown in figure 7. The  $<7$  ppm per  $^{\circ}\text{C}$  shown is typical for fibers cabled in loose tubes, but can be much worse for tightly jacketed fibers. The indicated hysteresis is in the measurement system.

Tests were made to verify that the delay through single-mode optical fibers is affected very little by bending. A 500-MHz signal was transmitted through a 1-km piece of single-mode fiber cable. The phase delay through the cable was monitored while the cable was moved and bent in different ways. With a phase noise floor of about 0.2 degrees (1 ps) no change occurred that could be related to the movement of the cable.

The 1300 nm wavelength lasers and photodiodes were not available until May of this year (1981) and had to be packaged before they could be used. The packaging has just been completed.

A high isolation low-phase noise distribution amplifier and a temperature-stabilized phase detector, needed for the cable stabilization system, were developed in the meantime.

The distribution amplifier (reference 5) specifications are,

- \* 25 to 225 MHz bandwidth,
- \* 3 dB nominal gain,
- \* +14 dBm output power,
- \* Power spectral density of phase noise is  $< -140$  dBc in a 1 Hz bandwidth, 10 Hz from a 100 MHz signal,
- \*  $> 100$  dB back to front isolation below 200 MHz and,
- \*  $> 100$  dB isolation between any pair of the 4 output ports up to 110 MHz.

The temperature-stabilized phase detector, Figure 8 (reference 6), uses a high-level Schottky diode mixer. It has a temperature coefficient of  $0.014$  ps/ $^{\circ}\text{C}$  or  $8.7 \times 10^{-6}$  radians/ $^{\circ}\text{C}$  at 100 MHz. The thermal time constant is  $\approx 500$  seconds. Good thermal control of these devices is achieved by winding the heater wire directly on the mixer and placing the thermistors at the most thermally sensitive location.

The control circuitry for the 1300 nm laser diode has been breadboarded and is being tested except for the modulation phase stabilizer. The laser diode is being simulated for these tests until the circuitry is proven.

A pin diode optical receiver design has been tested at 850 nm wavelength. It will be converted to 1300 nm wavelength when the 1300 nm laser diode is operating.

## CONCLUSION

Preliminary measurements have been made on optical fiber cable, optical system components and phase-stabilization system components. The results indicate that the goals can be approached. There are some problems and some gray areas, but the technology is moving rapidly, and solutions are expected soon.

## ACKNOWLEDGMENT

The author wishes to thank Richard Sydnor for technical assistance and suggestions throughout the course of this work.

## REFERENCES

1. G. Lutes, "Optical Fibers for the Distribution of Frequency and Timing References," NASA Conference Publication 2175, Proceedings of the Twelfth Annual Precise Time and Time Interval (PTTI) Applications and Planning Meeting, held at Goddard Space Flight Center, Greenbelt, Maryland, Dec. 2-4, 1980.
2. K. Y. Lau, "Signal-To-Noise Ratio Calculation for Fiber Optics Links," The Telecommunications and Data Acquisition Progress Report 42-58, Jet Propulsion Laboratory, Pasadena, CA, Aug. 15, 1980.
3. Barnes, J. A., et al., "Characterization of Frequency Stability," NBS Technical Note 394, National Bureau of Standards, Washington, D.C., 1970.
4. L. Bergman, et al., Plots of Delay vs. Temperature, to be published, Jet Propulsion Laboratory, Pasadena, CA, 1982.
5. Y. V. Lo, "A Four-Way Distribution Amplifier for Reference Signal Distribution," The Telecommunications and Data Acquisition Progress Report 42-62, Jet Propulsion Laboratory, Pasadena, CA, April 15, 1981.

6. Y. V. Lo, "Temperature Stabilized Phase Detector," The Telecommunications and Data Acquisition Progress Report 42-64, Jet Propulsion Laboratory, Pasadena, CA, June 15, 1981.

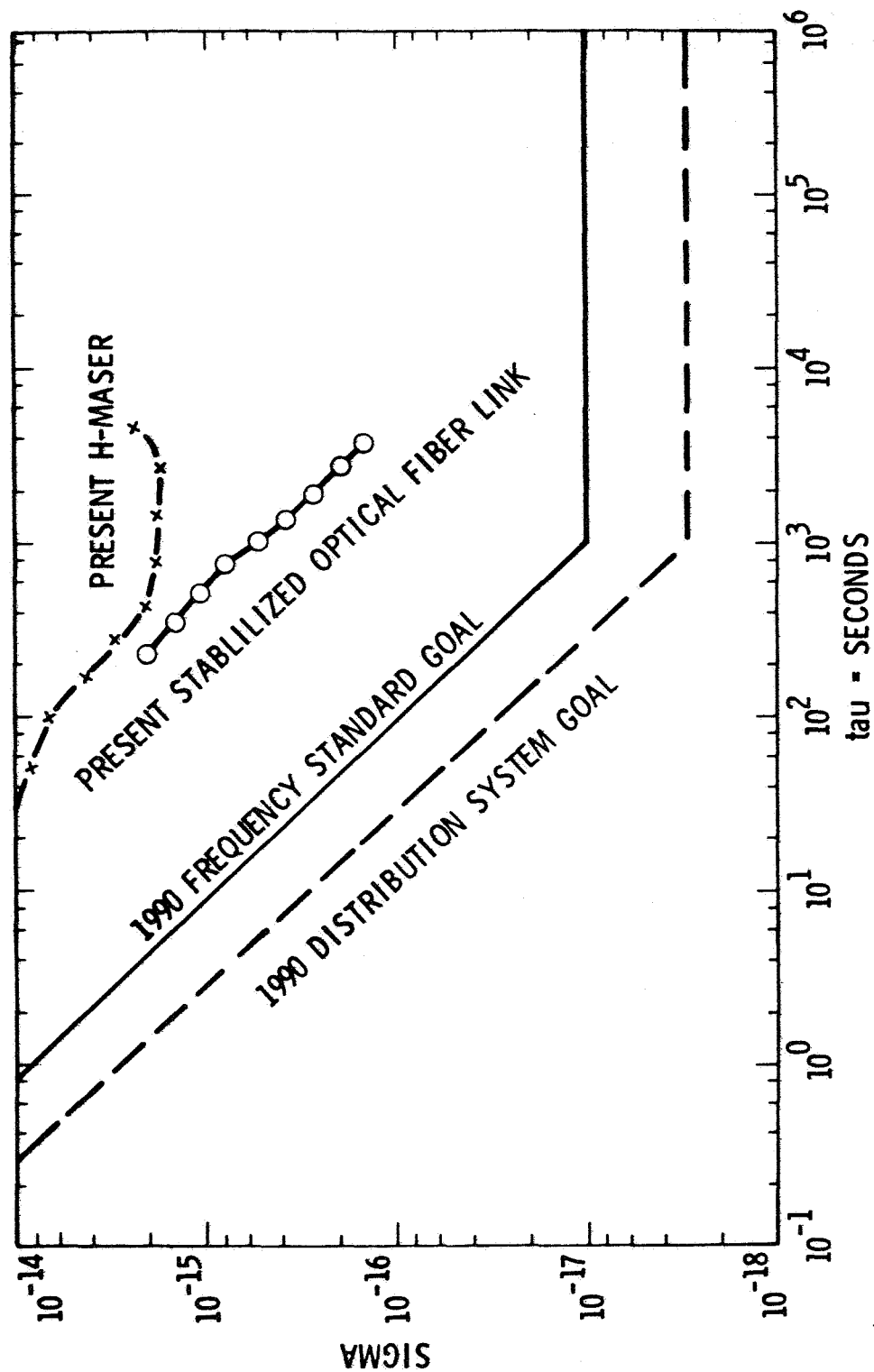


Figure 1. Present State-of-the-Art and Goals

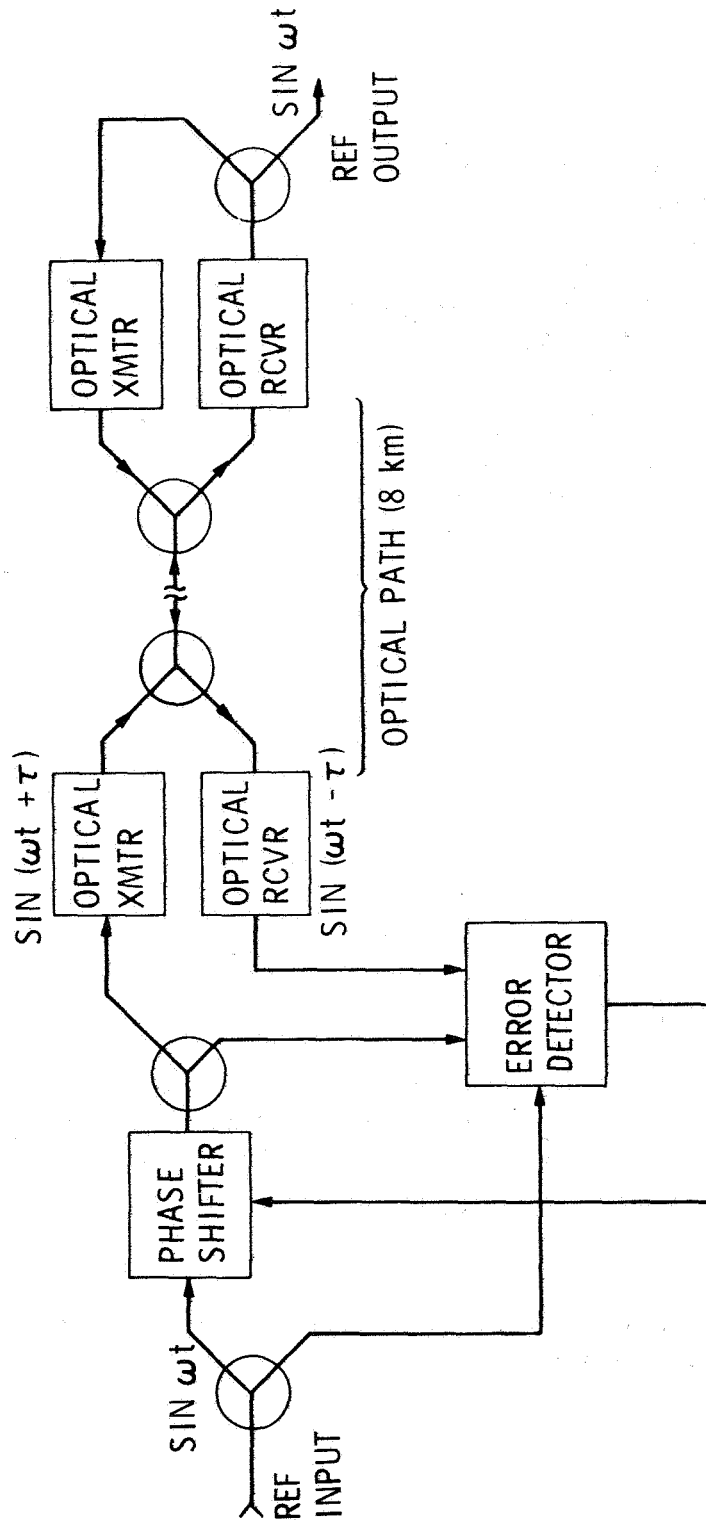


Figure 2. Conjugation Method of Phase Stabilization

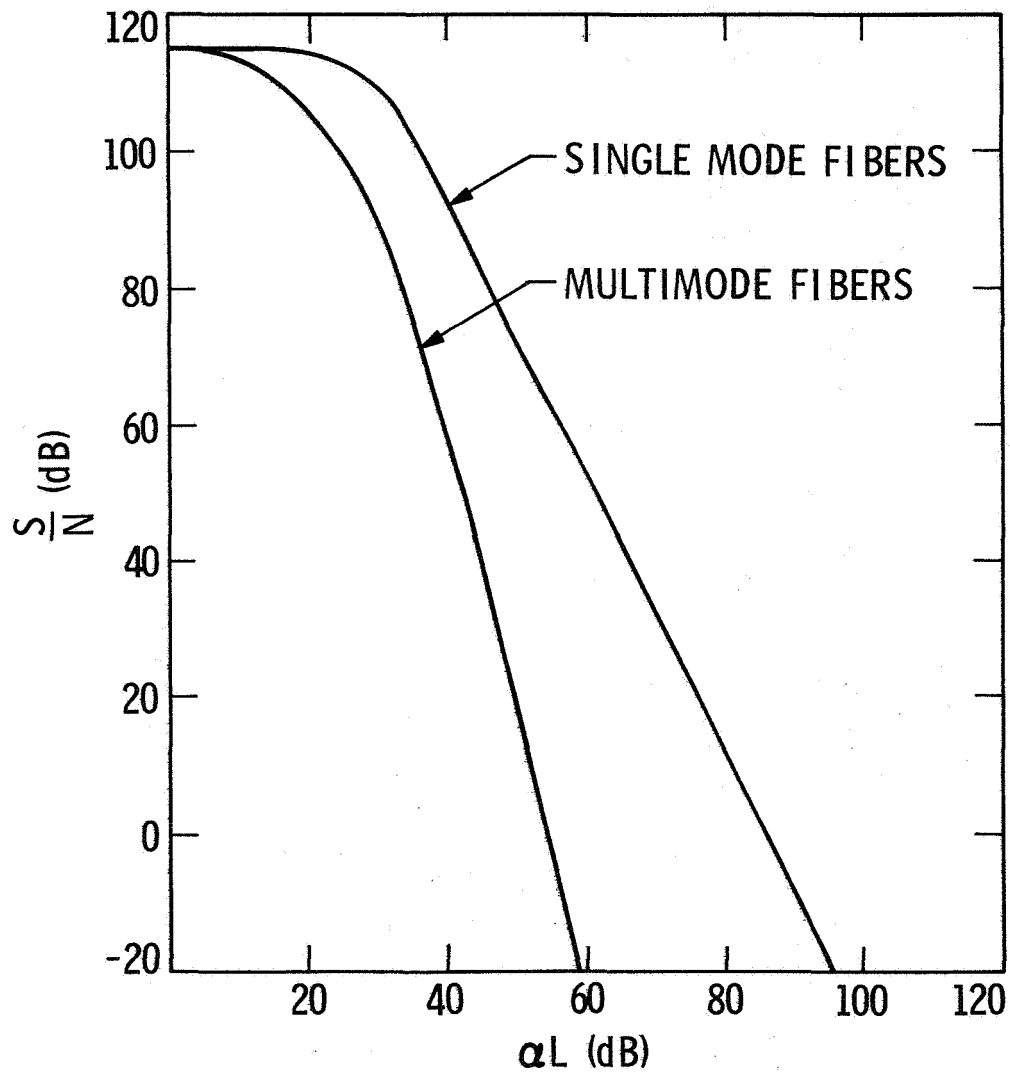


Figure 3. Signal-to-Noise Ratio vs Total Fiber Attenuation (10 Hz Bandwidth) at  $F_o = 100$  MHz

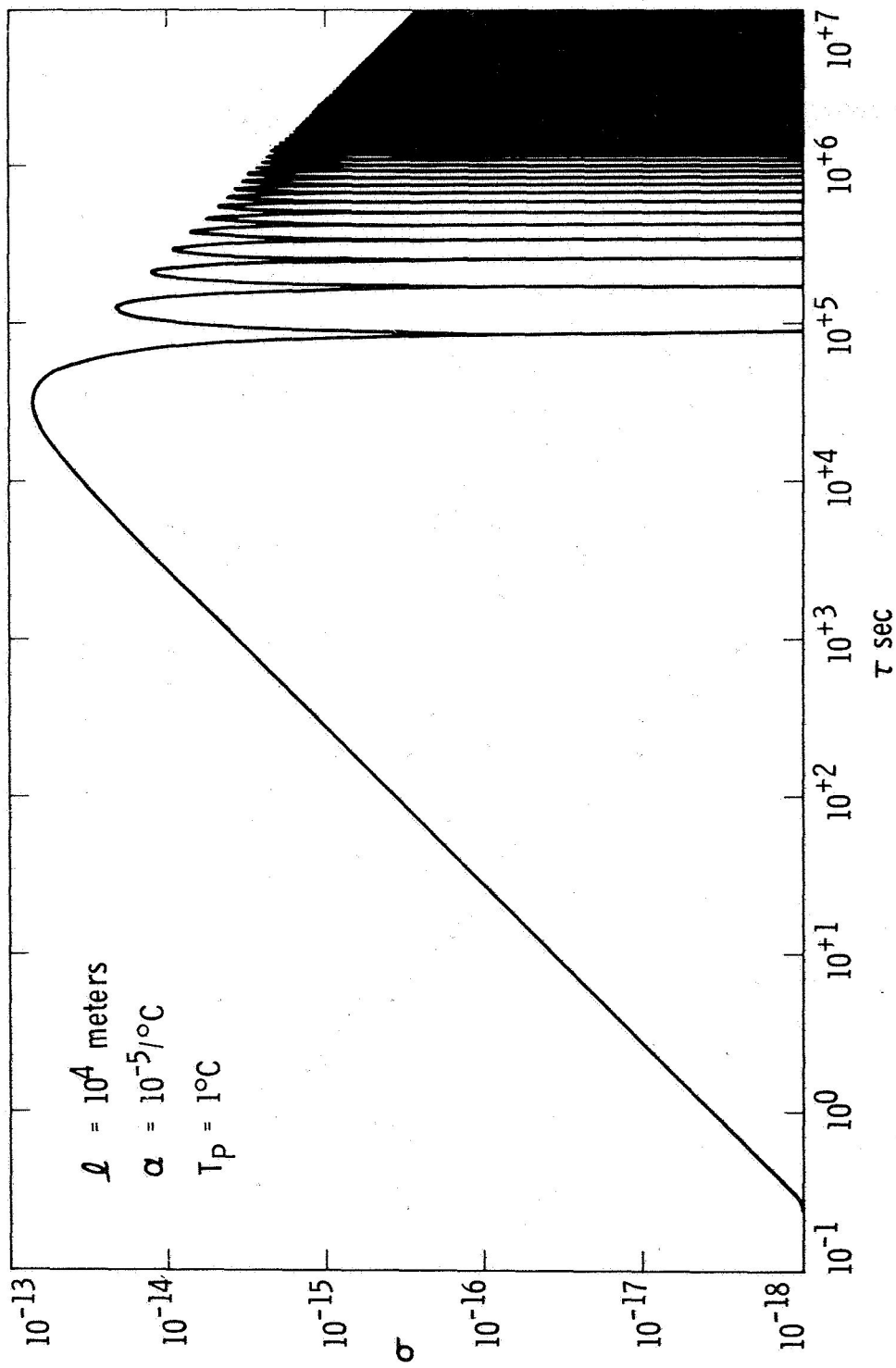


Figure 4. Estimated Frequency Stability vs Sampling Period for an Unstabilized Single Mode Optical Fiber Link



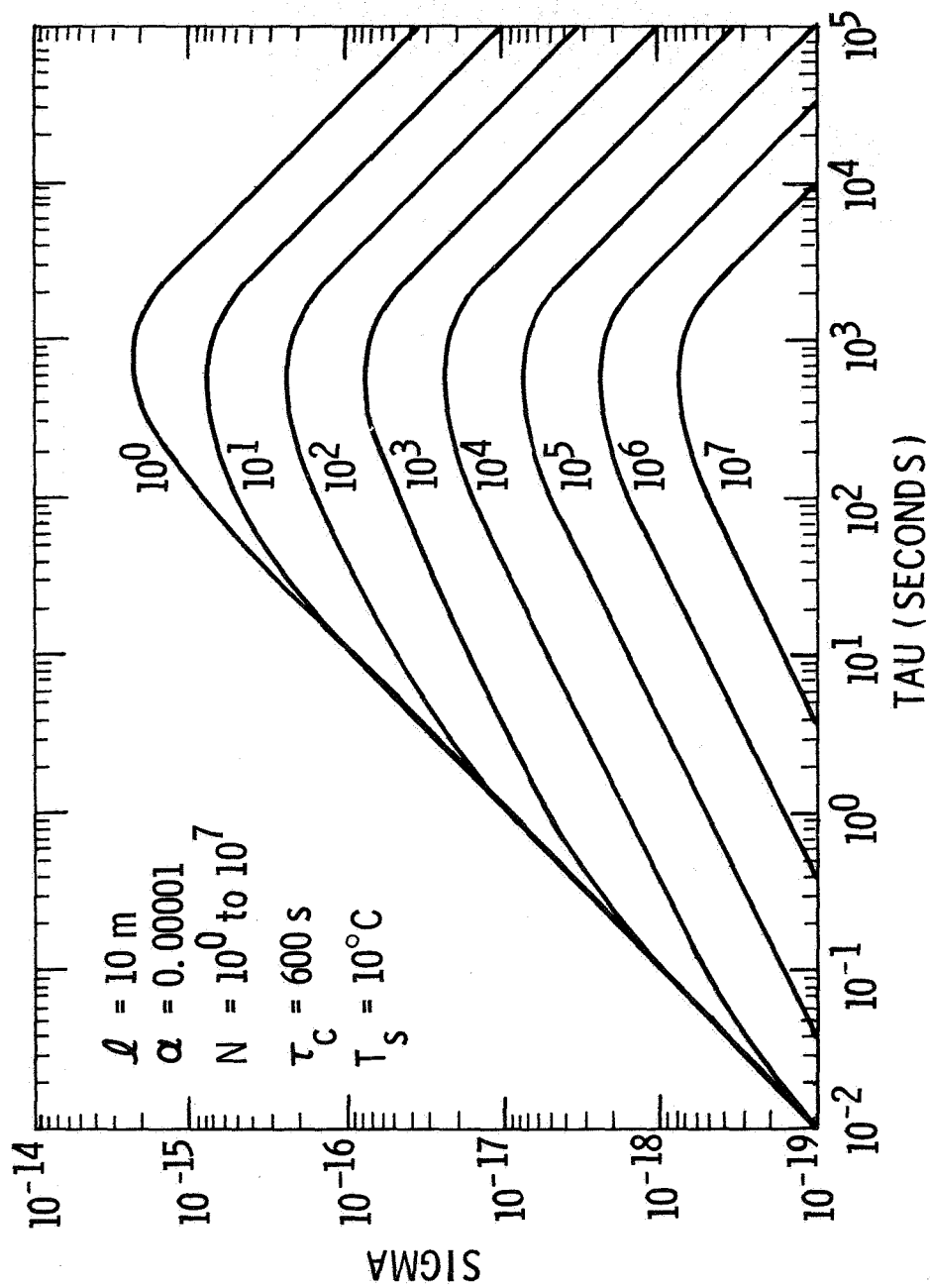


Figure 5. Stability as Affected by a Step Change in Temperature on a Cable

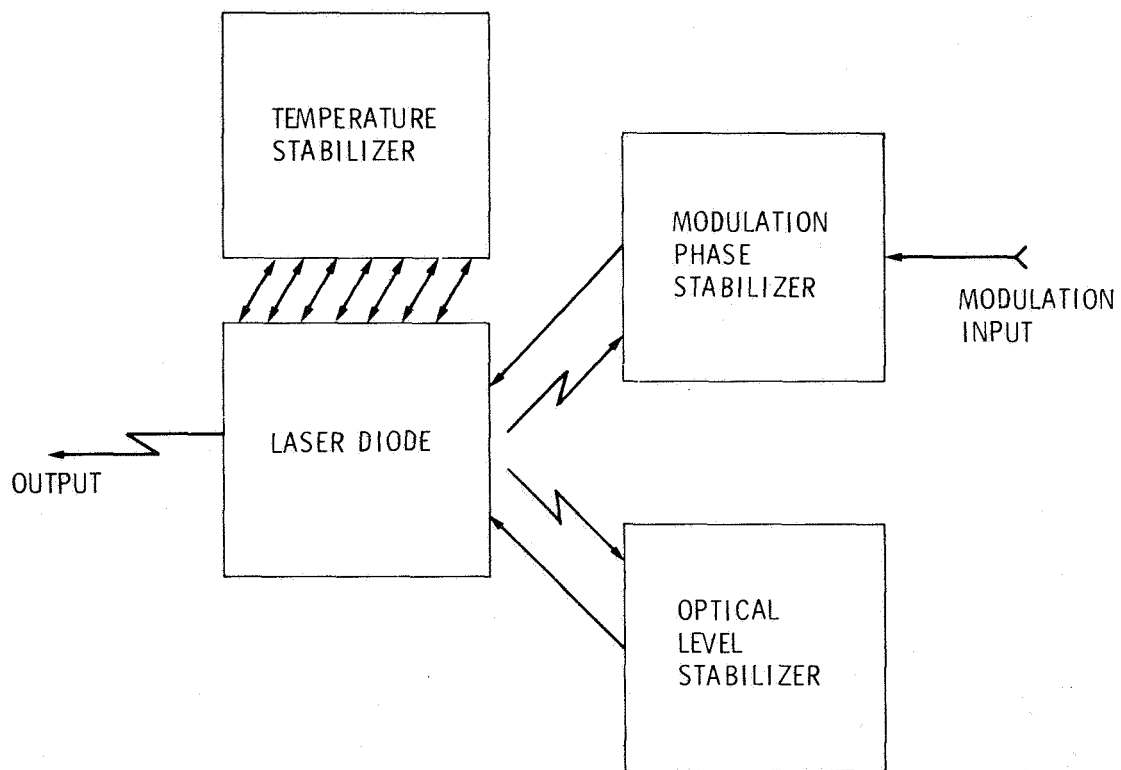


Figure 6. Block Diagram of the Laser Transmitter

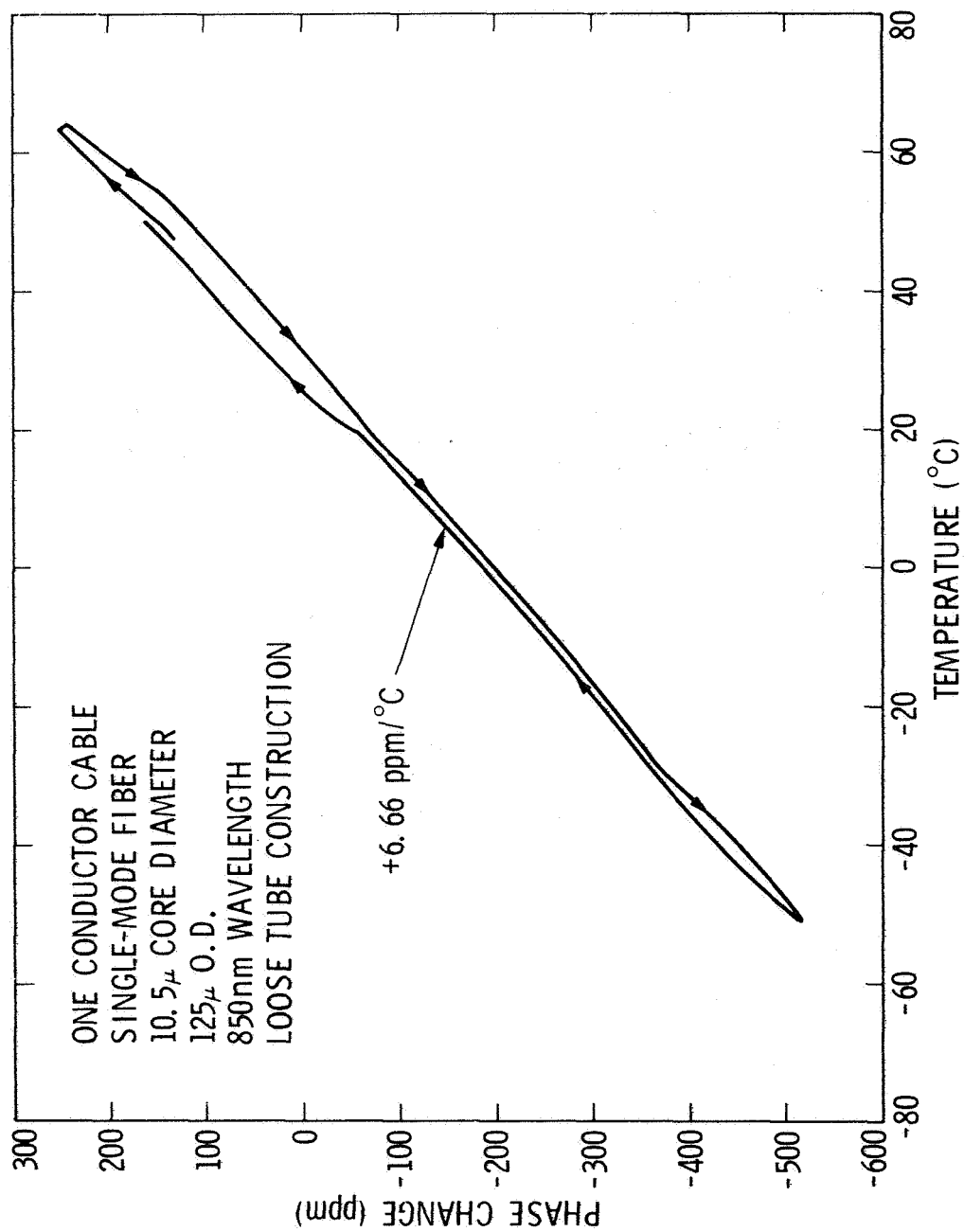


Figure 7. Phase Delay vs Temperature of a Single Mode Optical Fiber Cable

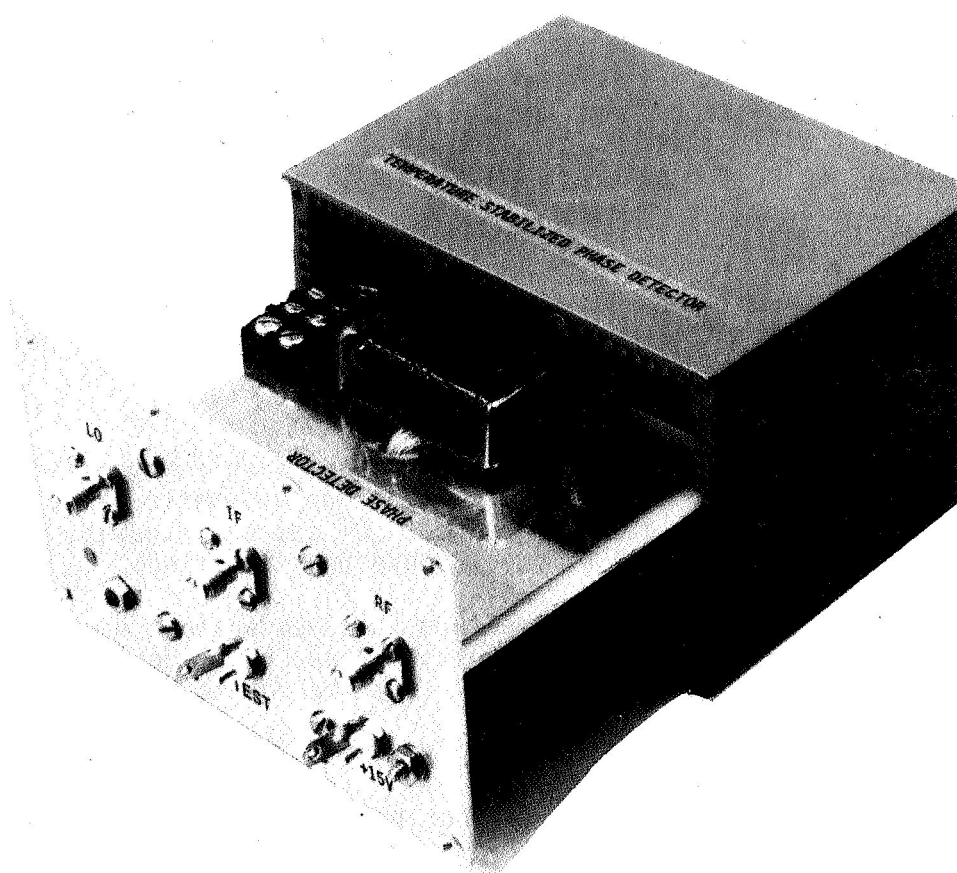


Figure 8. The Temperature Stabilized Phase Detector with the Insulation Removed

## QUESTIONS AND ANSWERS

MR. JIM KEMPARO, Aerospace Corporation

How concerned are you with spectral aging of the laser diode?

MR. LUTES:

Well, we're very concerned. We hope eventually to be able to put the diode in an inert environment and cool it below room temperature to protect it, and we believe that will greatly extend the life. Hopefully, it will extend it enough that we don't have a problem with that if we have a regular maintenance program.

MR. LAUREN RUEGER, JHU/APL

Are you doing anything to compensate for frequency dispersion over the large bandwidths you are trying to transmit on this fiber optic?

MR. LUTES:

The dispersion of the cable that we're buying, single mode fiber in the cable is such that we're hoping to get one gigahertz bandwidth to go over the eight kilometer distance. Of course, bandwidths as great as 30 to 35 gigahertz kilometer have been reported.

Nobody really knows how to measure that yet without having a long cable; so, we have a problem in that area, but I don't think it is going to be a problem at the levels that we're looking at.

DR. FRED WALLS, NBS

What's the level of sensitivity of your precision phase detector?

MR. LUTES:

I don't know off hand. It's a high-level Schottky Diode mixer.

DR. WALLS:

Sure. But if the amplitude of the signal changes by a couple of dB, how many picoseconds does that cost you?

MR. LUTES:

I don't know. I don't have those numbers.

DR. WALLS:

Thank you.

LOW NOISE BUFFER AMPLIFIERS AND BUFFERED PHASE  
COMPARATORS FOR PRECISE TIME AND FREQUENCY  
MEASUREMENT AND DISTRIBUTION

R.A. Eichinger, P. Dachel, W.H. Miller and J.S. Ingold  
Bendix Field Engineering Corporation  
Columbia, Maryland

ABSTRACT

Extremely low noise, high performance, wideband buffer amplifiers and buffered phase comparators have been developed for the NASA Goddard Space Flight Center Atomic Hydrogen Standards Program. These buffer amplifiers are designed to distribute reference frequencies from 30 KHz to 45 MHz from a hydrogen maser without degrading the hydrogen maser's performance. The buffered phase comparators are designed to intercompare the phase of state-of-the-art hydrogen masers without adding any significant measurement system noise. These devices have a 27 femtosecond phase stability floor and are stable to better than one picosecond for long periods of time. Their temperature coefficient is less than one picosecond per degree C, and they have shown virtually no voltage coefficients. When used in distribution amplifiers and phase comparison systems, these devices have greater than 90 dB of isolation.

INTRODUCTION

Extremely low noise buffer amplifiers, distribution amplifiers and buffered phase comparators have been developed by NASA Goddard Space Flight Center's Atomic Hydrogen Standards Program with engineering support from Bendix Field Engineering Corporation (BFEC). The buffer amplifiers are designed to distribute reference frequencies between 30 KHz and 45 MHz without degrading the hydrogen maser's performance. The distribution amplifiers are designed to provide multiple outputs with a minimum of cross talk. The phase comparators are designed to intercompare the phases of state-of-the-art hydrogen masers without adding any significant system noise.

BFEC has been building, testing and improving these buffer amplifiers and phase comparators. Both the electrical and the mechanical designs ensure their meeting the requirements of hydrogen maser performance.

These devices have been extensively tested. This paper will report on the results of those tests and the specialized test systems developed to perform these tests.

The contents of this paper have been divided into five sections. The first section will state what is meant by distribution and measurement requirements that do not degrade state-of-the-art performance of hydrogen masers. In the second section, an electrical and mechanical description of buffer amplifier and phase comparator design will point out the reasons for their high stability. The third section will describe the tests and measurements performed and will discuss in detail the systems used to perform those tests. Fourth, a detailed test result section will discuss the results of each test and discuss some design improvements that have increased performance. A final section will summarize the data for easy reference.

The tests and measurements are divided into three groups.

1. TIME DOMAIN PHASE TESTS
  - a. Temperature Coefficient
  - b. Power Supply Voltage Coefficient
  - c. Mechanical Shock Coefficient
  - d. Allan Variance Phase Stability
2. FREQUENCY DOMAIN TESTS AND MEASUREMENTS
  - a. Frequency Response
  - b. Harmonic Signal Generation
  - c. VSWR
  - d. Isolation (back-to-front, port-to-port)
3. SPECTRAL PHASE MEASUREMENTS
  - a. Phase Noise Spectrum
  - b. 60 Hz AC Magnetic Field Sensitivity

Time domain phase tests were run to test for phase changes due to environmental changes. The tests that were run include tests for temperature coefficient of phase, voltage coefficient of phase, mechanical shock coefficient of phase and Allan variance tests for phase

stability. Frequency domain tests and measurements are also included. Wideband frequency response, harmonic signal generation, and VSWR were measured. The buffer amplifiers and phase comparators were also tested for back-to-front isolation. When the buffer amplifiers were configured with a power splitter to form a distribution amplifier, port-to-port isolation tests were run. Spectral phase measurements were made of phase noise in a 10 Hz BW between DC and 1 KHz, and phase noise in a 100 Hz BW between DC and 100 KHz. The same measurement system was also used to test for 60 Hz AC magnetic field sensitivity.

#### REQUIREMENTS.

Hydrogen masers have phase stability floors of the order of 0.1 ps and long term stabilities of the order of 1 ps (1). In order not to degrade these stable signals, distribution and measurement devices must have extremely low additive noise, high stability and low sensitivity to environmental changes. Also, to minimize the effect of cross talk from multiple users, isolation factors from -110 dB to -90 dB are required at 5 MHz.

For this paper, except when talking about isolation, phase disturbances will be normalized to clock error units by:

$$x = \frac{\phi}{\omega_0}$$

but, for simplicity, will still be referred to as phase changes or phase stabilities. A phase error of 1 ps on a 5 MHz carrier corresponds to an isolation of -90 dB and 0.1 ps at 5 MHz corresponds to -110 dB. Small phase changes,  $\delta\phi$ , may be converted to units of dB by the relation:

$$\delta\phi = 20 \log \delta x + 20 \log \omega_0$$

where  $\delta x$  is a small time disturbance in seconds and  $\omega_0$  is the carrier frequency in radians per second.

The buffer amplifier and phase comparator devices described in this paper exceed the minimum requirements of hydrogen maser performance. As testing continues, the major contributors to phase errors are being isolated and improved upon by design modifications. A brief electrical and mechanical description follows.

#### DESCRIPTION OF DEVICES

The buffer amplifier was designed for use in 50  $\Omega$  RF systems. The gain can be adjusted from 0 to 10 dB to bring outputs up to 1 VRMS to compensate for the power splitter losses of distribution systems. Each buffer amplifier has its own voltage regulator to reduce indirect cross talk due to power supply changes under varying load conditions.



The essence of the buffer amplifier is in its high stability and high isolation. This is achieved not only by its electronic design (2) but by its mechanical design. A common heat sink for all semiconductor circuit elements has been essential in producing good temperature performance. The heat sink slows down the effects of ambient temperature changes and reduces gradients across semiconductor components improving the cancellation of temperature effects inherent in matched semiconductor components.

The phase comparator is used to compare the phases of two RF signals at nearly the same frequency with subpicosecond precision. The two RF signal inputs are highly isolated by buffering each port with a unity-gain buffer amplifier (see figure 1). These drive a double balanced mixer generating a beat frequency between the two RF inputs. The beat frequency is filtered by a passive low pass filter and then by an active low-passed, zero-crossing detector. A TTL compatible square wave is output with positive and negative going edges corresponding to the zero-crossings of the beat between the two RF signal inputs. If the epoch of these TTL edges is measured by a clock, the phase difference between the RF inputs can be constructed.

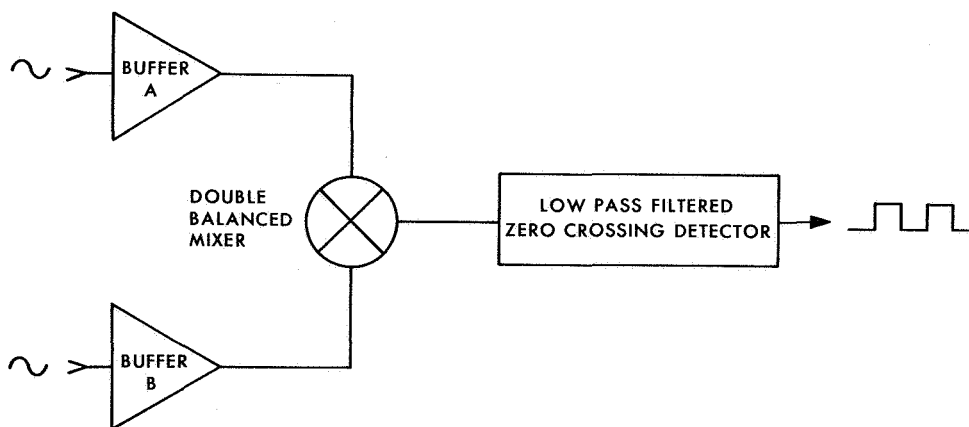


Figure 1. Buffered Phase Comparator Block Diagram

The phase comparator employs the same mechanical design as the buffer amplifier. A common heat sink is used for all the semiconductors in its two buffer amplifiers and double balanced mixer. Reducing temperature gradients across the double balanced mixer is especially important since it achieves its high stability by using four matched diodes.

## DESCRIPTION OF TEST SYSTEMS

### Time Domain Phase Tests

Many of the tests are run using a dual phase comparator test system (see figure 2). The test technique is based on the Picosecond Time Difference Measurement System used by the National Bureau of Standards (NBS) (3). Two TTL signals corresponding to the same phase difference between two crystal oscillators are intercompared by a time interval counter. To improve the system's phase stability floor, the RF cables are adjusted to cancel the phase noise from the crystal oscillators.

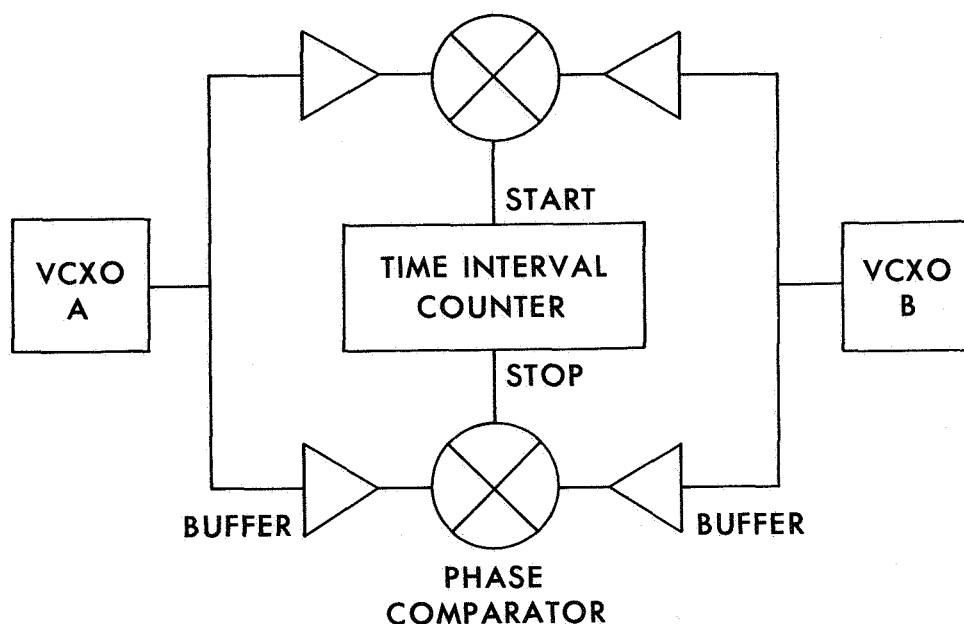


Figure 2. Dual Phase Comparator Test System

The dual phase comparator test system is a versatile test instrument. Once a test set-up has been characterized, test devices are substituted for known good devices. Device phase change characteristics versus time, temperature, power supply voltage, mechanical shock and 60 Hz AC magnetic fields are calculated from phase data.

The tests are automated by a programmable calculator. Most tests have operating programs that control programmable time interval counters, digital multimeters and digital plotters. Software has been written for the HP9815 and HP9825 calculators to run plots on two types of HP

plotters. Each of the programs allow the operator to select plotting scales and the number of data points to be averaged. A program to run two sample allan variance data may be run at any time during the tests.

#### Frequency Domain Tests and Measurements

Frequency domain tests and measurements were made with a tracking generator and a spectrum analyzer (see figure 3). The type of analyzer varied, depending on the frequency band of the measurement.

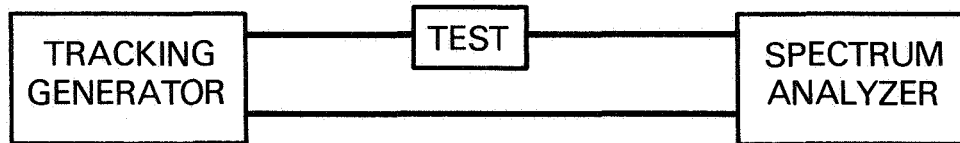


Figure 3. Frequency Domain Test and Measurement System

The buffer amplifiers and phase comparators are tested for back-to-front and port-to-port isolation. The test is performed simply by inputting a nominal signal (+13 dBm) into the output and examining the leakage signal at the input. Another method used in multiple buffer amplifiers systems is to short or open the output of one buffer while recording the phase of a signal through another buffer with the dual phase comparator system (see figure 2). Each test reveals a worst case phase disturbance as previously discussed.

Tests for harmonic distortion are made on all buffer amplifiers and phase comparators. The signal level of both the second and third harmonics are recorded relative to a +13 dBm output signal at 5 MHz. Although harmonic signals, which are phase coherent, pose no phase problem; they are of interest to those who use these devices with frequency multiplication or division circuits.

A similar configuration with a programmable network analyzer replacing the spectrum analyzer was used to measure voltage standing wave ratio (VSWR). The VSWR was run to ensure an accurate 50  $\Omega$  input and output impedance over the entire bandpass of the buffer.

## Spectral Phase Measurements

Spectral phase measurements were made using a single mixer test system (see figure 4). A 5 MHz signal is split and shifted 90 degrees by a quadrature hybrid phase shifter (4). The unshifted signal is fed through a buffer amplifier and input to one port of the mixer. The shifted signal is fed through a variable air line and another buffer to provide signals 90 degrees different in phase at the mixer. The mixer symbol, in figure 4, represents a modified phase comparator; in which, both the active filter and zero-crossing detector were by-passed. To minimize high frequency noise, a two-pole, low pass filter was used following the mixer. One stage was placed at the output of the mixer and the other stage was placed at the input of a low frequency spectrum analyzer.

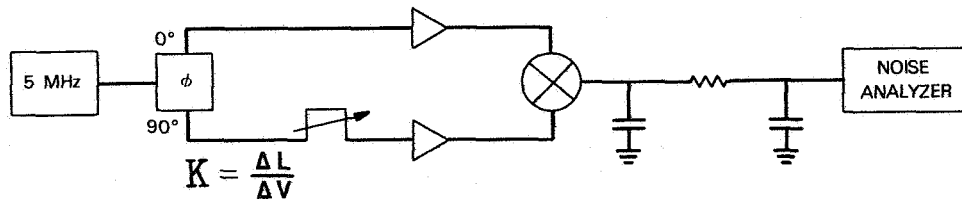


Figure 4. Spectral Phase Measurement System

The basic theory of this measurement technique is as follows. The mixer outputs a voltage that is proportional to small phase changes:

$$\phi \propto V$$

thus small changes in phase can be measured in terms of small changes in voltage. Phase disturbances may be written as:

$$\delta\phi = \frac{K\omega_0}{c} \delta V$$

where K is a calibration constant in centimeters per volt, made by increasing the path of one signal through the variable air line and recording the DC voltage change with a precision digital multimeter. The constants,  $\omega_0$  and c, are included to convert K to radians per volt. Small voltage disturbances are generally measured in dBV and can be converted to phase disturbances in dB by:

$$\delta\phi = \delta V + 20 \log \frac{K\omega_0}{c}$$

To measure the phase noise spectrum of one or more unity-gain buffers, they may be substituted for other buffers or added to either signal path. Then the additional phase noise is displayed on the spectrum analyzer. The test system was checked for flat, low frequency response by frequency modulating a small signal on one 5 MHz signal. The system's frequency response rolled off 3 dB at 900 KHz.

The test system was used to measure the phase spectrum in a 10 Hz bandwidth (BW) between DC and 1 KHz and the phase spectrum in a 100 Hz BW between DC and 100 KHz because a 1 Hz BW spectrum analyzer was not available at the time. The data were not corrected to a 1 Hz BW because the correction factor would be different for the phase noise spectrum and the spectral lines in the data. Another measurement made with this system was the 60 Hz AC magnetic field sensitivity of the buffer amplifiers, distribution amplifiers and phase comparators. An AC field was generated by using a spare maser field coil. The test device was oriented in its most sensitive position so that a worst case 60 Hz phase noise peak could be recorded.

#### TEST RESULTS

The previous section outlined the tests that have been run on buffer amplifiers, distribution amplifiers and phase comparators. This section will discuss raw data samples of typical test results. Also discussed, will be changes to the buffer amplifier and phase comparator design that were made to improve certain test results.

Figure 5 is a plot of phase comparator temperature performance. The plot of phase in picoseconds as measured by the dual phase comparator test system is shown. The temperature of the phase comparator under test is monitored on the chassis. Upon completion of the test, a temperature coefficient is then calculated from the phase change before and after the temperature step. Phase comparator test results are all better than 1.0 ps/°C. Please note the peak-to-peak phase noise on figure 5 and compare it with figure 6.

Figure 6 is a plot of buffer amplifier temperature performance. The peak-to-peak phase noise is noticeably higher. This increase in noise level was purposely caused by delaying one signal path so that the phase noise of the crystal oscillators could not be sufficiently cancelled. Time delays are normally held below 1 ns to ensure a 27 femto-second noise floor. A thirty-eight buffer sample was tested by this method. Their mean temperature coefficient was 0.41 ps/°C with a standard deviation of 0.27 ps.

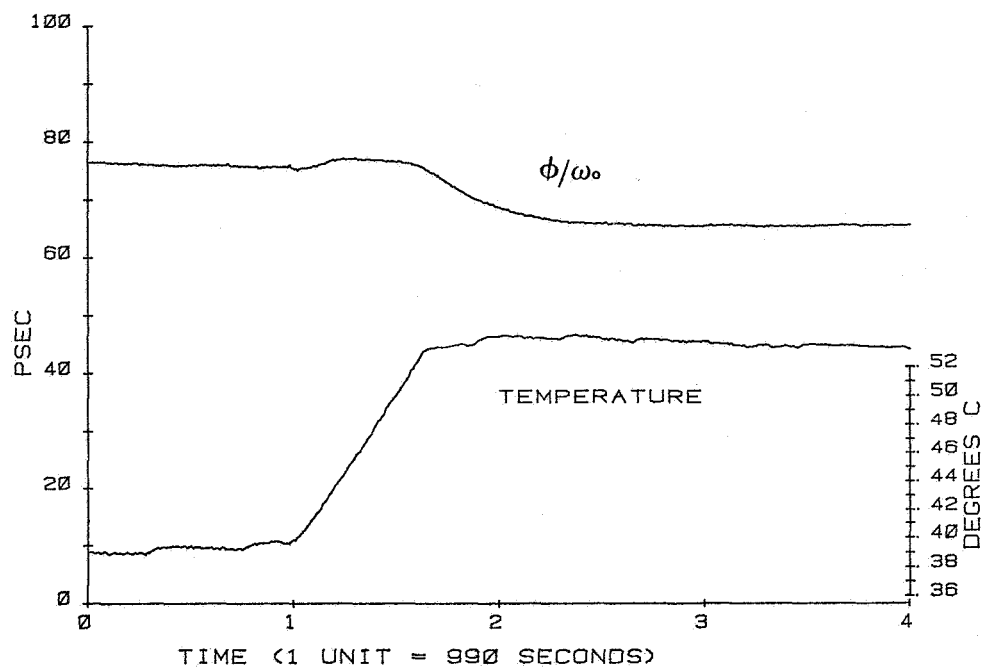


Figure 5. Typical Phase Comparator Temperature versus Phase Performance

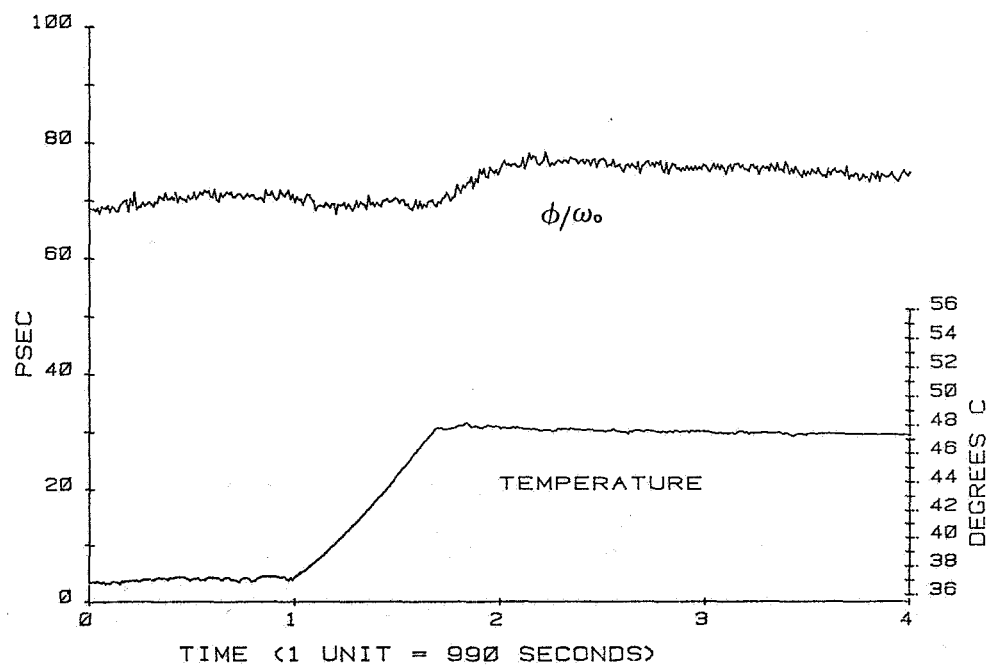


Figure 6. Typical Buffer Amplifier Temperature versus Phase Performance

Shock sensitivity was also tested for using the same dual phase comparator test system. A calibrated hammer blow was applied to several buffers' most sensitive chassis face. When it was discovered that small movements in the position of parts in the buffer amplifier caused relatively large phase jumps, a thermal conductive potting compound was used to reduce the phase jumps to less than 1 ps/10 g shock (see figure 7). One ps is the dual phase comparator system resolution since any band in the RF cables caused a 1 ps phase jump.

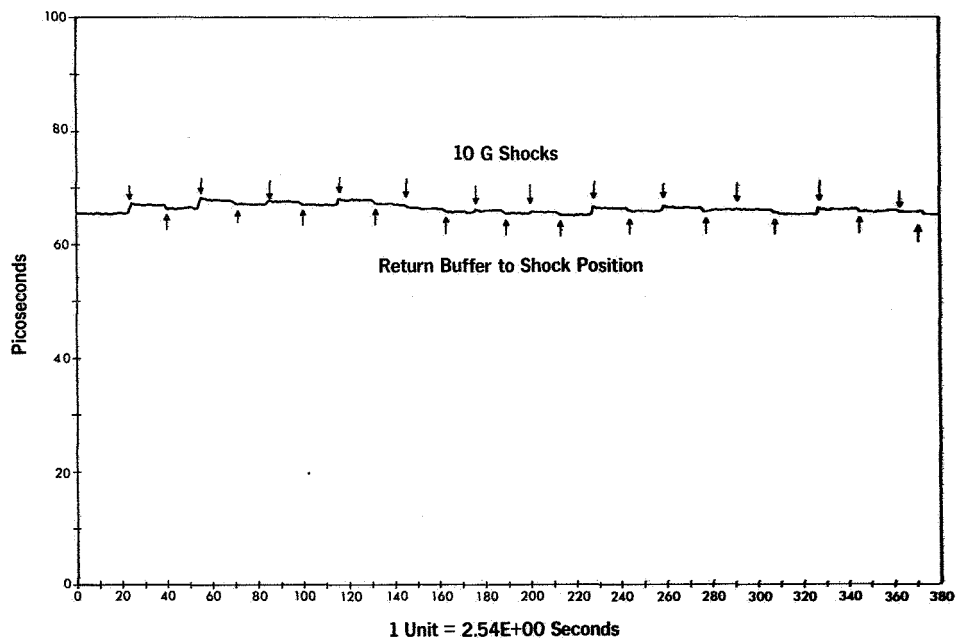


Figure 7. Typical Buffer Amplifier Mechanical Shock versus Phase Performance

Figure 8 is a plot of power supply voltage versus phase for a buffer amplifier. The power supply voltage was stepped from 25 to 32 volts. There were no phase changes, to the resolution of the measurement system, between 26 and 32 volts. Below 26 volts the buffer amplifier's voltage regulator does not work since a 2.7 volt drop must be maintained across the regulator.

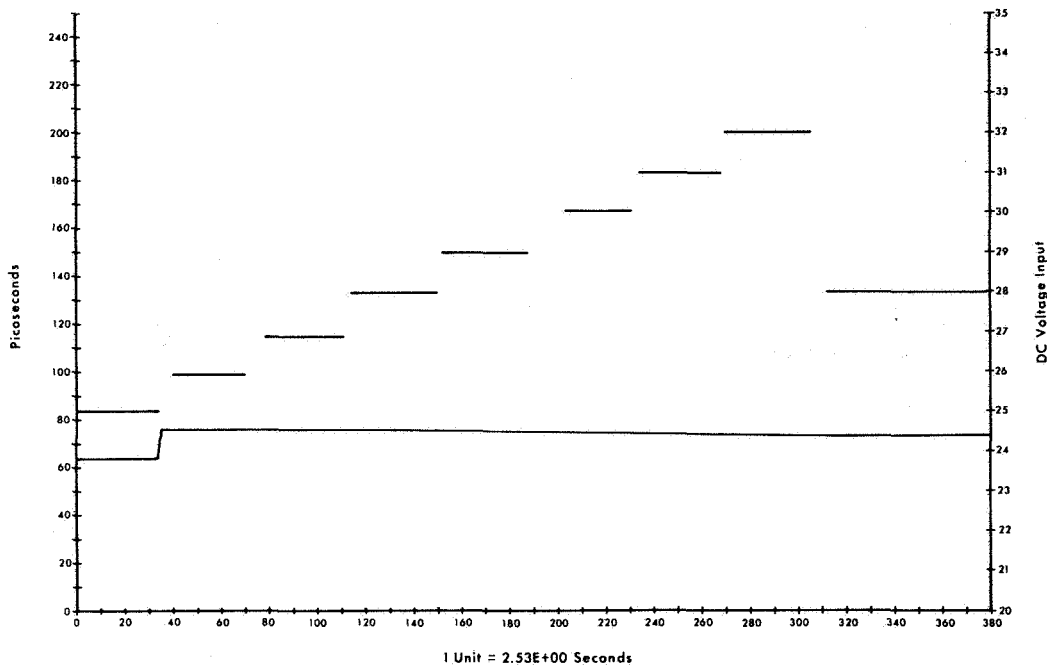


Figure 8. Typical Buffer Amplifier Power Supply Voltage versus Phase Performance

Sixty Hz AC magnetic field sensitivity can be tested for using the dual phase comparator system but the spectral phase test system has higher resolution. A 60 Hz response and corresponding odd harmonics are displayed on a spectrum analyzer. The spectrum analyzer has a few of its own 60 Hz peaks as shown in figure 9. The high peak at 0 Hz is also an intrinsic property of the spectrum analyzer. When a phase comparator was tested for 60 Hz magnetic field sensitivity in a 10 gauss field, the 60 Hz peak was -90 dB. The mixer calibration factor of  $20 \log K_{\omega_0/c}$  was +6 dB. This magnetic susceptibility, although tolerable, can be reduced to -120 dB by lining the phase comparator with a 0.005 in. sheet of co-netic foil.

Figure 9 also shows the phase noise spectrum of the phase comparator's output signal. The 6 dB mixer calibration correction is included in this data. The extremely good noise performance of the phase comparator is clearly shown in figure 9. Since both the 180 Hz and 300 Hz peaks are analyzer generated, the phase noise level in a 10 Hz BW between DC and 1 KHz is less than -138 dB.



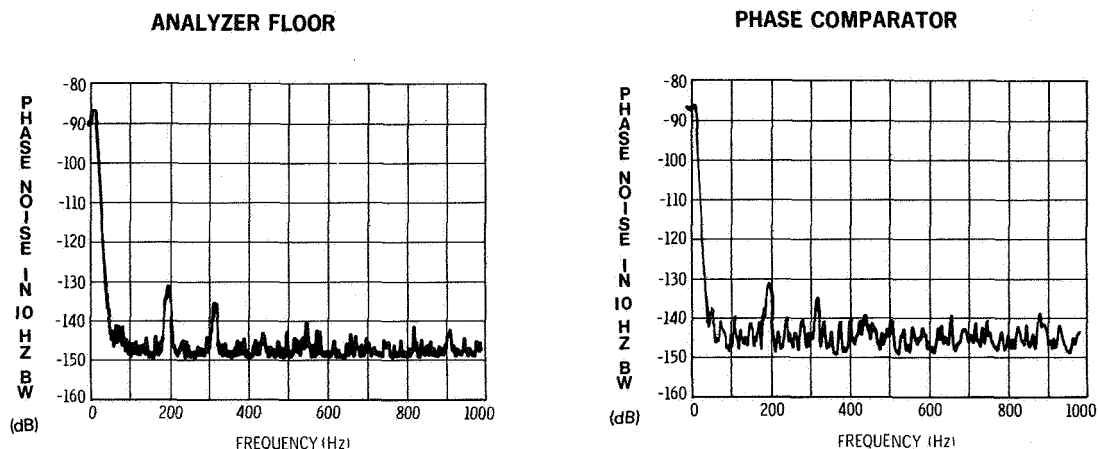


Figure 9. Phase Noise Spectrum of Spectrum Analyzer and Phase Comparator

Buffer amplifiers also have extremely low noise performance. In fact there were two buffers already in the test system during the phase comparator phase noise measurement. Figure 10 shows the phase noise level roughly doubled (+3 dB) when two more buffers were added to the test system. The increase indicates that the measurement system is actually resolving buffer amplifier phase noise.

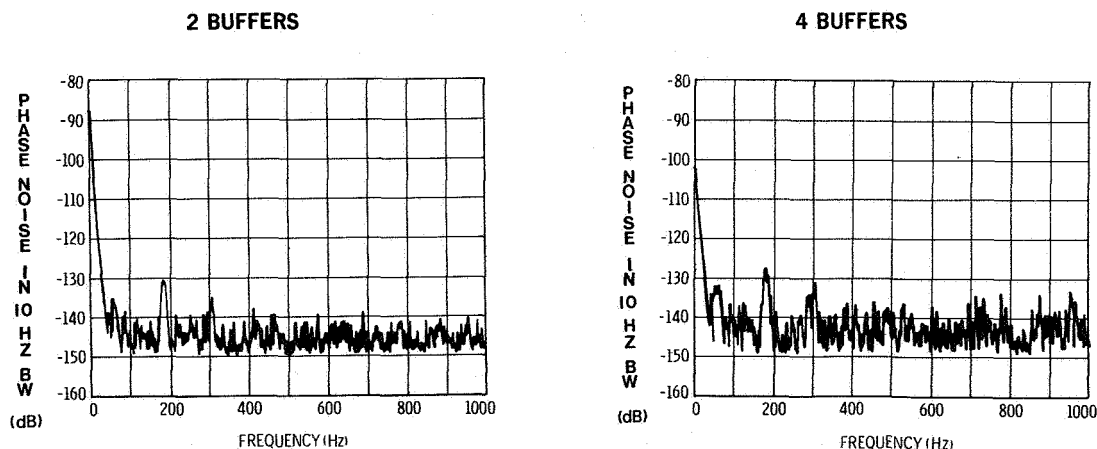


Figure 10. Phase Noise Spectrum of 2 and 4 Buffer Amplifier Measurement Systems

Figure 11 is another comparison of two and four buffer test results. But, these data are of phase noise in a 100 Hz BW between DC and 100 KHz. Again, the noise level increased 3 dB with more buffers. However, whether two or four buffer amplifiers are used, the phase noise level remains well below the required level of -110 dB.

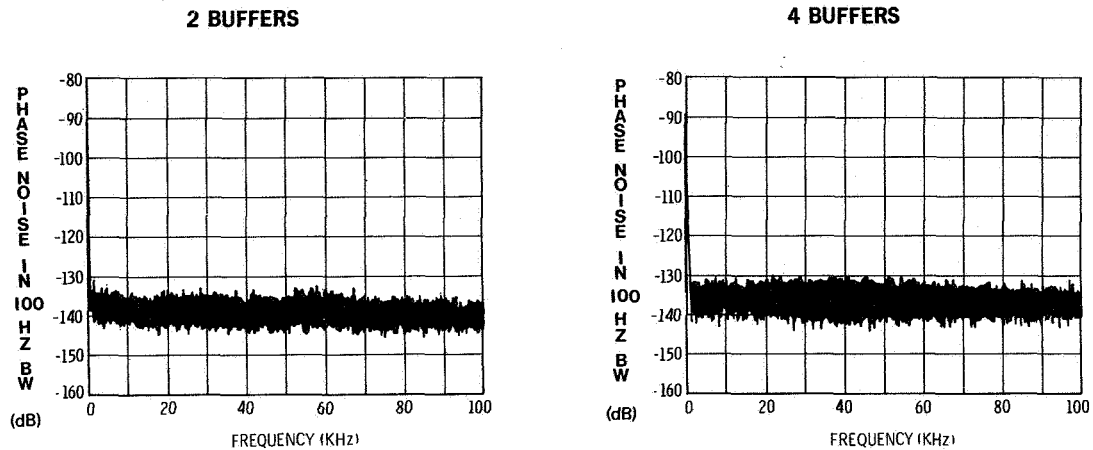


Figure 11. Phase Noise Spectrum of 2 and 4 Buffer Amplifier Measurement Systems

Table 1 shows the port-to-port isolation obtained from a distribution amplifier built for a NASA hydrogen maser. The distribution amplifier uses a Mini-Circuits Lab 8-way power splitter to distribute 5 MHz reference signals to eight output ports. The power splitter design limits the port-to-port isolation between ports on the same side of the power splitter to 25 dB. This causes a quadrant grouping of good and better isolation factors (see table 1).

#### Summary of Test Results

To summarize all the test and measurement results to date, a buffer amplifier data sheet is provided in table 2. The phase stability in a 12 Hz bandwidth of 27 femtoseconds for 1 second averaging times is a two sample Allan deviate statistic (1).

The temperature coefficient is less than  $1.0 \text{ ps}/^{\circ}\text{C}$ . The power supply voltage coefficient is less than  $0.1 \text{ ps/volt}$  which is the dual phase comparator system resolution. Permanent phase jumps from mechanical shocks of 10 G force are less than 1 ps. The 60 Hz AC magnetic field sensitivity, with the buffer turned to its most sensitive position,

		OUTPUT							
INPUT		1	2	3	4	5	6	7	8
	1	X	96	96	96	110	110	110	110
	2	95	X	93	93	110	110	110	110
	3	93	94	X	110	110	110	110	110
	4	93	93	100	X	110	110	110	110
	5	110	110	110	110	X	96	93	93
	6	110	110	110	110	110	X	94	96
	7	110	110	110	110	94	95	X	99
	8	110	110	110	110	95	95	100	X

ALL UNITS ARE IN dB

Table 1. A Typical Distribution Amplifier's Port-to-port Isolation

is -129 dB in a 10 gauss field. Buffer amplifiers configured in a distribution amplifier have a -125 dB sensitivity. Isolation tests at 5 MHz result in a minimum 67 dB back-to-front isolation for a single buffer. Forty buffers have recently been built and tested with 69 dB +2 dB back-to-front isolation. This result is an improvement over past results. When these new buffers are assembled in distribution amplifiers, higher back-to-front and port-to-port isolation test results are expected. The load isolation test result is from data of statistical measurements. Phase data were repeatedly averaged before and after a load change to each port of a distribution amplifier. The statistical mean and standard deviation resulted in a worst case -115 dB isolation factor. Harmonic signal generation is typically 56 dB below a 5 MHz carrier frequency. All other harmonics are lower, and there are no spurious signals out to 1 GHz. The 3 dB bandpass response is 15 KHz to 55 MHz at a nominal output level of +13 dBm. The gain can be adjusted easily between 1 and 10 dB by changing one resistor and one capacitor value. The VSWR at 5 MHz is less than 1.02 for both the input and the output. Power supply requirements can be either 60 mA at 24 volts or 50 mA at 28 volts. The newest buffer uses a 28 volt supply.

PHASE STABILITY .....	$2.7 \times 10^{-14}$ s AT 1 s AVERAGING TIME
TEMPERATURE COEFFICIENT .....	< 1.0 ps/°C
POWER SUPPLY VOLTAGE COEFFICIENT .....	< 0.1 ps/VOLT
MECHANICAL SHOCK SENSITIVITY .....	< 1.0 ps AT 10 G
60 Hz AC MAGNETIC FIELD (60 Hz NOISE RESPONSE) .....	-129 dB /10 GAUSS
ISOLATION AT 5 MHz	
BACK-TO-FRONT .....	-67 dB
BACK-TO-FRONT (WITH POWER SPLITTER) .....	-120 dB
PORT-TO-PORT (WITH POWER SPLITTER) .....	-90 dB
PORT-TO-PORT (SHORT/OPEN LOAD) .....	-115 dB
HARMONICS .....	-56 dB AT 10 MHz -68 dB AT 15 MHz
FREQUENCY RESPONSE (3dB) .....	15 KHz TO 55 MHz
MAXIMUM OUTPUT LEVEL .....	+13 dBm
GAIN .....	0 TO 10 dB
VSWR (50Ω/5 MHz) .....	< 1.02 AT INPUT AND OUTPUT
SIZE .....	2 x 2 x 1.25 IN.
POWER .....	60 mA AT 24 V OR 50 mA AT 28 V

Table 2. Buffer Amplifier Data Sheet

Table 3 is a data summary for the phase comparator. The phase stability is 27 femtoseconds for about 1 second averaging times (1). Phase comparators also have less than 1 ps/°C temperature coefficients. Their power supply voltage coefficients are less than 1.0 ps/volt for both  $\pm 15$  volt supplies and less than 0.1 ps/volt for the 24 volt supply. When placed in a 60 Hz AC magnetic field. The worst case 60 Hz peak is -120 dB. Port-to-port isolation at 5 MHz is -100 dB. The phase comparator's usable frequency range is between 100 KHz and 55 MHz. The phase comparator will respond to relatively low input levels and has been used to intercompare different carrier frequencies through internal harmonic generation. An RF input level of +13 dBm should not be exceeded to obtain the best performance. The phase comparator puts out a TTL compatible square-wave, phase coherent with the beat frequency of the two mixed RF signals. A 120 mA supply at 24 volts powers the buffers in the phase comparator. A  $\pm 20$  mA supply at  $\pm 15$  volts supplies the zero-crossing detector electronics.

PHASE STABILITY .....	$2.7 \times 10^{-14}$ s AT 1 s AVERAGING TIME
TEMPERATURE COEFFICIENT .....	< 1.0 ps/°C
POWER SUPPLY VOLTAGE COEFFICIENT .....	1.0 ps/VOLT FOR $\pm 15$ V < 0.1 ps/VOLT FOR $\pm 24$ V
60 Hz AC MAGNETIC FIELD .....	-120 dB AT 10 GAUSS (WITH SHIELD, 60Hz NOISE RESPONSE)
ISOLATION (PORT-TO-PORT, 5 MHz) .....	-100 dB
FREQUENCY RESPONSE .....	100 KHz TO 55 MHz
MAXIMUM INPUT LEVEL .....	+13 dBm
OUTPUT LEVEL .....	TTL
SIZE .....	6 x 4 x 1.5 in.
POWER .....	120 mA AT 24 V AND $\pm 20$ mA AT $\pm 15$ V

Table 3. Phase Comparator Data Sheet

#### CONCLUSION

These low noise buffer amplifiers, distribution amplifiers, and phase comparators are presently being built and tested at BFEC. Specialized tests and test systems are used to verify each devices' performance. The buffer amplifier design has been improved by shortening lead lengths to increase back-to-front isolation, by increasing the power supply level to reduce harmonic distortion at higher output levels, and by potting the buffer to reduce phase sensitivity to mechanical shocks. Distribution amplifier improvements are made by using a higher isolation power splitter for increased port-to-port isolation and by using higher isolation RF cables and connectors for increased back-to-front isolation. The phase comparator design has been improved by changing power supply connectors and securing circuit boards to increase their mechanical stability. All three devices are assembled in various configurations for use in many different precise time and frequency measurement and distribution systems.

Each of the devices and systems of devices are extensively tested to verify a performance level that does not add any significant measurement system noise to the phase of state-of-the-art hydrogen masers. Phase stability floors of 27 femtoseconds and long term stabilities of one picosecond have been measured on all measurement systems using these devices. They have shown temperature coefficients, power supply voltage coefficients and mechanical shock coefficients of less than one picosecond. The distribution amplifiers and the phase comparators presently have greater than 90 dB of isolation and later should have greater than 100 dB of isolation.

In conclusion, BFEC builds, tests and improves these devices to reliably exceed these performance results just outlined. These devices should have application in various other high stability measurement and distribution systems.

#### REFERENCES

1. V.S. Reinhardt, W.A. Adams, G.M. Lee and R.L. Bush, "A Modular Multiple Use System for Precise Time and Frequency Measurement and Distribution", 10th Annual PTTI Applications and Planning Meeting, (Washington, D.C., 1978).
2. A.E.E. Rogers, "Frequency Standard Buffer Amplifier for Use in Very Long Baseline Interferometry", Haystack Observatory Technical Note, 1975-3.
3. D.W. Allan and H. Daams, "Picosecond Time Difference Measurement System", 29th Annual Frequency Control Symposium, (Atlantic City, N.J., 1975).
4. Model QHF-2A-5, Merrimac Industries Inc., West Caldwell, N.J.

## QUESTIONS AND ANSWERS

DR. FRED WALLS, NBS

Let me ask my original question, again. Have you looked at the amplitude sensitivity of your phase detector?

MR. EICHINGER:

That 6 dB correction factor, are you interested in the slope of the zero crossing?

DR. WALLS:

No. What if you change the level of the signal in one of the ports of your phase detector by, say, 3 dB, what happens to the phase?

Our experience is that you will see a substantial phase excursion.

MR. EICHINGER:

I haven't checked that, but each time a different phase measurement was made, I recalibrated the mixer and used that correction factor on the data.

DR. WALLS:

Sure. That changes the slope, but if you're trying to measure phase between two signals and for some reason over a long period of time you have a change in amplitude, you may have a spurious change in phase which had nothing to do with the signals, it's just a measurement difficulty.

MR. EICHINGER:

Right. Well, most of the data was done at a short term, not over a long term.

TIME TRANSFER BY IRIG-B TIME CODE VIA  
DEDICATED TELEPHONE LINK

G. Missout, J. Béland, D. Lebel, G. Bédard      and      P. Bussière,  
Institut de recherche d'Hydro-Québec                      Hydro-Québec

ABSTRACT

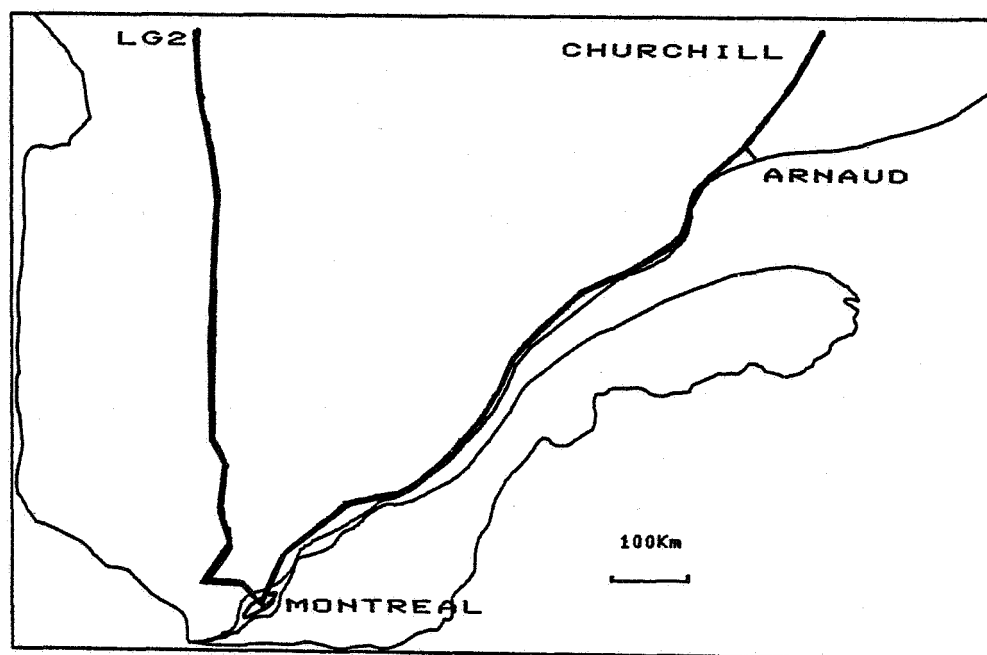
Measurements were made of the stability of time transfer by the IRIG-B code over a dedicated telephone link on Hydro-Québec's microwave system. The short-and long-term Allan Variance was measured on both types of microwave system used by Hydro-Québec, one of which is synchronized, the other having free local oscillators. The results promise a time transfer accuracy of 10  $\mu$ s. The paper also describes a prototype slave clock designed to detect interference in the IRIG-B code to ensure local time is kept during such interference.

1. INTRODUCTION

Hydro-Québec's requirements with regard to time dissemination cover a wide range.<sup>1</sup> As far as voltage phase angle measurements are concerned, it calls for an accuracy of 10  $\mu$ s on a round-the-clock basis, 365 days a year. The GOES system used for this purpose to date has yielded unsatisfactory results and Hydro-Québec is therefore exploring the possibility now of making maximum use of the IRIG-B system.<sup>2</sup>

This paper presents the results of measurements performed at two points on the Québec utility's power system and describes the measurement and calculation techniques. The operating principles of the slave clock to be used for detection purposes are also described.





HYDRO-QUEBEC MICROWAVE NETWORK  
SIMPLIFIED DIAGRAM

Figure 1.

## 2. STABILITY MEASUREMENTS

### 2.1 Hydro-Québec microwave system

Hydro-Québec's microwave system, illustrated in Fig. 1, comprises two main branches basically: Montréal-Churchill Falls Via Arnaud substation, and Montréal-LG2. The former, i.e. the Montréal-Churchill-Falls branch is the synchronized type. A pilot is transmitted from Montréal and used at the various substations to phase-lock the local oscillators of the multiplexer. The Montréal-LG2 branch, on the other hand, is the free-oscillator type in which the pilot serves only to generate alarms when the frequency error exceeds a given limit.

In practice, the synchronized system provides a guarantee that the frequency of the multiplexer input and output signals will be identical except in the case of loss of synchronization. Furthermore the phase between the input and output signals increases or decreases stepwise whenever a momentary loss of synchronization occurs.

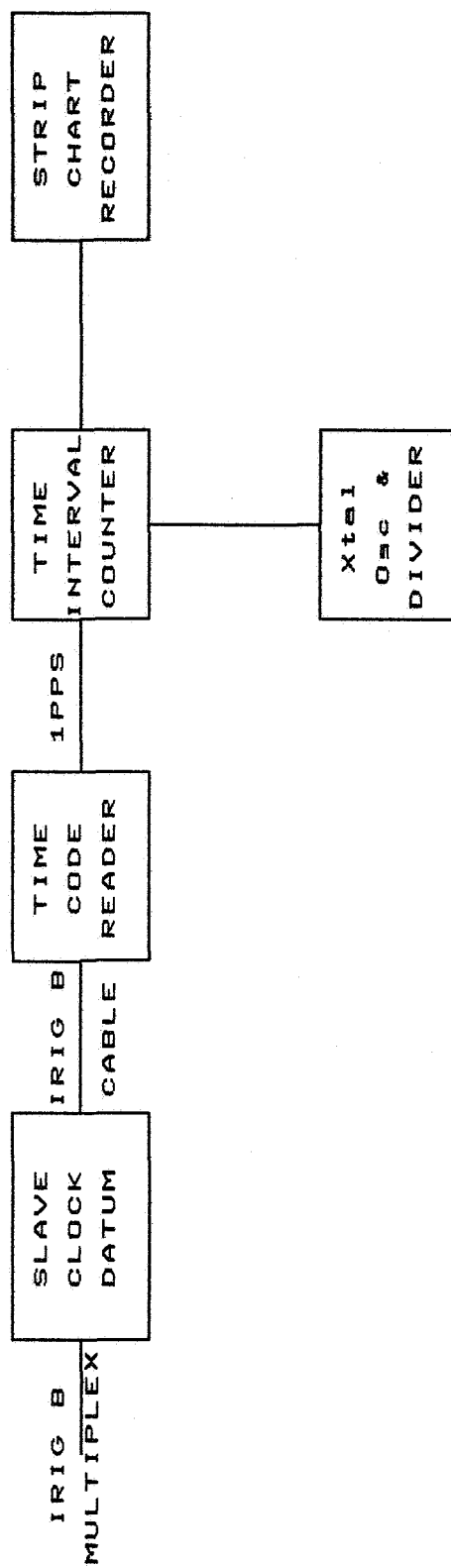
The nonsynchronized system can introduce a maximum error of 1 Hz in the transmitted signal, which would therefore be 1000 Hz at the input and 1001 Hz at the output. However, in practice, this error is more like 0.1 Hz, which results in a smooth phase drift.

These characteristics of Hydro-Québec's microwave systems mean that a corrector has to be used in order to rebuild a usable IRIG-B signal. Tests were therefore conducted on both types of multiplexer to study their performance. For this purpose we used an IRIG-B code originating in Montréal from a rubidium frequency standard HP 5065-Z. Measurements were made on the IRIG-B code received and corrected at LG-2 and at Arnaud substation.

## 2.2 Test setup

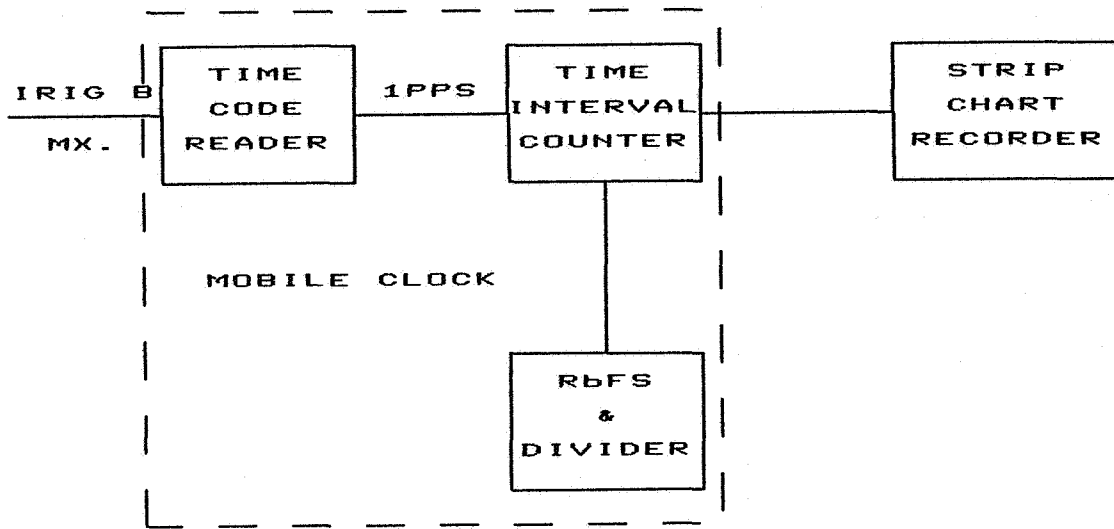
In the test setup at Arnaud Substation (Fig. 2) we used a time code reader and a synchronized generator (Datum 9390). A clock with a quartz oscillator was used while an interval counter and a strip chart recorder served to measure the accumulated line error between the two times scales (IRIG-B and crystal oscillator).

At LG2 (Fig. 3) we used our mobile clock<sup>1</sup> with a rubidium standard as reference (FRKH EFFATOM). This unit comprises the IRIG-B decoder, the corrector and the interval counter together with a separate recorder.



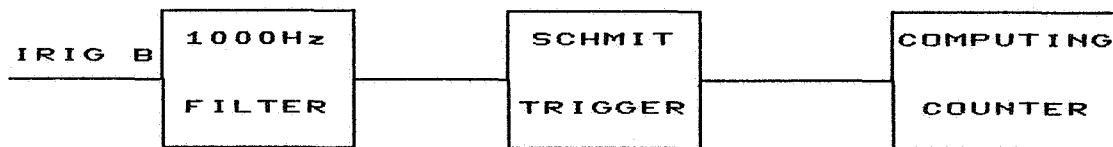
ARNAUD: MEASUREMENT APPARATUS

Figure 2.



LG2: MEASUREMENT APPARATUS

Figure 3



SHORT TERM MEASUREMENT APPARATUS

Figure 4

For the short-term measurements (Fig. 4) a computing counter HP 9360A, a band pass filter ( $Q=4$  at 1000 Hz) and a Schmitt trigger were used.

### 2.3 Experimental results

Typical curves obtained are presented in Fig. 5. Some synchronization losses were observed at Arnaud (Fig. 6). The accumulated time error values obtained were digitized. The following equation<sup>3</sup> served to calculate the frequency stability:

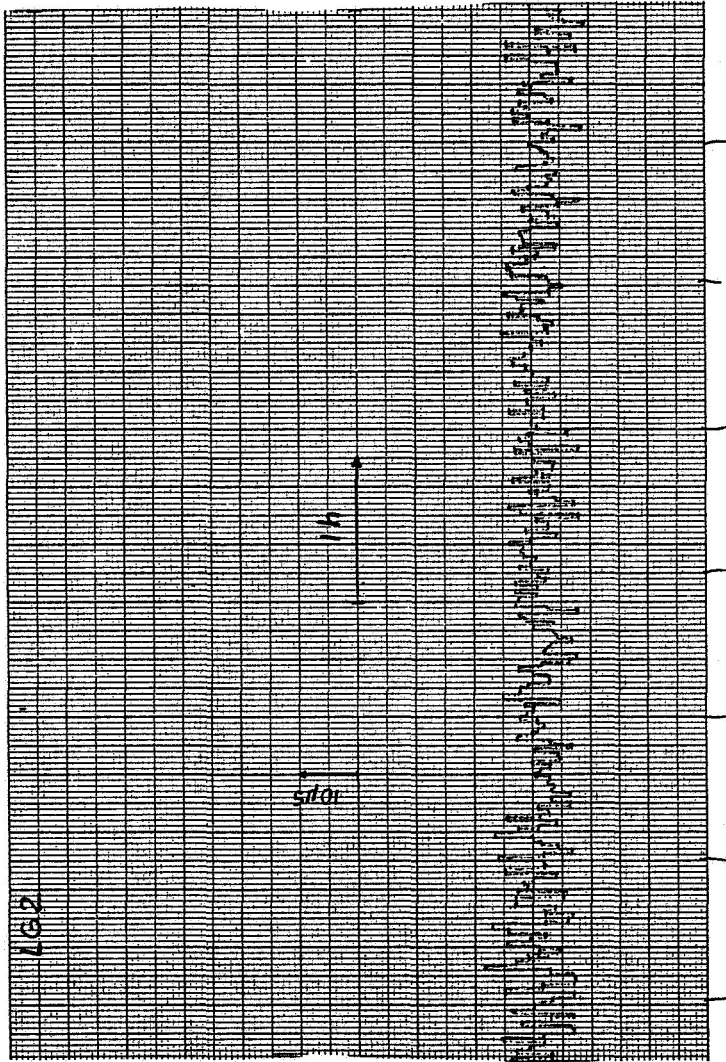
$$\sigma_y(t) = \frac{1}{2T^2} [4U_x(\tau) - (2\tau)]$$

$$\text{where } U_x(\tau) = \langle [x(t) - x(t+\tau)]^2 \rangle$$

$x(t)$  = variations in the time scale due to random frequency variations.

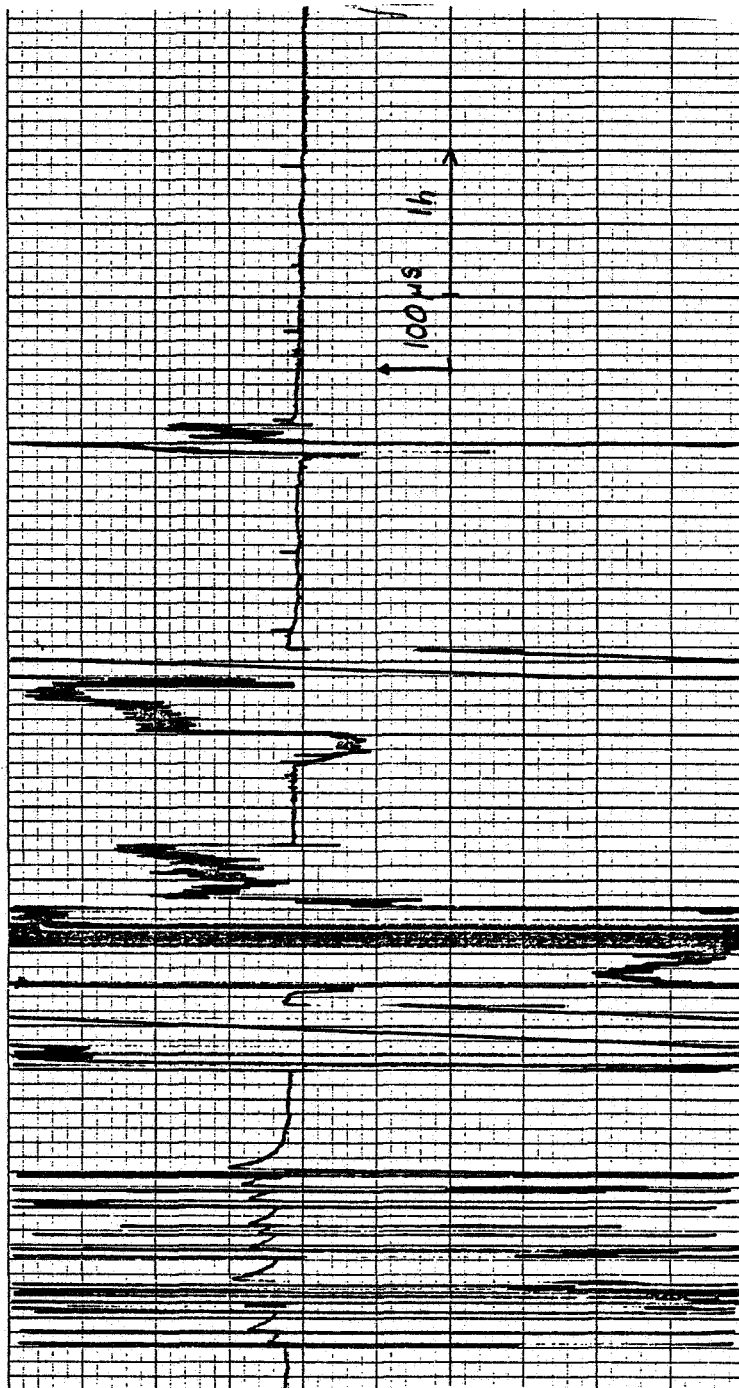
Two such curves were obtained, one at Arnaud, the other at LG2. The LG2 curve (Fig. 7) shows a long-term stability limit as well as the combined effect of the two rubidium references (master and mobile clocks). This explains the series of points above the typical frequency stability curve of a rubidium frequency standard. The circles indicate the short-term measurements made at IREQ. The curve for Arnaud (Fig. 8) shows the long-term frequency stability limits of the reference clock.

It is clear from these curves that a 10- $\mu$ s transfer time is possible, although this remains to be confirmed by longer-term discrete measurements (over months). In Figs. 9 and 10 we plotted the stability frequency curve in the case of a minor synchronization loss and it can be seen that already the stability has dropped one order of magnitude.



ACCUMULATED TIME ERROR AT LG2

Figure 5



9270-1012

10

ACCUMULATED TIME ERROR AT ARNAUD

IN PRESENCE OF NOISE

Figure 6

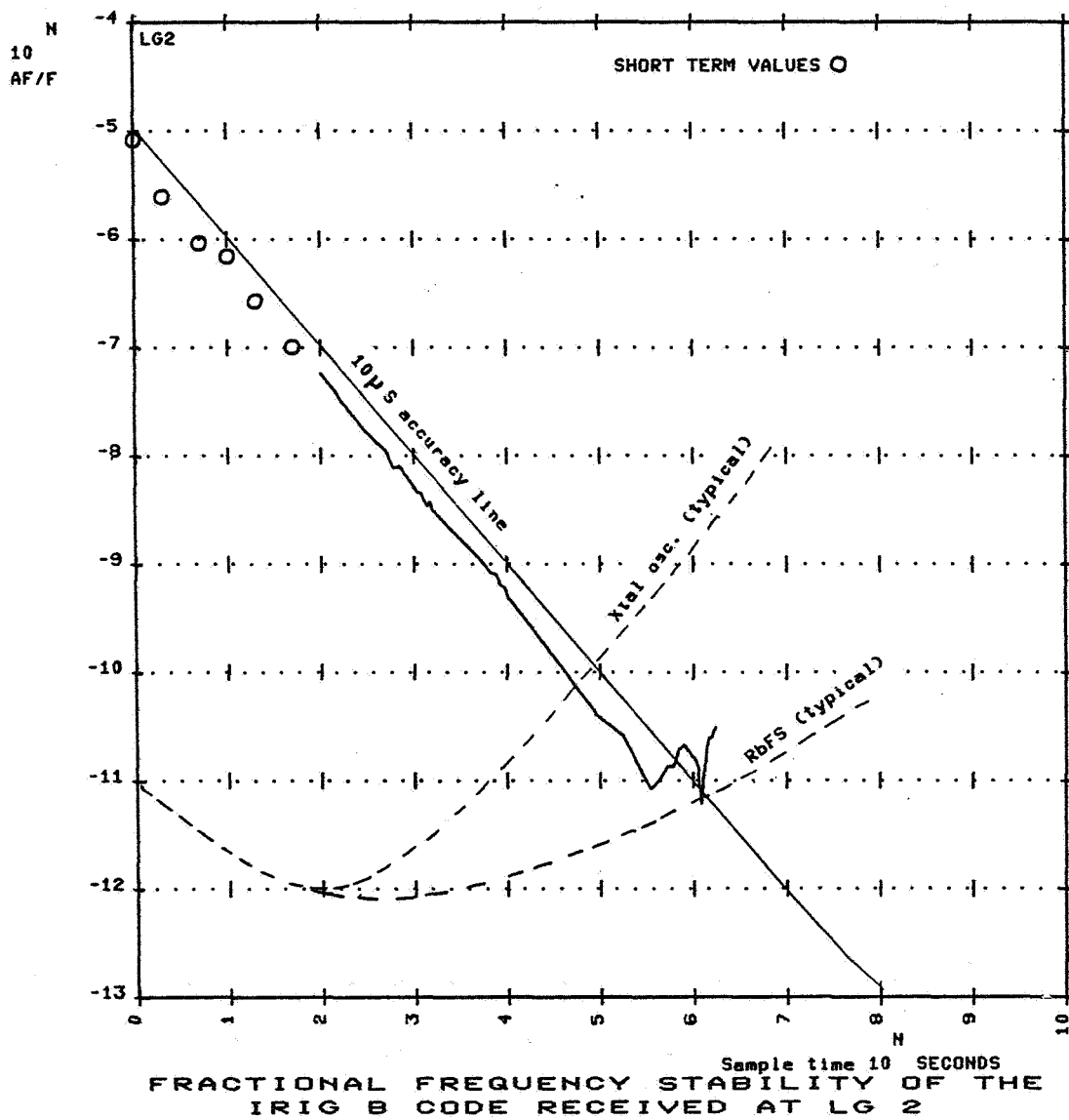


Figure 7



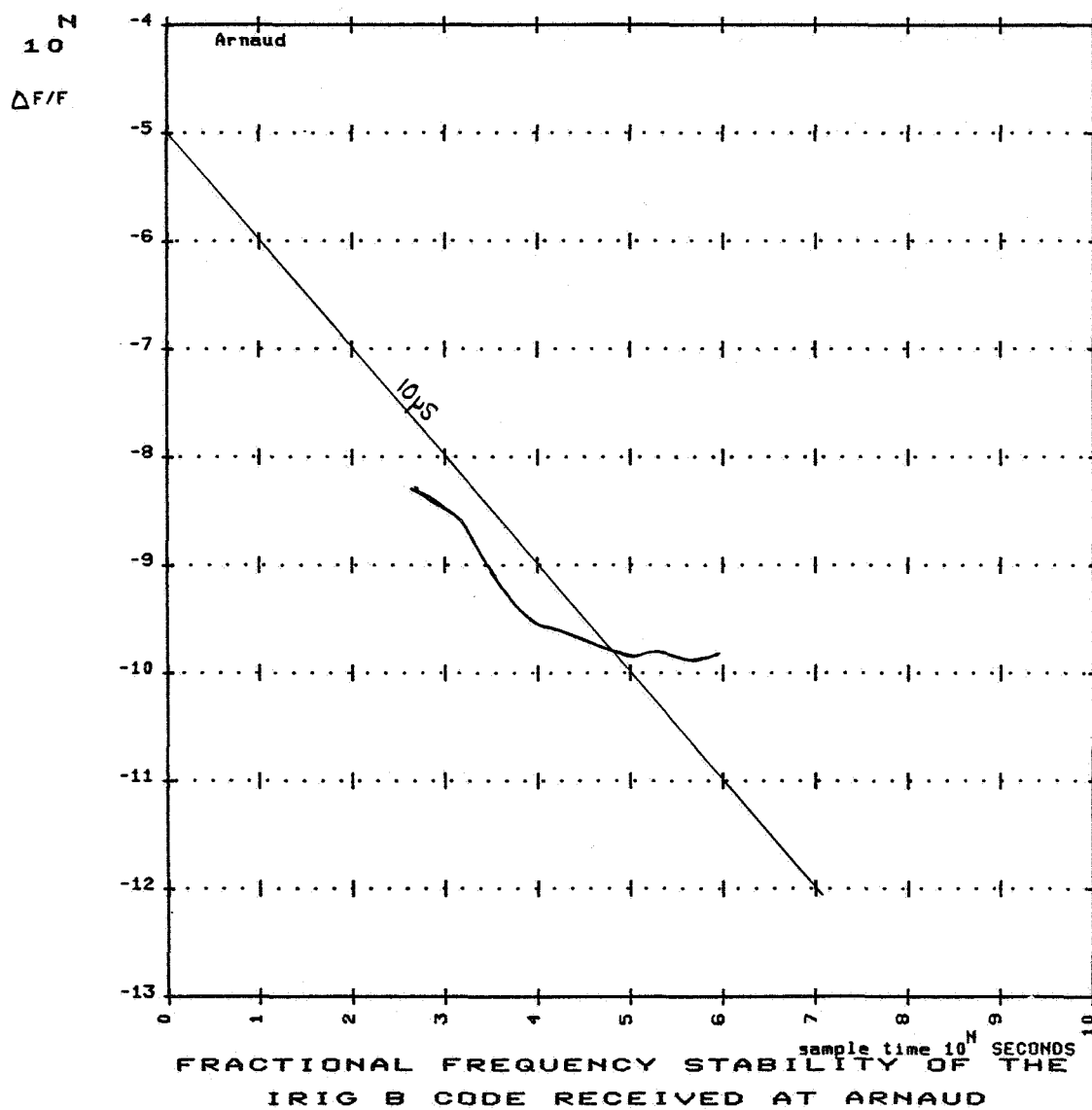
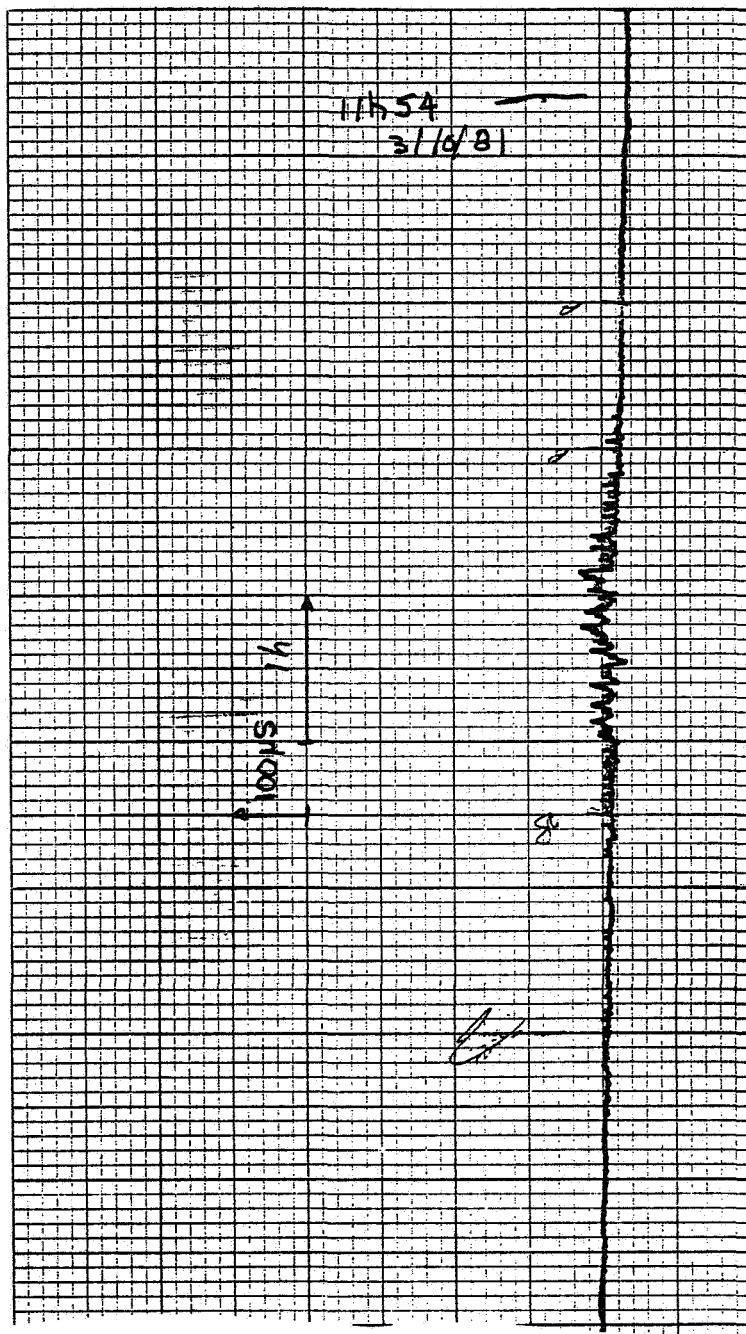


Figure 8.



HEWLETT

# ACCUMULATED TIME ERROR AT ARNAUD IN PRESENCE OF NOISE

Figure 9

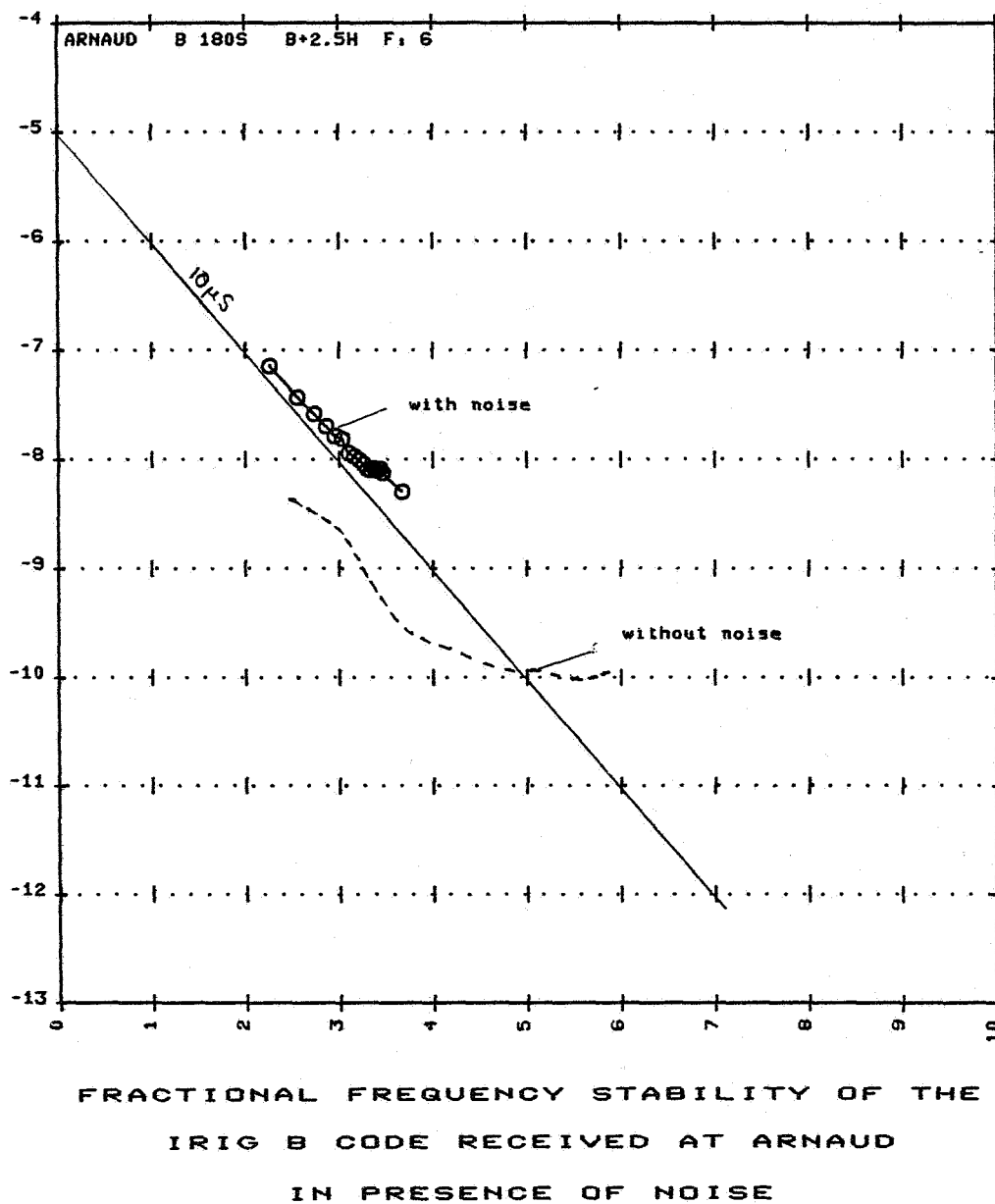


Figure 10

However, this can be put to good use, as will be explained in the next section.

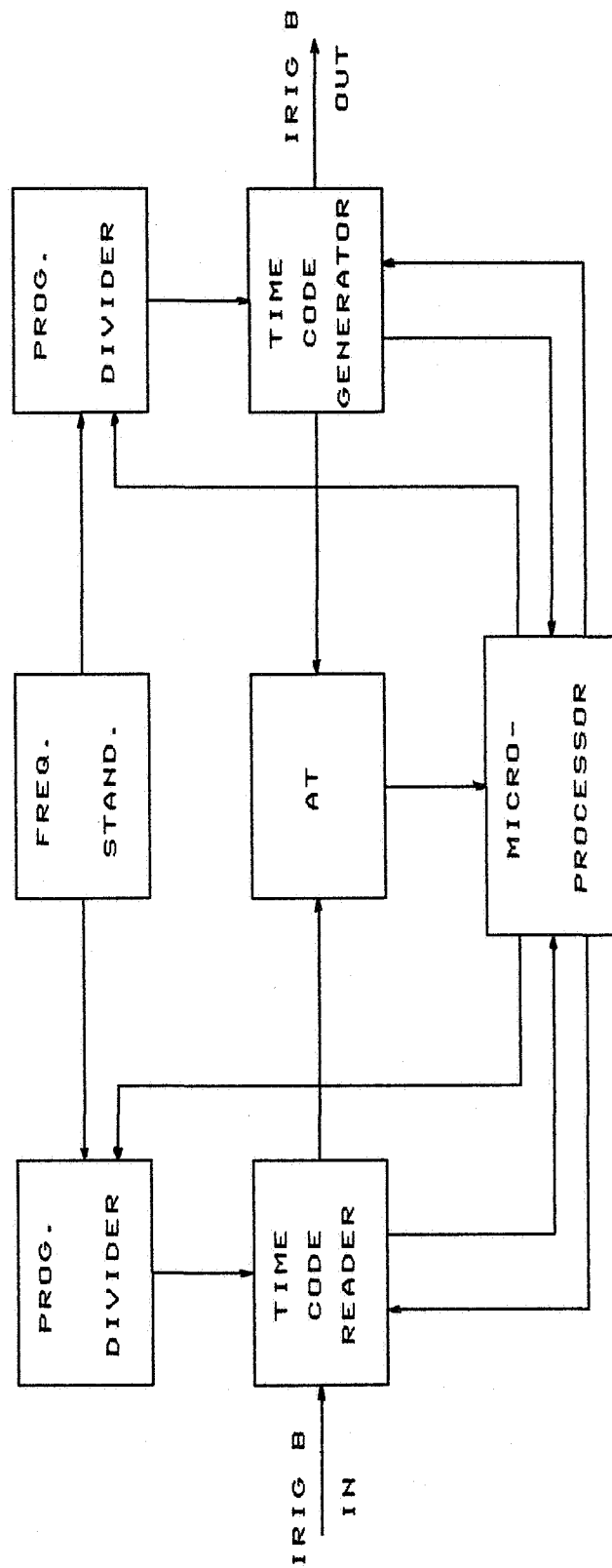
The curves presented in Figs. 6 and 9 show that a conventional slave clock tracks the input-signal drift with a relatively short time constant ( $\approx 5$  min or less). This is indispensable because the IRIG-B code reader must be sufficiently agile to follow the input signal; otherwise it risks losing the signal and will have to begin sweeping to relocate it. The coupled generator therefore has to follow the reader. We are now in the process of developing a unit in which the reader and the generator are controlled separately by the same microprocessor.

Figure 11 presents a block diagram of the prototype slave clock. The time code reader tracks the input code, eliminating the short-term noise (up to a few tens of seconds). The programmable divider A drives the time code reader.

On the other side we have a separate generator, which is corrected with another programmable counter B, and a unit for measuring the time difference between the reader and the generator.

This approach enables us to maintain a relatively short time constant (a few tens of seconds) for the reader, and consequently keep a check on any code drift while checking its consistency, without needing to shift the generator in time. The generator can in fact be corrected with a time constant of between a few hours and over one day if we use a rubidium standard.

Furthermore we can make note of corrections to the divider B so that we have an idea of the drift of the frequency standard, which can be systematically corrected whenever the input signal disappears. In this case we have a zero offset frequency equivalent at the outset. If

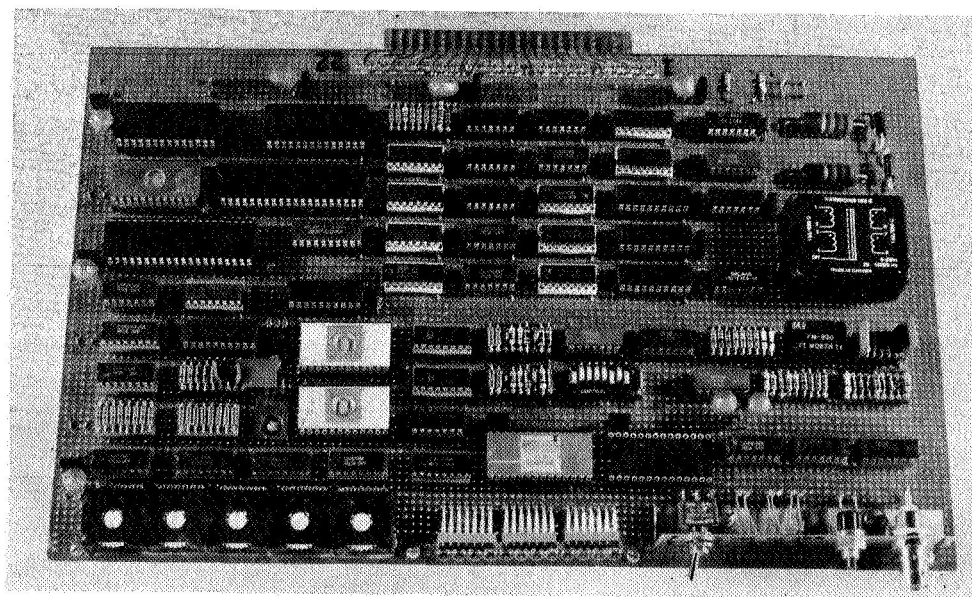


SLAVE CLOCK BLOCK DIAGRAM

Figure 11

a rubidium frequency standard is used, the corrections can be transmitted, thus providing an excellent means of remotely studying the clock performance without having to add an outside reference clock.

Furthermore, the  $\Delta T$  interval counter allows us to calculate the stability of the IRIG-B code as received and read, thus providing a reliable means of knowing whether or not we are in the presence of noise so as to ignore the input in the generator correction process. This approach is far more sensitive than the method presently employed, which consists in checking whether or not the input signal is present. A photograph of the prototype clock is shown in Fig. 12.



SLAVE CLOCK PROTOTYPE

Figure 12

## CONCLUSION

In this paper we have examined the stability of a time code disseminated on a microwave system. The measurements obtained reveal a possibility of time transfer with an accuracy of 10  $\mu$ s. The new prototype slave clock used should allow us to give a reliable time code despite interference in the microwave network by calculating the frequency stability of the signal received. This unit will also allow remote transmission of corrections to the generator and thus provides a possible means of control and measurement.

## REFERENCES

- (1) PTTI Application at Hydro-Québec, G. Missout, J. Béland, G. Bédard, p. 377-385, 12th PTTI, 1980.
- (2) Time Dissemination in the Hydro-Québec Network, G. Missout, W. Lefrançois, L. Laroche, p.343, 11th PTTI, 1979.
- (3) The NBS Atomic Time Scale: Generation, Stability, Accuracy and Accessibility, D. Allan, J. Gray, H. Machlam, NBS Monograph 140, Chap. 9, p.210.

## QUESTIONS AND ANSWERS

DR. WINKLER:

Thank you. I have a question concerning your filter. It is clear from the last slide that you reject time code information for your phase lock loop if the time limit exceeds a certain limit; is that correct? Or, do you reject the time code input if it is inconsistent over a couple of seconds.

There are two different methods, and I was wondering whether you have some kind of an algorithm to make the decision?

DR. MISSOUT:

Okay. The first thing to check is if the second of the time card follow them. That is, if you have 31, and so on, but also, you have to check if there is some noise because in some cases, you have a slight drift in the code. You still have consistency on the date, but actually we are not about to detect the slight drift. So, we try to make measurement of the Allan variance of the received signal and put some level over which we decide that the signal is too noisy to change output.

DR. WINKLER:

But that is exactly my question because you assume a White or Gaussian distribution, and these errors are definitely not Gaussian distributed. Any time you have a digital data transmission, your errors are completely non-Gaussian, as non-Gaussian as you can be, and, therefore, if you don't take that into account the algorithms are completely wrong and very inefficient.

So, my question is: What is the rejection criteria? What is the algorithm to reject noise in the phase lock loop?

DR. MISSOUT:

Okay. The fact is it's not clearly digital transmission. The problem is due to loss of synchronism in the micro system; so, what you observe at the time is a quick change of the time transfer in between the input and the output. So, the only means I see to measure the Allan variance, is by taking samples and if the value is too high, you will reject the input value.





Variations in Propagation Delay Times  
For Line Ten (TV) Based Time Transfers

M. C. Chiu and B. W. Shaw

The Johns Hopkins University, Applied Physics Laboratory  
Johns Hopkins Road  
Laurel, MD 20707  
(301)953-7100 X2571

ABSTRACT

Variation in the propagation delay for a 30 km TV (Line Ten) radio link has been evaluated for a series of 30 independent measurements. Time marks from TV Channel 5 WTTG in Washington, DC were simultaneously measured at JHU/APL and at the USNO against each stations' local cesium standard clocks. Differences in the stations' cesium clocks were determined by portable cesium clock transfers. Thirty independent timing determinations were made between May 1980 and August 1981. The RMS deviation in the propagation delay calculated from the timing determinations was 11 ns.

The variations seen in the propagation delays are believed to be caused by environmental factors and by errors in the portable clock timing measurements. In correlating the propagation delay variations with local weather conditions, only a moderate dependence on air temperature and absolute humidity was found.

Advantages and Disadvantages of TV Based Time Transfers

The TV Line Ten System provides a submicrosecond method for obtaining the timing of a local time standard relative to the U.S. Naval Observatory (USNO) timing. Time transfers based on TV Line Ten measurements can be an attractive alternative to time transfers using portable cesium clocks. TV Line Ten measurements take only minutes to perform and can be done with little advance preparation. These features are useful both for routine time transfers and in particular for varification and recovery of local clock operation following a power outage or other operational anomaly. In comparison, portable cesium clock transfers, for our location, require an average of three to four hours to complete for transporting the clock from the USNO to our facility at JHU/APL and back again.

The primary drawback in using the TV Line Ten System for time transfers has been in the resolution limitation of 10 ns or more and in the difficulty of accounting for the propagation delay and its variations between the TV transmitter and the receiver at the local time standard. As a consequence, these factors make the accuracy of the time transfer based on Line Ten measurements difficult to assess.

The propagation time of a TV signal from transmitter to receiver is influenced by many environmental conditions along its path, including the terrain and the local climate. These influences can not be incorporated into a calculation of propagation time along a given path with a high degree of accuracy. Compounding the problem, variation in the propagation time can result from localized environmental changes (particularly climatic) at any point along the transmitter-receiver path. Recognizing the difficulties in calculating propagation delays inherent in the TV based time transfer, an experiment was conducted at JHU/APL in which the propagation delay for our pathway was determined using the results of portable cesium clock time transfers.

#### Calculation of the Propagation Delay

Our TV Line Ten measurements were obtained from WTTG's (Channel 5) transmission originating in Washington, D.C. (See schematic of tuning measurement shown in Figure 1.) The pathway from WTTG's transmitter to our receiver at JHU/APL is approximately 30 km. The terrain along the propagation path varies from city environment to open fields and wooded areas. The propagation between the transmitter and receiver is not line of sight, but rather gently rolling hills.

The propagation delay along this path was calculated using both the results of the TV Line Ten measurements and of the portable clock time transfers. The TV Line Ten measurements were made to coincide with the portable cesium clock time transfers which are carried out between the USNO and JHU/APL on a weekly basis. These portable clock transfers give the timing of our local cesium standards (APL System Nos. 1-3) relative to USNO System No. 1 timing. Immediately following the measurement of our local standards against the portable cesium clock, the timing of APL System No. 2 was again measured using the TV Line Ten System\*. The measurement obtained from the TV Line Ten System is the sum of three elements, 1) the APL System No. 2 timing relative to the USNO System No. 1, 2) the emission timing of WTTG, and 3) the propagation delay between WTTG's transmitter and our TV receiver at JHU/APL. (All cable delays have been taken into account.) The emission timing data of WTTG at the instant of our TV Line Ten measurements was obtained over the phone from the USNO. This emission timing and the timing of APL System No. 2 relative to the USNO System No. 1 obtained from the portable cesium clock transfers, were then subtracted from the TV Line Ten measurements to determine the propagation delay.

---

\* An ILC Data Device Corporation, Model 5433 Timing System on loan from NASA was used for the measurement.

Twenty independent determinations of the propagation delay were made between May 1980 and January 1981. Ten additional determinations were made between April and August 1981. These propagation delays are shown in Figure 1. The mean value of the first twenty determinations is 88,402 ns with a standard deviation of 16 ns. The mean value of the entire 30 determinations is 88,408 ns with a standard deviation of 11 ns.

#### Variations in the Propagation Delay

The range of the propagation delay variation shown in Figure 2 is much smaller than expected. The variation seen in Figure 2 represents the fluctuations in the propagation time along the transmitter recovery path plus any errors resulting from the portable cesium clock transfer. In these tests, the primary source of error in a portable clock transfer resulted from the closure time. The closure of a time transfer is designated as the change in timing of the portable cesium clock relative to the USNO System No. 1 between the start and finish of the transfer. To determine the most probable value of the portable clock timing at the instant of measurement against our cesium standards, it was assumed that this timing varies linearly during the course of the transfer. The error in a time transfer resulting from the closure should then be only a fraction of the closure time. The RMS of the closures for the first 20 transfers used in the propagation delay determination was 19.7 ns. The closures for the ten additional determinations were not available but are assumed to have an equal or smaller standard deviation.

Unfortunately, for this data, there is no way to isolate errors in the portable clock transfers from the variations seen in the calculated propagation delay. However, assuming these errors to be relatively small an attempt was made to relate the propagation delay variation to climatic conditions of air temperature and absolute humidity. Local weather conditions recorded at the meteorological observatory at Washington National Airport (Ref. 1) were obtained for the dates and approximate times on which the first 20 propagation delay determination measurements were taken. Correlations were made between propagation delay variations and the air temperature and between the delay variations and the dew point temperature (which is a measure of absolute humidity). These correlations using a least squares fit are shown in Figures 3 and 4. The coefficient of determination was .48 for the air temperature dependence and .55 for the dewpoint temperature. Both indicate only a moderate dependence of the propagation delay variations on gross climatic conditions. Localized climatic disturbances along the actual propagation path may have been present which could have altered the propagation time. Time transfer errors in the calculated propagation delay may also have obscured the weather dependence.

### Significance of Propagation Delay Results

While the variation in the propagation delay determined for our TV Line Ten based time transfers could not be correlated with gross climatic conditions, again the range of the variation itself is significant. The propagation delay variation over 30 independent determinations, spanning 15 months had a standard deviation of only 11 ns. This indicates that TV Line Ten based time transfers, for our system, also have at best a standard deviation of 11 ns. Depending on the final use of the timing information, this accuracy could be sufficient.

It is difficult to apply the data on propagation delay variations obtained in our experiment, directly to another propagation path. Since the variations can result from a number of factors, a shorter or longer path may depart from proportionality in the propagation delay. Our data does indicate that if several determinations of the propagation delay along a specific path can be made over an extended period of time, the variations in the propagation delay can be bracketed for use in assessing the accuracy of a TV Line Ten based time transfer.

### References

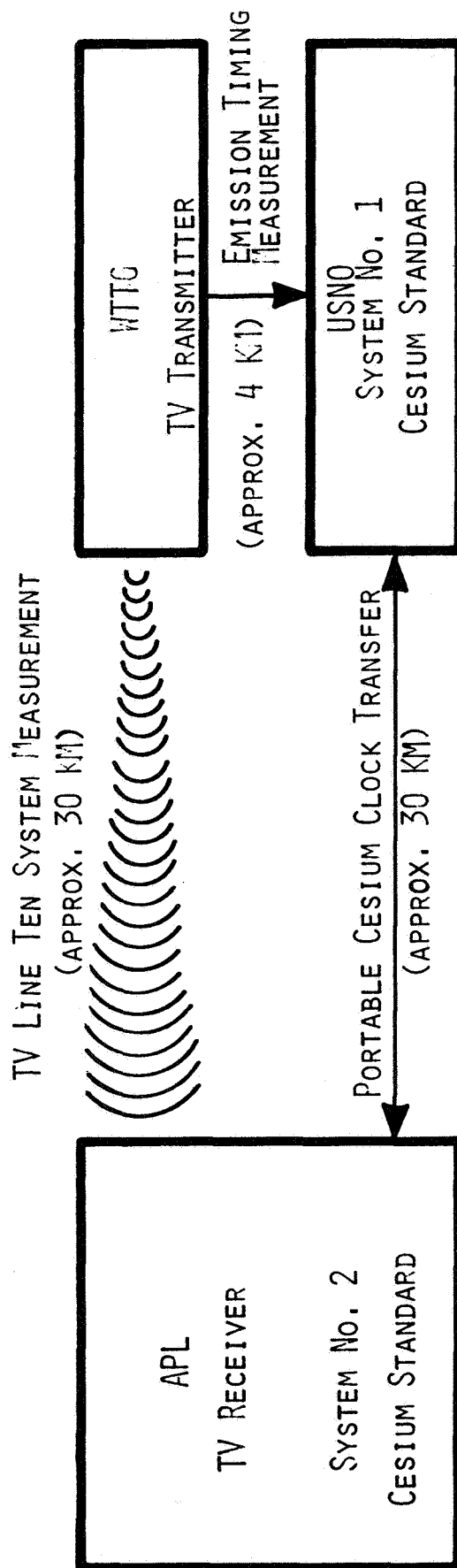
1. National Oceanic and Atmospheric Administration, Local Climatological Data, Washington National Airport, Monthly Summary.  
May 1980 Through January 1981.

### Acknowledgements

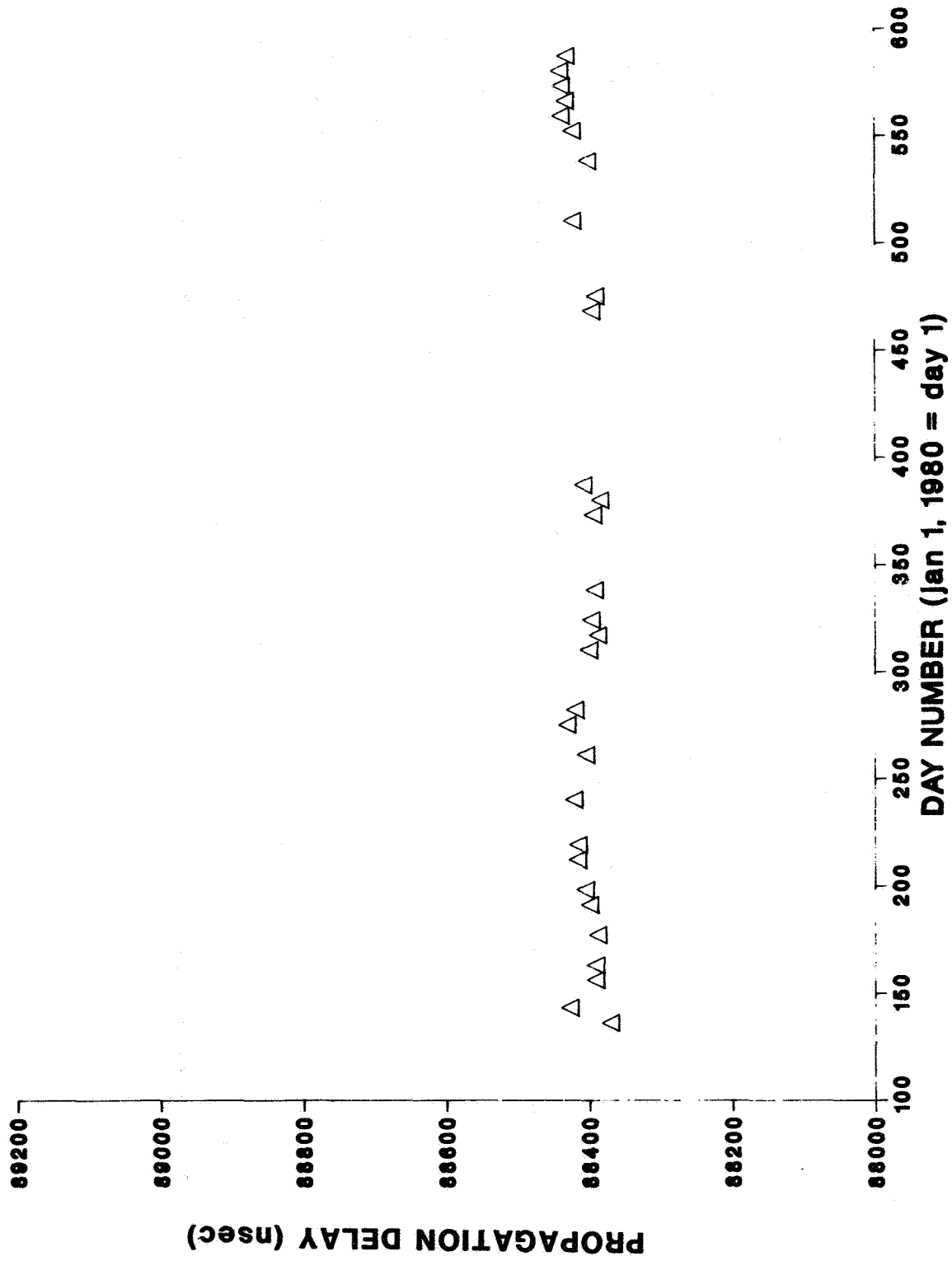
Data based on measurements initiated by B. H. Shaw who has since retired from JHU/APL. The TV (Line Ten) receiver was loaned to JHU/APL by the Goddard Space Flight Center as a part of a cooperative study for station time synchronization.

FIG. 1

SCHEMATIC OF TIMING MEASUREMENTS



# FIG. 2 PROPAGATION DELAY



**FIG. 3**  
**PROPAGATION VS TEMPERATURE**

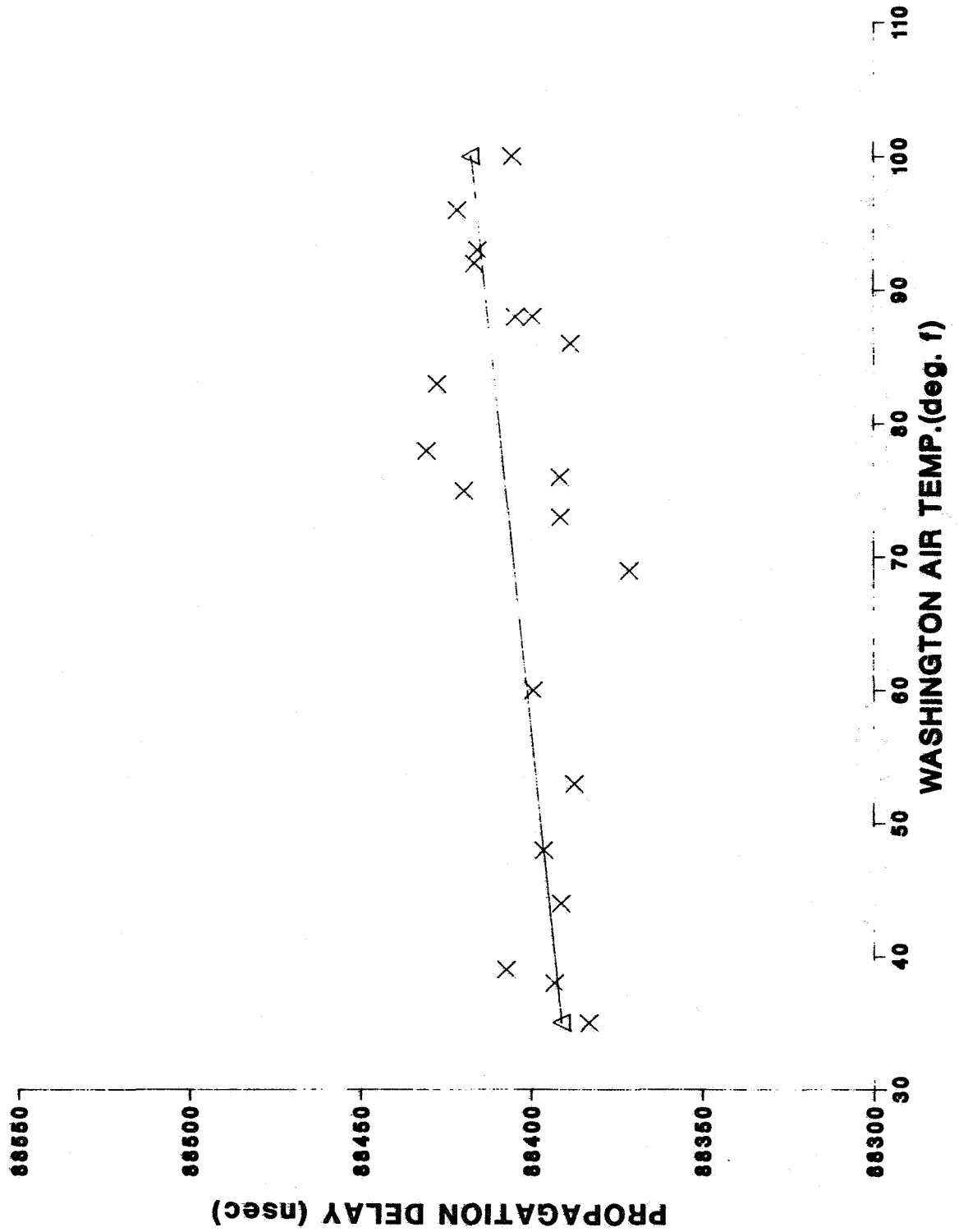
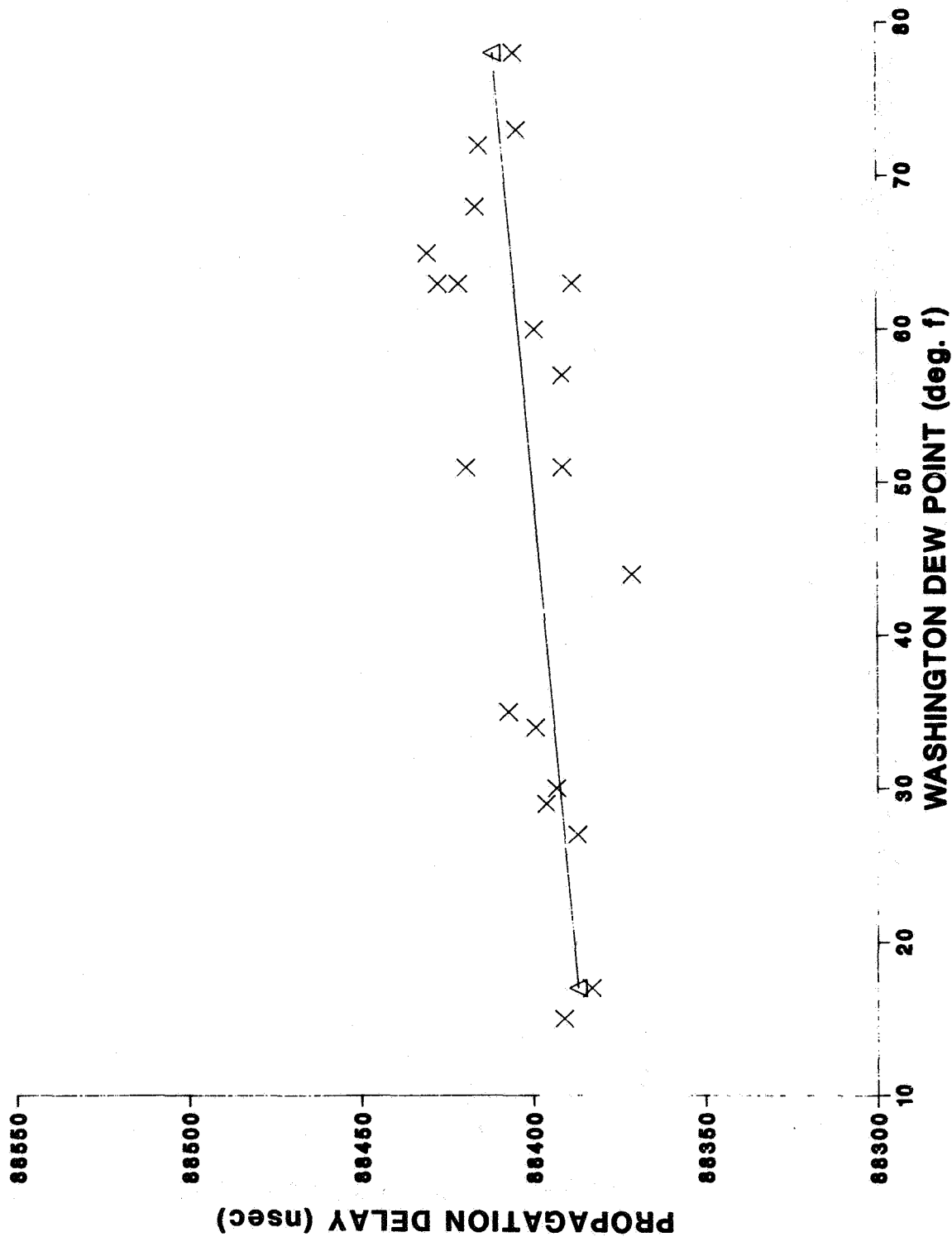




**FIG. 4**  
**PROPAGATION VS DEW POINT**



## QUESTION AND ANSWERS

DR. WINKLER:

I have a comment rather, because your correlation coefficient of about .5 with absolute humidity or a dew point temperature has to be the same order of magnitude as against temperature because both of them with each other have a very high correlation. Your dew point or your absolute humidity is much higher in summer than it is in winter, and it would be interesting to separate these correlations.

MRS. CHIU:

Yes.

DR. WINKLER:

I would suspect that there is a correlation with temperature, but not with humidity. But it would be a very interesting question to find out.

MRS. CHIU:

Yes, it would.

QUESTION FROM THE AUDIENCE:

One quick question. Were the regressions statistically significant?

MRS. CHIU:

As I say, there's only a moderate dependence. That's about all you could say.

QUESTION FROM THE AUDIENCE:

But you didn't do a "T" test on the coefficients.

MRS. CHIU:

No, I didn't.

QUESTION FROM THE AUDIENCE:

Thank you.



## THE ROLE OF PRECISE TIME IN IFF\*

William M. Bridge

The MITRE Corporation  
P.O. Box 208  
Bedford, MA 01730

### ABSTRACT

Precise knowledge of time of day can dramatically affect the design of military electronic systems. Small, inexpensive atomic clocks are becoming available that can provide free-running accuracies on the order of 10 to 100 microseconds for periods in excess of a month. Such clocks could revolutionize tactical communications, navigation, data links, IFF and ELINT systems.

This paper discusses the application of precise time to the IFF problem. The simple concept of knowing when to expect each signal is exploited in a variety of ways to achieve an IFF system which is hard to detect, minimally exploitable and difficult to jam. Precise clocks are the backbone of the concept and the various candidates for this role are discussed. The compact rubidium-controlled oscillator is the only practical candidate.

### INTRODUCTION

Time has played a role in the battlefield identification of friend or foe (IFF) since the beginning of organized war. The challenge (question-and-answer) system for sentries has always involved the element of time. Eventually the challenge/password pair is compromised and must be changed. A returning soldier who missed the update is susceptible to fratricide. Present IFF techniques, although more sophisticated, bear some resemblance to this primitive system. Instead of a single challenge/password pair, there is a large library of coded challenge words which are paired with relatively few passwords for the duration of any given code-validity interval.

\* This work was supported by the MITRE Independent Research and Development Program.

Security has always been a critical aspect of IFF systems. Any modern IFF system must have essentially perfect resistance to interrogation by the enemy or he (the enemy) will interrogate our forces and use our replies to determine whom and where to shoot. This situation is worse than no IFF at all and must be avoided at all costs.

The solution is a time-varying, cryptographic signalling scheme, and the security of such a system is improved by reducing the time interval for which the library of challenge/password pairs is valid (code-validity interval). However, as this interval is reduced, it becomes increasingly difficult to guarantee that all friendly forces receive a timely update of the challenge/password pairs. To be truly secure, the author believes that any new IFF system will have to be based on very accurate time synchronization.

#### SYSTEM CONSIDERATIONS

The current IFF system employs a signalling scheme where the library of challenge/password pairs remains valid for one day. Thus, if the enemy obtains even a single valid interrogation, he can interrogate and track our forces for the remainder of the day. The enemy can determine a valid interrogation by either listening to our IFF transmissions or by guessing interrogations until he receives a reply. The chances of guessing a valid interrogation are not all that bad and should yield results quickly. This condition seriously weakens the current system. One critical element of the answer is to drastically reduce the code-validity interval.

At this point we must distinguish between a code-validity interval and a cryptographic key-update interval. The key-update interval is related to the expected time that the enemy can be denied access to working IFF equipments. In peacetime the key-update interval can be fairly long provided there is a special, back-up key ready for immediate use when the war starts. Once the war starts, the length of the key-update interval becomes a complex question related to the progress of the war relative to the capture of our IFF equipment, the seriousness of IFF equipment compromise, and the difficulty of securely disseminating a new key under battle conditions. The latter two elements are the only ones that can be affected in the design of a new IFF system. Any new IFF system should certainly be designed so that the capture of working equipments, with or without the operators, is of minimal use to the enemy. The actual command and control information contained in an IFF transmission is of little use to the enemy and one might design the IFF system to take advantage of a public-key cryptographic system utilizing radio links rather than secure couriers for key distribution.

The code-validity interval can be much shorter than the cryptographic-key-update interval if each user has some form of synchronized clock. The actual encrypted IFF signal is then a function of time of day as well as the cryptographic key. As this code-validity interval shrinks, the system becomes increasingly difficult to exploit. Unfortunately, it also becomes increasingly difficult for our own forces to maintain time synchronization. If the code-validity interval can be made shorter than the time to guess a valid interrogation, this particular form of exploitation can be completely eliminated. However, the enemy still has the option of instantly repeating our valid interrogations omnidirectionally so that all friendly forces reply. The enemy can still track our forces but only when we choose to use the system. Unfortunately a minimum code-validity interval is set by the propagation time for the signal to reach the maximum range of the system. If this maximum range were 300 km, the minimum code-validity interval would be 1 ms. This minimum code validity interval still allows the enemy to instantly repeat interrogations from a short-range interrogator and elicit responses from all friendly forces out to the maximum range of the system. Thus, even with a minimum code-validity interval, the basic approach is vulnerable to repeat exploitation. However, a short code validity interval is certainly less vulnerable than a long one.

The reason that the minimum code-validity interval is set by the propagation time to maximum range is because IFF is thought of as a beacon-transponder system for the surveillance of friendly aircraft and not as an integral part of a fire-control system. The crucial difference is that a beacon-surveillance system demands replies from all friendly aircraft at all ranges and all azimuths, whereas a fire-control system needs an IFF reply only from aircraft that have been detected, tracked, and targeted by the weapon. The surveillance requirement proliferates the number of interrogations and replies, establishes a lower limit to the code-validity interval and results in a system that is inherently vulnerable to enemy exploitation.

#### TIME-SYNCHRONIZED APPROACH

If we give up the surveillance requirement and use IFF only as an adjunct to fire control, we can use accurate-time synchronization to achieve a system that is:

- hard to detect,
- virtually unexploitable, and
- difficult to jam.

Atomic clocks are available that can provide time with an accuracy on the order of one to ten microseconds for periods in excess of a day. Time synchronization with this accuracy allows spread spectrum signalling methods which include frequency hopping, time jitter, and a different intrapulse spreading code on each transmission. These essential characteristics of every transmission are known exactly to each friendly synchronized subscriber, but the enemy sees only an occasional, short-pulse, low-duty-factor signal which appears random in the dimensions of time, frequency, and intrapulse code.

Accurate-time synchronization can be employed in a variety of ways to achieve special ECCM features. The use of IFF as an adjunct to fire control requires selective interrogation of the tracked target in range and azimuth. Selective interrogation in range can be achieved by sending an interrogation pulse so that it will arrive at the target at a prescribed time of day known to both parties. The friendly responder simply opens a narrow gate at the prescribed time of day. The synchronized interrogator, knowing precisely the times that this receive gate is open, transmits his interrogation early by an amount equal to the propagation delay (measured a priori) to the tracked target. If the measured range is correct and the time synchronization is adequate the interrogation pulse should arrive at the desired target when the receive gate is open. This situation is depicted in figure 1. If the interrogation pulse subsequently arrives at a more distant friendly target within the antenna beamwidth ( $F_2$  of figure 1), the additional propagation delay to the second target causes the pulse to arrive after the receive gate on the second aircraft has closed. Receipt of a pulse in the selective-interrogation gate tells the interogatee that his range from the interrogator is approximately equal to the intended interrogation range. Of course, the specific times of day set aside for selective interrogation can be very frequent and ascribed in a pseudorandom fashion known only to friendly participants with accurately synchronized clocks.

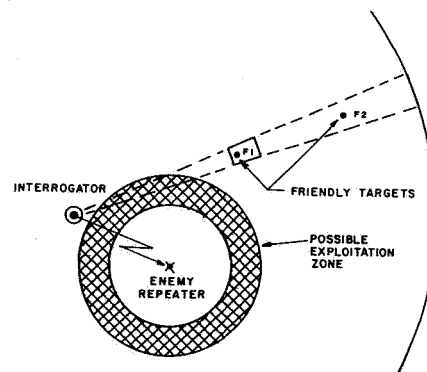
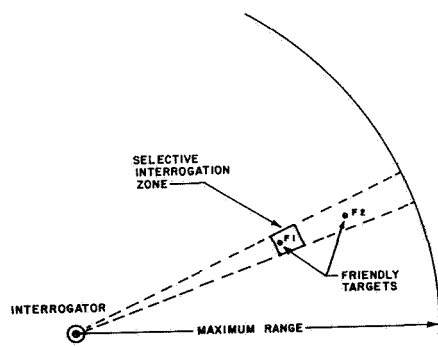


Figure 1. Selective Interrogation      Figure 2. Repeater Exploitation

The width of this receive gate must be sufficient to accommodate the combined clock error at both terminals and any range-measurement error. If range-measurement error is negligible, as it should be in a fire-control system, and timing uncertainty at each terminal is within  $\pm 10 \mu\text{s}$ , the receive gate could be as narrow as  $40 \mu\text{s}$ . This means that only those targets within  $\pm 6 \text{ km}$  of the intended range receive a valid interrogation.

This approach to selective interrogation is operationally advantageous. It minimizes the number of inadvertent replies, markedly reducing the problem of reply interference or "fruit." It also greatly reduces the effectiveness of enemy repeat exploitation, as seen in figure 2. If the enemy repeater employs an omnidirectional antenna, the effective zone of exploitation becomes an annular ring centered at the location of the exploiter. The width of this exploitation ring is  $12 \text{ km}$ , for the above example, and its radius is determined by the intended range of the interrogation. If the intended range is less than the range to the exploiter, the effective zone of exploitation shrinks to zero. For intended interrogations at longer ranges, the radius for the annular zone of exploitation is equal to the intended-interrogation range minus the range delay to the exploiter minus the equivalent range delay through the repeater itself. The dependence on the range delay through the repeater forces the enemy to use a continuous-repeater amplifier such as a TWT. The enemy has no knowledge of the specific time or direction of a given interrogation and the duty factor of the interrogation signal can be extremely low. The output of the enemy TWT repeater in the absence of an interrogation is high-power noise. This makes the enemy exploiter very vulnerable to detection and attack by friendly forces. It must also be remembered that the effective zone of exploitation is not under the exploiter's control and only occasionally does it coincide with the location of friendly forces. Thus repeat exploitation is not a severe threat because the time-synchronized approach results in an effective code-validity interval limited by clock errors and not by the maximum range of the system.

If clocks are available with accuracies sufficient to support the concept of selective interrogation by range, then the concept of range measurement at the interrogatee can also be supported. This concept allows the interrogatee to measure the approximate range to each active interrogator. This is of little value to the interrogatee unless he receives additional information defining the weapon type at the interrogator. This weapon information, coupled with range measurement and selective interrogation, can form a sufficient basis for making an automated decision to reply or not.



If the measured range (to the interrogator) is well beyond the weapon range, the appropriate decision might be not to reply, particularly if the aircraft is over enemy territory where electromagnetic radiation of any sort can be hazardous.

Implementing a range-measurement scheme is not difficult. If the interrogation pulse for range measurement is sent at the prescribed time of day, it arrives at the interrogatee with a propagation delay commensurate with the range between the two parties. The interrogatee simply opens a receive gate at the prescribed time of day and measures the range delay to each interrogator. The width of this receive gate is set by the maximum range of the system (1 ms for 300 km). The uncertainty of the measurement is limited by the clock error at both terminals ( $\pm 6$  km for  $\pm 10$   $\mu$ s error). This is not a very precise measurement of range, but it should be adequate for making the reply decision, and as improved clocks become available, the accuracy of this range measurement can be increased without involving a major redesign of the system.

The next question is how to send the few bits of information necessary to define the weapon at the interrogator. If this information is sent at a prescribed time of day exactly as the range-measurement pulse was sent, the interrogatee knows precisely when to expect the data pulse, independent of both range and clock error, provided his position has not changed appreciably between the previous range-measurement pulse and the current data pulse. This knowledge of the precise time of arrival of the data allows the interrogatee to set up an extremely narrow receive gate for the reception of this data. The width of this gate is related to the time resolution of the system, which might be on the order of 100 ns for an instantaneous bandwidth of 10 Mhz. Such an extremely narrow gate minimizes the risk of partial-time jamming.

Accurate-time synchronization can also be used advantageously in the reply signalling. The same spread spectrum techniques of frequency hopping, time jitter, and a different intrapulse spreading code on each transmission can be incorporated to achieve covertness and jam resistance on the reply. In order to take advantage of these techniques the exact characteristics (frequency hop, time hop, and PN code) must be known in advance to all friendly participants with synchronized clocks. This means that there need not be an exact one-to-one relationship between interrogations and replies. Multiple simultaneous, valid interrogations of an aircraft would result in a single reply at the prescribed, pseudorandom time, frequency, and PN code. This single reply would be available to all friendly interrogators whether they actually interrogate or just listen with their antenna aimed in the

direction of the replying aircraft. This is consistent with the concept of an automated decision process at the aircraft before a reply is made, and results in a number of interesting operational modes.

If the aircraft is subject to severe jamming it might, under pilot option, go into a mode of irregular, unsolicited replies. Each unsolicited reply would have the identical spread spectrum characteristics of a normal reply at that specific time and would be available to all friendly interrogators with synchronized clocks. The pilot might elect this option if he was severely jammed and over friendly territory where the risk of fratricide might be high. He might even be instructed to go into this mode over friendly territory so that all interrogators could remain silent without revealing their positions. The pilot might even elect a continuous-reply mode at every possible pseudorandom reply time. This could perform the function of an emergency beacon if the pilot has to ditch the aircraft. Even in this mode the signal would include pseudorandom time hopping, frequency hopping, and a different spread spectrum code on every transmission. Thus even the emergency-beacon mode would be difficult for the enemy to intercept and exploit.

Clock updating is a major concern in the design of any system requiring accurate-time synchronization. Eventually free-running clocks will drift outside the acceptable limits and require time updating. An aircraft mission time is fairly short and clock update information could be supplied just prior to or just after take off. The real problem for the aircraft is maintaining adequate time synchronization in the severe aircraft environment. Although not trivial, this problem can be addressed in the design and development of an airborne clock.

The ground-interrogation equipment associated with a Short-Range Air Defense (SHORAD) weapon system does not have the luxury of returning to a base for time calibration and update after each mission. Any viable IFF system must be designed to accommodate somewhat inferior clock synchronization for the SHORAD weapons systems, and clock update information should be automatically provided to these weapons systems as part of the normal reply signalling. This can be done based on the assumption that the clock in the aircraft is generally more precise than the one at the SHORAD interrogator. Thus the friendly aircraft can act as a portable secondary time standard for updating the SHORAD clocks.

The automatic-clock-update approach is based on a reply containing at least two pulses. If one pulse is sent at the prescribed pseudorandom reply time, it will arrive at the

interrogator after the appropriate range delay. The ground interrogation equipment knows the pseudorandom time that the pulse was sent and measures the apparent range delay relative to his clock. The term "apparent range delay" is used because it includes the relative clock error between the terminals as well as the true propagation delay. The second pulse of the aircraft reply is sent advanced or retarded from a prescribed pseudorandom reply time by an amount equal to the apparent range delay that the aircraft has measured for that interrogation. This offset reply pulse arrives at the interrogator after the same propagation delay as the previous pulse, provided the aircraft has not moved significantly since the previous pulse. The arrival time of this pulse, relative to the prescribed pseudorandom time at the interrogator, is exactly twice the propagation delay to the aircraft, independent of clock error at either terminal. Thus one reply pulse provides precise-range information while the other provides apparent-range information. This allows the SHORAD terminal to determine its clock error relative to the more accurate aircraft clock. This information can be collected, averaged, and eventually applied as an update to the SHORAD clock. It should be pointed out that an aircraft can provide clock update information for only one SHORAD at a time, and it is important that the SHORAD check for consistency in clock-update information before actually making a correction to the clock.

Precise timing allows the reply signalling to include additional information such as the specific tail number of the replying aircraft. This information would help the SHORAD equipment sort out enemy tag-along spoofers who simply repeat the reply signal from a friendly aircraft. The SHORAD equipment can easily recognize that the two replies give the same tail number, and the weapon operator can be alerted.

The basic IFF signalling scheme is shown in figure 3. All time is divided into interrogation periods followed by reply periods. Whenever an interrogation is initiated it will be accomplished in the next available interrogation period. The IFF responder listens at appropriate times during each interrogation period and collects the information to determine the validity and identity of the interrogation as well as its applicability to the specific responder. The responder evaluates this information and replies in the period immediately following the interrogation if a decision to reply is made. The interrogator then evaluates the reply information and either reinterrogates or makes a final determination of Friend, Spoofer or Enemy.

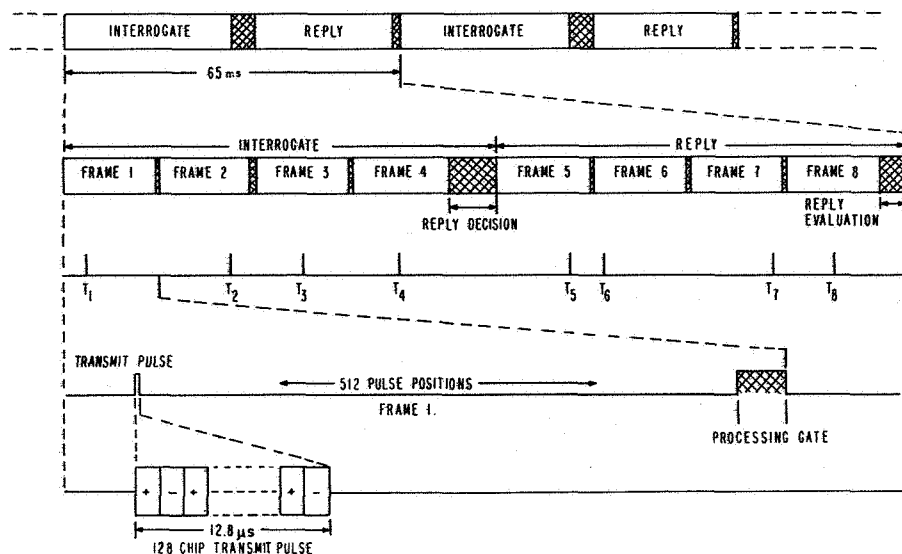


Figure 3. IFF Signalling Format

The interrogation and reply periods are each divided into four frames of about 8 ms each. The actual signalling consists of a short burst of RF energy 12.8  $\mu$ s long in each frame. The specific transmission time within each frame is pseudorandomly determined from 512 possible time slots. The remaining time in each frame is used for signal processing in preparation for the next frame. The actual 12.8  $\mu$ s transmission is phase modulated with 0.1  $\mu$ s chips. Both the chipping code and the carrier frequency are pseudorandomly selected on each transmission. There are 64 carrier frequencies for a total frequency hop bandwidth of 640 MHz and there are 128 different chipping codes. The combination of time hopping, frequency hopping and spread spectrum coding results in a processing gain of 66 dB. This provides the basis for a system which is hard to detect, virtually unexploitable and difficult to jam.

The above discussion has highlighted certain aspects of a new IFF scheme based on accurate-time synchronization. The details of this approach are presented in a paper which was published in the September 1980 issue of the IEEE Transactions on Communications. <sup>(1)</sup>

## TACTICAL CLOCKS

The entire concept of a time synchronized IFF system evolved out of the need to provide an "effective code-validity interval" (selective interrogation zone) which was much shorter than the maximum propagation delay of the system. If a minimum unambiguous range of 150 km is needed; the effective code validity interval should be much smaller than 500  $\mu$ s. The range-measurement accuracy and the exploitability of the system both improve as this effective interval is reduced, but the clock accuracy required becomes increasingly stringent. Requiring a clock precision better than 1  $\mu$ s is not realistic for tactical weapons, even with atomic clocks. A nominal system accuracy of  $\pm 10 \mu$ s was selected as being the least stringent specification capable of providing substantial ECCM improvement. The concept developed in Reference 1 included a special mode which would allow SHORAD interrogators with degraded clocks to continue functioning and receive automatic clock updating until their synchronization degraded beyond  $\pm 100 \mu$ s. A remaining question is the availability of practical, inexpensive clocks that provide the requisite performance in the tactical environment.

At this point we must distinguish between a precision oscillator and a precision clock. The precision oscillator is a device whose output frequency is extremely stable as a function of time and environment. The precision clock incorporates a precision oscillator and count-down circuits to provide an extremely accurate indication of time of day. Intermittent operation of a precision oscillator is acceptable provided the output settles down to the proper frequency within a reasonable time. Intermittent operation of a precision clock is totally unacceptable, even if the basic oscillator within the clock is extremely accurate and quickly settles down to the proper frequency, because its time indication is useless until its readout is synchronized with an adequate external standard.

The traditional approach to precision clocks since 1760, when Harrison invented the first chronometer, has been to never shut the instrument off and never re-set the read out. Current readings are compared periodically with a time standard, and a running tabulation of the error is dutifully kept. A long history of performance is thus developed which not only builds confidence but provides useful interpolation prior to the next check with a time standard. The resynchronization approach is less reliable because the benefit of a long history is lost. Furthermore the setting of time rate or frequency is a difficult task, requiring a significant history of performance. Setting the hands of a pendulum clock is quick and easy, but setting the rate (pendulum length) requires days or even months, depending on the accuracy desired.

The only real candidates for the precision oscillator in a tactical clock are the cesium-controlled oscillator, the rubidium-controlled oscillator, and the quartz crystal oscillator. Both cesium and rubidium rely on the extreme stability of an atomic resonance phenomenon. Although the rubidium and cesium resonances were both demonstrated in the 1950's, the cesium device has dominated for absolute-frequency-standard applications. The cesium device is a primary standard whose output frequency can be accurately predicted from measurements of fundamental parameters such as pressure, temperature, and axial magnetic field. The rubidium device is a secondary standard because the accuracy of this predictive process is less precise than that of the cesium device. In practice, the frequency of a rubidium-controlled oscillator is trimmed, after manufacture, to the frequency of a primary standard. The quartz crystal oscillator relies on the mechanical resonance of an accurately machined quartz plate and its fundamental accuracy and long-term stability are inferior to that of the atomic oscillators. The quartz crystal oscillator has not been considered as a primary frequency standard for half a century, but the extensive history and success of this device as a very stable working oscillator still make it a candidate for an extremely stable, if not precision, clock.

The cesium-controlled oscillator is designed as a primary frequency standard and, as such, achieves the ultimate in performance. However it is extremely expensive (\$26,000 to \$30,000), it is heavy (70 pounds), and it is not designed to function in a tactical environment.

The rubidium-controlled oscillator is a much smaller device. One company (Efratom of California) is producing a unit for tactical military aircraft that is approximately 4" x 4" x 5" and costs about \$6,000. This company is currently developing a smaller unit (2 1/4" x 3 1/2" x 4") for a tactical aircraft communications system<sup>(2)</sup>. This unit is expected to cost approximately \$3,000 in large quantities. It is certainly a candidate for the oscillator in any tactical clock<sup>(3)</sup>.

Some recent advances in quartz crystal oscillator technology make this device an interesting candidate. In particular, the new SC cut provides excellent spectral purity, low aging rate, and less sensitivity to vibration. These units are small (< 13 cubic inches), light (0.7 pounds), low-power (< 2W), and inexpensive (\$750); but they do not have the fundamental accuracy or long-term stability of the atomic oscillators.

Frequency stability and long-term frequency drift are dominant factors in the choice of an oscillator for a accurate tactical clock. Frequency drift is a more or less random function and its

cause is not well understood. It can vary markedly from one time interval to the next and from unit to unit. If this were not so, then frequency drift could be modeled and its deterministic effects removed. In a sense the drift specification of an oscillator is simply an upper bound on long term, unexplained effects, and there is no guarantee that the drift function is either smooth or monotonic.

Figure 4 is a simplified extrapolation based on the frequency-drift specification of one of the best double-oven crystal oscillators on the market. The drift specification is less than  $1 \times 10^{-10}$  per day after a 30 day warmup. The unit sells for about \$1800, consumes about 2.5 W of input power, and fits in a package  $2 \frac{3}{8}'' \times 3 \frac{3}{16}'' \times 5''$ . The dotted curve indicates that the nominal IFF system accuracy of  $\pm 10 \mu\text{s}$  could be maintained for the first 1.5 days without clock update and the degraded limit of  $\pm 100 \mu\text{s}$  could be maintained for about 5 days. The solid curves indicate the extrapolated performance with daily clock updates. After 5 days a clock update every day would be essential, and after 12 days the clock update interval would have to be less than 1 day even for the degraded mode of operation.

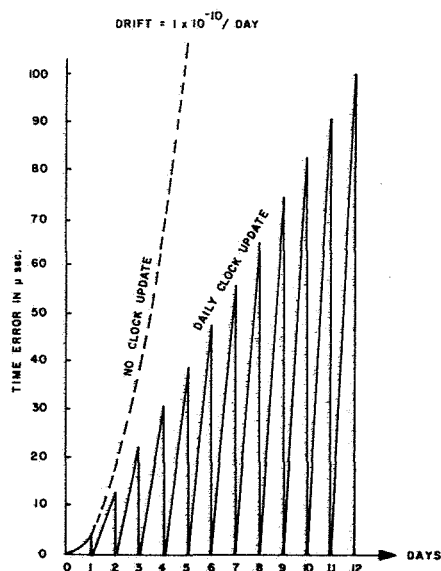


Figure 4. Crystal Oscillator  
Drift

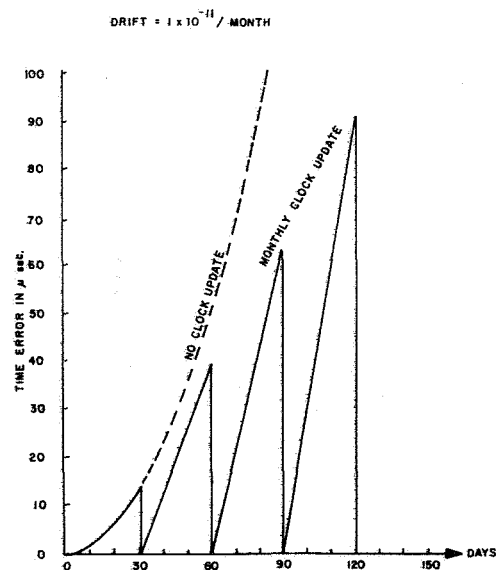


Figure 5. Rubidium Oscillator  
Drift

Figure 5 is a similar extrapolation for a small rubidium-controlled oscillator with a frequency drift specification of  $1 \times 10^{-11}$  per month. This unit sells for about \$6000, consumes 13 W of power, and fits in a package approximately  $4'' \times 4'' \times 5''$ .

The dotted curve indicates that the nominal accuracy of  $\pm 10 \mu\text{s}$  could be maintained for nearly 1 month without clock update and the degraded limit of  $\pm 100 \mu\text{s}$  could be maintained for nearly 3 months. The solid curves indicate that operation within the degraded limit could be extended to better than 4 months if clock updates were obtained as infrequently as once per month. The performance of the crystal oscillator is marginal, at best, for the IFF application, and there is certainly no latitude for degraded performance in the tactical environment. On the other hand, the performance of the rubidium-controlled oscillator is clearly superior, and considerable latitude is available for degraded performance in the tactical environment.

Commercial cesium frequency standards have a long term frequency drift specification of  $3 \times 10^{-12}$ . This is better than the performance of the rubidium-controlled oscillator and should certainly be adequate for the IFF application, but its size, weight, and cost make it practical only as a primary standard at a major base.

Although stability and long-term drift are the dominant factors in the choice of an oscillator for a precision tactical clock, the final decision depends on a number of practical factors as well. The significant parameters of the three candidate oscillators are summarized in Table I.

It is clear from Table I that, unless one is willing to update the clocks very frequently, atomic oscillators will be required. Both the cesium and rubidium oscillators can provide more than adequate stability for the IFF application, but the rubidium oscillator is the only practical choice for a tactical system. The rubidium oscillator has a considerable margin of safety for degraded performance in the tactical environment and, as experience is gained with these units, the system synchronization requirements might be tightened to yield more accurate range measurement and improved ECCM performance.

## CONCLUSION

Accurate time synchronization could form the essential basis of a new spread spectrum IFF system which offers substantial resistance to enemy jamming and makes spoofing and exploitation extremely difficult. The compact rubidium oscillator is the only viable candidate for a tactical clock with sufficient accuracy to support this IFF concept. The performance of these compact rubidium oscillators is extremely impressive for their current state of development, but additional production engineering is necessary to guarantee performance in the tactical environment. The application



Table I  
Comparison of Oscillator Characteristics

	<u>Cesium</u>	<u>Rubidium</u>	<u>SC Crystal</u>
Aging Rate	$3 \times 10^{-12}$ /mo	$1 \times 10^{-11}$ /mo	$1 \times 10^{-10}$ /day
Aging Rate	4 $\mu$ s/mo	13 $\mu$ s/mo	4 $\mu$ s/day
Warm up	30 min for $1 \times 10^{-11}$	4 min for $5 \times 10^{-10}$ 60 min for $1 \times 10^{-11}$	24 hrs for $5 \times 10^{-10}$ 30 days for $1 \times 10^{-10}$
Retrace After 24 hr Shut Off	$7 \times 10^{-12}$	$1 \times 10^{-11}$	$1 \times 10^{-9}$ after 2 hr warmup
Temperature	-40° to 75°C	-55°C to 68°C	-55°C to 60°C
Vibration	MIL-167-1	Not Established Spec = $4 \times 10^{-12}$ /G	Not specified
Size	9" x 17" x 16"	4" x 4" x 5" or 2 $\frac{1}{4}$ " x 3 $\frac{1}{2}$ " x 4"	2.4" x 3.2" x 5"
Weight	70 lb.	4.5 or 2 lb.	2 lb.
Power	43 W	13 W	2.5 W
Cost	\$26K	\$6K - \$3K	\$1K - \$2K

of accurate-time synchronization is not limited to IFF and its increasing use is expected to revolutionize the whole approach to secure, jam-resistant electronic systems for the military.

#### REFERENCES

1. W. M. Bridge, "IFF System Concept Based on Time Synchronization," IEEE Transactions Communication, pp. 1630-1637, September 1980.
2. H. Fruehauf, W. Weidemann, E. Jechart, "Development of a Sub-Miniature Rubidium Oscillator for Seek Talk Application," in Proc. 12th Annual Precise Time and Time Interval (PTTI) Applications and Planning Meeting, December 1980.
3. N. Houlding, "Clocks for Airborne Systems," Proc. 13th Annual PTTI Applications and Planning Meeting (this issue).

## QUESTIONS AND ANSWERS

DR. STOVER, Defense Communications Agency

My question really doesn't have to do with the clocks themselves, but back to your figure that showed the four frames. Have you looked into the possibility that the enemy having captured one of these devices could gain considerable information even though he didn't know the code from the information in those four frames just as when the pulse was received and so forth?

Aren't you perhaps giving him information even though we can't get the code?

MR. BRIDGE:

I don't think so. I think what we've done is we've put all our eggs in the basket of the cryptographic key. As long as he has a valid key, he can use the system exactly as we would. If he captured one, he could certainly use it the way we would. And, now, the problem boils down to: Can he deduce the performance of the box externally without knowledge of that key. And I think that's a NSA problem, and they feel that he can't.

DR. STOVER:

Let me ask one more extrapolation. I interpreted that only a couple of those frames actually were coded. Are you saying all eight of them are coded?

MR. BRIDGE:

I failed to mention that. Let me explain a little bit more. The signal in each frame is hopped in time pseudo-randomly. It's hopped in frequency pseudo-randomly over 600 megahertz and it's hopped in spread-spectrum coding over 128 chips. Each pulse is different in all three parameters, and it really makes it looking for a needle in the haystack for the enemy to try to even find that signal, let alone exploit it.

Okay.

DR. STOVER:

That answers the question. Thank you.

## DIGITAL PROCESSING CLOCK

David H. Phillips, Naval Research Laboratory, Washington, D.C.

### ABSTRACT

The Digital Processing Clock SG 1157/U has been developed by Naval Research Laboratory and is:

- (1) compatible with the PTTI world where it can be driven by an external cesium and built in test equipment shows synchronization with that cesium through the 1 PPS
- (2) built to be expandable to accomodate future time keeping needs of the Navy as well as any other time ordered functions.

Examples of this expandability are the recent inclusion of an unmodulated XR3 time code and the 2137 modulated time code (XR3 with 1 kHz carrier)

### INTRODUCTION

The Digital Processing Clock is designed to make precision time available in visual and electronic form. The system consists of one digital processing clock (SG 1157/U) four remote display units (ID 2170/U) and contains state-of-the-art electronic devices. In all instances where it has been available, military-specified hardware has been utilized. The clock provides all necessary timing information to enable the generation of a wide range of time codes and time related information for future applications.

The clock is human engineered for easy setting. It is designed to be driven by precision frequency standards such as cesium beams, rubidium vapor standards, disciplined time and frequency standards, or any other precision frequency standard providing an adequate 1 MHz output, but will operate on its own internal oscillator if no precision standard is available. The clock is capable of being set to an accuracy within 1 microsecond to an applied external pulse. This pulse need not occur on precise 1 second intervals; prior knowledge of when the pulse will occur is used to preset the thumbwheel switches on the front of the clock.

In addition to the display of the precise time in days, hours, minutes, and seconds, the Digital Processing Clock produces (a) a parallel time code output that is capable of driving from one to four remote display units at distances well removed from the clock itself,

(b) two separate selectable time of event output pulses which can be used to synchronize other equipments, and (c) pulse outputs of 1 PPS and 1 PP10S.

The Digital Processing Clock is presently incorporated in the 688 Class Navy Submarines and applications of it may be extended into other Navy platforms in the future.

#### FUNCTIONAL DESCRIPTION

Figure 1 shows the Digital Processing Clock as it is presently being installed in the 688 class submarines. Sixteen of these clocks have been delivered to the Navy at this time.

Figure 2 is a Block Diagram showing the Digital Processing Clock with four remote readout units daisy-chained to it. The remote display units are located at distances up to 100 ft. from the SG 1157/U clock on the submarines. The remote display units are fed by a 20 line parallel bus which allows the use of very simple and easily replaceable electronic parts. BCD to seven segment decoders are included on the LED readout chip.

Figure 3 is a block diagram for the Digital Processing Clock showing signal flow and functional operation and inputs on front and back of clock. The Digital Processing Clock takes the 1 MHz input signal from a frequency standard, for example a cesium beam standard, and divides it down to produce a one-pulse-per-second (1PPS) output tick and the time-of-day information. Should the external 1 MHz signal disappear from the input, an internal 1 MHz signal generated from an internal oscillator within the clock itself is automatically applied at the input. The accuracy of this signal, however, is one part in  $10^7$  over a temperature range of 0°C to 50°C and, therefore, the clock will accumulate time error rapidly when this mode of operation exists. The internal oscillator may be retuned with the screw-covered screw-driver adjustment on the top of the oscillator. Buffered outputs from all dividers in the countdown chain are available internally, and the 20 parallel lines of information containing hours, minutes, and seconds in a binary-coded decimal (BCD) format are fed to a multipin connector (Time Code Out) on the rear panel of the clock to drive the remote readout units.

Synchronization, time setting, or both, are accomplished by applying an external positive going transition to the External Sync Input on the front panel. If no external time signal is available, the lower Sync switch on the front panel can be put in the INT position and after the Arm button is pushed the next internally generated (1-pulse-per-10-s) 1 PP10S signal will set and synchronize the Digital Processing Clock.

An output pulse may be generated at any time desired with the Time-of-Event (TOE) output. There are two TOE output BNCs, A and B, on the back of the clock. The repetition rate of this event pulse is internally selectable at five different rates (1 PPS, 1 PP10S, 1 PPM, 1 PPHR, and 1 PPDAY) with DIP packaged rocker switches on the TOE Circuit Board. The TOE output (e.g., 10 microsecond wide one pulse per sec (1 PPS) output) can be delayed by the time set up on the subsecond (millisecond and microsecond) thumbwheel switches on the front of the clock. If the subsecond thumbwheel switches were set to zero, this 1 PPS signal would be synchronized with the 1 PPS output signal available on the front panel.

The Digital Processing Clock normally receives its power from an external power source of 115 V, 60 Hz, single phase. If the power source fails or is disconnected, or the power module develops a fault, the clock is diode switched to battery operation with zero time error.

Figure 4 shows the Clock Time Base and Display printed circuit card. This circuit contains the TCXO (temperature controlled crystal oscillator) and switching circuit which allows the transfer of external frequency reference with minimal time loss (in the order of one microsecond ( $\mu$ s)).

Figure 5 shows the 1 MHz to 1 PPS Countdown and Sync Function printed circuit card. The function of this circuit is to count pulses of the input 1 MHz square wave and produce an output of one-pulse-per-second (1 PPS). In addition, the occurrence of this output pulse must be capable of being set to within one microsecond ( $\mu$ s) of any time relative to an externally applied synchronizing pulse or any preset number of microseconds from the external pulse.

Figure 6 shows the Day, Hour, Minute, Second Counter Function printed circuit card. The function of this circuit is to take the 1 PPS signal produced by the card just described and divide it down further to produce second, minute, hour, and finally, day of the year information, which will be displayed on the clock's front panel. With external sync, it can be preset to any desired day, hour, minute, second with front panel thumbwheel switches.

Figure 7 shows the Time of Event Function printed circuit card. The function of this circuit is to compare the BCD output information from the clock's divider chain with the setting of the digital thumbwheel switches on the front panel. When this comparison indicates total agreement, this circuit gates out a 10  $\mu$ s Time of Event pulse whose leading edge occurs at the precise time when coincidence was achieved. The TOE card presents two selectable outputs on the back of the clock.

Figure 8 shows the Power Supply printed circuit card. This circuit regulates the 9.7 vdc from the power supply to 5 vdc for the printed circuit cards and provides diode switching for battery operation.

#### OPERATOR CONTROLS

Figure 9 shows the operator controls.

1. Thumbwheel Switches--15 unit decade used for time setting, delay insertion, and time of event operations.
2. Battery Standby/Off Switch--in Standby position supplies backup power for clock for 1/2 hour; in Off position battery is taken out of circuit to prevent discharging during shipping or storage.
3. LED Display--when on battery power, push to get display of day of year and time of day.
4. LED Test--when pushed display shows all 8s and decimal points lit.
5. Event Output/Inhibit--Time of Event outputs on back of clock are enabled in Output position.
6. Sync 1 PPS/Clock--in Clock position sets clock to time on thumbwheel switches and syncs to within one microsecond with sync signal when it arrives. In 1 PPS position only the subsecond timing is changed.
7. Sync Int./Ext.--in Int. position syncs clock with internally generated 1 PPS. In Ext. position syncs clock to applied Ext. Sync signal.
8. Sync Arm--push button to arm clock for arrival of sync signal.
9. Display--7 segment LED display of Day, Hour, Minute, Second information and flashing decimal point indicators for (1) clock armed (3 points to left of each day digit), (2) clock on Internal Oscillator (1 point to left of tens of minutes), (3) coincidence of Sync to within one microsecond (2 points to left of second digits).
10. Fuses--two 1.5A Line fuses and one spare.

The clock is started by tick start. It is easily started by an external tick which is the preferred method, but can also be started from the internal oscillator in several steps. This design is used to facilitate starting with information from other reference standards and for precision setting, the pulse need not arrive on an even second. However, if time of arrival is known in advance, this advanced information is set in the thumbwheel switches on the front and the clock armed before the arrival of the pulse. The clock starts on the positive going transistion which may typically start at 0.5 vdc and rise to 5 vdc.

## BUILT-IN TEST EQUIPMENT

The Digital Processing Clock has built-in test equipment (BITE) to ease the checking of proper operation. The status of the BITE indicators should be checked on a regular basis depending on usage. BITE indicators are:

1. LED test--when pushbutton switch on front panel is pushed, the display shows all 8's and decimal points are lit.
2. Flashing decimal point indicators:
  - a. Clock Armed (3 decimal points to left of each day digit light)
  - b. Clock on Internal Oscillator (1 decimal point to left of tens of minutes flashes)
  - c. Coincidence of Sync to within one microsecond (2 decimal points to left of seconds digits flash).

## EXPANDIBILITY

Figure 10 shows the SG 1157/U clock with the newly developed XR3 serial time code printed circuit card installed. This is the first of the additional add-on capabilities which uses the basic timing information available in the clock and delivers specific outputs, i.e., XR3 level shift code, 2137 code (XR3 time code, AM modulated on a 1000 Hz carrier), and 200 KHz. There is still additional room for future development of time ordered capability.

Figure 11 shows the SG 1157/U clock's back panel which has the output BNC connectors for the above mentioned three outputs as well as the original 1 PPS, 1 PP10S, TOE (time of event), and 20 line parallel time code outputs.

## BATTERY POWER

Figure 11 also shows the Gel-cell batteries used to power the SG 1157/U clock in case of Ship-to-Shore changeover power interruptions. The batteries will power the clock in excess of one hour in case of power interruption. The batteries are charged by a 9.7 vdc regulated power supply.

## SPARE CARDS

Figure 12 shows an SG 1157/U clock with a set of spare cards stored in the card cage. The reliability of the printed circuit cards has been very high and availability of spare cards from a supply center is made difficult by the high reliability of the cards themselves. Therefore a set of spare cards for possible future failures



and storage of these cards in the clock itself is recommended. This also eases the submarine's requirements on space and difficulty in attaining spares at sea.

#### FUTURE CAPABILITIES

Figure 13 shows possible future capabilities for the Digital Processing Clock.

1) Timekeeping station capability - The inclusion of a microprocessor card such as the Intel 8085 would enable the clock to monitor external precision standards and calculate the time differences between the external standards and the time in the SG 1157/U clock. This time difference information could then be multiplexed to the clock's LED readout and present the information to the operator via the display. The time difference information could be also made available by an RS232 output on the back of the clock.

2) Upgrade to 100 ns time steps - If increased accuracy is required a high precision sync card could take an external 5 MHz signal and double it to 10 MPPS, thus allowing the clock to be synchronized to the nearest 100 nanosecond pulse rather than nearest microsecond pulse as is now the case.

3) High Speed Recorder - With the basic timing information available in the SG 1157/U clock, a high speed recorder capability could be developed using an A/D converter storing the digitized information along with the time it was sampled. This information could be stored in RAM under the control of a microprocessor. The output could be displayed at a much slower rate and fed through a D/A converter to an external recorder for visual presentation.

It takes many years for new ideas to be implemented into the Fleet. This equipment represents several ideas on how technology transfer can be implemented in progressive steps without necessitating total equipment replacement.

#### ACKNOWLEDGEMENTS

The author would like to acknowledge the contributions of Joseph J. O'Neill and Ruth E. Phillips.

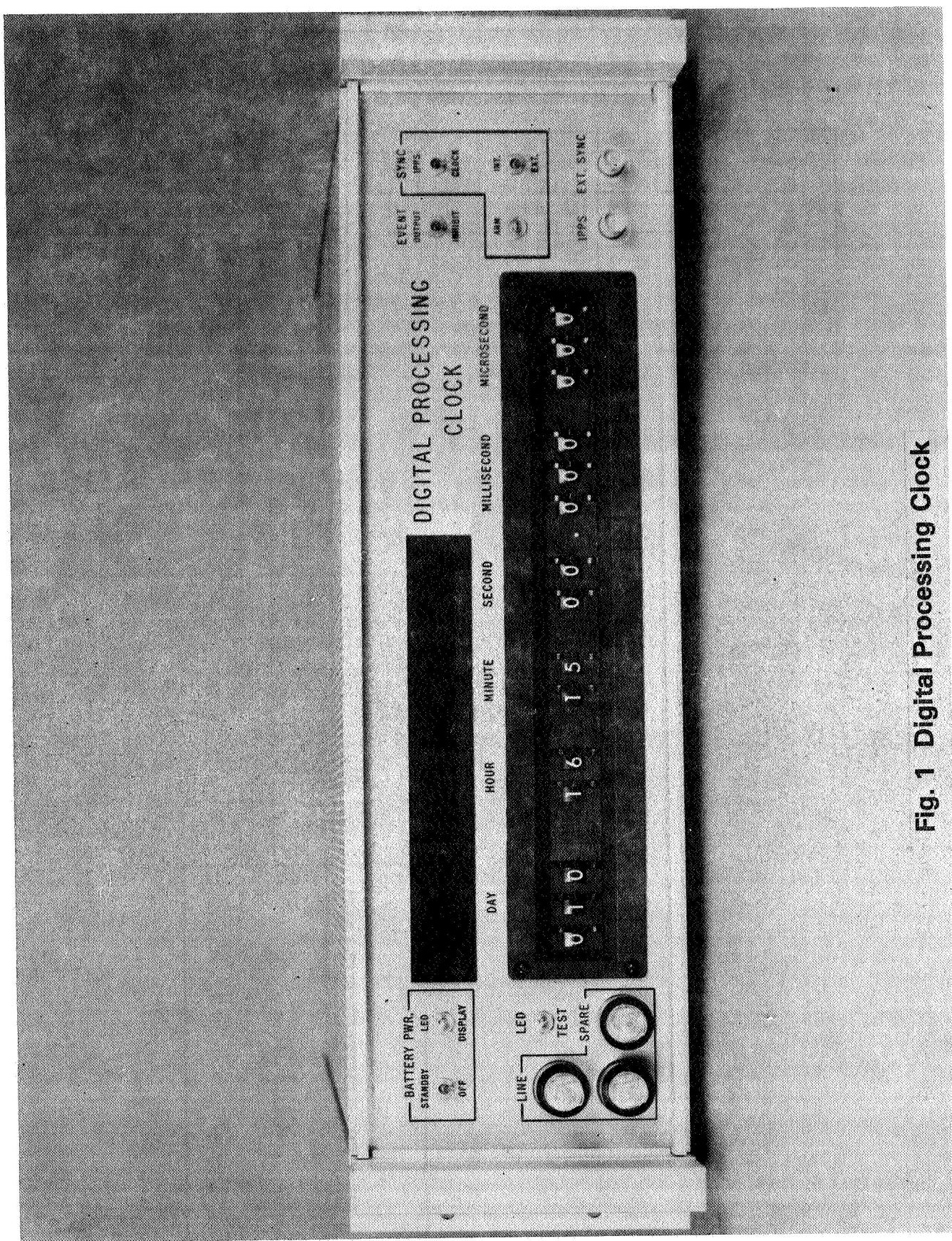


Fig. 1 Digital Processing Clock

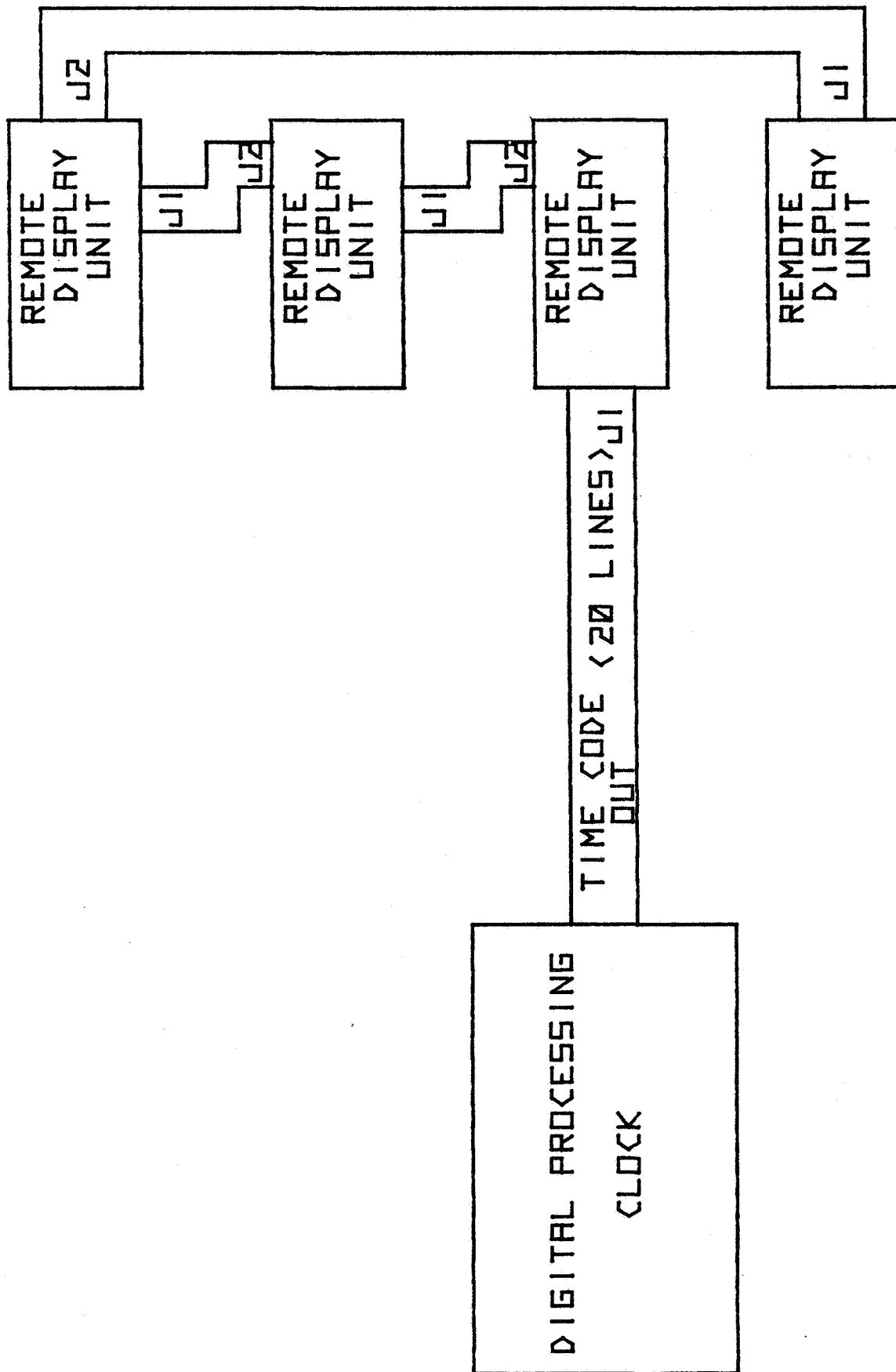


Fig. 2 System Block Diagram

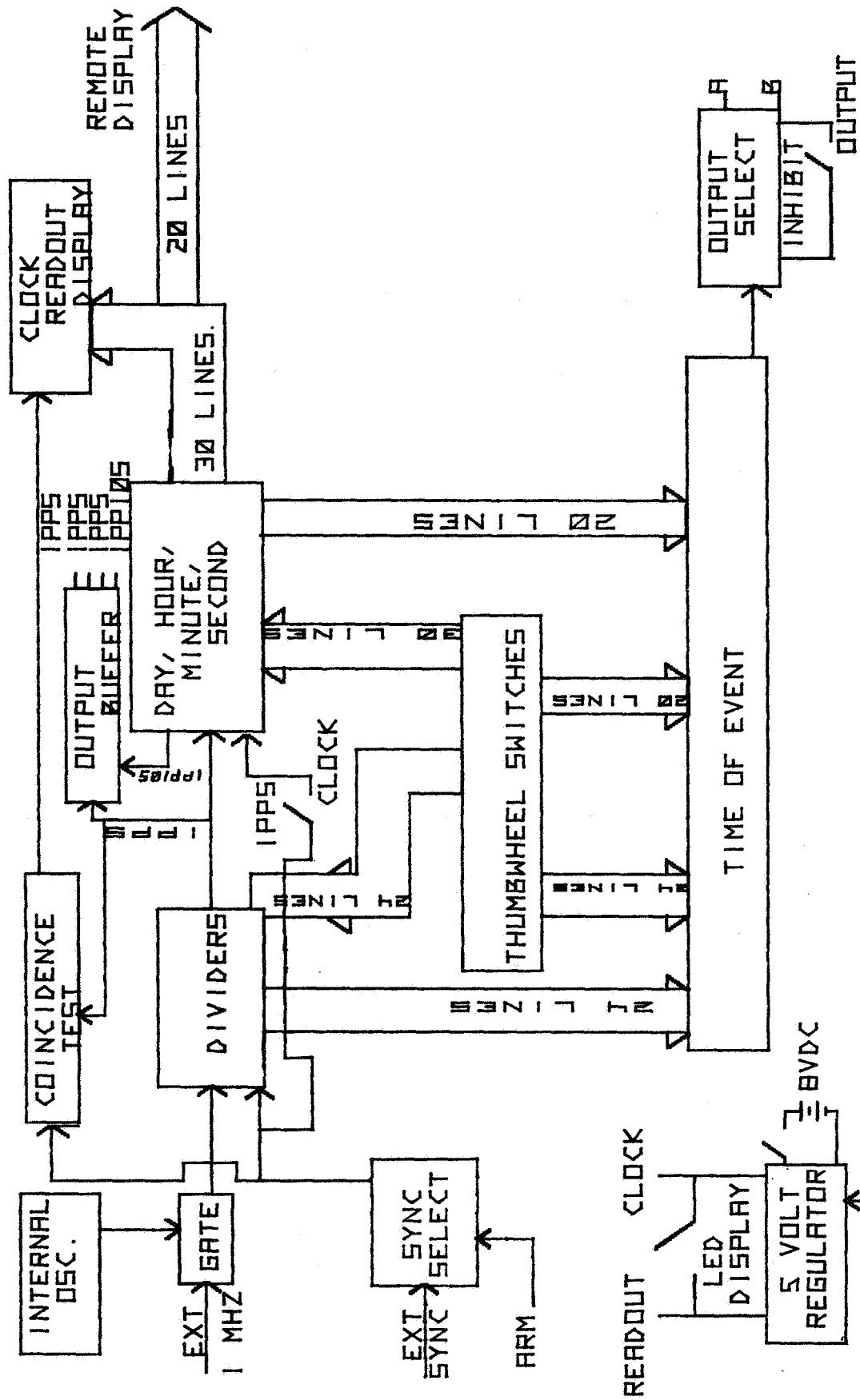
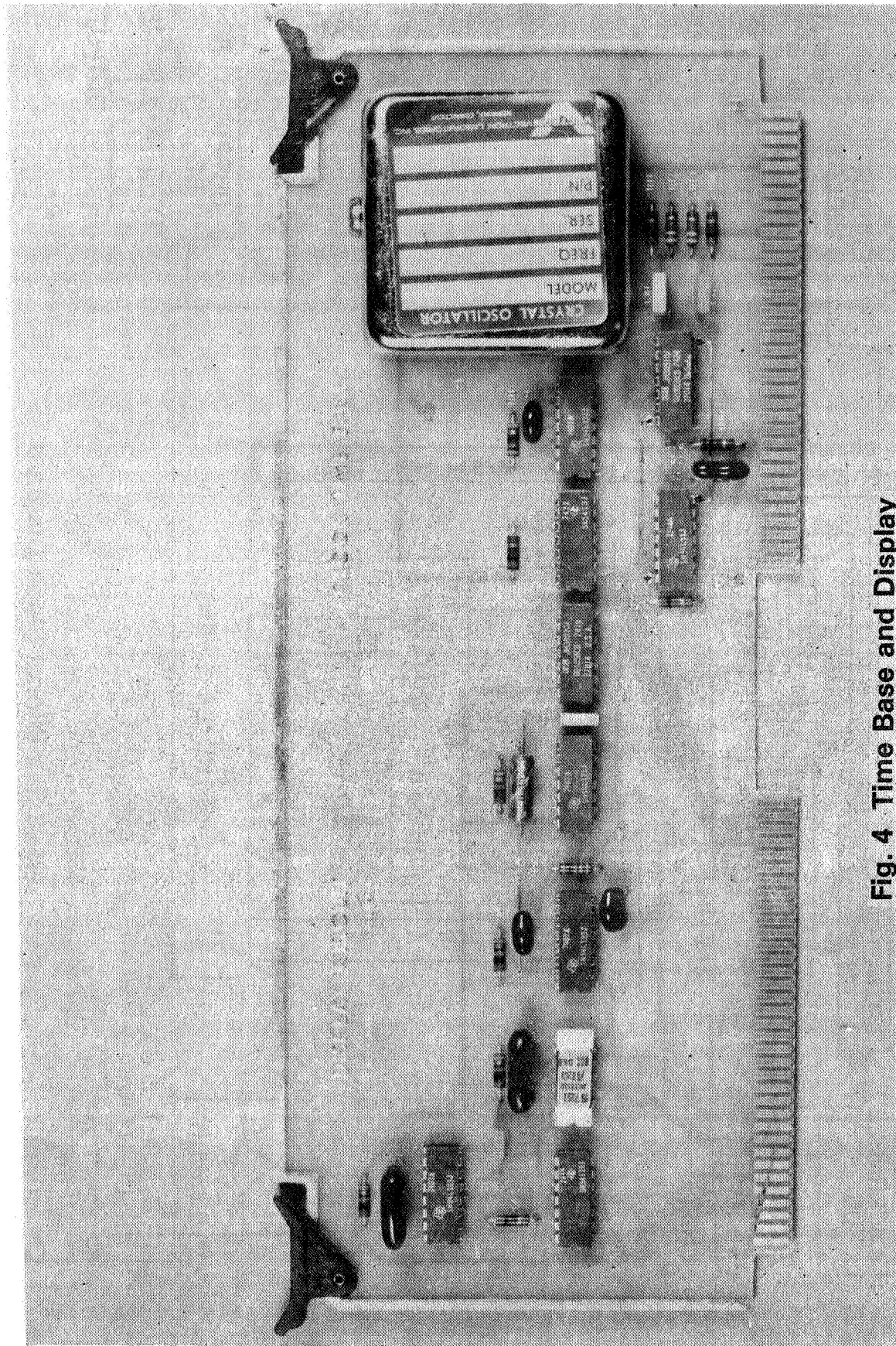
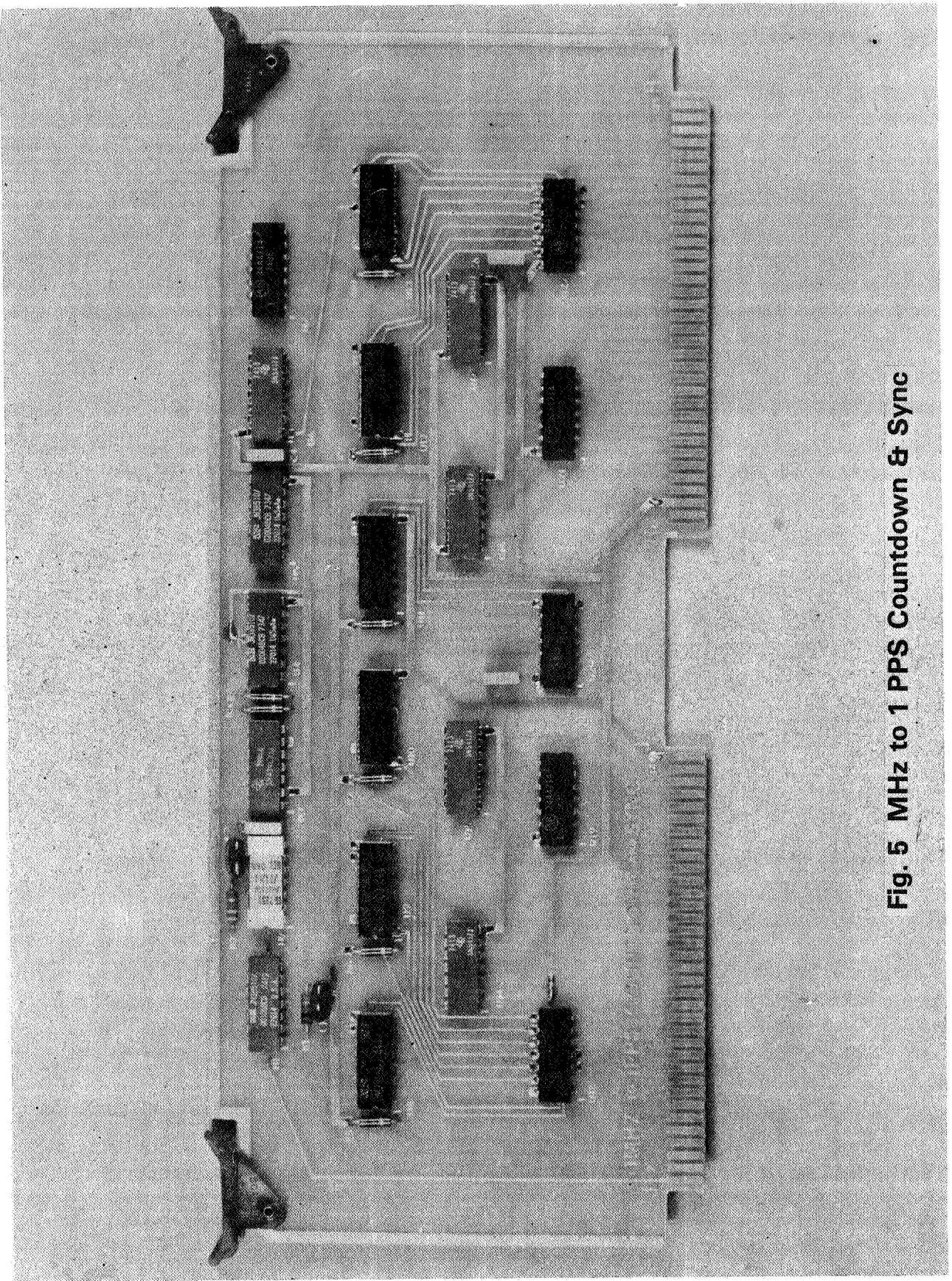


Fig. 3 Functional Block Diagram





**Fig. 4 Time Base and Display**



**Fig. 5 MHz to 1 PPS Countdown & Sync**



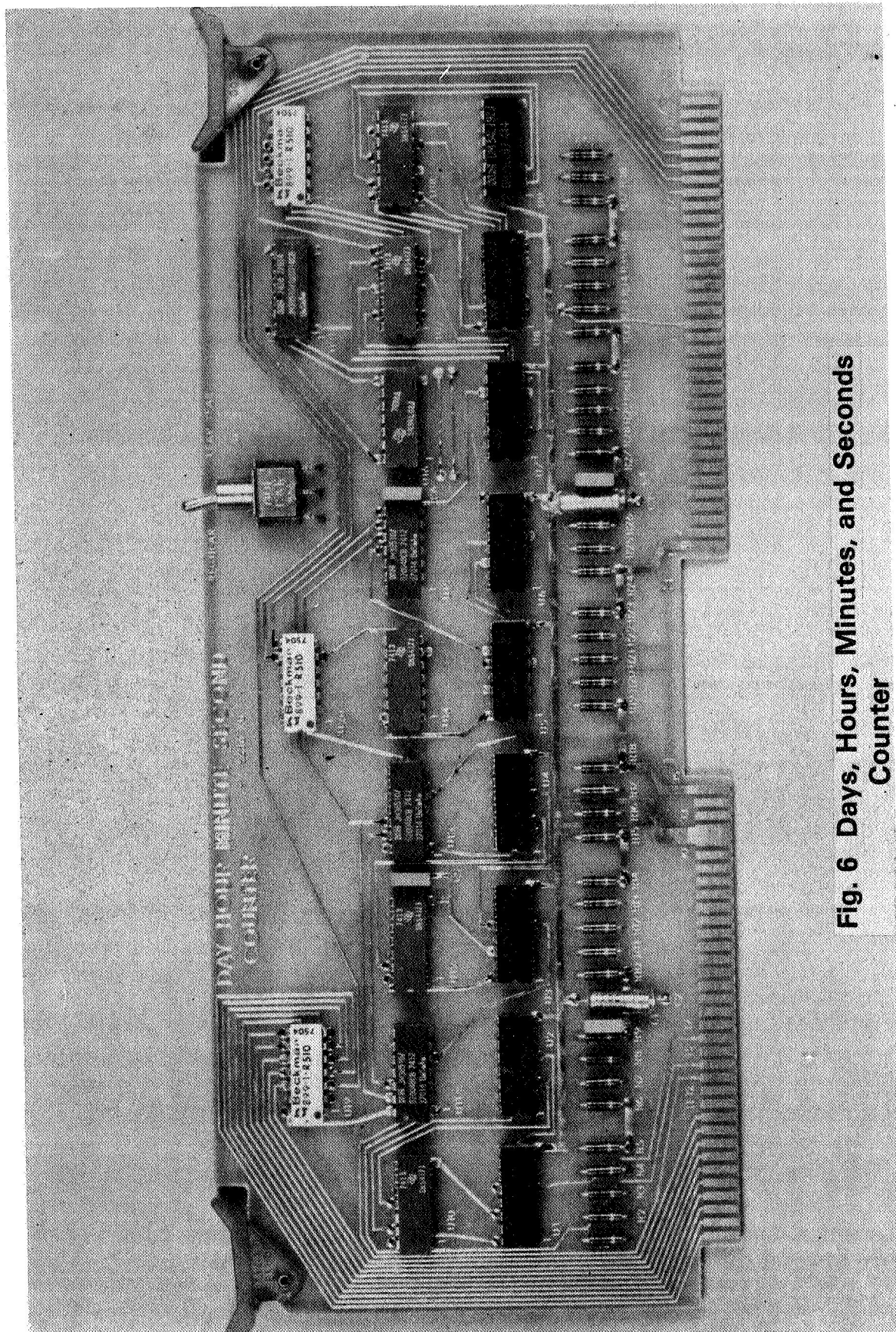


**Fig. 6 Days, Hours, Minutes, and Seconds Counter**

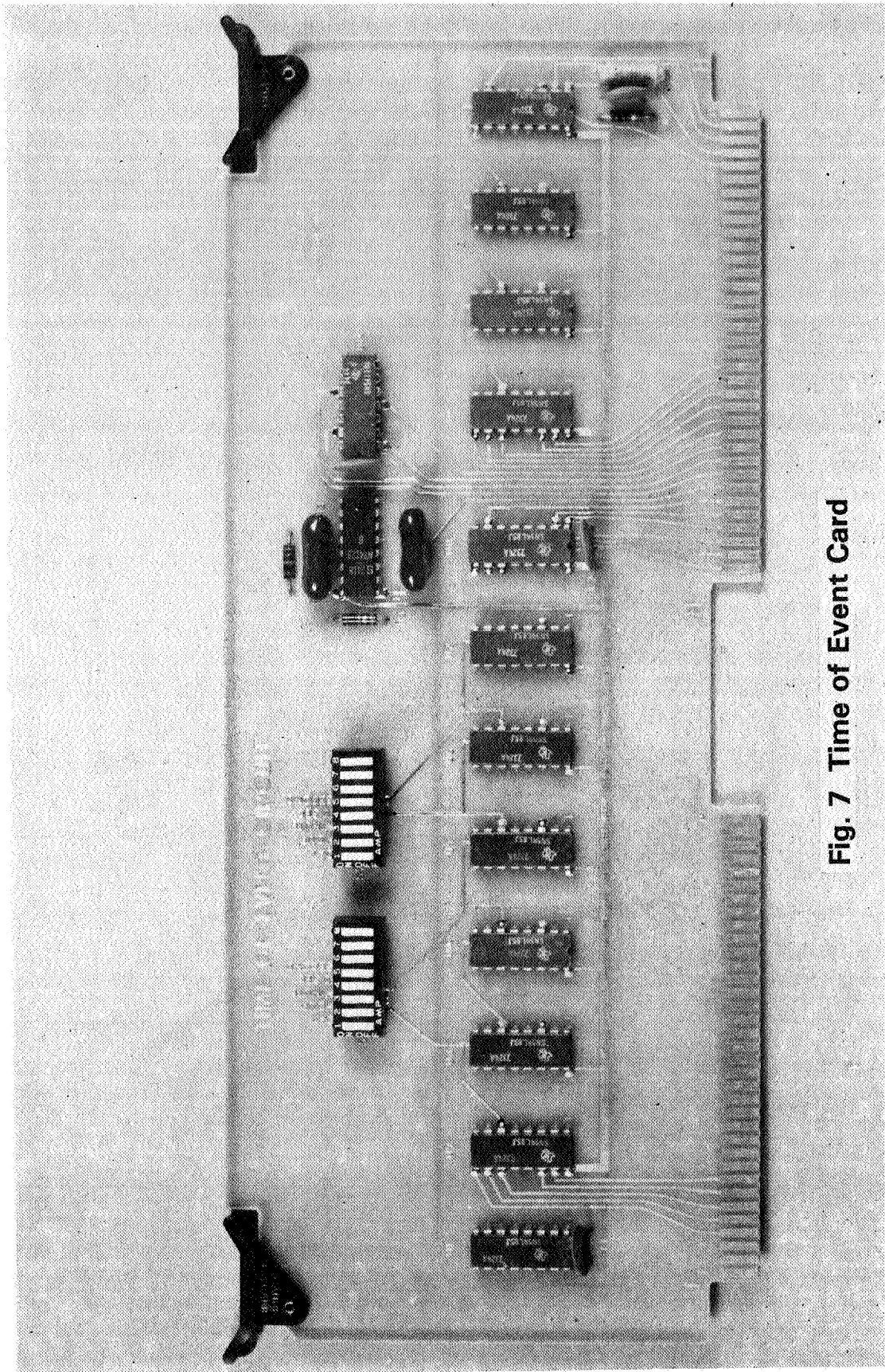


**Fig. 7 Time of Event Card**



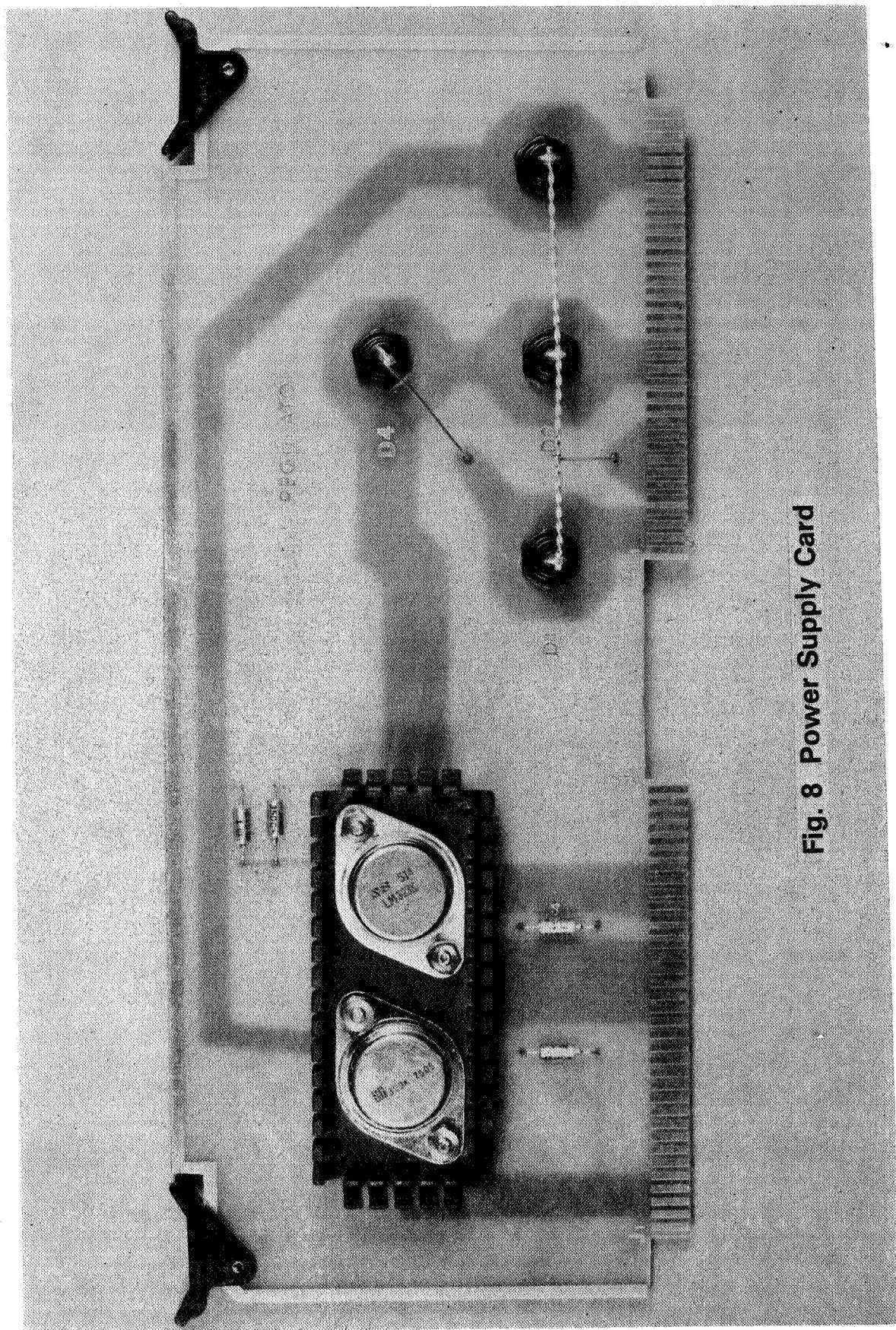
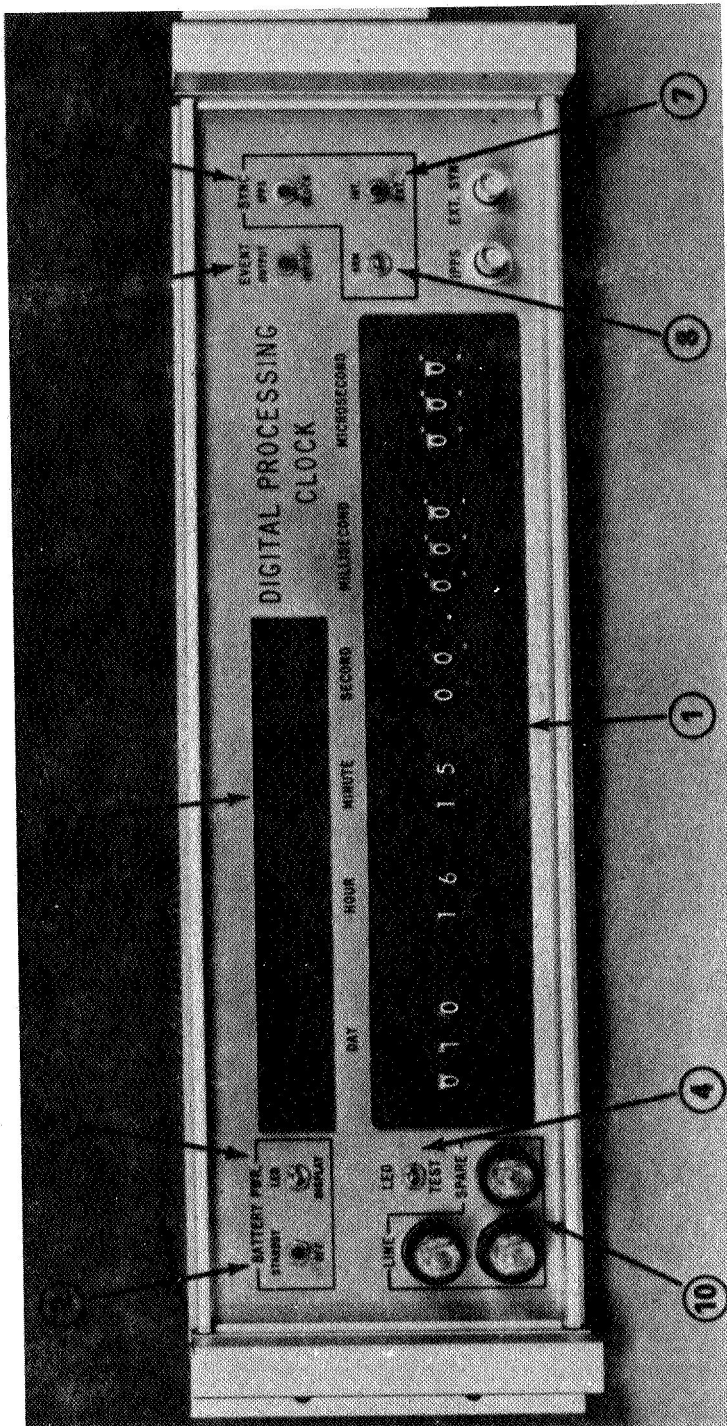


**Fig. 8 Power Supply Card**



1. Thumbwheel Switches—15 unit decade used for time setting, delay insertion, and time of event operations.
2. Battery Standby/Off Switch—in Standby position supplies backup power for clock for ½ hour; in Off position battery is taken out of circuit to prevent discharging during shipping or storage.
3. LED Test—when on battery power, push to get display of day of year and time of day.
4. LED Test—when pushed display shows all 8s and decimal points lit.
5. Event Output/Inhibit—Time of Event outputs on back of clock are enabled in Output position.
6. Sync 1 PPS/Clock—in Clock position sets clock to time on thumbwheel switches and syncs to within one microsecond with sync signal when it arrives. In 1 PPS position only the subsecond timing is changed.
7. Sync Int./Ext.—in Int. position syncs clock with internally generated 1 PPS. In Ext. position syncs clock to applied Ext. Sync signal.
8. Sync Arm—push button to arm clock for arrival of sync signal.
9. Display—7 segment LED display of Day, Hour, Minute, Second information and flashing decimal point indicators for (1) clock armed (3 points to left of each day digit), (2) clock on Internal Oscillator (1 point to left of tens of minutes), (3) coincidence of Sync to within one microsecond (2 points to left of second digits).
10. Fuses—two 1.5A Line fuses and one spare.

**Fig. 9 Operator Controls**



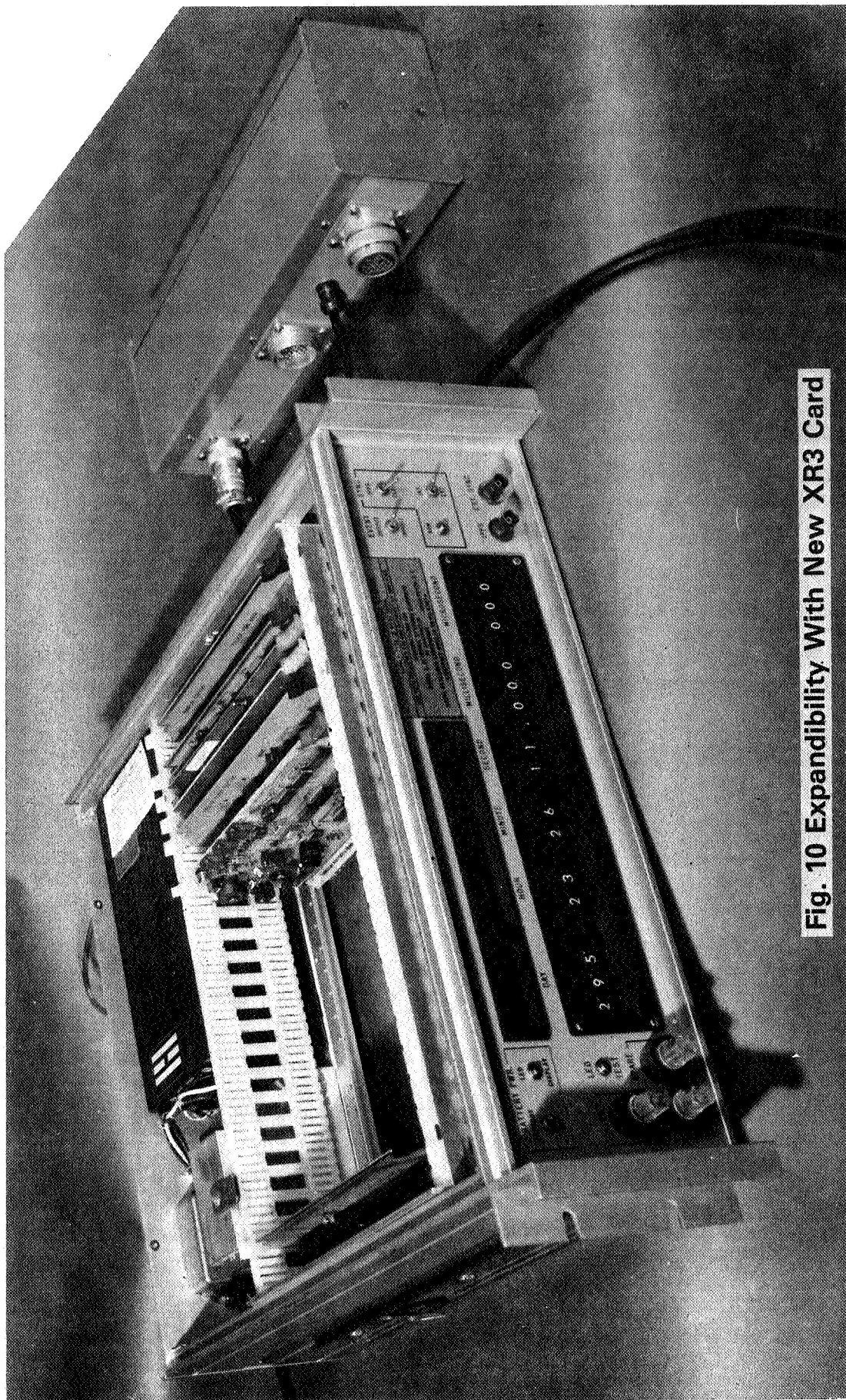


Fig. 10 Expandibility With New XR3 Card



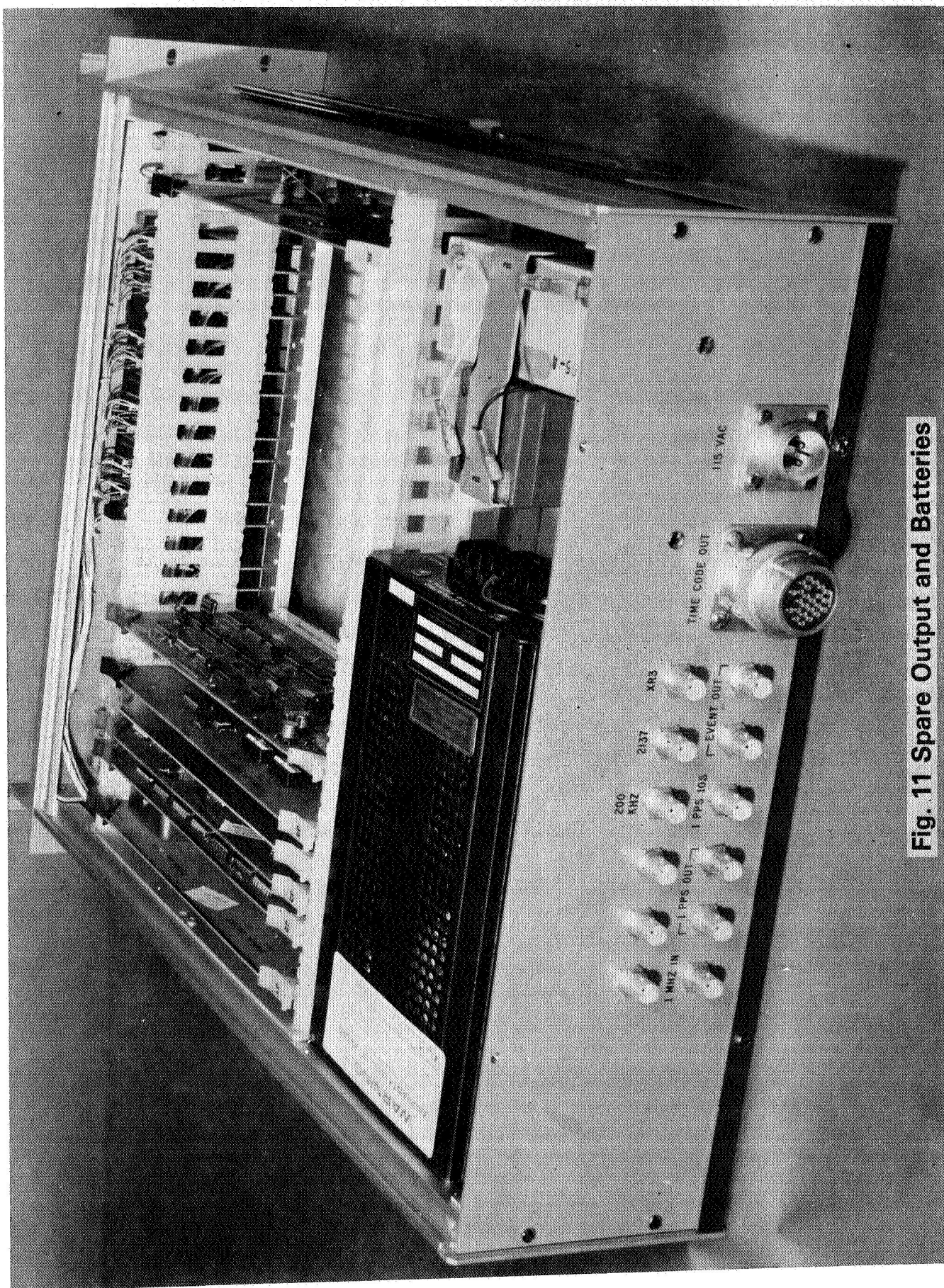


Fig. 11 Spare Output and Batteries

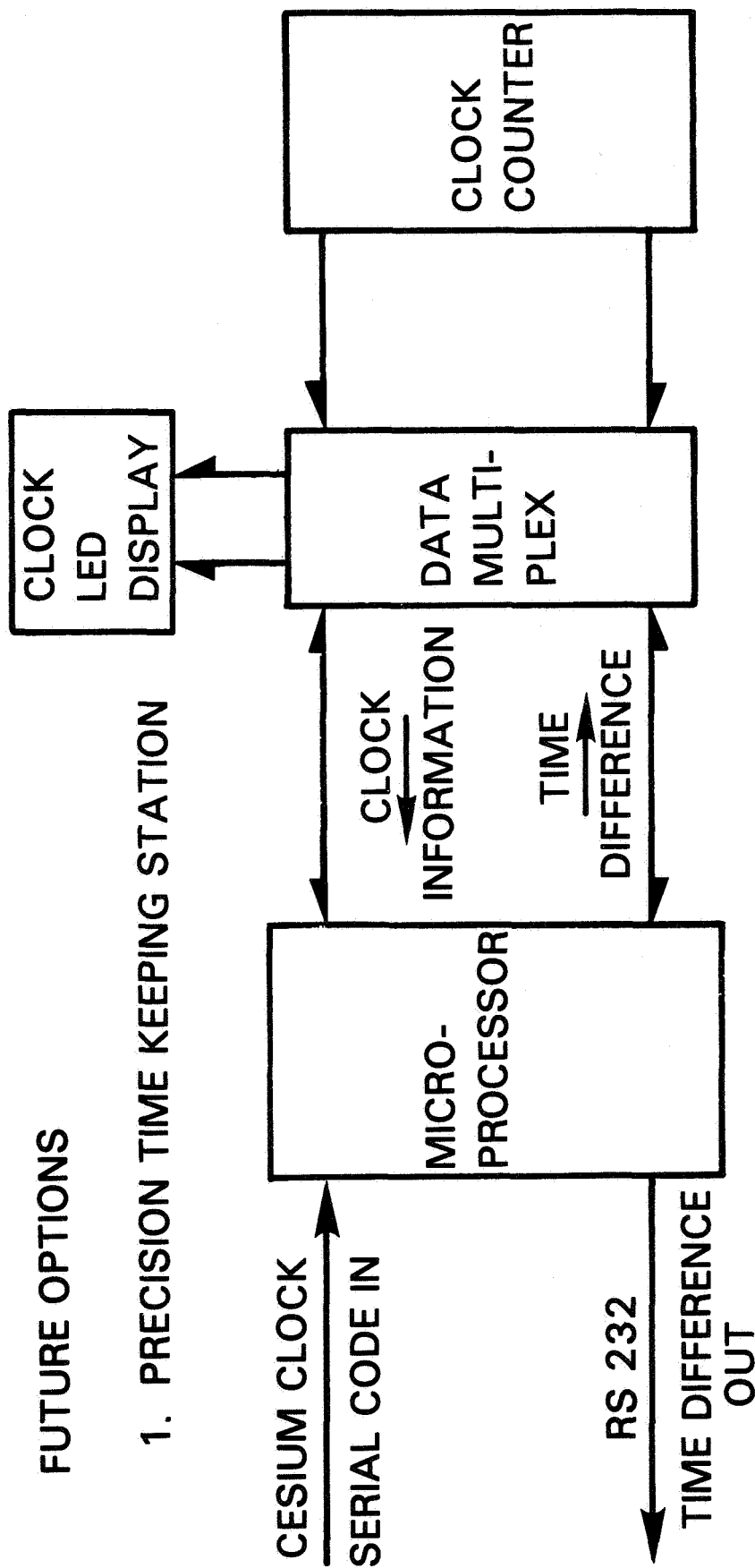




Fig. 12 Spare Card Storage

## FUTURE OPTIONS

### 1. PRECISION TIME KEEPING STATION



### 2. UPGRADE TO 100 n SEC SYNCHRONIZATION CAPABILITY

### 3. HIGH SPEED RECORDER CAPABILITY

Fig. 13 Future Options

## QUESTIONS AND ANSWERS

LT. CARL COLLETTE, GPS Program Office

You mentioned this was scheduled for installation aboard the 688 class submarine. Can you mention when that is planned to go into the fleet?

This is designed for the 688 class submarine, correct?

MR. PHILLIPS:

Yes.

LT. COLLETTE:

Can you tell me like when that's going to be on board, you know, the fleet installation?

MR. PHILLIPS:

We already have some clocks on board. We have delivered 16 clocks already and we have more deliveries to occur. Actually, we are in the process now of putting in this serial time code; so, some of them are actually coming back to us to put in the serial time code.

One reason that we don't anticipate all these things and put a microprocessor in immediately like we would like to is that we have to be in the real world of the user, and do only what he asks us to do. We can suggest, but we have to wait until he allows us to do it.

MR. REX BACKUS, True Time Instruments, Santa Rosa, California

I don't mean to seem to be picking on the Navy or any other time user, and my comment probably belonged in yesterday's discussion of user standards. I'm just curious to know if there's any attempt to diminish the number of serial time codes in use among the user community. We've heard IRIG-B, XR-3. Other user communities have other similar time codes, and we occasionally get requests from the field for time codes that are considered obsolete even by the unit -- even by the standardizing sponsors of these codes. I am just curious what we can do in the standardizing activity to kind of reduce the proliferation, or if not reduce the proliferation, at least reduce the utilization of so many different apparently similar time codes?

MR. PHILLIPS:

Yes, I think that is very appropriate. I certainly sympathize with you, and we are exactly in the same position. In fact, when we started out, we were informed that the time code we are now putting in would not be required, and we should not put it in. And, now, we are required to put it in. So, I think that this would be very impressive to me, to many of the users to have this group decide on the appropriate time code to be disseminated. It would be very useful to all of us to know which one is really the right one.

So far as we are concerned, the XR-3 seems to be.





## TIME COMPARISON VIA OTS-2

G.de Jong and R.Kaarl's, Van Swinden Laboratory (VSL), Delft,  
Netherlands

D.Kirchner and H.Ressler, Technical University (TUG), Graz,  
Austria

### ABSTRACT

Since 1980 time comparisons are carried out via OTS-2 between the Technical University Graz (Austria) and the Van Swinden Laboratory Delft (Netherlands).

The method has been based on the use of the synchronization pulse in the TV-frame of the daily evening broadcasting of a French TV-programme to Northern Africa.

Corrections, as consequence of changes in the position of the satellite coordinates are applied weekly after reception of satellite coordinates from ESOC.

A description of the method is given as well as some of the particular techniques used in both the participating laboratories.

Preliminary results are presented.

Starting January 1982 the experiment will be supported by the EEC and enlarged by participation of NPL, PTB, DFVLR, LPTF and IEN.

### INTRODUCTION

In order to improve (inter-)national time comparisons over long distances, as much as possible independent of atmospheric disturbances and other obstacles between the participating institutes, the application of several types of satellites and pulse transmission systems is investigated.

Although several satellite systems have proven to give possibilities for excellent time comparisons, so far most of the systems are limited from the point of view of continuous availability, continuous accessibility, on-site installation possibility, high costs and so on.

Therefore, an investigation is carried out after the application of always available, on-site receivable, easy accessible, low cost satellite systems.

The experiment described here, makes use of the OTS-2 satellite. The first stage is based on the application of a one-way method by making use of the TV-synchronisation method. In this case corrections must be applied for the changes in the position of OTS-2

In a later stage a partly two-way method will be considered.

## MEASURING PRINCIPLE

The time comparison is based on the measurement of the time of arrival of the same agreed event in the signal from a geostationary communications satellite at both sites A and B (figure 1).

The signal used is a TV-broadcast from a groundstation, which is relayed by the transponders on board of the satellite. At sites A and B receiving only stations have been installed. Therefore, the method is a one-way method.

The time difference of the clocks at A and B can be expressed as :

$$\begin{aligned}\Delta t &= [T_A - (t_A' + t_A'')] - [T_B - (t_B' + t_B'')] \text{ or} \\ \Delta t &= [T_A - \frac{(R_A}{c} + t_A'')] - [T_B - \frac{(R_B}{c} + t_B'')] \text{ or} \\ \Delta t &= (T_A - T_B) - \frac{(R_A - R_B)}{c} - (t_A'' - t_B'') \text{ where,}\end{aligned}$$

$T_A$  and  $T_B$  are the times of arrival of the same reference pulse as determined on the time scales in A and B respectively;

$t_A'$  and  $t_B'$  are the propagation times from the satellite to A and B respectively;

$t_A''$  and  $t_B''$  are the delay times of the signal in the stations A and B respectively;

$R_A$  and  $R_B$  are the ranges from the satellite to A and B respectively;

$c$  is the speed of light.

$t_A''$  and  $t_B''$  are constant and can be determined

$t_A'$  and  $t_B'$  are depending of satellite movements of the geostationary satellite.

In order to achieve high accuracy, the geographic position of the receiving stations and the position of the satellite must therefore be known with high accuracy.

Due to the relative small baseline from A to B and the large ranges  $R_A$  and  $R_B$  to the satellite a geometric configuration

exists in which the first order influences of the satellite movements are cancelled.

## OTS-2 SATELLITE

The satellite used is the Orbital Test Satellite (OTS-2), launched by the European Space Agency, on May 11, 1978 and positioned at 10 °E in the geostationary orbit. The expected lifetime of the satellite extends to 1983.

In the communications field several experiments are carried out with OTS-2.

Some details of the satellite and its payload are give in the figures 2 through 5.

The time comparison experiments are done by making use of a TV-signal sent from France to Northern Africa during the evening hours.

The received carrier frequency is 11.682 GHz. The TV-signal is FM-modulated and occupies a bandwidth of 36 MHz. The signal uses energy dispersal following CCIR-recommendations.

## OTS-2 ORBIT DETERMINATION

The satellite position is calculated by the European Space Operations Centre (ESOC) in Darmstadt (FRG).

The ranging data are determined by the ground stations Fucino (Italy) and--partially-- Villafranca (Spain).

From these data ESOC calculates the OTS-2 orbit, which gives an accuracy of about 2,6 km (1σ) for the position, when manoeuvres are absent. This orbit determination is carried out every week over a period which lasts from Wednesday to Wednesday.

Taking into account the geometry of the position of TUG, VSL and OTS-2 the next table shows the consequences of position uncertainty of OTS-2 on the accuracy of the time comparison.

position uncertainty	east-west	north-south	height
	2.5 km	2.5 km	2.5 km
resulting time error	175 ns	65 ns	8 ns

Table 1 : Time errors resulting from the uncertainty of the spacecraft position

## RECEIVING STATIONS

### TUG, GRAZ, AUSTRIA

The timekeeping station of the Department of Communications and Wave Propagation (INW) of the TUG is located at the Observatory Lustbühel, Graz.

The satellite receiving station, which is also managed by the INW is used for various propagation experiments and is therefore rather complex.

In figure 6 a simplified block diagram shows the configuration for the time comparison.

In table 2 some of the relevant station characteristics are given.

The antenna together with the antenna box is computer controlled in azimuth and elevation. The dish can be heated and the antenna box with the RF-equipment is fully airconditioned.

The received signal is converted down to 70 MHz and fed into an industrial type TV-receiver with a bandwidth of 36 MHz and provided with a threshold extension video demodulator and a videoclamp, which provides more than 40 dB rejection of the energy dispersal wave form.

The video signal ( $1V_{PP} + 3 \text{ dB}$  into 75 ohm) is transmitted by a coaxial cable  $_{PP}$  with a length of 50 m from the antenna building to the time keeping station in the observatory.

The station clocks are HP cesium beam frequency standards.

The laboratory is further equipped with several Loran-C and LF/VLF receivers.

VSL, DELFT, NETHERLANDS

The time-/frequency standards laboratory is part of the Van Swinden Laboratory of the National Service of Metrology (Ministry of Economic Affairs).

Figure 7 shows a simplified block diagram of the receiver configuration.

The most relevant station characteristics are given in table 2.

The antenna with the antenna box is remote controlled in azimuth and elevation, out from the time-/frequency standards laboratory.

The antenna is placed on top of the laboratory and is connected to the time-/frequency standards laboratory by a coaxial cable with a length of 140 m

The station clocks are HP cesium beam frequency standards. The laboratory is equipped with several Loran-C and LF/VLF receivers.

## THE REFERENCE POINT IN THE SIGNAL

The common reference point/event is the trailing edge of the first fieldsynchronization pulse of the video signal.  
See figure 8.

Special electronic circuitry has been developed in order:

- to reject the DC- offset and energy dispersal waveform;
- to clamp the synchronization pulses to zero volt level;
- to measure and to memorize the positive white peak voltage of the video signal;
- to extract the reference pulse at a fixed percentage of the maximum positive peak voltage of the video signal;
- to provide the positive reference pulse with an amplitude of more than 2 V into 50 ohm;
- to suppress the reference pulse, when the video signal to noise ratio is too bad, e.g. when there is no TV-transmission;
- to provide a positive video-output of half the input signal amplitude into 75 ohm for a video monitor; the digital sound-in-sync pulses are removed, so a stable line synchronization is possible.

The delay in the circuit for the reference pulse is about 10 ns and is very stable; the pulse to pulse jitter being only depending on the video signal to noise ratio.

## MEASURING SCHEME, DATA REDUCTION AND COMPUTATION

Since September 2, 1980 the time scales UTC (TUG) and UTC (VSL) are compared by making use of the TV-signals transmitted by the OTS-2 satellite.

Every day, beginning at 18h10min 00s UTC the first measurement is made, followed by one measurement every two seconds. up to a total of 20 measurements (last measurement 18h10min38s). This series of twenty measurements is repeated every hour with the last series ending at 22h10min38s UTC.

Each series of measurements is followed by a Loran-C measurement of the transmitter Sylt (7970W), which is one of the slaves of the Norwegian Sea chain. For the rest, the actual number of measurements per day depends mainly on the presence and duration of the TV-transmission.

The reference pulses have a repetition rate of 50 Hz.

The time difference between the local time at each station and the reference pulse is measured with an accuracy of 1 ns.

The measuring data are exchanged once a week.

The data are processed in the following way. From each series of 20 measurements a mean value is computed by an iterative process omitting all data outside an originally arbitrary limit ( $\pm 0.5 \mu s$ ) from the resulting mean value. Moreover, this mean value is only used for further computation if the number of measurements used to form this mean is greater than 50 % of the available measurements (on an average 91 % of the available measurements are used). The  $1 \sigma$  standard deviations are also computed and their mean value is about 30 ns.

Also the  $1 \sigma$  standard deviations for the readings of each station are evaluated after removing the systematics by a linear regression through the series of data points and result on an average in a figure smaller than 10 ns for the TUG station and 30 ns for the VSL station.

Next, corrections as consequences of the ranging data are applied. This leads to UTC (TUG) minus UTC (VSL).

Only, still a certain offset is present as a result of so far unknown equipment delays.

The determination of these delays has still to be carried out.

To identify the outliers after correcting for the ranging data, a linear best fit of certain length (50 data points, i.e. 50 hourly mean values or approximately 20 days) is applied.



If the data point in question deviates by no more than a given limit ( $\pm 0.5 \mu\text{s}$ ) from the estimate for this point, which is given by the above mentioned linear regression through the last 50 preceding and used data points, then this point is used and becomes the last point in the next calculated linear best fit.

A further condition is that only such data points are used which are the mean of at least 10 single measurements. For further processing of the data from the hourly mean values daily mean values were calculated and also the  $1 \sigma$  standard deviation for all measurements of one day (the  $1 \sigma$  values are on an average smaller than 35 ns). The measurements were then corrected for a step ( $1.6 \times 10^{-13}$ ) in the relative frequency difference of the both time scales. This step is evident from the OTS and LORAN-C data. Thereafter a linear best fit was subtracted from the data. The associated LORAN-C values were processed in the same way.

## RESULTS

Figure 9 shows a plot of the hourly mean values of the readings (TUG) minus readings (VSL).

A time step of 9  $\mu\text{s}$  in the UTC (TUG) scale at MJD 44744 (May 20, 1981) is removed and furthermore the values for UTC (TUG) before MJD 44564 (November 21, 1980) were replaced by the corresponding values of a second clock (HP 5061A with High Performance Tube) which was used later on to generate UTC (TUG). The overall slope of the curve is caused by the frequency difference (about  $7 \times 10^{-13}$ ) of the involved time scales UTC (TUG) and UTC (VSL) respectively. The characteristic shape is due to the change of propagation time resulting from the movements of the satellite.

Figure 10 is a plot of all points which meet the specifications in order to be taken into account for the calculation of UTC (TUG) minus UTC (VSL).

Also plotted in figure 10 are the values of portable clock visits by the U.S. Naval Observatory to both stations. Unfortunately however, the clock visits to both the stations were not carried out on the same trip. Therefore, the plotted values are extrapolations using the clock rates to obtain UTC (TUG) minus UTC (VSL) from UTC (USNO) minus UTC (TUG) and UTC (USNO) minus UTC (VSL).

Fig. 11 shows the residuals of the OTS-2 and the LORAN-C data plus arbitrary constants. The third trace of data points in Fig. 11 presents the difference of the OTS-2 and LORAN-C data for mean values of 10 days (a constant is added to the difference so that the first value is equal to zero). Also indicated are the differences between the OTS-2 results (regression line) and that obtained by the portable clock visits of the USNO ( 100 ns and - 43 ns respectively). No attempt was made to correct for the difference in the delays of the receiving equipments. The accuracy and precision of this result is mainly determined by the knowledge of the position of the spacecraft. Figs. 12 and 13 show a portion of Figs. 9 and 10 on an expanded scale to demonstrate this effect. The data in Fig. 13 are corrected for the frequency difference of the two time scales and clearly show the influence of the uncertainties caused by the ranging data. Fig. 14 is a stability plot (two sample Allan variance  $\sigma_y(2, \tau)$ ) of the UTC(TUG) - UTC(VSL) time scales compared by TV via OTS-2 and LORAN-C. For sampling times longer than 5 days the stability of the OTS-2 TV-link is better than that of the LORAN-C signal. Also plotted in that figure are the  $\sigma_y(2, \tau)$  values if one only uses the data period from MJD 44646 to MJD 44665 (see also Fig. 13). These figures give an estimate of what could be gained by time comparisons using the TV-signal transmitted by the OTS-2 satellite if better tracking data would be available.

## CONCLUSIONS

- The given results are not corrected for equipment delays, so the data have a certain offset.  
Also a direct transportable clock comparison should be carried out in the near future.
- The ranging data could be improved by the application of another best fit method by ESOC.  
This was discussed with ESOC and will be carried out by them.
- From one orbit determination period to the next an offset of up to 200 ns can be seen, especially when there was a spacecraft manoeuvre in between the periods of computation (see Fig. 13 : MJD 44645).
- The receiver at the VSL could be improved in order to achieve less scatter in the readings.  
This improvement has been carried out recently.

- The Loran-C data seem to have a strong seasonal dependence. The difference between the Loran-C and OTS-2 results reached 700 to 900 ns for a differential path length over land of 600 km. The 1 $\sigma$  standard deviation for the period of one year is 107 ns for the OTS-2 data and 270 ns for Loran-C.
- In January 1982 the OTS-2 experiment will be extended by the participation of NPL, PTB, DFVLR, LPTF and IEN. The experiment will be supported by the EEC.

#### ACKNOWLEDGEMENT

The authors would like to express their appreciation to S. Pallaschke and S.J. Arnold of ESOC-Darmstadt for their contributions and fruitful discussions. We also like to thank Mr. A. de Regt of VSL for his contribution in improving the datahandling.

#### REFERENCES

- O. Ortmann, D. Kirchner  
Zeitübertragung mittels Fernsehsignalen  
Internal Report, INW 7801, 1978
- D. Kirchner  
Die Automatisierung einer Zeitstation mittels des IEC-Bus-Systems am Beispiel der Station des Observatoriums Lustbühel der Technischen Universität Graz  
Proc. 10, Internat. Kongress für Chronometrie, p.p.111-117, Genf, 1979.
- G. de Jong  
High - accuracy time and frequency calibration with the aid of television signals  
VSL - report, June 1979
- R. Kaarls and G. de Jong  
Comparison of different time synchronization techniques  
Proceedings 11th PTTI-conference, November 1979
- G. de Jong and R.Kaarls  
An automated time-keeping system  
IEEE, I & M, Vol.IM-29 No.4.pp.230-233, Dec. 1980

table 2

## Main characteristics of the receiving stations

	TUG	VSL
geographical position	47°04'02.88" N 15°29'41.80"E 485.52 m above sea level	52°00'01.85" N 4°22'56.18" E 20.16 m
antenna diameter	3 m	3 m
pre-amplifier	uncooled parametric GaAs Fet low noise amplifier	low noise amplifier
noise temperature	190 K	817 K
down conversion	two stage first IF(750+ 250) MHz second 70 MHz	single stage (135 + 18) MHz
antenna gain	48 dB at 11 GHz	47.5 dB
system noise temperature	370 K	832 K
figure-of-merit	22,3 dB/K	18,3 dB/K
carrier to noise ratio	16,7 dB	12 dB
TV-receiver	double conversion	single conversion
filter bandwidth	36 MHz	40 MHz
time- interval counter	2 ns	1 ns acc.
data storage	magnetic tape	diskette

The geographical coordinates of the antennae at both the stations are determined by Doppler measurements carried out in Western Europe during the last years. The calculations were made by IFAG, Frankfurt a.Main, (FRG).

**Overall Characteristics of Communications Payload (Beginning of Life)**

Repeater Chains	Module designation	A				B	
		2	2	4	4	RL	LR
Repeater Chains	Chain designation						
	Centre frequency						
	- Receive	14172.5	14172.5	14302.5	14302.5	14457.5	14457.5
	- Transmit	11510.0	11510.0	11640.0	11640.0	11795.0	11795.0
	Nominal channel bandwidth	40	40	120	120	5	5
	Overall noise figure	5.0	5.0	5.0	5.0	5.0	5.0
	Max. output level	11.5	11.6	12.4	11.8	12.3	11.9
	Input level for max. output						
	- Max. gain setting	-101.5	-101.5	-101.5	-101.5	-123.0	-125.0
	- Min. gain setting	-87.5	-87.5	-87.5	-87.5	-93.0	-95.0
Beacons	Antenna beam-Polarisation						
	- Receive	Euro 'A' - X	Euro 'A' - Y	Euro 'A' - X	Euro 'A' - Y	Euro 'B' - R	Euro 'B' - L
	- Transmit	Euro 'A' - Y	Euro 'A' - X	Spot - Y	Spot - X	Euro 'B' - L	Euro 'B' - R
	Maximum EIRP at beam centre	38.0	38.4	47.9	47.3	41.4	41.0
	Maximum G/T at beam centre	-3.0	-3.0	-3.0	-3.0	-0.4	-0.4
	Beacon designation	TM	TM			B <sub>0</sub>	B <sub>1</sub>
	Frequency	11575.0	11575.0			11786.0	11786.0
	Output level	-7.0	-7.0			1.6	1.3
	Antenna beam-Polarisation	Euro 'A' - X	Euro 'A' - Y			Euro 'B' - R	Euro 'B' - L
	EIRP at beam centre	19.5	19.5			31.2	31.1

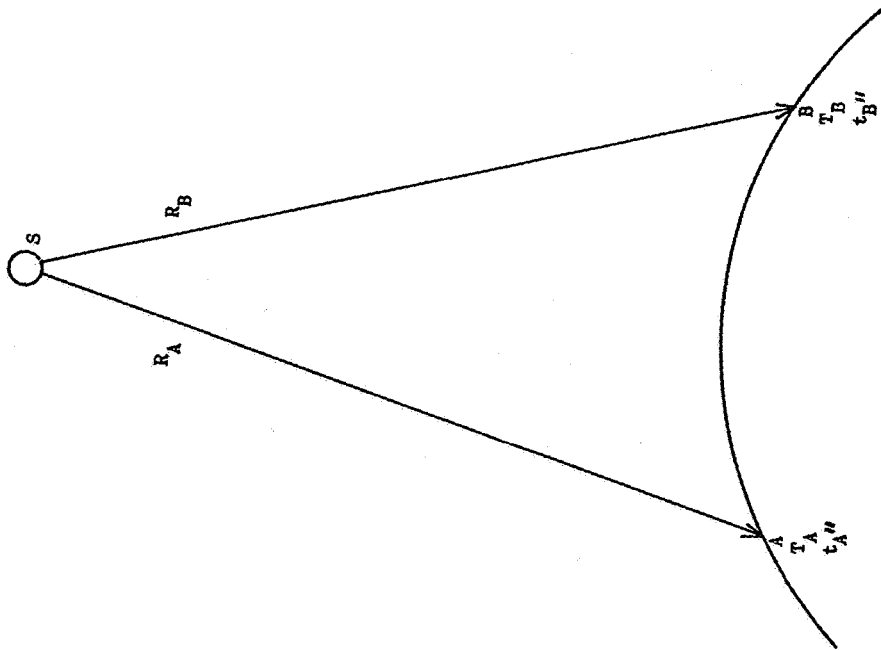


Fig. 1

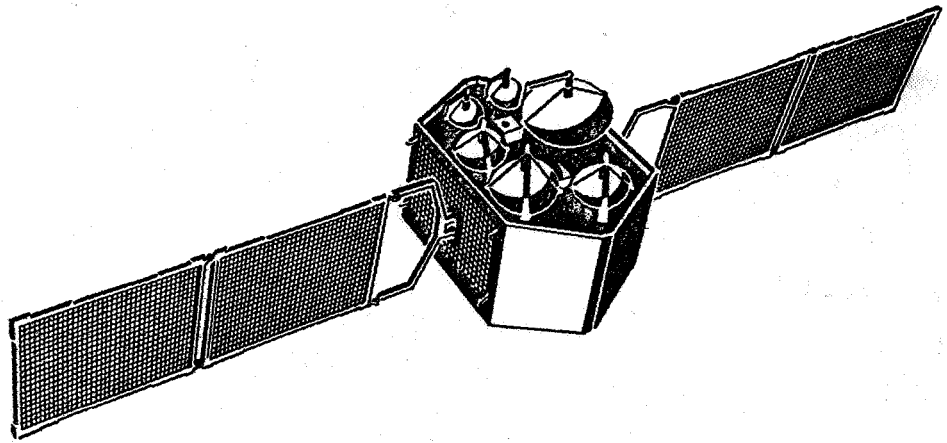


Fig. 2

# **OTS TRANSPONDER - SYSTEM**

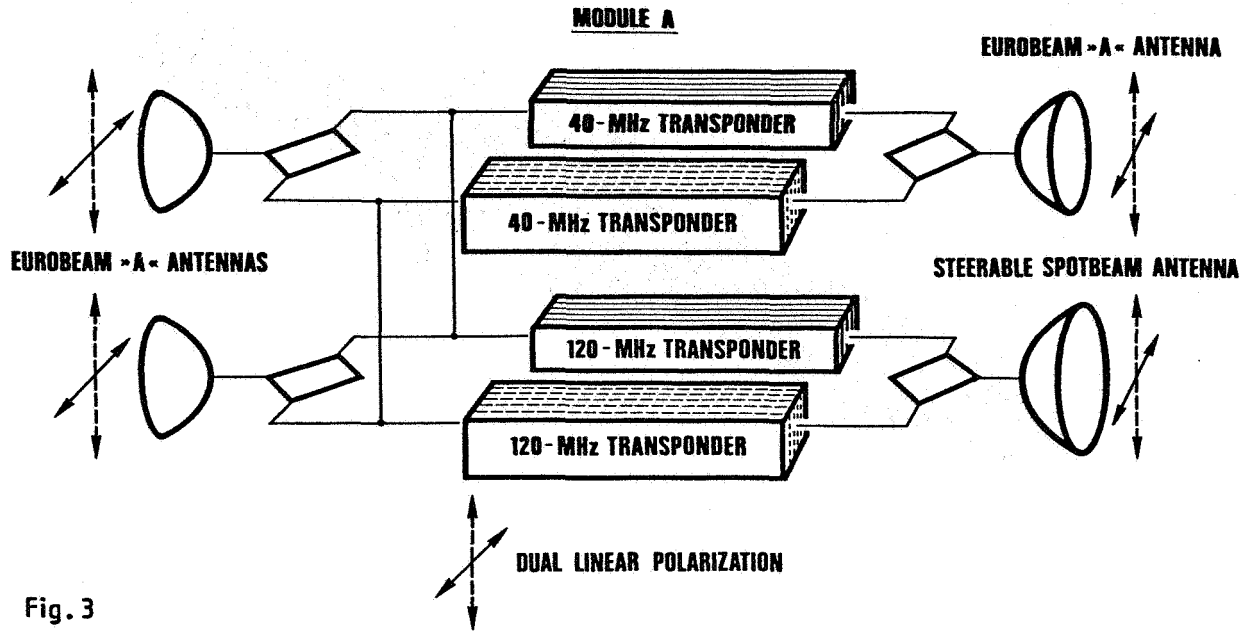


Fig. 3

## **OTS FREQUENCY PLAN MODULE A**

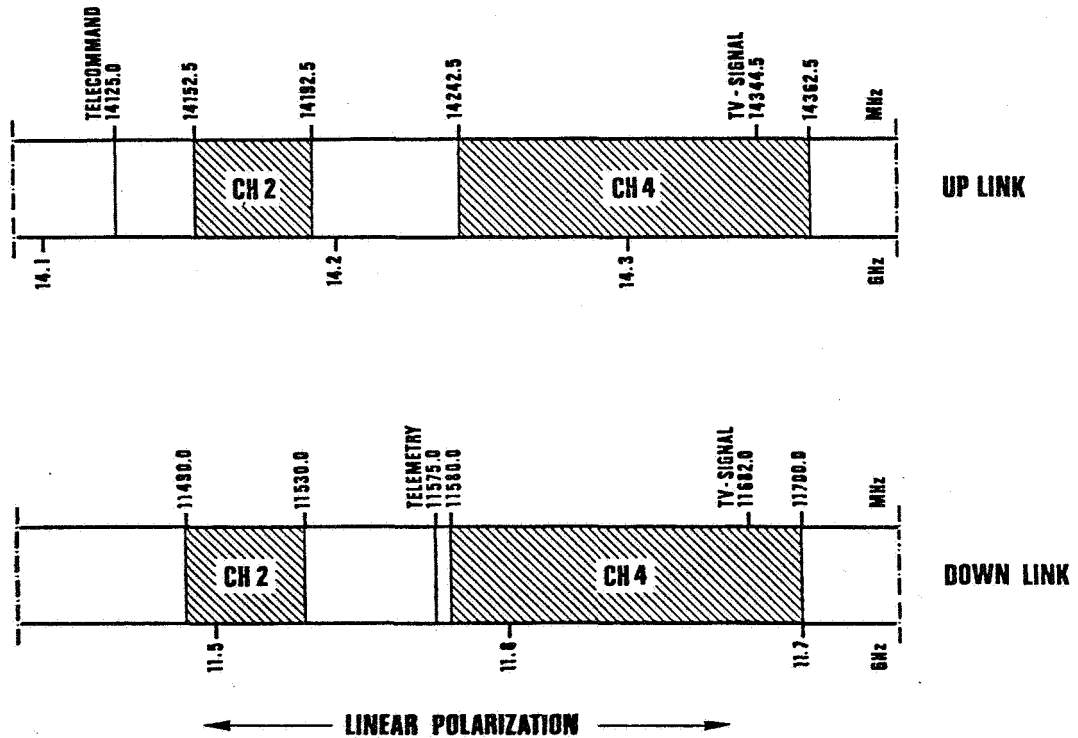
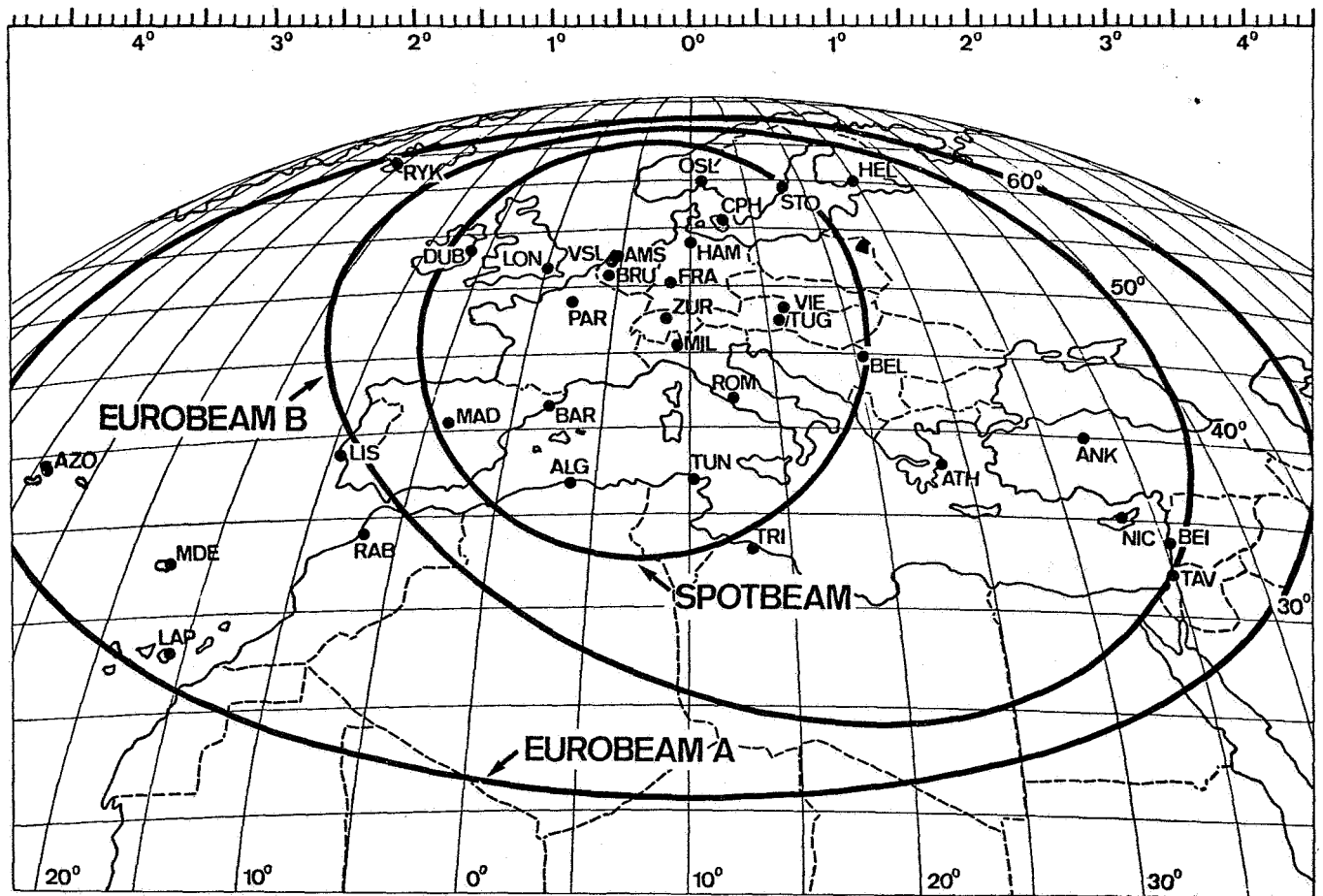


Fig. 4



OTS - COVERAGE ZONES

Fig. 5

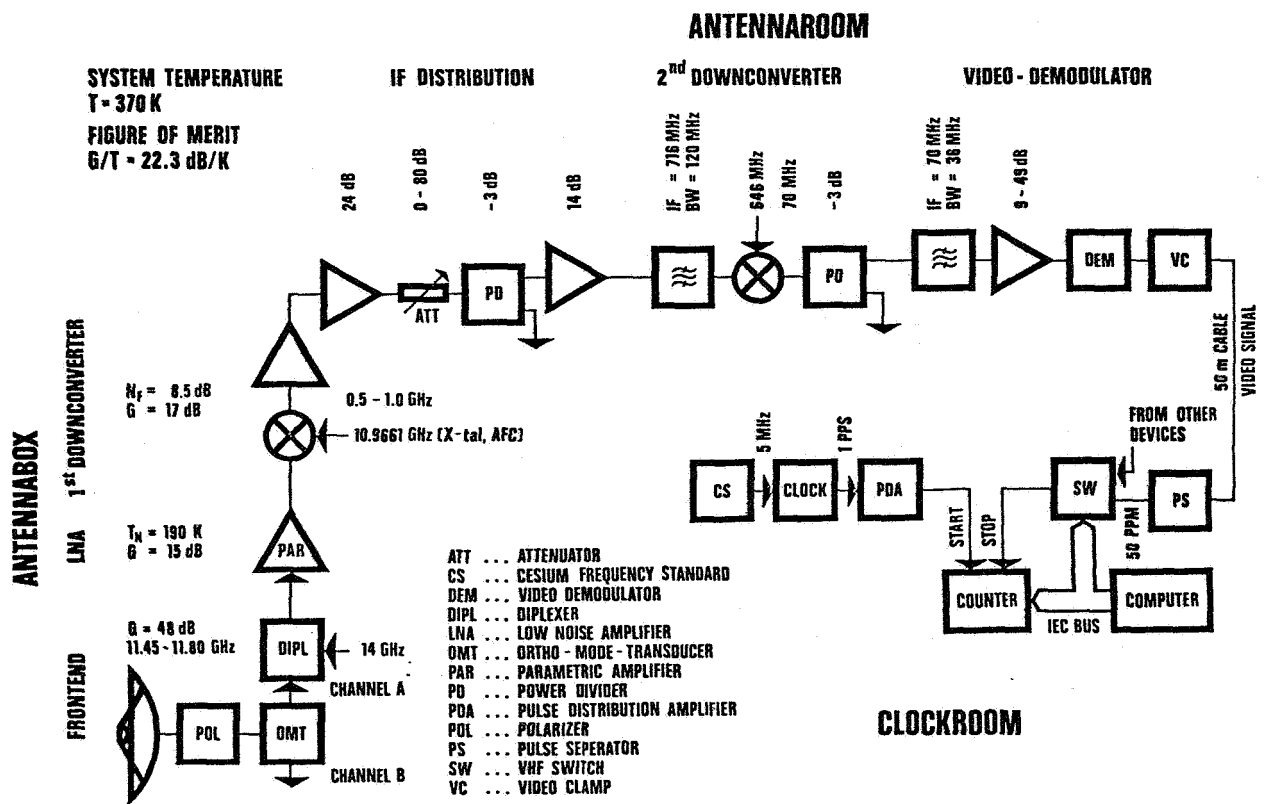


Fig. 6



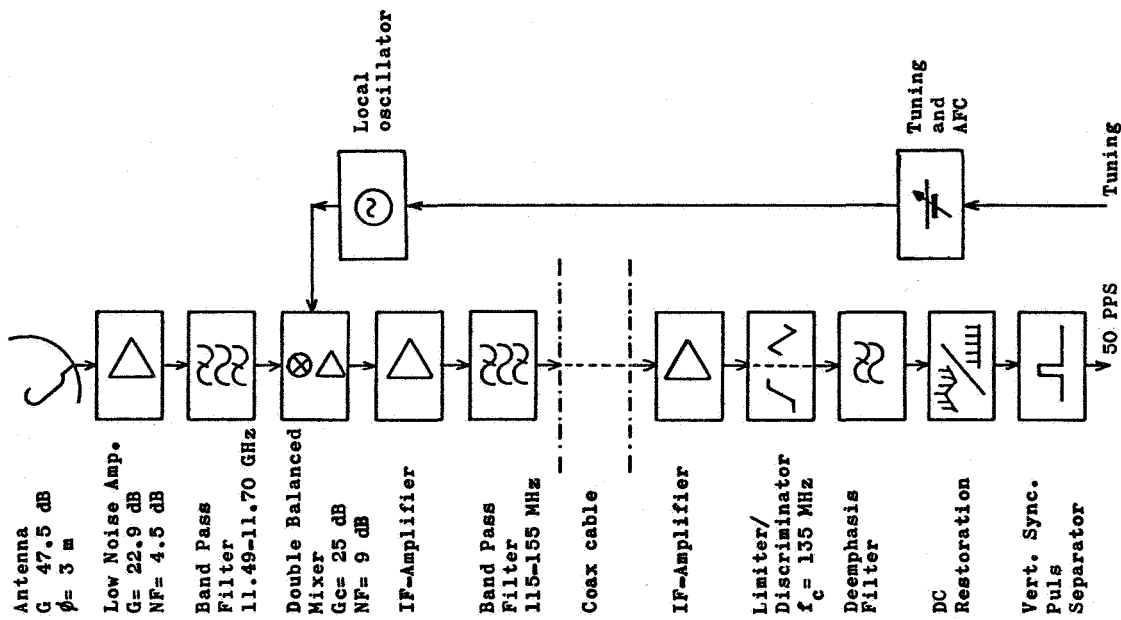


Fig. 7

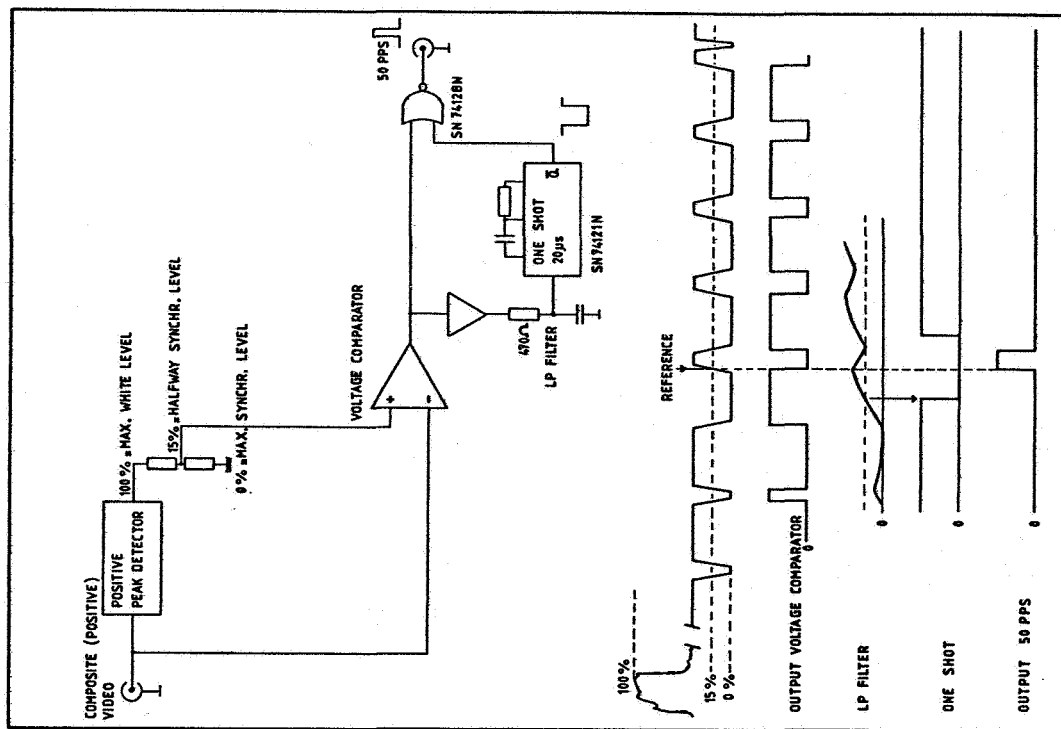
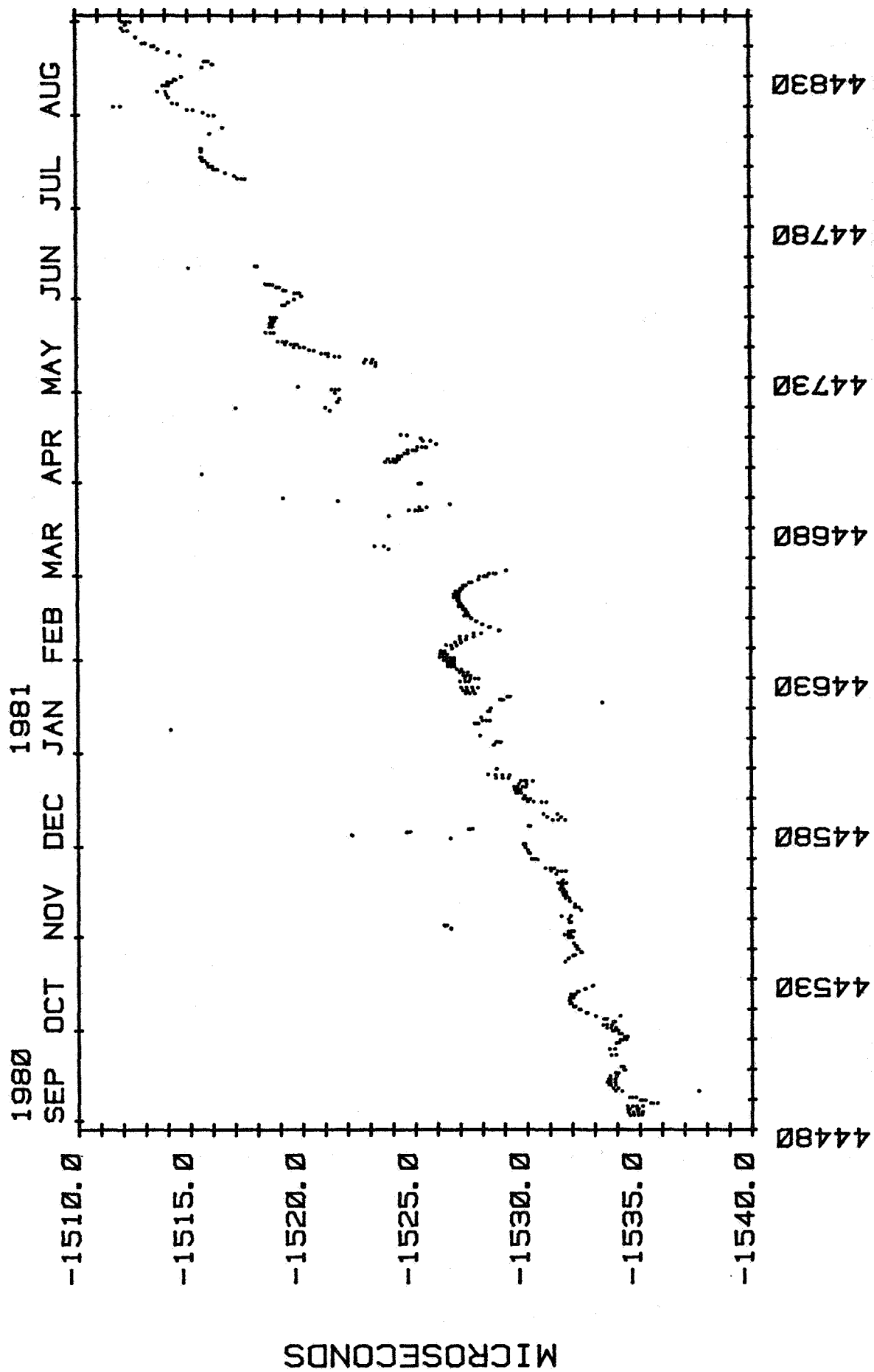


Fig. 8



MOD. JUL. DATE

Fig. 9

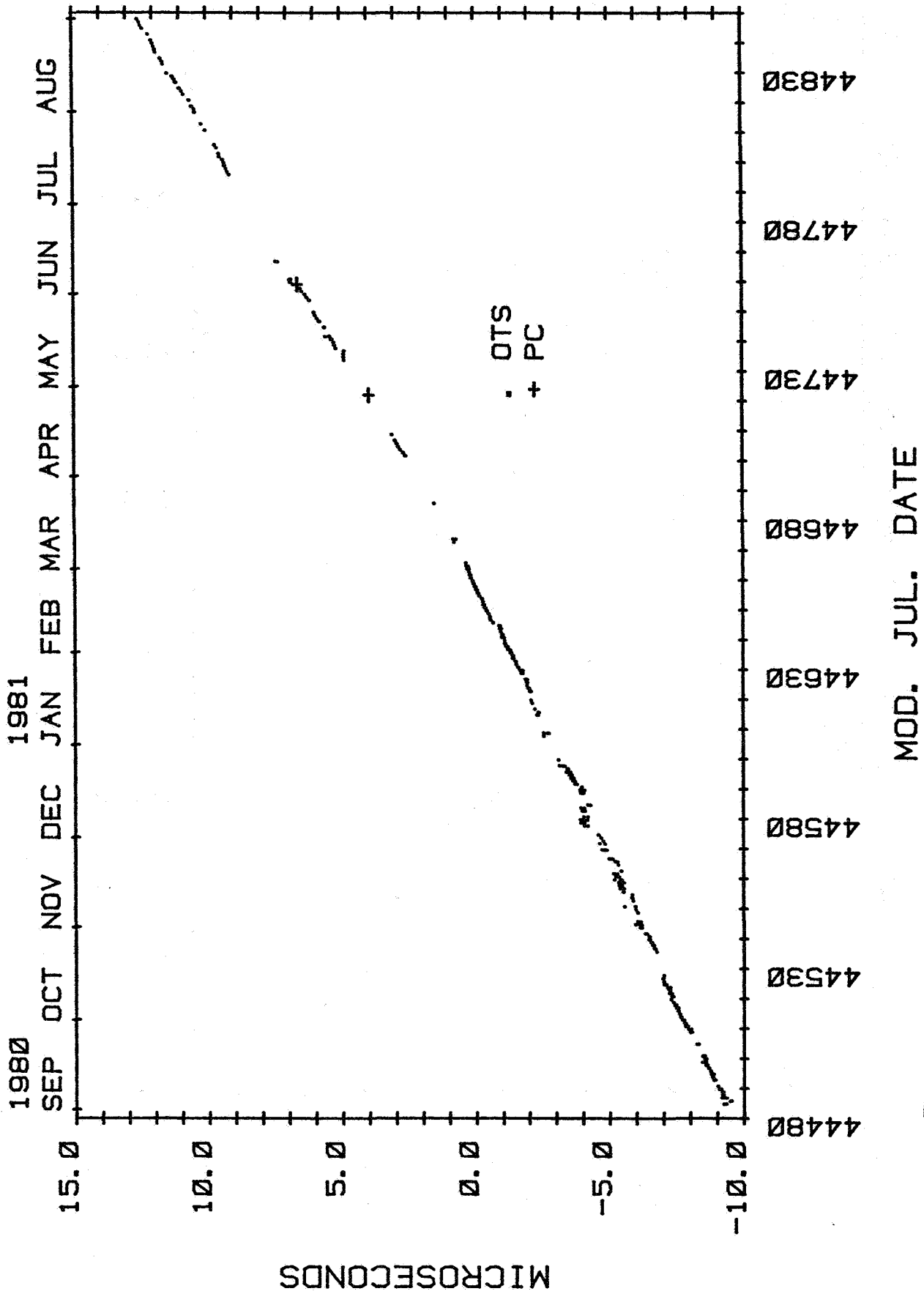


Fig.10

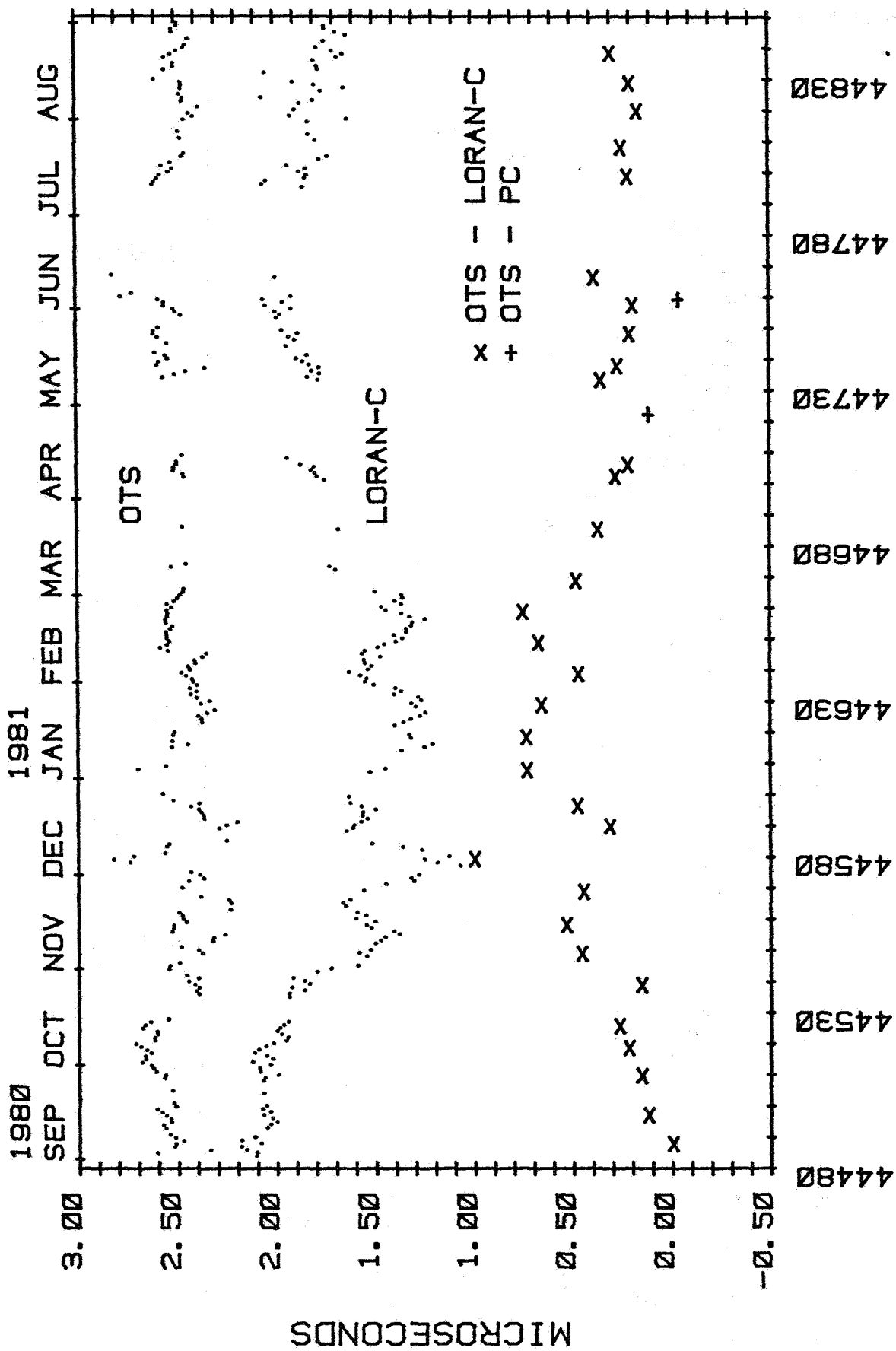


Fig.11

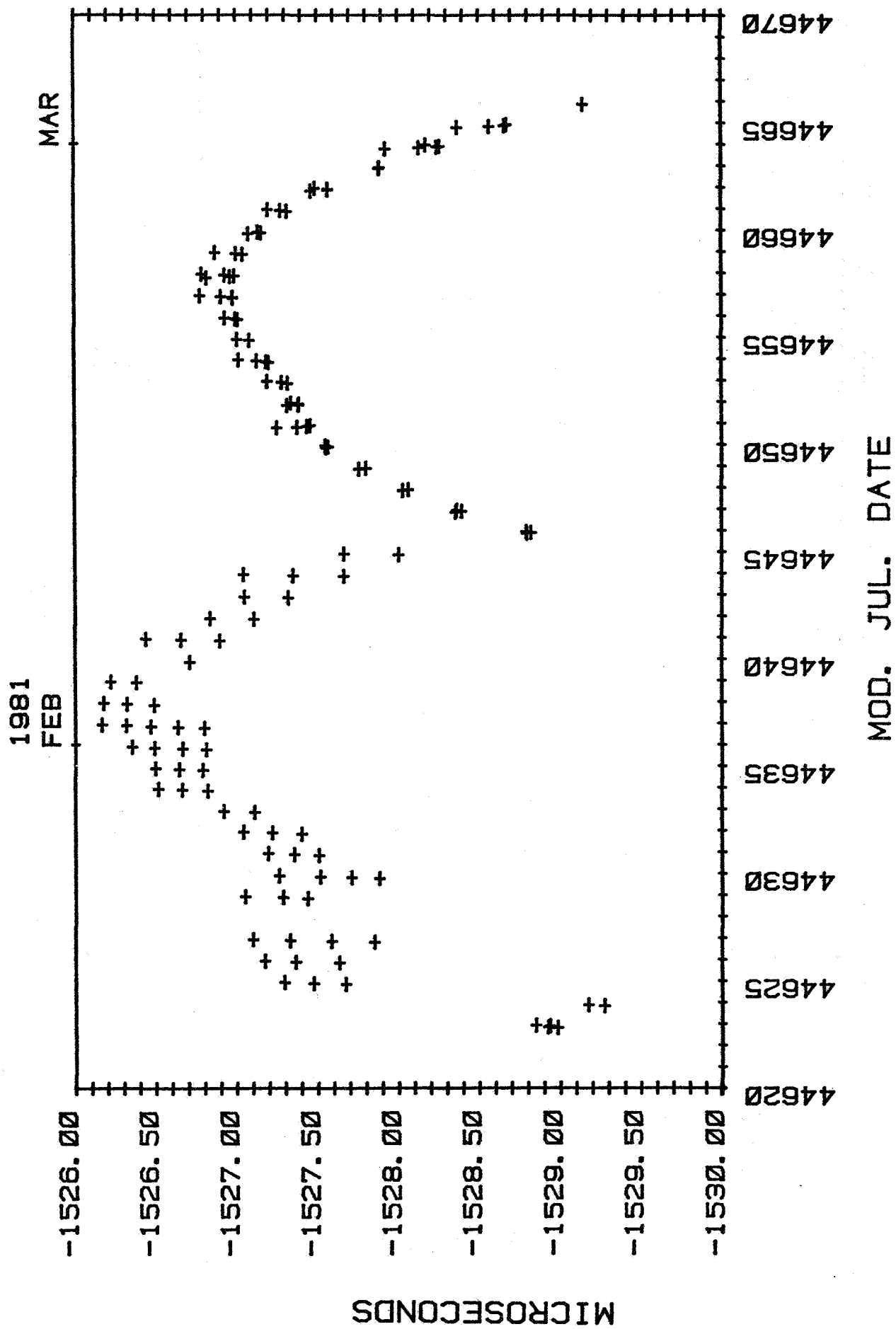


Fig.12

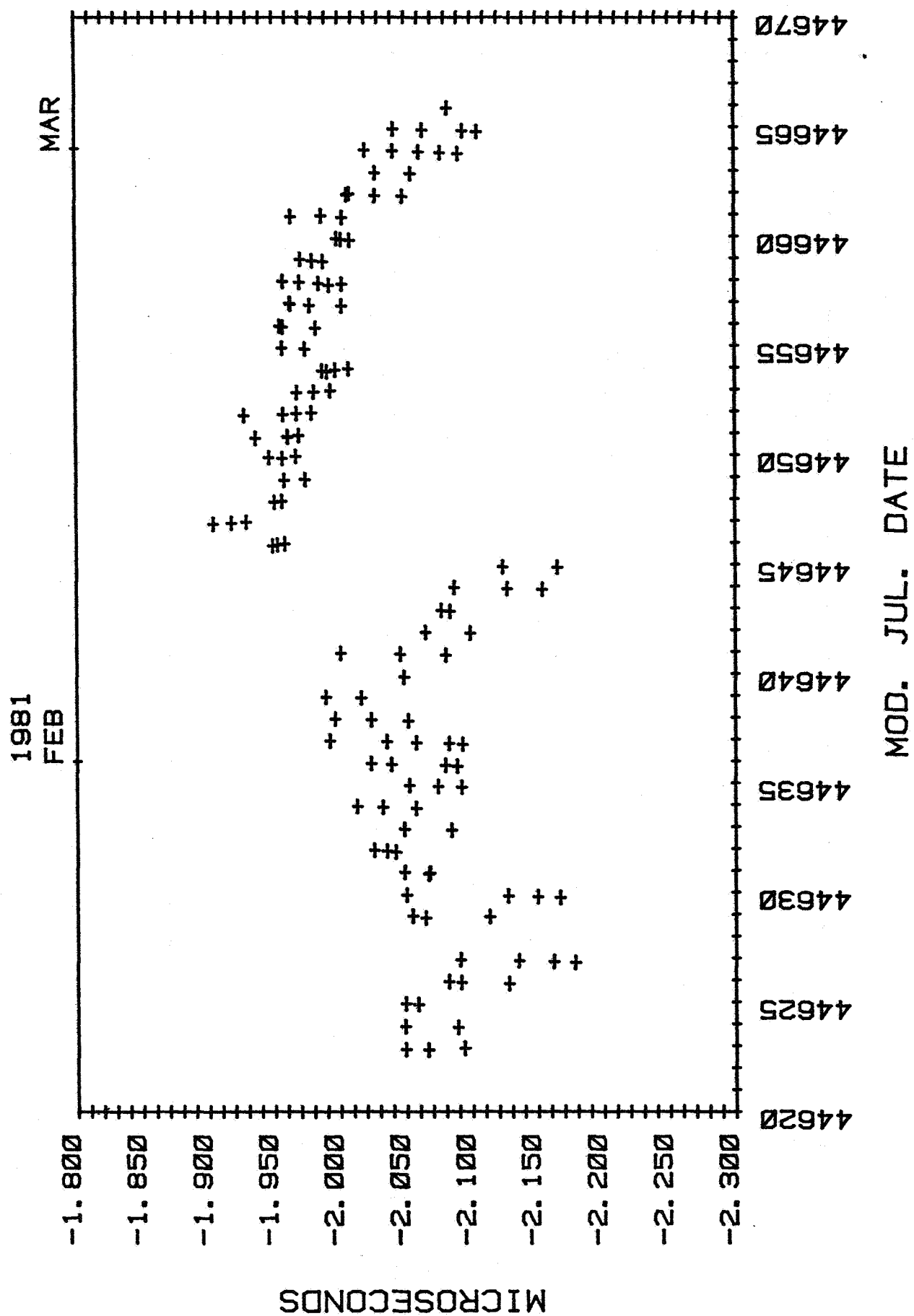


Fig. 13

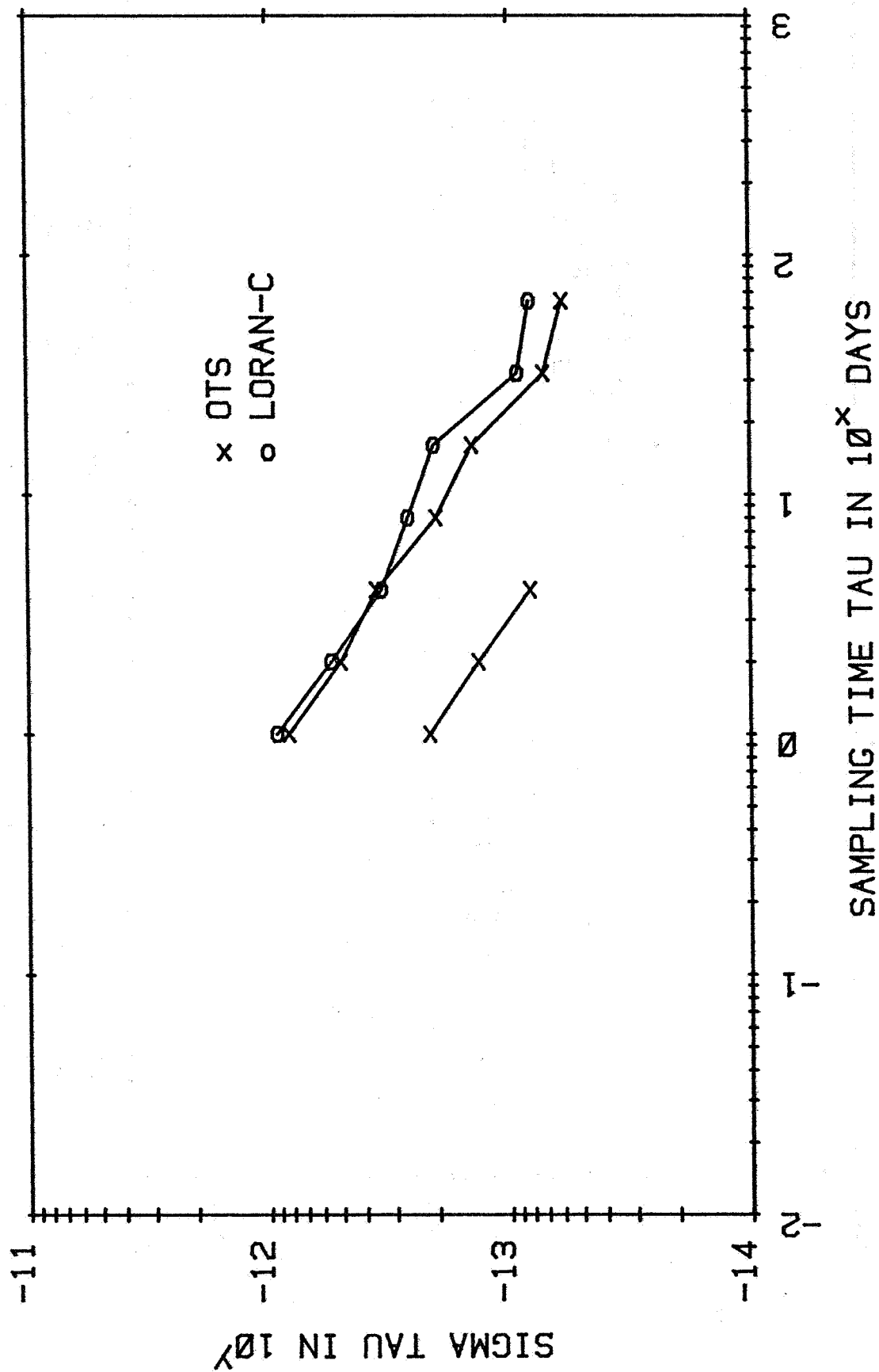


Fig.14

## QUESTIONS AND ANSWERS

MR. DAVID ALLAN, The National Bureau of Standards

As you move towards 10 nanosecond level of accuracy, I noticed in your original equations the sagnac was not included, and that between those two sites, it calculates to be about 25 nanoseconds interestingly?

DR. KAARLS:

What was the correction, I'm sorry?

MR. ALLAN:

The sagnac correction.

DR. KAARLS:

Okay. No, it was not included, you are right.

MR. ALLAN:

Yes. And especially as you go to North/South stations where the sagnac will be very small with respect to East/West stations, you will get incontinuity or discontinuities if you don't apply that correction as you get down to the 10 nanosecond region?

DR. KAARLS:

Yes. It might be a factor of importance, yes. Thank you.





**SESSION IV**

**GLOBAL TIME AND FREQUENCY TRANSFER**

**Mr. David W. Allan  
National Bureau of Standards**



## DESIGN APPROACH FOR A MICROPROCESSOR-BASED GPS TIME TRANSFER RECEIVER

P.C. Ould and R.J. Van Wechel,  
Interstate Electronics Corporation,  
Anaheim, California

### ABSTRACT

This paper describes the design concept and characteristics of a self-contained microprocessor-based GPS time transfer receiver. A prototype of this unit is currently in the test phase. It employs two-bit digital baseband correlation rather than analog IF correlation of the signals with the reference code. The correlator, numerically controlled oscillators (NCO) and code generator are implemented in a special-purpose digital signal processor. The time is recovered in the digital code tracking loop, and final corrections are applied in the control processor. By means of asynchronous sampling techniques for the digital correlator and NCO, the time transfer resolution limit is  $2^{-N}$  part of a code chip period, where  $N$  is 32 for a 32-bit accumulator in the NCO. Other features of this design are: drift-free digital mechanization, high reliability of digital circuits, flexible control capability of the microprocessor, and potential for a high degree of digital VLSI chip development leading to compact, low-cost units.

A description is given of the process by which the precise measurement is made between user clock and received signal code. The user-clock-derived sample times in the code tracking loop yield high-resolution uncorrected time sample words. These uncorrected time words are corrected for range to the satellite, satellite clock error, ionospheric error, and relativistic errors. They are then differenced with the user clock to yield user-clock error estimates.

User-clock outputs consist of 1-pps, time readout, and direct digital outputs of time and time error of the user clock.

Test data on random error of the approach are also presented.

## INTRODUCTION

The GPS receiver described in this paper consists of a baseband RF converter, digital signal processor, and general-purpose microprocessor. The design approach and components have been developed at Interstate Electronics during the past four years as part of an internally funded GPS applications research program. The goal of this research effort is to develop a reliable, low-cost, and highly accurate modular system that can be configured to satisfy a wide range of requirements in the areas of timing, tracking, and navigation.

Our design approach is primarily digital in that the received signal is converted to baseband and digitized before any signal processing is attempted. We intend to achieve reliability and low cost by employing the latest gate-array and custom-VLSI (Reference 1) techniques. System accuracy is achieved through use of digital correlation techniques (Reference 2) with asynchronous sampling to attain very high measurement resolution, and by using long (i.e., 32-bit) word lengths.

This paper emphasizes the characteristics of the digital signal processor that provide the capability of extracting time from the received signal directly as a numerical value.

Evaluation of this GPS time transfer technique is currently in progress at Interstate, and the results of initial tests of the system's tracking accuracy are included in the paper.

## BACKGROUND

Our work with GPS receivers began in the middle of the last decade with development of the Flight Test Support System (FTSS) for the Navy's Trident I (C4) strategic weapon system (Reference 3). The FTSS employed the early GPS satellites for metric (postflight analysis) tracking and time division multiple access (TDMA), pseudorandom-noise (PRN)-coded ground transmissions for range safety tracking. Many of the digital-baseband processing techniques we are now using for GPS processing originated in the FTSS.

We subsequently developed a breadboard GPS system that was used for test and evaluation at our facility about two years ago. This GPS receiving system employed clear/acquisition (C/A)-code, one-bit digital baseband correlation and was an all-digital system (Reference 2) except for the RF converter, which converted the received signal to baseband for digitization. The system's central processing unit was a Digital Equipment Corporation PDP-11 computer.

The time transfer receiver described here is a microprocessor-based system using a Motorola Corporation MC68000 as its central processing

unit. This version is a combined C/A- and P-code GPS receiver, with the P-code capability added to determine and compare the time-transfer accuracy and reliability achievable with each code, and to satisfy requirements for other applications.

#### GENERAL DESCRIPTION

Figure 1 is a functional block diagram of the GPS time transfer receiver. The RF converter is a straightforward, double-conversion device for L1. The carrier numerically controlled oscillator (NCO) drives the baseband converter to *tune* the receiver to the signal plus Doppler. (The structure of this second-order phaselocked loop is described later.) The digitizer (Figure 1) has been mechanized as either a one- or two-bit (Reference 2) analog-to-digital converter sampling at a rate slightly higher than twice the code chip rate.

The correlator processes the digitized in-phase (I) and quadrature (Q) data to generate a tracking-error signal. In response to the delay tracking error, the delay tracking filter drives the code NCO and code generator. This loop is the time transfer mechanism (described later in more detail with the clock and its associated components).

The integrated correlation data and loop feedback signals are sampled at 250 Hz.

In our system, the microprocessor accomplishes most of the signal processing. Figure 2 illustrates the algorithms and process flow. Note that the code generator is mechanized in a separate microprocessor (Reference 2) and that basic signal acquisition is not shown.

All computations except clock correction are completed in less than 4 milliseconds. Clock correction operates continuously on a priority basis.

#### CARRIER AND CODE TRACKING

Figure 3 shows the basic operation of the carrier and code tracking loops.

In acquisition, the carrier NCO and code generator are operated in a search pattern that results in a correlation function being centered in the early/on-time/late correlator output. The on-time correlator complex (I and Q) outputs are used for carrier tracking, and an estimate of the angle of these coefficients yields the carrier-loop phase error. This is analogous to conventional Costas-loop carrier tracking. The carrier-loop error is filtered in the loop filter for second-order carrier-loop tracking. The carrier frequency estimate controls the

carrier NCO and also is scaled to control the code NCO frequency, and to provide dynamic aiding for the first-order code tracking loop.

The code loop derives its delay error signal from the difference of the magnitudes of the early and late correlation coefficients, in the manner of a noncoherent code tracking loop. The code loop is first-order, with aiding from the carrier loop, and controls the delay of the code NCO/code generator directly rather than the more usual process of controlling the code chip frequency. This control mechanism offers some significant advantages in achieving very-high-resolution time transfer measurement.

#### BASIC APPROACH TO TIME TRANSFER

Figure 4 is a functional block diagram of the GPS time transfer process, the basic element of which is the code track loop that keeps a local reference code synchronously tracking the received code. The initial phase or time delay of the reference code is controlled at the start of each loop iteration (4 milliseconds) by the feedback from the code loop filter. The control word from the loop filter is split into integer and fractional parts in terms of code chip units; the integer part sets the starting chip number of the code generator, and the fractional part sets the starting phase of the NCO.

This control mechanism for the combined NCO/code generator is very precise and eliminates the need for a high-resolution time interval counter to perform the basic time difference measurement between reference time and received code epochs. Figure 5 illustrates how the 43-bit integer delay sets the starting code chip, and a 32-bit control word initializes the NCO starting phase. This, in effect, sets the starting phase to a resolution of  $2^{-N}$  part of a code chip, where  $N$  is 32 for a 32-bit accumulator in the NCO.

Figure 6 outlines the form of the NCO for this process. The NCO consists of an accumulator register that can be preset by the fractional chip phase command word from the code loop filter whenever each loop filter iteration begins. The frequency command word is then added to the accumulator on each clock time, causing the accumulator to overflow at an average frequency equal to the desired chip frequency. It is important in this process to maintain an asynchronous relationship between the NCO output frequency and the NCO accumulation rate over the entire Doppler range. When this is done, it is found that only the most significant bit (MSB) from the accumulator needs to be used as an NCO output, and it then advances the code generator a chip on each overflow of the NCO accumulator.

Although it may appear at first that such a code generation process would yield unacceptably high jitter in the code loop, this has not been the case, because of the broad spectral distribution of the NCO phase jitter. We use the same process in the carrier and code loops and see a phase jitter of about 2 degrees rms (for high-SNR signals) in the carrier track loop, as shown in Figure 7. Code track results are shown in Figure 8, which is a time history of the combined code NCO/code generator control words plotted for an actual satellite pass. No smoothing was used on the plotted data, in order to illustrate the resolution of the raw delay measurements.

Referring again to Figure 4, it can be observed that the nominal 4-millisecond loop iteration rate of the code loop is derived from the user clock. On each 4-millisecond loop iteration, an uncorrected time word in units of integer and fractional code chips is extracted from the code loop. This time word consists of the raw uncorrected time measurements that can be corrected for range, ionospheric error, relativistic error, satellite clock error, etc. They can be used as measurement values input to a Kalman filter to model various systematic and random clock errors. User clock error is determined by differencing with the user clock value at the same iteration time mark. The clock can be set to null the error by a combination of setting the clock counter in 200-nanosecond increments and, in finer increments, by phase control of the reference frequency input. Note (Figure 4) that uncorrected time measurements have a different significance, depending on whether the tracking mode is C/A- or P-code. In the P-code mode, the code state represents the time of the week (TOW) in direct unambiguous form. In the C/A-code mode, the TOW establishment and maintenance is somewhat less direct in that it involves a combination of measured C/A delay and resolution of the 1-millisecond C/A-code ambiguity.

#### DESIGN APPROACH

The components of the signal processor described in Figure 1 are designed to interface with the Motorola VERSAbus\*. Figure 9 shows the particular configuration used for the P-code time transfer processor.

The VERSAbus concept provides a dedicated section for the microprocessor functions and a user-definable section.

The microprocessor bus supports a multiprocessor system that can be used to support auxiliary processors for navigation, clock error estimation, and special-purpose I/O and display functions.

Figure 10 is a photograph of the enclosure for this design. Typical circuit boards, which have the physical characteristics of a Motorola EXORmacs\* board, are shown in Figures 11 and 12. The RF converter is

---

\*Registered trademarks of Motorola Corporation.



packaged in a module so that it plugs into the enclosure in the same manner as the processor boards. The present design includes a CRT, disk, and printer in addition to the basic control panel.

This modular design approach provides extensive flexibility to define systems for custom applications.

#### REFERENCES

1. C. Mead and L. Conway, *Introduction to VLSI Systems*, Addison-Wesley Publishing Company, 1980.
2. P.C. Ould and R.J. Van Wechel, "All-Digital GPS Receiver Mechanization," *Proceedings of the National Aerospace Meeting*, The Institute of Navigation, 8-10 April 1981; also to appear in *Navigation*, Vol. 28, No. 3, Fall 1981.
3. T. Thompson, "Performance of the Satrack/Global Positioning System, Trident I Missile Tracking System," *Proceedings of the 1980 IEEE Position, Location, and Navigation Symposium*, pp. 445-449.

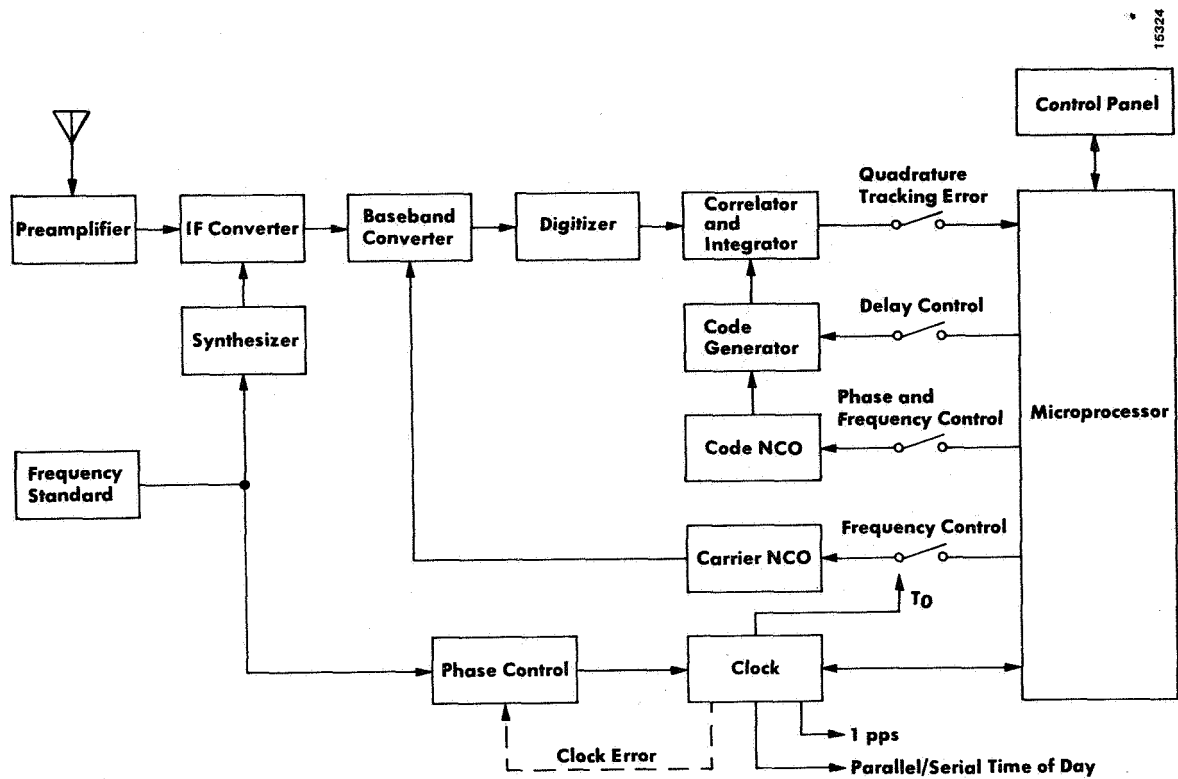


Fig. 1-Functional block diagram of GPS time transfer receiver

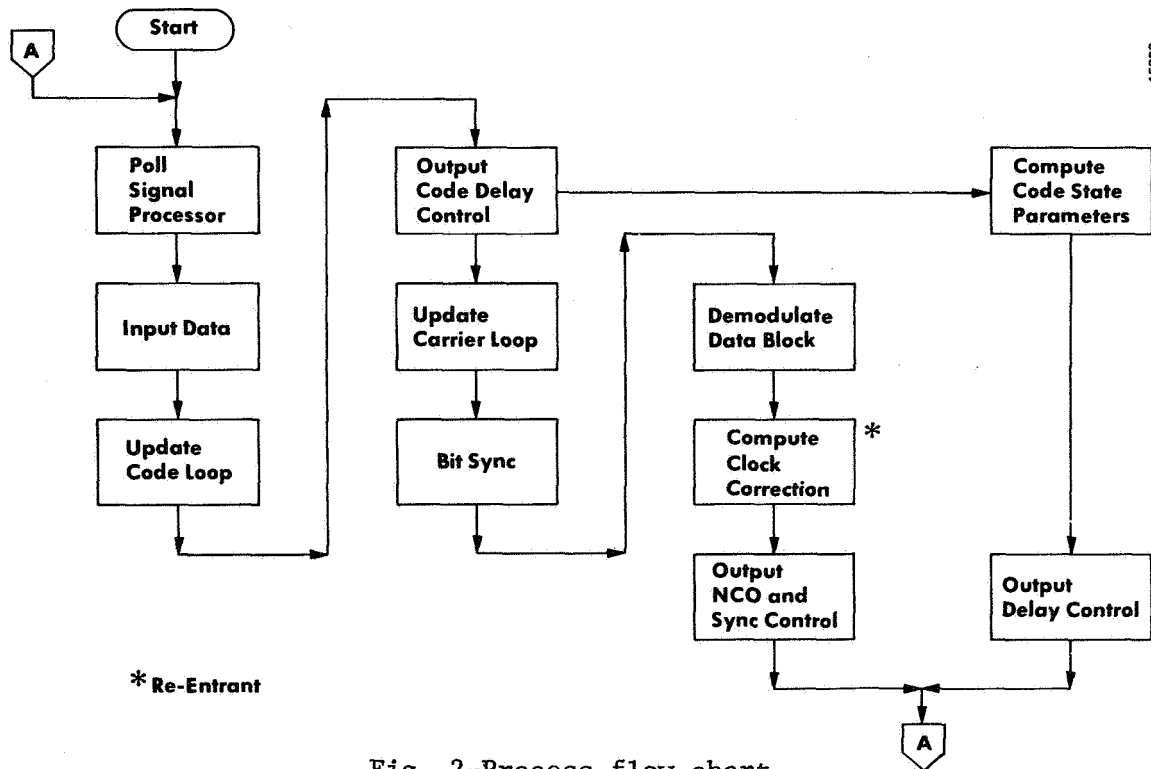


Fig. 2-Process flow chart

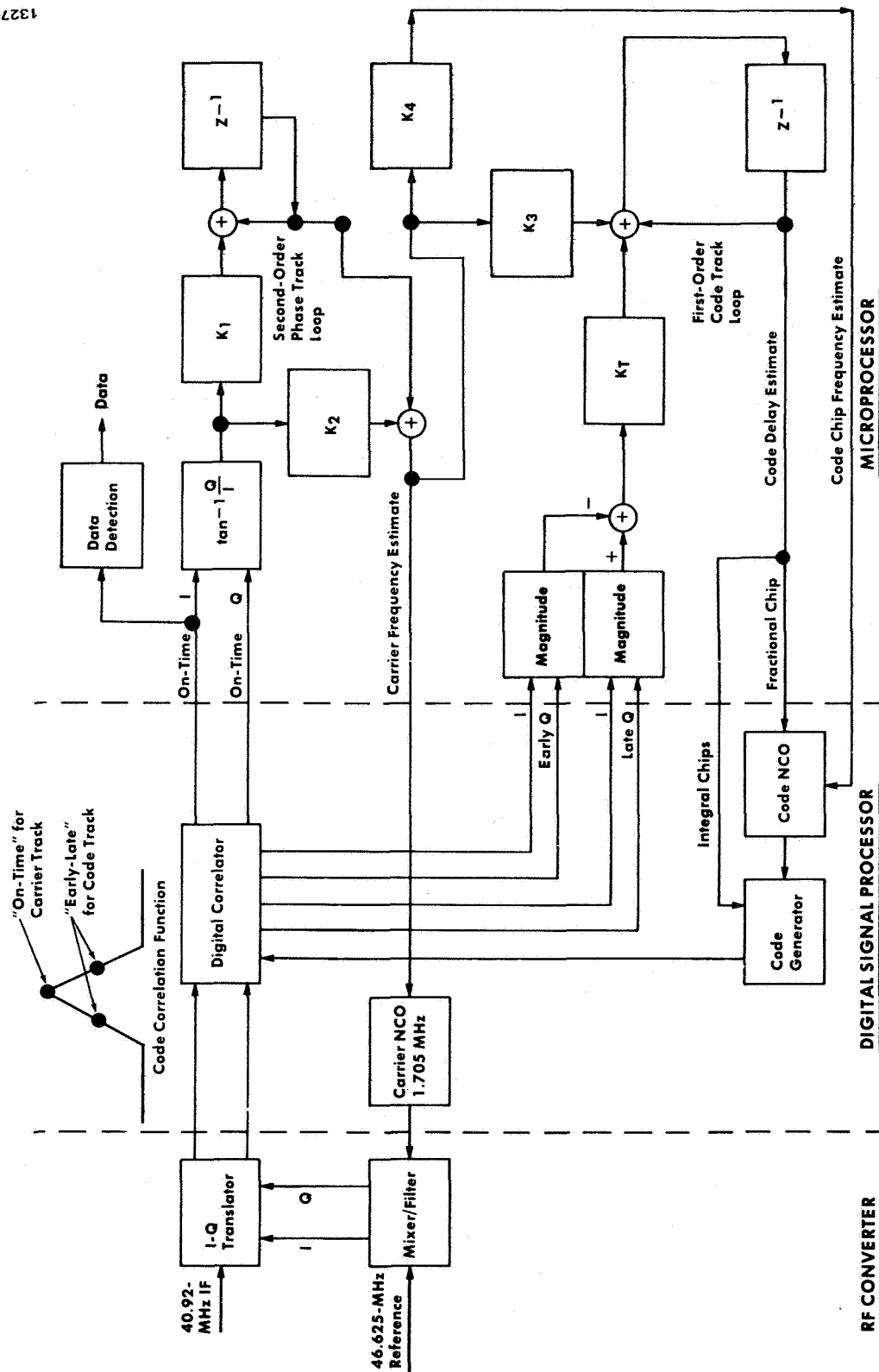
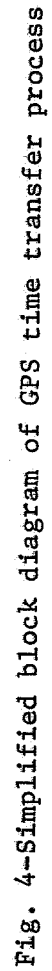


Fig. 3-Operation of carrier and code track loops



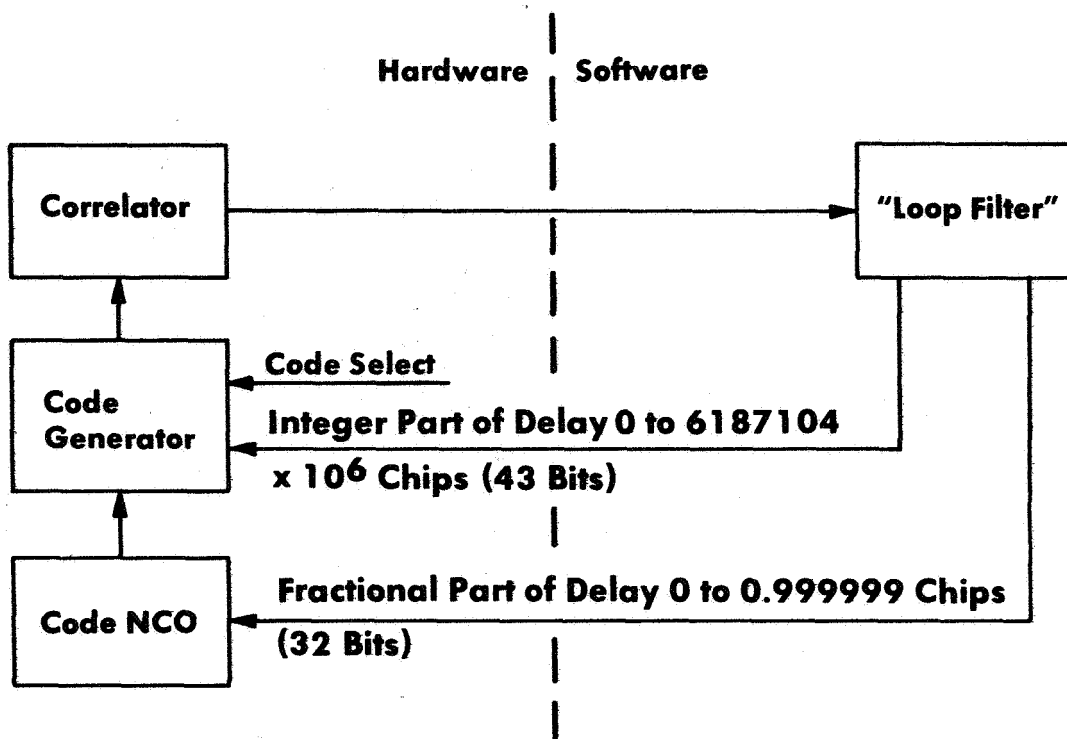


Fig. 5-NCO/code generator control

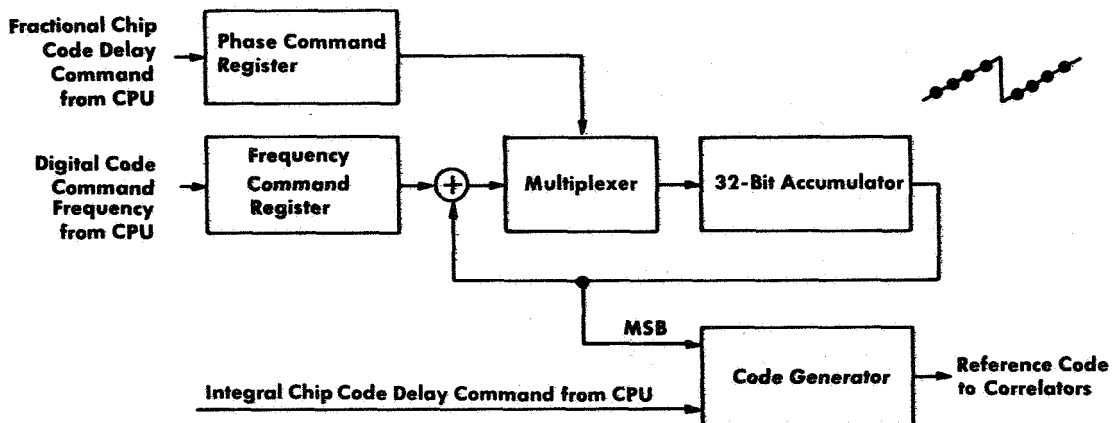


Fig. 6-Code NCO function

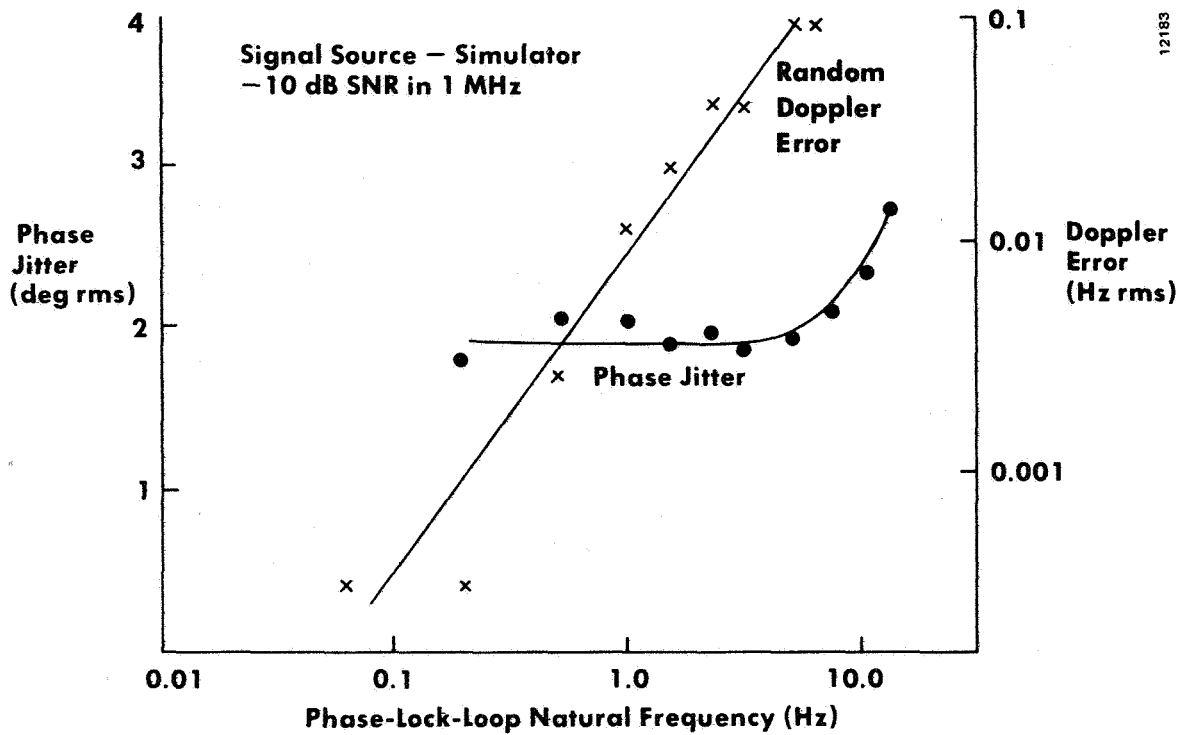


Fig. 7- Measured phase jitter and random Doppler error vs loop bandwidth

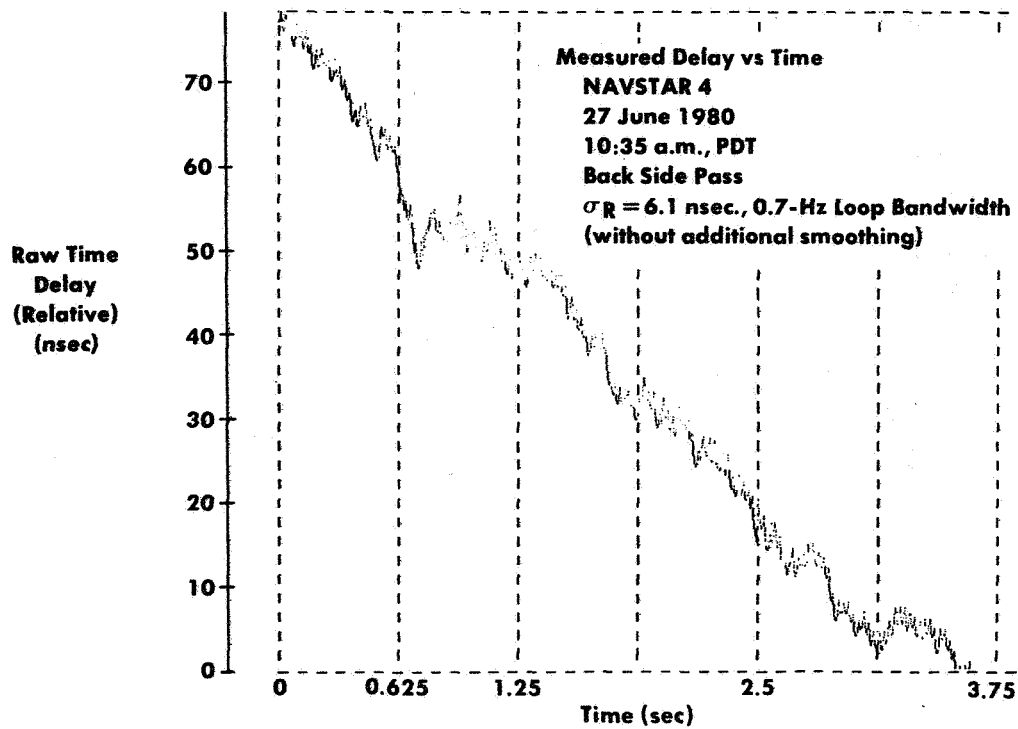


Fig. 8-Typical time-delay measurement test results

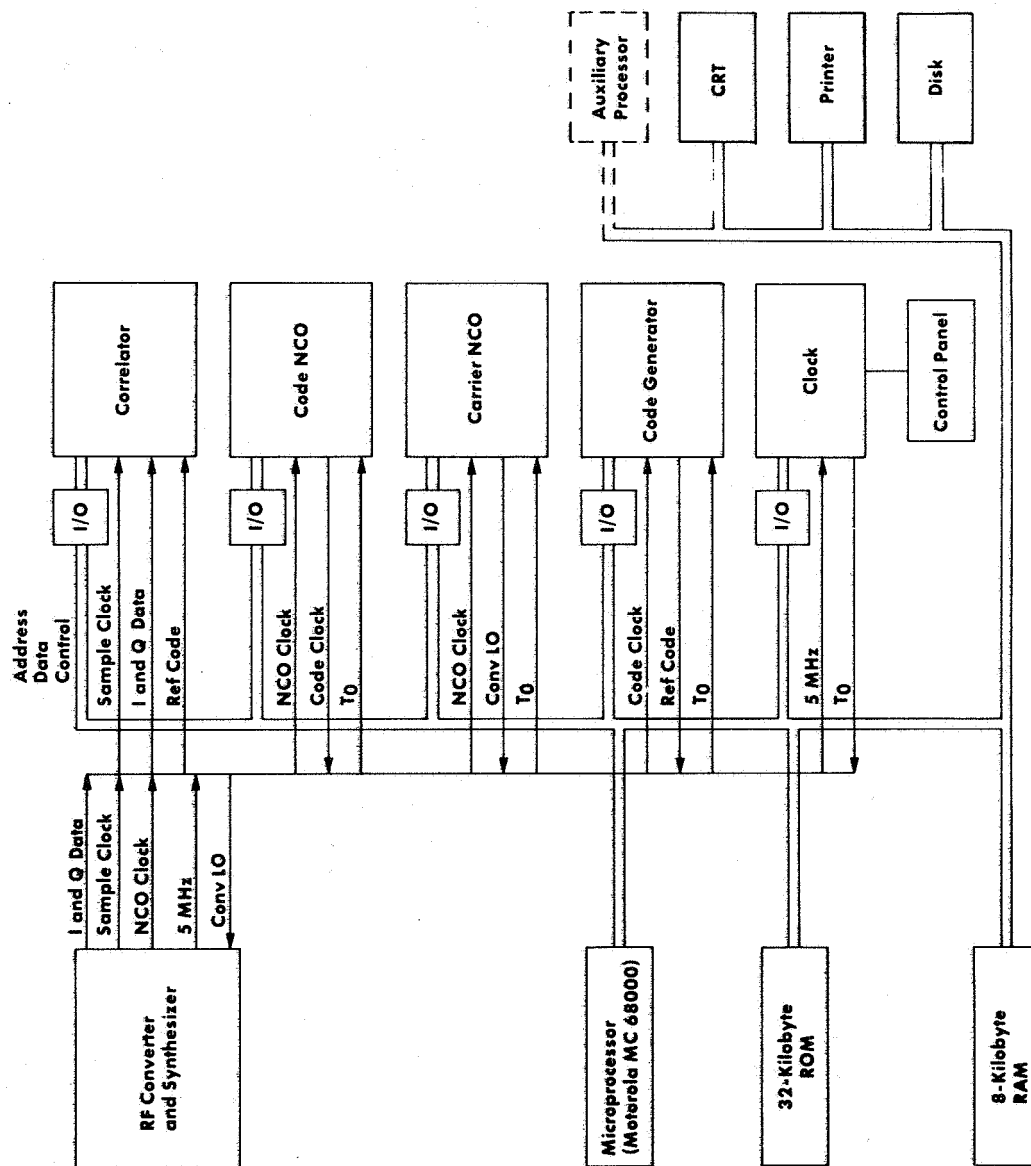


Fig. 9-System architecture

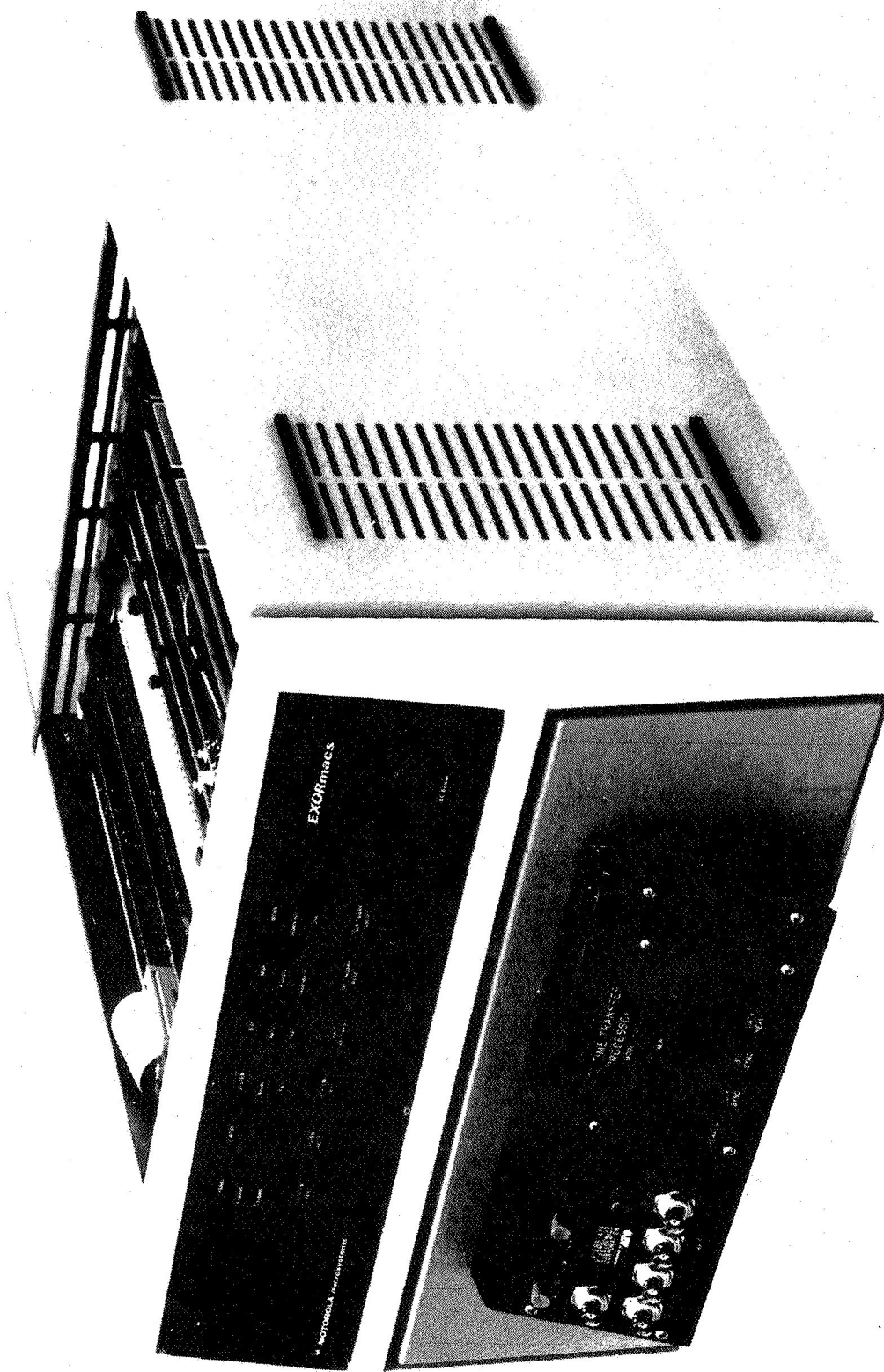


Fig. 10-Time transfer unit chassis

15319



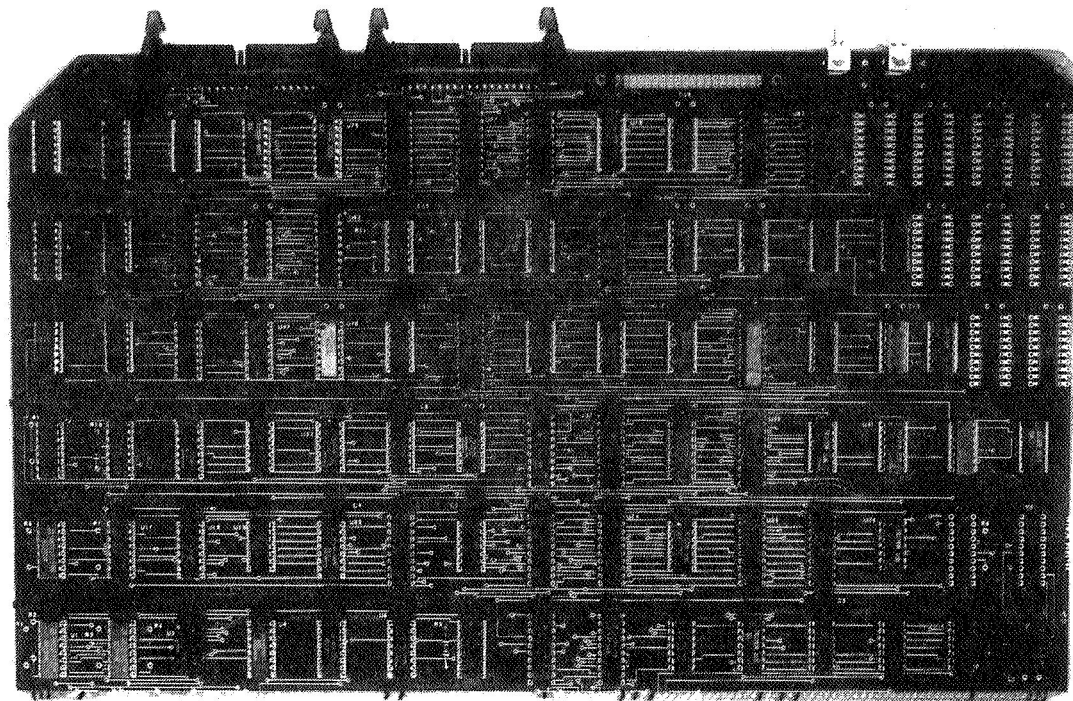


Fig. 11-Correlator printed-circuit board

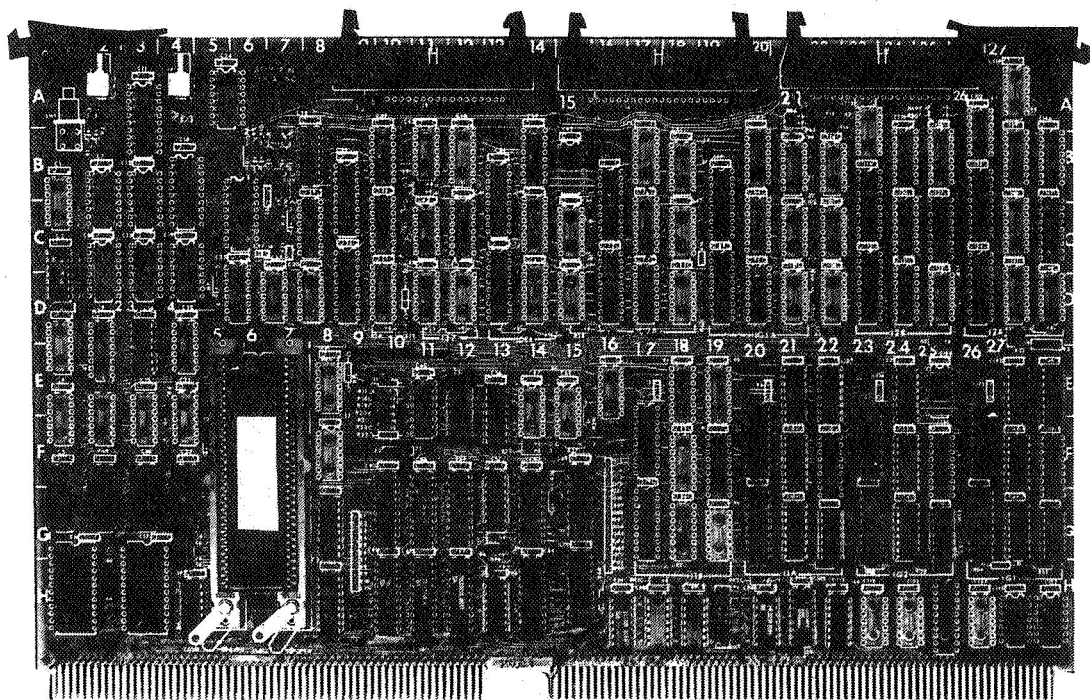


Fig. 12-Code generator printed-circuit board

## QUESTIONS AND ANSWERS

DR. VICTOR REINHARDT, NASA/Goddard

Do you have any idea when this will be available, and do you have any idea what the cost will be?

MR. OULD:

Available to carry away or observe?

DR. REINHARDT:

Available to carry away.

MR. VAN WECHEL:

Probably another year.

MR. OULD:

We could conceivably do it in six months, but I would hate to promise anything short of a year and that is primarily because we're a very limited staff. We're only talking about three to six people, and right now we're down to the three-people limit, and you are looking at two of them.

And Jim is back, just before we left, the RF Section crashed, and that is his responsibility. And yet that is the three people. So, I'd be sticking my neck out to promise anything short of six months to a year.

DR. REINHARDT:

Do you have any idea of what the cost would be?

MR. OULD:

I'd really rather not say right now. We, you know, being small, Interstate is not a product house, okay. We're in to this development. It is totally funded by the company. We are in to it because we can support the Trident Missile testing. That is our intent. Time transfer for the ranges, et cetera. I had to beg off on it like that.

MR. VAN WECHEL:

Tell him to come and see us afterwards.

MR. OULD:

Come and see me at coffee break.

DR. REINHARDT:

Thank you.

MR. ED CHRISTY, Offshore Navigation

I have two questions. One, were you receiving both the L-1 and L-2 channels in the receiver? And, secondly, you mentioned a synchronous sampling rate in your digitizer. Approximately what frequency of digitization were you employing?

MR. OULD:

Okay. Question one, L-1 only.

Question two, you know 20.462046 megahertz. In other words, it's a 10 to the fourth higher than the chip rate.

MR. CHRISTY:

And you digitized this to 16 bits at that rate?

MR. OULD:

No, we're digitizing to one bit at that rate.

MR. VAN WENCHEL:

Can I say something here?

MR. ALLAN:

Yes, please.

MR. VAN WENCHEL:

That chip rate is chosen to be outside of the Doppler range, that is the idea of the asynchronous sampling so that the sample rate never becomes coherent with the chip rate. If it ever becomes coherent, especially with one bit quantization, you get in big trouble because you have very coarse quantizing of the phase.

So, you choose it to be just outside the Doppler range, and that's why the one part in ten to the fourth.

## TIME TRANSFER USING NAVSTAR GPS

A. J. Van Dierendonck, Q. D. Hua, J. R. McLean, A. R. Denz  
Stanford Telecommunications, Inc. (STI), Sunnyvale, CA 94086

## ABSTRACT

The NAVSTAR Global Positioning System (GPS) allows extremely accurate and global determination of time, as well as position and velocity. An STI Time Transfer Unit (TTU) developed for the U.S. Naval Observatory (USNO) has consistently demonstrated the transfer of time with accuracies much better than 100 nanoseconds. A new STI Time Transfer System (TTS), the TTS 502, is currently in development and will be available on the market by the end of 1981. The TTS 502 will be a relatively compact microprocessor-based system with a variety of options that will meet each individual's requirements, and will have the same performance as the USNO system. This paper summarizes the time transfer performance of that USNO system and presents the details of the new system.

## INTRODUCTION AND SUMMARY

The NAVSTAR GPS is currently operating in its Concept Validation Phase (Phase I), while the operational system is under development. Rather than being repetitive on the description of the system, which has been described in numerous papers over the last 6 years, let it suffice to refer to a few of these papers in References 1 through 3. The important factor to note here, however, is that even though the system is not fully operational, it already provides the best overall time transfer capabilities in existence. Time transfer, using a Time Transfer Unit (TTU) designed and built for the U.S. Naval Observatory (USNO) by STI, has been demonstrated to be consistently better than 50 nanoseconds when done so with GPS satellites with good clocks.

Ultimately, GPS will allow continuous global determination of time when the complement of satellites in the system provides the appropriate coverage. (Only one satellite in view is required for time transfer.) At present, global determination is possible, but not continuously. Currently, the GPS program plan is to have an 18 satellite constellation<sup>4</sup>, which would provide global satellite visibility of 4-8 satellites above 5° elevation (7 satellites 28.7% of the time).<sup>5</sup> The original planned constellation of 24 satellites would have provided visibility of 6-11 satellites above 5° elevation. A possible near-term constellation of six satellites will provide one satellite time transfer coverage ranging from approximately 16.5 to 20 hours per day, depending upon location. As it turns out, one of the worst time coverages is the

continental United States (and the Indian Ocean) because the constellation was designed to provide a clustering of satellites for testing at Yuma, Arizona.<sup>5</sup> Examples of satellite coverage for those six satellites are presented in Figure 1.

The Time Transfer Systems, both old and new, operate on only the GPS L1 C/A (Clear/Acquisition) code at 1575.42 MHz. They do not operate on the L2 frequency (1227.60 MHz) because the C/A code will usually not be available on that frequency. The reasons for operating only on the C/A code are for simplicity and because, in the future, the P-code will not be available to all users. It will be obvious from later discussions that operating on the P-code would only improve the time transfer accuracy by about 30-35 nanoseconds (one sigma) when operating with large ionospheric propagation delays, to very little improvement when the delays are small. For most applications, this improved accuracy is not required, and for some users that need it, special purpose P-code time transfer systems can be developed.

The Time Transfer Systems also operate only from known surveyed (and stationary) locations. In future systems, position determination with limited motion is anticipated as an option. Position determination does degrade the time transfer accuracy because of Geometric Dilution of Precision (GDOP) and Time Dilution of Precision (TDOP) effects (see Reference 4 for definitions of GDOP and TDOP).

The USNO TTU is described in detail in References 7 and 8. This unit was delivered to the USNO late in 1979 and has been operating since mid-1980 very well.<sup>9</sup> A summary of results obtained from this unit will be presented later in this paper. It has been instrumental in the determination of the long-term performance of the GPS frequency standards in orbit, as well as the performance of GPS time.

The USNO TTU, because it was the first Time Transfer System built, is a large and not so portable unit. Because of that, STI has developed a new TTS, the TTS 502, that has similar performance characteristics, but is relatively small, even to the point of being portable (a near future option). The unit is shown in Figure 2. Details of this new system are presented later in this paper.

Also presented in this paper are the techniques for accomplishing the time transfer, a time transfer error analysis, a description of various applications of the TTS and some future considerations for the use of GPS for time transfer.

#### TIME TRANSFER TECHNIQUE

For users with known locations, only one satellite signal is required for time transfer purposes. The time transfer technique employed is illustrated in Figure 3 which shows the timing relationships between

the system (GPS) time, satellite time, and the user's time when an epoch transmitted from the satellite (at GPS time  $T_T^{GPS}$ ), arrives at the user's location (at GPS time  $T_A^{GPS}$ ). Time transfer is accomplished by computing the user clock error,  $\Delta T_A^U$ , with respect to system time, when an epoch is received. GPS satellites transmit continuous signals with readily identified subframe epochs every six seconds. The transmission time,  $T_T^{SV}$ , is determined by an on-board atomic standard which will, in general, differ by some amount,  $\Delta T_T^{SV}$  from system time.

When the epoch arrives at the station, the transit time is measured as observed by the user. This measurement, called pseudorange (PR), is, in essence, the time difference between the user time at epoch arrival  $T_A^U$ , and the satellite time at epoch transmission,  $T_T^{SV}$ , i.e.,

$$PR = T_A^U - T_T^{SV} \quad (1)$$

In terms of system time, the pseudorange can be expressed as

$$PR = T_A^{GPS} - T_T^{GPS} - \Delta T_T^{SV} + \Delta T_A^U \quad (2)$$

The term  $T_A^{GPS} - T_T^{GPS}$  is the "true" transit time (with respect to system time) representing the true time range,  $R$ , between the satellite and the station except for a propagation delay  $\tau$ :

$$T_A^{GPS} - T_T^{GPS} = R + \tau \quad (3)$$

The user clock error is readily obtained from (2) and (3) as

$$\Delta T_A^U = PR + \Delta T_T^{SV} - R + \tau \quad (4)$$

The propagation delay includes the ionospheric and tropospheric propagation time delays and a receiver equipment bias.

A raw time transfer is performed every six seconds at the reception of the satellite signal epoch (subframe epoch) by the following procedure:

- o Deriving satellite (epoch) transmission time,  $T_T^{SV}$ , from the Z-count contained in the broadcast data subframe (inferred after initial synchronization).

- o Computing satellite clock error,  $\Delta T_T^{SV}$ , and system transmission time,  $T_T^{GPS}$ , using clock correction parameters contained in the data frame.
- o Computing satellite position at system time  $T_T^{GPS}$  using the satellite's ephemeris contained in the data frame.
- o With the known user location, estimating the propagation delay  $\tau$  using (1) ionospheric correction parameters contained in the data frame, (2) a simple tropospheric correction model, and (3) receiver equipment bias calibration data provided by the user during system initialization.
- o Computing the satellite-to-station range  $R$ , taking into account the effect of earth rotation during signal propagation.
- o Collecting a pseudorange measurement,  $PR$ , when the epoch arrives, and finally, computing the user clock time error  $\Delta T_A^U$  according to equation (4).

These raw user clock time errors are then collected in a rotating buffer so that they can be smoothed to reduce the effect of the receiver noise and quantization errors. The smoothing is accomplished by applying a least squares fit on the values in the buffer. This smoothed error is then subtracted from the time of the epoch arrival to provide the GPS time of arrival

$$T_A^{GPS} = T_A^U - \overline{\Delta T_A^U} \quad (5)$$

where  $\overline{\Delta T_A^U}$  is the smoothed user clock time error evaluated at user time  $T_A^U$ . However, the time transfer is accomplished by providing the user with a time pulse that is either coincident with  $T_A^U$ , along with the correction, or with a time pulse that has been corrected with the past best estimate of  $\Delta T_A^U$ , and thus corrected to  $T_A^{GPS}$  or  $T_A^{UTC}$ . The corrected pulse is an option of the TTS. To correct to  $T_A^{UTC}$ , the epoch time of arrival in Universal Coordinated Time (UTC), a known difference between UTC and GPS time is applied. This known difference is presently supplied by the user. In the future it will be supplied in the GPS Navigation Message<sup>8</sup>.

#### THE TTS 502

A block diagram of the TTS 502 is shown in Figure 4. It is comprised of an STI Time Transfer Receiver Model 5026, an Omnibyte Motorola-based

MC68000 microcomputer and software, antenna, preamplifier and a display station. Also, options to the basic TTS-502 are illustrated. These options are:

- o 001 Precision internal 5 MHz crystal oscillator
- o 002 1 pps (pulse-per-second) output corrected to GPS or UTC time
- o 003 RS-232 interface for data output to external peripherals
- o 004 GPIB interface for data output to external peripherals
- o 005 Desk Top Cabinet Enclosure (not shown)

Other options will be added in the future and will be based on future user requirements. For example, for portability, an option for a portable chassis and a portable display and control terminal will be offered.

#### Timing Sources

The TTS's flexible relationship to external or internal frequency standards, oscillators, or digital clocks is illustrated in Figure 5, resulting in 3 time-source operating modes.

The TTS-502 can be controlled with a 3-position switch on the rear panel to operate in one of the following three modes:

Mode 1: Internal 5 MHz and Internal 1 pps Mode  
(Internal 5 MHz with Option 001 only)

In this mode, an external 1 pps signal is not required. With Option 001, the TTS-502 includes a precision 5 MHz quartz crystal oscillator generating an internal 5 MHz signal from which all the required frequency references and timing pulses are generated when operating in Mode 1. The GPS time transfer is made with respect to an internally derived 1 pps signal. A TTS-502 with Option 001 can also operate in Mode 2 or Mode 3.

Mode 2: External 5 MHz and Internal 1 pps Mode

In this mode, a user-supplied external 5 MHz signal is used to derive all of the required frequencies and timing pulses. The TTS-502 uses the 5 MHz input signal to internally derive a 1 pps signal for referencing the GPS time transfer.



### Mode 3: External 5 MHz and External 1 pps Mode

In this mode, a user-supplied external 5 MHz signal and a user-supplied 1 pps are input to the TTS-502. The GPS time transfer is made with respect to the externally supplied 1 pps signal.

In all of the above operating modes, the 5 MHz signal is passed through and available as an output at the rear panel. The 1 pps used to reference the GPS time transfer (internally derived in Modes 1 and 2, externally provided in Mode 3) is also available at the rear panel with the basic system. With Option 002, this pulse is time-shifted to correspond to GPS or UTC time.

### Preamplifier/Antenna

The preamplifier and antenna, which are included in the TTS-502 system, are off-the-shelf items. The preamplifier is an Avantek AM1664 modified to accept power via the RF cable to the receiver and high power input protection (Avantek M1664N103). This preamplifier is tuned to the L1 frequency with a minimum of 50 dB gain, and a noise figure of 3 dB and a bandwidth of 10 MHz. This will insure a receiver system noise figure of less than 4 dB, even for installations with very long preamplifier-to-receiver cable lengths. Its size is approximately 8 inches by 3 inches by 2 inches, including connectors.

The antenna is an omni-directional antenna. It is right-hand circular polarized and has greater than -2 dBIC gain above 10° elevation angle and greater than -3 dBIC gain above 5° elevation angle with hemispherical coverage (measured on a ground plane).

### Receiver/Processor

A block diagram of the Receiver/Processor subsystem of the TTS-502 is shown in Figure 6. This subsystem is the portion of the TTS that is housed in the 8-3/4-inch chassis shown in Figure 2 (which includes the Option 001 oscillator, if provided). The receiver has its baseband processing and control resident in firmware in a microprocessor. The receiver hardware consists of a downconverter, correlator, code generator, code and carrier NCO's (Number Controlled Oscillators), frequency synthesizer and timer and a 115 volts, 60 cycle, (both  $\pm 10\%$ ) power supply which also supplies DC power to the preamplifier. The receiver operates on the L1, C/A code signals only, and in conjunction with the microprocessor, acquires the satellite signals, tracks the code and carrier of the acquired signal, demodulates the navigation data, performs parity checking on the data, measures pseudorange and doppler and provides the data and measurements, upon request, to the MC68000 microprocessor. That control will occur at a maximum rate of once per second, either as an acquisition command or as a measurement request.

The receiver accepts the L1 C/A RF signal from the preamplifier. Its sensitivity is better than 132 dBm (at the preamplifier) and it has a dynamic range of greater than 20 dB, with a spurious response greater than 60 dB at 130 MHz from the carrier. Its 3 dB IF bandwidth is 25 MHz. Its pseudorange measurement resolution is 48.9 nanoseconds, which, in the time transfer algorithms, is smoothable down to a one sigma of 0.9 nanoseconds.

The MC68000 microprocessor, in addition to controlling the receiver, contains all of the time transfer software (firmware). Its basic duty cycle for computing time transfer values is once per six seconds. Some of the basic features of this processing are described below.

#### Time Transfer Software Processing

The TTS software package resident in the MC68000 microprocessor is written primarily in a FORTRAN language. However, the entire software system will be compiled and "burned" into Programmable Read Only Memories (PROM's) on the microprocessor card. In addition to volatile Random Access Memory (RAM) available for processing, nonvolatile RAM is used to store initialization parameters to circumvent reentering those parameters whenever power is lost or removed and then restored.

The software routines are designed to perform a variety of functions: operator input handling, receiver signal acquisition control, satellite data collection and processing, scheduling and schedule control, time transfer algorithm execution, data smoothing, data statistical analysis, data display, data output, etc.

The primary purpose of the software processing is to provide the user the flexibility of exercising various modes of operation to suit his requirements. Most important, the software processing provides an automatic mode of operation in which visible satellites are scheduled to be tracked under software control, permitting continuous time transfer operation. Once this mode is initiated, no further operator intervention is required, and the TTS is operated in a so-called "do forever" loop.

The TTS with its application software processing is designed primarily for the automatic controlling of the receiver to track a sequence of visible satellites based on a 24-hour tracking schedule, in support of continuous time transfer operation. The TTS provides two modes of control for setting up this schedule.

Under the full automatic mode of control, a 24-hour satellite tracking schedule is generated internally by the software based on a stored almanac and known user location. The criterion used for generating a schedule is such that every satellite chosen by the operator will be tracked at least once every day. This schedule is automatically

revised daily to account for the GPS satellite constellation precession. To override the full automatic schedule, the user may exercise the semi-automatic mode of control in which the user is allowed to set up a 24-hour schedule using any criterion he may choose.

In either mode, once a schedule is set up, it will be maintained by the program and, at the beginning of each tracking interval, the receiver will be automatically reset with a new satellite identification number and initial doppler estimate computed using stored almanac data. Since almanac data for all satellites are updated occasionally by the GPS Master Control Station, the stored almanac data to be used by the system are continuously and automatically refreshed once the system is in operation.

Starting with a new satellite acquisition command, the time transfer operation proceeds through three phases of operation. In the first phase, the signal acquisition phase, the receiver will acquire and track the selected satellite. During this phase, the receiver acquisition process is monitored by the program until the signal is successfully acquired and subframe synchronization is achieved. In the next phase, the initial data acquisition phase, satellite data subframes demodulated by the receiver are input and processed every six seconds until a complete set of error-free data is collected. Normally, these two phases will take much less than one to two minutes, depending upon whether time had been previously established. The final phase, time transfer solution phase, will last for the rest of the scheduled time. This phase consists of a number of time transfer cycles, each cycle occurring at 6-second subframe epochs.

At the beginning of each cycle, the processor inputs a 300-bit data subframe, receiver status information, and measured pseudorange and doppler from the receiver. Pseudorange and doppler measurements are taken every second and combined at the end of six seconds to provide a smoothed measurement for the time transfer computations. The receiver status information is used for monitoring the receiver performance, and for accessing the validity of the measured pseudorange. The purpose of the data subframe is threefold: first, to derive the satellite time of transmission from the subframe Z-count; second, to refresh satellite navigation and almanac data; and finally to check if the navigation data is being updated by the satellite. If so, a new set of satellite ephemeris data will be collected to keep the microprocessor data base current.

The time transfer algorithms are then applied to estimate user clock time error, to enter that error into the time offset smoothing process, to display data in a variety of forms, based on user's selected options, and to output data to the optional output ports. Typical displays show the station clock time error, the time of day (in GPS or UTC time),

date (in Modified Julian Date Number), age of data, receiver status, satellite identification number, and elevation and azimuth angles.

Besides the two major modes of operation described above, the TTS software processing also provides additional modes of operation which allow the user to initialize the data base, collect an initial set of almanac data, to obtain satellite constellation times of visibility, and to exercise the manual mode of control in which a particular satellite of interest can be tracked until terminated or until it is no longer in view.

#### TIME TRANSFER ERROR ANALYSIS

Various sources of error that could affect the accuracy of the time transfer to varying degrees are listed in Table I and are discussed below.

##### Satellite Group Delay and Clock Errors

Normally, satellite group delay, which is caused primarily by delays in satellite signal paths, are indistinguishable from the satellite's clock time offset. Therefore, they are included in the GPS Control Segment's estimate of that clock offset. However, that estimate is based on dual frequency (L1 and L2) measurements of pseudorange, absorbing any group delay differential between the L1 and L2 signal paths within the satellite. This differential has no effect on two-frequency users. However, since the TTS has an L1 only receiver, that differential, multiplied by a factor of 1.546, is not accounted for in the polynomial clock correction terms of the Navigation Message.<sup>11</sup> However, it is accounted for in the TGD term included in that message. The error in that term is affected, however, by the Control Segment's ability to measure it through the ionosphere at times of relatively small ionospheric delays. However, that error, along with perturbations in the absolute group delay in the satellite, is expected to be insignificant compared to the satellite's random clock drift described below. Therefore, they can be neglected.

The satellite clock errors are basically the error in the satellite's polynomial clock correction terms of the Navigation Message. That error is caused by three sources: the satellite's random clock drift, the group delay described above, and the Control Segment's inability to estimate and predict the clock drift exactly. These errors are very much related, so it makes no sense to try and differentiate them. Over a period of time, however, the random clock drift will normally dominate if the satellite's clock is reasonably stable. (In other words, a clock is one that meets specification - a nonanomalous satellite.) That assumption is made here, since that is the case for all but the first two satellites launched. In fact, the most recently launched satellites have very stable clocks.

Since these clocks do vary in stability, it makes more sense to discuss the specified stability rather than the actual stability. The numbers in Table I reflect those specifications<sup>12,13</sup>. For the Phase I satellites, the clock errors were specified for only two hours after upload of the satellite, obviously to cover specific testing periods. However, since the TTS could be used anywhere, that error budget has been extended to 24 hours here, using the clock Allan variance characteristics provided in Appendix III of Reference 13 and the time drift models of Reference 14. Since there are two types of frequency standards operating in the Phase I satellite (Rubidium and Cesium), a range is given for the clock error budget of 25.5-108 nanoseconds (one sigma) for 24 hours after upload (25.5 for Cesium, 108 for Rubidium). These are based on the equations:

$$\begin{aligned}\sigma^2(t) = & 10^{-20}(t-t_{\text{UPLOAD}}) \\ & + 1.44 \times 10^{-24}(t-t_{\text{UPLOAD}})^2 \text{ seconds}^2\end{aligned}\quad (6)$$

for the Rubidium standard, and

$$\begin{aligned}\sigma^2(t) = & 2.5 \times 10^{-21}(t-t_{\text{UPLOAD}}) \\ & + 5.76 \times 10^{-26}(t-t_{\text{UPLOAD}})^2 \text{ seconds}^2\end{aligned}\quad (7)$$

for the Cesium standard.

Although the drift of the Rubidium standard causes the TTS error budget to exceed the 100 nanoseconds advertised, the standards that are operational have been performing much better than specified.

For the operational GPS system, the Operational Control Segment (OCS) is simply specified to upload the satellites as often as required to maintain the combined clock and ephemeris errors to within 20 nanoseconds (6 meters), one sigma.

The nature of these clock errors are basically bias-like over the smoothing interval of the TTS (240 seconds, maximum).

#### Satellite Ephemeris Prediction Errors

These errors are primarily the Control Segment's inability to predict the satellite's ephemeris (position versus time) exactly plus any perturbations that are unpredictable. These errors, along the line-of-sight to the user, are budgeted to be 12 nanoseconds (3.6 meters), one sigma for the Phase I system for 24 hours after upload, and are combined with the clock errors as described above for the operational system. Actually, the errors are somewhat negatively correlated with the clock errors and tend to cancel somewhat over short periods of

time after upload. Therefore, it makes more sense to combine the error budget as it is for the operational system.

As for the clock errors, the ephemeris errors are basically bias-like over the smoothing interval of the TTS.

### Ionospheric/Tropospheric Delays/Multipath Errors

These errors are obviously independent of each other; however, they are worse at low elevation angle tracking and minimized at higher elevation angles. The multipath errors can be controlled with good installation practices. They can also have a relatively random component that could be lumped in with the receiver noise errors. The tropospheric delay is corrected with a simple model.

In any event, the ionospheric delay correction error will usually dominate, since the TTS has no capability of measuring pseudorange at two frequencies. It must rely on the ionospheric correction model provided in the Navigation Message.<sup>10,15</sup> In fact, under normal situations, the ionospheric delay correction error will dominate the TTS performance.

Reference 15 treats this correction error in detail. In summary, the ionospheric delay error is caused by the integrated electron content along the ray path between the satellite and the user. The delay effect is dependent on both the character of the ionosphere at the zenith and the elevation angle to the satellite. The character at zenith is highly dependent on geometric latitude of the user and the time of day, and is not very predictable. Figure 7 shows typical measurements of ionospheric delay for an L-band signal (near L1) received at vertical incidence.<sup>16</sup> The mean ionospheric delay at nighttime is on the order of ten nanoseconds. During the daytime the mean delay increases to as high as fifty nanoseconds. At low elevation angles the delay can be up to three times the values given above (30-150 nanoseconds). Although these delays are partially corrected with the Navigation Message model, that model will normally be in error by about 50 percent of the delay (one sigma).<sup>15</sup> Therefore, as a "ballpark" estimate, it is assumed that the ionospheric delay correction error, combined with the tropospheric correction and multipath error, ranges between 5-40 nanoseconds (one sigma), depending upon many variables. This error is the most important error source of the TTS time transfer error.

### Receiver Noise (and Random Multipath) Errors

Receiver noise is dominated by the thermal noise effects on the performance of the receiver's code loop (neglecting unintentional jamming, of course). Since the TTS receiver's code loop is aided by its carrier loop, and because pseudorange measurements are relatively infrequent

(once per second), its loop bandwidth is quite small, reducing the raw measurement receiver noise error to 15.5 nanoseconds, one sigma. Smoothing to one-second measurements reduces this error to 6.3 nanoseconds, one sigma. Also, this error is random in nature; therefore, since the TTS software processing smooths the raw time transfer results, this 6.3 nanoseconds can be further reduced to about 1.0 nanoseconds, one sigma (40 sample smoothing).

#### Pseudorange Quantization Errors

The least significant bit of the TTS pseudorange measurements is worth 48.9 nanoseconds (1/20th of a C/A code chip). This is reduced by the square root of 12 to a one sigma value of 14.1 nanoseconds, since it is a uniformly distributed error between  $\pm 24.4$  nanoseconds. (The bias is a time error that is part of the receiver's calibration correction, primarily because pseudorange, as measured, is always positive). As was the case for the receiver noise errors, these quantization errors are further reduced in the TTS software processing because they are smoothed, reducing the 14.1 nanoseconds down to about 5.8 nanoseconds, one sigma for the smoothed 6-second measurement and down to 0.9 nanoseconds, one sigma, in the time transfer smoothing (40 sample smoothing).

#### User Location Estimation and Receiver Bias

The TTS makes use of the user coordinate in the estimation of satellite-to-user range, and therefore must be known accurately. The error budget for this estimation depends on the surveying technique used to determine the coordinates. If a GPS Geociever is used for the survey, the GPS position can be derived quite accurately, to within about 1-2 meters<sup>17,18</sup> ( $\approx 5$  nanoseconds). Otherwise, the location error could be somewhat larger, and budgeted to be up to about 5 meters (15 nanoseconds), one sigma. This error is bias-like, and therefore cannot be smoothed over the TTS smoothing intervals.

The TTS receiver bias from the antenna to the input (or output) 1 pps, is calibrated prior to TTS delivery. The error and subsequent drift in that bias is well within the location error budget given above. Of course, any cable length changes require a new bias input.

#### Total (RSS) Time Transfer Error Budget

Table I lists the various individual error budget that makes up the total TTS time transfer error budget. The RSS totals are given as ranges, consistent with the ranges given for the individual budgets. Also, the smoothed error budget is given versus the raw error budget, assuming 40 sample smoothing (6 seconds per sample). For the Phase I GPS error budget, two totals are given - one for the Rubidium satellite frequency standards and one for the Cesium satellite frequency

standards. All budgets are well within the advertised budget of 100 nanoseconds for the TTS, except for worst case Rubidium frequency standard drifts, which to date have not been exhibited.

## USNO TTU RESULTS

### Acceptance Test Results

The acceptance tests of the USNO Time Transfer Unit were conducted for five days in November 1979, as part of the unit acceptance tests. The following is an excerpt from a paper by Dr. Kenneth Putkovich<sup>8</sup>, USNO representative at the time of the acceptance tests.

"Initial tests of the time transfer capability of the Time Transfer Unit (TTU) were carried out as part of the unit acceptance tests. A pair of portable atomic clocks was carried to the MCS (Master Control Station) at Vandenberg AFB in California. The ensemble of atomic clocks which constitute the GPS master clock were measured against the portable clocks with particular attention to the clock serving as reference for the Vandenberg Monitor Site. Pertinent system delays in the monitor receiver were also measured and verified with site personnel. The portable clocks were then transported to the STI facility in Sunnyvale, where a series of time transfers were made using the portable clocks as reference for the TTU. The clocks were then returned to Vandenberg (to establish a baseline for GPS time) and then taken back to Sunnyvale for a final series of measurements. The results of this initial series of measurements are presented in Figure 4 (Figure 8 in this paper). As can be seen from the plot, time transfers with a precision of better than  $\pm 50$  nanoseconds were achieved."

After the portable atomic clocks were shipped back to USNO, additional testing was performed, this time using a Cesium standard which was calibrated against the atomic clocks. These tests also produced similar results.

### Subsequent Testing and GPS Time Performance Monitoring<sup>8,19</sup>

Subsequent tests performed by the USNO involved the verification of GPS Time at the GPS Master Monitor Station via portable clocks and the acquisition and tracking of as many passes of the satellites currently in operation as possible. These tests resulted in the same level of performance as the initial acceptance testing, but revealed what appeared to be several discontinuities in GPS Time. An investigation showed the cause of these steps to be GPS master clock changes and failures in GPS Monitor Stations. Since then, due to a coordinated effort between USNO and the GPS program office, an improvement has been made as the magnitude and frequency of the discontinuities has decreased. More details of GPS Time monitoring are given in Reference 19, which covers a period of time up through about the end of 1980.



The TTU has also been used to monitor the performance of the frequency standards in the GPS satellites. Those performances are also presented in Reference 19 over the same time frame and have also been presented in terms of Allan variance numbers in Reference 20. That performance is monitored by "backing out" the satellite clock correction polynomial derived from the GPS Navigation Message<sup>11</sup>, which basically "uncorrects" the satellite clock time from GPS Time to the time of the satellite's subframe epoch transmission. In a sense, the accuracy in this TTS estimate of satellite time is better than that of GPS Time because it is not corrupted by the prediction errors in the clock correction polynomial, which is evident from results presented in Reference 19. However, this estimate is of little value to the normal TTS user, unless he is primarily interested in monitoring satellite clock performance, with one exception. Since the USNO publishes the difference between their Master Clock and each satellite's clock, a user can perform a time transfer to UTC via a satellite clock instead of via GPS Time. The published difference of a good satellite clock is more accurately predictable by extrapolation than that of GPS Time to the user's time of transfer. However, if the user does not extrapolate and uses data common to the USNO after the fact, it makes no difference because the clock correction polynomial prediction errors cancel. (In fact, in a common view time transfer performed while in communication with the USNO, all common errors such as satellite clock errors, ephemeris prediction errors, and part of the ionospheric delay correction errors cancel, resulting in a more accurate time transfer. This has been suggested and demonstrated by the National Bureau of Standards.<sup>21,22</sup>).

#### USNO GPS Time Service

Data from the GPS satellites are recovered daily by the USNO and are made available through the USNO Time Service Automated Data Service (ADS) via standard dial-up telephone line, using a modem and terminal. (See Reference 19.) This service was used to obtain more recent data than that presented in Reference 19 for a satellite that has had a Cesium beam standard operating for some time (SV#9). The data was retrieved for a period of 190 days starting on January 1, 1981. The results provided by the Time Service are plotted in Figure 9 for both the difference between GPS Time and the USNO Master Clock and the difference between SV#9's clock and the USNO Master Clock. The following polynomials (three point derived) were removed from the data before plotting:

$$\begin{aligned} \text{GPS Time: } & -35.811 \mu\text{s} - 1.3352 \times 10^{-12} \text{ s/s } \times t & (8) \\ & + (2.81436 \times 10^{-15} / 86400) \text{ s/s}^2 \times t^2 \end{aligned}$$

$$\begin{aligned} \text{SV\#9 Time: } & 346,428 \text{ ns} + 3.6651 \times 10^{-13} \text{ s/s } \times t & (9) \\ & + (6.04051 \times 10^{-16} / 86400) \text{ s/s}^2 \times t^2 \end{aligned}$$

where  $t$  is in seconds since 1 January. These coefficients are equivalent to drift values of:

$$\text{GPS Time: } \Delta f/f = -1.3352 \times 10^{-12}$$

$$D = 5.62872 \times 10^{-15}/\text{day}$$

$$\text{SV\#9 Time: } \Delta f/f = 3.6651 \times 10^{-13}$$

$$D = 1.2081 \times 10^{-15}/\text{day}$$

It is evident from these plots that the satellite's clock is better than the GPS clock. This should be expected since the GPS clock is much older than the satellite's clock. The fact is that both clocks are exhibiting normal "flicker" characteristics. The anomalous results that occurred around day 130 are due to transient conditions in the GPS system after a "Master" receiver failure. Time in the master GPS clock was reinitialized.<sup>23</sup>

The results of Figure 9 are consistent with the results presented in Reference 19 for a previous period of time.

#### TIME TRANSFER APPLICATIONS

The Time Transfer System can be employed in a variety of applications. As a stand-alone system it can provide an absolute time reference for users within GPS. By using the data provided by USNO's Time Services, GPS Time (or any of the SV times) can be translated to UTC. More stable timing can be achieved by operating the TTS with an external Cesium or Rubidium standard to bridge periods of nonvisibility to satellites in the current GPS system. Intermittent accurate time transfer can be achieved with the optional internal crystal oscillator, with accuracies on the order of microseconds during periods of nonvisibility.

The TTS can also be used as a calibration device to provide time alignment of other standards in the user's timing network.

For a timing network in which only relative time is required, the so-called "common mode-common view" technique of time transfer can be employed to provide even better accuracy.<sup>21</sup> In this mode, a highly stable TTS is used as the master clock (such as the one at USNO) and another TTS at a remote location will be simultaneously scheduled to track an identical satellite that is visible from both TTS's. When the time offsets obtained from these two TTS's are compared, better (relative) accuracy will be achieved due to the cancellation or reduction of common sources of error, e.g., satellite clock and ephemeris error, and some of the atmospheric time delay error.

As an example, Figure 10 shows the times that two TTS's located in Washington, D.C. and Paris, France may both see a particular satellite. Note that, even with the six-satellite constellation, the daily common view period can be as much as 15 hours.

This technique is similar to that employed in TV line-10 transfers, where simultaneous, common view measurements against a stable transmitter yield measurements with ten-nanosecond uncertainty. Intercontinental time transfer at ten nanoseconds should be possible with GPS TTS's.

#### FUTURE CONSIDERATIONS

In the near future, the TTS 502 will be available in a portable configuration. The receiver/processor chassis will be packaged as a portable unit. The preamplifier and antenna are already quite portable. Portable terminals are also available on the market or may already be available at remote sites. And the TTS does not need batteries. It can be plugged into any 115 VAC wall socket. Initialization parameters can be stored in nonvolatile memory (or PROM) at a laboratory or depot site, and the TTS can be shipped unattended to a remote site as a calibration device. The only starting parameter that is needed is an approximate time-of-day and day-of-year, which could conceivably be entered with other means besides a terminal (such as a set of thumbwheels, a start button, and an LED readout), eliminating the need for a terminal.

As the number of TTS's increase, they will become smaller than "Flying Clocks," and competitive in price. They are already lighter (no batteries), and much less expensive to maintain and transport (again, no batteries).

As GPS matures and more satellites become available, it is also conceivable that the TTS's will also replace frequency standards in the field. Over the short term they are not quite as accurate, but over the long term they will be nearly as accurate as UTC itself ( $\pm 100$  nanoseconds or less). And, they will never need calibrating. As with the flying clocks, the TTS will also eventually become competitive in price with accurate frequency standards.

#### ACKNOWLEDGMENT

The authors wish to thank Dr. Gernot Winkler and Dr. Kenneth Putkovich and their staff at USNO for their helpful response to inquiries made to them regarding the subject matter of this paper.

#### REFERENCES

- 1) GPS Special Issue, Navigation: Journal of the Institute of Navigation, Summer of Navigation, Summer 1978, Vol. 25, No. 2.

- 2) "Global Positioning System," Papers published in Navigation: Journal of the Institute of Navigation, 1980.
- 3) "Principles and Operational Aspects of Precision Position Determination Systems," AGARDograph No. 245, edited by C. T. Leondes, North Atlantic Treaty Organization Advisory Group for Aerospace Research and Development, July 1979.
- 4) P. S. Jorgensen, "Navstar/Global Positioning System 18 - Satellite Constellations," Navigation: Journal of the Institute of Navigation, Summer 1980, Vol. 27, No. 2.
- 5) P. S. Jorgensen, "Navstar Global Positioning System 18-Satellite Constellations," Air Force Systems Division GPS Constellation Briefing, June 5-6, 1980.
- 6) W. F. Brady and P. S. Jorgensen, "Worldwide Coverage of the Phase II Navstar Satellite Constellation," presented at the Institute of Navigation National Aerospace Meeting, Trevese, PA, 8-10 April 1981.
- 7) Q. D. Hua and H. A. Bustamante, "A GPS Time Transfer System," presented at Second Annual AFCEA Communications Electronics Exhibit and Technical Symposium, Palo Alto, CA, 12-14 November 1980.
- 8) K. Putkovich, "Initial Test Results of USNO GPS Time Transfer Unit," presented at 34th Annual Symposium on Frequency Control, May 1980.
- 9) Private Communication with Dr. Gernot Winkler, USNO, July 1981.
- 10) Navstar GPS Space Segment/Navigation User Interface, (Draft), ICD-GPS-200, Rockwell International Interface Control Document, May 27, 1981.
- 11) A. J. Van Dierendonck, S. Russell, E. Koptizke, and M. Birnbaum, "The GPS Navigation Message," included in References 1, 2, and 3 above.
- 12) "System Specification for the Navstar Global Positioning System, Phase I," U.S. Air Force Space and Missile Systems Organization document SS-GPS-101B, 15 April 1974.
- 13) "Requirements for the Control Segment of the Navstar Global Positioning System," U.S. Air Force Space Division (AFSD) document No. YEN-78-019, Revision VI, 10 March 1980.

- 14) A. J. Van Dierendonck, "Opportunities and Limitations with Satellite-Borne Time and Frequency Navigation Systems," lecture given at National Bureau of Standards Seminar on Time and Frequency Control, August 1977.
- 15) J. A. Klobuchar, "A First-Order, Worldwide, Ionospheric Time-Delay Algorithm," U.S. Air Force Cambridge Research Laboratories Report No. AFCRL-TR-75-0502, 25 September 1975.
- 16) B. D. Elrod, "Correction for Ionospheric Propagation Delay in ASTRO-DABS - The Dual Frequency Calibration Method," Mitre Report, MTR-6896, April 1975.
- 17) Patrick Fell, "Geodetic Positioning Using a Global Positioning System of Satellites," presented at IEEE Plans 80 Position, Location, and Navigation Symposium, Atlantic City, N.J., 8-10 December 1980.
- 18) J. M. H. Bruckner, R. W. Carroll, N. B. Hemesath, W. M. Hutchinson, "Low Cost-High Accuracy GPS Survey Receiver Design," presented at 13th Annual Offshore Technology Conference, Houston, Texas, 4-7 May 1981.
- 19) K. Putkovich, "USNO GPS Program," paper presented at 12th annual PTTI Applications and Planning Meeting, NASA Goddard Space Flight Center, Greenbelt, MD, 2-4 December 1980.
- 20) M. Levine, paper presented at 35th Annual Symposium on Frequency Control, May 1981.
- 21) Allan, D. W. and Marc A. Weiss, "Accurate Time and Frequency Transfer during Common-View of GPS Satellite," Proceedings, 34th Annual Frequency Control Symposium, Fort Monmouth, NJ, May 1980.
- 22) Davis, D. D., M. Weiss, A. Clements, and D. W. Allan, "Unprecedented Syntonization and Synchronization Accuracy via Simultaneous Viewing with GPS Receivers; Construction Characteristics of an NBS/GPS Receiver," 13th Annual Precise Time and Time Interval (PTTI) Applications and Planning Meeting, Naval Research Laboratory, Washington, DC, December 1981.
- 23) Private Communication with Walt Harbour, OAO Corporation, August 1981.

TABLE I  
TIME TRANSFER ERROR BUDGET

	PHASE I GPS SPECIFIED ONE SIGMA ERROR BUDGET <sup>12</sup> (nanoseconds)	OCS SPECIFIED ONE SIGMA ERROR BUDGET (nanoseconds)
SV GROUP DELAY AND CLOCK	9 (for 2 hrs) 25.5-108 (for 24 hrs)	20*
SV EPHEMERIS	12 (for 24 hrs)	
IONOSPHERIC/ TROPOSPHERIC DELAY/MULTIPATH	5-40**	5-40**
RECEIVER NOISE (RAW/SMOOTHED)	6.3/1.0	6.3/1.0
PSEUDORANGE QUANTIZATION (RAW/SMOOTHED)	5.8/0.9	5.8/0.9
USER LOCATION ESTIMATION AND RECEIVER BIAS	5-15	5-15
TOTAL (RSS) (RAW/SMOOTHED)	(18-117)/(17-117)*** (18-52)/(17-51)****	(23-50)/(21-47)

\* BETWEEN SUCCESSIVE UPLOADS<sup>13</sup>

\*\* ELEVATION ANGLE, LATITUDE AND TIME OF DAY DEPENDENT

\*\*\* RUBIDIUM FREQUENCY STANDARD IN SATELLITE

\*\*\*\* CESIUM FREQUENCY STANDARD IN SATELLITE

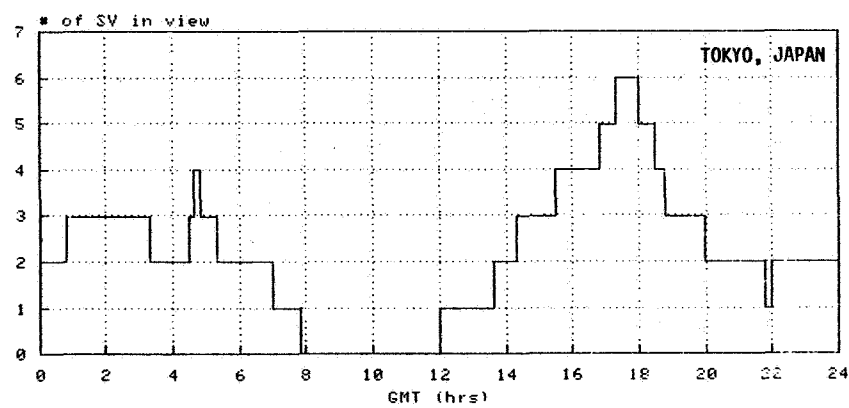
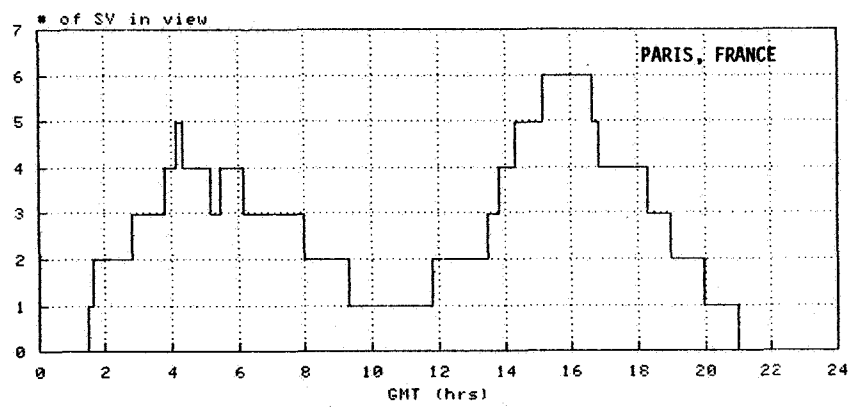
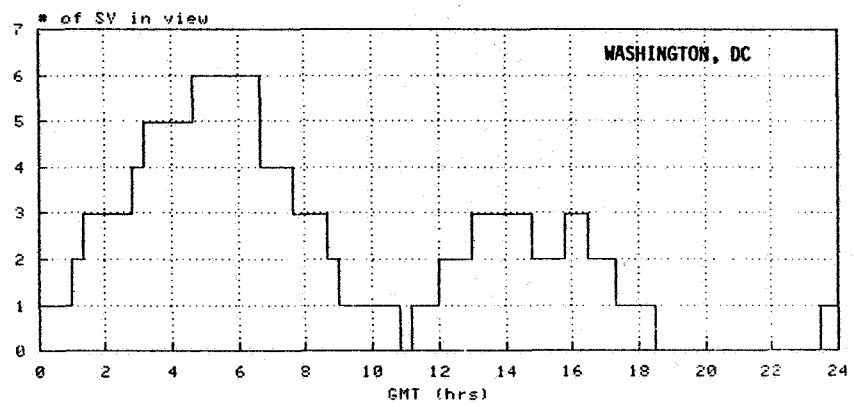


FIGURE 1 SIX SATELLITE COVERAGE

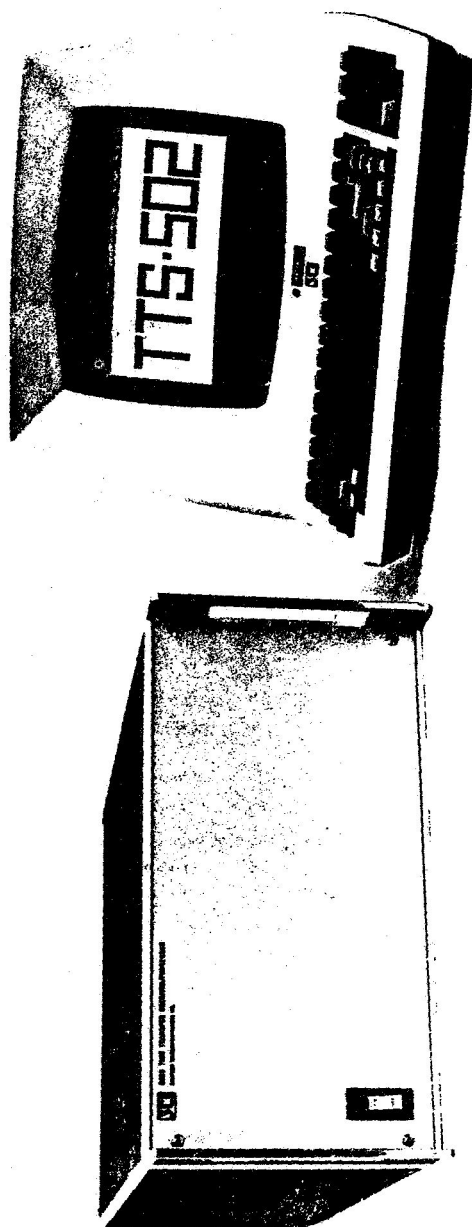
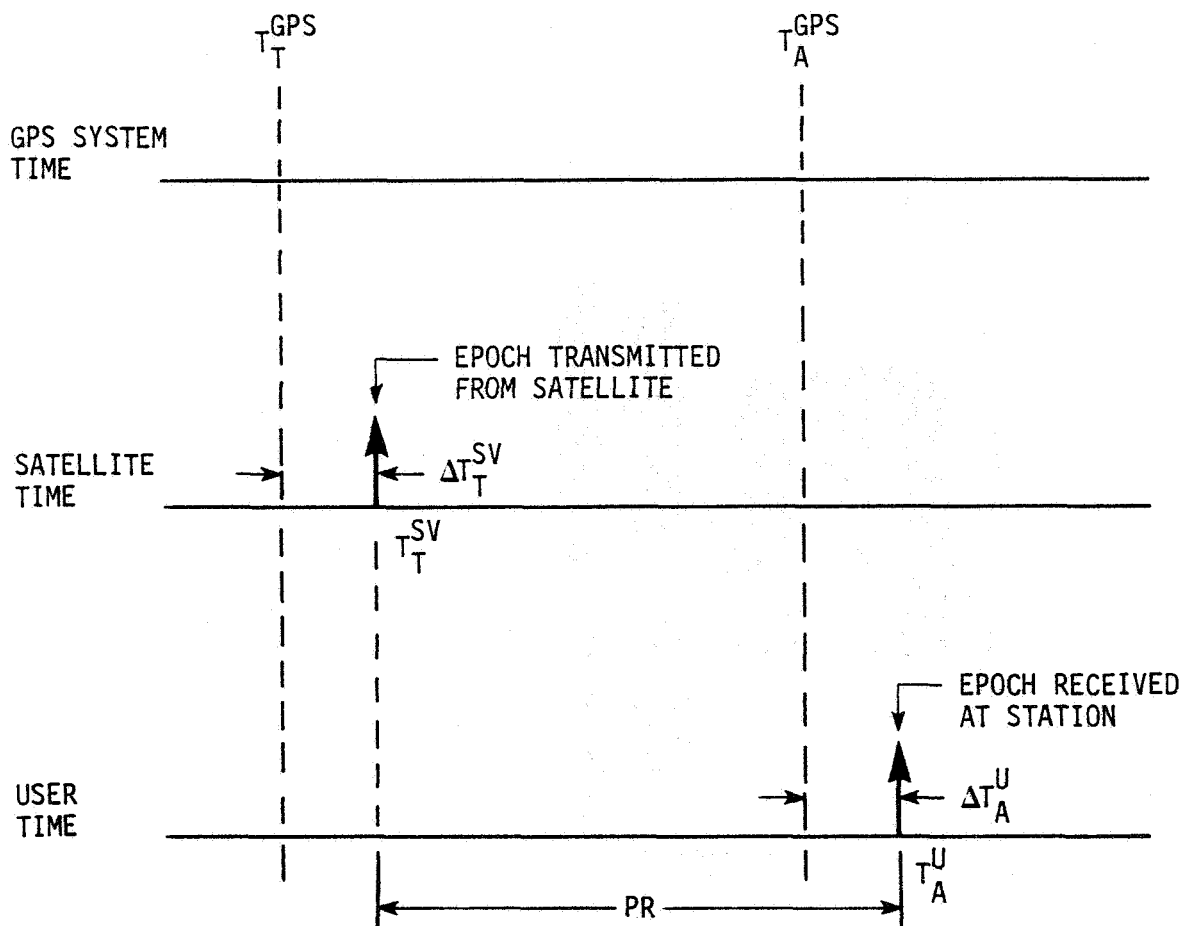


FIGURE 2 TTS-502 (ANTENNA AND PREAMPLIFIER NOT SHOWN)





- $T_T^{SV}$  : SATELLITE TIME AT EPOCH TRANSMISSION  
 $T_T^{GPS}$  : GPS TIME AT EPOCH TRANSMISSION  
 $\Delta T_T^{SV}$  : SATELLITE CLOCK ERROR AT EPOCH TRANSMISSION  
 $T_A^U$  : USER TIME AT EPOCH ARRIVAL  
 $T_A^{GPS}$  : GPS TIME AT EPOCH ARRIVAL  
 $\Delta T_A^U$  : USER CLOCK ERROR AT EPOCH ARRIVAL  
 PR = USER-MEASURED PSEUDORANGE

$$= T_A^U - T_T^{SV} = T_A^{GPS} - T_T^{GPS} - \Delta T_T^{SV} + \Delta T_A^U$$

FIGURE 3 TIMING RELATIONSHIPS

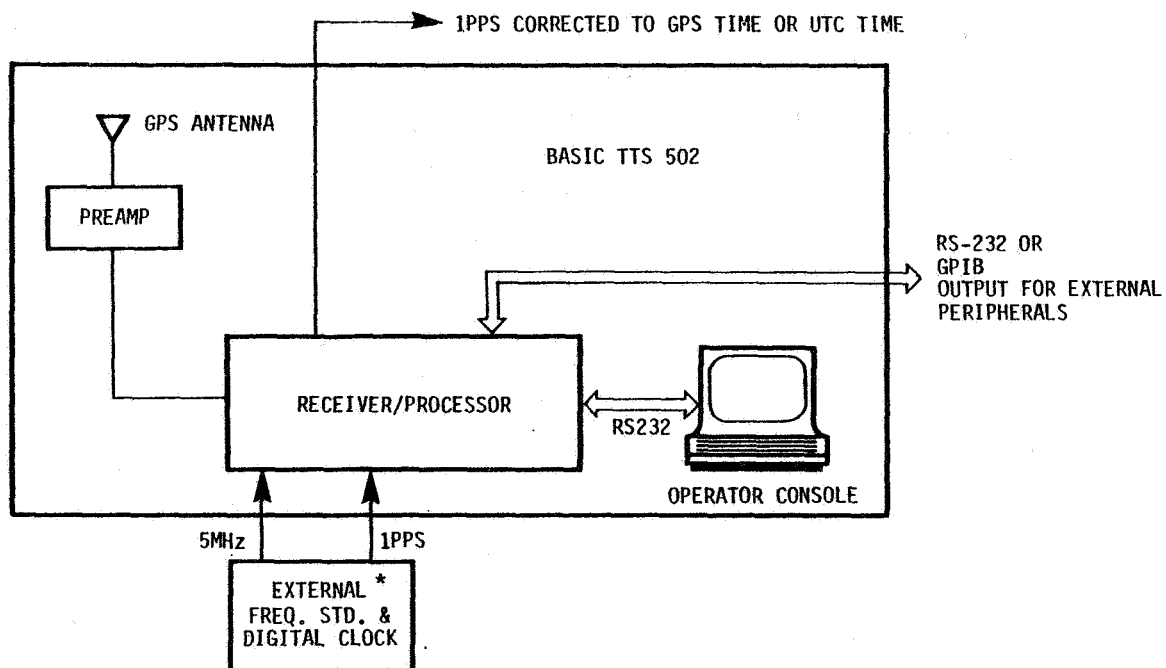


FIGURE 4 TIME TRANSFER SYSTEM 502

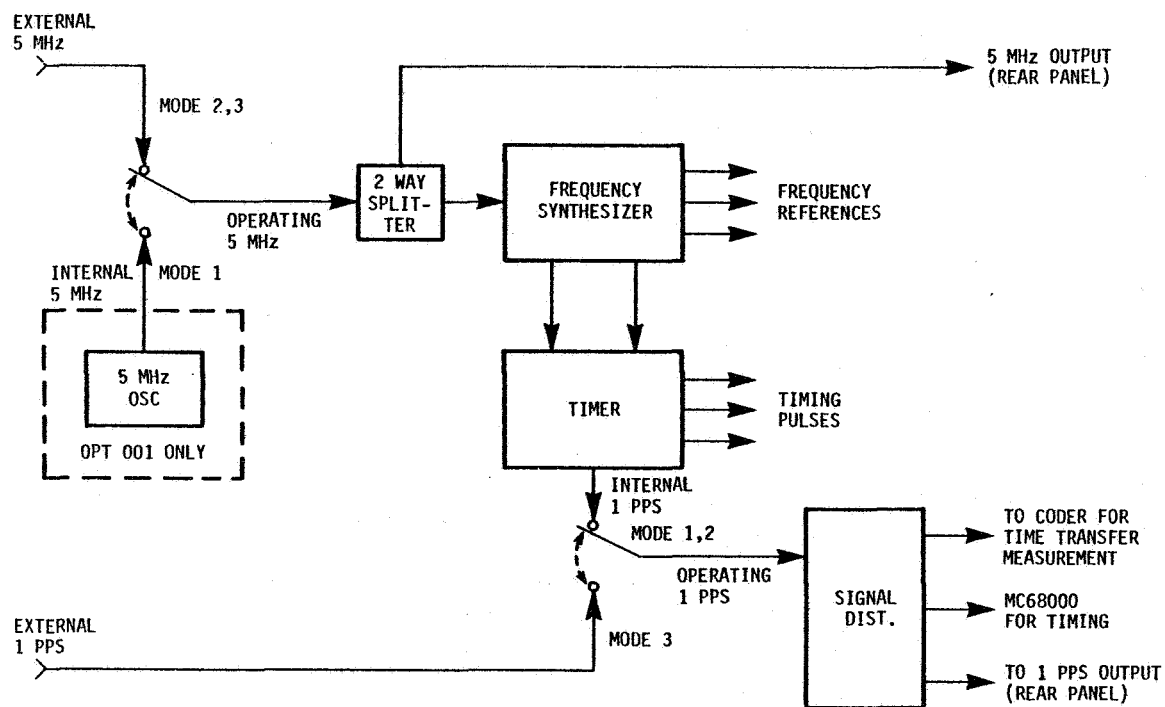


FIGURE 5 TTS-502 TIME SOURCE OPERATION MODES

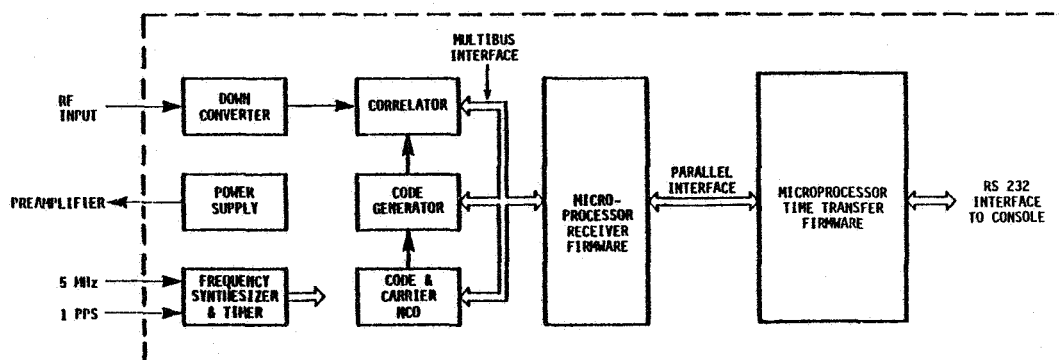


FIGURE 6 TIME TRANSFER RECEIVER/PROCESSOR MODEL 5026 BLOCK DIAGRAM

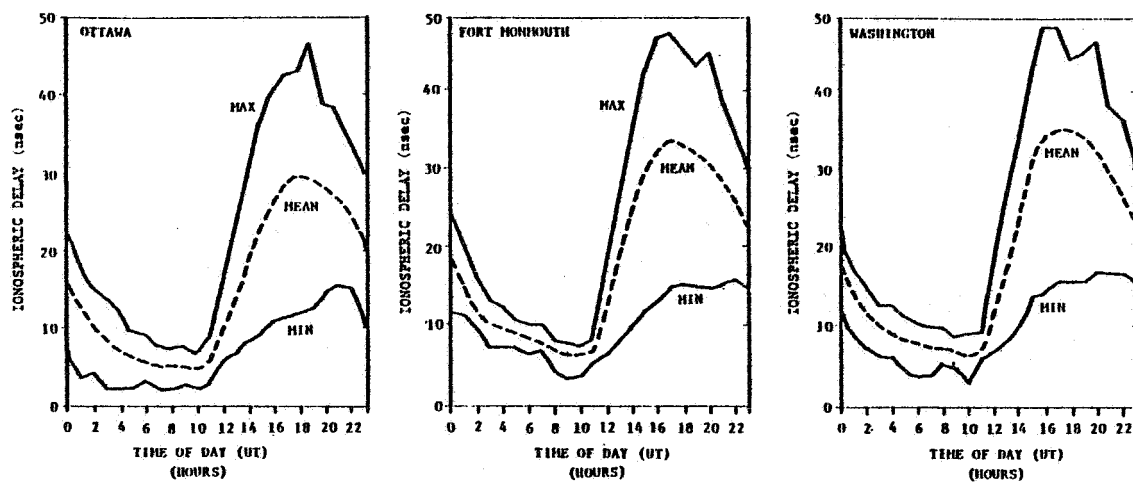


FIGURE 7 MEAN IONOSPHERIC DELAY AND ENVELOPE OF DELAY VARIATION VS. TIME OF DAY DURING -MARCH, 1958- SATELLITE AT ZENITH  $f=1.6$  GHz (FROM REFERENCE 16)

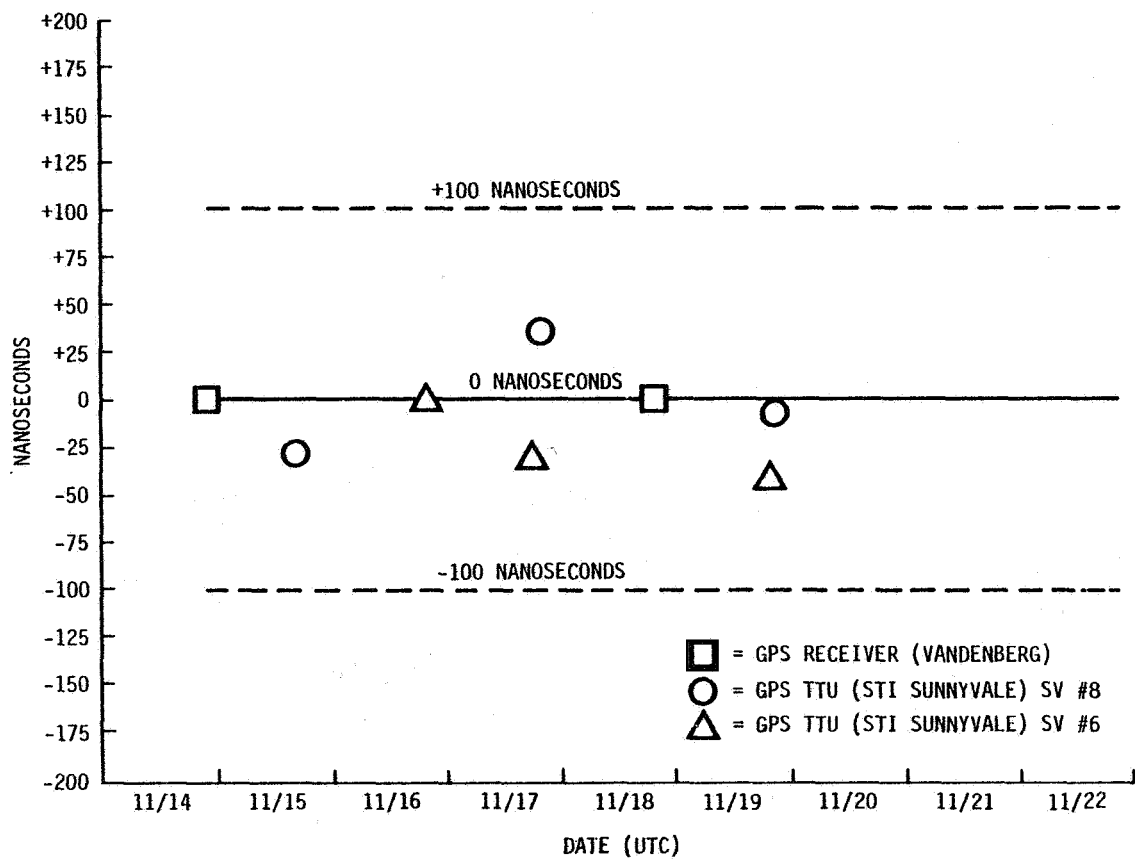


FIGURE 8 INITIAL TIME TRANSFER RESULTS

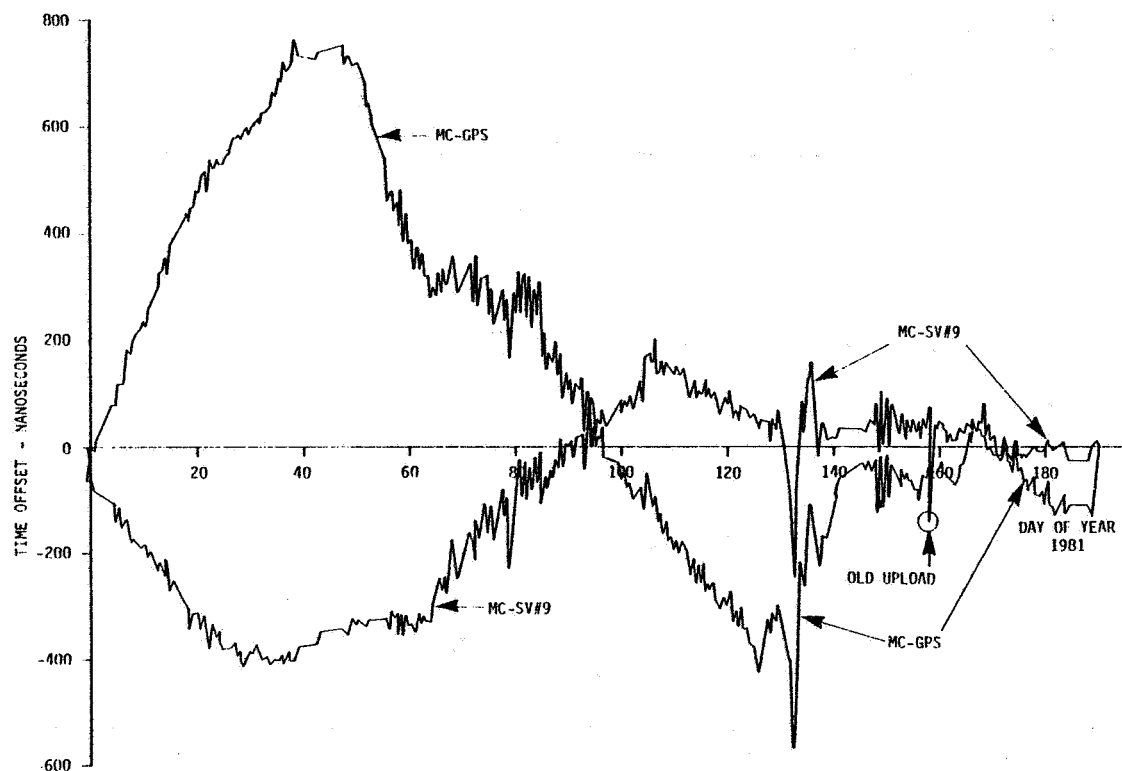


FIGURE 9 USNO TIME MONITORING RESULTS USING SV#9 FROM 1 JANUARY 1981 TO 11 JULY 1981

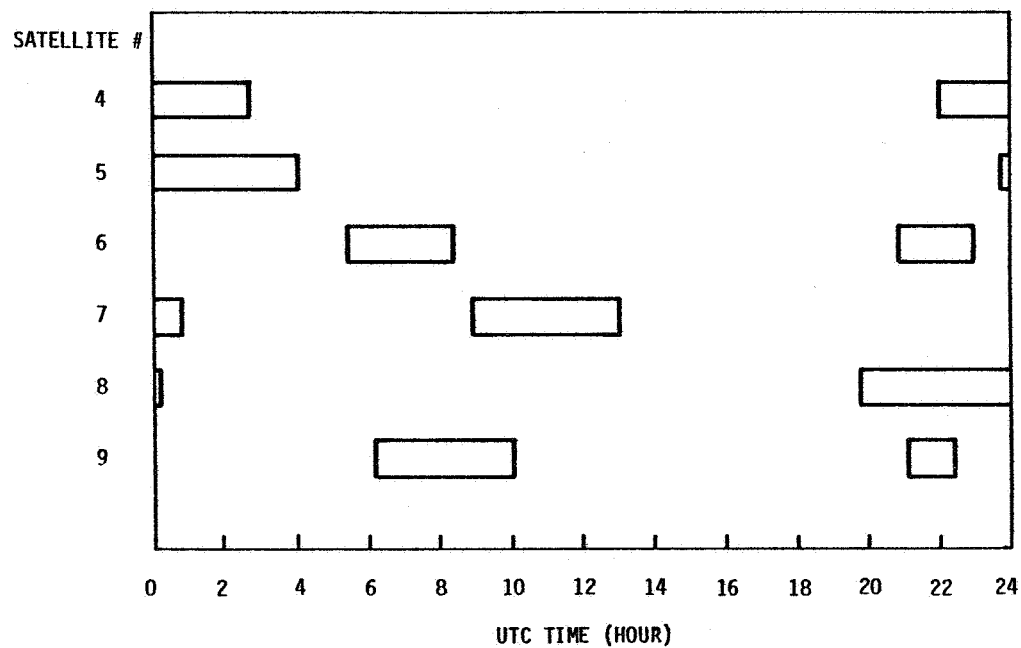


FIGURE 10 COMMON-VIEW TIME BETWEEN WASHINGTON,DC AND PARIS,FRANCE  
ON 2 OCT 1980



## QUESTIONS AND ANSWERS

MR. KELLOGG, Lockheed

In collecting the data and evaluating it, I noticed you have gone through the U.S. Naval Observatory time comparison with UTC; is that true or that is just a possibility?

MR. HUA:

That's true.

MR. KELLOGG:

Do you have any data which would permit evaluating whether we should have great confidence in the relativity corrections which have been built in to the standard on board the satellite?

MR. HUA:

I do not have any answer. I do not know much about that to answer your question about relativity.

MR. ALLAN:

I think I can answer that, and the corrections, I believe, are correct, and I think you can have great confidence in those.

MR. KELLOGG:

Thank you.

GLOBAL POSITIONING SYSTEM TIME TRANSFER  
RECEIVER (GPS/TTR) PROTOTYPE DESIGN AND  
INITIAL TEST EVALUATION

J. Oaks, A. Frank, S. Falvey, M. Lister, and J. Buisson  
Naval Research Laboratory  
Washington, D. C.

C. Wardrip  
NASA Goddard Spaceflight Center  
Greenbelt, Maryland

H. Warren  
Bendix Field Engineering Corporation  
Columbia, Maryland

ABSTRACT

Time transfer equipment and techniques used with the NRL Navigation Technology Satellites have been modified and extended for use with the GPS satellites. A prototype receiver was built and field tested at NASA's Kennedy Spaceflight Center.

The receiver uses the GPS L1 link at 1575 MHz with C/A code only to resolve a measured range to the satellite. A theoretical range is computed from the satellite ephemeris transmitted in the data message and the user's coordinates. Results of user offset from GPS time are obtained by differencing the measured and theoretical ranges and applying calibration corrections. These results may be referenced to Naval Observatory Time through published values of offsets of GPS Time from USNO Master Clock 1.

Results of the first field test evaluation of the receiver are presented. Measurements were made at NASA Goddard's MILA facility located in the Kennedy Spaceflight Center, Fla. Portable clock measurements were made for comparison, and all measurements were referenced to the Naval Observatory.

## INTRODUCTION

Present time synchronization techniques with the NASA laser network rely on LORAN-C and portable clocks to provide very accurate time tagging of laser ranging data. In applications where the data from two or more stations will be merged to determine baselines for geodetic work and polar motion determinations, it is necessary that the clocks at the several stations be synchronized to within  $\pm 1$  microsecond with respect to a master clock, such as that of the U.S. Naval Observatory (USNO). Best synchronization results using the LORAN-C system have been obtained from the West Coast chain at the Goldstone, California laser tracking station (MOBLAS 3). Figure 1 shows the MOBLAS 3 clock relative to the USNO Master Clock for the period of July 1980 through June of 1981. The x's are phase difference measurements made through LORAN-C referenced to USNO, and the O's are the phase measurements corrected for known offsets such that a linear least squares fit may be performed on the data. The standard deviation of the fit to this data shows a time synchronization of about a half a microsecond.

MOBLAS 5 located in Yarragadee, Australia has obtained a synchronization of only four microseconds using the LORAN-C Northwest Pacific chain as evidenced by the data in figure 2. Direct reception of LORAN-C signals is not possible at this location, and uncertainties in the path length of bounced signals cause large errors. In this instance MOBLAS 5 required frequent portable clock measurements (also shown in figure 2) to maintain microsecond synchronization.

Time transfers by satellite have been performed by NASA Goddard Spaceflight Center (GSFC) and the Naval Research Laboratory (NRL) initially using the NRL Navigation Technology Satellites (NTS).<sup>(1,2)</sup> Accuracies of several hundred nanoseconds were obtained.<sup>(3)</sup> As an outgrowth of the NTS effort, a Time Transfer Receiver (TTR) which operates with the NAVSTAR Global Positioning System (GPS) satellites is presently being developed jointly by GSFC and NRL. GSFC will use the GPS TTR in the Laser Ranging Network. The network consists of eight mobile vans, a permanent installation at GSFC, and eventually four highly transportable laser systems. The laser systems will be deployed to various locations around the world (figures 3 and 4) and will be used in support of the NASA GSFC Crustal Dynamics Program.

NAVSTAR GPS is a tri-service Department of Defense (DOD) program.<sup>(4)</sup> The first GPS satellite flown was NTS-II<sup>(5,6)</sup> which was designed and built by NRL personnel. GPS will provide the

capability of very precise instantaneous navigation and transfer of time from any point on-or-around the earth. At present six NAVSTAR satellites are on-orbit, providing instantaneous navigation over selected areas for limited parts of each day. This constellation is part of the GPS Phase I configuration. Additional space vehicles (SV) are to be launched during the next year.

The major objective of a satellite time transfer receiver is to determine precise time differences between a given satellite and a local ground clock referenced to the TTR (figure 5). Precise time can then be obtained between the SV and a single remote ground station clock or between the SV and any number of remote stations. The remote sites can then be synchronized among themselves.

#### THE NAVSTAR GLOBAL POSITIONING SYSTEM (GPS)

GPS is comprised of three segments. The space segment consists of a constellation of satellites for global coverage.(7) Phase III GPS will have a total of 24 satellites, eight in each of three orbital planes. The GPS orbits are near-circular at an altitude of approximately 10,000 nautical miles, inclined at 55 degrees to the equator. The period is adjusted such that a repeating ground trace is obtained for a given ground tracking station. Each satellite transmits its own identification and orbital information continuously. The GPS signal is spread spectrum in nature, formed by adding the data to a direct sequence code which is then biphase modulated onto a carrier.

The control segment consists of a master control station (MCS) and monitor stations (MS) placed at various locations around the world.(8) The current Phase I MCS is located at Vandenberg Air Force Base with the supporting monitor tracking stations at Alaska, Guam, Hawaii, and Vandenberg. The monitor stations collect data from each satellite and transmit to the MCS. The data is processed to determine the orbital characteristics of each satellite and the trajectory information is then uploaded to each satellite, once every 24 hours as the spacecraft passes over the MCS.

The user segment consists of a variety of platforms containing GPS receivers which track the satellite signals and process the data to determine position.(9,10) Coverage of the Phase III constellation is such that at least four satellites will always be in view from any point on the earth's surface.

## TIME TRANSFER METHOD

To perform a satellite time transfer with GPS, pseudo-range measurements are made that consist of the propagation delay in the signal plus the difference between the satellite clock and the ground station receiver reference clock. Data from the satellite is processed to obtain satellite position and satellite clock information (offset from GPS time). The propagation delay is subtracted from the pseudo-range by knowing the exact locations of the satellite and the station. This difference is then corrected by the GPS time offset to determine the final result of ground station time relative to GPS time. The Phase I GPS time is normally maintained at the Vandenberg MCS using a cesium oscillator. The Phase III GPS time is planned to be referenced from the MCS to the U.S. Naval Observatory (USNO) Master Clock. The final results obtained from a single-frequency receiver, such as the one described in this paper, will contain a small error due to the ionospheric delay which may be modeled and corrected.

## GPS TIME TRANSFER RECEIVER (TTR)

The GPS TTR is a microcomputer based system which was designed to replace existing receivers that formerly used the NTS satellites for time transfer. The design uses hardware and software from these receivers whenever possible. The following is a summary of the design requirements:

### A. GPS Signal Detection Characteristics

- 1) Operates at the single L1 frequency of 1575 MHz.
- 2) Has sufficient bandwidth to track satellites throughout their doppler range from horizon to horizon.
- 3) Uses only the course/acquisition (C/A) code of 1.023 MHz.
- 4) Tracks the C/A code to within 3% of a chip (30 nanoseconds).
- 5) Tracks any GPS satellite by changing to the appropriate code.
- 6) Detects and decodes the navigation data as required to determine a time transfer.

### B. Operational Characteristics

- 1) Requires a stationary platform during operation.
- 2) Determines the time difference between the 1 pps input station reference and GPS system time.

- 3) Measures the time difference once every six seconds.
- 4) Has an RMS of less than 50 nanoseconds on the time difference measurements.
- 5) Controls the operation of the receiver by inputs from a keyboard.
- 6) Outputs data to the CRT display and records on a flexible disc.

#### C. Input Requirements

- 1) Antenna position in WGS-72 coordinates.
- 2) 1 pps from the station time standard.
- 3) 5 MHz from the station time standard.

With these design requirements, the receiver block diagram in figure 6 was implemented. The following is a description of the major components shown in the diagram.

#### RF Subsystem

The RF subsystem provides carrier and code tracking capabilities for the GPS signal. It demodulates the data message into the non-return to zero (NRZ) format and provides the voltage controlled crystal oscillator (VCXO) frequency for coherent code generation. An external control voltage input to the VCXO is used for acquisition tuning.

#### C/A Code Generator

The C/A code generator accepts the code sequence of any GPS satellite from the microprocessor. It then derives the 1.023 MHz C/A code from the VCXO frequency and outputs it to the RF subsystem for code tracking. A satellite time epoch is derived from the C/A code period and output for the time interval pseudo-range measurement.

#### Time Interval Measurement

A time interval counter is controlled by the microprocessor to measure the time difference between the satellite epoch and the station reference. This measurement occurs once every six seconds as commanded by the microprocessor. The time difference, which is pseudo-range, is output to the microprocessor for determining the time transfer. The time interval counter is also used to determine the VCXO frequency for tuning control.

## I/O Terminal

The receiver contains a CRT display with a keyboard and a dual flexible disc drive recorder. The keyboard provides an operator interface for inputs and control of the receiver. The time transfer results are displayed on the CRT and recorded on the flexible disc.

## Microprocessor

The microprocessor controls hardware functions in the receiver, decodes the navigation message, and calculates the time transfer. Receiver tuning is provided during acquisition by taking frequency measurements of the VCXO, comparing these measurements to predicted values and outputting corrections to the control voltage through a digital-to-analog converter.

The appropriate satellite C/A code is loaded into the code generator after being calculated using a linear feedback shift register algorithm implemented in the microprocessor. The code phase is also controlled by the microprocessor until a correlation or "code lock" is established in the RF subsystem. After signal acquisition, the microprocessor decodes the navigation data and commands pseudo-range measurements to be performed using the time interval counter to calculate the final time transfer result. This result is output to the CRT display and recorded on a flexible disc once every six seconds.

## TIME TRANSFER FIELD TEST

The prototype GPS TTR was installed and tested at NASA's Merrit Island tracking site (MILA) at Kennedy Spaceflight Center, Fla. Figure 7 shows the horizon of the MILA facility and the portion of the orbit of NAVSTAR 5 in view at the MILA site. Figure 8 shows the orbits of all five NAVSTAR satellites along with approximate rise and set times for the period during which the tests were performed. Most of the data was taken during a segment of time when all the satellites passed through a high elevation angle ( $60^{\circ}$  to  $90^{\circ}$ ) with approximately the same azimuth. Figure 9 shows the segments of each orbit where the data collection was concentrated.

Figures 10 through 14 present data collected from individual satellite passes which gives the difference between the MILA station ground clock and the GPS spacecraft clocks. On each graph a calculated time transfer is presented for an epoch close to the mid-time of the observed period. The RMS of a least squared data fit is also given. The RMS of any one pass varies from 11 to 13

nanoseconds for a given satellite. Figure 15 is an extended track (two hour) of a NAVSTAR 6 pass and also shows an RMS of 13 nanoseconds. NAVSTAR 1 has a quartz crystal oscillator, NAVSTAR 3 and 4 have rubidium oscillators, while NAVSTAR 5 and 6 have cesium oscillators.

Figure 16 summarizes the results relating the MILA clock to the USNO clock as determined through GPS, LORAN-C and portable clock measurements performed during the test. The GPS results are presented as single points which are the average of the five satellite values. The bar over each point represents the range of the five values. The GPS results show peak-to-peak agreement of 200 ns or less with the portable clock measurements which are considered to be truth. During Phase I of the NAVSTAR GPS program, no attempt is being made to precisely synchronize the satellites. In Phase III of the program, it is planned to maintain satellite synchronization to within 100 nsec.

Figures 17 through 20 present results using only the data taken from NAVSTAR 1, which uses a crystal oscillator, and NAVSTAR 5, which uses a cesium oscillator. Figures 17 and 19 show the MILA station clock relative to GPS time as determined by the data from each satellite. Each point is the result of a linear least squares fit to approximately 20 minutes of data from an individual satellite pass. When another linear fit is performed on this day-to-day data, the results show that the time transfers have an RMS of 25 nsec and 24 nsec for NAVSTAR 1 and NAVSTAR 5 respectively. Figures 18 and 20 show the same satellite data referenced to USNO through published differences of GPS time and USNO time as determined by a GPS receiver at the Naval Observatory. The time transfer results again show an RMS of 25 nsec and 24 nsec. This result is within the expected noise of a single cesium to which all the data is referenced at the MILA ground station.

## CONCLUSIONS

Figure 21 presents a comparison of the resulting time transfer RMS of all the GPS satellites during the test. When data is considered on a single satellite basis, the results always yield a time transfer with better than a 100 nsec accuracy. No ionospheric corrections have been made to obtain these results, and tests are planned in the future to determine how much error this contributes. Also, it was determined that the receiver has small biases that are frequency dependent. Improvements are being made in the receiver to account for these biases, and it is expected that follow-on tests will demonstrate even better accuracies.



## FUTURE PLANS

Increased receiver performance and capabilities development is continuing based on results and operational feedback from field tests and on-going experiments. Extensive evaluation of the receiver is planned through several additional field tests. A joint experiment is scheduled with the Jet Propulsion Laboratory (JPL) to evaluate ionospheric delay error. Co-location tests are planned to compare nanosecond accuracy VLBI data with GPS TTR data. The co-location tests will involve VLBI stations at NRL Maryland Point, Haystack/Westford Observatory, NASA Deep Space Network (DSN), Goldstone, CA., and NASA DSN, Madrid, Spain. Future activities also include joint participation by GSFC, USNO, NBS, and NRL in the European Space Agency (ESA) SIRIO/LASSO time transfer experiment during 1982. This experiment will use a global baseline and will provide nanosecond accurate laser time transfers for comparison with the GPS time transfers.

The first operational field test of the GPS TTR is scheduled in the second quarter of fiscal year (FY) 1982 with the deployment of the NASA GSFC Transportable Laser Ranging System (TLRS) prototype to Easter Island. Four additional receivers are scheduled to be deployed with mobile laser systems later in FY 1982.

## REFERENCES

1. L. Raymond, O. J. Oaks, J. Osbone, G. Whitworth, J. Buisson, P. Landis, C. Wardrip, and J. Perry, "Navigation Technology Satellite (NTS) Low Cost Timing Receiver," Goddard Space Flight Center Report X-814-77-205, Aug. 1977.
2. J. A. Buisson, T. B. McCaskill and O. J. Oaks, "Initial Design for Navigation Technology Satellite Time Transfer Receiver (NTS/TTR)," NRL Report 8312, 16 May 1979.
3. J. Buisson, T. McCaskill, J. Oaks, D. Lynch, C. Wardrip, and G. Whitworth, "Submicrosecond Comparisons of Time Standards via the Navigation Technology Satellites (NTS)," Proc. PTII, Nov. 1978, pp 601-627.
4. B. W. Parkinson, "NAVSTAR Global Positioning System (GPS)," National Telecommunications Conference, Conference Record, Vol. iii, 1976, pp 41.1-1 to 41.1-5.
5. J. A. Buisson, R. L. Easton, and T. B. McCaskill, "Initial Results of the NAVSTAR GPS NTS-2 Satellite," NRL Report 8232,

May 25, 1978.

6. R. L. Easton, J. A. Buisson, T. B. McCaskill, O. J. Oaks, S. Stebbins, and M. Jeffries, "The Contribution of Navigation Technology Satellites to the Global Positioning System," NRL Report 8360, Dec. 28, 1979.
7. J. A. Buisson and T. B. McCaskill, "TIMATION Navigation Satellite System Constellation Study," NRL Report 7389, June 27, 1972.
8. S. S. Russell and J. H. Schaibly, "Control Segment and User Performance," J. Inst. Navigation 25(2), Summer 1978, pp. 166-172.
9. J. J. Spilker, "GPS Signal Structure and Performance Characteristics," J. Inst. Navigation, 25(2), Summer 1978, pp. 121-146.
10. A. Dierendock, S. Russell, E. Kipitzke, and M. Birnbaum, "The GPS Navigation Message." J. Inst. Navigation, 25(2), Summer 1978, pp. 147-165.

MOBLAS 3 VS. USNO JUL 1980 thru JUN 1981

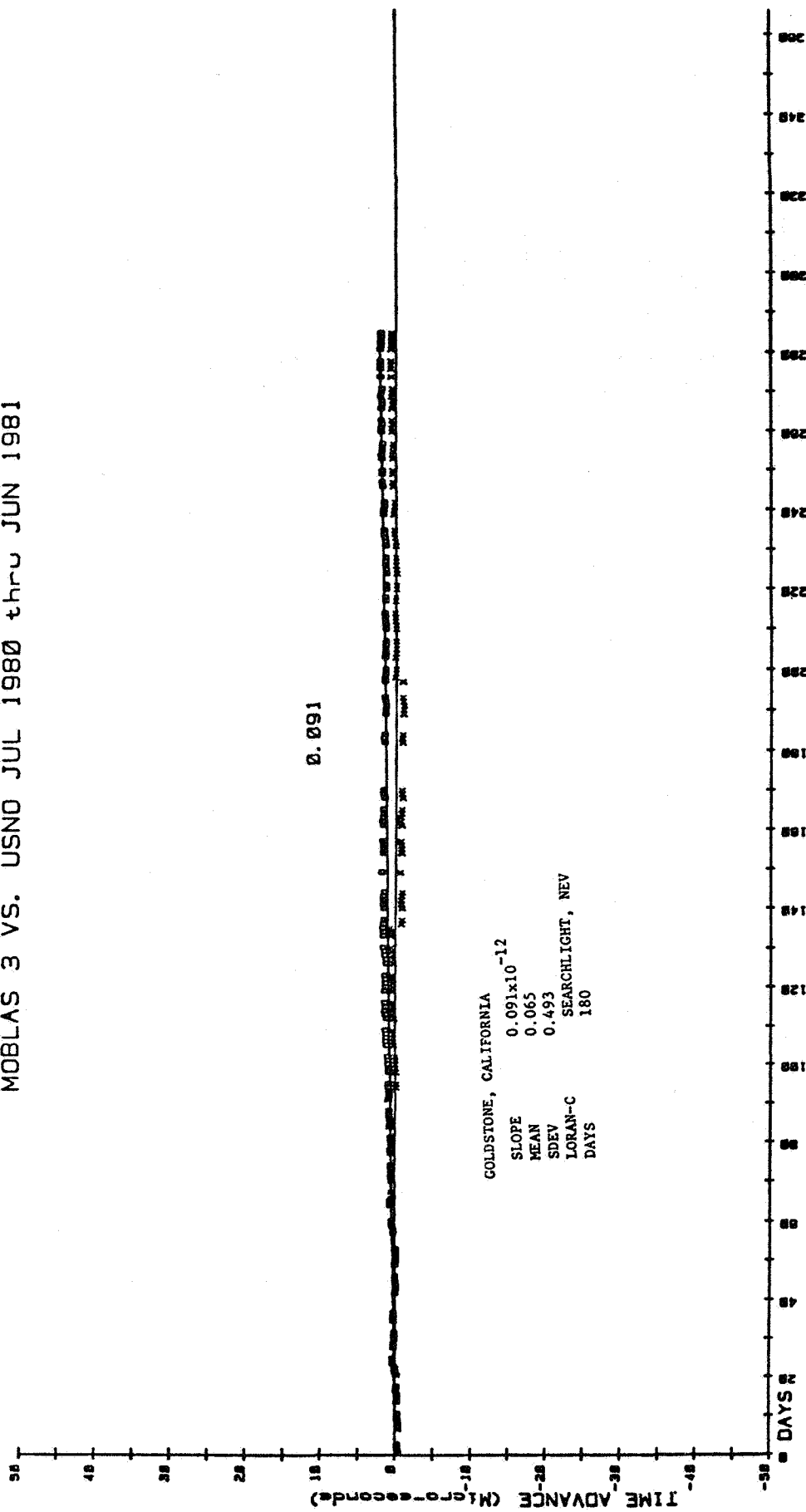


Figure 1

# MOBLAS 5 VS. USNO JUL 1980 thru JUN 1981

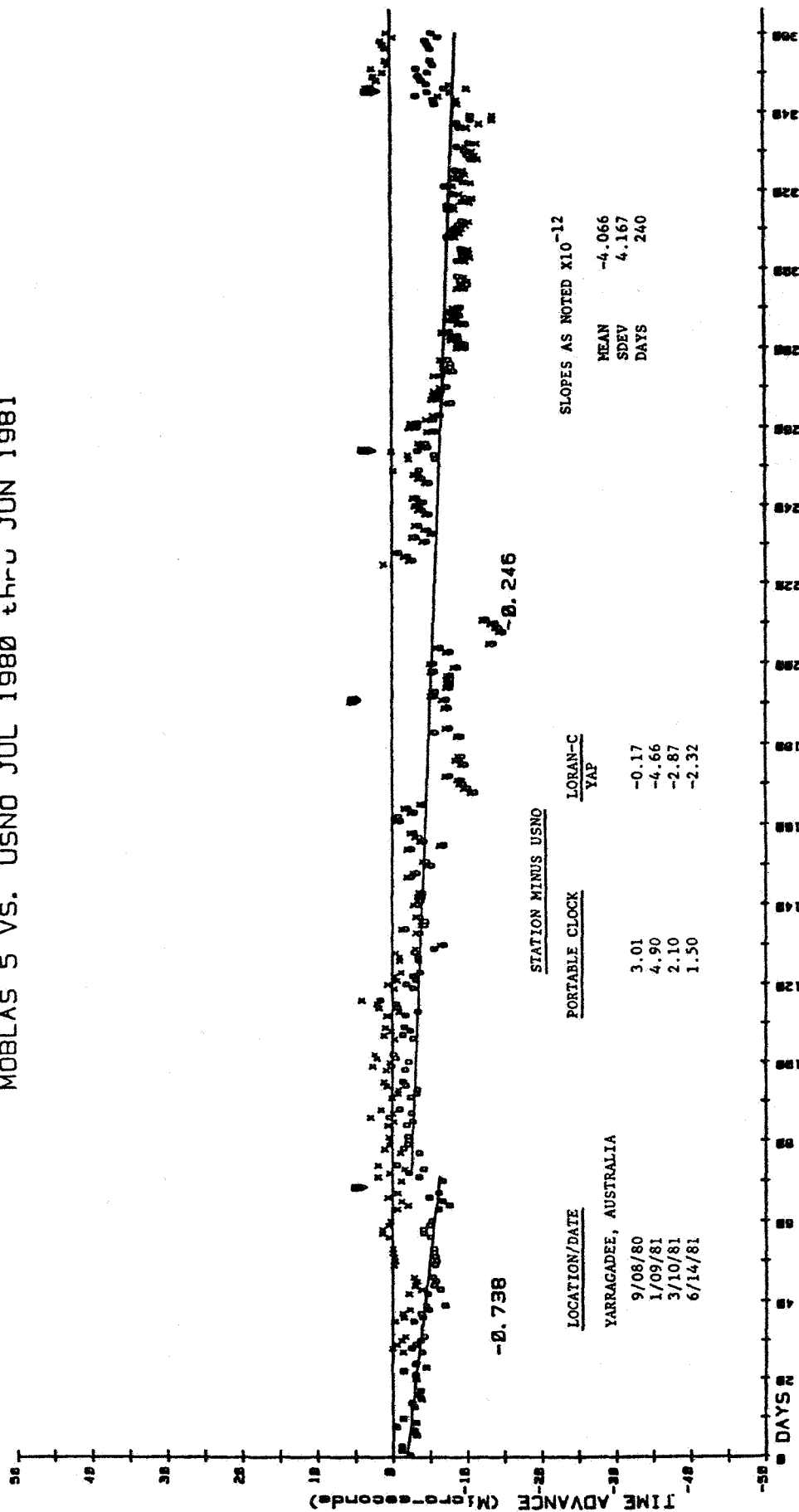


Figure 2

# NASA-GSFC LASER TRACKING SITES 1980 - 1986

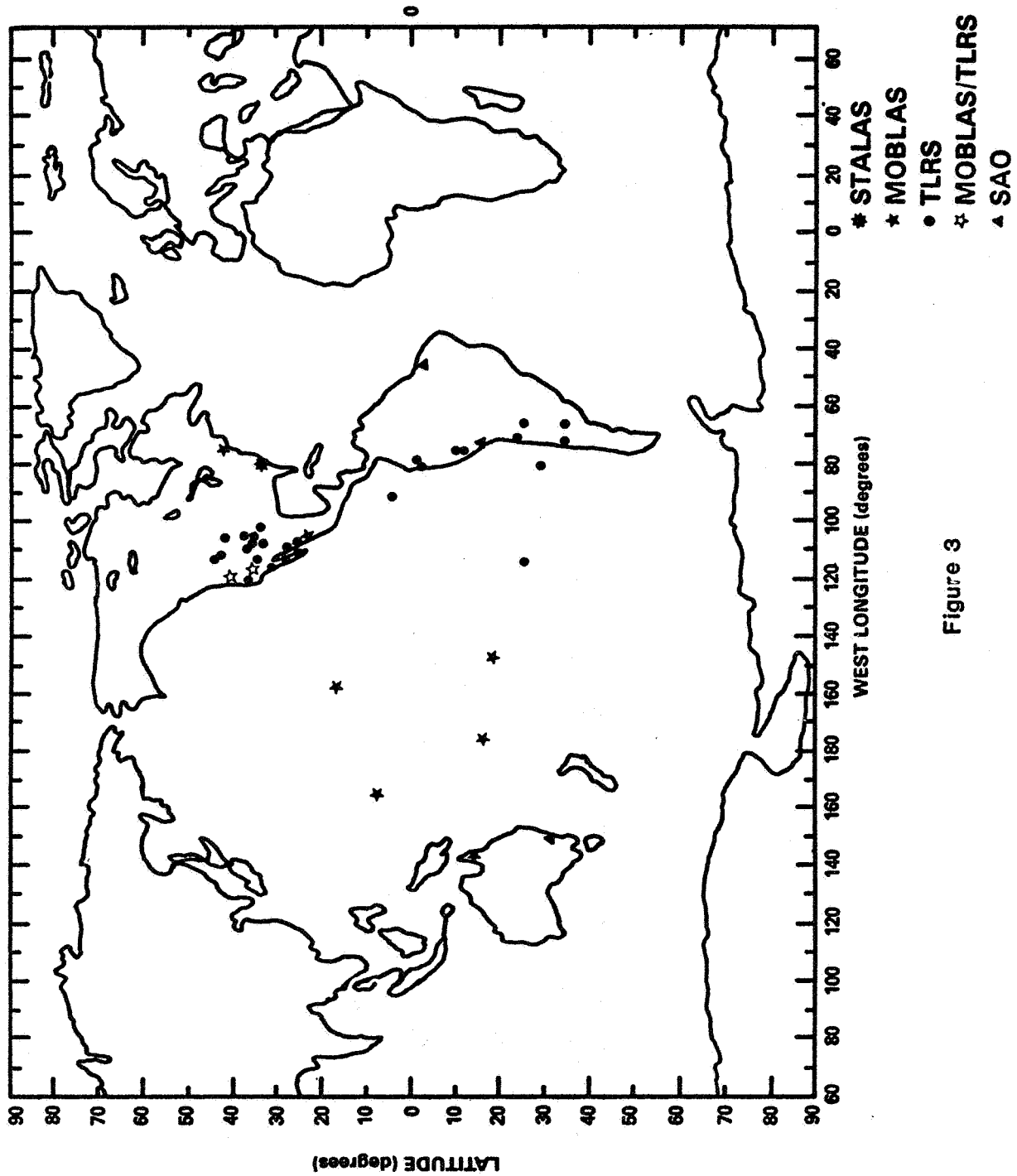
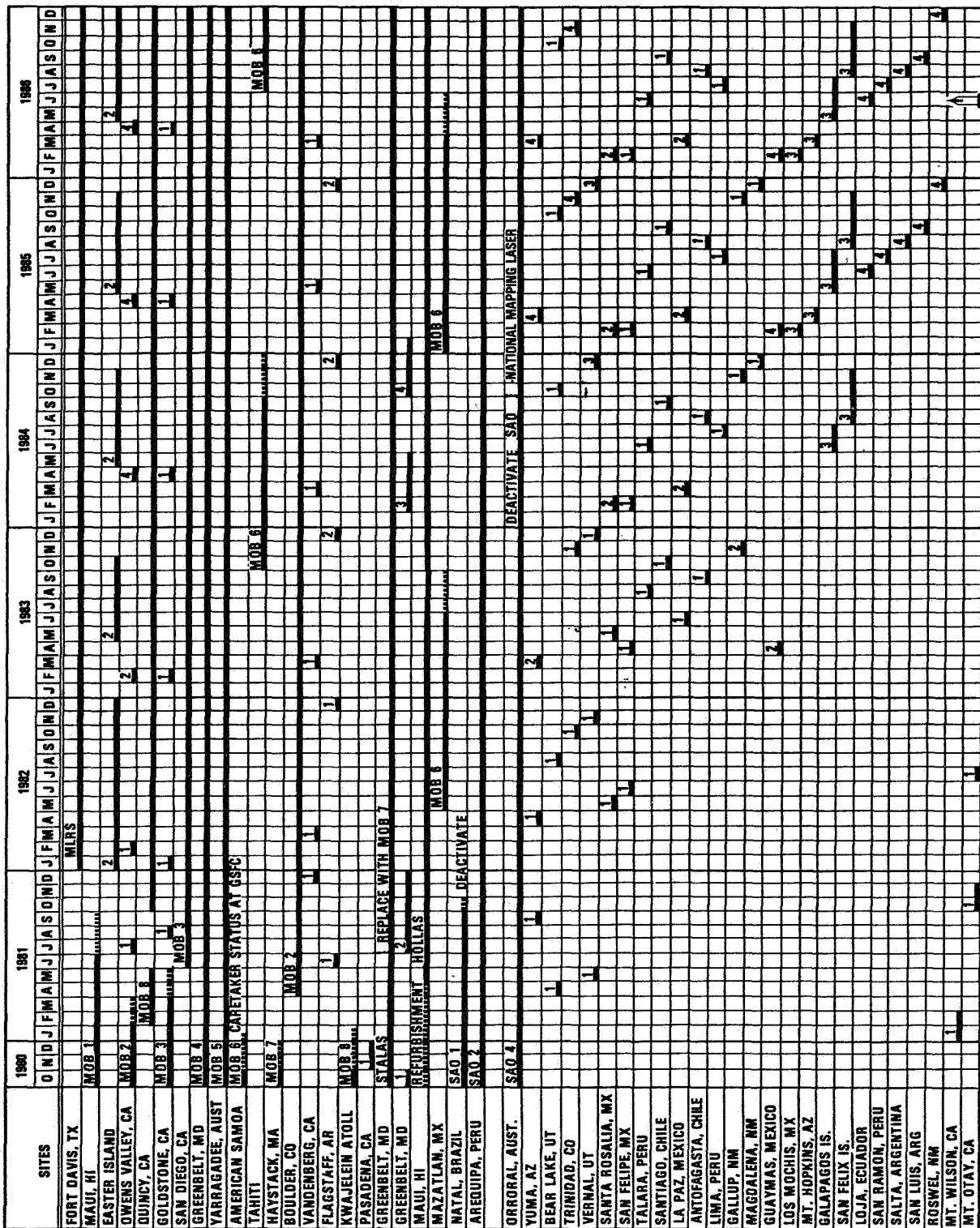


Figure 3

# TENTATIVE LASER DEPLOYMENT SCHEDULE



NOTES: ——— OPERATIONAL ..... PACKING, SHIPPING, SET-UP, CHECKOUT ▲ TLRS-1 ▲ TLRS-2 ▲ TLRS-3 ▲ TLRS-4  
 TLRS-TRANSPORTABLE LASER RANGING SYSTEM

*Robert D. Coates*  
 CRUSTAL DYNAMICS PROJECT MANAGER

*Andrew Odellman*  
 LASER PROJECT MANAGER

*Stacy St. White*  
 LASER NETWORK MANAGER

Figure 4

# NAVSTAR GPS STATION SYNCHRONIZATION BY TIME TRANSFER

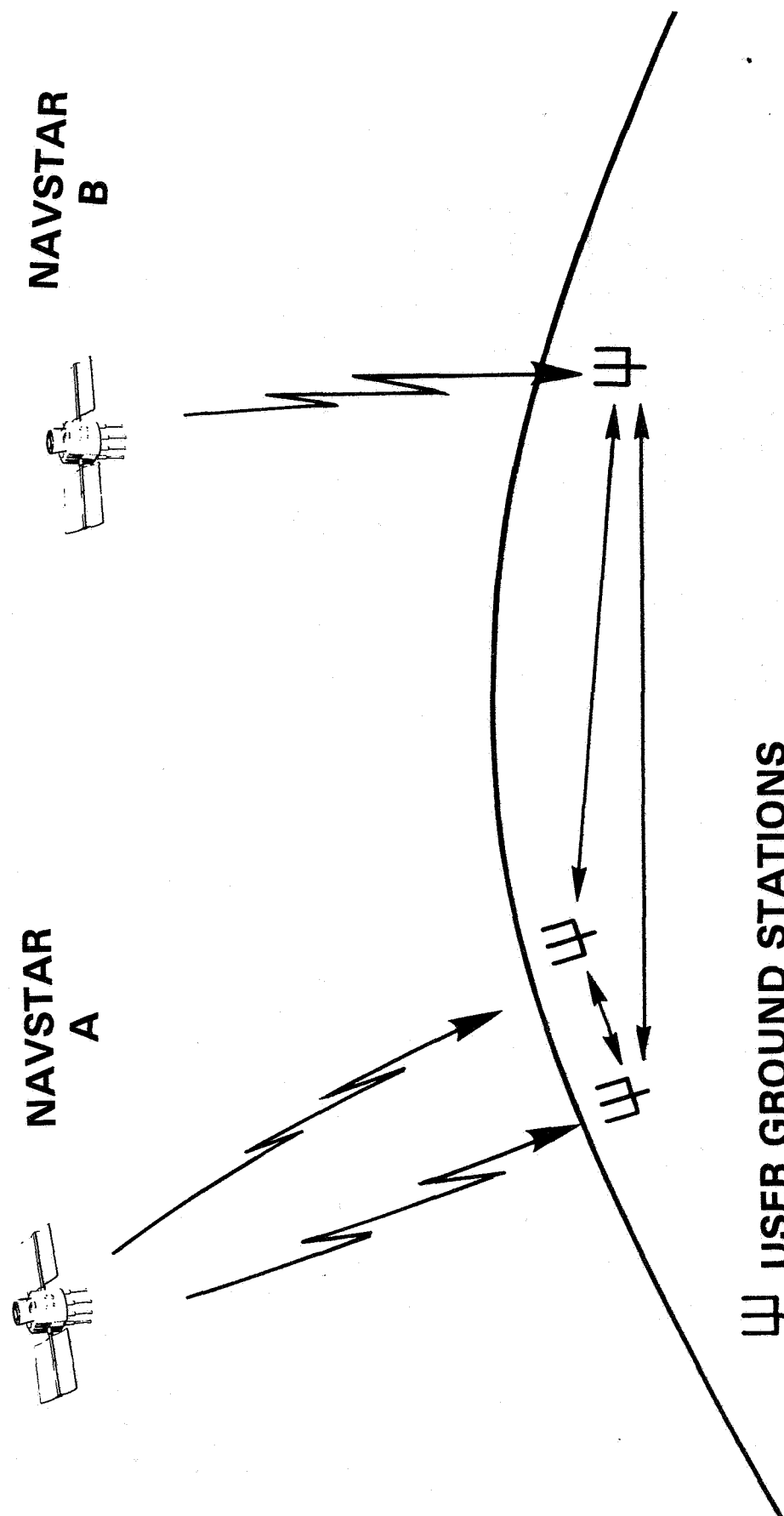
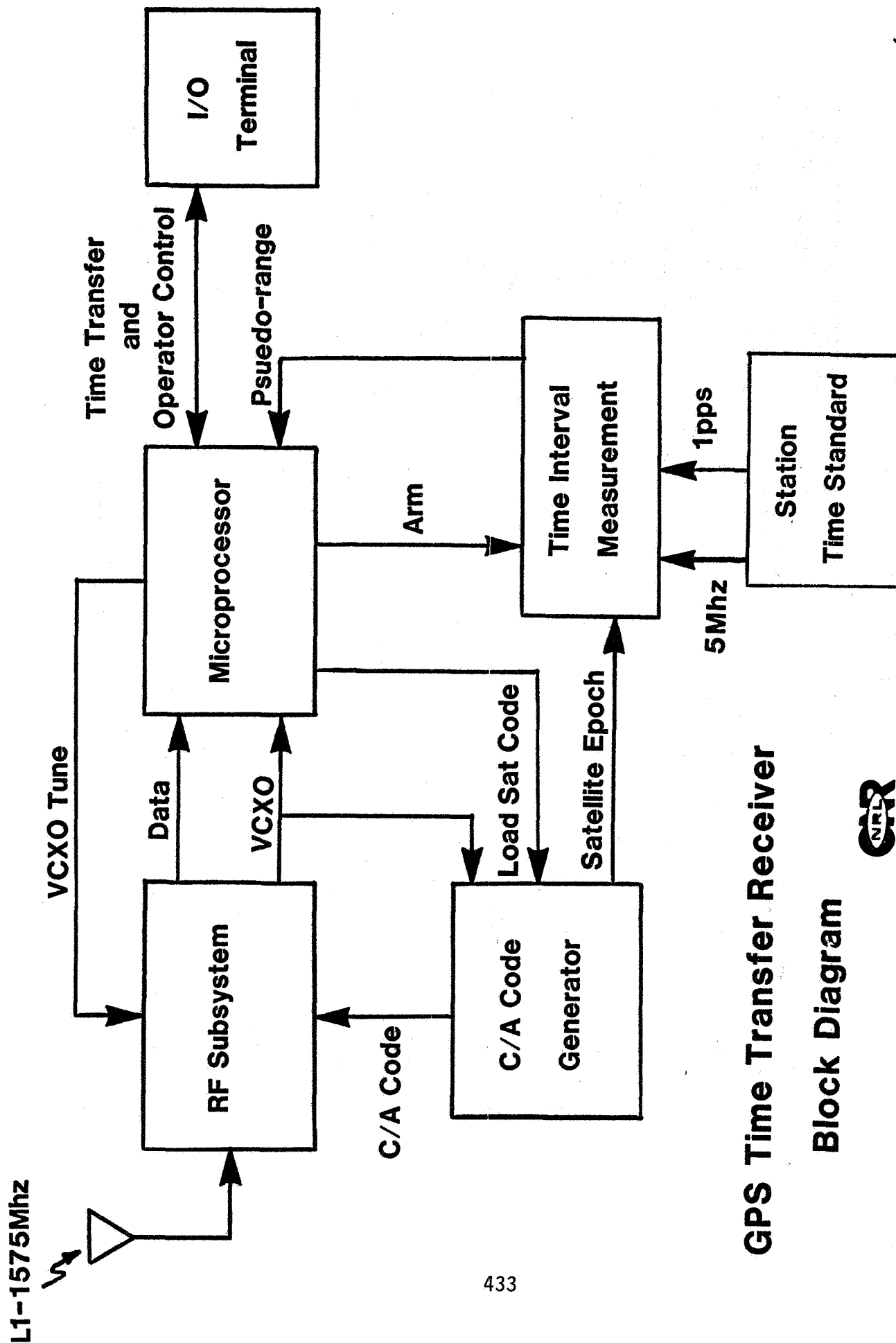


Figure 5



**GPS Time Transfer Receiver  
Block Diagram**



Figure 6



# GPS NAVSTAR MILA GROUND TRACK

(6/15/81)

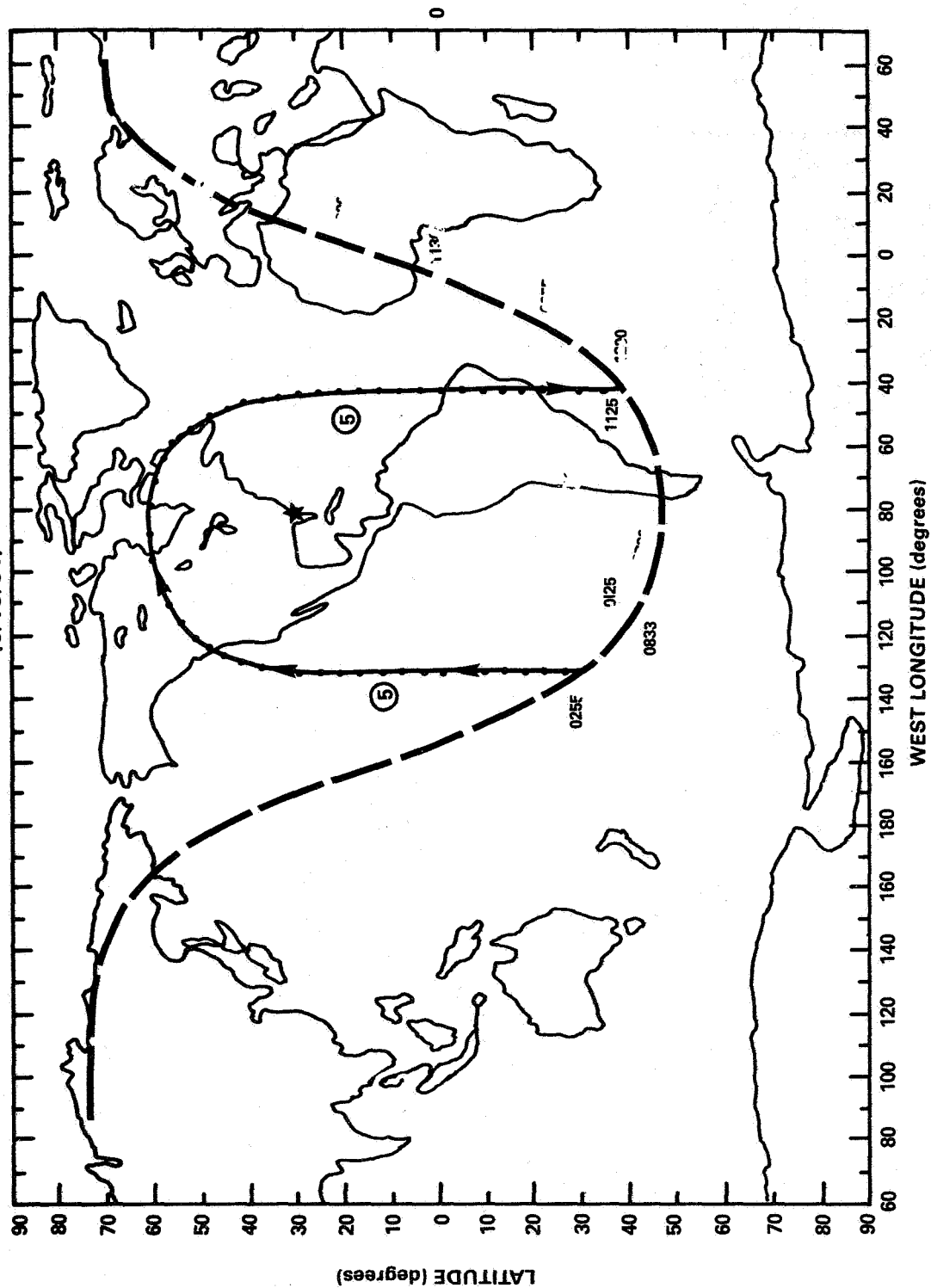


Figure 7

# GPS NAVSTAR MILA GROUND TRACK

(6/15/81)

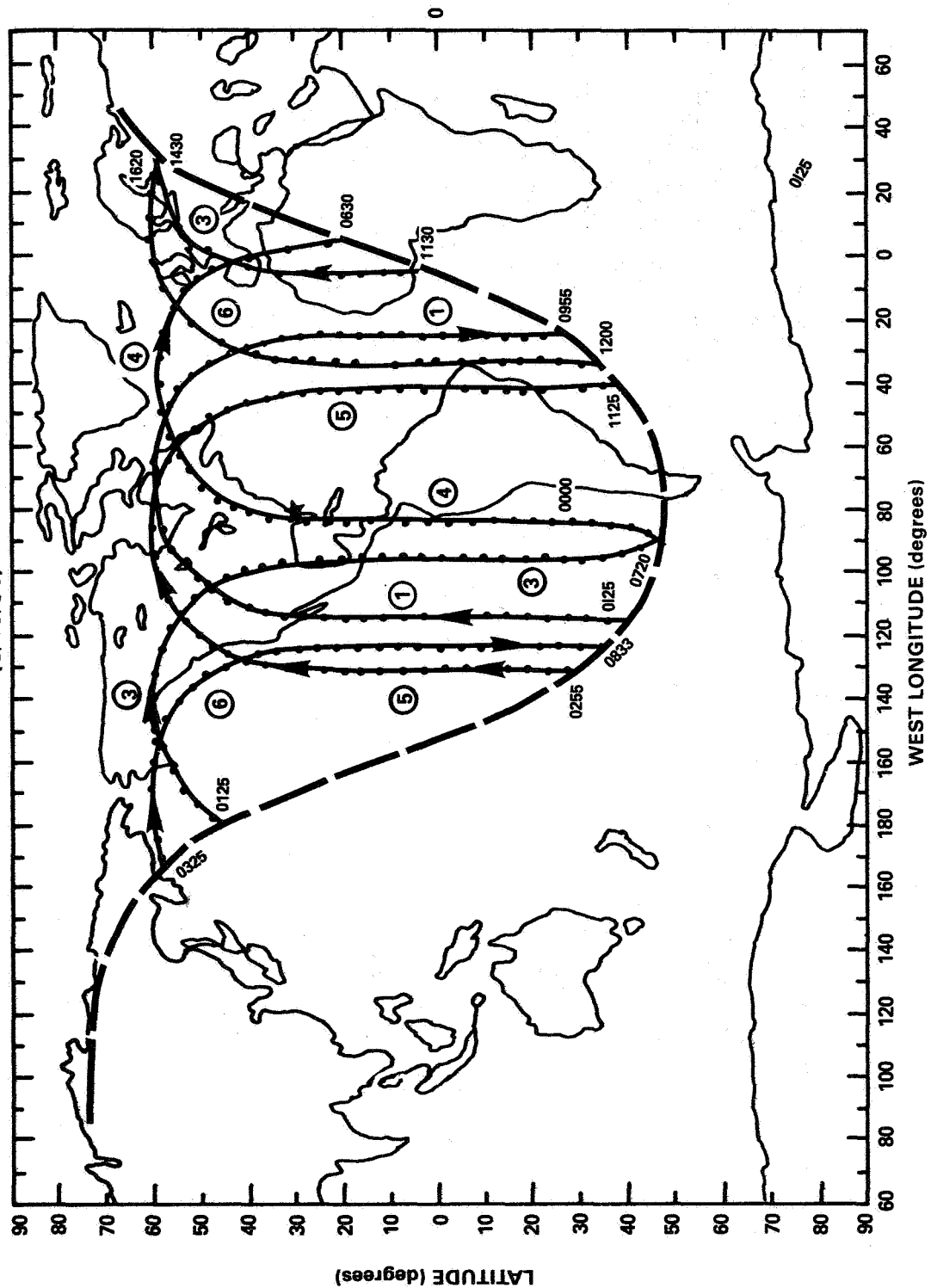


Figure 8

# GPS NAVSTAR MILA GROUND TRACK

(6/15/81)

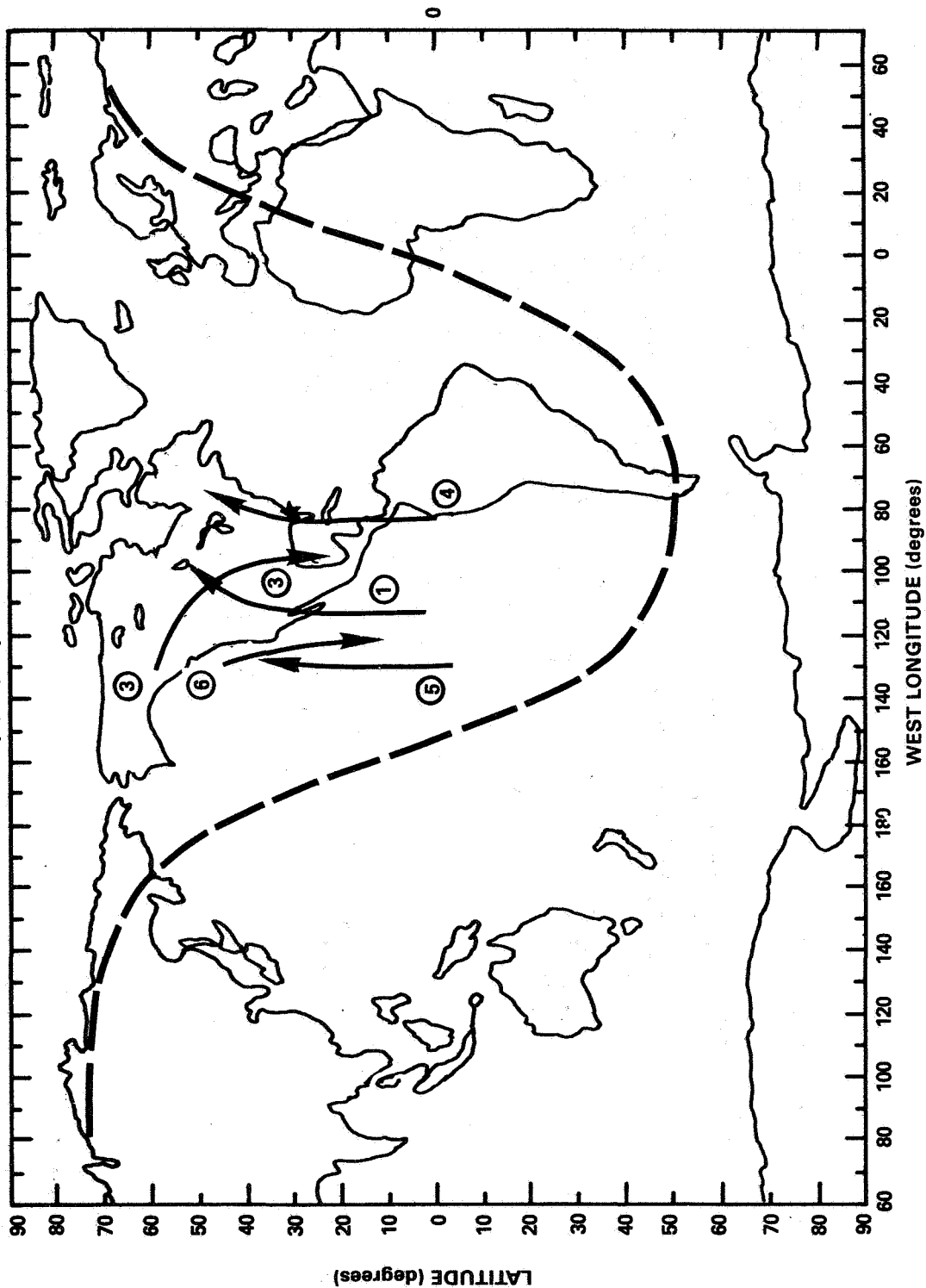
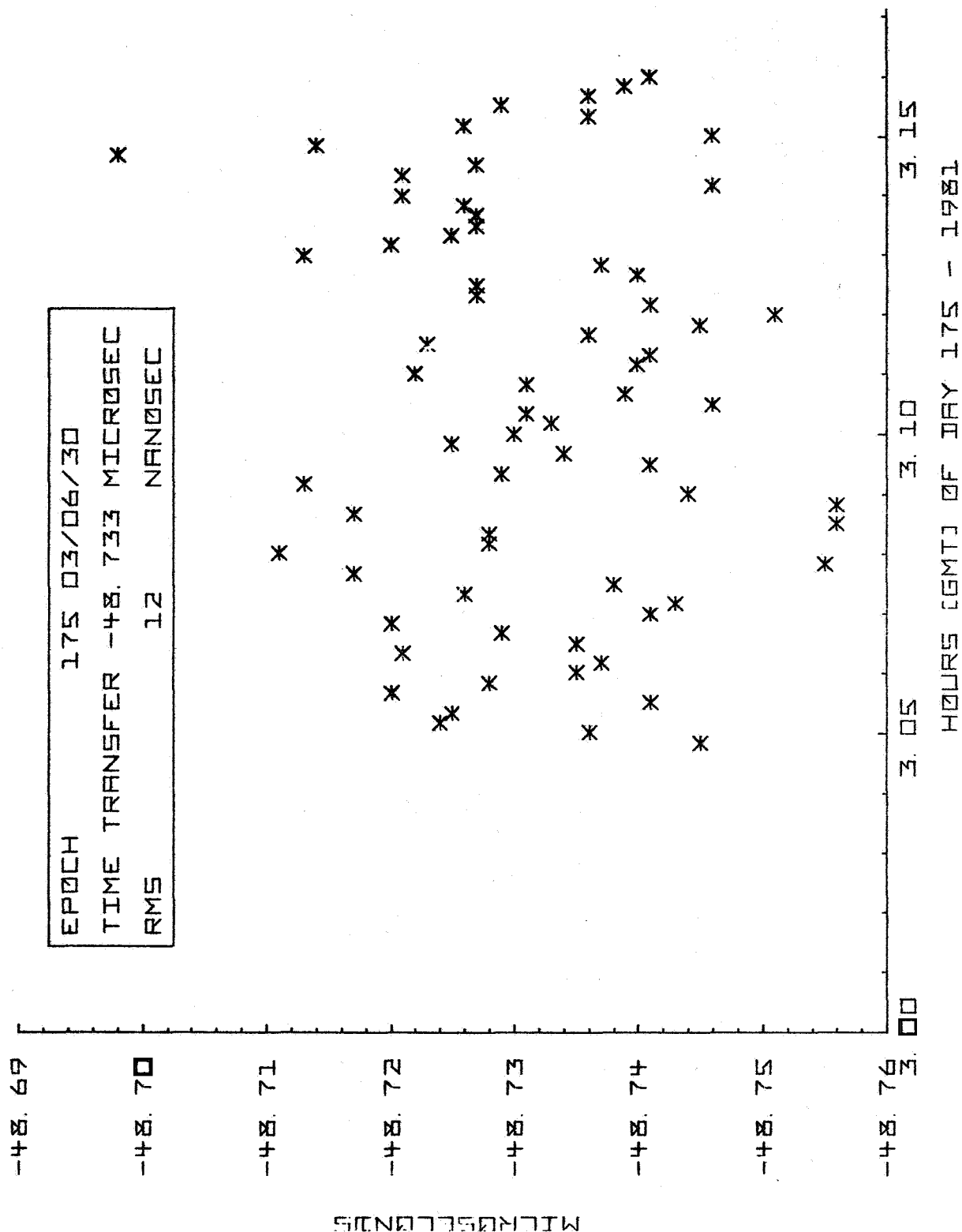


Figure 9

# MILA MINUS GPS VIA NAVSTAR 3



# MILA MINUS GPS VIA NAVSTAR 1

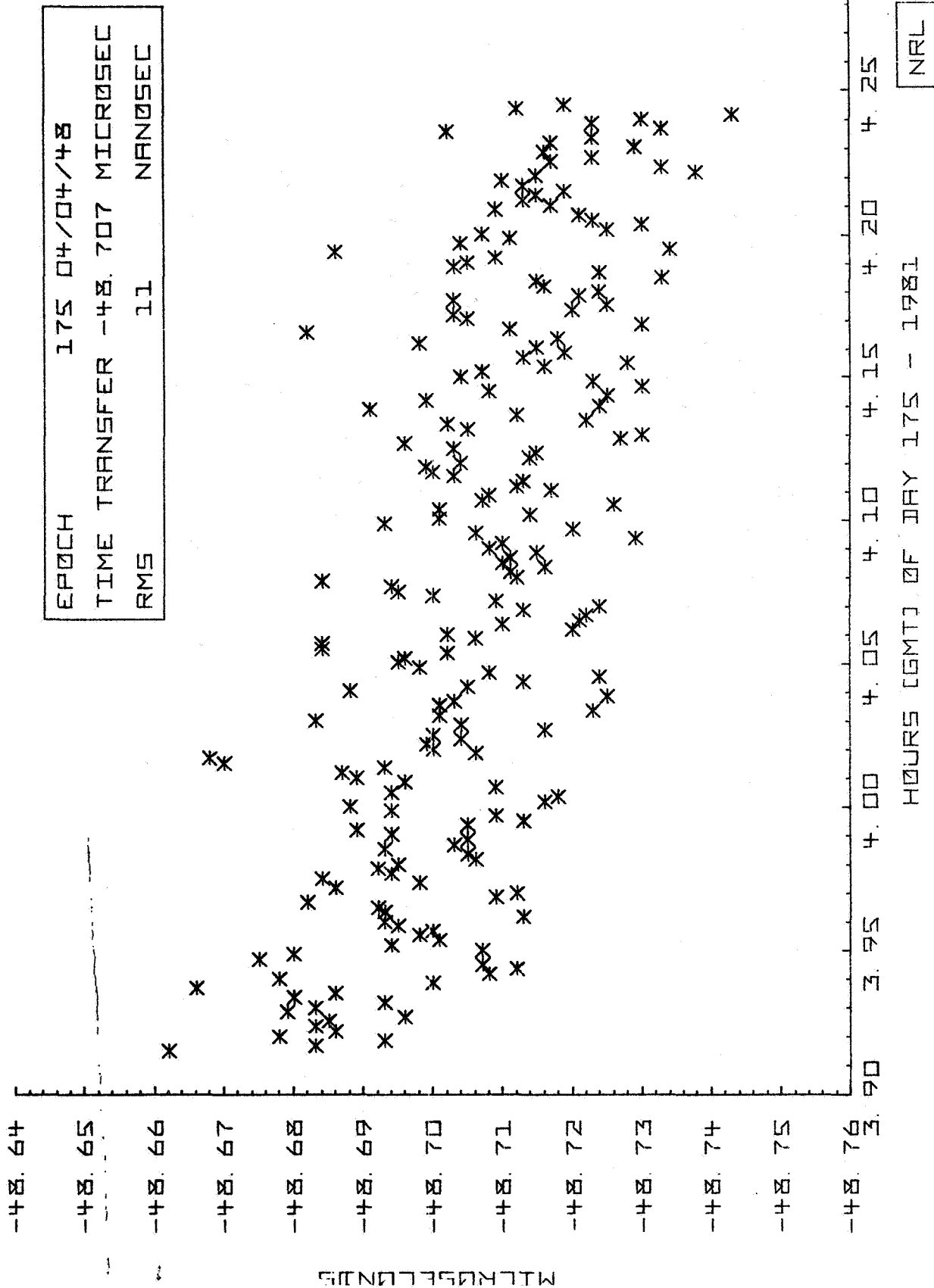


Figure 10

# MILA MINUS GPS VIA NAVSTAR 4

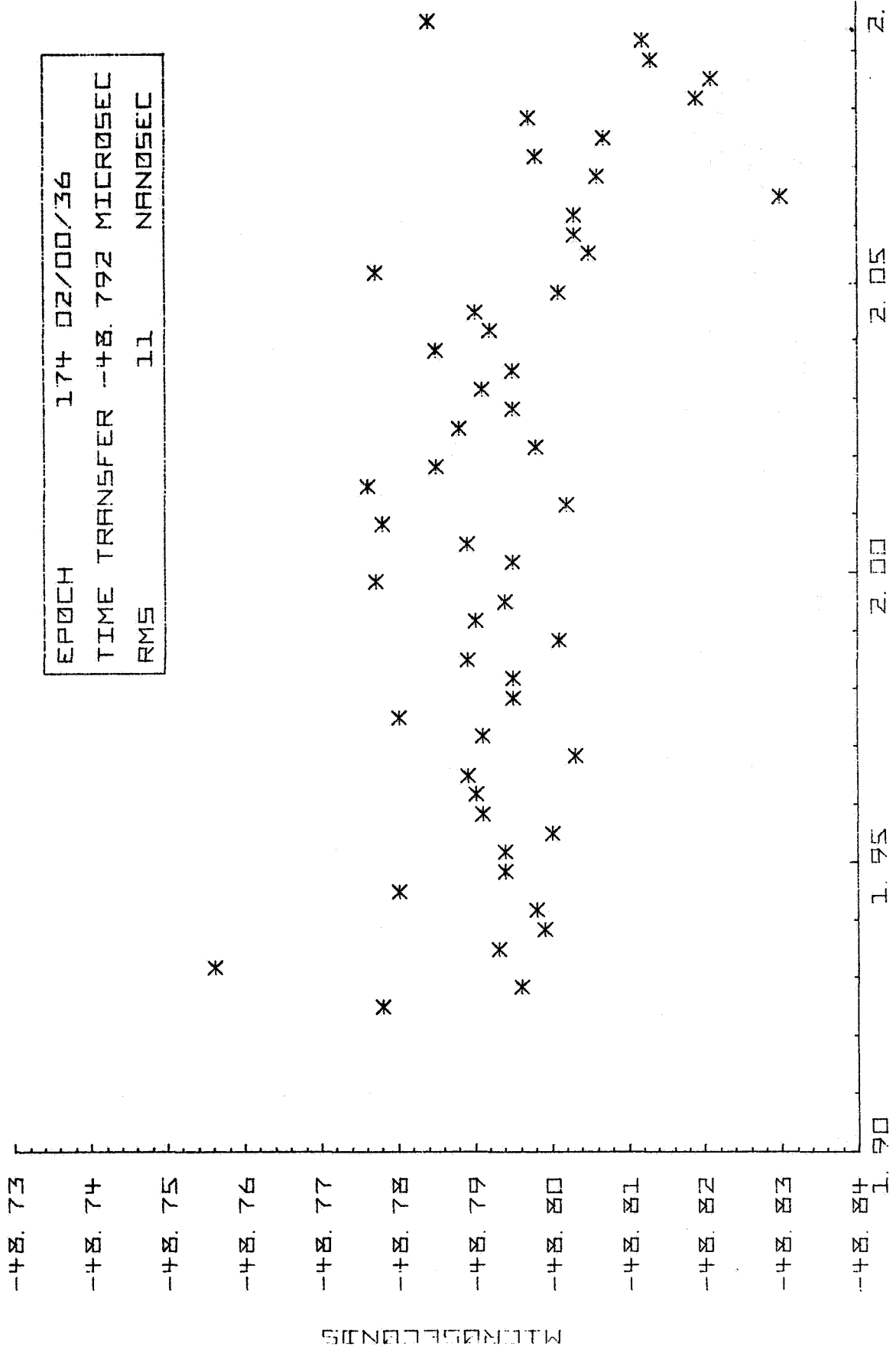
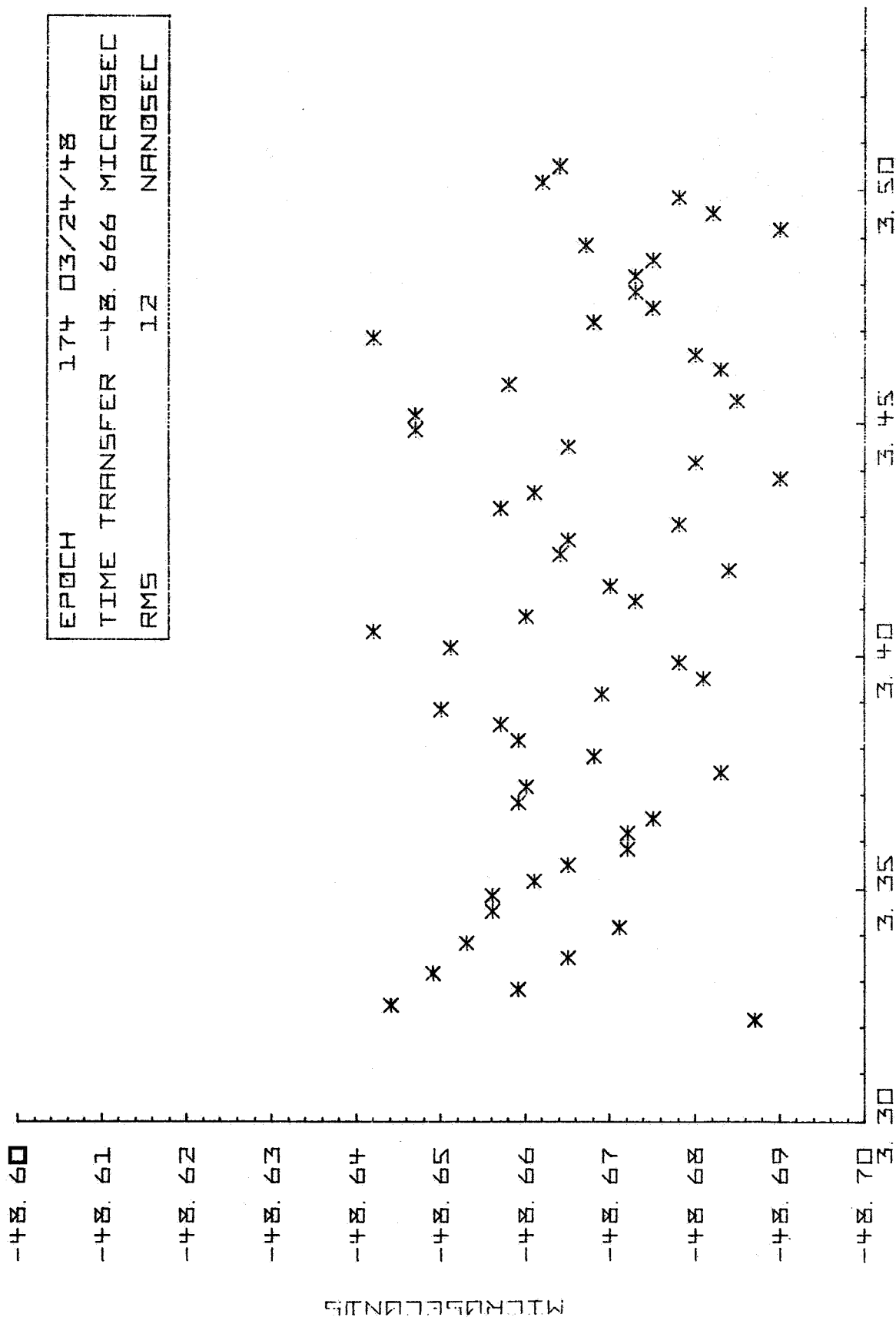


Figure 12

NRL

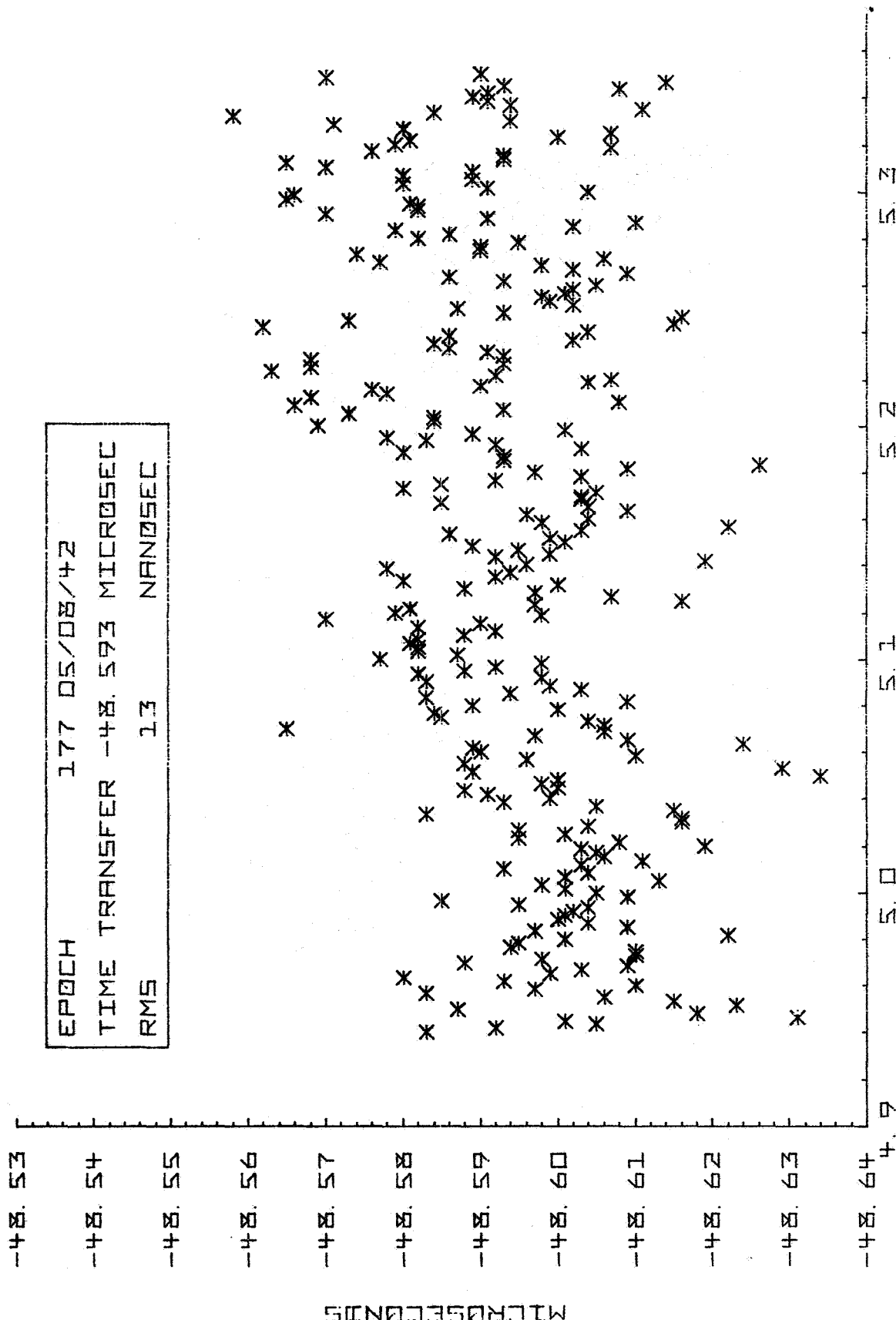
# MILA MINUS GPS VIA NAVSTAR S



NRL

Figure 13

# MILA MINUS GPS VIA NAVSTAR 6

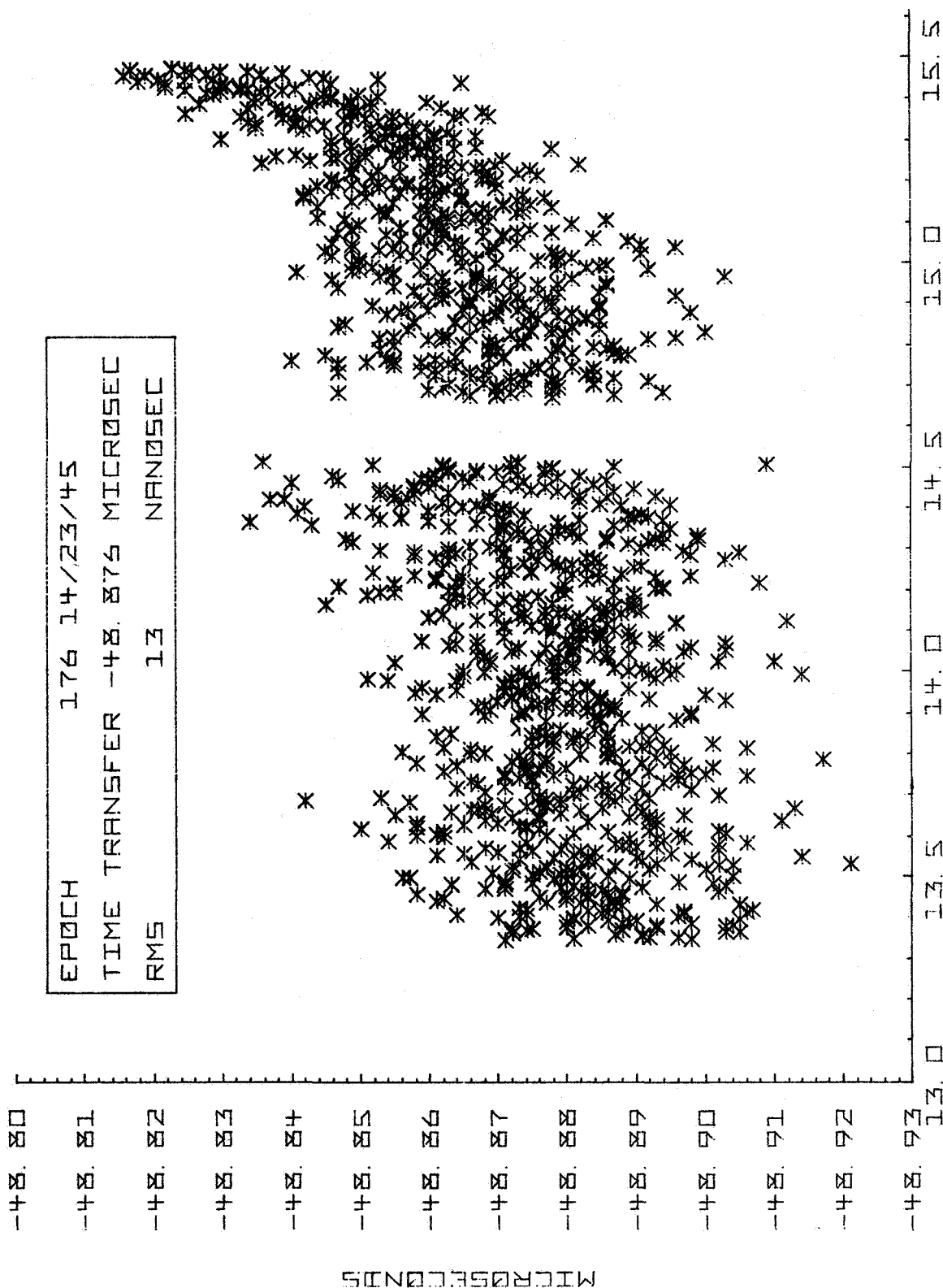


NRL

Figure 14



# MILA MINUS GPS VIA NAVSTAR 6



HOURS [GMT] OF DAY 176 - 1981

Figure 15

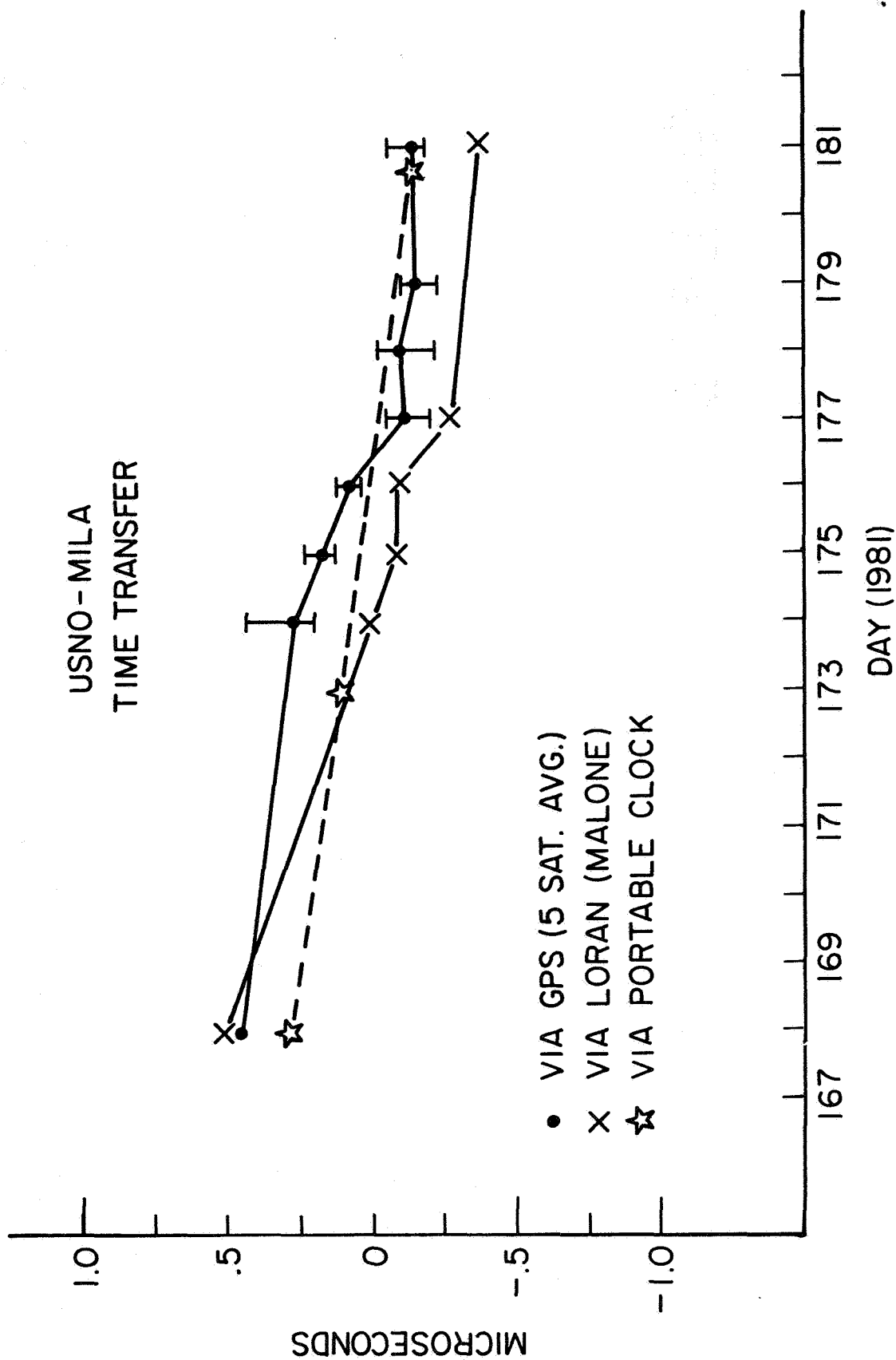


Figure 16

# MILIA MINUS GPS VIA NAVSTAR I

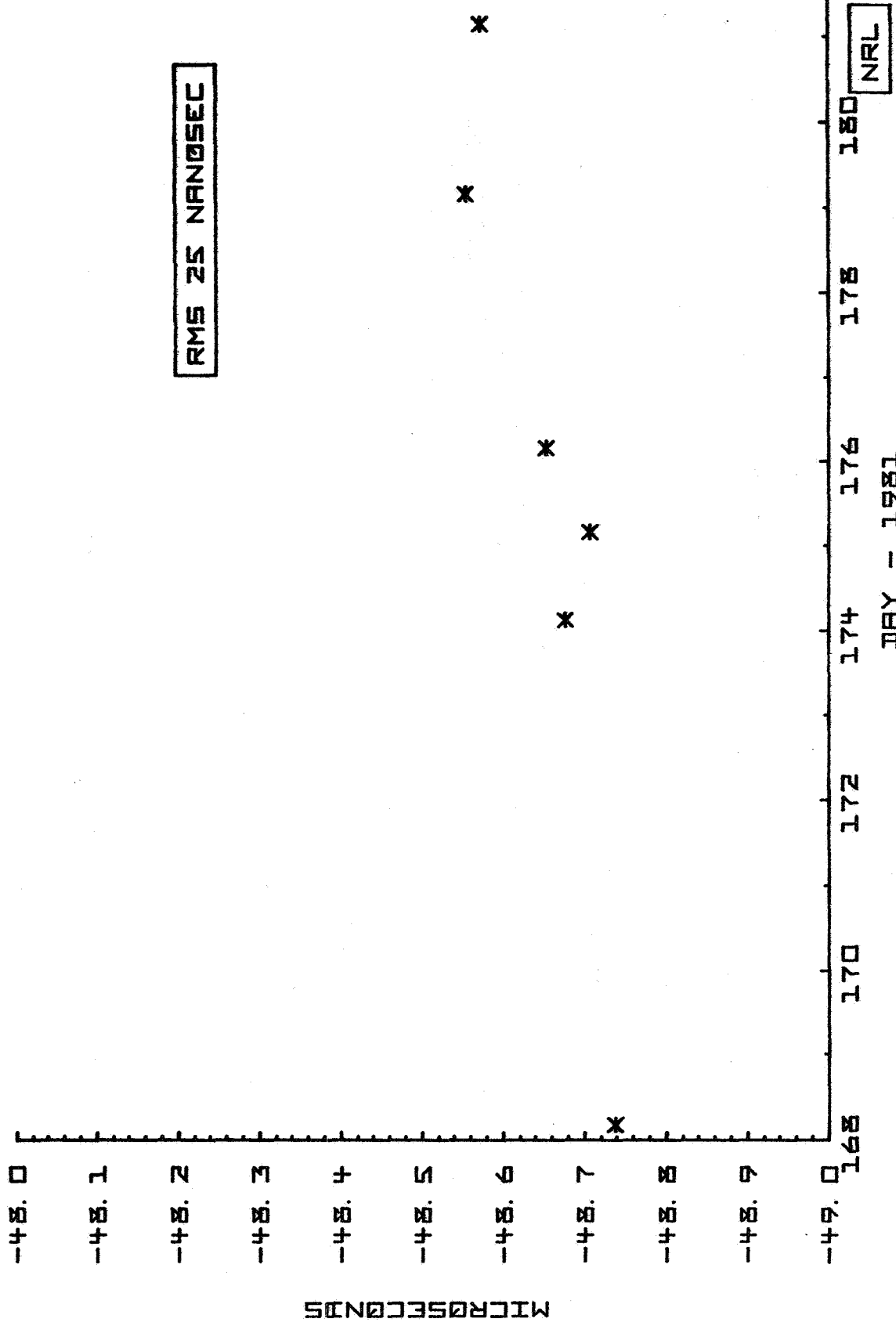


Figure 17

# USNO MINUS MILA VIA NAVSTAR 1

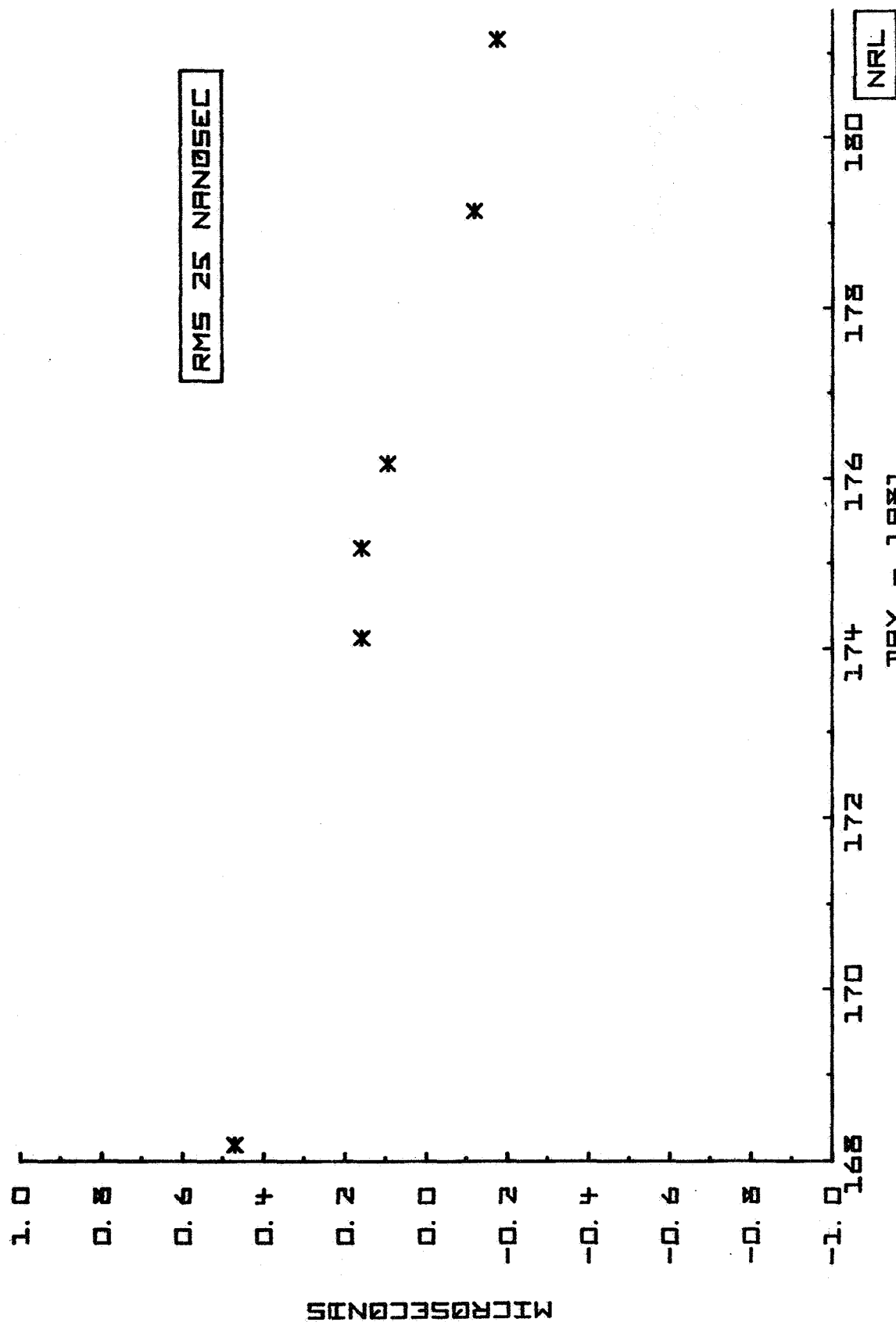


Figure 18

MILA MINUS GPS  
VIA NAVSTAR

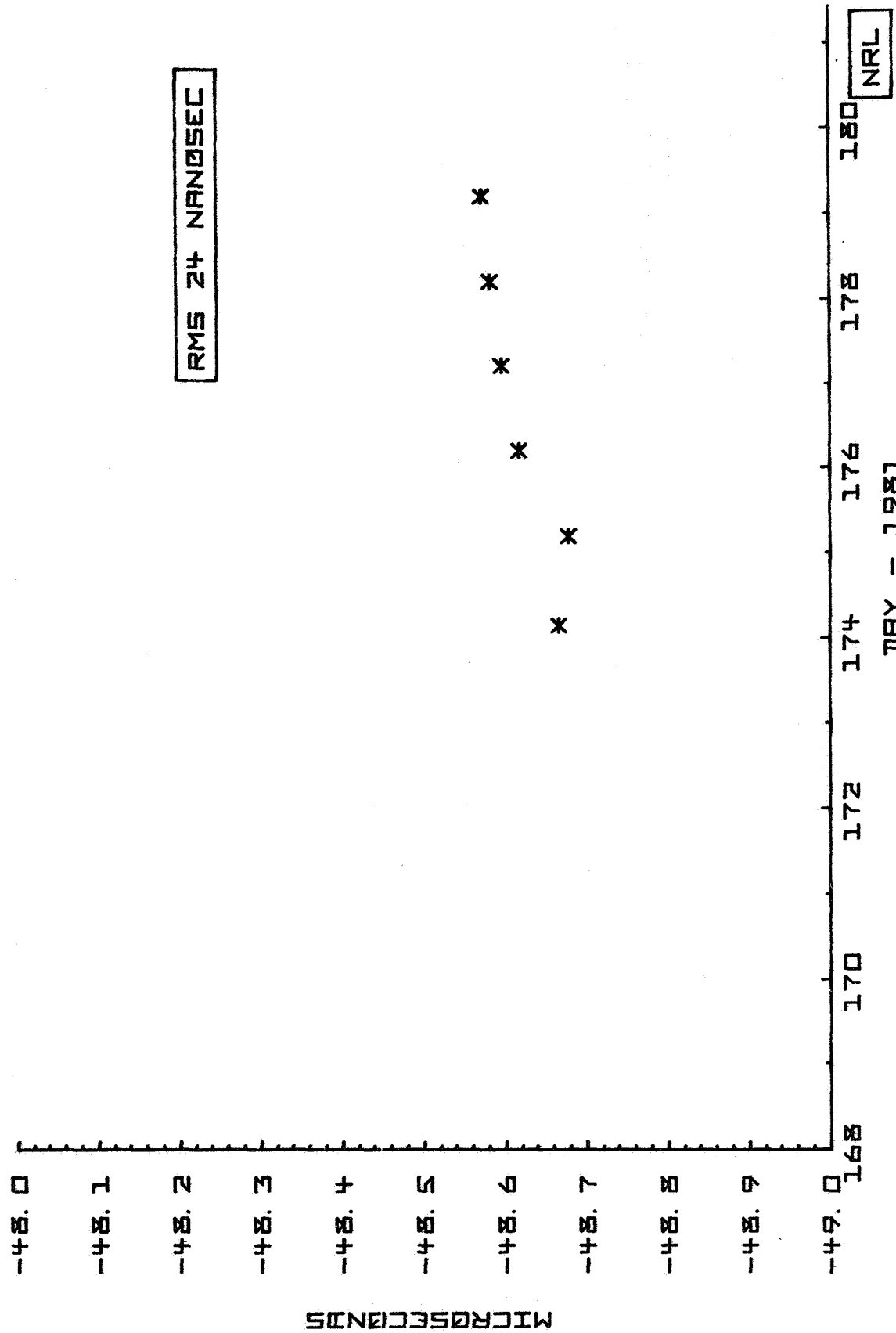


Figure 19

USNO MINUS MILA  
VIA NAVSTAR S

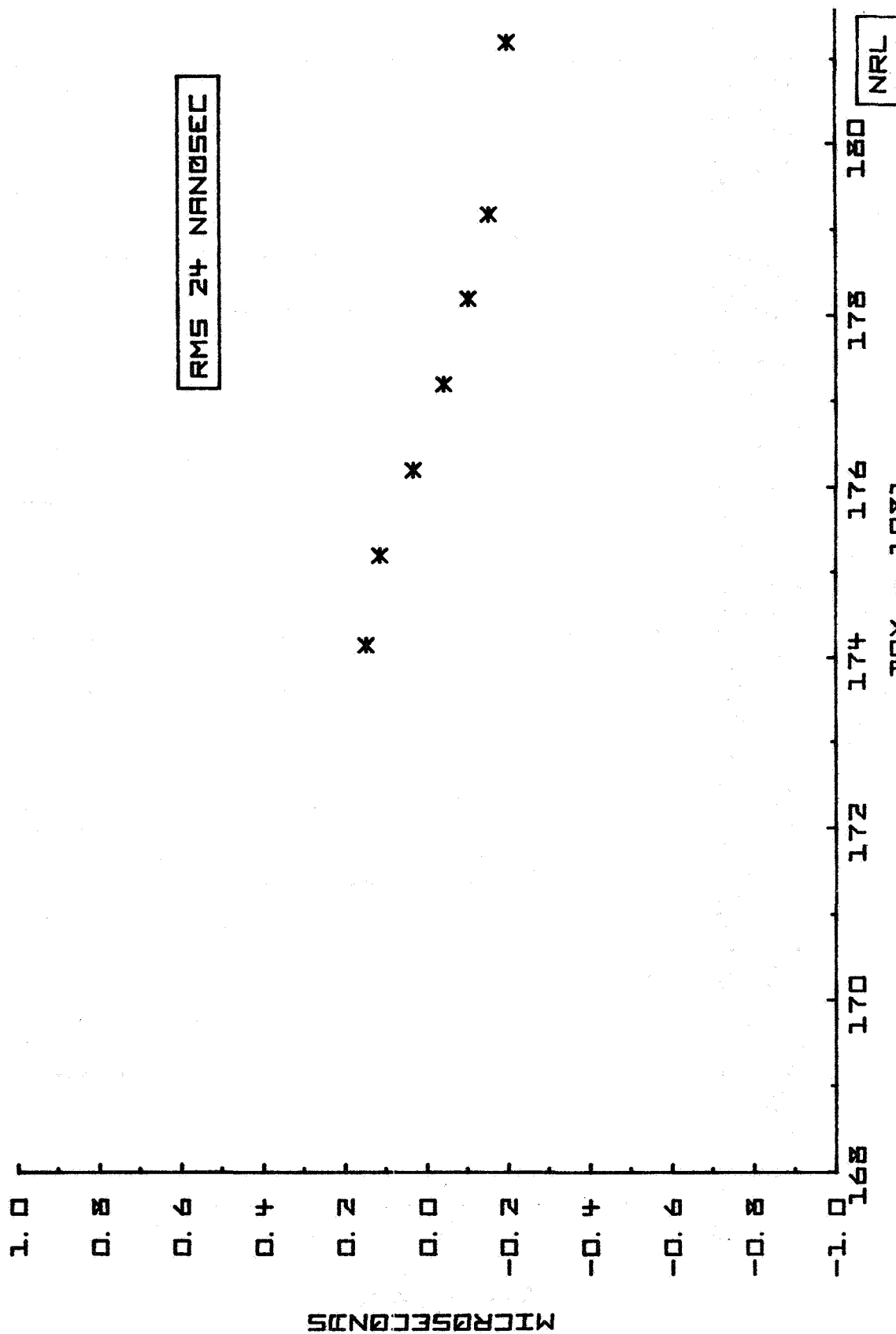
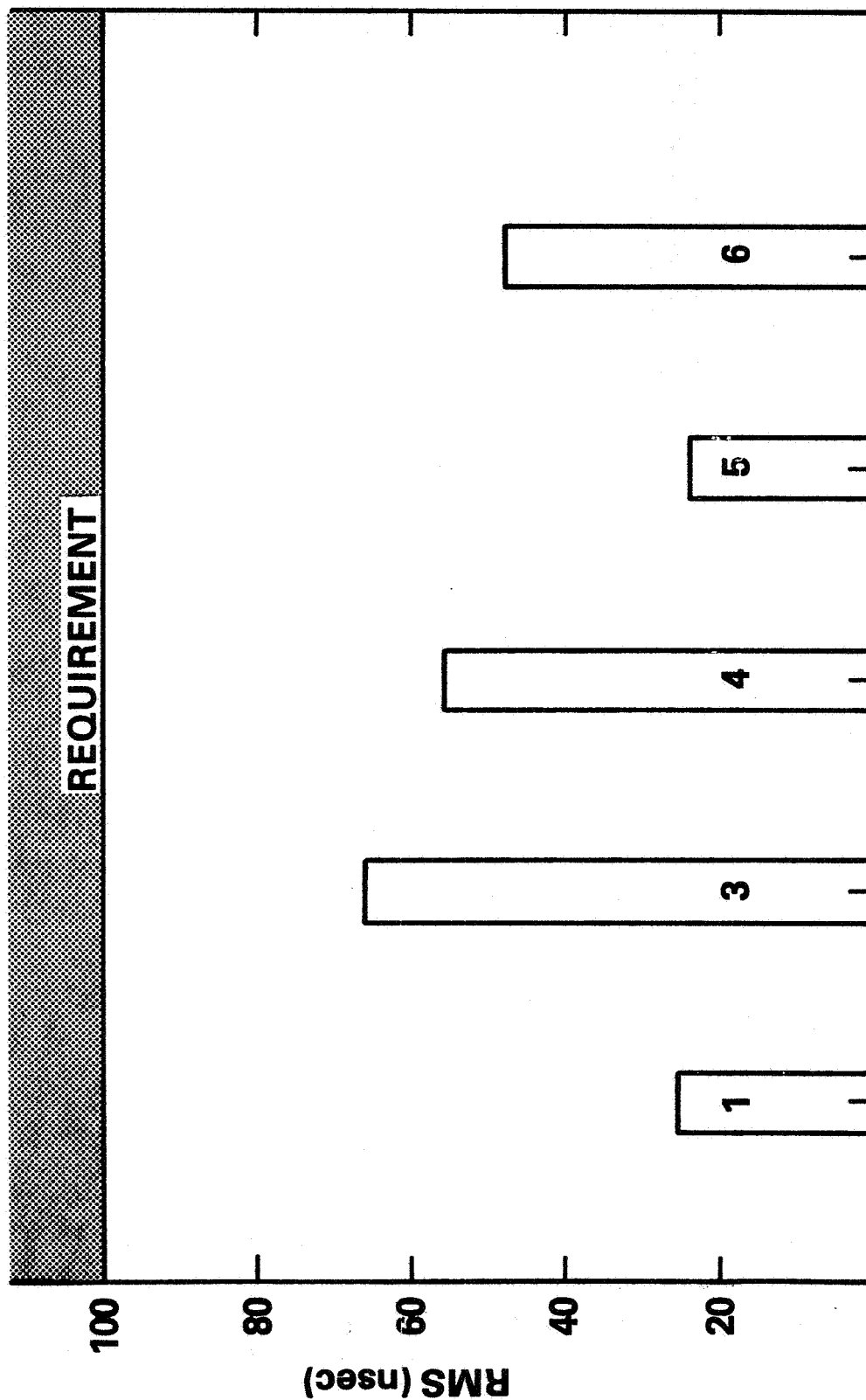


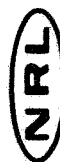
Figure 20

# TIME TRANSFER RMS OF USNO-MILA



GPS NAVSTAR NUMBER

Figure 21



## QUESTIONS AND ANSWERS

MR. ALLAN:

I might make one comment. In regard to the same noise from all the satellites, I think one can deduce from that that it is basically not anything in the satellite, but rather in the signal or in the receiver.

MR. OAKES:

Right.

MR. ALLAN:

And, secondly, I think you can also deduce from the long-term data, the 25 nanosecond RMS numbers. That says probably nothing about GPS, but only about the clocks.

MR. OAKES:

Yes. I didn't point that we were making a one clock comparison against the USNO ensemble.

MR. ALLAN:

Right.

In the long term, that is not bad performance for a clock, and that is what you are seeing. So, it really doesn't say anything about GPS per se.





LONG TERM FREQUENCY STABILITY  
ANALYSIS OF THE GPS NAVSTAR 6  
CESIUM CLOCK

Thomas B. McCaskill, Sarah Stebbins,  
Clarence Carson, James Buisson  
Naval Research Laboratory  
Washington, D. C.

ABSTRACT

Time domain measurements, taken between the NAVSTAR 6 Spacecraft Vehicle (SV) and the Vandenberg GPS Monitor Site (MS), by a pseudo random noise (PRN) receiver, have been collected over an extended period of time and analyzed to estimate the long term frequency stability of the NAVSTAR 6 onboard frequency standard, referenced to the Vandenberg MS frequency standard.

The technique employed separates the clock offset from the composite signal by first applying corrections for equipment delays, ionospheric delay, tropospheric delay, earth rotation and the relativistic effect. The data are edited and smoothed using the predicted SV ephemeris to calculate the geometric delay. Then all available passes from each of the four GPS monitor stations, are collected at 1-week intervals and used to calculate the NAVSTAR orbital elements. The procedure is then completed by subtracting the corrections and the geometric delay, using the final orbital elements, from the composite signal, thus leaving the clock offset and random error.

Frequency stability estimates of clock performance are then made using the clock offsets to calculate the Allan Variance,  $\sigma_y(\tau)$ , for the spacecraft oscillator, using sample times that vary from 1 to 10 days. The results indicate a combined clock/ephemeris frequency stability of  $1.3 \times 10^{-15}$ , or less, for sample times varying from one day up to ten days. Future work will include analysis of cesium standards on SV 5 and 6 as well as a rubidium standard on SV 5.

## INTRODUCTION

As part of the Navy support to the NAVSTAR GPS Clock Development Program, the Naval Research Laboratory (NRL) has continued (1) research and development of precise time and frequency standards. This paper describes the on-orbit performance evaluation of the NAVSTAR 6 cesium clock.

The cesium clock in NAVSTAR 6 is the fifth one to be orbited in the GPS clock development program. This cesium clock was built under contract to the Navy by Frequency and Time Systems (FTS). The NAVSTAR 6 cesium clock was activated on 26 April 1980 (Day number 117, 1980) and has been in continuous operation for more than one year.

The FTS clock is a preproduction model (PPM) which is designated as PPM-11. The preproduction series of cesium beam frequency standards is an evolutionary development from the prototype model orbited in the Navigation Technology Satellite II (NTS-2). The preproduction cesium frequency standards built by FTS are scheduled to be placed in the NAVSTAR 5, 6, 7, and 8 spacecraft.

The NAVSTAR 6 spacecraft is also known as SV 9. The SV identification is given as part of the navigation message.

## GPS SYSTEM DESCRIPTION

The NAVSTAR Global Positioning System is a Department of Defense (DOD) space-based system employing a constellation of satellites which broadcast signals that are synchronized in both time and frequency. Information is given in the ephemeris message which can be combined with measurements from four GPS satellites and used to calculate the user's instantaneous position and velocity in all three coordinates, as well as precise time and frequency. Signals from the GPS satellites can be rapidly acquired and processed independently of all other systems. The precise time and frequency information can be used to provide a common, worldwide time grid for referencing scientific measurements by laboratories all over the world.

The NAVSTAR GPS system is comprised of four segments:

- (1) Control Segment
- (2) Space Segment

### (3) User Segment

### (4) Engineering Segment

The Space, Control, and User segments of GPS will be discussed with emphasis on factors that are important to this paper.

The GPS Control Segment consists of a Master Control Station (MCS), located at Vandenberg, CA, and four remote Monitor Sites (MS), located at Vandenberg, Hawaii, Alaska, and Guam. These four stations track the GPS spacecraft vehicles (SV). Data from these sites are collected at the MCS and processed to determine SV health, orbits, and clock offsets.

The GPS Space Segment currently consists of six NAVSTAR SVs, with a total of 18 satellites scheduled to be operational in the 1986-87 time frame. These satellites are placed in (nominal) 12 hour near-circular orbits, with occasional orbit adjust maneuvers which maintain a repeating ground track for each SV. The configurations of the NAVSTAR have been under active study since the original recommended constellation (2). Recent studies (3) have produced configurations which result in a small improvement in the GPS coverage.

Each GPS spacecraft broadcasts spread spectrum modulated signals which are precisely related to the on-board clock. The spacecraft navigation message (4) is also modulated onto the signal at precise epochs which aid in defining GPS time.

The "precise", or P-code modulation is generated at two frequencies in the L-band; these are designated as the  $L_1$  and  $L_2$  signals. The P-code signals are modulated at a rate of 10.23 Mbps (million bits per second). The P-code modulation provides the capability for high precision time difference measurements, and is resistant to electronic countermeasures and multipath interferences. The P-code employs a very long code that is reset once per week. The second code which is designated as the coarse/acquisition code, or (C/A) code, is modulated at 1.023 Mbps and repeats every millisecond. It provides a coarse signal that is a factor of ten less precise than the P-code. The C/A signal is biphase modulated with the P-code and may be rapidly acquired by all users. Each GPS SV has an atomic frequency standard which controls the broadcast frequency of each satellite to the same nominal value. The use of the spread spectrum modulation and separate codes for each GPS SV permits multiple access to any of the satellites that are above the user's horizon.

A GPS user would be required to have an appropriate antenna, receiver, processor, and output device to receive the precise time and time interval signals and perform a navigation solution. A fully operational GPS user would select four NAVSTARs from the 6 to 9 satellites that would be available in such a fashion as to minimize the Geometrical Dilution Of Precision (GDOP), a quantity [5,2] that relates to the navigation accuracy available from GPS. The user would acquire and lock the receiver to signals broadcast from four of the SVs, and then make simultaneous measurements of time difference (pseudo-range) and frequency difference (pseudo-range-rate) between each of the SV clocks and the receiver clock. The user would then use the four pseudo-range measurements to calculate clock offset, latitude, longitude, and height. The four pseudo-range-rate measurements would be used to calculate frequency offset and velocity in all three components.

#### LONG TERM FREQUENCY STABILITY

The GPS system is capable of providing instantaneous precise navigation because the satellite clocks are synchronized in time and frequency. Therefore a fundamental measure of system performance is given by the long term frequency stability of each of the SV clocks.

The technique that has been developed for analyzing frequency stability performance of orbiting clocks and frequency standards was developed (6) at the Naval Research Laboratory (NRL) in 1975.

This procedure has evolved into an analytical procedure depicted in Figure 1. Each major component of the long term frequency stability analyses will be described in the development of this paper.

#### FREQUENCY STABILITY MODEL

The Allan variance was adopted by the IEEE as the recommended measure of frequency stability. Reference 7 presents a theoretical development which results in a relationship between the expected value of the standard deviation of the frequency fluctuations for any finite number of data samples and the infinite time average of the standard deviation. Equation (1) presents the Allan variance expression for M frequency samples with sample period T equal to the sampling time,  $\tau$ .

$$\text{Eq (1) } \sigma_y^2(2, \tau) = \frac{1}{(M-1)} \sum_{k=1}^{M-1} \frac{(\bar{y}_{k+1} - \bar{y}_k)^2}{2}$$

The average frequency values  $y_k$  are calculated from pairs of clock offsets,  $\Delta t$ , separated by sample time,  $\tau$ , is given by

$$\text{Eq (2)} \quad y_k = \frac{\Delta t_{k+1} - \Delta t_k}{\tau}$$

The clock offset is not directly observable from a pseudo-range measurement; other variables must be measured or estimated.

#### CLOCK DIFFERENCE MEASUREMENTS

Pseudo-range (PR) and accumulated delta pseudo-range (ADR) measurements are taken between the NAVSTAR SV clock and the MS clock using a spread spectrum receiver. The measurements are taken once every 6 seconds and then aggregated and smoothed once per 15 minutes. Figure 2 presents a plot of a typical pseudo-range signature obtained from a single NAVSTAR pass over a monitor station. Each measurement is corrected for equipment delay, ionospheric delay, tropospheric delay, earth rotation, and relativistic effects. Then the data are edited and smoothed using the predicted SV ephemeris to calculate the geometric delay. The clock offset at the mid point of the 15 minute data span is estimated, using both the pseudo-range and the pseudo-range rate measurements which are fitted to a cubic polynomial with epoch at time corresponding to the mid point of the data.

The pseudo-range measurements are resolved to  $(1/64)$  of a P-code chip, which corresponds to 1.5 nsec of time, or 46 cm in range. Nominal values for the pseudo-range noise levels are  $\sigma_{PR} = 1.3\text{m}$  for the  $L_1$  measurements and  $\sigma_{PR} = 2.0\text{m}$  for the  $L_2$  measurements. The  $L_1$  and  $L_2$  measurements are combined to correct for ionospheric refraction, which results in an increase to 4.53m for the corrected pseudo-range measurement. The accumulated delta pseudo-range measurement noise levels are 0.31cm for  $L_1$  and 0.56 cm for  $L_2$ . These measurements are also combined to correct for the accumulated pseudo-range measurements. The smoothing procedure uses the ADR measurements to aid the PR smoothing of each 15 minute segment of data. This process results in a smoothed pseudo-range measurement noise level of 18.5cm.

The equation which relates the pseudo-range measurements to the clock difference between the NAVSTAR SV and the monitor site (MS) is given by Equation (3).

$$\text{Eq (3)} \quad PR = R + c(t_{MS} - t_{SV}) + c \Delta t_A + \epsilon$$

where

PR = the measured pseudo-range

R = the slant, or geometric range, from the SV (at the time of transmission) to the MS (at the time of reception)

c = the speed of light

$t_{MS}$  = the MS clock time

$t_{SV}$  = the SV clock time

$t_A$  = ionospheric, tropospheric, and relativistic delay, with corrections for antenna and equipment delays

$\epsilon$  = the measurement error

The clock difference, denoted by  $\Delta t_k$  for the  $k_{th}$  measurement is obtained by rearranging Eq (3) into

$$\text{Eq (4)} \quad \Delta t_k = (t_{SV} - t_{MS}) = R/c + \Delta t_A + \epsilon/c - PR/c$$

The particular evaluation of Eq (4) that will be used in this paper is obtained by designating the NAVSTAR 6 by SV 9 and by designating the Vandenberg Monitor Site as VMS. This particular case of Eq (4) is given by

$$\text{Eq (5)} \quad \Delta t_k = (SV9 - VMS)$$

#### SMOOTHED ORBIT ESTIMATION

All of the smoothed pseudo-range measurements are collected from the four GPS monitor sites for one week. The Naval Surface Weapons Center (NSWC) then estimates a smoothed NAVSTAR orbit using an orbit estimation program which extensively models the dynamics of the satellite motion, including solar radiation pressure, and orbit adjust maneuvers. The NSWC post-fit ephemeris calculations employ the highly redundant set of range-difference (5) values, which are calculated from the smoothed 15 minute pseudo-range measurements.

The purpose of the smoothed orbit estimation is to separate the clock and orbital components by modeling the clock as a constant,

(but unknown frequency) during the one week span. The model incorporates the feature of inclusion of an (unknown) aging rate, which may be used for frequency standards that exhibit aging. The model also is capable of segmenting the clock bias solution to allow for frequency adjustments of the MS or SV clock.

The clock differences used for analyzing the spacecraft clock incorporate the smoothed orbit and the set of 15 minute pseudo-range measurements to calculate the clock difference at the time of each measurement according to Eq (4). The clock differences for each NAVSTAR pass are then used to estimate the clock differences at the time-of-closest-approach (TCA) of the NAVSTAR SV over the monitor site. This procedure results in either one or two points per day. The NAVSTAR orbit and the monitor site location determine whether one or two points per day will be available. For NAVSTAR 6, one pass per day is available from the Vandenberg Monitor Site (VMS).

The evaluation of the clock difference at the TCA point minimizes the effect of the NAVSTAR orbit estimation for along-the-satellite-track and out-of-plane errors. However this procedure does not reduce the effect of radial orbit errors. Hence the estimate of radial orbit error will be one of the factors that limit the accuracy of the long term frequency stability analysis. The effect of the radial error on the frequency stability is given by

$$\text{Eq (6)} \quad \sigma_y(\tau) = \frac{\sqrt{3}\sigma_{RR}}{c\tau}$$

where

$\sigma_{RR}$  = standard deviation estimate of radial component of orbit error

$c$  = the speed of light

$\tau$  = sample time

## NAVSTAR 6 RESULTS

The clock differences between the NAVSTAR 6 cesium clock and the Vandenberg Monitor Site (VMS) clock are presented in Figure (3). Each "X" symbol corresponds to a single measurement obtained from the smoothed 15 minute pseudo-range measurement. A total of 23 points are plotted for this NAVSTAR 6 pass over the VMS. These



23 points are analyzed and a subset of these data are used to estimate the clock offset at the TCA point.

The clock difference, which is denoted by (SV9 - VMS), corresponds to starting a time interval measurement with the NAVSTAR 6 clock, and stopping with the VMS clock (with corrections for the orbit and other delays). The clock offset changed by approximately 30ns during the SV pass. The clock offset presented here represents a clock difference which may be further processed to produce "GPS" time. The slope of these measurements indicates a frequency offset of  $-1.08 \times 10^{-12}$  between the NAVSTAR 6 clock and the VMS clock. The magnitude of this offset is normally what would be expected (8) after the correction for the relativistic clock effect.

The clock differences for one week are presented by Figure 4. In this figure, each "X" symbol denotes one clock difference obtained from the smoothed 15 minute pseudo-range measurements. There are seven groups of "X" symbols, each one corresponding to a single NAVSTAR 6 pass that was observed by the Vandenberg Monitor Site. The slope of the clock differences for this one-week segment is  $-1.56 \times 10^{-12}$ .

The clock differences for the entire 100 day data span are presented in Figure 5. Each vertical mark corresponds to the clock difference evaluated at the TCA point of a NAVSTAR pass over the Vandenberg Monitor Site.

Reference to Figure 5 indicates a total change in clock difference of about 10  $\mu$ s in 100 days, or approximately 0.1  $\mu$ s/day ( $-1.16 \times 10^{-12}$ ). It also indicates that a small frequency change, on the order of  $5 \times 10^{-15}$ , occurred between days 120 and 150. This small frequency shift will be further analyzed before computing the frequency stability.

The frequency differences for sample times of one, three, and ten days are presented in Figures 6, 7, and 8. Analysis of the results indicates that the total frequency change between the two cesium standards during the 100 day span was on the order of  $1 \times 10^{-12}$ . Reference to Figure 7 indicates three small frequency changes on the order of  $3 \times 10^{-13}$  occurred, with the majority of the frequency differences on the order of a few parts in  $10^{14}$ . Analysis of other GPS data (not included in this paper) indicates that the Vandenberg MS cesium clock was responsible for the largest frequency changes analyzed.

The frequency measurements were then used to calculate the Allan variance for sample times varying from one to ten days. An

interleaving (also called overlapping) data processing technique was used in order to obtain maximal use of the data. For instance, with a sample time of one day and the set of clock differences  $\{\Delta t_1, \Delta t_2, \Delta t_3, \Delta t_4\}$  two variances were calculated. The first variance used the subset  $\{\Delta t_1, \Delta t_2, \Delta t_3\}$  and the second variance was calculated using the subset  $\{\Delta t_2, \Delta t_3, \Delta t_4\}$ . Thus, the two  $\sigma_y(\tau)$  values have the subset  $\{\Delta t_2, \Delta t_3\}$  in common.

Frequency stability estimates, for the combined clock and ephemeris, are presented in Figure 9. The results are summarized by Table 1.

Sample Time (days)	Table 1	Frequency Stability $\sigma_y(\tau)$ Parts in 10 <sup>13</sup>
1		1.1
2		1.0
3		.9
4		.9
5		.9
6		1.0
7		1.1
8		1.2
9		1.3
10		1.3

The  $\sigma_y(\tau)$  may be characterized by four segments, using a model given by

$$\text{Eq (7)} \quad \sigma_y(\tau) = a \tau^\mu$$

The coefficients and sample times for the combined clock and ephemeris frequency stability are summarized in Table 2.

Table 2

Sample Time (days)	Coefficient "a" PP 10(13)	Exponent "μ"
$1 < \tau < 3$	1.10	-0.18
$3 < \tau < 5$	.90	0.00
$5 < \tau < 9$	.33	.63
$9 < \tau < 10$	1.30	0.00

Comparison of the exponents with the type of noise process identifiable in reference (7) in atomic frequency standards indicate that the segment for sample times from three to five days is classified as flicker noise frequency modulation (FM). The segment for sample times of nine to ten days may also be classified as flicker noise FM. The other two segments can not readily be classified, however the first segment has an exponent of -0.18, which is close to flicker noise FM, and the third segment has a slope of 0.633, which is close to that expected from a random walk in frequency (with an exponent of 1.0).

The error sources that are believed to be most significant in limiting this analysis are

- o the use of a single monitor station frequency standard
- o the radial component of orbit error

The first factor can be reduced by incorporating into the analysis multiple frequency standards at a single monitor station, or by analyzing the spacecraft clock performance using multiple monitor sites. For example, the use of the other three GPS monitor sites will permit the identification of frequency changes such as evidenced in Figure 7. A time scale could then be formed in a manner similar to that described in reference (8). The effect of the radial orbit error can be estimated by using equation (6). For the best fit ephemerides used in this analysis, the average radial error was 2.1m, which corresponds to  $1.4 \times 10^{-15}$  for a sample time of one day. Additional orbit smoothing could produce better estimates for the orbit; however, the exponent of -1 (from Equation (6)) is unchanged by additional smoothing. Ultimately, the 18cm noise level

obtained from the smoothed fifteen minute measurements yields a lower limit of  $1.2 \times 10^{-14}$  for a one day sample time.

#### CONCLUSIONS

- o The frequency stability performance of the NAVSTAR 6 cesium clock, to date, is acceptable and within specifications.
- o The combined (spacecraft clock, single monitor station clock, and ephemeris) frequency stability is equal to, or less than,  $1.3 \times 10^{-15}$  for sample times of one to ten days.

#### ACKNOWLEDGEMENTS

The authors want to express their appreciation to Captain Brian Masson of the Air Force Space Division for his efforts in supporting and expediting this work; to Robert Hill, James O'Toole, and Jack Carr of the Naval Surface Weapons Center for the smoothed ephemeris calculations; to Mr. Art Satin and Mr. William Feess of the Aerospace Corporation for technical consultation and assistance in acquiring the data; to Mr. Al Bartholomew, NRL GPS Program Manager, and to Ms Stella Scates for manuscript preparation.

#### REFERENCES

1. C. A. Bartholomew, "Satellite Frequency Standards", Journal of the Institute of Navigation, Volume 25(2), Summer 1978, pp 113-120.
2. J. A. Buisson and T. B. McCaskill, "TIMATION Navigation Satellite System Constellation Study", NRL Report 7389, June 27, 1972.
3. P. S. Jorgensen, "NAVSTAR/Global Positioning System 18-Satellite Constellations", Journal of the Institute of Navigation, Volume 27(2), Summer, 1980, pp 89-100.
4. A. J. Van Dierendonck, et al, "The GPS Navigation Message", Journal of the Institute of Navigation", Volume 25(2), Summer 1978, pp 147-165.
5. T. B. McCaskill, J. A. Buisson, and D. W. Lynch, "Principles and Techniques of Satellite Navigation Using the TIMATION II Satellite", NRL Report 7252, June 17, 1971.
6. T. B. McCaskill and J. A. Buisson, "Quartz - and Rubidium - Oscillator Frequency Stability Results", NRL Report 7932,

December 12, 1975.

7. David W. Allan, et al, "Statistics of Time and Frequency Data Analysis", National Bureau of Standards Monograph 140, 1974, Chapter 8.
8. J. A. Buisson, et al, "GPS NAVSTAR-4 and NTS-2 Long Term Frequency Stability and Time Transfer Analysis", NRL Report 8419, 30 June 1980.

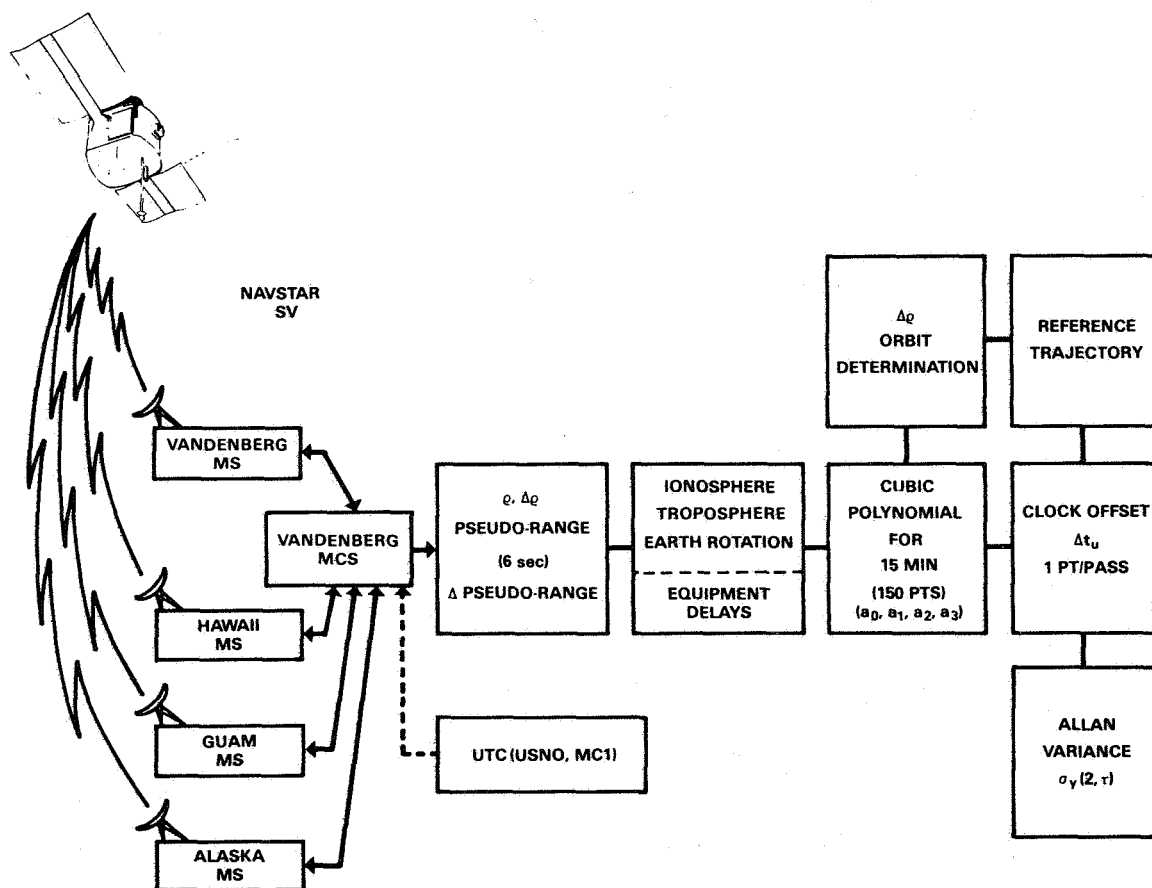


Figure 1 – GPS Frequency stability analysis procedure for analyzing on-orbit clock performance

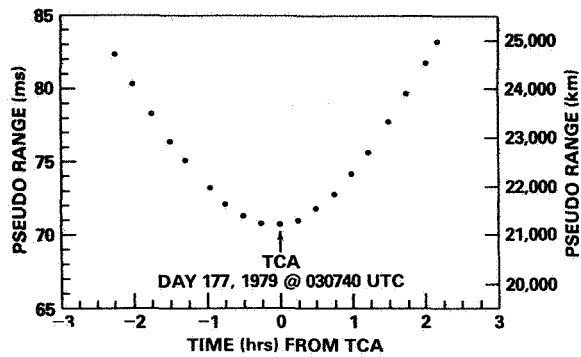


Figure 2—Typical NAVSTAR pseudo-range signature, plotted every 15 minutes

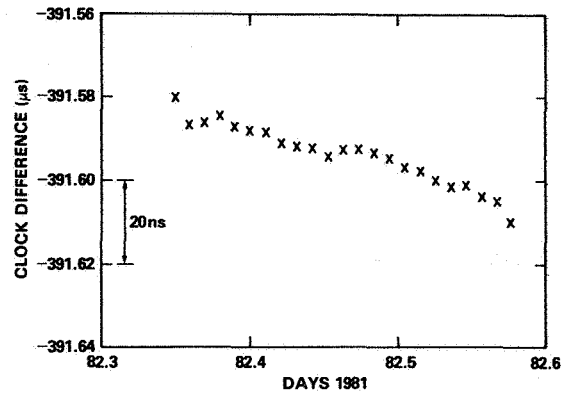


Figure 3—Single Pass Clock difference between NAVSTAR-6 (SV9) and the GPS Vandenberg Monitor Site (VMS)

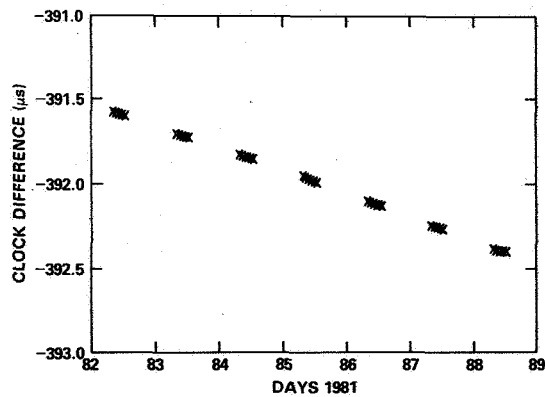


Figure 4—One week of clock differences between NAVSTAR-6 (SV9) and the GPS Vandenberg Monitor Site (VMS)

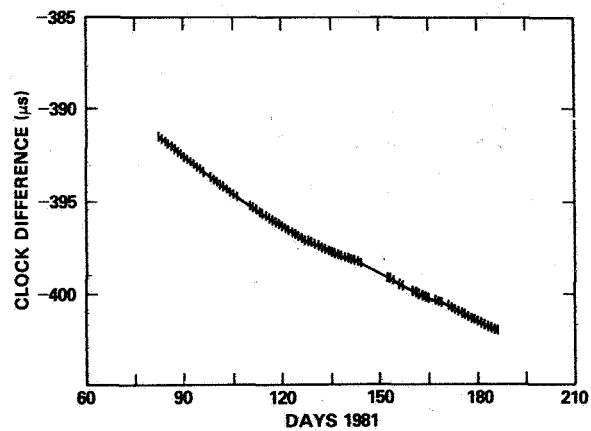


Figure 5—100 days of clock differences between NAVSTAR-6 (SV9) and the GPS Vandenberg Monitor Site (VMS)

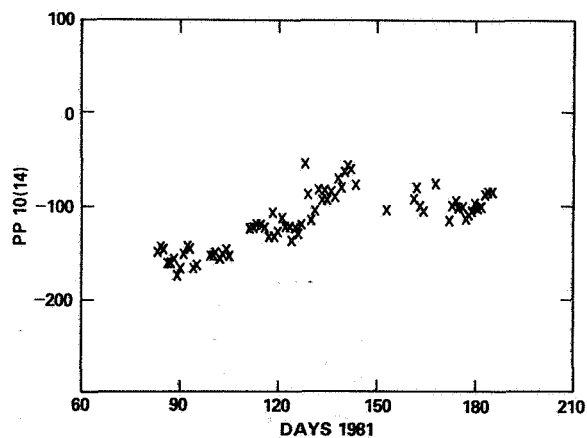


Figure 6 — 100 days of frequency differences between NAVSTAR-6 (SV9) and the GPS Vandenberg Monitor Site (VMS) for a one day sample time

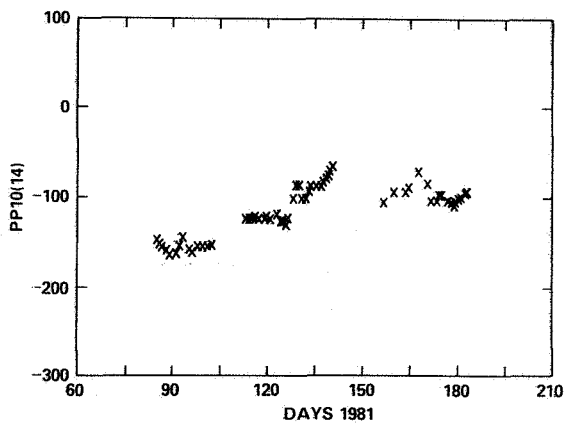


Figure 7 — 100 days of frequency differences between NAVSTAR-6 (SV9) and the GPS Vandenberg Monitor Site (VMS) for a 3 day sample time

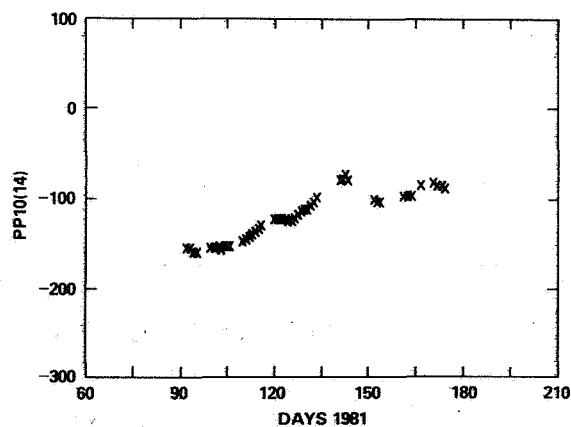


Figure 8 — 100 days of frequency differences between NAVSTAR-6 (SV9) and the GPS Vandenberg Monitor Site (VMS) for a 10 day sample time



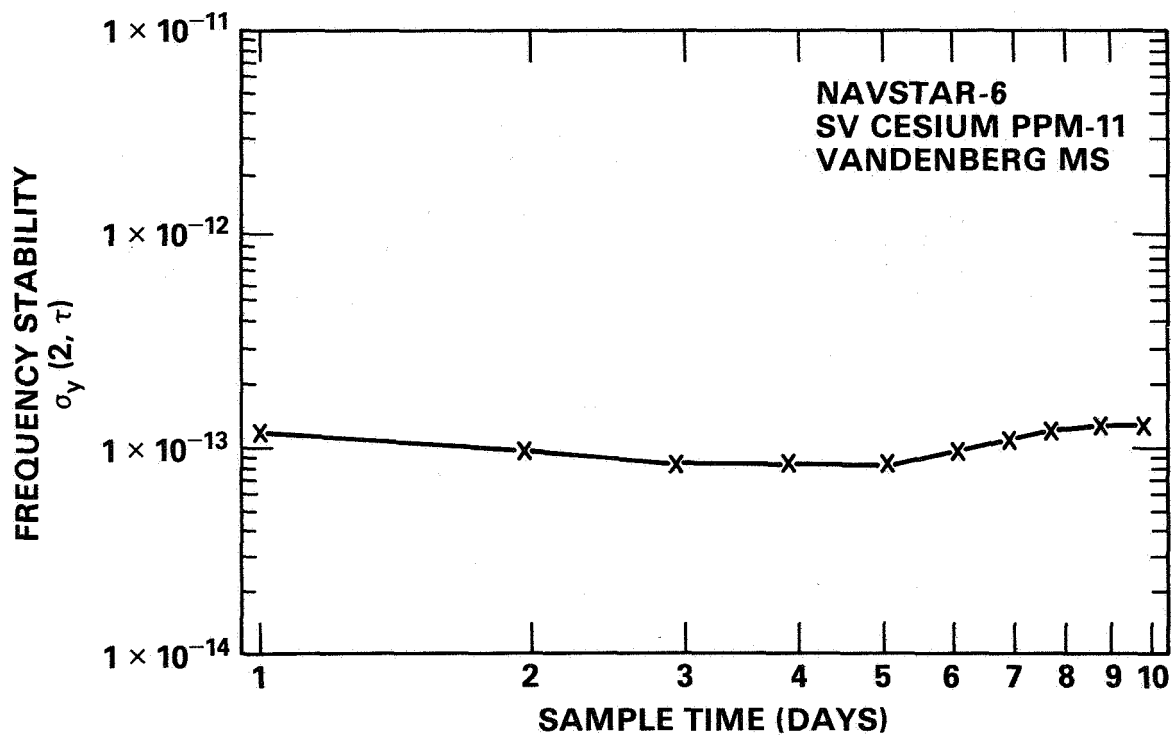


Figure 9—NAVSTAR-6 Cesium Clock (PPM-11) on-orbit clock/ephemeris frequency stability for 1 to 10 day sample times

## QUESTIONS AND ANSWERS

DR. VICTOR REINHARDT, NASA/Goddard

Looking at your historical data of frequency difference between the satellite clock and the Vandenberg clock, have you been able to correlate any of those changes with historical events at Vandenberg, or any place else?

MR. MCCASKILL:

We have been able to correlate that frequency change, and even though we do not have the results today, it appears that there was a small shift in frequency of the monitor site frequency standard. We are in hopes that at the Frequency Control Symposium that we would be able to pin it down a little further as to what causes frequency change.

DR. REINHARDT:

So, they have been monitoring the Vandenberg clock against USNO, but it is just not in the data there now; is that it? Or is there just no data?

MR. ALLAN:

I think Dr. Winkler can address that directly.

DR. REINHARDT:

I think there have been some portable clock trips; is that correct?

DR. WINKLER:

There have been portable clock trips and they have also made available the monitor data which go back to October 1980 of all the satellite clocks and the Vandenberg clock itself directly against the Observatory. I don't understand why you don't take these data into account because they show very clearly that the monitor station clock has a very poor performance, and, in fact, during that period has suffered a frequency change and on the basis of our data, which are publicly available, you can see that the space vehicle No. 9 clock was much better than the referenced clock.

Thank you.

MR. MCCASKILL:

Thank you for the comment.

MR. KELLOGG, Lockheed

In your future plans, do you still plan to stick with this batch average of a week to get the ephemerides data when you start comparing more of the clocks?

MR. MCCASKILL:

The answer is, yes, we do intend to stay with a batch type of estimation procedure. There could be some changes in that. I think there is actually room for a good paper by the Naval Surface Weapons Center in describing the type of orbit estimation procedure that is used. That it is a model that has been highly developed over a number of years, but to directly answer your question, yes, we will stay with a batch type of estimation procedure.

MR. KELLOGG:

And at some time further in the future, would you consider the suggestion that lasers which are to see whether the earth moves three centimeters might give you a better ephemerides data base from which to see whether it is errors in time or ephemerides that you are looking at?

MR. MCCASKILL:

There are no plans, to my knowledge, to put the laser retro-reflectors on the GPS satellites.

TIME CODE DISSEMINATION EXPERIMENT VIA THE SIRIO-1  
VHF TRANSPONDER<sup>(1)</sup>

E. Detoma  
Bendix Field Engineering Corporation, Columbia, Maryland

G. Gobbo  
Telespazio, Roma

S. Leschiutta  
Politecnico di Torino

V. Pettiti  
Istituto Elettrotecnico Nazionale, Torino

ABSTRACT

The advantages of employing synchronous satellites for time dissemination are well known, both in terms of coverage and continuity of service over the covered area. Many synchronous telecommunications satellites carry onboard VHF transponders; these are mainly used as ranging transponders during the launch phases and as beacons or telemetry backup transmitters during the satellite operational life, in which the ranging capabilities of these transponders are seldom used. The aim of the experiment described in this paper was to test the possibility of using these VHF transponders, in their ranging configuration, as repeaters to disseminate time information over a wide area. The experiment, proposed by the Istituto Elettrotecnico Nazionale (Torino, Italy), was performed during the summer of 1980, with the cooperation of Telespazio S.p.A., and using the VHF transponder onboard the synchronous experimental telecommunications satellite SIRIO-1.

- (1) The work was made possible by a grant from the Italian National Research Council/Italian National Space Plan.

## PURPOSE OF THE EXPERIMENT

The aim of the experiment was to evaluate the possibility of disseminating a time code via the SIRIO-1 satellite, by using the onboard VHF repeater. The precision in the synchronization of remote clocks was expected to be of the order of 0.1 to 1 ms.

The main features of the proposed experiment can be briefly summarized as follows:

- 1) the RF carrier was in the VHF band, so that low cost receivers could be used and then a broader class of users could be served;
- 2) an already existing repeater, even if not designed specifically for communications could be utilized; the operation of this repeater was not intended to affect any other function of the spacecraft (both the SHF repeater and the VHF telemetry link were active during the time code dissemination via the VHF transponder).

Moreover, the rising interest about methods of time dissemination using satellites is fostered. The European Space Agency (ESA) is in the process of evaluating the possibility to insert the same time code used by the U.S. GOES satellites in the telemetry message transmitted by Meteosat. In addition, the dissemination of a narrow-band time code is possible also using an MDD (Meteorological Data Dissemination) channel of SIRIO-2. A similar implementation is planned by the Indian National Physical Laboratory; in this instance a 10 kHz channel via the INSAT satellite will be used for frequency and time dissemination.

A geostationary orbit is the optimum choice for time dissemination purposes, since the coverage of a single geostationary satellite is about one third of the Earth surface. For a user located within this area, the satellite is always visible; this way a service continuity is easily implemented.

However, small variations in the position of the satellite affect seriously the uncertainty of the time code dissemination, since the propagation delays are not constant.

Two orbital elements are primarily responsible for these variations: the inclination  $i$  of the orbital plane, that

causes a variation of  $\pm i$  in the satellite declination over one day, and the orbit eccentricity  $e$ , on which the orbital velocity depends; this causes a periodic (period = 1 day) variation in the satellite hour angle.

In the time code dissemination the synchronous satellite acts usually as a repeater of the time signals transmitted by a ground station. Then, an onboard oscillator, a clock and related control equipment are not needed. Since almost all the equipment is on ground, the reliability of the service is very high; moreover, the ground located equipment can be easily serviced or substituted in case of failure. It is customary to refer to this mode of operation as a "one-way technique", since the signal travels from the ground station to the satellite and from the satellite to the users (fig.1).

Previous time code dissemination experiments or services are summarized in table I, along with the main specifications of each one.

#### THE VHF TRANSPONDER

We were particularly interested in using the onboard VHF transponder because it is seldom used during the operational lifetime of the satellite. The SIRIO-1 VHF transponder was used in the ranging mode only during the launch and the first months of operation of the satellite (August-December 1977). Afterwards, it was used only as a beacon for propagation experiments, as a backup telemetry link (the main link uses the SHF transponder) and as a commands receiver.

The repeater is basically a phase modulated (PM) transponder. In the ranging mode, several tones are transmitted to the satellite and from the satellite back to Earth.

By comparing the phase of the received tone with the transmitted signal, we get the range between the satellite and the ranging site. The baseband (video) bandwidth of the transponder in the ranging mode is about 20 kHz, that is the frequency of the highest tone employed.

The switching of the repeater in the ranging mode (normally it acts only as a telemetry transmitter and commands receiver)

is obtained by a "preset" command followed by the transmission of a 20 kHz holding-tone.

When the satellite receives this tone the onboard transponder is switched to the ranging mode, so that it acts as a "transparent" repeater. The holding tone must be received continuously to hold the transponder in the ranging mode, so that, in our experiment, the time code was simply added to the tone.

Under these conditions, since the time code and the holding tone are retransmitted by the satellite on two equally spaced ranging subcarriers (fig. 2), the telemetry transmission was not interrupted, but the telemetry carrier power is reduced.

So, in the ranging mode, it is possible to use the VHF transponder as an additional communication channel, and to obtain the time code dissemination without affecting the VHF telemetry link.

#### THE TIME SIGNAL

In the experiment we used the same IEN time code that is broadcasted over Italy by the National Broadcasting Company (ref. 1). This is a narrow-band time code (fig. 3), repeated every minute, starting at second 52. The duration of the code is 960 ms and it contains a complete date information, including hours, minutes, month, day of the month, day of the week and a flag indicating if the hours are referred to a daylight saving time; moreover, standard items such as start, stop and parity checking bits are added to the code.

This digital BCD code is transmitted by using an audio frequency shift keying (AFSK) modulation, whose bandwidth is compatible with the AM broadcast requirements, featuring a very narrow bandwidth; the two tones used are a 2 kHz tone to indicate a logical "0" and a 2.5 kHz tone to indicate a logical "1".

After the code, a train of six bursts of 1 kHz tone is transmitted, the duration of each burst being 100 ms, starting at seconds 54, 55, 56, 57, 58 and 00 of the following minute.

This provides an audio information easily recoverable by users that have not access to the special equipment for de-

coding the time code (ref. 2,3 and 4).

Because of the experimental nature of the tests and since the transmitting and receiving equipment was located at the same site so that the propagation delay was directly measurable, no information about the satellite position was added to the time code, the principal concern being the measure of the communication link capabilities with such a narrow-band time code.

Following tests performed in our laboratories to define the capabilities of the code alone, it has been shown (ref. 5) that a maximum precision between 1 and 10  $\mu$ s is possible in recovering the time information, with a good signal-to-noise ratio and by using the commercially available decoders.

#### EXPERIMENTAL SETUP AND RESULTS OF THE MEASUREMENTS

The transmitting and receiving equipment was located at the Fucino station, near Rome, which is operated by the Telespazio, the company in charge of space telecommunications in Italy.

The RF carriers are depicted in fig. 2 and in table II. Only one of the two ranging subcarriers was decoded, and since the transmitted power of the single subcarrier was very low, we had a very poor S/N. This could be improved by demodulating both subcarriers, but this operation was deferred to when the necessary equipment will become available.

The time signal TS(FUC) to be transmitted to the satellite (fig. 4) is locally generated by the time code generator AR1340 (fig. 5).

The time code TS(IEN), received via a ground microwave link from the IEN in Torino is used only as a reference to synchronize the station generator. The local 5 MHz time base is obtained by a Telespazio owned Rubidium clock. The reference 1 Hz and 0.1 Hz signals are obtained from this frequency by division.

The 20 kHz holding-tone is locally generated by synthesis from the 5 MHz standard frequency or from a separate crystal oscillator as a backup. When generated from the Rubidium fre-



quency, this holding tone can be used as a standard signal broadcasted along with the time code, allowing continuous phase or frequency comparisons and improving the resolution of the synchronization.

The code was transmitted once every ten seconds; the gating is obtained from the 0.1 Hz signal (fig. 4) generated by the local time base of the receiver RFM/C (fig. 6): this receiver/decoder is a commercially available unit.

The decoded output is a pulse every 10 seconds; such a pulse is generated when a time message is received and decoded. The decoded output pulses are fed to the start channel of the counter, while the stop channel is connected to the 1 Hz local time base.

Since the code is transmitted at 0 seconds in this local reference, it lasts 960 ms and the propagation delay is around 255-256 ms, then the start pulses are generated at about 215 ms of the minute following the transmission minute.

The counter measurements  $\epsilon_i$  are then the complement to 1 second of the reception time and their value is about 785 ms on the average.

Every measurement run consisted of 60 measurements  $\epsilon_i$ ; the data were then stored on magnetic tape for subsequent processing. The average value of each group of data is then computed as the arithmetic mean  $\epsilon$ , with an associated standard deviation  $\sigma$ .

The evaluation of  $\epsilon$  and  $\sigma$  is carried out by applying a 3-sigma width filter; that is any measured value  $\epsilon_i$  is rejected if the residual  $|\epsilon_i - \epsilon| > 3\sigma$ ; if any  $\epsilon_i$  has been rejected, a new  $\epsilon$  and  $\sigma$  are evaluated using the remaining data. This procedure is repeated until no more data are rejected.

Assuming a normal distribution of the data, the one-sided estimated error  $|\delta_\epsilon|$  in the determination of  $\epsilon$  is given, with the 99.5% confidence, as:

$$|\delta_\epsilon| = \frac{\sigma \cdot t_{0.995}}{\sqrt{n}}$$

where  $n$  is the number of available data and  $t$  is the Student distribution.

Some results are summarized in table III and in fig. 7; the magnitude of  $\sigma_e$ , with  $n \approx 60$  data, ranges usually between 0.4 and 0.6 ms.

## CONCLUSIONS

After the experiment and looking at the results, we can not only recognize the difficulties but also the possibility of using the satellite VHF transponder for time code dissemination. In spite of the very difficult conditions of the radio link, we were always able to obtain the desired accuracy (less than 1 ms).

However, in order to test the code capabilities by using a better channel, we performed a series of measurements via the satellite SHF transponder; the results of these tests are summarized in appendix A.

We would like to thank all the personnel at the Telespazio ground stations for their support and Messrs. E. Angelotti, F. Cordara, V. Marchisio and L. Pietrelli who actually carried out the measurements at the sites.

## APPENDIX A - SHF TESTS

The measurements were carried out in September 1980 at the Lario ground station in North Italy, by using the SHF transponder onboard the satellite, which provides a better communication channel than the VHF transponder. The uplink frequency was 17.10 GHz, the downlink frequency was 11.52 GHz. The modulation now was FM and the signal-to-noise ratio was larger than 30 dB. The measurements were carried out with the same equipment used at Fucino and shown in fig. 4. Typical results are given in fig. 8 and table IV, showing the improvement in  $\delta_{\xi}$  versus the VHF data: now  $\delta_{\xi}$  was down to 10-20  $\mu$ s. This has been proven to be the limit of the present decoding equipment, so the SHF channel appears to be really noise-free.

In fig. 8 is also easily noticeable the slow variation in the propagation delay due to the satellite approaching the station.

## REFERENCES

- 1 - S. Leschiutta, V. Pettiti, E. Detoma - Time coded distribution via broadcasting stations, Proc. of the 11th PTTI Meeting (NASA/DoD - Washington D.C. - December 1979).
- 2 - F. Cordara - Nuovo segnale orario codificato, Elettronica e Telecomunicazioni, n. 6 (1979), pp. 241-243.
- 3 - F. Cordara, V. Pettiti - Codici orari radiodiffusi per sistemi automatici di acquisizione dati, 27° Congresso Scientifico Internazionale per l'Elettronica (Roma, marzo 1980).
- 4 - E. Angelotti, S. Leschiutta - Segnali di tempo e codici orari radiodiffusi, L'Elettrotecnica, vol. LXVII, n. 5 (maggio 1980), pp. 449-453.
- 5 - V. Pettiti - Indagine sulla fluttuazione di decodifica del codice di tempo, Rapporto Interno IEN n. RI-2/80S (marzo 1980).

Table I - Time dissemination via satellites  
Experiments and services

Satellite	Country	Year	Mode of operation	Carrier frequency	Accuracy
Transit NNSS	U.S.A.	1967-1981	Onboard clock	VHF - UHF	1-10 $\mu$ s
ATS-3	U.S.A.	1973-1974	One-way	VHF	20-100 $\mu$ s
GOES	U.S.A.	1976-1981	One-way	UHF	10-20 $\mu$ s
GPS	U.S.A.	1979-1981	Onboard clock	Microwave	10-100 ns
SIRIO-1	Italy	1980	One-way	VHF SHF	1 ms 10-20 $\mu$ s

Table II - Main features of the RF link

1. - RF characteristics

- \* Uplink frequency: 148.260 MHz
- \* Downlink frequency (carrier): 136.140 MHz
- \* Ranging subcarriers frequency:  $\pm 775$  kHz  
(from the carrier)
- \* Modulation: phase modulation (PM)

2. - Equipment setup

- \* Diversity polarization combiner reception
- \* Diversity combiner: Electrac mod. 2150
- \* Phase lock demodulators: Electrac mod. 215

3. - Measurement conditions

- \* Tracking bandwidth: 100 Hz
- \* Demodulator output bandwidth: 1500 Hz
- \* Modulation phase shift:
  - holding-tone only 0.7 rad
  - complete signal 1.5 rad<sub>max</sub>  
(holding-tone + time code)
- \* Signal-to-noise ratio:  $2 < S/N < 5$  dB

SIRIO-1 TIME CODE DISSEMINATION EXPERIMENT

FILTERED DATA  
(3-sigma filter width)

Table III - Sample of VHF results

Elapsed time (min.)	$\epsilon$ (ms)	$\sigma$ (ms)	Number of measurements	$ \sigma\epsilon $ (ms) $[t_{0.995}]$
0	787.042	1.149	59	0.432
10	786.913	1.216	59	0.458
20	787.248	1.070	60	0.403
30	787.084	1.725	60	0.649
40	787.331	1.182	59	0.445
50	786.597	1.717	60	0.646
60	787.094	1.262	60	0.475

Date: 21 Aug. 80  
Elapsed time: from 1200 GMT  
Station: Fucino  
Link: VHF

SIRIO-1 TIME CODE DISSEMINATION EXPERIMENT

FILTERED DATA  
(3-sigma filter width)

Table IV - Sample of SHF results

Elapsed time (min.)	$\epsilon$ (ms)	$\sigma$ ( $\mu$ s)	Number of measurements	$ \delta\epsilon (\mu$ s) $[t_{0.995}]$
0	784.042	30.7	60	11.7
12	784.058	28.0	60	10.6
22	784.057	29.3	60	11.1
32	784.061	29.6	60	11.2
43	784.062	29.4	60	11.2
53	784.068	28.5	60	10.8
64	784.072	28.9	60	11.0
75	784.073	29.1	60	11.1
85	784.077	29.1	60	11.1
96	784.082	32.7	60	12.4

Date: 10 Sep. 80  
Elapsed time: from 1405 GMT  
Station: Lario  
Link: SHF



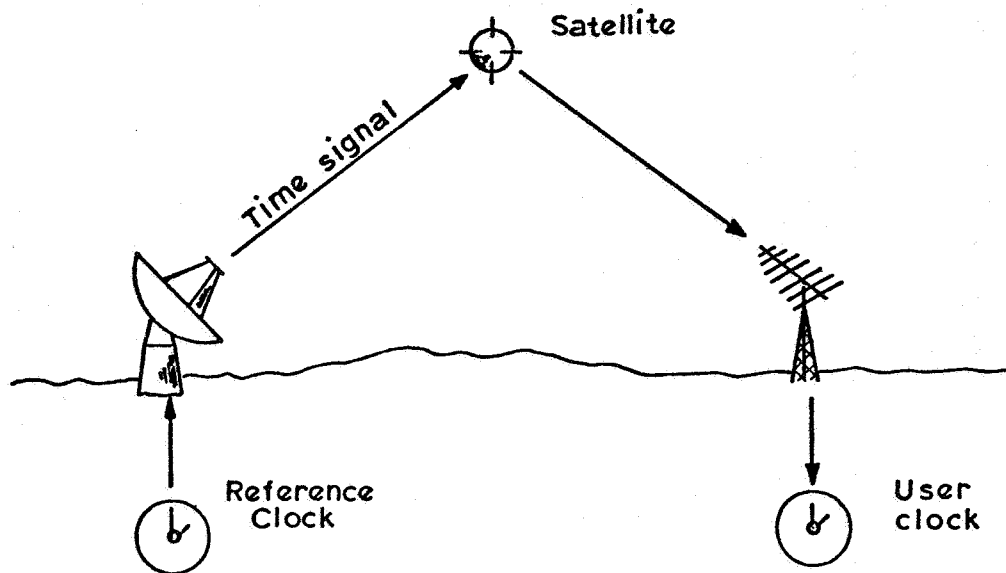
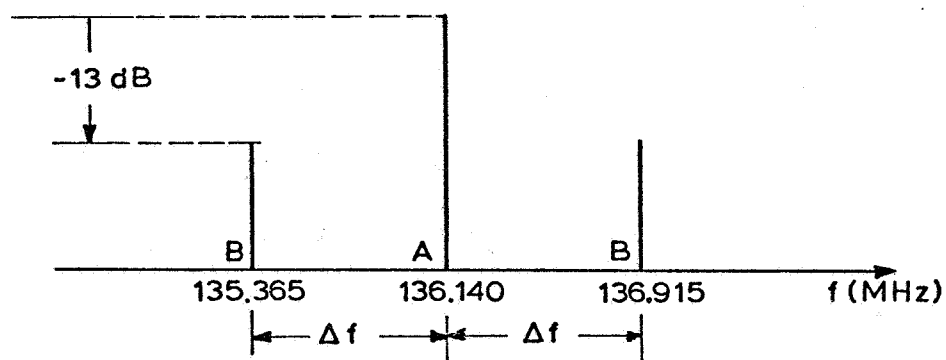


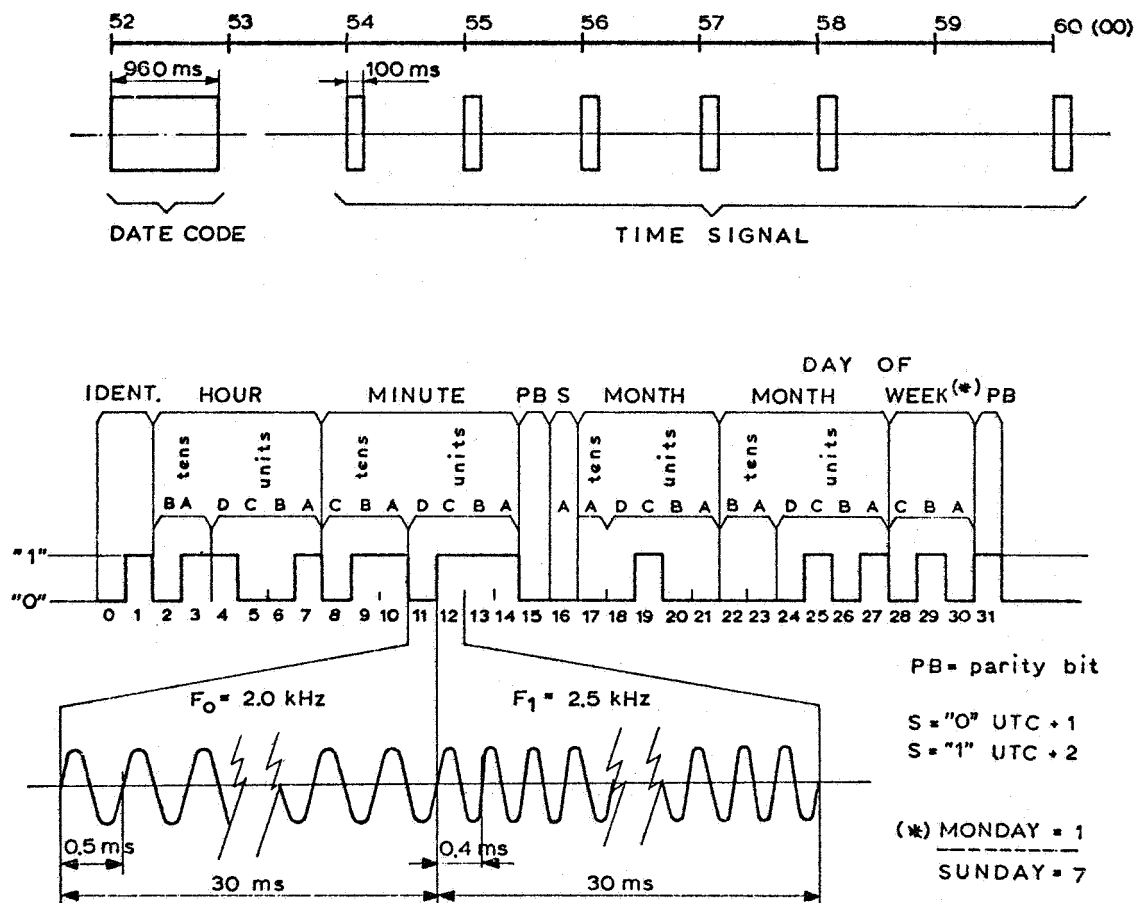
Fig.1 - One-way time dissemination via satellite



A = telemetry carrier at 136.140 MHz

B = ranging subcarriers:  $\Delta f = \pm 775$  kHz

Fig.2 - VHF spectrum transmitted by the satellite



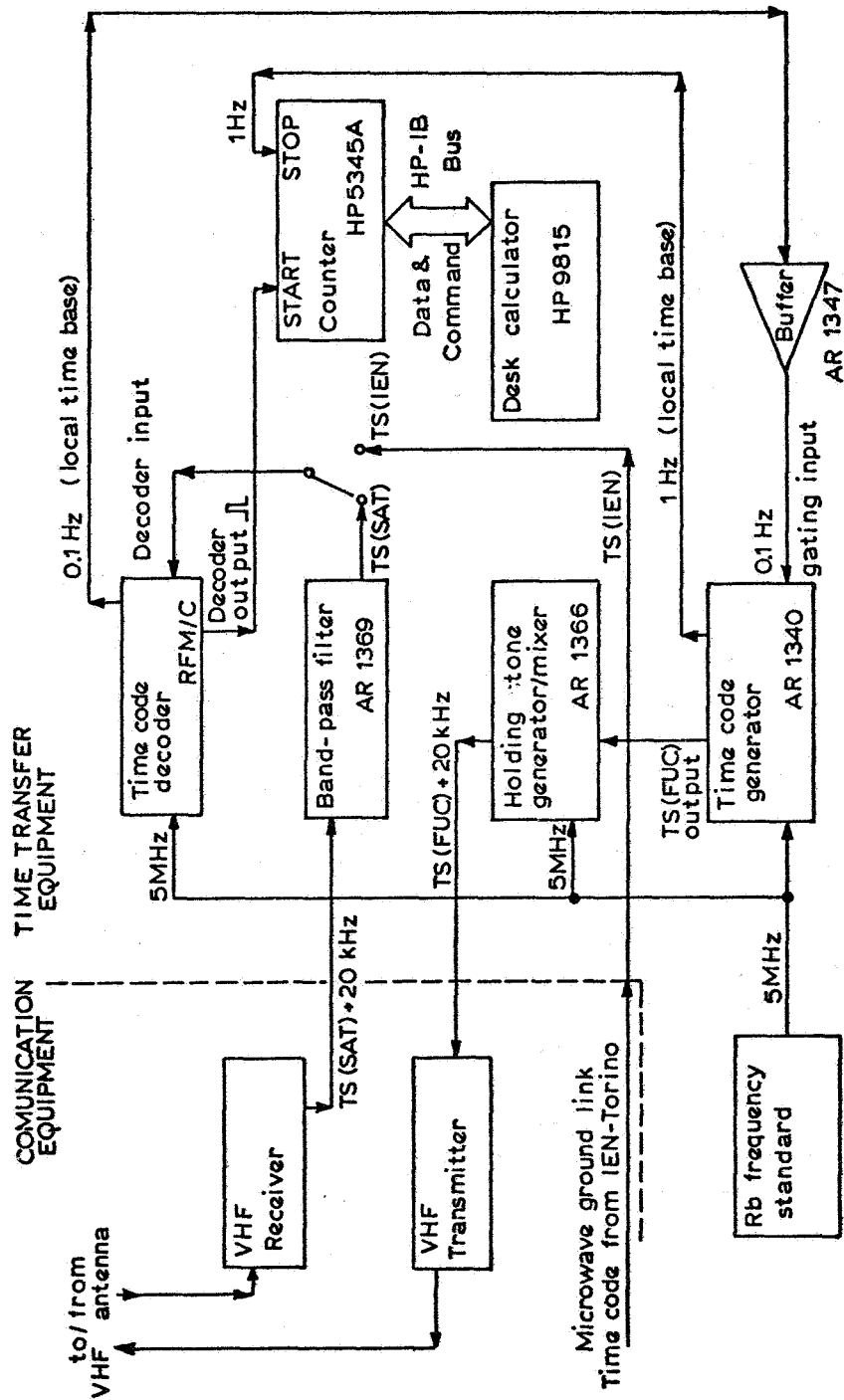
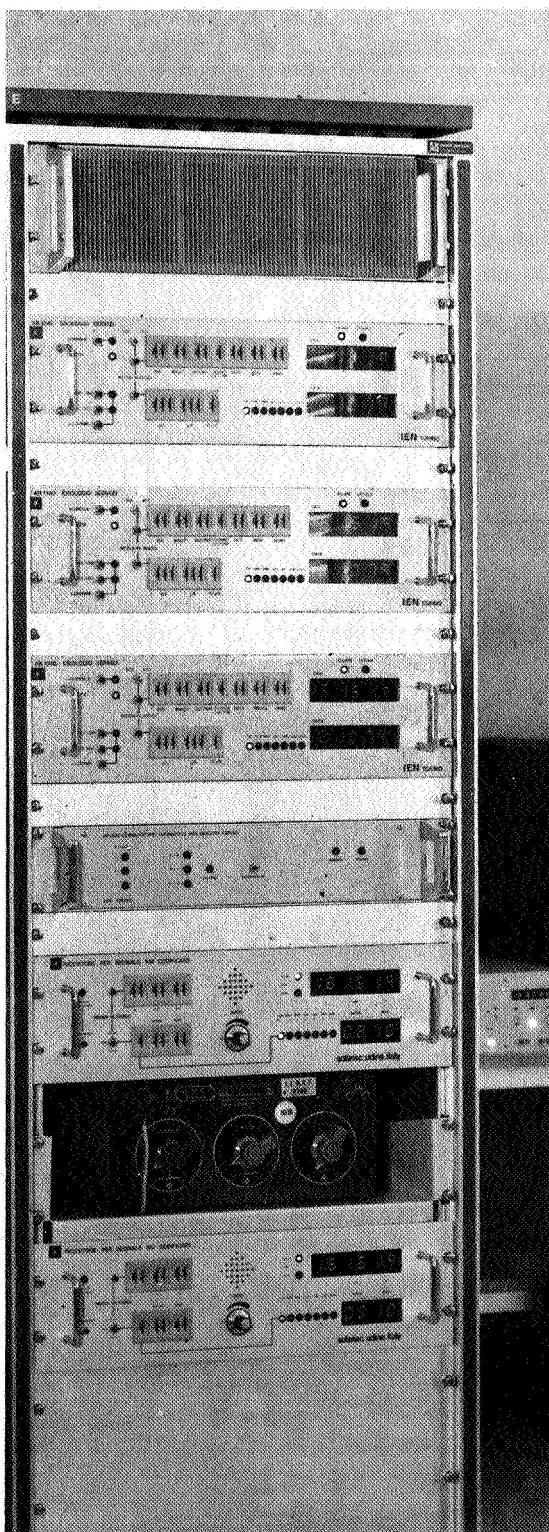
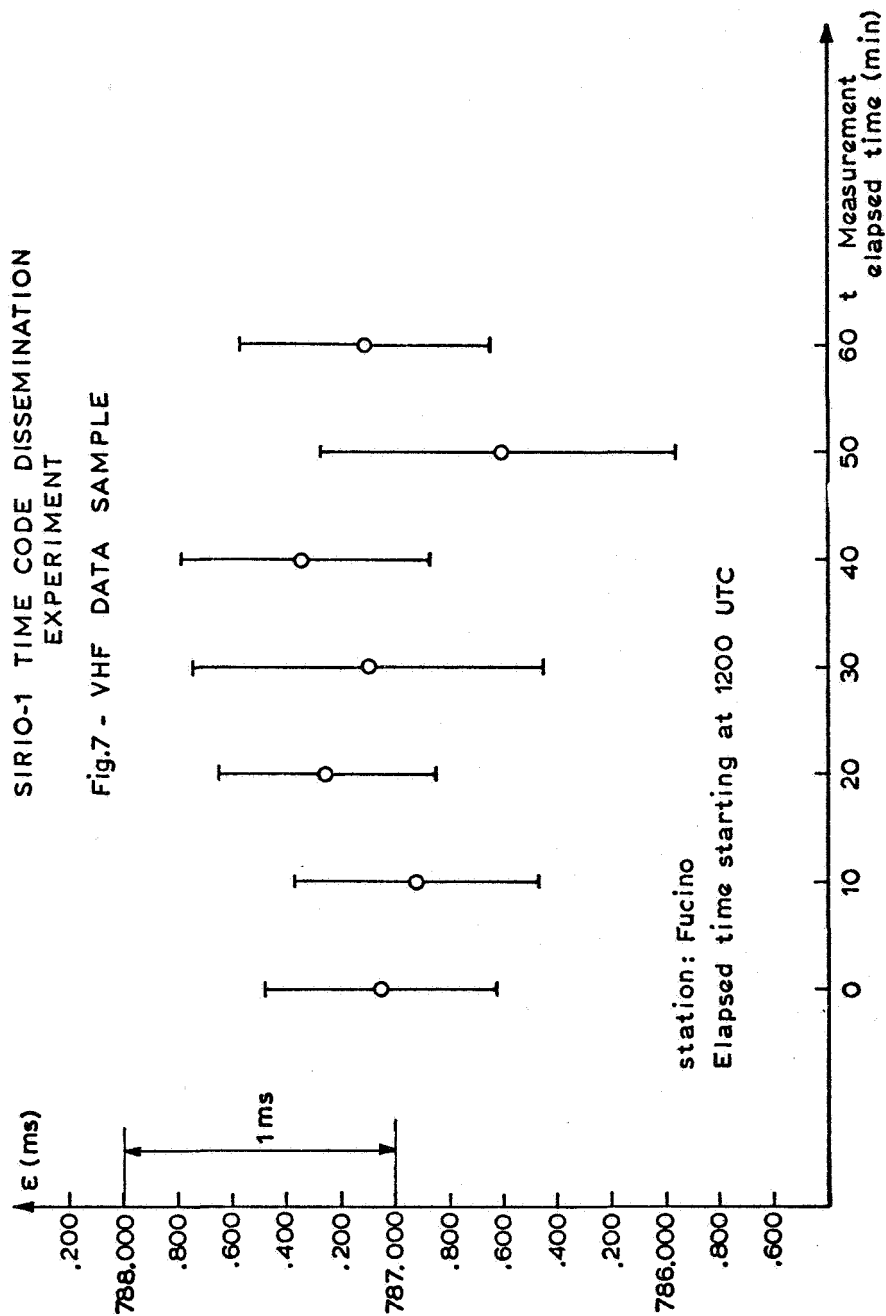


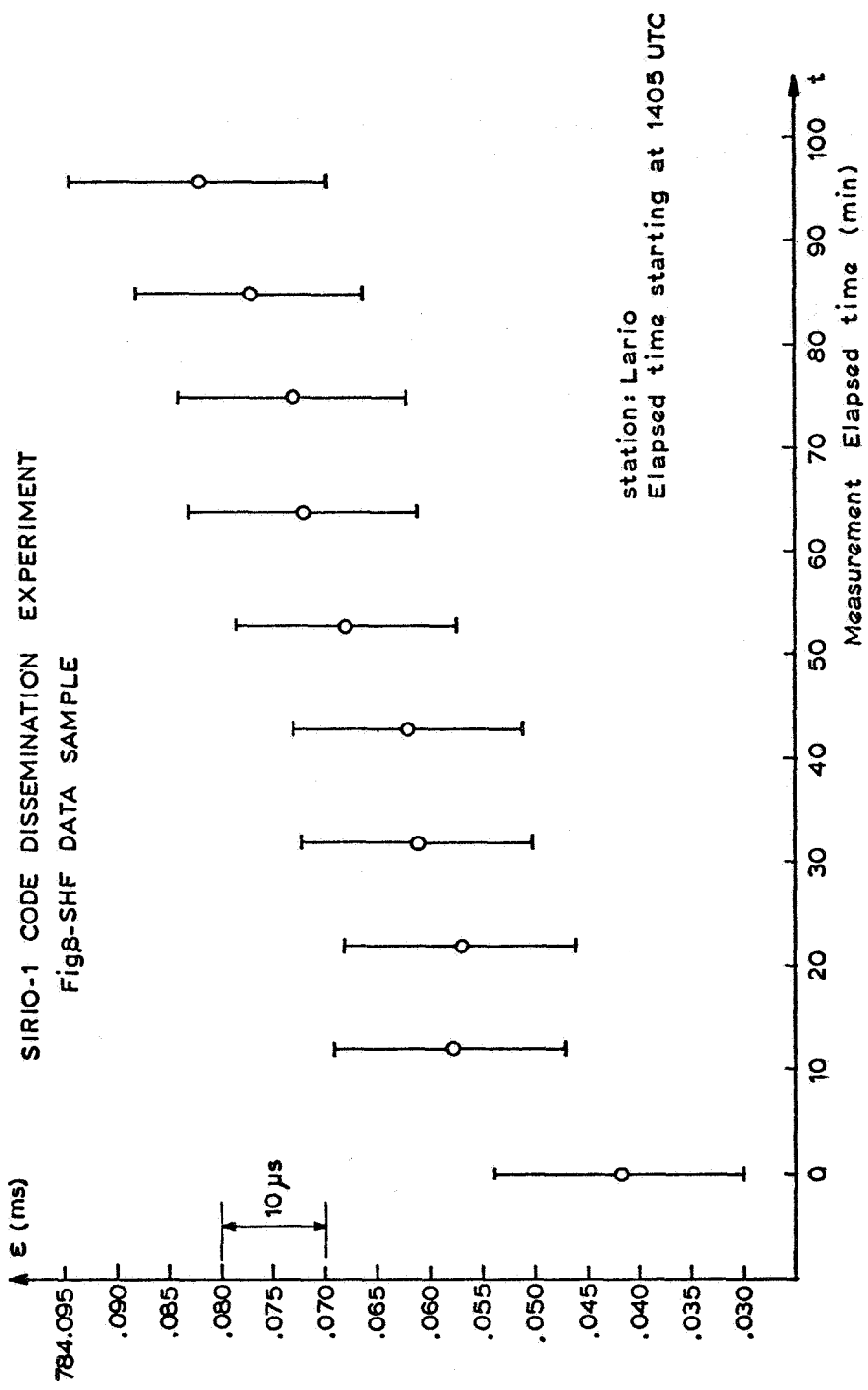
Fig.4 - Experimental set-up (Fucino ground station)



←Fig. 5 - The time code generator AR 1340

←Fig. 6 - The time signal receiver/decoder RFM/C





## QUESTIONS AND ANSWERS

DR. WINKLER:

What are the bandwidths of these two repeaters which you use in the satellite?

DR. DETOMA:

Yes. For the VHF repeater, the actual bandwidth is 20 kilohertz, but we were unable to use the full bandwidth because of a signal to noise ratio problem. For the SHF system, the bandwidth is very large. It's 40 megahertz, but we limited the code before transmission actually to 20 kilohertz again.

## INTERCONTINENTAL CLOCK SYNCHRONIZATION WITH THE BLOCK I VLBI SYSTEM

Mitchell G. Roth, Jet Propulsion Laboratory, Pasadena CA

### ABSTRACT

The Block I Very Long Baseline Interferometer (VLBI) operated by the Deep Space Network (DSN) is used to make weekly measurements of the relative epoch and rate offsets between the time standards in the global network of DSN stations. Over the past year, the precision of these measurements has routinely achieved sub-microsecond levels for epoch offset and accuracies of better than one part in  $10^{12}$  for rate offset. The implementation of the phase calibrator system will permit absolute measurement of epoch offset to better than 10 nanoseconds. With the near-real-time playback and on-line storage of VLBI data, the Block I system typically produces clock parameters within 48 hours from the time of observation.

### INTRODUCTION

The Block I VLBI (Very Long Baseline Interferometry) system [1] has been developed at JPL to provide Deep Space Station (DSS) clock synchronization, platform parameter determination (UT1 and polar motion-UTPM) and spacecraft navigation in nearly real time. The accuracy goals for the system in the 1981 time frame call for measurement of epoch offset to 150 ns, rate offset to 0.6 ps/s, and UTPM to 30 centimeters in each component. During critical events, such as planetary encounters, the results are to be available within 24 hours from the time of data acquisition. With the implementation of the phase calibrator system, now nearly completed, the accuracy of the epoch offset measurements will improve to better than 10 nanoseconds.

From 1980 December to 1981 August, system development was carried out concurrently with observations designed to monitor clock parameters and UTPM. This report describes the steps involved in conducting and processing the observations and the results that were obtained for the clock parameters.

### Block I VLBI System

The Block I system is implemented at the Deep Space Network (DSN) 64 meter radio telescopes located at Madrid, Spain (DSS 63) Canberra, Australia (DSS 43) and Goldstone, California (DSS 14). The hardware



configurations at all three stations are identical, consisting of S and X-band receivers, phase calibrators, channel multiplexers, analog to digital converters and tape recorders, as shown in Figure 1 for a pair of stations. The receivers use maser front ends to achieve system temperatures of 25°K over a 40 MHz bandpass at S-band and 100 MHz at X-band. Up to 4 channels may be recorded in each band by time multiplexing to obtain a maximum spanned bandwidth of 40 MHz. Individual channels have bandwidths of 250 KHz and are digitized by sign, time tagged and then recorded at 500 Kb/s on digital tape. The frequency and timing systems at the station are controlled by hydrogen masers with frequency stabilities of  $\Delta f/f < 10^{-14}$ . The recorded data are replayed from the stations to JPL over the NASCOM wide band data lines at 56 Kb/s, where they are stored on the discs of the VLBI processor for cross-correlation. When the data from both stations have been received at JPL, usually within 10 hours of the observations, they are cross-correlated. The resulting correlation function is analyzed by the post-correlation software of the VLBI processor to determine clock parameters and UTPM.

#### Observation Procedures

Beginning in 1980 weekly VLBI observing sessions were scheduled on both the California-Spain and California-Australia baselines for the purpose of monitoring clock parameters and UTPM and for Block I system development and testing. In most cases both baselines were observed in the same 24 hour period. Estimation of clock parameters requires only a single baseline, but UTPM estimates require two baselines to separate the three components.

For each baseline, 7 to 13 extragalactic radio sources from the JPL navigation source catalog [2] were observed for 200 seconds each. The sources to be observed were chosen to give an observation schedule which would minimize the correlations between the clock and UTPM parameters. For most of the 1981 observations, the scheduling of sessions was governed by DSS availability. However, during the period from DOY 136 through DOY 200, a sidereal schedule was employed, which permitted the same sources to be observed each week for 10 consecutive weeks. The sidereal schedule consisted of a set of 12 sources observed in the same sequence each time. The observing time shifted at the sidereal rate of approximately 4 minutes per day so the same sources could be used for each session. This schedule was very useful for distinguishing between random and systematic errors.

Initially, the data were acquired in 4 S-band and 4 X-band channels for bandwidth synthesis with a maximum spanned bandwidth of 30 MHz in each band. To improve the signal to noise ratios, the configuration was changed to 3 channels per band with a maximum span of 40 MHz on 1981 DOY 107.

Data were recorded at each station on digital tape at the rate of 500 Kb/s. The total on-source time per baseline was nominally 2000 seconds, corresponding to  $10^9$  bits. These data required about 5 hours for transmission to JPL via the 56 Kb/s wide band data lines. Beginning on 1981 DOY 86, the data were logged directly onto the disc storage units of the VLBI processor. Prior to DOY 86, the data were first recorded on magnetic tape when received at JPL and then read into the VLBI processor. With the advent of direct disc playbacks, the tape recordings were used as a backup capability in the event of a system malfunction.

#### Data Reduction

The first step in the reduction of the data was the cross-correlation of the two streams of data. The Block I correlator performs 16 simultaneous cross-correlations over a bitstream alignment (BSA) delay range of 32 microseconds. Since the principal component of BSA delay is the epoch offset between the station clocks, this offset must be known accurately enough to place the correlation function in the 32 microsecond window. If the offset was not known, the correlator operator would search for the correlation function in steps of 32 microseconds. Once found, the correlation function was centered by adjusting the epoch offset, and a data file containing the cross-correlation function and instrumental phase calibrations was produced.

The next **step** in the processing, phase tracking, estimated the correlation function parameters for each radio source. The correlation function for each data channel is completely described by four parameters: amplitude, phase, phase rate, and BSA delay. These were determined by a least squares fit to the correlator output. Bandwidth synthesis (BWS) delays were calculated from the phase differences between the data channels in each band. The BSA delays, BWS delays, and single channel phase rates were the VLBI observables from which the clock and UTPM parameters were estimated.

In the final step of processing, the clock and UTPM parameters were estimated from the VLBI observables. It is important to note that instrumental phase calibration is required for the absolute measurement of epoch offset. In the absence of phase calibration, the delay observables are corrupted by instrumental delays. However, the BSA delays may be used to measure relative epoch offsets containing an unknown bias due to the instrumental delays, provided that the instrumental delays are constant in time. This approach was used to obtain the epoch offset data presented in this report. Although the BWS delays are inherently much more precise than the BSA delays, they are useless for epoch offset measurements without phase calibration because of the difficulty in resolving BWS cycle ambiguities. However, uncalibrated BWS delays can be used for UTPM estimates. In this

context, the resulting epoch offsets are meaningless, but the corresponding sigmas are representative of the values that would be obtained if the BWS delays were properly calibrated. Frequency standard rate offsets were estimated from the X-band phase rate observables.

### Clock Synchronization Results

Of the 55 observing sessions conducted from 1980 December to 1981 August, 36 produced useful data for clock synchronization. These results are shown in Figures 2-5. Epoch offsets from Voyager 2 VLBI navigation data also plotted on these figures and are in good agreement with the clock synchronization data. The epoch offset uncertainties ranged from 35 to about 200 ns and the rate offset uncertainties varied from 0.13 to 1.52 ps/s. These data were processed without phase calibration for instrumental delays. Therefore, an unknown bias is present in the reported epoch offset values. Comparisons with the offsets measured by a travelling clock indicate that the bias was smaller than one microsecond on both baselines. The VLBI data gave independent confirmation of two known clock anomalies. The steep slope (1) in Figure 2 at the end of 1980 was due to the use of a Cesium standard at Madrid (DSS 63). The anomalous points denoted by hollow symbols (2) on Figures 2 and 3 were caused by a 1 microsecond retardation of the Goldstone (DSS 14) epoch as measured by the Frequency and Timing Systems standards laboratory. The cause of the erratic behavior (3) in Figure 2 is not yet known.

The long term clock rate calculated from the slope of the epoch data was found to be  $.05 \pm .02$  ps/s on the California-Spain baseline, excluding 1980 data and 1981 data after DOY 165. All points were equally weighted in the linear regression because it was felt that some of the reported uncertainties were exaggerated by systematic errors due to inconsistencies between the source catalog positions and the precession model in the rapid analysis software. The RMS of the residuals was 92 nanoseconds. On the California-Australia baseline, the long term rate offset was  $0.51 \pm .01$  ps/s. The RMS of the residuals was 89 nanoseconds. These values agreed with determinations made by LORAN on the California-Spain baseline and by travelling clocks combined with television time transfer on the California-Australia baseline. On both baselines the VLBI measurements were about 10 times more accurate. The X-band rate data for the California-Spain baseline shown in Figure 4 had a mean of  $-0.14 \pm 0.20$  ps/s with an RMS of 0.84 ps/s. While the mean was consistent with the long term rate, the comparatively large RMS of the residuals is believed to be caused by media effects and the previously mentioned problem concerning the precession model. The rate data for the California-Australia baseline in Figure 5 exhibited similar behavior. The mean was  $0.41 \pm 0.19$  ps/s with an RMS of 0.79 ps/s.

The sources of error in the epoch measurements are shown in Figure 6 for the cases of uncalibrated S-band BSA delays and calibrated X-band BWS delays. For BSA delays, the largest error is system noise, a direct result of the narrow 250 KHz channel bandwidths. The instrument phase and S band ionospheric effects also contribute significantly to the total error of 76 ns, which agrees fairly well with RMS values obtained in fitting the epoch data to a linear model. The slightly larger residuals in the data can be explained by noting that the actual number of sources per session was somewhat smaller than expected.

With phase calibration at X-band, the BWS delays provide an order of magnitude improvement in accuracy. In this case the dominant sources of error are the source position, troposphere and geophysical models, for a total error of 8.0 nanoseconds. Analysis of actual BWS data indicates that this level of accuracy is realistic. Using the master fitting software at JPL to solve for clock and UTPM parameters, the epoch uncertainties were typically 5 nanoseconds and the rate uncertainties were about 0.2 ps/s. These uncertainties should be slightly decreased by the introduction of phase calibration.

#### Summary

The Block I VLBI system has provided relative epoch offset measurements derived from BSA delays with a precision of better than 100 ns, typically within 24 hours of data reception. The long term rate offsets determined from these epochs have uncertainties of about .01 ps/s. These rates agree with LORAN determinations and are about 10 times more accurate. The VLBI data has independently confirmed known clock anomalies. The precession model in the rapid analysis software should be updated to match the source catalog to obtain the full precision of the rate offset measurements, which would be about 0.2 ps/s. The implementation of the phase calibration system will allow the BWS delays to be used for absolute epoch offset measurements with an accuracy of better than 10 nanoseconds.

#### Acknowledgements

Sam Ward provided invaluable assistance with the analysis and interpretation of the clock synchronization data. John LuValle, Phil Harmon, Tom Runge, and Marshall Eubanks assisted with the correlation and reduction of the VLBI data.

## References

- [1] "The DSN VLBI System Mark IV-85," W. D. Chaney, TDA Progress Report, 42-64, pp 61-76, 1981 May-June.
- [2] "Development of a Radio-Astrometric Catalog By Means of Very Long Baseline Interferometry Observations," J. L. Fanselow, et al., in Reference Coordinate Systems for Earth Dynamics, E. M. Gaposkin and B. Kolaczek (eds.), pp 351-357, Reidel (1981).

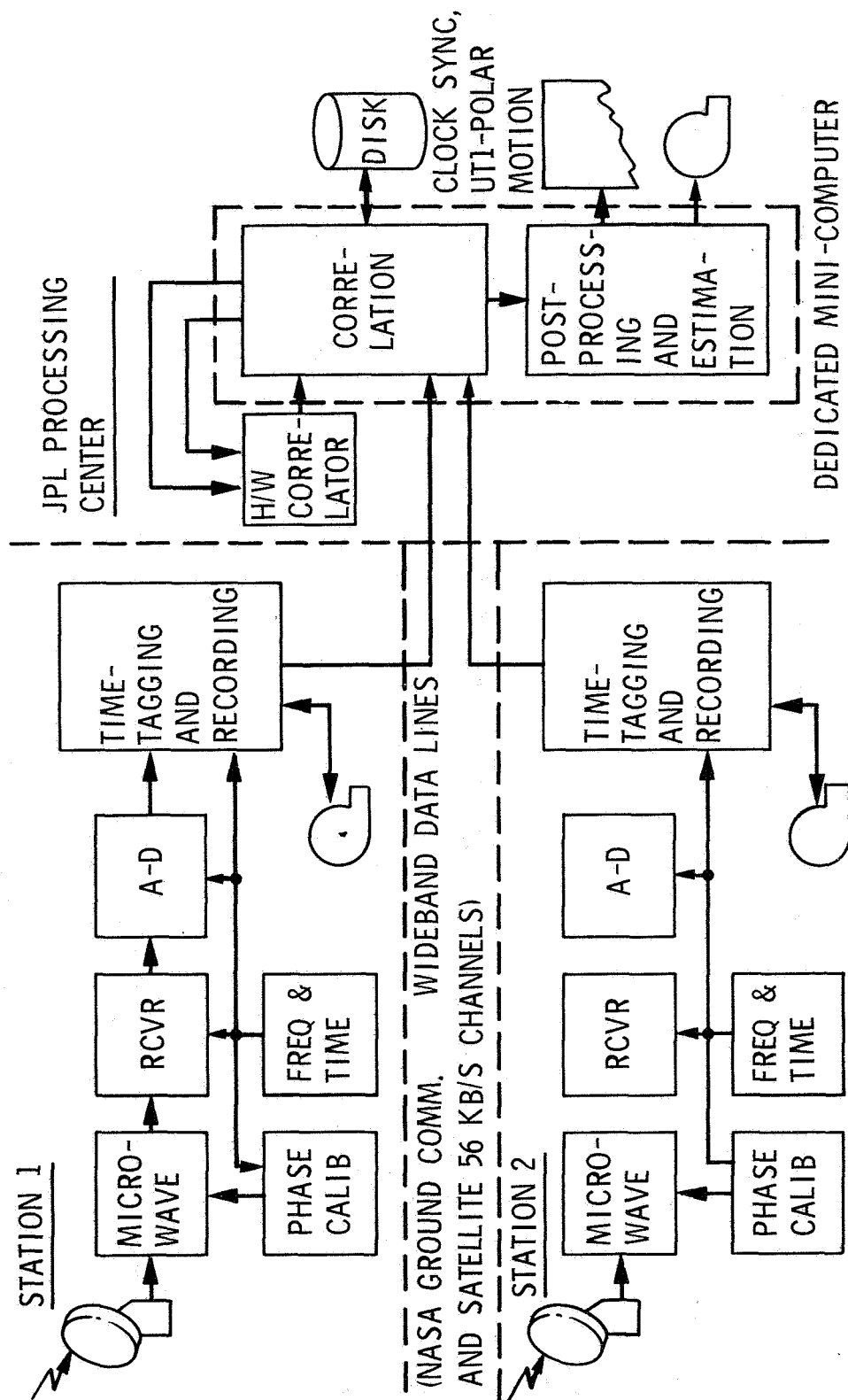
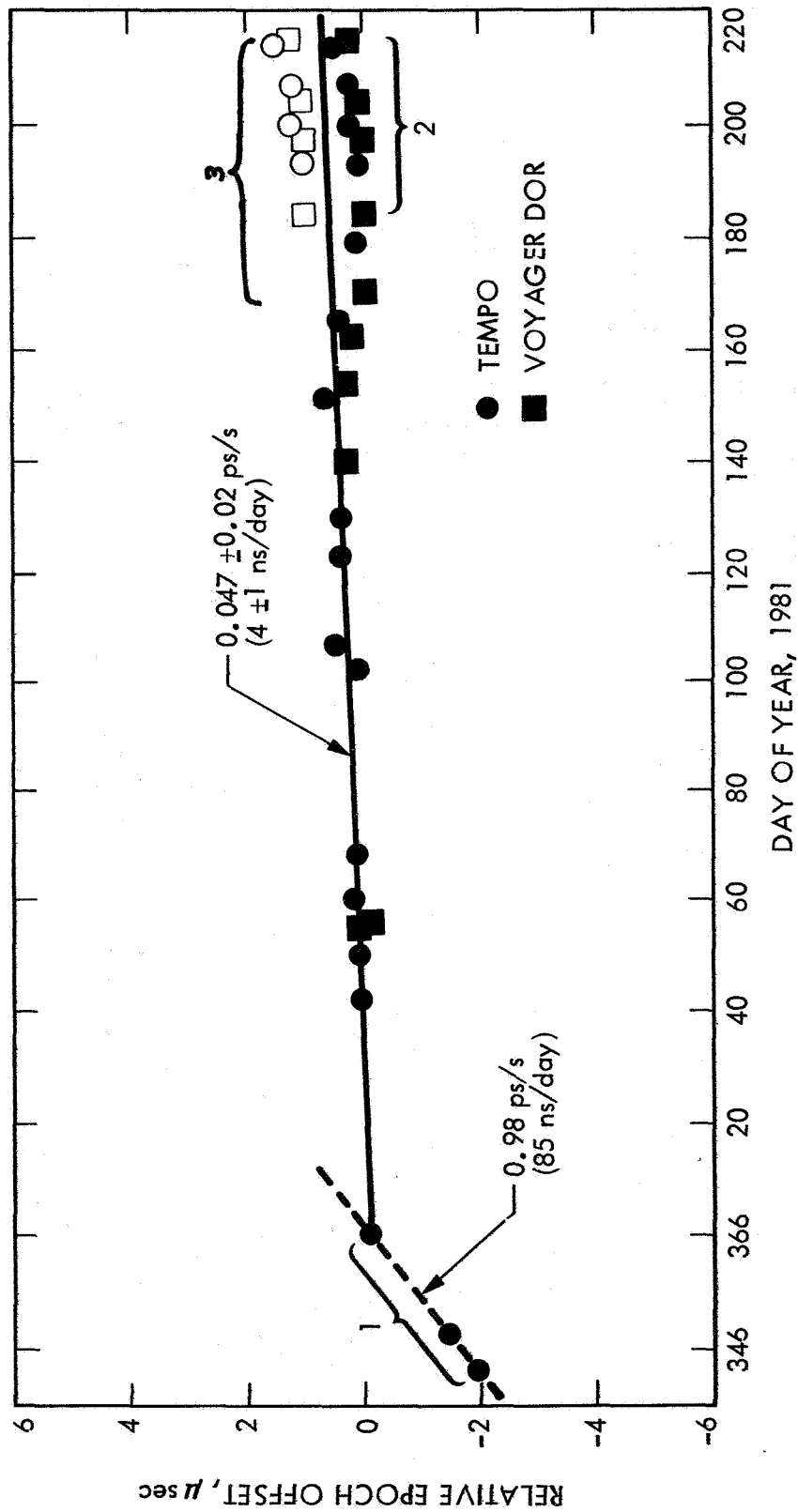


Figure 1. Block 1 VLBI System Configuration.



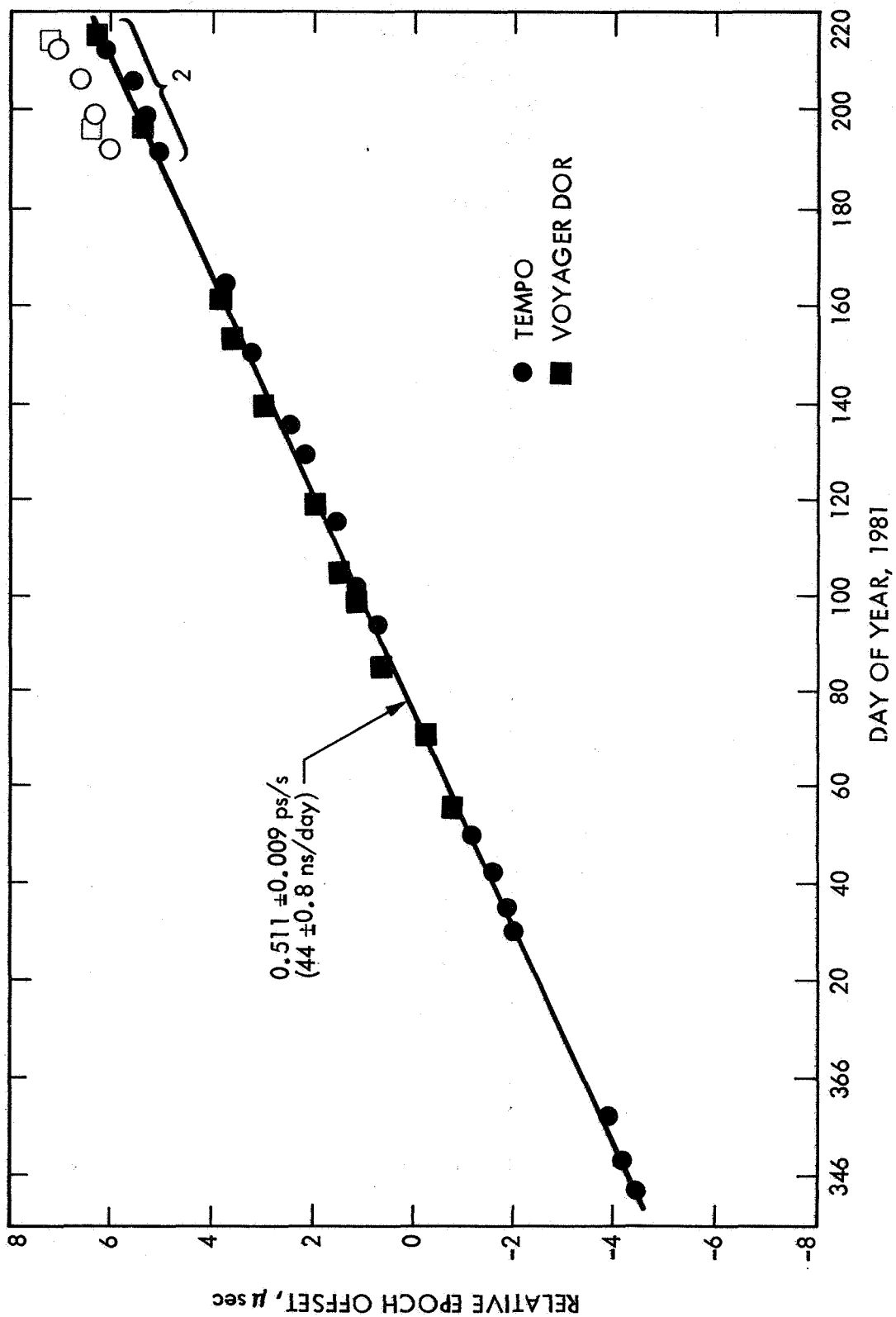


Figure 3. DSS 43-DSS 14 Epoch Offsets



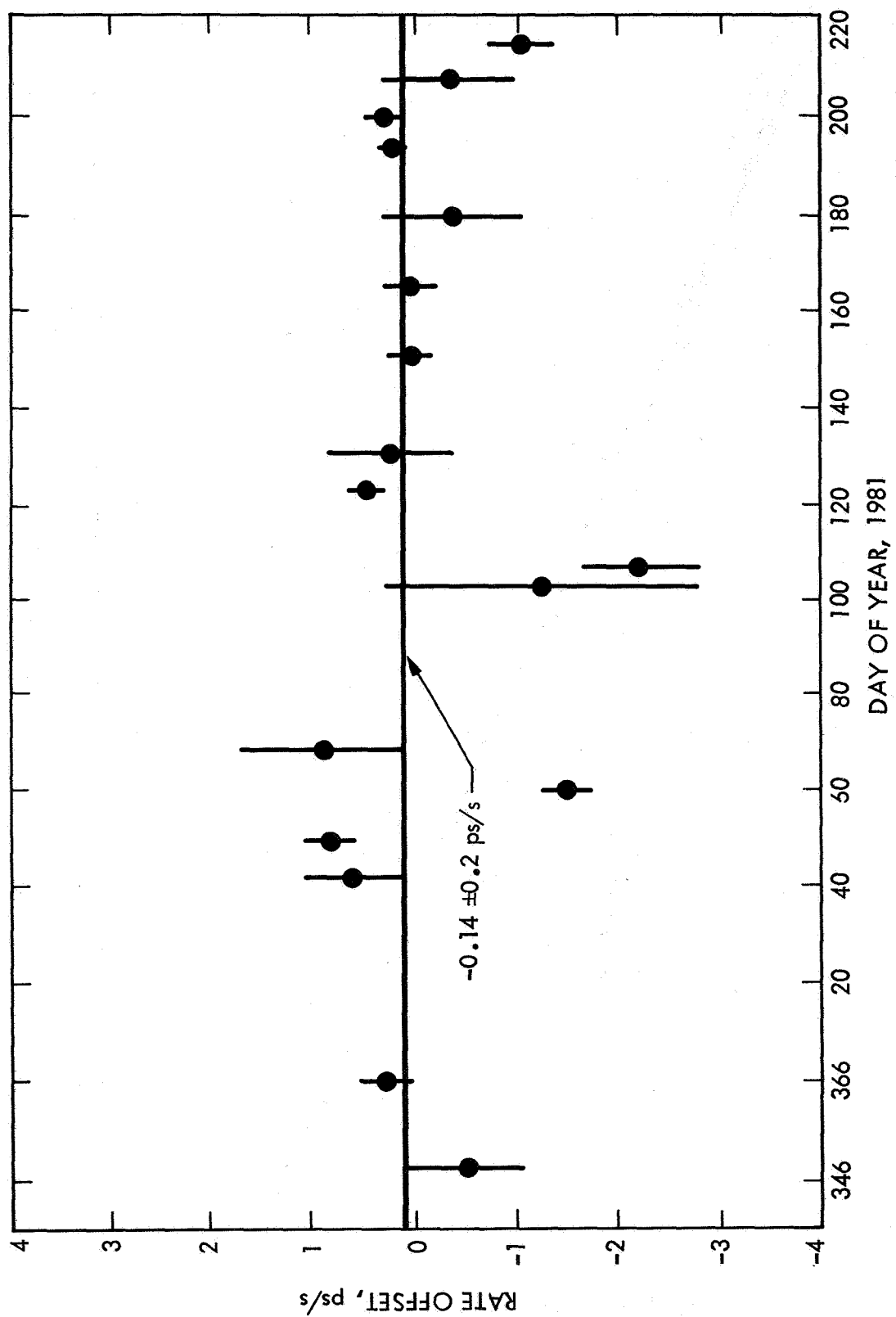


Figure 4. DSS 63-DSS 14 Rate Offsets

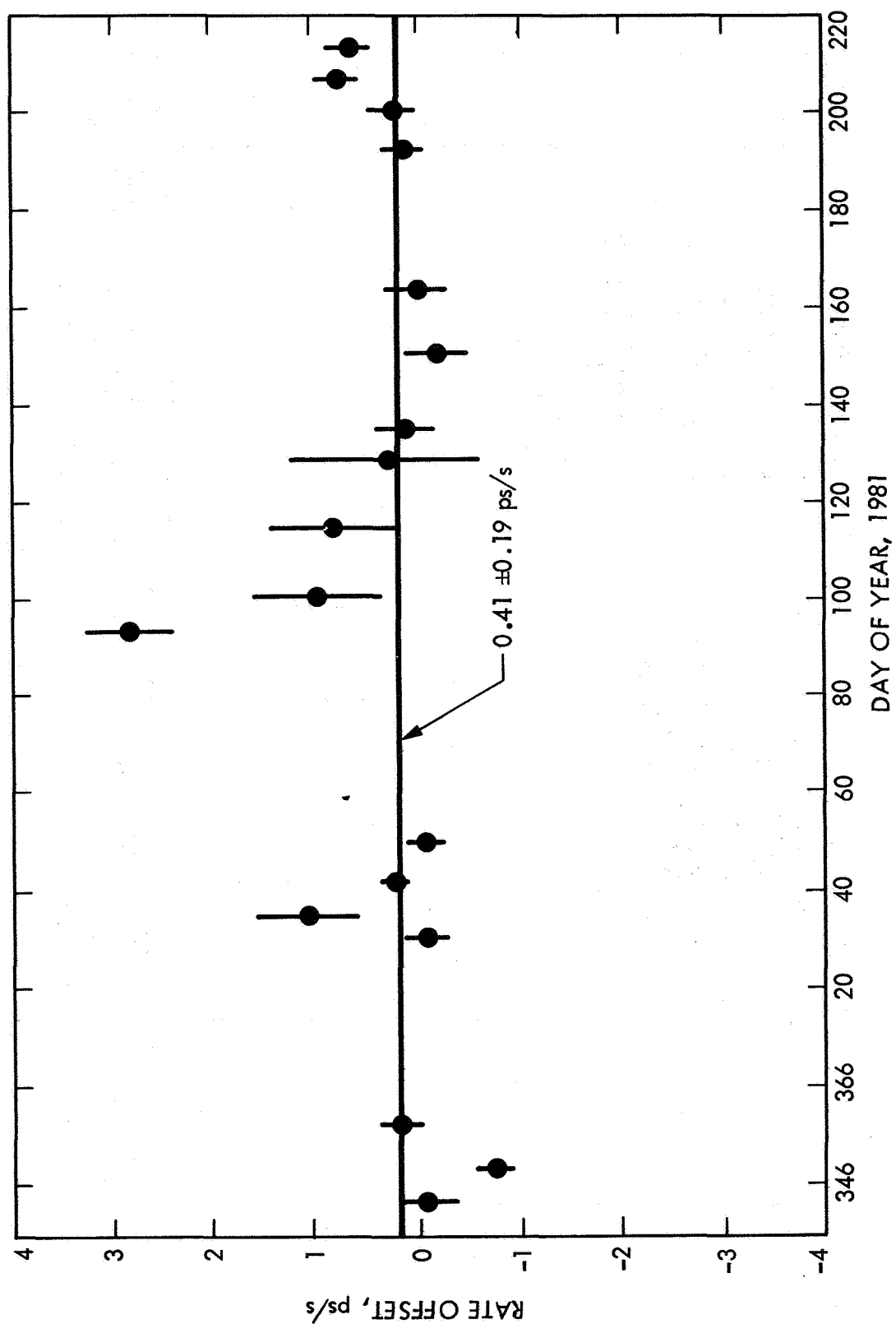


Figure 5. DSS 43-DSS 14 Rate Offsets

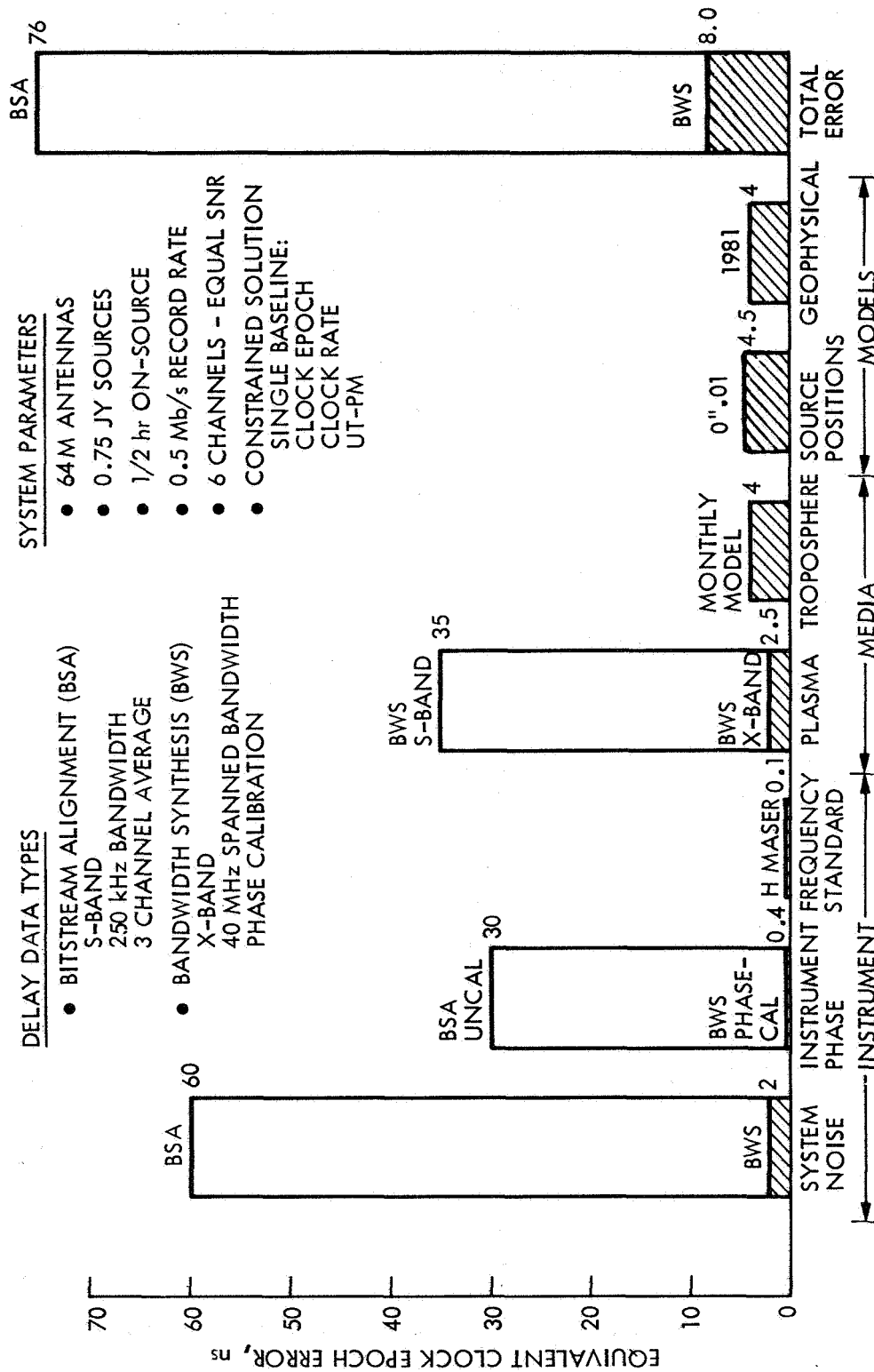


Figure 6. DSN Block I VLBI Error Sources

## QUESTIONS AND ANSWERS

DR. BILL KLEPCZYNSKI, U.S. Naval Observatory

You indicated that you were using cesium for a VLBI experiment. Could I ask at what frequencies, was that an S-band, and at what sources were you looking, could you get coherence over a long enough period of time to really use the cesium?

MR. ROTH:

Well, that cesium was an emergency situation when the hydrogen maser was out of service. And this was with S-band data that I was presenting, and it seemed to work as well at X-band, but that might be a better question to address to Sam Ward.

MR. WARD:

Could I answer that, please?

MR. ROTH:

Sure, okay.

MR. WARD:

As a part of the procedure when a maser is being serviced or repaired. Prior to taking it down, we set the cesium as close as possible to the maser offset and we use our best cesium when we do this, and so far no user has been able to detect the difference.

QUESTION FROM THE AUDIENCE:

Well, how long a time do you integrate for your observation time, 10 minutes or shorter?

MR. ROTH:

There are 10 observations, each of 200 seconds.

QUESTION FROM THE AUDIENCE:

Okay. 200 seconds.

MR. ALLAN:

I might comment in regard to the long term comparisons again. The same problem that we saw in the NRL data, that when you do an RMS of the time residuals around the linear of these squares, that really isn't a very good measure. It doesn't tell you much. It is dependent upon the data length, and it doesn't tell you really much about the propagation or the instrumentation. It's usually a function of the clock and how long you measure it. It really isn't a very good measure.

So, what I am saying is: I would discourgae the use of that. I think there are better ways to characterize long term performance sometimes called the Allan variance.

MR. ROTH:

It will be there in our next report.

# MAINTAINING HIGHLY ACCURATE GLOBAL SYNTONIZATION USING THE HYDROGEN LINE

Samuel C. Ward  
Frequency and Timing System Cognizant Operations Engineer  
Jet Propulsion Laboratory  
Pasadena, California

## ABSTRACT

The NASA-JPL Deep Space Network (DSN) supports spacecraft navigation requirements through the use of ensembles of atomic frequency standards located in Australia, California, and Spain. The syntonization of these widely separated reference frequency standards is maintained over long periods, >6 months, through use of a technique that exploits the phenomena that: the magnitude of the offset of the output frequency of a particular hydrogen maser (H2M) from the hydrogen line is constant throughout the life of the H2M.

The magnitude of an H2M's frequency offset ( $F_0$ ) from the hydrogen line is a function of  $\Delta F_m$ ,  $\Delta F_r$ ,  $\Delta F_t$ ,  $\Delta F_w$ , where  $m$  is the ambient magnetic field in the bulb,  $r$  is cavity mistuning,  $t$  is thermal motion of hydrogen atoms in the bulb and  $w$  is wall collision caused shifts. Of these four,  $\Delta F_r$  is the major contributor to drift of the output frequency.

Subsequent to a careful cavity tuning operation any residual frequency offset is due to the other three error sources ( $\Delta F_m$ ,  $\Delta F_t$  and  $\Delta F_w$ ). This residual  $F_0$  is largely a function of the manufacturer's design and the maser's geographic orientation. -Thus this residual  $F_0$ , for a particular H2M at a fixed location, will be constant throughout the life of the H2M.

In August-September 1980 the  $F_0$  of three Smithsonian Institution Astrophysical Observatory (SAO) model VLG-10B hydrogen masers at widely separate locations were measured against a "calibrated" model 5061A cesium beam frequency standard. In April-May 1981 after the three H2M's were returned to the hydrogen line, the  $F_0$  values returned to within  $\pm 4 \times 10^{-15}$  of the original "calibrated" values. Since the "calibrated" 5061A was calibrated against UTC (NBS), then the syntonization between H2M's and to UTC (NBS) was maintained within a few parts in  $10^{13}$  over a period of >8 1/2 months. More accurate syntonization may be obtained if the retuning is performed more frequently.

---

This paper was to present the results of one phase of research carried out at the Jet Propulsion Laboratory, California Institute of Technology, under Contract No. NAS7-100, sponsored by the National Aeronautics and Space Administration.

(ABSTRACT ONLY)

PAPER NOT SUBMITTED

## QUESTIONS AND ANSWERS

### QUESTION FROM THE AUDIENCE:

I have a question. What is the reference standard for tuning the maser, particularly in Spain and Australia, and what's the procedure of tuning the maser?

### MR. WARD:

Your first question first. The reference standard we use was 5061A, option 4, Hewlett-Packard cesium.

And the second question. In tuning the maser, you measure the Zeeman frequency, then using an independent reference such as a quiet cesium, but preferably a good specially prepared rubidium, such as the 5065, and you use that to tune the cavity over the hydrogen line.

### QUESTION FROM THE AUDIENCE:

Yes. What is the standard time for tuning the maser?

### MR. WARD:

It is a function of how quiet your source is. If you used another maser, you can do it in a few hours. If you use a rubidium, it perhaps will take you a day. If it's cesium, as we in many cases have to use, it may take five days.

### QUESTION FROM THE AUDIENCE:

Okay. Another question. Did you change the orientation of the maser, and how much does the frequency offset change? Because I was wondering even if you didn't change the position of the maser, but the surrounding magnetic would change for some reason?

### MR. WARD:

Well, first we have excellent shielding. And we try to put them in magnetically stable environment second, and the results show that nothing has happened in the magnetic domain or we couldn't get those numbers that you just saw.

## CLOCKS FOR AIRBORNE SYSTEMS\*

Norman Houlding  
The MITRE Corporation  
Bedford, Massachusetts

### ABSTRACT

Because of the need for an accurate clock for future airborne systems such as IFF, MITRE has investigated the potential performance of compact oscillators. In particular, extensive testing of rubidium oscillators manufactured by Efratom has been performed for more than two years. The results indicate that an accuracy of better than 10 microseconds should be achievable in tactical aircraft provided that appropriate measures are adopted to counter the many environmental factors. In a favorable environment a stability of better than  $5 \times 10^{-15}$  for one day is achievable with present commercial units, but improvements are required to suit operation in an aircraft. Results of some vibration tests show promise, but further investigation is required.

With further development of rubidium controlled clocks the ultimate limitation on time accuracy in aircraft will probably be associated with time dissemination, maintenance difficulties and doctrinal hurdles.

### INTRODUCTION

The design of a communications system and the study of an Identification Friend or Foe (IFF) scheme, both using absolute time,<sup>(1)</sup> have aroused the interest of the Air Force in the capabilities of small frequency standards. Preliminary investigation has led to the realization of the wide potential value of accurate airborne clocks, since accurate time can be used for many communication and navigational systems which, at present, are designed to use independent oscillators. Although there are now only a few AF systems in the development phase that require accurate time, the trend toward the use of coding to achieve security and the

---

\*This work was supported by the MITRE Independent Research and Development Program.



development of Time Difference of Arrival (TDOA) techniques for precise location suggest that an accurate clock may well be a vital part of the complex nerve center of future weapons of war.

The Navy has already taken action to coordinate the many systems in their service using precise time, and plans to provide a master clock (comprising three standard oscillators with cesium beam tubes) on Navy platforms.<sup>(2)</sup> Although a similar system cannot be implemented on aircraft, Air Force system requirements are not as onerous as those of the Navy in many respects. In particular, aircraft (unlike ships) are not required to operate autonomously for long time periods; some relaxation of independent clock performance should be tolerable. For Air Force needs, a unit must be light and compact.

When we learned that small rubidium cell units were being produced commercially, we decided to investigate the performance of this type of oscillator in some detail. Two commercial rubidium units were purchased from Efratom Systems Corporation in April 1979 and testing began that same month. Other units have been purchased for an experiment in which signals from aircraft were received at three sites and the times were recorded. The recorded results were then used to compute the positions of the aircraft. Consequently we have performed many tests on different versions of the commercial models. We have also tested an early version of the M-100 militarized model that was made available for Project SEEK TALK, and performed vibration tests on this unit and on one of the commercial units.

On the whole our results have confirmed the performance claims for these units and shown that there is a good prospect of achieving time accuracy of 10 microseconds for 10 hours. Many features of the present designs will require attention, and special procedures will have to be established before this accuracy in time keeping will be reliably obtained on tactical aircraft.

#### PRIMARY OBJECTIVES OF THE TEST PROGRAM

The immediate objectives of our preliminary testing were to establish, at first hand, the basic accuracy of the rubidium cell and to check the performance figures quoted by Efratom. We also needed to obtain more experience with precise time-interval measurements and accurate oscillators in order to be well-prepared for performing environmental tests on militarized versions of rubidium cells when they become available. Many measurements have been made to a higher resolution than would normally be required, in order to ensure satisfactory performance with our transportable units.

## THE COMMERCIAL EFRATOM UNITS

Figure 1 shows a photograph of two Efratom units. These are both fitted with the optional finned heat sink. With the heat sink attached, the major dimensions are approximately 4 in x 4 in x 5.7 in and the weight is 3.5 lbs. The output is +7 dBm (1 volt in series with 50 ohms) at 10 MHz.

The input power required is approximately 15 watts at 24 volts dc, but is a function of the temperature and the supply voltage which should be kept within 22 to 32 volts dc.

The two available commercial units are designated FRK-L and FRK-H, the latter being the more expensive unit. The specifications for the two differ in some important features, as shown in Table 1.

TABLE 1 Major Specification Features of Efratom Units

	FRK-L	FRK-H
Long-Term Stability	$<4 \times 10^{-11}$ /month	$<1 \times 10^{-11}$ /month
Short-Term Stability	$3 \times 10^{-11}$ ( $\tau=1\text{sec}$ )	$1 \times 10^{-11}$ ( $\tau=1\text{sec}$ )
	$1 \times 10^{-11}$ ( $\tau=10\text{sec}$ )	$4 \times 10^{-12}$ ( $\tau=10\text{sec}$ )
	$3 \times 10^{-12}$ ( $\tau=100\text{sec}$ )	$1 \times 10^{-12}$ ( $\tau=100\text{sec}$ )
Trim Range	$2 \times 10^{-9}$	$1 \times 10^{-9}$
Environmental Effects:		
Voltage Variation	$<1 \times 10^{-11}$ /10%	$<1 \times 10^{-11}$ /10%
Temperature (Base Plate)	$<6 \times 10^{-10}$ from $-40^{\circ}\text{C}$ to $+65^{\circ}\text{C}$	$<1 \times 10^{-10}$ from $-25^{\circ}\text{C}$ to $+65^{\circ}\text{C}$
Magnetic Field	$<3 \times 10^{-11}$ /oersted	$<3 \times 10^{-11}$ /oersted
Pressure	$<1 \times 10^{-13}$ /mbar	$<1 \times 10^{-13}$ /mbar

The warm-up characteristics are specified as reaching within  $2 \times 10^{-10}$  frequency error in 10 minutes. The retrace is not specified but data supplied by Efratom shows a retrace of  $1 \times 10^{-11}$  in 60 minutes at  $25^{\circ}\text{C}$ . This retrace is defined as the difference from the frequency before switching off. However, the measurement accuracy claimed is only  $\pm 1 \times 10^{-11}$ .

Some other options available give improved magnetic shielding, optimized performance at desired temperatures, and improved short-term stability. One option fitted to MITRE-purchased units is external resistance-control of the frequency adjustment, with a range of  $1 \times 10^{-10}$ .

The FRK-L units we have tested are not strictly representative because they have been given special attention. After our early testing gave us a better appreciation of high-performance oscillators, our objectives were expanded to include assessment of the scope for further improvements in small rubidium oscillators.

A brief history of the units is given below.

FRK-H 3368 Received April 1979. Has been operated almost continuously. Installed in special unit with temperature control of the fan in August 1980. Subsequently used as local reference.

FRK-L 3311 Received April 1979. Returned to Efratom June 1979 to correct intermittent fault. Deficiency in magnetic shield corrected by clamping (August 1980). Temperature compensation modified April 81. Used in test as transportable clock.

FRK-L 3610 Received June 79. Returned to Efratom for improvement of temperature coefficient and other minor changes in Sept. 79. Used intermittently in 1980, and continuously in 1981.

FRK-H 4548 Fitted with extra mumetal shield. Received June 80 and returned to Efratom because of non-reproducible turnover effects. Particularly susceptible to phase-lock but otherwise has proved to be exceptionally stable. The temperature compensation was modified in 1981.

FRK-H 3940 Ordered with special features. The mumetal shield was given special attention and the temperature coefficient adjusted for a heat sink temperature of  $42^{\circ}\text{C}$ . Received March 81. Operated continuously since April 81. Used for transportable clock.

FRK-H 5415 Ordered with the same features as H3940. The temperature coefficient was unsatisfactory and the unit was returned to Efratom for attention. Measurement since return to MITRE has shown that the short-term (minutes to hours) instability is about one order worse than for other units.

M100 018 Received March 1980 and returned to Efratom because of nonreproducible turnover effects caused by stray signal couplings between subunits. Returned to MITRE Aug. 80. Particularly susceptible to phase-lock. Tested through Oct. 80 and returned to Efratom for investigation.

#### MEASUREMENT CONDITIONS AND TECHNIQUES

The units have been operated in a widely used laboratory, and, on some occasions, room temperature changes which were not under our control affected the measurements significantly. Since the spring of 1981, three of the units have been mounted on vibration isolators with the optic axis vertical so that movement of their cabinets should not cause a change in the earth's magnetic field. The stabilized power supplies have a standby battery with capacity for about 30 minutes operation of the oscillators and their associated clocks. The resolution of the clocks is 100 ns. These three units are all fitted with a finned heat sink and a temperature-sensing thermistor to control the operation of a cooling fan.

Other units have been operated from a floating battery supply. The heat sink temperature can be monitored or recorded, and the temperature can be varied over a range of 10 to 20°C by control of the cooling.

Measurements have been purely relative with no attempt to obtain an absolute-time reference. The phase/time difference between two oscillators is recorded using an H-P 8405A Vector Voltmeter. For the more important measurements the differences between at least three oscillators have been recorded simultaneously.

From July 79 to August 80 we used an H-P 5062C Cesium Beam Reference Frequency\* as the standard, and measured the long-term drift of unit FRK-H3368. We have also used an Arbiter 1011C Frequency Comparator with the ABC-TV signal. Unfortunately, reception at MITRE is not line-of-sight, and the signal-to-noise ratio is usually inadequate for accurate frequency measurements.

We have found it necessary to provide special shielding of the oscillators to avoid phase-lock effects. For bench testing we enclose the units in an aluminum box with decoupling fitted to the four leads that are brought out (power supply, crystal oscillator varactor voltage, rubidium lamp voltage).

\*This unit was kindly lent by N. F. Yannoni (RADC).

## PHASE LOCKING AND STRAY COUPLING

All the units we have tested suffer from interaction effects when operated in the vicinity of other units. Some lock up to another unit even when the frequency difference is greater than  $1 \times 10^{-11}$ . The phenomenon is displayed as a constant phase-difference until the frequency difference exceeds the hold-in range, when the phase jumps. With proper shielding there is no evidence of phase lock.

An experiment in which the output of one unit was coupled into another showed that the signal required to achieve partial phase lock for a frequency difference of only  $1 \times 10^{-12}$  was 0.1 volt or 14 dB below the output level. Before proper shielding was fitted there were many false symptoms of coupling through the connections to the phase meter. Other experiments with unshielded units have shown that the frequencies of both units are affected.

When M100-018 was phase-locked to FRK-L 3610 the phase recording against an unlocked unit showed sinusoidal perturbations of 2 ns peak-to-peak at six periods per 100 ns of total change. Another small perturbation was detected at 42 periods per 100 ns of total change. Subsequent measurements of the output signal from another unit, H4548, showed harmonics of 60 MHz extending to the 21st (1260 MHz) and many harmonics of 10 MHz. The strongest harmonics were 20 MHz at 20 dB down and 240 MHz at 35 dB down. The 420 MHz component was 37 dB below the 10 MHz level. A non-harmonic output of 237.125 MHz was 39 dB below the 10 MHz output.

Many recordings have shown occasional cyclic phase changes in a period of approximately one to ten seconds without phase-locking and sometimes cyclic changes of only a few hundredths of a nanosecond or about one tenth of a degree. Some recent tests with H3940 and L3311 close together and inadequately shielded showed, in the phase comparisons against H3368, cyclic changes at  $1/7$  Hz and approximately  $1/100$  Hz. The effect on L3311 was the greater, with a peak to peak excursion of more than 3 ns. The  $1/7$  Hz was probably the difference between the frequencies of the two servo oscillators, indicating leakage of modulated signals between the two units. After refitting the shields at the rear of the cabinets, the leakage effects were no longer detectable.

The FRK-L units show noise of approximately  $1/100$  ns; for the FRK-H units the high frequency noise ( $>1$  Hz, but noise bandwidth only  $\sim 5$  Hz) displayed on the recorder is appreciably less. A recording of L3610 vs L3311 showed occasional cyclic modulation and occasional jumps of  $1/10$  ns.

For our time-keeping requirements, small modulation of the phase is of negligible concern. However, the evidence of leakage implies stray coupling between subunits. It is suspected that such coupling

may cause changes in the frequency when a unit is subjected to mechanical stress. Although the turnover effects are usually reproducible, M100-018 as originally submitted was found to suffer from variable stray coupling.

## CHARACTERIZATION RESULTS

### Warm-Up and Retrace

Measurements of warm-up and retrace have been made on an ad hoc basis so that the results given in Table 2 show values measured at some convenient time, rather than a detailed record as a function of time.

Retrace is not exactly defined, and the measurement of the frequency was made within two to eight hours of switching on. The frequency difference is referred to the value before shutting down. The overshoot measured on some of the tests shows the difficulty of defining retrace. It apparently would be unwise to rely upon achieving the limiting stability until a unit has been operated for ten days, although on all our tests the frequency reached after two hours was within  $2 \times 10^{-11}$  of the previously established value.

A frequency accuracy of  $1 \times 10^{-10}$  should be attained with 15 minutes after switching on, but more experimental data will be required in order to assess the practicality of starting an airborne clock just prior to take-off.

### Temperature Coefficient

M100-018 is the only unit we have measured over a wide range of temperature. Results are shown in Figure 2. The hysteresis indicates the difficulty of making accurate measurements of the temperature coefficient in the region of the minimum.

The unit was cooled from  $+37$  to  $-30^{\circ}\text{C}$  in two hours and then left overnight to reach the lowest temperature. The temperature was then raised to  $60^{\circ}\text{C}$  in three hours and again the unit was allowed to cool overnight. After settling at  $37^{\circ}\text{C}$  the frequency was in excellent agreement with the value measured at the start ( $1 \times 10^{-12}$ ). Following investigation of thermal transients in the region of  $60^{\circ}\text{C}$  the temperature cycle was repeated.

The compensation is well suited for a range of  $-50$  to  $+55^{\circ}\text{C}$ , giving a total change of only  $6 \times 10^{-11}$ . In the region of  $30$  to  $45^{\circ}\text{C}$ , corresponding to a range around normal ambient temperature with the large heat sink used for environmental testing, the coefficient is  $\pm 2 \times 10^{-12}$  per  $^{\circ}\text{C}$ .

Table 2

## Warm-up\* and Thermal Effects

Unit	Temperature Coefficient ( $^{\circ}\text{C} \times 10^{-12}$ )	Warm-up ( $\times 10^{-11}$ )	Retrace		Overshoot	
			Off-Time (Days)	Frequency Change ( $\times 10^{-11}$ )	Value ( $\times 10^{-11}$ )	Recovery
FRK-L 3311	<-0.15 after adjusting R28 April 81	-6 @ 11 min	1	1	small	7 days
			2	2	small	
			12	2	2.8	
FRK-L 3610	+1.3 to 2.0, increasing at higher temp. (30 to 50 $^{\circ}\text{C}$ ) +5 before return.	-10@9 min -1 @ 60 min	14	2	4	not measured
FRK-H 3368	-0.5 (30 to 60 $^{\circ}\text{C}$ )	-20@7 min -1 @50 to 90 min	1	0.5	small	- 10 days no record
			14	-	6 @ 2 days	
			18	0.5	2.6 @ 1 day	
FRK-H 4548	< + 0.5 (estimated .3 35 to 45 $^{\circ}\text{C}$ ) < - 0.2 after modification		10	-0.8	small	
FRK-H 3940	< +0.3 (30 to 50 $^{\circ}\text{C}$ )	-6 @ 8 min	0.5	-0.7	small	
M100 018	+2 (37 to 47 $^{\circ}\text{C}$ )	changed from + to - @ 13 min, -3 @ 20 min	3	<0.5	not checked	

\*at ambient 23  $\pm$  2 $^{\circ}\text{C}$

The other units have been measured over a limited region by cooling with a fan or raising the temperature by blocking the air flow. Following the example set earlier, the compensation of units L3311 and H4548 has been adjusted. We have found the value of the compensating resistor to be very critical; we are uncertain that results are reproducible. After reducing the value of R28 by 0.5% in unit H4548, the temperature coefficient was small, but measurement was uncertain, partly because the laboratory temperature varied appreciably and affected the frequency of the reference.

#### Effects of Magnetic Field

By placing the unit with the optic axis along the earth's horizontal component, H, reversal gives the effect of a change of 0.36 Oe (Bedford MA.) Since the change is instantaneous it can be measured with precision.

Our experience with L3311 is of special interest. When tested before its return to Efratom in 1979 the effect was  $1.6 \times 10^{-11}$ ; after the return to MITRE the effect was small. Then in July 1980 the result was the same as originally measured. Inspection revealed an appreciable gap between two sides of the outer shield and the mumetal plate fixed to the heat sink. By clamping these two sides the effect of a reversal of H was again small. A plastic spacer of .010 in, inserted in one side, gave a consistent effect of  $0.6 \times 10^{-11}$ .

Fitting a clamp to H3368 did not improve the magnetic shielding. Because we have used this unit continuously as a local reference we have not investigated further. However, the poor shielding resulted in problems from a choke in an adjacent power supply, and with one type of fan motor. The fan we finally fitted gave no detectable effect even at a spacing of only one inch.

The M100 is fitted with a folded lip on the heat sink mumetal and the results showed excellent shielding. However, after completion of vibration tests, measurements showed appreciable sensitivity to the earth's field.

#### Turnover (Constant Acceleration)

Most units display the largest turnover effect along the optic axis, possibly as a result of small physical movements of the "physics package" and is, perhaps, affected by inhomogeneity of the C Field<sup>4</sup>. Unit H4548 displayed small turnover effects, but appreciable change for a rotation of  $90^\circ$  around a horizontal axis which gave a maximum effect of  $12 \times 10^{-12}$ .



Table 3  
Effects of Magnetic Field

Unit	Fractional Frequency Change $\times 10^{-11}$	
	Reversal of Horizontal Component of Earth's Field (H = 0.18 Oe)*	Estimated** Effect of Reversal with Optic Axis Vertical (Z = 0.54 Oe)*
FRK-L 3311	small	small (see text)
FRK-L 3610	1.3 <sup>†</sup>	4 <sup>‡</sup>
FRK-H 3368	2.1 <sup>†</sup>	6.5 <sup>‡</sup>
FRK-H 4548	small (3 Mumetal shields)	small
FRK-H 3940	0.4 <sup>†</sup>	1.2 <sup>‡</sup>
M100 018	small (see text)	small (see text)

\* Information from R. Hutchinson (RADC)

\*\* The effect of a change of 2 Z in magnetic field was calculated using the results for a change of 2H.

† Lower frequency with fins North

‡ Higher frequency fins at the top

Table 4

Turnover Effects (Gravitational Changes)  
(parts  $\times 10^{-11}$  per 2g)

Unit	Fins Vertical* Optic Axis E-W	Fins Horizontal Optic Axis E-W	Optic Axis Vertical (corrected for magnetic field)
FRK-L 3311	0.4	0.2	$1.8 \pm 0.2^{\dagger}$
FRK-L 3610	1.7	1.6	$2.4^{\mp}$
FRK-H 3368	0.9	0.5	$4.0^{\mp}$
FRK-H 4548	0.2	0.3	$0.3^{\dagger}$
FRK-H 3940	0.7	0.1	$0.5^{\mp}$
M100 018	<0.2	<0.2	$1.0^{\mp}$

\* Fins Vertical is equivalent to Label Top/Bottom

$\dagger$  Higher frequency with fins at top

$\mp$  Lower frequency with fins at top

Because measurements were made on L3311 for three different conditions of the magnetic shield we are more confident of the measured result for the optic axis than for other units, although the accuracy for all should be within  $\pm 3 \times 10^{-12}$ .

In view of the early experience with M100-018 and the evidence of stray coupling effects, we suspect that some of the turnover effects may be the result of changes in signal coupling, although measurements have given consistent results.

After vibration testing of M100-018 the turnover tests gave different results (cf magnetic shielding changes). The sense of the change along the optic axis was reversed and the magnitude was twice the previous value.

The excellent stability of H4548 along the optic axis was demonstrated by drop tests on the bench. Only very small (barely detectable) phase transients occurred (whereas the M100 displayed phase changes as great as  $40^{\circ}$  (11 ns), and output level transients of 1 dB when given less severe shocks).

Most units show monotonic phase jumps for shocks along the optic axis with reversal of sense for the opposite sense of shock. The effects on the frequency are small.

#### Crystal Tuning and Aging

A change in crystal tuning equivalent to a varactor bias change of more than 10 volts caused a frequency change of no more than  $2 \times 10^{-12}$  on H3368, and  $8 \times 10^{-12}$  on L3311.

The tuning of H3368 was set to give a varactor bias voltage of 14 volts on Aug. 79. The crystal aging had been compensated by a change to 7.2 volts by Oct. 81.

#### Pressure Effects

With M100-018 the frequency change for a change from atmospheric pressure to vacuum ( $10^{-5}$  atmosphere) was no worse than  $-5 \times 10^{-11}$ . The temperature was kept constant within  $1^\circ\text{C}$  for this test.

#### Supply Voltage

Measurement on H3368 gave an average effect of  $+2 \times 10^{-12}$  per volt of change over the range 20 to 30 volts. Correction for temperature change would make the coefficient slightly greater, but the value is about half that given in the specification.

#### Stability and Aging

Measurements of the stability for periods of hours have shown that the temperature changes are the main factor. A typical value for the six hour Allan variance (for the three units with fan control circuits) is  $2.8 \times 10^{-15}$ . However, in one week, the result for H3940 was  $5.3 \times 10^{-13}$  whereas L3311 and H3368 both gave  $2.8 \times 10^{-13}$ . In some tests the effect of an apparent drift was significant, but the calculation was not corrected because such drifts appear to be random.

Unit H4548 has been operated without temperature control and the six-hour variance is clearly affected by the changes in temperature. The value for the combined variance with H3368 was  $3.5 \times 10^{-13}$  for one week when the temperature was relatively stable. It increased to  $7 \times 10^{-13}$  for a week when the temperature rose to  $30^\circ\text{C}$  during the day. For the favorable week the six-hour variance for L3311 and H3368 combined was only  $1.6 \times 10^{-13}$ .

Results for the six, twelve and twenty-four hour variances for H3940 and H3368 over one period of ten days are given in Table 5. The effect of diurnal changes in temperature can be seen in the dependence of the 12 hour variance on the time of sampling. An

assumption of a daily sinusoidal fluctuation of amplitude 5.5 ns would make the corrected values fit a  $\tau^{1/2}$  dependence, but the two weekends would distort the diurnal effect.

Aging data were obtained on H3368 by referring to the cesium reference, starting after two months of prior operation. This unit showed negative aging in the first four months with the rate slowing to approximately  $-5 \times 10^{-12}$  per month. After a three month gap the result for the subsequent five months was a positive change at an average rate of less than  $5 \times 10^{-12}$  per month. The records for other units are purely relative and mostly spoiled by interruptions. However, units H3940 and L3311 have recently been operated without interruption or adjustment. Their frequencies compared with H3368 four months after setting to a small difference were  $-4 \times 10^{-12}$  and  $+5 \times 10^{-12}$  respectively, although L3311 has changed as much as  $+8 \times 10^{-12}$  in one ten-day period, and  $-5 \times 10^{-12}$  in a five-day period. The clocks were resynchronized 10 weeks after the initial frequency adjustment, and the accumulated time differences after a further seven weeks were  $+4.1 \mu\text{s}$  for H3940 and  $+23.2 \mu\text{s}$  for L3311. One additional measurement with Unit H4548 showed a monotonic change of a total of  $-2.5 \times 10^{-11}$  in three months, compared with H3368.

We have not made extensive calculation of the variance for shorter periods because this requires recording with enhanced resolution. One measurement for L3311 and H3368 combined gave the two-hour variance value of  $2.3 \times 10^{-13}$  and the one-hour value of  $1.9 \times 10^{-13}$ . Unit H3940 is distinctly less stable for the shorter periods, and the one-hour variance for it combined with L3311 was  $3.7 \times 10^{-13}$ .

Unit H5415 was put on test in October 1981 but the frequency instability is so much worse than for any other unit that accurate characterization would require extraordinary care. Frequency changes of  $1 \times 10^{-11}$  in ten minutes and  $3 \times 10^{-12}$  in one hour were observed.

TABLE 5  
Combined Variances for 6, 12 and 24 Hour Intervals

Units H3940 and H3368. April 17 to 27, 1981

INTERVAL	STARTING TIME FOR INTERVALS						ALL TIMES
	1100	1300	1500	1700	1900	2100	
6 Hour Variance $\times 10^{-13}$	3.76	3.47	4.33				3.96
12 Hour Variance $\times 10^{-13}$	4.9	4.46	3.73	3.28	3.83	5.09	4.28
24 Hour Variance $\times 10^{-13}$	5.06	5.19	4.7	4.89	4.35	4.21	4.95

Unit H3368 has occasionally displayed a sudden positive jump in frequency lasting about half an hour and then returning to the previous value. The largest change seen was  $+5 \times 10^{-11}$ . Coincidentally, these changes have usually occurred at night or on weekends, although smaller changes have occurred while the recording was being observed.

On Sunday August 9, 1981, unit L3311 lost lock of three occasions in a six-hour period, operating in the search mode for approximately half an hour on the second occasion. Full recovery after regaining lock took five hours. The resultant effect was a time loss of  $6 \mu s$  in 11 hours equivalent to a mean frequency difference of  $-1.5 \times 10^{-10}$ . This is the only occasion when loss of lock has occurred without power failure.

Various difficulties were encountered in the experiments with the portable clocks but not with the rubidium oscillators. Two successful experiments gave a maximum change of 75 ns between any pair after returning some 7 hours later. This change is less than the 100 ns resolution of the counters. The tests were made in hot weather and temperatures were higher than allowed for during transportation.

#### VIBRATION

The effects of vibration were measured using a Ling Model A300 shaker at the Air Force Geophysics Laboratory. Preliminary tests showed that the stray magnetic-field effect on M100-018 was negligibly small after a few minutes delay.

Resonance effects were explored with sine wave excitation over the range 20-2000 Hz. The frequency difference compared with a reference was set to a small value before testing and both the phase difference and the varactor voltage were recorded. The recorder response falls above 2 Hz to about one tenth amplitude at 20 Hz.

When vibrated at a frequency close to the servo carrier frequency (nominally 127 Hz) the 10 MHz output changes were dependent upon the excitation rate of sweep. Results of a slow sweep, with reversals in sense around 130.5 Hz, using unit H4548, are shown in Figure 4. The varactor voltage showed modulation of approximately  $1 \times 10^{-9}$  peak-to-peak, which was undetectable as phase modulation until the vibration frequency was close to that of the servo. The phase excursions for low beat frequencies became quite significant, and in many of the tests the units lost lock for vibration at this frequency, or even at some harmonic.

M100-018 was vibrated along the optic axis and the two axes designated A & B in Figure 5. The inclination of  $22\frac{1}{2}^\circ$  with respect to the sides is a consequence of fitting the unit within the circle of bolt holes used on the shaker table.

The performance of M100-018 was clearly best for vibration along the optic axis, whereas the turnover effects were worst along this axis. Pronounced effects were produced in the frequency range 20 to 50 Hz, and 90 to 100 Hz, where the phase change averaged about 2 ns per second ( $2 \times 10^{-9}$ ) for excitation of 3g amplitude. There was no loss of lock, but strangely, there was as much effect when passing 250 Hz as when passing 125 Hz. The vibration frequency range of 20-2000 Hz was swept through in  $13\frac{1}{2}$  minutes, i.e. at a rate of 1% per 2 seconds. When vibrated along axis A there were marked effects. At 3g peak amplitude the average frequency change was more than  $+3 \times 10^{-9}$  when the vibration frequency was below 30Hz, but then changed sense to  $-5 \times 10^{-10}$  for vibration in the range 40 to 110 Hz. In the vibration frequency range 375 Hz to 750 Hz the unit was out of lock for two minutes.

For axis B the frequency change was as large as  $10^{-8}$  for vibration below 30 Hz. There was a phase transient at 125 Hz, a small effect at 250 Hz and loss of lock from 375 Hz to approximately 480 Hz (about one minute).

Unit H4548 performed much better, but when vibrated at 130 Hz along the optic axis the servo went out of lock for a vibration amplitude greater than 0.42g. Except for this problem, the phase changes were small although varactor voltage resonances were displayed at 105, 210, 330, 390, 1500 and 2020 Hz. Other effects were probably associated with vibration harmonics coinciding with 130 or 390 Hz. Only the resonance at 105 Hz caused a significant phase change, of about -12 ns with a vibration amplitude of 1g.

Tests on unit H4548 along the two axes normal to the sides showed that the axis normal to the labelled side was best, with only small changes in varactor voltage displayed at 130, 260 & 390 Hz. The biggest change of 0.2 volt occurred in the region 1950 to 2010 Hz. The only change in the 10 MHz phase was about 1 ns at about 45 Hz vibration.

Tests with noise excitation (white from 15 to 1000 Hz, falling by 6 dB at 2000 Hz, viz. MIL-STD-810C Figure 514.2-224) were made on M100-018, with the results summarized in Table 6. We suspect that the frequency change is mainly caused by the low frequency noise, in view of the effects observed with sinusoidal vibration.

Unit H4548 was tested for 15 minutes with noise excitation of  $.04g^2/\text{Hz}$ . This was the maximum time obtainable before the thermal overload switch of the shaker tripped open. Only brief tests with

noise were made for the other two axes since our objective was to prove that the deficiencies of M100-018 were not endemic to the basic design.

Figure 6 shows the record of the five-minute run on M100-018 for noise vibration of 6.4g rms along the optic axis. Figure 7 shows a portion of the 15 minute record for noise vibration of 8g along the best axis for H4548. The frequency fluctuated by 'parts' in  $10^9$ , but the average rate was only about  $2 \times 10^{-10}$  since the net change was less than 150 ns in 900 seconds, and should be compared with the results shown in Table 6.

Table 6

Noise Vibration M100-018

Noise Level		Average Frequency Difference
Density $g^2/Hz$	rms 'g'	
.0004	0.8	$-3 \times 10^{-11}$
.0016	1.6	$-11 \times 10^{-11}$
.0064	3.2	$-30 \times 10^{-11}$
.0256	6.4	Approximately $-100 \times 10^{-11}$

We believe that the difficulties encountered with vibration at the servo frequency will be overcome by using vibration isolators. However with units that are affected by vibration below 30 Hz, it will be necessary to use isolators having a very low resonant frequency.

#### FUTURE POSSIBILITIES

It is contended that, by the 1990s, there will be many avionics systems requiring accurate time and that the needs of all will be best satisfied by each aircraft carrying a master clock. We believe that clock should use a rubidium cell.

Many systems will be designed to operate from an internal standard that will, perhaps, be a common design of crystal oscillator.<sup>(5)</sup> However, with a master clock in the aircraft the systems could be designed so that when the master is available it automatically corrects all timing and provides a reference for the frequencies of internal oscillators. The planning of this conceptual use of absolute time will need to be flexible. We fear there is risk of

encountering major difficulties before the operational stage is reached because of unforeseen, or ignored, human factors.

Some of the areas requiring special attention are:

- engineering design of a clock package to reduce the environmental effects of vibration, temperature, pressure, magnetic fields and power supply transients;
- choice of the technique that will best serve to ensure accurate synchronization before take-off;
- provision of redundant dissemination techniques in the many links between the USNO and tactical aircraft.

We believe that the best way to transfer time to an aircraft from the local time center will be to carry on a small clock rather than a signal transmission (although a laser system could satisfy the need for covertness). Consequently, we envision that a crew member will carry the master clock on board where it will be plugged into its special mounting. The internal battery will have a capacity of, perhaps, only 10 minutes. Use of the master, directly, should be superior to carrying out a clock to synchronize the on-board clock after warm up.

To provide this facility every base will need a Time Center in which an appropriate number of portable units will be kept in continuous operation. The portable master clocks can be monitored and adjusted periodically. Pick-up of a clock will become a part of the scramble drill.

On the basis of our experience with compact rubidium-controlled oscillators we believe that it will eventually be possible to achieve better than one microsecond accuracy on tactical aircraft with a unit that can easily be carried on a belt or by hand.



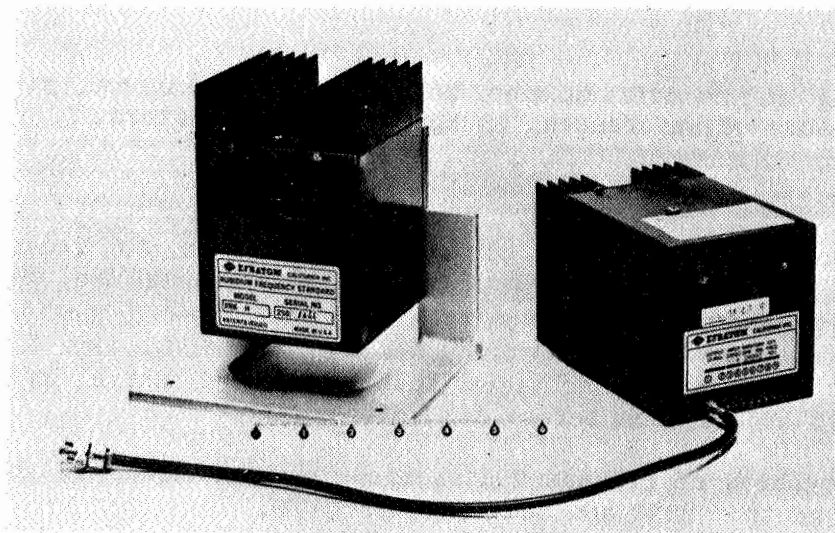


Figure 1. Efratom Units

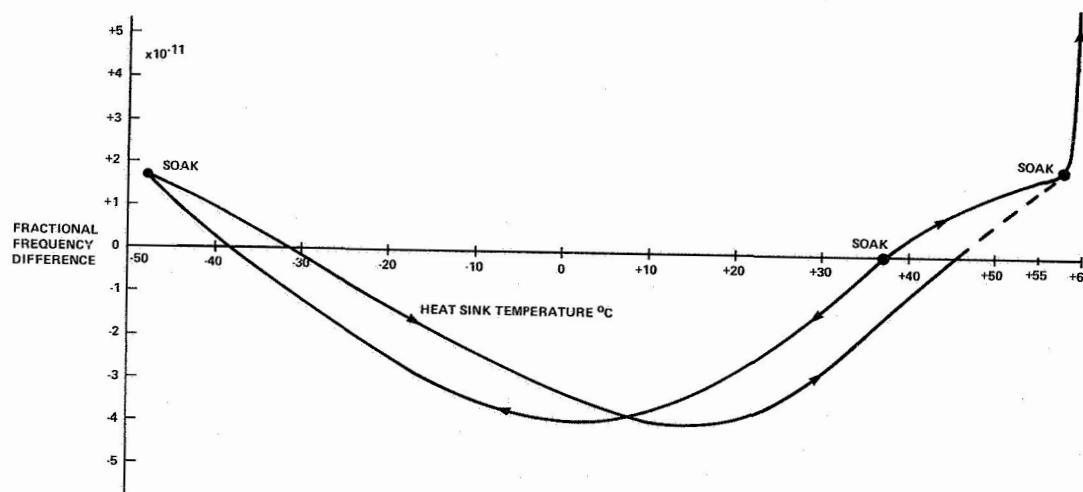


Figure 2. M100 Serial 018 Frequency Dependence On Temperature

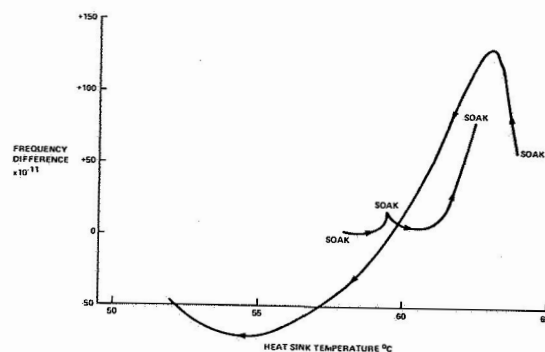


Figure 3. Thermal Transient Effects M100 Serial 018

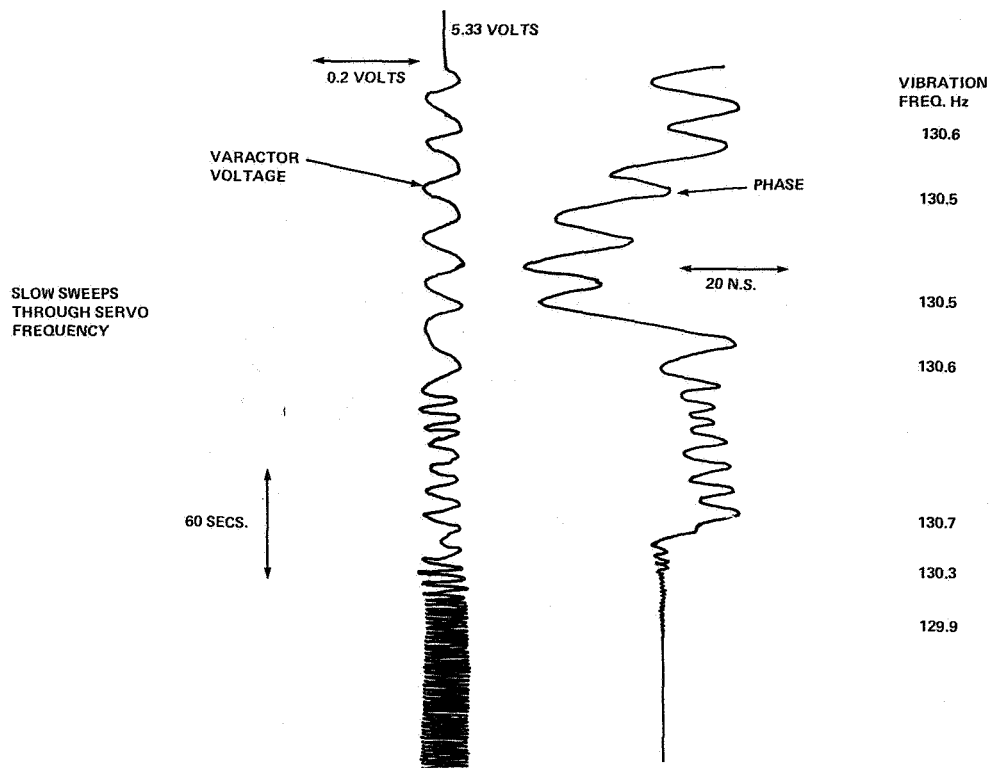


Figure 4. FRK-H 4548 Sine Wave Vibration 0.7g RMS  
Axis Normal To Labelled Side

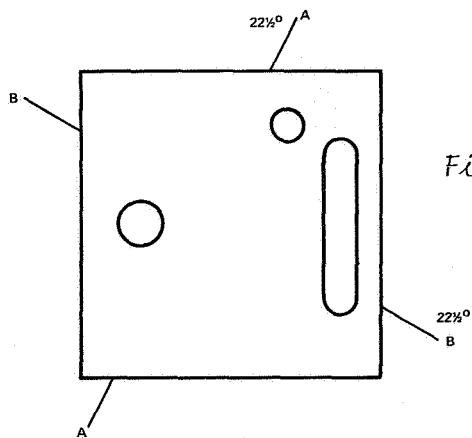


Figure 5. Vibration Axes M100

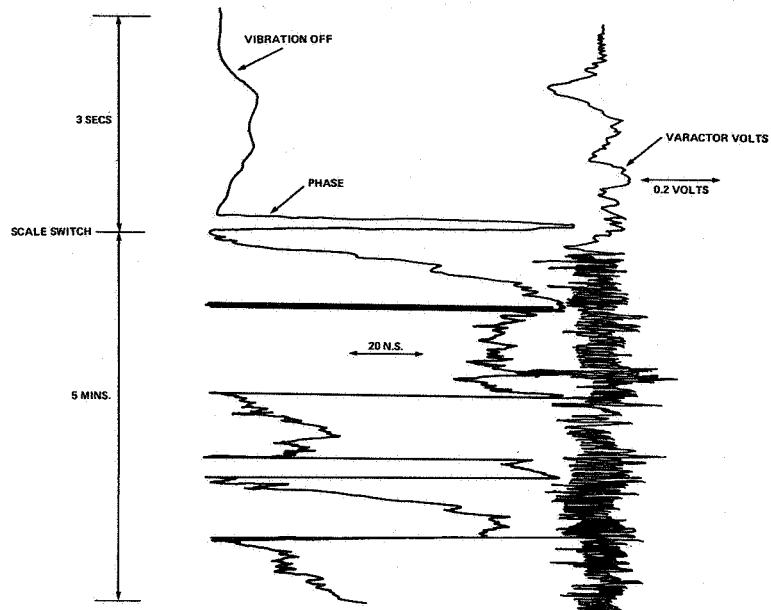


Figure 6. Noise Vibration M100-018.  
 $.026g^2/Hz$  Optic Axis Oct. 20/80

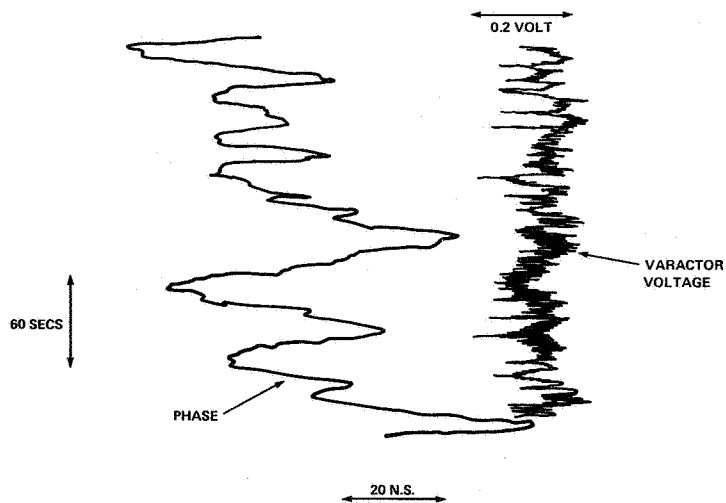


Figure 7. Noise Vibration FRK-H4548 Oct. 28/80  
 $.04g^2/Hz$  Normal To Labelled Side

#### REFERENCES

1. W. M. Bridge, "The Role of Precise Time in IFF," Proc. 13th Annual PTTI Meeting (this issue).
2. R. T. Allen, "A Review of the U.S. Navy's Precise Time and Time Interval Program," Proc. 10th Annual PTTI Meeting November 1978, NASA Tech. Memo 80250.
3. H. Hellwig and A. E. Wainwright, "A Portable Rubidium Clock for Precision Time Transport," Proc. 7th Annual PTTI Meeting, December 1975.
4. T. C. English, E. J. Jechart and T. M. Kwon, "Elimination of the Light Shift in Rubidium Cell Frequency Standards using Pulsed Optical Pumping," Proc. 10th Annual PTTI Meeting, November 1978.
5. N. F. Yannoni, "Precise Time Technology for Selected Air Force Systems: Present Status and Future Requirements," Proc. 12th Annual PTTI Meeting, December 1980, NASA Conference Publication 2175.

## QUESTIONS AND ANSWERS

DR. VICTOR REINHARDT, NASA/Goddard

Since you have measured the environmental performance of your rubidium, have you considered monitoring the ambient temperature and pressure, and fitting that out of your data before you take the Allan variance to see how well you can do?

MR. HOULDING:

The best units were actually operated with a simple bang, bang Servo controller, but even so if the room temperature varies about 8°C, as it sometimes does, things are not too good for the best results, shall we say.

In the paper, I do mention some results taken on the unit that didn't have temperature -- special control.

DR. REINHARDT:

What I mean is, instead of trying to control the temperature, since you have measured the temperature coefficient, just monitor it?

MR. HOULDING:

I don't believe in that. We have evidence that thermo transients do very odd things, and I find it very dubious. I don't believe in much of this modeling because you can't treat all these things as independent variables.

DR. REINHARDT:

That's true.

UNPRECEDENTED SYNTONIZATION AND SYNCHRONIZATION ACCURACY  
VIA SIMULTANEOUS VIEWING WITH GPS RECEIVERS;  
CONSTRUCTION CHARACTERISTICS OF AN NBS/GPS RECEIVER

Dick D. Davis, Marc Weiss, Alvin Clements, and David W. Allan  
Time and Frequency Division  
National Bureau of Standards

ABSTRACT

The NBS/GPS receiver has been designed around the concept of obtaining high accuracy, low cost time and frequency comparisons between remote frequency standards and clocks with the intent to aid international time and frequency coordination. The receiver has been tested by simultaneous viewing of the GPS satellites with the USNO GPS receiver as well as by several individual tests. The simultaneous viewing yielded syntonization accuracies of the order of parts in  $10^{15}$  over about a two-week average. Using a May '81 portable clock trip to calibrate the differential delay between the NBS and the USNO GPS receivers, July and August '81 portable clock trips agreed with the values given by simultaneous GPS satellite viewing between Boulder, CO and Washington, DC to better than the 10 ns accuracy of the portable clock trips.

The hardware and software of the receiver will be detailed in the text. The receiver is fully automatic with a built in 0.1ns resolution time interval counter. A microprocessor does data processing. Satellite signal stabilities are routinely at the 5ns level for 15s averages, and the internal receiver stabilities are at the 1ns level. The second generation receiver has a built in CRT and parallel keyboard for operator interface. Serial RS232 is provided for local hardcopy (printer) and telephone modem use.

## RECEIVER PHYSICAL CONSTRUCTION

The NBS/GPS receiver is housed in 3 rack mounted cabinets (plus a weather-tight case for the antenna electronics). The microprocessor, tape drive, 12.7cm(5 inch) CRT display and time interval counter are in a 17.8cm(7 inch) cabinet and the receiver and power supply are each in 13.3cm(5¼ inch) cabinets. It would be possible to fit everything except the antenna electronics into a single 17.8cm(7 inch) cabinet but access for testing would be much more difficult.

## MICROPROCESSOR BLOCK DIAGRAM

Figure 1 shows the microprocessor and its interfaces to the rest of the receiver system. The microprocessor card was specially designed for this application.

Major features are:

- 4MHz Z80A Processor Chip
- 32k Dynamic Ram
- 16k EPROM
- 2k Memory Mapped Video - 16 Lines x 64 Char
- 9 x 8 Bit Parallel Ports
- 2 USARTS (1 - RS232, 1 - Tape Drive)
- 24 Strobe Lines

Operator interface to the system is through a parallel keyboard and menu driven video display, a 12.7cm(5 inch) CRT is included in the processor box, with BNC out for an external TV monitor.

A micro-cassette tape drive is included for saving and loading (programs, tracking schedules and almanacs.)

An RS-232 interface is provided for connecting to a telephone modem to exchange tracking data.

A hard copy output is provided for printing tracking data and plots of satellite azimuth and elevation angle (AZ-EL) viewing times for any location and date.

A time interval counter card (ambiguity 1 sec, resolution .1ns) is included in the processor. The counter was designed for the GOES satellite system and improved for use in the GPS receiver. It is a start-stop interpolator counter with 5 MHz main channel time base. The processor calibrates the interpolators before each satellite pass. Repeatability of the counter is better than 1ns.

The receiver is controlled by the processor through a 34 line ribbon cable. The cable includes 8 parallel lines from the receiver, 2 x 8 parallel lines to the receiver, 4 strobes for multiplexing data to the receiver and 1 interrupt line from the receiver.

## RECEIVER BASIC FREQUENCY PLAN

The NBS receiver frequency plan is illustrated in Fig. 2. The receiver utilizes triple conversion, with the first IF at 75.42 MHz. This IF is wide band (25 MHz - 150 MHz) and provides about 50 to 55 dB of net gain. The correlation mixer converts the IF to 10.7 MHz. The post-correlation bandwidth is set by a 12 kHz crystal filter. The 10.7 MHz IF gain of 0 to 30 dB is controlled by the microprocessor during lock-up and by coherent AGC after lockup. The third IF of 700 kHz was chosen for ease of implementation of the phase coherent detectors using CMOS switches. Approximately 40dB of gain is provided in the 700 kHz IF. By limiting gain at each IF to less than 60 dB, we minimize stability problems. With this selection of IF frequencies we have no problems with carrier false lock due to spurious frequency interference.

## CORRELATION LOOP

The correlation loop is an early-late ( $\pm \frac{1}{2}$  chip) non-coherent type. The locally generated clear access (C/A) sequence bi-phase modulates 86.12 MHz from the carrier loop. The resultant signal is applied to the correlation mixer and, if the local and received sequences are aligned, the resultant 10.7 MHz IF out contains only the bi-phase (50Hz) data transitions (of course, with the early-late dither of the local code, one-half of each code chip is lost). Servo error voltage is obtained from the envelope detector during initial lock and from the in phase coherent detector through a 1 ms delay sampler when locked. Correlation loop bandwidth is set to 3 Hz during acquisition and 1 Hz while tracking.

## CARRIER LOOP

The carrier loop operates as a frequency synthesizer during correlation loop acquisition and a Costas loop when tracking. The companion microprocessor computes the expected Doppler from almanac data and sets the carrier synthesizer accordingly. Range is  $\pm 4800$  Hz, in 400 Hz steps. The carrier synthesizer will therefore be within  $\pm 200$  Hz of the carrier center frequency when the track mode is initiated. Carrier acquisition follows within one second.

## DETAILED RECEIVER BLOCK DIAGRAMS

Figures 3 and 4 show more detailed diagrams of the receiver and indicate the functions in the receiver that are controlled by the microprocessor.



## SOFTWARE

In this implementation of a GPS receiver, a single Z80A processor handles all the real time concurrent tasks of receiver control, satellite message acquisition, and control of a time interval counter making a pseudo range measurement each second. Without an interruption of any of the above functions, the processor computes a least squares quadratic fit of the pseudo range measurements each 15 seconds, evaluates the estimate at its mid-point, computes the slant range to the satellite at the time corresponding to the mid-point fit and arrives at a value for the local clock time minus the space vehicle clock time (LOCAL-SV) and LOCAL-GPS, where "GPS" denotes SV time plus the GPS computed SV clock correction. Each data point is displayed on the video display and is stored in memory for processing immediately after the end of the SV track time. The receiver is always responsive to the local keyboard interface and the RS-232 modem interface, even while tracking and processing data, thus allowing easy communication with the user. (We should note that 5 of the 8 interrupt driven programs are dedicated to making the machine friendly.)

For example, the operator can command the processor to erase an old almanac tape and write a new tape of the almanac that has just been collected while the unit is still tracking. The menu driven operator interface will even allow the operator to generate a 24 hour graph of satellite elevation/azimuth for any location and any date while the unit is tracking and collecting data. (The graph is limited to a maximum of 5 satellites at a time and is output to the printer).

All of these capabilities are made possible by a unique interrupt implementation. A total of 8 vectored interrupts are utilized:

Priority	Interrupt Rate	Function
1	50 Hz/1kHz	Control Receiver, collect serial satellite data
2	75Hz/200Hz	Read/write tape files
3	150 Hz	Receiver RS-232 data
4	100 Hz	Format video display
5	30 HZ	Make counter measurements (pseudo range)
6	30 Hz	Read KBD input, display on screen
7	150 Hz	Transmit/format RS-232 data
8	1 Hz	Run real time UTC clock

When an interrupt is taken, a complete context switch takes place, much as in a large time share system. This context switch requires about 70 $\mu$ s for each interrupt taken but the advantage is that the

interrupt driven program is written "in line" rather than having the same entry point each time an interrupt is taken. Each interrupt driven program is analgous to a program running on a time share system with one exception: on the time share system the central processor assigns a "time slice" to a single user and at the end of that time (say 10 milliseconds) the user's program is stopped and another user's program is taken up where it left off and is run for a few more milliseconds. The user is unaware of these "time slice" allocations and from his perspective, his program runs continuously to completion (unless the system is overloaded).

In our implementation the interrupt driven program's "time slice" starts when the interrupt is taken. The program continues to execute until the instruction "CALL INTERRUPT RETURN" is executed. All registers of the interrupt driven program are stored and the machine returns to the main program. When the next interrupt is taken, execution continues with the instruction following "CALL INTERRUPT RETURN", with all registers and status restored. The interrupt driven programs have been written so that no more than 500 $\mu$ s elapses before a "CALL INTERRUPT RETURN" is executed. All of the interrupt driven programs together utilize 5 to 15% of the total processor time.

With this introduction, we will examine the interactions of the MAIN (interruptable) program and the three interrupt driven programs that are responsible for locking to and tracking the satellite.

A satellite tracking operation begins when the 1 HZ interrupt driven program finds a match between its current hours, minutes, and seconds (HMS) clock time and any of the 48 user programmed satellite start track times. The 1 HZ program stores the SV# and SV class bytes in a reserved 2 byte variable area and loads the "start track" command byte into the main program's 16 byte circular command buffer. At the time this happens, the Main Program, and the Receiver and Counter programs may be idle (or) may be busy tracking another satellite. If they are tracking already, the main program recognizes this and will execute sequential commands "stop track", followed by "start track".

The 1 Hz program then sets a timer to count down for 7 minutes, 58 seconds at which time it will issue a "stop track" command to the main program. The 1 Hz program continues its timekeeping function and has no further direct interaction with the lockup/track sequence.

If the machine were idle at the time the 1 Hz program issued "start track", the main program would immediately vector to the start track program. It would first pick up the SV# and through a lookup table, set the proper C/A code into the receiver PN generator. It then sets the carrier loop synthesizer in the receiver to center frequency. Next, it picks up the binary almanac for the proper SV and converts it

to floating point decimal format. It then picks up an image of the UTC clock and computes the slant range to the satellite. It then increments the time of the UTC clock image by 100s and computes a second value of slant range to the satellite. From these 2 computations of slant range, it determines the expected carrier Doppler and sets the carrier synthesizer to the correct value.

At this point, the program is approximately 2 seconds into the lockup sequence. The main program now sets a flag to signal the receiver program to exit its idle loop and begin its lockup sequence. The main program continues on to the "calibrate counter routine" which will require approximately 8 seconds to complete. After the counter is calibrated, the main program returns to its idle loop. While the main program is calibrating the counter, the receiver program begins the receiver lockup sequence.

The amount of time required for the receiver program to lock up and find the HANDOVER WORD (HOW) in the SV data stream can vary from a minimum of 10 seconds to a maximum of 50 seconds, with the median being 30 seconds. At this point, the receiver program again needs the services of the main program to convert the binary HOW into DAY, HH, MM, SS and GPS seconds of the week (decimal). The receiver program issues a "Set Clock" command to the main program. The main program requires about 100 ms to set the GPS clock in the receiver. The receiver program then sets a flag to tell the counter program to exit its idle loop and start making a pseudo range measurement each second. The pseudo range measurements are stored in a modulo-30-second circular buffer.

The main program returns to its idle loop to await further commands. The receiver program continues to run the GPS clock and store serial 50 Hz data from the SV. It hangs in a loop until the end of Frame 5 of the GPS data format. (The end of frame 5 will be second 00 or 30 of the GPS minute).

At the end of frame 5, the receiver program enters a 30 second loop where it will remain until the track is terminated. In this loop, it continually collects serial SV data, runs the GPS clock, and outputs 1PPS for the pseudo-range measurements. It also gives commands to the main program at the appropriate times to convert data blocks I and II and verify parity and save the almanacs contained in data block III. Each 15 seconds, it gives a command to the main program to make a measurement computation.

A measurement computation involves doing a least squares quadratic fit to 15 seconds of pseudo-range data, evaluating the mid-point estimate of the fit, computing the slant range to the SV using data block II, making the sagnac correction, computing the SV clock correction using data Block 1, and storing a value for LOCAL-SV and LOCAL-GPS. This data is also output to the video display (and) to the hard copy device

if desired. A complete measurement computation sequence executes in 2.5 seconds. The main program is busy about 20% - 25% of the time and is in the idle loop the rest of the time.

The track time is terminated when the 1 Hz program timer counts down and the 1Hz program issues a "stop track" command to the main program. The main program forces the receiver program into a 1 second sequenced stop routine and sets a flag to signal the counter program to return to its idle loop when it completes its current measurement.

The main program then does a least squares linear fit on the 15 second data points for LOCAL-SV and LOCAL-GPS. It then stores the intercepts and slopes, along with the SV#, Ref time at beginning of track, AZ/EL at the end of the track, data age of DB II, and sigma for the fits. It then searches through all programmed track times and displays the next scheduled track time and returns to the idle loop.

The main program is by far the largest of the 9 programs running in the machine. As we have noted, it receives commands to do various functions through a 16 byte circular buffer. Up to 15 commands may be queued up at one time before the system blows up. Normally no more than 3 or 4 commands will be queued in the buffer. At present, a total of 18 different commands are executed by the main program, but this number will ultimately grow to the mid twenties when all the planned functions are added. All precise arithmetic functions are handled through a 15 decimal digit floating point package with hex interpreter, especially developed for this system. The floating point package occupies about 2K bytes.

All of the interrupt driven programs not discussed until now are concerned with input/output operations. The tape program reads and writes tape files. These may be data such as almanacs and track times or the "personalized" program that has the receiver coordinates for a particular location. The two RS-232 programs are concerned with communications over a telephone modem, and the video and keyboard programs provide the local operator interface.

The complete software package will approach 32 K bytes of machine language code, with 16K of firmware and display formatting in EPROM and 16K of program in RAM to be loaded from tape.

### Common View Data Analysis Results

As has been shown [1] one of the main advantages of the GPS in common-view approach is the cancellation of errors that are common in both legs of the viewing path when the same GPS satellite is viewed simultaneously. Therefore, the only errors in the time and frequency measurements between two remote sites are due to changes in the differential delays. The following analysis is an effort to characterize

the limitations of using GPS satellites in common-view measurements taken simultaneously at the U. S. Naval Observatory in Washington, DC with its GPS receiver and with the NBS constructed receiver located in Boulder, CO (a baseline of about 3,000 kilometers). We began collecting data using this mode on the 31st of May 1981 and performed the analysis over the period of June, July, August and September of '81. Three portable clock trips were made during this period and nearly daily values were taken on NAVSTAR satellites 3, 4, 5 and 6 which correspond to space vehicle (SV) 6, 8, 5 and 9 respectively. We agreed with USNO to measure at relatively high elevation angles after upload of the SV clock and ephemeris parameters from Vandenburg Air Force Base occurs; we also agreed to change the time once a week about 28 minutes to correspond with the movement of the ephemeris. Thus the satellites were viewed at nominally constant azimuth and elevation angles at each of the two sites. The USNO receiver applies ionospheric and tropospheric corrections. The NBS receiver collects the correction data, but the corrections were not applied. The viewing time for the constellation of the above four satellites moved from nominally midnight on the 31st of May to late morning for the September data--the data being taken over about a three-hour period for the four satellites. This moved the viewing through a significantly different period in the ionospheric profile--going from midnight delays to daytime delays. The coordinates of USNO and NBS used were  $38^{\circ} 55' 13.503''$  North Latitude,  $282^{\circ} 56' 0.151''$  East Longitude, + 47.68m elevation and  $39^{\circ} 59' 43.6220''$  North Latitude,  $254^{\circ} 44' 15.569''$  East Longitude, 1663.3m elevation respectively. Both sites are about the same latitude, which would make the differential delay in the ionosphere about the same.

The short-term stability has been analyzed in a previous paper [2]. Fig. 5, is a review of that stability showing the short-term white phase noise characteristics of the apparent propagation fluctuations from the satellite through the receiver, to the reference clock on the ground. If the white phase noise shown in Fig. 5 were the only limiting noise, the mean value of an 8 to 10 minute data set would have an uncertainty of less than one nanosecond. However, when we analyze the day-to-day fluctuations, they were of the order of 10 nanoseconds rms, which indicates that there is another random noise driving mechanism on the day-to-day fluctuations. A possible mechanism is the daily uncertainties in the ephemeris. Fortunately, in the common-view approach, the clock error goes to zero, and the ephemeris error is significantly reduced from the actual error realized in a navigation solution. Fig. 6 is a plot via the common-view approach of UTC(USNO) provisional-UTC(NBS) over the four-month period mentioned with a mean frequency of  $1.2 \times 10^{15}$  removed. The circles indicate the three portable clock trips made during this period. The first clock trip was simply used to calibrate the differential delay between the USNO and NBS receivers and amounted to 335 nanoseconds. The remaining two trips used that as a calibration value assuming it would remain con-

stant. The values were compared against quadratic least-squares fits to the data over the period in which the clock trip was taken. The portable clock values agreed to within three nanoseconds and two nanoseconds respectively of the estimated GPS measures of the USNO-NBS time difference. The uncertainties on the portable clock trips were at least 10 nanoseconds. The excellent agreement may be somewhat fortuitous, but is very encouraging. The four months of data were broken up into ten-day segments where continuous data were available. For each ten-day segment and for each of the space vehicles (SV6, 8, 5, and 9) NAVSTAR 3, 4, 5, and 6 respectively a linear-least-squares (LLS) fit to the USNO-NBS clock time differences was calculated. Each LLS fit gave an intercept and a slope. The consistency of these intercepts and slopes are a measure of the synchronization and syntonization accuracies respectively taken across the 4 satellites and as a time series given the ten-day average. Taken as a time series the uncertainty on the LLS fit for a single satellite was 4.7 nanoseconds and averaged across the four satellites was 2.2 nanoseconds. The uncertainty on the slope from a single satellite for the ten-day average was about 0.7 nanoseconds per day and averaged across the four satellites was 0.3 nanoseconds per day. A slight asymmetry in the intercept values was observed that seemed consistent from one ten-day interval to the next and amounted to a peak-to-peak of about seven nanoseconds which would indicate possibly an error in the coordinates at one or both of the sites.

Figure 7 shows a frequency stability analysis using modified  $\sigma_y(\tau)$  versus the sampling time [3]. The shaded area represents range of performance of the state-of-the-art standards that are currently being studied in various timing centers. The square blocks are stability measures for Loran-C taken over the last year for comparison purposes. The circles with the x in the middle are the frequency stability analysis of the data shown in Fig. 7 for the comparisons of the time scales UTC(USNO) versus UTC(NBS). The circles with the dots in the middle are estimates of the GPS measurement limit from the previous ten-day analysis. The one-day, two-day and ten-day values were calculated by measuring the same thing with the four satellites -  $\text{UTC(USNO)} - \text{UTC(NBS)}$ . It is interesting that the measures seem to follow a  $\tau^{-3/2}$  behavior, which would indicate white phase noise again, but at a higher level. There are no apparent indications of systematics for sample times out to ten-days, which allows us to have an incredible frequency comparison capability over ten-day samples of about three parts in  $10^{15}$ . It then becomes apparent that at the ten-day averaging time the GPS in common-view is about a factor of 26 times better than is Loran-C for the Washington, Boulder path. It is also interesting to note that for sample times of the order of four-days and longer, the instabilities of two of the best clock ensembles in the world are measurable using the GPS in common-view approach.

## CONCLUSION

The NBS developed GPS(C/A) receiver features hardware which has an intrinsic time stability of about 1ns when locking on to a GPS satellite signal. The Z80 based microprocessor software is very powerful, versatile, and friendly--with the ability to calibrate an internal 0.1 ns time interval counter as one of its many tasks. The design and parts selection for the receiver have been chosen to minimize cost and to maximize stability and reliability.

The receiver is also designed to be accessed through a modem so that it's data can be readily compared with receiver data taken simultaneously at a remote site, which is in common-view of the same satellite. Preliminary tests of this technique between Boulder CO and Washington D.C. indicate the ability to do accurate time transfer to better than 10 ns, and frequency measurements to better than 1 part in  $10^{14}$ .

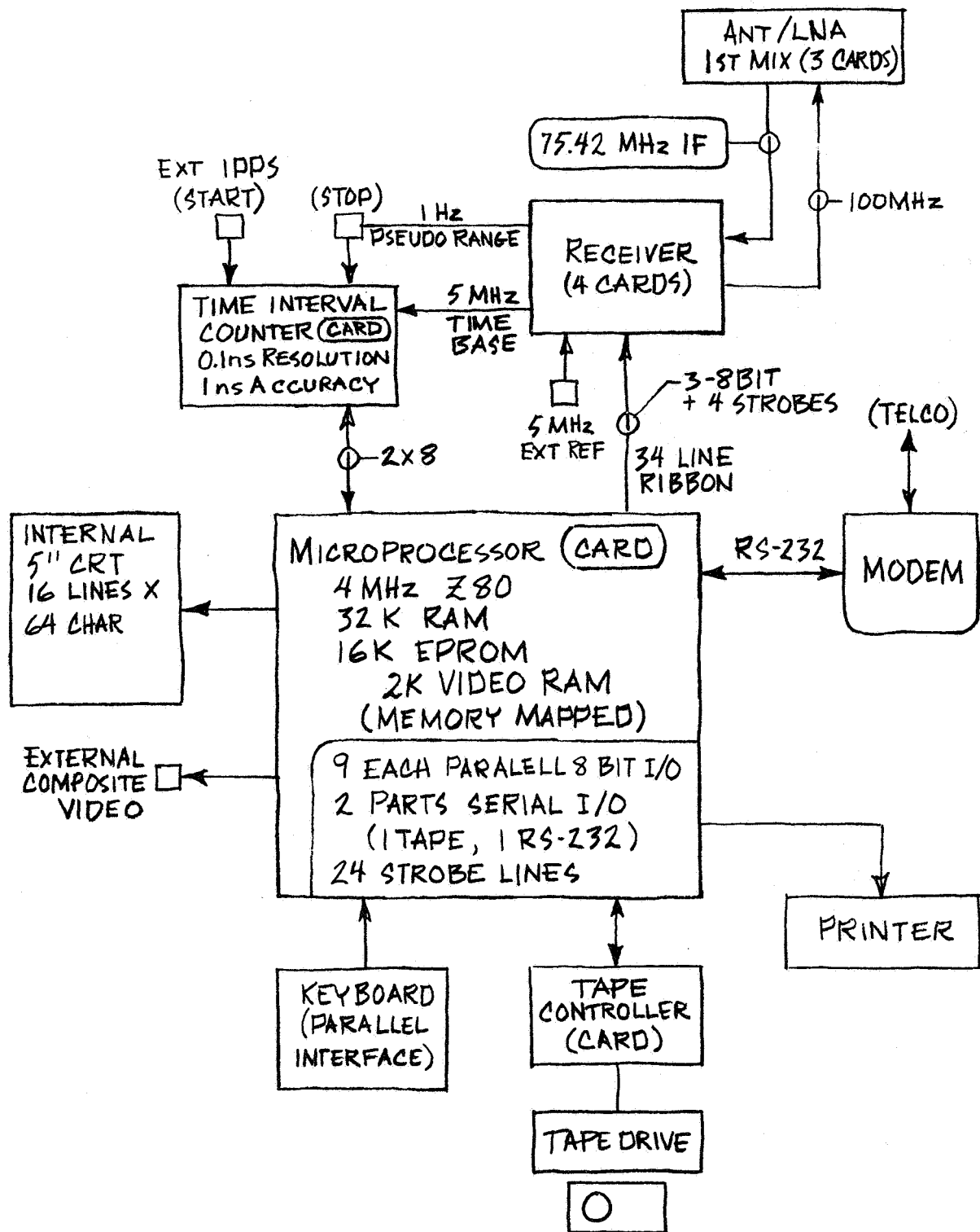
Because the GPS satellites orbit at about 4.2 earth radii and most of the T/F standards laboratories are at fairly high latitudes, the simultaneous common-view approach has the potential of working well for international time and frequency metrology. Experiments are planned to test these techniques internationally.

## ACKNOWLEDGEMENTS

The authors are deeply appreciative of the cooperation of the staff of the USNO. Also we wish to thank Mr. Roger Beehler and Professor Neil Ashby for their careful reading and comments on the paper. We are also grateful for the support of our sponsors: Air Force Space Division, Jet Propulsion Laboratories, Navy Metrology Engineering Center, and Naval Air Logistics Center. Without their support this project would most probably never have come to fruition.

## REFERENCES

- [1] D. Allan and M. Weiss, Accurate Time and Frequency Transfer During Common-View of a GPS Satellite, Proc. 34th Annual Symp. on Frequency Control (SFC), 334 (1980).
- [2] Davis. et. al., Construction and Performance Characteristics of a Prototype NBS/GPS Receiver, Proc. 35th Annual Symposium on Frequency Control (SFC) 1981.
- [3] D. Allan and J. Barnes, A Modified "Allan Variance" with Increased Oscillator Characterization Ability, Proc. 35th Annual Symposium on Frequency Control (SFC) 1981.

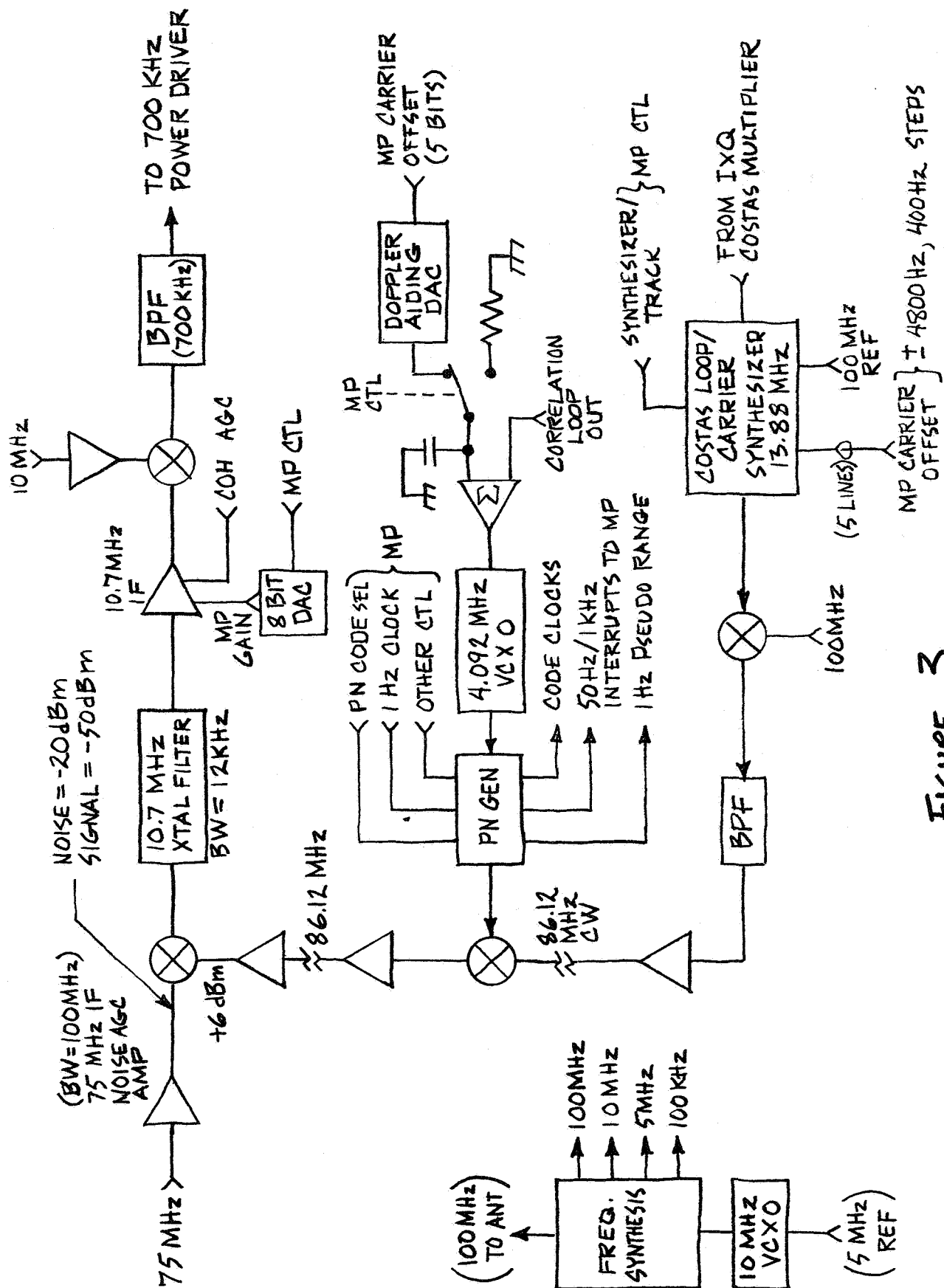


(UP TO 16K BYTE PROGRAM ON  
20 FOOT TAPE.  
LOAD TIME = 60 SECONDS)  
ALSO SAVES TRACKTIMES  
& ALMANACS.

FIGURE 1







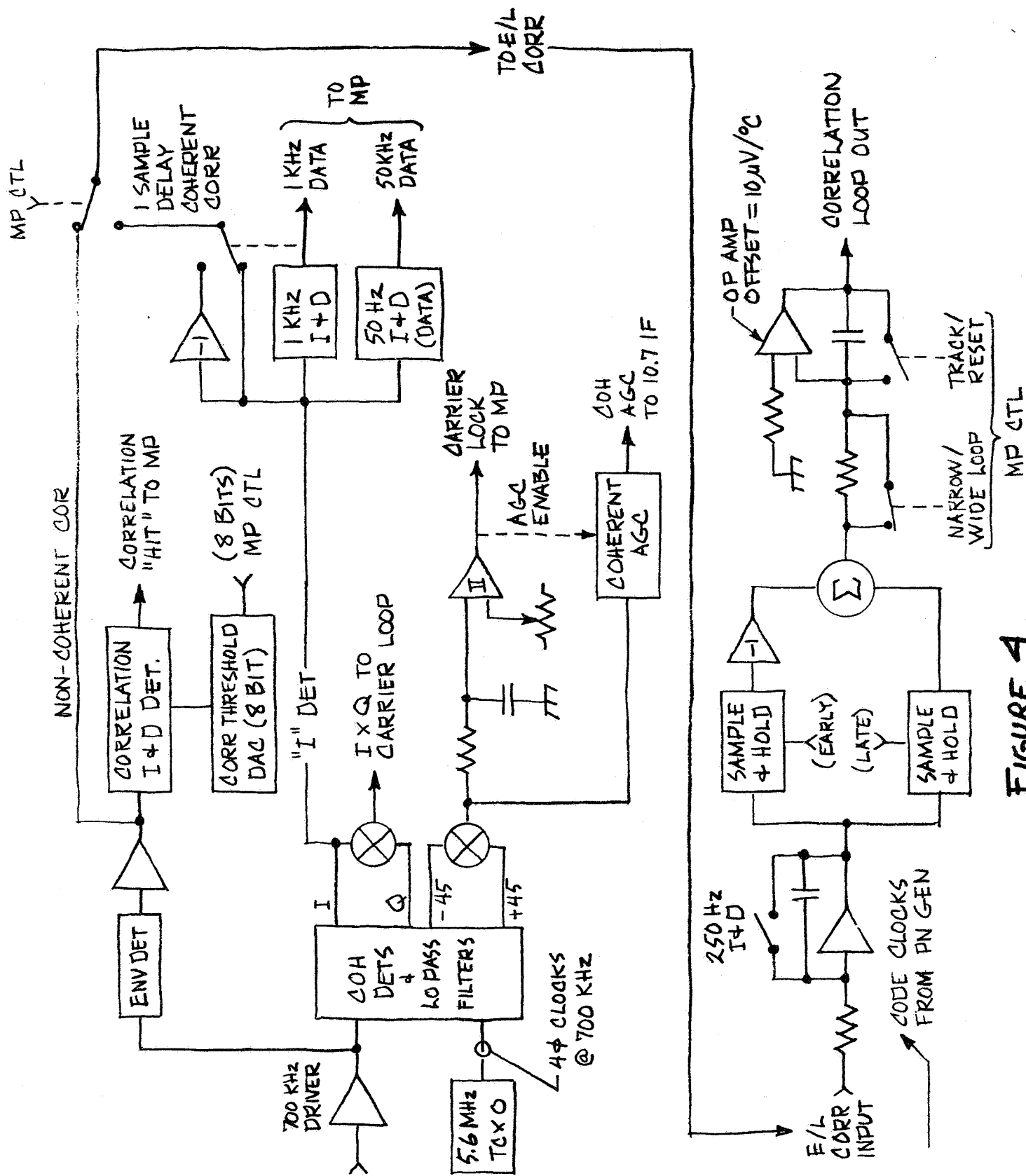
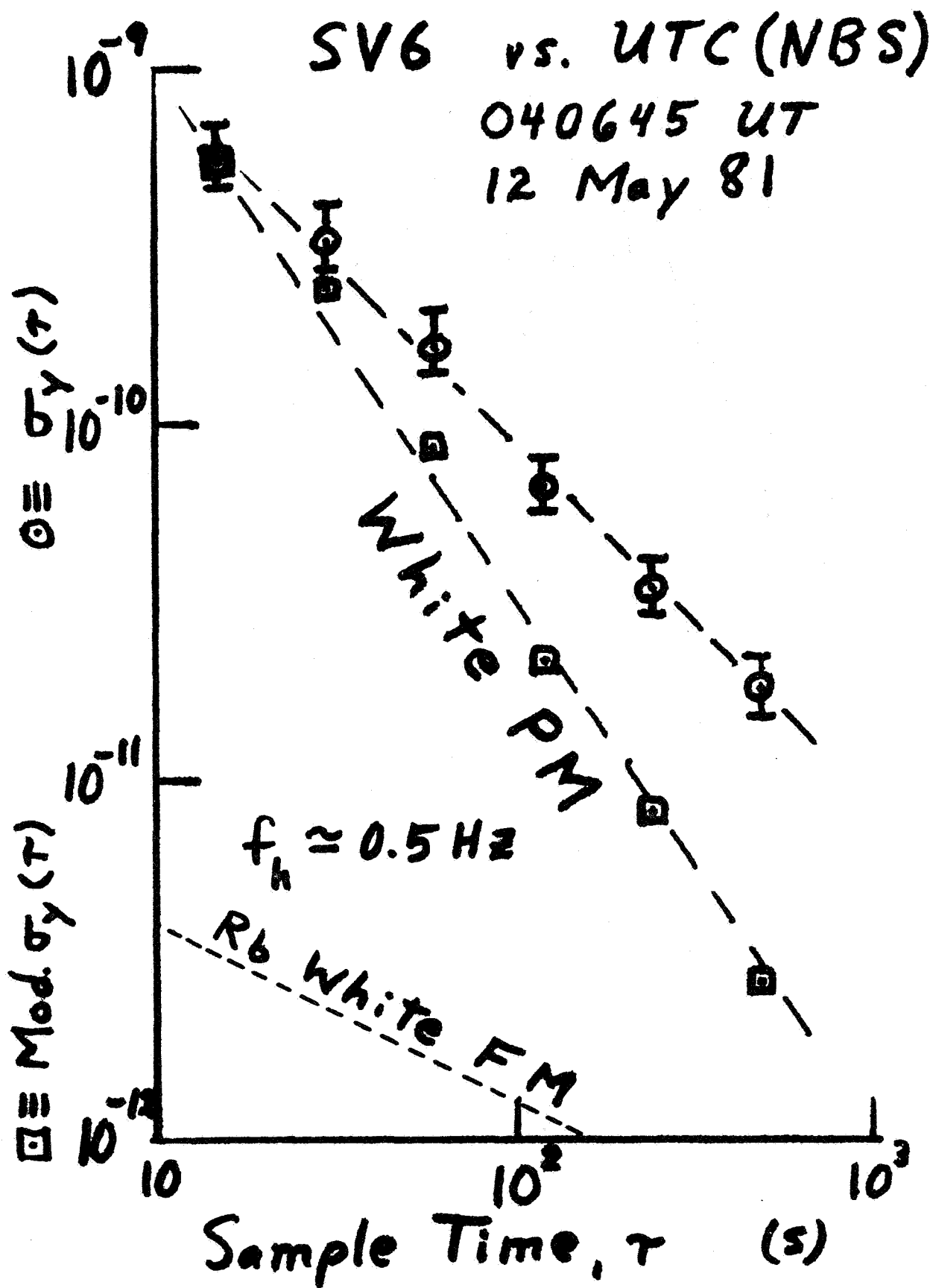


FIGURE 4

FIGURE 5



UTC(USNO) - UTC(NBS)

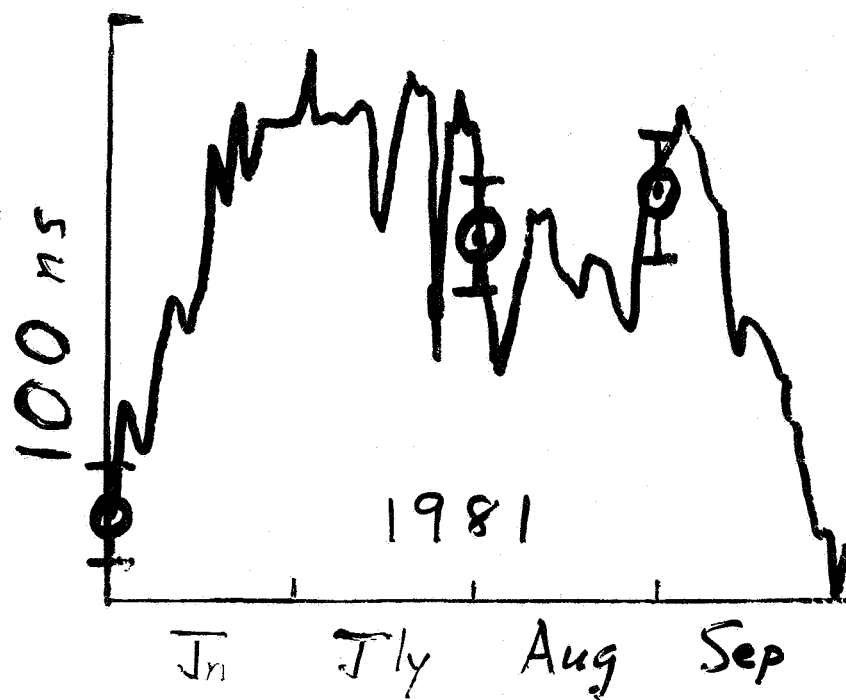
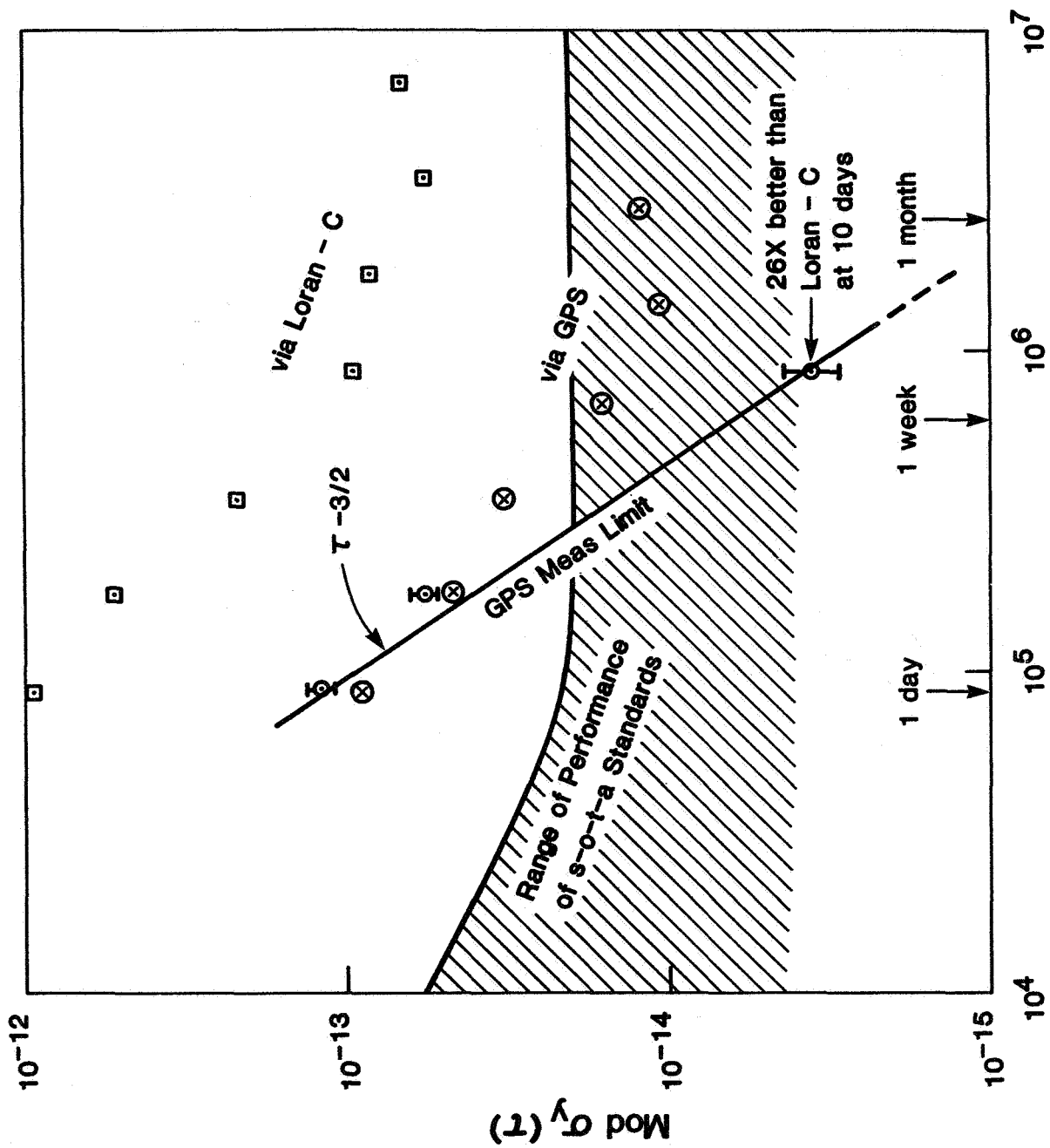


FIGURE 6

Frequency Stability  
UTC (USNO) vs. UTC (NBS)



Sample Time,  $\tau$  (s)

FIGURE 7

## QUESTIONS AND ANSWERS

MR. BOB VAN WECHER, Interstate Electronics

I had one question on your picture of the receiver with the antenna. It looked, at a quick glance, like the mixer was right on the antenna and there wasn't a pre-amp, or did I see wrong there?

MR. ALLAN:

There is a low-noise amplifier. A 40 dB low-noise amplifier immediately following the antenna, and then it goes through a very broad band seven pole filter. It's very flat over about 70 megahertz.

QUESTION FROM THE AUDIENCE:

I'd like to ask what type of ionospheric calibration, if any, were you using? How badly would the effects of different ionosphere degrade on intercontinental distances, say, Goldstone, Canberra, that type of thing?

MR. ALLAN:

It is a very, very good question. We don't know the answer. All we can do is calculate some numbers, and it looks like internationally we can from the results over this path 3,000 kilometered base-line, USNO/NBS, we would estimate we could probably do 10 nanoseconds dealing with the ionosphere models that we have.

SESSION V

INNOVATED FREQUENCY STANDARDS

Dr. Robert F. C. Vessot, Chairman  
Smithsonian Observatory





## CRYOGENIC MASERS

A. J. Berlinsky and W. N. Hardy  
Department of Physics, University of British Columbia  
Vancouver, B.C. V6T 1W5, Canada

### ABSTRACT

The long-term frequency stability of a hydrogen maser is limited by the mechanical stability of the cavity, and the magnitudes of the wall relaxation, spin exchange, and recombination rates which affect the  $Q$  of the line. Recent magnetic resonance studies of hydrogen atoms at temperatures below 1 K and in containers coated with liquid helium films have demonstrated that cryogenic masers may allow substantial improvements in all of these parameters. In particular the thermal expansion coefficients of most materials are negligible at 1 K. Spin exchange broadening is three orders of magnitude smaller at 1 K than at room temperature, and the recombination and wall relaxation rates are negligible at 0.52 K where the frequency shift due to the  $^4\text{He}$ -coated walls of the container has a broad minimum as a function of temperature. Other advantages of the helium-cooled maser result from the high purity, homogeneity, and resilience of the helium-film-coated walls and the natural compatibility of the apparatus with helium-cooled amplifiers, which are necessary to take advantage of the intrinsically low thermal noise of the cooled cavity.

### I. INTRODUCTION

The results on which this paper is based grew out of a program in which magnetic hyperfine resonance was used to study the behavior of hydrogen atoms at liquid helium temperatures ( $T < 4.2$  K). The primary motivation for this program was (and still is) the possibility of producing high densities of atomic hydrogen gas at sufficiently low temperatures that quantum degeneracy effects, similar to those which occur in superfluid  $^4\text{He}$ , might be observed. Since this paper is about masers, and not about superfluids, the latter subject will not be pursued any further. However the interested reader is referred to reviews by Berlinsky<sup>(1)</sup> and Hardy,<sup>(2)</sup> which discuss the problem of observing superfluidity in hydrogen gas and contain further details of our magnetic resonance work.

A natural dividend, accruing from our pursuit of superfluid hydrogen, has been the development of a practical working knowledge of the behavior of hydrogen atoms in a cryogenic environment. The ability, which we have developed, to maintain high densities of hydrogen atoms for long times and with extremely sharp magnetic resonance lines, is likely to lead to significant improvements in the stability of the hydrogen maser.

The idea of improving the frequency stability of hydrogen masers by lowering the maser temperature has been discussed by a number of authors. In particular Vessot et al.<sup>(3)</sup> noted that a thousand-fold improvement in the quality factor  $q$  (defined below) results from the fact that the spin exchange cross-section  $\sigma$  drops precipitously at low temperatures as does the thermal velocity  $\bar{v}$ . The main impediment to exploiting this advantage has been the lack of a suitable container for cold hydrogen-atoms. This problem has its analogue in room temperature masers where the development of fluorocarbon wall coatings was a necessary precursor to the successful operation of the hydrogen maser.

When a conventional maser, with Teflon-coated walls, is cooled to low temperatures, it stops operating somewhere below liquid nitrogen temperature (77 K) when the atoms begin to spend an excessive amount of time stuck to the Teflon, which both shifts their frequency and broadens the maser line. The natural solution is to use some less binding surface such as solid neon or, at lower temperatures still, solid  $H_2$ . However, at this point, the options quickly run out. The least binding surface, solid  $H_2$ , has a binding energy  $E_B$  for H of roughly 35 K.<sup>(4)</sup> This means that at very low temperatures ( $T < 5$  K) essentially all the hydrogen atoms are on the wall, and the magnetic resonance lifetime is too short for maser operation. An important breakthrough in our work was the discovery that liquid  $^4He$ -coated surfaces have a very low binding energy for hydrogen,  $E_B = 1.15$  K.<sup>(5)</sup> Liquid  $^3He$  is even better, with  $E_B = 0.40$  K.<sup>(6)</sup> However  $^3He$  is technically more difficult to work with, and hence we will concentrate in this paper on the use of liquid  $^4He$ -coated walls. (See, however, Hardy and Morrow<sup>(7)</sup> for more details on the use of  $^3He$  wall-coatings for hydrogen masers.)

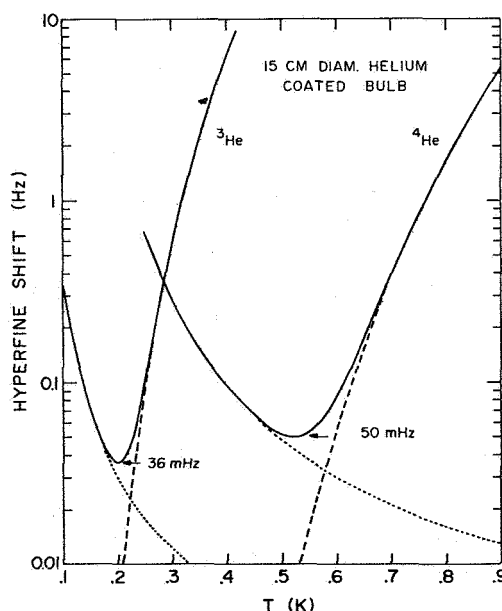


Fig. 1 - Predicted hyperfine shift vs temperature for a 15-cm-diameter bulb coated with liquid  $^3He$  and  $^4He$ .

Except at the lowest temperatures,  $T \ll 1$  K, the vapor pressure of  $^4\text{He}$  is substantial. This leads to a pressure shift of the hydrogen atomic resonance frequency, which is strongly temperature dependent, since it follows the vapor pressure of liquid  $^4\text{He}$ . To minimize this effect one would like to work at a temperature where the pressure shift is negligible, say at  $T \leq 0.4$  K. However this is just the region where the atoms start to stick to the  $^4\text{He}$  surface, which also causes a shift of the same sign. Thus there is a cross-over temperature where the total, pressure shift plus wall shift, has its minimum, as shown in Fig. 1. For the nominal maser dimensions that we assume in this paper (see below) the minimum occurs at  $T = 0.52$  K, which is thus the natural and, in fact, the only practical operating point for a  $^4\text{He}$ -cooled hydrogen maser.

The remainder of this paper is organized as follows: Section II contains a description of the various sources of frequency instability in a hydrogen maser, along with estimates of the size of these effects in conventional masers. In Sec. III, the various factors affecting the frequency stability, such as line Q and power, are related to maser design parameters, such as incident beam flux and storage time. In Sec. IV, we consider specific design parameters for a maser operating at  $T = 0.52$  K, and in Sec. V we estimate the stability that might be achieved in such a maser. We conclude that  $\Delta f/f$  of order  $2 \times 10^{-18}$  should be obtainable, which is about 300 times better than the stability of conventional hydrogen masers.

## II. SOURCES OF FREQUENCY INSTABILITY IN HYDROGEN MASERS

The main sources of frequency instability in a hydrogen maser are the following:

- 1) Thermal noise in the oscillator,
- 2) Receiver noise,
- 3) Time dependent frequency pulling due to fluctuations in the cavity frequency.

We will consider each of these in turn.

Thermal noise in the oscillator leads to random perturbations of the frequency of magnitude<sup>(8)</sup>

$$\left(\frac{\Delta f}{f}\right)_{\text{osc}} = \frac{1}{Q_\ell} \left(\frac{kT}{2P\tau}\right)^{1/2}, \quad (1)$$

where  $Q_\ell = \pi f_0 T_2$  is the Q of the maser line,  $f_0 = 1,420,405,751.773$  is the frequency of the maser,<sup>(9)</sup>  $P$  is the power radiated by the atoms, and  $\tau$  is the time of the measurement. In the situation in which the maser bulb, cavity, and isolator are all at the same physical temperature,  $T$  is that temperature. If the isolator is at a higher temperature, then the situation becomes more complicated.<sup>(7)</sup> Here, we assume that all components are at the same temperature.

The most important contribution to receiver noise arises in the first stage amplifier and contributes<sup>(3)</sup>

$$\left(\frac{\Delta f}{f}\right)_{\text{rec}} = \frac{1}{\omega_0 \tau} \left[ \frac{Bk(T + T_N)}{P_A} \right]^{1/2} \quad (2)$$

where  $B$  is the effective noise bandwidth,  $T_N$  is the noise temperature of the amplifier, and  $P_A$  is the power delivered to the amplifier. The relation of  $P_A$  to  $P$  is determined by the loaded  $Q$  of the cavity and the coupling  $Q$ ,  $Q_c$

$$P_A = \frac{Q}{Q_c} P \quad (3)$$

and

$$\frac{1}{Q} = \frac{1}{Q_0} + \frac{1}{Q_c} \quad , \quad (4)$$

where  $Q_0$  is the unloaded cavity  $Q$ . In general, conventional masers are lightly coupled while, as we shall see, it will usually be best to overcouple a helium-temperature maser.

Fluctuations in the cavity frequency,  $\delta f_c$ , pull the maser frequency by an amount

$$\Delta f = \frac{Q}{Q_l} \delta f_c \quad . \quad (5)$$

The source or sources of  $\delta f_c$  and their spectral distribution are not well understood. In conventional masers  $\delta f_c$  is often attributed to temperature fluctuations since the cavity frequency is quite measurably temperature dependent. However, mechanical instabilities almost certainly contribute also. The shift of the maser frequency  $\Delta f$  is proportional to the loaded  $Q$ . It may be minimized by overcoupling, which is only practical at low temperatures.

A measure of  $\Delta f/f$  is obtained by heterodyning two masers to a low difference frequency, say 1 Hz, and then measuring the time required to count a prescribed number of cycles of the difference frequency, say  $10^n$ ,  $n=0, 1, 2, \dots$ . The difference of two successive times allows calculation of the two-sample or Allan variance  $\sigma(2, T, \tau, B)$  where  $T$  (here only) is the time between the beginning of one measurement and the beginning of the next,  $\tau$  is the actual measurement time, excluding "dead time," and  $B$  is the bandwidth of the receiver. If the various contributions to  $\Delta f/f$  are independent then  $\sigma(2, T, \tau, B)$  is equal to the rms sum of these contributions. Measurements<sup>(3)</sup> of  $\sigma(2, T, \tau, B)$  for two VLG-11 masers are shown in Fig. 2. Both the short term  $\tau^{-1}$  behavior of Eq. 2 and the long term  $\tau^{-1/2}$  behavior of Eq. (1) are evident for  $\tau < 10^3$  s. For still longer times,  $\sigma$  begins to increase approximately as  $\tau^{1/2}$ , as the result of a systematic drift in relative frequency of the two masers.

This drift is caused by pulling due to changes in the cavity frequencies and the effect is smaller than  $10^{-15}$  at  $\tau = 10^3$  s. The minimum value of  $\Delta f/f$  achieved in Fig. 2 is about  $6 \times 10^{-16}$  for  $\tau \approx 1$  h.

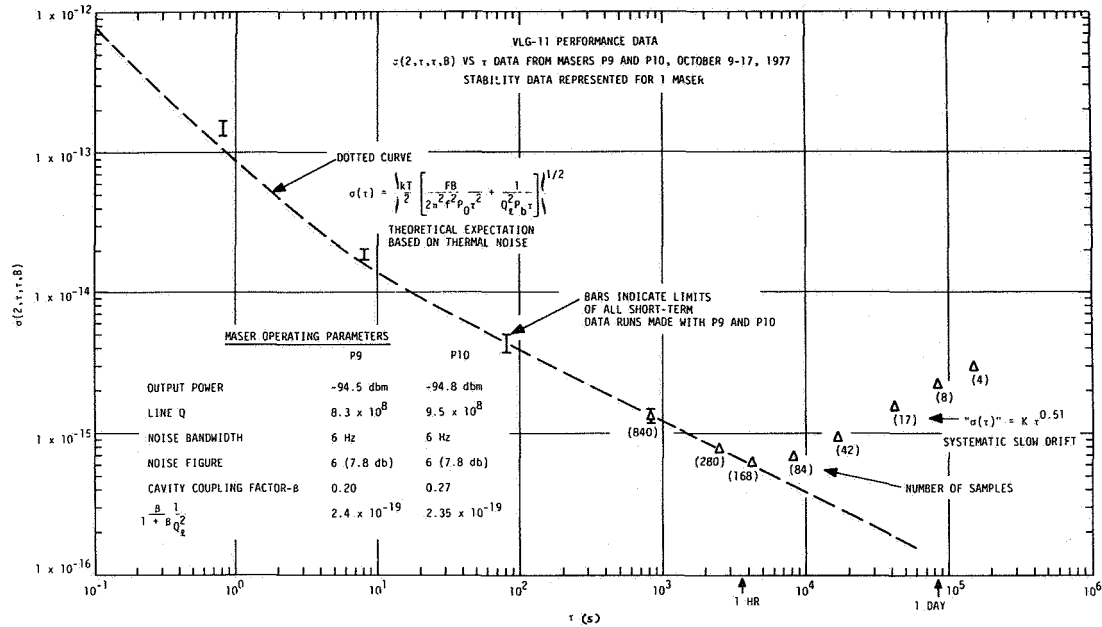


Fig. 2 - VLG-11 stability data.  $\sigma(2, \tau, \tau, B)$  vs  $\tau$  for masers P.9 and P.10, October 9-17, 1977.

### III. RELATION OF FACTORS DETERMINING FREQUENCY STABILITY TO THE OPERATING PARAMETERS OF A MASER

The condition for maser operation is simply that the power emitted by the atoms equal the power absorbed by or coupled out of the cavity. If the cavity is tuned to the maser frequency  $\omega = 2\pi f_0$ , then the power may be written as<sup>(10)</sup>

$$P = \frac{1}{2} \hbar \omega (I - I_0 T_b^2 / T_1 T_2) \quad , \quad (6)$$

where  $I$  is the net incident flux (i.e., the difference in flux of atoms in the  $F = 1, m_F = 0$  and  $F = 0, m_F = 0$  states, in atoms per second).  $T_b$  is the average time that an atom spends in the bulb, and  $T_1$  and  $T_2$  are, respectively, longitudinal and transverse relaxation times.  $T_1$  measures the rate with which the level populations achieve thermal equilibrium, and  $T_2$  is the time required for a collection of radiating atoms to lose phase coherence. The flux  $I_0$  is defined as

$$I_0 = \hbar V_c / (4\pi \mu_B^2 \eta Q T_b^2) \quad , \quad (7)$$

where  $V_c$  is the volume of the cavity,  $\mu_B$  is the Bohr magneton, and  $\eta$  is the "filling factor" defined as

$$\eta = \langle H_z \rangle_{\text{bulb}}^2 / \langle H^2 \rangle_{\text{cavity}} \quad . \quad (8)$$

Contributions to the relaxation rates,  $T_1^{-1}$  and  $T_2^{-1}$ , result from atoms leaving the bulb, from interactions with the wall and from spin exchange interactions between H atoms. Explicitly one has

$$\frac{1}{T_1} = \frac{1}{T_b} + \frac{1}{T_1^w} + \frac{1}{T_1^{se}} \quad (9a)$$

$$\frac{1}{T_2} = \frac{1}{T_b} + \frac{1}{T_2^w} + \frac{1}{T_2^{se}} \quad , \quad (9b)$$

where

$$\frac{1}{T_1^{se}} = \frac{2}{T_2^{se}} = \sigma \bar{v} n_H \quad . \quad (10)$$

Here  $\sigma$  is the spin-exchange cross section ( $\sigma = 2.31 \times 10^{-15} \text{ cm}^2$  at room temperature)<sup>(11)</sup> and  $\bar{v}$  is the thermally averaged relative velocity of pairs of hydrogen atoms ( $\bar{v} \approx 2 \times 10^4 \sqrt{T} \text{ cm/sK}^{1/2}$ ). Thus  $\sigma \bar{v} \approx 10^{-9} \text{ cm}^3/\text{s}$  at room temperature. The density of hydrogen atoms in the bulb  $n_H$  may be expressed in terms of the total flux  $I_{\text{tot}} \gtrsim 2 I$ , if magnetic hexapole state selection is employed, the volume of the bulb, and  $T_b$ ,

$$n_H = I_{\text{tot}} T_b / V_b \quad . \quad (11)$$

For liquid  $^4\text{He}$ ,  $T_2^w > 500 \text{ s}$  at  $T = 0.52 \text{ K}$  with  $A/V = 0.4 \text{ cm}^{-1}$  and  $T_1^w \gg T_2^w$ . Neglecting  $(T_1^w)^{-1}$  results in a great simplification in the analysis of Eq. (6). For the low temperature maser at low flux, spin exchange is unimportant, and  $T_1$  and  $T_2$  are essentially equal to  $T_b$ . Then Eq. (6) says that the maser turns on for  $I > I_0$ , the threshold flux. As  $I$  is increased,  $n_H$  increases and spin exchange causes  $T_1$  and  $T_2$  to become short. Eventually, at high flux the second term in Eq. (6) again dominates and the maser turns off. Somewhere in between, at  $I_{\text{max}}$ , the maser power passes through a maximum. The relevant scale of flux at which spin exchange becomes important can be inferred by examining the quantity

$$\frac{T_b}{T_2^{se}} = (I_{\text{tot}}/I) \frac{\sigma \bar{v} I T_b^2}{2V_b} \equiv (I/I_1) \quad . \quad (12)$$

The quantity  $I_{\text{tot}}/I \approx 2$  is innocuous. It differs from 2 only to the extent that state selection is imperfect or that there are Majorana transitions within the  $F = 1$  manifold. The quantity

$$I_1 = \frac{2V_b}{\sigma \bar{v} T_b^2} (I/I_{\text{tot}}) \quad (13)$$

is the flux at which the spin exchange width  $(T_2^{se})^{-1}$  equals the rate at which atoms leave the bulb,  $1/T_b$ . The ratio of the fluxes

$$q \equiv I_0/I_1 \quad (14)$$

is the same as the quality factor defined by Kleppner *et al.* <sup>(8)</sup> when  $1/T_1^W$  and  $1/T_2^W$  are negligible. Small values of  $q$ , which result when the spin exchange rate constant  $\sigma\bar{v}$  is small, correspond to a "good" quality factor. Kleppner *et al.* <sup>(8)</sup> showed that the maximum value of  $q$  for which a maser can operate is  $q = 0.172$ .

In terms of  $q$  and the quantity  $I/I_1$  the maser power is

$$P = \frac{1}{2} \hbar \omega I_1 [-q + (1 - 3q) (I/I_1) - 2q(I/I_1)^2] \quad (15)$$

This function is shown in Fig. 3a for  $0 \leq q \leq 0.16$  ( $q = 0.1$  is typical for conventional masers). In Fig. 3b Eq. (15) is plotted for  $q = 0.024$  and  $q = 0.0024$ , which are appropriate for low temperature. From Eq. (15) we find that for  $q \ll 1$  the maser threshold is  $I = qI_1 = I_0$ . The maximum in  $P$  occurs at  $I_{\max} = I_1/4q$ , and the maser turns off at  $I = I_1/2q$ . For small  $I$

$$P \approx \frac{1}{2} \hbar \omega I_1 [(I/I_1) - q] \quad (16)$$

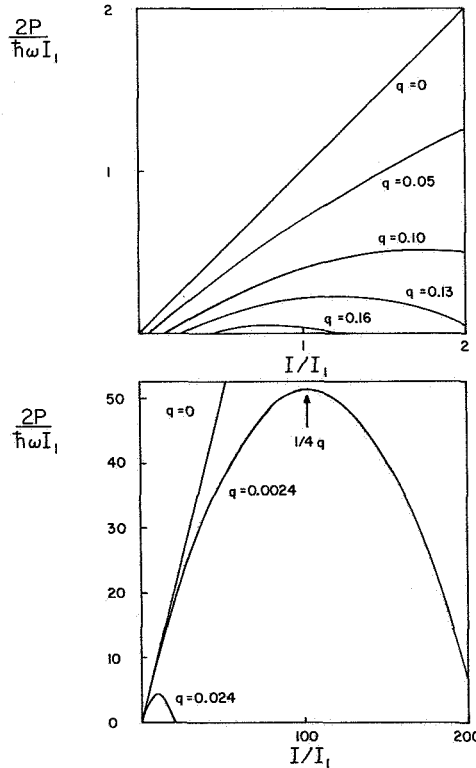


Fig. 3 — Power in units of  $\hbar\omega I_1/2$  versus incident flux in units of  $I_1$  as defined in Eq. (13) for various values of  $q$ , defined by Eqs. (7), (13) and (14). (a)  $0 \leq q \leq 0.16$  and (b)  $q = 0.024$  and  $0.0024$ .



For  $q \ll 1$  as is the case at low  $T$ , the long-term noise, Eq. (1), is minimized by operating at  $I = I_1$ . To see this define  $x = I/I_1$ . Then Eq. (1) may be written as

$$\left(\frac{\Delta f}{f}\right)_{\text{osc}} = \frac{2}{\omega T_b} \left(\frac{kT}{\hbar \omega I_1 \tau}\right)^{1/2} \frac{1+x}{\sqrt{x-q}}, \quad (17)$$

where we have used the fact the  $1/T_2 = (1+x)/T_b$  (cf. Eq. (12)).

Equation (17) is optimized by  $x = 1+2q \approx 1$  since  $q \ll 1$  by hypothesis. It is also noteworthy that, from Eq. (13) since  $I_1 \sim T_b^{-2}$ , Eq. (17) is independent of  $T_b$ .

For  $I = I_1$  and  $q \ll 1$  one obtains

$$\left(\frac{\Delta f}{f}\right)_{\text{osc}} = \left(\frac{8kT\sigma\bar{v}}{\hbar\omega^3 V_b \tau} \frac{I_{\text{Tot}}}{I}\right)^{1/2}. \quad (18)$$

Under the same assumptions the short-term receiver noise is given by

$$\left(\frac{\Delta f}{f}\right)_{\text{rec}} = \left[\frac{k(T_N + T) B\sigma\bar{v}}{\hbar\omega^3 V_b} \frac{Q_c}{Q} \frac{I_{\text{Tot}}}{I}\right]^{1/2} \frac{T_b}{\tau}, \quad (19)$$

which is proportional to  $T_b$ . Hence adjusting  $T_b$  affects the ratio of long-term noise to short-term noise for a given value of the averaging time  $\tau$ .

Other factors that can affect the stability of the maser are the spin exchange shift  $\Delta\nu_{\text{ex}}$ , which depends on the incident flux, and cavity pulling, if the cavity is mistuned, which also depends on the incident flux through the line  $Q_\ell$  (see Eq. (5)). Fortunately these two effects can be arranged to offset each other. Crampton<sup>(12)</sup> has shown that the sum of these two effects may be written as

$$\Delta\nu = \left[\frac{2Q}{\omega} (f_c - f_0) - \frac{1}{4\pi} qS \frac{I}{I_{\text{tot}}}\right] \frac{1}{T_2}. \quad (20)$$

The factor  $I/I_{\text{tot}}$  just cancels an identical factor in  $q$ , and  $S$  is the ratio of thermally averaged spin exchange shift to width cross section ( $S = \lambda^+/\sigma$ ). Equation (20) shows that if the cavity is properly mistuned then fluctuations in  $1/T_2$  will not affect the frequency. Of course the effect of fluctuations in  $f_c$  itself cannot be avoided by this technique.

#### IV. OPERATING PARAMETERS FOR $T = 0.52$ K

By now it is clear that the crucial difference between conventional masers and a helium temperature maser is the drastic reduction of the spin exchange broadening parameter  $\sigma\bar{v}$  at low  $T$ . This is illustrated in Fig. 4 where  $\sigma\bar{v}$  and the shift parameter  $\lambda^+\bar{v}$  are shown plotted versus  $T$ .  $\sigma\bar{v}$  is very close to  $10^{-12}$  cm<sup>3</sup>/s at 0.52 K, which is  $10^{-3}$  of its room temperature value. The curves in Fig. 4 are theoretical calculations by Allison<sup>(13)</sup> for  $T > 10$  K and by Berlinsky and Shizgal<sup>(14)</sup> for  $T < 10$  K. Experimental points<sup>(15-17)</sup> both at high

temperatures and at 1.2 K confirm the theoretical predictions. The shift parameter changes sign twice in going from room temperature to  $T < 1$  K. At  $T = 0.5$  K the ratio  $S$  of shift to width has the value 95 compared to room temperature where  $S = 0.2$ . However it is the product  $qS$  that appears in the tuning (Eq. (20)) and this product is smaller at 0.5 K than at 300 K for values of the loaded  $Q$  larger than about half the  $Q$  of the room temperature maser.

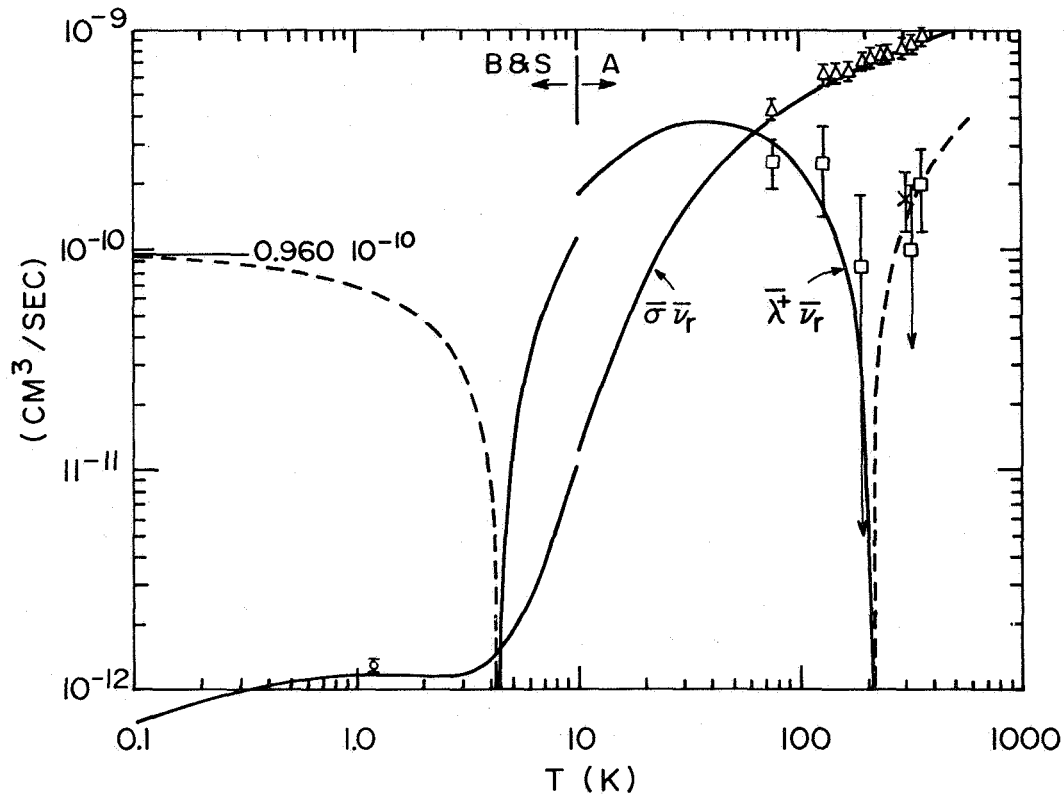


Fig. 4 - Spin exchange width ( $\sigma$ ) and frequency shift ( $\lambda^+$ ) cross sections times relative velocity. Dashed lines represent negative values of  $\lambda^+ \bar{v}$ . B+S refers to the theory of Berlinsky and Shizgal, Ref. 14. Symbols are experimental data:  $\Delta = \sigma \bar{v}$  and  $\square = \lambda^+ \bar{v}$  from Ref. 15.  $x = \lambda^+ \bar{v}$  from Ref. 16.  $o = \sigma \bar{v}$  from Ref. 17.

At this point it is useful to choose nominal values for the maser parameters so that estimates can be made of the operating conditions and potential stability of the low temperature maser. For convenience we choose parameters appropriate to conventional masers:  $V_b = 1.8 \times 10^3 \text{ cm}^3$ ,  $V_c = 1.3 \times 10^4 \text{ cm}^3$ ,  $\eta = 3$ . Our analysis will be quite insensitive to the value of the loaded  $Q$  although we assume  $Q \ll Q_0$ , the intrinsic  $Q$  of the cavity. We expect  $Q_0 \sim 10^5$  and  $10^2 < Q < 5 \times 10^3$ . The minimum possible value of  $Q$  is that which implies  $q = 0.172$ . From Eqs. (7), (13), and (14), taking  $I_{\text{tot}}/I = 2$  this value is  $Q_{\text{min}} = 14$  at  $T = 0.52$  K. For  $Q = 100$ ,  $q = 0.024$ , and the maximum in the power curve occurs at  $I \gg I_1$ . (See Fig. 3b.) For  $Q = 1000$  the condition  $q = 0.0024 \ll 1$  is well satisfied. The only advantage of the smaller value,  $Q = 100$ , is that the

effect of cavity pulling is further suppressed. However we shall see in the next section that this effect is likely to be negligible even for  $Q = 1000$ . We would like to comment at this point that the final choice of a value of  $Q$  may require consideration of additional contributions to  $\delta f_c$  arising from overcoupling. In fact it is the product  $Q\delta f_c$ , which should be optimized by a proper choice of  $Q$ .

The value  $Q = 1000$  implies a threshold flux  $I_0 = 4.2 \times 10^{12} \text{ s/T}_b^2$ . Independent of  $Q$  we have  $I_1 = 1.8 \times 10^{15} \text{ s/T}_b^2$ . Since  $I_{\text{Tot}} \approx 2 I_1$ , operating at  $I = I_1$  requires a total flux of  $3.6 \times 10^{15} \text{ s/T}_b^2$ . For  $T_b = 1 \text{ s}$ ,  $I_{\text{Tot}}$  is about 100 times larger than that of a conventional maser where the limitation results from the speed of the vacuum pumps. At low temperatures pumping is not such a problem because helium temperature surfaces cryopump molecular hydrogen with great efficiency. It may also be desirable to work with a larger value of  $T_b$  if the short term noise is not too severe. Taking  $T_b = 10 \text{ s}$  reduces  $I_1$  to quite a manageable rate.

A number of other advantages appear when operating at liquid helium temperature, which are peripheral to the maser bulb and cavity. For example, one has available liquid helium-cooled pre-amplifiers, based on GaAs FET's, with noise temperature  $T_N$  of 10 K, which greatly reduce receiver noise. Magnetic state selection is also more efficient at low  $T$  because atoms emerging from low temperature sources move more slowly and hence are easier to focus. On the other hand a variety of complications result from the presence of the liquid  $^4\text{He}$  film. For instance the vapor pressure of  $^4\text{He}$  at this temperature is slightly higher than one would like. The mean free path for hydrogen in the  $^4\text{He}$  vapor<sup>(7)</sup> will be about 1.4 cm at  $T = 0.52 \text{ K}$ , which will make it difficult to inject the hydrogen atoms in a beam. Also the tendency of the  $^4\text{He}$  film to flow toward warmer temperature regions where it evaporates and is then pumped back down into the bulb implies a region of refluxing  $^4\text{He}$  vapor near the entrance of the bulb. In certain circumstances this can act as a  $^4\text{He}$  vapor diffusion pump<sup>(18)</sup> for the hydrogen atoms, and this effect might possibly prove useful in the design of the apparatus.

## V. ESTIMATES OF THE POTENTIAL STABILITY OF A HYDROGEN MASER OPERATING AT $T = 0.52 \text{ K}$

We are now in a position to estimate the actual sizes of the various contributions to the frequency fluctuations of a maser operating at 0.52 K. The physical parameters of the maser that we consider are those mentioned above:  $V_b = 1.8 \times 10^3 \text{ cm}^3$ ,  $V_c = 1.3 \times 10^4 \text{ cm}^3$ ,  $\eta = 3$ . The values of  $T_b$  and  $Q$  will be left free to optimize the performance of the maser. Then for  $I_{\text{Tot}}/I = 2$ ,  $I = I_1$ , and  $\sigma\bar{v} = 10^{-12} \text{ cm}^3/\text{s}$ , Eq. (18) has the value

$$\left(\frac{\Delta f}{f}\right)_{\text{osc}} = \frac{2.9 \times 10^{-17}}{\tau^{1/2}} \text{ s}^{1/2}, \quad (21)$$

and for  $T_N = 10 \text{ K}$  and  $B = 6 \text{ Hz}$ , Eq. (19) gives

$$\left(\frac{\Delta f}{f}\right)_{\text{rec}} = 1.2 \times 10^{-16} T_b/\tau. \quad (22)$$

$T_b$  is then determined by equating the short and long term noise at a suitable averaging time such as  $\tau = 10^3$  s. The result is  $T_b = 8$  s, and then the rms sum of the two contribution is  $\sqrt{2}$  times the long term noise, i.e.,  $\Delta f/f = 1.3 \times 10^{-18}$  for  $\tau = 10^3$  s and  $T_b = 8$  s. The effect of choosing  $T_b$  is to determine the operating flux  $I_1$  through Eq. (13).  $T_b = 8$  s implies  $I_1 = 2.8 \times 10^{13}$  s $^{-1}$  and hence  $I_{\text{tot}} \approx 5.6 \times 10^{13}$  s $^{-1}$ , which is comparable to fluxes employed in conventional masers.

This value of  $I_{\text{tot}}$  determines  $n_H$ , the density of atoms in the bulb, to be  $n_H = 2.5 \times 10^{11}$  cm $^{-3}$ . We have measured the rate constant for recombination for H into H $_2$  at this temperature in the presence of liquid  $^4\text{He}$ . The rate constant which we measure implies a recombination lifetime  $\tau_b = 1.4 \times 10^5$  s at this density of hydrogen. Thus for  $T_b = 8$  s nearly all the atoms leave the bulb before they recombine.

Next we consider the effect of time dependent pulling due to fluctuations in the cavity frequency. At room temperature these fluctuations are thought to result from the nonzero temperature dependence of the frequency of the cavity. Such effects will be totally negligible below 1 K where thermal expansion coefficients of most technical materials are extremely small. For example the thermal expansion coefficient of copper at  $T = 0.5$  K is less than  $10^{-5}$  of its room temperature value. Mechanical instabilities are more difficult to analyze. However it is unlikely that they will be more severe at low  $T$ .

In any case one can minimize pulling effects by reducing the value of  $Q/Q_\ell$  in Eq. (5). At room temperature this quantity is typically around  $2 \times 10^{-5}$ . For the low temperature maser,  $Q_\ell = \pi f_0 T_2 = 1.8 \times 10^{10}$  for our optimal case ( $T_2 = T_b/2 = 4$  s). Then, taking  $Q = 1000$ ,  $Q/Q_\ell = 5.6 \times 10^{-8}$ , and cavity pulling should be down by a factor of  $3 \times 10^{-3}$ . Since cavity pulling effects are already well below the  $10^{-15}$  level for  $\tau = 10^3$  s at room temperature, this lower value of  $Q/Q_\ell$  should allow operation with stabilities  $\Delta f/f$  of order  $10^{-18}$ .

An obvious additional source of frequency instability in the low temperature maser is the temperature dependence of the wall shift. Near the minimum frequency  $f_{\text{min}}$  the temperature dependence may be represented as

$$f(T) = f_{\text{min}} - 3.73 (T - T_{\text{min}})^2 \quad (23)$$

If the fractional frequency stability required is  $\Delta f/f$  then the temperature must be maintained within  $\Delta T$  of  $T_{\text{min}}$  where

$$\Delta T = \left( \frac{\Delta f/f}{3.73/f} \right)^{1/2} \quad (24)$$

Taking  $\Delta f/f = 10^{-18}$  implies  $\Delta T = 20 \mu\text{K}$ . This level of temperature stability is well within the capability of modern low temperature technology. To illustrate this point we show in Fig. 5 recent high resolution measurements, by J.A. Lipa of Stanford University, of the heat capacity of liquid  $^4\text{He}$  near the  $\lambda$  transition at 2.2 K.<sup>(19)</sup> Controlled temperature drift rates in this experiment ranged from 1 K/s to  $9 \times 10^{-8}$  K/s and the temperature resolution was  $6 \times 10^{-10}$  K for a

bandwidth of 1 Hz at 2.2 K. Note that the entire width in temperature covered by Fig. 5a is the width within which a low temperature maser would have to be controlled.

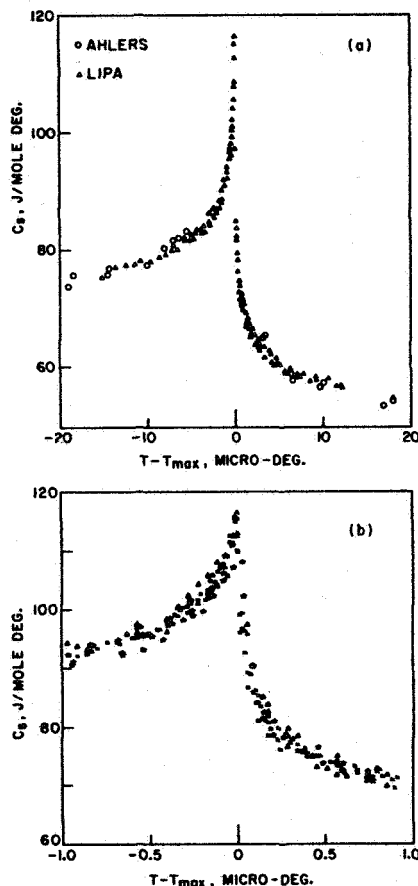


Fig. 5 — Heat capacity measurements close to  $T_{\lambda}$  for liquid  $^4\text{He}$  from Ref. 19. This figure illustrates the state of the art of temperature control at 2.2 K, which is not very different from the situation at 0.52 K.

We conclude that the achievement of frequency stability of order  $2 \times 10^{-18}$  for a measuring time  $\tau = 10^3$  s is a plausible objective for helium-cooled hydrogen masers operating at the temperature where the wall shift has its minimum. This will not be an easy goal to achieve, and one can say with confidence that many technical difficulties will arise in the course of development, which will have to be dealt with. However it is also true that we have learned quite a lot in the past few years about hydrogen atoms in the presence of liquid-helium-coated walls, and that this knowledge has allowed us to construct a fairly complete scenario of how a cold maser might operate. Based on this scenario the stability estimates given above appear reasonable.

We would like to acknowledge many useful discussions with Dr. R.F.C. Vessot of the Smithsonian Astrophysical Observatory. This work is supported in part by grants from the Natural Sciences and Engineering Research Council of Canada and from the Harvard-Smithsonian Center for Astrophysics. One of us (AJB) has also received the support of an Alfred P. Sloan Foundation Fellowship.

## REFERENCES

1. A.J. Berlinsky, J. Appl. Phys. 52, 2309 (1981).
2. W.N. Hardy, Int. Conf. Low Temp. Phys., Physica 107 B+C (1981).
3. R.F.C. Vessot, M.W. Levine, and E.M. Mattison, Proc. 9th Annual Precise Time and Time Interval Conference, 549 (1978).
4. S.B. Crampton, J. de Physique 41, C7-249 (1980).
5. M. Morrow, R. Jochemsen, A.J. Berlinsky, and W.N. Hardy, Phys. Rev. Lett. 46, 195 (1981); Erratum: Phys. Rev. Lett. 47, 852 (1981).
6. R. Jochemsen, M. Morrow, A.J. Berlinsky, and W.N. Hardy, Phys. Rev. Lett. 47, 852 (1981).
7. W.N. Hardy and M. Morrow, Third Symposium on Frequency Standards and Metrology, Aussois, France, 1981, to appear in J. de Physique C.
8. D. Kleppner, H.M. Goldenberg, and N.F. Ramsey, Phys. Rev. 126, 603 (1962).
9. P. Petit, M. Desaintfusicien, and C. Audoin, Metrologia 16, 7 (1980).
10. D. Kleppner, H.C. Berg, S.B. Crampton, N.F. Ramsey, R.F.C. Vessot, H.E. Peters, and J. Vanier, Phys. Rev. 138, A972 (1965).
11. M. Desaintfusicien, J. Vennet, and C. Andoin, Metrologia 13, 125 (1977).
12. S.B. Crampton, Ph.D. Thesis, Harvard, 1964 (unpublished).
13. A.C. Allison, Phys. Rev. A5, 2695 (1972).
14. A.J. Berlinsky and B. Shizgal, Can. J. Phys. 58, 881 (1980).
15. M. Desaintfusicien, J. Vennet, and C. Andoin, Metrologia 13, 125 (1977).
16. S.B. Crampton, J.A. Duvivier, G.S. Read, and E.R. Williams, Phys. Rev. 5, 1752 (1972).
17. W.N. Hardy, M. Morrow, R. Jochemsen, B.W. Statt, P.R. Kubik, R.M. Marsolais, A.J. Berlinsky, and A. Landesman, Phys. Rev. Lett. 45, 453 (1980).
18. I.F. Silvera and J.T.M. Walraven, Phys. Rev. Lett. 44, 164 (1980).
19. J.A. Lipa, Int. Conf. Low Temp. Phys., Physica 107 B+C, 343 (1981).

## QUESTIONS AND ANSWERS

DR. VESSOT:

There have to be questions. The reason that there have to be questions is we are now, I think, on the threshold of something that's very, very good. And I think the questions are more likely in the line of speculations to what can you do with two in 10 to the 18.

I can think of gravitational waves. But then that would be stealing other people's thunder, and that's another session this afternoon.

DR. REINHARDT:

In trying to achieve a maser at these low temperatures I think the real glitch is going to be state selection, because the interaction with the high temperature state selector and the low temperature environment.

However, there is an alternative which you can just use the natural occurring population difference and use an absorbing cell. That has many problems.

Do you want to comment on that?

DR. BERLINSKY:

Well, I guess if we made a frequency standard which was just looking at the magnetic resonance line, then the sense corresponds to what you say.

Let me comment in this way. The philosophy I believe that you have to use to design a low temperature maser is just to think of everything in terms of low temperatures.

Now I agree with you that it may be difficult to make a room temperature state selector which is compatible with a low temperature maser. But I would never do it that way. I would make a low temperature state selector, just as we have a low temperature amplifier, and somebody is going to have to build a low temperature isolator.

And I think that you can design a state selector for us in this environment, which would probably work extremely well. And, in fact, I'd love to talk about how to do that.

DR. VESSOT:

Let's have another question. And then you can argue that one over lunch.

DR. BERLINSKY:

Okay.

DR. MICHEL TETU, Laval University

I want to underline the fact that you used, in order to get provision of the short-term and mid-term stability of your maser, an equation that might be not exactly the right one. And at the end of this session I will give a talk in which I will recall these relations.

And I suggest that you look at a paper by Claude Audoin at the Philadelphia meeting on the 33rd Symposium on Frequency Control. To get there a reevaluation of the theoretical expression for short-term stability of maser.

And I think people have to be aware of this calculation.

DR. VESSOT:

Is it better or is it worse? Give us the bottom line Michel.

DR. TETU:

I think that it will be a little worse, but not really more than an order of magnitude.

DR. BERLINSKY:

Can you just say what factor it is different?

DR. TETU:

You have already a factor of four for the thermal noise spectral density, and also the fact that the noise from the receiver is not expressed exactly as the f-factor. But you have to add it separately with an f for the noise figure, minus one, times the spectral density of the thermal noise.

DR. WINELAND:

Is there any particular reason here for doing your calculations in terms of oscillating masers?



DR. VESSOT:

He's been prejudiced by me. But carry on.

DR. BERLINSKY:

Yeah, there are several aspects of my calculation which are tied to what look to me to be conventional maser designs. And I think as we get further into the business that many things will change.

DR. WINELAND:

But there's no particular reason?

DR. BERLINSKY:

No. I would say no.

DR. WALLS:

Except for the problem of a local oscillator. We don't have any local oscillators which are 10 to minus 15, or 10 to minus 16, or 17 at a second that would allow to realize these incredible numbers you are talking about.

I think a self-excited oscillator is probably the only way to reach those levels.

## A TRAPPED MERCURY 199 ION FREQUENCY STANDARD

Leonard S. Cutler, Robin P. Giffard, and Michael D. McGuire  
Hewlett-Packard Laboratories, Palo Alto, California

### ABSTRACT

Mercury 199 ions confined in an RF quadrupole trap and optically pumped by mercury 202 ion resonance light form the basis for a high performance frequency standard with commercial possibilities. This report describes some results achieved to date and gives estimates of the potential performance of such a standard.

### DESCRIPTION OF STANDARD

The mercury 199 ion has a number of desirable properties for a hyperfine frequency standard (1-3). It is massive and thus has relatively small, second order doppler shift. The hyperfine frequency is 40.5 GHz, high enough to give good line Q but not so high as to be very difficult to generate. The nuclear spin is  $1/2$  so the hyperfine levels,  $F=0$  and  $F=1$ , have only one and three states respectively, and the transition between the  $m=0$  levels has no first order magnetic field dependence. Since the hyperfine frequency is high, the second order magnetic field dependence is small, allowing good performance with relatively simple shielding. A simple optical pumping and detection scheme exists.

The energy levels of the mercury 199 and 202 ions are shown in Fig. 1 (2). Mercury 202 has no nuclear spin and consequently no hyperfine structure. The transition between its ionic ground state and the first excited state matches fairly well the transition between the  $F=1$  level in the mercury 199 ion and its first excited states at a wavelength of 194.2 nm. Consequently 199 ions will be pumped from the  $F=1$  level to the excited states from which they will decay back to both ground state levels. In the absence of relaxation they would all end up in the  $F=0$  level. A sample of ions so pumped would become transparent to the pumping radiation and the fluorescence would vanish. Microwave radiation at the resonance frequency between the  $F=0$  and  $F=1$  levels would re-populate the  $F=1$  level, making ions available for pumping and producing fluorescence. Observation of this fluorescence can thus be used to detect the hyperfine resonance.

The ions must have a long lifetime if they are to have a narrow linewidth. This is accomplished by using an RF quadrupole trap. Neutral mercury 199 inside the trap is bombarded with an electron beam to form ions which will stay in the trap if the potentials and drive frequency are suitable. Lifetimes of many seconds in the trap are easy to achieve. It is possible to store of the order of  $10^6$  ions. First order doppler shift in the trap averages to zero and the broadening can be kept under control.

With this number of ions and typical pumping intensities, the fluorescence and stray background levels are low enough for photon counting to be used. This simplifies the electronics since mostly digital circuitry can be used.

Fig. 2 is a schematic diagram of a standard on which we have been working. The trap is shown being illuminated with a focused and filtered light beam from the mercury 202 lamp. The fluorescence from the mercury 199 ions in the trap is collected by the optics at right angles to the input beam and focused into the photomultiplier tube. Since the incident and fluorescent light have the same wavelength, great care must be exercised to keep the stray, scattered light to a minimum. The output pulses from the photomultiplier are fed to a counter whose gate is controlled by the sequencer.

The operations the sequencer performs are shown in Fig. 3. After an interval of optical pumping the light is turned off and the ions are irradiated with the microwave frequency tuned to one side of the line. The microwaves are then turned off, the pumping light applied again, and the counter gate is opened for a time. After the gate is closed the electron beam is turned on for a short time to refresh the ion population. The whole process is then repeated with the microwave frequency tuned to the other side of the line. If the mean frequency of the microwave source, as it is switched between the two sides of the line, is not at the line center, there will be a difference in the counter readings which is used as the error signal for the mean frequency. The counter readings are differenced and digitally integrated by the computer and then converted to an analog signal. A second integration is performed and the control signal is fed to the VCXO and synthesizer. The double integration eliminates the effects of linear frequency drift in the flywheel oscillator. It also removes the effect of frequency jumps in the flywheel oscillator on time kept by the standard when it is used as a clock.

The light is switched off during the time the RF is applied to avoid light induced frequency shift and line broadening. The electron beam is also switched off to avoid its line broadening effect and to remove the electron induced fluorescence.

Rather than using first differences as the error signal, second differences are used. This removes any error due to linear drifts in system parameters such as light intensity, ion number, etc. The second differences are formed by the computer as follows. Consider a sequence of counts from the system

$C_1, C_2, C_3, C_4, \dots$

The computer forms the sequence

$+(C_1 - 2C_2 + C_3), -(C_2 - 2C_3 + C_4), +(C_3 - 2C_4 + C_5), \dots$

It is easy to show that each member of this sequence contains the error information and removes linear parameter drifts. This is similar to the scheme used by Jardino et al (3) and gives, in addition, new error information for each count, thus allowing faster loop response.

Some other aspect of the system should be mentioned. The mercury 202 lamp is excited by RF at a level of about 20 watts. Its intensity is controlled by a photodiode monitor feedback loop. The present microwave source is a phase-locked Gunn diode. For making measurements the system is operated open-loop with the VCXO phase-locked to a cesium standard. Most of the measurements reported here were done in this mode. Optical design is critical to achieving good signal to noise ratio. The design of the input and output light paths strives to maximize the ion fluorescence signal while minimizing stray light, which at present is the largest photon flux at the photomultiplier. The present experimental arrangement has no magnetic shields. The ambient field is partially cancelled with sets of Helmholtz coils and gradient coils. Fields as low as 10 mG have been achieved but with questionable homogeneity.

The most important source of frequency shift is the second order doppler effect. This is given approximately by the ratio of the average kinetic energy of the ions in the trap to their rest energy. For mercury 199 the shift amounts to  $-5.4 \times 10^{-12}$  per eV of kinetic energy. The energy of uncooled ions in a trap (4) is typically about one tenth the well depth or about 2.0 eV. Since the effect is second order in velocity it can also induce line asymmetry if there is a distribution of velocities. Another effect of the velocity distribution is line broadening. Consequently it is almost essential to cool the ions.

Laser cooling is very effective (5) but not attractive from a commercial standpoint. The approach under investigation here uses viscous drag cooling (6) in which the hot ions are cooled by making collisions with a cool, light, inert gas such as helium. Calculations show that effective cooling should take place at gas pressures as low as about  $1 \text{ E-6}$  torr. There is also a frequency shift due to the collisions with the cooling gas, but this should be small at the low pressures involved. More will be said about this later.

## MEASUREMENTS

A large number of measurements have been made during the course of the work. The experimental setup includes a small computer that can control many of the operating parameters and also collect and store data. Many of the experiments involve data gathering overnight or over a week-end.

Fig. 4 shows a line recorded overnight. In this case the sequence was one which allowed the RF irradiation and optical pumping to come into equilibrium before the fluorescence count rate was measured, resulting in a conventional CW lineshape. The FWHM is 1.55 Hz. The ambient field was 0.52 gauss. There was helium present at about  $2\text{E-6}$  torr. The line was swept 32 times at 16 seconds per point, and the resulting set of points is the average of all the 32 sets. The fitted curve is a Lorentzian line with free parameters height, width, and center frequency. The background was subtracted out by taking alternate measurements with the frequency far removed from the resonance.

Fig. 5 shows a pulsed line recorded overnight. The ambient field was 0.46 gauss and helium was present. The line was swept 60 times at 8 seconds per point and the resulting data is the average of the 60 sets of points. The valleys are due to the pulsed operation. The length of the RF pulse was 0.24 seconds. Again, the background has been subtracted out. The effective linewidth is about 3.5 Hz.

Fig. 6 shows a pseudo-derivative of the pulsed line. Conditions were approximately the same as those for Fig. 5. It was obtained by sweeping slowly through the resonance while the frequency was being switched back and forth 3.5 Hz. The difference in counts for the two conditions is plotted as a function of the average frequency and, of course, goes through zero at line center. This is very close to the actual discriminator action to be used in the operating standard. This plot also is the result of averaging over a long run.

Fig. 7 shows the effect of trap well depth variation on zero magnetic field ion resonance frequency. As mentioned earlier the mean kinetic energy of the ions in the trap has been reported to be about one tenth the well depth. This should lead to a second order doppler shift of  $-0.022$  Hz per eV of well depth. The depth was varied by changing the trap drive voltage and was calculated from the harmonic oscillator model using measured motional resonance frequencies for the ions. The hyperfine resonance frequency data shown in Fig. 7 were taken with the best vacuum attainable in the system at that time. This was about  $1 \text{ E-}7$  torr indicated and the system probably contained some residual helium. The straight line with slope  $-0.022$  Hz per eV that is the best fit to the data points is shown. Each data point is the mean of five measurements and the standard deviation of that mean is about  $0.01$  Hz. This is about half the height of the crosses. The departures from the straight line are much larger than the standard deviation and must represent real variations from the simple straight line model. This behavior is not understood and more work is needed.

Some measurements were made of the dependence of frequency on helium pressure. Only a few results have been obtained thus far. One experiment was to measure the frequency as the helium pressure was slowly increased from the best vacuum attainable to about  $5 \text{ E-}6$  torr. The frequency changed less than  $2 \text{ E-}12$ . This is a surprising result that could possibly be explained by a fortuitous cancellation of two effects: the second order doppler shift reduction induced by the helium cooling and the shift due to the helium. Another experiment involved varying the trap well depth as described earlier but with helium present at a pressure of  $5 \text{ E-}6$  torr. The change in frequency was plus or minus  $3 \text{ E-}13$  for a well depth change from  $17.5$  to  $23.2$  eV. This change is much smaller than the vacuum results and indicates that the helium cooling is effective. Other effects of the helium include narrower lines and a larger signal indicating cooling and perhaps storage of more ions. The gas technique for cooling is promising but needs more work.

The resonance line was studied as a function of the static magnetic field. As mentioned earlier, the apparatus is unshielded and the homogeneity of the field is questionable. At fields lower than about  $70$  mG the line became broadened, distinctly non-Lorentz shaped, and quite sensitive to externally applied gradients. Zeeman transitions were also observed. They were fairly broad and also indicated the presence of small amounts of low frequency AC magnetic field, most probably from the  $60$  Hz power lines and rotating machinery.

Measurements were also made of the effective signal to noise ratio for the pulsed mode of operation. The results would give a square root of the Allan variance of

$$\sigma_y(2, \tau) = 1.2 \text{ E-}12 (\tau)^{-1/2}$$

for times longer than the servo time constant. Due to the narrow line and the consequent slow data gathering rate, this time constant is presently about 20 seconds.

Measurements were made of relaxation and pumping rates. In the notation of Jardino and Desaintfusien (2) a set of measurements was:

$$\begin{aligned}\gamma_p &= 1.8 \text{ sec}^{-1} \\ \gamma_l + \gamma_s &= .43 \text{ sec}^{-1} \\ \Gamma_2 &= 4.9 \text{ sec}^{-1}\end{aligned}$$

$\gamma_p$  = pumping rate

$\gamma_s$  = (storage time) $^{-1}$

$\gamma_l$  = longitudinal relaxation rate

$\Gamma_2$  = total transverse relaxation rate

These do not necessarily represent the best conditions for frequency standard operation.

The background photon count rate depends strongly on a number of factors. The contributions to background are stray light scattered from the incident beam, atomic fluorescence from the background gas, residual fluorescence from the ions due to relaxation, and light from the heated electron gun. The electron beam is switched off during counting so there is no electron induced fluorescence. The background count rate also, of course, depends on the available light. For the line shown in Fig. 4 the background count rate was 11,500 per second while the signal count rate was 3,250 per second at a saturation factor of 3.2. Background rates of  $1.5 \times 10^5$  with signal rates of about  $1.7 \times 10^4$  have also been observed.

An estimate of the absolute hyperfine frequency in zero magnetic field and with zero second order doppler shift based on the results of Fig. 7 is

$$= 40,507,347,996.9 \pm 0.3 \text{ Hz}$$

The uncertainty is mainly due to the extrapolation to zero second order doppler shift. The uncertainty due to the cesium standards used as reference is no larger than 0.1 Hz referred to NBS. Measurements made with  $4 \times 10^{-6}$  torr of helium are slightly lower in frequency but still fall within the quoted uncertainty range.

## REFERENCES

1. F. G. Major and G. Werth; Appl. Phys. 15, 201 (1978).  
M. D. McGuire, Proceedings of the Frequency Control Symposium 1977, p 612.
2. M. Jardino and M. Desaintfusicien; IEEE Trans. Inst. Meas. IM29, 163 (1980).
3. M. Jardino, M. Desaintfusicien, R. Barillet, J. Viennet, P. Petit, and C. Audoin, Appl. Phys. 24, 107 (1981).
4. R. Ifflaender and G. Werth; Metrologia 13, 167 (1977).
5. W. Neuhauser, M. Hohenstatt, P. E. Toschek, H. G. Dehmelt; Appl. Phys. 17, 123 (1978).  
D. J. Wineland, R. E. Drullinger, and F. L. Walls; Phys. Rev. Lett, 40, 1639 (1978).
6. F. G. Major and H. G. Dehmelt, Phys. Rev. 170, 91 (1968).  
H. Schaaf, U. Schmeling, and G. Werth; Appl. Phys. 25, 249 (1981).



Measurements of stability of the mercury standard against a high performance cesium standard were made with averaging times of 100 sec. The measured fluctuations were essentially those of the cesium, at a level of  $5 \text{ E-13}$ . The mercury standard fluctuations were not detectable.

## CONCLUSIONS

The optically pumped trapped mercury ion frequency standard looks promising. A number of measurements have been made to ascertain its potential. While a great deal of work remains to be done, it appears that the following performance characteristics could be met in a commercial standard:

absolute accuracy	$1 \text{ E-12}$
Reproducibility	$2 \text{ E-13}$
$\sigma_y(2, \tau)$	$1 \text{ E-12 } (\tau)^{-1/2}$

## ACKNOWLEDGMENTS

The authors are grateful for useful discussions with Dr. C. Audoin and Dr. M. Desaintfuscien and for preprints they and Dr. M. Jardino have sent. Construction of much of the electronics was carried out by D. Weigel.

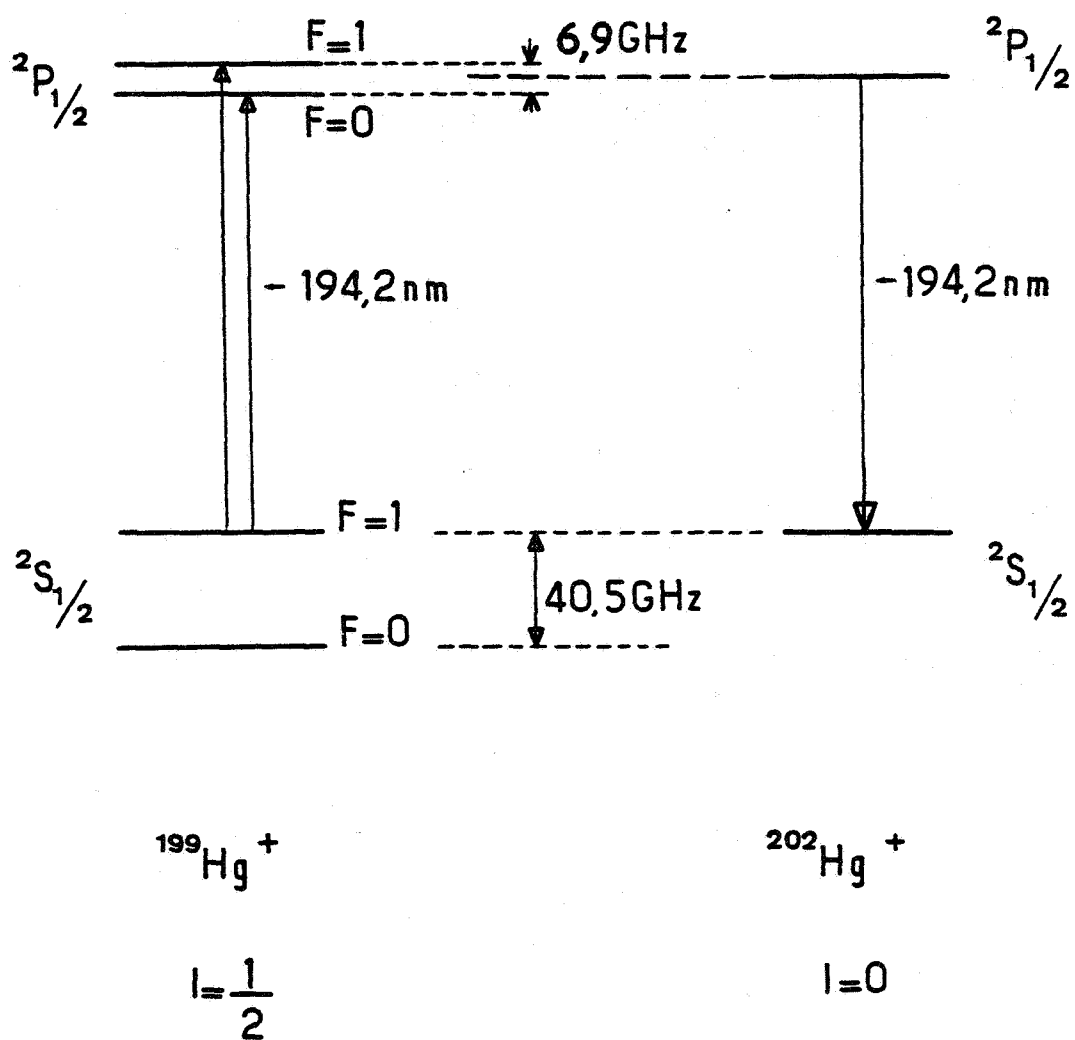


Fig. 1 - Energy levels of mercury 199 and 202 ions.

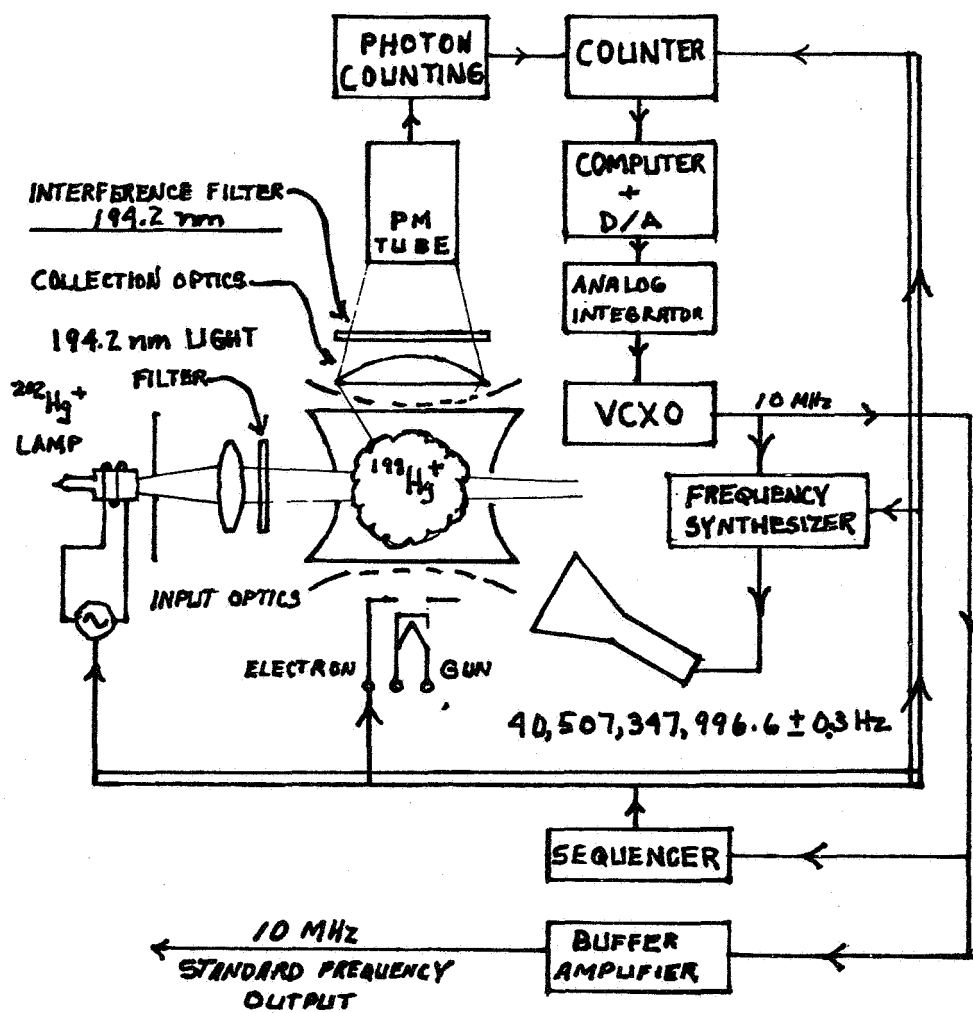


Fig. 2 - Schematic diagram of trapped mercury ion standard.

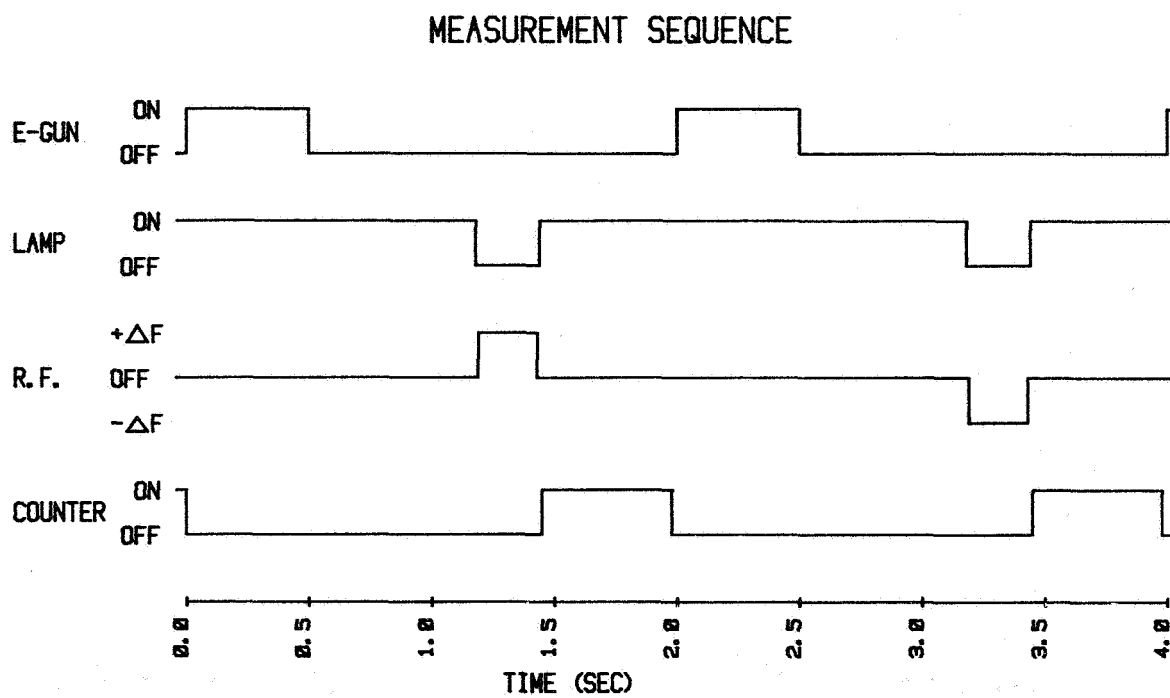


Fig. 3 - Sequencer Operation

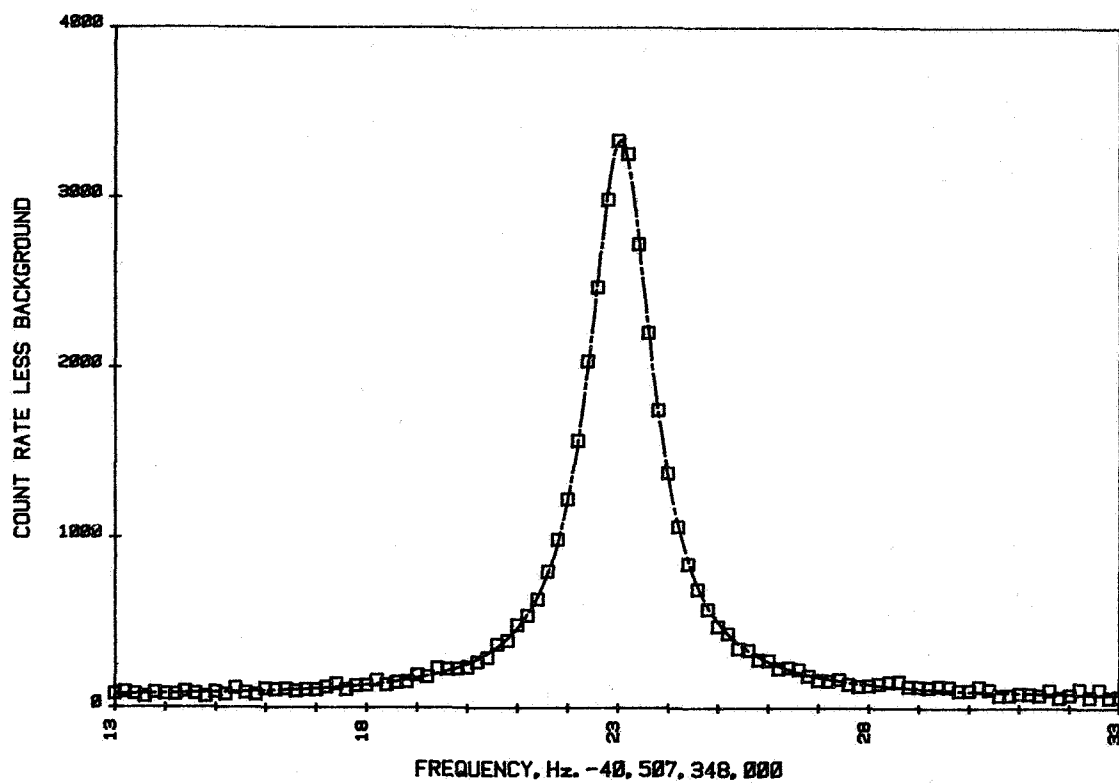


Fig. 4 - CW line with helium. FWHM is 1.55 Hz. The fitted curve is a Lorentz line.

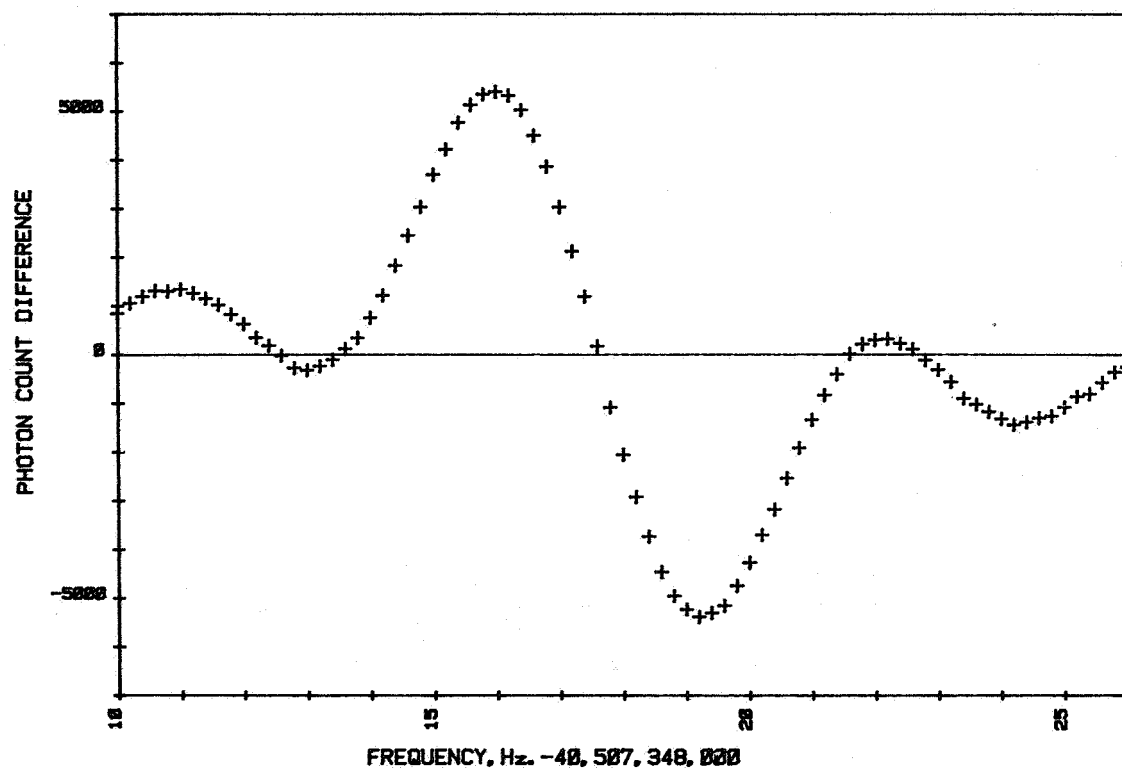


Fig. 6 - Pulsed line pseudo-derivative. This is a first difference error signal.

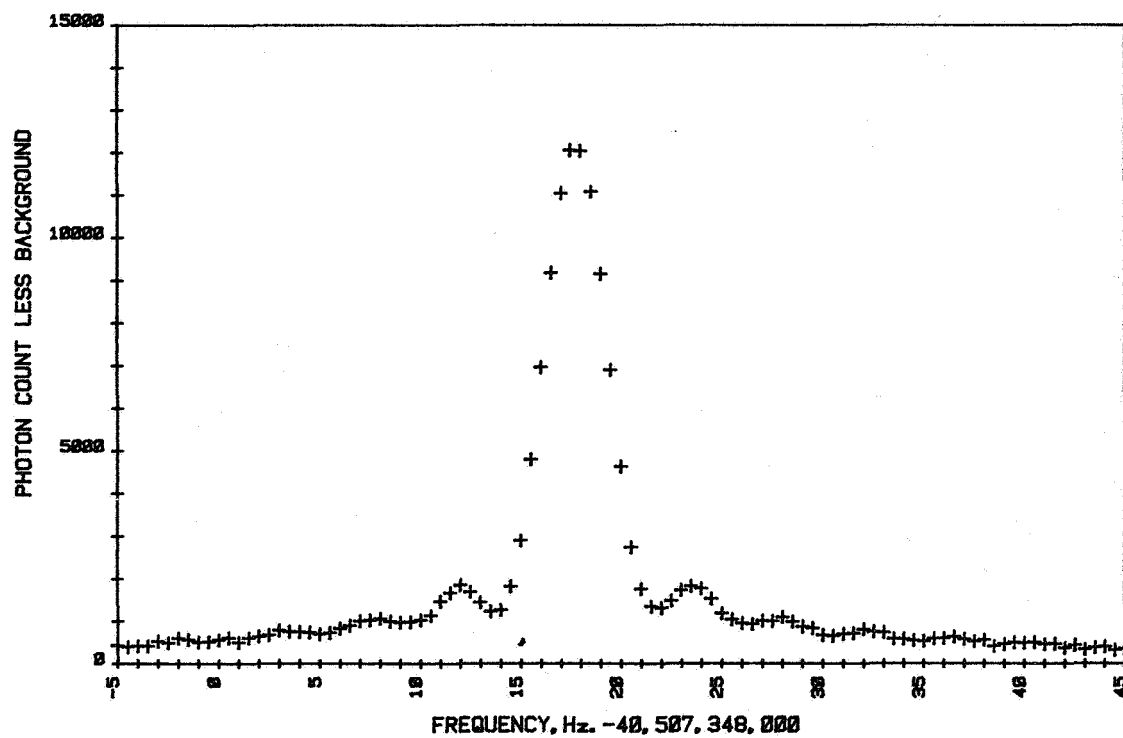


Fig. 5 - Pulsed line. The RF pulse width is 240 ms.  
FWHM is about 3.5 Hz.

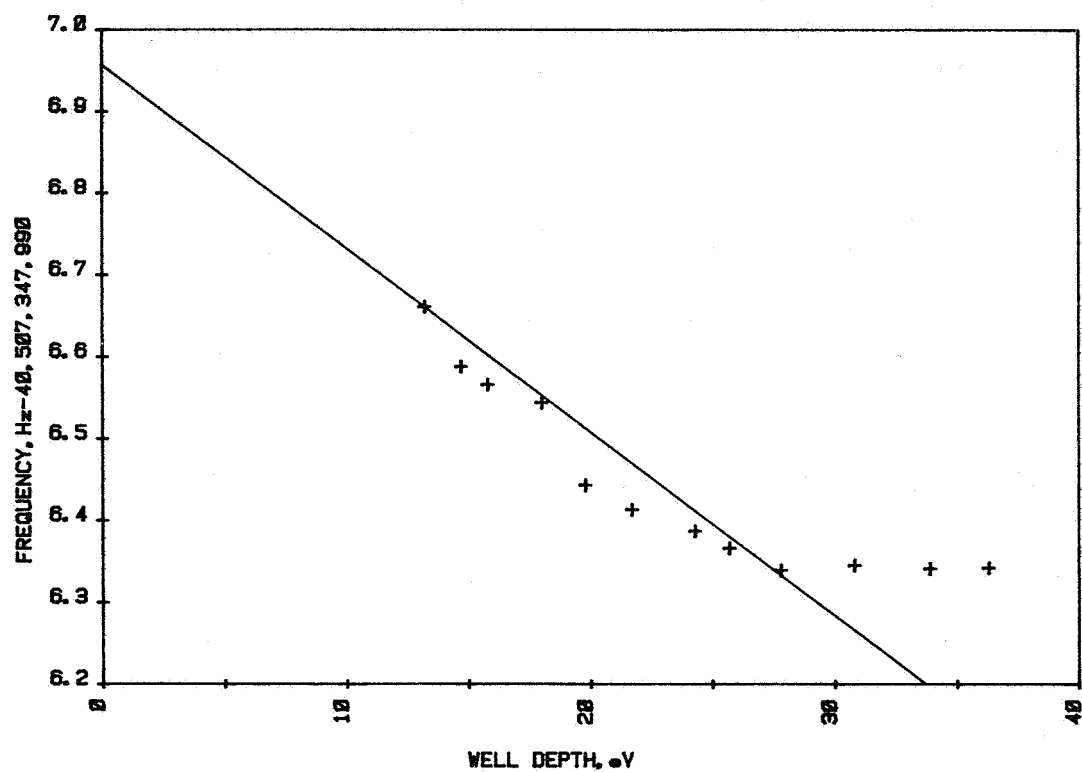


Fig. 7 - Hyperfine resonance frequency versus trap well depth. Standard deviation of each data point is less than 0.01 Hz. The straight line slope corresponds to second order doppler shift for ion energy equal to 0.1 well depth. Data points are corrected to zero magnetic field.



## QUESTIONS AND ANSWERS

DR. DAVE WINELAND, National Bureau of Standards

Len, what's the main decay mechanism in your lamps, do you know yet what the problem is?

DR. CUTLER:

Well, there's a bulb-darkening effect, which appears to be something that comes on the surface of the inside of the bulb. We tried to analyze this using ESKA and some other things. And it looks like there may be some silicates involved. These are fused quartz lamps. Since the radiation we are interested in is 1,940 angstroms, it has to be quite good quartz, so it's supercil. And that's one thing that we see.

Another thing is that eventually the mercury does seem to disappear. Probably combining chemically with something in the quartz.

We are going to attempt to use some sapphire and see what that does. But we don't have any results on that yet.

DR. WINELAND:

One other question, at each cycle of the RF do you dump the ions and then reload them?

DR. CUTLER:

No. We just turn on the electron gun again for a short time and pick up a few more ions.

DR. WINELAND:

One slight comment, I may be already aware of, is that when you do that, if your pumping is not complete, you'll get a light shift because of the phase coherence between light systems.

DR. CUTLER:

That's right.

DR. VESSOT:

I think we're running a little late. I'd like to suggest, if it's all right with you, Len, that we have all these questions towards the end of the three related papers, or I fear that we may not have lunch.

# PROSPECTS FOR STORED ION FREQUENCY STANDARDS

D. J. Wineland  
National Bureau of Standards, Boulder, Colorado

## ABSTRACT

Fundamental limitations of possible frequency standards based on stored ions are examined. Practical limitations are also addressed but without regard to size, power consumption, and cost. With these guidelines, one can anticipate that a stored ion frequency standard with accuracy and stability better than  $10^{-15}$  is now possible.

## INTRODUCTION

Since the pioneering work of Dehmelt and co-workers, who first observed high resolution microwave spectra on stored  $^3\text{He}^+$  ions, it has been clear that the ion-storage technique [1] provides the basis for an excellent frequency standard [2-20]. The goals of various groups in this field seem to be determined largely by a trade-off between desired performance and limitations on equipment, such as size, power consumption, cost, etc. In this paper, the fundamental limitations of stored ion frequency standards are addressed. Experiments possible with "available" technology are discussed, but restrictions on experimental equipment, such as size, power consumption, cost, etc., are not made.

In any case, the following assumptions will be made:

- (1) The only restriction on experimental equipment is that it be available at a "reasonable cost."
- (2) Only experiments where inaccuracy  $\leq 10^{-15}$  can be potentially achieved will be discussed.
- (3) With this in mind, we will assume that "laser cooling" is employed in all experiments in order to suppress Doppler shifts.
- (4) Both rf and Penning traps are considered with advantages and disadvantages of each noted.

Optical frequency standards as well as microwave frequency standards will be discussed. In a meeting on "precise time and time interval," this might seem a bit out of place because of the difficulty of providing time from frequency standards which operate much above 100 GHz [14]. However, these devices will also be discussed because of the other uses for frequency standards and because of the remarkable accuracies potentially achievable.

## MICROWAVE FREQUENCY STANDARDS

The dominant choice for a microwave frequency standard is one based on hyperfine transitions in the ground state of a singly ionized atom. Fine structure transitions in an ion such as  $B^+$  might be used [14], but here there are difficult problems with state selection and detection. Exotic choices such as  $Bk^+$  are interesting because of the large hyperfine structure, but this ion has other obvious practical drawbacks.

If we assume that the transition linewidth is fairly independent of the ion species (for example, this is true if the linewidth is determined only by the fundamental limit of interrogation time), then we would like to use an ion with as high a hyperfine frequency as possible. This is why  $Hg^+$  ions are attractive since  $\Delta\nu_{hfs}(^{199}Hg^+) \cong 40$  GHz and  $\Delta\nu_{hfs}(^{201}Hg^+) \cong 30$  GHz. Simple schemes for laser cooling and optical pumping/detection of hyperfine transitions such as was realized [21] in  $Mg^+$  are possible [22] in other ions like  $He^+$ ,  $Be^+$ ,  $Zn^+$ , and  $Cd^+$ . However, in the case of  $He^+$ , the required laser wavelength is too short and for all of these ions, the hyperfine frequencies are about three or more times lower than for  $Hg^+$ .

Because of its high hyperfine frequency, large mass (which gives a small second order Doppler shift at a given temperature) and availability of a  $^{202}Hg^+$  pumping lamp,  $^{199}Hg^+$  has so far received the most attention as a possible microwave frequency standard [2, 4, 5, 7, 10, 11, 19, 20]. If "laser cooling" is employed, the simple schemes [21] using only a laser for cooling and state selection are not possible. However, if the ground state energy levels are "mixed" [9, 16], then laser cooling and optical pumping/detection in  $Hg^+$  ions are possible. Using this "mixing,"  $Ba^+$  also becomes a possible choice [6, 9, 13], but the mixing schemes are more complicated than for  $^+Hg$ . Also, since the  $Ba^+$  hyperfine frequency is smaller than for  $Hg^+$ , then  $Hg^+$  still seems a better choice. Unfortunately, the first resonance line for  $Hg^+$  which would be used for laser cooling and pumping/

detection is at a wavelength  $\lambda = 194.2$  nm. Generating this wavelength in a c.w., narrow band ( $< 10$  MHz) way is difficult but possible using state-of-the-art techniques [16]. With this in mind, experiments have been initiated at NBS to realize a microwave frequency standard based on the 25.9 GHz  $(F, M_F) = (2,1) \leftrightarrow (1,1)$  transition in  $^{201}\text{Hg}^+$  at a magnetic field of 0.534 T [16]. For operation in a Penning trap, this transition is chosen because at 0.534 T, the transition frequency is independent of magnetic field to first order. Therefore, systematic effects due to magnetic field instabilities and inhomogeneities are reduced (see below). If a similar experiment is done in an rf trap, then the 40.5 GHz  $(F, M_F) = (1,0) \rightarrow (0,0)$  transition in  $^{199}\text{Hg}^+$  at low magnetic field would probably be a better choice.

Regardless of the transition or ion used, the prospects for obtaining high  $Q$  look very good. Transition linewidths of 0.012 Hz have already been observed [21] in  $\text{Mg}^+$ ; it is anticipated that these narrow linewidths and linewidths even smaller should be observable in  $\text{Hg}^+$  which would yield a  $Q$  significantly greater than  $10^{12}$ .

In addition to the high  $Q$  possible, we note that by observing the scattering of many optical photons (or the absence of many scattered photons) for each microwave photon absorbed, it should be possible to achieve the maximum signal-to-noise -- that is, where the limit is governed by the statistical noise in the number of ions that have made the transition [16, 17]. This will be important in any stored ion experiment, since the number of stored ions are typically rather low.

## OPTICAL FREQUENCY STANDARDS

Because of the practical difficulty [14] of producing time from an optical frequency standard, the utility of such a device is restricted. Nevertheless, there would be many uses for such a device used only as a frequency standard; this fact coupled with the potential performance make it interesting to examine. In this discussion, the term "optical" frequency standard is used loosely and will include frequencies above about 1 THz.

When we consider "optical" frequency standards, if we carry our thoughts to their logical conclusion, the obvious choice is to build a  $\gamma$ -ray clock based on a recoilless ("Mossbauer") nuclear transition. The reason we don't think about such things yet is that we don't have the required narrowband, tunable,  $\gamma$ -ray local oscillator. (Not to mention the problems of frequency comparison.) The optical frequency standard problem is similar, but it now appears that very narrow band, tunable, laser sources will be available in the not-too-distant future. Hopefully, in the next few years, tunable lasers will achieve

linewidths less than 1 Hz and stabilities over short times of  $< 10^{-15}$  [22,23]. With this in mind, the prospects for an optical ion storage frequency standard look very promising.

Again, our choices are somewhat restricted because for the laser cooling and optical pumping/detection functions we require a fairly strongly allowed electric dipole transition. For the frequency standard transitions, however, we desire a very weakly allowed transition in order to obtain a narrow bandwidth. Dehmelt [24] was first to suggest using the intercombination lines of group III B singly ionized atoms for an optical frequency standard; an experiment based on a  $Tl^+$  was suggested. (Note that the highest resolution so far obtained in the visible is on the  $^1S_0 \leftrightarrow ^3P_1$  (657 nm) intercombination line in neutral calcium [25,26].) For  $Tl^+$ , laser cooling and optical pumping/detection could be accomplished using the fairly strong  $^1S_0 \leftrightarrow ^3P_1$  line (191 nm). The optical frequency standard would be obtained on the  $^1S_0 \leftrightarrow ^3P_0$  line which has a Q of  $5 \times 10^{14}$ ! Although difficult, it is certainly within the state of the art to produce these wavelengths by doubling and mixing tunable dye lasers. (With this in mind, a more favorable choice appears to be  $In^+$ .) Another possibility which is more attractive from the standpoint of available lasers is to drive the two-photon  $^2S_{1/2} \leftrightarrow ^2D_{5/2}$  transition in  $Ba^+$  [18, 27] or  $Hg^+$  [15, 16]. These transitions have comparable Q to  $Tl^+$  but can suffer from the problem of ac Stark shifts. For example, in  $Hg^+$  if the  $S \rightarrow D$  transition is driven with two photons of equal wavelength ( $\lambda = 563$  nm), then the ac Stark shift is about  $10^{-15}$  [16]. To make the ac Stark shift negligible, one could drive the  $^2S_{1/2} \leftrightarrow ^2D_{5/2}$  single photon quadrupole transitions [17].

For single photon transitions, it will be desirable to achieve or approximately satisfy the Dicke criterion (confinement dimensions  $\lesssim \lambda/2\pi$ ). This condition is most easily satisfied for a single trapped ion. A single ion is also the most desirable case from the point of reducing systematic effects (see next Section), but suffers, of course, from the standpoint of signal-to-noise ratio. For a single ion which approximately satisfies the Dicke criterion, it is interesting to note that the power required to saturate a transition (assuming the natural radiation decay process is the same as the excitation process) is given by assuming the ion has an absorption cross-section of about  $\lambda^2/2\pi$  (case for ions unpolarized). If the laser is focused to about a 1  $\mu m$  diameter, then a power of only  $2 \times 10^{-15}$  W is required to saturate the 202 nm transition in  $Tl^+$ . These small required powers may make practical the possibility of producing these short wavelengths by very weak nonlinear processes. Unfortunately, the initial preparation of laser cooled single ions would require substantially higher powers.

For the experiments on single ions, the rf trap may ultimately have an advantage because the confinement can be tighter. It should be noted, however, that even if the Dicke criterion cannot be satisfied, the performance is not severely degraded, since the line is only slightly broadened [24] and more noisy.

## SYSTEMATIC SHIFTS

Here we discuss the more important fundamental systematic shifts in possible ion storage frequency standards. They are basically the same in microwave and optical frequency standards, but may differ in magnitude.

(1) Magnetic Fields: In the rf trap, very low magnetic fields would be desirable, and although there would be slight field sensitivities [12, 19], these could be stabilized and calibrated out of the system by locking the field to a Zeeman transition. For example, in the case of the  $^{199}\text{Hg}^+$  microwave frequency standard, the problem would be the same as in the hydrogen maser. It is sometimes noted that a drawback of the Penning trap is the required large magnetic fields, and the influence these fields have on transition frequencies. These problems can be made very small, however, by operating at a magnetic field where the transition frequency is independent of field to first order.

For the  $(F, M_F) = (2, 1) \leftrightarrow (1, 1)$  transition in  $^{201}\text{Hg}^+$  discussed above [16], the second order field dependence is given by  $\Delta\nu/\nu_{\text{hfs}} = (\Delta H/H)^2/6$ . For the  $S \leftrightarrow D$  optical transitions, we obtain a further reduction in sensitivity by approximately the ratio of the hyperfine frequency to the optical frequency ( $\sim 10^{-4}$ ). Since a good magnet system has drift rates  $< 10^{-8}$  and inhomogeneities  $< 10^{-8}$  over 1 cm dimensions, field instabilities should not be a problem until well below the  $10^{-15}$  level of accuracy.

(2) Second Order Doppler and Electric Field (Stark) Shifts: The fundamental limits on these two effects will scale together, so they are treated at the same time. Usually only second order "Stark" shifts will be important; therefore, we will be interested only in  $\langle E^2 \rangle$ .

For single ions, laser cooling has already achieved temperatures between 10 mK and 100 mK [18, 28]. Theoretically, when the motional oscillation frequencies  $\Omega_i$  ( $\omega_z$  and  $\omega_r$  for the rf trap and  $\omega_z$ ,  $\omega_c$ , and  $\omega_m$  for the Penning trap) are less than the natural linewidth ( $\gamma$ ) of the optical cooling transition, then the limiting "temperature" in each degree of freedom is given by  $k_B T \cong \frac{1}{2} \hbar \gamma$  [18, 29, 30], where  $k_B$  is Boltzmann's constant. (For a single ion, the precise minimum temperature depends on the angle of incidence of the laser beam and on the spatial distribution of recoil photons [30].) For strongly allowed transitions as in  $\text{Ba}^+$  or  $\text{Hg}^+$ , this limiting temperature is

about 1 mK. For more weakly allowed transitions, the temperature is correspondingly less, but other limits such as recoil can come into play, limiting the temperature to about  $10^{-6}$  K.

When the opposite condition ( $\Omega_i \gg \gamma$ ) is fulfilled and  $\hbar\Omega_i \gg$  recoil energy, then the limiting energy [27, 29] is given by  $E_i = \hbar\Omega_i (\langle n_i \rangle + \frac{1}{2})$  where  $\langle n_i \rangle \cong 5\gamma^2/(16\Omega_i^2)$ . Therefore the limiting kinetic energy is given by  $E_{ki} \cong \hbar\Omega_i/4 \ll \hbar\gamma/4$ . For simplicity, we will assume only the case  $\Omega_i \ll \gamma$  and  $\hbar\gamma \gg$  recoil energy below; however, even better results are potentially obtained for the opposite condition ( $\gamma \ll \Omega_i$ ).

For a single ion in an rf trap, when  $U_0$  (D.C. applied potential) = 0, the nonthermal micromotion has an average kinetic energy equal to that of the secular motion (1); this is approximately true in the spherical trap. In the Penning trap the kinetic energy in the nonthermal magnetron motion can be much less than in the cyclotron or axial modes [30]. Therefore, the minimum second order Doppler shifts are given approximately by [31]:

$$\frac{\Delta\nu_D}{\nu_0} = \frac{E_K}{Mc^2} = \begin{matrix} \frac{3}{2} \hbar\gamma/Mc^2 & \text{rf trap} \\ \frac{3}{4} \hbar\gamma/Mc^2 & \text{Penning trap} \end{matrix}$$

For a single ion in a spherical rf trap,  $\langle E^2 \rangle$  is primarily due to the oscillating rf fields and is largest for the z motion. A simple calculation gives  $\langle E^2 \rangle_z = M\Omega^2\hbar\gamma/e^2$  for maximum laser cooling or  $\langle E^2 \rangle_z = 2M\Omega^2k_B T/e^2$  for a given temperature in the z secular motion. For a single ion in a Penning trap, it is usually possible to make  $r_m, r_c \ll z$  [28, 30], therefore Stark shifts from the static fields are primarily due to the z motion. We find  $\langle E^2 \rangle_z = \hbar\gamma M\omega_z^2/(2e^2)$  for maximum laser cooling or  $\langle E^2 \rangle_z = k_B T M\omega_z^2/e^2$  at temperature T. In the Penning trap, a larger effect can be caused by the motional electric field  $\vec{E}_M = \vec{v} \times \vec{B}/c$ . We have  $\langle E^2 \rangle_M = \hbar\gamma B^2/(Mc^2)$  (maximum laser cooling) and  $\langle E^2 \rangle_M = 2k_B T B^2/(Mc^2)$ . In table I are shown examples of the second order Doppler shift and  $\langle E^2 \rangle$  for single ions in rf and Penning traps.

To get an idea of the effect of electric fields, we note that the fractional Stark shift of Hg<sup>+</sup> hyperfine structure has been estimated to be [32]

$$\Delta\nu/\nu_{hfs} \cong 1.43 \times 10^{-18} E^2$$

where  $E$  is in volts/cm. (The shift for  $\text{Ba}^+$  is about 24 times higher [32].) For the  $^2S_{1/2} \leftrightarrow ^2D_{5/2}$  transitions in  $\text{Hg}^+$  we have [16]

$$\Delta\nu/\nu \cong 1.4 \times 10^{-18} E^2.$$

This shift should be similar in magnitude in other optical transitions. We note that in many cases, the electric fields from black-body radiation ( $\langle E^2 \rangle_{\text{bb}} \cong (8.3 \text{ V/cm})^2$  at  $T = 300 \text{ K}$ ) [32] can be much larger than those due to trapping conditions. Therefore, operations at reduced environmental temperatures may ultimately be required.

For clouds of identical ions, we first consider the electric fields due to collisions between ions. For the rf trap, we neglect the energy in the micromotion since the ions are driven in phase, therefore ion collisional effects in the rf and Penning traps are treated the same.  $\langle E^2 \rangle$  due to collisions will, of course, depend on the cloud density and temperature, but some idea of the magnitude can be given by calculating the electric field for one ion on another at the distance of closest approach. Assuming the maximum energy available for closest approach is given by  $3k_B T$ , we have  $E_{\text{max}} = 6.7 \times 10^{-8} \text{ V/cm}$  ( $\gamma/2\pi = 10 \text{ MHz}$  and maximum laser cooling) and  $E_{\text{max}} = 7.4 \text{ V/cm}$  at  $T = 4\text{K}$ . Therefore at modest temperatures, ion-ion collision induced Stark shifts can be quite small.

For clouds of ions, other effects can contribute to Stark and second order Doppler shifts. We will consider only theoretical limits and therefore neglect effects such as rf heating in an rf trap, which may be the real limitation in a practical experiment. We will assume that the secular motion in an rf trap and the axial and cyclotron modes in a Penning trap have been cooled to negligible values. For both traps we will assume that it is desirable to maximize the number of ions  $N$ .

In an rf trap we must consider the effects of the micromotion and corresponding electric fields for ions on the edge of the cloud. We impose the constraint that the maximum fractional second order Doppler shift ( $\Delta\nu/\nu$ ) not exceed a certain value ( $\epsilon$ ). Therefore, for spherical clouds in an rf trap we find [31]

$$N_{\text{max}} = 6.48 \times 10^{15} r_i M \epsilon$$

where  $M$  is in  $u$  (atomic mass units), and  $r_i$  is the cloud radius.

For a spherical cloud of ions in a Penning trap, the maximum second order Doppler effect is due to the magnetron motion of ions on the edge of the cloud ( $r_m = r_i$ ,  $z=0$ ). We find [31]

$$N_{\text{max}} = 1.96 \times 10^{13} B \sqrt{\epsilon} \left[ r_i^2 - \frac{440 M \sqrt{\epsilon}}{B} r_i \right]$$



where B is in tesla, M in u. Negative solutions are not physical because they correspond to parameters where the magnetron second order Doppler shift cannot be made as large as  $\varepsilon$  (for a spherical cloud).

We can also calculate the corresponding electric fields. As before, for the rf trap, the maximum fields occur on ions for  $z=r_i$  and  $r=0$  and we have [31]

$$\langle E^2 \rangle_{z(\max)} = \frac{2M\Omega^2 N}{r_i}$$

In the Penning trap, the electric fields cancel along the z axis. Along the radial direction [31]

$$\langle E^2 \rangle_{r(\max)} = [2Mc^2\varepsilon/(er_i)]^2$$

In table II are shown some representative values of maximum numbers of stored ions and Stark shifts for various values of  $\Delta\nu_D/\nu_0$  and  $r_i$  on clouds of ions. In certain configurations, second order Doppler and Stark shifts could still be a problem; however, with small enough numbers of ions these can be overcome.

The values in tables I and II are only examples, and of course each experiment would vary. However, table II seems to emphasize that in experiments on clouds of ions, one must be careful to account for Doppler shifts and electric fields due to either the forced micro-motion in the rf trap or the magnetron motion in the Penning trap. We also note that in order to obtain very small second order Doppler shifts, very shallow well depths are required [31].

With these extremely low levels of anticipated systematic effects, the search for other effects continues. For example, Dehmelt has pointed out [12] that the shift due to atomic quadrupole moments must be accounted for. In nearly all of the microwave experiments, however, this small shift is negligible; moreover, in single ion experiments it can be calibrated to extremely high levels of precision ( $\ll 10^{-17}$ ).

## STABILITIES

With the anticipated high Q's, the expected stabilities are quite high even though the number of ions is rather small. If, as in the microwave case, the linewidths are limited by the interrogation time, then we could expect [16]:

$$\sigma_y(\tau) = (2\omega_0 N_i T \tau)^{-1/2} \quad \tau > 2T$$

where T is the interrogation time, assuming the time domain Ramsey method is used. For  $^{201}\text{Hg}^+$  ( $\omega_0 = 2\pi \cdot 25.9 \text{ GHz}$ ), assuming  $T = 50\text{s}$  and  $N_i = 8.2 \times 10^4$ , we obtain

$$\sigma_y(\tau) = 2 \times 10^{-15} \tau^{-\frac{1}{2}} \quad \tau > 100s$$

which emphasizes the need for extremely stable oscillators to drive the transition.

In the optical domain, anticipated stabilities are even more dramatic. For the  $^2S_{1/2} \leftrightarrow ^2D_{5/2}$  transition in  $Hg^+$  we expect [16]

$$\sigma_y(\tau) \cong 2 \times 10^{-18} \tau^{-\frac{1}{2}} \quad \tau \geq 2s$$

for  $N_i = 8.2 \times 10^4$  and even for one ion:

$$\sigma_y(\tau) = 6 \times 10^{-16} \tau^{-\frac{1}{2}} \quad \tau \geq 2s$$

Of course, these anticipated stabilities would be limited by available lasers, but perhaps in the future, these theoretical limits may be approached.

## CONCLUSIONS

From the above, it is not unrealistic to contemplate frequency standards with inaccuracies  $\ll 10^{-15}$ . These projections have assumed that the experiments would not be limited by local oscillators; however, this clearly is an important limit -- particularly in the case of optical frequency standards. Since this limitation may well be overcome, the future of ion frequency standards looks very promising indeed.

## ACKNOWLEDGEMENTS

The author wishes to thank both the Office of Naval Research and the Air Force Office of Scientific Research for continued support.

	T(K)	300	4	$2.4 \times 10^{-4}$
	$\gamma/2\pi$	----	----	10 MHz
rf	$\Delta v_D/v_0$	$8.3 \times 10^{-13}$	$1.1 \times 10^{-14}$	$6.6 \times 10^{-19}$
	$\langle E^2 \rangle_z$ ( $V^2/cm^2$ )	200	2.67	$1.6 \times 10^{-4}$
	$z_{rms}$ ( $\mu m$ )	170	20	0.15
Pen.	$\Delta v_D/v_0$	$4.2 \times 10^{-13}$	$5.5 \times 10^{-15}$	$3.3 \times 10^{-19}$
	$\langle E^2 \rangle_z$ ( $V^2/cm^2$ )	$4.0 \times 10^{-2}$	$5.4 \times 10^{-4}$	$3.2 \times 10^{-8}$
	$\langle E^2 \rangle_M$ ( $V^2/cm^2$ )	499	0.067	$4.0 \times 10^{-6}$
	$z_{rms}$ ( $\mu m$ )	1300	145	1.1

TABLE I.

Fractional second order Doppler shifts ( $\Delta v_D/v_0$ ), Stark fields ( $\langle E^2 \rangle$ ), and classical r.m.s. axial amplitudes ( $z_{rms}$ ) for single ions in rf and Penning traps. When  $\gamma/2\pi$  is given, we assume maximum theoretical laser cooling ( $\Omega_i \ll \gamma$ ). For both traps we assume  $M = 100u$ . For the rf trap where the trap potential is  $\phi(r,z) = A_0 \cos \Omega t (r^2 - 2z^2)$ , we assume  $\Omega/2\pi$  (rf drive frequency) = 1 MHz,  $A_0 = 300 V/cm^2$ . For the Penning trap,  $\omega_z/2\pi = 20$  kHz,  $B = 1$  T.  $T$  is the temperature of the secular motion for the rf trap and the temperature of the cyclotron and axial motion for the Penning trap.  $\langle E^2 \rangle_z$  is the mean square electric field for motion along the  $z$  axis,  $\langle E^2 \rangle_M$  is the mean square "motional" electric field for the  $\vec{v} \times \vec{B}/c$  force in the Penning trap. Note that  $z_{rms}$  for the Penning trap can be reduced at expense of increasing  $\langle E^2 \rangle_z$ .

$\Delta v_D/v_0$		$10^{-12}$	$10^{-12}$	$10^{-15}$	$10^{-15}$
$r_i$ (cm)		0.5	0.01	0.5	0.01
rf	$N_{\max}$	$3.2 \times 10^5$	6500	320	$\sim 6$
	$\langle E^2 \rangle_z$ ( $V^2/\text{cm}^2$ )	760	760	0.76	0.76
Pen.	$N_{\max}$	$4.9 \times 10^6$	---	$1.5 \times 10^5$	53
	$\langle E^2 \rangle_{r_i}$ ( $V^2/\text{cm}^2$ )	0.14	---	$1.4 \times 10^{-7}$	$3.5 \times 10^{-4}$

TABLE II

Maximum numbers, ( $N_{\max}$ ) and electric fields ( $\langle E^2 \rangle$ ) for "cold" spherical ion clouds in rf and Penning traps. A maximum fractional second order Doppler shift  $\Delta v_D/v_0$  is assumed. The secular motion for the rf trap and the axial and cyclotron motion for the Penning trap are assumed to be frozen out (i.e., cooled to negligible values).  $r_i$  = ion cloud radius;  $M = 100u$ ,  $\Omega/2\pi = 1$  MHz for the rf trap and  $B = 1$  T for the Penning trap.

## REFERENCES

1. H. G. Dehmelt, *Advan. Atomic and Mol. Physics* 3, 53 (1967) and 5, 109 (1969).
2. F. G. Major, NASA Report X-521.69.167, Goddard Space Flight Center (1969).
3. H. A. Schuessler, E. N. Fortson, and H. G. Dehmelt, *Phys. Rev.* 187, 5 (1969).
4. H. A. Schuessler, *Metrologia* 7, 103 (1971).
5. F. G. Major and G. Werth, *Phys. Rev. Lett.* 30, 1155 (1973) and *Appl. Phys.* 15, 201 (1978).
6. R. Ifflander and G. Werth, *Metrologia* 13, 167 (1977).
7. M. D. McGuire, R. Petsch, and G. Werth, *Phys. Rev. A* 17, 1999 (1978).
8. F. Strumia, Proc. 32nd Ann. Symp. on Freq. Control (Fort Monmouth, NJ, May 1978) p. 444.
9. F. L. Walls, D. J. Wineland, and R. E. Drullinger, *ibid.* p. 453.
10. M. Jardino, M. Desaintfuscien, R. Barillet, J. Viennet, P. Petit, and C. Audoin, Proc. 34th Ann. Symp. on Freq. Control (Fort Monmouth, NJ, June 1980) p. 353 and *Appl. Phys.* 24, 1 (1981).
11. M. D. McGuire, *Bull. Am. Phys. Soc.* 26, 615 (1981).
12. H. G. Dehmelt, Proc. 35th Ann. Symp. on Freq. Control (Philadelphia, PA, June 1981) and Proc. 3rd Symp. on Freq. Stds. and Metrology (Aussois, France, October 1981).
13. G. Werth, Proc. 3rd Symp. on Freq. Stds. and Metrology (Aussois, France, October 1981).
14. D. J. Wineland, Proc. 11th PTTI (NASA Publ. 2129, Nov. 1979) p. 81.
15. P. L. Bender, J. L. Hall, R. H. Garstang, F. M. J. Pichanick, W. W. Smith, R. L. Barger, and J. B. West, *Bull. Am. Phys. Soc.* 21, 599 (1976).
16. D. J. Wineland, W. M. Itano, J. C. Bergquist, and F. L. Walls, Proc. 35th Ann. Symp. Freq. Control (Philadelphia, PA, June, 1981).

17. D. J. Wineland, J. C. Bergquist, R. E. Drullinger, H. Hemmati, W. M. Itano, and F. L. Walls, Proc. 3rd Symp. Freq. Stds. and Metrology (Aussois, France, October 1981).
18. W. Neuhauser, M. Hohenstatt, P. E. Toschek, and H. G. Dehmelt, *Phys. Rev. A* 22, 1137 (1980).
19. M. Jardino, M. Desaintfuscien, and F. Plumelle, Proc. 3rd Symp. Freq. Stds. and Metrology (Aussois, France, October 1981).
20. See also talks by L. S. Cutler and L. Maleki at this conference.
21. W. M. Itano and D. J. Wineland, *Phys. Rev. A* 24, 1364 (1981).
22. J. L. Hall, *Science* 202, 147 (1978).
23. J. L. Hall, Proc. 3rd Symp on Freq. Stds. and Metrology (Aussois, France, October 1981).
24. H. G. Dehmelt, *Bull. Am. Phys. Soc.* 18, 1521 (1973) and 20, 60 (1975).
25. R. L. Barger, in *Laser Spectroscopy* (Plenum, New York, 1974) p. 273.
26. R. L. Barger, J. C. Bergquist, T. C. English, and D. J. Glaze, *Appl. Phys. Lett.* 34, 850 (1979).
27. W. Neuhauser, M. Hohenstatt, P. Toschek, and H. Dehmelt, Proc. 5th Int. Conf. on Spectral Lineshapes (West Berlin, July 1980).
28. D. J. Wineland and W. M. Itano, *Phys. Lett.* 82A, 75 (1981).
29. D. J. Wineland and W. M. Itano, *Phys. Rev. A* 20, 1521 (1979).
30. W. M. Itano and D. J. Wineland, *Phys. Rev. A*, to be published.
31. D. J. Wineland, Proc. Conf. on Prec. Meas. and Fundamental Constants (Gaithersburg, MD, June 1981).
32. W. M. Itano, L. L. Lewis, and D. J. Wineland, *Phys. Rev. A*, to be published.



# RECENT DEVELOPMENTS AND PROPOSED SCHEMES FOR TRAPPED ION FREQUENCY STANDARDS

L. Maleki  
Jet Propulsion Laboratory  
California Institute of Technology  
Pasadena, California

## ABSTRACT

Ion traps are exciting candidates as future precision frequency sources. Recent developments have demonstrated that mercury ion frequency standards are capable of a stability performance comparable to commercial cesium standards. Novel schemes proposed recently may prove promising for the improvement of the frequency stability of ion traps. In this paper we will discuss new developments and prospects of proposed schemes currently under investigation for the achievement of this goal. Possible difficulties that new schemes may encounter will also be discussed.

## Introduction

Since 1966 when Dehmelt and co-workers first proposed the application of ion traps for the development of a frequency standard<sup>1</sup>, there has been considerable effort in various laboratories in the US and abroad to achieve this objective. The intrinsic properties of trapped ions, namely, their isolation and relative insensitivity to environmental influences, makes them ideally suited for application as a frequency standard. Ions with appropriate electronic energy level structure may be contained for relatively long periods of time, and interrogated spectroscopically with little perturbations. In this way it is possible to utilize suitable electronic transitions in ions to establish a precision frequency source.

The development of a trapped ion microwave frequency standard was first attempted by Major<sup>2</sup>, who investigated the feasibility of this concept with <sup>199</sup>HgII contained in an rf trap. A microwave-optical double resonance method was then utilized by Major and Werth<sup>3</sup> to determine the



magnetic hyperfine spectrum of this ion. Since then, various attempts at NBS and Hewlett Packard in the US, Universities of Mainz and Heidelberg in Germany, and the University of Paris-Sud in France have been successful in determining hyperfine structure of a number of ion systems with the utilization of ion traps. While all this work contributed both directly and indirectly to the development of trapped ion frequency standards, it was only recently that Audoin and co-workers in France constructed an operational trapped mercury ion microwave standard and investigated its performance<sup>4</sup>.

At JPL there has been continued interest in the development of advanced frequency standards in connection with various applications in navigation, communications, VLBI, and other related areas. A study was therefore initiated in 1979 to evaluate the usefulness of a trapped ion frequency standard in meeting the present and future requirements for the application mentioned above. This study resulted in the establishment of an effort, presently under way, to develop a trapped ion microwave frequency standard. In this paper some salient features of trapped ion frequency standards will be discussed, and some areas which might challenge the development will be identified. An attempt will be made to indicate possible approaches to overcome the difficulties and facilitate further development of trapped ion frequency standards.

#### JPL Study

Based on our study at JPL, we determined that trapped ion frequency standards offered a unique potential for two diverse areas of application. Because of their relatively small size and low power consumption, the development of a trapped ion standard capable of performance similar to that of the cesium standard will be particularly useful for application as on-board standards in space crafts. Such a standard would be quite attractive for use in the areas of deep space navigation and communications, as well as other near earth applications, such as Global Positioning System where a reliable, high performance on-board clock is

required. On the other hand, since trapped ion frequency standards represent a viable approach for the development of an optical frequency standard, their development for this particular application is significant and desirable. The ultimate development of a mono-ion oscillator as proposed by Dehmelt<sup>5</sup>, can provide a significant improvement in the capability of conventional frequency standards presently in use.

While our efforts at JPL are presently aimed at the development of a trapped ion microwave frequency standard, we are also interested in the investigation of certain approaches that may aid the development of the trapped ion optical frequency standard.

#### Trapped Ion Microwave Frequency Standard

The 199 isotope of mercury has been the most widely used system for the development of a microwave frequency standard. The reason for the popularity of this ion system lies on the simple hyperfine structure of its  $^2S$  ground state ( $F = 0$  and  $1$ ), the size of the separation of the hyperfine levels ( $40.5$  GHz) and the relatively large mass of the mercury ion. The advantage of the simplicity of the hyperfine structure is obvious. Such a hydrogenlike structure implies the attractive attribute of large number of ions participating in  $\Delta m_F = 0$  transition, which has the smallest sensitivity to magnetic field variations. The size of the splitting at  $40.5$  GHz implies a large line  $Q$ , an important parameter for precision frequency standard applications. Finally, the relatively large mass of mercury minimizes the undesirable effects of second order Doppler broadening, which sets the limit of stability for the trapped ion standard.

The scheme employed for the use of mercury 199 in previous works has involved utilization of light from mercury 202 lamp, which has an emission line at  $1942 \text{ \AA}$ . Because of the energy level structure of 202 HgII, the wavelength of this transition coincides with the wavelength required to pump  $^2S_{1/2}$  ( $F = 1$ ) to  $^2P_{1/2}$  transition of the isotope 199 ion. The optically excited Hg 199 ions decay from the  $^2P_{1/2}$  state

into both the  $F = 0$  and  $F = 1$  hyperfine levels. Thus, in a double resonance scheme similar to that employed in the rubidium clock, it is possible to lock a 40.5 GHz signal from an oscillator to the intensity of the fluorescence due to the  $^2P_{1/2} \rightarrow ^2S_{1/2}$  transition and establish a frequency standard. This scheme, however, suffers from an intrinsic difficulty. Since the wavelength of the pump light at 1942 Å is the same as the fluorescence, the scattering of the pump light from the trap and other surfaces produces a large background which severely degrades the signal-to-noise ratio<sup>2</sup>. This condition does not constitute a difficulty in studies where a laser can be employed for pumping the optical level. But since a suitable laser with a light output at the UV wavelength of 1942 Å is not available at the present time, this difficulty has impeded the development of a trapped mercury ion microwave frequency standard.

As part of our investigation at JPL to seek an approach for improving the signal-to-noise ratio, we proposed in 1980 to utilize a different pumping scheme with the  $^{199}\text{Hg}$  ion<sup>6</sup>. An inspection of the energy level diagram of this ion indicated that a two photon pumping scheme could be utilized to pump the  $^2S_{1/2} (F = 1) \rightarrow ^2D_{5/2}$  transition (Fig. 1). In the case of the mercury ion, the decay of the "forbidden"  $^2D_{5/2}$  state to the ground state was observed previously in the literature<sup>7</sup> with a relatively strong emission at 2815 Å. We proposed to utilize the light from a single mode dye laser at 5630 Å to pump the  $^2S_{1/2} (F = 1) \rightarrow ^2D_{5/2}$  transition via two photons<sup>8</sup>. The fluorescent light at 2815 Å could then be detected without a background contribution from the pump light. The result would be a significant improvement of the signal to noise ratio. This approach was also proposed by Wineland<sup>9</sup>, in a presentation given at the 1981 Frequency Control Symposium, in connection with the development of an optical frequency standard, based on a previous theoretical study at JILA<sup>10</sup>.

While this laser induced two photon pumping scheme with  $^{199}\text{Hg}^+$  could significantly contribute to an experimental determination of the

performance capability of the trapped mercury ion microwave standard, it is obvious that its usefulness is limited to that of a laboratory device. The required dye laser system makes it impractical for space-borne, as well as ground based applications, requiring a long term reliable performance. We have therefore pursued, in parallel with the study of this scheme, an effort to design improved optics for the detection of the fluorescence signal which would enhance the signal-to-noise in the conventional pumping scheme. In the design of Jardino et al<sup>4</sup> a signal-to-noise ratio of about 10 to one was reported. We have designed an optical detection system which we believe can improve their value by a factor of 10. The details of this design, presently under construction, will be published after the required tests are concluded. With this improvement we should be able to obtain a satisfactory level of performance, and still use a conventional mercury ion light source. We also determined that the success of such a device would depend on a reliable operation of the mercury ion lamp. Presently we are engaged in efforts aimed at the improved operational life of mercury ion lamps; we believe that it is possible to extend the operational life of the lamp by a factor of 5, through a careful determination of the relevant parameters. Finally, mention should be made of the choice of an appropriate trap. The use of an rf trap as opposed to a Penning trap is pertinent for this particular application because rf traps eliminate the need for a magnet with very high stability, as required by Penning traps. The influence of rf heating however is an undesirable feature in the trade off. Recent studies involving the use of a buffer gas for cooling the trapped ions appear quite promising. In particular, Schaaf et al have achieved a factor of 3 reduction in the temperature of  $\text{Ba}^+$  ions stored in an rf trap, through collisions with a helium buffer<sup>11</sup>. Based on the above consideration, the development of a trapped mercury ion microwave standard suitable for space applications appears quite feasible.

### Optical Frequency Standard

The development of an optical frequency standard is expected to make the achievement of stabilities of a part in  $10^{18}$  and higher possible. Presently efforts to develop cryogenic hydrogen masers<sup>12</sup> and superconducting cavity stabilized oscillators are also aimed at the same objective. Optical frequency standards utilizing Terahertz frequencies and extremely high line Q's are particularly promising for the development of ultra-stable frequency standards. Application of ion traps in this area can greatly aid the study of relevant concepts for the realization of this goal. In particular Dehmelt's proposed mono-ion oscillator utilizing optical transitions of a single ion confined in an rf trap seems to hold considerable promise. Because of its state of complete rest, the single ion may be shielded almost totally from interaction with the environment. With the application of minute laser powers and suitable photon detection, this device could have the capability of producing stabilities in the range of parts in  $10^{18}$ .

The  $^2D_{5/2}$  transition of mercury ion with a calculated lifetime of 0.1 s and 10 Hz line width is also a promising candidate in optical frequency applications. With a two photon pumping of this level from the ground state with counter-propagating laser beams, the first order Doppler effect will be completely eliminated. There are however some difficulties that are anticipated with this scheme. First, as mentioned before, the problem of the second order Doppler shift proves an obstacle if an rf trap is used. With a Penning trap, the ions may be cooled to very low temperatures, as demonstrated at NBS<sup>13</sup>, and thus the second order Doppler may be essentially eliminated. There could, however, be a line broadening effect due to the quadrupole perturbation of the static electric field of the Penning trap on the ions. Second, the effect of the quadratic Stark shift associated with the two photon pumping should also be carefully investigated, particularly because a large laser intensity may be required for the two photon pumping of this magnetic quadrupole transition. Nevertheless it is expected that an effort

utilizing this approach would provide valuable information concerning the possibility of pumping a narrow metastable state to be used in the development of an optical frequency standard, or in applications where solid state lasers could be used to replace conventional pump lights.

### Conclusion

Recent results from various laboratories have clearly demonstrated the potential of ion traps as precision frequency standards. Nevertheless considerable work remains to be done before the full potential of such devices could be realized. With respect to microwave frequency standards, the concept demonstration phase is already complete, and a working unit has been constructed<sup>4</sup>. There is however considerable room for improvement with regard to the signal to noise problem. The 40 GHz microwave frequency implies that a careful design should be implemented to ensure the elimination of the unwanted side bands in the microwave pump signal. The development of a long life, high performance light source to be used in a trapped mercury ion microwave standard requires attention. Finally, the long term performance of a trapped mercury ion microwave standard is yet to be investigated. This is a necessary step since such devices are expected to have high stabilities for long averaging intervals.

While newly proposed two photon pumping schemes in conjunction with mercury ions promise exciting developments for both microwave and optical frequency standards, it would be useful to carry out investigations with other ions that may be potential candidates<sup>14</sup> to evaluate their usefulness for this application. The concept of trapped ion frequency standards has come a long way since the early work of Major; yet we may expect to see exciting new developments in not too distant a future.

This paper presents the results of one phase of research carried out at the Jet Propulsion Laboratory, California Institute of Technology, under contract No. NAS 7-100, sponsored by the National Aeronautics and Space Administration.

## REFERENCES

1.     Frostor, E.N., Major, F.G., and Dehmelt, H.G., Phys. Rev. Lett. 16, 221 (1966).
2.     Major, F.G., NASA Report No. X-521-69-167, (1969).
3.     Major, F.G., and Werth, G., Phys. Rev. Lett. 30, 1155 (1973).
4.     Jardino, M., Desaintfuscien, M., Barillet, R., Viennet, J., Petit, P., and Audoin, C., Appl. Phys. 24, 107 (1981).
5.     Dehmelt, H.G., Proceedings of Third Symposium on Frequency Standards and Metrology, Aussois, France, Oct. 1981. In press.
6.     Proposal to JPL's DDF, July, 1980.
7.     Morozowski, S., Phys. Rev. 57, 207 (1940).
8.     Bloembergen, N., and Levenson, M.D., in: "High Resolution Laser Spectroscopy", ed. by K. Shimoda (Springer-Verlag, New York 1976) chapter 8.
9.     Wineland, D.J., Itano, W.M., Berquist, J.C., and Walls, F.L., Proceedings of 35th Annual Frequency Control Symposium, Philadelphia, PA., May 1981. In press.
10.    Bender, P.L., Hall, J.L., Gartstang, R.H., Pichanick, F.M., Smith, W.W., Barger, R.L., and West, J.B., Bull. Am. Phys. Soc. 21, 599 (1976).
11.    Schaat, H., Schmelding, V., and Werth, G., Appl. Phys. 25, 249 (1981).
12.    Crampton, S.B., Souza, S.A., and Krupczak, G., Proc. Third Symposium on Frequency Standards and Metrology, Aussois, France, Oct. 1981. In press.



13. Drullinger, R.E., Wineland, D.J., and Berquist, J.C.,  
Appl. Phys. 22, 365 (1980).
14. Strumia, F., Proceedings of 32nd Annual Symposium on  
Frequency Control, June 1978, p. 444.

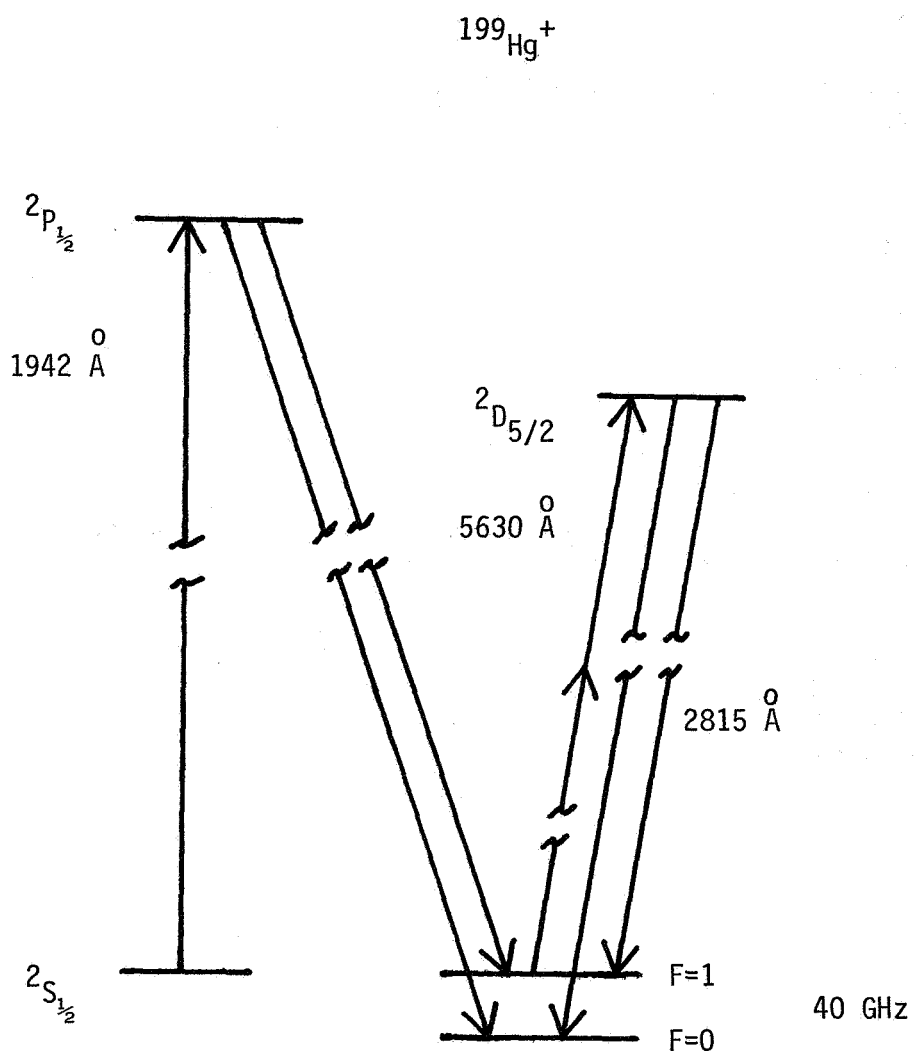


FIG. 1-SIMPLIFIED DIAGRAM OF MERCURY ION LEVEL STRUTURE

## QUESTIONS AND ANSWERS

RELATIVE TO PAPERS: 28, 29, 30, & 31

PROFESSOR ALLEY:

You alluded to a new optical detection scheme, but you did not say what it was.

MR. MALEKI:

That's right.

PROFESSOR ALLEY:

Can you say something.

MR. MALEKI:

Well, essentially it is nothing dramatic. What we are talking about is sitting down and determining precisely the proper parameters. And determining, in particular, the proper components, optical components. I think we can do that.

Like I said, our models show that. This, as I explained, is right now being built. And I believe we are going to have some data in the not too distant future at which time, then, you will get all the details.

PROFESSOR ALLEY:

Thank you.

May I ask another question of Len Cutler? Len, have you tried coherently phased RF pulses in some sort of power of two pulse, or something like that, to shift populations?

DR. CUTLER:

No, we haven't, Carroll. We've thought of this. The lifetime in the trap is certainly long enough. There's no problem there. But there are other relaxations. For example, if you have helium present there are relaxations caused by that. So we haven't actually tried it.

PROFESSOR ALLEY:

Thank you.

Could I address one more question, Bob, please to Dr. Wineland?

What is the type of laser that you are now using, the whole scheme, to do your laser cooling?

DR. WINELAND:

The experiments we've done so far, both on magnesium and beryllium, but those aren't very good frequency standard candidates. The reason is that we can drive the optical transitions with doubled dye-lasers.

The scheme we're working on to do mercury is fairly complicated, but looks feasible for the low powers that we need. That is where we double an argon laser and mix the output of that with a dye-laser to get 194 nanometers. But we haven't realized that source yet.

PROFESSOR ALLEY:

It's all CW?

DR. WINELAND:

It's all CW.

PROFESSOR ALLEY:

You haven't tried any short pulse in the doubling?

DR. WINELAND:

Well, the problem there is to do the laser cooling we basically want a laser line which is less than the optical transition line. And it's not inconceivable you could do that with lasers. But then the problem is that the repetition rate of lasers, pulse lasers, is just too short to do effective laser cooling.

So we really want it to be CW.

DR. HARRY WANG, Hughes Research Laboratory

I'm just addressing my question to Len or Dave. My question is can you eliminate the ion pumps -- the vacuum pumps from your standard? You know, in view of the realization you might increase

in closed system. What is the possibility for a closed ion standard so that you can eliminate ion pumps? And what is the price you have to pay for such a system?

DR. CUTLER:

I think it is possible to have a closed system. All of the components that go inside are such that you can bake out at a very high temperature, and get a very good vacuum.

Fortunately, in the system that we have built so far we had a seal break. And so the vacuum deteriorated as a result of that. But that's not a fundamental problem.

So I think it's possible to have a closed system. You may very well want to have an ion pump present, though, if you are going to use viscous drag cooling with a gas to control the pressure of this gas.

The mercury is very well limited by a number of materials. For example, if you have a lot of copper around, the mercury sticks to the copper very well. So the background pressure of mercury is not much of a problem.

DR. VESSOT:

I think we'll eat into our coffee break for another one or two minutes.

DR. JOHN VIG, U.S. Army Electronics Technology & Devices Lab

Len Cutler gave some projections of stability and accuracy of a commercial standard. I wonder if you have some other projections, such as size, power consumption, relative cost, and the probability that we might see a commercial standard, say, in five years?

DR. CUTLER:

Okay. Tackling the last one first. I think it is possible barring some unfortunate, unforeseen, really bad thing that would prevent it, that we will see something within, say, five years.

As far as size and weight are concerned, I think it's entirely possible to put a complete standard inside a box that's roughly the same size as a commercial cesium box.

Weight could possibly be a little bit less than cesium.

Power consumption; if we use an Rf excited lamp, mercury 202 lamp, probably will be somewhat higher than cesium, just because of the lamp power.

I would suspect that costs could be about comparable with cesium.

And expect the performance to be considerably improved as the numbers I talked about earlier.

DR. WINELAND:

Well, I have a comment and a question for Lou Maleki.

First of all, I don't think the signal to background problem has to really be a problem. Just as an example, in some of the experiments we're doing now on beryllium on a few hundred ions we see a signal to background of about 1,000. So good optical filtering, and so on, it doesn't have to be a problem.

The question is what do you think the principal uses for an optical frequency standard will be?

MR. MALEKI:

The first comment is half true, in the sense that the signal to background problem that I'm talking about is one that Major has had to deal with and Giardino has had to deal with.

I suspect some of the chopping scheme that Len is using is to circumvent that problem.

The second thing as to what it is going to be good for. Well, I was hoping you would tell me that yourself. But I could at least mention that some of the experiments, regular science experiments that they are talking about they are interested in very high stability.

It turns out that application of the quantum nondemolition schemes that are going to be used, gravity waves, makes it useful in the future -- now by future I -- may be beyond my life time -- but in the future to use frequency standards upwards of 10 to the minus 21.

But, finally, it is the challenge of it. I mean it is there. And you have to get there. I thought that was the drive that NBS needed.



## A RUBIDIUM CLOCK FOR GPS

William J. Riley  
EG&G, Inc., Frequency and Time Department  
Salem, Massachusetts

### ABSTRACT

The work at EG&G, Inc. on a second-source rubidium frequency standard for use in the GPS navigation satellites has now reached the prototype stage. This paper describes (1) the design objectives and approach, (2) the more important design features, (3) the signal parameters and error budget, and (4) the early results of this program up to the present.

### INTRODUCTION

Since March 1980, EG&G, Inc., has been engaged in a program to develop a rubidium frequency standard (RFS) for the Department of Defense, NAVSTAR Global Positioning System (GPS). This paper describes the RFS design objectives and approach as well as the early test results obtained up to the present prototype stage of development.

The basic objective in the RFS development is to meet the stringent stability, reliability, and radiation hardness requirements of the Phase III NAVSTAR satellites. A summary of the general specifications is contained in Table 1.\* The overall design approach has been to choose a configuration that favors the highest possible performance and, wherever possible, uses mature S-level quality parts. All parts will be subjected to extensive screening.

The design objective of radiation hardness will be met by circuit design, component selection, and passive shielding.

To ensure the highest possible performance, the design utilizes a discrete filter cell arrangement to permit separate control of the optical pumping spectrum. This allows the light shift effect to be independently nulled and reduces inhomogeneities in the absorption cell.

---

\*Tables are located at the end of the paper.



The synthesizer is based on a 10.23 MHz output and uses a direct primary loop multiplier chain for high spectral purity. The physics package makes effective use of the vacuum environment for thermal insulation, thus reducing oven operating power.

The early results obtained during the prototype development are encouraging, and the unit uses less than half the power than the original GPS rubidium clock (12 versus 28 watts), although it is somewhat larger (260 versus 170 cubic inches) and heavier (10.5 including radiation shielding versus 9.7 pounds). The weight factor has only recently increased in importance, and a weight reduction effort is currently underway.

It is expected that one of the prototype units will be subjected to extended stability testing, which will be followed by the building and testing of qualification units. This program should result in the production of the most stable rubidium clocks yet manufactured.

#### SYSTEM BLOCK DIAGRAM

A block diagram of the complete RFS system is shown in Figure 1. The major sections, which are discussed separately on the following pages, are listed below:

- (1) The physics package that serves as a frequency discriminator by generating an error signal whose magnitude and sense indicates the difference in frequency between the microwave excitation and the stable atomic resonance.
- (2) The supporting electronics that allow proper operation of the physics package.
- (3) The primary loop that produces an output signal whose frequency is locked to an exact submultiple of the atomic resonance.
- (4) The secondary loop that synthesizes the desired 10.23 MHz output.
- (5) The control circuits that allow remote tuning, mode selection, and monitoring.
- (6) The power supply.

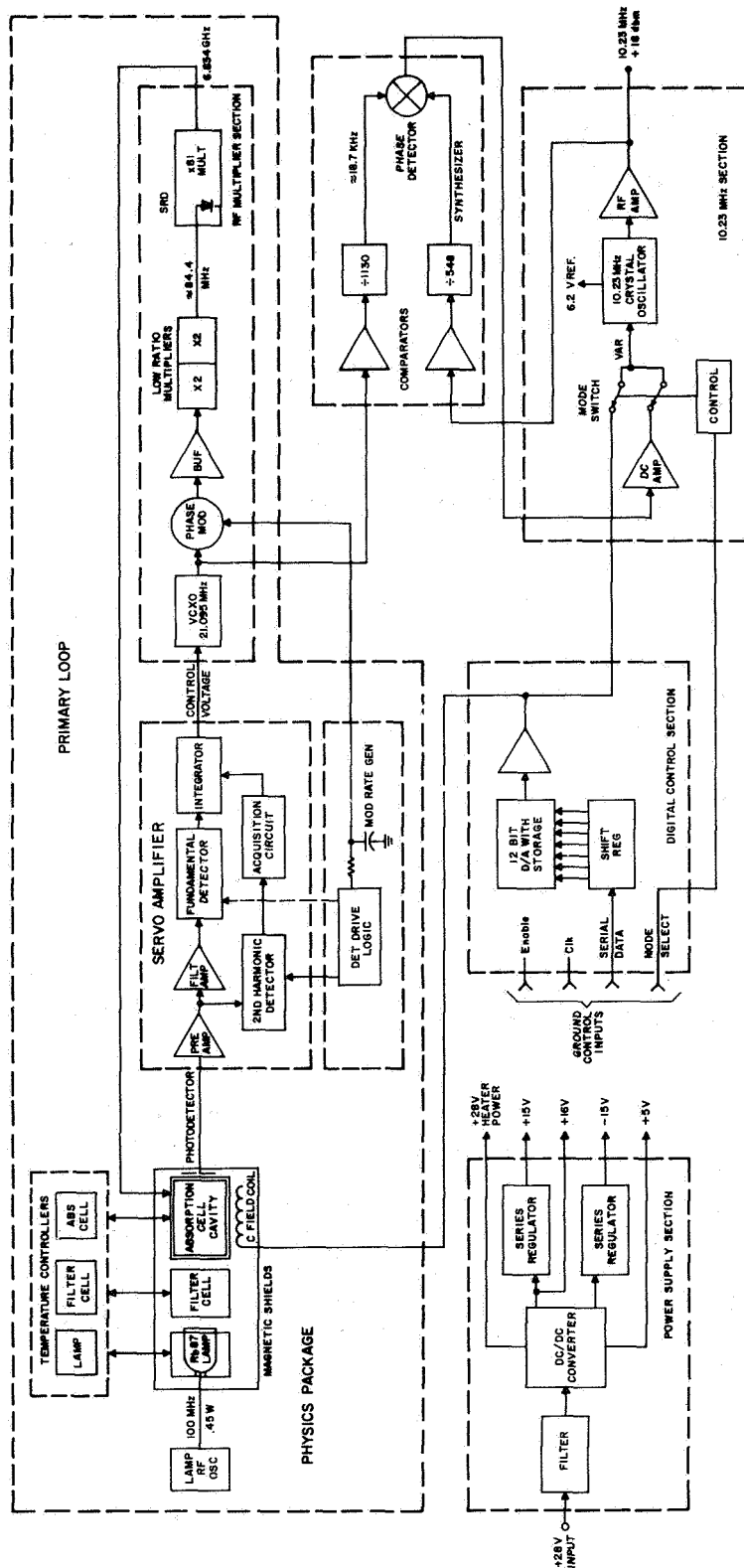


Figure 1 — GPS RFS system block diagram

## Physics Package

The physics package design is based on classical rubidium frequency standard principles, except for the use of a smaller TE<sub>111</sub> cavity. This approach gives the highest performance consistent with allowable size. The discrete filter cell gives zero light shift (ZLS) over a range of light intensity and a high S/N ratio. This permits operation at a relatively low light level, thus reducing temperature and rf power dependencies.

The characteristics of the lamp, filter, and absorption cell are shown in Table 2. The lamp operates in the Kr-Rb mixed mode and is excited with 0.45 watt of rf power at 110 MHz. The lamp D<sub>1</sub> line emission at 794.7 nm is shown in Figure 2a; it is free of self-reversal. Lamp life is aided by tight heat sinking, alkali resistant glass, high vacuum processing, and calorimetric measurement of rubidium fill.

An example of calorimetric measurement is shown in Figure 3. A differential scanning calorimeter, Perkin-Elmer DSC-2C, is used to measure the heat energy required to melt the rubidium in a lamp. This allows (using the known heat of fusion of Rb) the amount of rubidium to be determined with a resolution of a few  $\mu$ G. A test program is underway to evaluate lamp life using this technique.

The filter cell is operated in a separate oven whose temperature is adjusted for ZLS. The spectrum of the filtered light is shown in Figure 2b. Notice that ZLS filtration corresponds to only a slight attenuation of the skirt of the unwanted hyperfine optical component. Heavier filtration with a longer or hotter isotopic filter gives a stronger signal and lower filter cell TC but only at the expense of a large negative light shift coefficient. The filter cell buffer gas and pressure were chosen to give optimum signal and lowest TC under ZLS conditions.

The absorption cell buffer gases are chosen for narrow linewidth and low TC. The mix ratio is adjusted for a slightly positive TC to partially compensate for the filter cell TC. The nominal fill pressure is determined by the synthesizer ratio and is sufficient to reduce the wall relaxation rate without excessive buffer gas collisional broadening. The absorption cell length is optimized for maximum signal at the chosen light intensity and temperature, the latter being the coolest practical value for the required upper ambient limit of 45°C.

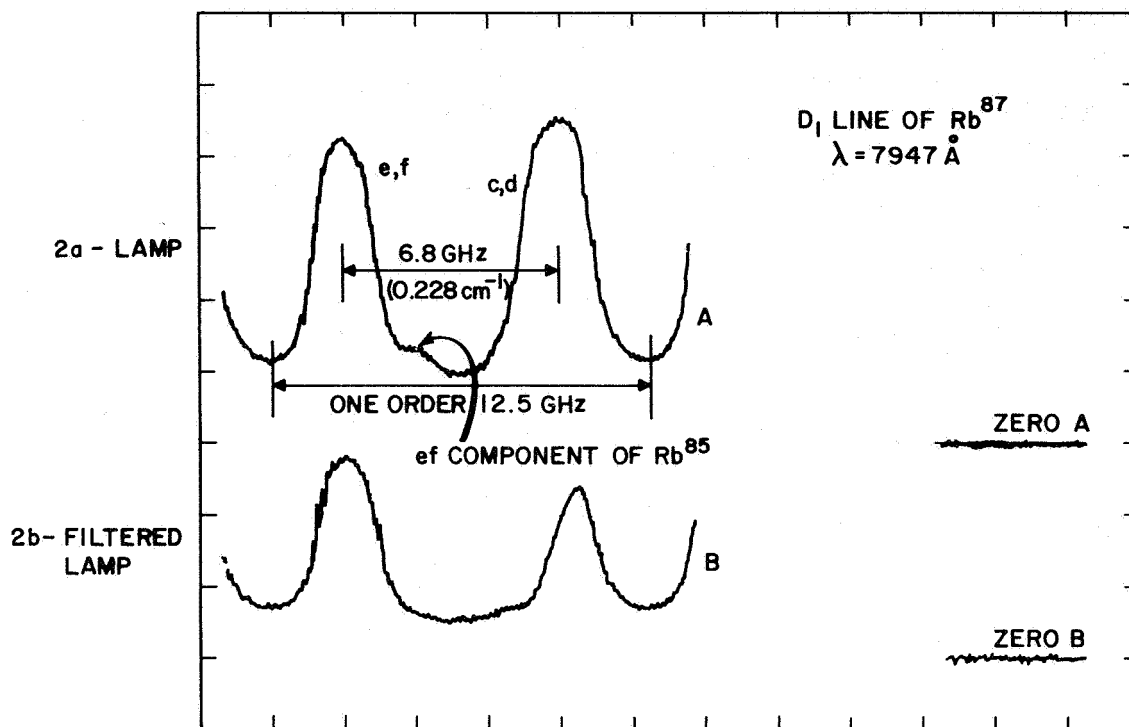


Figure 2 — Hyperfine light spectra

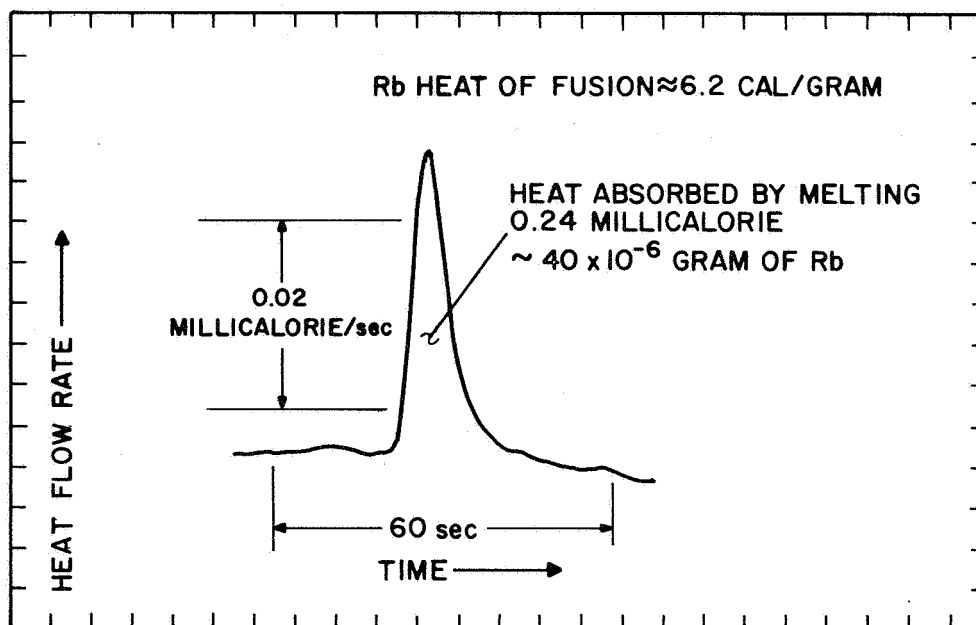


Figure 3 — Rb determination by calorimetry

A cross-sectional view of the physics package is shown in Figure 4. The three ovens are supported by a fiberglass structure with finger-like tabs that combine rigidity with low thermal conductance. This makes effective use of the vacuum environment for thermal insulation. Low thermal conductivity leads and low emissivity gold foil further reduce losses so that the entire physics package requires only 1.8 watts of oven power under nominal operating conditions.

It is important to avoid any condition that can distort the shape of the absorption line, because any such inhomogeneity will contribute to the rf power dependence. A lens is used to collimate the lamp output and provide a uniform light distribution, the filter cell is adjusted for ZLS, a two-section C-field coil configuration provides a uniform magnetic bias field, and a well bonded absorption cell with modest pressure shift coefficient provides low temperature gradients. All oven windows are sapphire for high thermal conductivity.

Another consideration is the residual magnetic field of the oven heaters which, particularly for the cavity, can induce a pseudo temperature coefficient. Precise registration of a thin double-layer blanket heater and low oven supply current reduce this effect to  $2 \mu\text{G}/\text{mA}$  or  $2 \times 10^{-14}/^\circ\text{C}$ .

The microwave cavity is excited with an E-probe and has slotted end covers that support the desired  $\text{TE}_{111}$  mode while allowing light transmission without significant microwave leakage.

The physics package includes two 0.025 inch Hipernom cylindrical magnetic shields. The major physics package parts are shown in Figure 5.

#### Supporting Electronics

Directly associated with the physics package are the temperature controllers, lamp exciter, photodetector preamplifier, and magnetic bias current supply. These circuits determine, to a large extent, the overall frequency stability that is achieved.

The temperature controllers (Figure 6) are dc thermistor bridges and dissipative regulators, with static thermal gains of about 2000. The oven demand power is determined by the one hour warmup required for ground testing in air. Vacuum conditions not only reduce the oven losses but also raise the thermal gains and servo stability margins. Care is taken to hold thermistor self-heating constant at a fraction of a degree C.

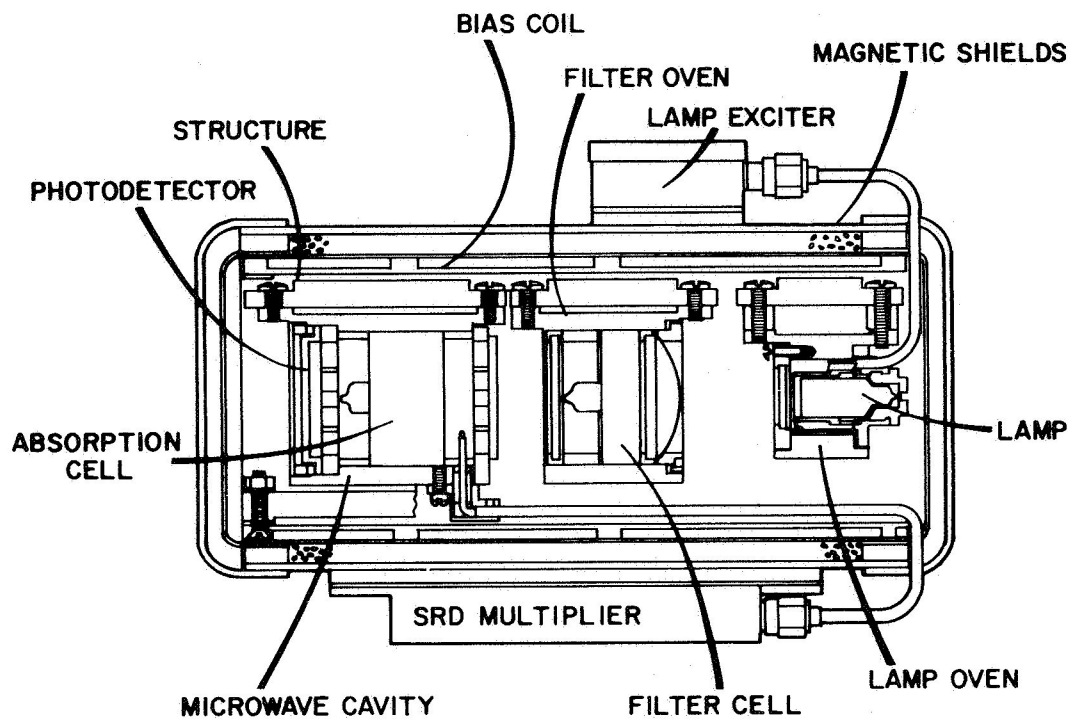


Figure 4 — Breadboard physics package cross-sectional drawing

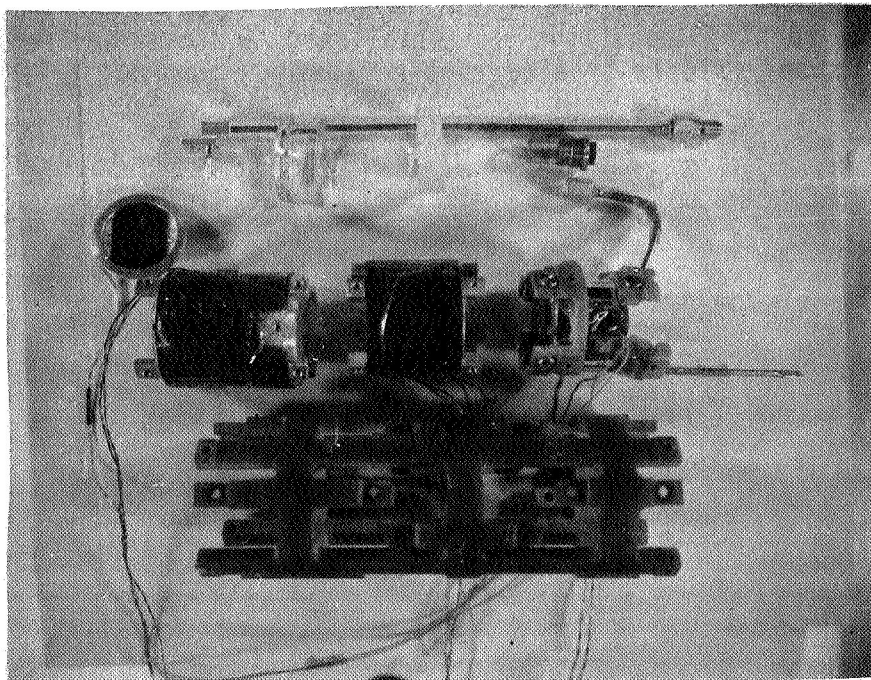


Figure 5 — Breadboard physics package parts

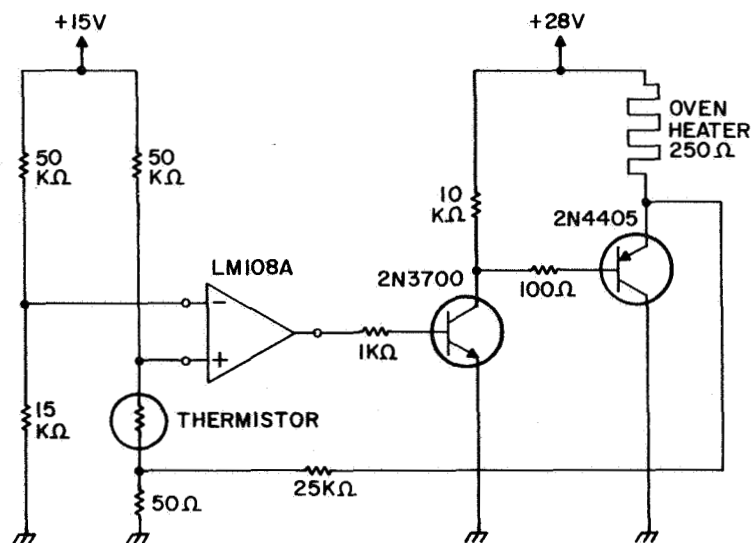


Figure 6 — Basic temperature controller circuit

The lamp exciter (Figure 7) is a straightforward Clapp power oscillator with the lamp located inside the series-tuned coil. The lamp network presents a range of loads as a function of lamp mode, and the circuit has been characterized under these various conditions to ensure proper operation. Starting may require the exciter to redistribute condensed rubidium inside the lamp by rf induction heating. Ignition takes place when sufficient voltage exists across the lamp coil. The running condition is stabilized against environmental changes and supply ripple by a current regulator circuit.

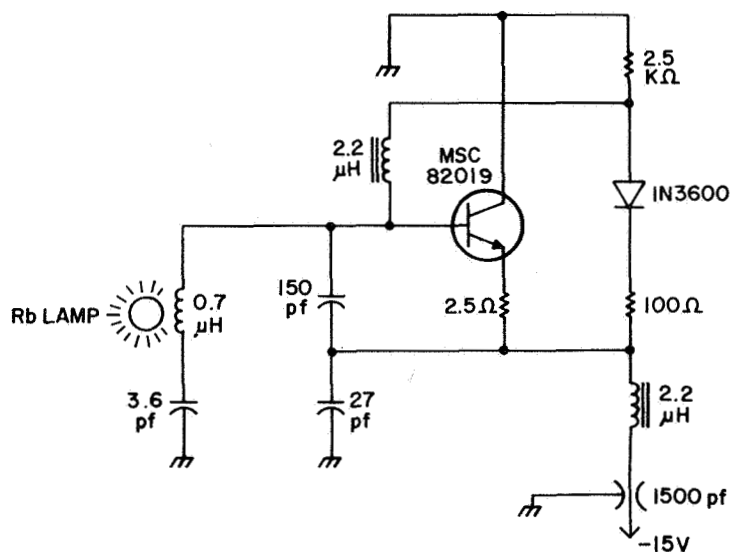


Figure 7 — Basic lamp exciter circuit

The photodetector preamplifier (Figure 8) is a two-stage configuration with dc and ac transimpedances of  $100\text{ k}\Omega$  and  $5\text{ M}\Omega$ , respectively. The ac gain is broadly peaked at the fundamental modulation frequency.

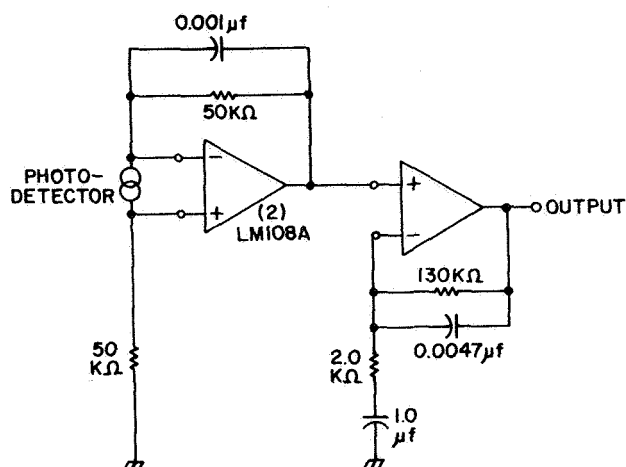


Figure 8 – Basic preamplifier circuit

The magnetic bias supply (Figure 9) is an active current source, programmable under ground control with a resolution of  $3 \times 10^{-12}$ . Relay switched fixed resistors are used for the four most significant of 12 bits, in order to minimize temperature effects on this critical circuit. The reference voltage for the C-field supply is derived from a precision zener diode located inside the oven of the secondary loop crystal oscillator. Provision is made for the direct use of this oscillator in a backup mode independent of the rubidium reference.

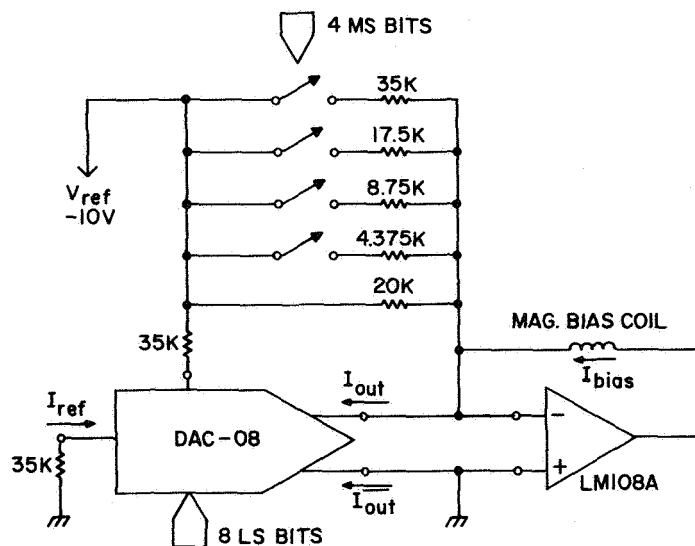


Figure 9 – Basic magnetic bias supply circuit



## Primary Loop Electronics

The servo amplifier, crystal oscillator, and rf multiplier chain that complete the primary loop are shown in Figure 10. No synthesis or mixing is done in this loop to avoid instability caused by asymmetrical components on the microwave spectrum. The amount of frequency offset caused by a single spurious component scales directly with its power and inversely with its separation from the main carrier. A typical sensitivity is  $5 \times 10^{-13}$  for a component equal in power and 5 MHz away. Direct multiplication essentially eliminates this effect. The most critical components are at  $\pm 18.7$  kHz (from the secondary loop synthesizer) that are well suppressed ( $> -60$  dBC) and symmetrical.

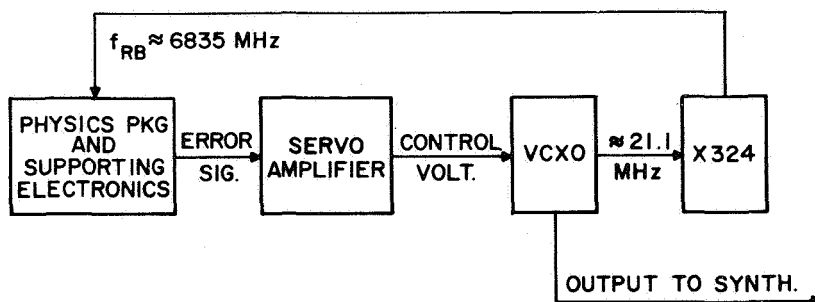


Figure 10 - Primary loop block diagram

The servo amplifier (Figure 11) consists of a main fundamental detector/integrator channel, a second harmonic/acquisition channel, and the modulation reference logic. The modulation rate is derived by division of the 10.23 MHz output to approximately 146 Hz. The servo amplifier circuits, although straightforward, require care in execution and component selection, since the system is a frequency lock loop and offsets directly cause frequency errors.

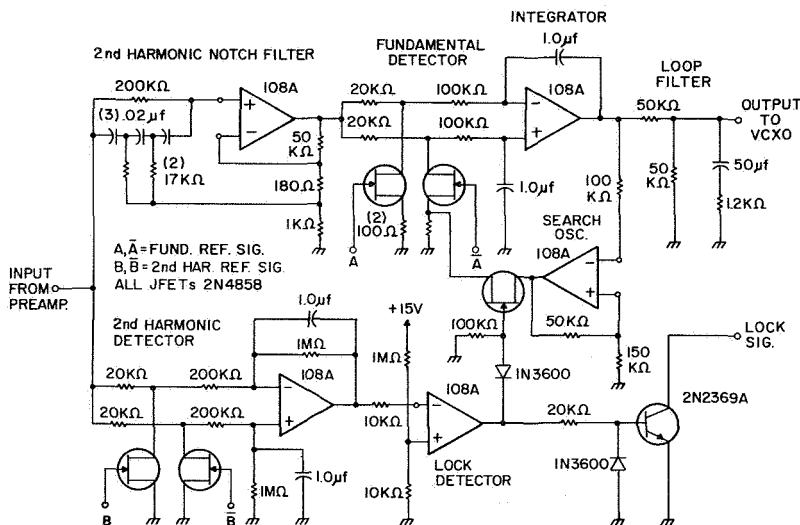


Figure 11 - Basic servo amplifier circuit

The crystal oscillator (made by Frequency Electronics, Inc.) uses an FC-type crystal which, by virtue of its excellent temperature characteristic, avoids the need for ovenization.

The rf multiplier chain (Figure 12) consists of a phase modulator, two push-push doublers, and a X81 step recovery diode (SRD) multiplier. An ALC loop is used to maintain constant drive to the SRD multiplier. This approach gives high stability and spectral purity with minimum complexity. Particular care is taken to avoid frequency offsets caused by even-order modulation distortion. A relative second harmonic distortion level of -70 dB can cause an offset of  $5 \times 10^{-12}$  and thus must be constant to a few percent to obtain good frequency stability. A pure modulation waveform is generated by passive integration of a precision squarewave, and a highly linear phase modulator characteristic is obtained by applying small excursions to a hyper-abrupt varactor diode biased at an "S" shaped inflection point. A more subtle factor is the distortion caused by AM and subsequent AM-to-PM conversion in the multiplier chain. A simple RC phase shifter circuit introduces equal amounts of AM and PM and thus can cause considerable distortion. The all-pass phase modulator configuration shown in Figure 12 provides about 26 dB of AM rejection and thus greatly reduces this problem.

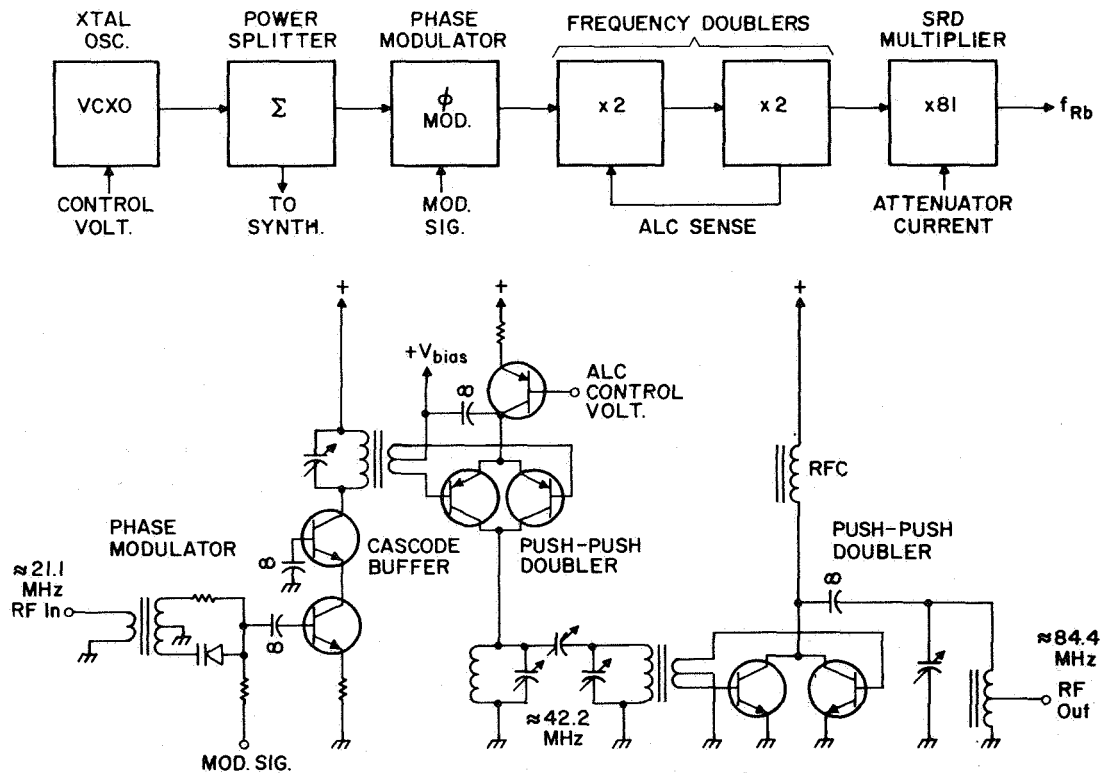


Figure 12 – Basic rf multiplier chain and circuit.

The SRD multiplier (made by Frequency Sources, Inc.) uses a low capacitance diode in a shunt mode with external dc bias. A temperature stability of 0.01 dB/°C is typical for the  $\approx 50$   $\mu$ W microwave output which can be adjusted to the optimum level by an internal PIN diode attenuator.

### Secondary Loop and Synthesizer

The 10.23 MHz output is derived from a precision ovenized crystal oscillator (made by Frequency Electronics, Inc.) that is phase locked to the primary loop by the synthesizer. (See Figure 13.) The +18 dBm output is obtained via an output amplifier that has sufficient tank circuit Q to maintain a phase-continuous output under transient radiation. Sufficient isolation is provided by the divider input circuits to keep the output spectrum free (-100 dBC) of synthesizer spuri.

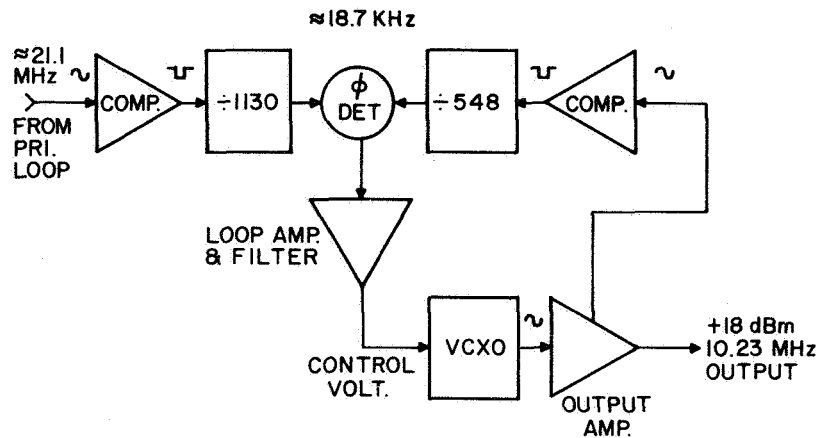


Figure 13 – Synthesizer block diagram

The synthesizer consists of a pair of dividers that divide the primary and secondary loop frequencies down to their common factor of  $\approx 18.7$  kHz. A phase detector and loop filter generates a control voltage for the 10.23 MHz crystal oscillator. Rapid lock acquisition is accomplished by logic that presets the dividers to the proper phase relationship. This also provides fast recovery from a radiation-induced upset.

### Power Supply

The power supply consists of an input filter, a dc/dc converter, and two linear regulators as shown in Figure 1. The dc/dc converter (Figure 14) uses a single-ended flyback configuration that provides both dc isolation and regulation. Its +28 V and +5 V outputs are used directly as heater and logic supplies respectively while the  $\pm 16$  V outputs are further stabilized by precision linear regulators before

supplying the analog circuits. Under normal operating conditions in vacuum, the RFS circuits consume under 10 watts. The total dc input is expected to be 28 watts demand during warmup and 12 watts steady state.

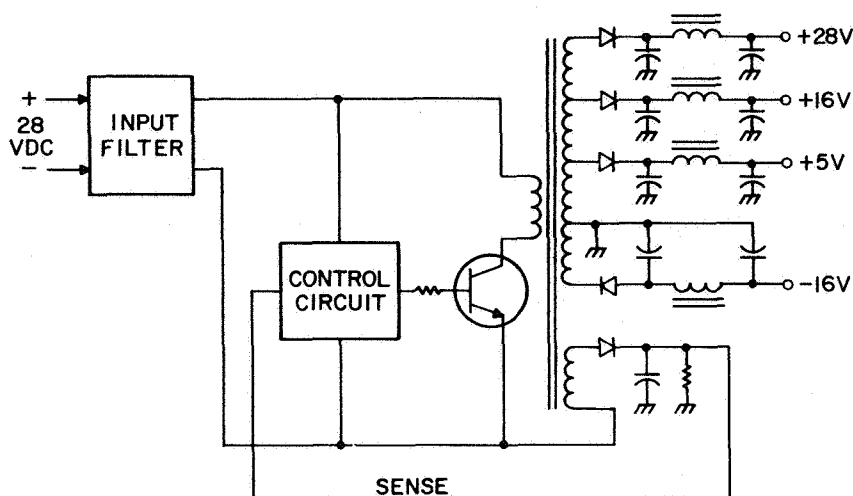


Figure 14 — Basic power supply circuit

### Packaging

The overall RFS package, shown in Figure 15, consists of an aluminum structure with aluminum and Hipernom covers for magnetic, EMI, and radiation shielding. The hollow center of the structure holds the physics package, secondary crystal oscillator, the lamp exciter, preamplifier, and SRD multiplier. The other electronic circuits are on 13 circuit boards located inside compartments that comprise the outside walls of the structure. Additional local radiation shielding is used as required. This approach meets all thermal, electrical, mechanical, magnetic, and radiation requirements as well as allowing good access to most circuit boards.

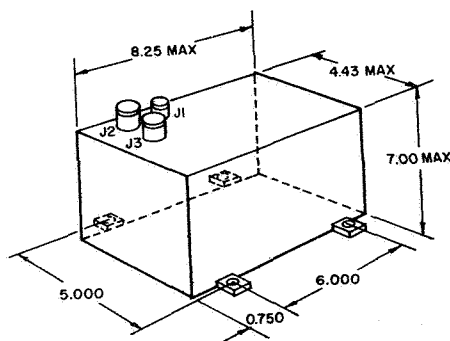


Figure 15 — RFS outline drawing

### Signal Parameters

The operating conditions and signal parameters of the physics package are summarized in Table 3. In general, these values indicate a good signal and exceptionally low sensitivities.

The S/N ratio of a passive rubidium frequency standard is limited by the shot noise of the dc photodetector current,  $I_0$ , which sets a level of white frequency noise and gives a time-domain frequency stability that varies as  $\tau^{-1/2}$ , where  $\tau$  is the averaging time.

The frequency stability can be estimated simply from the values of  $I_0$  and the discriminator signal,  $D$ . For  $I_0 = 82 \mu\text{A}$ , the shot noise current,  $i_n$ , is:

$$i_n = \sqrt{2eI_0\Delta F} = 5.1 \text{ pA}/\sqrt{\text{Hz}}$$

This establishes the white frequency noise level in relation to the  $D$  value of 240 pA per  $1 \times 10^{-10}$ , giving a fractional frequency noise power spectral density of:

$$S_y(f) = h_0 = \left(\frac{5.1}{240} \times 10^{-10}\right)^2 = 4.5 \times 10^{-24}(\text{Hz})^{-1}$$

This results in a time-domain stability of:

$$\sigma_y(\tau) = \sqrt{\frac{h_0}{2}} (\tau)^{-1/2} = 1.5 \times 10^{-12}(\tau)^{-1/2}$$

which may be converted to a frequency-domain value of:

$$\mathcal{L}(f) = [\sigma_y(\tau)]^2 \nu_0^2 \tau f^{-2}$$

where  $\nu_0$  is the carrier frequency of 10.23 MHz. Then,

$$\mathcal{L}(f) = 2.4 \times 10^{-10} f^{-2} \text{ and } \mathcal{L}(1) = -96 \text{ dBC/Hz.}$$

The measured noise level is  $5.5 \text{ pA}/\sqrt{\text{Hz}}$  rather than the  $5.1 \text{ pA}/\sqrt{\text{Hz}}$  value expected from shot noise only. The noise level is  $0.7 \text{ pA}/\sqrt{\text{Hz}}$  without light, also indicating a negligible contribution from the

photodetector and pre-amplifier. This is possible primarily because of the use of a very high quality EG&G custom photodetector that has a high leakage resistance ( $>50K \Omega$ ) at the  $65^{\circ}C$  operating temperature.

The actual noise results in an estimated time-domain stability of  $1.6 \times 10^{-12} \tau^{-1/2}$ . The observed value is  $4 \times 10^{-12} \tau^{-1/2}$  uncorrected for the (unknown) contribution of the reference.

The S/N ratio can be defined as the rms value of the maximum fundamental error signal current divided by the rms noise current in a 1 Hz bandwidth.

Values of over 90 dB have been obtained with this design by operating the lamp in the more intense red (all Rb) mode, and over 80 dB in the mixed (Kr-Rb) mode. However, higher light intensity also results in larger temperature coefficients, rf power shift, and other sensitivities. For the GPS application, it is considered a better tradeoff to favor long-term and environmental stability by operating at modest light intensity where the S/N ratio is about 75 dB.

#### ERROR BUDGET

The RFS frequency is influenced by a number of factors that can affect its stability. Some of these factors involve dependencies of the physics package and others are a result of electronic circuit sensitivities. The largest of these factors are listed in Table 4. Also shown in Table 4 are the resulting individual temperature coefficients and the total worst-case and rms values expected. These factors also govern the aging rate and radiation sensitivity of the unit.

#### TEST RESULTS AND CONCLUSIONS

Tests of a breadboard version of the RFS have given encouraging results. The results of stability tests conducted on the primary loop with the physics package in a thermovac chamber and most electronic circuits on the bench in air are shown in Figure 16. The measured time-domain stability is within the goal specification. The results are uncorrected for the contribution of the reference and are probably limited by the reference stability in the medium term region. The region near  $\tau = 1$  second will be determined by the secondary loop crystal oscillator, which has a measured stability of  $4 \times 10^{-12}$ . The RFS stability in the medium term region is at least as low as  $4 \times 10^{-12} \tau^{-1/2}$  and reaches below  $1 \times 10^{-13}$  between  $\tau = 10^4$  and  $10^5$  seconds. The Rb reference is better in the medium term region, but the Cs reference has been found to be better at  $10^4$  seconds and longer, probably because of the barometric sensitivity of the rubidium reference unit. The GPS RFS is immune to this effect in the thermovac chamber. A drift rate of under  $1 \times 10^{-13}$  per day and a physics

package temperature coefficient of  $1 \times 10^{-13}/^{\circ}\text{C}$  has been obtained. It is reasonable to assume that the  $10^5$  second stability will be even better in the prototype version, when all circuits are packaged and operated within the controlled thermovac environment. Overall, the RFS program is on schedule and all objectives are being met.

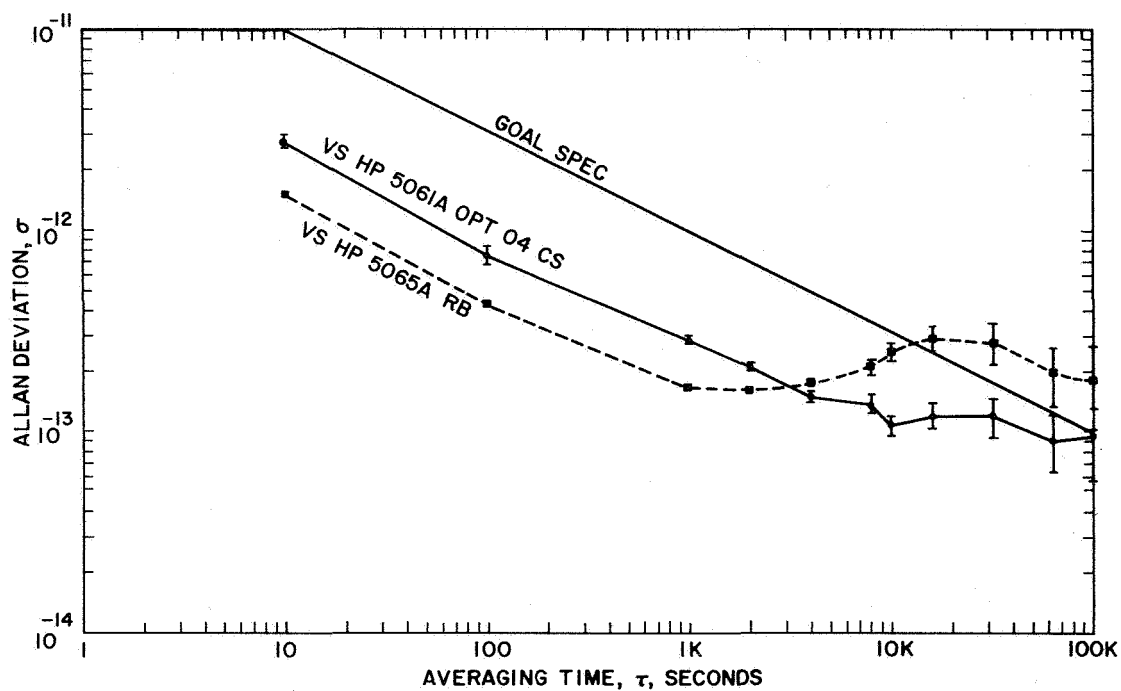


Figure 16 — Time-domain stability of the breadboard

## ACKNOWLEDGMENTS

The author wishes to acknowledge the support of Rockwell International, Space Division, and the Department of the Air Force, Headquarters Space Division (AFSC), Directorate of Space Navigation Systems for their sponsorship of this work. The program has benefited by technical advice from the Aerospace Corporation and the radiation hardening expertise of JAYCOR Inc. Also, we received valuable consultation from Professor J. Vanier of Laval University and Mr. H.P. Stratemeyer.

The work at EG&G has been a team effort and important contributions have been made by all staff members. Particular credit should be given to Mr. T. Lynch in the area of thermal-mechanical design and for the concept of calorimetric rubidium measurement; Mr. E. Sullivan for power supply and synthesizer design; and Mr. S. Goldberg for his overall scientific direction. Other design contributions were made by F. Chang, J. Kirby, K. Lyon, and J. McDonald.



Table 1 — Condensation of specifications for the Phase III GPS RFS

Output	$f = 10.23 \text{ MHz nominal, } +18 \text{ dBm nominal}$
Operating Temperature	$+ 20 \text{ to } +45^{\circ}\text{C}$
Frequency Stability (Figure 16)	$\sigma_y(\tau) = 1 \times 10^{-11}$ for $\tau = 1$ and 10 seconds decreasing as $\sqrt{\tau}$ to goal of $1 \times 10^{-13}$ at $10^5$ seconds
Phase Noise	$\mathcal{L}(1) = -83 \text{ dBC/Hz maximum, decreasing}$ at 10 dB/decade to 5 kHz
Spurious	-100 dBC maximum, 5 kHz to 20 MHz from carrier
Temperature Coefficient	$\frac{\Delta f}{f} \leq 1 \times 10^{-12}/^{\circ}\text{C}$
Drift	$\frac{\Delta f}{f} \leq 1 \times 10^{-13}/\text{day}$
Voltage Sensitivity	$\frac{\Delta f}{f} \leq 1 \times 10^{-12}/\text{volt}$
Mag Susceptibility	$\frac{\Delta f}{f} \leq 1 \times 10^{-12}/3 \text{ Gauss}$
Warmup Time	1 hour
Reliability	73% for 7.5 years' operation

**Table 2 — Lamp and cell characteristics**

	Lamp	Filter Cell	Absorption Cell
Glass (Corning #)	1720	7070	7070
Outside Diameter, inches	0.31	1.09	1.09
Inside Length, inches	0.54	0.18	0.45
Isotope	87	85	87
Buffer Gas	Kr	Ar	N <sub>2</sub> /Ar = 0.731
Pressure, Torr	7	120	14.2*
Operating Temperature, °C	120	85	65
Temperature Coefficient pp10 <sup>11</sup> /°C	~0	-6	+3

\*Offset = +2.78 kHz.

Table 3 — Breadboard RFS operating characteristics

<u>Signal</u>	
Second Harmonic Signal:	45 mV rms*
Maximum Fundamental Signal:	165 mV rms*
Light:	8.23 Vdc*
Discriminator Slope:	1.2 mV per $1 \times 10^{-10}$ *
Linewidth:	252 Hz†
<u>Sensitivities</u>	
Light Shift:	$\sim 0 \pm 1 \times 10^{-12}/\%$
Lamp Oven TC:	$\sim 0 \pm 3 \times 10^{-12}/^{\circ}\text{C}$
Filter Cell TC:	$\approx -6 \times 10^{-11}/^{\circ}\text{C}$
Absorption Cell TC:	$\approx +3 \times 10^{-11}/^{\circ}\text{C}$
RF Power Shift	$\approx \pm 2 \times 10^{-12}/\text{dB}$
Lamp Exciter TC:	$\sim 0 \pm 5 \times 10^{-14}/^{\circ}\text{C}$
<u>Noise</u>	
Shot Noise:	$5.1 \text{ pA}/\sqrt{\text{Hz}}$
Total Noise:	$5.5 \text{ pA}/\sqrt{\text{Hz}}$
Signal:	33 nA rms
(S/N):	76 dB in 1 Hz BW
Line Q:	$16 \times 10^6$
Predicted Stability:	$\sigma_y(\tau) = 1.6 \times 10^{-12} \tau^{-1/2}$

\*At preamp output with  $Z_T(\text{ac}) = 5 \text{ M}\Omega$ ,  $Z_T(\text{dc}) = 100 \text{ K}\Omega$ .

†Full width between inflection points with normal light and rf.

Table 4 — Frequency error budget

Factor	Sensitivity	TC, pp10 <sup>14</sup> /°C
Magnetic Bias Current	+ 3 x 10 <sup>-14</sup> /ppm	± 6.0
Lamp Exciter TC	± 5 x 10 <sup>-14</sup> /°C	± 4.0
Filter Cell TC	- 6 x 10 <sup>-11</sup> /°C	- 3.0
dφ/dt Effects	---	± 2.5
RF Level Shift	± 2 x 10 <sup>-12</sup> /dB	± 2.0
Residual Heater Field	± 5 x 10 <sup>-14</sup> /mA	± 2.0
Absorption Cell TC	+ 3 x 10 <sup>-11</sup> /°C	+ 1.5
VCXO Dynamic TC	---	± 1.5
Servo Integrator	± 1 x 10 <sup>-14</sup> /°C	± 1.0
Power Supply	± 1 x 10 <sup>-12</sup> /%	± 1.0
Modulation Deviation	± 1 x 10 <sup>-13</sup> /%	± 1.0
Miscellaneous	---	± 1.0
Total		Worst-case 23.5
		rms 9.2

## QUESTIONS AND ANSWERS

PROFESSOR ALLEY:

What are the dimensions?

MR. RILEY:

I have them right here. Let me just read them off, so that I get it right.

The height of the package is seven inches. That's what really increased over the existing one because the height was available. The footprint area is about the same as the existing one which is, call it five by eight. Rough numbers.

INVESTIGATIONS OF LASER PUMPED GAS  
CELL ATOMIC FREQUENCY STANDARD

C. H. Volk, J. C. Camparo and R. P. Frueholz  
The Aerospace Corporation, P.O. Box 92957, Los Angeles, CA 90009

ABSTRACT

Recently it has been suggested that the performance characteristics of a rubidium gas cell atomic frequency standard might be improved by replacing the standard rubidium discharge lamp with a single mode laser diode. Since the short term stability of the rubidium frequency standard is limited by the shot noise of the photodetector,<sup>1</sup> an increased signal to noise ratio, from the more efficient laser diode pumping, might significantly improve the short term performance. Because the emission wavelength of the laser diode can be tuned, improved long term performance could be attained through the control of the light shift effect. However, work done by Lewis et al<sup>2</sup> at NBS Boulder indicates that a new source of instability is present in the laser pumped clock; the frequency instability of the laser induces instability in the frequency standard.

We have been investigating various aspects of the laser pumped gas cell atomic clock. Our investigations include effects due to laser intensity, laser detuning and the choice of the particular atomic absorption line. Our studies indicate that the performance of the gas cell clock may be improved by judicious choice of the operating parameters of the laser diode.

The laser diode has also proved to be a valuable tool in investigating the operation of the conventional gas cell clock. Our results concerning linewidths, the light shift effect and the effect of isotopic spin exchange in the conventional gas cell clock are reported here.

---

<sup>1</sup> C. Audoin and J. Vanier, J. Phys. E: Scient. Inst. 2. 697 (1976).

<sup>2</sup> L. L. Lewis and M. Feldman, 35th Symp. on Freq. Control (1981).

## INTRODUCTION

The recent advances that have been made in the semiconductor laser diode technology have been followed very closely by numerous applications for this type of laser in practical devices. The laser diode is extremely attractive because it possesses the features of high light intensity in a small package requiring only moderate to low power for operation.

The rubidium gas cell atomic clock is one such device, among others, that could possibly be improved by the incorporation of a laser diode which would be used in place of the conventional rubidium discharge lamp. Figure 1 is a schematic representation of the rubidium gas cell clock. In the 'classic' design of the clock,<sup>1</sup> the physics package consists of an optical absorption cell contained within a microwave cavity, a hyperfine filter cell and a rubidium lamp providing the optical pumping radiation. The absorption cell and the lamp usually contain  $^{87}\text{Rb}$  while the hyperfine filter employs the  $^{85}\text{Rb}$  isotope. A simplification of this design uses an 'integrated' absorption cell in order to avoid the necessity of the hyperfine filter cell.<sup>2</sup> From Figure 1, it is readily apparent that the use of a laser diode as the optical pumping source in the rubidium clock could be quite beneficial. The laser would provide a much more intense beam of light with better collimation and a spectral linewidth sufficiently narrow to allow for the elimination of the filter cell. Additionally, because of the tuneability of the laser diode, frequency offsets due to the light shift effect could be readily controlled.

Although the idea of using laser diodes in place of discharge lamps is not a new idea, it has only been very recently that single mode laser diodes of sufficiently long life have become commercially available at prices that make their use somewhat reasonable. In addition to our effort in this area at The Aerospace Corporation, there is a very active effort at NBS Boulder<sup>3</sup> to investigate the possible uses of laser diodes in atomic clocks.

However, as is normally the case, no simple substitution of one component in a device for some other, although much better, component is ever possible. The new component itself, in this case the laser diode, must be made to conform to the constraints of the device; the clock. Additionally, new aspects of the device normally appear upon the incorporation of the improved component. We report here on our observations of new characteristics of the rubidium clock when operated using a laser diode pump source.

## DISCUSSION

Our experimental apparatus is shown schematically in Figure 2. The emission from a Mitsubishi ML 4001 GaAlAs laser diode was collimated and used to illuminate the absorption cell of an Efratom FRK-L rubidium frequency standard. This particular standard employs the integrated absorption cell. The laser diode linewidth was measured to be approximately 400 MHz and the laser provided output power of up to 6 mW/cm<sup>2</sup>. The rubidium lamp from the frequency standard was removed to allow access for the laser light. Since the laser diode electronics were sufficient to keep the wavelength of the laser from drifting for about an hour, no further wavelength stabilization of the diode was used for these particular experiments. The laser diode was tuned to the proper hyperfine absorption line of the <sup>87</sup>Rb by observing the transmitted light through the absorption cell, and due to the particular diode used we tuned to the D<sub>1</sub> (5S<sub>1/2</sub>-5P<sub>1/2</sub>) resonance of rubidium at 794.7 nm. The 10 MHz clock frequency was monitored with an HP-5345A frequency counter and a gate output indicated locking of the crystal frequency to the rubidium hyperfine transition.

Figure 3 shows the absorption spectrum of the gas cell as the laser was tuned across the D<sub>1</sub> resonance. The two central peaks at a tuning of 2 and 5 GHz correspond to the F = 3 and F = 2 hyperfine absorption lines of the <sup>85</sup>Rb present in the cell for the normal operation of this clock. The shoulder that appears on the F = 3 hyperfine line of the <sup>85</sup>Rb near 0.5 GHz corresponds to the F = 2 hyperfine line of <sup>87</sup>Rb, and the peak at 7.3 GHz corresponds to the F = 1 hyperfine line of <sup>87</sup>Rb. This line appears to be asymmetric because of the unequal contributions from the two hyperfine states of the first excited state.

Figure 3 also shows those regions of laser tuning where the clock locked, and it should be remembered that the clock will only lock when there is a population imbalance between the two <sup>87</sup>Rb hyperfine states. Not surprisingly, the figure clearly shows that the clock locked when the laser was tuned to either of the <sup>87</sup>Rb hyperfine absorption lines. However, when the laser was tuned to the F = 3 absorption line of <sup>85</sup>Rb, the clock locked to the <sup>87</sup>Rb microwave resonance. This effect shows that hyperfine polarization is being shared between the <sup>85</sup>Rb and <sup>87</sup>Rb populations. The most obvious mechanism to account for this sharing of polarization is spin-exchange between the two isotopes.<sup>4</sup> The presence of spin exchange between the <sup>85</sup>Rb and <sup>87</sup>Rb may result in a frequency shift in the clock that is proportional to the rubidium density. Whether this proposed frequency shift has any deleterious effect on the operation of the clock is not presently known.



Our preliminary investigation of the light shift effect in the gas cell clock involved its dependence on laser intensity and wavelength. The laser diode emission was first centered on the  $F = 1$   $^{87}\text{Rb}$  absorption line and then subsequently tuned to the high and low side of this line. The laser intensity was  $6 \text{ mW/cm}^2$ . Since the 10 MHz output and the Rb hyperfine transition frequency are directly proportional, it is a straightforward procedure to relate a change in the clock's output to a shift in the Rb hyperfine transition frequency. The results of this light shift measurement are displayed in Figure 4.

From top to bottom the four curves of Figure 4 represent laser detuning from the  $5S \frac{1}{2} (F = 1) - 5P \frac{1}{2} (F = 2)$  resonance of approximately -700 MHz, -200 MHz, 0, and +200 MHz respectively. All of these curves show the same general behavior: they are linear at low laser intensity, reach an extremum, and finally saturate to a light shift value dependent only on the laser detuning from the atomic resonance. The linearity of these curves at low light intensity and their symmetry about zero frequency detuning are consistent with the standard theory of light shifts first developed by Barrat and Cohen-Tannoudji<sup>5</sup> and treated semi-classically by Happer and Mathur.<sup>6</sup> We believe that the new features of the light shift curve, the extrema and saturation regions, are due to an Autler-Townes type splitting<sup>7,8</sup> of the microwave resonance. This splitting would occur because the microwaves are no longer probing a nearly unperturbed Rb atom; they are probing a Rb atom while it is interacting with the intense laser emission. Arditi and Picque proposed a similar mechanism for distortions that they observed in the microwave signals from a Cs vapor optically pumped with a GaAs laser diode<sup>9</sup>, and we have seen similar distortions in our microwave lineshapes.

As evidenced by Figure 4, the light shift is a sensitive function of laser frequency detuning. In fact, even when the laser is tuned on resonance there is a very small light shift effect which we believe is due to the overlap of the  $^{87}\text{Rb}$  ( $5S \frac{1}{2} (F = 1) - 5P \frac{1}{2} (F = 1 \text{ and } 2)$ ) absorption lines. In order to more fully understand the effect of laser detuning, we measured the light shift as the laser was tuned across the  $F = 1$  hyperfine resonance for a fixed laser intensity. Figure 5 shows the results of one such experiment where the relative laser intensity was held fixed at about  $0.3 \text{ mW/cm}^2$  and the zero of frequency detuning corresponds to the  $5S \frac{1}{2} (F = 1) - 5P \frac{1}{2} (F = 2)$  atomic resonance. The solid curve is a calculation of the light shift as a function of detuning based on the theory of Happer and Mathur. The discrepancy between theory and experiment in the region of large negative detuning may be due to spin exchange shifts resulting from the pumping of  $^{85}\text{Rb}$  by the wing of the laser line. We presently do not have enough data to definitively determine the origin of this discrepancy.

Two important factors which effect the shape of Figure 5 are the excited state hyperfine splitting and the broad laser line. It is the combination of these two factors which produces the nearly flat region at a laser detuning of  $\sim -.015 \text{ cm}^{-1}$  (-450 MHz), and indicates that the atomic hyperfine frequency is relatively insensitive to slight changes in the laser frequency. We refer to this flat region as the "decoupling" region, since the clock frequency could be considered as decoupled from laser frequency noise if the laser was tuned into this region.

The two curves of Figures 4 and 5 suggest a novel technique for operating a laser diode gas cell clock which might result in improved performance. The laser diode would be operated at high intensity so as to be in the saturation region of Figure 4, and detuned into the decoupling region of Figure 5. In this way the atomic response to the optical pumping conditions would decouple laser intensity and frequency noise from the clock output. We are in the process of performing Allan Variance measurements on a gas cell clock operated with this optical pumping scheme, and the results will determine if any improvement occurs.

#### REFERENCES

1. G. Missout and J. Vanier, *Can. J. Phys.* 53, 1030 (1945).
2. E. Jechart, 27th Annual Frequency Control Symposium (1981).
3. L. L. Lewis and M. Feldman, 35th Annual Frequency Control Symposium (1981).
4. W. Happer, Optical Pumping, *Rev. Mod. Phys.* 44 (2), 169 (1972).
5. J. P. Barrat and C. Cohen-Tannoudji, Elargissement et Déplacement Des Ries De Resonance Magnetique Causes Par une Excitation Optique, *J. de Phys. et le Rad.* 22, 443 (1961).
6. B. S. Mathur, H. Tang, and W. Happer, Light Shifts in the Alkali Atoms, *Phys. Rev.* 171 (1), 11 (1968).
7. S. H. Autler and C. H. Townes, Stark Effect in Rapidly Varying Fields, *Phys. Rev.* 100 (2), 703 (1955).
8. P. L. Knight and P. W. Milonni, The Rabi Frequency in Optical Spectra, *Phys. Rep.* 66 (2), 21 (1980).
9. M. Arditi and J-L Picque, Precision Measurements of Light Shifts Induced by a Narrow-Band GaAs Laser in the 0-0  $^{133}\text{Cs}$  Hyperfine Transition, *J. Phys. B* 8 (14), L331 (1975).1

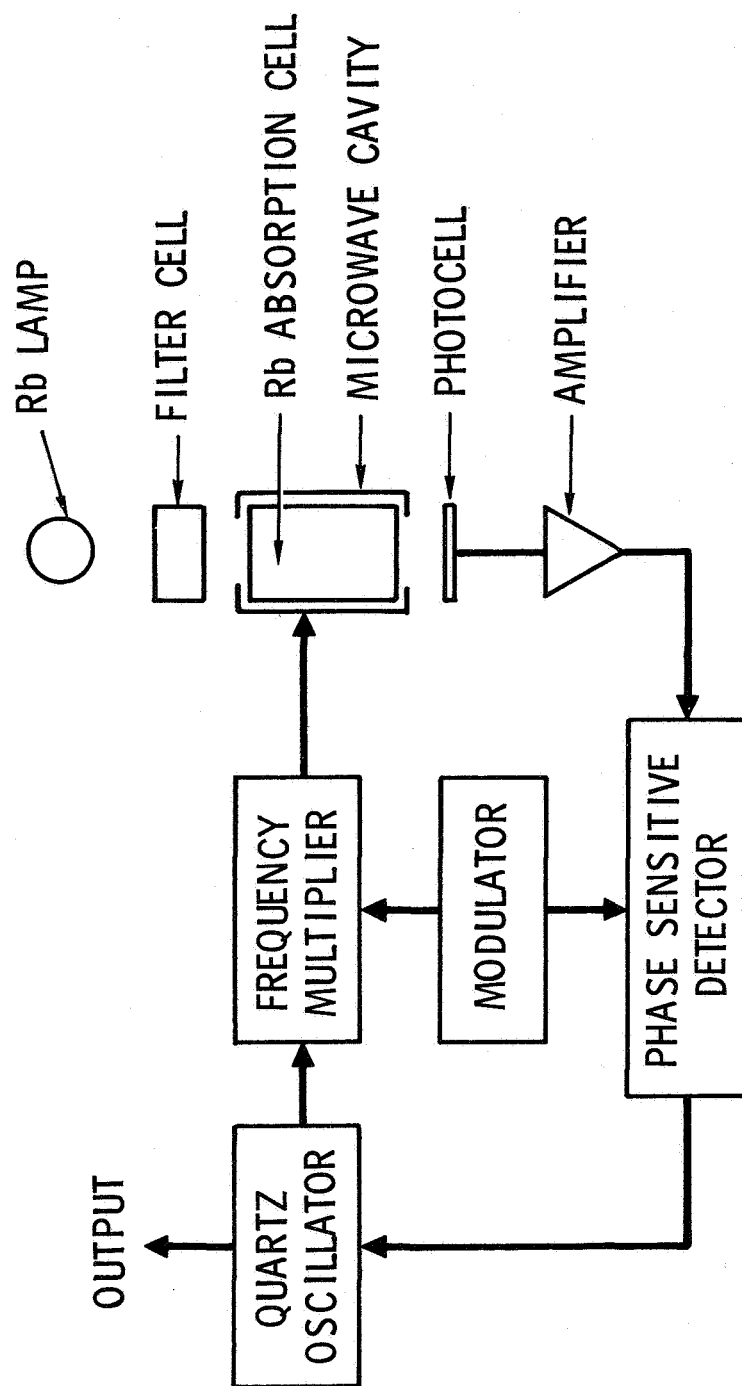


Figure 1. Schematic Diagram of a Passive Rubidium Gas Cell Frequency Standard

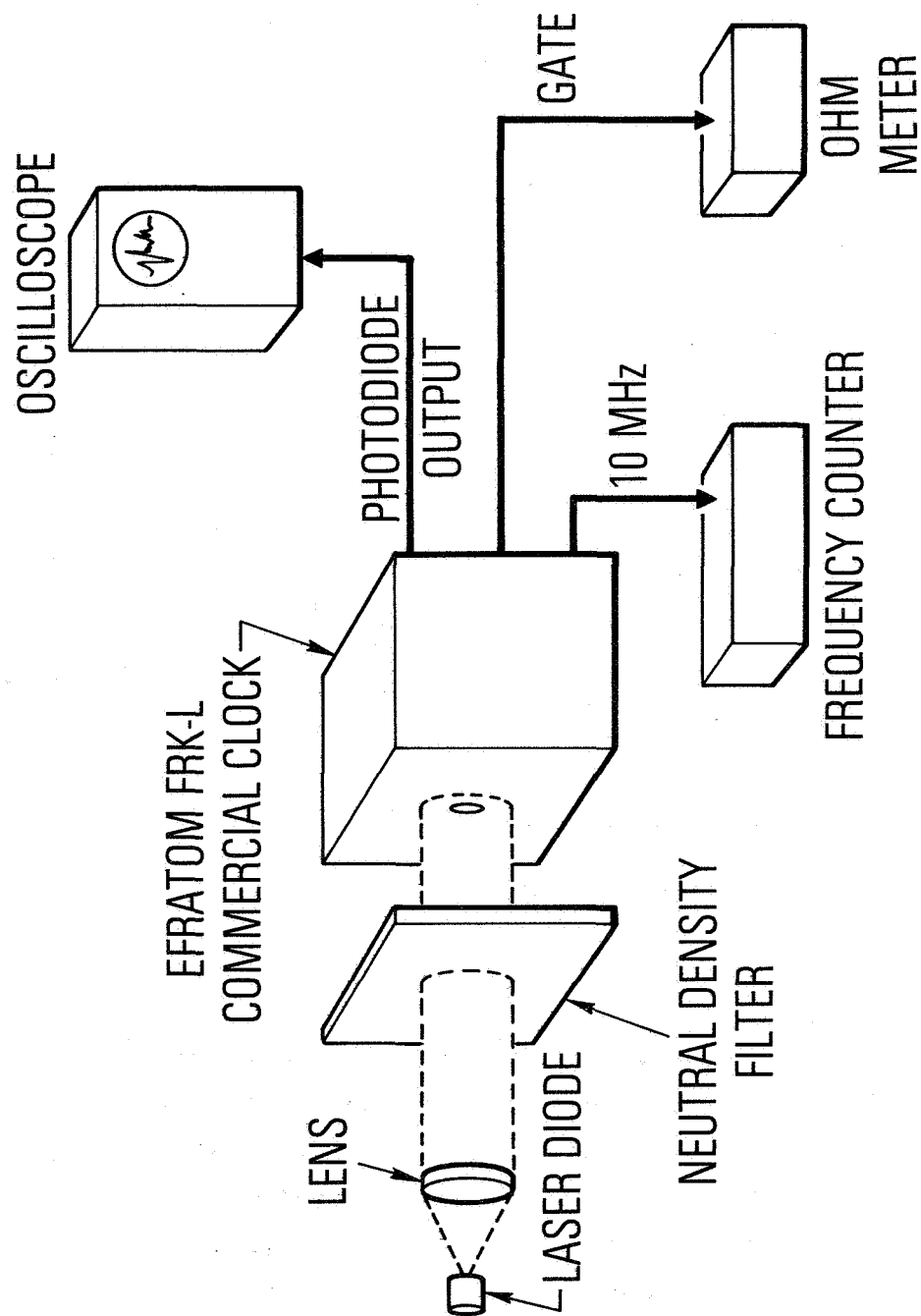


Figure 2. Schematic Diagram of the Experimental Apparatus

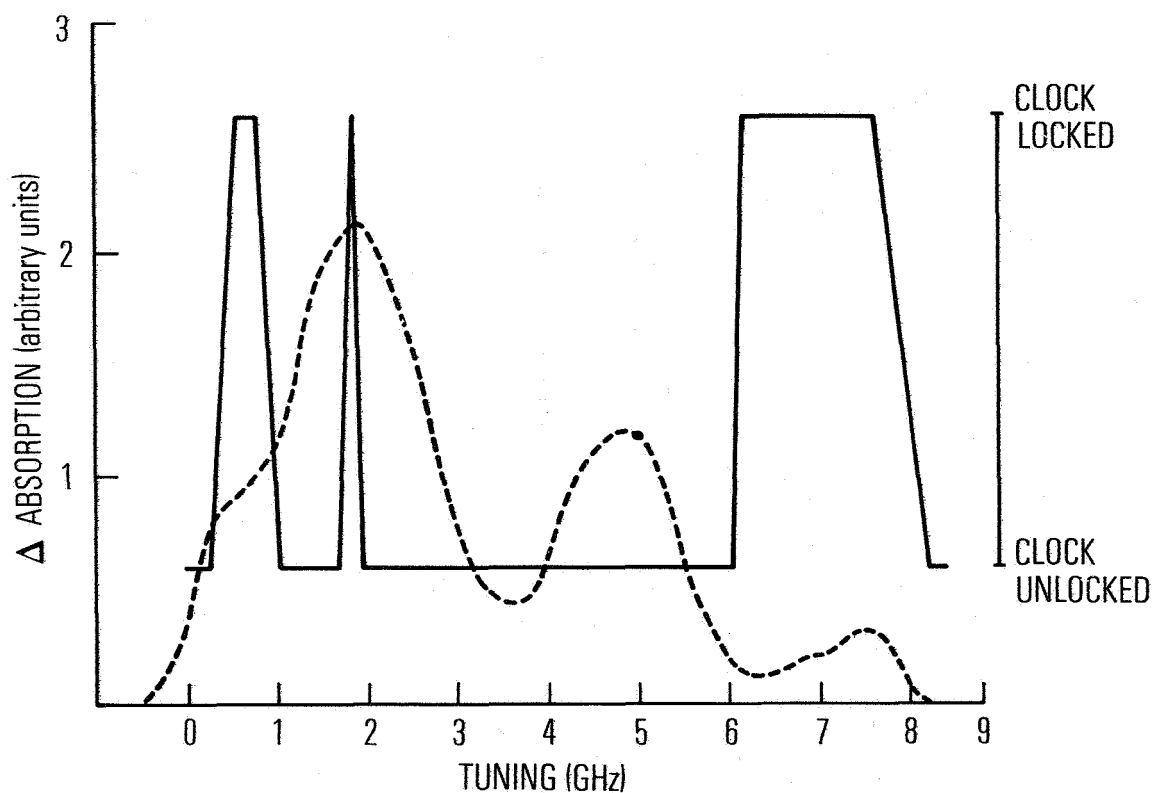


Figure 3: Rb absorption spectrum in the integrated cell showing the hyperfine structure of both  $^{87}\text{Rb}$  and  $^{85}\text{Rb}$ . The solid line represents the locked condition of the clock. This was determined by observing the current flow in the phase lock indicator. We observed conditions between unlocked and full-lock of the feedback loop, and thus this plot essentially maps potential operating points of the clock.

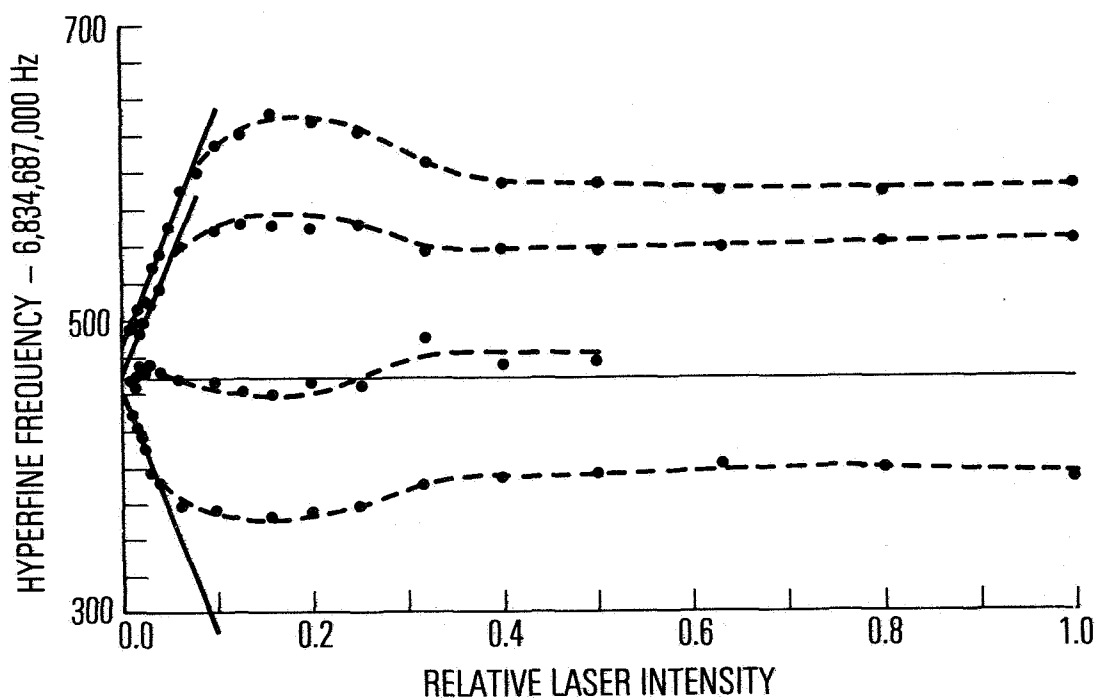


Figure 4: Microwave resonance frequency as a function of light intensity for various laser detunings from the  $5S \frac{1}{2}$  ( $F = 1$ ) -  $5P \frac{1}{2}$  ( $F = 2$ ) optical resonance. The detunings from top to bottom are = -700 MHz, -200 MHz, 0, and 200 MHz. Maximum laser intensity is  $6 \text{ mW/cm}^2$ . The solid lines are linear fits of the low intensity light shift points. This linear relationship is expected from the classic theory of the light shift effect. The dashed lines are for the convenience of the reader to follow the light shift along a particular laser detuning.

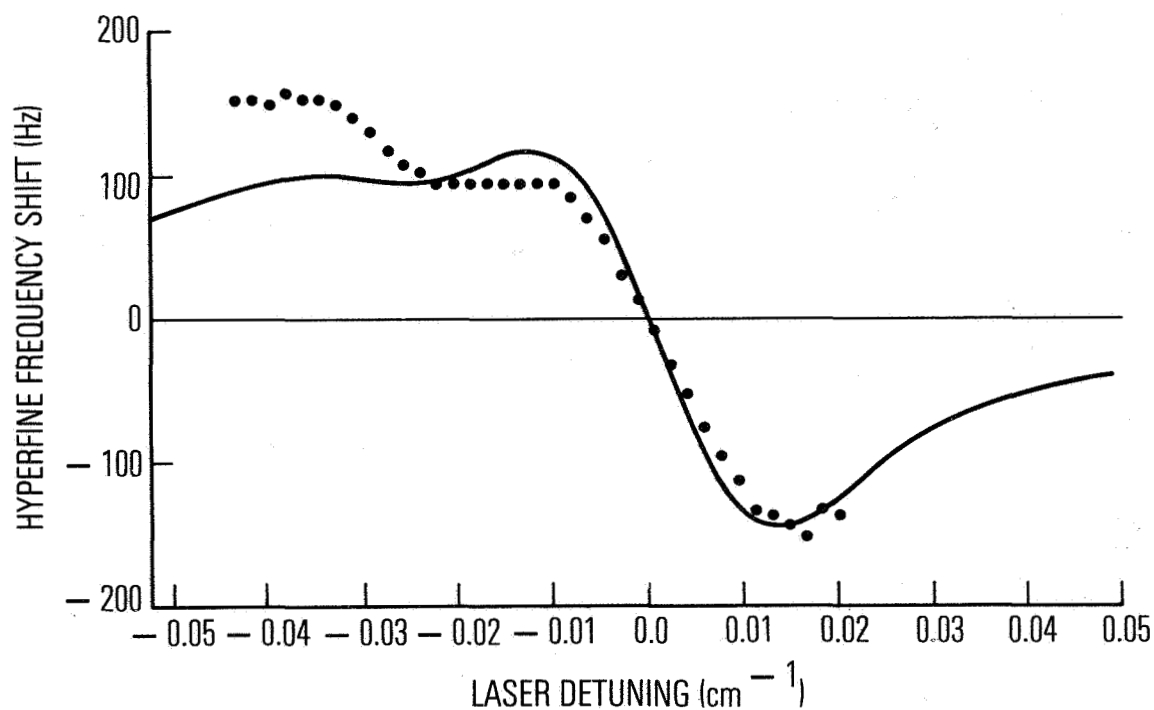


Figure 5: Microwave resonance frequency shift as a function of laser detuning for a fixed relative intensity of about  $0.3 \text{ mW/cm}^2$ . The zero of detuning corresponds to the  $5S \frac{1}{2} (F = 1) - 5P \frac{1}{2} (F = 2)$  optical resonance, and the solid curve is a theoretical estimate of the light shift.

## QUESTIONS AND ANSWERS

PROFESSOR ALLEY:

What do you use to laser these chisels by?

MR. COMPARO:

Current.

DR. DAVE WINELAND:

One minor point. When you tuned on resonance, what you call a resonance condition, don't you get poling, don't you pole the other hyperfine level in the ground state, since you're off resonance with that line?

MR. COMPARO:

Oh, you mean the splitting there?

DR. WINELAND:

Yes.

MR. COMPARO:

That excited state splitting?

DR. WINELAND:

No, no. The ground state splitting. You're tuned to one ground state -- you know, from one of the ground state levels to the excited state.

And don't you pole then the other ground state level?

MR. COMPARO:

Oh, because I'm detuned?

DR. WINELAND:

Yes. Or is that just a negligible effect at this point?

MR. COMPARO:

I think it would be negligible because my laser line which is 400 megahertz, and that's six gigahertz away.



DR. WINELAND:

Okay. That was really the question I meant. At this point, anyway, it is negligible.

MR. COMPARO:

I would think so.

DR. WINELAND:

The other question -- and maybe I just didn't understand -- when you say -- the numbers you got, where you were at line center, and the stability turned up, were you actually locked to line center? Or were you just nominally tuned to line center?

MR. COMPARO:

No. Just nominally tuned.

DR. WINELAND:

Okay.

MR. COMPARO:

The thing is the only way that the laser is really stabilized to the atomic absorption line is as long as the current and temperature don't cause you to drift away.

DR. WINELAND:

Okay. So presumably you might be able to improve, if you actually locked.

MR. COMPARO:

Exactly. Exactly. And that's one thing we want to do. We've talked to Lyndon Lewis about his locking scheme. And we're going to be doing something similar to see what happens to those measurements when the clock is locked to the absorption line, so you don't have to worry about drift.

DR. FRED WALLS, National Bureau of Standards

Another possible scheme, of course, is to pulse the light on and off. That has a couple of advantages. One, of course, is that it

removes the frequency pulling from the source. And the other thing is that you can have an improvement in the line width, because part of the microwave line width is the fact that you're disturbing it with a pumping process.

MR. COMPARO:

I think that's absolutely true. And I don't know if we'll be getting to some type of scheme like that in the near future, but it's definitely something that should be looked into.



# MAGNETIC STATE SELECTION IN ATOMIC FREQUENCY AND TIME STANDARDS

H. E. Peters

Sigma Tau Standards Corporation  
1014 Hackberry Lane, P.O. Box 1877  
Tuscaloosa, Alabama 35403-1877

## ABSTRACT

Atomic standards such as those based upon cesium and hydrogen rely upon magnetic state selection to obtain population inversion in the hyperfine transition levels. Use of new design approaches and improved magnetic materials has made it possible to fabricate improved state selectors of small size, and thus the efficiency of utilization of beam flux is greatly improved and the size and weight of the standard is reduced. The sensitivity to magnetic perturbations is also decreased, so that the accuracy and stability of the standard is improved. Several new state selector designs are illustrated and the application to standards utilizing different atomic species is analyzed.

## INTRODUCTION

The geometry and properties of the magnetic state selector are crucial elements in achieving beam standards of optimum performance. However, the overall design of the standard must be carefully considered to obtain the best balance of performance, reliability, and longevity. This paper gives a brief review of the factors which relate to the efficient utilization of beam flux and the optimization of the atomic beam state selection process, and also reviews some of the considerations which enter into the choice of atom for a standard. The design of quadrupole and hexapole state selectors is next discussed, and an idealized analysis of beam trajectories is presented for the different types. Finally, several small, efficient, magnetic state selectors are illustrated.

## MAGNETIC STATE SELECTORS AND BEAM STANDARD ELEMENTS

The essential features of the atomic beam standard<sup>1</sup> which relate to state selectors and atomic trajectories are illustrated in Figure 1.

For beam devices designed to use velocity focussing trajectories to achieve maximum efficiency, the quadrupole or the hexapole state selector may be used, depending upon the physical properties of the particular atom. Quadrupole state selectors have a magnetic field which increases linearly with radius about the beam axis, while hexapole state selector fields increase with the square of the radius.

The source for metallic atoms is an oven, and for gaseous molecular atoms an RF discharge dissociator. The atoms emerge from the source through a collimating exit hole of large length to radius ratio to conserve flux and then pass through the state selector wherein atoms in certain magnetic quantum states are caused to converge towards the axis, while others are deflected. Atoms in the desired state pass through an interaction region to a detector in the case of magnetic resonance standards, or to a storage region within an RF cavity in the case of maser standards.

#### BEAM INTENSITY FACTORS

The flux utilization efficiency is the product of several factors, the most important of which are:

$F_1$  = (Velocity Distribution)

$F_2$  = (Source Dissociation Efficiency)

$F_3$  = (Source Collimation Factor)

$F_4$  = (Magnetic Hyperfine Structure of the Atom)

$F_5$  = (State Selector Properties)

$F_6$  = (Target Distance and Aperture)

$F_7$  = (Detector Efficiency or Maser Parameters)

Figure 2 shows the normalized distribution of intensities in the beam emerging from the source as a function of velocity and temperature. For an oven source a most important consideration is that the distribution is relatively broad, and a state selector system may select atoms having considerably higher or lower velocity than the most probable, if desired. For example, in the case of cesium standards it is common practice to select velocities 50% or more lower than the peak of the distribution so as to achieve the highest line Q.

Another important result of the broad distribution is that it is not essential that the atomic state or the state selector have exact focussing properties to achieve maximum intensity, since atoms in some velocity range at a particular source emergent angle will be focussed

as long as the system is only approximately idealized.

The distribution of velocities from an RF dissociator source is much less ideal than the oven source. The distribution varies with many factors such as RF power, source bulb size and material, and the degree to which thermallization occurs before emerging. The most prominent features of a discharge source are the large population of hotter than ambient atoms, and less than perfect dissociation efficiency. For a device such as the hydrogen maser the most important functions of the state selector are to capture the largest fraction of the atoms in the right state, and most importantly, to deflect strongly the wrong state atoms.

Figure 3 shows the effect of the source collimator in conserving atoms.<sup>2</sup> This gives the intensity in an increment of solid angle emerging from the source collimator as a function of the emergent angle. It is clear that a large improvement in flux utilization may be obtained with the collimator, but a peak is reached when the radius to length ratio of the collimator becomes comparable to the state selector acceptance angle. In the case of discharge sources one must be aware that recombination may occur on the collimator wall, and in practice  $a/L$  is usually no smaller than .05.

#### MAGNETIC HYPERFINE STRUCTURE AND FORCES ON THE ATOM

Reference (1) may be referred to for most of the theoretical basis for this paper and for the experimental data on hyperfine frequencies and other atomic and nuclear data as well as for atomic and molecular beam early history. For the purposes of trajectory analysis several approximations will be made which are entirely valid within the accuracy required. Thus the nuclear magnetic moment is considered negligible in magnitude in relation to the electronic moment, angles measured normal to the beam axis are very small so that sines equal tangents equal angles in radians, and the magnitude of the  $z$  axis velocity is equal to the total velocity magnitude.

The starting point for energy and force considerations for  $J = 1/2$  atoms, which are almost invariably the ones of concern, is the Breit-Rabi equation (Reference 1, pp 80.) The force on the atom in the radially symmetric field magnitude and field gradient of the state selector is the first derivative of the energy with respect to the radius. Figure 4 is a plot of the energy levels of an atom with nuclear moment  $I = 1/2$  as a function of the magnetic field. The force on atoms with  $I$  greater than  $1/2$  and  $m = 0$  are the same, while the forces on levels with maximum  $|m|$  are the same as for the  $|m| = 1$  levels shown. The  $m = 0$  levels are usually the ones of primary interest for focussing in atomic standards.

For atomic beam magnetic resonance standards it is desirable to direct

atoms in a particular state through an interaction region to a relatively distant detector target. For a state with a permanent moment, or with  $H_1$  considerably smaller than the state selector fields, a hexapole magnet provides the desired focussing fields. However, if  $H_1$  is much greater than the state selector fields, or if some velocity dispersion is allowable in the detected atoms, the quadrupole state selector will usually provide a much more intense detected beam.

For maser standards the choice depends upon the target distance and aperture, but for the compact geometry of recent maser designs the quadrupole state selector provides very significant advantages as will be discussed later. It is seen in figure 4 that the value of  $H_1$  for a particular atom is important in considering the dynamical behavior of the atom within the state selector. Typical quadrupole tip fields at saturation are 10 kilogauss or greater, while hexapole tip fields of 7 kilogauss may be obtained.

Chart I below gives the approximate value of  $H_1$  calculated for several interesting atoms as well as other pertinent data. The calculations for this chart use data from Reference 1.

CHART I

ATOM	I	$\nu_0$ GHz	$H_1$ GAUSS	$\Delta\nu/H^2$ -Hz/(Gauss) <sup>2</sup>	MULTIPLICITY
H 1	1/2	1.42	510	2,750	4
Na 23	3/2	1.77	630	2,210	8
Al 27	5/2	1.51	1,610	290	12
Ga 69	3/2	2.68	2,870	160	8
Rb 85	5/2	3.04	1,080	1,290	12
Rb 87	3/2	6.84	2,440	570	8
Ag 107	1/2	1.71	610	2,290	4
Ag 109	1/2	1.98	710	1,980	4
Cs 133	7/2	9.19	3,280	430	16
Au 197	3/2	6.11	2,180	640	8
Tl 203	1/2	21.1	22,600	20.6	4
Tl 205	1/2	21.3	22,800	20.4	4

In calculating beam efficiencies it is important to note that atoms with  $I$  greater than  $1/2$  suffer a significant loss due to the multiplicity of the states. The number of ground state hyperfine levels for each atom is listed in the last column. Not only does the multiplicity reduce the percentage of atoms in the selected state, but there are serious problems with nearby ( $\Delta m = 0$ ) transitions which force one to use relatively high "C Fields" within the interaction region to maintain separation of the several resonances. For example, with cesium, one must use "C Fields" of the order of .04 Gauss or greater, while with  $I = 1/2$  atoms such as thallium, silver, or hydrogen, one may use fields as low as 100 microgauss or less if desired, and there is negligible inaccuracy due to lack of knowledge of the field or due to distortions from overlapping resonances.

#### CURVED BORE STATE SELECTORS

To make a state selector as small as possible and to maximize the acceptance angle, the magnet bore radius should ideally be as close as possible to the beam. It is possible to make such a state selector, and in addition to achieve a focussing field for certain of the magnetic quantum states. Figure 5 illustrates the geometry of this design. The state selector may be either hexapolar or quadrupolar. It is assumed in the analysis that atoms of the largest radius are near to and have a velocity vector tangent to the bore radius. The equations defining the magnet curve are also given in Figure 5. For an atom such as thallium a strong focussing action could be obtained for the (1,0) state, while the  $m = 1$  as well as the deflected states would be very "unfocussed." This is one example where a "pure" beam of (1,0) atoms could be obtained so that a "point" detector would not have a large noise flux of other atomic states.

In nearly all cases of interest it is not necessary (or practical) to use a curved bore state selector since the ideal bore dimensions are so small and the required curvature so slight. However, tapered bore state selectors can be made which give results nearly as good, and they are more practical to fabricate.

#### TAPERED BORE AND UNIFORM BORE STATE SELECTORS

Both hexapole and quadrupole state selectors with tapered bores are more efficient than uniform bore state selectors for beam resonance devices. For atoms such as hydrogen, sodium, or silver, with  $H_1$  very much less than the magnet tip field, a hexapole magnet would be the likely choice, although for selecting very cold atoms from a higher temperature velocity distribution a relatively weak, large bore, quadrupole would be used.

In most other cases a quadrupole state selector will give the best results. It should be emphasized that for all atoms emerging from



the source at a particular angle within the maximum acceptance angle there is always one velocity for which focussing occurs upon a given target. Thus if the range of focussed velocities falls within the more probable part of the velocity distribution, a very efficient selection of the desired state may be obtained. For most atoms a quadrupole state selector may be configured to obtain the best results, even though  $H_1$  is only a fraction of the magnet tip field.

Figure 6 diagrams the coordinates and defines the parameters which are used in subsequent equations for both the tapered bore and the constant bore state selectors. (For constant bore  $\alpha = 0$ )  $\theta_w^2$  is defined by the ratio of maximum potential energy the atom incurs in traversing the field from the axis to the bore tip divided by the thermal kinetic energy. It should be noted that the thermal kinetic energy of the atom in the beam,  $1/2mv^2$ , is equal to  $3/2 KT$ , and is independent of the particular atomic mass. It is assumed the state selector tip iron is saturated and the tip field is constant.

Figure 7 gives the trajectory equations for the quadrupole state selector for states which have a constant magnetic moment or in which the moment is essentially constant due to the magnet fields being generally greater than  $H_1$ . Figure 8 gives the results for other cases noted therein.

The equations given in the figures, if used with judgement, provide a good basis for approximating the best state selector type, as well as the bore radius and length, for a particular atom and detector target aperture and distance.

If desired, the equations of motion may be solved exactly for all cases. Thus, if  $W_w$  is the magnetic potential energy (derived from the Breit-Rabi equation), the differential equation to be solved is:

$$m\ddot{r} \pm \frac{dW_w}{dr} = 0 ,$$

which solves immediately for the angle  $\theta = dr/dz$ :

$$\theta^2 = \theta_0^2 \mp \frac{W_w}{(\frac{1}{2}mv^2)} .$$

From here  $r$  may be solved for by elementary means for either the hexapole or quadrupole.

The accuracy achieved by exact computation usually far exceeds the practical necessity in view of the uncertainties due to mechanical tolerances of the state selector, alignment inaccuracies, or the imperfection of the magnetic field pattern. Several papers on beam calculation methods have been published, one of which is given in Reference 3.

## STATE SELECTORS FOR HYDROGEN MASERS

The hydrogen maser and similar devices present a different problem than beam resonance devices. Traditionally, masers used hexapole state selectors which were placed a relatively large distance from the bulb, and were designed to focus atoms near the peak of the modified Maxwellian velocity distribution. This system is quite inefficient due to the small solid angle the bulb entrance subtends and the loss of the atoms in the higher temperature part of the real velocity distribution.

A quadrupole with very small bore diameter, and length to radius ratio much greater than that dictated by the peak of normal velocity distribution, will "capture" the largest possible flux of atoms from a source. Due to its small size and the small level of stray fields caused by the magnet, it may be placed within 1 cm or less of the maser shields without incurring shielding problems. Thus the state selector to bulb distance can be minimized. Typical state selector entrance maximum capture angles are .04 radians or less (much less for higher velocity atoms) thus if the bulb distance is 2 inches, a bulb entrance diameter of .16 inches will "capture" essentially all of the atoms "captured" in the state selector. Most importantly though, an atom which is in a state to be deflected and which starts out with a zero entrance angle will have a relatively large exit angle. Calculations for the small magnet indicate that essentially all of the "wrong state" atoms will not enter the bulb in the above example.

Due to the high state selection efficiency of the small quadrupole in a compact maser design, the source exit collimator diameter may be very small, and the idealization assumed in the calculations that the atom enters the state selector from a point source is closely realized. Hydrogen atom flux efficiencies 1,000 times better than obtained with early hydrogen masers are thus possible with recent maser designs.<sup>4,5</sup>

### STATE SELECTOR DESIGNS

Figure 9 is a picture showing 3 state selectors recently made at Sigma Tau Standards Corporation which are examples of the state of the art at this writing. On the left is a tapered bore quadrupole with a bore entrance diameter of .30 mm, exit diameter 1.4 mm, length 38 mm, and  $\alpha = .0145$ .

On the right in Figure 9 is a tapered bore hexapole with entrance diameter .90 mm, exit diameter 1.70 mm, length 38 mm and  $\alpha = .011$ .

In the center in Figure 9 is a very small tapered bore quadrupole with entrance diameter .46 mm, exit diameter .97 mm, length 25.4 mm and  $\alpha = .010$ . This state selector has been designed for a high flux compact hydrogen maser. The maximum diameters that may be used with this small state selector and still maintain magnetic saturation is

about 1.2 mm and the minimum, dictated by present mechanical tolerances, is about .25 mm. Within this range and with a length of 25.4 mm (1 inch) it may easily be configured to the requirements of atomic beam resonance standards using many of the different atoms described in this paper. The particular dimensions of the small state selector shown in Figure 9 are ideal for compact hydrogen masers with state selector to bulb distances of 2 inches to 8 inches or over, depending upon bulb aperture.

#### CONCLUSION

This paper illustrates that with new state selector designs and new and improved atomic beam standard configurations it is possible to achieve much more efficient use of source flux and to focus very large intensities of a variety of atoms. It is thus very possible to improve the efficiency, stability, and accuracy of existing standards or to design new standards based upon atoms which have fundamental properties which may be superior to those of standards presently in use.

#### ACKNOWLEDGEMENTS

Consideration of the optimum design of the beam optics for a small hydrogen maser<sup>4</sup> stimulated much of the work on this paper. The research and development program for the "Small Hydrogen Maser" was supported by the United States Air Force, RADC, Deputy for Electronic Technology, Hanscom AFB, MA. The author greatly acknowledges this support.

#### REFERENCES

1. N.F. Ramsey, MOLECULAR BEAMS, Oxford University Press, 2nd Ed., 1963.
2. H.E. Peters, T.E. McGunigal and E.H. Johnson, "Hydrogen Standard Work at Goddard Space Flight Center," Proceedings of the 22nd Annual Symposium on Frequency Control, 1968.
3. C. Adoin, M. Desaintfuscien, and J.P. Schermann, Nuclear Instruments and Methods, 69, 1969, pp. 1.
4. H.E. Peters, "New Hydrogen Maser Design," Proceedings of the 34th Annual Symposium on Frequency Control, 1980.
5. D.A. Howe, F.L. Walls, H.E. Bell and H. Helwig, "A Small Passively Operated Hydrogen Maser," Proceedings of the 33rd Annual Symposium on Frequency Control, 1979.

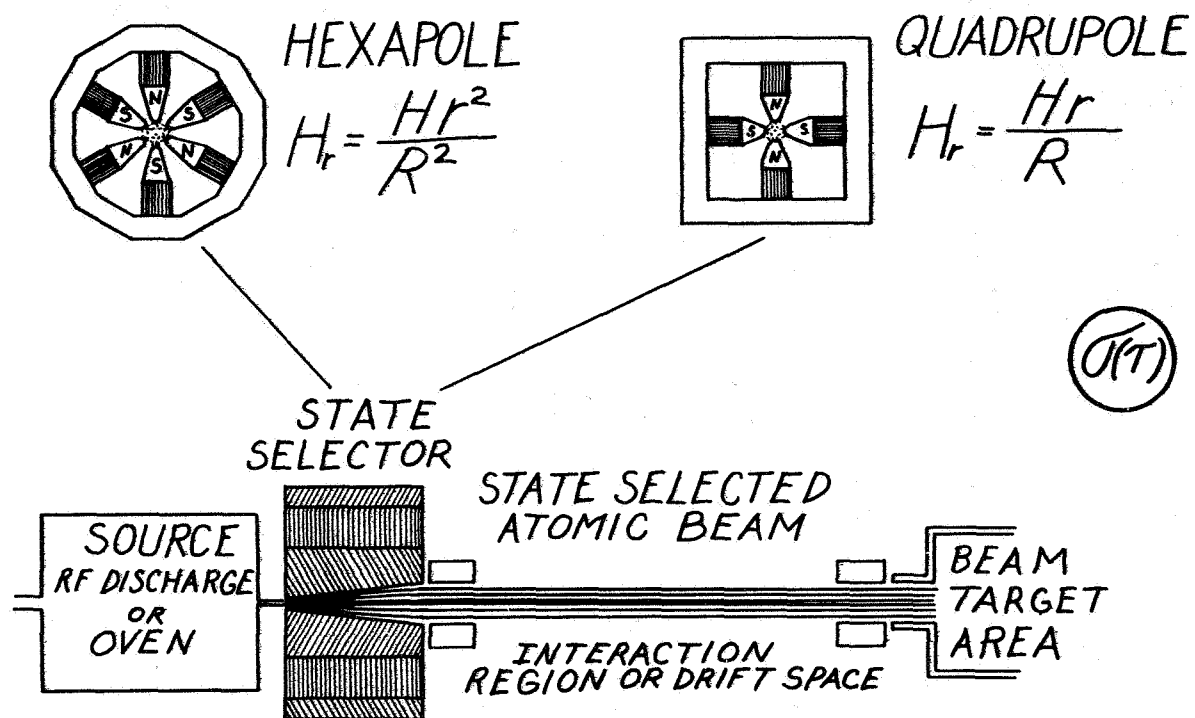


Figure 1. Magnetic State Selectors And Beam Standard Schematic.

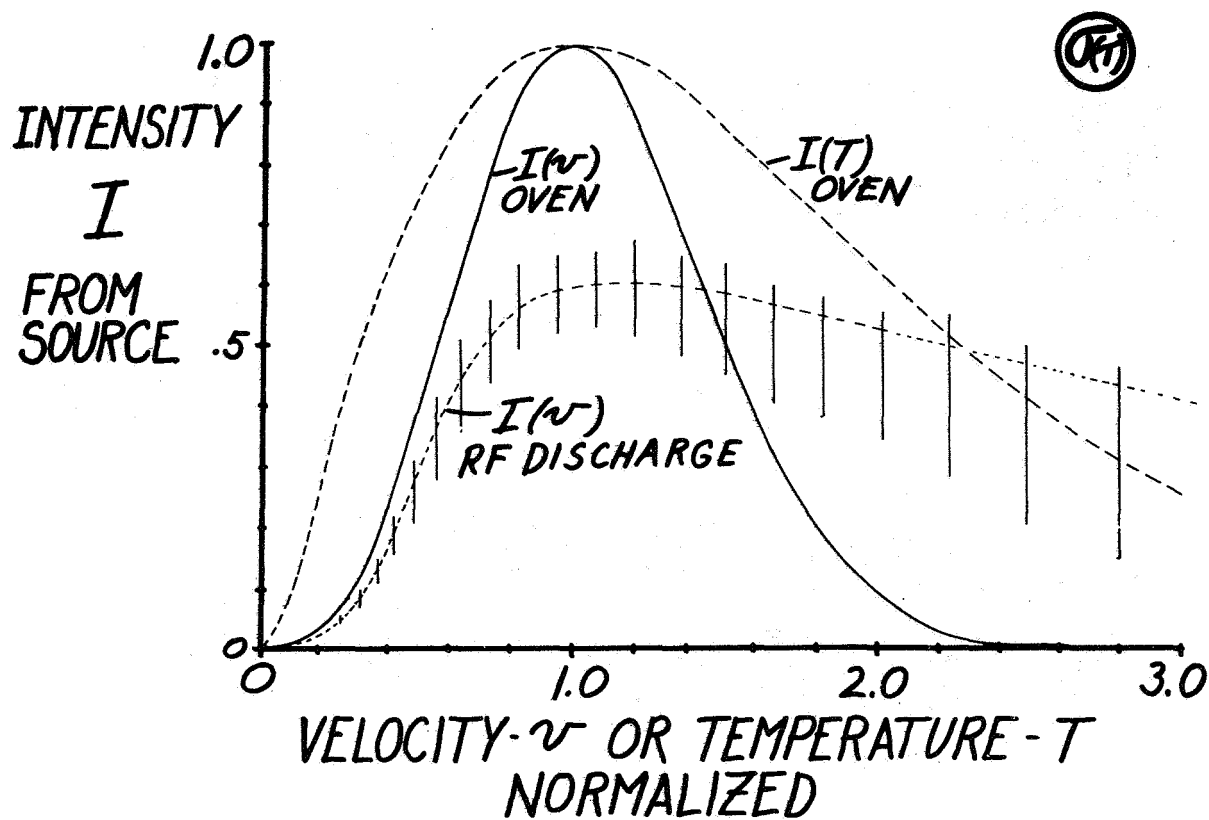


Figure 2. Intensity Distribution Of Atoms In A Beam Emerging From An Oven Or Discharge Source.

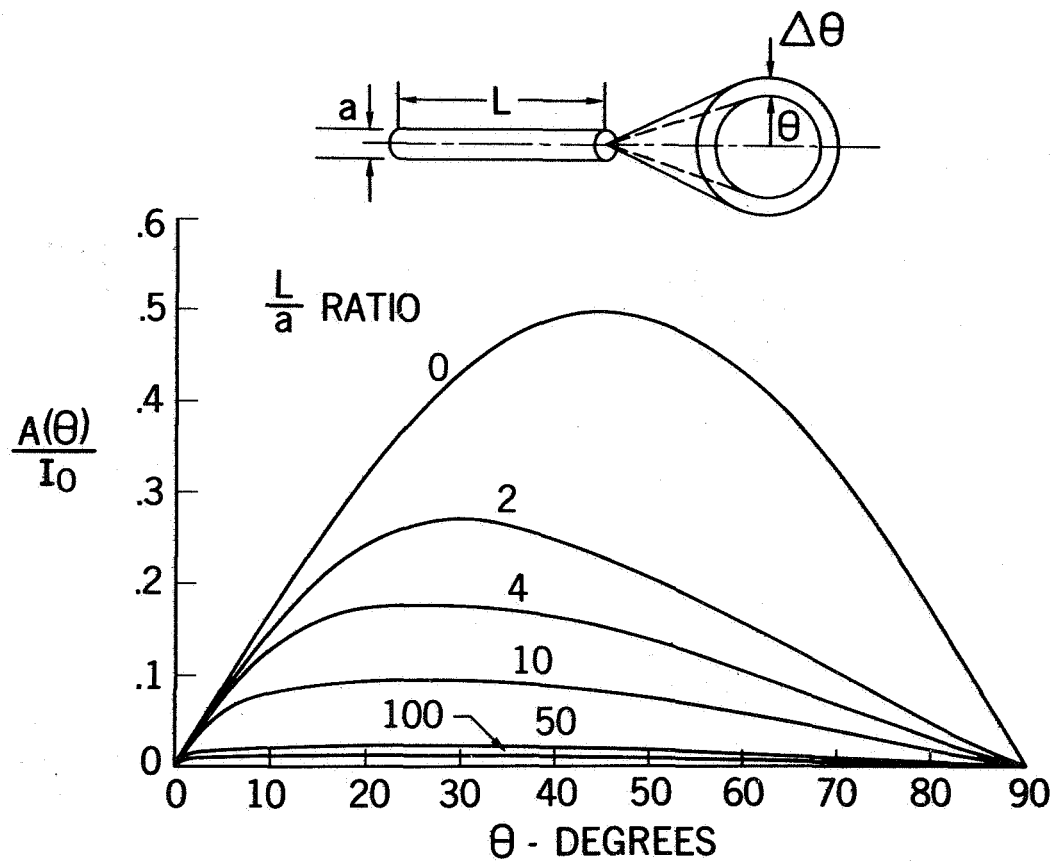


Figure 3. Intensity Of Beam In An Increment Of Solid Angle Emerging From A Source Collimator Versus The Emergent Angle.

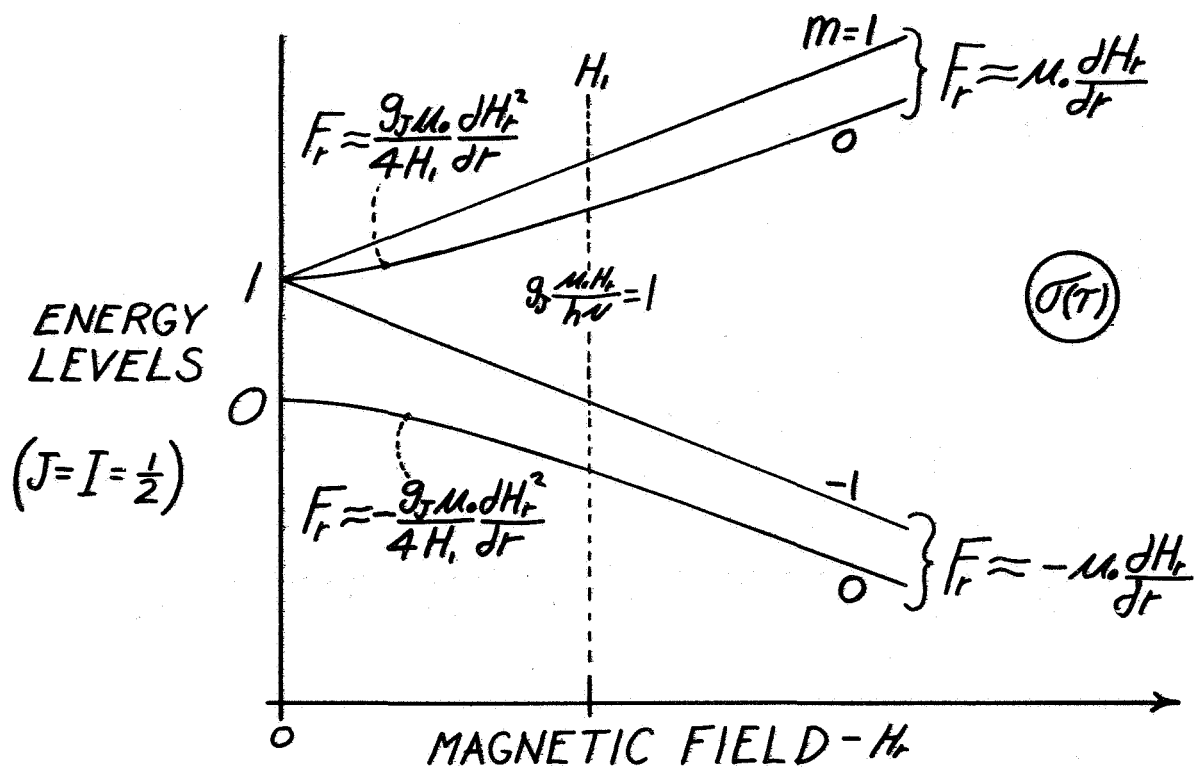


Figure 4. Magnetic Hyperfine Energy Levels Of An Atom With  $J = 1/2$  And  $I = 1/2$  Versus Magnetic Field.

For  $\Theta_L = 0$ ,  $\frac{dR}{dz} = \sqrt{2} \Theta_w S$

$$v_z \doteq v, \quad S \equiv \sqrt{\ln\left(\frac{R_k}{R}\right)}, \quad L_H = \frac{\sqrt{2} R_k}{\Theta_w} \int_0^S e^{-y^2} dy$$

$$\Theta_w^2 = \frac{g_J H}{4 H_i} \Theta_T^2, \quad \Theta_T = \sqrt{\frac{\mu_B H}{\frac{1}{2} m v^2}}$$

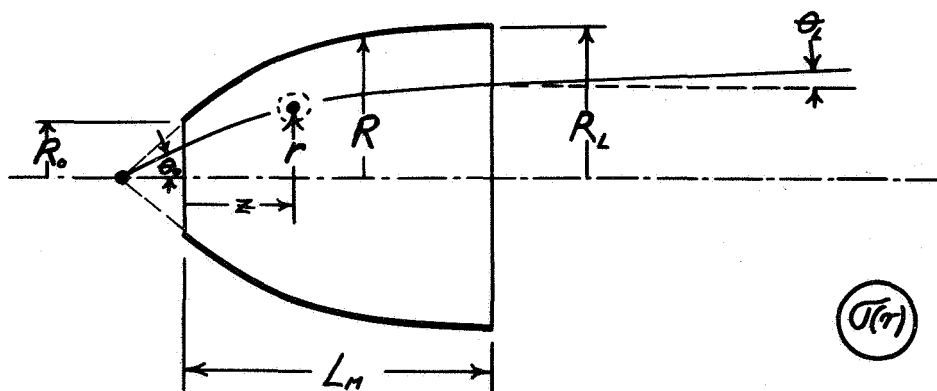


Figure 5. Curved Bore State Selector Diagram And Curvature Analysis.



$$\text{SLOPE } \frac{\Delta R}{\Delta z} = \frac{R_L - R_0}{L_N} = \alpha$$

$$R = R_0 + \alpha z$$

(U(T))

$$\Theta_0^2(\text{Max}) = \Theta_w^2 + \alpha^2$$

$$v_r = \frac{dr}{dt} \quad v_z = v = \frac{dz}{dt}$$

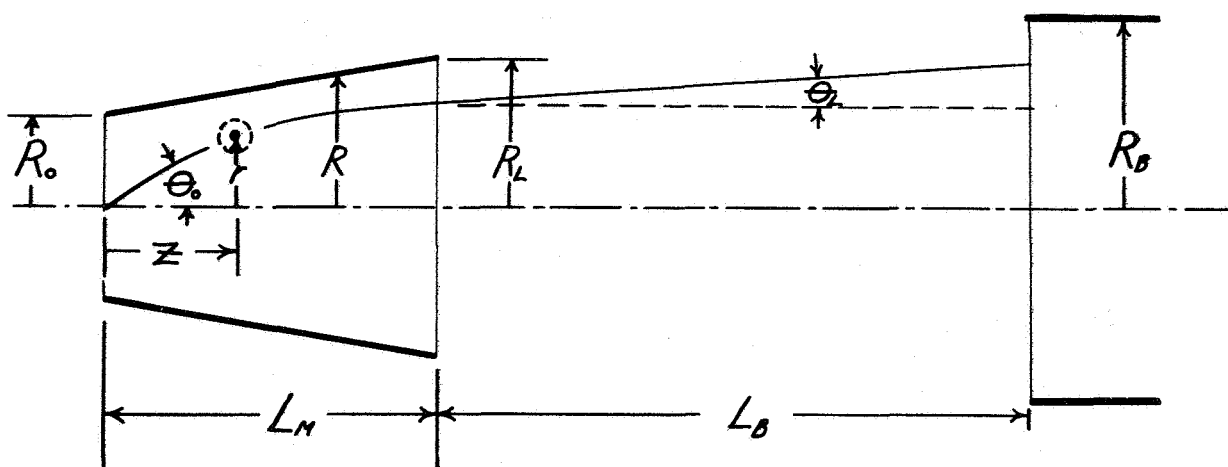


Figure 6. Diagram Of Coordinates And Parameters For Analysis Of Atom Trajectories Within State Selectors.

ATOM PATH IN QUADRUPOLE STATE SELECTOR  
FOR  $F(1, \pm 1)$  STATES OR  $F(\frac{1}{2}, 0)$  WITH  $H > H_c$

$$r_0 = 0, \quad R = R_0 + \alpha Z, \quad \Theta_r^2 = \frac{\mu_0 H}{\frac{m \omega^2}{2}} = \Theta_w^2$$

$$\frac{d^2 r}{dZ^2} + \frac{\Theta_r^2}{2R} = 0 \quad \begin{matrix} (+ \text{ATTRACTING}) \\ (- \text{DEFLECTING}) \end{matrix}$$

$$r = \Theta_0 Z + \frac{\Theta_r^2}{2\alpha^2} \left[ R \left\{ \ln \left( \frac{R}{R_0} \right) - 1 \right\} + R_0 \right]$$

$$\Theta = \Theta_0 + \frac{\Theta_r^2}{2\alpha} \ln \left( \frac{R}{R_0} \right)$$

AS  $\alpha \rightarrow 0$  (NO TAPER)

$$r = \left( \Theta_0 + \frac{\Theta_r^2 Z}{4R_0} \right) Z, \quad \Theta = \Theta_0 + \frac{\Theta_r^2 Z}{2R_0}$$

Figure 7. Equations Of Motion Within State Selector For Cases Where The Magnetic Moment Is Constant, Or Nearly So.

ATOM PATH IN QUADRUPOLE STATE SELECTOR  
 FOR  $F(1,0/0,0)$  STATES ( $H < H_1$ ) OR HEXAPOLE  
 FOR  $F(1,\pm 1)$  STATES.  $r_0 = 0$ ,  $R = R_0 + \alpha z$

$$\Theta_w^2 = \frac{g_H \Theta_r^2}{4 H_1} \quad (H < H_1, F(1,0/0,0))$$

$$\Theta_w^2 = \Theta_r^2 = \frac{\mu_0 H}{(\frac{m_N \gamma}{2})} \quad (H > H_1 \text{ or } F(1,\pm 1))$$

---

ATTRACTING:  $\Phi_1 \equiv B_1 \ln(\frac{R}{R_0})$ ,  $B_1 \equiv \sqrt{\frac{\Theta_w^2}{\alpha^2} - \frac{1}{4}}$

$$r = \frac{\Theta_0 \sqrt{R R_0}}{B_1} \sin \Phi_1, \quad \theta = \frac{\Theta_0 \sqrt{R R_0}}{2 B_1} [\sin \Phi_1 + 2 B_1 \cos \Phi_1]$$


---

DEFLECTING: Replace  $\sin$  With  $\sinh$ ,  $\cos$  With  $\cosh$   
 &  $\Phi_2 \equiv B_2 \ln(R/R_0)$ ,  $B_2 \equiv \sqrt{\frac{\Theta_w^2}{\alpha^2} + \frac{1}{4}}$

---

LIM  $\alpha \rightarrow 0$  ATT:  $r = r_{MAX} \sin \Phi_3$ ,  $\theta = \Theta_0 \cos \Phi_3$

$\Phi_3 \equiv \Theta_w \frac{z}{R_0}$  DEF:  $r = r_{LMAX} \sinh \Phi_3$ ,  $\theta = \Theta_0 \cosh \Phi_3$

Figure 8. Equations Of Motion Within Quadrupole State Selector For ( $m = 0$ ) Cases Where  $H$  Is Less Than  $H_1$  Or Within Hexapole In Cases Where The Magnetic Moment Is Constant, Or Nearly So.

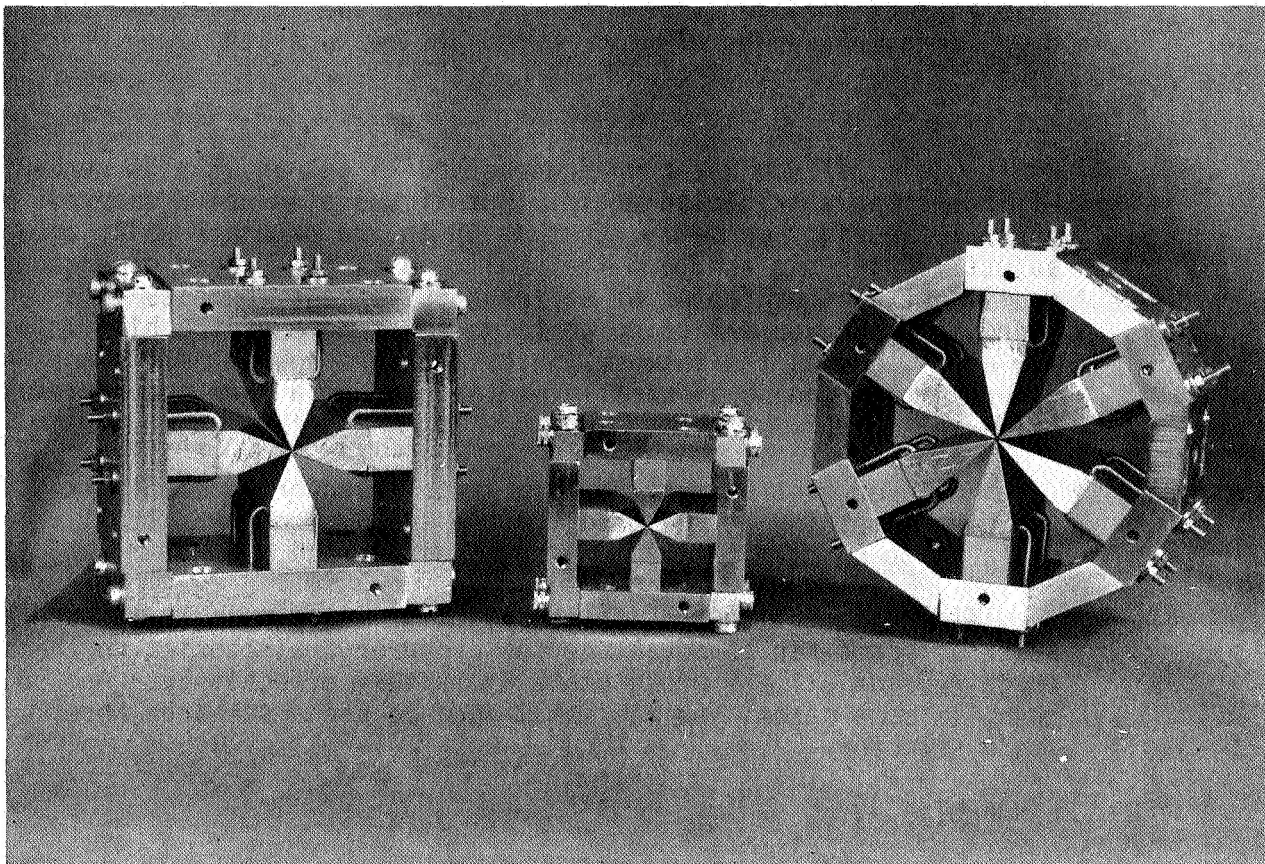


Figure 9. Quadrupole And Hexapole State Selectors Produced At Sigma Tau Standards Corporation. For Dimensional Reference The Small Quadrupole In The Center Has A Tapered Bore With Entrance Diameter of .46 mm, Exit Diameter .97 mm, And Is 25.4 mm Long. The Poles Are Saturated And Have Tip Fields Of Approximately 10 Kilogauss In The Quadrupole Units, And 7 Kilogauss In The Hexapole.

## QUESTIONS AND ANSWERS

DR. VICTOR REINHARDT, NASA/Goddard

What kind of efficiency improvement do you see in a tapered bore over a non-tapered bore? And how do you measure it?

MR. PETERS:

Okay. Well, if you use a quadrupole you'll get about a 50 percent efficiency in total solid angle. But if you also use a tapered bore of the right geometry, that is up to the saturate point and adjust it, the big end, and the small end is the proper dimensions, you'll get another factor of at least 50 percent, because in a hydrogen maser you are going to focus a lot more of the high velocity atoms, due to the intense fields near the source. It's an indeterminate increase in atoms over the case of a more conventional state selector.

Now over just a straight bore state selector, probably it would be something on the order of the small geometry. It'll probably be no more than a 50 percent difference.

I should mention that the straight geometry on a small bore state selector has an advantage for close up trajectories in that it defocusses all the wrong state atoms very effectively. And so, then, in some cases, you may still want to use a straight bore state selector.

DR. REINHARDT:

Have you experimentally verified that?

By looking at a hydrogen maser. Tapered bore versus straight bore.

MR. PETERS:

No, Victor, I haven't.

DR. REINHARDT:

Thanks a lot.

DR. WINKLER:

Your talk brought back memories of 1959 when Professor Kusch suggested very strongly in an analysis to use thallium. And from almost all points of view it would be a superior choice. Except that

work which then was started in a couple of laboratories was stopped because of the difficulty to detect it.

And now, of course, you could consider schemes of optical pumping and optical detection. And then that would be an entirely different situation. Have you thought about that?

MR. PETERS:

Yes, indeed, Dr. Winkler. I think that we can. Of course, the earlier schemes with thallium Zeeman transitions were to boot the one state down to the one zero state. And this has its advantages or disadvantages.

But if we can focus an intense, very intense beam of the one zero -- relatively, I should say, you lose about a factor of 12, but you gain by focussing the one zero state.

You can gain part of this back by selecting a lower temperature from the distribution. And this is done in cesium, for example. But, if you get a very intense beam, a relatively very intense beam, and you should be able to get, maybe, three or four orders of magnitude more atoms at the detector than you do with a cesium beam, which is only about 10 to the sixth, or 10 to the seventh, atoms per second, to get the marvelous performances they are getting.

You could use a modern mass spectrometer, commercially available, probably, to get the same signal to noise ratio.

You could probably use laser techniques. I think you might use a penning trap or another type of trap ionizer to ionize the thallium atoms.

So I think this problem could be solved. And it certainly deserves looking into.

DR. JOHN BERLINSKY, University of British Columbia

I didn't mention this, but in our low temperature experiments we make the RF discharge at the temperature of the dilution refrigerator, which is about half a degree.

And some of our competitors have demonstrated that you can make a beam where the nozzle at the outlet is at four degrees, and the beam temperature, the temperature distribution looks like a five degree distribution.

Our needs, on the other hand, are more or less the same as you described. We would like to have a small state selector with good acceptance.

How much could you improve things, if you could work the beam at low temperatures?

MR. PETERS:

I don't see -- well, of course I don't know exactly the design of state selector that you are presently acquainted with, or using.

DR. BERLINSKY:

Well, we don't, of course, in our present experiments use a state selector. But if we made a maser we might.

MR. PETERS:

Well, the only problem that I can see off-handedly, I haven't looked at the low temperature properties, the materials in the state selector in detail, it seems to me would be the thermal expansion coefficients between the cerium cobalt magnet parts and the soft iron parts. And I think they're all good materials and retain their magnetism, and it's far below the Curie point.

The small magnet you saw here used epoxy, which we'd probably have to do away with, and they can easily be fastened, just as the larger ones were, with screws and the adjustables. So I see no reason why that couldn't be applied.

Also I started to put together, but it was a little tedious, one which was only a half an inch long, and as small a bore diameter as I could realistically work with under the microscope. But I didn't bring it. I said in the program, perhaps, I was going to. But I didn't.

But this could give you one this big. And I don't know if you're worried about the proximity of the source to the region. But I suspect that within this range of sizes something would probably apply very realistically to your apparatus.

DR. REINHARDT:

One quick comment, to further answer that question.

Because the atoms are moving much slower at low temperature, your efficiency theoretically should go up as the ratio of the temperature.

MR. PETERS:

Oh, I forgot that. Yes, my yes.

DR. REINHARDT:

But I think the angles would get so large that you'd limit to two  $\pi$  solid angles.

DR. VESSOT:

Things look awfully good when things get cold, Victor. There's no question about it. And anything Harry said would apply in space.

MR. PETERS:

If I could answer that question further. I think that a tapered or curved pole state selector with a parabolic curve like a space antenna would probably do the job without any further calculations at the moment.

And it probably is very feasible. But your poles won't be saturated if you get a larger bore. You'll have to deal with a little bit different calculation.





FREQUENCY STABILITY OF MASER OSCILLATORS  
OPERATED WITH ENHANCED CAVITY Q

Michel Têtu and Pierre Tremblay  
Laboratoire de Recherches sur les Oscillateurs et Systèmes  
Université Laval, Québec, Canada

and

Paul Lesage, Pierre Petit and Claude Audoin  
Laboratoire de l'Horloge Atomique  
Université de Paris-Sud, Orsay, France

ABSTRACT

This paper presents an experimental study of the short term frequency stability of masers equipped with an external feedback loop to increase the cavity quality factor. The frequency stability of a hydrogen and a rubidium maser are measured and compared with theoretical evaluation. It is observed that the frequency stability passes through an optimum when the cavity Q is varied. Long term fluctuations are discussed and the optimum mid term frequency stability achievable by small size active and passive H-masers is considered.

INTRODUCTION

Much effort has been devoted recently to hydrogen masers in order to reduce their size, their weight, and to increase their long term frequency stability. New technology and design improvements applied to conventional masers [1] led to the realization of the most stable atomic frequency standards in the mid term region of averaging time [2], and to a sufficiently light and rugged device to be space-borne [3]. Small size masers with various types of microwave cavities were proposed and tested [4,5]. Masers with dielectric loaded cavities operated as passive frequency standards were also investigated [6,7]. The latest development is a small cavity oscillating maser, equipped with an external loop to enhance the quality factor [8,9].

A theoretical model, established to evaluate the amplitude noise and the phase noise in actively and passively operated masers [10,11] made possible the prediction of the short term frequency stability of a maser equipped with an external feedback loop [12]. Subsequently, the ultimate performance of such a device were evaluated and compared to the corresponding passive standard [13]. The following gives an experimental check of that theory applied to a hydrogen maser and a rubidium maser of conventional design [14,15], so equipped.

## THEORY

The time domain frequency stability of an oscillator is expressed by the two sample variance of the relative frequency fluctuations over an averaging time  $\tau$ , with no dead time (Allan variance) [16]. In the case of a maser, the dominant frequency fluctuations considered arise from both the thermal noise within the electromagnetic cavity and the thermal noise added in the receiver necessary to detect the signal [17]. When the spectrum of the fluctuations is limited by a low-pass filter of cut-off frequency  $f_c$ , it can be shown [15,18] that the short term frequency stability, in the time domain, is expressed by the relation:

$$\sigma_y^2(\tau) = \frac{4k\theta_c}{P_0} \left\{ \frac{3\pi f_c}{2\omega_0^2} \left[ 1 + (F_r - 1) \frac{Q_{\text{ext}}}{Q_c} \frac{\theta_r}{\theta_c} \right] \frac{1}{\tau^2} + \frac{1}{8Q_\ell^2} \frac{1}{\tau} \right\}, \quad (1)$$

where  $k$  is the Boltzmann constant,  $\theta_c$ ,  $Q_c$  and  $Q_{\text{ext}}$  are respectively the temperature, the loaded and the external quality factors of the cavity,  $\theta_r$  and  $F_r$  are the temperature and the noise factor of the receiver,  $\omega_0$  is the maser angular frequency,  $Q_\ell$  is the atomic line  $Q$  and  $P_0$  is the power delivered to the cavity by the atoms.

The first two terms of equation (1) come from the thermal noise added to the maser signal by the cavity and the receiver respectively; they correspond to white phase noise. The third term is white frequency noise resulting from the stimulated emission of radiation by the cavity's thermal noise within the atomic linewidth. The atomic power can be expressed simply, in terms of the cavity  $Q$ , by the following [19]:

$$P_0 = \frac{1}{2} S \hbar \omega_0 \frac{Q_c - Q_t}{Q_c} \quad (2)$$

where  $S$  is a flux term,  $\hbar$  is the Planck constant divided by  $2\pi$  and  $Q_t$  is a threshold  $Q$  value determined by various maser parameters.

A feedback loop, external to the cavity, can be utilized to increase the quality factor; a schematic diagram is given in figure 1. Part of the maser signal is taken out, amplified and re-injected into the cavity. If the phase of the injected signal is properly adjusted, it will add to the signal already in the cavity, thus simulating a lower loss cavity. In this set-up, the cavity is used in transmission, with coupling loop coefficients  $\beta_1$  and  $\beta_2$  at the injection and output ports respectively. The loaded cavity  $Q$  becomes [20]:

$$Q_c = \frac{Q_0}{1 + \beta_1 + \beta_2} \quad (3)$$

where  $Q_0$  is the unloaded cavity  $Q$  associated with ohmic losses. Two external cavity  $Q$ 's are defined as follows:

$$Q_{\text{ext},1} = \frac{Q_0}{\beta_1} \quad \text{and} \quad Q_{\text{ext},2} = \frac{Q_0}{\beta_2} \quad (4)$$

The enhanced cavity  $Q$  has a maximum value given by:

$$Q_e = \frac{Q_0}{1 + \beta_1 + \beta_2 - 2G\sqrt{\beta_1\beta_2}} \quad (5)$$

where  $G$  is the total voltage gain of the feedback loop. The atomic power of such a maser will now be:

$$P_0 = \frac{1}{2} S \hbar \omega_0 \frac{Q_e - Q_t}{Q_e} \quad (6)$$

The presence of the feedback loop alters the thermal noise within the cavity. Part of the cavity noise undergoes the same process as the maser signal and the loop amplifier adds a certain amount of thermal noise. These supplementary contributions give to the cavity an effective noise temperature which can be written [21]:

$$T_c = \theta_c \frac{Q_e}{Q_c} \left[ 1 + \beta_1 (F_a - 1) G^2 \frac{Q_c}{Q_0} \frac{\theta_a}{\theta_c} \right] \quad (7)$$

where  $\theta_a$  and  $F_a$  are the temperature and the noise figure of the loop amplifier.

If we substitute equations (3), (4), (5), (6) and (7) into equation (1), we obtain for the time domain short term frequency stability of a maser equipped with an external feedback loop, an expression of the form:

$$\sigma^2(\tau) = K_{-2} \tau^{-2} + K_{-1} \tau^{-1} \quad (8)$$

where the white phase noise contribution is:

$$K_{-2} = \frac{12\pi k \theta_r f_c}{S \hbar \omega_0^3} \frac{Q_e}{(Q_e - Q_t)} \left\{ \frac{\theta_c}{\theta_r} \frac{Q_e}{Q_0} \left[ 1 + \beta_1 + \beta_2 + \frac{\theta_a}{\theta_c} (F_a - 1) \frac{1}{4\beta_2} \left( 1 + \beta_2 + \beta_2 - \frac{Q_0}{Q_e} \right)^2 \right] + (F_r - 1) \frac{1 + \beta_1 + \beta_2}{\beta_2} \right\} \quad (9)$$

and the white frequency noise contribution is:

$$K_{-1} = \frac{k\theta_c}{\sin\omega_0 Q_\ell^2} \frac{Q_e^2}{(Q_e - Q_t)} \frac{1}{Q_0} \left[ 1 + \beta_1 + \beta_2 + \frac{\theta_a}{\theta_c} (F_a - 1) \frac{1}{4\beta_2} \left( 1 + \beta_1 + \beta_2 - \frac{Q_0}{Q_e} \right)^2 \right] \quad (10)$$

These equations are explicitly expressed in terms of the fixed cavity parameters  $\beta_1$ ,  $\beta_2$  and  $Q_0$  and its enhanced  $Q$ .

Computation of equation (8) with the parameters given in table 1 for a conventional H-maser and a conventional Rb-maser yields the results shown in figure 2.

	H-maser	Rb-maser
$\omega_0$	$2\pi(1.42 \times 10^9)$ rad/sec	$2\pi(6.83 \times 10^9)$ rad/sec
$Q_\ell$	$2.2 \times 10^9$	$5.5 \times 10^7$
S (normalization parameter)	$7.15 \times 10^{11}$ at./sec	$3.65 \times 10^{15}$ ph./sec
$Q_t$	40 000	22 500
$Q_0$	64 400	28 000
$\beta_1$	0.157	0.60
$\beta_2$	0.171	0.55
$\theta_c$	300 K	337 K
$F_r = F_a$	1.78	2.24
$\theta_r$	293 K	290 K
$\theta_a$	300 K	290 K
$f_c$	5 Hz	50 Hz

Table 1: Maser parameters used to evaluate equation (8).

The behavior of the two types of noise is drawn from the two asymptotical lines obtained for the very short averaging times and for the long averaging times respectively.

#### EXPERIMENTAL STUDIES

In order to verify the model just described, both an hydrogen and a rubidium maser were equipped with a feedback loop as illustrated in figure 1. The cavity  $Q$  was varied by changing the value of the attenuator and measured with the usual technique of the r.f. pulse decay [19]. For the

H-maser phase of the loop was adjusted, at each attenuator setting to cause no frequency shift from non-enhanced operation. In the case of the Rb-maser, the phase was adjusted to make the output power maximum.

The short term frequency stability for various values of  $Q_e$  with the parameters shown in table 1 are given in figure 3. It is observed that the stability decreases when the cavity  $Q$  reaches high values. In the case of the Rb-maser, a roll-over is observed in the very short term region ( $\tau < .02$  sec). In both systems, unpredicted sources of instabilities dominate for long averaging times. The solid lines are best fit polynomials.

From the coefficient of the polynomials we can extrapolate the white phase noise contribution,  $K_{-2}$ , and the white frequency noise contribution,  $K_{-1}$ . The square root of each contribution is shown in figure 4. The solid lines are the result of the evaluation of equations (9) and (10) as a function of  $Q_e$ . They are normalized with the flux term,  $S$ , so that the  $\sqrt{K_{-2}}$  curve passes over the experimental point indicated by an arrow. These results are experimental evidence that each noise contribution can be minimized by choosing the proper value for  $Q_e$ . Consequently, if the overall frequency stability is to be optimized, the  $Q_e$  value will be selected according to the averaging time considered.

A comparison between the experimental observation and the theoretical evaluation of the frequency stability at different averaging times, as functions of the enhanced  $Q$ , is given in figure 5. We see that the stability is optimum for a certain value,  $Q_e^{opt}$ . This value depends slightly on the averaging time chosen since the dominant type of noise evolves from the white phase noise to the white frequency noise when the averaging time is varied from very short term to mid term. In this last comparison, the averaging time was limited to values smaller than 300 sec for the H-maser and .07 sec for the Rb-maser in order to reduce the influence of the long term instabilities.

In figure 3 frequency instabilities other than the ones predicted by equation (8), are evident. Since their contribution increases with the cavity  $Q$ , we are tempted to relate them to a cavity pulling effect. We measured the relative frequency shift due to temperature variation of the feedback loop components for different cavity  $Q$ 's. The results are given in figure 6 for each maser. The coefficients are approximately  $1 \times 10^{-13}/^{\circ}\text{C}$  at 40 000 for the H-maser and  $3 \times 10^{-11}/^{\circ}\text{C}$  at 25 000 for the Rb-maser. These shifts are due to a phase pulling effect related to a change in the length of the feedback loop and explain some of the long term instabilities. It is seen from these measurements that a very precise control of the loop temperature will be necessary if high performance is required. Automatic cavity tuning such as the fast auto-tuning system [7,22] would then improve the long term

frequency stability of masers actively operated with an external feedback loop.

#### SMALL SIZE HYDROGEN MASER

The theoretical model seems to fit well the reality observed. We will now use it to predict the ultimate frequency stability achievable by small size active H-maser with enhanced cavity Q. To do so, the maser parameters found in equation (8) are expressed in terms of more fundamental parameters which are associated with the gain and linewidth of the atomic system. They are the spin exchange parameter [1]:

$$q = \frac{\sigma \bar{v}_r \hbar}{2\mu_0 \mu_B} \frac{T_b}{T_t} \frac{1}{V_b} \frac{V_c}{\eta Q_c} \frac{I_{tot}}{I} \quad (11)$$

and the threshold flux:

$$I_{th} = \frac{\hbar}{\mu_0 \mu_B^2} \frac{V_c}{\eta Q_c} \frac{1}{T_t^2} \quad (12)$$

In these equations  $I_{tot}$  is the total atomic flux entering the bulb,  $I$  is that portion of the flux in the upper active quantum state,  $\mu_0$  is the magnetic permeability of vacuum,  $\mu_B$  is the Bohr magneton,  $\eta$  is the filling factor,  $V_c$  is the cavity volume,  $\sigma$  is the spin exchange cross-section,  $\bar{v}_r$  the relative average hydrogen velocity,  $T_b$  is the bulb storage time constant,  $V_b$  is the bulb volume and  $T_t = \sqrt{T_1^0 T_2^0}$  with  $T_1^0$  and  $T_2^0$  the longitudinal and transversal relaxation time constants.

Considering only the effect of the white frequency noise contribution, it has been shown [13, eq. 44] that the frequency stability of an active maser, with enhanced cavity Q, is expressed by the relation:

$$\sigma_{a,e}^2(\tau) = \frac{4kT}{\hbar^2 \omega_0^3} \mu_0 \mu_B^2 \frac{\eta Q_c}{V_c} \left( \frac{Q_e}{Q_c} \right)^2 H_{a,e} \left( q, \frac{I}{I_{th}} \right) \frac{1}{\tau} \quad (13)$$

The function  $H_{a,e}(q, I/I_{th})$  [13, eq. 17] has to be minimized in order to reach the ultimate frequency stability. If the parameters of currently existing small size masers are substituted in equation (13), we obtain:

$$\sigma_{a,e,opt}^2(\tau) \simeq 0.6 \times 10^{-26} \tau^{-1}$$

The same approach can be applied to the case of a passive H-maser. One can show [13, eq. 25] that the optimum frequency stability is expressed by:

$$\sigma_p^2(\tau) = \frac{4kT}{\hbar^2 \omega_0^3} \mu_0 \mu_B^2 \frac{\eta Q_c}{V_c} H_p \left( q, \frac{I}{I_{th}} \right) \frac{1}{\tau} \quad (14)$$

Here again the function  $H_p(q, I/I_{th})$  must be minimized by a proper choice of  $q$  and  $I/I_{th}$ . When evaluating equation (14) with the parameters of existing passive masers [13, table 1] we have the value:

$$\sigma_{p,op}^2(\tau) \simeq 3.6 \times 10^{-26} \tau^{-1}$$

Both types of small size H-masers have then approximately the same ultimate frequency stability in the mid term region.

#### CONCLUSION

This experimental study as well as the previous one on amplitude noise [11] give great confidence in the theoretical model developed to consider the effect of thermal noise on the amplitude and the phase of actively or passively operated masers. When a maser is operated with a feedback loop to enhance the cavity  $Q$ , an optimum is found where the frequency stability is best. Small size H-masers of the same design can then be operated either actively or passively; they will offer about the same mid term frequency stability when all the parameters are optimized. Automatic cavity tuning is needed on both devices to improve the long term stability: the electronic complexity will then be of the same level.

#### REFERENCES

- [1] D. Kleppner, H.C. Berg, S.B. Crampton, N.F. Ramsey, R.F.C. Vessot, H.E. Peters and J. Vanier, "Hydrogen Maser Principles and Techniques", Phys. Rev., Vol. 138, No 4A, A972-A983, 1965.
- [2] R.F.C. Vessot, M.W. Levine and E.M. Mattison, "Comparison of Theoretical and Observed Hydrogen Maser Stability Limitation due to Thermal Noise and the Prospect for Improvement by Low-Temperature Operation", Proc. Ninth Annual Precise Time and Time Interval (PTTI) Applications and Planning Meeting, pp. 549-569, Washington, D.C., 1978.
- [3] R.F.C. Vessot, M.W. Levine, E.M. Mattison, T.E. Hoffman, E.A. Imbier, M. Têtu, G. Nystrom, J.J. Kelt, Jr., H.F. Trucks and J.L. Vaniman, "Space-Borne Hydrogen Maser Design", Proc. Eighth Annual Precise Time and Time Interval (PTTI) Applications and Planning Meeting, pp. 277-333, Washington, D.C., 1978.
- [4] E.M. Mattison, M.W. Levine, R.F.C. Vessot, "New  $TE_{111}$ -Mode Hydrogen Maser", Proc. Eighth Annual Precise Time and Time Interval (PTTI) Applications and Planning Meeting, pp. 355-380, Washington, D.C., 1978.



- [5] H.E. Peters, "Small, Very Small, and Extremely Small Hydrogen Masers", Proc. 32nd Annual Symposium on Frequency Control, pp. 469-476, 1978.
- [6] F.L. Walls and H. Hellwig, "A New Kind of Passively Operating Hydrogen Frequency Standards", Proc. 30th Annual Symposium on Frequency Control, pp. 473-480, 1976.
- [7] D.A. Howe, F.L. Walls, H.E. Bell, H. Hellwig, "A Small Passively Operated Hydrogen Maser", Proc. 33rd Annual Symposium on Frequency Control, pp. 554-562, 1979.
- [8] H.T.M. Wang, "An Oscillating Compact Hydrogen Maser", Proc. 34th Annual Symposium on Frequency Control, pp. 364-369, 1980.
- [9] H.E. Peters, "Feasibility of Extremely Small Hydrogen Masers", Proc. 35th Annual Symposium on Frequency Control, to be published.
- [10] P. Lesage, C. Audoin and M. Têtu, "Amplitude Noise in Passively and Actively Operated Masers", Proc. 33rd Annual Symposium on Frequency Control, pp. 515-535, 1979.
- [11] P. Lesage, C. Audoin, M. Têtu, "Measurement of the Effect of Thermal Noise on the Amplitude of Oscillation of a Maser Oscillator", IEEE Trans. Instrum. Meas., Vol. IM-29, No 4, pp. 311-316, 1980.
- [12] P. Lesage and C. Audoin, "Frequency Stability of an Oscillating Maser: Analysis of the Effect of an External Feedback Loop", IEEE Trans. Instrum. Meas., Vol. IM-30, No 3, pp. 182-186, 1981.
- [13] C. Audoin, J. Viennet and P. Lesage, "Hydrogen Maser: Active or Passive?", Proc. 3rd Symposium on Frequency Standards and Metrology, Aussois, France, to be published, 1981.
- [14] P. Petit, J. Viennet, R. Barillet, M. Desaintfuscién and C. Audoin, "Hydrogen Maser Design at the Laboratoire de l'Horloge Atomique", Proc. Eighth Annual Precise Time and Time Interval (PTTI) Applications and Planning Meeting, pp. 229-247, Washington, D.C., 1976.
- [15] M. Têtu, G. Busca and J. Vanier, "Short Term Frequency Stability of the  $\text{Rb}^{87}$  Maser", IEEE Trans. Instrum. Meas., Vol. IM-22, No 3, pp. 250-257, 1973.
- [16] J.A. Barnes, A.R. Chi, L.S. Cutler, D.J. Healey, D.B. Leeson, T.E. McGunigal, J.A. Mullen, W.L. Smith, R.L. Sydnor, R.F.C. Vessot and G.M.R. Winkler, "Characterization of Frequency Stability", IEEE Trans. Instrum. Meas., Vol. IM-20, No 2, pp. 105-120, 1971.
- [17] L.S. Cutler, "Coulomb Corrections to Inelastic Electron Scattering and Maser Oscillator Thermal Noise Analysis", Ph.D. thesis, Stanford University, 1966, unpublished.
- [18] P. Lesage and C. Audoin, "Effect of Dead-Time on the Estimation of the Two-Sample Variance", IEEE Trans. Instrum. Meas., Vol. IM-28, No 1, pp. 6-10, 1979.

- [19] C. Audoin, "Le maser à hydrogène en régime transitoire", D.Sc. thesis, Université de Paris-Sud à Orsay, 1967, unpublished.
- [20] G. Boudouris, "Cavités électromagnétiques", Dunod, Paris, 1971.
- [21] P. Lesage, "Caractérisation des fluctuations de fréquence et analyse du bruit d'amplitude dans le maser à hydrogène", D.Sc. thesis, Université de Paris-Sud à Orsay, 1980, unpublished.
- [22] C. Audoin, "Fast Cavity Auto-Tuning Systems for Hydrogen Masers", *Revue de Physique Appliquée*, Vol. 16, p. 125, 1981.

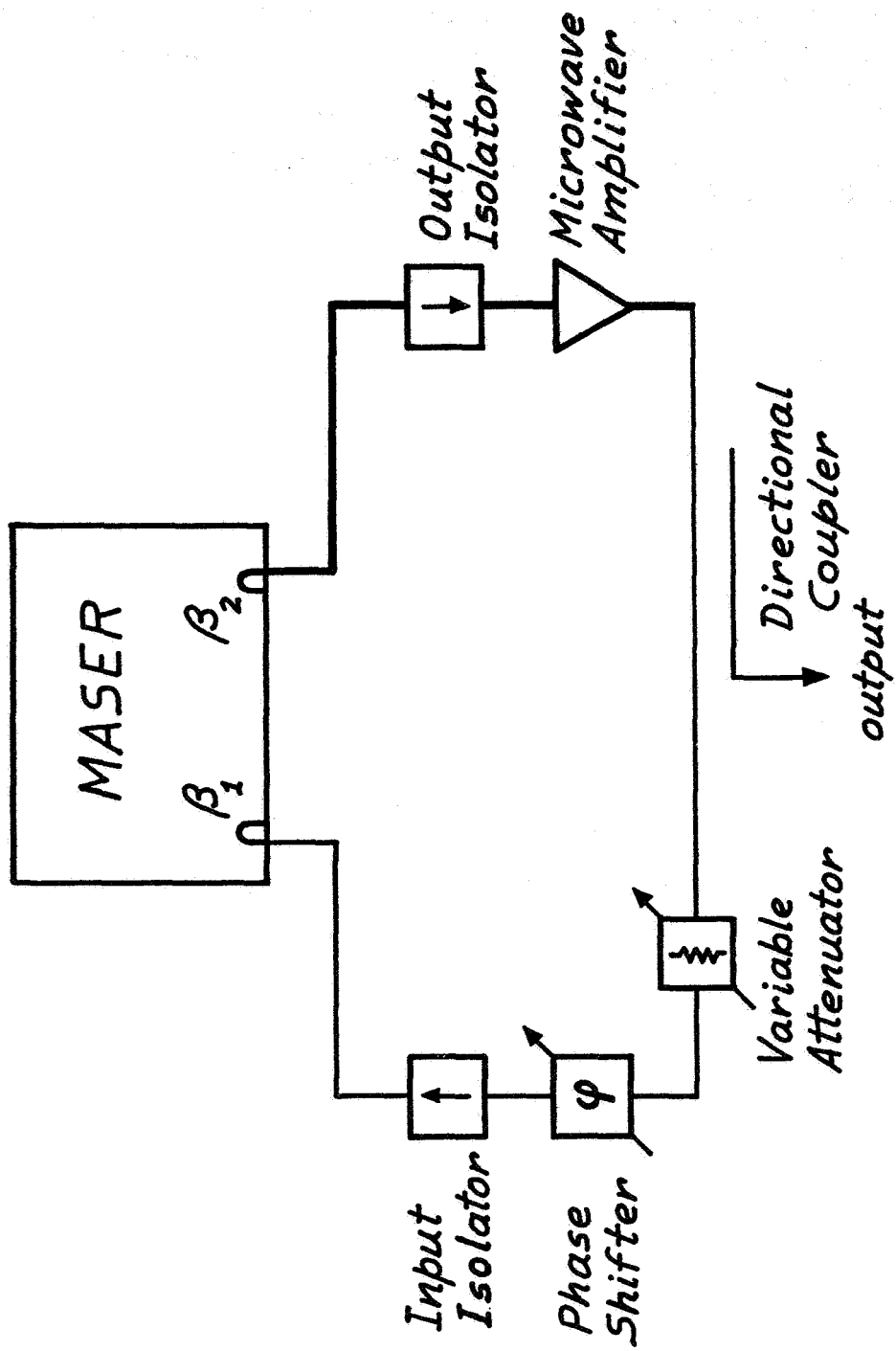


Fig. 1 Schematic diagram of the feedback loop associated with a maser cavity.

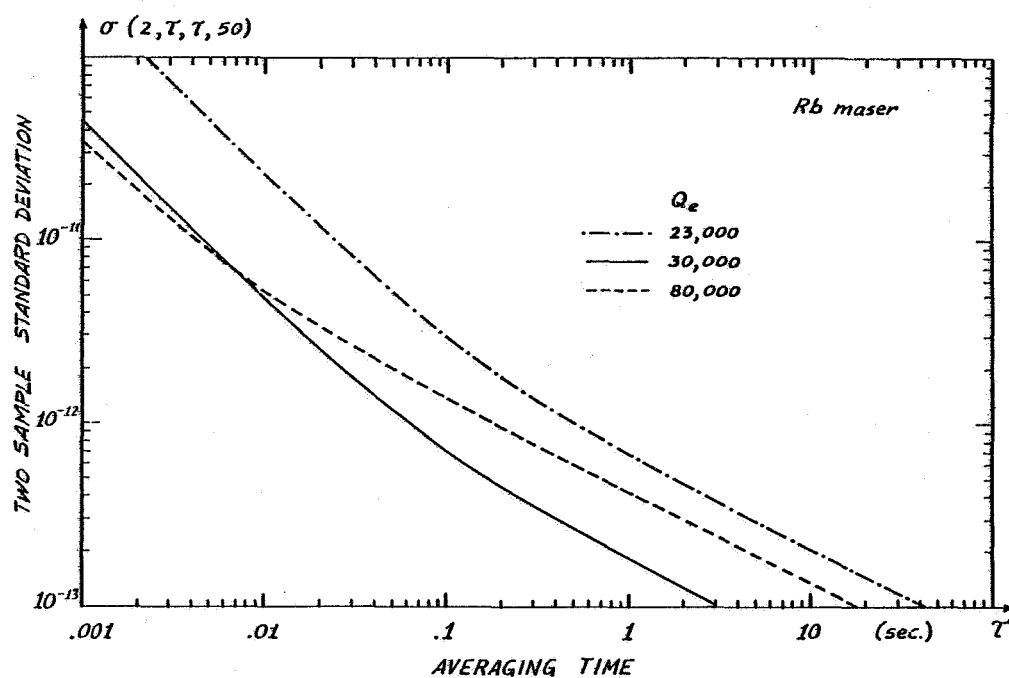
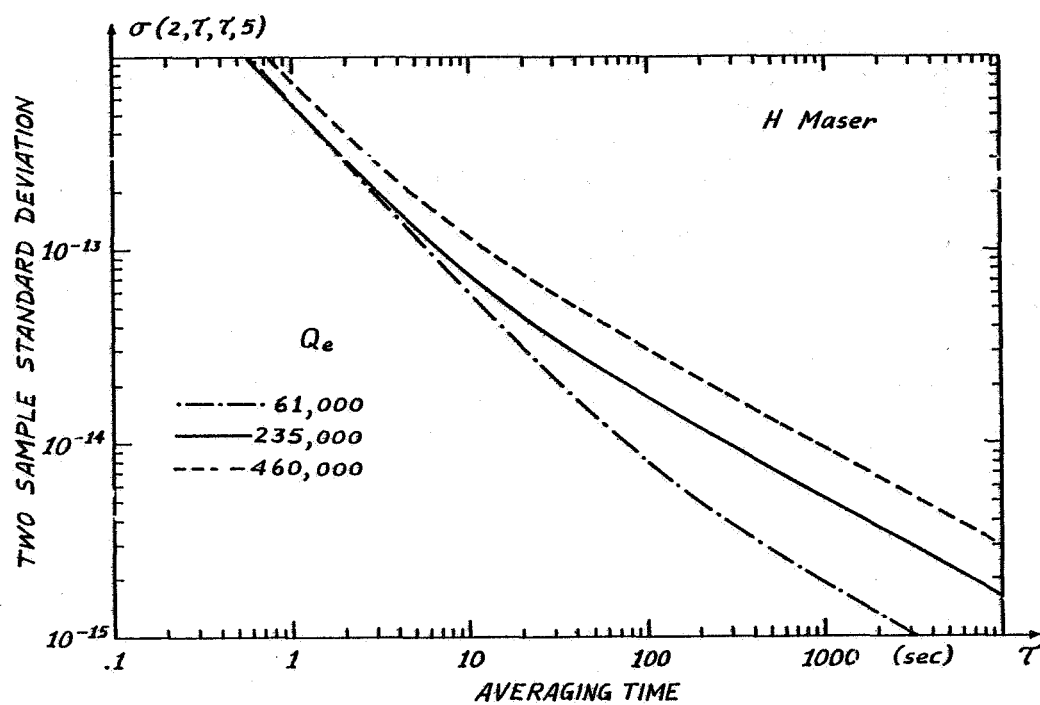


Fig. 2 Short term frequency stability: theoretical evaluation.

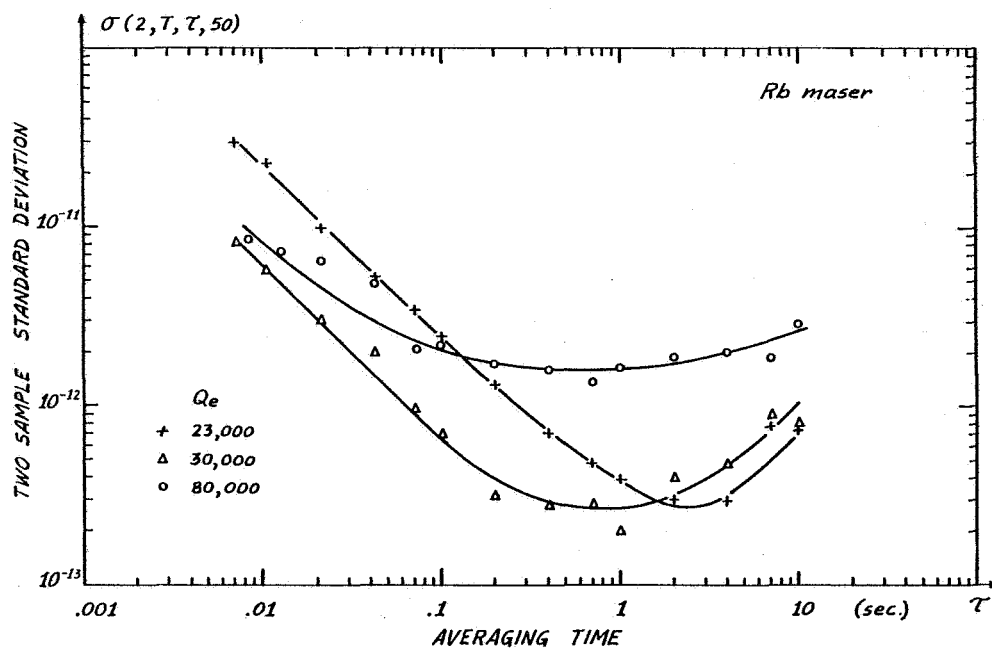
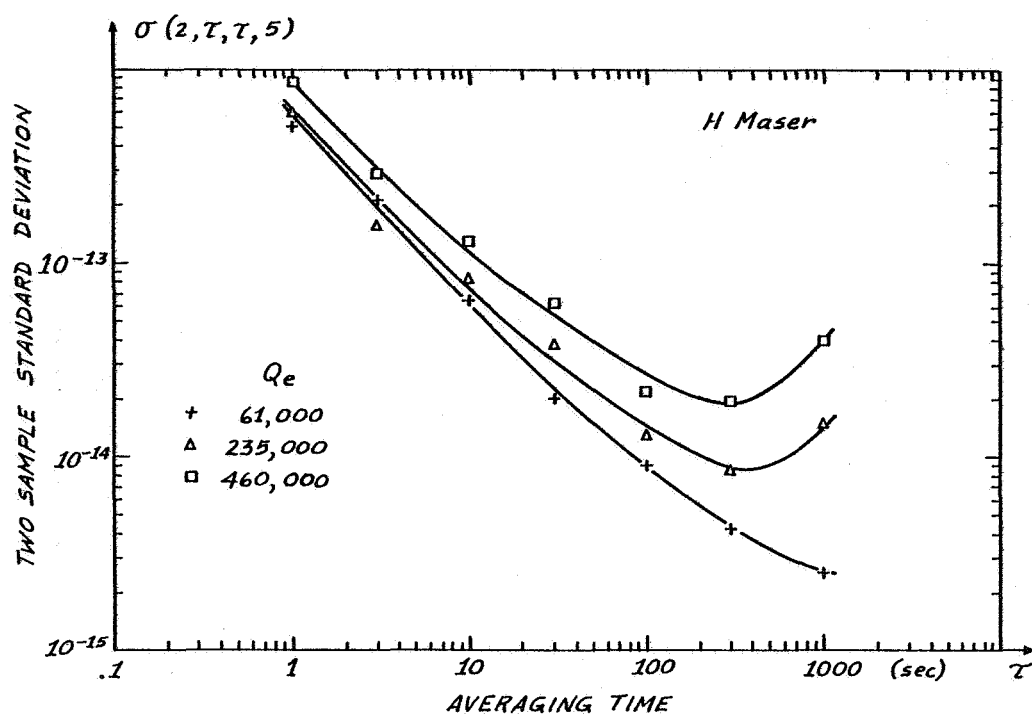


Fig. 3 Short term frequency stability: measurement.

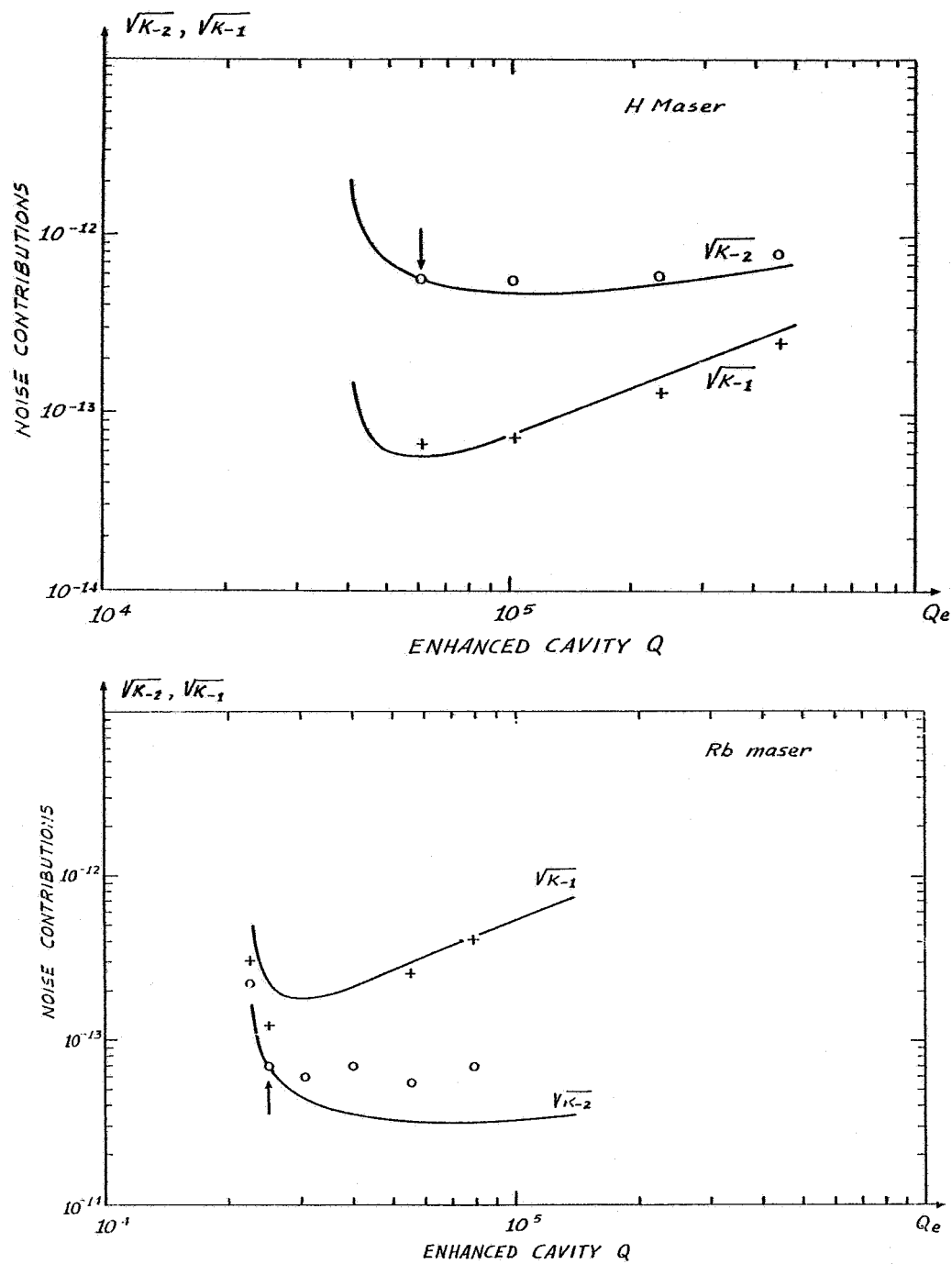


Fig. 4 White phase noise and white frequency noise contributions.

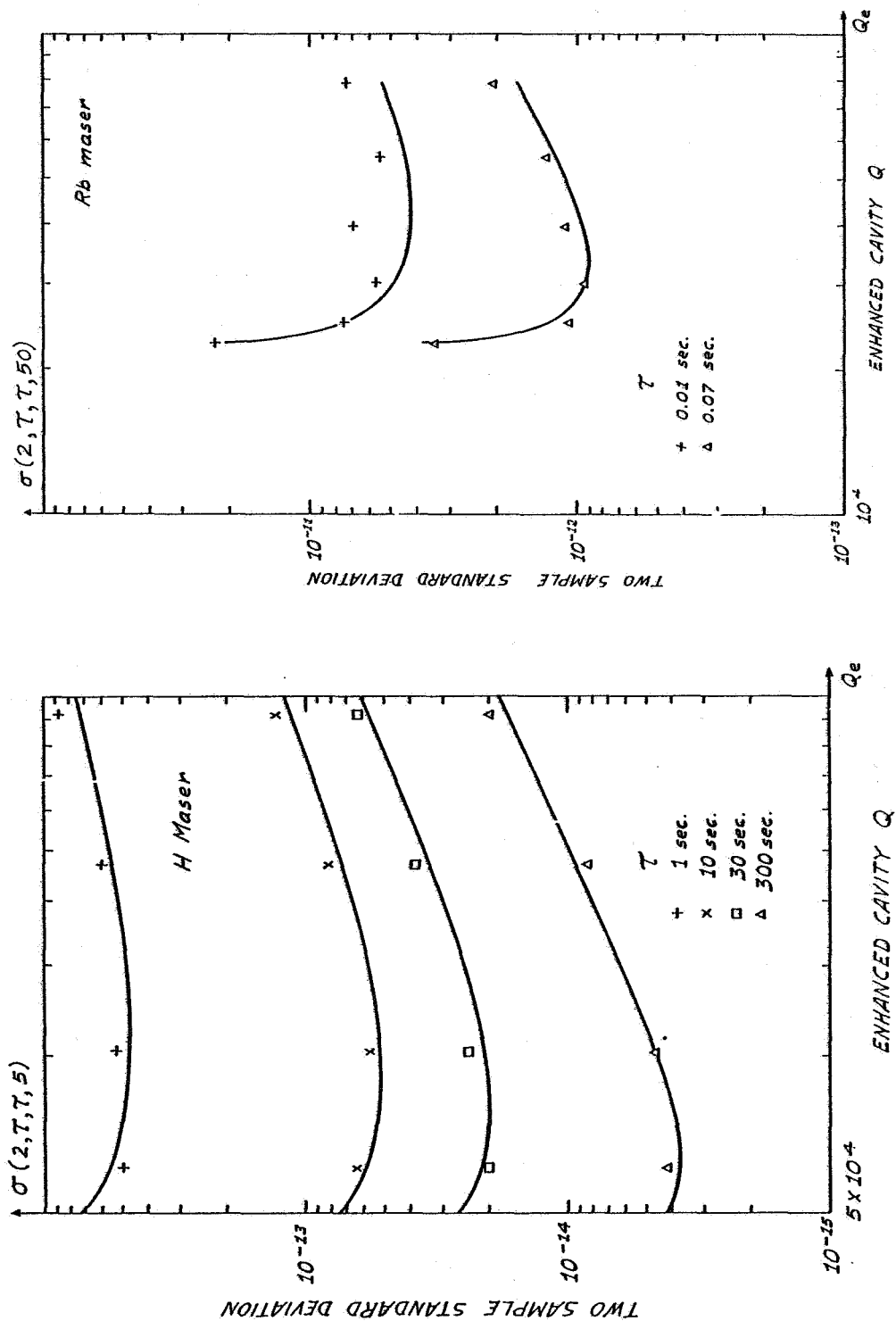


Fig. 5 Overall short term frequency stability.

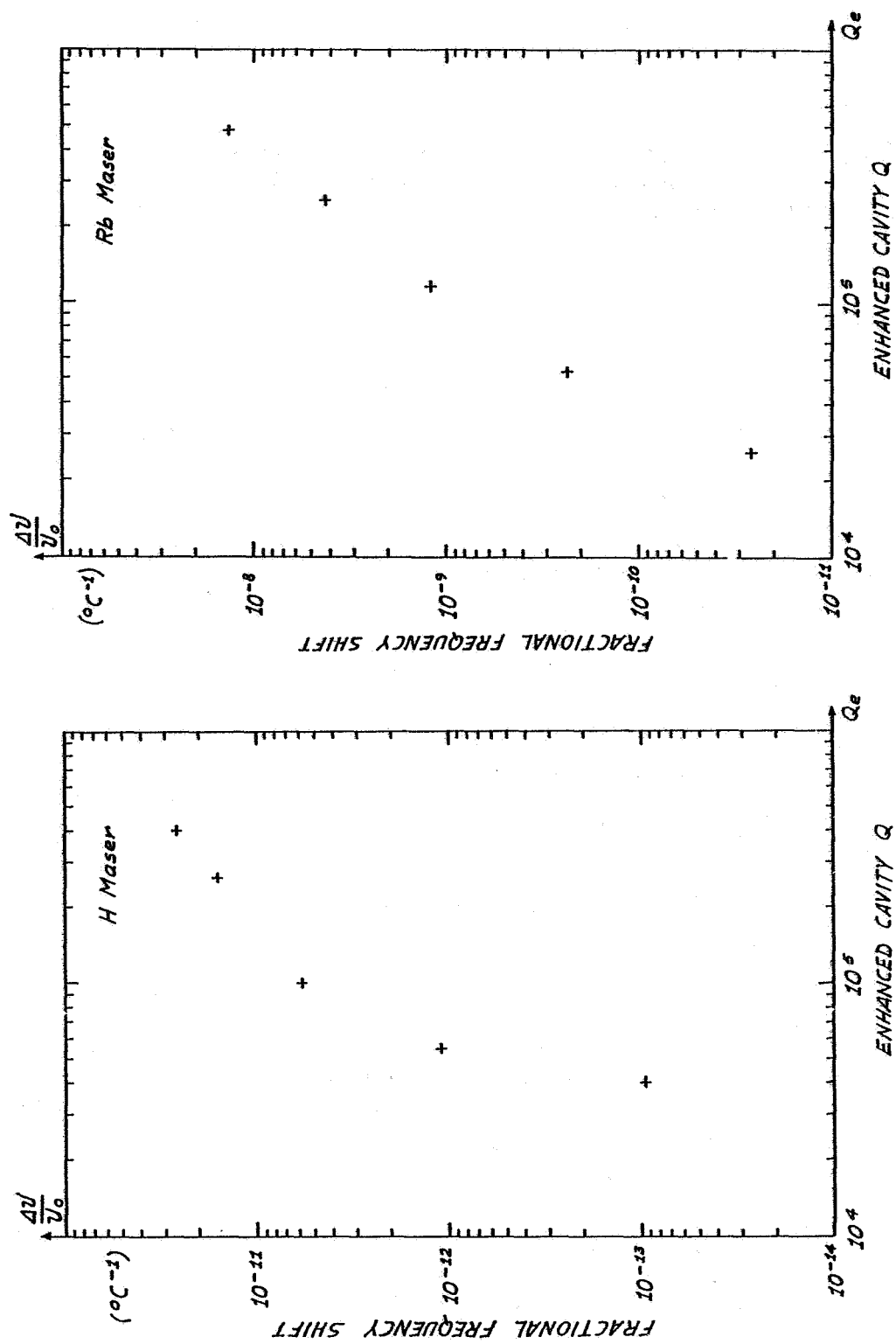


Fig. 6 Relative maser frequency shift associated to a variation of 1  $^{\circ}\text{C}$  of the loop temperature.



## QUESTIONS AND ANSWERS

DR. VESSOT:

I would like to point out that this represents experimental work. Those dots require a person to make a number. It's nice to see real numbers, Michel.

DR. TETU:

Well, I must say we spent a lot of time.

DR. VESSOT:

I can appreciate the amount of effort. I just hope others can, too.

DR. VICTOR REINHARDT, NASA/Goddard

Have you considered the effect of flicker of phase noise being converted to flicker of frequency noise. And in your curves I didn't see any evidence of it in the experimental curves. But have you done any theoretical considerations of it?

DR. TETU:

Well, you see in the theoretical model we have no way to generate the flicker of frequency noise or the flicker of phase noise. But as seen in the case of the rubidium maser, it seems that for a very high value of the enhanced Q we observed flicker of frequency type of noise. But we don't know, yet, the origin of it.

So we are expecting to do more work on it before we are ready to start talking about that.

DR. REINHARDT:

I have seen experimental evidence of that when I've Q multiplied. What I'm saying is that the flicker of phase noise in the amplifier, because of the loop that's converted to flicker of frequency.

DR. TETU:

Yes, I think I saw some work done by a worker in Montreal who looked at frequency stability of cavity oscillator using a feedback loop. And he observed this type of flicker of frequency noise. So probably you are right about that.

DR. VESSOT:

You could get a measure of that by putting in an arbitrary phase shift and determining what the response was to that phase shift.

I'd treat the flicker as systematic, which is a very close idea to my heart at least.

DR. HARRY WANG, Hughes Research Laboratory

I have a couple of comments. We have used a similar technique in compact maser Q-enhancement. And the first observation I'd like to point out is when you use the Q-enhancement the cavity is really not an isolated device any more. The feedback loop transmission line forms a part of the cavity.

So your isolators in the circuits become superfluous. In fact, in our earlier work we found that removing those isolators improved your performance.

DR. TETU:

For us, you see, it was one way to be sure of the noise figure of the amplifier.

DR. WANG:

And the second observation is we have, realizing that problem, we have incorporated an active electronic cavity stabilizing zero system. And we have measured stability of four parts in 10 to the 15th, at 10 to the five second averaging time.

DR. FRED WALLS, National Bureau of Standards

Your work there is really very nice. And what it tends to point to is that the enhanced cavity mode could be very useful for short-term stability. Stabilities out to a few hours, maybe even approaching a day. But it makes it considerably more difficult to get long-term stability, from day to months.

And with active cavity stabilization on the passive masers you, perhaps, give up some short-term stability in the few seconds out to a few hours. But we've measured frequency drifts over 72 days of much less than a part in 10 to 15 per day. Actually only a few parts in 10 to 16.

And I don't think such things would have been nearly as easy to obtain with the Q-enhanced system because of the amplification of the phase difficulties.

DR. TETU:

I ought to say two things on that. What is important at the beginning is the relative ratio of the Q that you need. So we have shown here a hydrogen maser having an enhanced Q of 400,000 which is a way too much. It's fairly forbidden. But that's one point. You see, it depends on the ratio that you have to give to the maser.

And it is also obvious that a kind of auto-tuning of the cavity is needed. You are right.

SESSION VI

RELATIVITY AND GRAVITY WAVES

Professor Carroll O. Alley, Chairman  
University of Maryland



INTRODUCTION TO SOME FUNDAMENTAL CONCEPTS OF GENERAL RELATIVITY  
AND TO THEIR REQUIRED USE IN SOME MODERN TIMEKEEPING SYSTEMS\*

by

C. O. Alley

Department of Physics and Astronomy  
University of Maryland  
College Park, Maryland

ABSTRACT

This is a largely tutorial lecture on the basic ideas of General Relativity - Einstein's theory of gravity as curved space-time - emphasizing the physical concepts and using only elementary mathematics. For the slow motions and weak gravitational fields which we experience on the earth, the main curvature is that of time, not space. Recent experiments demonstrating this property (Alley, Cutler, Reisse, Williams, et al, 1975 and Vessot and Levine, 1976) will be briefly reviewed.

The extraordinary stability of modern atomic clocks makes it necessary to understand and to include the fundamental effects of motion and gravitational potential on clocks in many practical situations. These include the NAVSTAR/Global Positioning System and time synchronization using ultra stable clocks transported by aircraft.

In future system such as global time synchronization using clocks in low earth orbit, the accuracy may be limited by uncertainties in the calculated proper time of the travelling clock, rather than by intrinsic clock performance.

INTRODUCTION

This talk will be in the same general vein as one I gave at the time of the Einstein Centennial two and half years ago at the 33rd Annual Frequency Control Symposium<sup>1</sup>, so I apologize to those of you who

\* This paper is an edited version of a tape recording of the invited tutorial talk.

<sup>1</sup> C. O. Alley, "Relativity and Clocks", Proceedings, 33rd Annual Symposium on Frequency Control, U.S. Army Electronics Research and Development Command, Fort Monmouth, N.J., pp 4 - 39A (1979). Copies available from Electronic Industries Association, 2001 Eye Street, N.W., Washington, D.C. 20006.

Reference should be made to this paper for details of some results given here and for further references.

may have heard that talk. But for a tutorial talk, perhaps it is excusable, or even desirable, to repeat important things. The emphasis here is somewhat different from Reference 1, however.

The concept of proper time in relativity is really central to the whole subject. The proper time is the ordinary time actually kept by a clock, its own time, or, in German, eigenzeit. The high stability that has been achieved by the time keeping community with modern atomic clocks allows the effects of motion and gravity to be actually measured, with results in agreement with Einstein's predictions. Einstein's ideas are no longer just a matter of great scientific interest, actually forming the basis of the view of the universe that we now have from modern astronomy, but also a matter of practical engineering concern. These timekeeping applications are the first practical applications of General Relativity which go beyond Newtonian gravity.

The subject can be understood. In the past, the subject was largely taken over by mathematicians, from about 1920 until the 1950's. The central physical ideas were rarely brought to the fore. The ideas were obscured by the Tensor Calculus with all of its bristling indices and the higher mathematics associated with differential geometry. The actual way in which Einstein got to these concepts was generally ignored in the teaching of the subject (at the few places where it was taught) and those of us in the academic community have to take some responsibility for not having understood these things properly and for not having taught them to many generations of engineering and physics students. But that situation has now changed.

In addition to these practical applications, many modern discoveries in astrophysics require the use of General Relativity in order to comprehend them. There's the whole notion of compact objects with the extreme being the black holes which probably exist. They may be the power sources of quasars. The energy conversion resulting from matter falling down the deep potential well of a black hole is something like 30% of the rest energy compared with only 0.7% for thermo-nuclear fusion. The expanding universe could have been predicted by Einstein, except that it was uncongenial to the world view in the teens of our century, and he modified his equations to avoid it. It was probably his greatest mistake (in his own evaluation) but General Relativity does describe its growth from the "Big Bang". The changes in the orbit of the Binary Pulsar<sup>2</sup>, revealed by precise timing of its periodic radio pulses with atomic clocks, seems to show the emission of the gravity waves predicted by General Relativity. We will hear more this afternoon about attempts to detect low frequency gravity waves left from the early

<sup>2</sup> J. M. Weisberg, J. H. Taylor, and L. H. Fowler, "Gravitational Waves from an Orbiting Pulsar", Scientific American, Vol. 245, No. 4, pp. 74-82 (October, 1981).

universe, using the atomic clock controlled tracking of interplanetary probes, opening a new window on the universe, if successful.

Now, let me give you some good introductory references. I like to approach the subject from an historical point of view, the way I think Einstein actually developed it. There's a great book by Banesh Hoffmann called Albert Einstein: Creator and Rebel (Plume Books, 1973). I recommend this to all of my students and I recommend it to you to read both for Einstein's physics and for his life. Nigel Calder has recently written a popular book called Einstein's Universe (Penguin Books, 1979) which was made into a two-hour BBC television film of the same name, which is highly recommended. I'm going to use an approach to relativity called the k-calculus by its developer, Hermann Bondi. It is described in a book called Relativity and Common Sense (Dover Books, 1980) and in another, Assumption and Myth in Physical Theory (Cambridge University Press, 1967). On the astrophysics, there are excellent books by Robert Wall, Space Time and Gravity: Theory of the "Big Bang" and Black Holes (University of Chicago Press, 1977), and by Roman and Hannelore Sexl, White Dwarfs and Black Holes (Academic Press, 1979).

The plan of the talk is the following. I will give you an introduction to General Relativity by adding gravity to special relativity through Einstein's Principle of Equivalence. This is the historical approach I mentioned. Then I will discuss some recent experiments which have measured the relativistic effects on clocks. This include experiments with aircraft and lasers in which Len Cutler and I collaborated with some of the students and staff at Maryland, with the support of the Navy and Air Force, and, very briefly, the rocket probe experiment with a hydrogen maser and microwave frequency detection, which Bob Vessot and Marty Levine have done with the support of NASA. Finally, I will talk about the influence of these effects in some actual systems: the NAVSTAR/Global Positioning System, the LASSO (Laser Synchronization from Stationary Orbit) experiment, and a technique called the Shuttle Time and Frequency Transfer (STIFT), which some of us are planning and hoping to persuade NASA to develop. The relativistic effects on clocks transported by air craft will also be discussed.

#### REVIEW OF SPECIAL RELATIVITY

Figure 1 shows Einstein in his study at the age of about 40, several years after he completed General Relativity. (Some of us take great solace from the disorderliness of his shelves.) Einstein began to think about relativity when he was 16 years old. Figure 2 shows him at age 16 in a classroom in Aarau, Switzerland (he is on the far right). He began to think along the lines of: "What would happen if I could catch up with a beam of light? Suppose I were looking at a mirror and could run with the speed of light, what would I see?" At his last lecture in Princeton in 1954, before he died in 1955, I was privileged



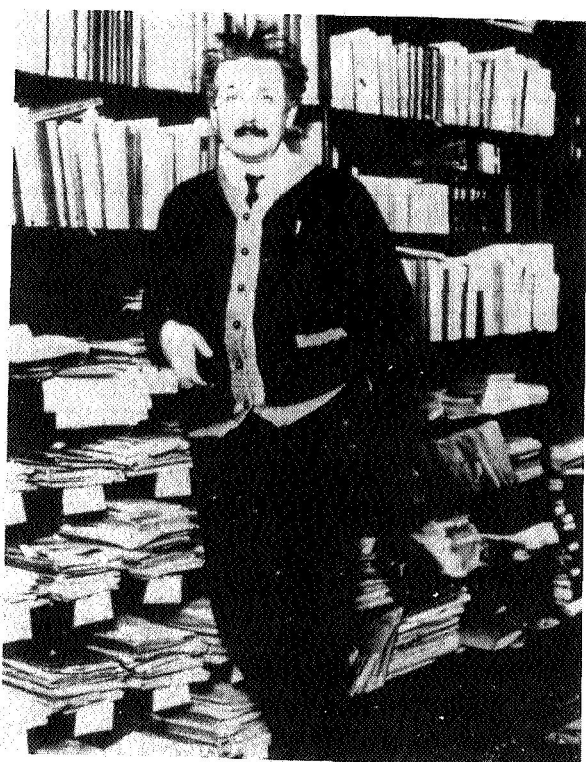


Figure 1

present. But Maxwell's theory doesn't allow that. Therefore, you can never catch up with light. No matter how fast you move, it recedes with the speed  $c \approx 3 \times 10^8$  m/sec. This was one of the real clues to his realization at the age of 26, at the Patent Office in Bern, Switzerland (Figure 3), that time is not absolute, and that this is the key to the question: How do you reconcile the classical Principle of Relativity, that any inertial observer should formulate in the same way the laws of physics, with the notion that the speed of light should be the same for all inertial observers?

Einstein wanted to have this restricted Principle of Relativity (restricted, that is, to inertial observers) include all of physics, not just mechanical physics: electro-magnetism and everything else. He also wanted to say that the velocity of light should be the same for all observers independent of the speed of the source. Now these requirements seem incompatible, because, if you imagine two space shuttles going by each other (Figure 4), each with a light source in the center of its bay, which emits beams of light, forward and backward, A would want to see the two waves spreading out with the velocity  $c$  in each direction. But then A would observe, from his point of view, that



Figure 2

to be present when he reminisced about some of these things. He mentioned that his independent study of Maxwell's Electromagnetic Theory as an undergraduate gave him the answer: that if you could catch up with a beam of light, you would see a static electric field and a static magnetic field at right angles to each other, with no charges and no currents



Figure 3

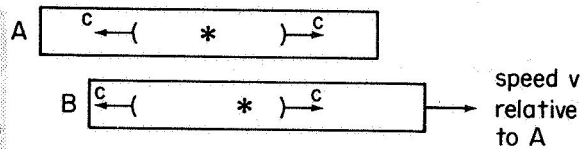


Figure 4

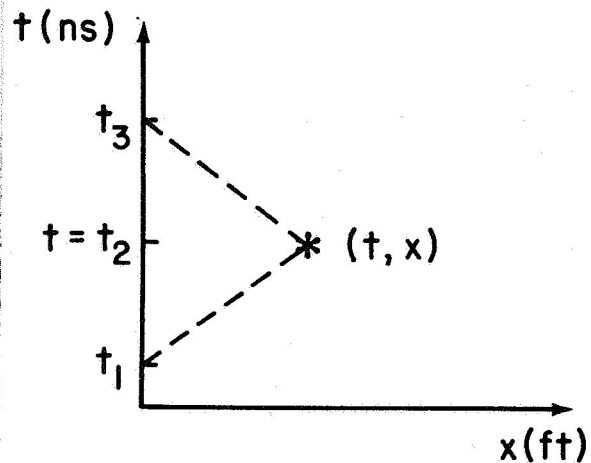


Figure 5

in B's system the light going forward would be travelling, with respect to B, with a smaller velocity than the light going backward. But B ought to be able to maintain the same point of view as A! How do you reconcile these things? Well, in 1905, at the age of 26, according to Hoffman, Einstein sat bolt upright in bed one morning, after having pondered these matters for ten years, with the realization that time is not absolute; that the simultaneity of separated events is relative to the inertial observer. This was the key to reconciling this whole thing. It has had profound consequences for all of physics. Let's formulate these ideas in terms of Minkowski space-time diagrams, and the so-called k-calculus.

In Figure 5 time is plotted vertically in units of nanoseconds, and distance horizontally in units of 30 centimeters, so that a light pulse has a slope of  $45^\circ$ . The dashed line is the worldline of a light pulse that would be sent out and reflected back from some event. Events are the raw materials of relativity: the time and place where something happens. If you send the light pulse out at a certain time,  $t_1$ , and get the pulse back at a time,  $t_3$ , then you would say you'd be sending out at  $t_1 = t - x/c$ , and getting it back at  $t_3 = t + x/c$ , where  $x$  is the position coordinate and  $t$  is the time coordinate of the reflection event. The time of reflection for you is naturally taken as midway between the emission and reception events,

$$t = t_1 + \frac{1}{2} (t_3 - t_1) = t_1 + \frac{1}{2} t_3 - \frac{1}{2} t_1 = \frac{1}{2} (t_1 + t_3) .$$

This is Einstein's original prescription for defining time at a distance when comparing clocks which are not adjacent to one another, which he gave in 1905 in his paper on restricted relativity. You get the distance of an event by taking the difference between the emission and reception times and multiplying by the speed of light and dividing by 2:

$$x = (t_3 - t_1) c/2 .$$

This is the basis for all the laser ranging measurements, including the ranging to corner reflectors on the moon<sup>3</sup>, whose motion has been monitored since 1969 with an accuracy of ten centimeters or so. It turns out that this method of comparing time between distant clocks is not only conceptually very clear, but it's practically the best way, the most accurate way, of comparing distant clocks which we know at the present time.

Modern observers now would be equipped with atomic clocks, short pulse lasers, fast photo detectors, and event timers to measure the epoch of arrival of light pulses. Let's consider two such observers, A and B, B moving with some relative velocity with respect to A, as shown in Figure 6. A sends out pulses with the separation T between them, and it's clear that they will be received by B with the separation kT, because of his motion. It is very easy (See Ref. 1) to show that k, this relativistic Doppler factor, is

$$k = \left[ \frac{1 + v/c}{1 - v/c} \right]^{1/2}$$

Now, how would A define his axis of simultaneity? (Refer to Figure 6) He would send out a pulse and get it reflected back. If it is sent out at the same time before his origin event as the time he

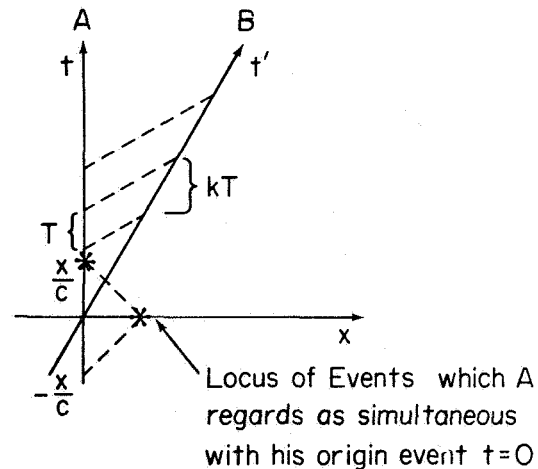


Figure 6

<sup>3</sup> C. O. Alley, "Apollo 11 Laser Ranging Retro-Reflector (LR<sup>3</sup>) Experiment: One Researcher's Personal Account", in Adventures in Experimental Physics, edited by B. Maglich, α 1972.

gets it back after his origin event, he would say that the event is simultaneous with his origin event. This procedure defines his X axis, the locus of events which he regards as simultaneous with his origin event. B can do the same thing. But both A and B measure the same speed of light, represented by the dashed lines in Figure 7, so that when B sends out his pulse and gets it back the same time before his origin event (taken to be the same as A's) as afterward, the reflection must occur as shown in Figure 7. This procedure defines a tilted space axis, which is B's locus of events which are simultaneous with respect to his origin event. So, B's time axis is tilted with respect to A's time axis, and his space axis is tilted with respect to A's space axis. This is the famous Minkowski diagram. Hermann Minkowski was one of Einstein's teachers at the technical university in Zurich, who was very negatively impressed with Einstein as a student, but later came to recognize his great accomplishments. It was Minkowski who contributed the space-time geometry to the physics of relativity that Einstein had developed.

We've had observers A and B, now suppose we have C. If C is moving to the left then his axis of simultaneity is tilted down, as shown in Figure 8. The several observers will register different relative times for two events. Consider the events, labelled 1 and 2 in Figure 9. Then it's clear that A would regard these as occurring at the same time since they're on his axis of simultaneity. But for B, he has to project over parallel to his axis of

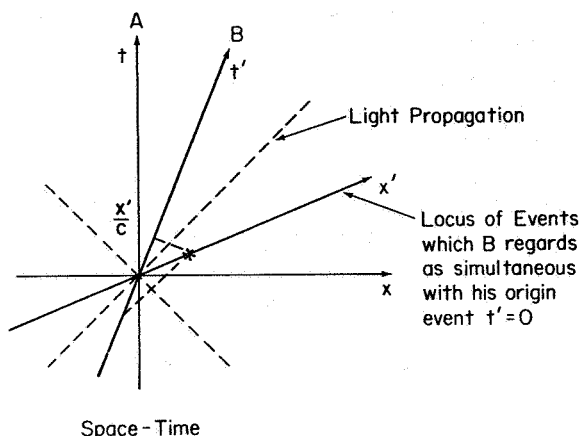


Figure 7

Minkowski's Absolute Space-Time (1907)

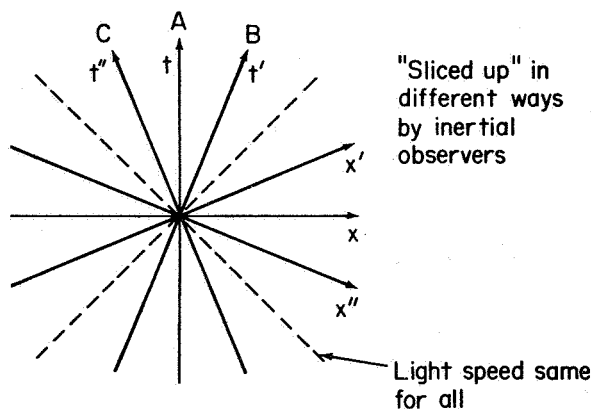


Figure 8

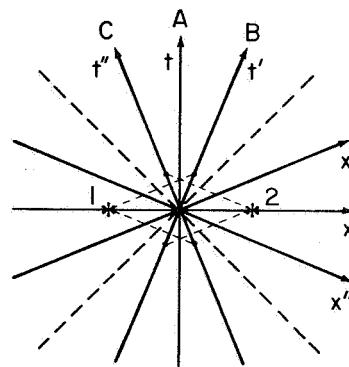


Figure 9

simultaneity and it is clear that Event 2 occurs before Event 1, according to B's time. C must project parallel to his axis of simultaneity and he will conclude that Event 1 occurs before Event 2. So they don't agree on which occurs first. They also don't agree on the magnitude of the time interval between two events. They won't agree either on the distance interval between two events. But Minkowski showed that they do agree on something! What they agree on is the so-called invariant interval,  $\Delta s$ , which is given by:

$$(\Delta s)^2 = c^2(\Delta t)^2 - (\Delta x)^2 \quad (A)$$

$$= c^2(\Delta t')^2 - (\Delta x')^2 \quad (B)$$

$$= c^2(\Delta t'')^2 - (\Delta x'')^2 \quad (C)$$

where unprimed, primed, and double-primed refer to A, B, and C respectively. They all get the same value when they make this combination of time and space intervals. The quantity  $\Delta s$  is invariant with respect to a change of inertial observers with their respective time and space coordinates. It's a very important result. It forms the basis for Einstein's whole development of gravity as curved space-time.

Einstein was often tempted to change the name of the theory of relativity to the theory of invariance because it wasn't so much, in his view, the way different observers see things in relative fashion, but what is unchanged for the various observers. But that suggested change of name never caught on. It is not hard to demonstrate the invariance of the interval. Because of limited time, I'm not going to do it. It can be done in only a few algebraic steps using the k-calculus and space-time diagrams (See Ref. 1). You don't have to introduce Lorentz transformations, and other complications to prove it.

Here's how Minkowski described his result in a talk in 1908:

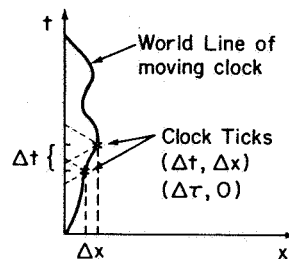
"The views of space and time which I wish to lay before you have sprung from the soil of experimental physics and therein lies their strength. Henceforth, space by itself and time by itself are doomed to fade away into mere shadows and only a kind of union of the two will preserve an independent reality."

He's talking about his slicing up of space-time with the tilted axes in Figure 8. I think of the axes tilting for different observers like the blades of a pair of scissors pivoted at the origin.

Now we have all we need in order to deduce the effect of motion on clocks. Consider Figure 10, which shows the worldline of a moving clock with the events corresponding to a couple of ticks on the clock in the

space-time diagram for some inertial observer. Between the two ticks, the inertial observer will say there's a certain interval of time,  $\Delta t$ , which we will call the coordinate time interval. The moving observer, of course, will record the interval between his own ticks and we will call that the interval of proper time,  $\Delta \tau$ . For the coordinate observer there's also a space interval between these two ticks: the clock is moving. But for the clock itself there is no spacial difference because the clock is always at the origin of its own instantaneous coordinates. So, in terms of this notion of proper time, we can deduce the difference between it and coordinate time by appealing to the invariance of the interval.

#### The Effect of Motion on Clocks



Reading of moving clock is its own time, Proper Time. Denote by  $\tau$

Figure 10

$$\Delta s^2 = c^2(\Delta t)^2 - (\Delta x)^2 = c^2(\Delta \tau)^2 - (\Delta x')^2$$

where the prime now refers to the moving clock. But we've agreed to identify  $\Delta \tau$  with  $\Delta \tau$ , the proper time interval, and we've agreed that  $\Delta x' = 0$ , so if we substitute that into the equation, and further note that  $\Delta x = v \Delta t$  where  $v$  is the instantaneous velocity, we have

$$(\Delta s)^2 = c^2(\Delta \tau)^2 - (\Delta x')^2 = (c^2 \Delta t)^2 - (\Delta x)^2 = c^2(\Delta t)^2 - (v \Delta t)^2$$

$$(\Delta \tau)^2 = (1 - v^2/c^2) (\Delta t)^2$$

$$\Delta \tau = [1 - v^2/c^2]^{1/2} \Delta t$$

proper time interval	coordinate time interval
----------------------------	--------------------------------

This famous equation, of course, is one of the basic equations that we will be dealing with. If we consider two clocks, A and B, which are moving along different paths in space-time, as shown in Figure 11, the elapsed proper time for each will be different. "Your time is not my time." If we synchronize the clocks when they are together and they then go on different paths and rejoin, one must evaluate an integral to get the elapsed proper time for each clock with respect to the coordinate time for some inertial observer.

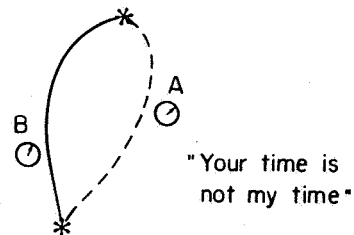


Figure 11

$$\tau_A(\text{final}) - \tau_A(\text{initial}) = \int (1 - v_A^2 / c^2)^{1/2} dt$$

$$\tau_B(\text{final}) - \tau_B(\text{initial}) = \int (1 - v_B^2 / c^2)^{1/2} dt$$

And since  $v_A^2$  will be different from  $v_B^2$  over the paths, these are not equal. There's a route dependence for proper time.

Einstein recognized these implications for clocks in 1905, and he actually made a prediction and suggested an experiment. He said that a clock (excluding one whose rate depends on the local value of the apparent acceleration of gravity, like a pendulum clock) at the Equator will run slow with respect to a similar clock at the Pole, because of the surface velocity produced by the earth's rotation, as shown in Figure 12. If you put in the value 0.46 kilometer per second for the equatorial

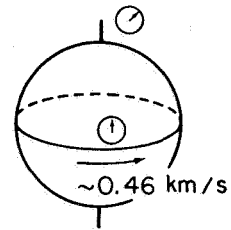


Figure 12

surface velocity, you get 102 nanoseconds per day, according to the time dilation equation for the difference in rate between an equatorial clock and a polar clock. If one could have done that experiment in 1905 -- if sufficiently stable clocks had existed then -- a different result would have been obtained than he predicted: a null result! His 1905 prediction ignores the effect of gravity. It was to be two years before he discovered the effect of gravity on time as a consequence of his famous Principle of Equivalence. I will come back to this question and describe an experiment we've done recently transporting clocks from Washington, D.C. to Thule, Greenland and back.

I'd like to quote from the Presidential Address at the American Association for the Advancement of Science in 1911 by Professor W. F. Magie of Princeton University.

"I do not believe that there is any man now living, who can assert, with truth, that he can conceive of time, which is a function of velocity."

That was six years after Einstein's paper of 1905 by which time most of the leading physicists had accepted his ideas. But to this day, there are people who do not believe that clocks behave in this fashion.

#### INCLUSION OF GRAVITY: THE PRINCIPLE OF EQUIVALENCE

Let me now turn to gravity. How does gravity get into the relativity picture? This is an excerpt from an essay that Einstein wrote in 1919 that was published in the New York Times when his papers began to be edited in 1972 (he was recalling what he was doing in 1907);

"At that point there came to me the happiest thought of my life in the following form: Just as in the case where an electric field is induced by electromagnetic induction, the gravitational field similarly has only a relative existence. Thus, for an observer in free fall from the roof of a house, there exists, during his fall, no gravitational field, at least not in his immediate vicinity. If the observer releases any objects, they will remain relative to him in a state of rest or in a state of uniform motion independent of their particular chemical and physical nature. The observer is therefore justified in considering his state as one of rest."

This is Einstein's own statement of the Principle of Equivalence between an accelerated system and a system in a gravitational field.

There is a story, probably apocryphal, that while Einstein was at the Patent Office in Bern, a workman fell off of the roof of a house and reported that his tools fell along with him. They all landed in bushes, and so he survived to tell the tale, thereby influencing Einstein. But I think that's really not true.

In a system falling freely under the influence of gravity, there is no local gravitational field. Of course, we're very familiar with this now, from the space flights of the Apollo Program, the Skylab, Space Shuttle and the Soviet Soyuz spacecraft, and so on. Objects that are put out in front of an astronaut will stay there, as shown in the upper left part of Figure 13. I'm told that on the Skylab, some of the astronauts made a basketball-size drop of water, which would just stay there, held together by surface tension (and of course oscillating just a bit). Consider now, in a region where gravity is not present, an accelerated lab, an "Aclab", which is pushed by a rocket engine. Then, if you release objects of whatever composition they would seem to approach the floor in the same way, equivalent to what you would see in a gravitational lab, "Gravlab", in the presence of a gravitational field, for example, on the surface of the earth. There have been many experiments showing that all objects, whatever their composition, fall (in a vacuum) with the same

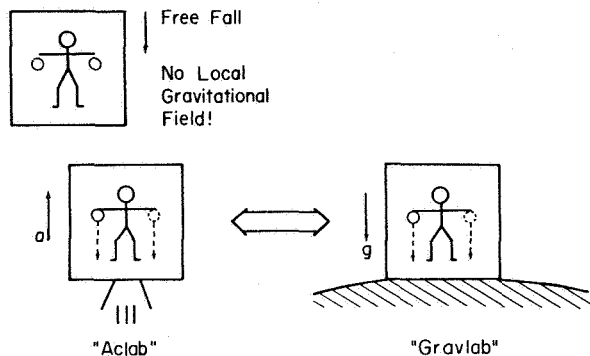


Figure 13



acceleration. In technical language, one says that the inertial mass is the same as the gravitational mass. In recent years, this has been shown by R. H. Dicke<sup>4</sup> and by V. Braginsky<sup>5</sup> to be valid to parts in  $10^{11}$  to  $10^{12}$ . Lunar laser ranging has shown this also to be true for the earth and moon falling to the sun, with the same precision<sup>6</sup>. Einstein's idea was not to stick with the mechanical properties only but to ask what are the consequences of the Principle of Equivalence for other parts of physics, in particular for electromagnetic phenomena, which includes light. Suppose you had light sent across this "Aclab", as shown in Figure 14. Think of it as rows of marching soldiers corresponding to the wavefronts. The lab is accelerated, so it would appear inside it as though the light beam were being bent. If the equivalence idea is true then in a gravitational field, you would see this bending of light, and the marching soldier analogy tells you that the soldiers at the top would have to move faster than those at the bottom in order to make the curve. So you predict that light paths should be bent by a gravitational field, and that the speed of light increases with the height. There's no mathematics in this deduction at all, just physical ideas.

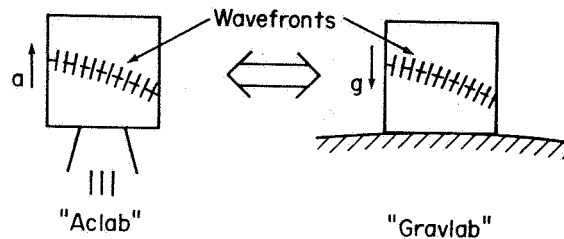


Figure 14

There's a little mathematics needed to deduce the properties of clocks in a gravitational field. Suppose you have this "Aclab" with a low clock on the floor and a high clock on the ceiling and you are exchanging laser pulses between them, as displayed in Figure 15. We can calculate what would happen in this situation, and I'll do it in just a moment. If the "Gravlab" is equivalent to the "Aclab", then what we

<sup>4</sup> P. G. Roll, R. Krotkov, and R. H. Dicke, "The Equivalence of Inertial and Passive Gravitational Mass," Ann. Phys. (U.S.A.), Vol. 26, pp. 442 - 517 (1964).

<sup>5</sup> V. B. Braginsky and V. I. Panov, "Verification of the Equivalence of Inertial and Gravitational Mass," Zh. Eksp. & Teor. Fiz., Vol. 61, pp. 873 - 879 (1971). English translation in Sov. Physics - JETP Lett., Vol. 10, pp 80 - 283 (1972).

<sup>6</sup> J. G. Williams, R. H. Dicke, P. L. Bender, C. O. Alley, W. E. Carter, D. G. Currie, D. H. Eckhardt, J. E. Faller, W. M. Kaula, J. D. Mullholland, H. H. Plotkin, S. K. Poultney, P. J. Shelus, E. C. Silverberg, W. S. Sinclair, M. A. Slade, and D. T. Wilkinson, "A New Test of the Equivalence Principle from Lunar Laser Ranging", Physical Review Letters, Vol. 36, pp 551 - 554, (1976).

calculate in the "Aclab" should apply for the "Gravlab", and we will see that the high clocks are predicted to run fast with respect to the low clocks. One can deduce this result easily by using the ideas of the k-calculus which we introduced earlier.

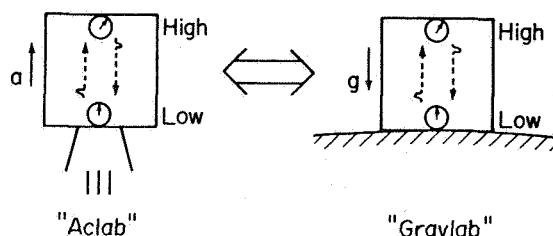


Figure 15

It is not true that you cannot consider accelerated motions in special relativity. Let us consider them. The left of Figure 16 shows the curved worldlines plotted in an inertial system Minkowski diagram of the low and high clocks of Figure 15 in the "Aclab". Let us send light pulses from the low clock to the high clock, as shown on the right of Figure 16. There will be a stretching factor  $kT$  just as we have discussed

Comparison of Clocks in "Aclab"

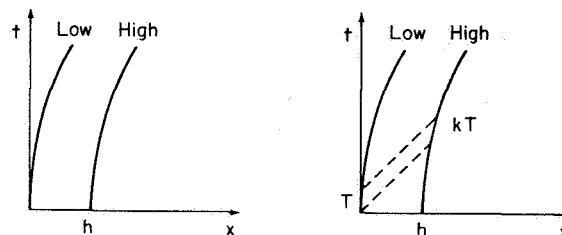


Figure 16

earlier, because there is some velocity of the high clock at the time of reception. Even though the high clock started off with zero velocity with respect to the inertial system, the acceleration produces some velocity according to  $v = at$ . If we substitute for  $v$  in the equation, and make a few manipulations, we find for  $k$

$$k = [(1 + v/c) / (1 - v/c)]^{1/2} = [(1 + at/c) / (1 - at/c)]^{1/2} \\ \approx (1 + 2at/c)^{1/2}$$

But  $t = h/c$  where  $h$  is the separation of the clocks. Therefore,

$$k = (1 + 2ah/c^2)^{1/2}$$

But by the Principle of Equivalence, the acceleration of gravity  $g$  is equivalent to  $a$ , so we substitute  $g$  for  $a$  and get

$$k = (1 + 2gh/c^2)^{1/2}$$

Then we remember that, according to Newtonian physics, the gravitational potential difference  $\phi$  is  $gh$ , so we have

$$k = (1 + 2\phi/c^2)^{1/2}$$

In the "Gravlab", as shown in Figure 17, the worldlines of the low and the high clocks will be straight, since they are not moving. However, if we send light pulses from the low clock to the high clock, we would still get a stretching factor given by the above equation because of the Principle of Equivalence. This straightened space-time diagram exhibits the curvature of space-time, in this case, the curvature of time, that is at the heart of Einstein's theory of gravity, General Relativity. Let's look a little more at that.

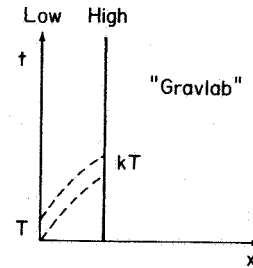


Figure 17

To compare a low clock with a high clock in a gravitational field, we can use the same Einstein prescription we discussed earlier: send out a light pulse, get it reflected back, and identify the mid-point between sending and receiving with the time of reflection, as shown in Figure 18. These two events are simultaneous for the low observer. A little bit later, the low observer could do the same thing and identify the mid-point time with the reflection time as being simultaneous. But what we've just seen is that the elapsed time for the high clock,  $\Delta\tau$ , is going to be different from the elapsed time for the low clock,  $\Delta t$ , defined this way:  $\Delta\tau \neq \Delta t$ .

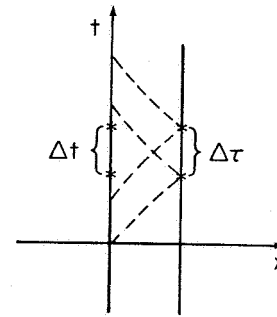


Figure 18

Now, how to incorporate this gravitational effect into the metric structure that Minkowski had proposed, the invariant interval? Einstein's idea was to retain the identification of  $(\Delta s)^2 \equiv c^2(\Delta\tau)^2$ ,  $\Delta\tau$  being the proper time interval, and to insert a metric coefficient in the invariant interval expression in order to make things come out the way we have just calculated for a static situation. So here is the presence of a metric coefficient in this invariant interval which is a manifestation of time curvature.

$$(\Delta s)^2 = (1 + 2\phi/c^2) c^2(\Delta t)^2 - (\Delta x)^2 = c^2(\Delta\tau)^2$$

metric  
coefficient

For the stationary high clock, we have then that

$$\Delta\tau = (1 + 2\phi/c^2)^{1/2} \Delta t$$

We can get the speed of light by noting that for light pulses, the two events lying along a light line,  $(\Delta s)^2$  is going to be 0, so if you put this equal to 0, we can solve for  $\Delta x/\Delta t$ , the coordinate speed of light,

and we get

$$\frac{\Delta x}{\Delta t} = (1 + 2\phi/c^2)^{1/2} c$$

This shows that the higher you go, the faster the light must move, as we had concluded already. We can now ask what happens to a moving clock. Let's bring in three dimensions, and include  $\Delta x$ ,  $\Delta y$  and  $\Delta z$  in the metric,

$$(\Delta s)^2 = c^2(\Delta \tau)^2 = (1 + 2\phi/c^2) c^2(\Delta t)^2 - (\Delta x)^2 - (\Delta y)^2 - (\Delta z)^2$$

The sum of the squares of these is just  $v^2(\Delta t)^2$ . Making that substitution, and carrying out a few lines of algebra,

$$c^2(\Delta \tau)^2 = (1 + 2\phi/c^2) c^2(\Delta t)^2 - v^2(\Delta t)^2$$

$$(\Delta \tau)^2 = (1 + 2\phi/c^2 - v^2/c^2) (\Delta t)^2$$

we get that in this gravitational case the relationship between the proper time interval and the coordinate time interval is given by

$$\begin{array}{ll} \Delta \tau &= (1 + 2\phi/c^2 - v^2/c^2)^{1/2} \Delta t \\ \text{proper} & \text{coordinate} \\ \text{time} & \text{time} \\ \text{interval} & \text{interval} \end{array}$$

We can expand this when  $\phi/c^2$  and  $v^2/c^2$  are small, which is certainly the case on the surface of the earth, and we get

$$\Delta \tau = (1 + \phi/c^2 - v^2/2c^2) \Delta t$$

One can synchronize clocks to the coordinate time (which we are taking as the time kept by clocks on the surface of the earth) by using the laser pulse technique illustrated in Figure 18. The light line is drawn slightly curved in Figure 18 to illustrate the speed of light changing with altitude. To make the high clock run at the same rate as the low clock, one must physically adjust it (See the later discussion on the GPS).

The above equation is the basic one needed in order to understand these effects of General Relativity on proper time. I'd like to give an analogy to the curved surface of the earth in Figure 19. Here we have a coordinate increment of longitude, call it  $\Delta \alpha$ , with  $\Delta \alpha$  being one degree. You know that at the equator the actual proper distance on the earth is about 112 kilometers, whereas, if we go to a latitude of  $45^\circ$  and consider the same longitude interval, it's only about 79 kilometers. There is a proper

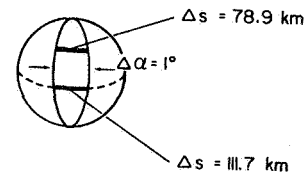


Figure 19

distance interval  $\Delta s$  which is related to the coordinate distance interval  $\Delta \alpha$  by the following equation

$$\Delta s = R \cos \beta \Delta \alpha$$

Proper	Coordinate
Distance	Distance
Interval	Interval

and there is a coefficient, called the metric coefficient,  $R \cos \beta$ , where  $\beta$  is the latitude and  $R$  is the radius of the earth. This is an excellent analogy to the situation in curved space-time. There, we have, when the clock is not moving

$$(\Delta s)^2 = c^2 \Delta \tau^2 = (1 + 2\phi/c^2) c^2 (\Delta t)^2 = g_{00} c^2 (\Delta t)^2$$

$$\text{or} \quad \Delta s = g_{00}^{1/2} c \Delta t$$

where  $g_{00}$  is the name given by relativists to the metric coefficient  $(1 + 2\phi/c^2)$ . The proper time interval  $\Delta \tau$  is related to the coordinate time interval  $\Delta t$  in this way for stationary clocks:

$$\Delta \tau = (1 + 2\phi/c^2)^{1/2} \Delta t = g_{00}^{1/2} \Delta t$$

One can often establish on two-dimensional curved surfaces a metric formula. In the case of the sphere when we consider both latitude and longitude we get

$$(\Delta s)^2 = R^2 \cos^2 \beta (\Delta \alpha)^2 + R^2 (\Delta \beta)^2$$

For a different choice of coordinates on a two-dimensional surface, as shown in Figure 20, there can be cross-product terms

$$\begin{aligned} (\Delta s)^2 = & g_{11} (\Delta x_1)^2 + g_{12} \Delta x_1 \Delta x_2 \\ & + g_{21} \Delta x_2 \Delta x_1 + g_{22} (\Delta x_2)^2 \end{aligned}$$

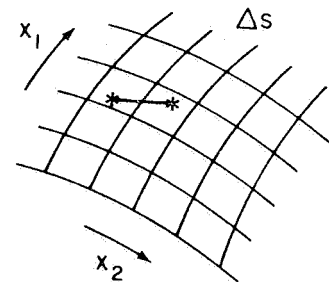


Figure 20

The great mathematician Gauss and his successors Riemann and Levi-Civita and many other differential geometers, have extended this to any number of dimensions and have written the proper interval of distance as a quadratic form with metric coefficients, which are always called  $g$  now, because of their application to gravity by Einstein in his curved space-time.

$$\begin{aligned}
 (\Delta s)^2 &= g_{11}(\Delta x_1)^2 + g_{12}\Delta x_1\Delta x_2 + \dots \\
 &= g_{21}\Delta x_2\Delta x_1 + g_{22}(\Delta x_2)^2 + \dots \\
 &= g_{31}\Delta x_3\Delta x_1 + \dots \\
 &\vdots
 \end{aligned}$$

Unfortunately, we cannot go into the mathematics of differential geometry for lack of time. It is highly interesting and enlightening and very powerful for calculations, but in many ways it has obscured the physics of General Relativity.

Einstein got these ideas about including metric coefficients in the expression for  $(\Delta s)^2$  to describe gravity around about 1911/1912. During the years 1912-1914, he worked with his long-time friend, the mathematician Marcel Grossmann, to develop the General Theory of Relativity. They wanted to allow curvature of space as well as curvature of time, and they proposed field equations to describe how matter will curve space and time. That is, how the metric coefficients will be determined by the distribution of matter. Matter curves space-time. Einstein proposed that objects would move in this curved space-time along geodesics: the shortest path or the extremal path. A geodesic between two points on the surface of the earth is the shortest path -- the arc of a great circle. In the case of curved space-time, if you imagine a clock attached to a particle which is moving, the motion will be such that the elapsed proper time will be a maximum. Bertrand Russell wittily called this the "Principle of Cosmic Laziness".

There is the prescription: "Curved space-time tells objects how to move; matter tells space-time how to curve." This is the way Professor John Wheeler likes to summarize General Relativity. There is no more Newtonian force. Objects move under the influence of gravity because of the way clocks behave. A clock will run faster the higher it is, and it will run slower the faster it moves. The primary curvature for slow speeds

and weak gravitational fields is the curvature of time, not the curvature of space, as you read in so many of the popular books. How can you represent this curvature of time? We can do it in terms of the diagram in Figure 21. Imagine the sun on the left, and plot the gravitational potential  $\phi$  of the sun, as a function of the distance  $r$  from its center (or, better, plot  $\phi/c^2$  since this combination occurs in the relation between proper time and coordinate time).

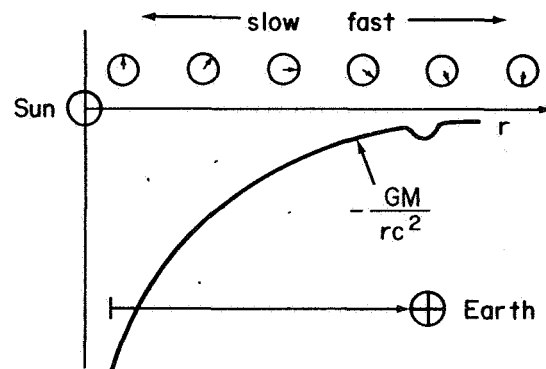


Figure 21

$$\frac{\phi}{c^2} = \frac{-GM_{\odot}}{R_{\odot} c^2} \left( \frac{R_{\odot}}{r} \right)$$

where  $G$  = Newtonian Gravitational Constant

$M_{\odot}$  = Mass of the Sun

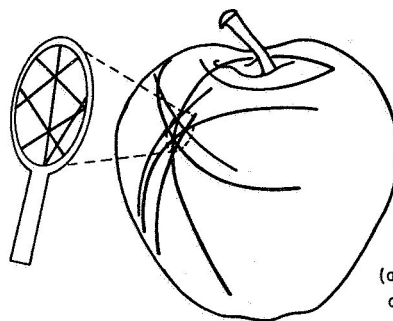
$R_{\odot}$  = Radius of the sun

This plot is often called the "potential well" of the sun. Its "depth" is  $GM_{\odot}/R_{\odot} c^2 \approx 2 \times 10^{-6}$ . The much smaller potential well of the earth is shown superimposed (in exaggerated form) on the curve for the sun. Its depth is  $GM_{\oplus}/R_{\oplus} c^2 \approx 7 \times 10^{-10}$  ( $M_{\oplus}$  = mass of the earth;  $R_{\oplus}$  = radius of the earth). With respect to a clock at a great distance (at the "top" of the potential well), a clock will run slower as it is placed deeper in the potential well.

To dramatize this effect, consider Figure 22 which is a drawing made by Herblock, the great cartoonist of the Washington Post, at the time of Einstein's death in 1955. Imagine that an observer at a great distance from the sun is observing events on earth. One hundred years on earth (for example, the time between Einstein's birth and his centennial celebration on March 14, 1979) would appear to this observer as 100 years plus 41 seconds: 29 seconds from the ascent from the earth up the potential well of the sun; two seconds from the potential well of the earth; and 15 seconds from the  $-v^2/2c^2$  effect of the earth's velocity around the sun.



Figure 22



(after Misner, Thorne, and Wheeler)

Figure 23

Wheeler likes to demonstrate the motion along geodesics in space-time by considering ants on an apple. Figure 23 is a sketch from the cover of the great book, Gravitation, by Misner, Thorne and Wheeler. Suppose you imagine ants that try to move as straight as they can locally (this is one way to define a geodesic). Since the surface of the apple is curved, they tend to move in curved paths, and this is analogous to the motion of objects in curved space-time. Locally, they try to go as straight as possible and they end up going in curves, which manifests itself in an acceleration, the acceleration of gravity. So his Principle of Equivalence gave the clue to Einstein: gravity is to be described by the metric coefficients in curved space-time, including not only the  $g_{00}$  coefficient, but all the other coefficients that could come in from the different products of  $\Delta t$ ,  $\Delta x$ ,  $\Delta y$ , and  $\Delta z$ .

$$\begin{aligned}
 (\Delta s)^2 = & g_{00} c^2 (\Delta t)^2 + g_{01} c \Delta t \Delta x + g_{02} c \Delta t \Delta y + g_{03} c \Delta t \Delta z \\
 & + g_{10} c \Delta t \Delta x + g_{11} (\Delta x)^2 + g_{12} \Delta x \Delta y + g_{13} \Delta x \Delta z \\
 & + g_{20} c \Delta t \Delta y + g_{21} \Delta y \Delta x + g_{22} (\Delta y)^2 + g_{23} \Delta y \Delta z \\
 & + g_{30} c \Delta t \Delta z + g_{31} \Delta z \Delta x + g_{32} \Delta z \Delta y + g_{33} (\Delta z)^2
 \end{aligned}$$

A certain symmetry is imposed

$$\begin{aligned}
 g_{10} &= g_{01} ; g_{20} = g_{02} ; g_{30} = g_{03} ; \\
 g_{12} &= g_{21} ; g_{13} = g_{31} ; g_{23} = g_{32}
 \end{aligned}$$

so that you end up with only ten metric coefficients which can be arrayed in this fashion.

$$g_{\mu\nu} = \begin{array}{cccc}
 g_{00} & g_{01} & g_{02} & g_{03} \\
 g_{10} & g_{11} & g_{12} & g_{13} \\
 g_{20} & g_{21} & g_{22} & g_{23} \\
 g_{30} & g_{31} & g_{32} & g_{33}
 \end{array}$$

This is the famous metric tensor; these  $g_{\mu\nu}$  are functions of space and time in general. Einstein wanted to allow any coordinates, not just inertial coordinates (inertial observers), but for an inertial observer (realizable locally by a freely falling laboratory), this array of metric coefficients reduces to a simple form

$$g_{\mu\nu} = \begin{array}{cccc}
 1 & 0 & 0 & 0 \\
 0 & -1 & 0 & 0 \\
 0 & 0 & -1 & 0 \\
 0 & 0 & 0 & -1
 \end{array} .$$

This represents the Minkowski metric that we have seen earlier:

$$(\Delta s)^2 = c^2 (\Delta t)^2 - (\Delta x)^2 - (\Delta y)^2 - (\Delta z)^2 .$$



When you make a change of coordinates, the metric coefficients are going to have to change also in order to keep  $\Delta s^2$  invariant. The metric coefficients play the role of generalized gravitational potentials. I wish there were more time to elaborate on these things.

#### SUMMARY OF GENERAL RELATIVITY

Einstein wrote the quadratic form that implies summation on repeated indices:  $\mu$  and  $\nu$  run from 0 to 3,

$$(\Delta s)^2 = g_{\mu\nu} \Delta x_\mu \Delta x_\nu .$$

invariant      metric  
interval      coefficients

The coefficients  $g_{\mu\nu}$  are to be obtained by solving the famous field equations which are shown here in symbolic form.

$$R_{\mu\nu} - \frac{1}{2} R g_{\mu\nu} = \frac{8 \pi G}{c^4} T_{\mu\nu}$$

Contracted	Curvature	$\frac{8 \pi G}{c^4}$	Stress
Riemann	Scalar		Energy
Curvature			Tensor
Tensor			

These are ten second order partial differential equations. They are non-linear in that they involve products of the first derivatives of the metric coefficients. The source term on the right-hand side  $T_{\mu\nu}$ , is the general stress energy tensor of matter; it includes the effects of matter, energy, and pressure, all of which produce gravitational fields. On the left-hand side are various curvatures from differential geometry involving first and second order partial derivatives with respect to time and space of the metric coefficients  $g_{\mu\nu}$ .  $R_{\mu\nu}$  is the contracted Riemann Curvature Tensor and  $R$  is the Curvature Scalar. In 1917, Karl Schwarzschild solved these equations and got the famous Schwarzschild metric, which I display here.

$$(\Delta s)^2 = \left(1 - \frac{2GM}{rc^2}\right) c^2 (\Delta t)^2 - \frac{(\Delta r)^2}{(1 - 2GM/rc^2)} - r^2 \cos^2 \beta (\Delta \alpha)^2 - r^2 (\Delta \beta)^2$$

$c^2 (\Delta \tau)^2$	Curvature	Curvature
for moving	of	of
objects	Time	Space

This is the metric that is to exist outside of an isolated spherical body of mass  $M$ . The coefficient  $g_{00}$  of the  $c^2 (\Delta t)^2$  term involves  $-GM/r$ , which is the Newtonian potential  $\phi$ . It describes the curvature of time as we have seen earlier. There's also a similar expression in the denominator of the  $(\Delta r)^2$  term, when one uses spherical coordinates as here. This describes the curvature of space. But, for

ordinary motion (that is, in weak gravitational fields, like on the earth, and for velocities much less than the speed of light), you can neglect the curvature of space. All of Newtonian physics follows from the curvature of time alone.

It is the Schwarzschild metric that leads to the famous concept of the black hole. This is a phrase coined by John Wheeler. Suppose you ask, <sup>2</sup> can <sup>2</sup> the coefficient of the  $c^2(\Delta t)^2$  term, the  $g_{00}$  coefficient, go to 0? Well, it can:

$$g_{00} = 1 - \frac{2GM}{rc^2} = 0$$

$$\text{for } r = \frac{2GM}{c^2}$$

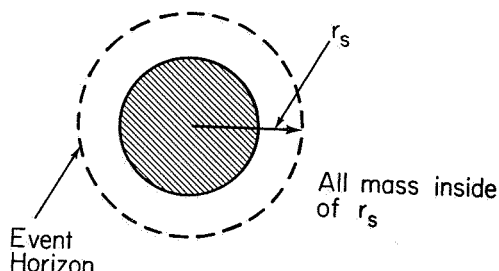


Figure 24

One calls this value of  $r$  the Schwarzschild Radius and often denotes it by  $r_s$ . You can calculate its value for various masses. In the case of the earth, it's about nine millimeters. In the case of the sun, it's three kilometers. Now suppose you could compress all of the mass of the sun into a sphere with a radius of less than three kilometers? Then you would have a very singular surface outside the mass, which is shown as a dashed line in Figure 24. The surface, often called the event horizon, has remarkable properties, because the coefficient  $g_{00}$  vanishes there. If you imagine watching a clock moving in towards the event horizon from a great distance, its time and motion would slow down and you would never see it get there. For this reason, the Russians call an object of this sort a frozen star, just because of the property that matter would fall in and seem to never get beyond the event horizon. You cannot get any information out from inside this event horizon. However, if you are riding in with some of the falling matter, and recording things in your proper time, it takes a finite proper time to get in and through the event horizon. If there is a supernova explosion and subsequent collapse of the central material to form a black hole, this can happen in a few milliseconds. Such collapses are, perhaps, potent sources of gravity waves, about which we will hear in the next talk.

I want to correct a widespread misconception about black holes: that they are all very, very dense. This is certainly the case for the examples of black holes with a solar mass or an earth mass as discussed above. Note, however, that the Schwarzschild radius  $r_s$  is proportional to the mass  $M$ , and that the density varies as  $M/r_s^3$ . Therefore, the density depends on mass as  $1/M^2$ . For a black hole with very large mass, the density can be very small. Figure 25 shows the galaxy M87 in the Virgo cluster. This is a weak exposure so that you can see this bright

jet coming out of the center unobscured by outer parts of the galaxy. There is some evidence, for example the high velocities of stars near the center of this galaxy, that suggests that there is a black hole of several billions of solar masses present there. The jet is probably associated with the rotation of that black hole; matter being converted into energy as it falls into the black hole, and somehow propelling the jet along the axes of rotation. There are many jets of this sort in galaxies. There may be a black hole in the center of our own galaxy. There's some evidence for it, but no time to discuss it here.



Figure 25

#### EXPERIMENTAL MEASUREMENTS OF RELATIVISTIC CLOCK EFFECTS

Let me now talk some about experiments very quickly. We have done experiments with aircraft and lasers to illustrate, measure and demonstrate these effects. My chief collaborator was Len Cutler who was the designer of the Hewlett-Packard 5061 Cesium atomic beam standards which we used. Bob Reisse<sup>7</sup> and Ralph Williams<sup>8</sup> did their theses as part of these experiments. There were many other participants at the University of Maryland and the Naval Observatory. Dr. Gernot Winkler, Director of the Time Services Division, very kindly lent the clocks and gave much, much support to these activities.

We were able to fly clocks in an airplane, suitably packaged so that they didn't suffer from environmental degradation of their performance. Figure 26 shows a schematic diagram of the flights. We could send light pulses up and get them reflected back from a lunar-type corner reflector on the plane, also registering the time of their arrival with the airplane clocks in just the way Einstein prescribed. We tracked the air craft with radar beams in order to have an independent knowledge of the position and velocity from which to calculate the proper time differences. We used minicomputers and event timers both on the ground and on the plane. There's no time to go into details; these have been discussed in other places<sup>1</sup>. The plane would fly for about 15 hours over the Chesapeake Bay from the Patuxent Naval Air Test Center in a racetrack pattern, taking about 20 minutes to go around a path shown

<sup>7</sup> R. A. Reisse, "The Effects of Gravitational Potential on Atomic Clocks as Observed with a Laser Pulse Time Transfer System," University of Maryland Ph.D. dissertation (May, 1976).

<sup>8</sup> R. E. Williams, "A Direct Measurement of the Relativistic Effects of Gravitational Potential on the Rates of Atomic Clocks Flown in an Aircraft," University of Maryland Ph.D. dissertation (May, 1976).

in Figure 27. We would accumulate, during one of these flights, a typical time difference of about 50 nanoseconds. These measurements were in good agreement with the proper time integral. The time difference between the airborne and ground clocks would be given by integrals of this sort.

$$\tau_A = \int_0^T \left( 1 + \frac{\phi_A}{c^2} - \frac{v_A^2}{2c^2} \right) dt$$

$$\tau_G = \int_0^T \left( 1 + \frac{\phi_G}{c^2} - \frac{v_G^2}{2c^2} \right) dt$$

$$\tau_A - \tau_G = \int_0^T \left( \frac{\phi_A - \phi_G}{c^2} - \frac{v_A^2 - v_G^2}{2c^2} \right) dt$$

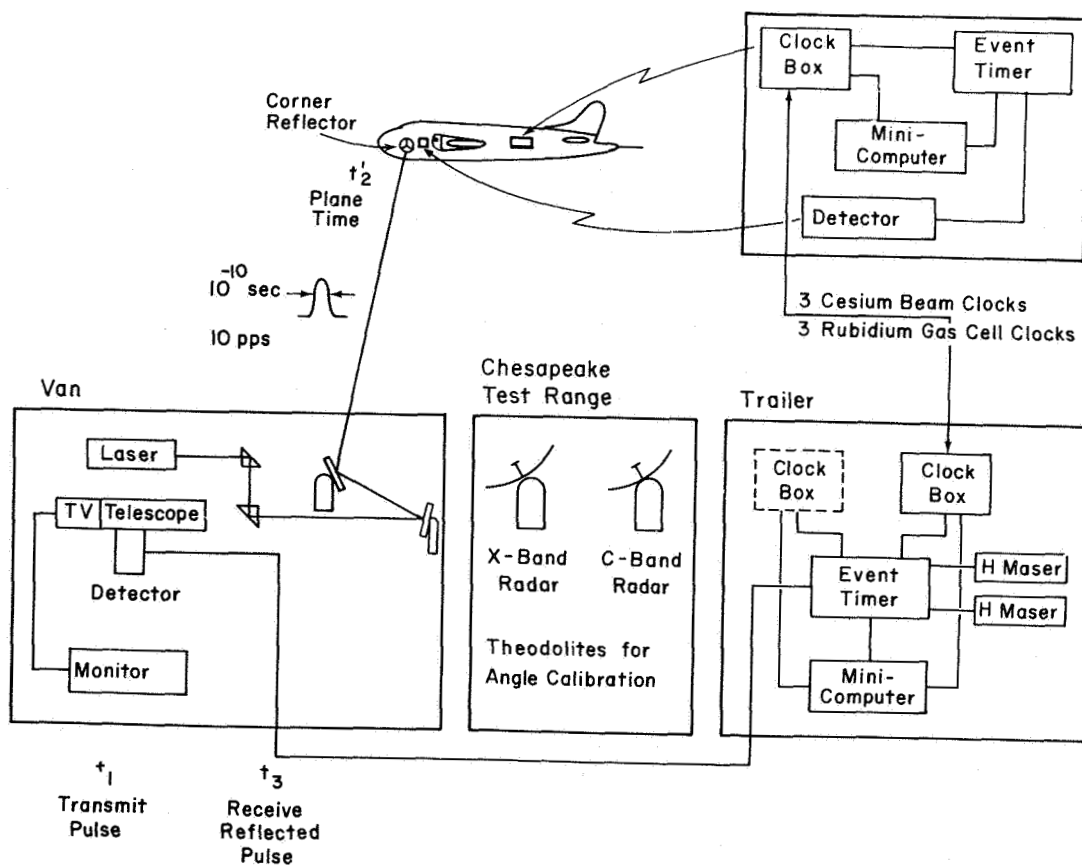


Figure 26

We allowed for higher terms in the earth's gravitational potential due to its oblate shape, and for the rotational effects of the earth. We evaluated the proper time integral in a reference frame centered on the earth which is non-rotating with respect to distant matter, as shown in Figure 28.

The clocks were modified in order to give the performance needed. Following suggestions by Len Cutler and others at Hewlett-Packard, we increased the beam current by a factor of 2, we added an integrating loop in the crystal control, and there was a proprietary modification of the beam tube (now standard on all high performance tubes). All in all, we could achieve stabilities over the 15 hours at a couple of parts in  $10^{14}$  with standard commercial clocks, as shown in Figure 29. We paid much attention to providing a stable environment for the clocks. Let us look at some pictures to show you the equipment and give you some feeling for the experiment.

Figure 30 is the plane which we used. Figure 31 shows it on the ground; the clocks were in the trailer, and the laser equipment was in the bus. Figure 32 is the detector on the plane behind one of the observation windows. Figure 33 shows the corner reflector outside the observation window. Figure 34 is the beam directing optics. Figure 35 shows the laser, below which is the 7.5 inch telescope which receives the reflected laser pulses. Both the detector and a closed circuit TV camera for guiding are coupled to it with a beam splitter. Figure 36 shows Len Cutler adjusting some of the six Cesium beam clocks. Figure 37 is the clock box that protected them from environmental changes. It contained magnetic shields, vibration isolators with near critical damping at a resonant frequency of several

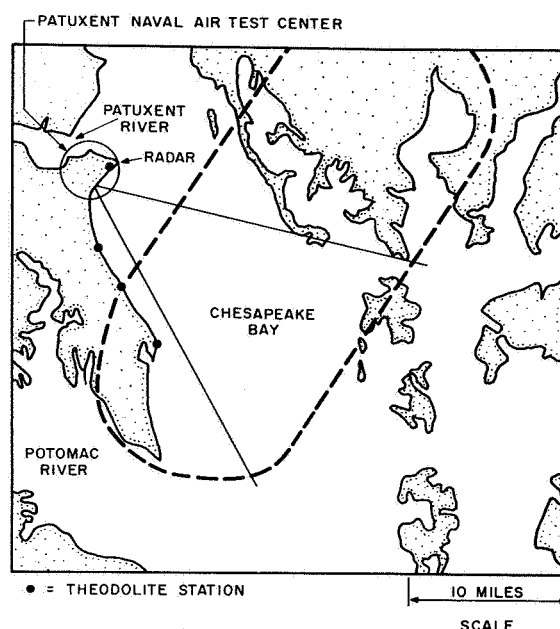


Figure 27

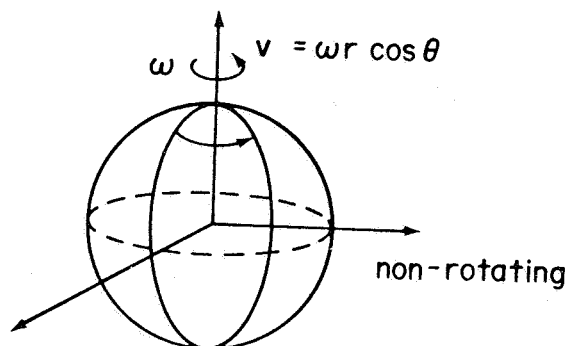


Figure 28



Figure 30

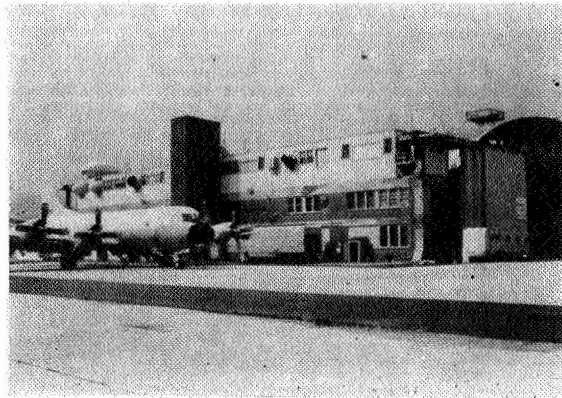


Figure 31

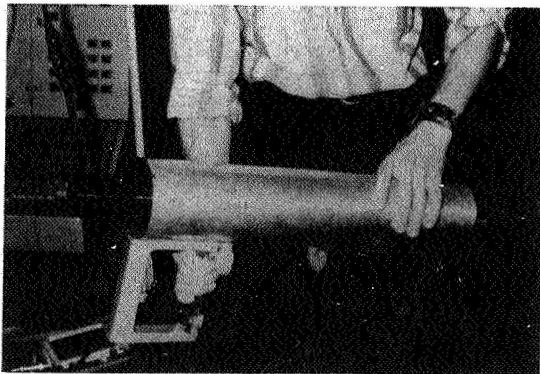


Figure 32

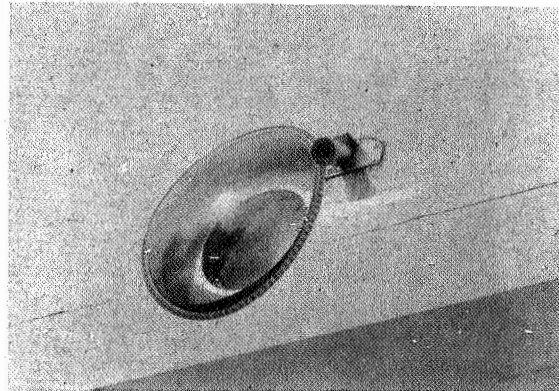


Figure 33

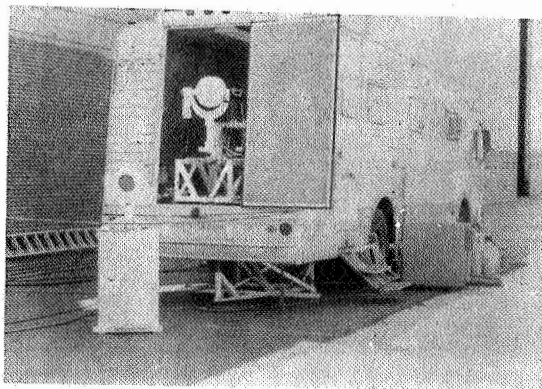


Figure 34

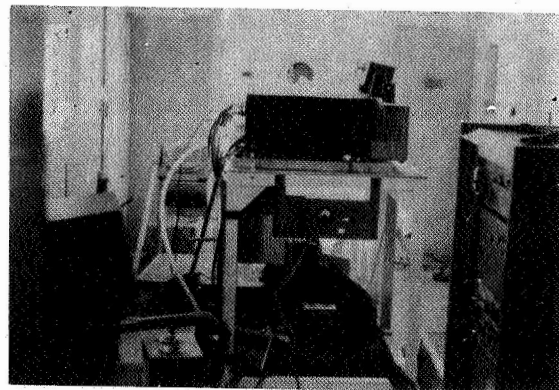


Figure 35

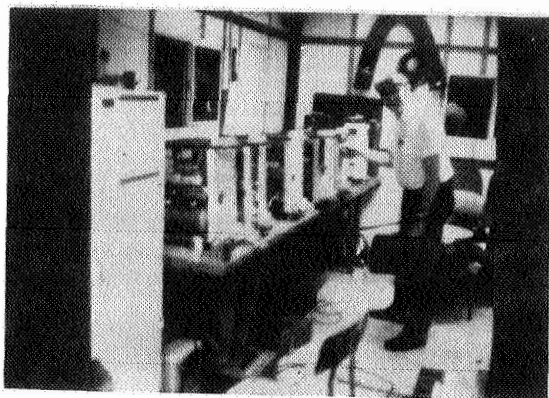


Figure 36

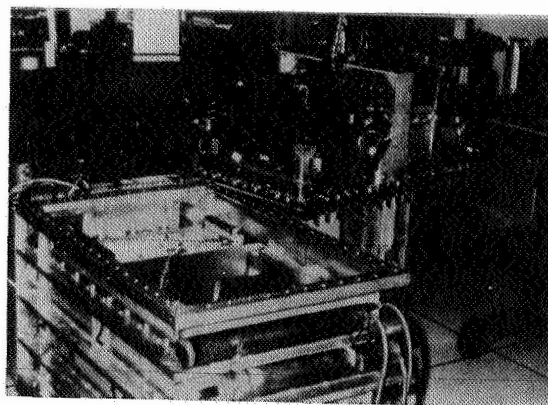


Figure 37

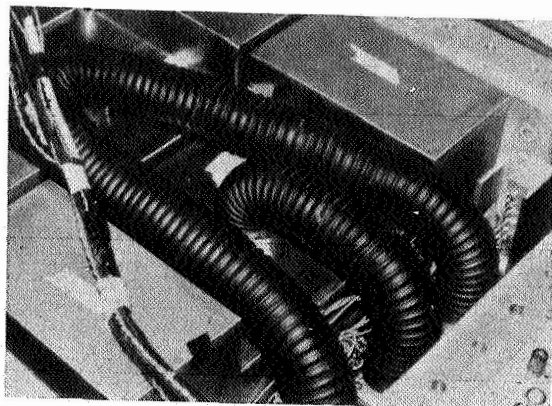


Figure 38

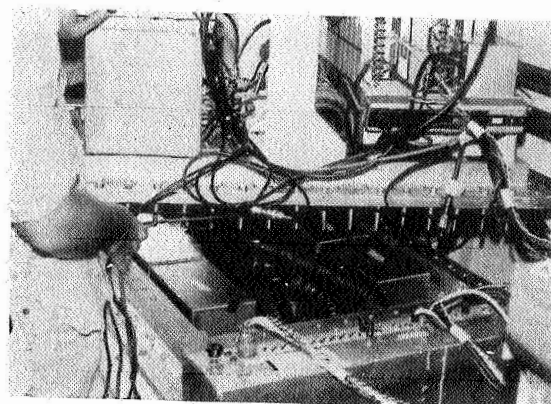


Figure 39

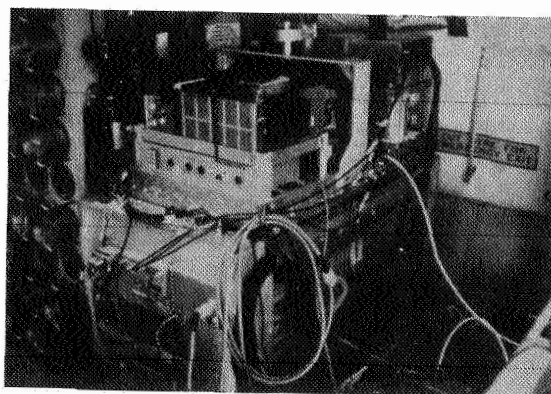


Figure 40

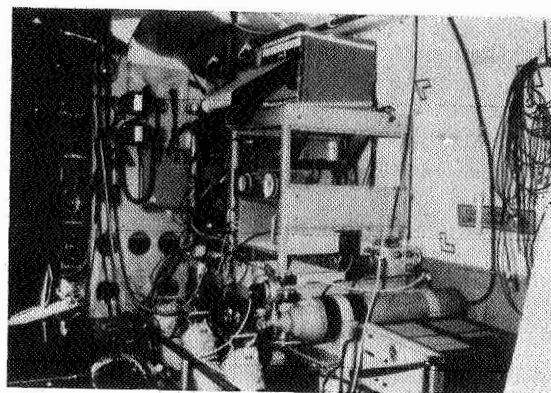


Figure 41



Hertz, and constant pressure and constant temperature controls. Air was circulated through the boxes to get the heat out and to keep the temperature constant, as shown in Figure 38. Figure 39 shows the lid which supported voltage and pressure regulators. Figure 40 shows the clock box mounted in the P3C airplane. Figure 41 is the electronic equipment to measure and record the relative performance of clocks on board and to record the epoch of the arrival of the laser pulse. On the right of Figure 41 is a travelling clock, whose environment was not controlled.

The kinds of data that one could get are shown in Figure 42 for a flight on November 22, 1975. We flew for five hours at 25,000 feet, and for another five hours at 30,000 feet to burn off fuel, concluding with another five hours at 35,000 feet. So there were steps in the potential difference. The vertical scale is parts in  $10^{12}$ . There were changes of velocity due to wind as the aircraft circled, shown in the lower part of Figure 42 (the  $v^2/c^2$  effect). The integral of these curves is shown in Figure 43. The potential effect integrates out to about 53 nanoseconds, the velocity effect to about -6 nanoseconds, with the net effect being about 47 nanoseconds. The error bar points are the laser pulse time comparisons. The actual data before flight and after flight can be seen in Figure 44 with the direct side-by-side clock comparison represented by the solid line, the laser comparison shown again by error bar points. The agreement between the prediction and the measurements is quite good. The relative rate of the airborne and ground clocks ensembles is represented by the slope and is seen to be the same both before and after flight. There was a similar effect for each of the individual clocks. Figure 45 illustrates the effects of the steps in altitude. They produced changes in relative clock rates which were measured by the laser pulse time comparison. The technique can serve as a crude altimeter! Figure 46 shows the time of an on-board clock with respect to the average of all on-board clocks. You can't even tell where the flight occurred! If that same clock is compared with the ground ensemble as shown in Figure 47, there is a step of some 47

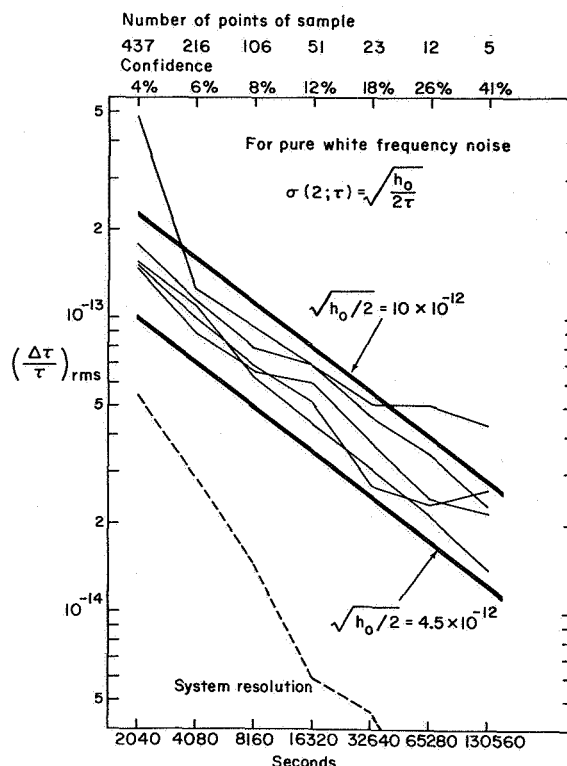


Figure 29



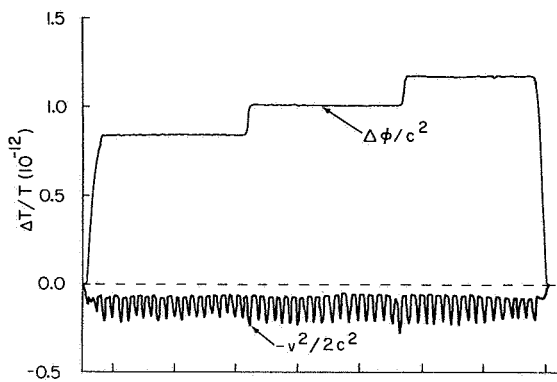


Figure 42

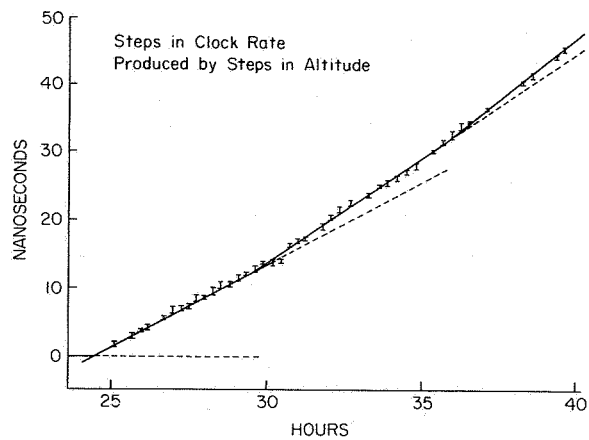


Figure 45

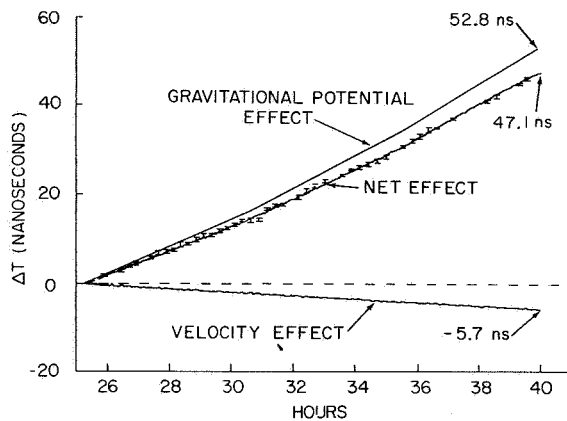


Figure 43

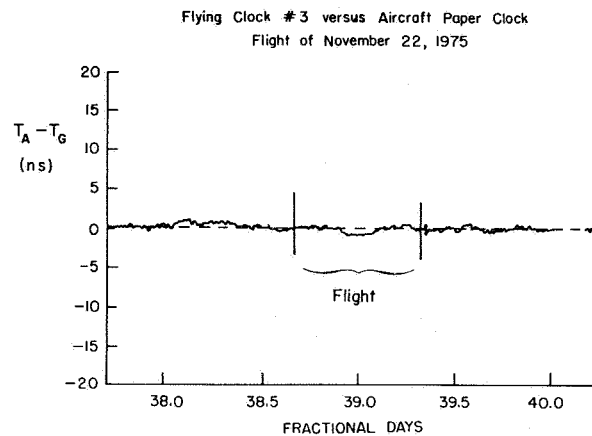


Figure 46

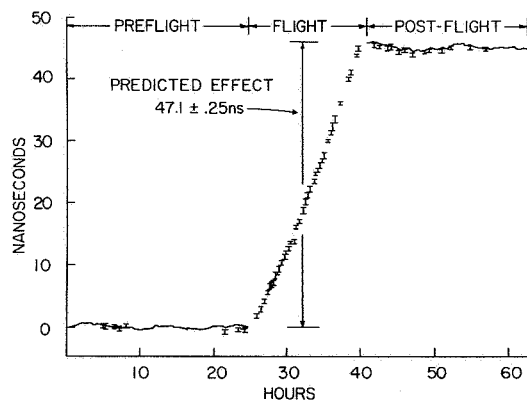


Figure 44

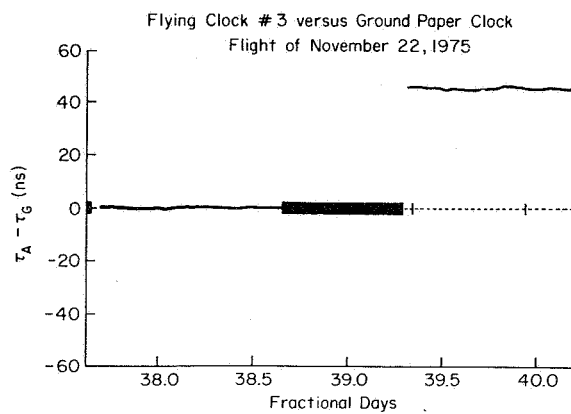


Figure 47

nanoseconds or so, as expected. Five separate 15-hour flights of this type were carried out, each yielding similar results.

We have done other aircraft clock experiments on a global scale. You will recall Einstein's "error" that we referred to earlier, the equator to the pole clock comparison. The surface velocity, if we consider only that, gives a prediction of 102 nanoseconds a day for the relative clock rates. But this is wrong, because you must also consider the gravitational potential difference. In going from the equator to the pole on an oblate earth there is a change in potential, as shown in Figure 48. The earth is an oblate spheroid and the mean ocean surface is an equipotential of  $\phi - v^2/2$ , the so-called geopotential. You remember that's exactly what comes into the relation between proper time and coordinate time:

$$d\tau = \left[ 1 + \frac{1}{c^2} \left( \phi - \frac{v^2}{2} \right) \right] dt$$

$\phi - v^2/2$  is constant along the mean ocean surface on the oblate earth. So the proper time is going to be constant along the mean ocean surface. Thus, one would expect a time difference to be produced only by flight conditions, the altitude above the ocean surface and the velocity contributing to the proper time integral, as we have discussed. We flew clocks to Thule, Greenland, left them four days, and brought them back. We measured a time difference of  $38 \pm 5$  nanoseconds, and we calculated  $35 \pm 2$  nanoseconds from inertial navigation and air to ground data. There is no anomalous latitude effect. The "Einstein error", if that prediction were calculated for Washington to Thule, would have been 224 nanoseconds over four days from a predicted rate of 56ns/day. The experiment provides another demonstration, from this point of view, of the effect of the gravitational potential difference which just compensates the velocity effect.

We have also done experiments with Einstein's freely falling laboratory in which we've used the earth itself as the falling laboratory. The earth is always falling freely towards the sun, but it moves in orbit around the sun and never falls in. Its spin axis is tilted 23.5 degrees with respect

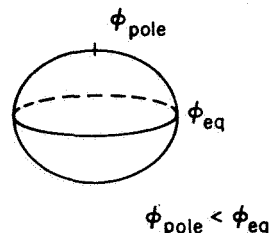


Figure 48

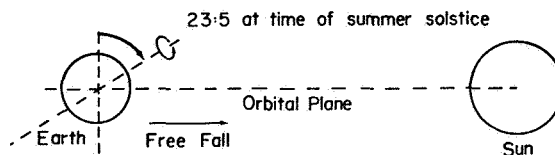


Figure 49

to the plane of its orbit, so that at the time of the summer solstice, clocks in the Northern Hemisphere are closer to the sun than clocks in the Southern Hemisphere, as shown, with an exaggerated tilt, in Figure 49. There's been a long-standing puzzle, or confusion, on the part of some people: on the earth, should the high clocks in the sun's potential run fast with respect to the low clocks in the sun's potential?<sup>9,10,11</sup>

The answer is no, by the Principle of Equivalence. You will remember that gravity is cancelled locally in a freely falling laboratory. We actually did the experiment by flying clocks from Washington to Christchurch, New Zealand and back again. The disagreement and the confusion in the literature, results from people wanting to retain the linear term in the expansion of the potential about the center of the earth, as sketched in Figure 50. There is

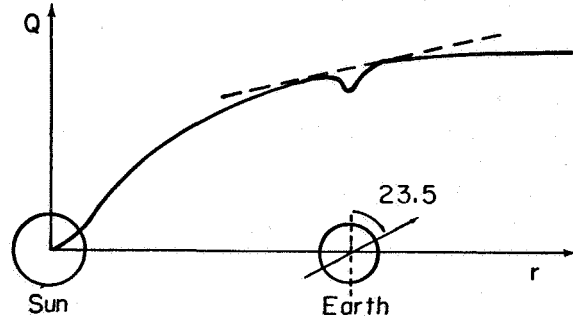


Figure 50

an excellent paper by J.B. Thomas from JPL<sup>12</sup>, which does this calculation correctly. There are remaining second order terms in the expression of the potential which cause tidal effects, but these can be neglected in their effects on currently available clocks. In our experiments we found agreement between the calculated proper time difference and the measured proper time difference. The results are shown in the following Table.

<sup>9</sup> B. Hoffmann, "Noon-Midnight Red Shift," Physical Review, Vol. 121, pp 337ff (1961).

<sup>10</sup> R. U. Sexl, "Seasonal Differences Between Clock Rates," Physics Letters, Vol. 61B, pp 65ff (1976).

<sup>11</sup> W. H. Cannon and O. G. Jensen, "Terrestrial Timekeeping and General Relativity: A New Discovery," Science, Vol. 188, pp 317ff (1975). The errors in this paper have been pointed out in many letters in "Acceleration and Clocks," Science, Vol. 191, pp 489-491 (1976). The authors have retracted their claims.

<sup>12</sup> J. B. Thomas, "Reformulation of the Relativistic Conversion Between Coordinate Time and Atomic Time," Astronomical Journal, Vol. 80, No. 5, pp 405ff (1975).

		FLIGHT 1 (10 - 17 July 1977)	FLIGHT 2 (23 - 30 July 1977)
$(\tau_A - \tau_G)$ measured	(ns)	$115 \pm 10$	$131 \pm 10$
$(\tau_A - \tau_B)$ calculated	(ns)	$129 \pm 2$	$122 \pm 2$
(Measured - Calculated)	(ns)	$-14 \pm 12$	$11 \pm 12$
Calculated Effect of Linear Term	(ns)	$80 \pm 2$	$70 \pm 2$

Note that there is no evidence for the alleged effect of the linear term.

These flights also point up the effect on proper time of clock transport by aircraft. The following table displays the calculated proper times using data from the on-board inertial navigation units and plane-to-ground radar for the different legs of the trips.

#### EFFECT OF EARTH'S ROTATION

	FLIGHT 1 (ns)	FLIGHT 2 (ns)
Andrews AFB to Travis AFB (E - W)	35	31
Travis AFB to Hickam AFB (E - W)	35	31
Hickam AFB to Christchurch (E - W)	47	52
Christchurch to Hickam AFB (W - E)	16	16
Hickam AFB to Andrews AFB (W - E)	-1	-4
Dwell Time on Ground	-3	-3

Note the large difference between East-West and West-East legs caused by the earth's rotation: In the West-East direction the surface velocity of the earth adds to the surface velocity of the aircraft, giving a large velocity in the inertial frame attached to the center of the earth where the calculations are best made. The large  $v^2/2c^2$  very nearly cancels the  $\phi/c^2$  in the proper time integral. The entries in the table are typical of the effects to be expected for an air speed of 500 knots and an altitude of 35,000 feet, characteristic of jet aircraft.

Let me show you a few pictures of our global flights. Figure 51 is a polar view of a National Geographic globe on which is marked the path of the flight from Washington to Thule and back. You can see there is a large change in distance from the earth's spin axis, producing a large

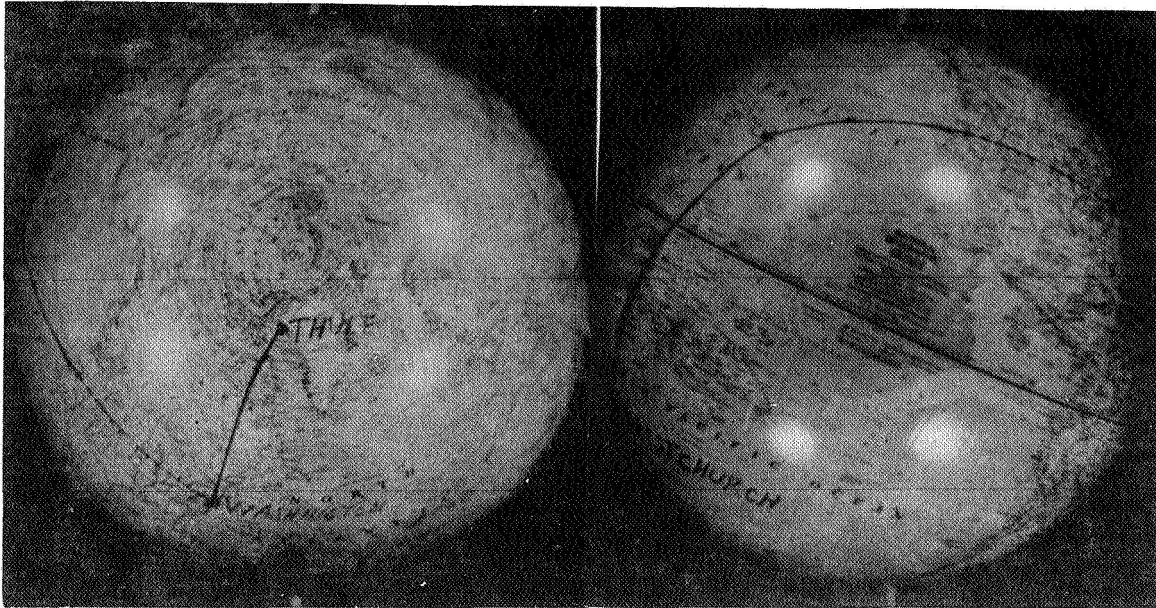


Figure 51

Figure 52

change in surface velocity. Figure 52 shows the tilted earth, the sun being off to the right at the time of the summer solstice. The path from Andrews AFB in Washington to the Travis AFB in California to Hickam Field in Hawaii, and down to Christ Church is marked. Figure 53 shows the repackaged equipment for flying on an Air Force C141 transport plane. Figure 54 shows the equipment mounted on a cargo pallet with the surrounding thermal protection enclosure. Figure 55 shows the pallet carrying the equipment being loaded into the C141. Figure 56 shows a later step in the loading process. Figure 57 is a picture taken during one of the flights. The equipment for recording the inertial navigation systems and air-to-ground radar information from which to calculate the proper time integral is on the table on the left.

Other experiments were done recently by Bob Vessot and Marty Levine<sup>13</sup>, with a hydrogen maser in a rocket probe, in which the ratio of the measured to predicted value was  $1 + (2.5 \pm 70) \times 10^{-6}$ . This is better than a hundredth of a percent confirmation. They measured frequency rather than time directly, but the same basic equation that we've been working with had to be used. The great thing about their experiment was the ability to essentially cancel out the Doppler effect, and ionospheric, which is two parts in  $10^5$ , sufficiently well to measure

<sup>13</sup> R. F. C. Vessot and M. W. Levine, "A Test of the Equivalence Principle Using a Spaceborne Clock," General Relativity and Gravitation, Vol. 10, No. 3, pp 181 -204 (179).

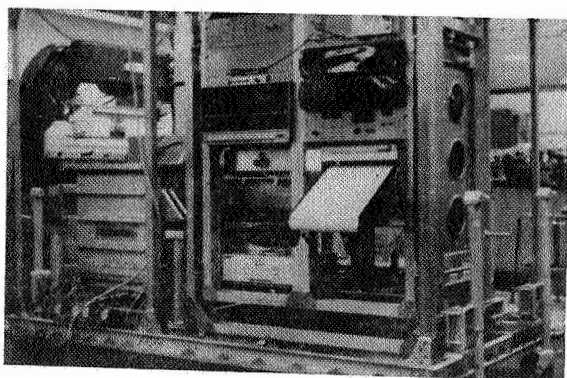


Figure 53

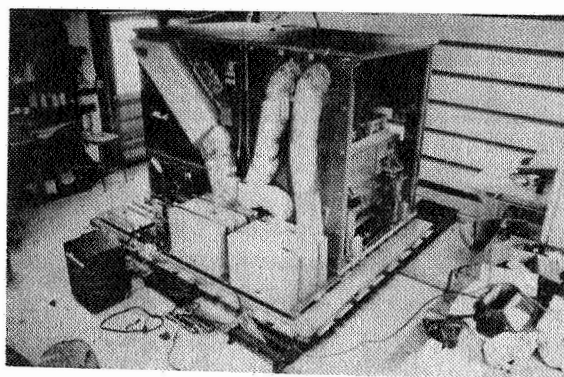


Figure 54

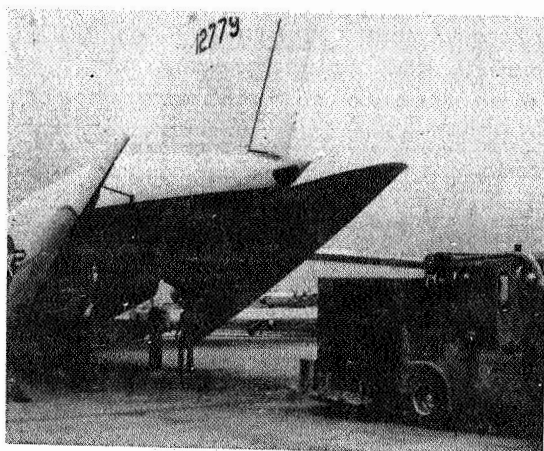


Figure 55

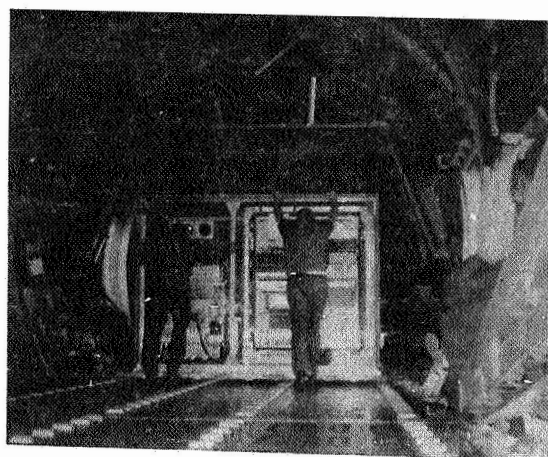


Figure 56

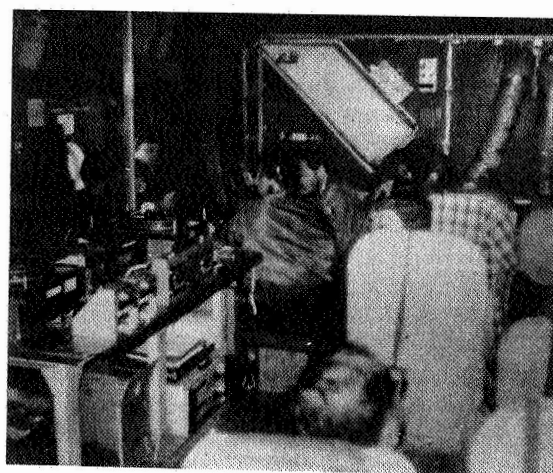
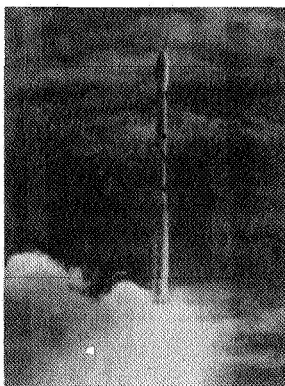
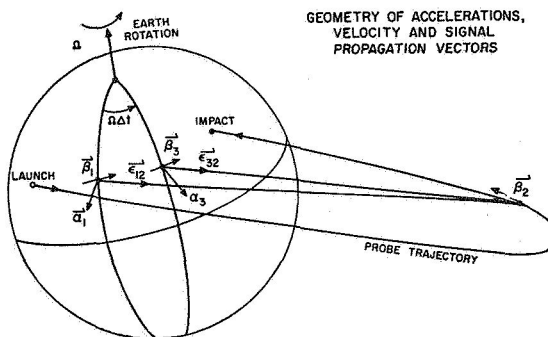


Figure 57



Left:  
Figure 58



Right:  
Figure 59

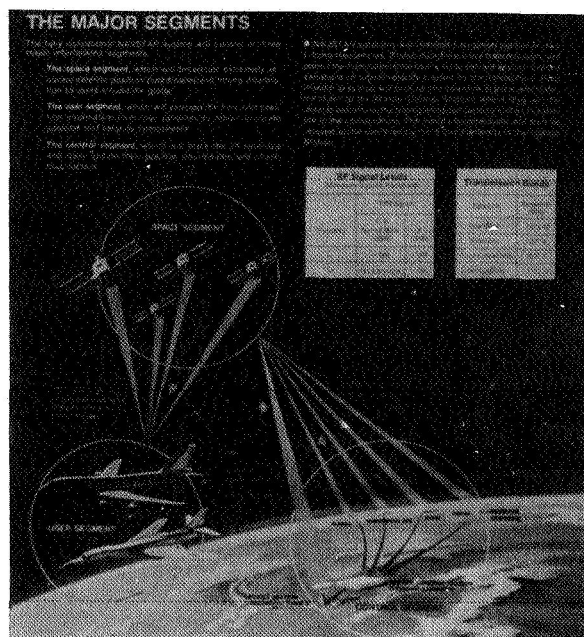
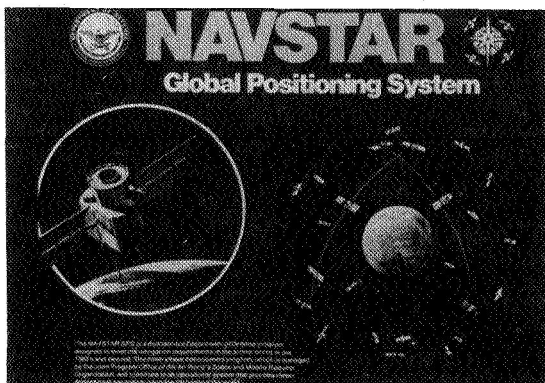
to  $10^{-4}$  the effect of the potential, which is only four  $\gamma 10^{10}$ , by a very clever three-frequency cancellation scheme. Figure 58 shows the Scout rocket that was used in that experiment, and Figure 59 shows its trajectory rising to several earth radii and falling back into the Atlantic Ocean. Unfortunately, there's no time to go into more details.

#### SOME APPLICATIONS

Let us now consider some practical engineering applications. Figure 60 is an artist's view of the GPS/NAVSTAR system, which I think now has only 18 satellites planned rather than the 24 shown here. They are in 12 hour period orbits, and they carry very good atomic clocks. The circular orbits are about 14,000 kilometers above the earth's surface. Figure 61 illustrates the way in which the system works. A

Right:  
Figure 61

Below: Figure 60



user receives L-band signals from each of several satellites, consisting of a coded bit stream whose rate is set by the onboard atomic clock at 10.23 MHz. The user's receiver is equipped with the same code, which is shifted in time to lock on to the satellite bit stream. By doing microprocessor calculations from four satellites, the user's equipment finds out where he is and also what the time is. But for all of this to work, the satellite clocks must be synchronized with the GPS master station. You have to allow for the gravitational potential and motional effects of General Relativity, which we have been discussing.

In the Global Positioning System, the calculations can be made in the way we have demonstrated.

$$\begin{aligned} d\tau_{\text{sat}} &= \left( 1 + \frac{\phi_{\text{sat}}}{c^2} - \frac{v_{\text{sat}}^2}{2c^2} \right) dt \\ d\tau_{\text{ground}} &= \left( 1 + \frac{\phi_{\text{ground}}}{c^2} - \frac{v_{\text{ground}}^2}{2c^2} \right) dt \end{aligned}$$

Dividing the equations, and retaining only the constant and first order terms,

$$\frac{d\tau_{\text{sat}}}{d\tau_{\text{ground}}} = 1 + \frac{\phi_{\text{sat}} - \phi_{\text{ground}}}{c^2} - \frac{v_{\text{sat}}^2 - v_{\text{ground}}^2}{2c^2}$$

Evaluating this expression for the NAVSTAR circular orbit, one finds,

$$\frac{d\tau_{\text{NAVSTAR}}}{d\tau_{\text{ground}}} = 5.1 \times 10^{-10} = 44,000 \text{ ns/day}$$

This result means that if a NAVSTAR atomic clock has a certain relative rate to the GPS master clock when they are side by side at an elevation corresponding to the mean ocean surface (the surface used for reference in the GPS system as well as for UTC) -- say 20 ns/day -- this rate will be increased by 44,000 ns/day when the clock is placed in orbit. This was observed in 1977 by the Naval Research Laboratory with the NTS-2 satellite.<sup>14</sup> But before that, there had been some doubt on the part of some people associated with the GPS program whether these effects were actually there. I remember well a meeting at the GPS offices in the Spring of 1976, when Gernot Winkler, Len Cutler and I presented the

<sup>14</sup> T. McCaskill, J. White, S. Stebbins, and J. Buisson, "NTS-2 Frequency Stability Results," Proceedings of the 32nd Frequency Control Symposium (1978).



results of our P3C aircraft clock experiments when such questions were raised.

If there is some eccentricity to the orbit, there will be a periodic change in the distance of the satellite from the center of the earth. For an eccentricity  $5 \times 10^{-3}$ , the change in gravitational potential is enough to produce an amplitude of 12 nanoseconds (peak to peak of 24ns) with a 12 hour periodic in the onboard clock reading. This would produce an error in position of 24 feet, if not allowed for.

One must understand and include these effects correctly, as the GPS now does. For the large relativistic offset in clock rate in orbit of +44,000 ns/day, one adjusts the clock so that on the ground it would have a rate of -44,000 ns/day with respect to the reference GPS clock. This compensates for the relativistic effect when it is put into orbit. Once this is done, there is no longer a "gravitational red (blue) shift" on transmitted frequencies from the satellite to the ground, even though the radiation passes through a difference of gravitational potential  $\Delta\phi$ . This mistake was made by one of the GPS contractors during the development of the system. It is a natural mistake following from an often presented derivation of the blue shift in terms of the energy of a photon,  $E = h\nu$ , at the satellite; the mass equivalent of the photon,  $m = h\nu/c^2$ ; and the gravitational energy change  $m\Delta\phi$ . If  $h\nu'$  is the energy of the photon at the ground, energy conservation gives the equation

$$h\nu' = h\nu + (h\nu/c^2)\Delta\phi$$

$$\text{or } \frac{\nu' - \nu}{\nu} = \Delta\phi/c^2$$

This argument does not hold if the clocks have been adjusted as described above.

There is an upcoming experiment called LASSO, Laser Synchronization from Stationary Orbit, being done by the European Space Agency<sup>15</sup> with the first operational launch of the ARIANE rockets, currently scheduled for April 1982. The experiment is on the Sirio 2 satellite, as shown in Figure 62. There will be corner reflectors, an avalanche photodiode detector, an event timer and a crystal clock on the satellite. Laser pulses will be fired at this synchronous satellite from the 1.2m telescope at the Goddard Optical Research Facility in a cooperative undertaking by the U. S. Naval Observatory, the University of Maryland, and NASA; and from several laser stations in Europe. The technique is

<sup>15</sup> B. E. H. Serene, "Progress of the LASSO Experiment," Proceedings of the Twelfth Annual Precise Time and Time Interval (PTTI) Applications and Planning Meeting; NASA Conference Publication 2175, pp 307 - 327, December 2 - 4, 1980.

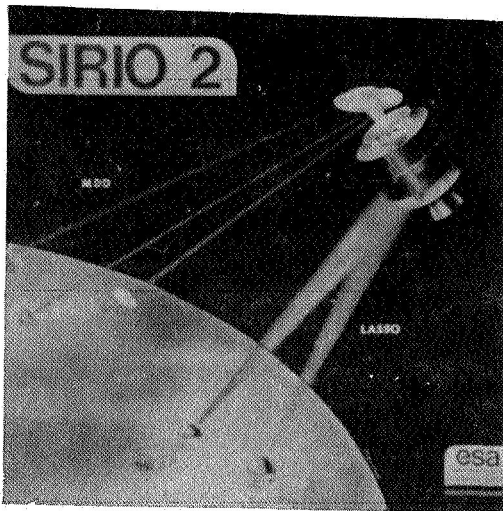


Figure 62

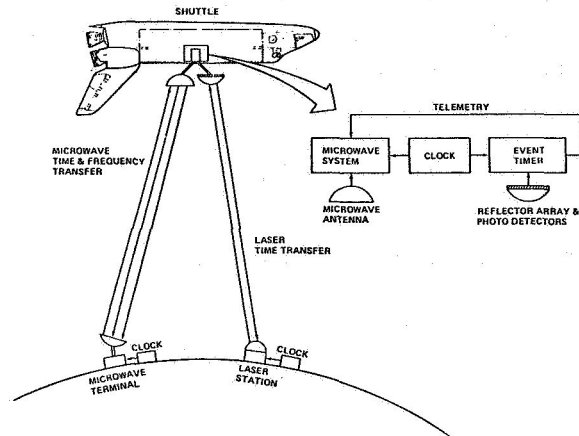


Figure 63

essentially the same as that used in the P3C aircraft experiments. The goal for the first experiments is one nanosecond synchronization between the United States and Europe. It is hoped that this will be the first of a series of satellite experiments with the goal of one tenth of a nanosecond synchronization later on. Since the comparisons on the satellite will be made rather close in time, we don't have to worry too much about the relativistic effect, but we just note that it is on the order of 50,000 nanoseconds per day, or about 6/10ths of a nanosecond per second. So if one has a goal of one nanosecond and one lets the reception between pulses spread over a few seconds, you may have to worry a bit about this effect.

There is a third space experiment which I wish to discuss this afternoon. This is the proposed Shuttle Time and Frequency Transfer experiment which we call STIFT. The plan has been developed by D. W. Allan of the National Bureau of Standards, Rudolf Decher of the Marshall Space Flight Center, Gernot Winkler of the U.S. Naval Observatory, and the speaker.<sup>16</sup> The idea is shown in Figure 63. There would be a hydrogen maser and other clocks on the shuttle, along with microwave frequency comparison equipment of the type developed by Vessot, et al., for the rocket probe relativity experiment, and laser pulse time comparison equipment of the type developed by Alley, et al., for the P3C

<sup>16</sup> R. Decher, D. W. Allan, C. O. Alley, R. F. C. Vessot, and G. M. R. Winkler, "A Space System for High-Accuracy Global Time and Frequency Comparison of Clocks," Proceedings of the Twelfth Annual Precise Time and Time Interval (PTTI) Applications and Planning Meeting; NASA Conference Publication 2175, pp 99 - 111, December 2 - 4, 1980.

aircraft relativity experiments. It now appears that the principal uncertainty in the STIFT technique will be that imposed on the calculation of the proper time integral by lack of knowledge of the velocity of the space shuttle.

$$\tau_S - \tau_G = \int \left[ \frac{\phi_S - \phi_G}{c^2} - \frac{(v_S^2 - v_G^2)}{2c^2} \right] dt$$

For a several hundred kilometer orbit,

$$\frac{v_S^2}{2c^2} = 3 \times 10^{-10}$$

If we wish to maintain a fractional time uncertainty  $\Delta\tau/\tau = 10^{-14}$  which the hydrogen maser is capable of, one must have

$$\frac{\Delta(v_S^2/2c^2)}{(v_S^2/2c^2)} = \frac{2\Delta v}{v} = 3 \times 10^{-5}$$

This requires that  $\Delta v = 10\text{cm/sec}$ . This may be very difficult to know without special instrumentation such as high quality inertial navigation systems. For this technique, the limiting performance for time transfer may be set by relativity rather than by clock performance!

## QUESTIONS AND ANSWERS

DR. WINKLER:

Maybe one comment is in order and that is in Professor Wheeler's concept that the space geometry, or space time geometry has to tell the planets where to go.

This, to me, seems like a step backwards. Because 300 years ago Kepler had much more definite ideas. He had an angel pushing the planets.

PROFESSOR ALLEY:

Some of Wheeler's recent thinking goes much beyond that. What this is, though, if you want to be a genuine relativist, as, say, interpreted by Wheeler and his school in the last 30 years, you think of no more Newtonian forces, no more angels. You have curve space time as displayed by this metric, with these metric coefficients. And then you try to move as straight as you can in the curve space time. And you end up going around the sun in an elliptical orbit. And, furthermore, you get the precession of the perihelion. You get the defraction of light. Plus all these rather remarkable things that people are now calculating busily.

Suppose you've got a rotating black hole and matter falling in. This whole theory has to be applied. And you can get these jets coming out, and enormous energies, and what not.

VOICE:

With regard to the suggestion you can multiply and get from the base line, do you anticipate the source is going to be closer than a parsec? Or are you going to get down into billionths of a parsec?

MR. MANKINS:

For what? The source of the gravitational wave?

VOICE:

Yes.

MR. MANKINS:

The source would be very, very distance. Many parsec.

VOICE:

May I suggest you forget your second experiment?

MR. MANKINS:

Well, if the gravity wave propagates at the speed of light, then for a maximum angle, i.e., say it came perpendicularly on the base line between the two stations, there would be some time delay between its arrival at the two stations on the order of a 30th of a second. Which is very large from frequency and timing values. Microseconds.

And that's all you would be looking for is the time delay between the arrival at the two stations.

VOICE:

The other question had to do with the uniqueness of this particular event. In your experimental considerations, do you have any basis for looking to see whether this is an act of nature, a gravity wave, an accident in data processing?

MR. MANKINS:

Well, that would be one of the good points about having two stations. With a single station and a single spacecraft you are more subject to some accident.

Where if you had two stations, and both of them independently recorded the event, you're safer from accidents.

Also if you've got some real correlation.

SECOND VOICE:

How frequently do these gravity waves occur, so that you know how long to look for them?

MR. MANKINS:

I believe in the paper by Thorne and Breginski, circa 1975, that they anticipated periods somewhere between a week and 10 years for a single event.

But the, like I say, those numbers were very cosmological, i.e., subject to change.

PROFESSOR ALLEY:

It is possible that the low frequency gravity waves that you might detect this way could be a result of primordial conditions in the universe, if the big bang, and so on, is correct.

There could well be some rumbling, rumbling thunder of gravity waves throughout the whole universe.

MR. MANKINS:

Still wandering about.

PROFESSOR ALLEY:

Might be picked up.



THE ROLE OF THE DEEP SPACE NETWORK'S  
FREQUENCY AND TIMING SYSTEM IN THE DETECTION OF  
GRAVITATIONAL WAVES

John C. Mankins

Jet Propulsion Laboratory, California Institute of Technology\*  
Pasadena, Calif. 91109

ABSTRACT

A review of the projected role of the Deep Space Network (DSN) in the planned detection of gravitational waves using precision doppler-tracking of deep space vehicles is presented. The review emphasizes operational and configurational aspects; considering: 1. the projected configuration of the DSN's Frequency and Timing System during the experiment, 2. the environment within the DSN provided by the precision atomic standards within the Frequency and Timing System--both current and projected and 3. the general requirements placed on the DSN and the Frequency and Timing System for both the baseline and the nominal gravitational wave experiments.

A comment is made concerning the current probability that such an experiment will be carried out in the foreseeable future.

\*This paper presents the results of one phase of research carried out and the Jet Propulsion Laboratory, California Institute of Technology, under Contract No. NAS 7-100, sponsored by the National Aeronautics and Space Administration.



## I. INTRODUCTION

A variety of astronomical events, both catastrophic and periodic, theoretically result in the generation of gravitational radiation. Of these, periodic events should generate periodic gravity waves while a catastrophic event (although it may be recurring) should result in emission of a "large" gravitational wave-burst.

An example of an event which may be generating periodic gravitational radiation is a star-pulsar binary pair. In such a case, a close examination of radio doppler data from the pulsar<sup>1</sup> may show a gradual decay of the pulsar's orbit and hence allow indirect confirmation of the existence of gravity waves.

Conversely, the gravitational wave bursts which are expected to result from "catastrophic" events such as the collapse of several solar masses of normal matter to form a black hole, may be directly observable by measuring the effect of their passage through the Solar System on some "local" experimental apparatus. Of the various experiments designed to observe such gravity wave bursts, one of the most promising involves the close examination of coherent doppler data which result from the tracking of deep space probes.

This paper will briefly discuss the anticipated effect of the passage of a gravity wave on an experimental configuration consisting of a Deep Space Tracking Station (DSS), a deep space probe and the coherent radio link between them. It will then review the configuration of a prototypical DSS in so far as it is involved with the experiment and in particular examine the varied ways in which the experiment depends upon the frequency stability performance 'environment' which the Frequency & Timing System provides. It will also note the performance constraints which the physical situation places on a DSS and a comparison will be made between these and the capabilities of the Deep Space Network; current (Mark III System), planned (Mark IV-A System) and anticipated (circa 1987-1990).

## II. GRAVITATIONAL WAVES

As an idealization, gravitational waves may be envisioned as being small 'ripples' in the shape of spacetime which are propagating outward in all directions from their point of origin--whether periodic or catastrophic.<sup>2</sup> It is assumed in theoretical analyses of such events that the generators of the waves are at great distances from ourselves and that the gravity waves which are believed to pass through our Solar System are essentially planar. See figure 1 for a graphic representation of the experimental configuration.

In a suitable frame of reference<sup>3</sup> (i.e., one which is soluble using the methods of general relativity) the earth and the spacecraft may be regarded as "fixed" and the entire effect of the gravitational wave placed upon the radio link between them. Theoretically, this effect may be regarded as the result of forcing the radio beam to travel through a "changing" spacetime. However, as a mnemonic device, the resultant effect on the experiment of the gravity waves' passage may be thought of in terms of three factors:

1. At Earth: Red-shifting of the frequency output by the Hydrogen Maser (clock speed-up.)
2. At Earth: Physical Buffeting (movement) of the DSS.
3. At Spacecraft: Physical Buffeting of the Spacecraft.

Each of these may be thought of as leading to the introduction of a distinctive, although minute, fluctuation (fractional frequency shift) in the measured doppler shift of the spacecraft. Together with the 'reflections' of effects 1 & 2, these form a unique three-pulse signature for gravitational wave events. See figure 2 for a detailed development of this signature; using this mnemonic device. (Appendix A contains a suggested enhancement of the single spacecraft/single DSS experiment discussed in the body of this paper.)

It results<sup>4</sup> that for gravitational wave bursts originating from the collapse of normal matter to form a black hole that the amplitude of the burst is related to the burst duration according to:

$$(h) \approx (2 \times 10^{-17}) \times T / (90 \text{ seconds}),$$

where  $(h)$  = A dimensionless, polarization-averaged amplitude parameter  
and  $T$  = The Burst Duration. See figure 3 for a plot of this relation.

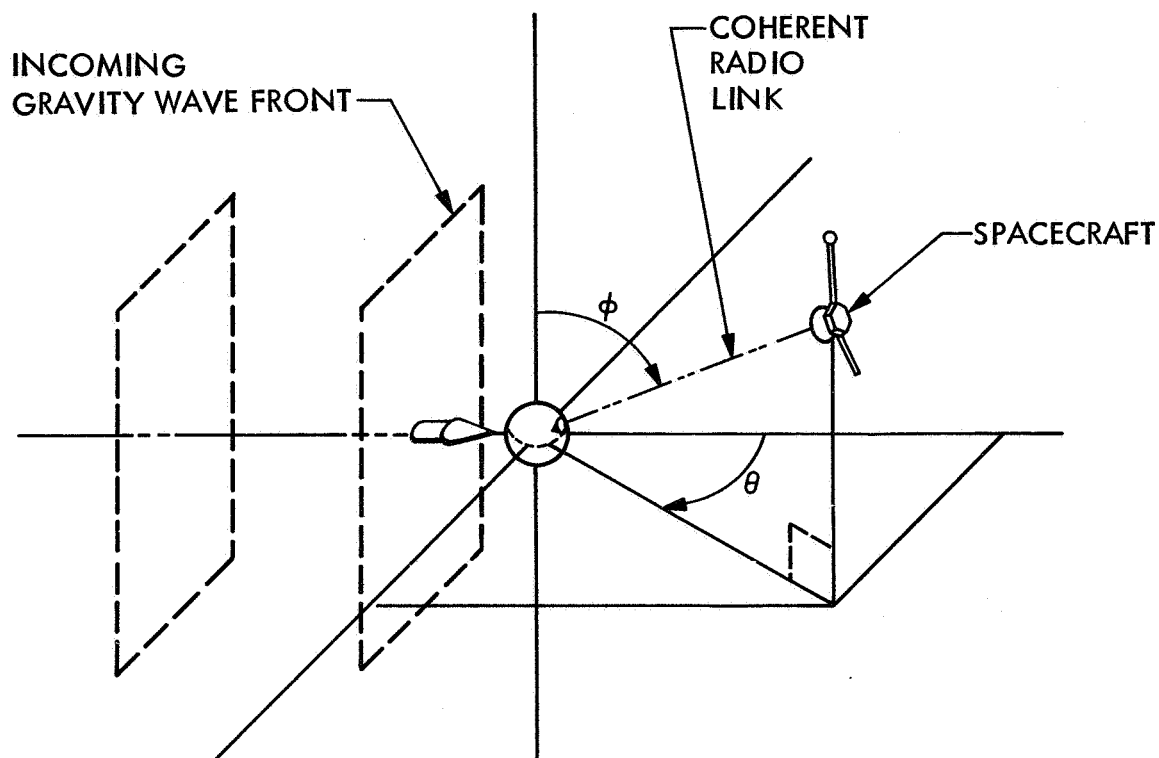
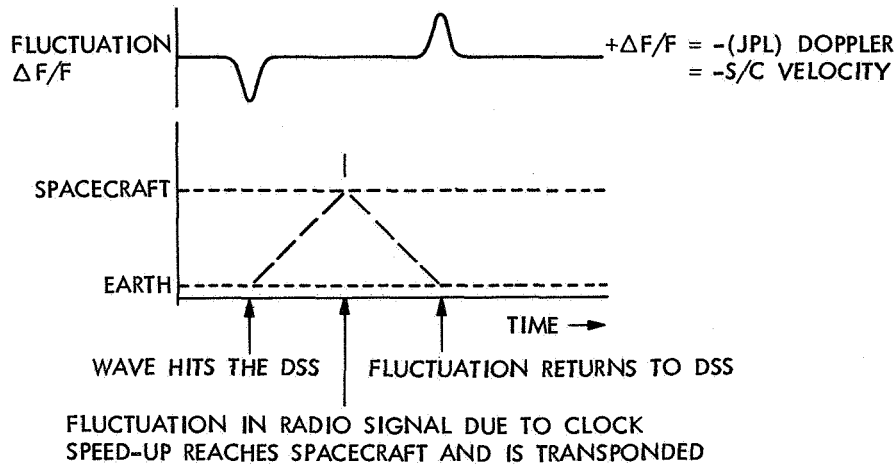
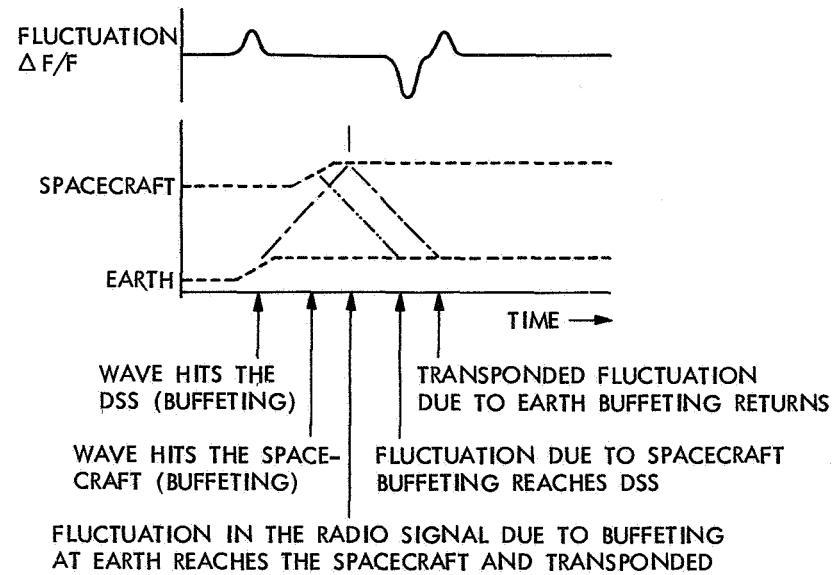


Figure 1. Gravitational Wave Experiment Tracking Geometry.  
 Events: 1. Wave passes Earth (causing clock speed-up & buffeting)  
 2. Wave passes Spacecraft (causing buffeting.)

### 1. CLOCK SPEED-UP EFFECT



### 2. EARTH/SPACECRAFT BUFFETING EFFECT



### 3. NET GRAVITY WAVE SIGNATURE ( $\theta = 60^\circ$ )

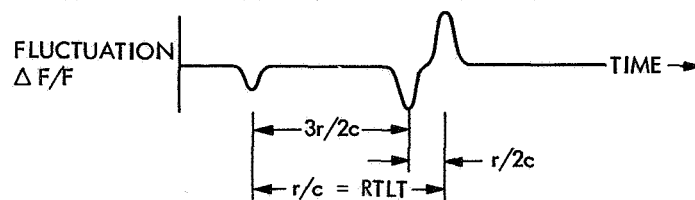


Figure 2. Details of Three-Pulse signature associated with gravity waves  
 Note: In point 3,  $\theta^* = 60^\circ$  refers to the angle  $\theta$  in figure 1 with  $\phi = 90^\circ$ .

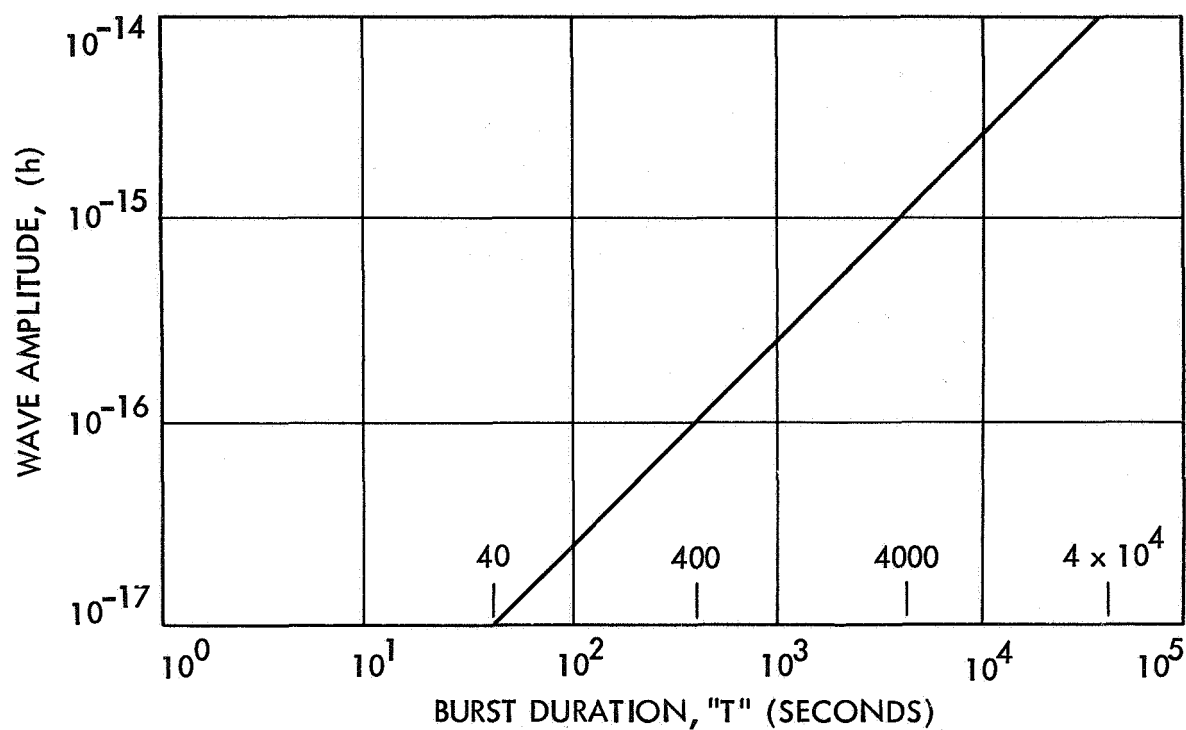


Figure 3. Plot of the Wave Amplitude, (h), vs. Burst Duration, T.  
(This relation is approximate.)

The anticipated ranges on these parameters are:

$$40 \text{ seconds} \leq T \leq 40,000 \text{ seconds}$$

$$10^{-17} \leq (h) \leq 10^{-14}$$

The range noted above is, however, highly dependent upon certain specific assumptions which were made during its derivation. The actual characteristics of gravity waves may be larger or smaller by some considerable factor. We will consider them as guidelines.

### Experimental Constraints

As a result, the following parameters have been suggested as constraints for the Deep Space Network in any attempt to measure gravitational waves<sup>5</sup>:

BASELINE EXPERIMENT :  $\Delta F/F \leq 10^{-15}$  Total Measurement System  
(Waves with  $(h) 10^{-15}$ )

$\Delta F/F \leq 10^{-16}$  Each Component (FTS)

for  $50 \text{ sec.} \leq T \leq 5000 \text{ sec.}$

DESIRABLE EXPERIMENT :  $\Delta F/F \leq 10^{-17}$  Total Measurement System  
(Waves with  $(h) 10^{-17}$ )

$\Delta F/F \leq 10^{-18}$  Each Component (FTS)

for  $50 \text{ sec.} \leq T \leq 5000 \text{ sec.}$

### III. THE DEEP SPACE NETWORK

Deep Space Tracking Stations (DSS) of the Deep Space Network (DSN) regularly maintain a coherent radio link over a period of hours with the various spacecraft of the Planetary Exploration Program. These stations transmit a precise radio frequency signal which is currently at S-Band (2.3 GHz) to the spacecraft. This "uplink" signal is received by the particular probe and transponded back to the Earth at S-Band (the downlink is the Uplink S-Band Frequency x 240/221) and/or at X-Band (this downlink is at the Uplink S-Band Frequency x 880/221; around 8.3 GHz). These "downlinks" (coherent with each other as well as with the uplink reference) are received by either the transmitting

DSS or by a second DSS which is coherent with the first. The former mode of communication (reception by the transmitting station) is referred to as being "two-way," while the latter (reception by a second DSS) is referred to as being "three-way."

The received frequency will differ (aside from the numerical factor) from the transmitted frequency by the amount of doppler shifting on the transponded signal. This doppler shift is due primarily to two factors:

1. The motion of the Spacecraft relative to the Earth,
2. The motion of the DSS due to the Earth's rotation.

(These factors were removed from the diagrams shown in figure 2.) Further, as we've noted, it is expected that the passage of a gravity wave through the System will result in a distinct fractional frequency shift in the doppler record.\* The amplitude of the pulses which make up the signature are very, very small, however, and hence each factor of noise which is inherent in the various components of the experiment is important.

We will list in some detail those points within the system where noise in the Frequency and Timing System's (FTS) outputs may be introduced into the experiment. We will consider in turn:

1. The Frequency and Timing System (FTS)  
Primary Component: Hydrogen Maser (H2M)
2. The Receiver/Exciter Subsystem (RCV)  
Primary Components: Closed-Loop Receiver (CLR)  
Open-Loop Receiver (MMR)
3. The Tracking Subsystem (DTK)  
Primary Component: Metric Data Assembly (MDA)
4. The Radio Science Subsystem (DRS)  
Primary Component: Occultation Data Assembly (ODA).

See figure 4 for a general block diagram of the configuration of the pertinent sections of a typical DSS during tracking.

---

\*Note: We're not considering media effects here.

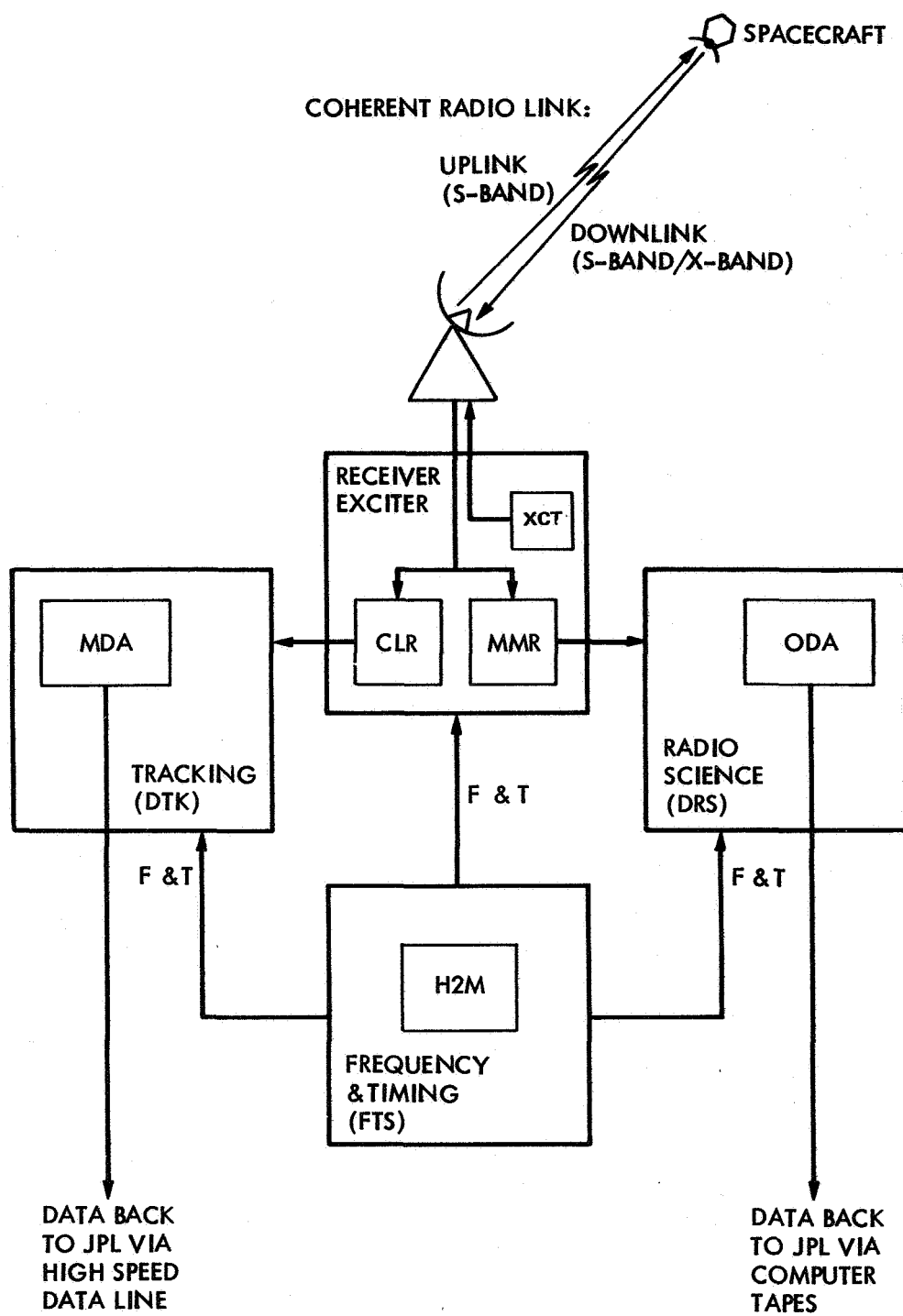


Figure 4. General Block Diagram of DSN Experimental Configuration  
(Note: "F & T" = Frequency and Timing products.)



## The Frequency and Timing System

The Frequency and Timing System (FTS) at a Deep Space Station provides virtually all reference frequencies and timing pulses as well as epoch times which are required by the DSS to perform its tracking function. The following are some of the major components of the FTS and their impact on performance. See figure 5 for a current (Mark III) functional block diagram of the FTS. This section will consider the following components of the FTS: The Coherent Reference Generator, the Time Format Assembly and the Hydrogen Maser.

### The Coherent Reference Generator

The Coherent Reference Generator (CRG) produces the various reference frequencies which are used in the station's subsystems. Currently the CRG outputs the following frequencies:

- 0.1 MHz
- 1.0 MHz
- 5.0 MHz
- 10.0 MHz
- 10.1 MHz
- 45.0 MHz
- 50.0 MHz
- 55.0 MHz

For the gravity wave experiment, among the most critical of the constraints placed on the CRG's outputs is that they not degrade the coherence of the recorded phase and time in the doppler data within the Tracking System. Problems with the outputs of the CRG can impact this performance in several ways. These include:

1. An increase in the noise of the reference signal can increase the overall noise in the doppler system and thus degrade resolution.
2. Errors in timing pulses can result in varied sample times and resultant doppler jitter. This can cause 'smearing' of the recorded frequencies. (Note, however, that the clocks which generate these pulses are typically noisier than the CRG.)

The stability of the CRG's products is also critical within the Receiver/Exciter Subsystem where they are used at various points to directly mix the incoming signal down into usable ranges.

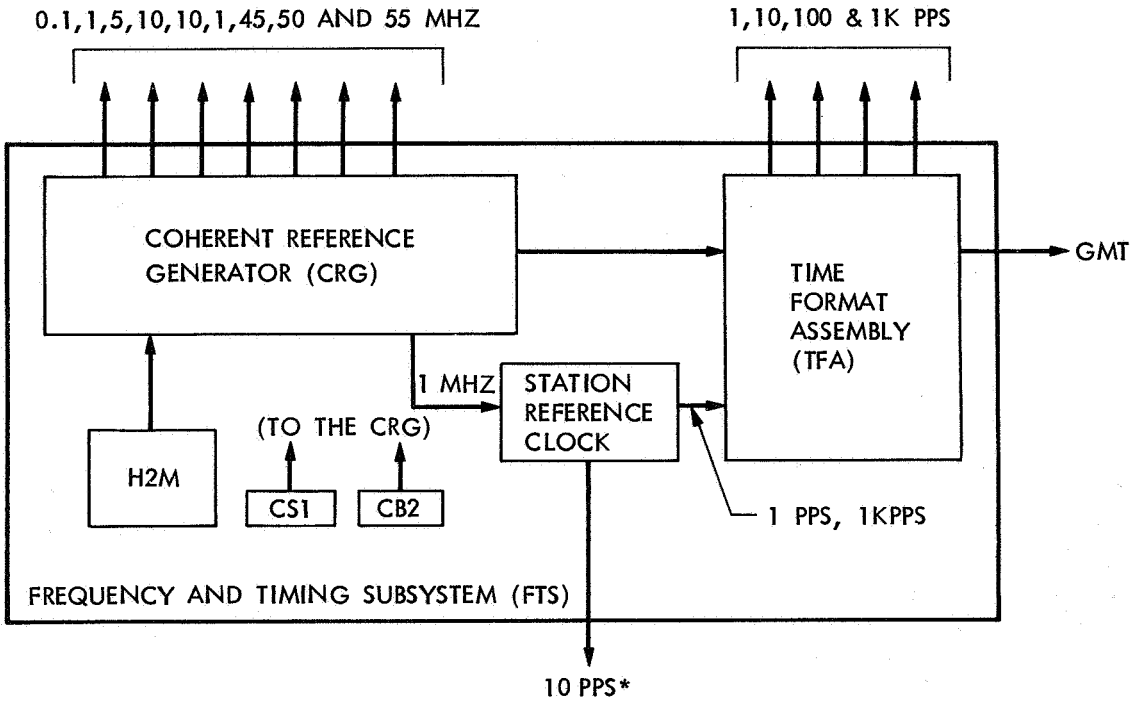


Figure 5. Functional Block Diagram of the Frequency and Timing Subsystem (FTS) showing the various F & T products; Mark III System. (Note: CS1 and CS2 are back-up Cesium Standards, for use in the event of Hydrogen Maser (H2M) failure.)  
 \*The 10 pps is for the DTK and DRS.

## The Time Format Assembly

The Time Format Assembly (TFA) provides precision timing pulses to the various subsystems. TFA outputs include:

Timing Pulses: 1 pps  
10 pps  
100 pps  
1 kpps

Epoch Time Code: GMT

The stability of these pulses depends upon the output of the CRG (see point 2 under Coherent Reference Generator.) Note that some users require a 10 pps reference timing pulse from the Master Clock (see figure 5) rather than from the TFA. (This pulse provides a 10 ns/second rms jitter.)

## The Hydrogen Maser

The Hydrogen Maser (H2M) is the central factor in any attempt to utilize the DSN as part of a gravitational wave experiment. Its ultra precision frequency products provide the baseline stability 'environment' upon which the stability of the DSS is determined. And hence, whether an experiment is feasible. Within the maser's cavity, a frequency of 1420 MHz is generated. This is in turn monitored by the unit's instrumentation and used directly in synthesizing several frequency products which are delivered to the CRG. These products are: 0.1 MHz, 1.0 MHz, 5.0 MHz and 10 MHz. In addition, a 100 MHz reference frequency is generated and this will become available to the CRG for use by the open-loop receiver under the Mark-IVA era (1984).

See Table 1 for a Summary of the Specifications imposed upon the Frequency and Timing System by the current requirements of the Deep Space Network. It includes specifications: 1. on the Frequency Standard, 2. between different Deep Space Network Complexes (DSCC's), 3. between the DSN and USNO/NBS, 4. on timing pulses, and 5. on the CRG.

Table 1. Summary of Current Specifications

Knowledge of time synchronization between DSCC's :  $\pm 10$  us  
Knowledge of frequency offset between DSCC's :  $\pm 3 \times 10^{-13}$   
Frequency Offset between DSCC's maintained within:  $\pm 1 \times 10^{-12}$   
Knowledge of time synch. between DSN & USNO/NBS :  $\pm 5$  us

---

The frequency standard at a DSS (the Hydrogen Maser) must conform to the following stability performance standards:

$1 \times 10^{-12}$  for 1 second  
 $1 \times 10^{-14}$  for  $10^4$  seconds  
 $1 \times 10^{-14}$  for 12 hours  
 $1 \times 10^{-13}$  for 10 days

These numbers apply also to CRG outputs (sine waves with harmonic distortion of no greater than 5% for the output frequencies.) In addition, the master clock must provide timing pulses with no more than 10 ns/second rms jitter.

---

## The Receiver/Exciter Subsystem

Within the Receiver/Exciter Subsystem (RCV), there are three components which are of interest in terms of the experiment:

1. The Exciter; which provides the basis for the uplink (S-Band) frequency.
2. The Closed-Loop Receivers which provide the downlink signal to the Doppler Extractor and thence to the Tracking Subsystem (DTK).
3. The Open-Loop, Multi-mission Receivers which provide the downlink signal to the Radio Science Subsystem (DRS).

Each of these rely upon FTS inputs. See figure 6 for a Block diagram of the Receiver/Exciter Subsystem.

Within the Exciter, the primary exciter reference frequency, upon which the uplink is based, is directly derived from a CRG-provided 50 MHz reference frequency.

The Closed-Loop Receivers use a phase-locked loop to follow the downlink signal. The signal is fed by these receivers to the Doppler Extractor where it is mixed with the present output of the Exciter. The resultant signal coming from the Doppler Extractor (whether S-Band or X-Band) is mixed-down using a combination of 1 MHz and 50 MHz frequencies supplied by the CRG. The Closed-Loop Receivers also use the following FTS products; from the TFA: 1, 10, 100 and 1k pps; from the CRG: 0.1 MHz, 1.0 MHz, 5 MHz, 10 MHz, 10.1 MHz, 45 MHz, 50 MHz and 55 MHz. (In short, all of the present CRG outputs are used by the Closed-Loop Receivers in some fashion.)

The Open-Loop Multimission Receiver uses a 50 MHz reference signal supplied by the CRG to mix the signal down into the range of the Narrow Bandwidth filters within the receiver prior to sending the signal to the ODA. This is a particular instance where FTS performance can directly impact data since any noise in the 50 MHz reference frequency will be mixed directly into the signal.

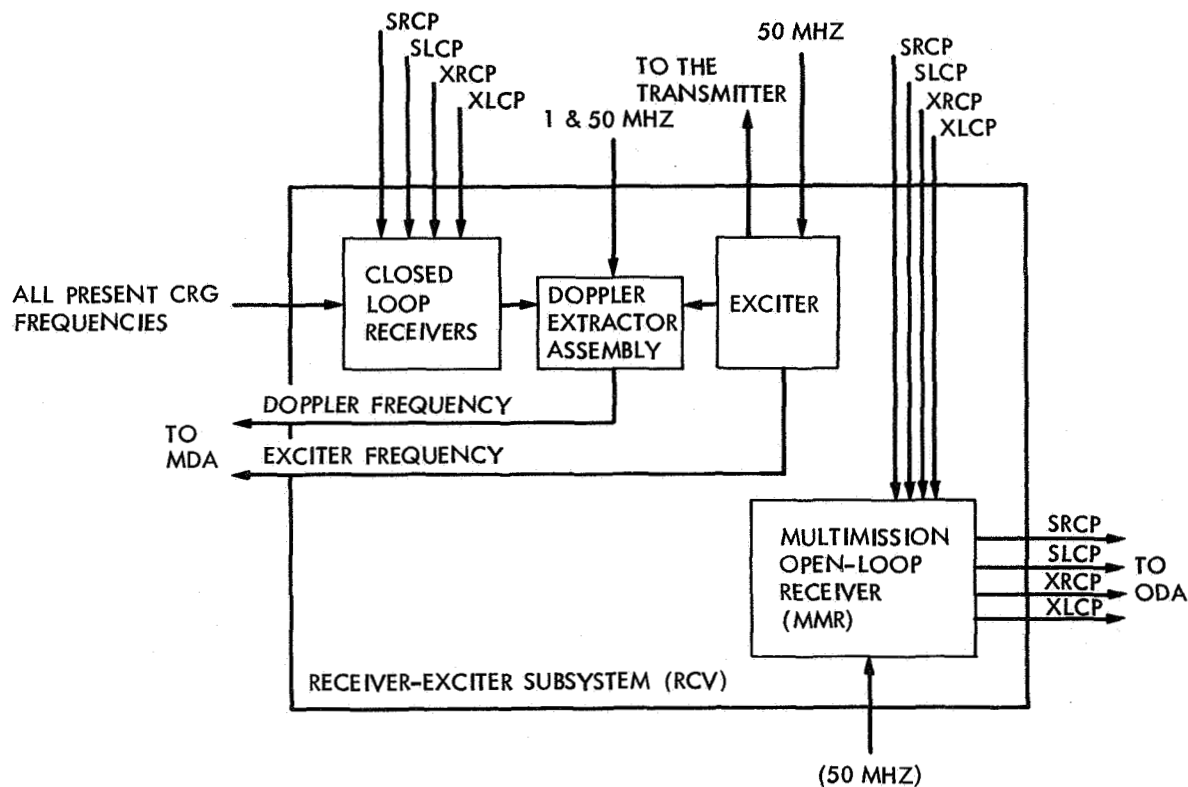


Figure 6. Block Diagram of the Receiver-Exciter Subsystem (RCV). Note that the input frequencies shown are SRCP = S-Band (Right-Circular Polarization), SLCP = S-Band (Left-Circular Polarization), XRCP = X-Band (Right-Circular Polarization) and XLCP = X-Band (Left-Circular Polarization.)

## The Tracking Subsystem

The primary user of frequency and timing products in the DSS Tracking Subsystem (DTK) is the Metric Data Assembly (MDA). The MDA utilizes:

1. From the TFA,
  - a) Timing pulses (1, 10, 100 and 1k pps)
  - b) GMT Epoch
2. From the CRG,
  - a) Frequencies: 1 MHz, 5 MHz and 10 MHz  
(to the frequency counters)
3. From the FTS Master Clock,
  - a) 10 pps (to the frequency counters).

Using inputs from the Receiver/Exciter Subsystem, the frequency counters of the MDA measure both the exciter reference frequencies and the resultant doppler frequencies. Following receipt of a timing pulse from the TFA, the frequency counters count radio frequency (RF) cycles and measure any fractional portion of an RF cycle which has occurred. (These counters are driven by the Master Clock's 10 pps reference timing pulse.) The resulting phase data are sent to the MDA's computer (a Mod Comp II/25) for collection and transmission back to the Jet Propulsion Laboratory (in real-time) via High Speed Data Lines (HSDLs). The data is ultimately recorded at JPL. This forms the basis for the closed-loop experiment. See figure 7 for a block diagram of the essentials of the Tracking Subsystem.

## The Radio Science Subsystem

The DSS Radio Science Subsystem (DRS), takes the baseband signal provided by the Multimission Receiver, digitizes and then records it on magnetic tapes which are ultimately delivered to JPL. The primary component of the DRS is the Occultation Data Assembly (ODA). See figure 8 for a block diagram of the DRS. From the various frequency and timing products, the DRS accepts:

1. From the TFA, a) Timing pulses (1 pps)  
b) GMT Epoch
2. From the CRG, a) Frequencies: 10 MHz (to the ODA)
3. From the FTS a) 10 pps. (to the Freq. Monitor Subassembly).  
Master Clock,

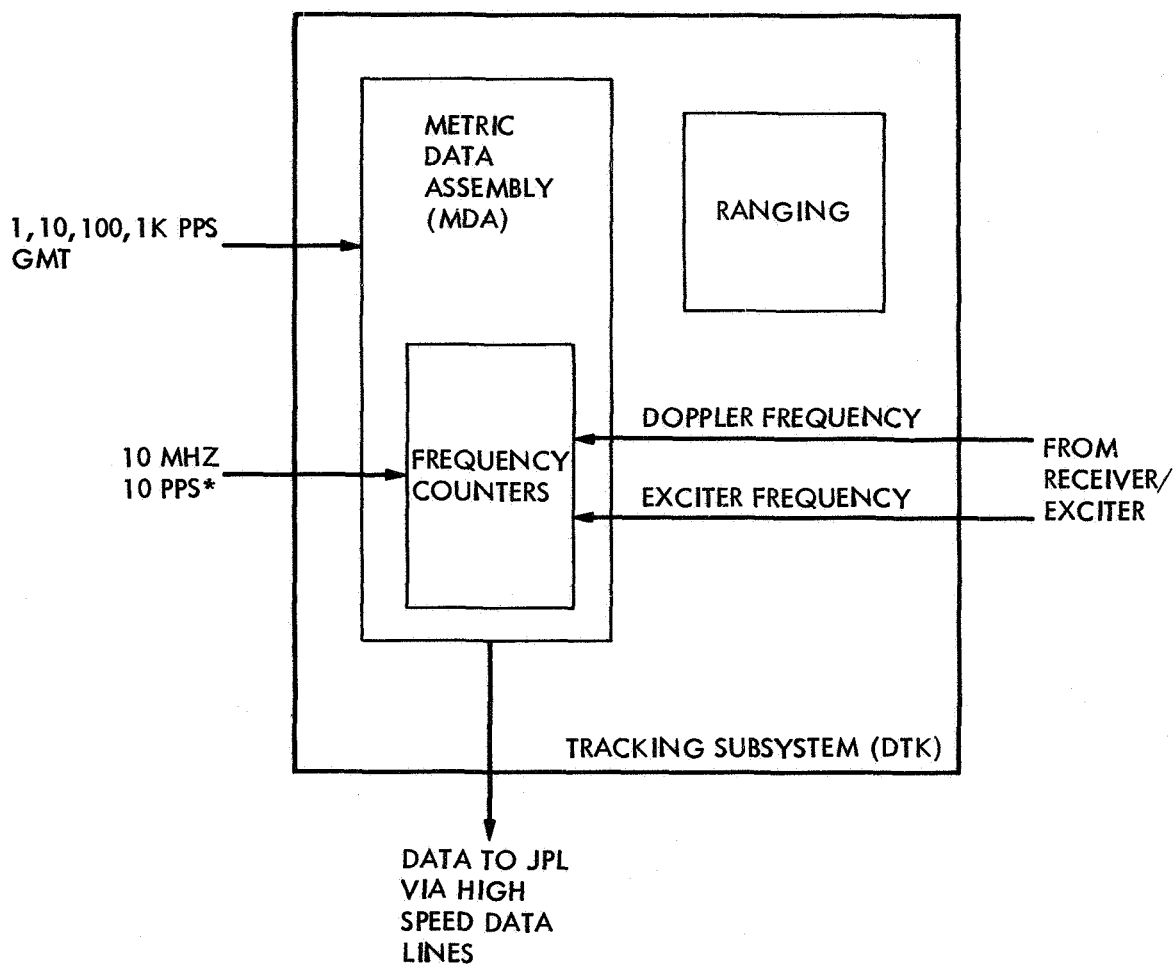


Figure 7. Block Diagram of the Tracking Subsystem (DTK).  
\*From the Station Reference Clock.



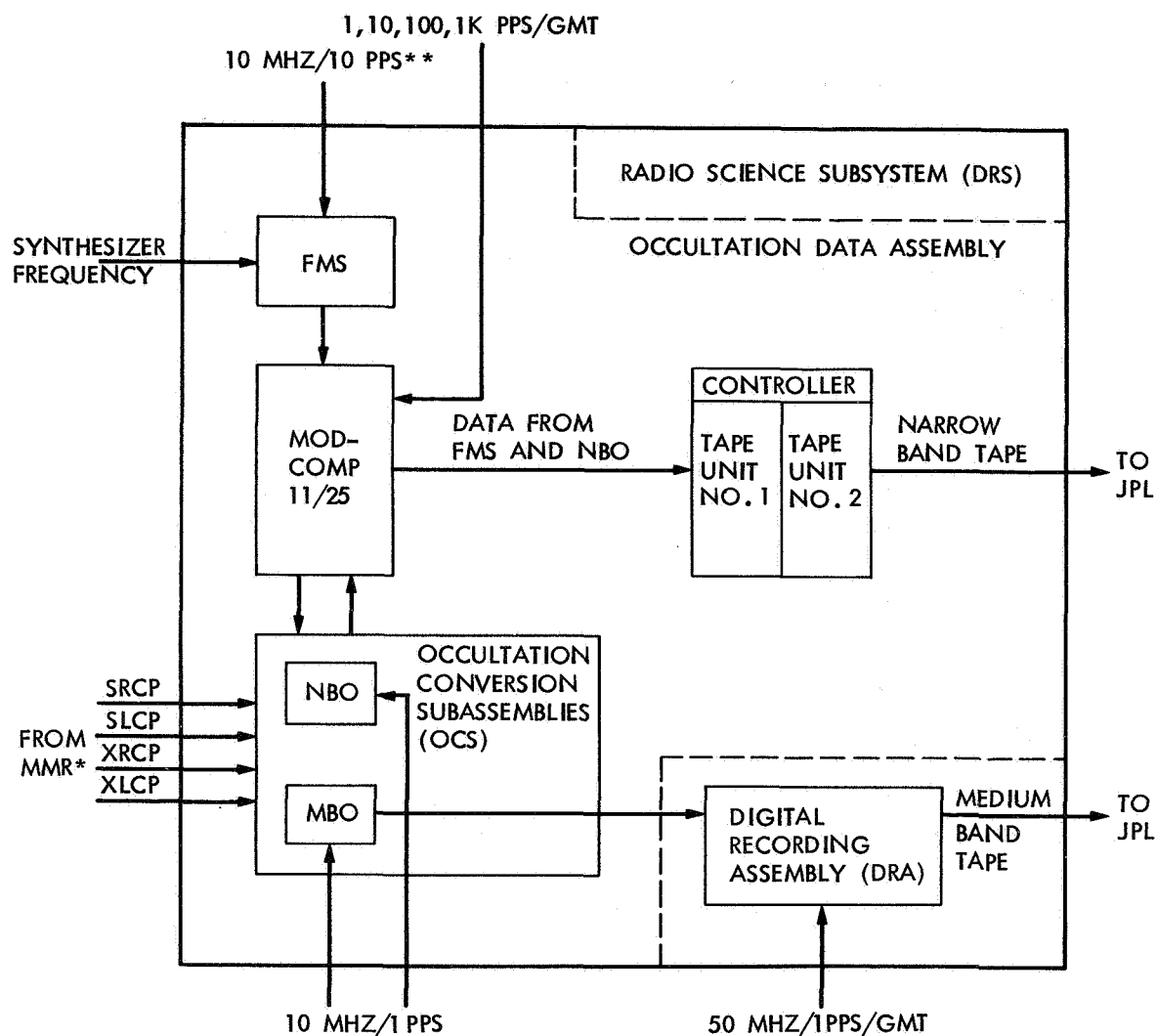


Figure 8. The Radio Science Subsystem (DRS). Note that the following acronyms are used above: "NBO" = Narrow Band Occultation Data Conversion Subassembly; "MBO" = Medium Band Occultation Data Conversion Subassembly; "FMS" = Frequency Monitor Subassembly.

\*These frequencies have been mixed down to audio levels.

\*\*The 10 pps is from the Station Reference Clock.

It is anticipated that during any gravity wave experiment that the DRS will operate in the 'Narrow-Band Mode' due to the narrow bandwidth of the MMR filters which are available in that mode and the resultant high values of the signal-to-noise ratio in the input to the ODA.\* (This can be an important factor when the spacecraft being used in the experiment is distant from the Earth.) In the Narrow-Band Mode, the DRS will digitize and format the incoming signal within the ODA's Narrow Band Occultation Conversion Subassembly (NBO). At this point, the experiment can be impacted by FTS performance as the analog-to-digital converters within the NBO rely upon a 10 MHz reference frequency provided by the CRG. Once digitized, the ODA records the data on magnetic tapes which again rely upon the FTS for precision time-tagging. These tapes are ultimately shipped back to JPL.

#### Planned Capabilities (Mark IVA Era)

In the coming years, a number of changes will be made in the current Frequency and Timing System within the DSN to supply improved mission support. The Mark IVA specifications will include:

CRG Outputs: Sine Waves with Harmonic distortion = 5% at the following frequencies: 0.1 MHz, 1.0 MHz, 5.0 MHz, 10.0 MHz, 10.1 MHz, 45.0 MHz, 50.0 MHz, 55.0 MHz and 100.0 MHz. (The 100 MHz is for the MMR.)

TFA Outputs: Timing pulses with a general stability of 10 ns/sec. rms at: 1 pps, 10 pps, 100 pps and 1 kpps. In addition, an improved 10 pps timing pulse with an rms jitter of 2 ns/sec. will be provided to the MDA/ODA.

---

Note: The Digital Recording Assembly (DRA) records data taken while the ODA is in the Medium Band Mode. It will not be used during this experiment. (It receives a 50 MHz reference from the CRG.)

\*Note: The Narrow Band filters' bandwidths range from  
100 Hz to 8180 Hz (S-Band)  
100 Hz to 30 KHz (X-Band)

Each Deep Space Communications Complex (DSCC) (as regards this experiment, "DSCC" may be taken as being equivalent to the term "DSS" used previously) will have 2 Hydrogen Maser frequency standards (1 prime and a back-up) as well as 2 Cesium Beam standards (as back-up references.) Each of the Hydrogen standards will continue to have a setability within  $7 \times 10^{-15}$  and will conform to the following stability performance levels<sup>6</sup>.

$1 \times 10^{-12}$	over 1 second
$1 \times 10^{-14}$	over $10^4$ seconds
$1 \times 10^{-14}$	over 12 hours
$1 \times 10^{-13}$	over 10 days.

In addition, critical FTS products will be distributed to the various subsystems via stabilized transmission lines with performance levels comparable to those above. (CRG outputs to be sent via these lines include 5 MHz reference frequencies to the closed-loop receivers and a 100 MHz for the MMR.)

#### DSN Capabilities circa 1987-1990

Anticipating the requirements of a gravitational wave experiment, the following numbers may be taken to represent the "best-case" capabilities of the DSN's Frequency and Timing System in the 1987-1990 era<sup>7</sup>:

1. Frequency Standards Stabilities better than:  $3 \times 10^{-16}$  for periods  $300 \text{ seconds} \leq T \leq 30 \text{ days}$ ,
2. 10 ns/second rms jitter accuracy timing pulses, with certain 2 ns/second rms jitter pulses for the DTK and DRS.
3. Time Synchronization to  $\pm 10 \text{ ns}$  between DSCC's,
4. Time Synchronization to  $\pm 100 \text{ ns}$  between the DSN Master Clock and UTC (USNO/NBS).

#### IV. SUMMARY

Table 2 contains a comparison of the capabilities of the Deep Space Network and the nominal requirements of the gravitational wave experiment.

Table 2. FREQUENCY STANDARD/DELIVERED PRODUCTS DESIRED STABILITIES

DSN Capabilities	$\Delta F/F$	Burst Duration, T
Current (Mark III)	$\leq 3 \times 10^{-13}$	over $10^4$ seconds
Planned (Mk IVA)	$\leq 1 \times 10^{-14}$	over $10^4$ seconds
Suggested ('87-90)	$\leq 3 \times 10^{-16}$	300 sec. $\leq T \leq$ 30 days

Expt. Requirements	$\Delta F/F$	Burst Duration, T
Baseline Expt.	$\leq 1 \times 10^{-16}$	50 sec. $\leq T \leq$ 5000 sec.
Desirable Expt.	$\leq 1 \times 10^{-18}$	50 sec. $\leq T \leq$ 5000 sec.
Range of Events	$10^{-14}$ to $10^{-17}$	40 sec. $\leq T \leq$ 40000 sec.

Although the stability requirements for the "baseline experiment" will not be approached for a number of years, the uncertainties which were involved in the derivation of the Range of Events and the efficacy of current post-processing techniques (which are not discussed here) suggests that experiments should be carried-out during the 1980's. (In point of fact, an experiment is currently being conducted by the DSN using the Pioneer 10 Spacecraft.)

# REFERENCES:

- <sup>1</sup> J.M. Weisberg & J.H. Taylor; General Relativity and Gravitation, Vol. 13, #1; (1981), pp 1-6.
- <sup>2</sup> C.W. Misner, K.S. Thorne & J.A. Wheeler; "Gravitation"; W.H. Freeman and Company, San Francisco California; (1973), pp 943-1044.
- <sup>3</sup> Private Communication with R. Hellings; JPL, (Nov. 1981.)
- <sup>4</sup> K.S. Thorne & V.B. Braginsky; Astrophysical Journal, 204; (15 Feb. 1976), pp L1-L6.
- <sup>5</sup> N.A. Renzetti & A.L. Berman; JPL Publication 80-93: "The Deep Space Network--An Instrument for Radio Science Research"; (15 Feb. 1981).
- <sup>6</sup> R.C. Coffin, D.E. Johnson & P.F. Kuhnle; "Frequency and Timing System for the Consolidated DSN & STDN Tracking Network"; Proceeding of the 12th Annual PTTI Meeting, Nasa Conference Publication 2175;(Dec. '80)
- <sup>7</sup> D.E. Johnson (prepared by); JPL Document: 824-13 "DSS (Mk III-77) and DSCC (Mark IVA) Subsystem Requirements: Frequency and Timing Subsystem"; (1 Sept. 1981).

Acknowledgements: Many thanks for the assistance of R. Kursinski, P. Wolken, J. LuValle and S. Ward.

## APPENDIX A

The following is suggested as an enhancement of the utilization of the DSN's Frequency and Timing System in some future gravitational wave experiment:

It has been suggested<sup>A1</sup> that by tracking two spacecraft simultaneously that the direction of propagation of an incoming gravitational wave could be resolved. (A single spacecraft merely resolves the direction of propagation to within some family of directions which forms a cone.)

Alternately, the simultaneous tracking of a single spacecraft by two stations (one of them in the three-way mode) could also resolve the direction of incidence of the wave via a correlation of the doppler tracking records from the two DSS's. Such a correlation could, if the rise-time of the pulse caused by the gravitational wave were sharp enough, yield the time-delay between the incidence of the plane wave on the two stations. Given that gravitational waves propagate at the speed of light, this yields a second family of directions (i.e., a second cone) and hence could resolve the direction of incidence.

---

<sup>A1</sup> R. Hellings; Physical Review D, Vol. 17, #12; (15 June 1978), pp 3158-3163.

## QUESTIONS AND ANSWERS

PROFESSOR ALLEY:

Thank you, very much. That's an excellent review.

I greatly admire this kind of approach, where you are trying to measure with what we have got, and not taking the theorists too seriously.

I mean, one could well be surprised and find something in this approach.

MR. ANDERSON:

It's an experimental approach is it not? Yes. We do have something that's tantalizing, and should be applied, I think.

I agree. Yes. Thank you.

DR. WINELAND:

For your modes coherent source, what kind of strains do you expect?

MR. ANDERSON:

Probably nothing about 10 to the minus 15. This would be orbiting black holes at the galactic center, or perhaps in a galactic halo.

DR. WINELAND:

In terms of known binary systems?

MR. ANDERSON:

Well, that goes way down below that. I'm not sure in this frequency region. But it's probably below, certainly below 10 to the minus 16. I don't know the exact magnitude region.

But I don't think you'd see any of that kind of thing. That probably is better picked up at higher frequencies by ground-based antennas, or laser interferometry techniques, or some such thing. Use the higher frequency gravity waves, rather than these low frequency waves we're looking for.

PROFESSOR ALLEY:

May I ask another?

In the gravity radiations you might expect, say a supernova collapsed in the Virgo cluster, the dimensions amplitude is very small. Like  $10$  to the minus  $21$ , or so. Yet, even with that kind of an amplitude, the weakness of coupling and so on -- this corresponds to an analog of the pointing vector. The energy per second per square centimeter that is on the order of hundredths or tenths the solar constant.

Now do you know a corresponding number in these longer wave lengths regions. Say you have a strain of  $10$  to the minus  $16$ , the actual energy per second per unit area is quite large.

MR. ANDERSON:

Well, that's right. It is. I haven't done that calculation. No. But that's a fascinating question.

PROFESSOR ALLEY:

I did the calculations and got at the energy flux for even this very weak Virgo cluster kind of thing.

DR. WINKLER:

It has to correspond, somehow, to  $10$  to minus  $29$  grams per cubic centimeter, which is the average -- the corresponding energy  $MC^2$ . Because it would have to be that missing mass to close the universe.

PROFESSOR ALLEY:

You are talking maximum --

DR. WINKLER:

That's right, that's right.

PROFESSOR ALLEY:

I guess you could make some estimates that way.

MR. ANDERSON:

That was a few parts in  $10$  to the  $14$ th over a  $1,000$  seconds wasn't it? Yes.



PROFESSOR ALLEY:

People, I think, ought to be aware that if the power is the weakness of coupling of these things. Not the amount of energy that is actually, presumably, fallen, if these ideas are correct.

MR. ANDERSON:

Yes.

PROFESSOR ALLEY:

It's very disheartening to hear that one can't get an X-band transponder on before the 1990's because of the paucity of space missions and so on.

There is another spacefaring nation, or even other -- several spacefaring nations. Do you know of any plans to put the appropriate equipment on planetary probes, so that one could make the kind of measurements you have indicated in the last few minutes?

MR. ANDERSON:

Unfortunately, there are no plans. No international --

PROFESSOR ALLEY:

The Soviets are not planning anything?

MR. ANDERSON:

Oh, I have no idea about the Soviets. I was thinking more in terms of the Japanese or Europeans. But, no, as far as I know, there are no plans to put our transponders on foreign spacecraft to do this kind of experiment.

There's no international cooperation on that level that I know of.

Of course, we had a spacecraft where we planned to do that. This was the ISPM mission. And we were going to put an X-band transponder in the American spacecrafts. Then the American spacecraft was scrubbed. Right.

So we only have an European spacecraft there now. And there are no -- that's an S-band system.

PROFESSOR ALLEY:

The opportunities are really going amiss.

MR. ANDERSON:

Yes.



## THE IMPLICATIONS OF PRECISE TIMEKEEPING FOR DOPPLER GRAVITATIONAL WAVE OBSERVATIONS

John D. Anderson, F. B. Estabrook, and J. W. Armstrong,  
Jet Propulsion Laboratory, California Institute of Technology,  
Pasadena, California

### ABSTRACT

Gravitational radiation from galactic and extragalactic astrophysical sources will induce spatial strains in the solar system, strains which can be measured directly by the Doppler radio link to distant spacecraft. We delineate current noise sources in Pioneer and Voyager Doppler data and make a comparison with expected signal levels from gravitational wave sources. The main conclusion is that it is possible to detect gravitational radiation with current DSN hydrogen maser systems stable in fractional frequency to  $\pm 2 \times 10^{-14}$  over 1000 sec. In the future, however, a serious Doppler observational program in gravitational wave astronomy will require frequency systems stable to at least  $10^{-16}$ , but at the same time the current single frequency S-band uplink transmission will have to be replaced by a dual frequency capability. In the meantime it is more likely that the S-band uplink will be replaced by a single X-band link, thereby improving the overall system frequency stability to the limit of the hydrogen maser system itself. This option, though attractive, seems more limited by the lack of X-band transponders on distant spacecraft than by the development of ground systems by the DSN. Earth tropospheric effects will not be a problem until stabilities of  $\pm 5 \times 10^{-15}$  or better are realized.

### INTRODUCTION

Gravitational radiation arises from the Einstein theory of gravitation (general relativity) which modifies the Newtonian concept of the gravitational force acting instantaneously at a distance to a modern view of a gravitational field which travels at finite speed  $c$  away from a source. The Einstein field equation, which is analogous to the Maxwell equations of electromagnetism (EM), is  $G = 8\pi T$ , where  $T$  is a second rank stress energy tensor representing the source of the gravitational field and  $G$  is a second rank tensor made up of

quantities describing the curvature of the four dimensional space-time continuum. Exact solutions of the Einstein field equations are few in number, and numerical techniques are now yielding most of the interesting descriptions of material interactions and associated Gravitational Waves (GW) [1]. Much of the physics of the generation of GW and their propagation can be understood by considering gravitation as a weak perturbation to an empty, flat space of special relativity. Under this restriction, it is possible to derive a wave equation from the Einstein field equations [2], and to predict gravitational radiation from material events in direct analogue to EM radiation from moving charges. However, unlike EM where both positive and negative charges exist, matter is made up of only positive mass, and as a result, the lowest order form of gravitational radiation is quadrupole, in contrast to the fundamental dipole EM radiation. Also, a spherically symmetric source of GW is impossible, and thus large deviations from spherical symmetry are required in sources useful for detection. For these reasons, in addition to the fact that energies of GW are about  $10^{-43}$  times smaller than EM energies from a comparable source, laboratory experiments of the type performed by Hertz are practically impossible for gravitational radiation. Yet few theorists doubt the existence of GW, for the reason that once one has transformed gravitation from the Newtonian concept of action at a distance to a modern concept of disturbances in a gravitational field which propagate at a finite velocity, it is difficult to avoid the consequence that GW carry energy, and interact with matter. In fact, the existence of GW is more widely accepted than the continuing validity of general relativity.

If GW cannot be produced and detected in the laboratory, then we must look to strong natural sources. The coupling of gravitational waves to matter is weak, and only the most violent astrophysical events generate waves of sufficient amplitude for detection at earth. For example, the current Doppler gravitational radiation search with Pioneer 10 could marginally detect the waves from a collision of two black holes with a total mass of 10,000 times the mass of the sun at the distance of the center of the galaxy. However, a beneficial consequence of weak coupling is that gravitational radiation has an enormous penetrating capacity which would give astronomers a clear window onto parts of the Universe that are totally opaque to even the hardest X-rays, a view which would include the internal structure of supernovae and the details of gravitational collapse of objects with masses of  $10^6$  solar masses or more.

The technique of using Pioneer or other distant spacecraft to detect GW is to monitor the Doppler shift of the radio signal, continuously transmitted to the spacecraft and coherently transponded back to earth. If the velocity induced Doppler shift is removed from

the records, then the remaining data can be analyzed for GW. The characteristics of the GW signal, embedded in a Doppler time series, have been discussed previously [3] and will not be repeated here.

#### CURRENT EXPERIMENTS

We are currently using two spacecraft, Pioneer 10 and Pioneer 11, for the detection of GW. The first acquisition of GW data started on November 15, 1981, from Pioneer 10, and will continue until December 8, 1981. During this interval Pioneer 10 will be at opposition where the noise from interplanetary plasma scintillations is at a minimum and the chances for the detection of GW are greatest. About six months later, Pioneer 11 will be at opposition and data will be acquired again. We plan to follow this pattern for several oppositions, thereby obtaining three weeks of relatively low-noise data about every six months.

The uplink to Pioneer 10/11 is a 20 kW S-band (2.2 GHz) signal radiated from one of the 64-meter parabolic antennas of the Deep Space Network (DSN). The signal is tracked in a phase-locked loop on board the spacecraft and coherently transponded at S-band at a power of 8 watts. In normal DSN operation, the received signal is tracked in a phase-locked loop, a hydrogen maser clock being used to beat the frequency down to the Doppler tone.

The two important limiting noise sources on the Pioneer Doppler system are the weak signal levels at distances of 20 to 40 AU, and scintillations in the Doppler signal caused by scattering of the S-band signal by free electrons in the interplanetary medium. Our estimate for the Doppler noise in  $\Delta f/f$  for the Pioneer spacecraft with its high gain 2.74m parabolic antenna fed by an 8 watt transmitter and using a 64m DSN receiving station is

$$\sigma_y \approx 7 \times 10^{-15} \left( \frac{100 \text{ sec}}{\tau} \right) \left( \frac{D}{5 \text{ AU}} \right)$$

where  $\tau$  is the integration time for the Doppler signal,  $D$  is the distance of the spacecraft, and  $\sigma_y$  is the square-root Allan variance of  $y \equiv \Delta f/f$ . For a distance of 20 AU, and a 100 sec integration time, the noise in the Doppler link because of a weak signal is about  $3 \times 10^{-14}$ . Pioneer 11 will not exceed a distance of 20 AU until 1986, but Pioneer 10 is beyond that distance now and will reach nearly 40 AU by 1986. However, the noise in the Pioneer 10 Doppler link can be held to an acceptable level of 2 or  $3 \times 10^{-14}$  by increasing the integration time to 200 or 300 sec. Signal to noise limitations are not a serious problem for either spacecraft.

Another significant limiting error source for the Pioneer Doppler link is interplanetary phase scintillation associated with refractive

index fluctuations in the solar wind. Armstrong, Woo, and Estabrook [4] have reported observations of radio wave phase scintillation, using the Viking spacecraft. The phase power spectrum level varies by seven orders of magnitude as the Sun-Earth-spacecraft (elongation) angle changes from  $1^\circ$  to  $175^\circ$ . It is noteworthy that a broad minimum in the S-band (2.3 GHz) phase fluctuation occurs in the antisolar direction; the corresponding fractional frequency stability (square root Allan variance) is  $6 \times 10^{-14}$  for 1000s integration times. The ionospheric contribution is significant but it is dominated by the contribution from the interplanetary medium. Nondispersive tropospheric scintillation was not detected in the Viking data, and more recent work by Armstrong and Sramek [5], using data from the National Radio Astronomy Observatory's Very Large Array (VLA), indicates that tropospheric noise should not be evident in either the Viking or the Pioneer data.

In summary, it is realistic to expect a sensitivity of  $6 \times 10^{-14}$  in the Pioneer Doppler link at opposition, even under additional considerations of limits in the stability of the hydrogen maser frequency standard system, kT noise in the various electronic subsystems, nongravitational translational forces on the spinning spacecraft, and resolution limits in the Doppler extraction system.

#### FUTURE REQUIREMENTS FOR FREQUENCY STABILITY

We have shown in the previous section that current Doppler searches for GW are not limited by the DSN hydrogen maser systems, but instead by plasma noise in the S-band radio link. While Pioneer is equipped with only an S-band transponder, Viking and Voyager have both S-band and X-band on the down link in an 11:3 frequency ratio. This difference in frequency can be used to remove most of the plasma noise on the down link by making use of the dispersive nature of electron scattering [6]. Unfortunately, it is not possible to establish enough spatial and temporal coherency between the uplink and downlink to reduce the plasma noise significantly on the S-band uplink. We have learned from experience that the advantage of the Voyager radio system over the single frequency Pioneer system is that the plasma noise can be reduced by about a factor of two; there is one noisy S-band link on Voyager (uplink), and two noisy S-band links (uplink and downlink) on Pioneer. Therefore, while the best low-noise environment on Pioneer is at about  $6 \times 10^{-14}$ , on Voyager it is at about  $3 \times 10^{-14}$ , still slightly above the DSN hydrogen maser system. The radio system being integrated into the 1985 Galileo mission to Jupiter is essentially the same as Voyager, so there is no real prospect for improvement over current systems in the 1980's. One exception might be a mission to the Sun (Starprobe) in the late 1980's; it could be used for GW detection [7] because of its required flyby of Jupiter for a gravity assist.

The Doppler search for GW over the next decade will probably be carried out in the noise environment displayed in Fig. 1. Here, we plot the error in the Doppler frequency, expressed as square-root Allan Variance, as a function of the Doppler integration time for a number of significant noise sources. In the region of 1000 sec, a representative region for the GW search, the solar plasma noise clearly dominates. The dotted line is representative of current DSN hydrogen masers, although the present overall frequency system may be an order of magnitude worse. However, with sufficient effort, stabilities on the order of  $10^{-15}$  over 1000 sec could be obtained.

We now address the problem of whether there are any GW sources of sufficient power to be detected in the noise given by Fig. 1. Estimates of the dimensionless amplitude of GW reaching the solar system from a variety of sources have been made by Thorne [8] and are shown in Fig. 3. The dimensionless amplitude represents the spatial strain in the gravitational field and is the quantity that is measured directly by the spacecraft Doppler technique. Thus at frequencies of GW in the VLF region of  $10^{-4}$  Hz, we would not violate anyones "cherished beliefs" if we detected Doppler shifts  $\Delta f/f$  of a few parts in  $10^{13}$  from bursts of GW, but we would not expect to see bursts above a level of  $10^{-15}$ . However, we might see a stochastic background of GW at a level of  $10^{-14}$ , a level that is just a little beyond the reach of Pioneer and Voyager. A clear detection of GW could be achieved with bursts of unexpectedly large magnitude. In the absence of such bursts, we can report a limit on the magnitude of bursts hitting the solar system during the times when spacecraft are being used for detection purposes, and also we can place a limit on the stochastic background in the region of  $10^{-4}$  Hz. This is rather useful negative information which has been reported to various levels of accuracy at various frequency bands by other experimenters over the past 15 or 20 years. By analyzing long records of Doppler data, extending over several days, it might be possible to detect coherent sources of GW at a level below the plasma curve (2) in Fig. 1. However, it is doubtful that any coherent sources exist in the Doppler detection band with strain amplitudes much above  $10^{-15}$  [9].

The probability of detecting GW by the Doppler technique can be increased substantially by simply replacing the current S-band uplink with an X-band link. The resulting noise environment is shown in Fig. 2. At the same time, improvements could be made in the DSN ground systems. We reflect this by a much improved, but reasonable, noise curve (1) for the receiver. The hydrogen maser curve (4) is based on the performance of selected "good" DSN masers now in hand. A comparison of Fig. 2 with Fig. 1 shows about an order of magnitude improvement with the addition of X-band uplink. The problem with



achieving the noise performance of Fig. 2 is that with the paucity of planetary missions planned for the 1980's there is presently no candidate spacecraft to carry an X-band transponder to the outer solar system.

If we look further ahead into the 1990's, it is possible that spacecraft radio systems will be flown with multifrequency capabilities. Plasma noise will not be a problem. Then, if the frequency standard is the limiting noise source, it will be important to use systems that are stable to  $10^{-16}$  over 1000 sec. At this level, the Doppler system could be an important tool of observational astronomy in the VLF region of the GW spectrum. At this point, though, we would have to be concerned with tropospheric noise. Some improvement over line (3) in Fig. 2 could be achieved by atmospheric monitoring, but in the long run the best solution would be to remove the tracking station from the surface of the earth. Possibilities that come to mind are an orbiting space station or a permanent lunar base.

# REFERENCES AND NOTES

1. Smarr, L. L., Sources of Gravitational Radiation, Cambridge University Press, Cambridge, 1979.
2. Misner, C. W., Thorne, K. S., and Wheeler, J. A., Gravitation, Chaps. 18 and 35, Freeman, San Francisco, 1973.
3. Estabrook, F. B. and Wahlquist, H. D., "Response of Doppler Spacecraft Tracking to Gravitational Radiation," GRG 6, 439-447, 1975; Hellings, R. W., "Testing Relativistic Theories of Gravity with Spacecraft Doppler Gravity Wave Detection," Phys. Rev. D. 17, 3158, 1978; Mashoon, B., "On the Detection of Gravitational Radiation by the Doppler Tracking of Spacecraft," Ap. J. 227, 1019-1036, 1979.
4. Armstrong, J. W., Woo, R., and Estabrook, F. B., "Interplanetary Phase Scintillation and the Search for Very Low Frequency Gravitational Radiation," Ap. J. 230, 570, 1979; Erratum, Ap. J. 240, 719, 1980.
5. Armstrong, J. W., JPL Interoffice Memo 3333-81-070, July 20, 1981.
6. Muhleman, D. O. and Anderson, J. D., "Solar Wind Electron Densities from Viking Dual-Frequency Radio Measurements," Ap. J. 247, 1093-1101, 1981.
7. Estabrook, F. B., "Gravitational Wave Detection with the Solar Probe. II. The Doppler Tracking Method," in A Close-Up of the Sun, M. Neugebauer and R. W. Davies, eds., JPL Publication 78-70, September 1, 1978.
8. Thorne, K. S., "Gravitational-Wave Research: Current Status and Future Prospects," Rev. Mod. Phys. 52, 285-297, 1980.
9. Wahlquist, H. D. and Estabrook, F. B., manuscript received from the authors.
10. We acknowledge several significant contributions to the ideas expressed in this paper by H. Wahlquist, R. W. Hellings, and J. M. Rotenberry of JPL. This research was carried out at the Jet Propulsion Laboratory, California Institute of Technology, under NASA contract NAS7-100.

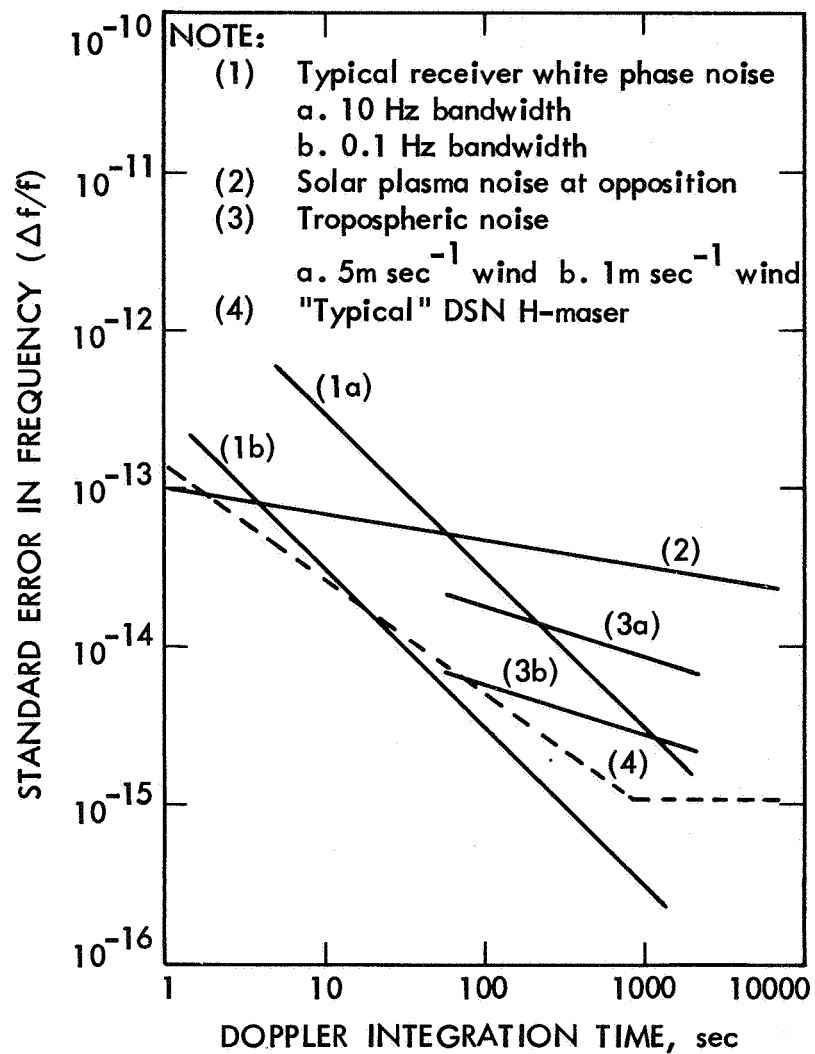


Fig. 1 Doppler Noise for Current S Band Systems

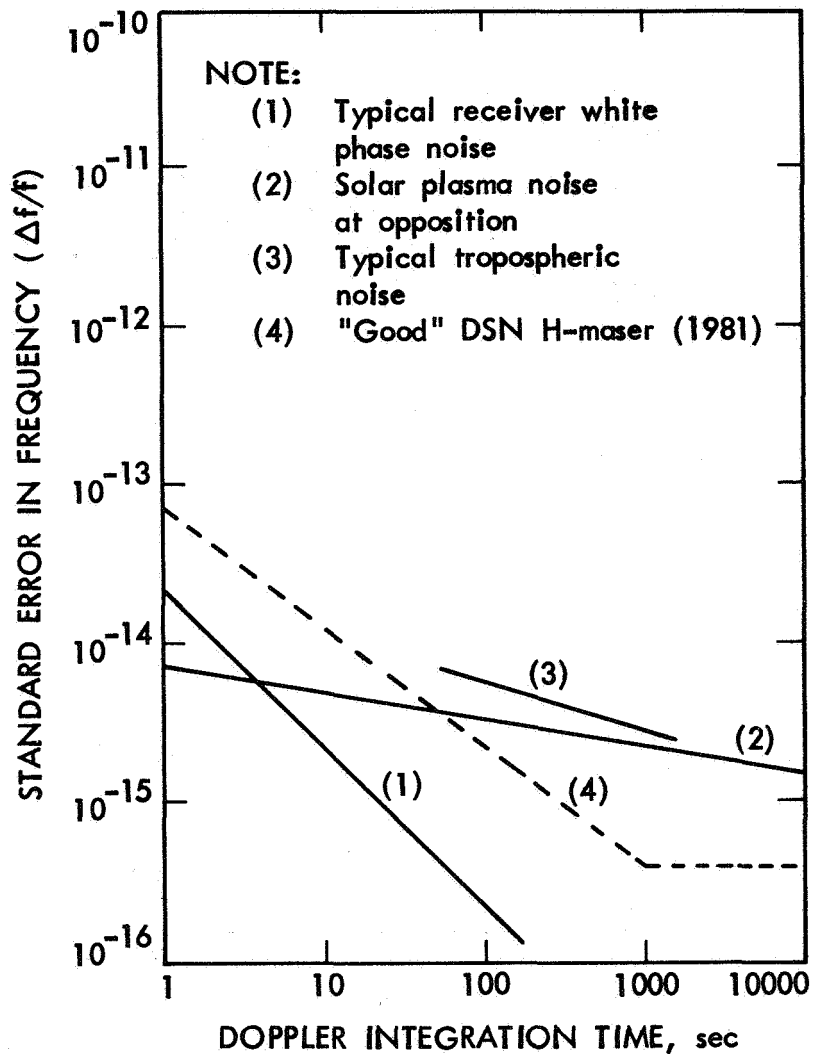


Fig. 2 Doppler Noise for Projected X-Band Systems

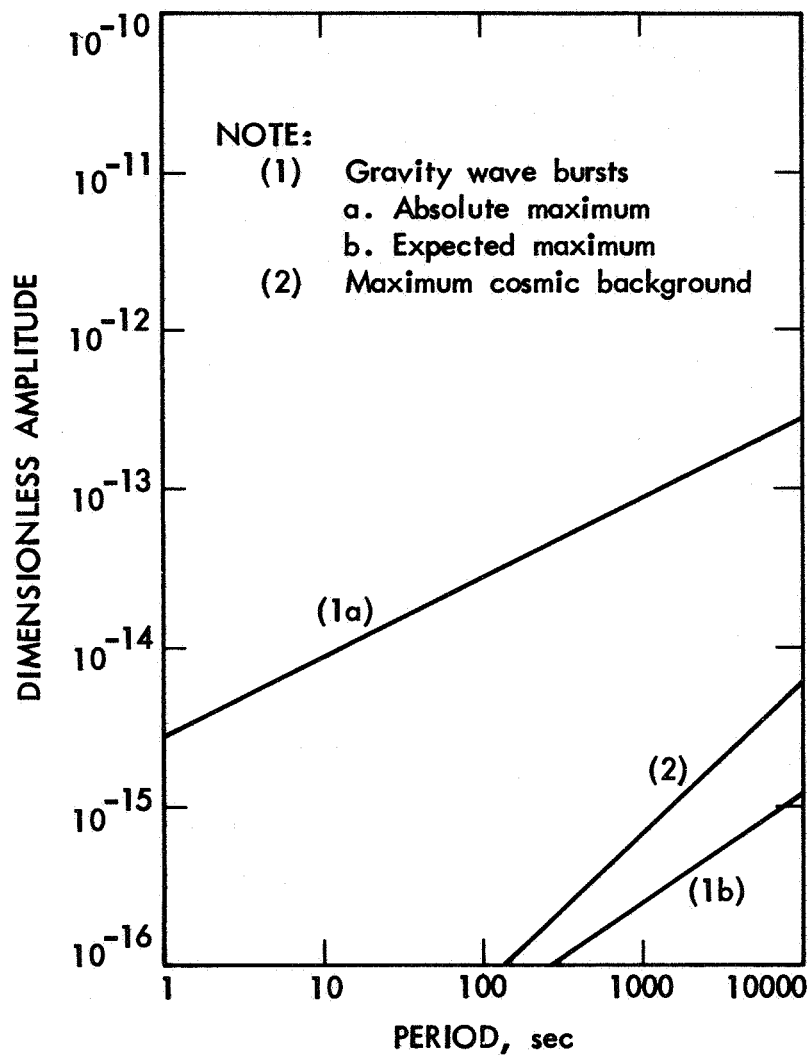


Fig. 3 Estimates of the Amplitude of Various GW Sources  
(After Thorne [8])

## LAMP RELIABILITY STUDIES FOR IMPROVED SATELLITE RUBIDIUM FREQUENCY STANDARD

R. P. Frueholz, M. Wun-Fogle, H. U. Eckert, C. H. Volk and P. F. Jones  
The Aerospace Corporation, P.O. Box 92957, Los Angeles, CA 90009

### ABSTRACT

In response to the premature failure of Rb lamps used in Rb atomic clocks onboard Navstar GPS satellites The Aerospace Corporation has initiated experimental and theoretical investigations into their failure mechanism. The primary goal of these studies is the development of an accelerated life test for future GPS lamps.

At this time the primary failure mechanism has been identified as consumption of the lamp's Rb charge via direct interaction between Rb and the lamp's glass surface. The most effective parameters to accelerate the interaction between the Rb and the glass are felt to be rf excitation power and lamp temperature. Differential scanning calorimetry is used to monitor the consumption of Rb within a lamp as a function of operation time. This technique has already yielded base line Rb consumption data for GPS lamps operating under normal conditions.

In order to insure acceleration methods do not alter the mechanism of the Rb-glass interaction detailed surface studies yielding information about the mechanism of interaction are in progress. It has been found that penetration profiles of Rb into pyrex surfaces can be analyzed in terms of one-dimensional diffusion models. Diffusion coefficients may be extracted via these models. The surface studies also indicate that Rb exists in at least two forms in pyrex, a thin colored surface layer and the major colorless penetration component. Further experiments are in progress to extend these results to a wide variety of glasses.

### INTRODUCTION

Rubidium (Rb) atomic frequency standards are currently in use onboard Navstar Global Positioning System (GPS) satellites. The premature failure of several of the satellite-borne devices has been attributed to the failure of the Rb lamps used for optical pumping in the Rb clocks. The Aerospace Corporation has responded to these events by initiating investigations into Rb lamp failure mechanisms. The primary goal of these studies is to develop an acce-

lerated life test to insure the reliability of future GPS Rb lamps. The test must be such that its application for a reasonable period of time will indicate that under normal operating conditions the Rb lamp will function for the required GPS mission lifetime.

There are several steps involved in developing such an accelerated life test:

- i) Identify the primary lamp failure mechanism
- ii) Determine the factors which accelerate this mechanism and quantify their effects
- iii) Insure that the acceleration procedure does not alter the failure mechanism.

In the body of this paper our results in each of these areas are discussed.

## II. FAILURE MECHANISM IDENTIFICATION

The GPS Rb lamps are of the standard Bell, Bloom, and Lynch [1] electrodeless discharge design. The current envelopes, composed of Corning 1720 glass, are cylindrical, approximately 1 cm in diameter and 2 cm in length. They contain both rare gas buffer, xenon (Xe), and an excess Rb metal charge which has a current GPS specification of from 300 to 500 $\mu$ g. During operation, the base of the lamp, which is its coldest point, is thermostated to the desired temperature to maintain constant Rb vapor pressures.

Several possible failure mechanisms may be proposed. It can be suggested that the electronically excited Rb is being quenched by vapor phase impurities prior to radiative emission. These impurities result from glass envelope outgassing. Another possibility is that outgassed impurities, for example water (H<sub>2</sub>O) or oxygen (O<sub>2</sub>), react directly with atomic Rb converting the lamp's Rb charge to nonvolatile compounds. The consumption of Rb charge through either reaction with or diffusion into the lamp envelope is also possible. Finally, the actual failure process may be some combination of the above mechanisms.

### A. Quenching of Excited Rubidium

A number of experimental results indicate that quenching of the excited atomic Rb is not significant. Emission spectra from both good and failed lamps have been obtained with a 3/4 m spectrometer and analyzed over the spectral range from 400 nm to 800 nm. Literally hundreds of lines are assigned to either atomic transitions

of Xe, Rb, or trace amounts of potassium and cesium normally found as impurities in the Rb. In the failed lamps only emission lines present in good lamps were observed. No emission lines from possibly outgassed impurities such as hydrogen ( $H_2$ ), nitrogen ( $N_2$ ), or  $O_2$  were detected. These results are consistent with an absence of quenching species.

Comparisons of emission intensities of the Rb 780.0 nm line and the Xe 823.2 nm line as functions of lamp base temperature for both good and failed lamps are shown in Figure 1. In addition, the Rb vapor pressure curve is plotted on Figure 1a. At low base temperature ( $< 100^\circ C$ ) Xe emission intensities are the same for both good and failed lamps. This indicates that the rf discharge has not changed due to the failure of the lamp. The most obvious difference between the good and failed lamps is that the Rb emission intensity is less in the failed lamp. The magnitude of the intensity reduction varies among failed lamps, depending on how far the failure process has proceeded. In Figure 1b the failed lamp's Rb intensity is nearly three orders of magnitude lower than that of a typical good lamp.

A reduction in emission intensity could result from quenching, however, careful examination of these curves shows conclusively that quenching is not significant in failed lamps. If quenching were the only process occurring, the entire Rb emission versus temperature curve would be expected to shift to lower magnitudes. This is not observed. While the Rb emission intensity of the good lamp increases monotonically (for temperatures less  $140^\circ C$ ) as the lamp base temperature is increased, the failed lamp displays nearly constant Rb intensity over the  $20^\circ C$  to  $70^\circ C$  range. This constant intensity portion of the curve implies the existence, in failed lamps, of a mechanism yielding vapor phase Rb which is essentially temperature independent. If rather than quenching, a reduced vapor phase density causes the diminished Rb intensity in failed lamps, the relative magnitude of Rb released by the temperature independent mechanism would be small compared to normal vaporization. It is speculated that the temperature independent mechanism may involve release of Rb imbedded in the glass via a plasma sputtering process.

At temperatures where the Rb vapor density is low enough so that self-absorption is not significant, ( $< 100^\circ C$ ), the emission intensity of a good lamp follows the vapor pressure curve closely. As the temperature,  $T$ , increases (above  $100^\circ C$ ) the emission intensity begins to drop below the vapor pressure curve due to increasing self-absorption. However, Rb emission from the failed lamp ( $110^\circ < T < 150^\circ$ ) displays no slope change due to self-absorption. Since self-absorption should not be affected by quenching it appears that the vapor density of Rb in a failed lamp is significantly lower than in a good lamp. At approximately  $145^\circ C$  the emission intensities on

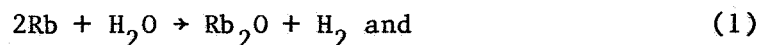


Figure 1a change dramatically. This happens as the plasma changes from a mixed mode in which both Rb and Xe are excited to a Rb only mode in which Rb is primarily excited. This mode change is found to be dependent on the Rb vapor density. At a specified rf excitation power the plasma will change to a Rb only mode when the Rb vapor pressure has reached a sufficient level. Looking at Figure 1b no mode change is observed to occur. This is again consistent with a reduced Rb vapor density in a failed lamp.

Finally, applying the integrated form of the Clausius-Clapeyron equation [2] to data of the type found on Figure 1 allows determination of the heat of vaporization of Rb in both good and failed lamps. For good lamps the experimental heat of vaporization is found to be  $18.1 \pm 0.3$  kcals per mole. The reported value for elemental Rb is 18.11 kcals per mole [3]. However, for failed lamps the heat of vaporization is found to be  $23.9 \pm 0.2$  kcals per mole. This implies that a liquid reservoir of Rb is not present in the failed lamp. Quenching, if it occurred, would not affect the heat of vaporization. Consequently, lamp failure results from a lack of Rb rather than its quenching.

#### B. Rubidium Reaction with Impurities

The second postulated mechanism for the failure of Rb lamps in the GPS Rb frequency standard is the loss of Rb by reaction with species outgassed from the glass envelope to form nonvolatile rubidium oxide ( $\text{Rb}_2\text{O}$ ). The most likely reactions are,



Experiments which tested for the presence of  $\text{H}_2$  in failed lamps prove that reaction with  $\text{H}_2\text{O}$  is not significant. Rf-induced emission spectra from a series of standard lamps containing  $\text{H}_2$  and Xe were analyzed to obtain a detection limit of  $\text{H}_2$  in the presence of the Xe buffer. Comparison of these spectra with those of failed lamps indicates that the pressure of  $\text{H}_2$  in a failed lamp is less than 1 torr. A subsequent removal of the evolved  $\text{H}_2$  through either formation of rubidium hydride,  $\text{RbH}$ , or permeation through the glass envelope has been ruled out.  $\text{RbH}$  is known to photodissociate when exposed to UV radiation [4], such as found in abundance within the lamp due to numerous Xe transitions. The permeation velocity constant for  $\text{H}_2$  [5, 6] is too low to allow for a significant loss of  $\text{H}_2$  through the glass. Thus less than 10 $\mu\text{g}$  of rubidium could be consumed by the postulated mechanism.

The fact that the amount of water desorbed from the glass envelope does not consume a significant amount of Rb has a bearing on the importance of reaction 2. Todd [7] states that the gas evolved from glasses of temperatures below their softening points is primarily water. Todd's studies covered a wide range of glasses including Corning 1720. His results are also consistent with data presented by Dushman [8] which indicate  $H_2O$  outgassing is greater than that of  $O_2$ . A question arises whether  $O_2$  outgassing might be preferentially accelerated by the rf discharge present in the lamp. Studies of electron bombardment of glass surfaces indicate this bombardment can release  $O_2$  [9, 10]. However, keV electrons were required to induce significant outgassing. From spectroscopic measurements the average kinetic energy of the electrons in the GPS lamp discharge is estimated to be less than 1 eV. In light of this information it is strongly believed that insufficient  $O_2$  is released by the lamp envelope to consume any significant amount of Rb.

#### C. Interaction of Rubidium with Glass

It has long been reported in the literature that alkali vapors react directly with glass surfaces [11-13]. Glasses exposed to alkali vapors are known to discolor as the interaction processes proceed. Failed GPS lamps display this discoloration implying reaction of Rb with the glass envelope. In light of this, surface analysis techniques have been applied to lamp envelopes. They indicate that Rb penetrates many micrometers into the glass. On the vapor-exposed surface the Rb's chemical form is found to be similar to that of an oxide or silicate, again implying reaction with the glass. In light of these results, it is believed that the primary failure mechanism in GPS lamps is the consumption of Rb via its direct interaction with the lamp's glass envelope. The mechanisms of this interaction are discussed in terms of the surface analysis studies in Section IV.

### III. ACCELERATION PARAMETERS AND QUANTIFICATION OF RUBIDIUM CONSUMPTION

#### A. Acceleration Parameters

With the identification of the primary failure mechanism it is possible to suggest parameters to accelerate the mechanism. Two such parameters under current investigation are lamp temperature and rf excitation power. Whether the interaction is a simple reaction whose rate is dependent on a rate constant,  $k$ , or a more complicated process involving diffusion effects characterized by a diffusion coefficient,  $D$ , the temperature would be expected to play an important role.

In the simplest approximation, rate constants, in general, obey the following proportionality,

$$k \propto \exp (-\Delta E/RT) \quad (3)$$

where  $\Delta E$  is the activation energy for the reaction of interest,  $R$  is the gas constant, and  $T$  is the absolute temperature. Over limited temperature ranges (several hundred °C) diffusion coefficients have been found to obey a similar proportionality,

$$D \propto \exp (-Q/RT) \quad (4)$$

where  $Q$  is an effective activation energy for the diffusion process. For both  $k$  and  $D$ , increasing temperature increases their magnitudes and due to their exponential relation to temperature this increase may be rapid. An increase in temperature may increase the interaction between Rb and glass in an additional manner. A higher reservoir temperature will cause a higher Rb vapor density resulting in the more rapid consumption of Rb via either a reactive or diffusive mechanism.

To aid in understanding the effects of rf excitation power and the plasma itself on the interactions of Rb vapor with the lamp envelope theoretical modeling of the plasma has been carried out. This model assumes electron production takes place in the lamp plasma by electron impact with Rb atoms. Electron loss is assumed to occur via ambipolar diffusion to the wall and subsequent recombination of electrons and ions. With these assumptions rate equations for the populations of the atomic and ionic Rb species may be set up. Solution of those equations in a cylindrical geometry yields atomic Rb and electron densities as a function of radial position. The salient results of these calculations are shown in Figure 2 [14].

In Figure 2a and b the left-hand ordinate describes the electron density while the right-hand ordinate gives the Rb density. The glass wall occurs at  $r = 4$  mm. In the absence of the Rb discharge the distribution of Rb atoms is given by the dashed lines. In Figure 2a, for 0.3 W/cm rf power the calculation yields a Rb atom density at the wall of approximately  $3.5 \times 10^{14}$  atoms/cc. This is 3.5 times the nonplasma density of  $1 \times 10^{14}$  atoms/cc. The results for an rf excitation power of 3 W/cm are shown in Figure 2b. In this case the presence of the plasma increases the wall Rb atom density by more than a factor of nine over the nonplasma density. It is seen that with increasing rf power into the plasma the concentration of Rb at the lamp wall also increases. This higher density will accelerate the consumption of Rb whether the interaction mechanism is reaction, diffusion or a combination of both.

## B. Experimental Determination of Rubidium Consumption

It is expected that both temperature and rf power will be useful in accelerating the interaction of Rb with the glass envelope. To establish these acceleration effects the baseline Rb consumption rate for GPS lamps operating in normal environments must be determined. However, in order to obtain this rate it is first necessary to develop a technique to monitor Rb consumption within a lamp.

In the current experiments the technique of differential scanning calorimetry (DSC) has been used to determine the amount of Rb contained within GPS lamps. This technique to measure the Rb content in a lamp was first proposed by workers at EG & G, Inc. [15]. In DSC, sample and reference objects are both heated such that their temperatures increase at the same rate. Heating rates are measured in °C/min. The instrument measures the heat flow, in calories per minute, required to maintain this heating rate for both sample and reference. The difference between these two heat flows is the instrument output, which is typically plotted versus time.

The sample object is a GPS lamp while the reference is a GPS lamp envelope containing no Rb. When the melting point of Rb (38.9°C) is reached, the excess heat required to melt the Rb contained in the sample lamp appears as a peak on the heat difference versus temperature plot. The area of this peak can be equated to the heat required to melt the Rb and division of this heat by Rb's heat of fusion, 6.14 cal/gram, yields the lamp's Rb content. Figure 3 is a typical DSC curve for a Rb lamp. Rb content is typically determined to  $\pm 10\%$  at 100  $\mu\text{g}$  and  $\pm 50\%$  at 10  $\mu\text{g}$ .

The DSC technique has been applied to GPS lamps operating in both vacuum and normal atmospheric pressure under standard temperature and rf power conditions. No significant difference in rate of Rb consumption between vacuum and atmospheric operation has yet been observed. Consequently in Figure 4, consumption data as a function of running time for lamps operating in both environments have been combined.

In Figure 4, the data span operating times from several hundred hours to 5,000 hours. The amount of Rb consumption can be fit to a power relation of the form,

$$M_{\text{Rb}} = 1.1 t^{0.54}, \quad (5)$$

where  $t$  is the operation time in hours and  $M_{\text{Rb}}$  is the amount of Rb consumed in micrograms.

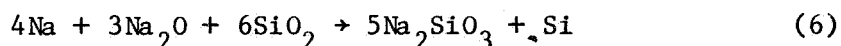
Currently, Rb consumption is being monitored for lamps under normal conditions, elevated temperatures, and high rf powers to ascertain whether accelerated consumption can indeed be induced. At this point the result of these studies are still preliminary and will not be discussed.

#### IV. MECHANISMS OF THE RUBIDIUM-GLASS INTERACTION

##### A. Results of Previous Investigations

As Rb lamps are subjected to a wider variety of operating conditions in an attempt to accelerate the Rb-glass interaction, care must be taken to insure the interaction mechanism occurring under normal operating conditions is not altered. To accomplish this a detailed knowledge of this mechanism must be obtained. Prior to our investigations very little work had been aimed at understanding the Rb-glass interaction. The majority of alkali-glass studies have focused on the sodium (Na)-glass interaction which occurs much more rapidly than Rb-glass processes. It is interesting to note that a major rationale of the prior investigations has been the possible improvement of alkali vapor lamps. However, virtually none of the previous studies has been conducted with an electrical discharge present.

In the case of Na, the consensus is that no single mechanism explains its interaction with glass [16-18]. Typically, one of two effects is observed. The first effect often occurs in glasses with high SiO<sub>2</sub> content. Exposure to Na results in the formation of a brown crystalline layer containing nearly 20% Na by weight [16]. The edge of this layer is found to advance into the glass at a rate proportional to the square root of the time of exposure [16], which is consistent with a Na-glass reaction limited by a diffusion-controlled step [19-20]. Elyard and Rawson [12] have suggested several reactions which are thermodynamically favored resulting in a variety of sodium silicates. Using x-ray diffraction, Brinker and Klein [16] have shown the crystalline phase was sodium metasilicate (Na<sub>2</sub>SiO<sub>3</sub>). Consequently, they suggest that the most probable of Elyard and Rawson's proposed reactions is the following,



$$\Delta G_{400^\circ\text{C}} = 1583 \text{ Kj/mole.}$$

The second effect, typically observed in glasses containing less than 70% (mole) SiO<sub>2</sub> [16], is characterized by a brownish discoloration of the glass. The discolored glass has apparently not undergone any devitrification and the crystalline material observed in the first effect is not present. The discoloration is described

as advancing into the glass with a sharp boundary [16]. This boundary has also been observed to advance into the glass at a rate proportional to the square root of time, again indicating a diffusion-controlled process. Brinker and Klein [16] believe that this process is the result of atomic Na diffusing into the glass.

What information may be drawn from the previous studies of the Na-glass interactions and applied to Rb's interactions with Corning 1720? Corning 1720 is a calcium aluminosilicate glass [21] containing less than 70% (mole)  $\text{SiO}_2$ . While this seems to imply the second effect would be most likely, care must be exercised. Corning 1720 also contains aluminum and boron oxides ( $\text{Al}_2\text{O}_3$  and  $\text{B}_2\text{O}_3$ ). The presence of these modifiers can significantly affect how a glass reacts when exposed to Na and most likely to Rb. Further, the parameters of greatest interest, the rates of Rb consumption, are not obtainable from the previous Na studies. Consequently, investigations specifically aimed at understanding Rb-glass interactions are required.

#### B. Current Surface Analysis Studies

In Figure 5, a "typical" Na penetration profile is compared to a Rb penetration profile representative of those currently being analyzed. Na-glass studies generally immersed glass samples in liquid Na at elevated temperatures. A profile similar to Figure 5a results when a glass sample is placed in  $400^\circ\text{C}$  Na for about 100 hours. Due to the rapidity of its progress into the glass, the Na profile can be followed using absorption spectroscopy, magnified examination of a glass cross section, or wet chemical etching techniques. The rate of progress of this penetration front yields the Na diffusion coefficient. In contrast, the reaction of Rb with glass under the conditions of current interest is orders of magnitude slower than that of Na. Exposure of glass to Rb vapor, whose density is specified by the Rb vapor pressure at temperatures near  $200^\circ\text{C}$ , for several thousand hours will yield a Rb profile similar to that in Figure 5b. In this case it is necessary to analyze the functional form of the profile rather than the penetration depth to determine the diffusion coefficient.

##### 1. Secondary Ion Mass Spectrometry (SIMS) Studies

To obtain the highly accurate penetration profiles needed to analyze Rb permeation of glass the technique of SIMS has been applied to cross-sectional pieces of Rb-exposed lamp walls. In the SIMS technique a  $1.5\text{ }\mu\text{m}$  diameter beam of oxygen ions is aimed at the sample. Secondary ions sputtered from the surface are mass spectrometrically analyzed allowing determination of elemental composition. Our initial tests were performed on Rb lamp with pyrex envelopes under plasma and nonplasma conditions. In both cases lamps

were thermostated in oil baths to maintain constant vapor pressures. Pyrex was selected for those studies because it is known to react with alkali vapors.

Figure 6 shows the raw SIMS profiles of silicon (Si) and Rb for a lamp exposed to a plasma discharge. Zero micrometers is the inner surface of the lamp wall. The gradual increase of Si and Rb concentrations near zero is due to the finite width of the SIMS beam. Treating these data as simple one-dimensional diffusion allows fitting them to the form [20]

$$\frac{C(X,t)}{C_0} = \operatorname{erfc} \frac{X}{\sqrt{4 D t}}, \quad (7)$$

where  $X$  is the penetration depth,  $t$  is the exposure time,  $C_0$  is Rb concentration at the wall, and  $D$  the diffusion coefficient resulting from the fitting process.

Experimental Rb data along with fit curves for pyrex lamps with and without plasma present are given in Figure 7. In both cases the diffusion coefficient is approximately  $3 \times 10^{-14} \text{ cm}^2/\text{sec}$ . This is in good agreement with high temperature diffusion coefficient data [22] extrapolated into the low temperature regime (about  $140^\circ\text{C}$ ).

The SIMS Rb penetration profiles indicate that Rb has penetrated many micrometers into the glass. This is particularly clear in Figure 7b whose sample was exposed to Rb vapor for a longer period of time than that of Figure 7a. The depth of Rb penetration cannot be attributed to a smearing of the true profile resulting from the finite width of SIMS ion beam. This beam, which is only approximately 1.5 micrometers in diameter, would smear a surface layer to a depth of at most 2 micrometers. In fact, in Figure 7b the amount of Rb which has diffused beyond 2 micrometers is greater than the amount found in this surface region.

Analysis of the SIMS data yields support for the theoretical plasma model. Using only vapor pressure/temperature considerations results in a ratio of the vapor density at the glass surface with plasma present,  $P_p$ , to the vapor density at the glass surface for the nonplasma sample,  $P_{np}$ , equal to approximately 0.1. However, if the plasma model is correct, the vapor density at the glass surface in the plasma case should be higher than expected from vapor pressure considerations. This could result in a larger  $P_p/P_{np}$  value. Integrating the SIMS curves allows determination of the total amount of Rb which has penetrated the glass. Combining these amounts with the extracted diffusion coefficients, the known exposure times, and the one-dimensional diffusion model allows calculation of the relative vapor densities exposed to the glass surfaces with and without plasma

present. The experimental  $P_p/P_{np}$  ratio is found to be approximately 1. The fact that this ratio is larger than would be predicted by only vapor pressure/temperature considerations is consistent with the plasma model predictions.

## 2. Electron Spectroscopy for Chemical Analysis (ESCA) Experiments

The chemical form of the Rb within the glass has been investigated using ESCA. In this method the surface of the sample is exposed to monochromatic X-rays and the photoejected electrons are energy analyzed. The resulting core electron binding (ionization) energies are characteristic of both a given element and its chemical form.

Table I summarizes the current ESCA results. Pure rubidium hydroxide (RbOH) and  $Rb_2O$  were analyzed as standards. Pyrex samples exposed to Rb were also analyzed. These pyrex samples had a yellow-brown discoloration as long as they were kept in dry atmospheres. However, upon exposure to moist air they became colorless in a matter of seconds. The rapidity of this discoloration indicates Rb exists in a colored form on a thin surface layer, probably less than  $0.1 \mu m$  thick. However, from the SIMS data it was seen that most of the Rb has diffused into the glass many micrometers. Consequently, Rb exists in at least two forms in pyrex. The minor form is a colored surface layer, while the major form extending more deeply into the glass is not significantly colored. The ESCA studies have thus far yielded information about the surface layer. Prior to water vapor exposure the Rb in the surface layer of pyrex is similar in form to a rubidium oxide or possibly a rubidium silicate. However, on exposure to moist air it becomes RbOH.

Currently, it appears the interaction mechanism between Rb and a glass surface is not dependent on whether a plasma is present or not. From this it may be inferred that varying the rf power into the plasma will not significantly affect the nature of the Rb-glass interaction. This will be important if increased rf power does indeed accelerate the interaction. Further, the nature of the diffusive mechanism apparent in these glass samples should not be significantly affected by temperature changes over several hundred degrees Celsius. Consequently, temperature should also be a reasonable acceleration parameter. Additional experiments on different glasses including Corning 1720 at elevated temperatures and rf powers are currently underway to further substantiate these statements.



Table I. ESCA Results

	<u>Rb (<math>3d_{5/2}</math> <math>3d_{3/2}</math>)</u> <u>Binding Energy (eV)</u>	
RbOH	109.8 $\pm$ 0.2	
Rb <sub>2</sub> O	110.3	
	<u>Non-plasma</u>	<u>Plasma</u>
Rb + Pyrex	110.7	110.5
Rb + Pyrex (Air Exposed)	—	109.8

V. DISCUSSION

The studies described in this paper represent a systematic investigation into the failure mechanisms of one portion of the Rb atomic frequency standard's physics package. The current investigations have resulted in the identification of the primary lamp failure mechanism along with obtaining baseline Rb consumption data for GPS type lamps. Additionally, insights into the mechanisms of the Rb consumption process have been gained. These studies will not only yield an accelerated life test for the GPS program but also allow reliability estimates to be made for Rb lamps. We consider the current investigations to be the first step in understanding the failure mechanisms of, and obtaining reliability estimates for, the entire physics package of the frequency standard.

## REFERENCES

1. W.E. Bell, A.L. Bloom, and J. Lynch, *Rev. Sci. Instr.* 32, 688 (1961).
2. K. Denbigh, *The Principles of Chemical Equilibrium*, Third Edition, Cambridge University Press, London, p. 202, 1971.
3. *Handbook of Chemistry and Physics*, Forty-Ninth Edition, The Chemistry Rubber Company, Cleveland Ohio, D 33, 1968.
4. R. Hilsch, *Ann. Physik.* 32, 155 (1938).
5. F.J. Norton, *J. Am. Ceram. Soc.* 36, 90 (1953).
6. V.O. Altemose, *J. App. Phys.* 32, 1309 (1961).
7. B.J. Todd, *J. Appl. Phys.* 26, 1238, (1955).
8. S. Dushman, *Scientific Foundations of Vacuum Technique*, John Wiley and Sons, Inc., New York, pp. 509-527, 1949.
9. B.J. Todd, J.L. Lineweaver, and J.T. Kerr, *J. Appl. Phys.* 31, 51, (1960).
10. J.L. Lineweaver, *J. Appl. Phys.* 34, 1786 (1963).
11. G.R. Fonda and A.H. Young, *Gen. Elect. Rev.* 37, 331 (1934).
12. C.A. Elyard and H. Rawson, *Advances in Glass Technology*, Plenum Press, New York, p. 270, 1962.
13. W. Happer, *Rev. Mod. Phys.* 44, 169 (1972).
14. H.U. Eckert, a complete presentation of these calculations will be published.
15. T. Lynch, EG & G, Inc., private communication.
16. C.J. Brinker and L.C. Klein, *Phys. Chem. Glass* 21, 1414 (1980); *Phys. Chem. Glass* 22, 23 (1981).
17. A.J. Burggroof and H.C. Van Velzen, *J. Am. Ceram. Soc.* 52, 238 (1969).
18. A.J. Burns, *Glass Technol.* 6, 17 (1965).
19. R.H. Doremus, *J. Non-Cryst. Solids* 25, 263 (1972).

20. J. Crank The Mathematics of Diffusion, Oxford University Press, London, Chapter 8, 1957.
21. Kirk-Othmer Encyclopedia of Chemical Technology, V. 11, M. Grayson ed., John Wiley and Sons, Inc., New York, p. 826, 1980.
22. A. Kolitsch, R. Kuchler, E. Richter, Silikatechnik 29, 369 (1978).

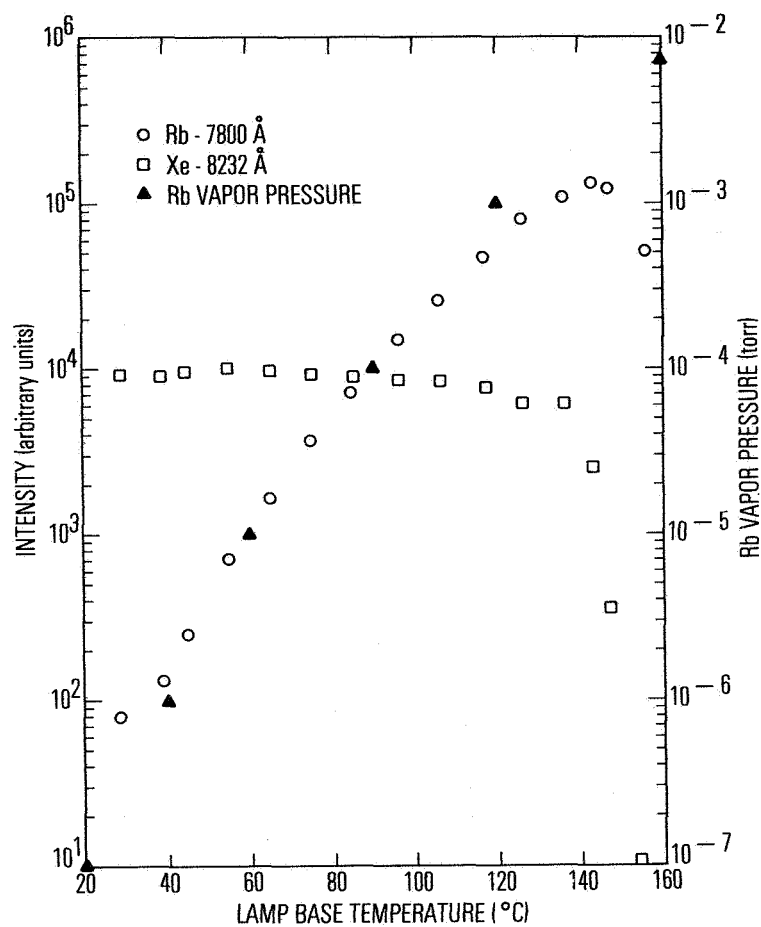


Figure 1a. Emission intensities of Rb 7800Å line (○) and the Xe 8232Å line (□) for a good Rb lamp as a function of base temperature. (▲) are Rb vapor pressure values

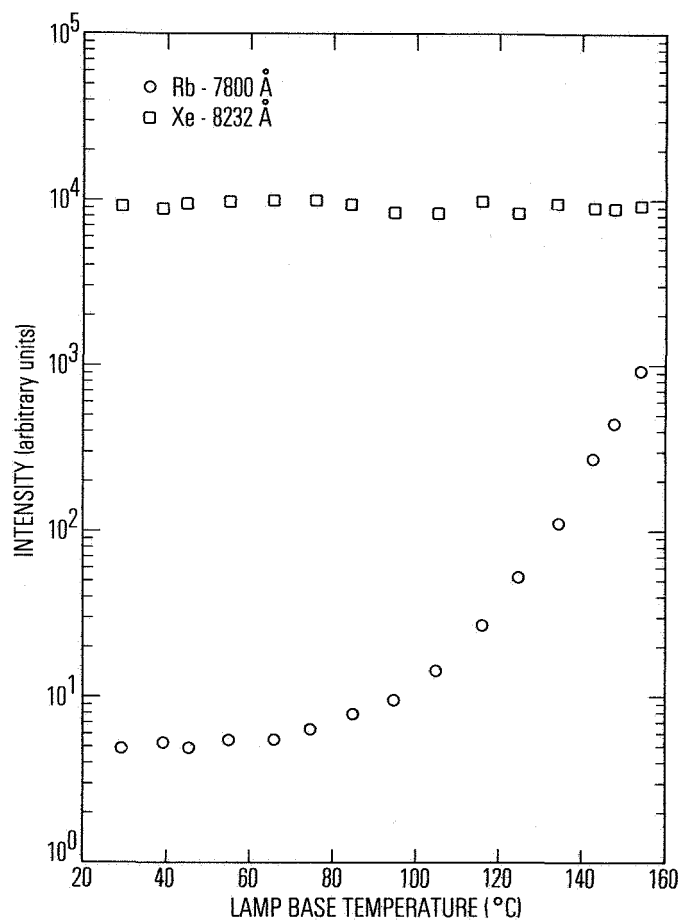


Figure 1b. Emission intensities for Rb 7800Å line (○) and Xe 8232Å (□) for a failed Rb lamp as a function of base temperature

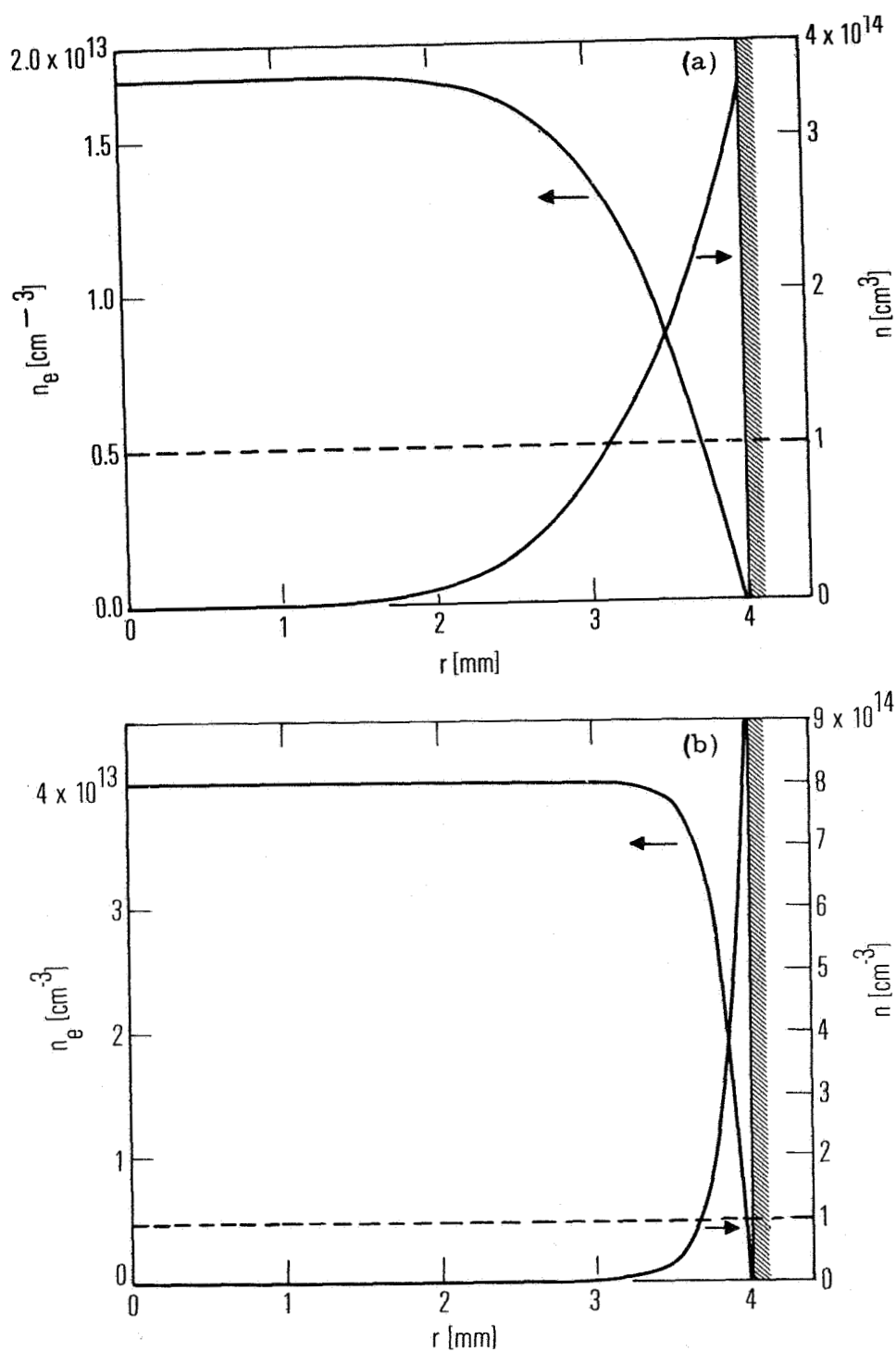


Figure 2. Theoretical calculations of Rb and electron densities as a function of radial position in a plasma discharge for a) 0.3 W/cm and b) 3.0 W/cm excitation power

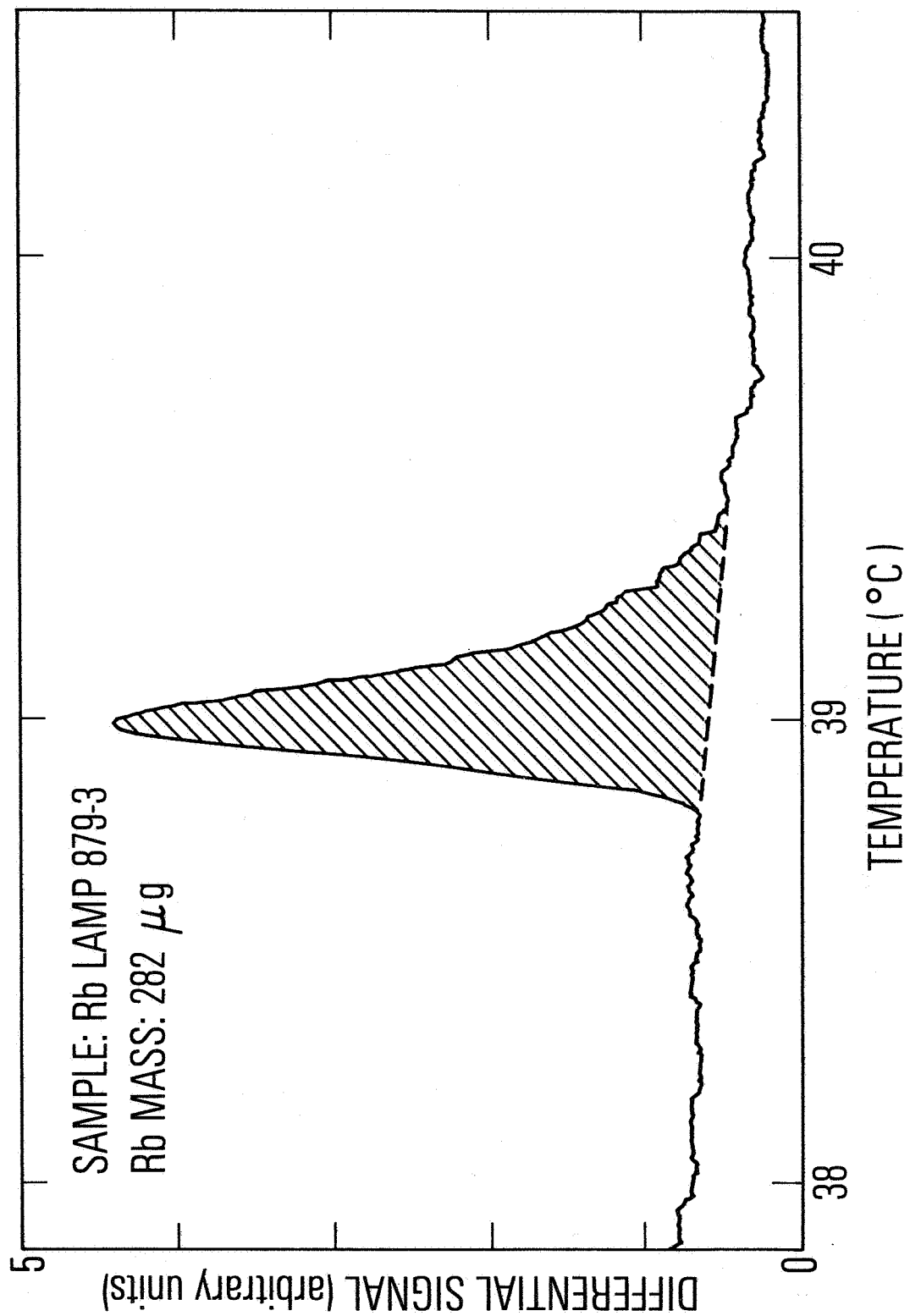


Figure 3. DSC curve for Rb lamp

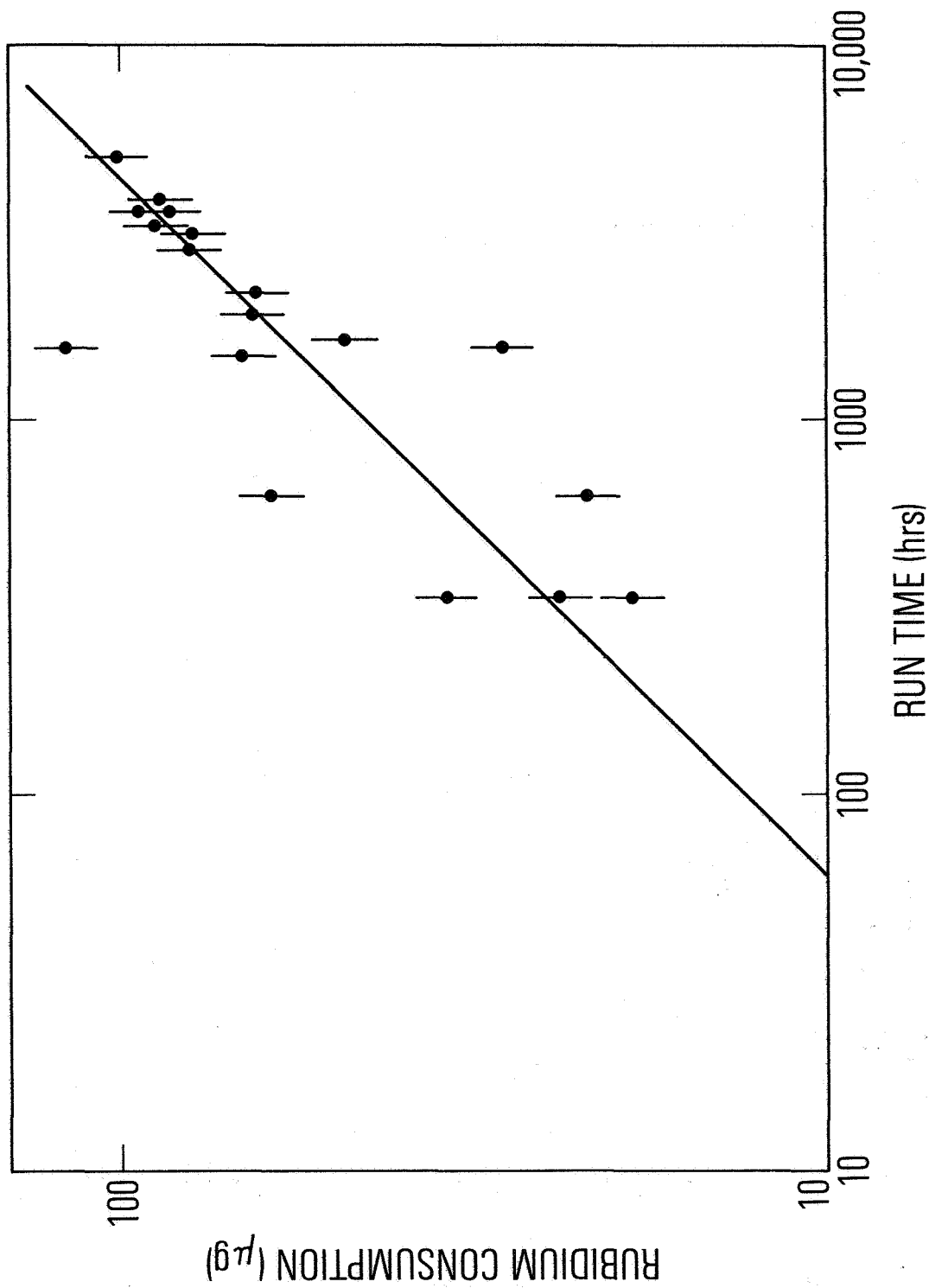


Figure 4. GPS lamp Rb consumption versus operating time



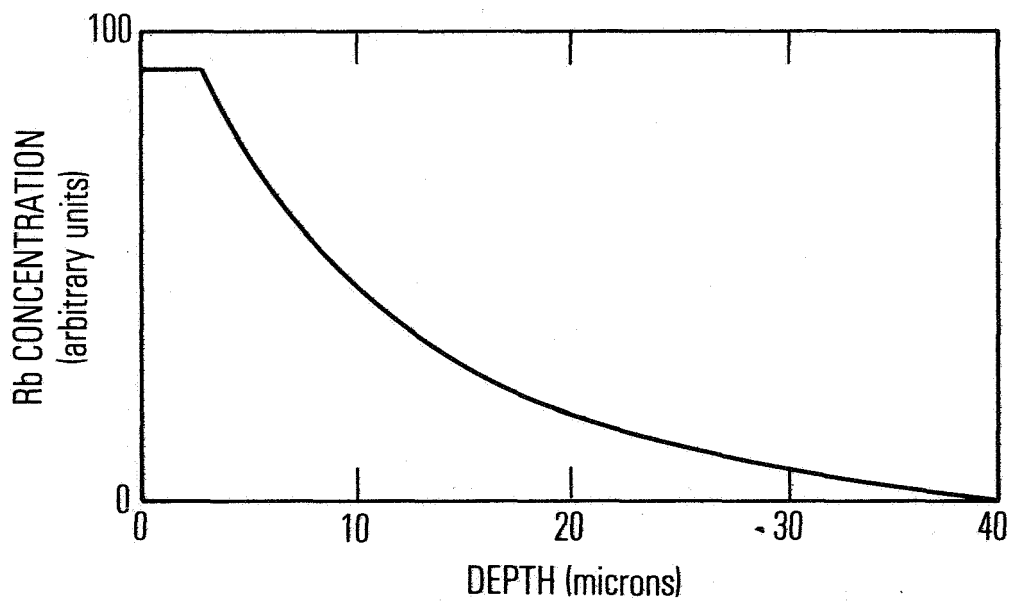
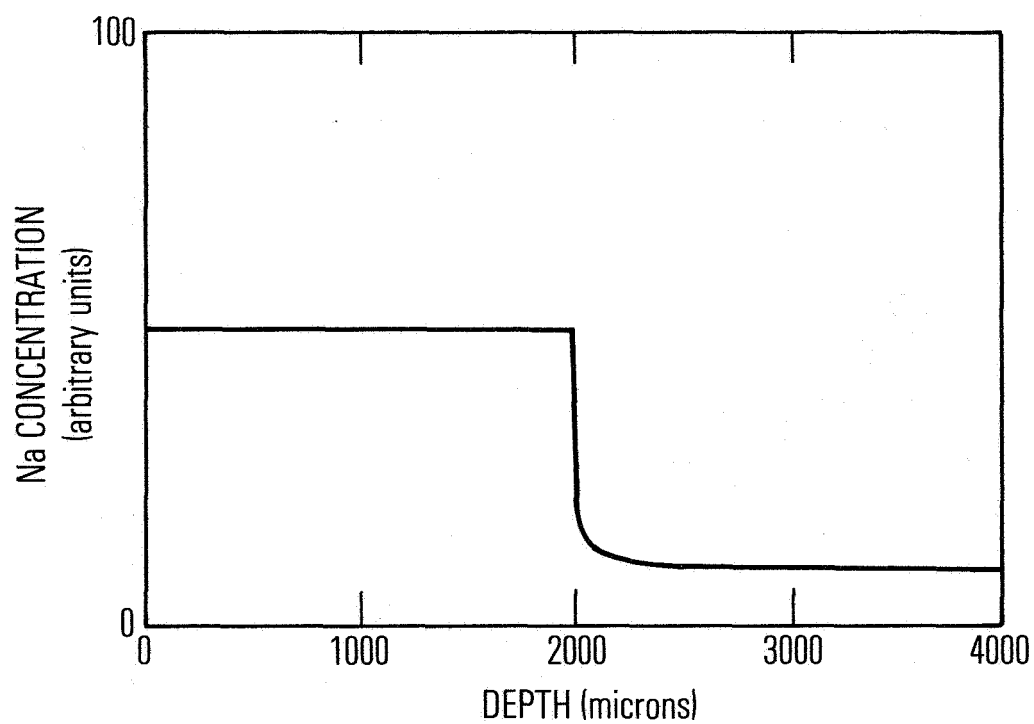


Figure 5. Schematic representation of a) Na and b) Rb penetration profiles into glass

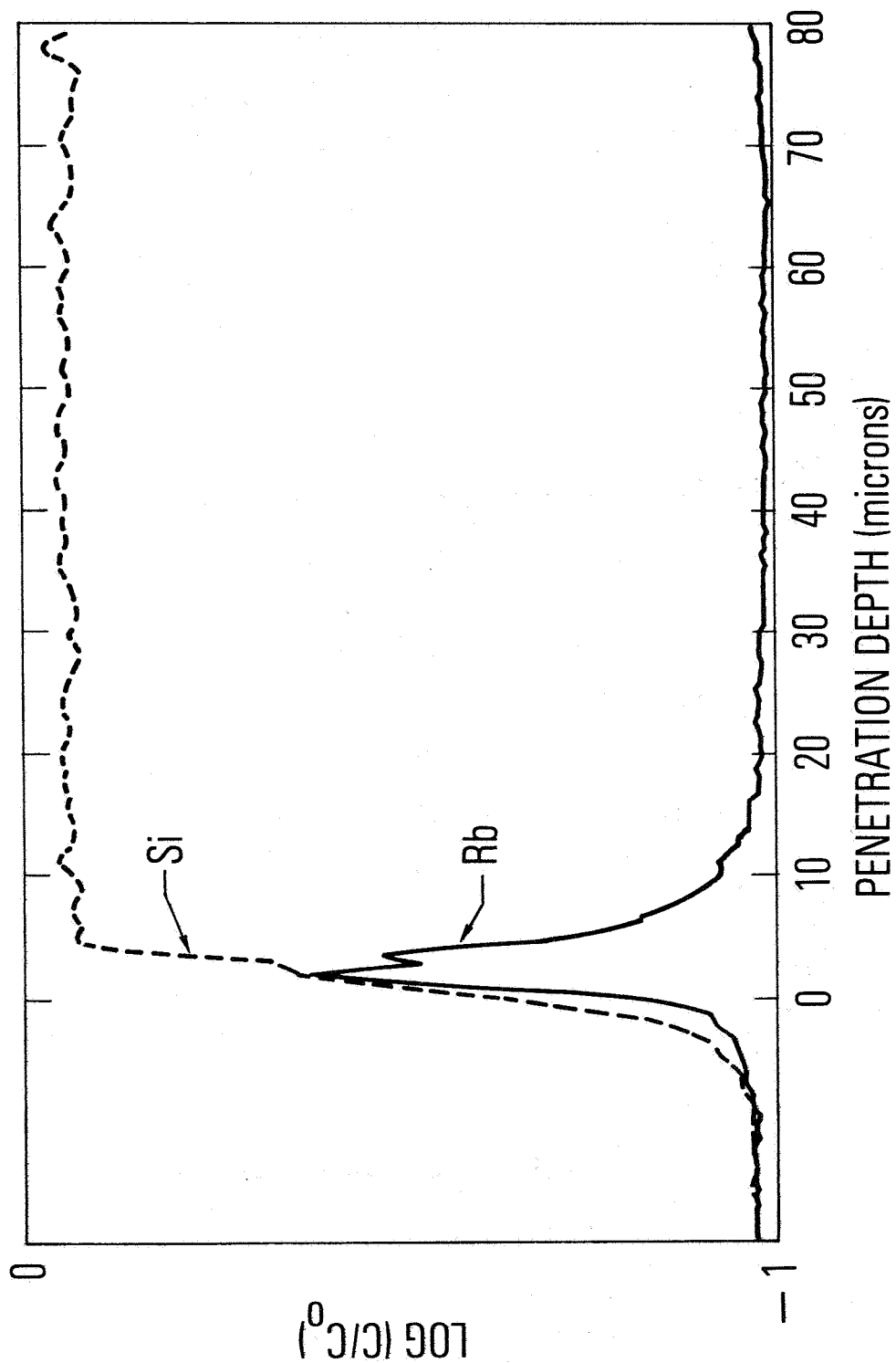


Figure 6. Raw SIMS data for Rb penetration into a pyrex glass surface. The surface occurs at 0 microns. The sharp decrease and increase in Rb concentration near 4 microns is believed to be due to inhomogeneities in the glass and not related to the penetration mechanism

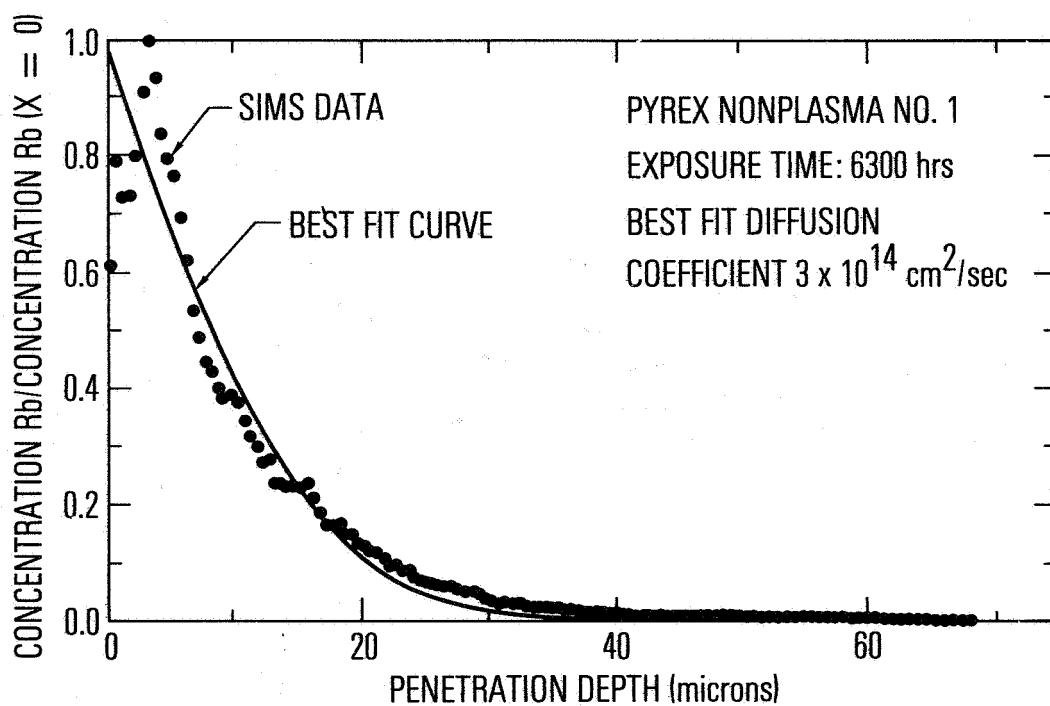
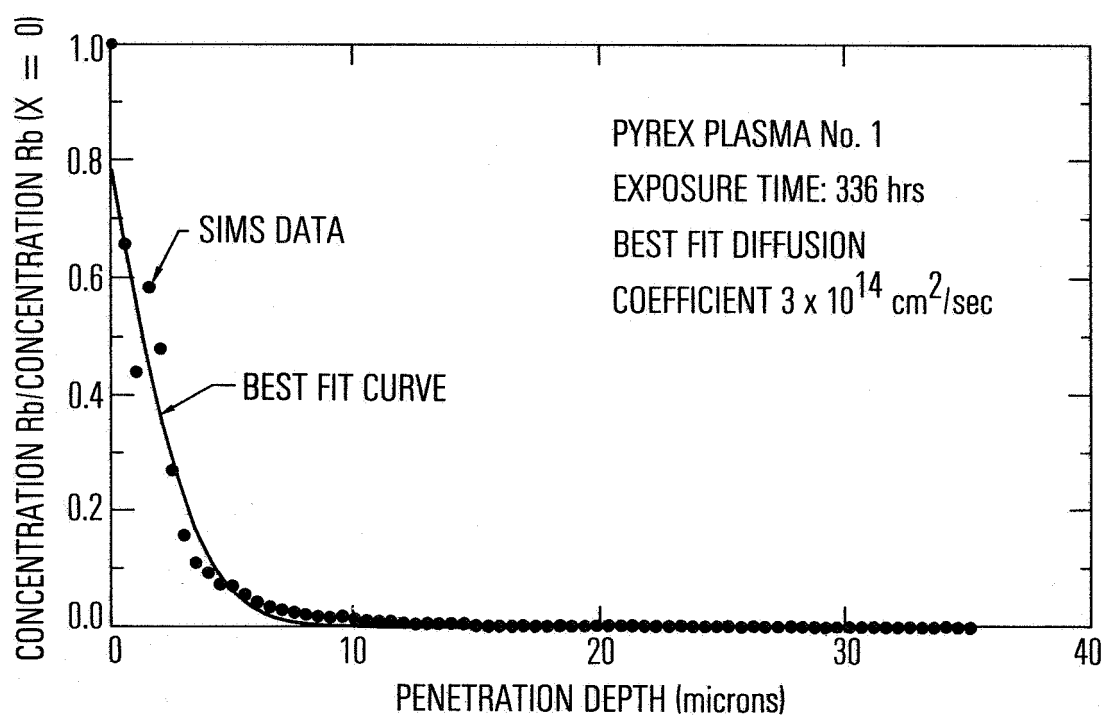


Figure 7. Experimental SIMS data (●) and fit curve (—) for pyrex glass samples a) with discharge present and b) without discharge

## QUESTIONS AND ANSWERS

MR. JOHN VIG, U.S. Army

It seems to me you have the inverse problem that we have in the quartz crystal field. We are worried about diffusing alkali ions out of the quartz to make the quartz more radiation hardened.

And the proposal has been made to grow quartz -- normally it is grown in a sodium hydroxide solution, but the proposal has been made to grow quartz in rubidium hydroxide in order to prevent the incorporation of the alkali into the quartz because apparently rubidium will not go into single crystal quartz.

Has anybody considered the possibility of building lamps out of single crystal quartz?

MR. VOLK:

I have heard it said that if you prepare the quartz correctly, they make much better absorption cells in lamps. However, in our work I have never seen that, which may mean that I don't prepare it correctly. It has been my sort of common experience that quartz is a bad material around rubidium, I don't know.

MR. VIG:

Single crystal quartz?

MR. VOLK:

I would have to check on that. Our techniques though would allow us to look at that rather quickly.

MR. VIG:

It would be interesting.

DR. LUKE MALEKI, Jet Propulsion Laboratory

Could you explain to me -- you had a couple of slides showing the ESCA results and at the end the plasma and non-plasma conditions, comparisons. I am not so sure I understand, when you have the plasma condition, how long do you run it and under what conditions, as opposed to the non-plasma conditions?

On the time scale how is the comparison made?

MR. VOLK:

Well, we ran the non-plasma for much longer. In the plasma it was run for a little over 300 hours and in the non-plasma, just heating with 6300 hours.

It takes a lot longer, of course, to react, that was the whole point of the model, is that you build up this density with the plasma to very large values.

DR. MALEKI:

Okay, maybe I can discuss that with you later.

One other thing, in view of the comment made on this single crystal quartz and so forth. Have you looked into the ion implantation influence in there? That is, the ions, in fact, because of the energy that they have, would --

MR. VOLK:

We don't see any evidence of that, of the ions penetrating, no.

DR. MALEKI:

Okay, thank you.

DR. MICHEL TETU, Laval University, Canada

When the temperature of the lamp is changed the usual observation is that the lamp goes from a ring mode to a pink mode, which means that the temperature is not too high, the density of the rubidium is, as you mentioned, close to the wall of the bulb and you have there a model which seems to explain very well the atomic distribution.

Now, if the temperature is slightly increased, the light seems to come from all over the bulb, which means that you have -- or we observe what we call the pink mode.

Is there any possibility to explain the atomic distribution with your model?

MR. VOLK:

Not at the present, we are working on that. Our model doesn't change modes, unfortunately.

MR. KUHNLE:

Thank you very much.

## Magnetic Shielding and Vacuum Test for Passive Hydrogen Masers

D.U. Gubser, S.A. Wolf, A.B. Jacoby, and L.D. Jones  
Naval Research Laboratory  
Washington, DC 20375

### ABSTRACT

Vibration tests on high permeability magnetic shields used in the SAO-NRL Advanced Development Model (ADM) hydrogen maser have been made. Magnetic shielding factors were measured before and after vibration at the Goddard Space Flight Center, magnetic field facility. Preliminary results indicate considerable ( $< 25\%$ ) degradation.

Test results on the NRL designed vacuum pumping station for the ADM hydrogen maser are also discussed. This system employs sintered zirconium carbon getter pumps, supplied by SAES Getters, to pump hydrogen plus small ion pumps to pump the inert gases. In situ activation tests and pumping characteristics indicate that the system can meet design specifications.

### INTRODUCTION

Hydrogen masers to be used as clocks aboard navigation satellites must be light but rugged enough to withstand shock and vibration introduced during launch. For the past several years, we have been developing both the magnetic shielding system and the vacuum pumping system for such a hydrogen maser. In part I of this two part article we report on preliminary shock and vibration tests performed on magnetic shields designed for a space-worthy hydrogen maser. In part II, we report on vacuum and pumping characteristics of our small, lightweight hydrogen maser pumping system.

#### I. MAGNETIC SHIELDS

A compact, lightweight magnetic shielding system using high permeability material has been designed, and tested by us and previously described<sup>1</sup> (Fig. 1). It consists of 4 nested shields, each 0.35 mm thick, with an OD of 19.4 cm, and ID of 13.8 cm, and overall length of 30 cm. In order to test the vulnerability of these shields to shock and vibration they were assembled within a special harness in a manner which duplicated as close as possible the actual hydrogen maser mounting arrangement including heaters, thermal blankets and a "dummy" load

replicating the mass of the maser cavity. At various locations on each individual shield, accelerometers were mounted to measure the magnitude of the vibration and to test for unwanted system resonances. The shields were vibrated at NRL's shock and vibration laboratory in a manner which simulated expected launch levels. Figure 2 shows the vibration table with the instrumented shielding system attached.

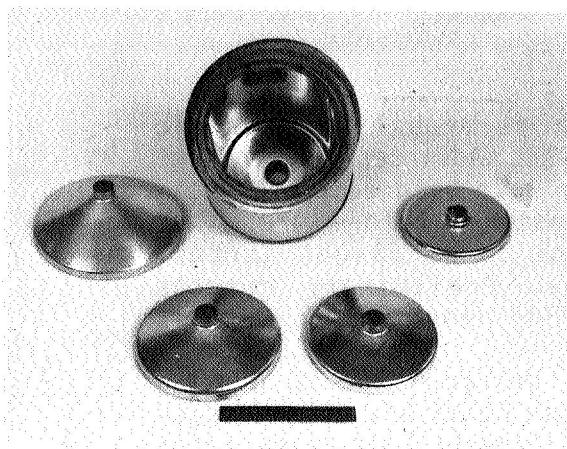


Fig. 1. Photo of Magnetic Shield system for hydrogen Maser.

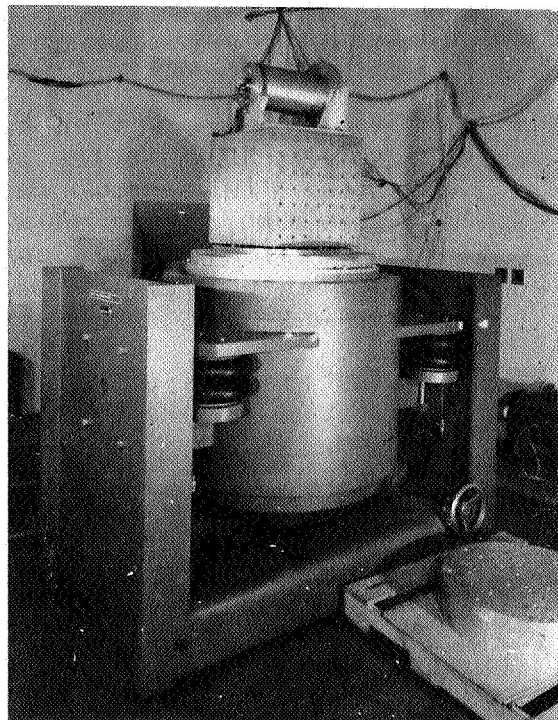


Fig. 2 Photo of Assembled Shield system showing instrumented mounting harness atop NRL vibrating table.

The magnetic shielding factor was measured before and after vibration at the Goddard Space Flight Center where homogeneous fields of  $\pm 60\mu\text{T}$  could be externally applied. Internal fields were measured with a flux gate magnetometer with  $\pm 1\text{nT}$  resolution. The shielding factor  $\Delta H_{\text{ext}}/\Delta H_{\text{int}}$  before vibration testing was 55,000. This value is 50% lower than previous shields of similar design and indicates that fabrication strains in the high permeability material were not completely removed during the factory annealing procedure.

Figure 3 is a plot of the power spectral density of vibration as a function of frequency. Curve "a" is from a "control" accelerometer

mounted on the harness of the system during vibration tests. Curve "b" is the power spectra density from an accelerometer mounted on one of the shields during the same test. As can be seen there is a considerable difference in the two curves. The shield at the location of the accelerometer is experiencing significant, frequency dependent resonances indicating shield flexing during vibration. Spectra from accelerometers located at other spots on the shields varied in detail, but all showed frequency dependent resonances.

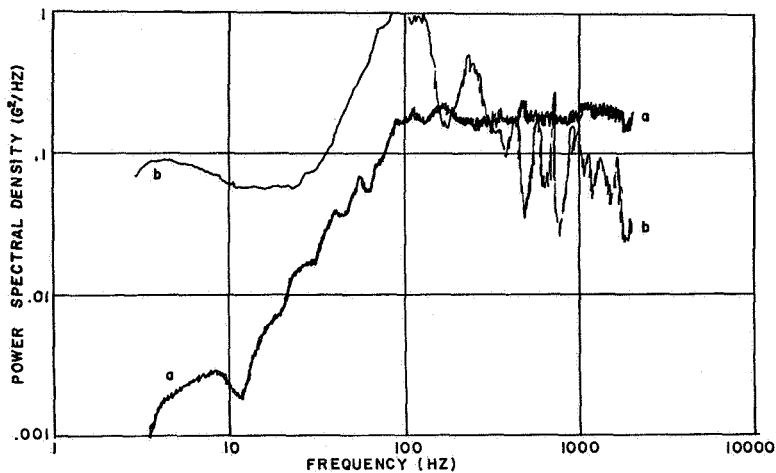


Fig. 3. Power spectral densities of vibration as measured on mounting harness "a" and on one of the shields "b".

Following the vibration tests, the shielding factor was again measured and found to be reduced from 55,000 to 40,000 - a degradation of 25%! This amount of degradation is quite large. It is possible that the initial strains in this poorly annealed set of shields may have predispositioned the shields to a more rapid degradation. We will soon be testing a more carefully annealed shield set in order to ascertain the degradation level in a shielding system more likely to be employed in an operating maser.

Different mounting arrangements for the magnetic shields may alleviate some of the problems observed with vibration induced shielding degradation. More shock absorbing or cushioning material between the shields may prevent some of the resonances. Alternatively one could increase the thickness of the shields which will give them more rigidity while at the same time provide a greater initial shielding factor for safety margin against degradation. Increasing the shield thickness by 20% will double the shielding factor for a 4-shield system, i.e. changing the shield thickness from .35 to .43 mm should provide an adequate safety margin even using the present mounting arrangement.

## I. SUMMARY/CONCLUSION

We have demonstrated a potential shock and vibration problem associated with the magnetic shield system of a space-borne hydrogen maser.



Shielding factor reduction of 25% have been seen on a poorly annealed shield set. Future tests on better annealed shields and different mounting arrangements should suggest ways to alleviate some of the problem.

## II. VACUUM/PUMPING SYSTEM

The vacuum/pumping system was designed to be compact, lightweight and structurally strong. A complete review of the various design considerations was presented last year.<sup>2</sup> The system as finally constructed is schematically shown in Fig. 4. It consists of a Ti-6Al/4V chamber which houses the state selector magnet and 2 ST 171 Zr-C getter pumps built by SAES Getters. Attached to one port on this chamber were 2 small Varian appendage ion pumps ( $\frac{1}{2}$  l/s) for assisting the getter pumps with residual gases (other than  $H_2$ ). This chamber was welded to the hydrogen maser and the hydrogen disassociator was attached with a viton "O"-ring to the bottom flange. The vacuum/pumping system tests were designed to determine i) the activation procedure ii) the system pumping speed and total hydrogen capacity of the getter pumps and iii) residual gas contamination levels and operation of small appendage ion pumps. The maser was initially operated using the described pumping system but with a turbo-molecular pump instead of the getter pumps in order to ascertain the initial operating condition of the complete system prior to the in situ getter pump tests.

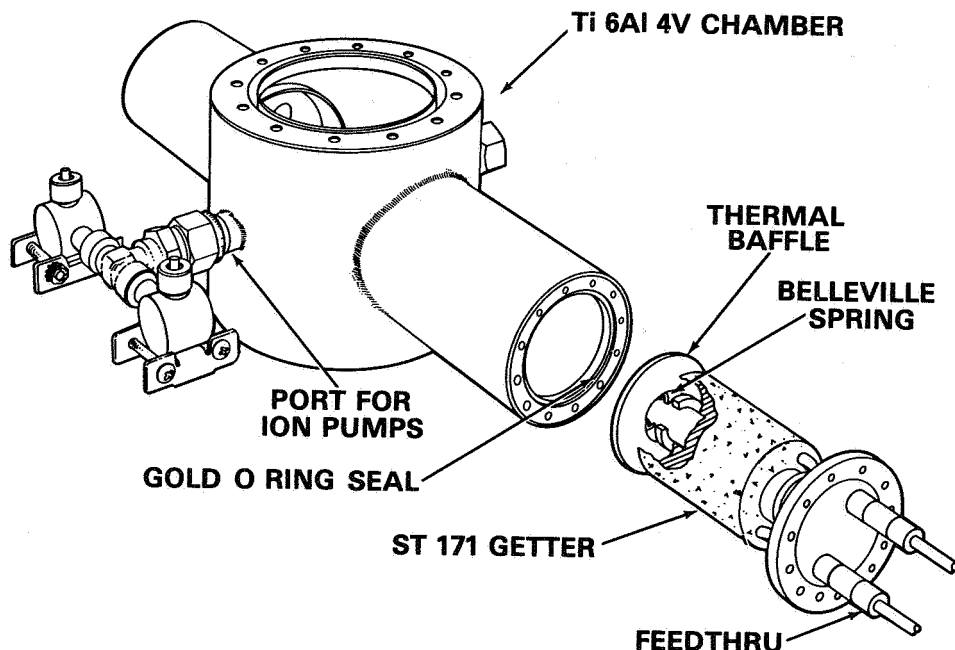


Fig. 4. Schematic drawing of Lightweight pumping system for  $H_2$  Maser.

We used only 1 Zr-C getter pump in the performance tests. The second getter pump port was used to attach a turbo-molecular pump for system evacuation during activation and for insertion of thermocouple (TC) leads into the vacuum space. One TC was attached to the getter pump to monitor its temperature while the 2nd was attached to the state selector magnet (AlNiCo VII, hexapole) immediately facing the getter pump. The two appendage ion pumps were attached to one of the remaining small ports while a partial pressure analyzer (Perkin-ELMER/Ultek Inc. Model 607-1000) was attached to the remaining port. Thus we were able to monitor partial pressures of all gases present in the system at all times.

#### i) Activation Tests

The getter pumps were equipped with an internal heater for activation. Initial attempts to activate the pumps were thwarted by heater burn out and shorts (a manufacturing problem hopefully being corrected) and by a large thermal leakage from the pumps to the outside world. A design modification involving insertion of several internal radiation shields located 1) inside the Ti pumping arm surrounding the getter pump, 2) between the inner diameter of the getter pump and the central support rod and 3) between the feed thru flange and the face of the pump. These design changes reduced the power required to activate the pumps by 75%. During activation, the Ti arm housing the getter pump was water cooled on the outside by slipping a double "O"-ring sealed brass cooling collar over it. The cooling water was thus directly in contact with the Ti metal itself. Activation was accomplished by maintaining the getter material at 900°C for 30 minutes as recommended by SAES Getters. 475 watts of power (8.5 amps at 55 volts ac) were required for activation. During activation the state selector magnet reached a maximum temperature of 195°C - well below the range where degradation is anticipated. The vacuum was maintained in the  $10^{-5}$  torr range or below with the turbo-molecular pump. Predominate gases emitted during activation were  $H_2O$ , CO,  $N_2$ , and hydrocarbons. After activation, the system was allowed to cool, the turbo-molecular pump was valved off, and an ultimate pressure of  $4 \times 10^{-7}$  torr was attained with the two ion appendage pumps and the getter pump. (See Table I)

#### ii) Pumping Speed and Capacity

Initial tests of the pumping speed were attempted using a variable leak valve (Granville-Phillips, Model 203) attached to a container of 5-9 purity Hydrogen. Even this high purity gas had enough Ar and N impurities to vitiate a long term test. The ion pumps could not maintain low Ar and N levels at the accelerated flow rate desired for the test. Following this discovery, a Pd value was inserted in the  $H_2$  gas stream in order to further cleanse the gas.

After insertion of the Pd value in the H<sub>2</sub> flow, the entering gas was free from any detectable impurities except a small amount of He. The pumping speed was determined by filling an external container of known volume V<sub>ext</sub> (8.3 liters) with 800 Torr H<sub>2</sub> and monitoring the pressure drop with a Quartz Manometer as the gas flowed into the maser, dP<sub>ext</sub>/dt. The pressure inside the maser P<sub>int</sub> was measured with the PPA (total pressure) and the flow rate was calculated from the formula

$$S \text{ (ℓ/sec)} = \frac{V_{\text{ext}}}{P_{\text{int}}} \frac{dP_{\text{ext}}}{dt} .$$

The measured average pumping speed was 20 liters/sec during the 1st 30 days of the test. Since the reported pumping speed of the Getter pump is >100 ℓ/sec, we assume that 20 ℓ/sec represents a conduction limited speed dependent on the geometry of the baffles and support mechanisms of the getter pumps. The flow rate for this test was 10<sup>-4</sup> torr ℓ/sec which is approximately 5 times larger than during maser operation. The total capacity of the H<sub>2</sub> pumped as of the writing of this article is 400 torr liters - 1/5 the expected useful capacity. These numbers are listed in Table I.

### iii Residual Gas Contamination - ion pump operation

A primary concern in these tests was the residual gas levels (≠ H<sub>2</sub>) in the system which might contaminate the getter pumps, limiting their useful lifetime and capacity. Associated with this same concern was the operation of the small ion pumps which were incorporated into the system to alleviate these residue gas problems.

For a clean system, calculations suggested that two small Varian appendage pumps would suffice to maintain stable maser operation provided the ion pumps were not degraded with time due to operation in a high partial pressure of H<sub>2</sub>. To increase the lifetime of the ion pumps operating in a hydrogen atmosphere, the operating voltage was reduced. The pumping efficiencies for lighter elements (such as H<sub>2</sub>) is reduced to a much greater extent than the heavier elements (such as N, O, Ar, and hydrocarbons) as the operating voltage of the pumps is lowered. To determine the optimum operating voltage, we measured the residual gas levels in the system as a function of ion pump voltage for two conditions: 1) H<sub>2</sub> flow with no Pd value (Fig. 5a) and 2) H<sub>2</sub> flow with Pd value (Fig. 5b).

In Fig. 5a one notes substantial levels of Ar and N<sub>2</sub> which were in the H<sub>2</sub> gas itself. With the ion pump off, the Ar and N levels quickly rose and the total pressure of the system increased continuously, i.e. the getter pumps could not pump these gases sufficiently well to maintain a

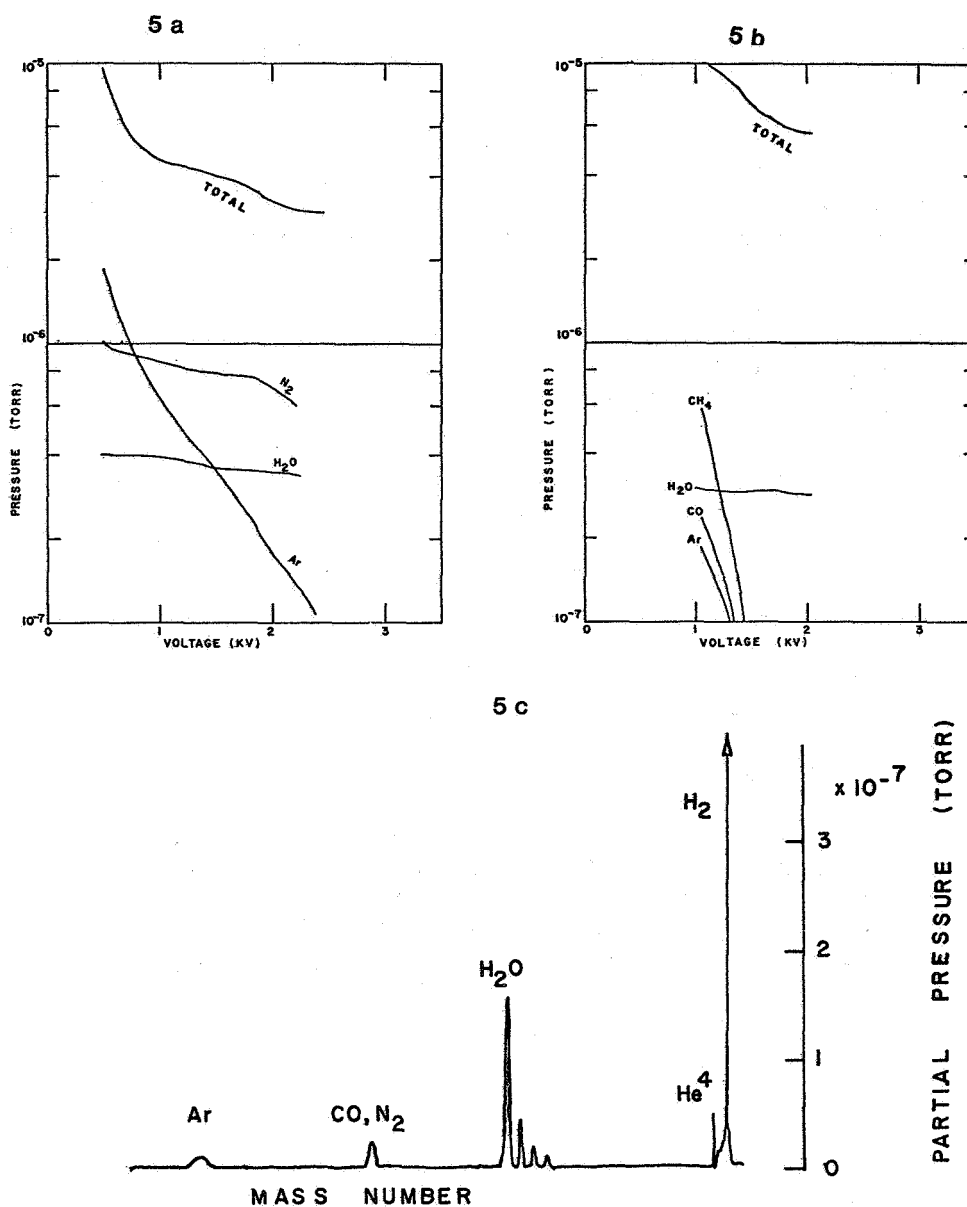


Fig. 5. Residual gas levels in  $H_2$  Maser. (See discussion Ref. 3).  
 (5a)  $H_2$  flow with no Pd value  
 (5b)  $H_2$  flow with Pd value  
 (5c) Gas spectrum after 40 days of operation at a flow rate of  $10^{-4}$  torr  $\ell$ /sec.

constant total system pressure at the flow rate used. With an operating voltage of 1 Kvolt, the system would maintain a stable pressure (albeit at a low flow rate), due to the ion pumps assistance with pumping. Ar partial pressure remained relatively high since the getters do not pump Ar. It appears that low voltage levels  $1 < V < 2$  Kvolts can effectively pump most contaminants in the maser.  $H_2$  does not appear to be significantly pumped at these voltage levels.

The same test was again performed after insertion of the Pd valve. Figure 5b shows the gas levels vs ion voltage for this test. As can be seen, the system is much cleaner, i.e. the Pd valve removed the contaminants in the  $H_2$  gas. At 1 Kvolt,  $CH_4$ , CO,  $H_2O$  and some Ar was detected in the  $10^{-7}$  torr range.<sup>3</sup> At 1.5 Kvolt, all gas contamination levels had fallen into the  $10^{-8}$  range except water. Thus it appears, that one can maintain a clean system operating the Varian appendage pumps at voltages as low as 1.5 Kvolts. We chose to operate the pumps at 1.75 Kvolt for the lifetime tests which are in progress. A PPA trace showing the detectable gas levels of the system after operation for 40 days is shown in Fig. 5c. Note the  $H_2O$  peak is 50% lower after 40 days than it was when the data in Fig. 5b was obtained after 5 days of operation, i.e. the system is cleaning up with time.

## II. SUMMARY/CONCLUSIONS

We have now demonstrated that the major design features of the lightweight Vacuum Pumping System are attainable. Major problems/uncertainties remaining are associated with 1) manufacturers reliability for delivering quality getter pumps with internal heater and 2) long lifetime tests for both the getter pumps and the ion pumps.

TABLE I

Pump System Characteristics

Activation power	475 watts
Activation temperature	900°C
Activation time	30 minutes
Ultimate Vacuum	$4 \times 10^{-7}$ getter + ion $9 \times 10^{-7}$ getter
Pumping speed	20 /sec
System pressure	$5.5 \times 10^{-6}$ torr (at flow rate of $10^{-4}$ torr l/sec)
Total pumped capacity at time of article	(40 days) 400 torr liters
Ion Pump Power	< 1 watt per pump

REFERENCES

1. D.U. Gubser, S.A. Wolf, and J.E. Cox, Rev. Sci. Instru. 50, 751 (1979).
2. S.A. Wolf, D.U. Gubser, and L.D. Jones, Proceedings of the 12th Annual PTTI meeting.
3. The partial pressures measured and reported are only nominal. The Ultek PPA does not accurately determine partial pressures of residual gasses, but rather gives a signal approximately proportional to their relative abundance in the system. The total pressure readings, however, are quite accurate since in this mode the PPA operates as an ionization guage.



A PHASE-COHERENT LINK USING THE ANIK-B SATELLITE  
FOR GEODETIC VLBI

W. B. Waltman, S. H. Knowles  
Naval Research Laboratory, Washington, D.C.

W. H. Cannon, D. A. Davidson, W. T. Petrachenko  
York University, Toronto, Canada

J. L. Yen  
University of Toronto, Toronto, Canada

J. Popelar  
Earth Physics Branch  
Energy Mines and Resources, Ottawa, Canada

D. N. Fort  
Herzberg Institute of Astrophysics, Ottawa, Canada

and

J. Galt  
Dominion Radio Astrophysical Observatory  
Penticton, B.C., Canada

ABSTRACT

A joint U.S.-Canada experiment is in progress to demonstrate the capabilities of phase-coherent VLBI for the measurement of Universal Time and Polar Motion. This paper was to present the results of the satellite link evaluation experiments. The 12/14 GHz transponder of the ANIK-B synchronous communications satellite has been used to provide a phase-coherent link between radio observatories in Maryland, Ontario and British Columbia. The system operates in a shared-user mode with television transmissions and makes only modest power and bandwidth demands on the satellite channel. A two-tone scheme is used with two-way transmissions on each path. The performance of the link can be separated from that of the frequency standards by use of the phase closure relationship for the three stations. The measured phase stability of the link is  $2 \times 10^{-15}$  for a period of one day. This result is comparable to that of the best separated hydrogen masers. When combined with the VLBI results the error in the UT measurement is  $\pm 200$  microseconds.

(ABSTRACT ONLY)

PAPER NOT PRESENTED





COMPOSITE-TYPE <sup>87</sup>Rb OPTICAL-PUMPING LIGHT SOURCE  
FOR THE RUBIDIUM FREQUENCY STANDARD

Nobunori Oura, Naimu Kuramochi, Shigeya Naritsuka,  
and Teruhiko Hayashi

Research Laboratory of Precision Machinery and Electronics,  
Tokyo Institute of Technology,  
4259, Nagatsuta, Midori-ku, Yokohama 227, Japan

ABSTRACT

This paper describes the experimental results and theoretical analysis of a newly devised compact light source for the Rubidium Frequency Standard (RFS). The light source is composed of a cylindrical Rb-87 lamp 10 mm diameter and a Rb-85 filter cell 3-7 mm long attached to the front flat face of the lamp. This composite-type device is operated in an oven at about 100°C. Thus a light source for Rb-87 hyperfine optical pumping less than 4 cm long by 3 cm diameter has been constructed.

INTRODUCTION

Among the various types of atomic frequency standards, the passive rubidium-gas-cell type frequency standard (so called "Rb Frequency Standard (RFS)") is the smallest, simplest, and least expensive one(1). Improvement of this type of standards is now making progress for satisfying various requirements(2-4).

One of the requirements is the miniaturization of the standard. The use of the optical-microwave unit without a filter cell may be an approach to meet this requirement(5). A miniaturized RFS without a filter cell has been on the market for seven to eight years, but its operating mechanism is not clearly understood(6). In addition, the lamp installed in the filterless optical-microwave unit is applicable to the passive RFS only.

In a previous paper, we proposed a new composite-type Rb-87 optical-pumping light source incorporating the lamp with the Rb-85 filter cell(7). From this light source, light suitable for the Rb-87 hyperfine

optical pumping ( $5S_{1/2}, F=1 \rightarrow 5P_{1/2}$  and  $5P_{3/2}$ ) is directly obtained. This device can be used for the miniaturized RFS. The idea of this device can be also applied to the Rb maser (Rb-87 and Rb-85 maser) and other optical pumping experiments.

In this paper, we clarify the operating mechanism of the composite-type device from the viewpoint of the spectral profile of the pumping light. This light source was applied to the RFS, and the resonant signal of the Rb-87 hyperfine frequency ( $f=6834$  MHz) was detected as a discriminator pattern. An attempt to make the composite-type device using natural Rb is also discussed.

#### SPECTRAL PROFILE OF THE PUMPING LIGHT

The composite-type Rb-87 pumping light source consists of the cylindrical Rb-87 lamp and the short-length Rb-85 filter cell as shown in Fig.1. The lamp is excited by an rf magnetic field of about 100 MHz in the coil. A simple self oscillator (transistor 2SC549) is used as the lamp exciter.

An elementary explanation of the Rb-85 filtering action is shown in Fig.2 in the case of the Rb D-1 line. If the spectral profiles of the Rb-87 and Rb-85 D-1 line are shifted and broadened by the foreign gas as shown in the figure, the combined cd component is greatly absorbed by the Rb-85 spectral profile. On the other hand, the combined ef component is less absorbed and almost unweakened. Efficient pumping light is thus obtained. The problems are in the designing of the filter-cell length  $l$ , the foreign-gas pressure  $P$ , the operating temperature  $T$ , etc.

The composite-type device was first evaluated from the spectral profiles of the D-1 line by using a Fabry-Perot interferometer scanned piezo-electrically(8). The photodetector is an R374 photomultiplier tube.

Figure 3 shows the temperature dependence of the Rb-87 D-1 line spectral profiles emitted from the composite-type device having a filter cell of 3 mm long(A) and 7 mm long(B). As the temperature rises to 100 - 110 °C, the ef component which is necessary for pumping increases, while the cd component which is unnecessary is much absorbed by the filter cell.

To discuss the quality of the pumping light source, the evaluation values  $r$  and  $d$  which express the ratio of the intensity of  $cd'$  to  $ef'$  and the difference of the intensity,  $ef'$  minus  $cd'$ , are introduced:

$$r = I_{cd'} / I_{ef'} = a' / b' \quad (1)$$

$$d = I_{ef'} - I_{cd'} = b' - a' \quad (2)$$

These values indicate the criteria for showing the filtering action of the Rb-85 cell. The smaller value of  $r$  and the greater value of  $d$  are desirable for pumping.

Figures 4 and 5 show the variations in the values of  $r$  and  $d$  against temperatures, which are calculated from the profile measurement of the composite-type light sources. The parameter is the length of the filter cell. A curve for  $\ell = 0$  shows the value obtained by the Rb-87 lamp only (without a filter cell).

From Fig.4, we find that the device with the longer filter-cell ( $\ell = 6 - 7$  mm) emits excellent pumping light around  $100^\circ\text{C}$ . Figure 5 prepares a different evaluation. As is mentioned in the former paper (10), the value of  $d$  corresponds to the intensity of the microwave resonance signal. From such a stand point, the composite-type source having 3-mm-long filter cell has excellent pumping power at about  $110^\circ\text{C}$ , although the value of  $r$  is not small compared to others.

On the other hand, the value of  $d$  for the composite-type light source with 7-mm-long filter cell is almost constant in the temperature range of  $95 - 110^\circ\text{C}$ . That is, the pumping light intensity of the present light source is stable against the environmental temperature variation. Because an increase of the light intensity of the lamp as a result of a temperature increase is killed by the increase of the absorption in the filter cell. Thus, we can get a light source with almost constant pumping power. This is a merit of the source using single oven.

The procedure for the analysis is shown in Fig.6. We applied the self-absorption model to the formulation of the temperature dependence of Rb-87 lamp profiles. It is assumed that the temperatures of the lamp and filter cell are equal and vary at the same time. In this calculation, values of the parameters such as the spectral line width of the component lines, pressure shift, and equivalent absorption-atom-layer thickness in the lamp, are assumed to be the same as in the references(10,11), which analyzed Rb-85 filtering action and Rb-87 lamp profiles.

Calculated results for the composite-type light source with the 7-mm-long filter cell are shown in Fig.7. These results agree well with the observed ones.(Fig.3(b)) From the calculated profiles, the temperature dependence of the values of  $r$  and  $d$  are obtained as shown in Figs.8 and 9.

#### THE DISCRIMINATOR PATTERN OF THE Rb-87 DOUBLE RESONANCE

Using the Rb-87 resonant cell containing 21 Torr of mixed gases ( $\text{N}_2 : \text{Kr} = 55 : 45$ ), the discriminator patterns were observed. Measurement was performed with the experimental setup for the RFS(9). The resonant cell

temperature was kept at 50°C and the composite-type light source was operated at temperatures between 80 and 110°C.

The block diagram of the measurement is shown in Fig.10. When the frequency-modulated interrogating signal in the microwave cavity is swept around the Rb-87 resonant frequency ( $f=6834$  MHz) through VCXO, the derivative of the resonance line, i.e. the discriminator pattern, is obtained on the phase sensitive detector output.

Figure 11(a) shows the discriminator patterns of the Rb-87 resonant cell pumped by the composite-type light source with 3-mm-long filter cell. At 80°C, the peak to peak value  $V_{pp}$  in the discriminator pattern is less than 0.1V. From 90 to 110°C,  $V_{pp}$  is increasing steadily. At 110°C,  $V_{pp}$  is greater than 8V. Figure 11(b) shows the discriminator patterns using the composite-type device with 7-mm filter. The temperature variation from 95 to 110°C did not remarkably change the discriminator patterns. These results agree well with the spectral profile characteristics.

#### COMPOSITE-TYPE DEVICE USING NATURAL Rb

The above discussion was concerned with the composite-type device using isotope Rb. Next, the same approach was taken into the device using natural Rb. Figure 12 explains schematically how the desirable Rb-87 pumping light is obtained by the combination of the natural Rb lamp and the natural Rb filter cell(12,13). Absorption profile of the filter cell is shifted to the longer wavelength side and broadened by the foreign gas such as nitrogen. If we choose the appropriate gas pressure, temperature, and length of the filter cell, unwanted components of the natural Rb line (EF, CD, cd components in the D-1 line) are much absorbed by this filter cell, and ef' component, which is necessary for pumping, remains as it is.

Through our experiments, the desired profile has been obtained under the following conditions: the natural Rb lamp had a pressure of 1.8-Torr krypton, the natural Rb filter cell was 5.5 mm long and had a pressure of 100-torr nitrogen. Spectral profiles of the D-1 line emitted from this device are shown in Fig.13. An optimum profile is obtained at about 110°C.

Although the output light intensity was reduced to one-third that of the device using isotope Rb, discriminator patterns of the Rb-87 hyperfine frequency were obtained with sufficient intensity for RFS operation.

#### DISCUSSION

To discuss the spectral profiles of the pumping light source, we introduced the evaluation values of  $r$  and  $d$  in Eqs.(1) and (2). If we compare these values with the experimental (Figs.4 and 5) and the calculated results (Figs.8 and 9), respectively, we find that there are some differences between them in the details. Especially, concerning the value of  $d$ , the discrepancy is distinguishable for the shorter length filter cell. The causes for this discrepancy are inferred as follows.

In the analysis of the profile as shown in Fig.7, we assume that the temperatures of the lamp and filter cell are equal and vary at the same time by the heater. In reality, the filter cell is positioned by the window glass of the oven, and the lamp radiate heat by itself due to excitation. Then the temperature of the filter cell tends to be lower than the lamp's. If the temperature of the filter cell is lower, the absorption by the filter cell is less, and higher output is obtained. This suggests that the temperature difference between the lamp and the filter cell must be taken into account in the analysis, especially, at higher temperature.

In the analysis we adopted the self-absorption model for the electrodeless spherical lamp(11). In this composite-type device, however, the shape of the lamp is cylindrical and the filter cell is attached to the front flat face of the lamp. Then the equivalent self-absorption atom layer in the model of Fig.6 is probably different from that of the spherical lamp. Some modification must be needed to clarify the characteristics completely.

Next we will discuss the profiles of the output light from the source with natural Rb only, not isotope Rb, both in the lamp and filter cell. The necessary component  $ef'$  at  $80^{\circ}\text{C}$  is low compared with the other unwanted components. However, the necessary component becomes higher as temperature increases, whereas the unwanted components hardly becomes higher. At  $109^{\circ}\text{C}$ , only the  $ef'$  component remains, while the unwanted components rather diminish. Although the output light intensity was reduced to one-third that of the device using isotope Rb, discriminator patterns of the Rb-87 hyperfine frequency were obtained with sufficient intensity for RFS operation.

These two kinds of the light source, made of isotope Rb or natural Rb, are available for not only RFS but also pumping light sources in other physical experiments and a maser. A parallel operation of the source is possible, if the output intensity of a single source is insufficient for maser oscillation. The size of the device is small as shown in Fig.1, and it is installed in a single oven, whereas the conventional source requires two ovens, one for the lamp and another for the filter cell with independent controls.

About the quality of the pumping light profile, it is necessary to discuss the symmetry of the spectral line. Some of the requisites to obtain the stable frequency from the RFS are that the spectral profile of the pumping light does not fluctuate in intensity and is symmetric. As is mentioned in Fig.3, the composite-type device having 3-mm-long filter cell has an excellent pumping power at about 110°C. However, if we look carefully at the pumping light profiles, we find the small dip near the peak of the  $ef'$  component line. This is so called self-reversal resulting from the self-absorption in the lamp. As a result, the line is asymmetric. This is a cause of the frequency shift in the RFS due to "light shift". On the contrary, the  $ef'$  component line's profiles from the device having 7-mm-long filter cell show symmetry. This source has two properties described above, that is, the symmetry in the profile and less variation in the intensity against the temperature.

When Rb-87 is enclosed in the lamp, and Rb-85 and 100-Torr nitrogen are in the filter cell, the length of the filter cell and the operating temperature of the composite-type device should be designed as follows according to the purposes. (1) To obtain the strong pumping power,  $l$  should be about 3 mm and operated at about 110°C. The pumping profile is a little asymmetric. (2) To obtain the constant power against the environmental temperature variation of 95 to 110°C,  $l$  should be about 7 mm. Though the pumping power is less than that of 3mm, the pumping profile is symmetric.

#### CONCLUSION

We have established designing methods for constructing a compact Rb-87 optical-pumping light source. By using isotope Rb, we can not only reliably miniaturize the size of RFS but also obtain a powerful pumping light source for use in applications such as a Rb maser. By using natural Rb, we can construct a compact RFS at low cost.

#### ACKNOWLEDGEMENT

The authors express their gratitude to Professor Emeritus H.Fukuyo and Professors T.Tako, T.Musha, and K.Iga for their helpful discussion. They also thank Mr.M.Shibata of Suwa Seikosha for his help in the early stage of the experiment, and Prof.I.Matsuda of Tokyo Institute of Polytechnics for his helpful discussion. This work was partly supported by Hōsō-Bunka Foundation.

#### REFERENCES

- (1) T.C.English, "Discussion forum: Atomic frequency standards -

Rubidium," Proc. Tenth Annual PTTI Applications and Planning Meeting (1978)pp.199-220.

- (2) F.K.Koide and D.J.Dederich,"Rubidium frequency standard test program for NAVSTAR GPS," Proc. Tenth Annual PTTI Applications and Planning Meeting (1978)pp.379-391.
- (3) T.C.English and E.Jechart,"Development of a sapphire lamp for use in satellite-borne atomic rubidium clocks," Proc. 35th Ann. Sympo. Freq. Control (1981) to be published.
- (4) T.Hashi, K.Chiba, and C.Takeuchi,"A miniature, high-performance rubidium frequency standard," Proc. 35th Ann.Sympo.Freq.Control (1981) to be published.
- (5) E.Jechart,"A new miniature rubidium gas cell frequency standard," Proc.27th Ann.Sympo.Freq.Control (1973) pp.387-389.
- (6) A.Risley and G. Busca,"Effect of line inhomogeneity on the frequency of passive  $^{87}\text{Rb}$  frequency standards," Proc. 32nd Ann. Sympo. Freq.Control (1978)pp.506-513.
- (7) N.Kuramochi, S.Naritsuka, and N.Oura,"Composite-type  $^{87}\text{Rb}$  optical-pumping light source," Opt.Lett., 5(1981)pp.73-75.
- (8) N.Kuramochi, H.Fukuyo, I.Matsuda, and N.Shioimi,"Spectral profiles of the  $^{87}\text{Rb}$  pumping light source," Jpn.J.Appl.Phys., 15(1976) pp.949-954.
- (9) I.Matsuda, N.Kuramochi, N.Shioimi, and H.Fukuyo,"Signal intensity characteristics of the  $^{87}\text{Rb}$  double resonance due to the pumping light," Jpn.J.Appl.Phys., 16(1977) pp.391-396.
- (10) N.Kuramochi, I.Matsuda, and H.Fukuyo,"Analysis of the effect of foreign gases in the filtering action of a  $^{85}\text{Rb}$  cell," J.Opt.Soc.Am., 68(1978)pp.1087-1092.
- (11) N.Kuramochi, I.Matsuda, N.Oura, and H.Fukuyo,"Analysis of the temperature dependence of  $^{87}\text{Rb}$  lamp profiles," J.Opt.Soc.Am., 70(1980)pp.1504-1507.
- (12) T.Tako, Y.Koga, I.Hirano, and M.Ohi,"Absorption of Rb-D lines by Rb filter cell," Jpn. J.Appl.Phys., 14(1975)pp.1641-1646.
- (13) N.Kuramochi, I.Matsuda, N.Oura, and H.Fukuyo,"Analysis of Rb optical pumping light sources," Jpn.J.Appl.Phys., 18(1979) pp.381-382.



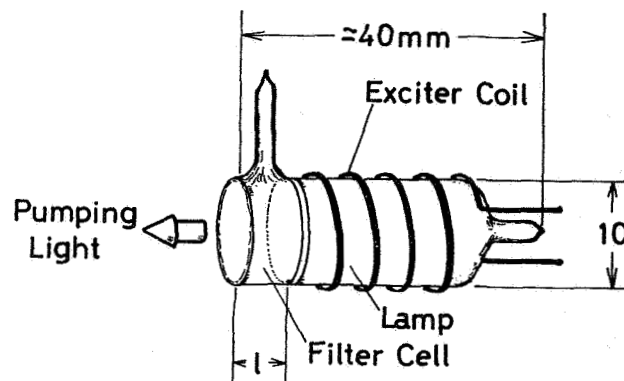


Fig. 1  
Composite-type Rb-87 optical pumping light source.

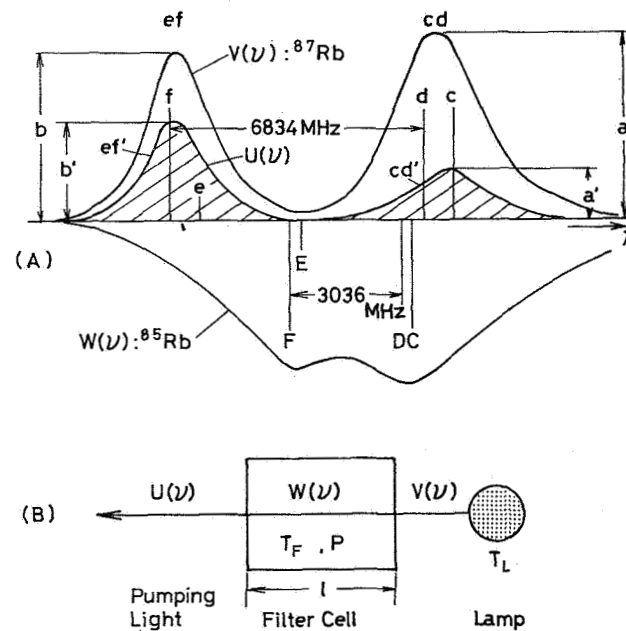


Fig. 2  
Schematic diagram of the Rb-85 filtering action for the Rb-87 lamp. (A) Spectral profiles of the Rb-87 D-1 line. Hatched areas are the pumping light profiles filtered by a Rb-85 filter cell. The Rb-85 spectral profile includes the shift and broadening due to foreign gas. (B) Arrangement of the usual Rb-87 pumping light source.

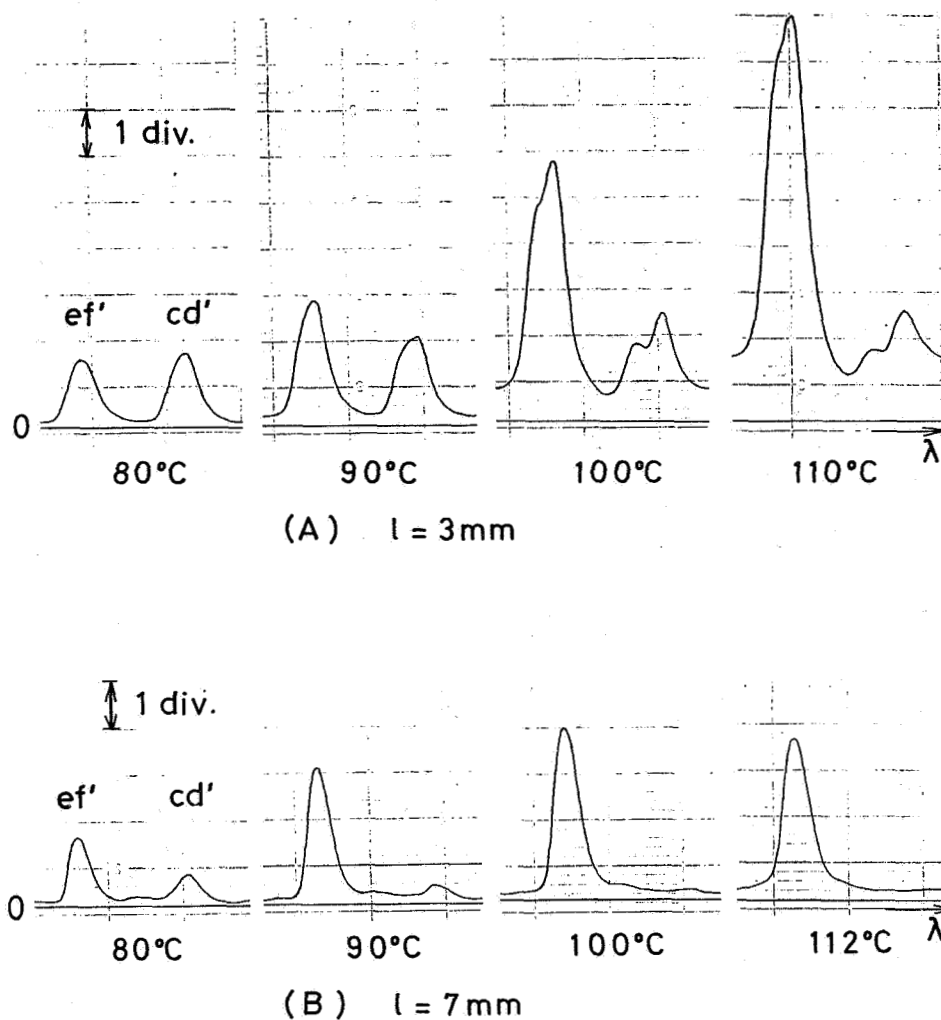


Fig 3.  
 Observed profiles of the Rb-87 D-1 line from the composite-type light source. 1.8-Torr krypton is in the Rb-87 lamp as a starting gas. Foreign gas in the filter cell is 100-Torr nitrogen. One division on the ordinate is 100  $\mu$ V.  
 (A) Filter-cell length is 3 mm. The lamp is excited by an rf magnetic field from an oscillator whose dc input is 1.1 W. (B) Filter-cell length is 7 mm. dc input to the exciter is 1.2 W.

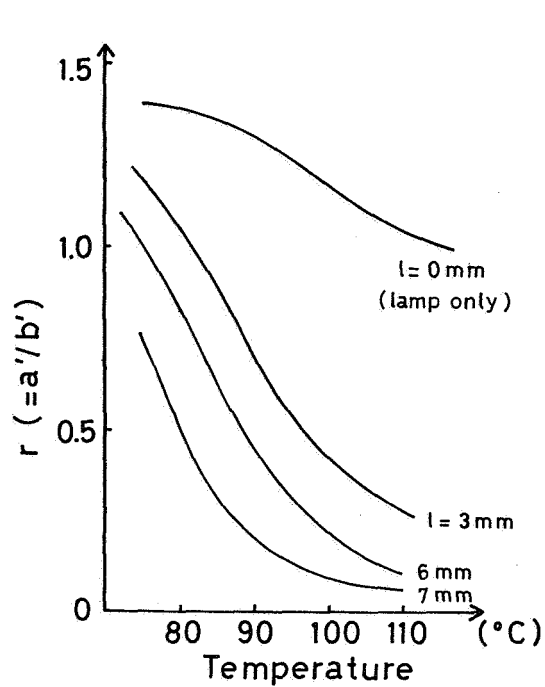


Fig.4  
Values of  $r$  vs. temperature of the source, which are calculated from the experimental results.

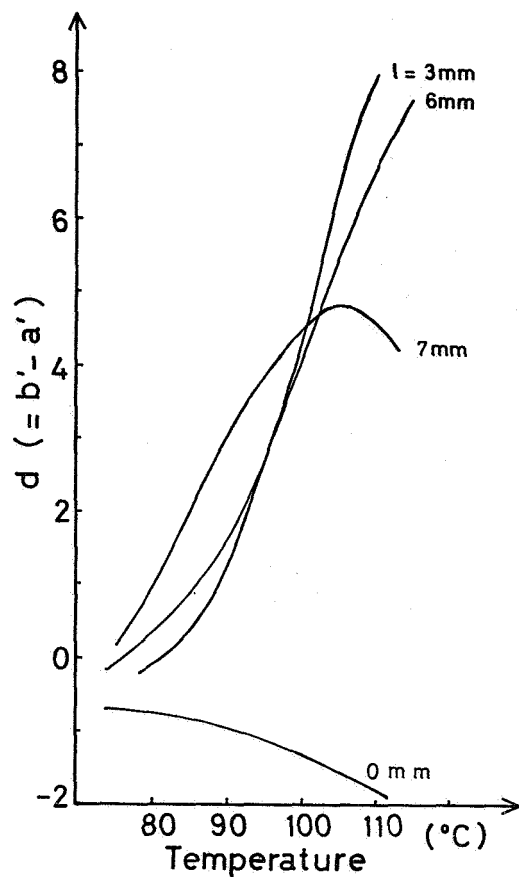
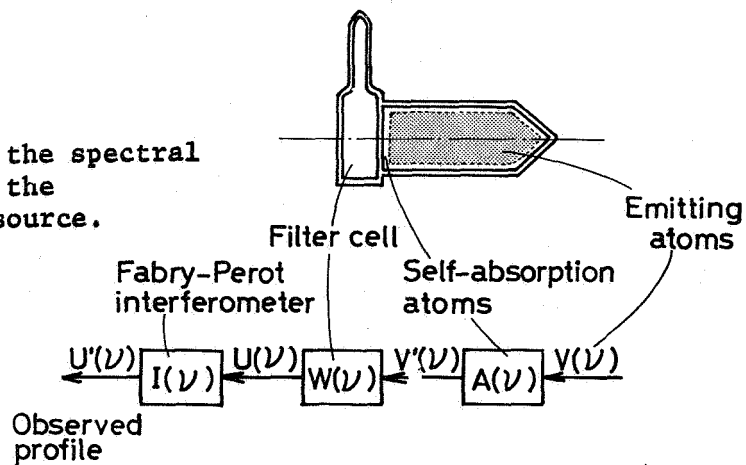
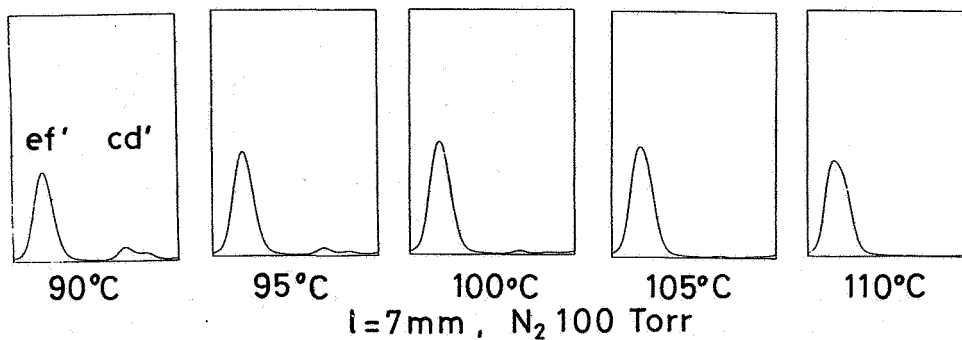


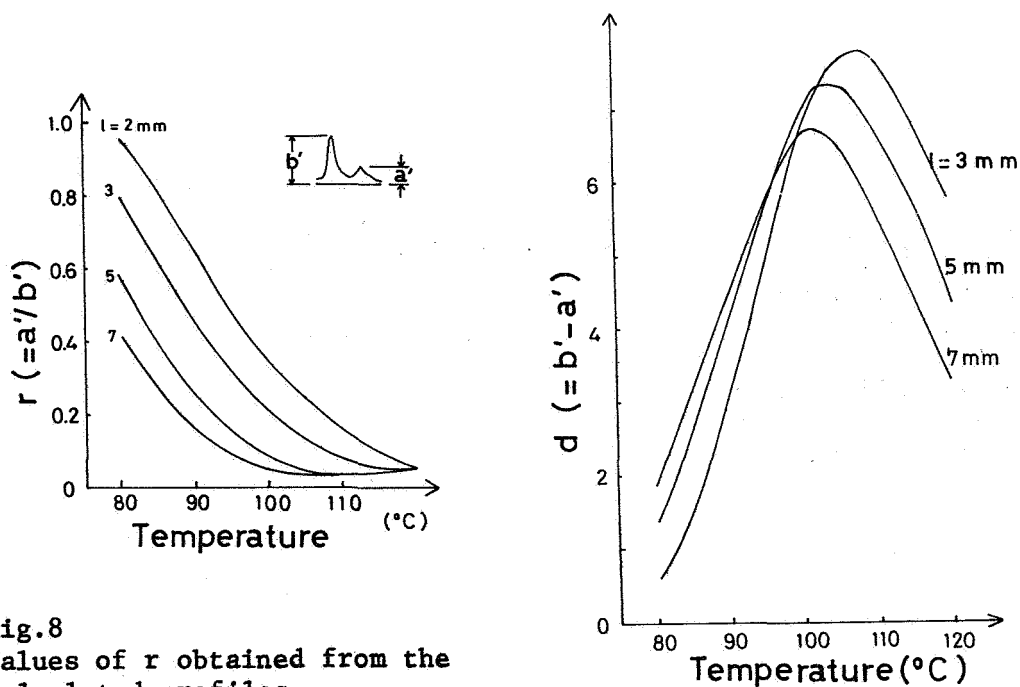
Fig.5  
Values of  $d$  vs. temperature of the source, which are calculated from the experimental results.

Fig.6  
A model for analyzing the spectral profiles emitted from the composite-type light source.





**Fig.7**  
Calculated profile of the Rb-87 D-1 line from the composite-type pumping-light source.



**Fig.8**  
Values of  $r$  obtained from the calculated profiles.

**Fig.9**  
Values of  $d$  obtained from the calculated profiles.

Fig.10  
Block diagram for  
measuring the discriminator  
pattern.

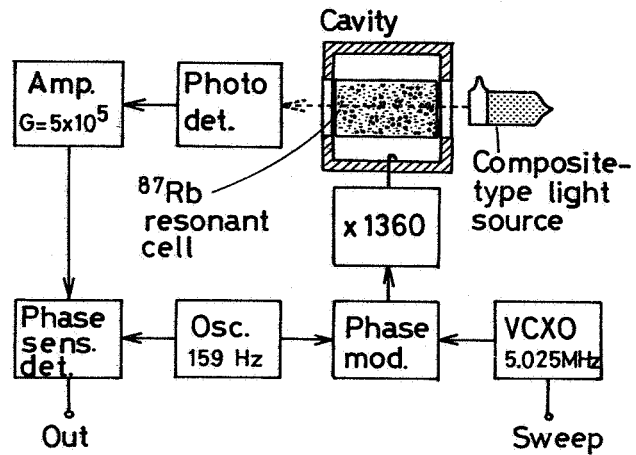


Fig.11  
Discriminator patterns  
of the Rb-87 resonance  
line pumped by the  
composite-type light  
source. (A) Filter-cell  
length is 3 mm. (B)  
Filter-cell length is  
7 mm.

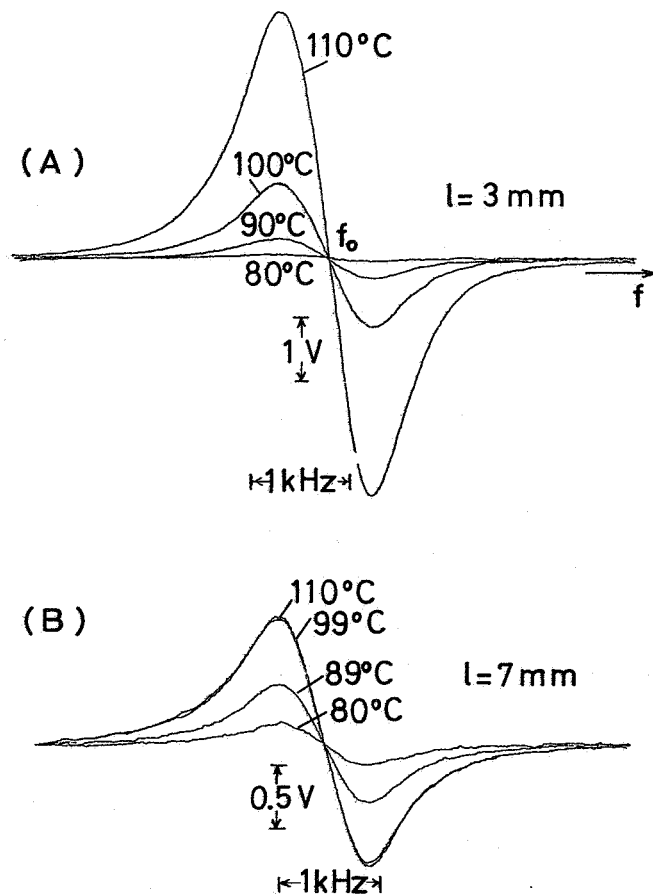


Fig.12  
Schematic diagram of the filtering action of the natural Rb cell for the natural Rb lamp. Absorption profile of the filter cell includes the shift and broadening due to foreign gas.

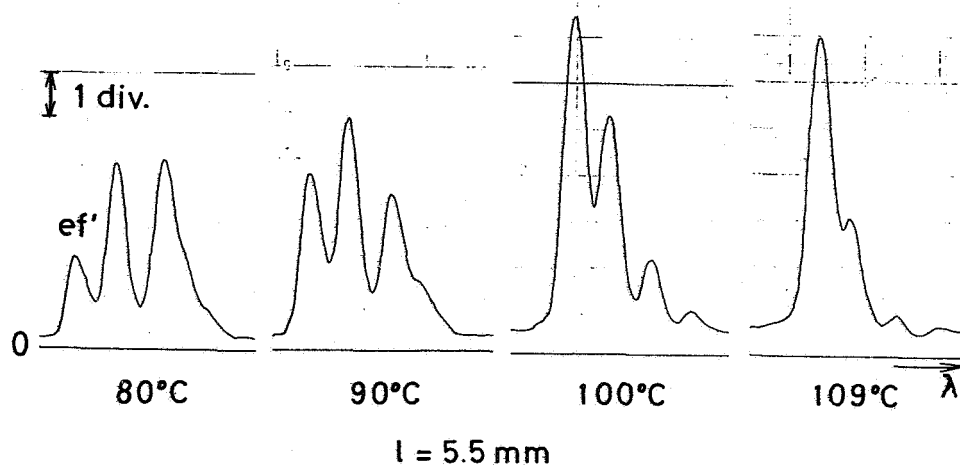
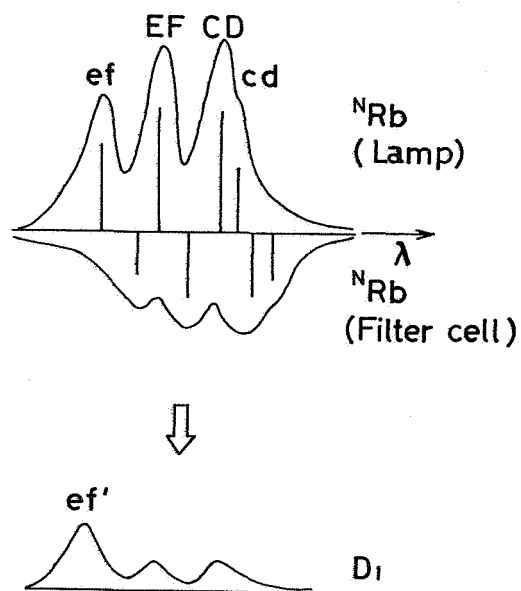


Fig.13  
Observed profiles of the Rb-87 D-1 line from the composite-type device including natural Rb both in the lamp and filter cell. Foreign gas in the filter cell is 100-Torr nitrogen. One division on the ordinate is 30  $\mu$ V. dc input to the exciter is 1.4 W.



# AN NNSS SATELLITE TIMING RECEIVER

BY

C.L.Jain\*, K. Kumar\*, H.I. Andharia\*, Mohan Singh+,  
V.D'Souza+, V.K. Goel+, A.K. Sisodia \*\*

Space Applications Centre  
(Indian Space Research Organisation)  
Ahmedabad-380053, INDIA

## ABSTRACT

The U.S.Navy Navigation Satellite System termed as NNSS offers a unique worldwide facility for the precise Time Synchronisation. To take the advantage of such a facility for tracking Indian Satellites, Space Applications Centre (SAC) has developed a simple Timing Receiver. Using this Timing Receiver first the internal time consistency of NNSS was studied and then its performance to synchronise time was compared with that of National Time Standard. This paper describes in detail the methodology of data analysis, results and the various sources of error which affects the time transfer accuracy. The main source of error was found to be the receiver delay which varies with signal strength. It is possible to apply this delay correction empirically provided signal strength is recorded.

---

\* Geodesy Division

+ Electronics Service Division

\*\* Digital Communications Division



## INTRODUCTION

The Navy Navigation Satellite System (NNSS) is a fully operational navigation system that enables the Navy Fleet or commercial users to accurately obtain their position anywhere on the Globe, day or night and in any weather. The NNSS commonly known as TRANSIT, consists of a constellation of five operational satellites in fixed circular polar orbits at an altitude of approximately 1100 km. The TRANSIT system requires accurate time to accomplish its navigational mission. For this reason the satellites transmit a precisely timed fiducial time mark (FTM) every two minutes. The transmission of FTM has provided a unique world wide facility for time Synchronisation. In fact Transit satellites are like unattended flying clocks and user can tap precise time as and when the satellites come on the horizon with a proper type of receiver. This unique facility has become a bonanza to users of precise time even in remote areas. Maintenance of precise time is as difficult as keeping an Olympic Flame. In case of failure it would be necessary in either situation to go back to the source. But the TRANSIT has solved this problem and 5 operational satellites provide excellent service reliability.

To take advantage of NNSS facility for maintaining time at ISRO Telemetry & Tracking Command Network (ISTRAC) Space Applications Centre (SAC), Ahmedabad under took the fabrication of a simple Timing Receiver. This receiver after getting locked to 400 MHz satellite carrier detects FTM and sets the 1PPS of the local clock. The path delay correction to 1PPS is applied using broadcast ephemerides and ground station coordinates manually.

## TIME TRANSFER METHODOLOGY - SATELLITE FRAME TO GROUND FRAME

The time mark in the satellite signals are referenced to UTC (Universal Coordinated Time maintained by U.S. Naval Observatory). The time mark consists of a "Zero", 23 "ones" and a "Zero", followed by a 400 Hz beep signal and is shown in fig. 1. The exact point of transition between the final binary zero and the beginning of 400 Hz beep is the exact two minute mark. This time mark is known as Fiducial Time Mark (FTM). In every two minute, synchronised with FTM, the satellites also transmit 26 orbital words. The first 8 words are known as variable parameters and the rest are known as fixed parameters. The fixed parameters describe the satellites nominal orbit where as the variable parameters describe the fine structure in the satellite nominal orbit as a function of time. The accuracy of the satellites position derived from these parameters (known as Broadcast Ephemeris) are 25 m in-track, 15 m cross-track and 10 m in radial direction.

The NNSS Timing Receiver detects the FTM and synchronises 1 PPS of its internal clock. The correction to this 1PPS is given by:

$$\text{Correction} = D_0 + R/C$$

where  $D_0$  = Mean receiver delay at a given signal strength.

$R$  = Slant range of the satellite from receiver antenna in km.

$C$  = Velocity of electromagnetic waves in km.

The satellite transmits the five orbital parameters viz. semi-major axis ( $a_{t_p}$ ), eccentricity ( $e$ ), inclination ( $i$ ), argument of perigee ( $\omega_{t_p}$ ) and right ascension of the ascending node ( $\Omega_{t_p}$ ), the precession rate of  $\omega$  and  $\Omega$  ( $\dot{\omega}$  &  $\dot{\Omega}$ ), the mean motion ( $n$ ) and Greenwich sidereal time ( $GAST_{t_p}$ ) at a certain time  $t_p$  along with  $\Delta a$ ,  $\Delta E$  and  $\eta$  where  $\Delta a$  and  $\Delta E$  are the corrections to be applied to the semi-major axis and the eccentric anomaly and  $\eta$  is the out of plane component.

The satellite coordinates at any instant  $t$  with respect to the orbital coordinate system are

$$\begin{bmatrix} x_t \\ y_t \\ z_t \end{bmatrix} = \begin{bmatrix} a_t (\cos E_t - e) \\ a_t \sin E_t \\ \eta_t \end{bmatrix}$$

where  $a_t =$  semi-major axis at time  $t$   
 $= a_{t_p} + \Delta a_t$   
 $E_t =$  Eccentric anomaly at time  $t$   
 $= M_t + e \sin M_t + \Delta E_t$   
 $M_t =$  Mean anomaly at time  $t$   
 $= n (t - t_p)$

The transformation of the satellite coordinates from the orbital plane system to the equatorial coordinate system is accomplished by three rotations viz

- (i) the rotation in the x-y plane by  $(-\omega_t)$
- (ii) the rotation in the y-z plane by  $(-i)$
- (iii) the rotation in the x-y plane by  $(-\Omega_t)$

where

$$\omega_t = \text{argument of perigee at time } t$$

$$= \omega_{t_p} - |\dot{\omega}| (t-t_p)$$

$$\begin{aligned}\Omega_t &= \text{right ascension of ascending node at time } t \\ &= \Omega_{t_p} + \dot{\Omega}(t-t_p)\end{aligned}$$

The rectangular geocentric coordinates are, therefore,

$$\begin{bmatrix} X_t \\ Y_t \\ Z_t \end{bmatrix} = R_1(-\omega_t) \cdot R_3(-i) \cdot R_1(-\Omega_t) \begin{bmatrix} x_t \\ y_t \\ z_t \end{bmatrix}$$

$$\begin{bmatrix} X_t \\ Y_t \\ Z_t \end{bmatrix} = \begin{bmatrix} \cos \omega_t & -\sin \omega_t & 0 \\ \sin \omega_t & \cos \omega_t & 0 \\ 0 & 0 & 1 \end{bmatrix} \begin{bmatrix} 1 & 0 & 0 \\ 0 & \cos i & -\sin i \\ 0 & \sin i & \cos i \end{bmatrix} \begin{bmatrix} \cos \Omega_t & -\sin \Omega_t & 0 \\ \sin \Omega_t & \cos \Omega_t & 0 \\ 0 & 0 & 1 \end{bmatrix} \begin{bmatrix} x_t \\ y_t \\ z_t \end{bmatrix}$$

In order to obtain the coordinates in the earth fixed system, a sidereal rotation by an angle equal to the Greenwich sidereal time at the instant is applied,

$$\text{i.e. } \lambda_t = \text{GAST}_t = \text{GAST}_{t_p} + \omega_e (t-t_p)$$

$\omega_e$  = rotation rate of the earth

$$\text{Thus } \begin{bmatrix} X_s \\ Y_s \\ Z_s \end{bmatrix} = \begin{bmatrix} \cos \lambda_t & \sin \lambda_t & 0 \\ -\sin \lambda_t & \cos \lambda_t & 0 \\ 0 & 0 & 1 \end{bmatrix} \begin{bmatrix} X_t \\ Y_t \\ Z_t \end{bmatrix}$$

The coordinates of the station are expressed in terms of the geodetic latitude  $\phi$  and longitude  $\lambda$ . They can be transformed into cartesian coordinates by the formulae,

$$\begin{aligned}X_o &= (N+h) \cos \phi \cos \lambda \\ Y_o &= (N+h) \cos \phi \sin \lambda\end{aligned}$$

$$Z_o = \left\{ (1-e^2) \nu + N+h \right\} \sin \phi$$

where,

$$\nu = \frac{a_e}{(1-e^2 \sin^2 \phi)^{1/2}}$$

$a_e$  = equatorial radius of the earth

$e$  = eccentricity of the earth

$N+h$  = height of the station above the reference ellipsoid.

Knowing the station position and the satellite position at any time  $t$ , we can calculate the slant range as follows:

$$R = \left\{ (X_s - Y_o)^2 + (Y_s - Y_o)^2 + (Z_s - Z_o)^2 \right\}^{1/2}$$

Using above relation slant range is determined. The mean receiver delay is added with the propagation delay and clock correction factor is obtained in microsecond. The clock is advanced by this clock correction factor.

#### EXPERIMENTAL SET UP

The Timing Receiver developed at Space Applications Centre is a single channel phase locked receiver operating at 400 MHz. The orbital data is stored in receiver memory and read manually for computing propagation delay. The receiver design was kept extremely simple in order to develop a concept for time transfer.

The experimental set up used to study the internal consistency of NNSS as well as the capability of receiver to transfer time with respect to National Standard is shown in fig. 2. In the first case for studying the internal time

satellites was found to be around  $\pm 75$  microsecond (1 sigma level) and is shown in fig. 3A. This one sigma ( $1\sigma$ ) level value may improve after applying the receiver delay correction for each data point (Delay variation with signal strength).

- (ii) For studying the performance of Timing Receiver to transfer time with respect to National Standard maintained at National Physical Laboratory, New Delhi, data were taken from 9th to 12th February 1981. The one sigma value for time transfer accuracy was found to be about  $\pm 70$  microsecond and is shown in Fig. 3B.
- (iii) The internal consistency of NNSS is found to be as good as the time transfer accuracy of Timing Receiver with respect to National Standard.

#### SOURCES OF ERRORS.

The accuracy to which time can be transferred from the satellite clock to the user's clock using an NNSS Timing Receiver depends on many factors. The following sources of error limit the overall accuracy of the system.

- (i) Time jitter in FTM detection
- (ii) Offset in FTM transmitted by satellite
- (iii) Receiver delay variation with signal strength.
- (iv) Ionospheric & Tropospheric delay

The error due to factor No. II is not under user's control. The transit satellite report series 17 published by U.S. Navy Astronautics Group, Point Mugu, C.A. gives the offset of each satellite clock with respect to UTC, can be obtained on request and one can apply the correction. The

consistency the Cesium Beam Atomic clock was synchronised using NNSS Timing Receiver. For this purpose a good satellite pass was selected and at the time of closest approach the FTM was detected and used to set 1PPS of receiver clock. Using the satellite orbital data the delay was computed and then the 1PPS of Cesium Beam Clock was synchronised. In the actual set up the 1 PPS of the Cesium Beam Clock was given to the start input of the Time Interval Counter and 1PPS from Timing Receiver was given to the stop input. For each satellite pass two sets of data were recorded near the closest approach. The corresponding time interval between 1PPS of cesium beam clock and 1PPS of Timing Receiver were noted down.

Just before starting the experiment the Timing Receiver clock was set to the nearest second of UTC. With the help of a satellite alert programme the rise time, the time of closest approach and time of setting for all the 5 satellites were predicted.

## RESULTS.

- (i) For studying the internal consistency of NNSS, the receiver was operated from 21st to 27th January 1981. Satellite passes occurred during office hours were used for time transfer purpose. Low elevation passes (elevation less than  $30^{\circ}$ ) were rejected manually and the data points for which the time difference between 1PPS of Cesium Beam clock and 1PPS of NNSS timing receiver after applying propagation delay correction, was more than 100 microsecond were rejected. The RMS for rest of the data points was computed. The internal consistency of all the 5

propagation delay error contributed by ionosphere and troposphere at 400 MHz is less than a microsecond and is negligible. The major error is contributed by the receiver delay which varies with signal strength as shown in Fig. 4. The correction can be applied using the relation given by

$$d = \pm ms + D_0$$

where

- $d$  = Delay in microsecond
- $s$  = Signal strength
- $D_0$  = Receiver mean delay at a give signal strength
- $m$  = Slope of delay curve

#### APPLICATIONS.

Time is one of the basic standards in science and its measurement related with the happening of an event (epoch) in the infinite flow of time is one of the most important problems of users. For all the experiments where time accuracy (epoch) requirement is of the order of 100 microsecond or better the TRANSIT system provides a unique facility. Tracking of satellites using Laser Ranging is one of the fields where this finds application. The optical satellite tracking stations (at least in India) are located at remote places and it is just not possible to take flying clocks due to the obvious limitations of transportation, the TRANSIT technique is found to be quite handy.

While analysing the data an arbitrary error was made in the antenna position by as much as 10 km and it was found that such error in the position does not affect much the accuracy of time transfer. A table giving position error and



time error is given below. This technique also provides facility for experiments located at unsurveyed places.

Position error	RMS Time error
10 km in Latitude	$\pm 11$ microsecond
10 km in Longitude	$\pm 10$ microsecond
10 km in Radial	$\pm 7$ microsecond
1 km in Radial	$\pm 1$ microsecond

For a country like India which is not hooked up by TV network as is the case in Europe and U.S. it is not possible to transfer time using either TV active or passive technique, the TRANSIT system finds a lot of potentiality.

#### REFERENCES.

1. L.M. Laidet. "World wide synchronisation using Transit Satellite System". Proceedings of IEEE P. 630, Vol.60, May 1972.
2. G.A. Hunt, R.E. Cashion "A Transit Satellite Timing Receiver". Proceedings of the 9th Annual Precise Time and Time Interval (PTTI) Applications and Planning meeting, December 1977.
3. T. Hara and K.H. Sato "Time Synchronisation Via the Transit Satellite At Mizusawa". Proceeding of the 10th Annual Precise Time and Time Interval (PTTI) Applications and Planning meeting, November 1978.
4. Theodore. D. Finsod. "Transit Satellite System Timing Capabilities" Proceedings of 10th Annual Precise Time and Time Interval (PTTI) Applications and Planning Meeting, November 1978.

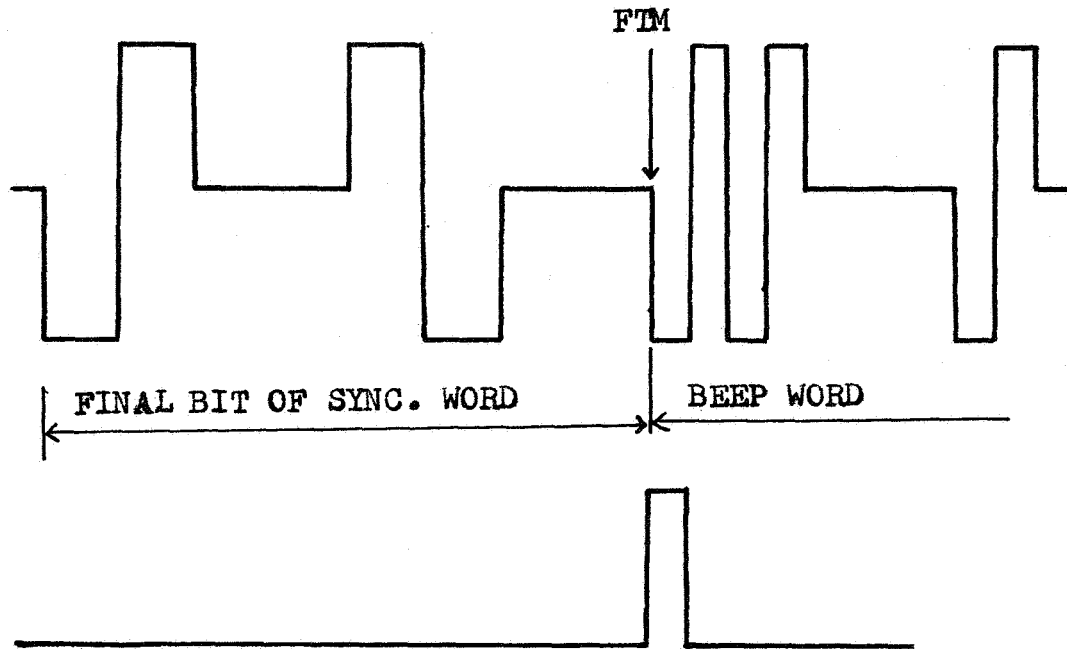


FIG. 1 - FTM DERIVATION

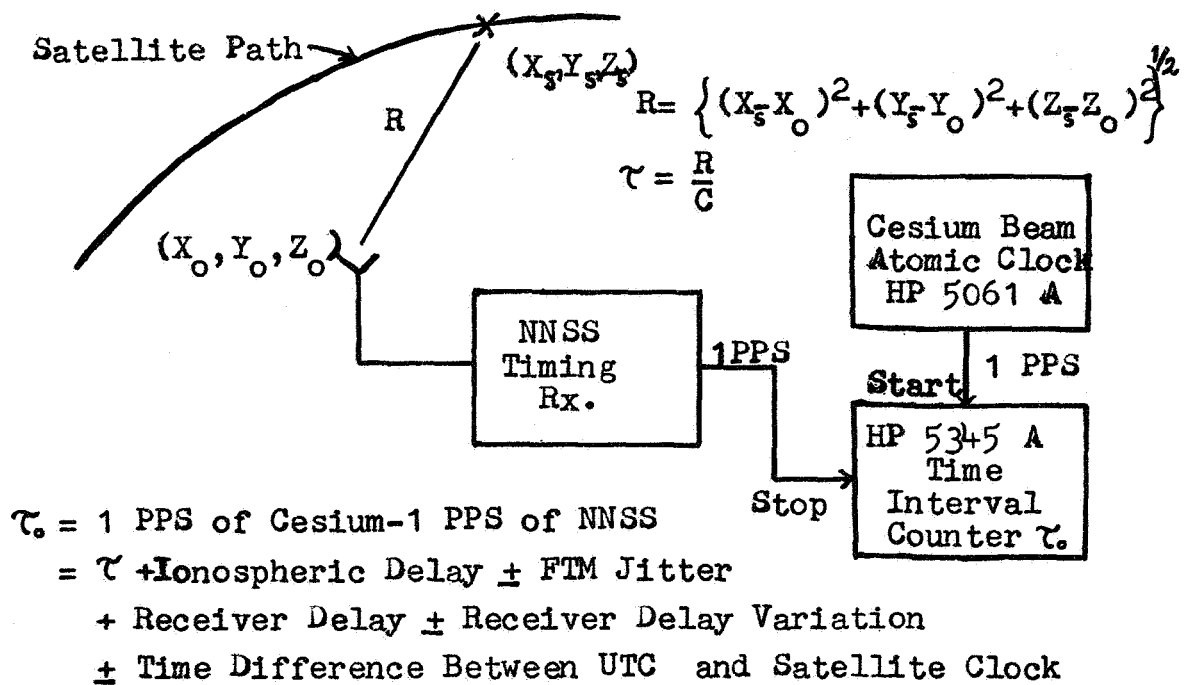


FIG. 2 - EXPERIMENTAL SET UP

5. R.E. Beehler, D.D. Davis, J.V. Cateora, A.J. Clements, J.A. Barner and E. Méndezquónones. "Time Recovery Measurements using Operational GOES and Transit Satellites" Proceedings of 11th Annual Precise Time and Time Interval (PTTI) Applications and Planning meeting, November 1979.

#### **ACKNOWLEDGEMENT.**

The authors would like to thank Director, SAC and Chairmen of Remote Sensing Area, Communication Area and Technical Service Group for taking keen interest in the Timing Activities and in the development of NNSS Timing Receiver. The authors are also grateful to the Heads of Digital Communication Division and Electronics Service Division of SAC for providing necessary support needed to fabricate this receiver. The authors appreciate and acknowledge the help rendered by Head, TESC of SAC and Dr. B.S. Mathur, Assistant Director, Time & Frequency Group of NPL, New Delhi, for providing Cesium Beam Atomic Clock and other facilities for testing the receiver.

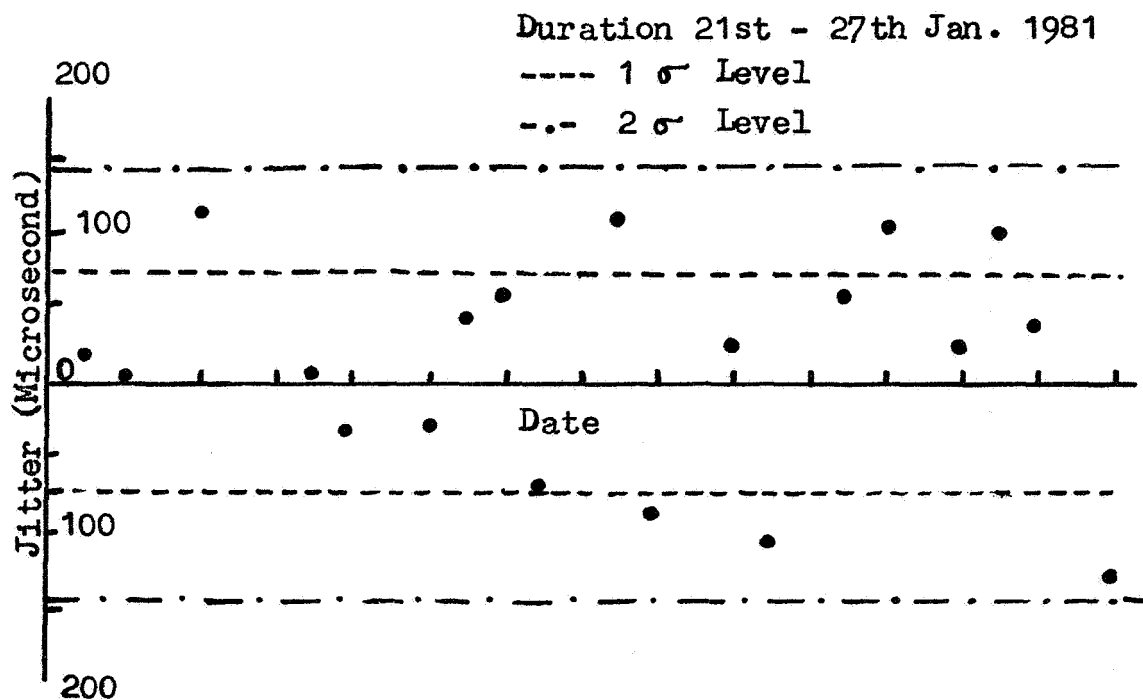


FIG. 3A - INTERNAL CONSISTENCY OF NNSS

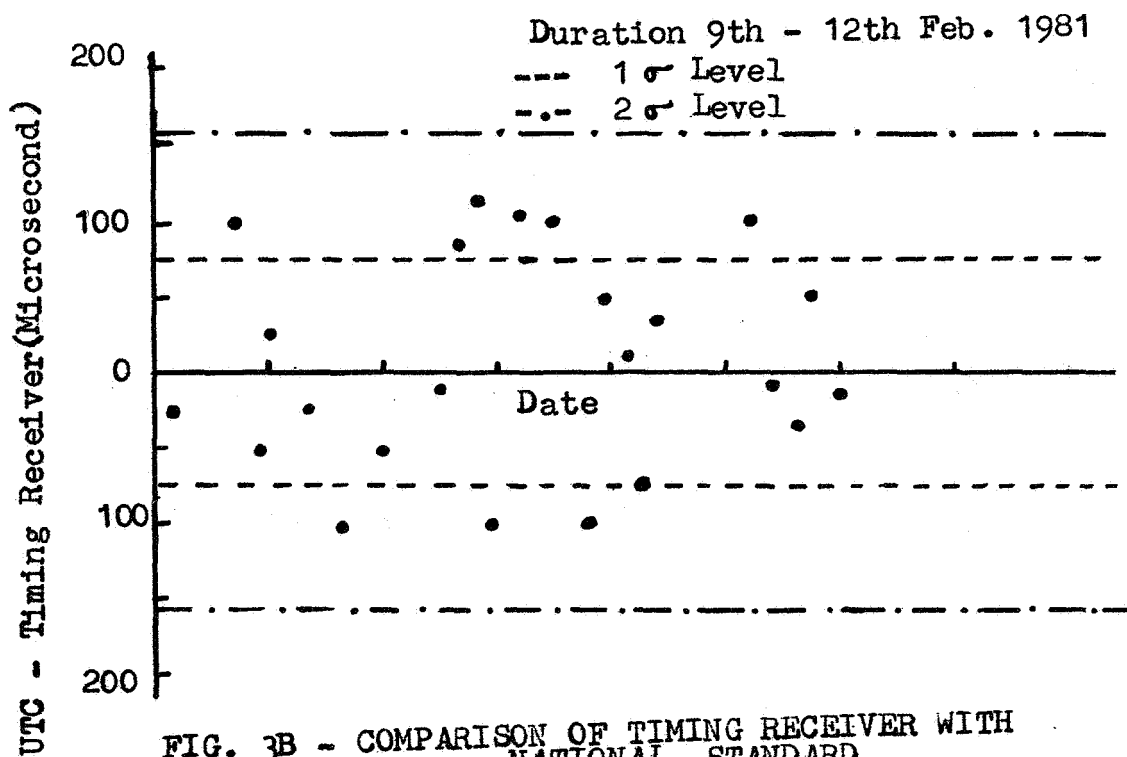


FIG. 3B - COMPARISON OF TIMING RECEIVER WITH  
NATIONAL STANDARD

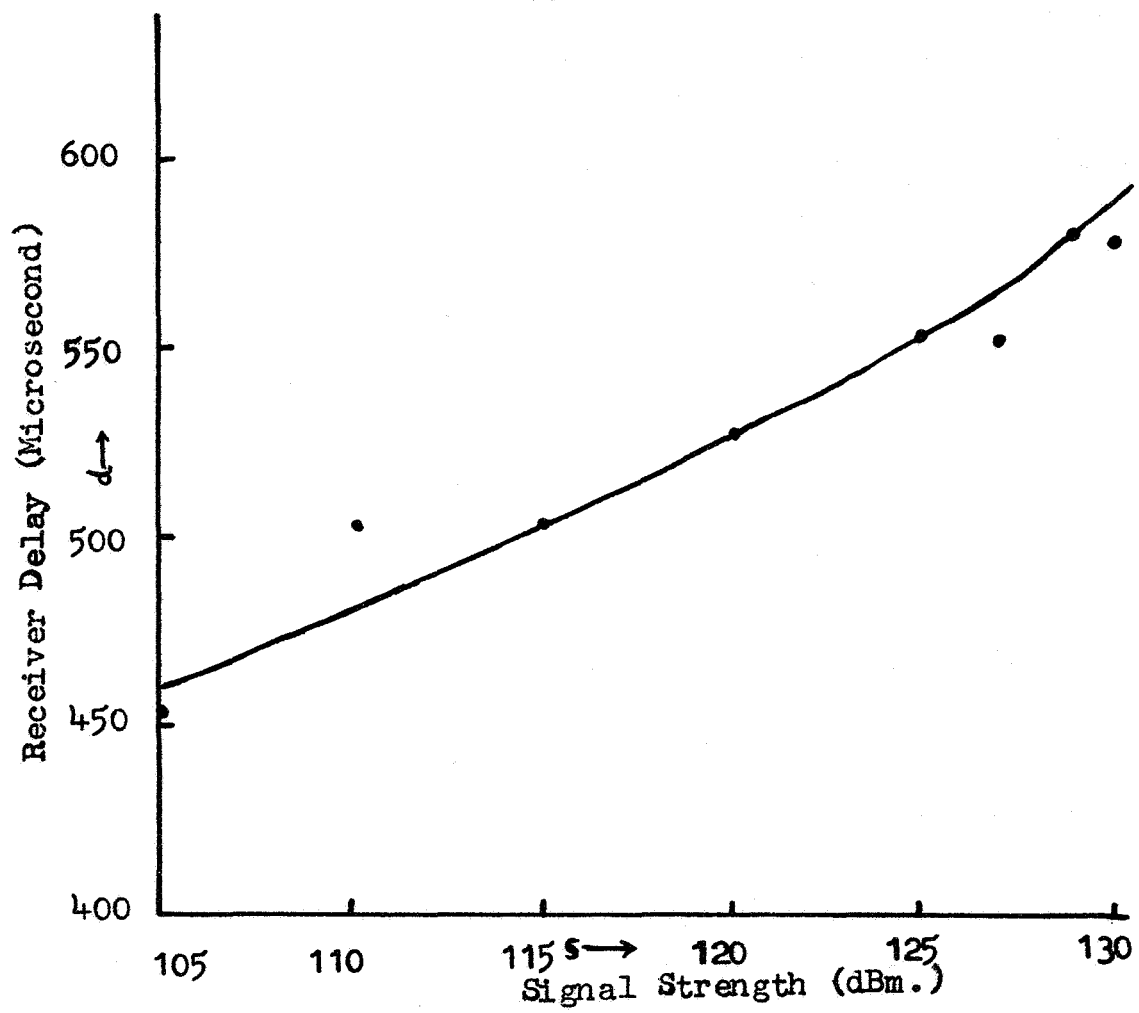


FIG. 4 - SIGNAL STRENGTH V/S RECEIVER DELAY

## No Warmup Crystal Oscillator

David H. Phillips, Naval Research Laboratory, Washington, D.C.

### ABSTRACT

During warmup, crystal oscillators often show a frequency offset as large as 1 part in  $10^5$ . If timing information is transferred to the oscillator and then the oscillator is allowed to warmup, a timing error greater than 1 millisecond will occur. For many applications, it is unsuitable to wait for the oscillator to warmup.

For medium accuracy timing requirements where overall accuracies in the order of 1 millisecond are required, a no warmup crystal concept has been developed. The concept utilizes two crystal oscillators, which are used sequentially to avoid using a crystal oscillator for timing during the trauma of warmup.

One oscillator may be a TCXO which preserves timing information during the warmup of the second crystal oscillator, which has a much higher frequency accuracy once warmed up.

This paper will show the accuracy achieved with practical TCXOs at initial start over a range of temperatures. A second design utilizing two oven controlled oscillators will also be discussed.

### TYPICAL WARMUP FOR AT CUT CRYSTAL

Figure 1 shows the warmup curve for a typical AT cut crystal oscillator with oven control. This particular warmup was done from room temperature ( $23^{\circ}\text{C}$ ) to crystal oscillator oven control temperature of  $85^{\circ}\text{C}$ . If one observes the point at which the curve crosses zero (nominal frequency) this oscillator has already gained approximately 11 milliseconds. During the next 5 minutes the oscillator loses approximately 60 microseconds. The negative overshoot due to stress is far too small to compensate for the large positive time error accumulation during oven warmup. If one cannot wait 20 minutes for the crystal oscillator to warmup and it is necessary to have less than 1 millisecond time error, another approach is required.

### TCXO TURNON

Figure 2 shows the phase difference between a TCXO (temperature compensated crystal oscillator) and a cesium beam standard from turnon of the TCXO to the end of the first minute. This shows a very regular beat frequency and is virtually the same as the nominal accuracy (2 parts in  $10^7$ ) of the TCXO. There is very little trauma occurring with turnon of a TCXO.

## TIME ERROR OF CRYSTAL OSCILLATOR AND TCXO COMBINED

Figure 3 shows the theoretical time error accumulated if a clock is started with a TCXO oscillator at time  $T_0$  and switched to an oven controlled crystal oscillator at time  $T_1$ .  $T_2$  is the time at which the time error accumulated is determined,  $f_0$  is the nominal frequency of 1 MHz,  $f_1$  is the TCXO's frequency,  $f_2$  is the oven controlled oscillator's frequency and  $\Delta T$  is the accumulated time error.

In practice precision frequency sources are not readily available to determine when the oven controlled crystal oscillator goes through zero (nominal frequency). One source of information available for switching is the oven cutback of the oven controlled crystal oscillator. An experiment was performed at Naval Research Laboratory (NRL) using a TCXO with switching circuitry which allowed the TCXO to drive the clock when no other standard frequency was available.

## EQUIPMENT

Figure 4 shows a printed circuit card with a commercial TCXO and the switching circuitry required to switch quickly enough to avoid losing more than one microsecond during switching.

Figure 5 shows the modular construction of an AN/URQ-23 developed by NRL and containing a double proportional oven controlled crystal oscillator with a 5 MHz, fifth overtone AT cut crystal.

Figure 6 shows six SG 1157/U clocks with each containing the TCXO card shown in Figure 4. To the left of the clocks is the AN/URQ-23 shown in Figure 5. All of the equipment is in a temperature chamber.

## EXPERIMENT

Seven experimental data runs were conducted at seven different temperatures ranging from  $-18^{\circ}\text{C}$  to  $55^{\circ}\text{C}$ . In between data runs, the equipment was allowed to equalize at the new temperature before power on. Prior to the first data run all clock oscillators were set to nominal frequency. Synchronization of the clocks with NRL's master clock occurred within 10 seconds of power on for each run. In these experimental runs,  $T_1$  (switching time) was chosen as the time when cutback of the inner oven of the AN/URQ-23 occurred.

Figure 7 shows the data of the first run at  $-18^{\circ}\text{C}$ . This temperature was below the spec limit for the TCXOs and so the data for the two clocks shown yield a larger than normal time error accumulated, but which is still less than 1 millisecond. The vertical line at 40 minutes shows the switching time  $T_1$  (oven cutback of AN/URQ-23).

Figure 8 shows the data of the second run at  $-8^{\circ}\text{C}$ . The data for clocks 1, 2, 3 and 5 are shown here and each yield an accumulated time error of less than 0.25 milliseconds. The vertical line at 25 minutes shows the switching time  $T_1$ .

Figure 9 shows the data of the third run at  $7^{\circ}\text{C}$ . Switching time  $T_1$  is shown by the vertical line at 18 minutes. The accumulated time error for each clock is less than 0.25 millisecond. Clock #3 shows a negative time accumulation and a change in slope is noted when the switch over to the oven controlled oscillator occurs at time  $T_1$ . After switching, the positive slope of the oven controlled oscillator is observable in all the clocks and this slope becomes less as the stress on the crystal is relieved.

Figure 10 shows the data of the fourth run at  $23^{\circ}\text{C}$  (room temperature). Switching time  $T_1$  is shown by the vertical line at 20 minutes. This plot shows data for two hours after power on. The oven controlled oscillator by itself over its entire warmup curve yielded an accumulated time error of -10 milliseconds while the ensemble of TCXOs and oven controlled crystal oscillator each yielded an accumulated time error of 0.1 millisecond or better.

Figure 11 shows the data of the fifth run at  $27^{\circ}\text{C}$ . Switching time  $T_1$  is shown by the vertical line at 22 minutes. This plot shows the data for two hours after power on and the accumulated time error is less than 0.25 millisecond for each clock.

Figure 12 shows the data of the sixth run at  $43^{\circ}\text{C}$ . Switching time  $T_1$  is shown by the vertical line at 22 minutes. This plot shows the data for 30 minutes. Clocks 1, 3, and 5 each yielded an accumulated time error of less than 0.2 millisecond.

The seventh and final run of data at  $55^{\circ}\text{C}$  is shown in Figure 13. This shows the performance of the TCXOs at  $55^{\circ}\text{C}$  for 30 minutes. The switching time  $T_1$  would have occurred at 14 minutes. The oven controlled oscillator warms up much more quickly at this temperature and with less overshoot.

#### IMPROVEMENT WITH SC CUT CRYSTAL

When a crystal is warmed up very rapidly internal stresses are set up which cause a frequency perturbation. The use of a stress compensated crystal such as the SC cut improves the performance, but even with it there will be a minimum warmup time.

Figure 14 shows the SC cut crystal in fast warmup [1] showing less frequency dependence on temperature than the AT cut and no stress



related overshoot. The warmup could be as short as 90 seconds. If a TCXO is used as an initial oscillator the optimum warmup time may in practice be several minutes to achieve the minimum accumulated time error.

#### ALTERNATIVE TECHNIQUE

An alternative technique using two oven controlled crystal oscillators is shown in Figure 15. The oscillators shown have a self tuning capability so that an external frequency may be utilized to assure accurate initial frequency. In step 1 when oscillator A is holding, it maintains the external frequency while oscillator B is warming up.

It requires only a second for the serial time code to be shifted into the shift register and shifted into the counter driven by oscillator A. The counter of oscillator B is continually updated until oscillator B is warmed up. Oscillator B now becomes the master and in step 2 it holds the time while oscillator A warms up. In step 3, when oscillator A has warmed up, it also becomes a master and two independent clocks are now available for intercomparison.

#### CONCLUSIONS

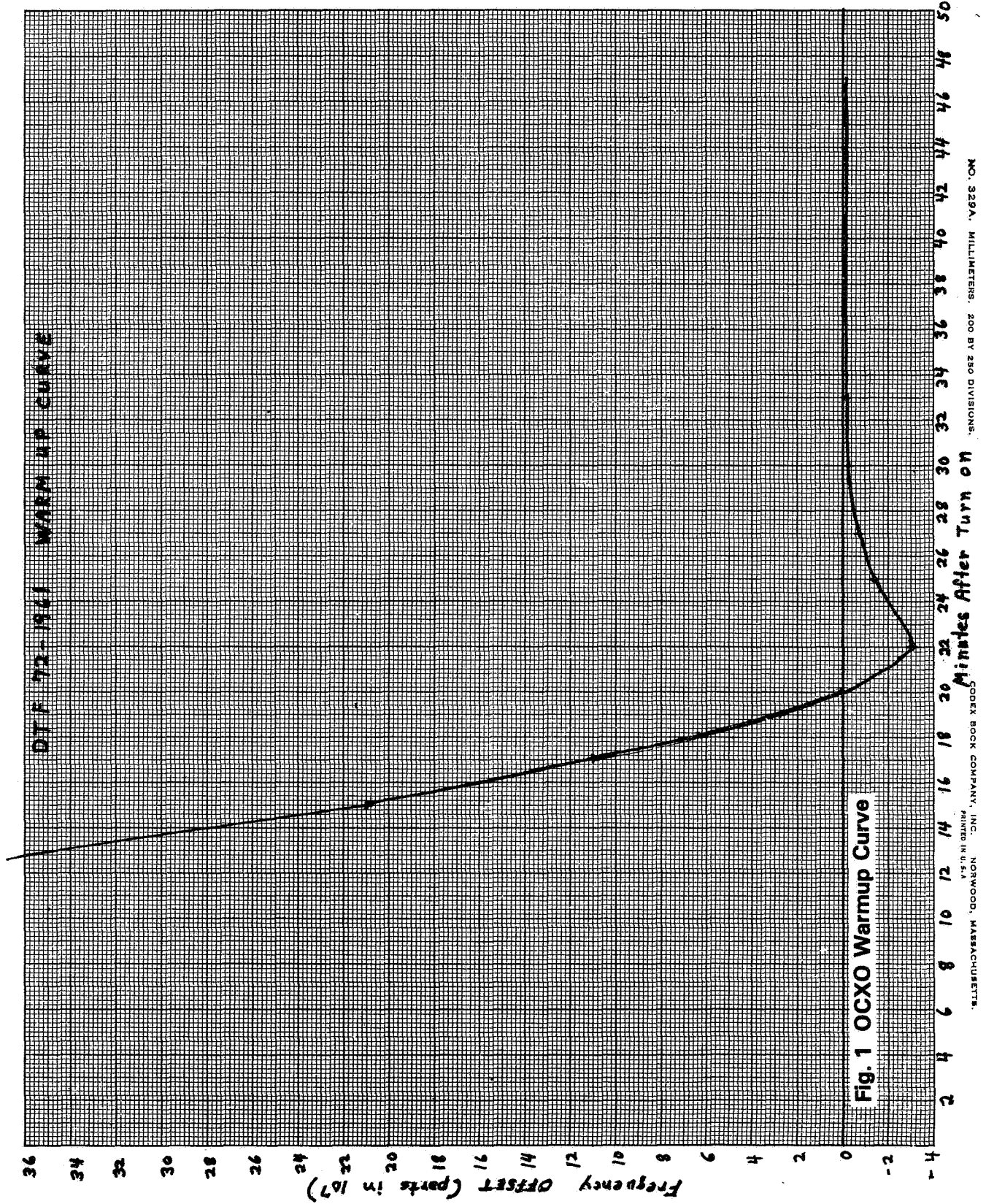
The experimental results show that the no warmup concept has an order of magnitude increase in timing accuracy for situations requiring instant turnon and deployment. If timing requirements are more stringent than the simple model tested, then the alternative suggestions should be utilized.

#### ACKNOWLEDGEMENTS

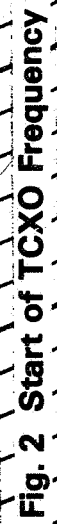
The author would like to acknowledge the contributions of Joseph J. O'Neill and Ruth E. Phillips.

#### REFERENCES

- [1] Robert Burgoon and Robert L. Wilsen, Proc. 33rd Annual Symposium on Frequency Control, 1979, "Performance Results of an Oscillator Using the SC Cut Crystal" p 408



↑  
1 MIN  
↓



$$\Delta T = \int_{T_0}^{T_1} \frac{\Delta f_1}{f_0} dt + \int_{T_1}^{T_2} \frac{\Delta f_2}{f_0} dt$$

$T_1$  = SWITCH IN TIME (OVEN CUTBACK TIME)

$T_0$  = STARTING TIME

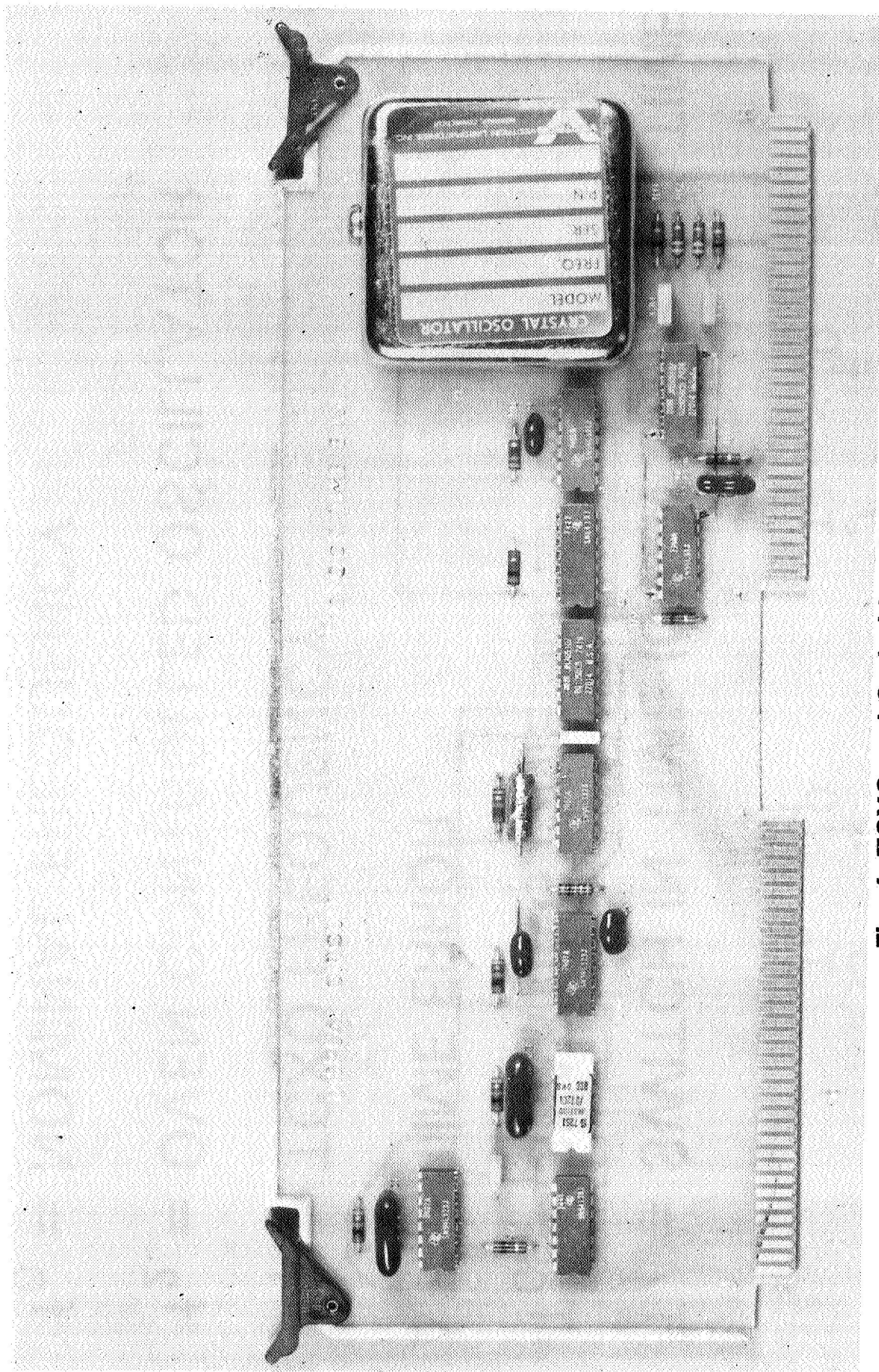
$\Delta T$  = TIME ERROR

$f_1$  = TCXO FREQUENCY

$f_2$  = OVEN CONTROLLED OSCILLATOR

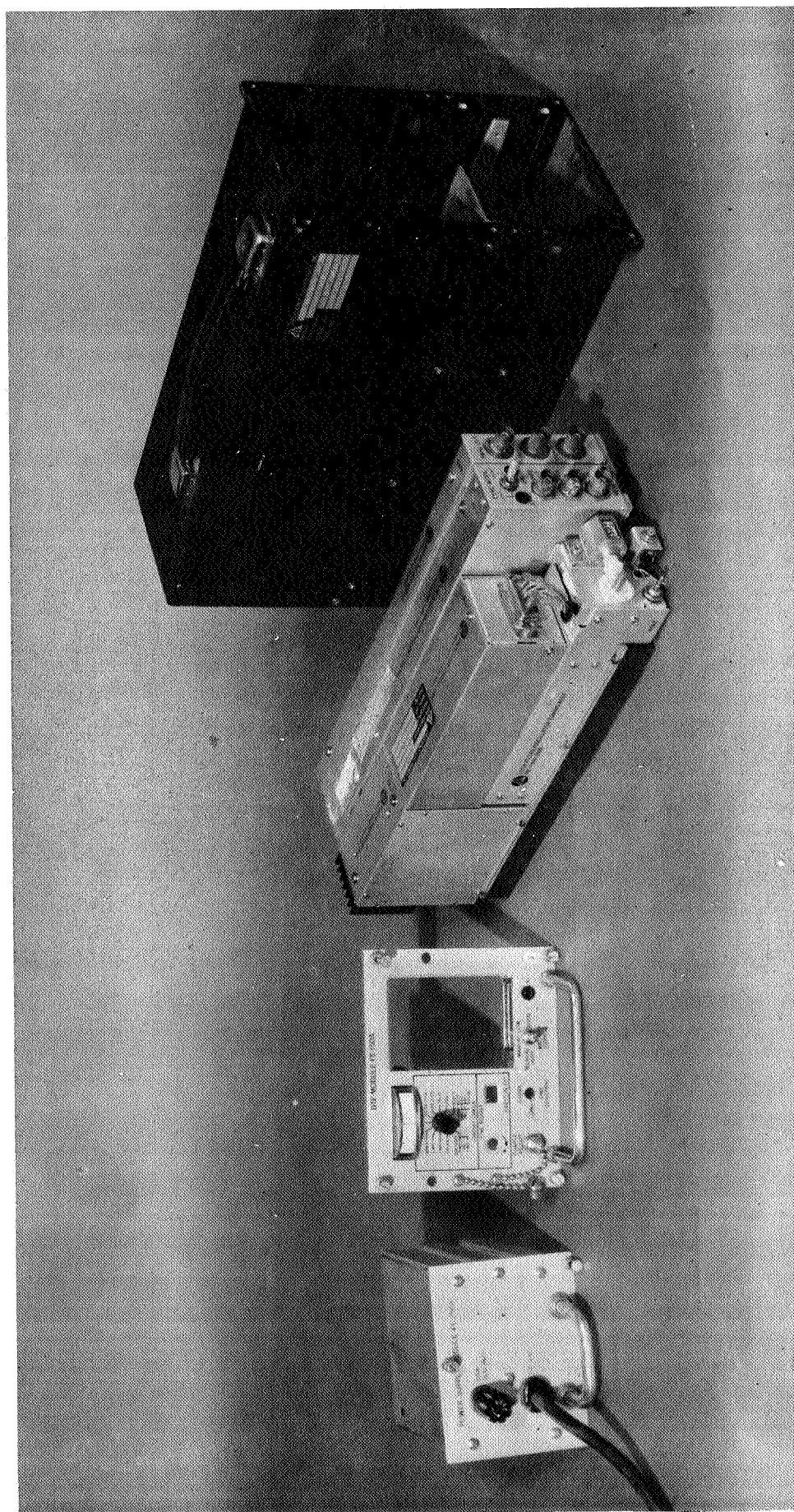
$f_0$  = NOMINAL FREQUENCY

Fig. 3 Equation of No Warmup



**Fig. 4 TCXO and Switching Circuit**





**Fig. 5 Modular AN/URO-23 Showing OCXO**

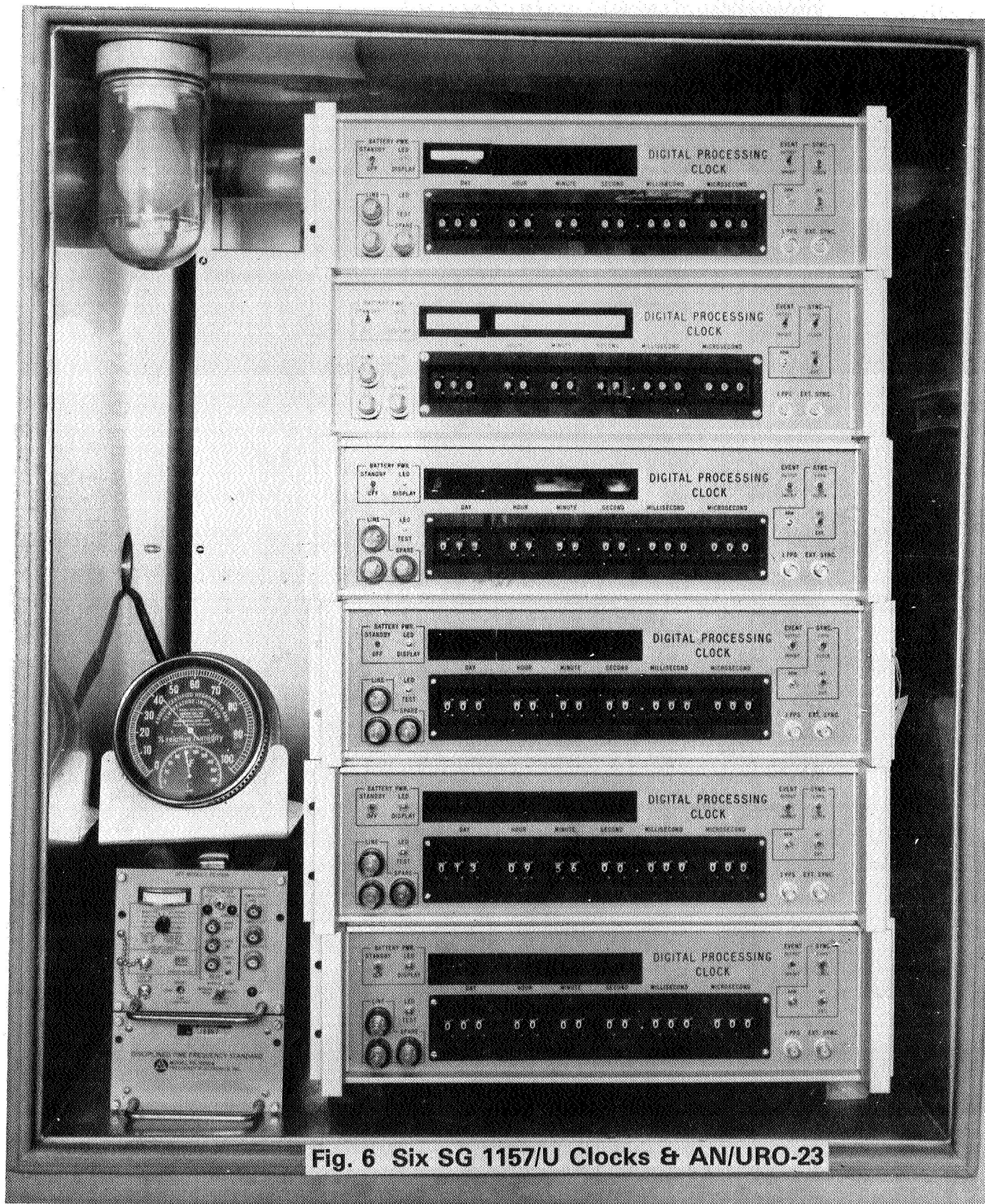


Fig. 6 Six SG 1157/U Clocks & AN/URO-23

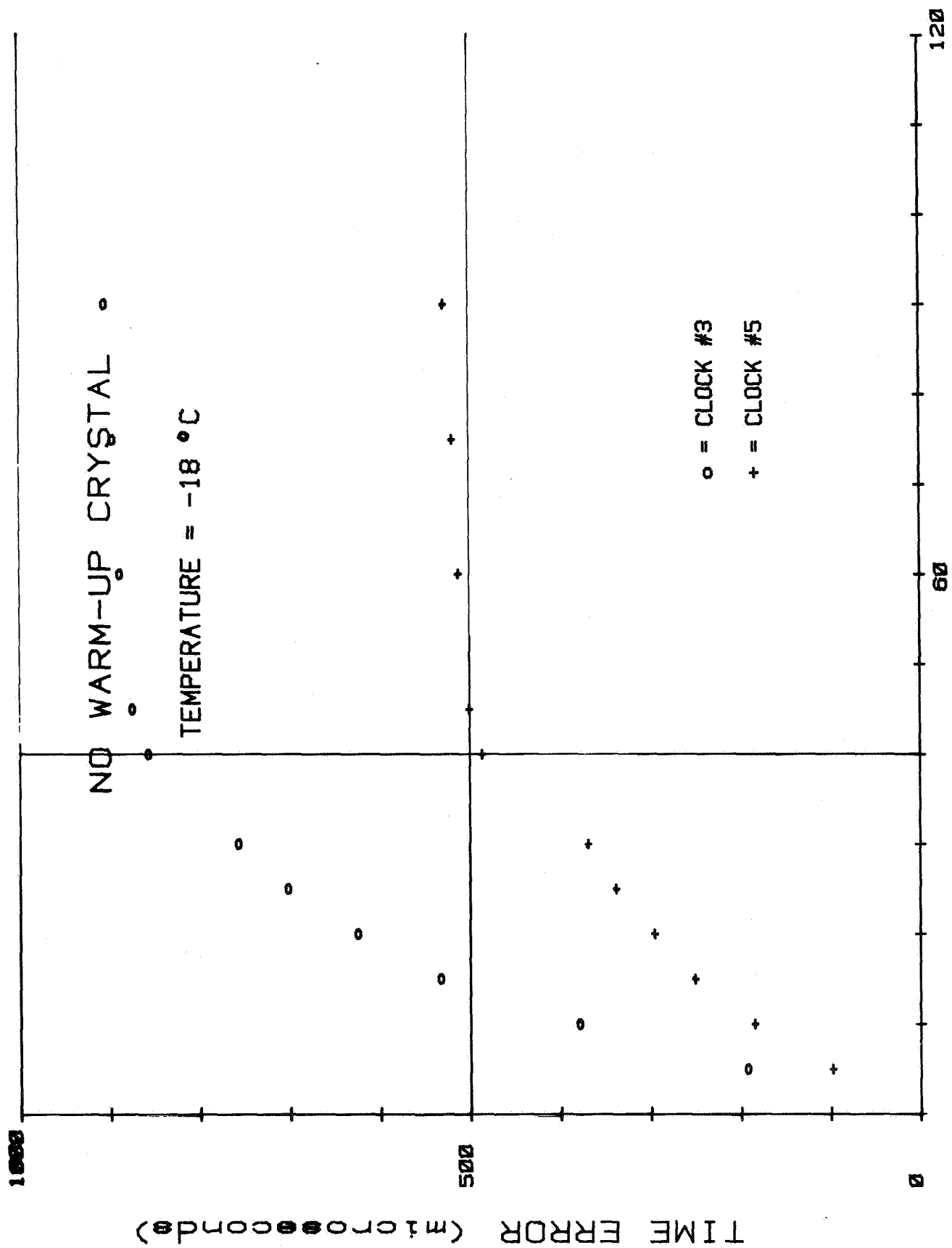


Fig. 7 Performance at -18°C TIME (minutes)



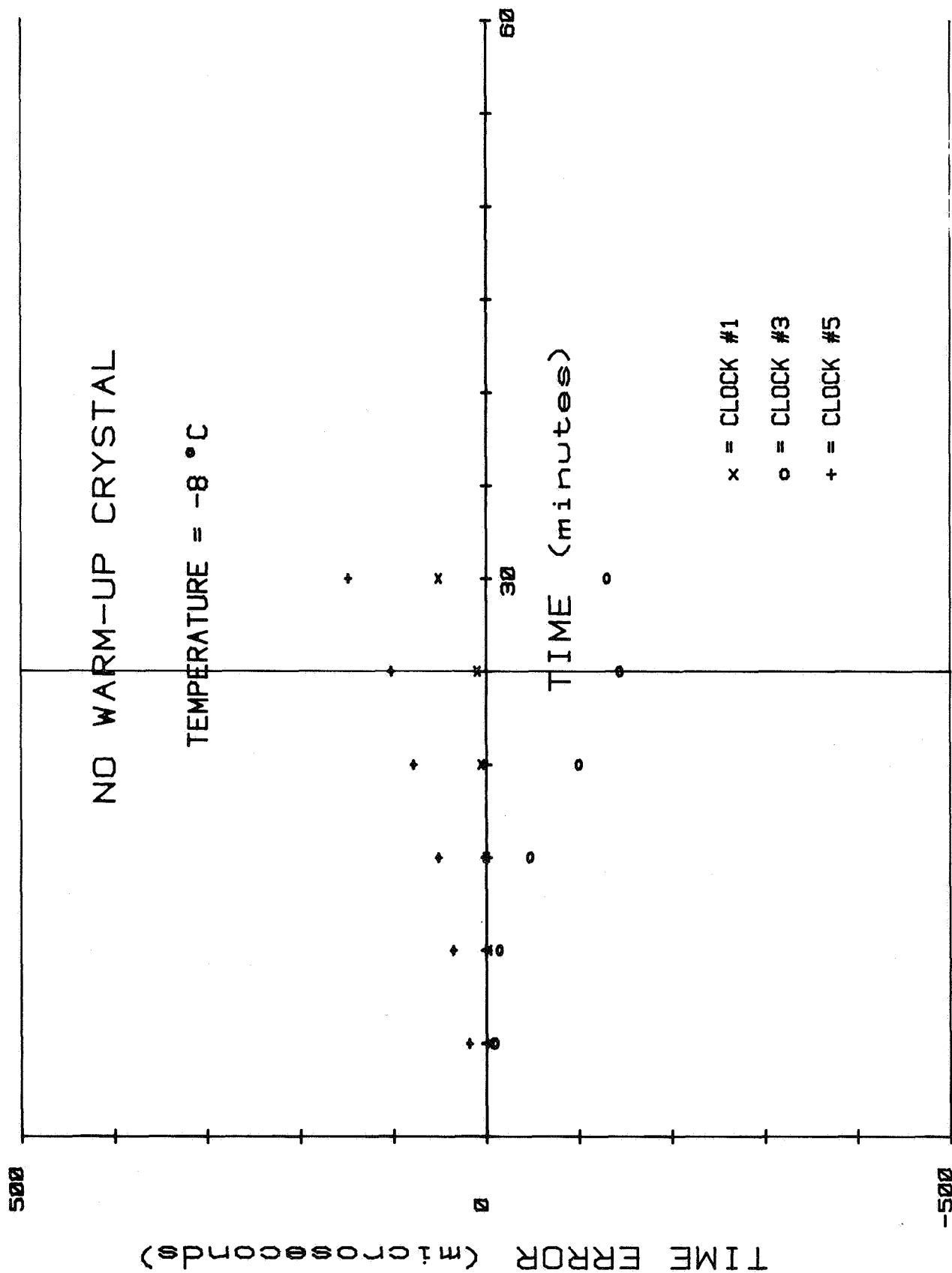


Fig. 8 Performance at  $-8^{\circ}\text{C}$

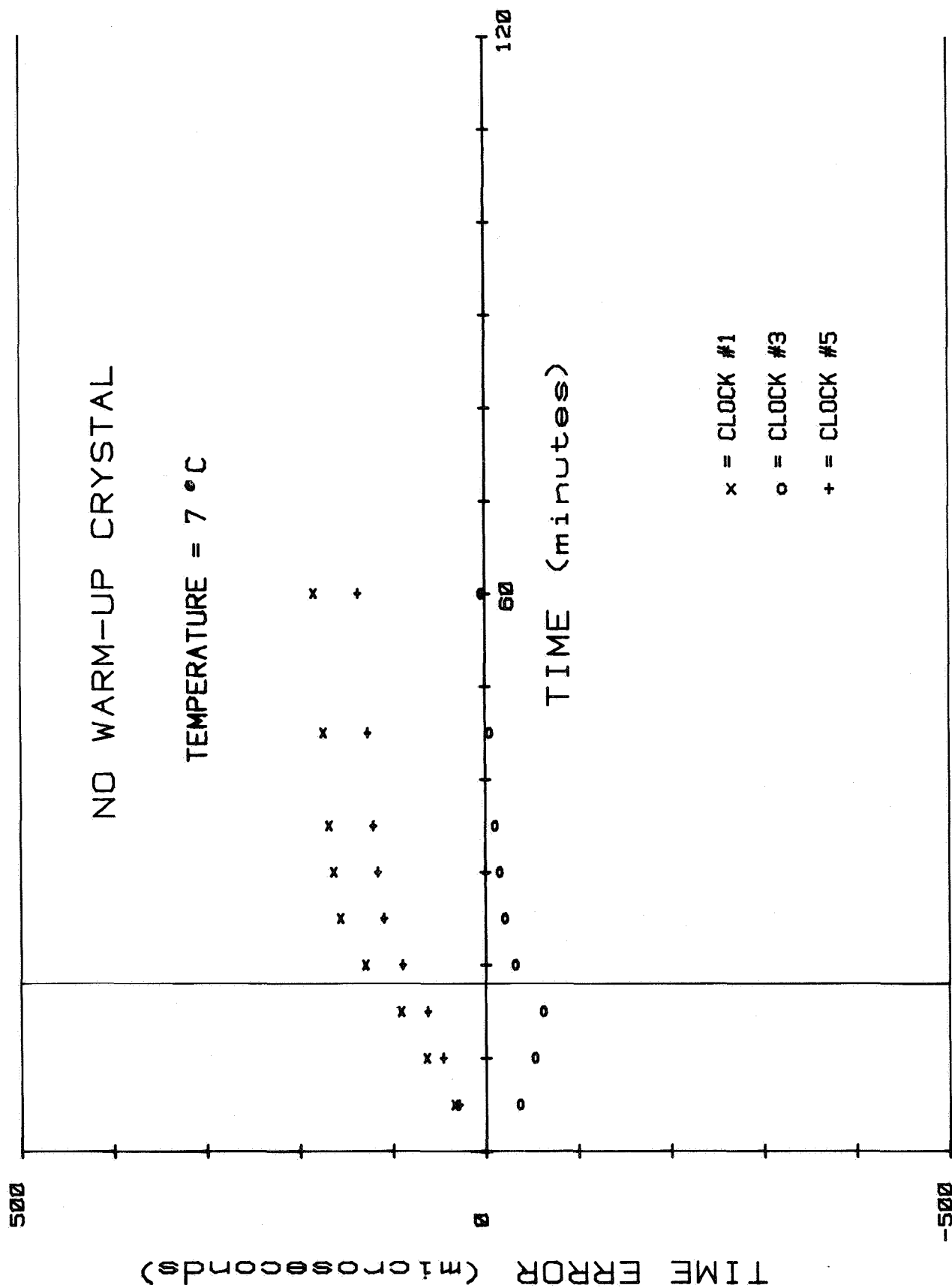


Fig. 9 Performance at 7°C

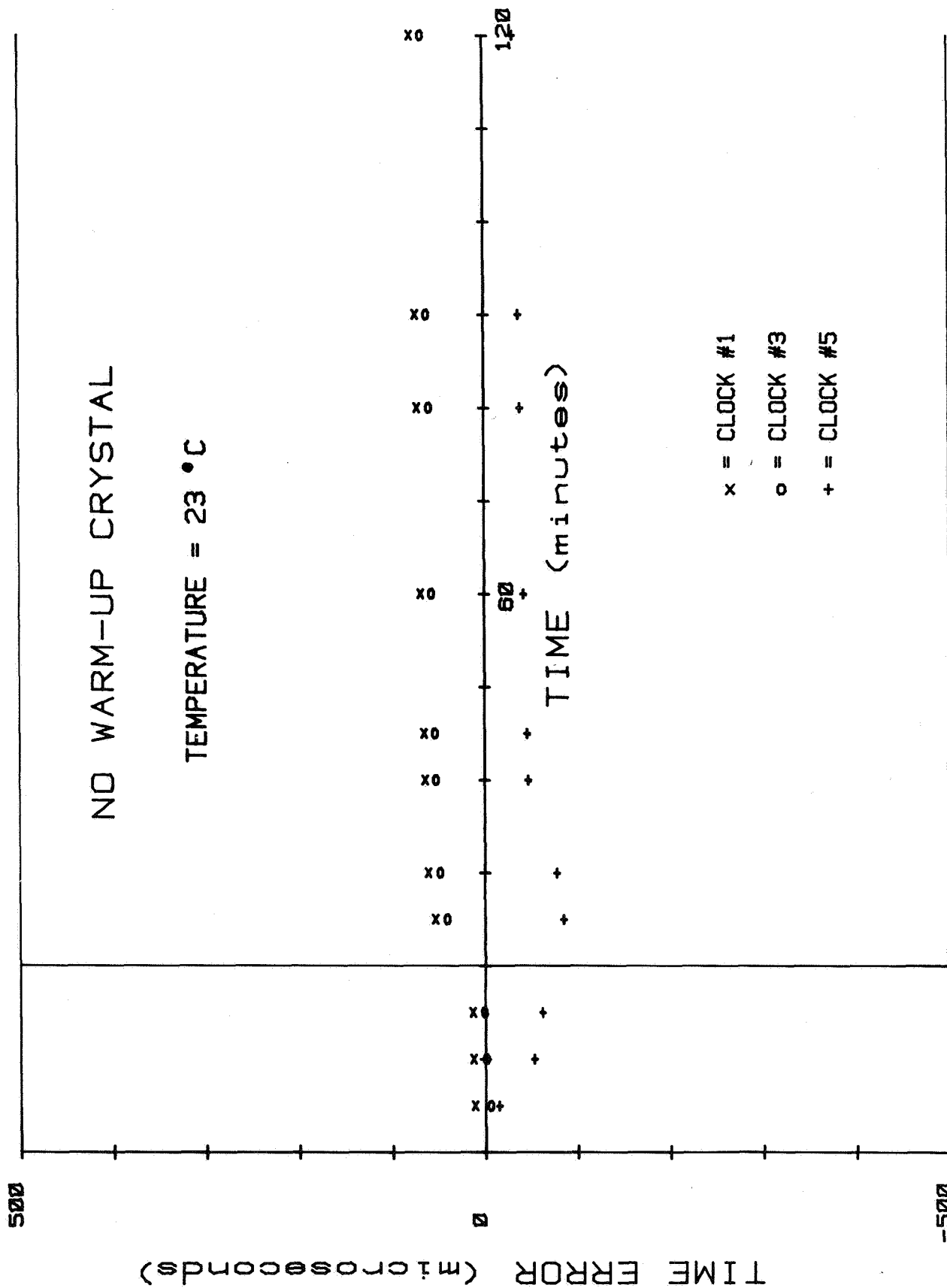


Fig. 10 Performance at 23°C

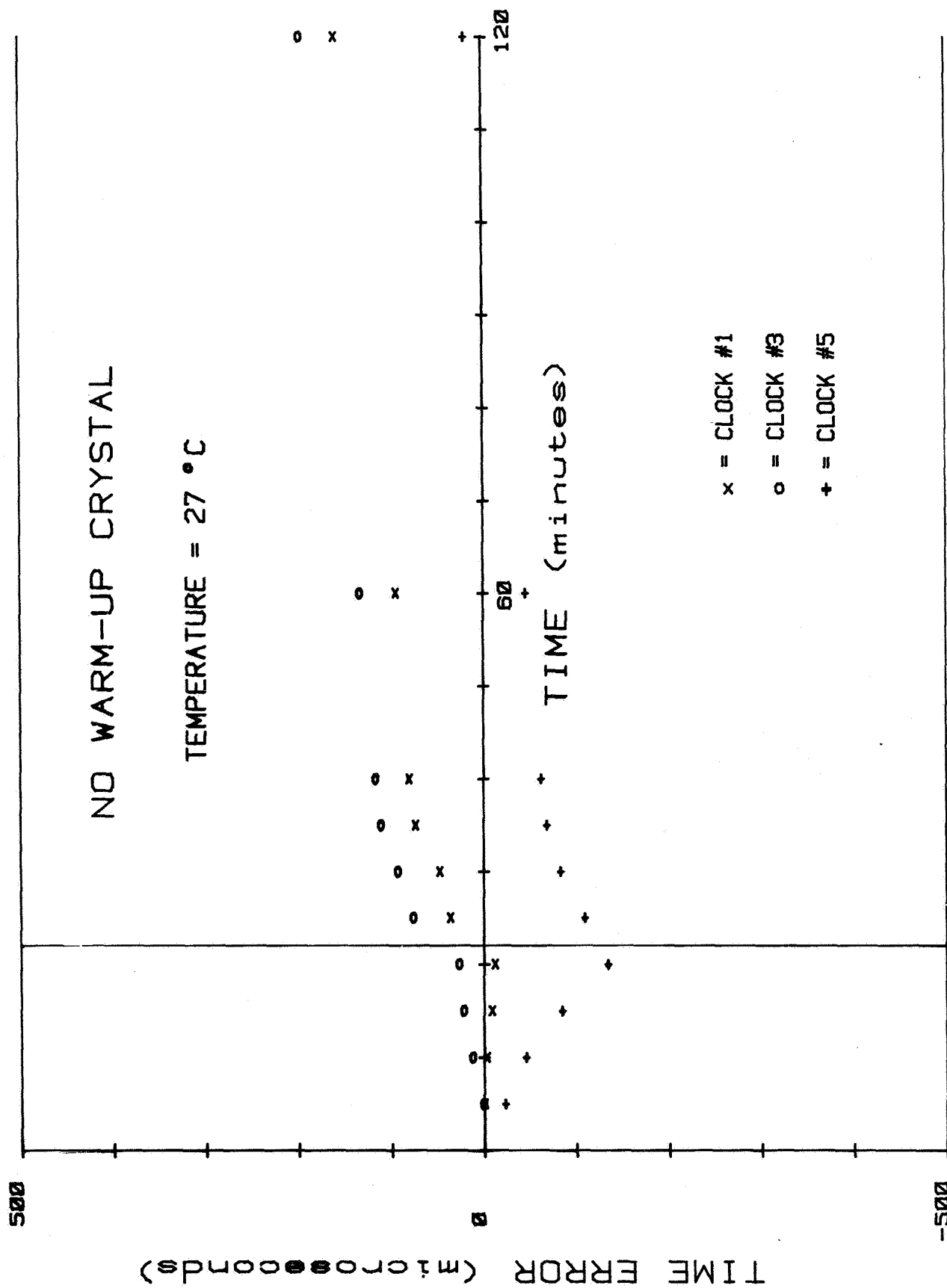


Fig. 11 Performance at 27°C

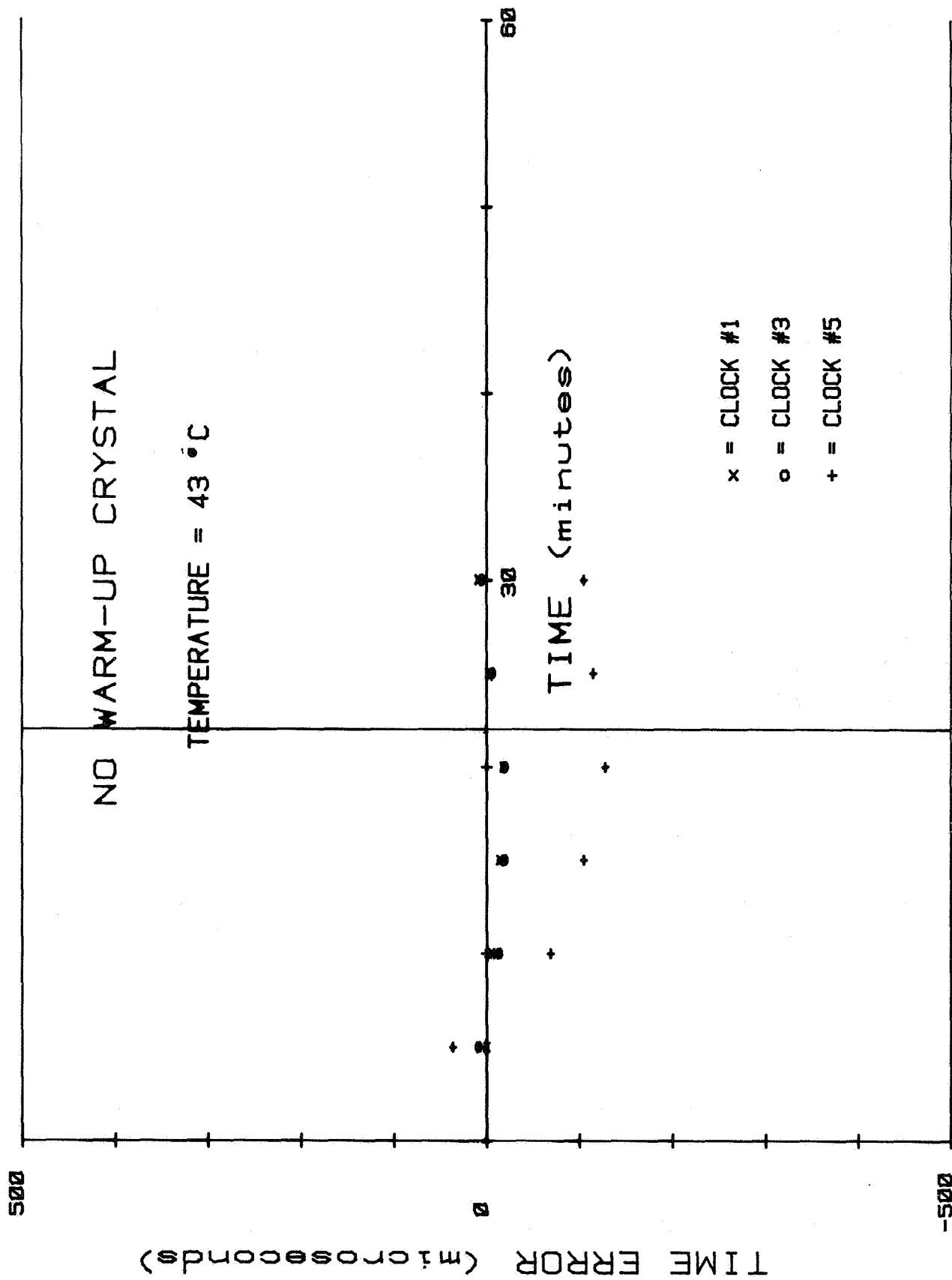


Fig. 12 Performance at 43°C

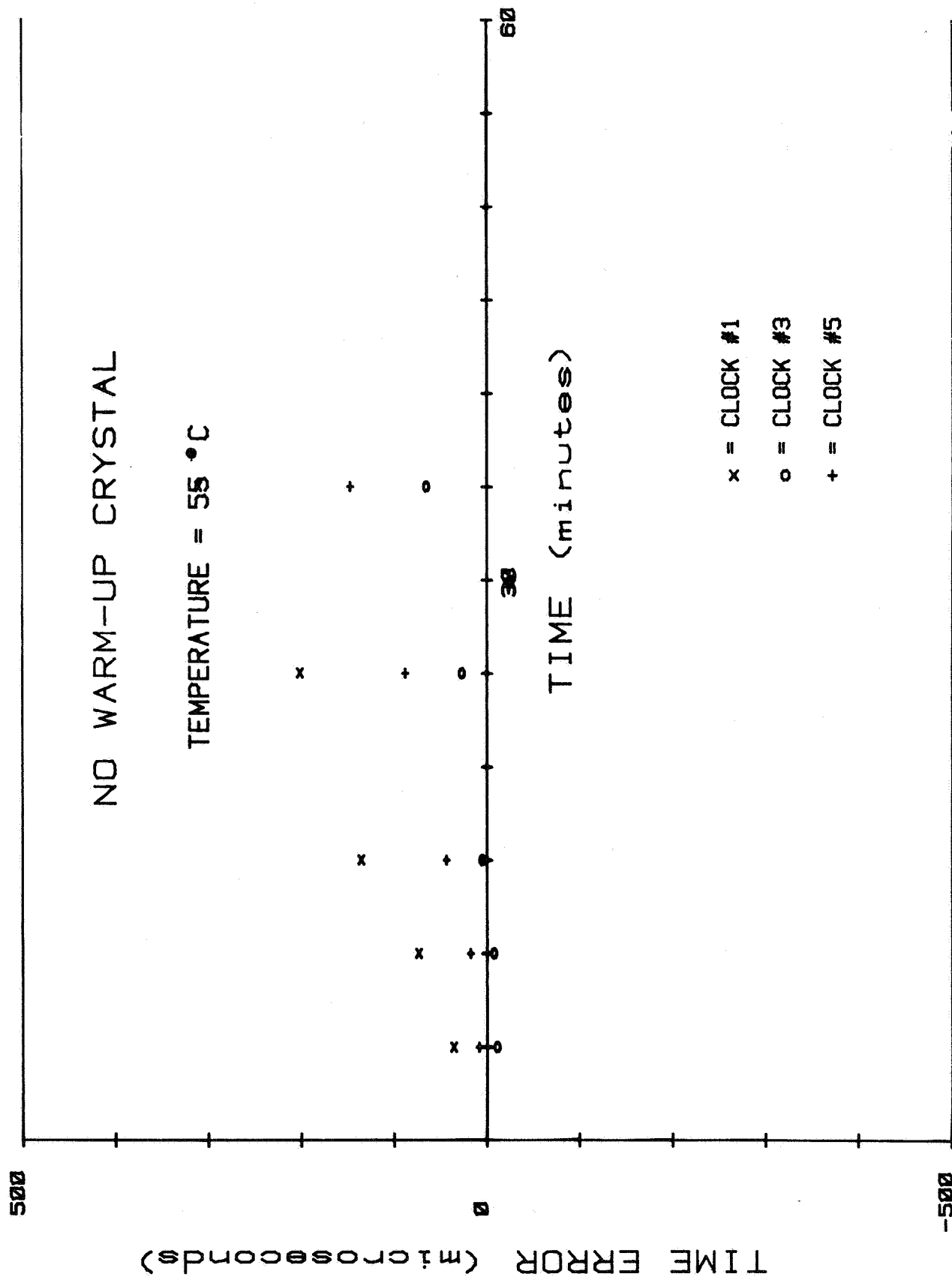


Fig. 13 Performance at 55°C

# PROCEEDINGS OF THE 33rd ANNUAL SYMPOSIUM ON FREQUENCY CONTROL 1979

PERFORMANCE RESULTS OF AN  
OSCILLATOR USING THE SC CUT CRYSTAL

Robert Burgoon and Robert L. Wilson  
Hewlett-Packard Company  
Santa Clara, Ca.

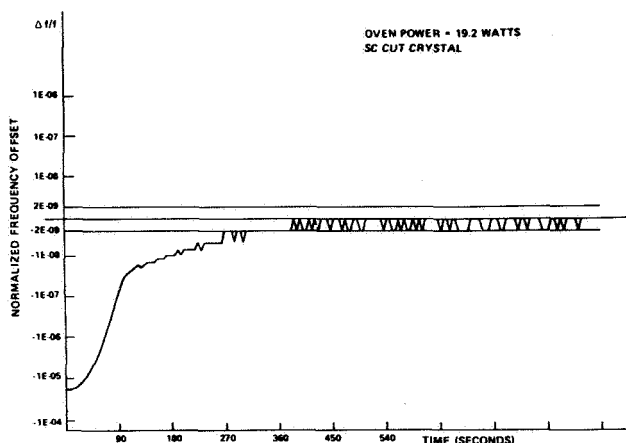


Figure 3. Oscillator Warmup for an HP 10544 Oscillator with an SC Cut Crystal

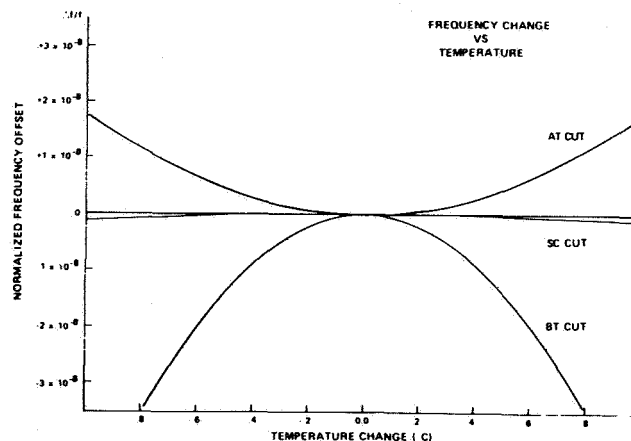
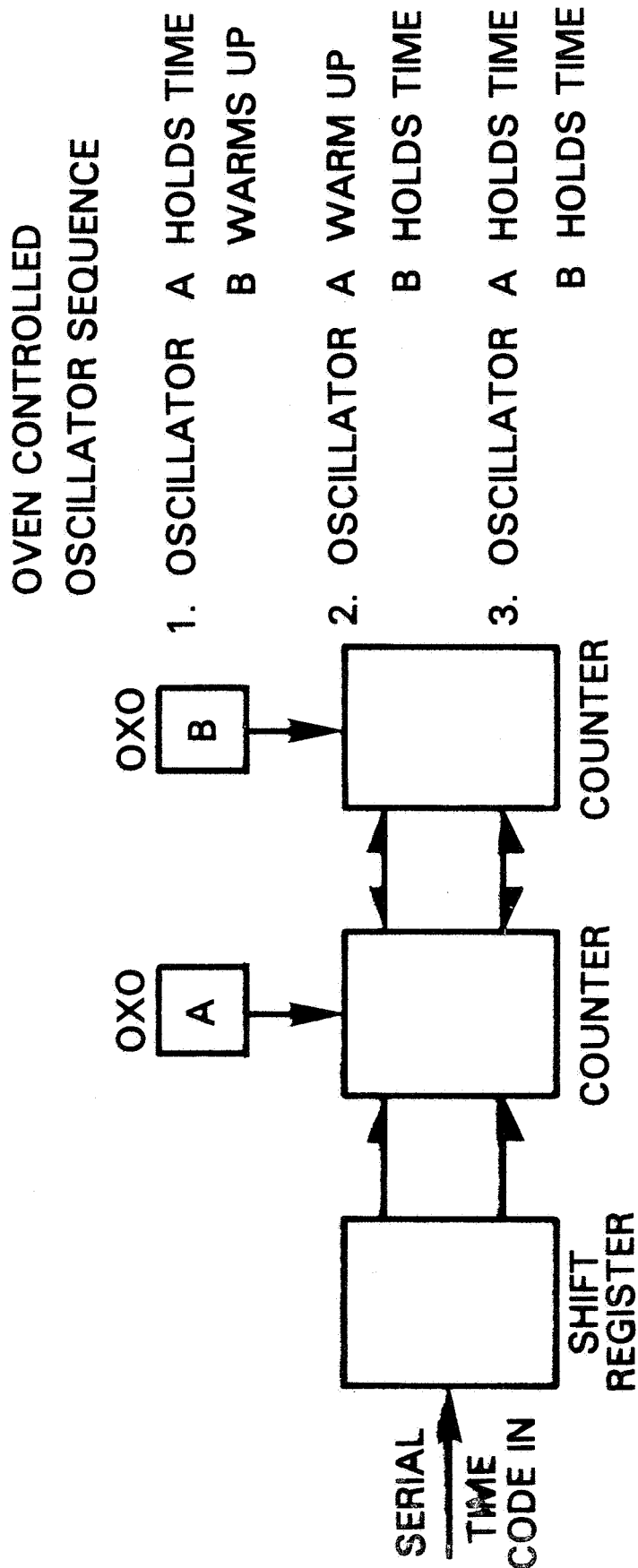


Figure 5. Crystal Temperature Performance Close to the Turnover Temperature

Fig. 14 SC Cut Performance

# NO WARM UP CRYSTAL OSCILLATOR



**Fig. 15 Two OCXO Design**





## CONCLUSION

MR. ANDY CHI, General Chairman

I am glad to see the persistence of the audiences here. They stay until the last minute.

And, of course, the success of the meeting, to a large extent, was due to the members of the Executive Committee, who made the advance planning, and, also, the hard work of the Chairman of the Technical Program Committee. Dick Sydnor, and his members of the Technical Program Committee, who also served as the session Chairmen.

You can see that they were very enthused. And they led very interesting sessions.

I hope that you are inspired, you have been enriched by this meeting.

For those who did not go to the banquet, I would like to tell you that we have, this year, 200 registrants. There are 18 from foreign countries. Attendees from nine countries in the meeting this year.

As you also see that the number of sponsorship keeps on growing. It reminds me almost like some authors after the Second World War. Usually you have one or two, and the authorship keeps on increasing to the extent it is longer than the abstract.

I hope that we are benefited by the number of authors, but only to the extent that it would be shorter than the program.

Of course, this large number of sponsorship, you will see is an indication of our support, but also the interest expressed by different agencies, who want to participate in the planning and in the application of the meeting.

We hope that we will be able to maintain that direction, and maintain the interest of the attendees, and give the proper mixture of the program, such that people will feel, under the present constraint of budget reductions, that you still feel, these three days you came, it's quite worthwhile for your trip and your time.

I would like to express my appreciation for the support of all the members of the Executive Committee, in particular, Clark Wardrip, and Jim Murray and Al Bartholomew, who actually did much of the work behind the scenes.

And I'm also sorry to see that there are several papers which could not be presented because of lack of time. However, they will be printed in the Proceedings.

For this reason, I would like to urge all the authors to please turn in your manuscript to the Editor of the Proceedings, the Chairman of the Editorial Committee, Lauren Rueger. The sooner he has the manuscripts, the sooner we can publish the Proceedings.

And I want to also use this opportunity to thank our host, the Naval Research Laboratory. They have accommodated much of the security clearance for us. In a sense, made life easier for us to come in and go out. So when you leave, all you have to do is show the badge, or turn them in at the gate, so you will not have any delay.

The next meeting will be held at Goddard. This will be on November 30 to December 2nd, 1982. And I hope you will have the occasion, opportunity to come and we will be happy to see you next year.

In the meantime, I hope you all have a nice stay here, if you have come from a long distance to Washington, D.C.; or if you are going home, have a safe trip home.

And the meeting is now come to a conclusion.

13TH ANNUAL PRECISE TIME AND TIME INTERVAL REGISTRATION

David W. Allan  
NBS  
325 Broadway  
Boulder, CO 80303

Ralph T. Allen  
Naval Electronic Systems Command  
PME 110-2315  
Washington, DC 20360

Carroll O. Alley  
University of Maryland  
Dept. of Physics & Astronomy  
College Park, MD 20742

Mohan P. Ananda  
Aerospace Corporation  
2350 E. El Segundo Blvd.  
El Segundo, CA 90009

John D. Anderson  
JPL  
4800 Oak Grove Dr.  
Mail Stop 264/626  
Pasadena, CA 91109

John C. Arnold  
Bendix Field Engineering Corp.  
9250 Route 108  
Columbia, MD 21045

Rex A. Backus  
True Time Inst.  
3243 Santa Rosa Ave.  
Santa Rosa, CA 95401

Heinz W. Badura  
Efratom Cal. Inc.  
18851 Bardeen Ave.  
Irvine, CA 92715

Otto J. Baltzer  
TRACOR, Inc.  
6500 Tracor Lane  
Austin, TX 78721

James A. Barnes  
NBS  
Boulder, CO 80303

Andrew Barszczewski  
National Research Council Canada  
N.A.E. Bldg U-61  
Ottawa Ontario, Canada KIA OR6

Charles A. Bartholomew  
NRL  
Code 7960  
Washington, DC 20375

Alvin G. Bates  
Johns Hopkins Univ. APL  
Johns Hopkins Rd.  
Laurel, MD 20707

Ronald L. Beard  
NRL Code 7969  
4555 Overlook Dr.  
Washington, DC 20375

Roger E. Beehler  
National Bureau of Standards  
325 Broadway  
Boulder, CO 80303

Jose S. Benavente  
Instituto Y Observatorio de Marina  
(Spanish Naval Observatory)  
Avenida Del Observatorio S/N  
San Fernando (CADIZ) Spain

Walter J. Bergman  
Vitro Laboratories  
14000 Georgia Ave.  
Silver Spring, MD 20910

A. John Berlinsky  
University of British Columbia/MIT  
Dept. of Physics MIT Rm 13-2025  
Cambridge, MA 02139

Martin B. Bloch  
F.E.I.  
3 Delaware Dr.  
New Hyde Park, NY

Eric L. Blomberg  
KERNCO, Inc.  
28 Harbor Street  
Danvers, MA 01923

John R. Howell  
Austron, Inc.  
1915 Kramer Lane  
Austin, TX 78758

James R. Bowser  
Vitro Laboratories, Automation Ind.  
14000 Georgia Ave.  
Silver Spring, MD 20910

William M. Bridge  
MITRE Corp.  
P.O. Box 208, Mail Stop E-090  
Bedford, MA 01730

Ellis H. Bryant, Jr.  
Weatherchron Co.  
4881 Powers Ferry Rd.  
Atlanta, GA 30327

James A. Buisson  
NRL Code 7966  
4555 Overlook Dr.  
Washington, DC 20375

Lee E. Burpee  
Arbiter Systems Incorporated  
1402 Norman Firestone Road  
Goleta, CA 93117

Jose E. Calavia  
Bendix Field Engineering  
3204-E Normandy Woods Dr.  
Ellicott City, MD 21043

Robert W. Camp  
CINOX  
4914 Gray Rd.  
Cincinnati, OH 45232

James C. Camparo  
Aerospace Corp  
P.O. Box 92957  
Los Angeles, CA 90009

John T. Carr  
NSWC  
Dahlgren, VA 22448

Clifford F. Casey  
Computer Sciences Corporation  
6565 Arlington Blvd.  
Falls Church, VA 22046

Robert C. Caudill  
21st CRS Elmendorf AFB AK  
1402 Eagle River Rd.  
Eagle River, AK 99577

David N. Chalmers  
U.S. Naval Observatory Time Service  
34th & Massachusetts Ave.  
Washington, DC 20390

Fritz Chang  
EG&G  
35 Congress St.  
Salem, MA 01970

Randy N. Chesnutt  
United States Air Force  
6520 Test G/Enree Stop 235  
Edwards AFB, CA 93523

Andrew R. Chi  
NASA - GSFC, Code 850  
Greenbelt, MD 20771

Mary C. Chiu  
Johns Hopkins Univ/APL  
Johns Hopkins Rd.  
Laurel, MD 20707

Carl S. Christensen  
Jet Propulsion Lab.  
7010 Tyndale St.  
McLean, VA 22101

Edmund H. Christy  
Offshore Navigation Inc.  
P.O. Box 23504  
Harahan, LA 70123

Robert V. Clark  
Vitro Laboratories  
14000 Georgia Ave.  
Silver Spring, MD 20910

Randolph T. Clarke III  
Nav. Obs. Time Service  
Washington, DC 20390

David A. Clayton  
Offshore Navigation, Inc.  
5728 Jefferson Hwy.  
Harahan, LA 70183

Richard C. Coffin  
Jet Propulsion Lab.  
4800 Oak Grove Dr.  
Pasadena, CA 91103

Jimmie B. Collie  
NESEC Portsmouth  
6341 Rt. 29  
Columbia, MD 21046

Richard C. Collum  
ISOTEMP Research, Inc.  
916 Preston Avenue  
Charlottesville, VA 22901

Robin B. Conley  
USAF Space Division/YEE  
P.O. Box 92960  
World Way Postal Center  
Los Angeles, CA 90009

Steve A. Cresswell  
Federal Electric Corporation  
Systems Performance Analysis Dept.  
P.O. Box 1886  
Vandenberg AFB, CA 93437

Richard C. Crutchfield  
IBM Corporation  
21 First Field Rd.  
Gaithersburg, MD 20760

Jay B. Curtright  
Jet Propulsion Lab  
4800 Oak Grove Dr.  
Pasadena, CA 91109

Leonard S. Cutler  
Hewlett Packard  
3500 Deer Creek Rd.  
Palo Alto, CA 94304

Peter R. Dachel  
Bendix  
9250 Route 108  
Columbia, MD 21045

Fredrick Danzy  
U.S. Naval Research Lab.  
4555 Overlook Ave., S.W.  
Washington, DC 20375

Charles L. Daves, Jr.  
Hughes Aircraft Company  
P.O. Box 31979  
Aurora, CO 80041

B. Louis Decker  
DMA Aerospace Center  
402 Devon Court  
Ballwin, MO 63011

Bearl F. Dennison  
Hughes Aircraft Co.  
6926 S. Spruce Dr., West  
Englewood, CO 80112

Edoardo Detoma  
Bendix Field Engineering Co.  
Goddard Space Flight Center, Code 854  
Greenbelt, MD 20771

Michael A. Dials  
EFRATOM  
18851 Bardeen Ave.  
Irvine, CA 92715

John S. Doby  
Defense Communications  
Engineering Center  
1860 Wiehle Ave.  
Reston, VA 22090

Lawrence Doepke  
DMAAC  
9418 Oakwood Manor  
St. Louis, MO 63126

Robert W. Donaldson  
Westinghouse Electric Corp.  
P.O. Box 1897, MS 935  
Baltimore, MD 21203

William Donnell  
TRACOR, Inc  
6500 Tracor Lane  
Austin, TX 78721

Mary S. Ealum  
DMAAC  
7014 Christopher Dr.  
St. Louis, MO 63129

James D. Echols  
Austron, Inc.  
1915 Kramer Lane  
Austin, TX 78758

Warren E. Edwall  
RCA Corporation  
1901 N. Moore St.  
Arlington, VA 22209

Richard Allen Eichinger  
Bendix Field Engr. Corp.  
9250 Route 108, M.S.: EOG/MAS  
Columbia, MD 21045

Robert F. Ellis  
Austron, Inc.  
1915 Kramer Lane  
Austin, TX 78758

Thomas C. English  
EFRATOM  
18851 Bardeen  
Irvine, CA 92626

Glen E. Eubanks  
OP 952  
U.S. Naval Observatory  
34th and Mass. Ave.  
Washington, DC 20390

James H. Ewing  
Gawler-Knoop Co.  
9209 Wendell St.  
Silver Spring, MD 20901

Michael Fischer  
Hewlett-Packard  
5301 Stevens Creek Blvd.  
Santa Clara, CA 95050

Terry M. Flanagan  
JAYCOR  
P.O. Box 85154  
San Diego, CA 92138

Vincent J. Folen  
NRL  
Code 6892  
Washington, DC 20390

Hugh S. Fosque  
NASA Hdq., Code TP  
Washington, DC 20546

D. Earl Fossler  
Trak Systems  
Division of Trak Microwave Corp.  
4726 Eisenhower Blvd.  
Tampa, FL 33614

George T. Fouratt  
I.T.T.  
P.O. Box 1886  
Lompoc, CA 93437

Harold C. Friend  
DCA, DCEC  
1860 Wiehle Ave.  
Reston, VA 22090

Dan Fryberger  
Interstate Electronics Corp.  
1745 Jefferson Davis Highway  
Arlington, VA 22202

Hitohiro Fukuyo  
2-19 Yoyogi, Shibuyaku  
Tokyo, Japan

Jean C. Gaignebet  
CNRS GRGS/CERGA  
Av Copernic  
Grasse, France F06130

Davis R. Gamble, Jr.  
Defense Communications  
Engineering Center  
1860 Wiehle Ave.  
Reston, VA 22090

Thomas H. Gattis  
Naval Research Lab.  
4555 Overlook Ave.  
Washington, DC 20375

Michel Granveaud  
Bureau International de L'Heure  
67 Av. Observatoire  
Paris, France 75074

David L. Hall  
HRB Singer, Inc.  
P.O. Box 60, Science Park Rd.  
State College, PA 16801

R. Glenn Hall  
3612 Spring St.  
Chevy Chase, MD 20815

Eugene P. Hamilton  
Systron Donner  
2727 Systron Dr.  
Concord, CA 94518

Donald W. Haney  
Haney's Electronic Systems  
10412 Scaggsville Road  
Laurel, MD 20707

Samuel N. Harmatuk  
1575 Odell St.  
Bronx, NY 10462

Nelson J. Hayes  
TRW  
One Space Park  
Redondo Beach, CA 90278

Robert J. Hesselberth  
Spectracom Corp.  
320 N. Washington St.  
Rochester, NY 14625

Norman Houlding  
MITRE Corp.  
P.O. Box 208  
Bedford, MA 01730

Quyen D. Hua  
Stanford Telecommunications, Inc.  
1195 Bordeaux Dr.  
Sunnyvale, CA 94186

John F. Hynes  
USAF  
Scott AFB/EETST, IL 62225

Edward A. Imbier  
Smithsonian Astrophysical  
Observatory  
60 Garden St.  
Cambridge, MA 02138

Jeffrey S. Ingold  
Bendix Field Eng.  
9250 Route 108  
Columbia, MD 21045

Andrew Johnson  
U.S. Naval Observatory Time Service  
34th & Massachusetts Ave.  
Washington, DC 20390

Kenneth J. Johnston  
NRL  
Code 4130  
Washington, DC 20375

Robert Kaarls  
Van Swinden Laboratory  
Natl. Service of Metrology  
13 Klaverwydenstraat  
Zoeterwoude, Netherlands 2381VX

Lou Franklin Kalil  
Goddard Space Flight Center/NASA  
Greenbelt Rd.  
Greenbelt, MD 20771

Edward J. Kasnicki  
Computer Sciences Corp.  
6565 Arlington Blvd.  
Falls Church, VA 22046

William W. Kellogg  
Lockheed Missiles and Space Co., Inc.  
1111 Lockheed Way, P.O. Box 504  
Sunnyvale, CA 94086

Dieter Kirchner  
Technical University Graz  
12 Inffeldgasse  
Graz, Austria A-8010

Richard A. Kitzerow  
U.S. Air Force, AFWAL/AARM  
253 Debs Drive  
Xenia, OH 45385

Chester J. Kleczek  
NRL Code 7969  
Washington, DC 20375



William J. Klepczynski  
U.S. Naval Observatory  
Washington, DC 20390

Frank K. Koide  
Rockwell International  
3370 Miraloma Avenue  
Mail Code HC02  
Anaheim, CA 92803

Karl L. Kovach  
USAF Space Division/YEU  
P.O. Box 92960  
World Way Postal Center  
Los Angeles, CA 90009

Robert M. Kramer  
Lockheed-California Co.  
1235 Jefferson Davis Hwy.  
Arlington, VA 22202

Bernard A. Kreigsman  
C.S. Draper Lab  
555 Tech. Sq. MS73  
Cambridge, MA 02139

Ralph A. Kriss  
Bendix Field Eng. Corp.  
9250 Route 108  
Columbia, MD 21045

Robert L. Kruger  
Bendix Field Engineering Corp.  
6118 Loventree Rd.  
Columbia, MD 21044

Anthony J. Kubik  
U.S. Naval Observatory  
34th and Mass. Avenue  
Washington, DC 20390

Paul F. Kuhnle  
Jet Propulsion Lab.  
4800 Oak Grove Drive  
Pasadena, CA 91109

Ryszond Kunki  
Bendix Field Engineering Corp.  
Columbia, MD 21045

Naimu Kuramochi  
Tokyo Institute of Technology  
4259 Nagatsuta, Midori-ku  
Yokohama 227, Japan

Tae M. Kwon  
Litton Guidance & Control  
5500 Canoga Ave.  
Woodland Hills, CA 91360

Ronald Lake  
N.P.R.L. of the C.S.I.R.  
P.O. Box 395 Pretoria 0001  
Republic of South Africa

Algie L. Lance  
TRW-Electronics & Defense  
One Space Park S-2471  
Redondo Beach, CA 90278

Leonard R. Lathrem  
Bendix Field Engr. Corp.  
9250 Route 108  
Columbia, MD 21061

Jean-Daniel Lavanceau  
LT International  
4907 Asbury Lane  
Bethesda, MD 20814

Felix Lazarus  
Hewlett-Packard (Schweiz) AG  
19 Chemin Chateau-Bloc  
1219 Le Lignon  
Geneva, Switzerland

David L. Lerner  
Technical Services  
P.O. Box MM  
Lytle Creek, CA 92358

Sigfrido Leschiutta  
Politecnico Di Torino-Elettronica  
24 Corso Duca D'Abbruzzi  
Torino, Italy

Vestal R. Lester  
Hughes Aircraft Co.  
19631 Strathern St.  
Reseda, CA 91335

Lionel Lipschultz  
Applied Physics Lab.  
Johns Hopkins Univ.  
412 E. Franklin Ave.  
Silver Spring, MD 20901

Mark J. Lister  
NRL  
4555 Overlook Ave.  
Washington, DC 20375

Melchiorre G. Lombardo  
European Space Agency  
(c/o Telespazio)  
42 Corso Italia  
Rome, Italy

Carl Lukac  
U.S. Naval Observatory Time Service  
34th & Massachusetts Ave.  
Washington, DC 20390

George F. Lutes  
Jet Propulsion Laboratory  
4800 Oak Grove Drive  
Pasadena, CA 91109

Donald W. Lynch  
Naval Research Lab.  
4555 Overlook Ave., S.W.  
Washington, DC 20375

Lute Maleki  
JPL  
4800 Oak Grove Dr.  
Pasadena, CA 91108

John C. Mankins  
Bendix/JPL  
240 W. Verdugo, Apt. V  
Burbank, CA 91502

Alvin A. Marquis  
Bendix Field Eng. Corp./NRL  
6416 85th Place  
New Carrollton, MD 20784

James A. Marshall  
Hewlett-Packard Co.  
5301 Stevens Creek Blvd.  
Santa Clara, CA 95050

Thomas D. Martin  
Electrospace Systems, Inc.  
1601 N. Plano Rd.  
P.O. Box 1359  
Richardson, TX 75074

Edward M. Mattison  
Smithsonian Astrophysical  
Observatory  
60 Garden St.  
Cambridge, MA 02138

Thomas B. McCaskill  
NRL  
Overlook Avenue  
Washington, DC 20375

Arthur O. McCoubrey  
National Bureau of Standards  
Washington, DC 20234

Kathy J. McDonald  
NRL  
4555 Overlook Ave., SW  
Washington, DC 20375

John E. McKeever  
U.S. Coast Guard  
8413 Ravenswood Rd.  
New Carrollton, MD 20784

Stephen R. McReynolds  
General Electric  
15 Patriot Circle  
Devon, PA 19333

Marvin Meirs  
Frequency Electronics, Inc.  
3 Delaware Drive  
New Hyde Park, NY 11040

Walter C. Melton  
Stanford Telecommunications, Inc.  
1195 Bordeaux Dr.  
Sunnyvale, CA 94086

John L. Metcalf  
Naval Electronic Systems  
Engineering Activity  
024 Division  
St. Inigoes, MD 20684

Wendell D. Metcalf  
Naval Electronic Systems  
Engineering Activity  
024 Division  
St. Inigoes, MD 20684

Paul G. Miller  
Litton  
L'Enfant Plaza  
Washington, DC 20546

G. Missout  
HYDRO Quebec  
1800 Montee Ste Julie  
Varenes PQ, Canada J3V2R3

Donald H. Mitchell  
Kentron International  
P.O. Box 4819  
Yuma, AZ 85364

Billy B. Moon  
U.S. Air Force, PTTI Training  
17124 E. Brown Circle  
Aurora, CO 80013

Craig R. Moore  
National Radio Astronomy  
Observatory  
P.O. Box 2  
Green Bank, WV 24944

Patrick J. Moran  
Pacific Missile Test Center  
Code 3533  
Point Mugu, CA 93042

Derek Morris  
Physics Division  
National Research Council  
Montreal Road  
Ottawa, Ontario, Canada K1A 0R6

Ivan I. Mueller  
Ohio State University  
Dept. of Geodetic Science &  
Surveying  
1958 Neil Avenue  
Columbus, OH 43210

Francis H. Mullen  
Frequency & Time Systems  
34 Tozer Rd.  
Beverly, MA 01915

James A. Murray  
Naval Research Lab.  
Code 7962  
Washington, DC 20375

Toshimitsu Musha  
Tokyo Institute of Technology  
4259 Nagatsuta, Midoriku  
Yokohama, Japan

Frank J. Narr  
Vitro Laboratories  
14000 Georgia Ave.  
Silver Spring, MD 20910

Stephen Nichols  
Naval Electronics System Command  
PME 106-6  
Washington, DC 20360

Jerry R. Norton  
Johns Hopkins Univ/APL  
Johns Hopkins Rd.  
Laurel, MD 20707

Michael J. Nugent  
Department of Defense W36  
9800 Savage Rd.  
Ft. George G. Meade, MD 20755

Jay Oaks  
Naval Research Laboratory  
4555 Overlook Ave., S.W.  
Code 7966  
Washington, DC 20375

William S. Orr  
18131 East 4th Street  
Tulsa, OK 74108

Eugene J. O'Sullivan  
Mitre Corp.  
P.O. Box 208  
Bedford, MA 01730

Peter C. Ould  
Interstate Electronics Co.  
707 E. Vermont Ave.  
Anaheim, CA 92803

Nobunori Oura  
Tokyo Institute of Technology  
4259 Nagatsuta, Midoriku  
Yokohama 227, Japan

Dorothy M. Outlaw  
231 Nicholson St., N.E.  
Washington, DC 20011

Xiaopei Pan  
Shaanxi Astronomical Observatory  
P.O. Box 18  
Lington, Shaanxi  
People's Republic of China

Harry E. Peters  
Sigma Tau Standards Corp.  
Box 1877  
1014 Hachberry Lane  
Tuscaloosa, AL 35403

H.E. Petrey  
Def. Map Agy.  
Al 6424 N. 54th Ave.  
St. Petersburg, FL 33709

Edward A. Pettit  
Eastern Space & Missile Center  
Range Systems Management  
ETR/RSM  
Patrick AFB, FL 32925

David H. Phillips  
Naval Research Lab.  
Washington, DC 20375

Paul J. Pointer  
Dept. of Defense  
9800 Savage Rd.  
Ft. Meade, MD 20755

Joseph M. Przyjemski  
C.S. Draper Labs. MS-92  
555 Technology Sq.  
Cambridge, MA 02138

Gerard L. Punt  
Interstate Electronics  
707 E. Vermont Ave.  
Anaheim, CA 92803

Ken Putkovich  
U.S. Naval Observatory  
34th St. & Mass. Ave., N.W.  
Washington, DC 20390

Victor S. Reinhardt  
NASA/GSFC  
Code 854  
Greenbelt, MD 20771

Joseph Rhodes  
4605 Post Oak Tritt, NE  
Marietta, GA 30062

Jerry L. Ricks  
Bendix Field Eng. Corp.  
P.O. Box 578  
LaPlata, MD 20646

William J. Riley  
EG&G, Inc.  
35 Congress St.  
Salem, MA 01970

Ronald C. Roloff  
Bendix  
8005 McKenstry Dr.  
Laurel, MD 20707

Mitchell G. Roth  
Jet Propulsion Lab.  
4800 Oak Grove Dr.  
Pasadena, CA 91109

Lauren J. Rueger  
The Johns Hopkins University  
Applied Physics Laboratory  
Johns Hopkins Road  
Laurel, MD 20707

John G. Schmid  
USAF AFSC WSMC  
1528 W. Cherry Ave.  
Lompoc, CA 93436

Malvin C. Schwalje  
Frequency and Time Systems, Inc.  
34 Tozer Road  
Beverly, MA 01915

Bengt A. Selin  
Swedish Telecommunications  
Administration, Rlm  
Marbackagatan 11  
Farsta, Sweden S-12386

Bernard E.H. Serene  
European Space Agency  
18 Avenue Edouard Belin  
31055 Toulouse  
Cedex, France

Dan S. Serice  
NASA Hq.  
600 Md. Ave.  
Washington, DC 20546

Barry L. Shoop  
Tobyhanna Army Depot  
U.S. Army  
Tobyhanna, PA 18466

Alexander Skopetz  
NASA/GSFC  
11911 Galaxy Lane  
Bowie, MD 20715

James A. Slater  
Defense Mapping Agency  
6500 Brookes Lane  
Washington, DC 20315

Arthur E. Smith  
Data Collection Div., Code 3412.3  
Range Inst. System Dept.  
Pt. Mugu, CA 93048

Willard J. Smith  
USAF Bolling AFB OLA89 FMS/PMEL  
Bolling AFB  
Washington, DC 20336

John H. Spencer  
NRL  
Code 4134.2  
Washington, DC 20375

Thomas M. Stalder  
Bendix Field Engineering Corp.  
5707 Thunderhill Rd.  
Columbia, MD 21045

James R. Steele  
Litton Industries  
5500 Canoga Ave.  
Woodland Hills, CA 91360

Samuel R. Stein  
National Bureau of Standards  
325 S. Broadway  
Boulder, CO 80302

Gary Stephens  
Stephens Applied Science, Inc.  
645 Governors Bridge Rd.  
Davidsonville, MD 21035

John E. Stephens  
Hewlett-Packard Co.  
5301 Stevens Creek Blvd.  
Santa Clara, CA 95050

Mac W. Stinson  
RCA International Service Co.  
Box 4608, GBI  
Patrick AFB, FL 32925

Harris A. Stover  
Defense Communications  
Engineering Center  
1860 Wiehle Ave.  
Reston, VA 22180

John T. Strain  
FET  
13975 Conn. Ave., #210  
Silver Spring, MD 20906

Herbert D. Stringer  
E-Systems/Garland Division  
MS 50380  
P.O. Box 226118  
Dallas, TX 75266

Peter P. Strucker  
Navy Metrology Engineering  
Center  
P.O. Box 2456  
Pomona, CA 91769

Lawrence C. Swenson  
Naval Electronic Systems  
Engineering Activity  
024 Division  
St. Inigoes, MD 20684

Richard L. Sydnor  
JPL  
4800 Oak Grove Drive  
Pasadena, CA 91109

Arthur C. Taber  
San Francisco State University  
560 Rockdale Dr.  
San Francisco, CA 94127

Philip E. Talley  
Aerospace Corp.  
550 Margo Ave.  
Long Beach, CA 90803

Michel Tetu  
E.E. Dept., Universite Laval  
Pavillon Pouliot  
Ste-Foy, Canada G1K-7P4

William J. Thrall  
U.S.C.G.  
3413 Austin Ct.  
Alexandria, VA 22310

James W. Tomlin  
Hughes Aircraft Co.  
2000 Mathews Ave., #3  
Redondo Beach, CA 90278

Pierre Tremblay  
Genie Electrique  
Universite Laval  
Quebec, Quebec, Canada G1K 7P4

Kenneth M. Uglow  
Box 2260  
Sarasota, FL 33578

Vinicio Vannicola  
G-ONSOD/43  
U.S. Coast Guard  
2100 2nd St., S.W.  
Washington, DC 20593

Robert J. Van Wechel  
Interstate Electronics Co.  
707 E. Vermont Ave.  
Anaheim, CA 92803

Robert F.C. Vessot  
Smithsonian Institution  
60 Garden Street  
Cambridge, MA 02138

John R. Vig  
U.S. Army Electronics  
Technology & Devices Lab  
Attn: DELET-MQ  
Fort Monmouth, NJ 07703

Charles H. Volk  
Aerospace Corporation  
P.O. Box 92957  
Los Angeles, CA 90009

Elbert S. Walker  
Hughes Aircraft Co.  
P.O. Box 31979  
Aurora, CO 80041-0979

William C. Walker  
Pan Am World Airways  
Bldg. 989 MU 840  
Patrick AFB, FL 32925

Fred L. Walls  
National Bureau of Standards  
325 Broadway  
Boulder, CO 80303

Elizabeth B. Waltman  
Naval Research Lab.  
Code 4134  
Washington, DC 20375

Harry T.M. Wang  
Hughes Research Laboratories  
3011 Malibu Canyon Road  
Malibu, CA 90265

Samuel C. Ward  
Jet Propulsion Laboratory  
4474 El Prieto Rd.  
Altadena, CA 91001

Clark S. Wardrip  
NASA-GSFC Code 854.1  
Greenbelt, MD 20711

Hugh E. Warren  
Bendix  
2946 Waterford Ct.  
Vienna, VA 22180

Werner A. Weidemann  
Efratom Cal., Inc.  
18851 Bardeen Ave.  
Irvine, CA 92715

Walter L. Welch  
Hughes Aircraft Co.  
P.O. Box 31979  
Aurora, CO 80041-0979

Gart Westerhout  
U.S. Naval Observatory  
Washington, DC 20390

Robert W. Wettingfeld  
Naval Research Lab.  
Washington, DC 20375

Paul T. Wheeler  
U.S. Naval Observatory  
Mass. Ave.  
Washington, DC 20390

Joseph D. White  
U.S. Naval Research Lab.  
Mail Code 7962  
Washington, DC 20375

Gary G. Whitworth  
Applied Physics Lab/JHU  
Johns Hopkins Rd.  
Laurel, MD 20707

Phillip C. Wildhagen  
Aerospace Corp.  
Box 92957  
Los Angeles, CA 90009

John J. Wilson  
Naval Ocean Systems Center  
Code 813  
San Diego, CA 92103

Warren L. Wilson  
Fairchild Test Systems  
1725 Technology Dr., MS 36-501  
San Jose, CA 95115

David J. Wineland  
NBS-Boulder, Div. 524.11  
325 Broadway  
Boulder, CO 80303

G.M.R. Winkler  
U.S. Naval Observatory  
Time Service  
34th & Massachusetts Ave.  
Washington, DC 20390

Sidney M. Wood  
Naval Electronic Systems  
Engineering Activity  
024 Division  
St. Inigoes, MD 20684

William H. Wooden  
DMAHTC  
6500 Brookes Lane  
Washington, DC 20315

Warren K. Wordsworth  
Austron, Inc.  
12024 Canter La.  
Reston, VA 22091

James L. Wright  
Pan American Airways-ASD  
Bldg. 989, MU840  
Patrick AFB, FL 32925

Nicholas F. Yannoni  
Rome Air Development Center  
Hanscom AFB  
Bedford, MA 01731

Plato Zorzy  
DELTEK  
P.O. Box 2074  
Salem, MA 01970

## BIBLIOGRAPHIC DATA SHEET

1. Report No. CP 2220	2. Government Accession No.	3. Recipient's Catalog No.	
4. Title and Subtitle Proceedings of the Thirteenth Annual Precise Time and Time Interval (PTTI) Applications Planning Meeting		5. Report Date March 1982	
		6. Performing Organization Code 814.2	
7. Author(s) Schuyler C. Wardrip, Editor		8. Performing Organization Report No.	
9. Performing Organization Name and Address Goddard Space Flight Center Greenbelt, Maryland 20771		10. Work Unit No.	
		11. Contract or Grant No.	
		13. Type of Report and Period Covered	
12. Sponsoring Agency Name and Address Naval Observatory NASA Goddard Space Flight Center Naval Electronic Systems Command Naval Research Laboratory		14. Sponsoring Agency Code	
15. Supplementary Notes			
16. Abstract <p>These proceedings contain the papers presented at the Thirteenth Annual Precise Time and Time Interval (PTTI) Applications and Planning Meeting, including questions and answers following presentations. The purpose of the meeting was to give PTTI managers, systems engineers, and program planners a transparent view of the state-of-the-art, an opportunity to express needs, a view of important future trends, and a review of relevant past accomplishments; to provide PTTI users with new and useful applications, procedures, and techniques; to allow the PTTI researcher to better assess fruitful directions for research efforts.</p>			
17. Key Words (Selected by Author(s)) Time, Time transfer, Time dissemination, time measurement, Hydrogen masers, masers		18. Distribution Statement Unclassified Unlimited STAR Category 36	
19. Security Classification Unclassified	20. Security Classif. (of this page) Unclassified	21. No. of Pages 864	22. Price*